

**TNO report****TNO 2019 R10335 | 1.0****Porthos - CO2 injection****Energy**Leeghwaterstraat 44  
2628 CA Delft  
P.O. Box 6012  
2600 JA Delft  
The Netherlands[www.tno.nl](http://www.tno.nl)T +31 88 866 22 00  
F +31 88 866 06 30

Date	11 April 2019
Author(s)	S.P.C. Belfroid
Copy no	
No. of copies	
Number of pages	89 (incl. appendices)
Number of appendices	
Sponsor	EBN - Porthos consortium
Project name	Flow Assurance Porthos
Project number	060.33502

All rights reserved.

No part of this publication may be reproduced and/or published by print, photoprint, microfilm or any other means without the previous written consent of TNO.

In case this report was drafted on instructions, the rights and obligations of contracting parties are subject to either the General Terms and Conditions for commissions to TNO, or the relevant agreement concluded between the contracting parties. Submitting the report for inspection to parties who have a direct interest is permitted.

© 2019 TNO

## Summary

This report presents the results of a flow assurance analysis of the first elements of an offshore CO<sub>2</sub> transport and storage network that is being designed by the Porthos consortium. The network is intended to transport CO<sub>2</sub> from industrial sources in the Rotterdam harbour to offshore depleted gas fields. The scope of the flow assurance study was the offshore pipeline from the compressor outlet, from the Maasvlakte to the P18-A platform, and up to four injection wells in the P18-2 and P18-4 fields. These activities are part of TNO project 060.33502.

The goal of the simulations is to evaluate the operating envelope within pre-described boundary conditions and restrictions. The goal of this project is to:

- Define the required compressor discharge conditions (pressure and temperature)
- Evaluate potential start-up and shut-in procedures and evaluate any showstoppers in these processes.

Evaluation of the sizing of the main pipeline was part of the phase-1 activities and as such is not covered in this report.

To obtain the goals the following activities have been done:

- Transient simulations to obtain steady state operating conditions.  
In the simulations, the effect on the steady state results were evaluated for:
  - o Variation well diameter
  - o Variation reservoir parameter (pressure and accompanying injectivity index)
  - o Variation wellhead temperature (for single well models)
  - o Variation compressor outlet temperature
  - o Variation pipeline pressure control
- Start-up simulation
  - o Different starting conditions (gas, two-phase, liquid) conditions in the pipeline.
  - o Variation of the reservoir pressure.
- Shutin/turn-down simulations
  - o Variation reservoir pressures.
  - o Variation shutin valve closure time.

For steady state conditions the following conclusions are found:

- At low reservoir pressure (20-40 bar), no steady state solution is found which comply with both the topside and downhole temperature restrictions when the pipeline pressure is maintained in the liquid state. Therefore, at low reservoir pressure the pipeline must be operated in gas or two-phase conditions. This puts limitations on the maximum injection rates per well or for all four wells combined.
- At reservoir pressures (40-300 bar), the required flow rate (170 kg/s) is achieved using four wells.
- At close to the maximum reservoir pressures, the compressor outlet temperature needs to be reduced. Otherwise no injection is possible.

For depressurization the following conclusions are found:

- The heat ingress in the pipeline is limited. Therefore, during depressurization or emptying the pipeline the temperature follows the pressure via the phase line and low temperatures conditions can occur in the complete pipeline. Therefore, a pressure control of the pipeline is recommended.

For shutin simulations the following conclusions are found:

- During well shutin, low fluid temperatures will occur in the well downstream of the choke. The temperature will go down to the corresponding phase line temperature. At a reservoir pressure of 20 bar, this means a temperature of -37 °C. At lower reservoir pressures this will lower even further. At higher reservoir conditions, the temperature will increase. -17, -5 and +30 °C at reservoir pressures of 60, 100 and 340 bar.
- During ramp-down, low temperatures occur mainly in the top part of the well. These temperatures go well below -10 °C.
- During ramp-down also the temperature in the pipeline itself will drop down to values below -20 °C.
- The low temperatures during shutin/ramp-down are difficult to avoid and as such it is recommended that all piping should be able to withstand the low temperatures.

From the start-up simulations the following conclusions are found:

- For all reservoir conditions, at initial choke valve opening, a short period of low temperature will occur downstream of the control valves. For the start-up, a faster valve-opening is beneficial with respect to the temperatures.
- In the sequencing of well opening and compressor ramp-up, the flow rates from the pipe to the wells must not decrease too quickly to avoid too low pressures (and therefore temperatures in the well and pipeline). Therefore, the compressor ramp-up must be done relatively soon after the well opening. The compressor can be ramped-up before the well opening at higher reservoir pressures with the limit that the pipeline pressure must not be higher than 85 bar.
- At low reservoir pressure, the system could be started up from low pressure (10, 30 bar) or medium pressure (60 bar). In case of medium-pressure conditions, the downhole temperature is too low for a limited period of time (less than 500 minutes).
- At low reservoir pressure, starting from high pressure pipeline conditions leads to long periods of too low temperatures (longer than 2000 minutes).
- At medium and higher reservoir pressures start-up can be done from medium-pressure (two -phase conditions) conditions within the temperature restrictions.

The base recommended operations (based on the set restrictions) are:

- At low reservoir pressure, the pipeline is operated in the gas phase and all well chokes are kept open to avoid pressure drop. The compressor outlet temperature is set to 80 °C.
- At mid to high reservoir pressures, the compressor outlet temperature is set to 40 °C. The setting is an optimization between cooling power and compressor power.

- At very high reservoir pressures, compressor outlet temperature must be set to 40 °C, otherwise injection is not possible.

Reservoir pressure [bar]	Compressor outlet temperature [°C]	Pipeline control	Well operations
20 – 40 bar	80	30	Full open
40 – 300 bar	40 - 80	30	1 well on pressure control. Other wells on mass control
300 – 340 bar	40	30	1 well on pressure control. Other wells on mass control

During well shutin, a fast closure the choke valves leads to very low temperatures. At low reservoir pressures the shutin procedure should be leaving the wells open while shutting down the compressor.

The main recommendations include:

- All piping material should be designed for extreme low temperatures (-40°C, based on expected wellhead pressures of 10 bar).
- Update simulation model to include full heat transfer (rather than U-value approach) at the time the well design and pipeline design is set.. This to get more detailed temperature information on pipe wall temperatures and annulus fluid temperatures.
- Considering the fact that fluid temperatures less than -10°C are probably not avoidable, the restriction of -10°C for the topside temperature should be reconsidered/re-evaluated.
- The criterion of 15°C downhole temperatures is restrictive. Alternatives for hydrate preventions should be evaluated.
- An operational guidebook should be set up which describes the number of wells and control settings for each mass flow rate.

This guidebook should also contain guidelines of start-up and shutin procedures

# Contents

	<b>Summary.....</b>	<b>2</b>
<b>1</b>	<b>Introduction .....</b>	<b>8</b>
1.1	Introduction .....	8
1.2	Project goals .....	8
1.3	Project activities .....	8
1.4	Report layout.....	8
<b>2</b>	<b>Boundary conditions and assumptions .....</b>	<b>10</b>
2.1	Introduction .....	10
2.2	Boundary conditions .....	10
2.3	Simulation goals.....	10
<b>3</b>	<b>General discussion .....</b>	<b>11</b>
3.1	Introduction .....	11
3.2	CO <sub>2</sub> injection behaviour in wells free flow.....	11
3.3	CO <sub>2</sub> injection with controlled pipeline pressure.....	21
<b>4</b>	<b>Simulation model(s) .....</b>	<b>24</b>
4.1	Introduction .....	24
4.2	Basic model.....	24
4.3	Pipeline geometry.....	25
4.4	Well geometry .....	25
4.5	Reservoir.....	26
4.6	Heat transfer .....	27
<b>5</b>	<b>Shutin-wellhead conditions .....</b>	<b>28</b>
<b>6</b>	<b>Steady state.....</b>	<b>30</b>
6.1	Introduction .....	30
6.2	Simulation cases .....	30
6.3	Overview conclusions.....	35
<b>7</b>	<b>Start-up simulations.....</b>	<b>37</b>
7.1	Introduction .....	37
7.2	Simulations overview.....	38
7.3	Remarks valve openings .....	43
7.4	Discussion start-up reservoir pressure 20 bar– low pipeline pressure.....	44
7.5	Discussion start-up reservoir pressure 20 bar– mid pipeline pressure .....	45
7.6	Discussion start-up reservoir pressure 20 bar– high pipeline pressure .....	56
7.7	Discussion venting.....	60
7.8	Discussions alternatives .....	61
7.9	Discussion start-up reservoir pressure 60 bar – mid pipeline pressure .....	61
7.10	Discussion start-up reservoir pressure 100 – 340 bar – mid pipeline pressure.....	63
<b>8</b>	<b>Depressurization .....</b>	<b>67</b>
<b>9</b>	<b>Shut-in/turn-down.....</b>	<b>68</b>
9.1	Introduction .....	68

9.2	Simulation cases .....	68
9.3	Results well shutin for different reservoir pressures.....	69
9.4	Results turn-down reservoir pressure 20 bar.....	74
9.5	Results turn-down reservoir pressure 100 bar.....	77
9.6	Results turn-down reservoir pressure 340 bar.....	78
<b>10</b>	<b>Discussion/ general remarks .....</b>	<b>80</b>
<b>11</b>	<b>General conclusions &amp; recommendations.....</b>	<b>82</b>
11.1	General conclusions.....	82
11.2	Recommedations .....	84
<b>12</b>	<b>Signature .....</b>	<b>85</b>

## **Appendices**

A Steady state results

# 1 Introduction

## 1.1 Introduction

This report presents the results of a flow assurance analysis of the first elements of an offshore CO<sub>2</sub> transport and storage network that is being designed by the Porthos consortium. The network is intended to transport CO<sub>2</sub> from industrial sources in the Rotterdam harbour to offshore depleted gas fields. The scope of the flow assurance study was the offshore pipeline from the compressor outlet, from the Maasvlakte to the P18-A platform, and up to four injection wells in the P18-2 and P18-4 fields. These activities are part of TNO project 060.33502.

## 1.2 Project goals

The goal of the simulations is to evaluate the operating envelope within pre-described boundary conditions and restrictions (Chapter 2). The goal of this project is to:

- Define the required compressor discharge conditions (pressure and temperature)
- Evaluate potential start-up and shut-in procedures and evaluate any showstoppers in these processes.

Evaluating of the sizing of the main pipeline was part of the phase-1 activities and as such not covered in this report.

## 1.3 Project activities

To obtain the goals the following activities have been done:

- Transient simulations to obtain steady state operating conditions.  
In the simulations, the effect on the steady state results were evaluated for:
  - o Variation well diameter
  - o Variation reservoir parameter (reservoir pressure)
  - o Variation wellhead temperature (for single well models)
  - o Variation compressor outlet temperature
  - o Variation pipeline pressure control
- Start-up simulation
  - o Different start conditions (gas, two-phase, liquid) conditions in the pipeline.
  - o Variation reservoir pressure.
- Shutin/turn-down simulations
  - o Variation reservoir pressures.
  - o Variation shutin valve closure time.

## 1.4 Report layout

Prior to discussing the simulation results an overview of the main trends in CO<sub>2</sub> injection are covered in Chapter 3. In Chapter 2, the boundary conditions and restrictions are presented with in Chapter 4 a discussion on the model used.



The results are presented in the Chapters 6 (steady state results), Chapter 7 (Start-up simulations), Chapter 8 (depressurization/venting) and Chapter 9 (Shutin/turn down ). The Chapters 10 and 11 cover the main conclusions and discussion.

## 2 Boundary conditions and assumptions

### 2.1 Introduction

This section describes the boundary conditions and restrictions at the start of the project.

### 2.2 Boundary conditions

The following boundary conditions/assumptions are set in the project:

- Compressor outlet temperature  $35 < T < 80$  °C.
  - In the simulations a range of 40 to 80 °C is used as Gasunie had indicated that the last 5 °C required a huge investment.
- Desired flow total rates of 15 – 170 kg/s.
- A preferred mass flow rate of up to 70 kg/s per well.
- 4 wells available for injection (1 well in P18-4 compartment and 3 wells in the P18-2 compartment).
- Start reservoir pressure 20 bar; maximum Pres = 340 bar.
- Compressor control is based on suction pressure control.
  - This means that all CO<sub>2</sub> delivered to the low pressure network needs to be injected.
  - This means that not all the wells can be at mass flow control. This is important as from Chapter 2 it is clear that there are restrictions in mass flow rate.
- Pipeline Constraint
  - Preferred operation in single liquid phase condition.
  - Minimum discharge pressure compressor of 60 bar.
- Well Constraints
  - Downhole temperature  $T > 15$  °C
  - Topside piping  $T > -10$  °C
  - Erosion, Tubing vibrations, thermal/mass flow rate constraints for reservoir, thermal gradients in well (radial and axial)) are not considered at this stage

### 2.3 Simulation goals

The goal of the simulations are:

- Steady state results to obtain required compressor envelope
- Start-up scenarios
- Shut-in scenarios
- Discussion of cold vs warm start-up

## 3 General discussion

### 3.1 Introduction

In this chapter, some typical behaviour of CO<sub>2</sub> injection is discussed. This is done based on results for a simple pure vertical monobore geometry.

In section 3.2, results are presented for a free well. That means no pipeline is attached and no control choke is present at the wellhead. In section 3.3 results are presented with a control action at topside. This means for instance a pipeline pressure of pressure 85 bar and a mass controlled injection into the well.

### 3.2 CO<sub>2</sub> injection behaviour in wells free flow

#### 3.2.1 *Model description*

The model used for this chapter is a simple monobore, pure vertical well of depth 3000m with a topside section of 100m horizontal (0.15m ID), with a heat transfer of 9.5 W/m<sup>2</sup>K with a vertical thermal gradient of 10 to 123 °C.

#### 3.2.2 *Base result*

Some base results are given in Figure 1 with the downhole temperature and the wellhead pressure as function of mass flow rate. The behaviour can be divided into low and high reservoir pressures. Low reservoir pressure typically means up to a reservoir pressure of 50 bar. At that pressure, the accompanying phase line temperature is 15°C (for discussion on limitations and boundary conditions: Chapter 2).

At low reservoir pressure the important features are:

- The required wellhead pressure is strongly dependent on the wellhead temperature (higher temperatures require higher pressures).
- For a large range of mass flow rates, the required wellhead pressure is constant due to the fact that the wellhead is in two-phase conditions.
- The required wellhead pressure at low flow rates is (very) low.
- The downhole temperature decreases with increasing mass flow rate up to the point that two-phase conditions occur downhole. In that case the downhole temperature increases due to an increase in bottomhole pressure due to an increase reservoir pressure drop. When in two-phase conditions, the downhole temperature is independent of the wellhead temperature but only a function of the downhole pressure.
- The range of downhole temperatures higher than 15°C increases with increasing wellhead temperature.

At higher reservoir pressures the important features are:

- An almost constant wellhead pressure for all mass flow rates.
- The downhole temperature is almost always higher than 15°C and the remaining trend is that the bottomhole temperature decreases with increasing mass flow rate.

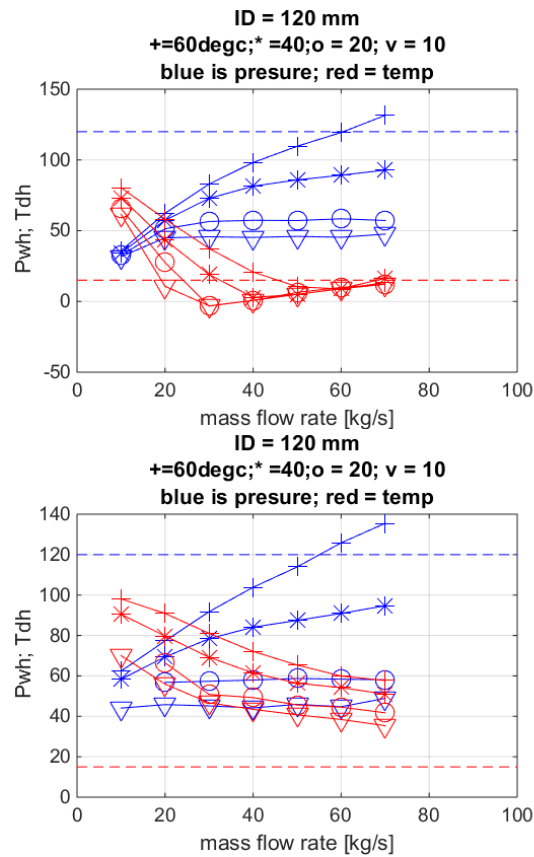


Figure 1: Wellhead pressures (blue) and downhole temperatures (red) as function of mass flow rate for a reservoir pressure of 20 bar (top) and 100 bar (bottom). Dashed lines indicate critical boundary conditions (120 bar and 15 °C). Each line is for a different wellhead temperature (10, 20, 40, 60 °C).

As example the pressure and temperature profiles in the well are plotted for:

- Reservoir pressure 20 bar, Wellhead temperature 10 °C    Figure 2
- Reservoir pressure 20 bar, Wellhead temperature 40 °C    Figure 3
- Reservoir pressure 100 bar, Wellhead temperature 10 °C    Figure 4
- Reservoir pressure 100 bar, Wellhead temperature 40 °C    Figure 5
- Reservoir pressure 300 bar, Wellhead temperature 10 °C    Figure 6
- Reservoir pressure 300 bar, Wellhead temperature 40 °C    Figure 7

The difference in behaviour between low and high pressures are directly clear. At low reservoir pressure, the well is mainly in the two-phase regime for the major part of the well. At high reservoir (300 bar), the complete well is in single phase supercritical conditions.

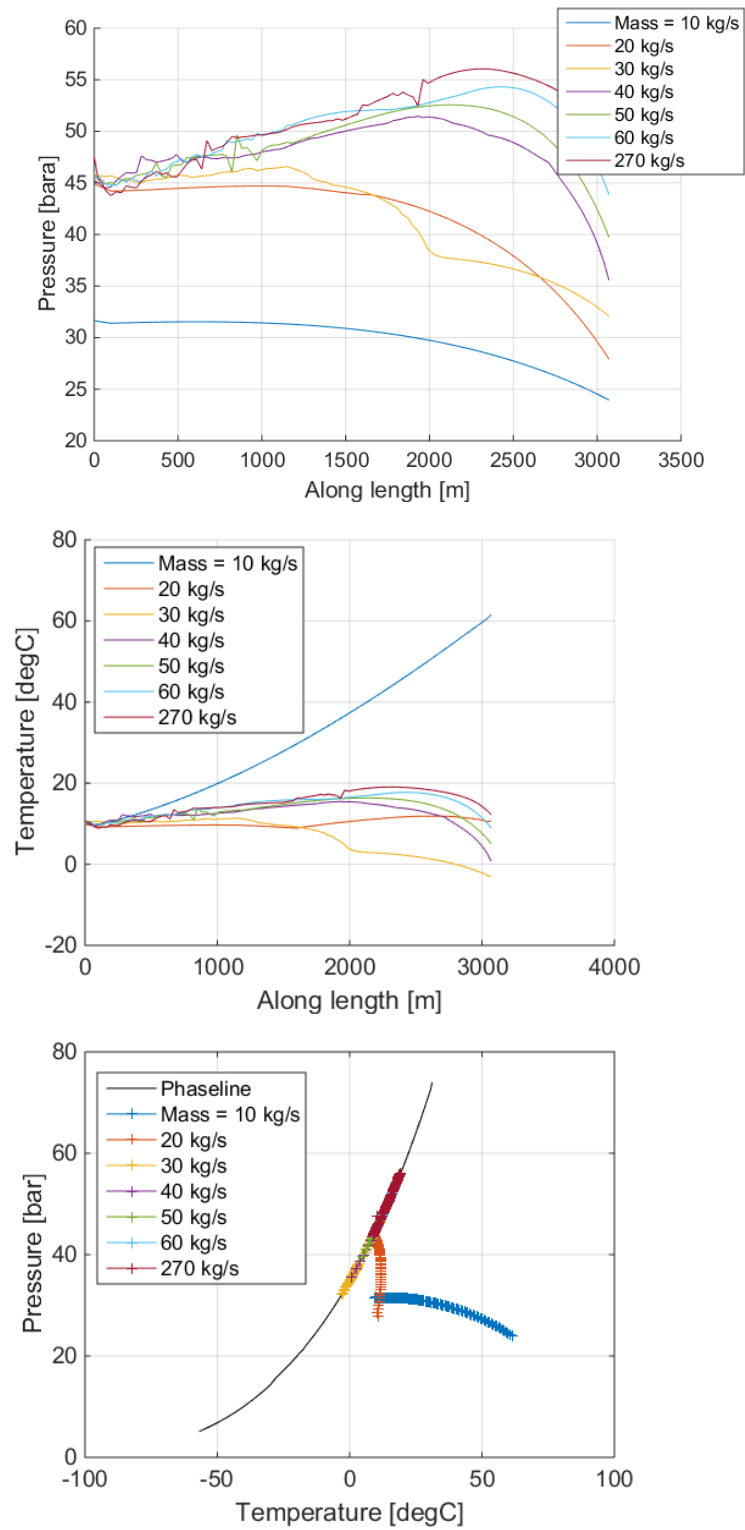


Figure 2: Pressure profile (top), temperature profile (middle) and P,T profile for a reservoir pressure of 20 bar and a wellhead temperature of 10°C. The mass flow ranges from 10 to 70 kg/s (edit one caption is wrong to be changed).

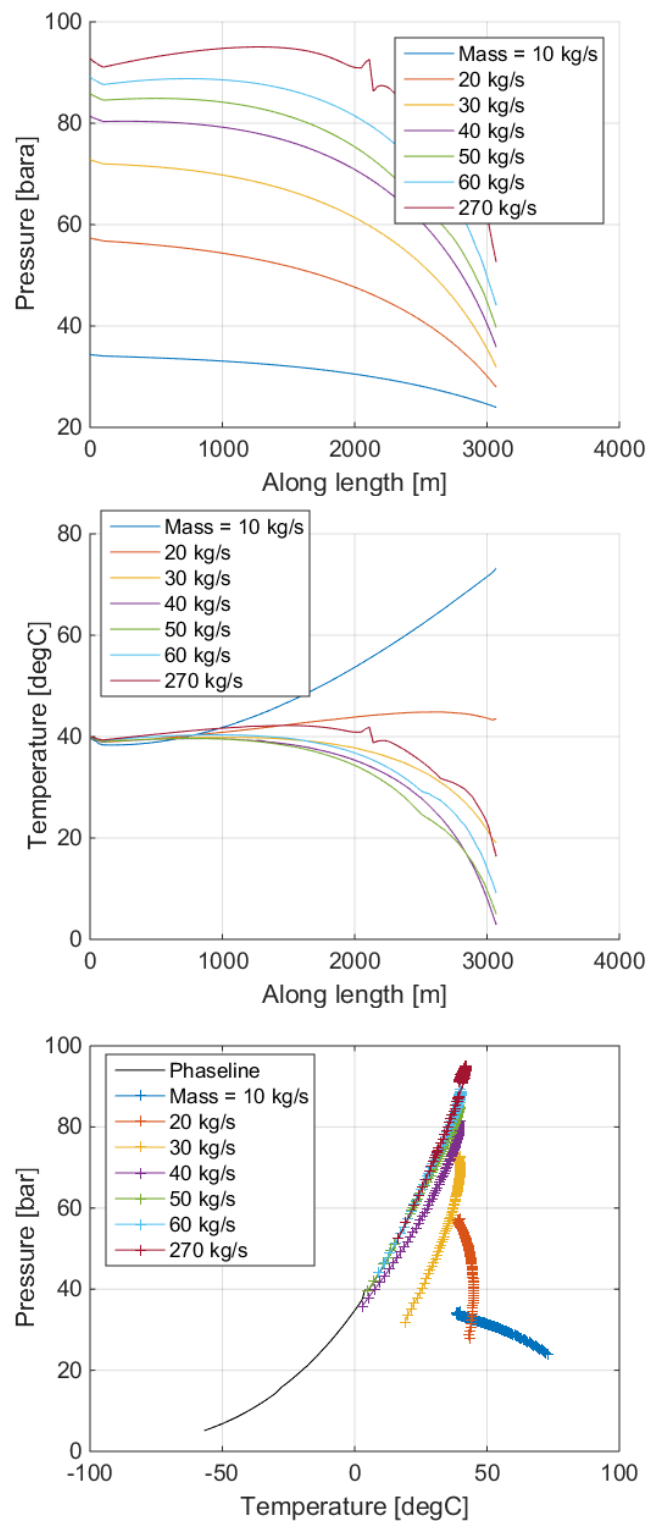


Figure 3: Pressure profile (top), temperature profile (middle) and P,T profile for a reservoir pressure of 20 bar and a wellhead temperature of 40°C. The mass flow ranges from 10 to 70 kg/s (edit one caption is wrong to be changed).

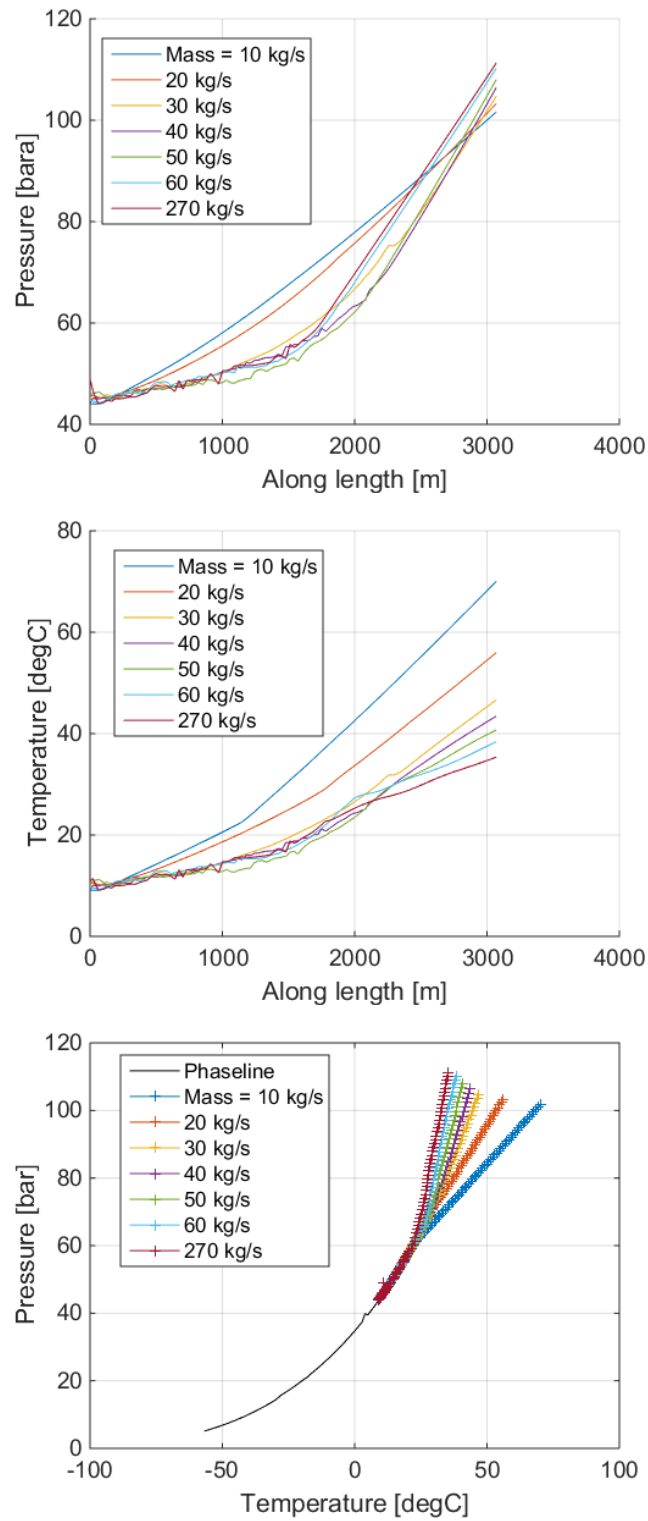


Figure 4: Pressure profile (top), temperature profile (middle) and P,T profile for a reservoir pressure of 100 bar and a wellhead temperature of 10°C. The mass flow ranges from 10 to 70 kg/s (edit one caption is wrong to be changed).

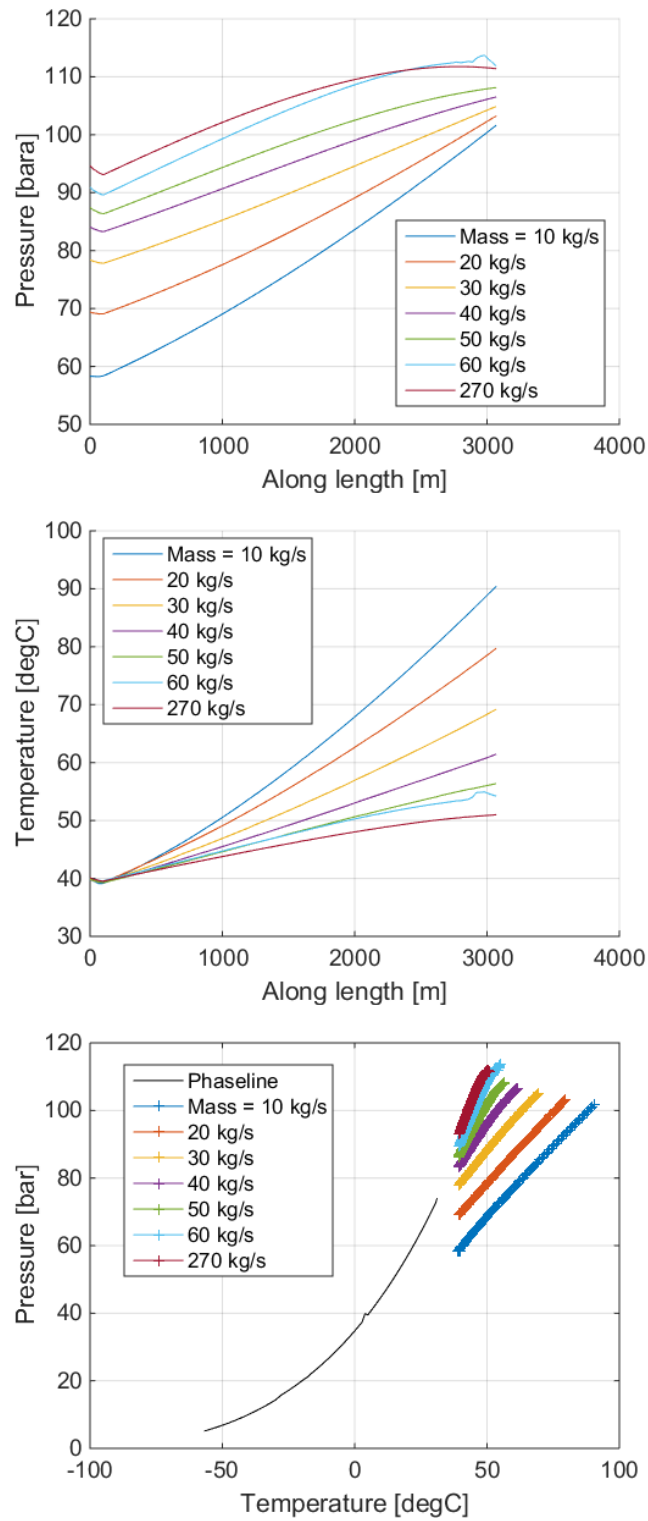


Figure 5: Pressure profile (top), temperature profile (middle) and P,T profile for a reservoir pressure of 100 bar and a wellhead temperature of 40°C. The mass flow ranges from 10 to 70 kg/s (edit one caption is wrong to be changed).



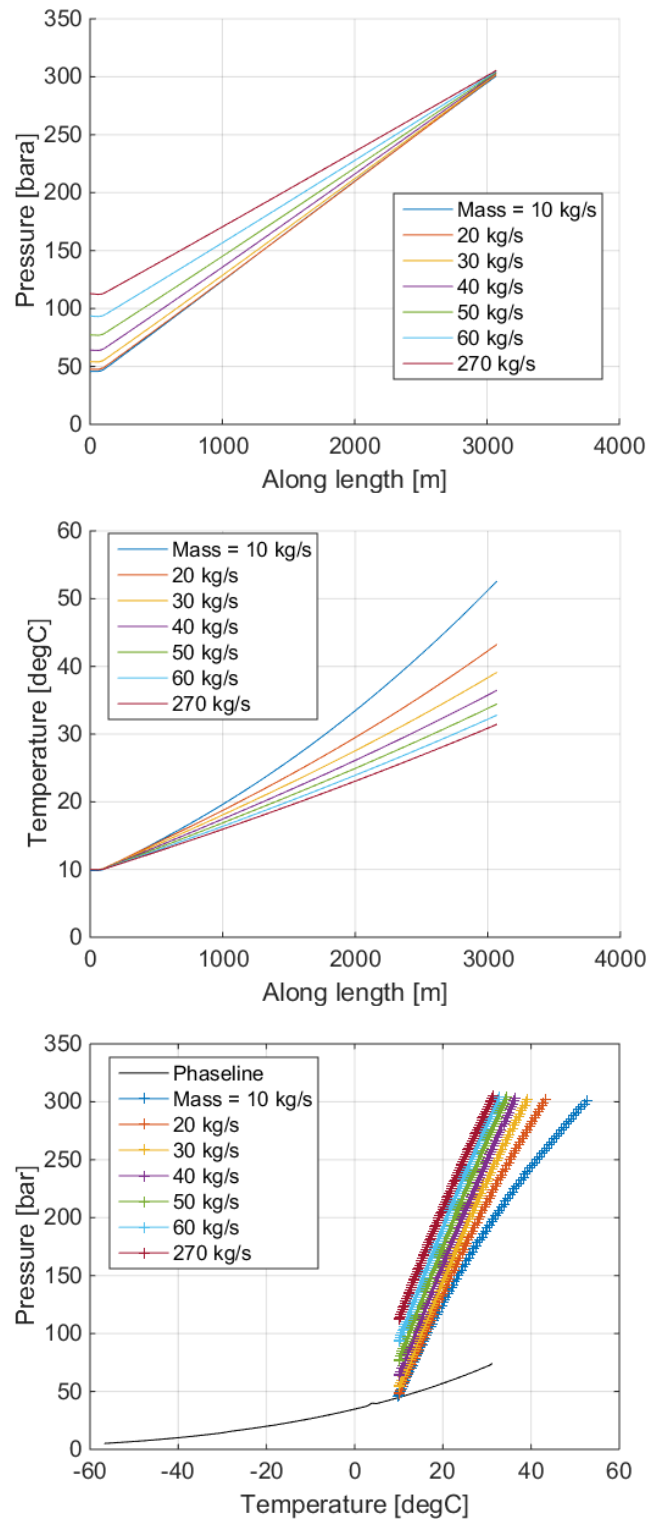


Figure 6: Pressure profile (top), temperature profile (middle) and P,T profile for a reservoir pressure of 300 bar and a wellhead temperature of 10°C. The mass flow ranges from 10 to 70 kg/s (edit one caption is wrong to be changed).

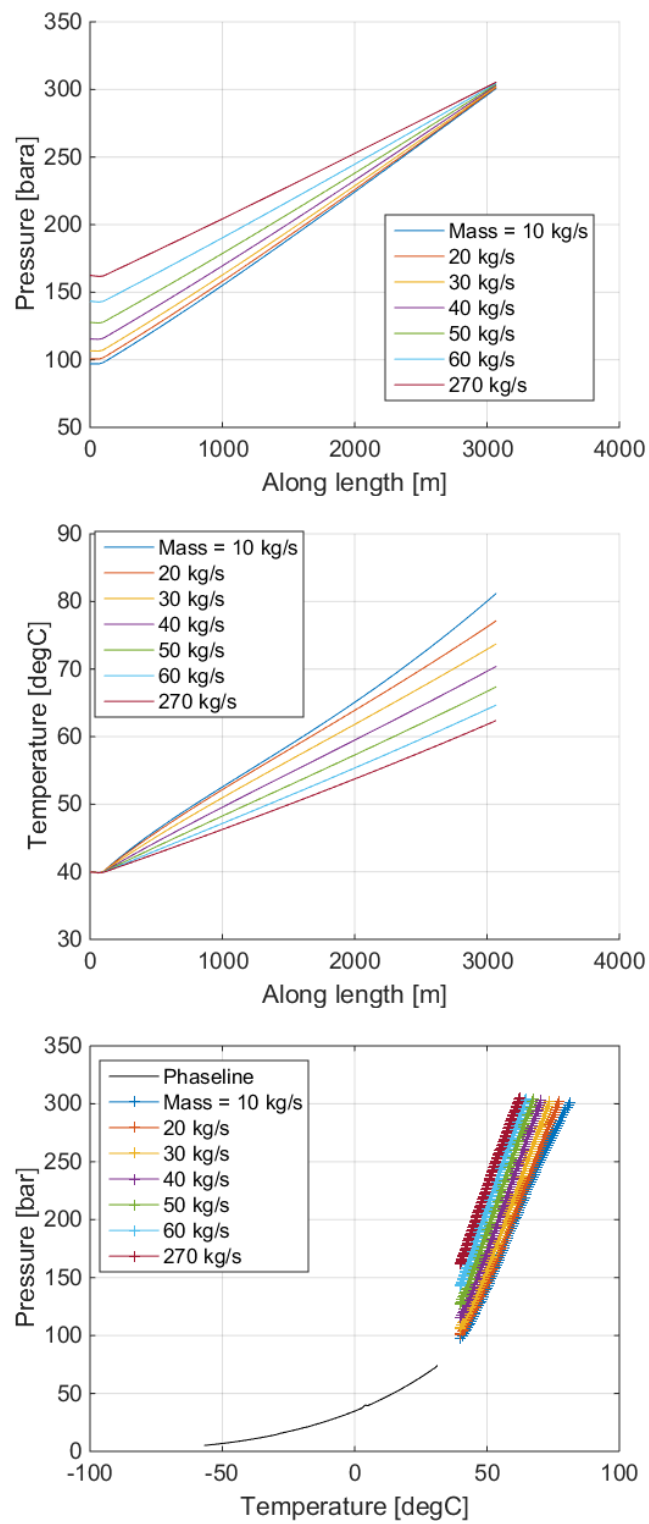


Figure 7: Pressure profile (top), temperature profile (middle) and P,T profile for a reservoir pressure of 300 bar and a wellhead temperature of 10°C. The mass flow ranges from 10 to 70 kg/s (edit one caption is wrong to be changed).

### 3.2.3 *Results influence reservoir pressure & influence well ID*

The influence of the well ID is plotted in Figure 8 in which the wellhead and downhole temperature are plotted as function of mass flow rate for a well with 50, 70, 90, 120 and 150 mm. These diameters are chosen based on 2 3/8", 3 1/2", 4 1/2", 5 1/2" and 7" tubing (approximate mid strength class).

At low reservoir pressure it is found that:

- The range of allowed flow rates with respect to the bottomhole temperature increases for increasing diameter.
- At larger diameters, the required wellhead pressure decreases.
- At temperatures lower than the critical temperature, the required wellhead pressure is constant for a range of mass flow rates. The minimum mass flow rate for when the required wellhead pressure becomes constant, increases for larger diameters..
- At smaller diameters, the required wellhead pressure is severely limiting. At a diameter of 70mm, the maximum flow rate is just 30 kg/s (at 10°C).

At mid reservoir pressures it is found:

- For diameters larger than (and including) 90 mm, there are basically no downhole temperature restrictions.
- For diameters smaller than (and including) 90 mm, the wellhead pressure is limiting to the mass flow rates for all temperatures.

At higher reservoir pressures it is found:

- For diameters smaller than (and including) 120 mm, the wellhead pressure is severely limiting for the allowed injection rate at higher temperatures.

Based on this set, a number of aspects can be concluded:

- At low reservoir pressure, a high temperature and large diameter is better with respect to the downhole temperature.
- At high reservoir pressures, a smaller diameter is rapidly restricting with respect to the mass flow rate. In other words, at smaller diameters, the required mass flow rates cannot be injected within the available wellhead pressure envelope.

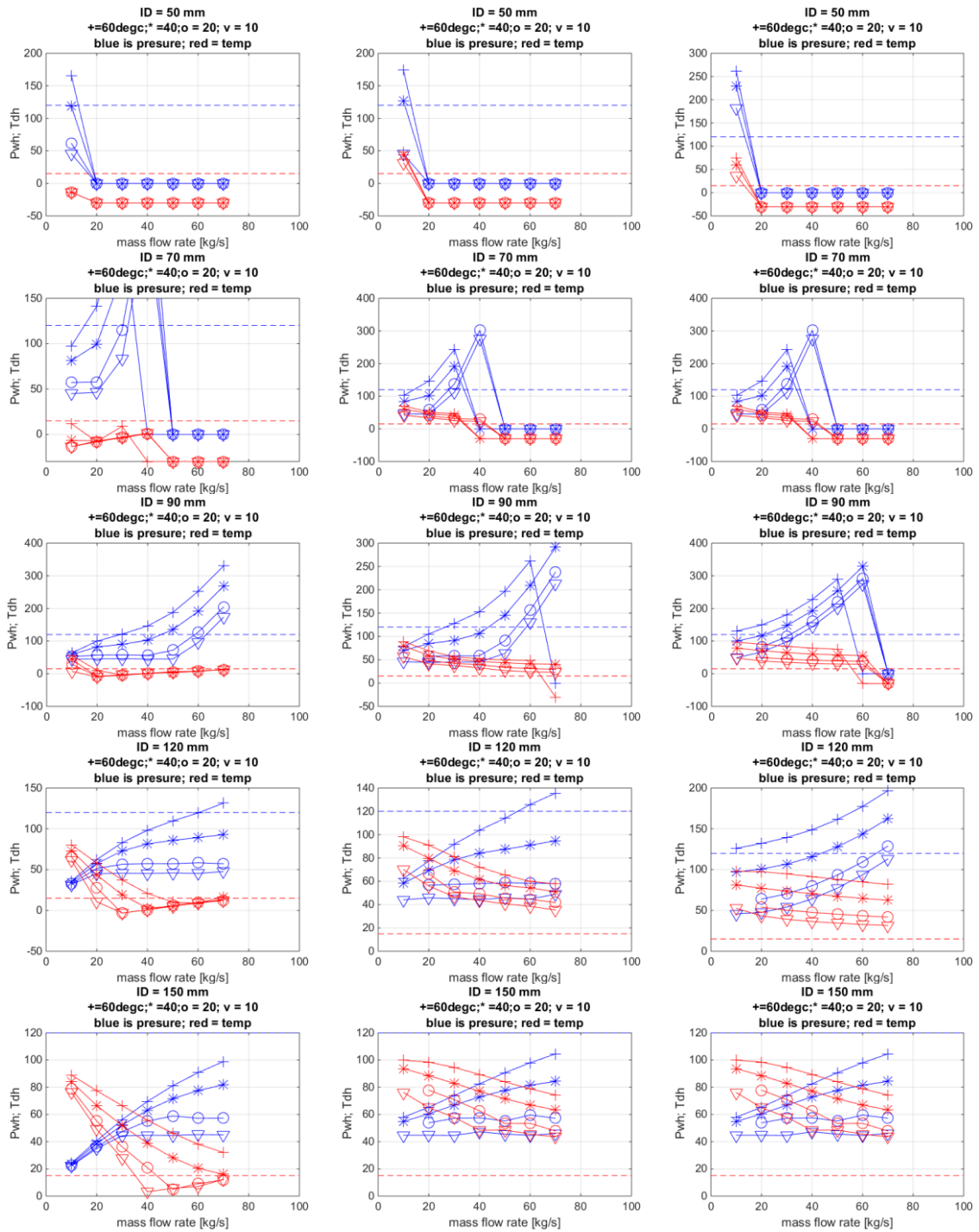


Figure 8: Influence well diameter (top to bottom rows) for a reservoir pressure of 20 bar (left), 100 bar (middle) and 300 bar (right). The simulations are limited to 350 bar. All cases with conditions higher than 350 bar are plotted as a pressure of 0 bar and a temperature of -30 °C.

### 3.3 CO<sub>2</sub> injection with controlled pipeline pressure

The results in the previous section are with a 'free' wellhead pressure. That is, there is no control choke at the wellhead. In this section a control valve is added. This control valve will keep the upstream pressure to a set value (or higher). It must be remarked that a section of 400m horizontal is used on the topside. This length was not set to very short as this would lead to numerical problems (with opening and closing of the choke the mass flow rate from the upstream side increases/decreases rapidly. This can lead to fast pressure variations in small volumes). Unfortunately that also meant some heat transfer was allowed in that section (for future cases, the heat transfer could be set to zero at those sections). This means the temperature arriving at the choke was not always similar to the 'inlet' temperature. This is especially true for low flow rates.

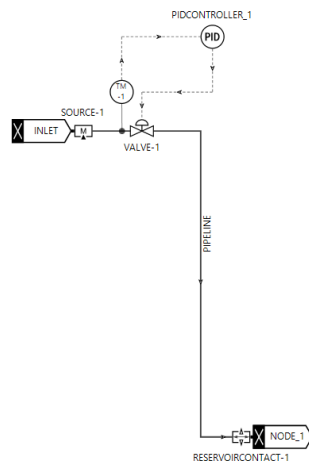


Figure 9: Model with control.

In this section results are given for:

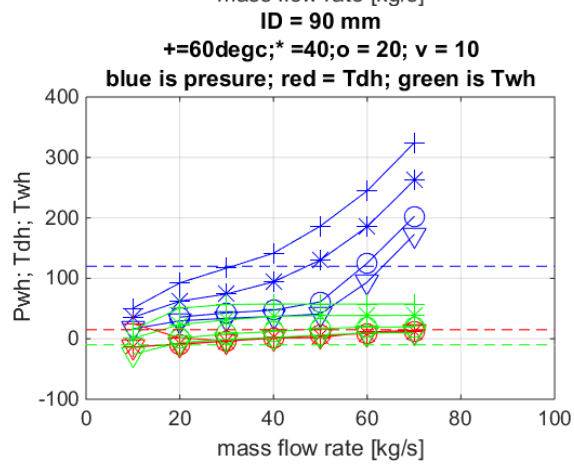
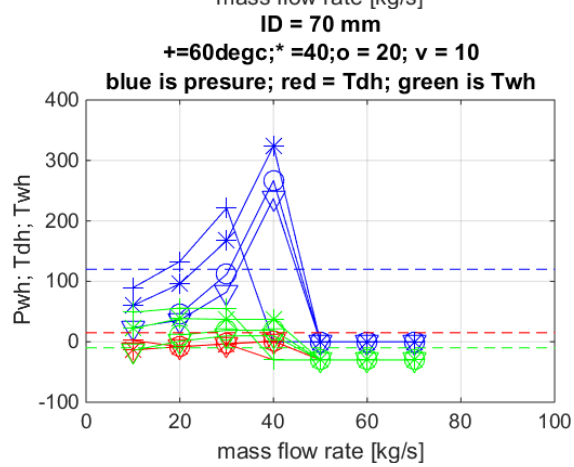
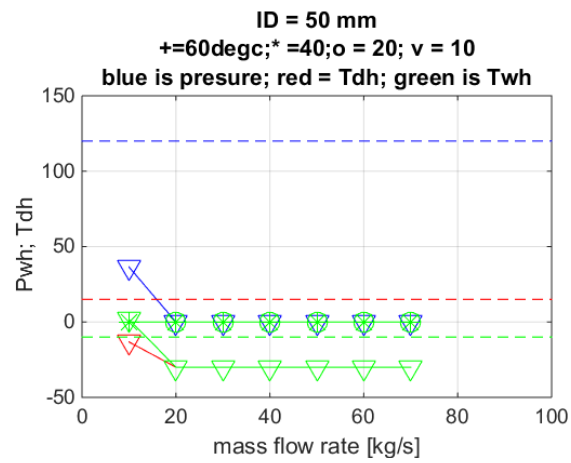
- Reservoir pressure 20 bar
- Pipeline pressure is minimally 85 bar

This condition is chosen as the low reservoir pressure is a strong limiting conditions as was shown in section 3.2.3.

The results are given in Figure 10. The figures are complex but the important conclusions are:

- At larger diameters, due to the low required wellhead pressures, a large pressure drop and therefore temperature drop occurs across the choke.
- The range of possible flow rates due to the downhole restriction (see Chapter 2) is limited due to this pressure drop across the control chokes.

This means that at low reservoir pressure, either the downhole temperature restriction is not achieved or the wellhead restriction. Only for the highest temperatures there is a margin of operation up to a flow rate of 40 kg/s in case of a ID = 120mm well. A side issue is that a low flow rates the cooling in the pipeline is such that 60 °C is difficult to achieve. This is only possible for high flow rates.



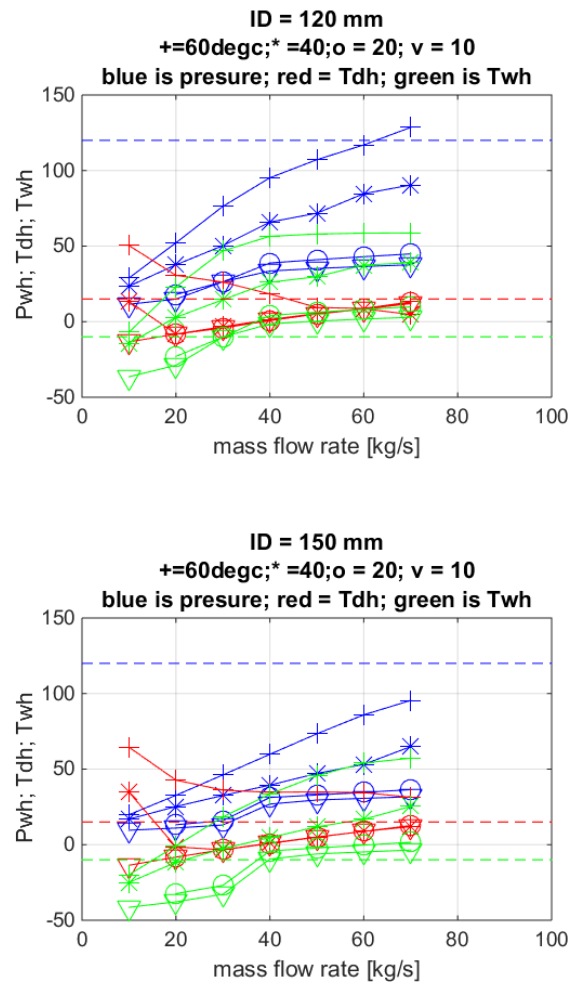


Figure 10: Wellhead pressures (downstream choke), wellhead temperatures (downstream choke) and downhole temperatures. The simulations are limited to 350 bar. All cases with conditions higher than 350 bar are plotted as a pressure of 0 bar and a temperature of -30 °C.

## 4 Simulation model(s)

### 4.1 Introduction

The simulations as presented have been done using OLGA 2017.1.0 with the single component CO<sub>2</sub> module using the P-H methodology. All simulations are done in transient mode simulating long enough to reach steady conditions (if any).

### 4.2 Basic model

The basic model is given in Figure 11. It consists of:

- Pipeline.
- 4 wells.
- A control valve at the pipeline inlet (to maintain a minimum discharge pressure of 60 bar).
- A control valve at the pipeline outlet to maintain the pipeline pressure at a minimum pressure.
- Each well has a control valve which is used in either mass flow or pressure control mode.

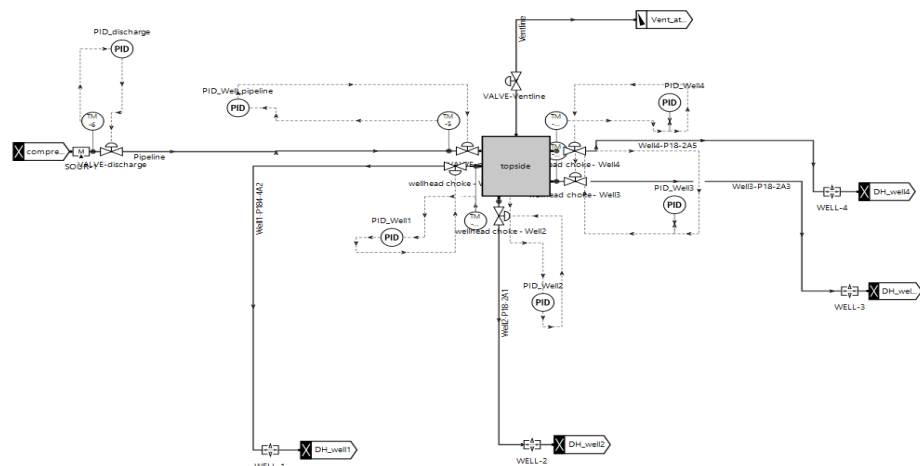


Figure 11: Olga model.

The controllers are all PID controllers with settings for the pressure controllers of:

Amplification: 2e-8

Bias: 0

Derivativeconst: 0 s

Error: 0

Integralconst: 5 [s]

The maximum change: 0.2

The mass flow controllers are set to:

Amplification: -0.0005

Bias: 0

Derivativeconst: 0 s

Error: 0



Integralconst: 5 [s]  
 The maximum change: 0.2

The control settings are not varied between cases and are relatively 'soft'. That is the gain could be put higher (and still avoid unstable control). However, these settings seemed to work for almost all conditions and as such it was chosen to keep the settings more or less constant.

### 4.3 Pipeline geometry

The pipeline is modelled as:

- 22km, horizontal, (Inner) diameter = 0.4318m
- 25m, vertical, (Inner) diameter = 0.4318m
- 50m, horizontal, (Inner) diameter = 0.254m

The vertical diameter has been kept large as that is worst case for instabilities (in case we have two phase flow) but a 10" section was added for pressure drop.

Two controllers are added to the pipeline:

- Compressor outlet valve at a pressure control of 60 bar.
- Pressure controller at the horizontal section at 'the platform'.

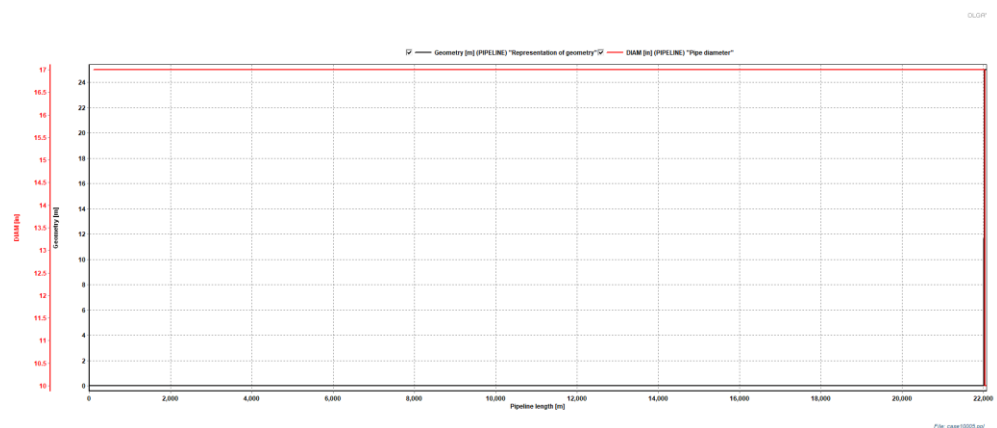


Figure 12: Pipeline geometry.

### 4.4 Well geometry

For the base model, the well inclination profiles of the wells P18-4A2, P18-2A1, P18-2A3 and P18-2A5 are used. For the base case, a tubing of 5.5" (0.12m ID) is used. The tubing diameter is used up to the point it could fit the casing/liner (as not for all a 5.5" tubing would fit down to the perforations). The detailed geometry used is given in Figure 13.

Well1 = P18-4A2	ID = 0.12m (5.5")
Well2 = P18-2A1	ID = 0.12m (5.5")
Well3 = P18-2A3	ID = 0.12m (5.5")
Well4 = P18-2A5	ID = 0.12m (5.5")

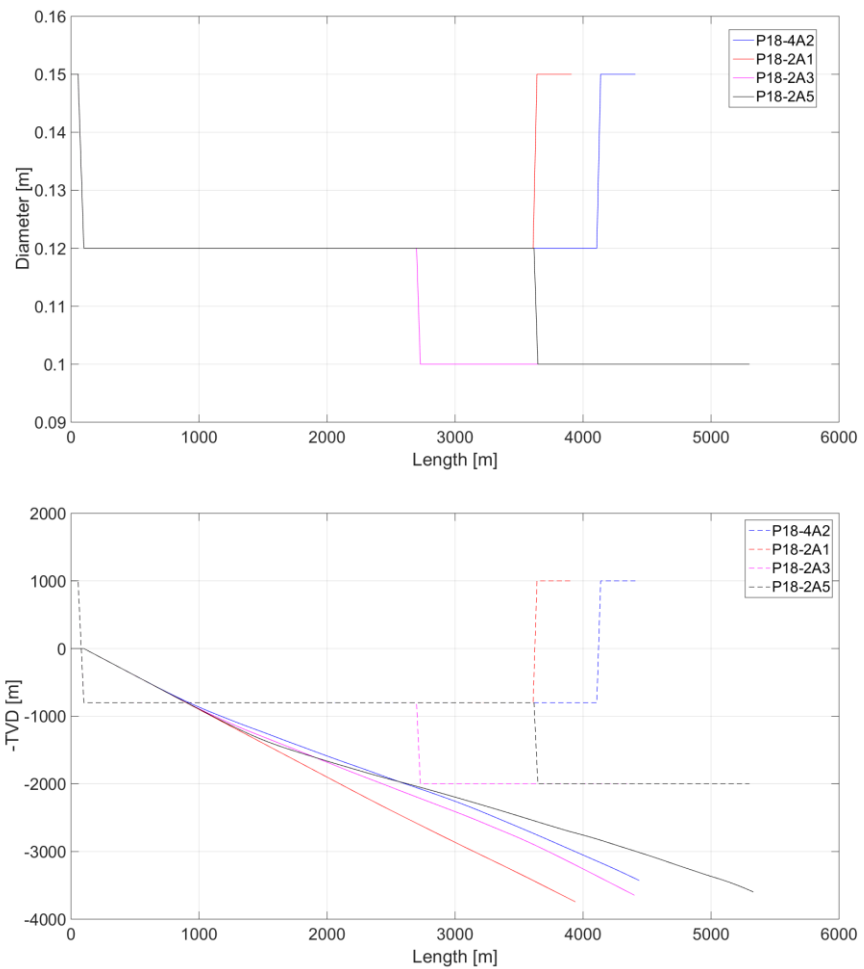


Figure 13: Well geometries used for the four wells. Diameter in bottom figures are scaled for visualisation.

The choice of diameters is based on :

- A larger diameter is 'better' for the downhole temperature (higher temperatures up to higher flow rates)
- A larger diameter is 'better' at high reservoir pressure
- A smaller diameter is 'better' with respect to topside temperature considerations (a smaller diameter builds up pressure faster with respect to mass flow rate and as such the pressure drop is less across control chokes at the wellheads.

A more detailed 'optimization' was done for 10°C injection cases. These are not reported in this report.

## 4.5 Reservoir

For the reservoir injectivity, a reservoir pressure dependent value is used. For all four wells the same injectivity (PI) index is used (based on P18-4 data). The injectivity is defined according:

$$m [kg/s] = PI \cdot \Delta p [Pa]$$

Table 1: Injectivity index used. \* For 340 bar no data was available and the same value as for 300 bar was used.

Reservoir pressure [bara]	Injectivity index [(kg/s)/Pa]
20	2.53e-5
60	4.04e-5
100	6.14e-5
200	0.000109
300	0.000129
340	0.000129*

#### 4.6 Heat transfer

For the heat transfer, at this stage an overall U value methodology is used. That is basically a steady state approach and less appropriate for dynamic simulations as the heat capacity of the walls are not included. However, as details on pipeline construction (insulation materials, burial depth, soil properties ) and well selection (well used, annuli fluids) are not known the choice was made to use a U value methodology.

The pipeline is calculated using:

Ambient temperature: 10 °C

U value: 1.5/ m<sup>2</sup>-K (based on ID)

This includes the 'riser' and 'topside' part of the platform.

The wells are calculated using:

Vertical thermal gradient from 10 to 123 °C

U value: 9.5/ m<sup>2</sup>-K (based on ID)

## 5 Shutin-wellhead conditions

The shutin pressure for well P18-4A2 was calculated by ramping up the reservoir pressure after shutin. In Figure 14, the wellhead pressure is plotted as function of the reservoir pressure. This figure is obtained for a simulation in which the reservoir pressure was (linearly) increased slowly from 20 to 340 bar in 500000s (5.8 days). As the details of the results are determined by heat transfer, deviations might occur in case the details of the heat transfer and outer temperature will be different.

There are three regimes:

- At low reservoir pressure, the wellhead conditions are closely to single phase gas. In this region, the shutin wellhead pressure increases with the reservoir pressure (as the static head is in that case purely density and therefore pressure dependent).
- In the mid region, the wellhead is at two-phase conditions and all is dominated by heat transfer details (Figure 15). The wellhead pressure will be more or less constant as function of reservoir pressure and will be determined by the temperature.
- At high reservoir pressures, the wellhead is at liquid (supercritical) conditions and the wellhead pressure will increase with the reservoir pressure.

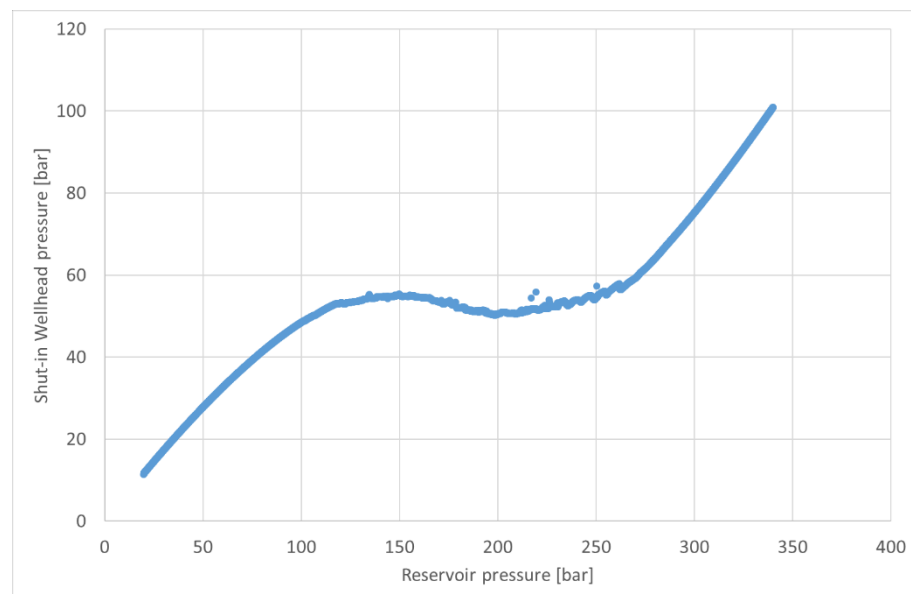


Figure 14: Shutin wellhead pressure for well P18-4A2. The reservoir pressure was increased from 20 to 340 bar in 500000s (5.8 days). For long term shutin case results of 12, 45, 45, 70 bar were obtained for 20, 100, 200, 300 bar reservoir pressure. The difference is due to the time allowed to reach steady state.

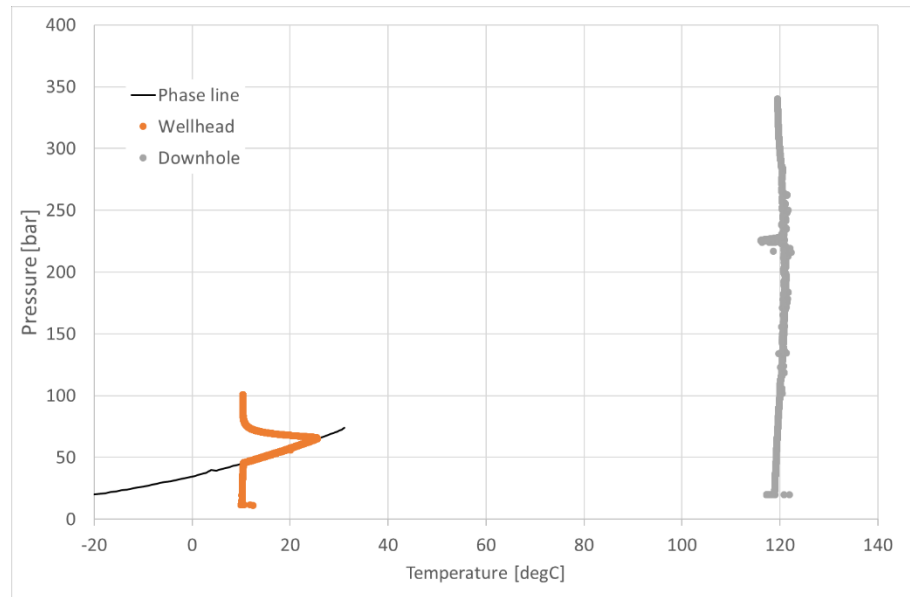


Figure 15: Wellhead and downhole condition for simulation with reservoir pressure increase.

## 6 Steady state

### 6.1 Introduction

In this chapter, the steady state results (final results of transient simulations) are discussed. These steady state simulations were done for a large range of models, flow rates and conditions. In this report only those results are presented with the model as described in Chapter 4. Previous models had no pipeline, a single well, no pipeline control valve or no compressor outlet control valve. When one well is used this is typically well-1 (P18-4A2).

In Section 6.2, an overview is given of the cases which have been simulated. The results of these cases are given in Annex A. In Section 6.3 a summary is given of the results.

### 6.2 Simulation cases

<b>Case</b>	<b>Pres</b>	<b>Tcompr</b>	<b>Wells</b>	<b>control</b>	<b>Mass flow</b>
4000	300	40	1 open	Platform (85 bar)	15
4001	300	40	1 open	Platform (85 bar)	30
4002	300	40	1 open	Platform (85 bar)	60
4002_45	300	40	1 open	Platform (85 bar)	45
4003	300	40	1 + 2 open	Platform (85 bar)	60
4004	300	40	All wells open	Platform (85 bar)	170
4119	300	80	All wells open	Platform (85 bar)	60
4120	300	80	All wells open	Platform (85 bar)	50
4005	340	40	All wells open	Platform (85 bar)	170
4006	340	40	All wells open	Platform (85 bar)	140
4110	340	80	All wells open	Platform (85 bar)	140
4111	340	80	All wells open	Platform (85 bar)	100
4113	340	80	All wells open	Platform (85 bar)	40
4114	340	80	All wells open	Platform (85 bar)	5
4130	340	40	1	Platform (85 bar)	30
4131	340	40	1	Platform (85 bar)	45
4132	340	40	1	Platform (85 bar)	38
4078^	100	40	All wells open	Platform (85 bar)	170
4079	200	40	All wells open	Platform (85 bar)	170
4080	100	40	1 open	Platform (85 bar)	60
4081	200	40	1 open	Platform (85 bar)	60
4082	100	40	1 open	Platform (85 bar)	30
4083	100	40	1 open	Platform (85 bar)	15
4084	200	80	1 open	Platform (85 bar)	30
4085	200	80	1 open	Platform (85 bar)	15
4118	200	80	All wells open	Platform (85 bar)	100
4127	100	80	All wells open	Platform (85 bar)	100
4124	100	80	1	Well (85)	15
4125	100	80	1	Well (85)	30

4127	100	80	1	Well (85)	60
4007	60	40	1 open	Platform (85 bar)	15
4008	60	40	1 open	Platform (85 bar)	30
4009	60	40	1 open	Platform (85 bar)	60
4010	60	40	1 open	Platform (85 bar)	100
4011	60	40	1 + 2 open	Platform (85 bar)	100
4012	60	40	All wells open	Platform (85 bar)	170
4013	60	40	All wells open	3 * mass; 1 P (85 bar)	170
4115	60	80	All wells open	3 * mass; 1 P (85 bar)	170
4116	60	80	All wells open	3 * mass; 1 P (85 bar)	100
4117	60	80	All wells open	3 * mass; 1 P (85 bar)	110
4121	60	80	1	Well 85	
4122	60	80	1	Well 85	
4123	60	80	1	Well 85	
4014	20	40	1 open	Platform (85 bar)	15
4015	20	40	1 open	Platform (85 bar)	30
4016	20	40	1 open	Platform (85 bar)	60
4017	20	80	1 open	P control at well (85)	15
4018	20	80	1 open	P control at well (60)	15
4019	20	80	1 open	P control at well (60)	60
4020	20	80	All open	3 * mass; 1 P (60 bar)	170
4021	20	80	All open	3 * mass; 1 P (60 bar)	120
4022	20	80	1 open	P control at well (60)	45
4023	20	80	1 open	P control at well (60)	30
4024	20	80	1 open	No control	15
4025	20	80	1 open	No control	30
4026	20	80	1 open	No control	45
4027	20	80	All wells open	No control	170
4028	20	80	All wells open	No control	140
4128	20	80	All wells open	No control	100
4129	20	80	All wells open	No control	90

### 6.2.1 Results overview

An overview of the results is given in Table 2 to Table 5. In these tables the main pressures and temperatures are given.

P<sub>comp</sub>: Compressor discharge pressure

T<sub>comp</sub>: Compressor discharge temperature

P<sub>platform</sub>: Pressure upstream of well control valves

T<sub>downstream</sub>: Temperature downstream of well control valves

T<sub>downhole</sub>: Downhole temperature at injection position

For a reservoir pressure of the 20bar, no case, with a liquid filled pipeline, adheres to both the wellhead and downhole temperature restriction (see Annex A).

Therefore, only cases in which the pipeline pressure was not controlled are presented.

In general results have been calculated with for a single well starting at low flow rate and determining the maximum flow rates with respect to the temperature restriction (either wellhead or downhole), and for scenarios with all wells open, determining the maximum allowed flow rate with respect to the compressor pressure.

Table 2: Examples of results for a reservoir pressure of 20 bar. \* The minimum wellhead temperature (T<sub>downstream</sub>) and downhole temperature are given if more than one well is used.

Reservoir pressure [bar]	Case	# wells	Mass flow rate [kg/s]	P comp [bar]	T <sub>comp</sub> [°C]	Control	P Platform [bar]	T* Down stream [°C]	T down hole* [°C]
20	4024	1	15	60	80	None	46	17	47
20	4025	1	30	80	80	None	80	42	17
20	4028	4	140	115	80	None	103	64	19
20	4128	4	100	90	80	None	81	58	35
20	4129	4	90	83	80	None	75	56	40



Table 3: Examples of results for a reservoir pressure of 60 bar. \* The minimum wellhead temperature (T<sub>downstream</sub>) and downhole temperature are given if more than one well is used.

Reservoir pressure [bar]	Case	# wells	Mass flow rate [kg/s]	P comp [bar]	T comp [°C]	Control	P Plat form [bar]	T* Down stream [°C]	T down hole* [°C]
60	4007	1	15	85	40	Pipe: 85	30	-6	25
60	4008	1	30	85	40	Pipe: 85	56	18	27
60	4009	1	60	89	40	Pipe: 85	87	37	32
60	4011	2	100	89	40	Pipe: 85	75	31	31
60	4013	4	170	95	40	Well: 85	85	19	29
60	4121	1	15	86	80	Well: 85	85	-5	41
60	4122	1	30	87	80	Well: 85	85	39	46
60	4123	1	60	138	80	Well: 85	136	65	38
60	4115	4	170	155	80	3*well; P(85)	143	41	38
60	4116	4	100	100	80	3*well; P(85)	93	46	57
60	4117	4	110	119	80	3*well; P(85)	111	33	47

Table 4: Examples of results for a reservoir pressure of 100 bar. \* The minimum wellhead temperature (T<sub>downstream</sub>) and downhole temperature are given if more than one well is used.

Reservoir pressure [bar]	Case	# wells	Mass flow rate [kg/s]	P comp [bar]	T comp [°C]	Control	P Plat form [bar]	T* Down stream [°C]	T down hole* [°C]
100	4083	1	15	85	40	Pipe 85	33	-2	50
100	4082	1	30	85	40	Pipe 85	52	15	53
100	4080	1	60	90	40	Pipe 85	87	37	51
100	4078	4	170	93	40	Pipe 85	76	32	50
100	4126	4	100	98	80	Pipe 85	90	60	82
100	4124	1	15	86	80	Well 85	85	9	60
100	4125	1	30	87	80	Well 85	85	45	71
100	4127	1	60	142	80	Well 85	139	64	60

Table 5: Examples of results for a reservoir pressure of 300 and 340 bar. \* The minimum wellhead temperature (Tdownstream) and downhole temperature are given if more than one well is used.

Reservoir pressure [bar]	Case	# wells	Mass flow rate [kg/s]	P comp [bar]	T comp [°C]	Control	P Plat form [bar]	T* Down stream [°C]	T down hole* [°C]
300	4000	1	15	85	40	Pipe 85	58	21	64
300	4001	1	30	92	40	Pipe 85	90	35	73
300	4002_45	1	45	108	40	Pipe 85	105	33	62
300	4002	1	60	136	40	Pipe 85	133	32	58
300	4003	2	60	94	40	Pipe 85	91	37	77
300	4004	4	170	116	40	Pipe 85	108	36	68
340	4006	4	140	123	40	Pipe 85	116	36	68
340	4005	4	170	138	40	Pipe 85	130	36	66

### 6.3 Overview conclusions

For the different reservoir pressures the following is concluded:

- Reservoir pressure = 20 bar

Cases calculated with  $T_{\text{compressor}} = 40\text{ °C}$  and  $80\text{ °C}$

Cases with  $T = 40\text{ °C}$  have a too low bottomhole pressure

With a pipeline at a pressure control of 85 bar, the minimum flow rate leads to a too low bottomhole temperature.

With a pipeline at a pressure control of 60 bar, the maximum flow rate is 30 kg/s.

At a pressure control of 60 bar, the maximum flow rate for all wells open is 120 kg/s

At open flow, the maximum flow rate for Well 1 is ~ 40 kg/s

At open flow, the maximum flow rate for all wells is ~ 140 kg/s

- Reservoir pressure = 60 bar

The cases are calculated with a compressor discharge temperature of

$T_{\text{compressor}} = 40\text{ °C}$ . At those conditions, there are no limitations in mass flow rate due to the wellhead temperatures or downhole temperatures.

Due the compressor limit of  $P = 120\text{ bar}$ , the maximum mass flow rate is between

60 and 100 kg/s for a single well and higher than 170 k/s in case all wells are open.

With platform control, downstream of the choke control, two phase flow occurs

Recommended to use individual control (1 pressure control, rest mass flow control)

- Reservoir pressure = 300 bar

The cases are calculated with a compressor discharge temperature of

$T_{\text{compressor}} = 40\text{ °C}$ . At those conditions, there are no limitations in mass flow rate due to the wellhead temperatures or downhole temperatures.

Due the compressor limit of  $P = 120\text{ bar}$ , the maximum mass flow rate is 45 kg/s for a single well and higher than 170 k/s in case all wells are open.

- Reservoir pressure = 340 bar

The cases are calculated with a compressor discharge temperature of

$T_{\text{compressor}} = 40\text{ °C}$ . At those conditions, there are no limitations in mass flow rate due to the wellhead temperatures or downhole temperatures.

Due the compressor limit of  $P = 120\text{ bar}$ , the maximum mass flow rate is 140 kg/s in case all wells are open.

A summary of these conclusions is given in Table 6.

Table 6: Overview maximum flow rates.

Reservoir pressure	Maximum flow 1 well	Maximum flow 4 wells
20 bar - Tcomp = 80 °C	30 kg/s	140 kg/s
60 bar - Tcomp = 40 °C	60 kg/s	> 170 kg/s
300 bar - Tcomp = 40 °C	45 kg/s	> 170 kg/s
340 bar - Tcomp = 40 °C		140 kg/s
60 bar - Tcomp = 80 °C		110 kg/s
200 bar - Tcomp = 80 °C		100 kg/s
300 bar - Tcomp = 80 °C		45 kg/s
340 bar - Tcomp = 80 °C		0 kg/s

## 7 Start-up simulations

### 7.1 Introduction

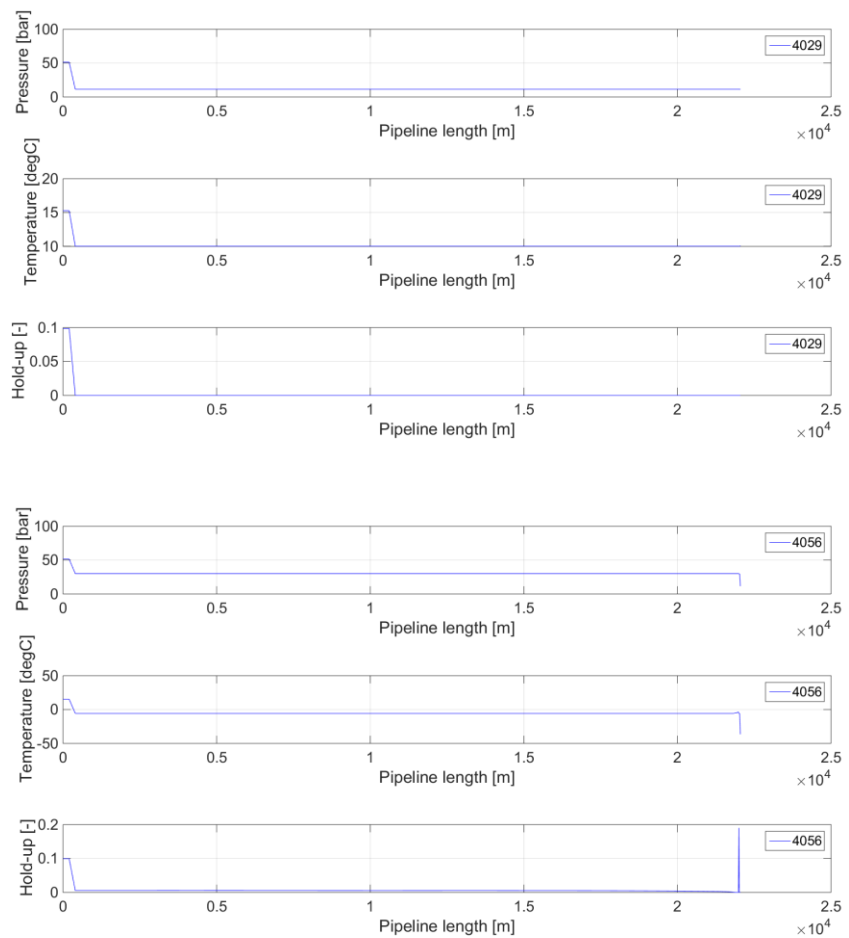
In this Chapter an overview of start-up simulation are presented. In principle only low temperature start-up cases have been simulated as these are almost always worst cases.

Start-up simulations are done starting from three conditions (Figure 16):

- Low pressure (12 or 30 bar, 10°C; gas phase)
- Mid pressure (60 bar, 21°C; two-phase)
- High pressure (115 bar, 14°C; liquid phase)

The mid pressure conditions were obtained by closing in the pipeline at approximate 85 bar, 40 °C. When cooling down the conditions shift to the two-phase line conditions such that the total mass remains constant.

The high pressure conditions are assumed to be a near critical cases.



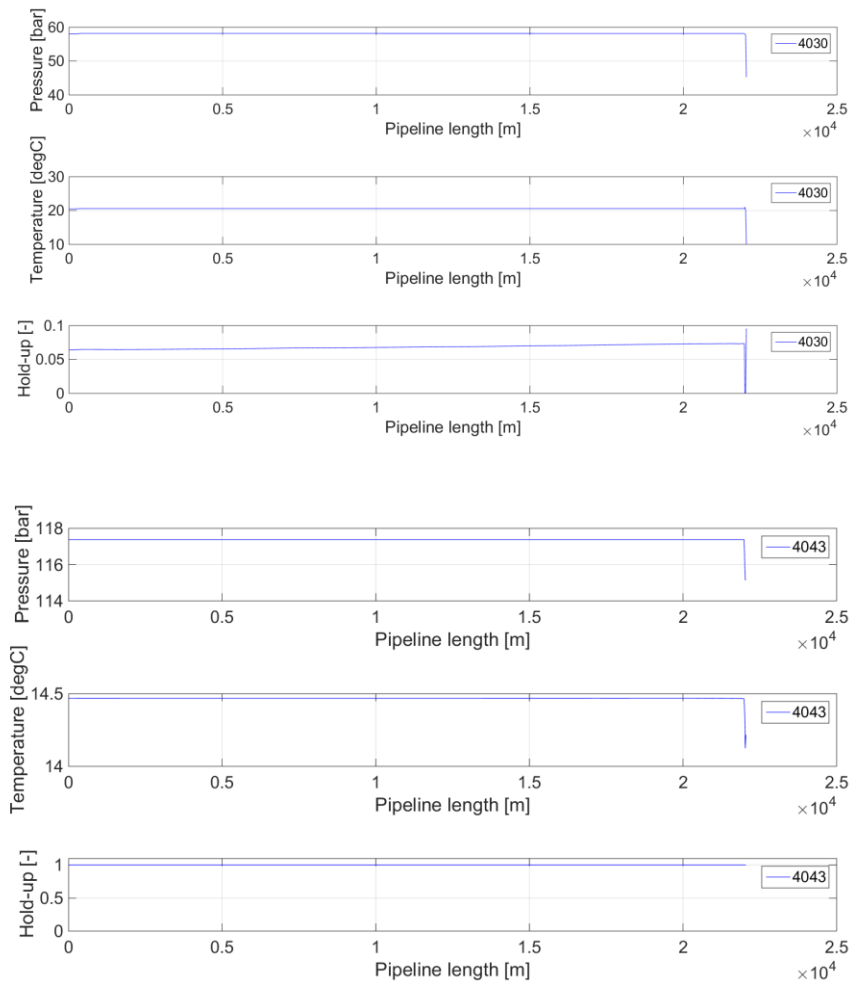


Figure 16: Pressure, temperature and hold-up profile for low (top 2 figures), middle and high pressures.

An overview of simulations ran is given in Section 7.2, with in Section 7.4, Section 7.5 and Section 7.6 start-up simulations at low reservoir pressure. In Section 7.9 and 7.10 the start-up cases for higher reservoir pressures are presented. Section 7.7 and Section 7.8 give a discussion on alternatives for low reservoir pressure start-up.

## 7.2 Simulations overview

In Table 7 an overview is given of the simulations ran. The different heading indicate:

Case:	Simulation case number
Pres:	Reservoir pressure [bar]
Tcmp:	Compressor outlet temperature [°C]
Wells:	Number of wells open or case number from which is restarted
Control:	Indication on how control is done
	None means the control settings are such that valves are full open (except discharge pressure control valve)

Pipe N indicates that the pipeline pressure control valve is set to N bar

Mass flow Compressor discharge mass flow rate [kg/s]

Table 7: Overview of simulations.

<b>Case</b>	<b>Pres [bar]</b>	<b>Tcmp [°C]</b>	<b>Wells</b>	<b>Control/ number of wells open</b>	<b>Mass flow [kg/s]</b>
4029	20	80	All wells open	Initialization at T = 10°C	
4030	20	80	All wells closed	Initialization at P ~85 bar (leading to a pipeline pressure of ~60 bar)	
4031	20	80		Shutin wells from 4028 (lading to a pipeline pressure of ~115 bar)	
<b>Low pipeline pressure start-up with no control</b>					
4032	20	80	Start from 4029	none	15
4033	20	80	Start from 4029	None	30
4034	20	80	Start from 4029	2 wells	60
4054	20	80	Start from 4029	4 wells	60
4055	20	80	Start from 4029	4 wells	170
<b>Mid pipeline pressure start-up</b>					
4035	20	80	Start from 4030		0
4036	20	80	Start from 4030	1 well full open	15 at t = 5000s
4037	20	80	Start from 4030	1 well full open	15 at t = 0s
4038	20	80	Start from 4030	2 wells Full open	60 at t = 5000s
4039	20	80	Start from 4038	3 wells Full open	90 at t = 1000s
4065	20	80	Start from 4030	Pipeline = 30 bar	0
4066	20	80	Start from 4030	Pipeline = 30 bar 1 well full open	15 at t = 5000s
4067	20	80	Start from 4030	Pipeline = 30 bar 1 well full open	Opening valve 10, 100, 300, 1000s
<b>High pipeline pressure start-up</b>					
4043	20	80		Initialization at t=10, 120 bar	
4044	20	80	Start 4043	Full open	15 at t = 5000s
4045*	20	80	Start 4043	Well 2 Control on 30 kg/s	15 at t = 5000s
4047*	20	80	Start 4043	Well 2 Control on 10 kg/s	15 at t = 5000s
4048	20	80	Start 4043	Well 2	15 at t = 5000s

				Control on 60 kg/s	
4046**	20	80	Start 4043	Full open @ t = 5000	15 at t = 0
4049	20	80	Crashes	Pipe 85 bar Well 60	
4050	20	80	Crashes	Pipe 0.05 Well 0.05	
<b>Venting solution</b>					
4051	20	80	Start 4043	Temporary vent	
4052	20	80	Start 4043	venting Well 1 open at 14000	15 at t = 10000
4053	20	80	Start 4043	Start at full open Well 1 + well 2	
4068	20	80	Start 4043	vent	
4069	20	80	Start 4068	Well 1 full open	15 at 5000s Well open at 1000
4071	20	80	Start 4068		Valve opening times
4072	20	80	Start 4068		15 at 1000 Well open at 5000
4074	20	80	Start 4068	Well 2 control	Control 15, 30, 45, 60 kg/s (60 *)
4075	20	80	Start 4068		15 at 1000 Well open at 6000
4076^	20	80	Start 4068	30 bar 4 wells open	15 at 10000s Well open at 1000
<b>Low Pipeline pressure startup with pressure control</b>					
4056	20	80	Pipe 30 bar	Initialization at T = 10°C	
4057	20	80	Start 4056	Pipe 30 bar (1 well full open)	30
4058+	20	80	Start 4056	None (1 well open)	30
4059++	20	80	Start 4056	None (1 well open)	30
4060	20	80	Start 4057	Open well 2	
4061	20	80	Start 4056	None (2 wells open)	60
4062	20	80	Start 4061	Open well 3	
4063	20	80	Start 4061	Open well 3 Variation opening time	topen = 10s, 100s 300s, 1000s
4064	20	80	Start 4060	Open well 2 Variation opening time	topen = 10s, 100s 300s, 1000s
4070	20	80	Start 4056	Pipe 30 bar (1 well full open)	15

<b>High pipeline pressure start-up with Well ID = 0.09m</b>					
5000	20	80		Vent	Well 1 0.09
5001	20	80	Start 5000		15 kg/s
<b>High pipeline pressure start-up with choke in well (variation ID and position)</b>					
6000	Initialization DHC position 4000m				
6001	20	80		Start 6000	15



6002	Initialization DHC position 3700m				
6003	20	80		Start 6002	15
6004	Initialization DHC position 3200m				
6005	20	80		Start 6004	15
6006	Initialization DHC position 2200m				
6007	20	80		Start 6006	15
6008	Initialization DHC position 1200m				
6009	20	80		Start 6008	15 kg/s
6010	20	80		Start 6000	Pressure control DHC

\* Hydrodynamic slugging is turned -off; otherwise no convergence.

\*\* This scenario is not useful as the pipeline pressure will rise too fast.

+ The maximum time step is limited

++ Hydrodynamic slugging is turned -off; otherwise no convergence.

^ Slip is turned-off otherwise no convergence

<b>Case</b>	<b>Pres</b>	<b>Tcmp</b>	<b>Wells</b>	<b>control</b>	<b>Mass flow</b>
4100	All 60	80	All wells closed	Pipe 85	For initialisation
4101	1*60 3*20	80	All wells closed	Pipe 85	For initialisation
4102	All 60	80	Start 4100	Pipe 85	15
4103	60; 3*20	80	Start 4101	Well 85	30
4104	60; 3*20	80	Start 4103	Well 85 Mass 15	30
4105	All 60	80	Start 4101	Well 1 open Pipe 30	15
4106	All 60	80	Start 4100	Well 1 open Pipe 30	30
4107	All 60	80	Start 4100	Well 1 open Pipe 30	60
4108	All 60	80	Start 4106	Opening well 2	60

<b>Case</b>	<b>Pres</b>	<b>Tcmp</b>	<b>Wells</b>	<b>control</b>	<b>Mass flow</b>
4200	All 100	40	All wells closed	Pipe 85	For initialisation
4201	All 100	40	Start 4200- 1 well	Pipe 85	15
4202	All 100	40	Start 4200- 1 well	Pipe 85	30
4203	All 100	40	Start 4200- 1 well	Pipe 85	60

<b>Case</b>	<b>Pres</b>	<b>Tcmp</b>	<b>Wells</b>	<b>control</b>	<b>Mass flow</b>
4300	All 200	40	All wells closed	Pipe 85	For initialisation
4301	All 200	40	Start 4300- 1 well	Pipe 85	15
4302	All 200	40	Start 4300- 1 well	Pipe 85	30
4303	All 200	40	Start 4300- 1 well	Pipe 85	60

<b>Case</b>	<b>Pres</b>	<b>Tcmp</b>	<b>Wells</b>	<b>control</b>	<b>Mass flow</b>
4400	All 300	40	All wells closed	Pipe 85	For initialisation
4401	All 300	40	Start 4400- 1 well	Pipe 85	15
4402	All 300	40	Start 4400- 1 well	Pipe 85	30

4403	All 300	40	Start 4400- 1 well	Pipe 85	60
------	---------	----	--------------------	---------	----

<b>Case</b>	<b>Pres</b>	<b>Tcmp</b>	<b>Wells</b>	<b>control</b>	<b>Mass flow</b>
4500	All 340	40	All wells closed	Pipe 85	For initialisation
4501	All 340	40	Start 4500 – 1 well	Pipe 85	15
4502	All 340	40	Start 4500 – 1 well	Pipe 85	30
4503	All 340	40	Start 4500 – 1 well	Pipe 85	60
4504	All 340	40	Start 4500 – 2 wells	Well 1:85 Well 2:30 kg/s	60

### 7.3 Remarks valve openings

Before the general start-up behaviour is discussed, the detailed temperature behaviour around valves is discussed. As example, in Figure 18, the fluid temperature is plotted as function of time of well-2. This well is opened while well-1 is running at 30 kg/s (Figure 17). The opening time of the valve is varied from 10s to 1000s.

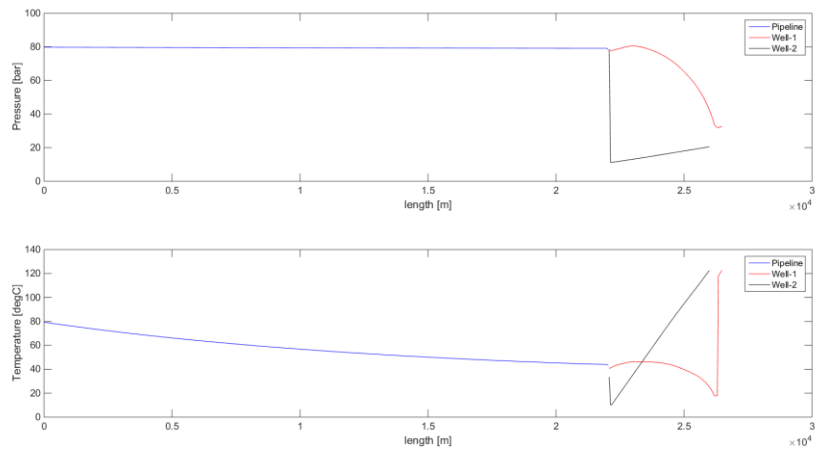


Figure 17: Initial conditions for case 4064.

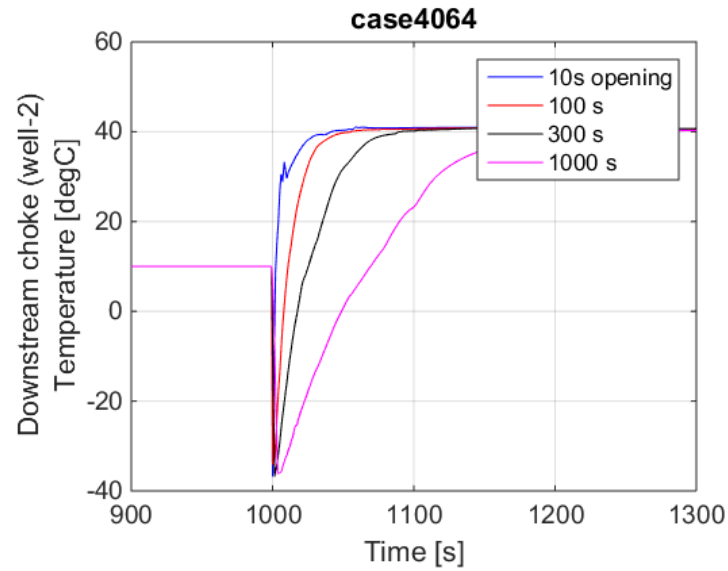


Figure 18: Temperature downstream choke of well-2 with different valve openings speeds (10s means the valve is opened from fully opened to fully closed in 10s).

As the conditions at the valve opening downstream of the valve are approximately 12 bar, when the CO<sub>2</sub> is expanded over the valve, the downstream conditions are for a short period at low temperature corresponding to the wellhead pressure and phase line temperature of approx. -38 °C. With a faster opening of the valve, the mass flow rate increases more rapidly through the valve resulting in

- A higher back pressure and therefore higher temperature
- A faster higher temperature arriving at the valve.

This will basically always occur when a new well is opened. A faster opening of the valves limits the period of low temperatures.

It must be remarked that the temperatures are fluid temperatures and not wall temperatures. When piping arrangements are known, a more detailed simulation can be done to determine actual wall temperatures when pipe thermal capacity is included.

#### 7.4 Discussion start-up reservoir pressure 20 bar– low pipeline pressure

The start-up simulations are run from a low pressure pipeline conditions ( Figure 19).

The sequence for the start-up are (Figure 20):

- The compressor mass flow rate is ramped up from 0 to a given flow rate from t = 1000s to 1600s.
- The pipeline pressure control valve is at p = 10 bar at t= 0s.
- For case 4032 and case4033, the well control was set to 10 bar at t= 0s (meaning full open).
- For case4033, the well 2 control was set to 1000 kg/s at t= 0s (meaning full open).

The sequence is setup such that the wells are first opened but that the pipeline pressure has not reduced too far down before the compressor is started up. However, the compressor is not started up too soon such that the pipeline is pressurized before the wells are opened.

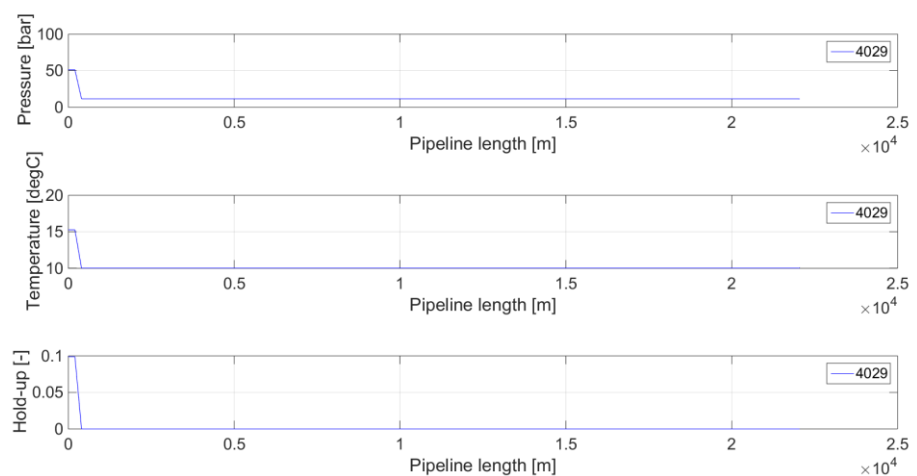


Figure 19: Initial conditions for start-up.

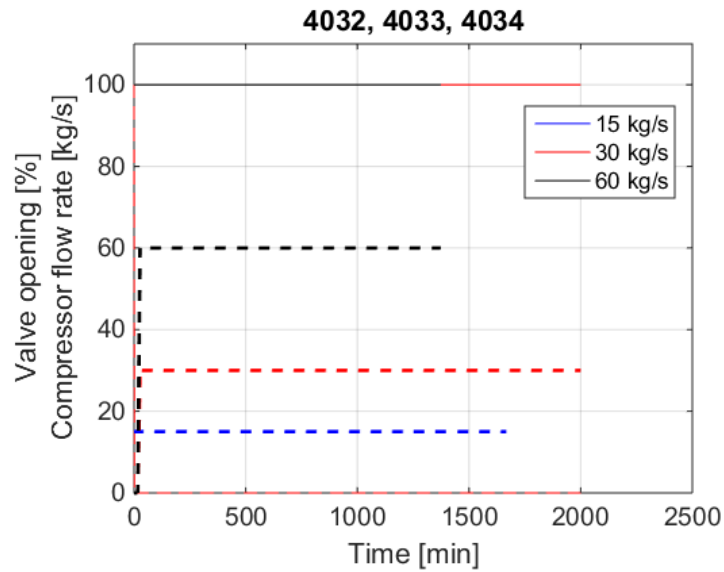


Figure 20: Compressor and valve openings.

The main parameters such as pipeline inlet pressure, the temperatures downstream of the choke valves and the downhole temperature are plotted as function of time in Figure 21. All pressures and temperatures comply with the restrictions. When the high temperatures have arrived at the platform other wells might be opened.

It must be remarked that the stabilization time before steady conditions are reached is nearly 500 – 1000 minutes (8-17 hrs).

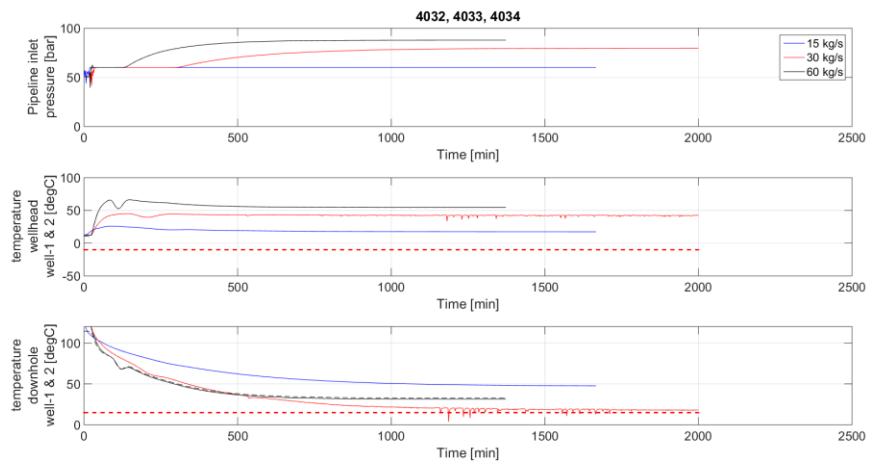


Figure 21: Pipeline inlet pressure, wellhead temperature (downstream choke valve) and downhole temperatures.

### 7.5 Discussion start-up reservoir pressure 20 bar– mid pipeline pressure

If the pipeline is at mid pressures (Figure 22), two potential start-up scenarios could be done:

- One in which the pipeline inventory is first emptied in the well by opening the well chokes prior to compressor start-up.
- Start-up the compressor while the pipeline is still flowing.

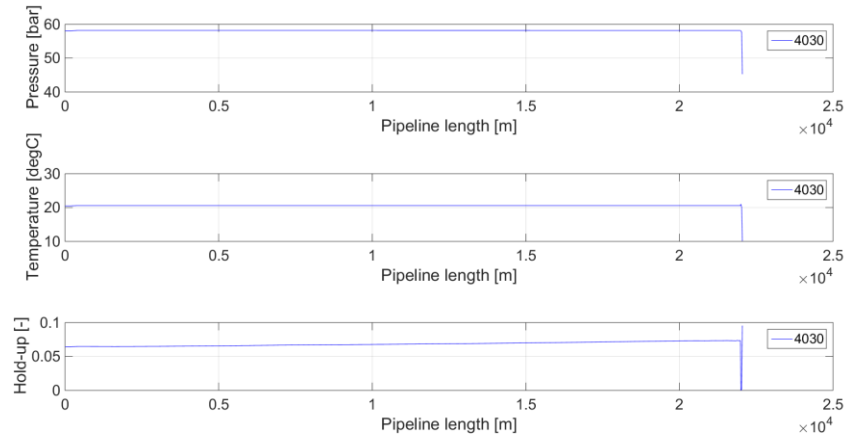


Figure 22: Initial conditions for start-up.

### 7.5.1 Empty pipeline (no pipeline pressure control) (case4035)

For case4035 the sequence is (Figure 23):

- The pipeline pressure control valve is set to  $p = 10$  bar at  $t = 0$ s.
- The control valve of well-1 is set to 10 bar at  $t = 1000$ s.

The resulting temperatures are plotted in Figure 24. The wellhead temperatures are for a prolonged period too low (700 min).

Therefore, this scenario is not advised.

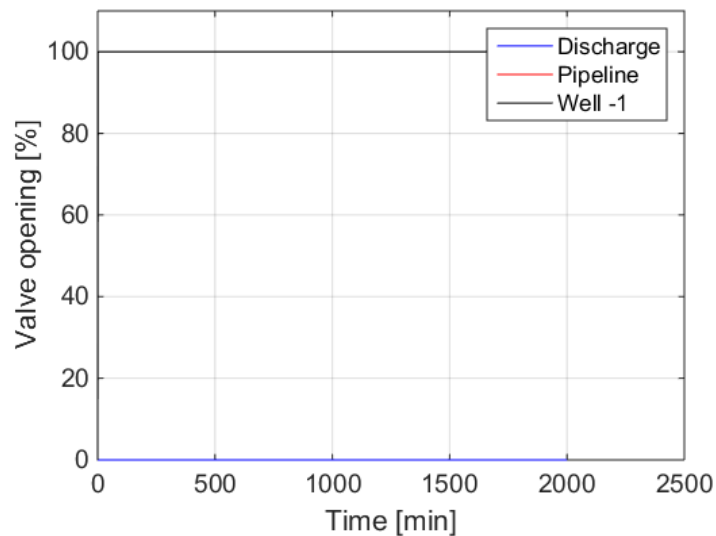


Figure 23: valve openings as function of time.

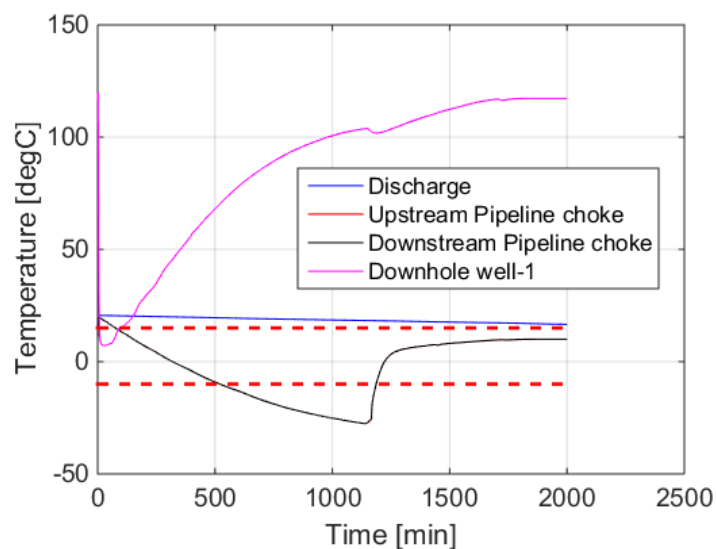


Figure 24: Resulting temperatures.

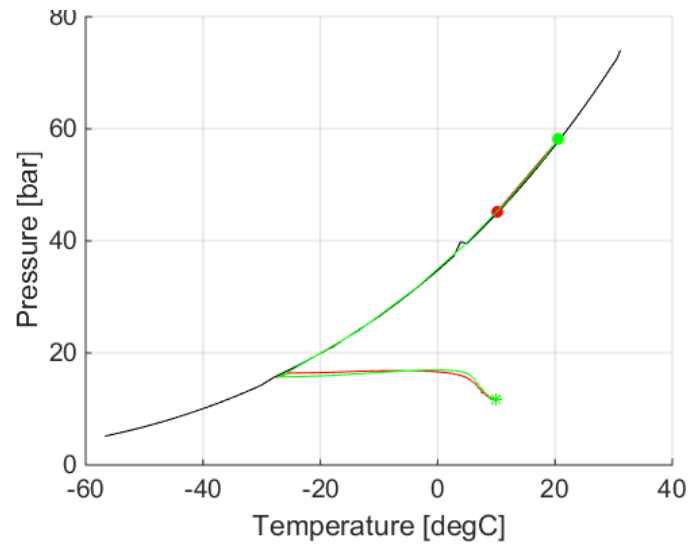


Figure 25: Pressure/temperature profile in the phase envelope. Black is the phase line. Green is downstream of the pipeline pressure control valve. Red at the pipeline inlet.

### 7.5.2 Start-up without pipeline control (case 4036, 4037) (1 well)

The second scenario is that the compressor is started up while the pipeline is emptied.

For case4036 the sequence is (Figure 26):

- The pipeline pressure control valve is set to  $p = 10$  bar at  $t = 0$ s.
- The control valve of well-1 is set to 10 bar at  $t = 1000$ s.
- The compressor is ramped up from  $t = 5000$  to 5600s.

For case4037 the sequence is (Figure 26):

- The pipeline pressure control valve is set to  $p = 10$  bar at  $t = 0$ s.
- The control valve of well-1 is set to 10 bar at  $t = 1000$ s.
- The compressor is ramped up from  $t = 1$  to 601s.

The resulting pressures & temperatures are given in Figure 27. Only for a short time ( 500 min) the downhole temperature criterion is just not met.



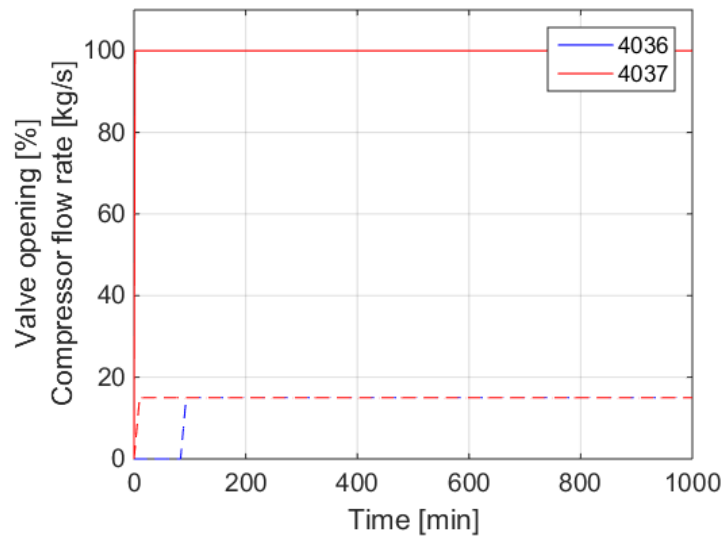


Figure 26: Valve (solid lines) and mass flow rates (dashed lines).

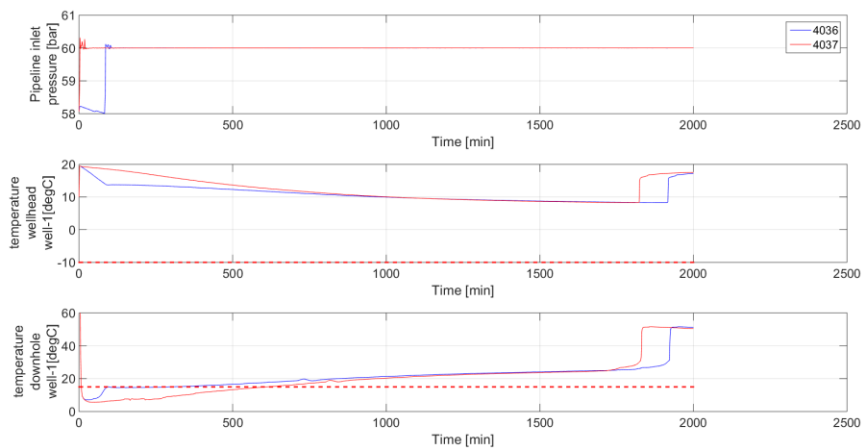


Figure 27: Resulting pressures and temperatures.

### 7.5.3 Start-up without pipeline control (case4038) (2 wells)

Case4038, is a start-up at higher mass flow rates with two wells open.

For case4038 the sequence is (Figure 28):

- The pipeline pressure control valve is set to  $p = 10$  bar at  $t = 0$ s.
- The control valve of well-1 is set to 10 bar at  $t = 1000$ s.
- The control valve of well-2 is set to 1000 kg/s at  $t = 0$ s.
- The compressor is ramped up from  $t = 5000$  to 5600s.

As with the previous start-up (Figure 27), for a short period, the downhole temperature criterion is not met but again this is for a shorter period (~200 minutes).

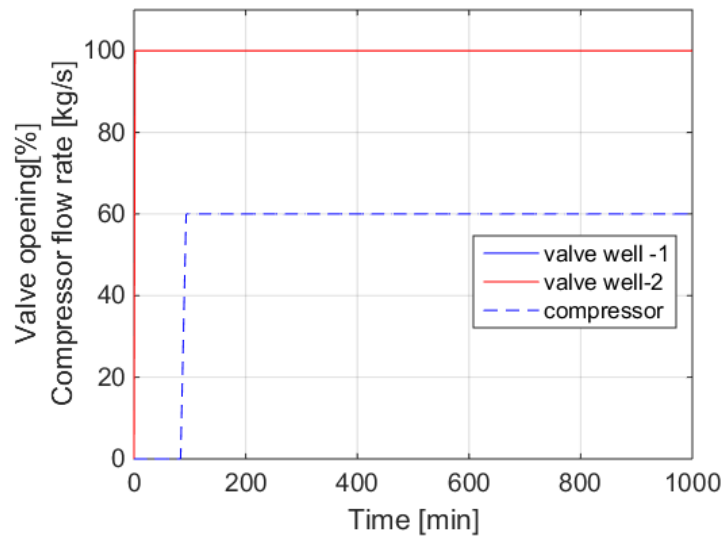


Figure 28: Valve opening (solid lines) and mass flow rate (dashed line).

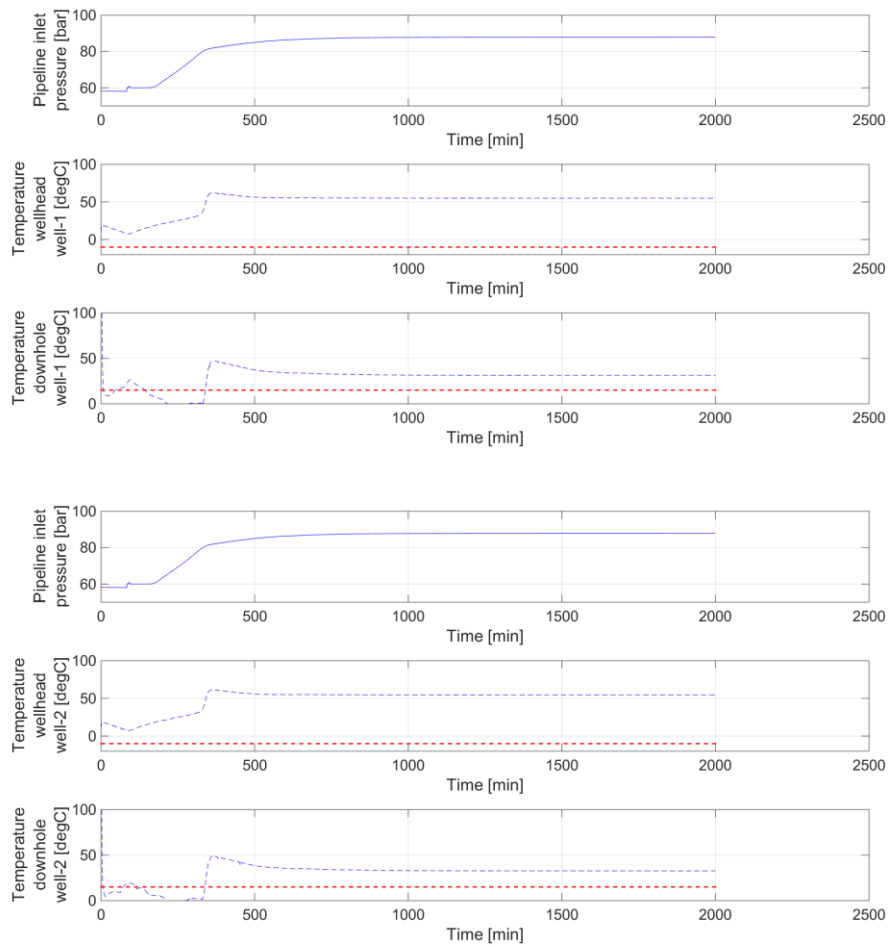


Figure 29: Pressures and temperatures for well-1 (top) and well-2 (bottom).

#### 7.5.4 Start-up without pipeline control (case4039) (3 wells)

Finally, a large mass flow start-up with three wells is calculated.

For case4039 the sequence is:

- The pipeline pressure control valve is set to  $p = 10$  bar at  $t = 0$ s.
- The control valve of well-1 is set to 10 bar at  $t = 1000$ s.
- The control valve of well-2 is set to 1000 kg/s at  $t = 0$ s.
- The control valve of well-3 is set to an opening 0, 0.05, 0.1, 0.2, 0.5 and 1 at  $t = 0, 100, 200, 300, 600, 700$  s. (This sequence was chosen to open the well-3 in a controlled way. No variations for other sequences have been tried).
- The compressor is ramped up from  $t = 1000$  to 1600s (from 60 to 90 kg/s).

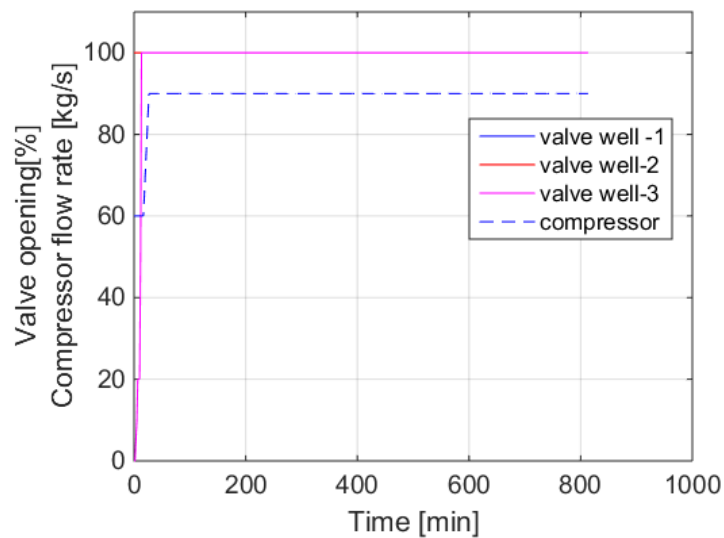
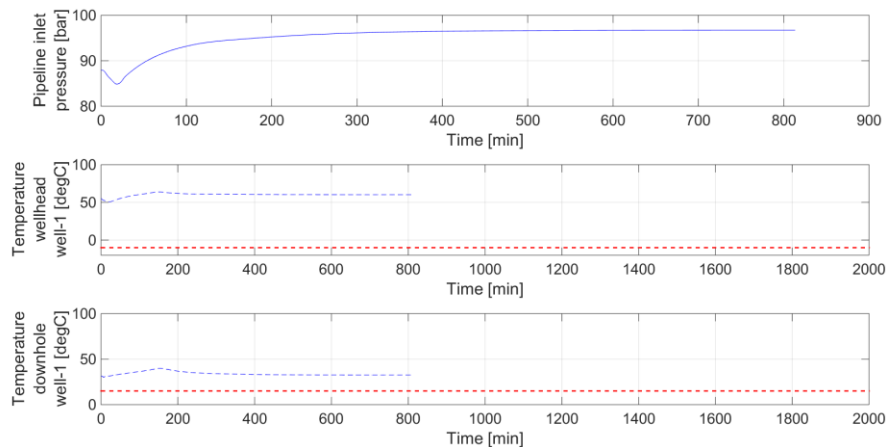


Figure 30: Valves (solid lines) and mass flow rate (dashed line).

The pressures and temperatures for the three wells are given in Figure 31. All conditions are met.



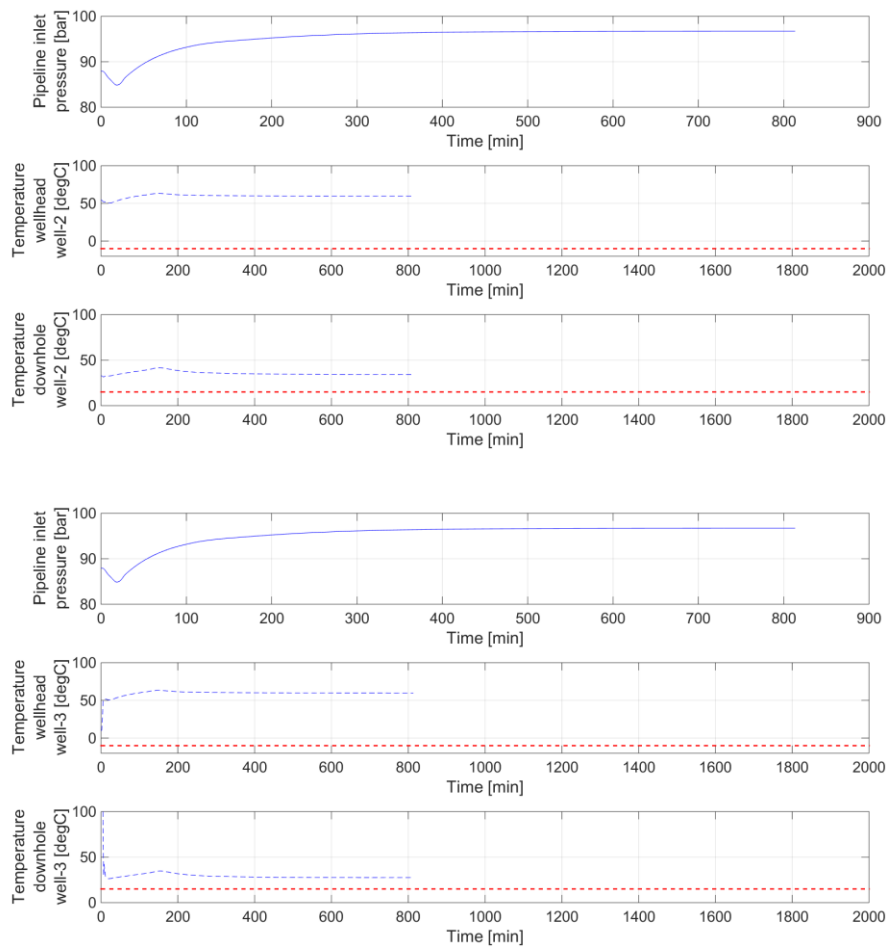


Figure 31: Pressures and temperatures for well-1, 2 and 3.

### 7.5.5 Empty pipeline (with pipeline pressure control) (case4065)

The previous start-up cases were without a pipeline pressure control. Case4065 is a case in which the pipe is emptied while there is a pressure control of 30 bar.

For case4065 the sequence is (Figure 32):

- The pipeline pressure control valve is set to  $p = 30$  bar at  $t = 0$ s.
- The control valve of well-1 is set to 10 bar at  $t = 1000$ s.

As with the full pipeline emptying, the pressure and temperature drop (Figure 33, Figure 34). At a time of 440 min, the pressure control valves starts to close. Downstream of the valve the flow expands further down to 12 bar. This results again to temperatures of  $-38$  °C before the heat transfer starts to kick-in.

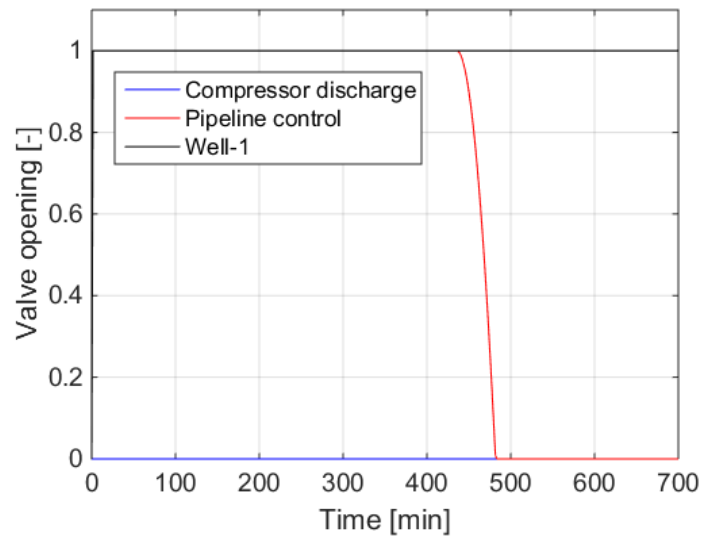


Figure 32: Valves as function of time.

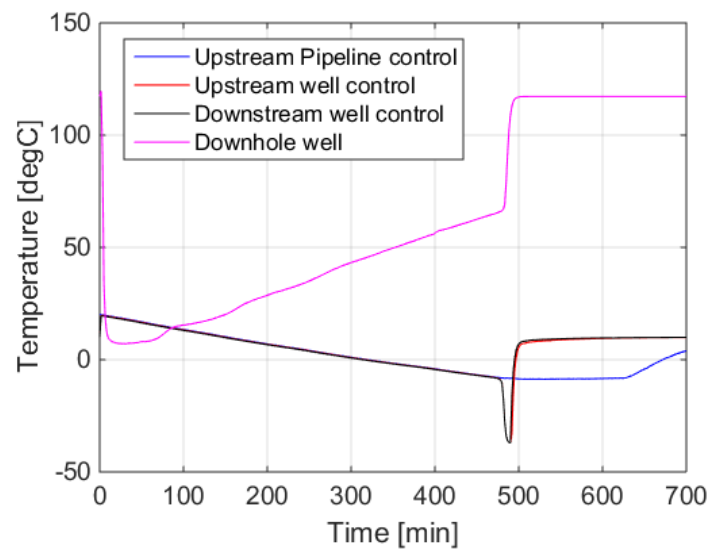


Figure 33: Temperatures as function of time.

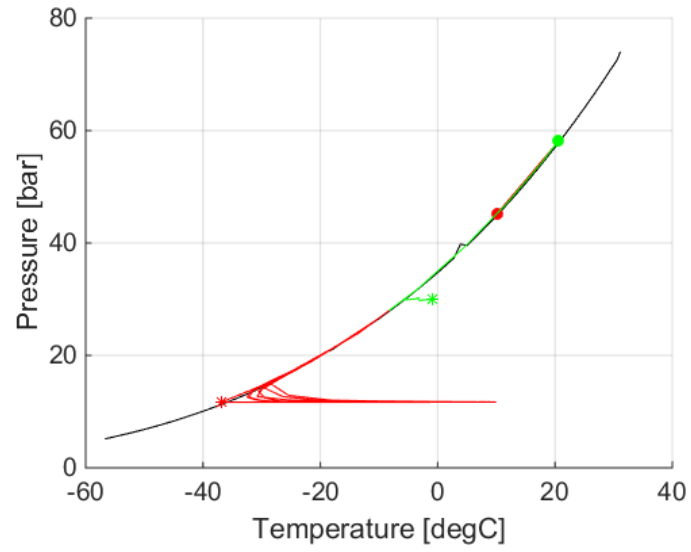


Figure 34: Pressure/temperature conditions in the phase envelope. Red indicated the conditions downstream of the pressure control valve. Green the conditions at the pipeline inlet.

7.5.6 Start-up without pipeline control (case 4066) (1 well)

For case4066 the sequence is (Figure 35):

- The pipeline pressure control valve is set to  $p = 30$  bar at  $t = 0$ s.
- The control valve of well-1 is set to 10 bar at  $t = 1000$ s.
- The compressor is ramped up from  $t = 5000$  to  $5600$ s. (This means the pipeline pressure if emptied partly before the compressor is ramped up).

The resulting temperatures are given in Figure 36. Only a very short time the downhole temperature is too low.

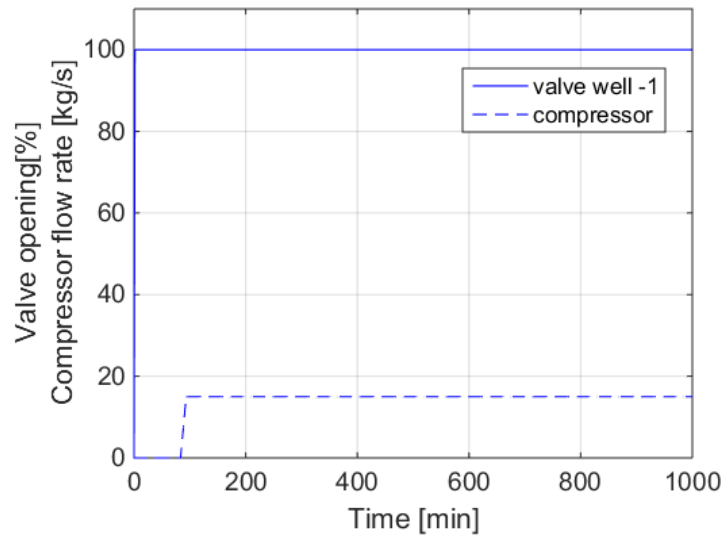


Figure 35: Valves (solid lines) and flow rates (dashed lines).

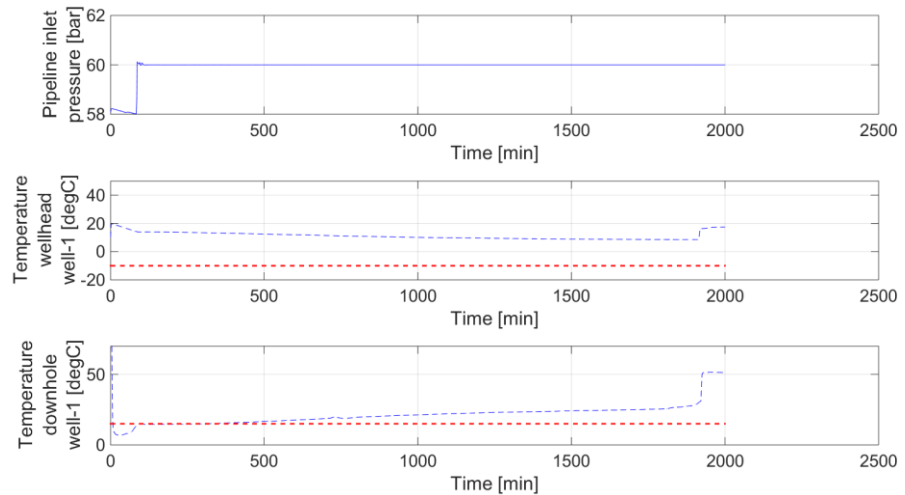


Figure 36: Pressures and temperatures as function of time.

## 7.6 Discussion start-up reservoir pressure 20 bar– high pipeline pressure

For the high pressure initial conditions (Figure 37), different strategies have been tried:

- First emptying the pipeline (case4044).
- Start up with the well (well2) the mass flow was limited (4045, 4047, 4048).
- A double pressure control (the pipeline at 85 bar and the well at 60 bar) (4049). (This case did not converge).
- Both the pipeline and well are at a limited opening (0.05) .

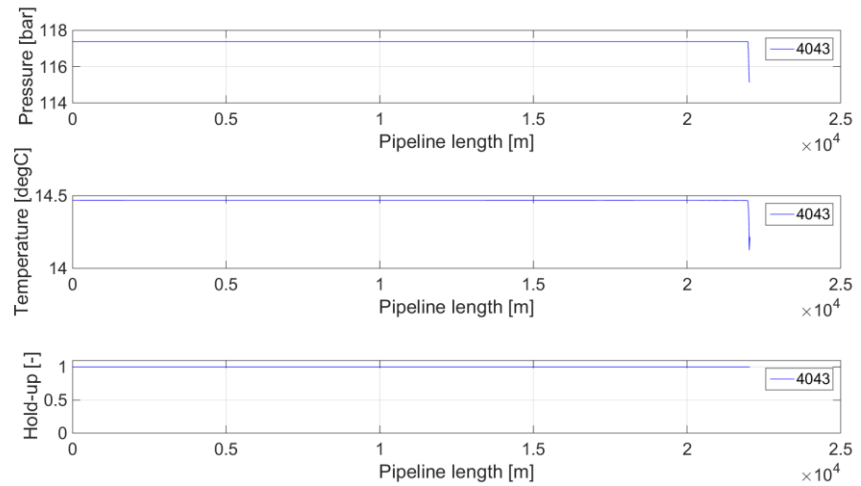


Figure 37: Initial conditions for high pressure start-up.



7.6.1 Results case4044

In case4044, the pipeline is emptied in to well-1 trying to release pressure (Figure 38 and Figure 39). However, this procedure leads to long periods of low downhole temperatures.

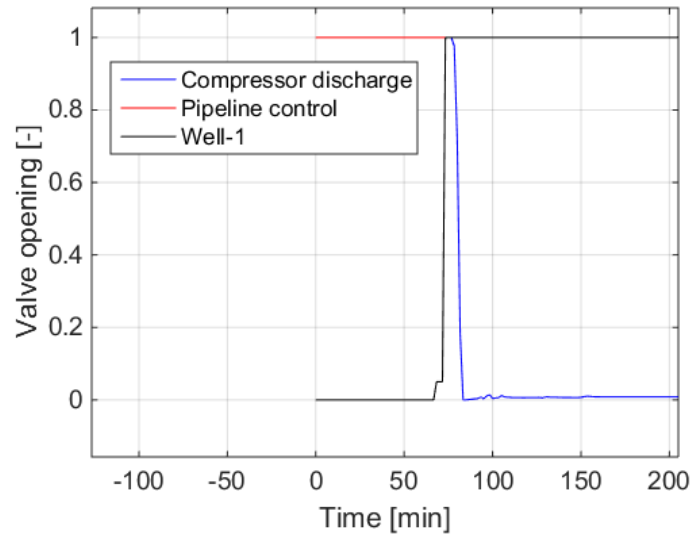


Figure 38: Valves as function of times.

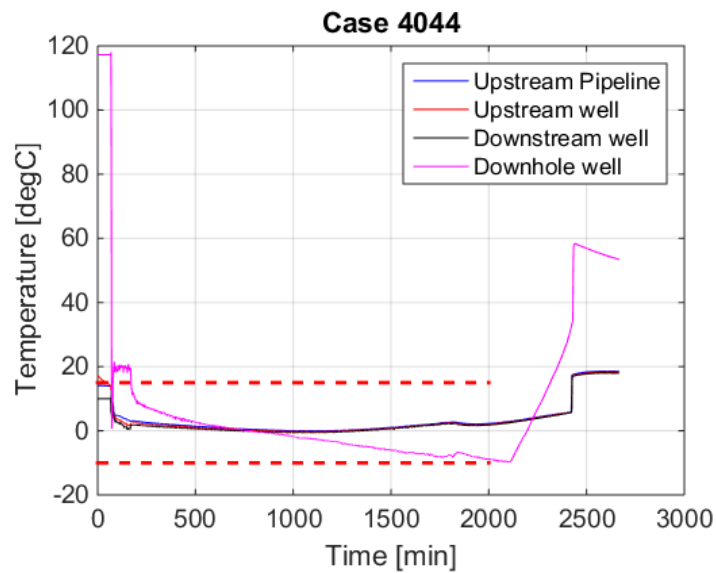


Figure 39: Resulting temperatures as function of time.

7.6.2 Results case4045

In case 4045, well-2 is used for injection and to limit the downhole temperature, the mass flow rate was constraint to 30 kg/s. However, both the topside wellhead temperature becomes too low as well as the downhole temperature.

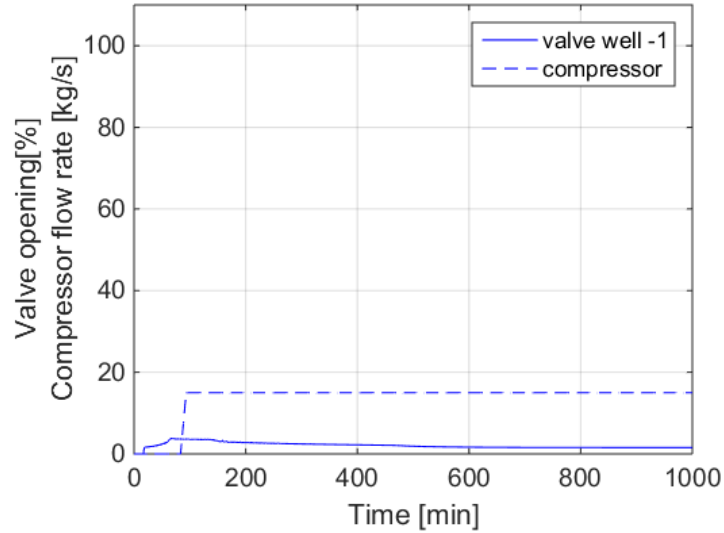


Figure 40: Valves and mass flow rates (dashed line).

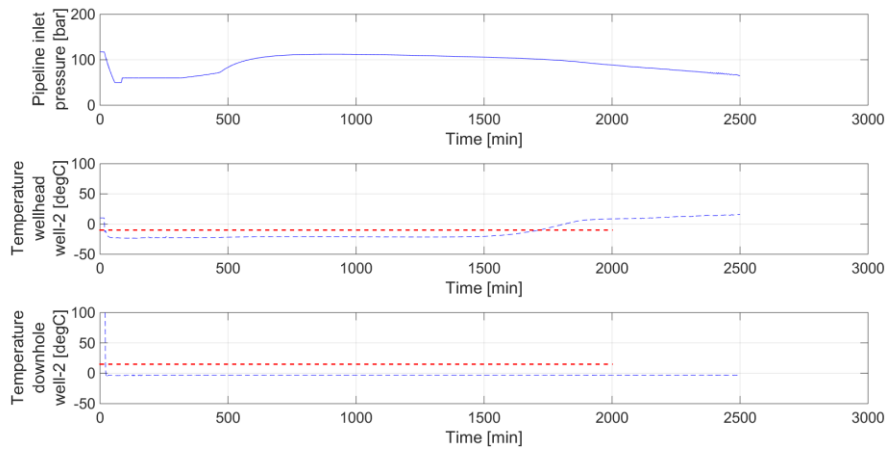


Figure 41: Temperatures and pressures as function of time.

7.6.3 Results case4047 & 4048

For completeness, the results of case4047 and case4049 are plotted in Figure 42 and Figure 43. In all these cases the temperatures are too low.

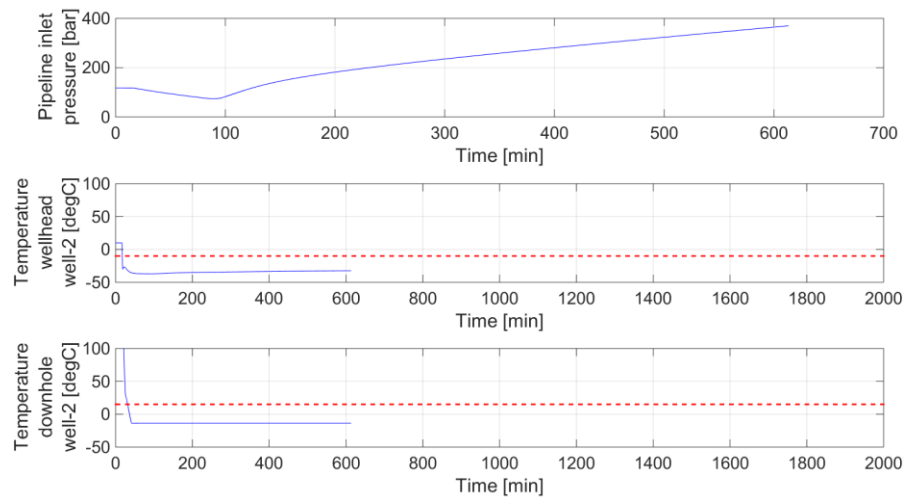


Figure 42: Results case4047.

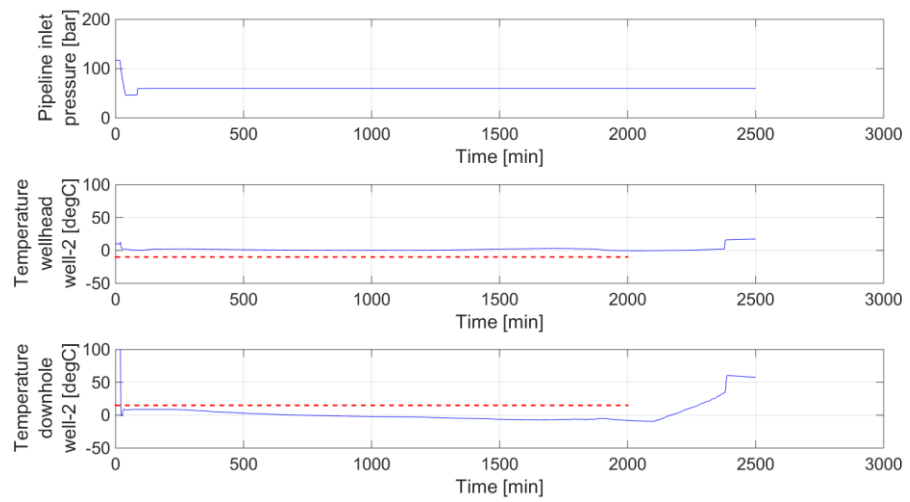


Figure 43: Results case4048.

## 7.7 Discussion venting

The high pressure start-up leads to long periods of too low temperatures. Therefore a set of venting solutions have been tried. The pipeline is vented down to a given pressure from which the system is started up again. (cases4051-4076).

If vented down to approximately 40 bar, the temperature in the pipeline is approximately 5 °C (for instance case4052). Different start-up scenarios, starting from this conditions were evaluated:

- First opening the wells
- First pressurizing the pipeline
- Mass flow control on the wells

Venting down to 40 bar, did lead to long periods of too low temperatures (Figure 44).

Venting down to 60 bar should lead to similar start-up sequences as discussed previously.

An alternative is that instead of venting, the pipeline pressure is slowly released into the well and that the topside piping is protected from the cold temperatures by local heating. As the bleed rate is low, the total heat capacity should be low. This scenario has not been calculated yet.

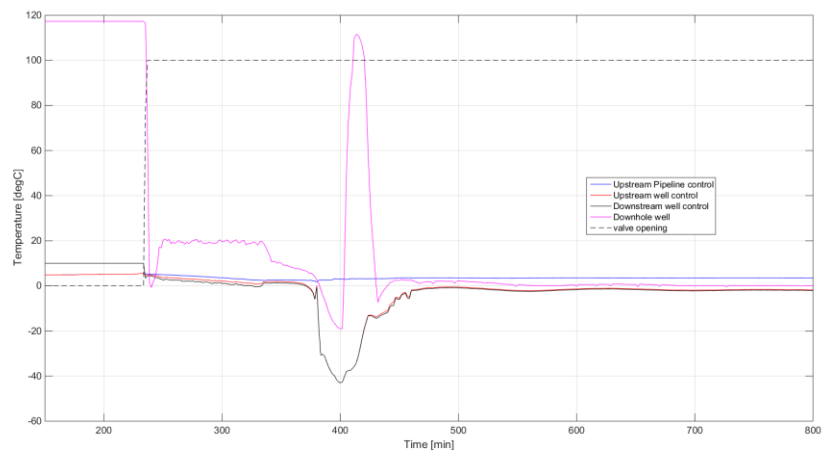


Figure 44: sharp peak is due to control action on the pipeline pressure control valve.

## 7.8 Discussions alternatives

Instead of venting a number of alternatives have been evaluated:

- Use of a very small ID well (0.09m). This increases the topside pressure at lower flow rates and keeps the flow rates at a given pipeline pressure limited.
- Adding N<sub>2</sub> (5% mole fraction) in the hope that the temperature effects are reduced.
- Adding downhole chokes (different sizes and different depts).

These were trial simulations and more scenarios could potentially be simulated. However, the cases tried did not pass the temperature boundary condition limitations.

## 7.9 Discussion start-up reservoir pressure 60 bar – mid pipeline pressure

For the start-up with a reservoir pressure of 60 bar two sets of cases are analysed. The first set is that all wells are at a reservoir pressure of 60 bar (cases 4105, 4106, 4107). In addition to the basic start-up, the effect of opening a 2<sup>nd</sup> well is evaluated (4108).

### 7.9.1 Results 4105 – 4107

The initial pipeline conditions at a pipeline pressure of approximately 63 bar, 24°C with a liquid hold-up of approximately 0.26 (Figure 47).

For all cases a sequence of events has been used defined by:

- The chokes of wells 2, 3, and 4 (P18-2 wells) are closed.
- The choke valve of well-1 is set to a pressure control of 85 bar at t= 0s.
- The pipeline control valve is set to a pressure control of 1 bar at t= 0s (this is already open in the initialisation cases).
- The compressor is ramped from t= 1000s to t = 1300s from a flow rate of 0 kg/s to the desired flow rate.

The results are given in

Figure 45. For all three start-up scenarios, the calculated temperatures are higher than the temperatures limitations.

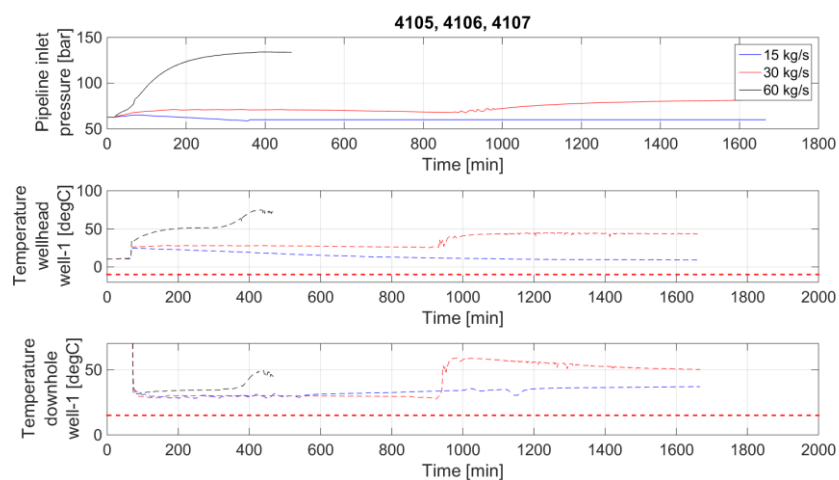


Figure 45: Resulting pressure and temperatures.



### 7.9.2 Results 4108 (opening 2<sup>nd</sup> well)

Case4108 is started from case4106 (with a reached steady conditions with a total mass flow rate of 30 kg/s).

The sequence of events is:

- The mass flow rate is increased to 60 kg/s at  $t = 0$ s.
- The choke at the second well well-2 is opened from 0 to 1 at  $t = 1000$ s.

Except for a very short period directly at opening of the choke valve (Figure 46) all temperatures meet the requirements.

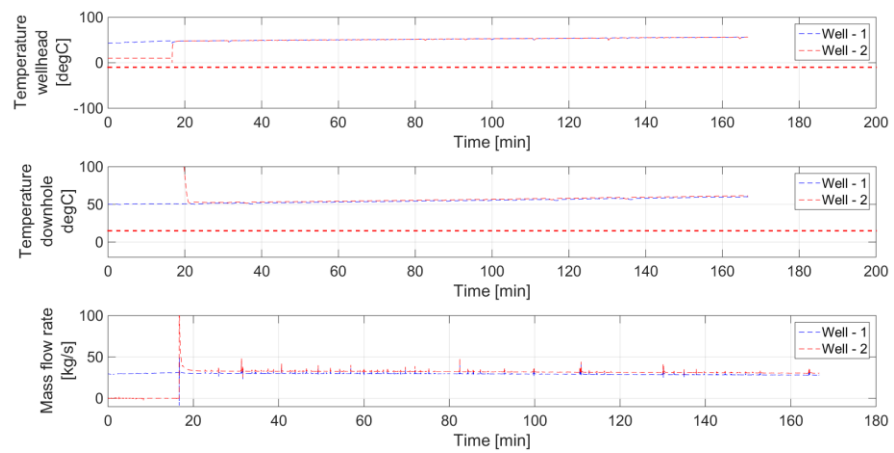


Figure 46: Resulting pressure and temperatures.

### 7.10 Discussion start-up reservoir pressure 100 – 340 bar – mid pipeline pressure

The higher pressure start-up cases have been done with pipeline conditions at a pipeline of approximately 63 bar, 24°C with a hold-up of approximately 0.26 (Figure 47).

For all cases a sequence of events has been used defined by (Figure 48):

- The chokes of wells 2, 3, and 4 (P18-2 wells) are closed
- The choke valve of well-1 is set to a pressure control of 85 bar at  $t = 0$ s.
- The pipeline control valve is set to a pressure control of 1 bar at  $t = 0$ s (this is already open in the initialisation cases).
- The compressor is ramped from  $t = 1000$ s to  $t = 1300$ s from a flow rate of 0 kg/s to the desired flow rate.

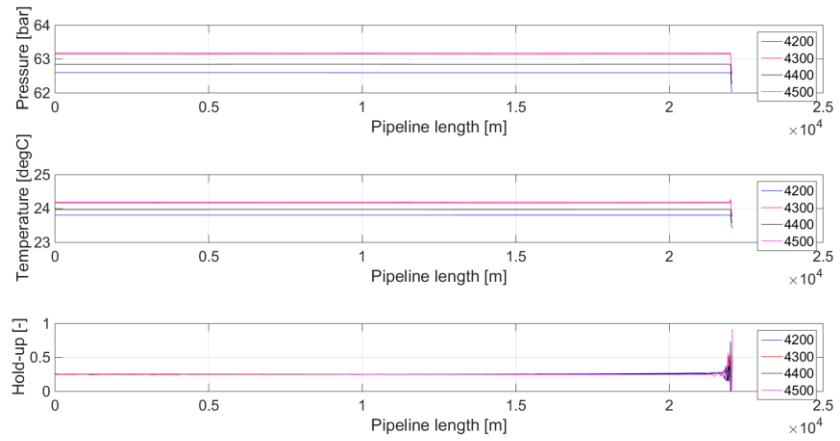


Figure 47: Pressure, temperature and hold-up profile at the start of the start-up sequence.

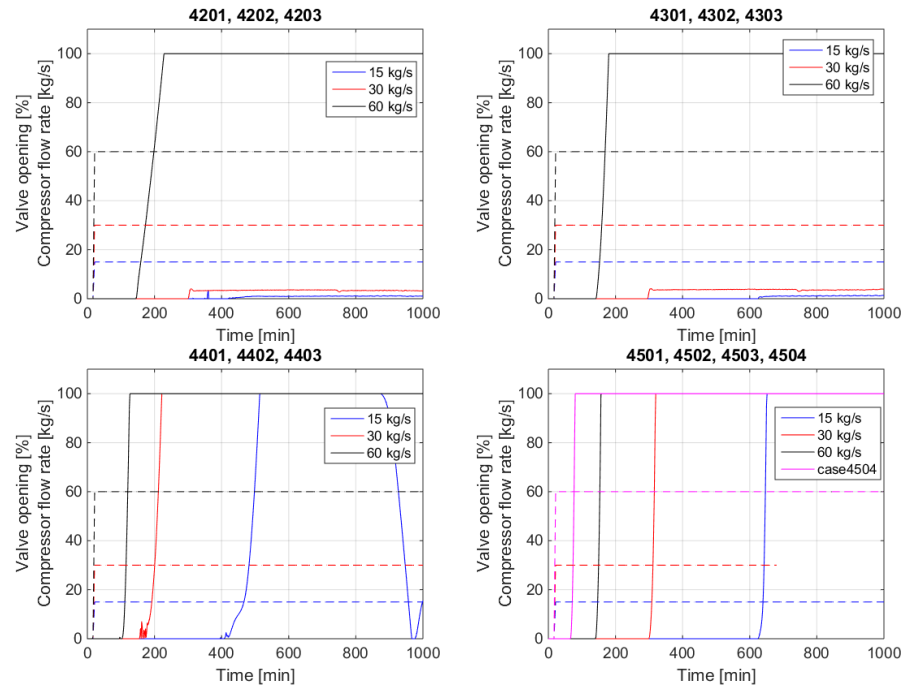


Figure 48: Compressor flow rates and valve openings at well 1 for the 4200, 4300, 4400 and 4500 series. Solid lines the valve opening [%]. Dashed lines indicate the compressor flow rates.

7.10.1 Results reservoir pressure 100 bar

For a reservoir pressure of 100 bar, the resulting pressures and temperatures are given in Figure 49. For all times, the temperatures are high enough both topside as well as downhole.



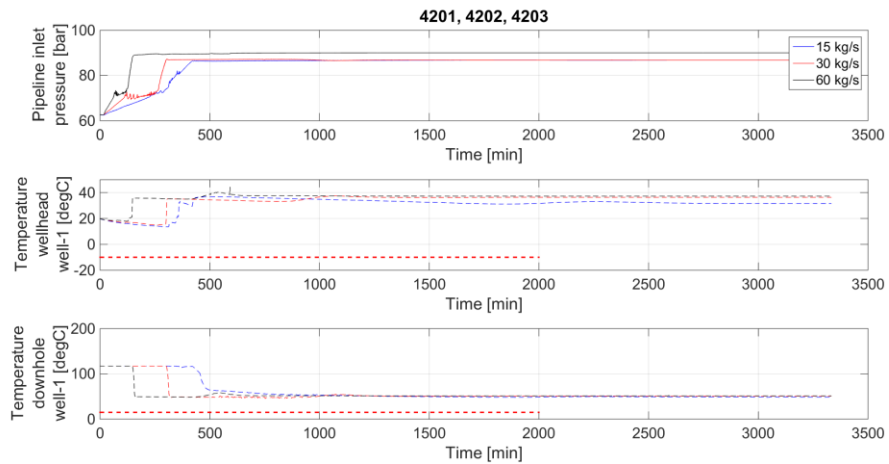


Figure 49: Pressures and temperatures as function of time.

7.10.2 Results reservoir pressure 200 bar

For a reservoir pressure of 200 bar, the resulting pressures and temperatures are given in Figure 50. For all times, the temperatures are high enough both topside as well as downhole.

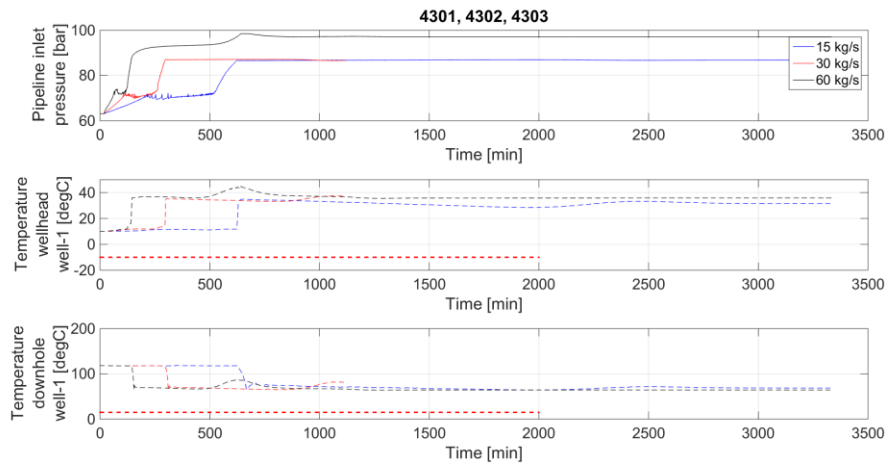


Figure 50: Pressures and temperatures as function of time.

7.10.3 Results reservoir pressure 300 bar

For a reservoir pressure of 300 bar, the resulting pressures and temperatures are given in Figure 51. For all times, the temperatures are high enough both topside as well as downhole. The high mass flow rate start-up might take longer than calculated as the maximum calculated compressor pressure is nearly 150 bar. Therefore, this start-up rate must be done with more than one well open.

Although, this specific case is not representative for the real life situations, no difficulties are expected as there are no temperatures limits downhole and the temperature effects topside are limited as the fluid is in the liquid state.

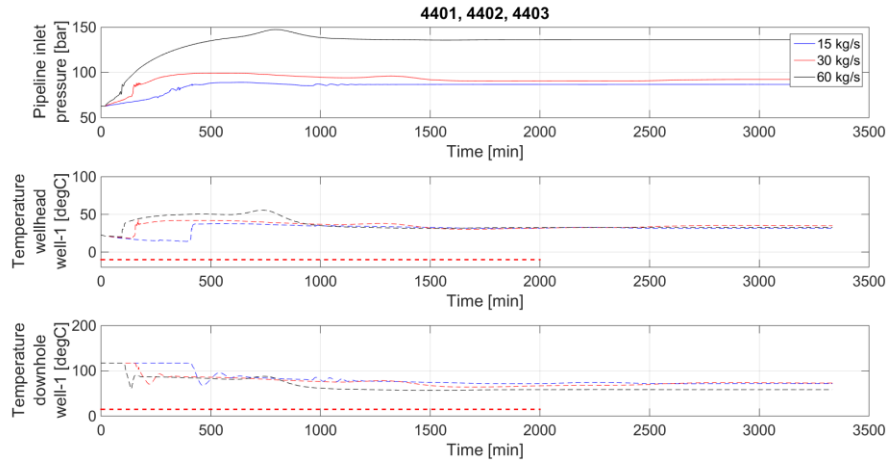


Figure 51: Pressures and temperatures as function of time.

7.10.4 Results reservoir 340 bar

For a reservoir pressure of 300 bar, the resulting pressures and temperatures are given in Figure 52 and Figure 53 For all times, the temperatures are high enough both topside as well as downhole. The high mass flow rate start-up might take longer than calculated as the maximum calculated compressor pressure is higher than 120 bar. Therefore, this start-up rate must be done with more than one well open.

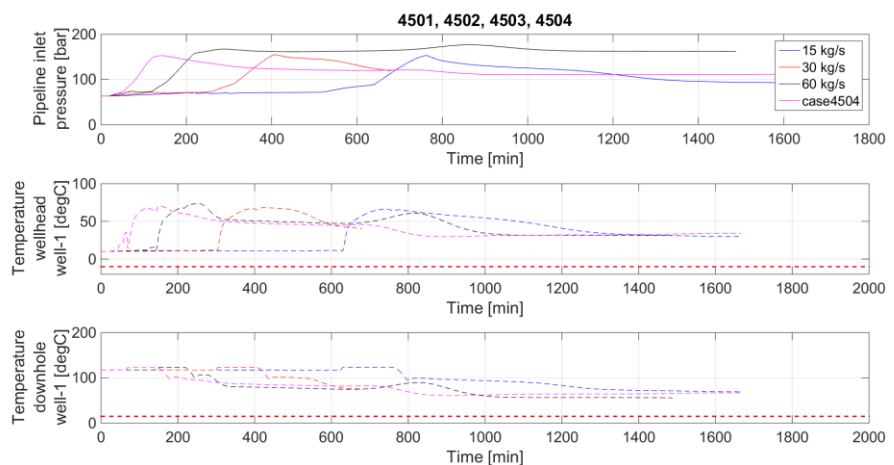


Figure 52: Pressures and temperatures as function of time.

## 8 Depressurization

An important event is venting or depressurizing the system. As most of the pipes are well insulated, there is no to little heat ingress. That means that the fluid temperature is almost adiabatic.

As an example, the pipeline is vented with initial conditions at the liquid state (115 bar, 15°C) (Figure 53). As soon as the venting starts, the pressure decreases rapidly as the pipeline is in liquid state. With the venting, the pipeline comes into two-phase conditions. With a continuation of the venting, the pipeline pressure decreases and the resulting temperature decreases fast.

This means that if venting continues to atmospheric conditions, solid CO<sub>2</sub> will be formed and the temperature will drop down to extreme low temperatures. To avoid this it is recommended to keep venting/depressurization limited down to 30 bar. This 30 bar is chosen based on the fact that the phase line temperature for 30 bar is -5 °C. Even with some pressure undershoot this will limit fluid temperatures.

It must be remarked that this effect will occur with all venting or depressurization event. All sections which must be able to be depressurized fast will need to be designed for extreme low temperatures.

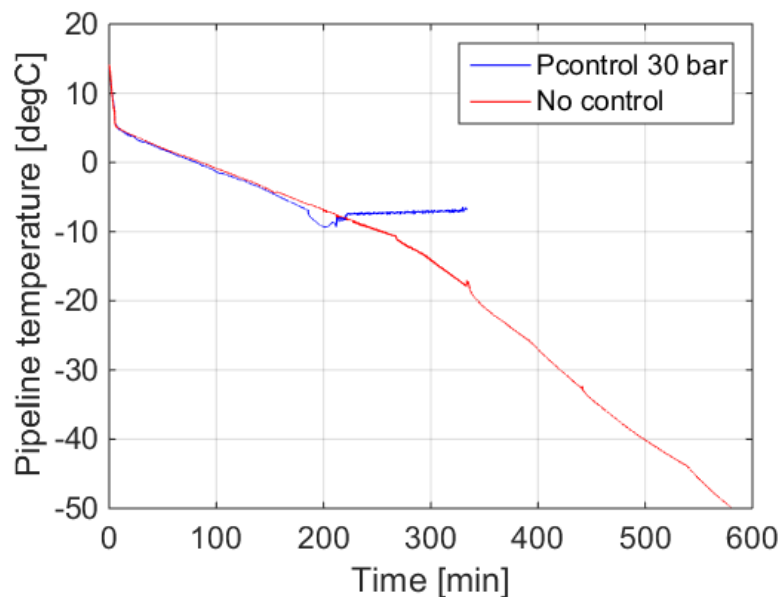


Figure 53: Pipeline temperature as function of time during a venting action with no pipeline control (red) or with the pipeline pressure control at 30 bar.

## 9 Shut-in/turn-down

### 9.1 Introduction

In this chapter two sets of simulations are presented. In the first set there are scenarios in which the mass flow is ramped down. The second set is a set in which the wells are shutin.

### 9.2 Simulation cases

Shutin at Pres = 20 bar

<b>Case</b>	<b>Pres</b>	<b>Tcmp</b>	<b>Wells</b>	<b>control</b>	<b>Mass flow</b>	<b>Start from</b>
7000	20	80	1	30	15->0; dt=300	4024
7001	20	80	1	30	30->0; dt = 300	4025
7002	20	80	4	30	140->0; dt = 300	4028
7005	20	80	1	no	15->0; dt=300	4024
7006	20	80	1	no	30->0; dt = 300	4025
7009	20	80	1	No	Well shutin	4025
7016	20	80	1	No	Well shutin 100	4025
7017	20	80	1	No	Well shutin 300	4025
7018	20	80	1	No	1000s	4025

Shutin at Pres = 60 bar

<b>Case</b>	<b>Pres</b>	<b>Tcmp</b>	<b>Wells</b>	<b>control</b>	<b>Mass flow</b>	<b>Start from</b>
7015	60	40	1	1 well	Well shutin	4009

The cases 7012-7014 have been wrongly initialised and are not reported

Shutin at Pres = 100 bar

<b>Case</b>	<b>Pres</b>	<b>Tcmp</b>	<b>Wells</b>	<b>control</b>	<b>Mass flow</b>	<b>Start from</b>
7008	100	40	4	Pipe (85)	170 -> 0	4078
7011	100	40	1	1 well	Well shutin	4078

Shutin at Pres = 340 bar

<b>Case</b>	<b>Pres</b>	<b>Tcmp</b>	<b>Wells</b>	<b>control</b>	<b>Mass flow</b>	<b>Start from</b>
7007	340	40	4	Pipe (85)	140->0	4006
7010	340	40	1	1 well	Well shutin	4006

### 9.3 Results well shutin for different reservoir pressures.

Well shutin simulations are done at different reservoir pressures. For a reservoir of 20 bar, the speed with which the valve was shutin was varied between 20 – 1000s (7009, 7016-7018). For reservoir pressures of 60, 100 and 340 bar only fast shutin cases were simulated.

For the shutin cases 7009, 7016-7018, the following sequences are calculated (Figure 54):

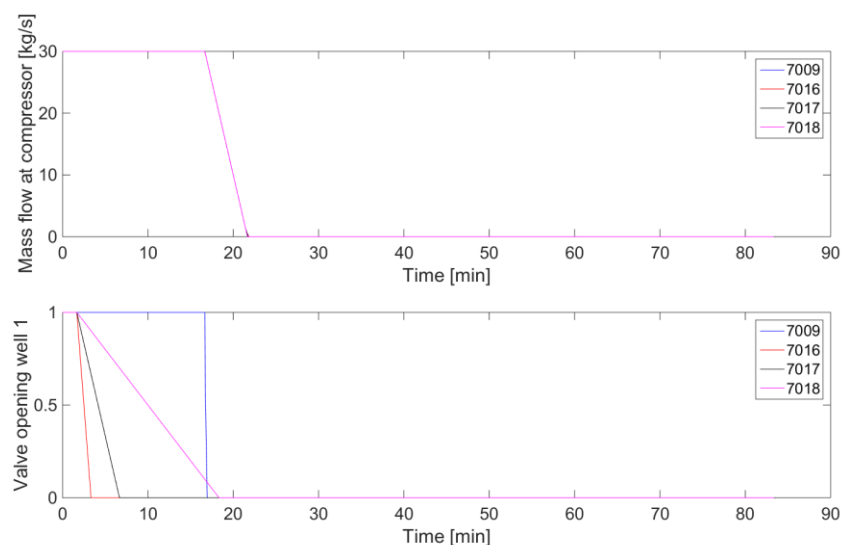
- Initial conditions are simulations at fixed mass flow ran long enough to obtain steady conditions.
- The mass flow is ramped down from  $t=1000s$  to  $t= 1100s$
- The choke at well-1 is shutin at  $t = 1000s$  (7009) and at  $t = 100s$  (7016-7018).
- Similar sequences are done for the higher pressure cases.

During shut-in/depressurization low temperatures in the well will occur due to expansion. This occurs typically in the top region (top 1000 m) but at fast shut-in of the wellhead choke, the complete well can go down in temperature (basically following pressure gradient and following phase line). The well control valve shut-in-time does practically not matter (Figure 55).

At higher reservoir pressures, the minimum temperatures increase

- Reservoir pressure 20 bar      -37 °C
- Reservoir pressure 60 bar      -17 °C
- Reservoir pressure 100 bar    -5 °C
- Reservoir pressure 340 bar    +30 °C

For the higher pressures, the wellhead temperature is plotted in Figure 57. From this figure, it is more clear that the low temperature period can be in the order of 30 minutes. It must be remarked again, that for the current simulation model uses Uvalue methodology and therefore no heat-capacity of the walls and annulus fluids are included. This means that the heating up also occurs faster then will be in real-life but that the wall temperatures will be higher than the calculated temperatures.



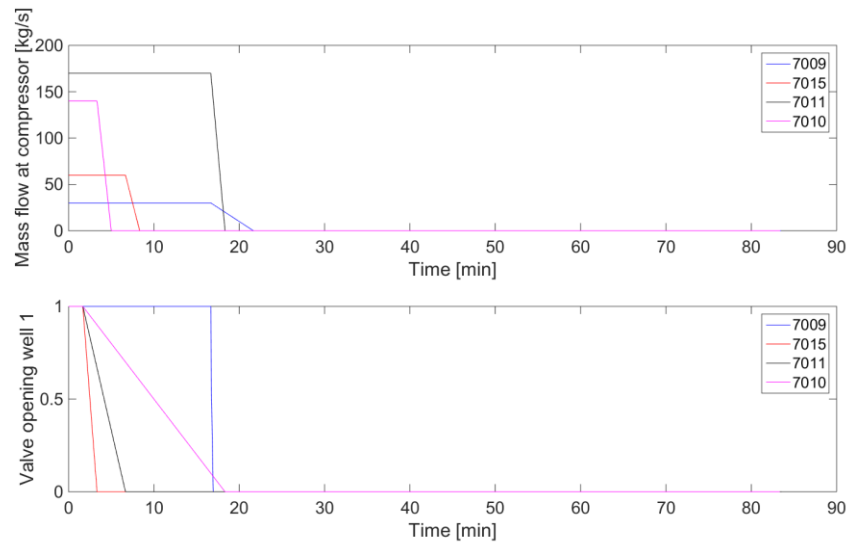


Figure 54: Sequences of flow rates and valves.

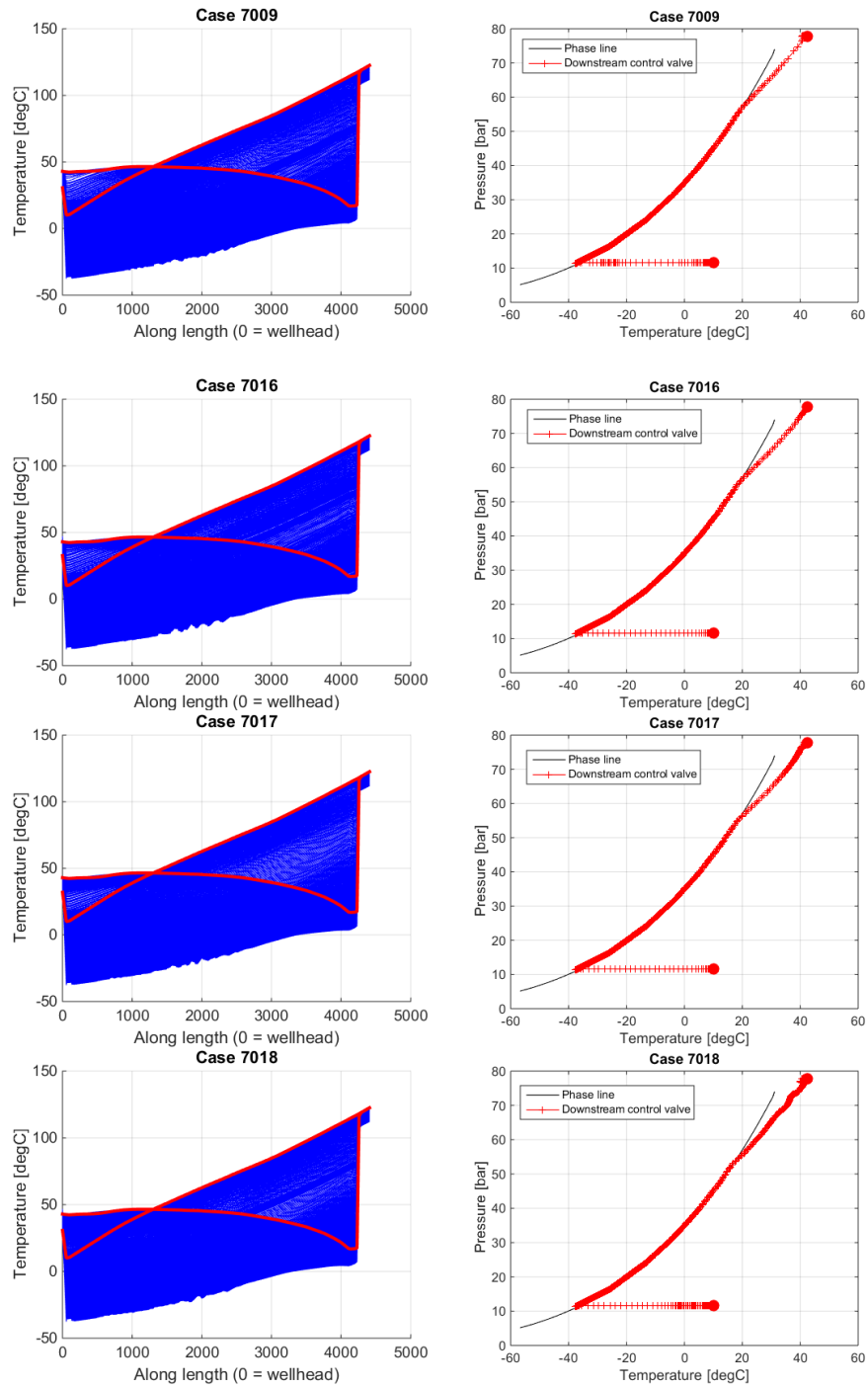


Figure 55: Temperature profile in the wells during ramp-down. The red lines indicate the initial and final profile. Each blue line is at a time step of 1 s. Right figures give pressure/temperature as function of time downstream of the choke at well-1. Cases 7009, 7016, 7017, 7018 are for cases without pipeline pressure control.

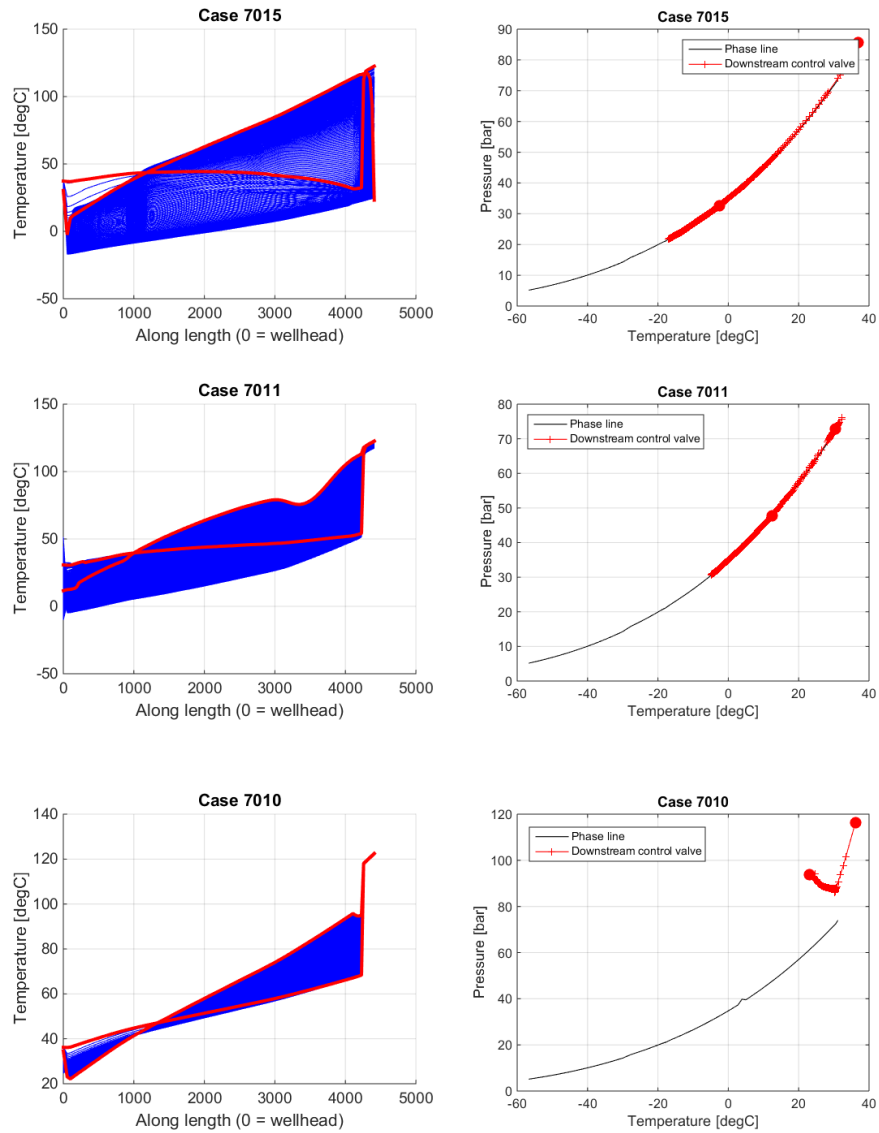


Figure 56: Temperature profile in the wells during ramp-down. The red lines indicate the initial and final profile. Each blue line is at a time step of 1 s. Right figures give pressure/temperature as function of time downstream of the choke at well-1. Cases 7015, 7011 and 7010 are for a reservoir pressure of 60, 100 and 340 bar.



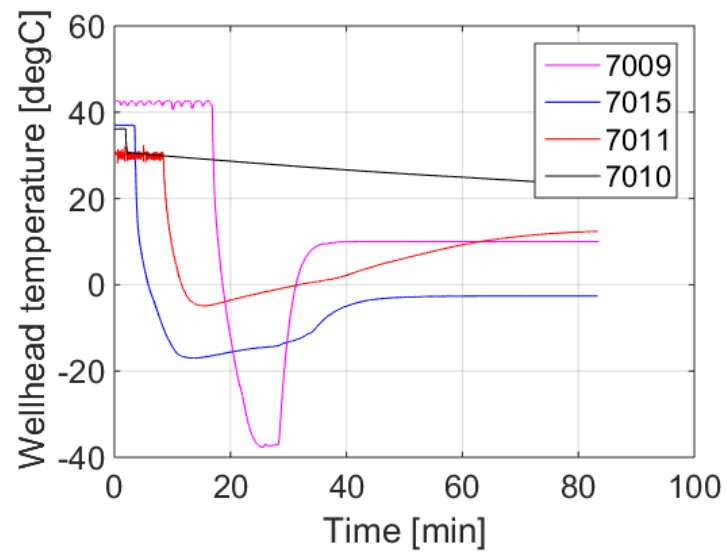


Figure 57: Wellhead temperature as function of time for the cases 7009 (20 bar), 7015 (60 bar), 7011 (100 bar), 7016 (340 bar).

## 9.4 Results turn-down reservoir pressure 20 bar

The cases with a reservoir pressure of 20 bar and including a pipeline control valve, the turn-down cases 7000, 7001, 7002, 7005 and 7006 are done. The sequences is mainly for (Figure 58):

- Mass flow rate is ramped down in 300s at  $t = 1000$ s.
- The well valves are kept open.

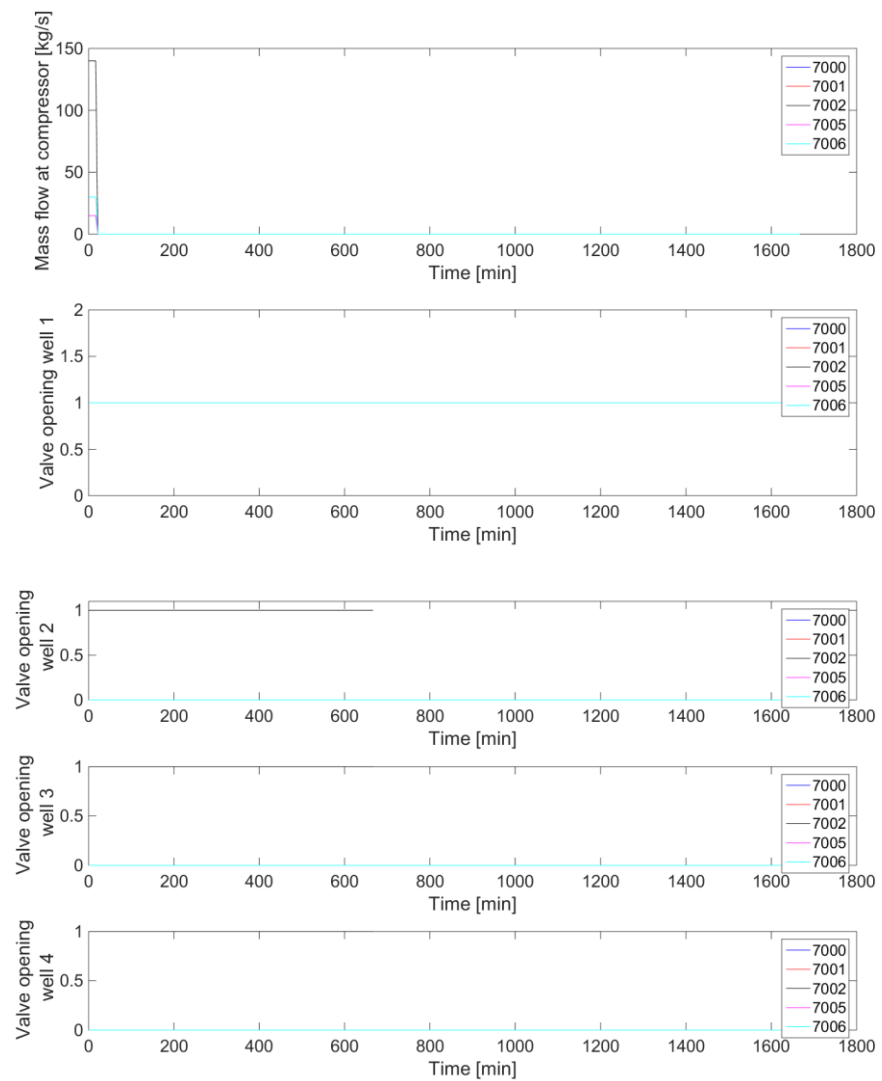


Figure 58: Mass flow rates and valve opening as function of time.

The resulting temperature profiles in well-1 are plotted in Figure 59 and the pipeline in Figure 60. The low temperature zone is mainly restricted to the topside in the well but the pipeline can get very cold with low temperatures down to  $-20\text{ }^{\circ}\text{C}$  in the whole pipeline and very low temperatures downstream of the pipeline control valve.

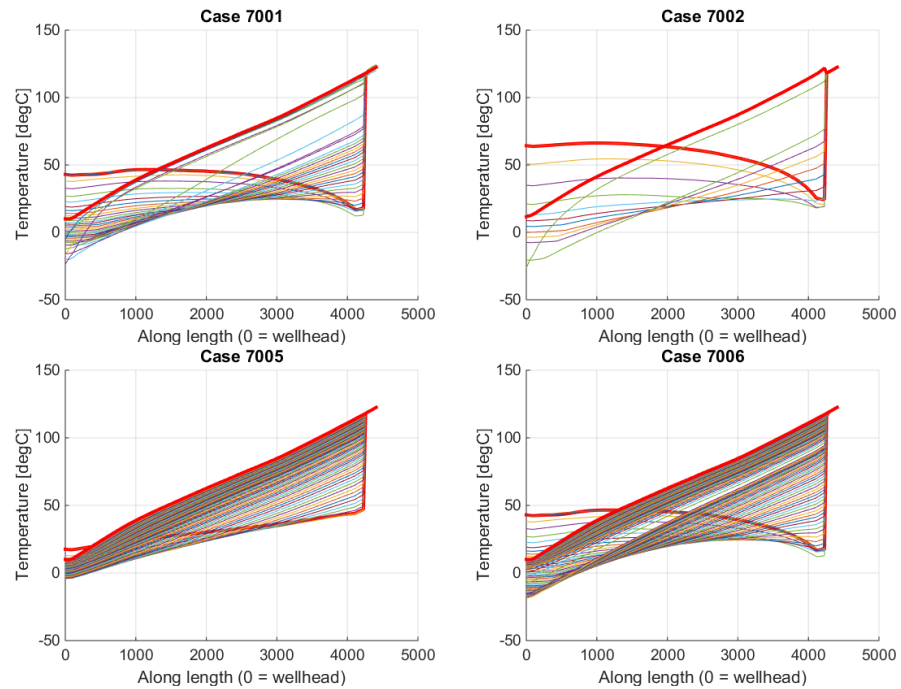


Figure 59: Temperature profile in the wells during ramp-down. The red lines indicate the initial and final profile. Each blue line is at a time step of 1000 s.

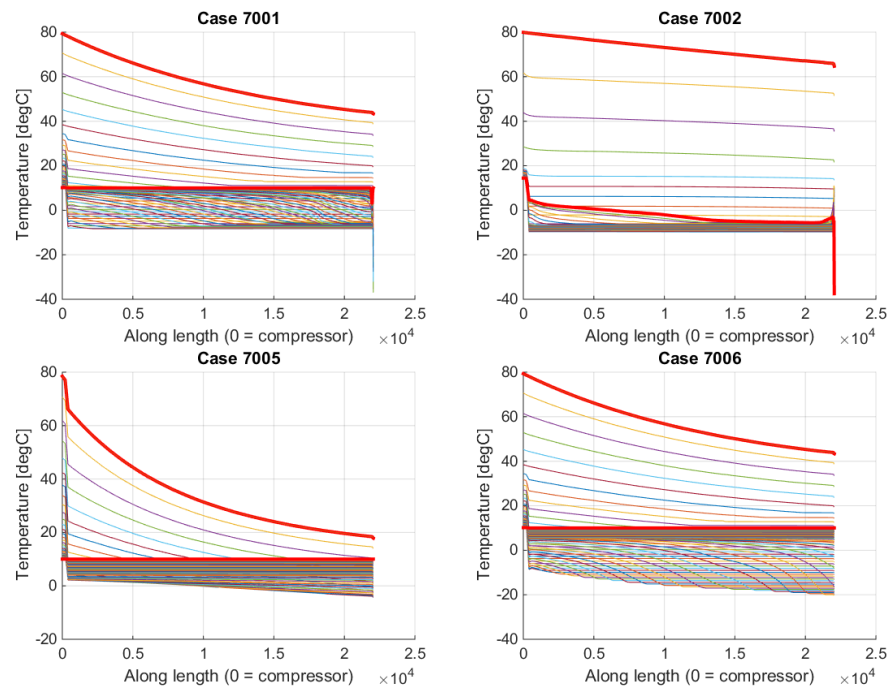


Figure 60: Temperature profile in the pipeline during ramp-down. The red lines indicate the initial and final profile. Each color line is at a time step of 1000 s. Cases 7001 and 7002 have a pipeline control of 30 bar. This means that downstream the valve, the expansion is deeper. This explains the sharp decrease observed in 7001 and 7002 results.

### 9.5 Results turn-down reservoir pressure 100 bar

For the case7008 with a reservoir pressure of 100 bar, the sequence of events simulated are (Figure 61):

- The mass flow rate is ramped down from t=0 to 100s
- The pipeline pressure controller is set to 85 bar
- Well-1 is at a pressure control of 10 bar (meaning full open)
- Well-2, 3, 4 is at a mass flow control at 1000 kg/s (meaning full open)

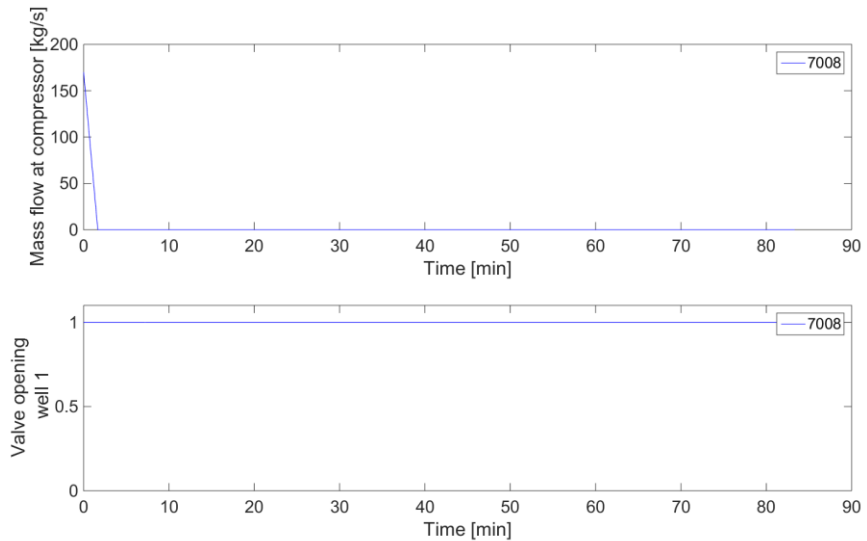


Figure 61: Mass flow rates and valve opening as function of time.

The resulting temperatures in all four wells and the pipeline is given in Figure 62 and in Figure 63. The minimum temperatures only just drop below 0 °C.

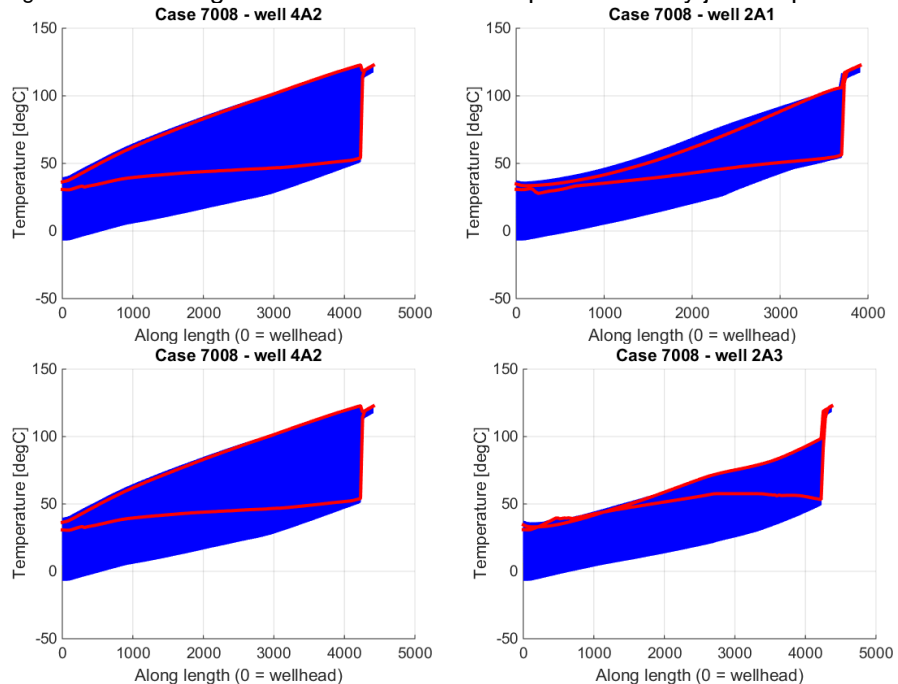


Figure 62: Temperature profile in the wells during ramp-down. The red lines indicate the initial and final profile. Each blue line is at a time step of 1 s.

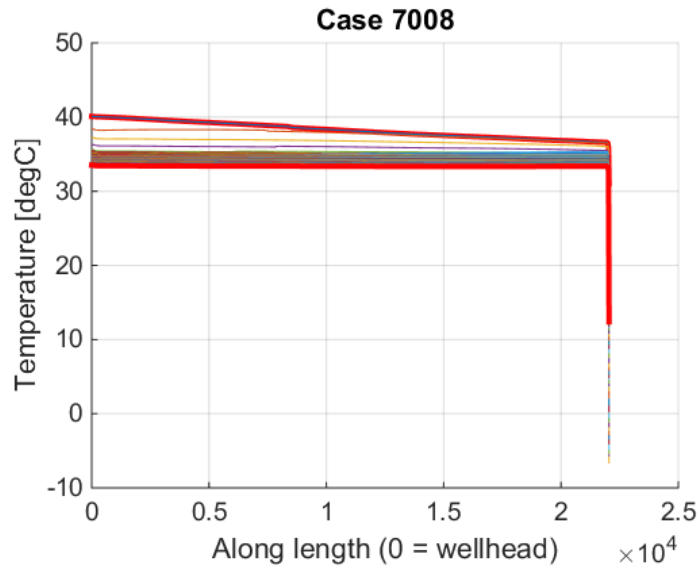


Figure 63: temperature profile in the pipeline. The red lines indicate the initial and final profile. Each coloured line is at a time step of 100 s

### 9.6 Results turn-down reservoir pressure 340 bar

Finally, for the case7007 with a reservoir pressure of 340 bar, the sequence of events simulated are (Figure 64):

- The mass flow rate is ramped down from t=0 to 100s
- The pipeline pressure controller is set to 85 bar
- Well-1 is at a pressure control of 10 bar (meaning full open)
- Well-2, 3, 4 is at a mass flow control at 1000 kg/s (meaning full open)

The resulting temperatures (Figure 65) all remain high.

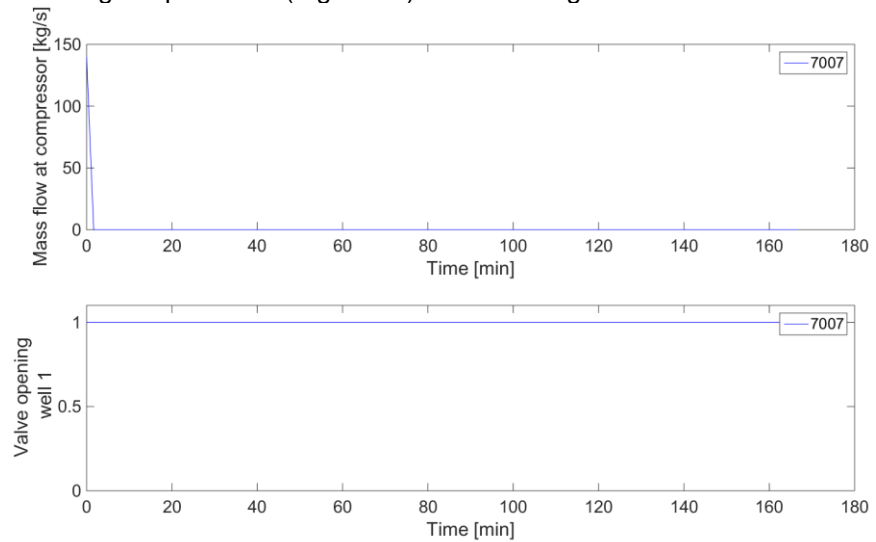


Figure 64: Mass flow rate and valve openings as function of time.

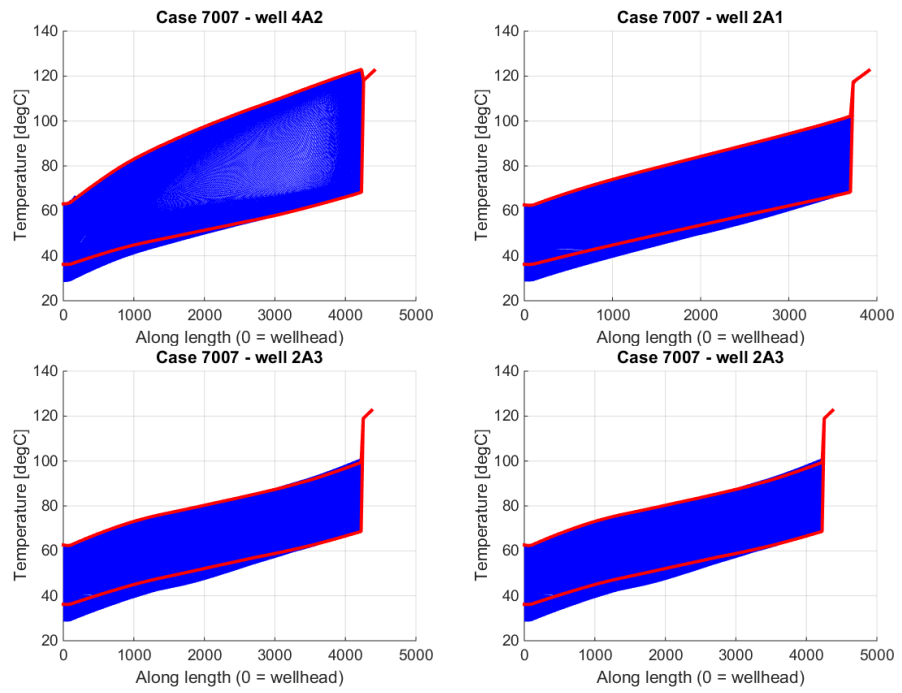


Figure 65: Temperature profile in the wells during rap-down. The red lines indicate the initial and final profile. Each blue line is at a time step of 1 s.

## 10 Discussion/ general remarks

This chapter summarises the conclusions and key results from the previous chapters.

The main concepts which determine injection:

- Phase line conditions link the temperature and pressure.
- The critical bottomhole pressure is 50 bar as this corresponds to a phase line temperature of 15 °C (which is the set downhole temperature limit).
- Keeping the mass flow rate and keeping the wellhead pressure high avoids low temperatures during steady operations. Smaller ID wells keep the wellhead pressure high already at low flow rates. However, small ID well limit the injection rate at low reservoir pressure due to too low downhole temperatures and at high reservoir pressures the rates are limited due to too high compressor pressures (too high friction).
  
- Scenario's in which the tubing diameter is changed after a period of operation have not been included in this report.
  
- Only a limited set of runs with more complicated well designs are done. Downhole valves, ICD's tuneable orifices etc are not included as this complicated the well design significantly and might risk of local freezing of components.
  
- The compressor discharge control valve is now set downstream of the compressor after-cooler. This as this is worst case for the simulations as we lose temperature across the valve. In reality this valve might be installed upstream of the cooler if so desired.
- In the simulations a dedicated pipeline pressure control valve is used. Downstream of the valve there is often two-phase flow.
  - The pipeline pressure control might also be done via a control on one of the wells. The other wells must be set on mass flow control.
  - The benefit of this is that upstream of the well control valves, there is single phase flow. This might be beneficial for metering.
  
- The flowing wellhead pressure is for a large range of conditions constant and not a function of mass flow rate but is mainly a function of temperature.
- The shutin wellhead pressure is for a large range of reservoir pressures constant.
  - Both conditions mean that the wellhead pressure is not a good control parameter and that his parameter cannot be used for flow allocation. Therefore, downhole gauges (pressure and temperature) are strongly recommended.
  
- The temperature downstream of valves is determined by a number of aspects:
  - Pressure drop and therefore temperature drop (mainly for a pressure drop across a valve with both upstream and downstream gas phase)



- Phase line temperature (mainly for expansion across a valve from liquid to low pressure resulting in two phase conditions downstream of the valve)
  - Back pressure at the valve. At high flow rates, the well provides back pressure to the valves resulting in less temperature drop.
- 
- A critical temperature of 15°C is used for downhole conditions. It has not been taken into account that the CO<sub>2</sub> expands in the reservoir resulting in lower temperatures in the near-well zone.
  - The injectivity index is based on single phase assumption at reservoir temperature. Therefore it is likely that the pressure drop in the reservoir will be higher than calculated.
- 
- In this report, no alternatives for hydrate prevention are evaluated.
  - As low fluid temperatures might be unavoidable and piping (manifold, valves etc) needs to be designed for low temperatures, the topside low temperature restriction might be re-evaluated.
- 
- The depressurization of the pipeline at high shutin pressure conditions is done via venting in this report. It might be evaluated whether slowly depressurizing and local heating of the pipe materials might work.

# 11 General conclusions & recommendations

## 11.1 General conclusions

For steady state conditions the following conclusions are found:

- At low reservoir pressure (20-40 bar), no steady state solution is found which comply with both the topside and downhole temperature restrictions when the pipeline pressure is maintained in the liquid state. Therefore, at low reservoir pressure the pipeline must be operated in gas or two-phase conditions.
- This puts limitations on the maximum injection rates per well or for all four wells combined.
- At reservoir pressures (40-300 bar), the required flow rate (170 kg/s) is achieved using four wells.
- At close to the maximum reservoir pressures, the compressor outlet temperature needs to be reduced. Otherwise no injection is possible.

For depressurization the following conclusions are found:

- The heat ingress in the pipeline is limited. Therefore, during depressurization or emptying the pipeline the temperature follows the pressure via the phase line and low temperatures conditions can occur in the complete pipeline. Therefore, a pressure control of the pipeline is recommended.

For shutin simulations the following conclusions are found:

- During well shutin, low fluid temperatures will occur in the well downstream of the choke. The temperature will go down to the corresponding phase line temperature. At a reservoir pressure of 20 bar, this means a temperature of -37 °C. At lower reservoir pressures this will lower even further. At higher reservoir conditions, the temperature will increase. -17, -5 and +30 °C at reservoir pressures of 60, 100 and 340 bar.
- During ramp-down, low temperatures occur mainly in the top part of the well. These temperatures go well below -10 °C.
- During ramp-down also the temperature in the pipeline itself will drop down to values below -20 °C.
- The low temperatures during shutin/ramp-down are difficult to avoid and as such it is recommended that all piping should be able to withstand the low temperatures.

From the start-up simulations the following conclusions are found:

- For all reservoir conditions, at initial choke valve opening, a short period of low temperature will occur downstream of the control valves. For the start-up, a faster valve-opening is beneficial with respect to the temperatures.
- In the sequencing of well opening and compressor ramp-up, the flow rates from the pipe to the wells must not decrease too quickly to avoid too low pressures (and therefore temperatures in the well and pipeline). Therefore, the compressor ramp-up must be done relatively soon after the well opening.

The compressor can be ramped-up before the well opening at higher reservoir pressures with the limit that the pipeline pressure must not be higher than 85 bar.

- At low reservoir pressure, the system could be started up from low pressure (10, 30 bar) or medium pressure (60 bar). In case of medium-pressure conditions, the downhole temperature is too low for a limited period of time (less than 500 minutes).
- At low reservoir pressure, starting from high pressure pipeline conditions leads to long periods of too low temperatures (longer than 2000 minutes).
- At medium and higher reservoir pressures start-up can be done from medium-pressure (two -phase conditions) conditions within the temperature restrictions.

### 11.1.1 Base operation

The base recommended operations (based on the set restrictions) are:

- At low reservoir pressure, the pipeline is operated in the gas phase and all well chokes are kept open to avoid pressure drop. The compressor outlet temperature is set to 80 °C.
- At mid to high reservoir pressures, the compressor outlet temperature is set to 40 °C. The setting is an optimization between cooling power and compressor power.
- At very high reservoir pressures, compressor outlet temperature must be set to 40 °C, otherwise injection is not possible.

Reservoir pressure [bar]	Compressor outlet temperature [°C]	Pipeline control	Well operations
20 – 40 bar	80	30	Full open
40 – 300 bar	40 - 80	30	1 well on pressure control. Other wells on mass control
300 – 340 bar	40	30	1 well on pressure control. Other wells on mass control

During well shutin, a fast closure the choke valves leads to very low temperatures. At low reservoir pressures the shutin procedure should be leaving the wells open while shutting down the compressor.

### 11.1.2 Shutin philosophy

During well shutin, a fast closure of the choke valves lead to very low temperatures. At low reservoir pressures the shutin procedure should be to leave the wells open while shutting down the compressor.

## 11.2 Recommendations

The main recommendations include:

- All piping material should be designed for extreme low temperatures (-40°C, based on expected wellhead pressures of 10 bar).
- Update simulation model to include full heat transfer (rather than U-value approach) at the time the well design and pipeline design is set. This to get more detailed temperature information on pipe wall temperatures and annulus fluid temperatures.
- Considering the fact that fluid temperatures less than -10°C are probably not avoidable, the restriction of -10°C for the topside temperature should be reconsidered/re-evaluated.
- The criterion of 15°C downhole temperatures is restrictive. Alternatives for hydrate preventions should be evaluated.
- An operational guidebook should be set up which describes the number of wells and control settings for each mass flow rate.
- This guidebook should also contain guidelines of start-up and shutin procedures.

## 12 Signature

Delft, April 2019

TNO



E.D. Nennie, MSc.  
Research Manager  
Heat Transfer and Fluid Dynamics



S.P.C. Belfroid  
Author

## A Steady state results

In this annex, the results for the steady state results are added.

<b>Case</b>	<b><i>Twh</i></b>	<b><i>Tdh</i></b>	<b><i>Pplatform</i></b>	<b><i>Pcomp</i></b>	<b><i>Mass flow</i></b>
Reservoir pressure = 300 bar					
4000	21	64	58	85	18
	10	116			0
	10	118			0
	10	116			0
4001	35	73	90	92	28
	10	117			0
	10	118			0
	10	115			0
4002	32	58	113	136	60
	10	117			0
	10	118			0
	10	115			0
4002_45	33	62	105	108	45
4003	37	77	91	94	24
	37	78			36
	10	118			0
	10	115			0
4004	36	68	108	116	42
	36	69			53
	36	69			39
	36	70			36
Reservoir pressure = 340 bar					
4005	36	66	130	138	42
	36	66			53
	36	66			40
	36	67			35
4006	36	68	116	123	33
	36	68			45
	36	69			33
	36	69			29
Reservoir pressure = 200 bar					
4079	33	75	79	93	43
	33	74			50
	33	74			39
	33	74			37
4081	36	62	95	97	60
	13	118			0
	13	119			0
	12	116			0
Reservoir pressure = 100 bar					
4078^	32	55	76	93	40
	32	54			38

	32	51			40
	32	51			45
4080	37	51	87	90	60
	11	117			0
	11	118			0
	12	115			0
4082*	15	52	52	85	30
	11	117			0
	11	118			0
	12	115			0
4083	-2	50	33	85	15
	11	116			0
	11	118			0
	11	115			0
Reservoir pressure = 60 bar					
4007	-6	25	30	85	15
	10	116			0
	10	118			0
	10	115			0
4008	18	27	56	85	28
	10	116			0
	10	118			0
	10	115			0
4009	37	32	87	89	60
	10	116			0
	10	118			0
	10	115			0
4010	35	35	143	147	100
	10	116			0
	10	118			0
	10	115			0
4011	31	31	75	89	48
	31	32			53
	8	118			0
	8	115			0
4012	30	31	72	93	59
	30	33			56
	30	30			44
	30	29			41
4013	20	29	85	95	40
	19	29			40
	20	29			40
	29	30			50
Reservoir pressure 20bar – control 85 bar					
4014	-10	-11	27	85.1	15
	10	116			0
	10	118			0
	10	115			0
4015	17	-3	53	85.3	30

	10	116			0
	10	118			0
	10	115			0
4016	37	9	86	89	60
	10	116			0
	10	118			0
	10	115			0
4017*	0.4	4.9	85	86	15
	10	116			0
	10	118			0
	10	115			0
Reservoir pressure 20bar – control 60 bar					
4018	7	36	61	61	15
	10	116			0
	10	118			0
	10	115			0
4019	64	9	134	137	60
	10	116			0
	10	118			0
	10	115			0
4020	77	12	126	140	50
	47	11			40
	61	6			40
	63	5			40
4021	62	29	96	106	33
	52	32			30
	62	25			29
	62	24			28
4022	57	7	109	111	46
	10	116			0
	10	118			0
	10	115			0
4023	43	18	79	81	30
	10	116			0
	10	118			0
	10	115			0
Reservoir pressure 20 bar – no control					
4024**	17	47	46	60	15
	10	116			0
	10	118			0
	10	115			0
4025	42	17	78	80	30
	10	116			0
	10	118			0
	10	115			0
4026***	58	8.3	107	109	43
		116			0
		118			0
		115			0



4027	67	16	116	131	44
	66	19			48
	66	12			39
	67	11			38
4028	64	24	103	115	37
	64	27			40
	64	20			32
	64	19			31

\* No hydrodynamic slugging used

\*\* single phase

\*\*\* not 100% converged

^ crashes

<b>Case</b>	<b><i>Twh</i></b>	<b><i>Tdh</i></b>	<b><i>Pplatform</i></b>	<b><i>Pcomp</i></b>	<b><i>Mass flow</i></b>
4128	58	40	81	90	26
	58	42			28
	58	35			23
	58	35			22
4129	56	45	75	83	24
	56	46			25
	56	40			21
	56	40			20

Princetonlaan 6  
3584 CB Utrecht  
P.O. Box 80015  
3508 TA Utrecht  
The Netherlands

[www.tno.nl](http://www.tno.nl)

T +31 88 866 42 56  
F +31 88 866 44 75

## TNO report

TNO 2019 R11635

# CO<sub>2</sub> storage feasibility in the P18-2 depleted gas field

Date	October 2019
Author(s)	Filip Neele Ton Wildenborg Kees Geel Daniel Loeve Lies Peters Siavash Kahrobaei Thibault Candela Mariëlle Koenen Paul Hopmans Kaj van der Valk Bogdan Orlic Vincent Vandeweijer

\*

Copy no	
No. of copies	
Number of pages	232 (incl. appendices)
Number of appendices	
Sponsor	
Project name	P18-2 storage study
Project number	060.35859

All rights reserved.

No part of this publication may be reproduced and/or published by print, photoprint, microfilm or any other means without the previous written consent of TNO.

In case this report was drafted on instructions, the rights and obligations of contracting parties are subject to either the General Terms and Conditions for commissions to TNO, or the relevant agreement concluded between the contracting parties. Submitting the report for inspection to parties who have a direct interest is permitted.

© 2019 TNO

## Summary

### *Objective*

This study presents the results from a CO<sub>2</sub> storage feasibility study on the P18-2 depleted gas field that is located in the Netherlands offshore. The aim of the study was to understand the risks associated with injecting CO<sub>2</sub> into the field, to outline injection strategies that lead to safe and secure storage and, finally, to propose an approach to risk management and monitoring during injection. The results from this study are to form the geoscientific basis for a CO<sub>2</sub> storage permit application.

### *Background*

The study was carried out for the Porthos consortium that plans to transport CO<sub>2</sub> from several industrial sources in the Port of Rotterdam to three P18 fields operated by Taqa: P18-2, P18-4 and P18-6. TAQA already obtained a storage permit for the P18-4 field in 2013, with the aim to store CO<sub>2</sub> for the ROAD project, with a mass of about 5 Mt. However, the ROAD project was cancelled in 2017.

The Porthos consortium builds onto the work done by the ROAD project. The consortium plans to transport and store an amount of CO<sub>2</sub> that is larger than the 5 Mt target of the ROAD project and, hence, will need storage capacity in addition to that offered by the already permitted P18-4 field. Operated from the same P18-A platform and also close to the end of production, the P18-2 and P18-6 fields represent a maximum storage capacity 32.3 Mt and 1.5 Mt (in both cases for a final reservoir pressure of just under original gas pressure). The current study is directed to the P18-2 field only.

In 2010 already a CO<sub>2</sub> storage feasibility study of the P18 fields was done. The present study provides an update for the P18-2 field based on new data and improved methods and workflows to investigate the response of the depleted field to injection of CO<sub>2</sub>.

### *Study approach*

The requirements for a CO<sub>2</sub> storage permit application are set out in the Dutch Mining Act which was amended in 2011 to include a transposition of the EU Storage Directive (EU, 2009). The results presented in this report cover the requirements described in the EU Storage Directive. The present study follows a workflow that was developed in a consortium of several EU Member States, building on combined experience in CO<sub>2</sub> storage feasibility assessments.

The workflow is risk-based, with the aim to understand the site-specific risks associated with CO<sub>2</sub> storage, to reduce them to a level that is as low as reasonably possible through site-specific design of injection scenarios and to develop a monitoring program and mitigation plan aimed at the most relevant, remaining risks.

### *Overall conclusion regarding storage of CO<sub>2</sub> in the P18-2 field*

The overall conclusion of the study is that CO<sub>2</sub> can be stored safely and securely in the P18-2 field. The CO<sub>2</sub> can be injected into the field in a way that is safe; during and after the end of injection, the P18-2 field will retain the CO<sub>2</sub> securely. There is no reason to assume that CO<sub>2</sub> could migrate out of the field after proper decommissioning of the injection wells after the end of injection.

### *Managing relevant risks*

The identified risks that are related to the potential leakage of CO<sub>2</sub> out of the P18-2 storage complex during or after CO<sub>2</sub> injection have been studied in detail and classified in a risk register. Most of the risks have been classified as 'low', with 'very low likelihood' that a small ('nil to negligible') amount of CO<sub>2</sub> that could migrate out of the reservoir; this corresponds with the lowest possible risk class. The remaining risks, with slightly higher likelihood and/or consequence, are related to (1) lateral CO<sub>2</sub> migration out of the storage reservoir, (2) the integrity of the wells in the field and (3) the stability of the faults in the storage system.

- (1) Simulation of the flow of CO<sub>2</sub> during injection into the storage formations shows that there is a possibility for the CO<sub>2</sub> to move into the attached water-filled formation, but remain within the storage complex. Simulations show that when CO<sub>2</sub> injection is stopped before the initial reservoir natural gas pressure is reached, the CO<sub>2</sub> will be retained within the original gas-filled reservoir formation and will not leave the storage complex.
- (2) Analysis of available data on the integrity of the wells in the P18-2 field shows that a workover is required for each of the potential injection wells to make them suitable for CO<sub>2</sub> storage operations or to decommission them. Once these are performed, the risk of CO<sub>2</sub> leaking along the wells, based on pre-injection status, is considered low.

The initial low reservoir pressure leads to low temperature of the injected CO<sub>2</sub> at the bottom of the well, causing significant temperature gradients in the well. This might lead to de-bonding of well liner (casing) and cement, potentially allowing leakage pathways to form (microannuli) for CO<sub>2</sub>. However, only when the pressure in the reservoir is above hydrostatic pressure could CO<sub>2</sub> enter these micro-annuli and potentially migrate into overlying aquifers. Therefore, the pressure in the reservoir is to be maximized at hydrostatic pressure, to reduce the likelihood of CO<sub>2</sub> flowing through these micro-annuli to small to negligible.

- (3) The cold CO<sub>2</sub> is injected into the reservoir formations, where it will create a low-temperature zone around the injection wells. If this zone reaches faults that are present in the reservoir, fault stability is affected; at the same time, faults become more stable during the injection process due to re-pressurizing the reservoir the reservoir. Monitoring of injection rate and temperature is required to track the pressure and temperature development in the reservoir and ensure that faults remain stable. All analysis points to small to negligible probability of fault reactivation; the caprock of 450 m to 750 m thick, fault destabilization will not lead to CO<sub>2</sub> movement through the caprock.

### *Recommendations*

- (1) In the study presented here the modelling of the injection process was performed with an isothermal reservoir simulator that could not simultaneously handle pressure and temperature variations in the reservoir. The impact of the low temperature of the injected CO<sub>2</sub> was estimated through the use of an additional simulator and analytical approaches and of scenarios that emphasise potential effects. While the results obtained thus far are considered sufficient for the assessment of the risks associated with CO<sub>2</sub> storage, detailed coupled

modelling of pressure and temperature in the storage formations is required prior to the start of injection. This is needed for pressure and temperature predictions that are sufficiently reliable for the management of the injection process and for the interpretation of monitoring data.

- (2) The aim of the present study was to provide the basis for a storage permit application, by understanding the current status of the storage formations, the caprock, the faults and the wells, and their response to the injection of CO<sub>2</sub>. The study established that conditions can be found under which CO<sub>2</sub> can be injected and stored safely and securely in the P18-2 field. The study did not aim to arrive at a complete and detailed description of these conditions. Such an 'operational plan' for CO<sub>2</sub> injection into the P18-2 field will be required prior to the start of injection, as a basis for the detailed monitoring plan and for the operational management of the injection process. The present study is the first step towards the P18-2 operational plan.

# Contents

	<b>Summary .....</b>	<b>2</b>
<b>1</b>	<b>Introduction .....</b>	<b>8</b>
<b>2</b>	<b>Reading guide .....</b>	<b>10</b>
2.1	Definitions .....	10
<b>3</b>	<b>Methodology .....</b>	<b>12</b>
3.1	Legal background .....	12
3.2	Feasibility study .....	12
3.3	Risk assessment.....	13
<b>4</b>	<b>P18-2 field overview .....</b>	<b>17</b>
4.1	Introduction .....	17
4.2	Geological description .....	17
4.3	Caprock .....	22
4.4	Naturally sealing formations .....	25
4.5	Overview of wells.....	26
<b>5</b>	<b>Injection scenario .....</b>	<b>28</b>
5.1	Injection wells and well completion.....	28
5.2	CO <sub>2</sub> supply scenarios .....	28
5.3	CO <sub>2</sub> quality.....	29
5.4	Summary of injection conditions.....	30
<b>6</b>	<b>Evaluation of reservoir performance and integrity .....</b>	<b>31</b>
6.1	Introduction .....	31
6.2	Setup of injection simulations .....	31
6.3	CO <sub>2</sub> storage capacity and CO <sub>2</sub> dispersion .....	32
6.4	Temperature development in the reservoir .....	44
6.5	Chemical interactions .....	52
6.6	Conclusions .....	55
<b>7</b>	<b>Fault stability.....</b>	<b>57</b>
7.1	Introduction .....	57
7.2	Fault stability: pressure effect.....	57
7.3	Fault stability: temperature effect .....	63
7.4	Fault stability: geochemical effects.....	68
7.5	Conclusions .....	71
<b>8</b>	<b>Caprock integrity .....</b>	<b>72</b>
8.1	Introduction .....	72
8.2	Pressure effect on caprock integrity .....	72
8.3	Temperature effect on caprock integrity .....	72
8.4	Geochemical effects .....	74
8.5	Conclusions .....	76
<b>9</b>	<b>Well integrity .....</b>	<b>78</b>
9.1	Introduction .....	78

9.2	Status of the well barriers .....	79
9.3	Influence of cooling on well cement.....	102
9.4	Well abandonment.....	115
9.5	Conclusions .....	116
<b>10</b>	<b>P18-2 storage site and storage complex.....</b>	<b>118</b>
10.1	Introduction .....	118
10.2	Definitions in the Netherlands Mining Law and the EU Storage Directive .....	118
10.3	Definition of the storage site .....	119
10.4	Definition of the storage complex .....	119
10.5	Differences with the P18-4 storage complex definition .....	121
10.6	Barriers .....	121
<b>11</b>	<b>Migration paths .....</b>	<b>123</b>
11.1	Introduction .....	123
11.2	Available data and workflow .....	123
11.3	Geological model of the overburden.....	124
11.4	Migration scenarios.....	126
11.5	Methods .....	127
11.6	Results .....	127
11.7	Present day hydrocarbon migration.....	131
11.8	Conclusions .....	132
<b>12</b>	<b>Risk assessment and preventative measures.....</b>	<b>133</b>
12.1	Reservoir .....	134
12.2	Caprock .....	136
12.3	Fault zones .....	138
12.4	Wells .....	140
12.5	Conclusion .....	143
<b>13</b>	<b>Monitoring and corrective measures plan .....</b>	<b>145</b>
13.1	Introduction .....	145
13.2	Foundation of the monitoring and corrective measures plan .....	146
13.3	Philosophy of the monitoring plan .....	150
13.4	Interpretation.....	154
13.5	The monitoring plan .....	155
13.6	Conclusion .....	160
<b>14</b>	<b>Conclusions .....</b>	<b>162</b>
<b>15</b>	<b>References .....</b>	<b>164</b>
<b>16</b>	<b>Appendix A. compliance with EU Storage Directive site characterisation and assessment .....</b>	<b>169</b>
16.1	Data collection (step 1).....	169
16.2	Building the 3-D static geological earth model (step 2) .....	170
16.3	Characterisation of storage dynamic behaviour, sensitivity characterisation, risk assessment (step 3) .....	171
<b>17</b>	<b>Appendix B. Subsurface model descriptions .....</b>	<b>174</b>
17.1	Static model .....	174
17.2	Seismic interpretation .....	174

17.3	Time-depth conversion .....	176
17.4	Petrel model building .....	176
17.5	Differences with 2010 model and implications .....	192
17.6	Adjustments made to the static model.....	195
17.7	Dynamic model.....	196
17.8	History Match of the dynamic model .....	203
17.9	Geomechanical model.....	217
17.10	Well degradation model.....	221
<b>18</b>	<b>Appendix C. Risk Register.....</b>	<b>223</b>
<b>19</b>	<b>Appendix D. Monitoring Plan .....</b>	<b>227</b>



# 1 Introduction

This report presents the results of a study into the technical feasibility of storing CO<sub>2</sub> in the depleted offshore gas field P18-2. This field is one of several fields in the P18 cluster. The Porthos consortium<sup>1</sup> is developing plans for a multi-user CO<sub>2</sub> transport and storage network that connects industrial emitters of CO<sub>2</sub> in the Rotterdam harbour area with geological storage capacity in the Dutch sector of the North Sea. The consortium is targeting the P18 cluster as the first candidate for CO<sub>2</sub> storage. Operation of the network is planned for 2022 / 2023<sup>2</sup>.

The Porthos network is still in its planning stage and no certainty exists at this point in time about the supply of CO<sub>2</sub>. A recent study of the P18 gas field cluster suggested that the fields P18-2, P18-4 and P18-6 together can accommodate a supply rate of the order of 2-3 Mt/yr (million tonnes per year) and possibly up to 5 Mt/yr (Vandeweyer et al., 2011). With a combined storage capacity of about 37 Mt, storage at a rate of 2-3 Mt/yr could continue for about 15 years.

The P18-4 gas field has a CO<sub>2</sub> storage permit in place. This permit was awarded irrevocably in 2013. The P18-4 field was planned to be part of the “Rotterdam afvang en opslag demonstratieproject” (ROAD), which aimed to capture CO<sub>2</sub> at a coal-fired power plant at the Maasvlakte, compress the CO<sub>2</sub> and transport it by offshore pipeline to the P18-A platform, located at a distance of about 20 km from the Maasvlakte. The ROAD project was cancelled in 2017; all close-out reports are available online (ROAD, 2018).

The Porthos consortium now builds onto the ROAD legacy. The Porthos network is planned to be a multi-user transport and storage network, building up to much higher CO<sub>2</sub> supply rates than those considered in the ROAD project. In addition, the Porthos network has a longer horizon. This means that more depleted gas fields are required for storage, in addition to P18-4. The first candidates are the P18-2 and, potentially, the P18-6 gas fields.

The starting point of the present study was the storage feasibility study of the P18 cluster that was performed under the CATO-2 R&D programme (Vandeweyer et al., 2011). While the scope of that study was the entire P18 complex – including the P18-2, P18-4 and P18-6 compartments – the focus of the analyses was on the P18-4 structure. The P18-4 storage feasibility study was used in a storage permit application that resulted in the permit granted in 2013. The analyses of the P18-2 and P18-6 compartments presented by Vandeweyer et al. (2011) were not sufficient for a subsequent storage permit application for these compartments.

This report presents the results of a technical CO<sub>2</sub> storage feasibility study of the P18-2 structure. The aim of the feasibility is to identify risks for the containment of CO<sub>2</sub> in the storage complex, how to minimize those risks and the best way to monitor remaining risks. The study, which extends the analyses and results of the CATO-2 study by using the latest production data and deploying state-of-the-art

---

<sup>1</sup> See <https://rotterdamccus.nl/>.

<sup>2</sup> See Notitie Reikwijdte en Detailniveau – Rotterdam CCUS Project (Porthos), available at <https://www.rvo.nl/sites/default/files/2019/02/Porthos%20concept%20NRD%20-%20versie%20finaal.pdf>

workflows and tools, will provide the necessary input for a CO<sub>2</sub> storage permit application under the Dutch Mining Act and a 'Milieu Effect Rapportage'(MER) (which is a required element for the permit application). In 2011, the Dutch Mining Act transposed the EU Storage Directive (EU, 2009), thus ensuring that a storage permit application submitted under the Dutch Mining Act will comply with European legislation concerning CO<sub>2</sub> storage.

## 2 Reading guide

This report presents the results of a technical CO<sub>2</sub> storage feasibility study for the P18-2 depleted gas field. The setup of the report is as follows.

Sections 3 through 5 set the scene for the storage feasibility study. Section 3 introduces the risk-based approach taken in assessing the feasibility of storing CO<sub>2</sub> in the P18-2 field. The geological setting of the P18-2 field is described in Section 4. Section 5 describes some of the key boundary conditions and assumptions used in the study: the CO<sub>2</sub> supply profile until 2035, as well as the preliminary approach to the injection process. The latter includes the number of wells that are assumed to be used. Section 5 also provides a brief summary of relevant results from a flow assurance study that was performed previously; this includes the conditions of the CO<sub>2</sub> at the bottom of the injection wells, which follow from the modelling of CO<sub>2</sub> flow from the compression station, through a subsea pipeline and down the injection well. These conditions are used in the present study as the starting point for the modelling of the behaviour of the CO<sub>2</sub> inside the reservoir.

Sections 6 through 11 present the results from the storage feasibility analysis. The behaviour of CO<sub>2</sub> in the reservoir and its effect on the temperature and pressure distribution is presented in Section 6. Sections 7 and 8 discuss the impact of injecting CO<sub>2</sub> on reservoir and caprock integrity and stability of the faults within and bounding the reservoir. Well integrity is covered in Section 9, evaluating the current status of the wells and discussing simulation results on the effect of CO<sub>2</sub> injection on the long-term structural integrity. Section 10 defines the storage site and storage complex and contains a description of the barriers in the storage site to CO<sub>2</sub> migration. Section 11 presents an analysis of potential migration of CO<sub>2</sub>, if it leaves the storage complex. All results are pulled together in Section 12 to assess the risks associated with injecting CO<sub>2</sub> into the P18-2 field.

Section 13, finally, outlines the system that will be designed to monitor the injection process and the behaviour of the CO<sub>2</sub> in the subsurface.

### 2.1 Definitions

The following definitions are used throughout this document.

<b>Block</b>	An area on a map (e.g., block P18)
<b>License areas</b>	Part or all of a block (e.g., P18a)
<b>Field</b>	A bounded structure where the hydrocarbons were discovered and produced from and includes the sealing faults, rocks, gas-water contact (GWC) and other structural elements (e.g., P18-2)
<b>Reservoir</b>	Part of the field where the reservoir fluids are contained and where the CO <sub>2</sub> will be stored, i.e. the porous rock
<b>Compartment</b>	Part of a field and includes the bounding elements, (e.g. three compartments in P18-2 field)
<b>Storage Site</b>	Defined under the CO <sub>2</sub> Storage Directive and under the Dutch Mining Act and includes the storage reservoir and the wellbores penetrating the storage reservoir

- Storage Complex** Includes the storage reservoir, the wellbores penetrating the reservoir and the surrounding and bounding formations and faults which make up the storage field.
- Migration of CO<sub>2</sub>** Movement out of the storage reservoir but remaining in the storage complex
- Leakage of CO<sub>2</sub>** Under the CO<sub>2</sub> Storage Directive means movement of CO<sub>2</sub> out of the storage complex
- Emission of CO<sub>2</sub>** Under the ETS Directive (ETS directive, 2009) means escape of CO<sub>2</sub> from the storage site to the atmosphere or the water column
- Injection facilities** Include well completions and wellheads; *not* included are other facilities on the platform, nor the platform itself.

## 3 Methodology

### 3.1 Legal background

This technical CO<sub>2</sub> storage feasibility study has the aim to provide the basis for a permit application for CO<sub>2</sub> storage in the P18-2 field. The Dutch Mining Act sets out the requirements for a storage permit application. A transposition of the EU Storage Directive (EU, 2009) was included in the Mining Act in 2011<sup>3</sup>. Previous work on the P18-4 field (Vandeweyer et al., 2011) resulted in a successful application for a CO<sub>2</sub> storage permit, proving that the workflow used provided a basis that was both sufficiently detailed and complete.

The present study follows the workflow that was used by Vandeweyer et al. (2011), and that was described in detail by Nepveu et al. (2015), who combined experience from several EU Member States in CO<sub>2</sub> storage feasibility assessments. The workflow covers the full list of requirements set out in Annex II of the EU Storage Directive (EU, 2009). Section 16 shows the link between the elements of site characterisation mentioned in Annex I of the EU Storage Directive and the present report.

### 3.2 Feasibility study

The workflow is risk-based and site specific, with the aim to understand the storage risks involved, to reduce them to a level that is as low as reasonably possible through site-specific design of injection scenarios and to develop a monitoring program aimed at monitoring and managing the most relevant, remaining risks.

This study uses the workflow described by Nepveu et al. (2015). Figure 3-1 illustrates this workflow.

- Phase 1 of the workflow represents a screening study, to find one or multiple sites that meet selection criteria, such as location, storage capacity or expected cost of storage.
- Phase 2 of the workflow represents the detailed CO<sub>2</sub> storage feasibility study that is presented in this report, for the P18-2 depleted gas field. The first part of phase 2 is a 'quick scan' of available data. The purpose of the quick scan is to identify the key risks to storage and 'showstoppers', if any, before entering the detailed assessment, which represents the second part of phase 2. This detailed assessment is shown in the diagram in the figure as the central, large rectangle labelled 'RA' (risk assessment), with several disciplines revolving around the RA. This is the key element of a storage feasibility assessment, with several disciplines analysing the response of the storage system on the injection of CO<sub>2</sub>.

In the present case, screening was already completed and outside the scope of this report. In addition, a 'quick scan' of available data was already performed in a previous study of the P18 gas fields (Vandeweyer et al., 2011). No showstoppers were identified for the P18-2 field. However, as the previous study was focused on the P18-4 depleted gas field, the detailed assessment of the P18-2 was incomplete;

---

<sup>3</sup> See <https://www.nlog.nl/en/licences-and-legislation> for links to relevant government internet sites.

the present report repeats the previous assessment with improved tools and experience where possible and fills the gaps where needed.

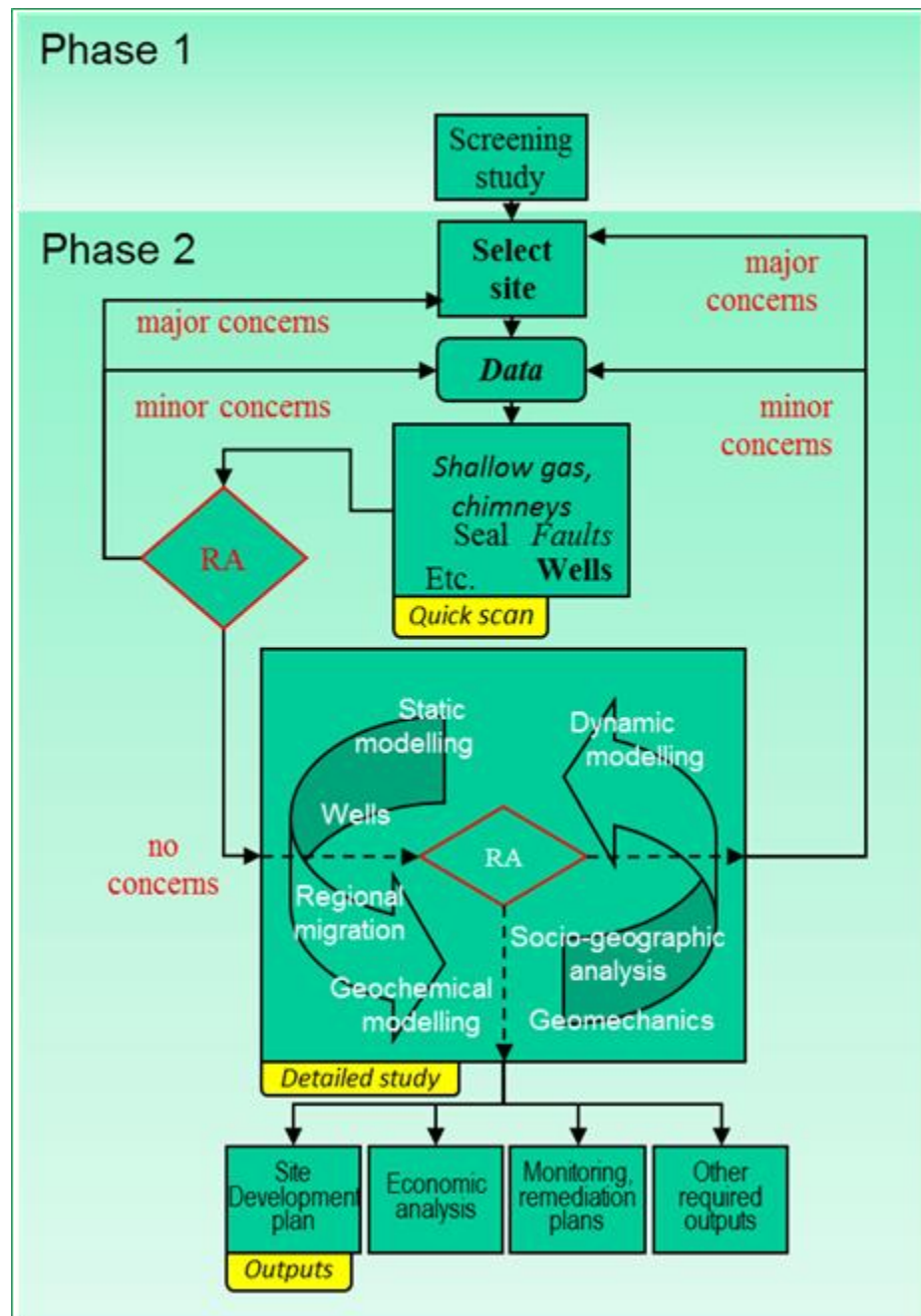


Figure 3-1 Workflow for site screening and characterization (Nepveu et al., 2015). RA is Risk Assessment

### 3.3 Risk assessment

The approach pursued in the risk assessment, e.g. the assignment of risk classes, is basically qualitative of nature and expert-based, although the underlying information used is often of a quantitative nature, e.g. output from model simulations or measurements of physical parameters like pressure.

The risk assessment consists of the following steps:

1. Identification of (a combination of) factors, which directly influence the containment of CO<sub>2</sub>
2. Detailed assessment of these (combined) factors and definition of potential risk reduction measures
3. Risk classification

Step 1 was performed in a workshop prior to the project in order to define the required assessment. Step 2, the detailed assessment of the risk factors and definition of potential risk reduction measures is reported in the present report in Sections 6 to 9; step 3 is described in Section 12.

Typically, the results of risk characterisation and classification are listed in a risk register (see Section 0) and summarized in accompanying risk matrices. For the classification of the risks, a risk matrix with classes of likelihood and consequences has been designed (see Figure 3-2), which is inspired by the work done by Van Eijs et al. (2011) and the risk assessment matrix included in the toolkit of the Energy Institute (2019) (website, version 15 Oct 2019). The definition of the classes of consequences has been linked to the concept and definition of the storage complex as described in the EU Storage Directive (EU, 2009).

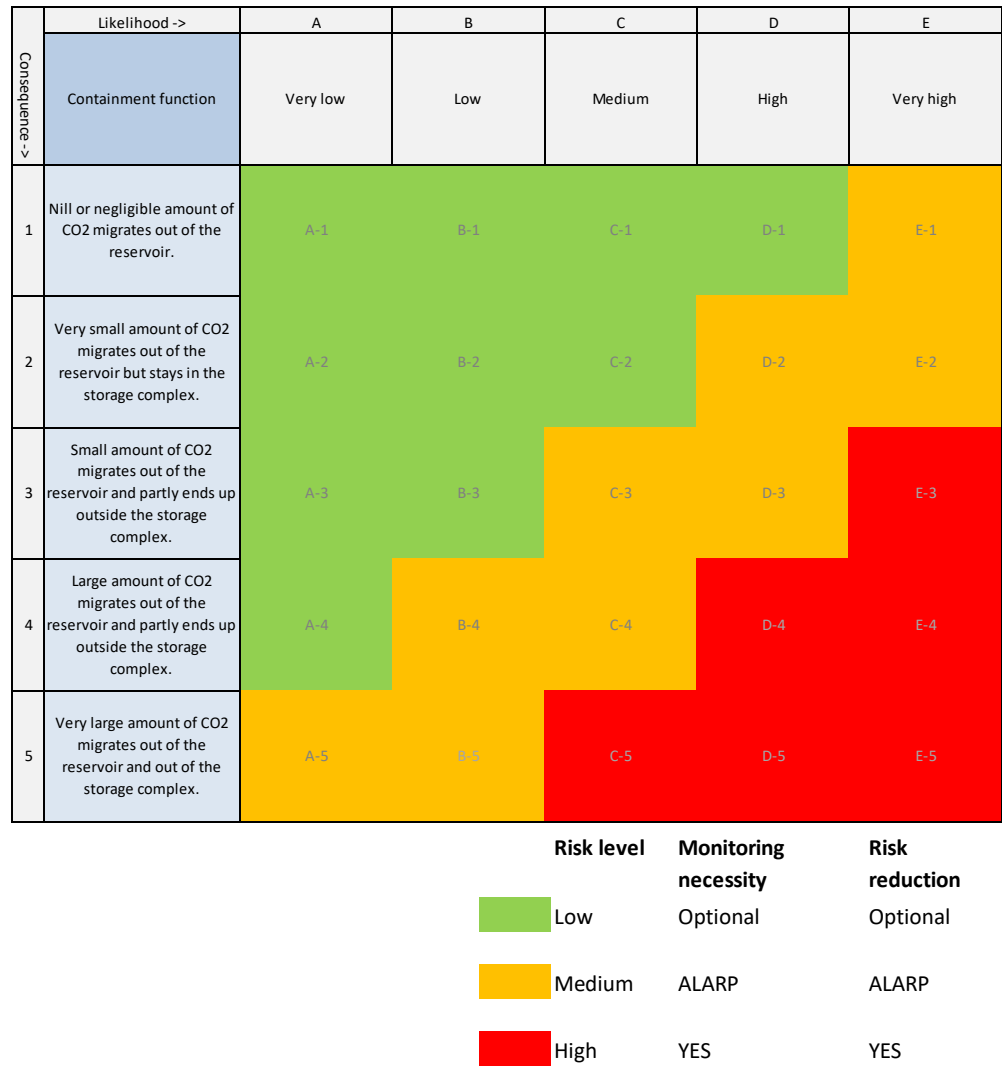


Figure 3-2 Proposed risk matrix nomenclature (modified after Van Eijs et al., 2011; Energy Institute, 2016).

Five classes of likelihood have been defined with the following definitions:

- Very low    Positive evidence for containment and large safety factor
- Low         No positive evidence and large safety factor
- Medium     Positive evidence and no large safety factor
- High        No positive evidence and no large safety factor
- Very high   No positive evidence and small or nil safety factor

The classes of consequence have been defined as follows:

- Negligible    Within natural variation and cannot be monitored
- Very small    Can be monitored and no impact on biosphere
- Small         Can be monitored and possible minor impact on biosphere
- Large         Can be monitored and possible impact on biosphere
- Very large    Can be monitored and possible adverse impact on biosphere

The resulting risk classes have been split in three categories (see Figure 3-2):

- Low risk      Strive for continuous improvement; monitoring and risk reduction are optional;



- Medium risk    Apply monitoring and risk reduction measures according to ALARP (As Low As Reasonably Practicable) principle;
- High risk      Risk reduction to acceptable levels and monitoring are obligatory.

## 4 P18-2 field overview

### 4.1 Introduction

The gas fields P18-2, P18-4, and P18-6, drilled from platform P18-A, are situated at approximately 3500 m depth below sea level and are located some 20 km NW from the port of Rotterdam (Figure 4-1). The reservoir rocks consist of sandstones which belong to the Triassic Main Buntsandstein Subgroup. The primary seal for the gas fields consists of unconformably overlying siltstones, claystones, evaporites and dolostones. The P18 gas fields are located in a heavily faulted area and consist mainly of fault bounded compartments, which are (at least on production time scales) hydraulically isolated from their surroundings. The bounding faults (which are well defined and clear to see on seismic) are sealing on a geological time scale due to juxtaposition of reservoir rock against impermeable rock.

High-calorific gas is being produced from these reservoirs since 1993. The gas is produced through the P18-A satellite platform and the P15-ACD processing and accommodations facilities in the adjacent P15 block, from where it is transported to the coast by a 40-km-long gas pipeline.

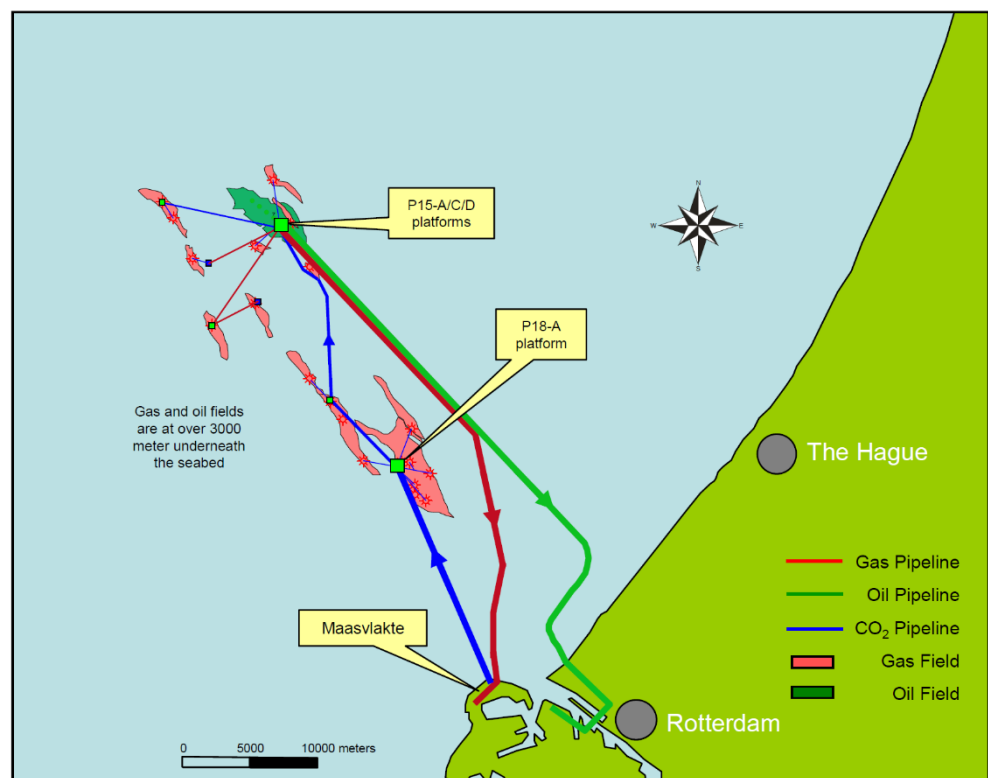


Figure 4-1: Overview of the locations of P15 and P18 fields (After TAQA, 2009)

### 4.2 Geological description

The P18 cluster consists of three fields, the P18-2, P18-4 and P18-6 fields (Figure 4-2). P18-2 was discovered in 1989 with the exploration well P18-02. It consists of three main compartments, 2-I, 2-II, and 2-III. This last compartment is now

considered to be consisting of two compartments (see Appendix B), and is therefore split into 2-III and 2-IV. Compartment 2-I came on stream first, in 1993. It contains three production wells: P18-02-A1, P18-02-A3ST2, P18-02-A5ST1, and the exploration well P18-02. Compartment 2-III contains one production well, P18-02-A6, and came on stream in 1997. Compartment 2-II came on stream in 2003, and also contains one production well, P18-02-A6ST1. For a while, this side track produced from Compartment 2-II only. After the whipstock had been perforated in 2005, well P18-02-A6 produced simultaneously from the 2-II and 2-III compartments. Field P18-4 was discovered in 1991, and production started from well P18-04-A2 in 1993. Field P18-6 was discovered in 2003, and production started from well P18-06-A7ST1 in 2003.

Peak production was reached in 1998, with a cumulative annual production of 2.2 bcm. At the end of June 2018, the total cumulative production of all P18 fields was 13.5 bcm. According to the updated Winningsplan from 2016, abandonment of the different fields is expected in 2024. Recovery factors by that time are expected to be 98% for P18-2 and P18-4, and 90% for P18-6.

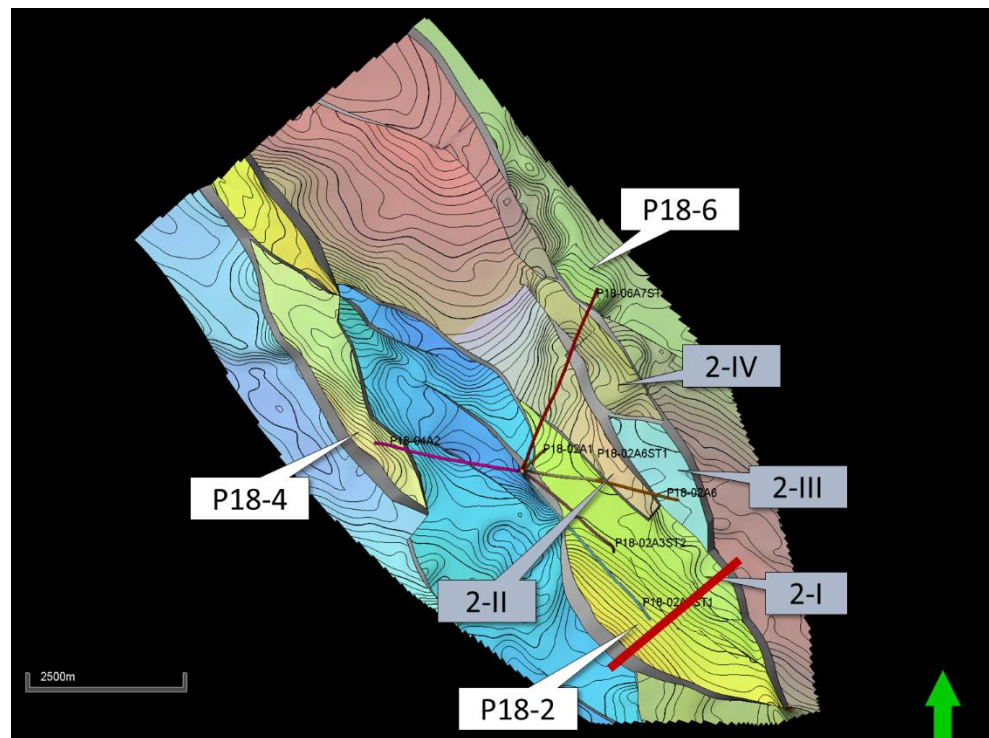


Figure 4-2: Overview of the three P18 fields (P18-2, P18-4, and P18-6), and the compartments of the P18-2 Field (2-I, 2-II, 2-III, and 2-IV). Red line indicates the position of the cross section shown in Figure 4-3.

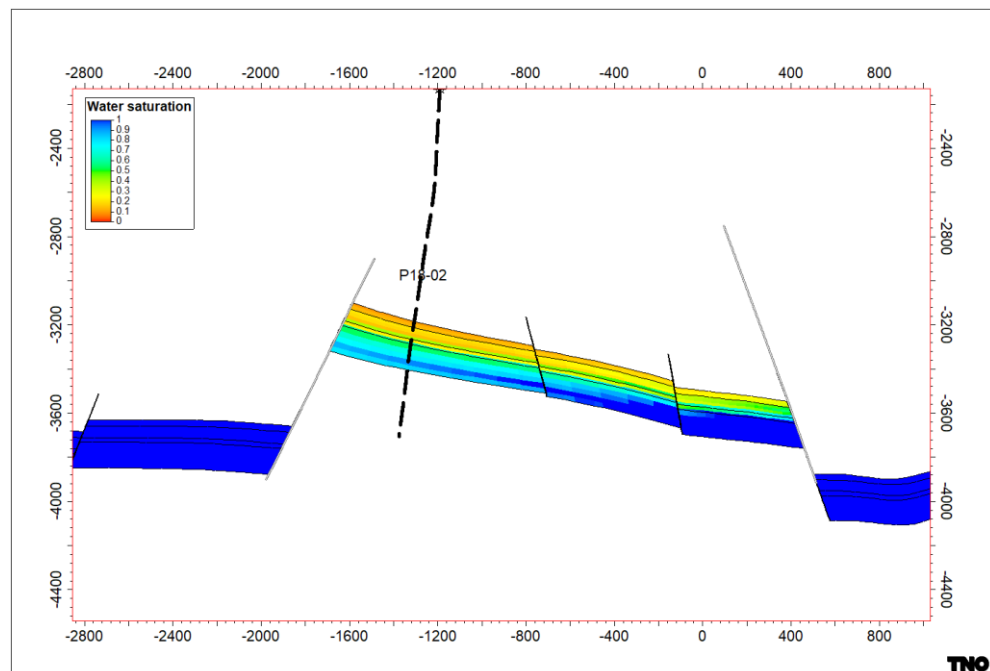


Figure 4-3: Cross section through the P18-2 field, showing compartment 2-I with initial water saturation. The location of the cross section is shown in Figure 4-2.

The structures that contain the reservoirs are bound by a system of NW-SE oriented faults in a horst and graben configuration, with a sinistral strike-slip component. The top of the reservoir compartments lies at a depth between 3175 m and 3455 m below sea level.

Compartment 2-I is the main compartment, and is bounded by two normal faults, F10 and F19/F20. A closer look at the offsets of these reservoir-bounding faults (Figure 4-3 and Figure 4-4) shows that they are sealing due to juxtaposition of reservoir zones against impermeable shales of the overlying Upper Triassic and Altona Groups (Figure 4-5).

Compartment 2-I is separated from compartment 2-II by fault F17, the offset of which is insufficient to be sealing by juxtaposition. Indeed, production data suggest that there is partial communication between the two compartments across this fault.

Compartment 2-III is separated from 2-II and 2-I by fault F19, which has enough offset to be sealing by juxtaposition, except for a small region at the northern end (Figure 4-4). However, no or very minor pressure communication was observed between the 2-I / 2-II compartments and the 2-III compartment, which suggests that fault F19 is sealing.

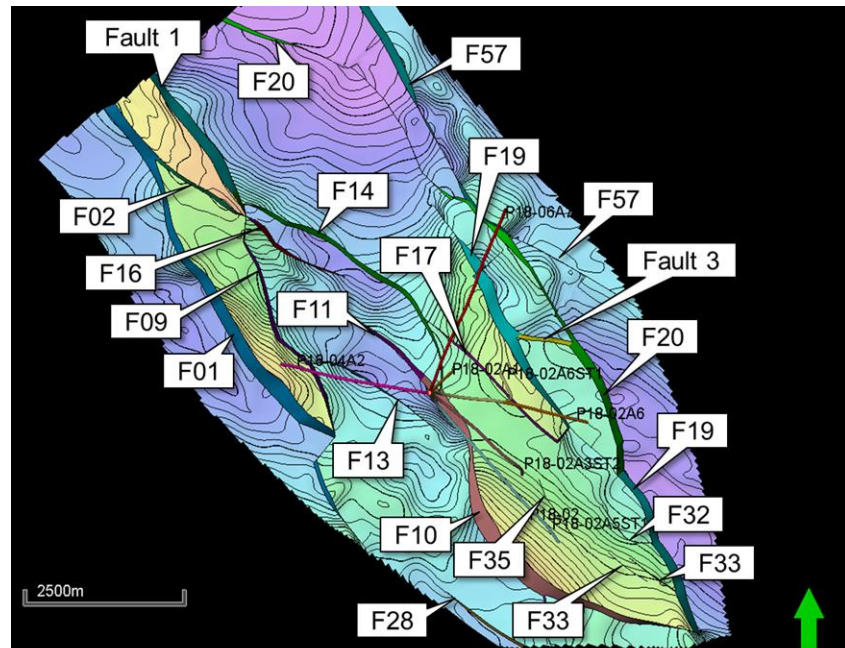


Figure 4-4: Map view of the Top Bunter in the P18 area with fault names used in this report.

The reservoir rocks of the P18 fields consist of four sandstone formations that belong to the Lower Germanic Trias Group, informally called Bunter. From top to base these are the Hardegsen, Upper Detfurth, Lower Detfurth and Volpriehausen Formations. (Figure 4-5). Each formation has highly variable porosity and permeability values. The Hardegsen Formation has in general the best reservoir properties.

Across a small zone at fault F14 low-permeable sandstones of the Volpriehausen and Lower Detfurth Formations in Compartment I are juxtaposed to permeable sandstones of the Hardegsen Formation (see Figure 4-4 for the location of fault F14). Figure 4-6 and Figure 4-7 show a cross section through fault F14 and an Allan diagram, respectively, with gas-filled formations juxtaposed against Hardegsen, Upper and Lower Detfurth and Volpriehausen. Communication – and flow of gas and CO<sub>2</sub> – across the fault cannot be established, as the impact of the volume of gas is too small to be visible on p/Z data. If this part of fault F14 is open to flow, the impact of CO<sub>2</sub> flow is negligible: potential communication applies only to the lower-quality reservoir formations which limits flow rate and the CO<sub>2</sub> would be remain structurally trapped against fault F14.

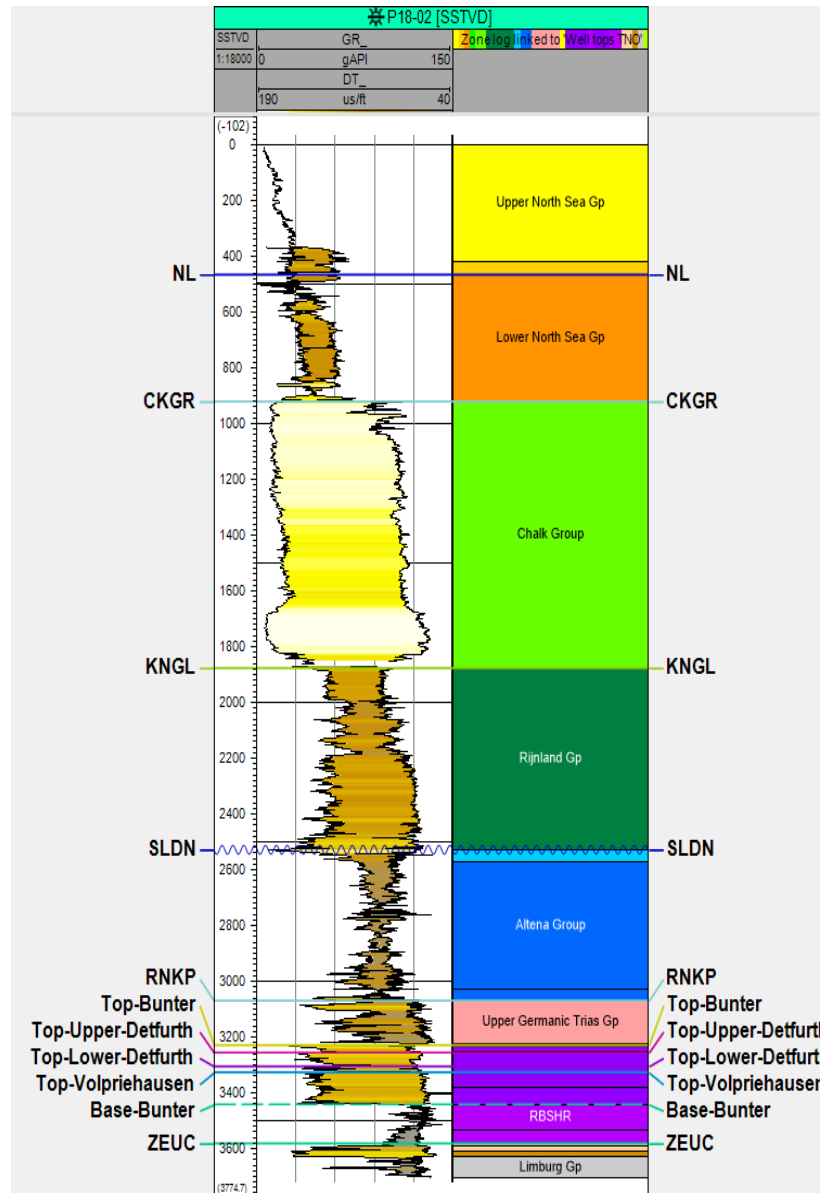


Figure 4-5: Stratigraphy and well logs of the reservoir interval and overburden of the P18 field

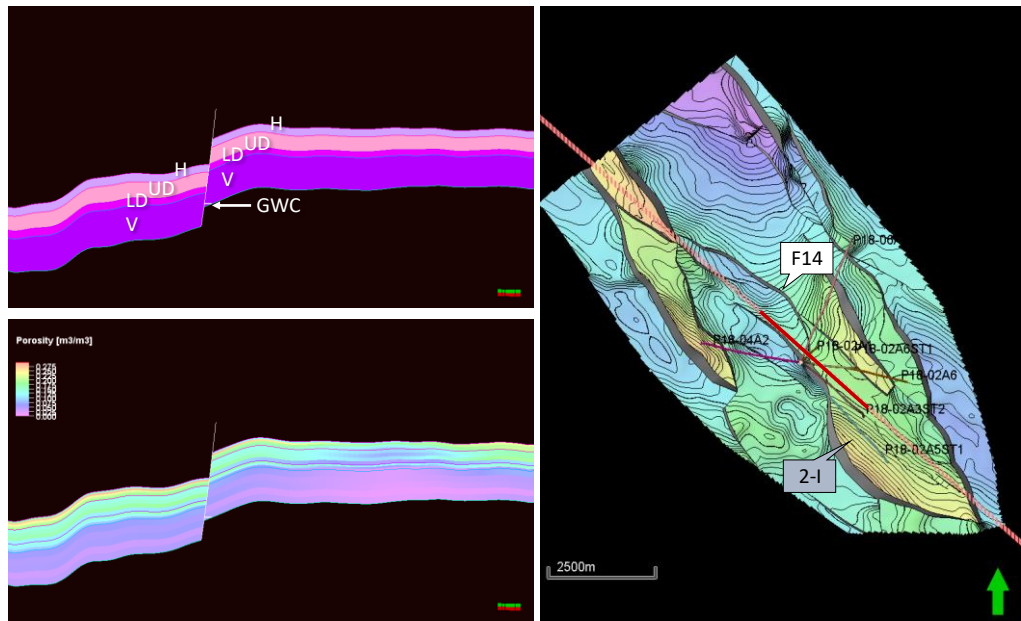


Figure 4-6: Cross section through fault F14, showing juxtaposition of gas-filled Upper Detfurth (UD), Lower Detfurth (LD), and Volpriehausen (V) against Hardegsen (H), Upper Detfurth, Lower Detfurth, and Volpriehausen. Upper left: Bunter formations, lower left: effective porosity, right: position of cross section (solid red line). GWC: gas water contact.

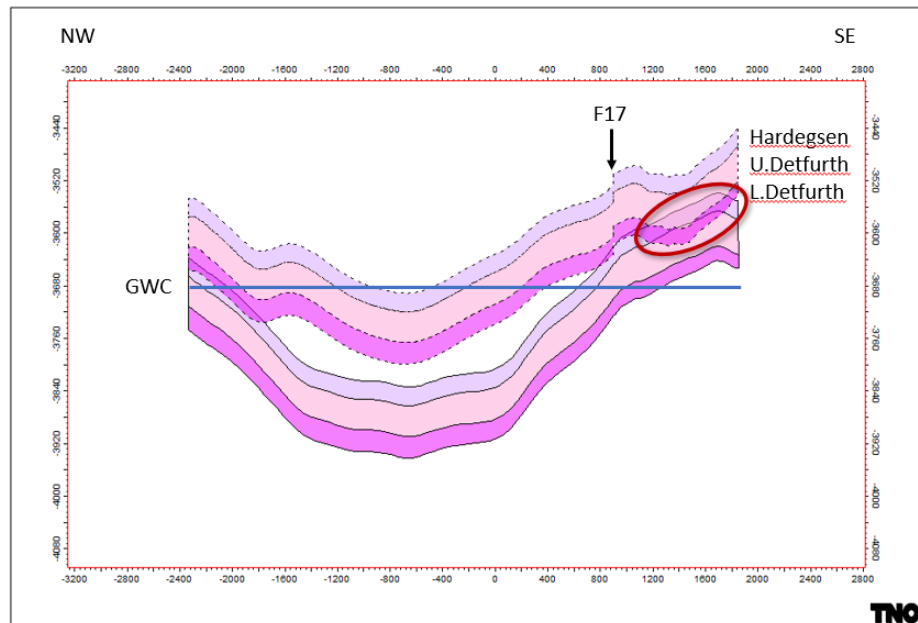


Figure 4-7: Fault juxtaposition diagram (Allan diagram) of fault F14. Blue line is the Gas Water Contact (GWC). Red ellipse indicates the area where the Hardegsen Fm is juxtaposed against Upper and Lower Detfurth.

### 4.3 Caprock

The seal to the P18 reservoirs is formed by the Upper Germanic Trias Group and the Jurassic Altona Group. The Upper Germanic Trias Group consists of siltstones, claystones, evaporites and dolostones. In well P18-02 it has a thickness of approx. 155 m. Directly above the Upper Germanic Trias Group lies the approx. 500 m thick

Altena Group (Figure 4-5), a thick succession of marine claystones, siltstones and marls of Early Jurassic age with excellent sealing quality. It includes the Posidonia Shale Formation that is easily recognized on seismic due to its excellent reflectivity.

The total thickness of the caprock of the P18 fields varies between 450 m and 750 m. The seal is excellent, as proven by the fact that it holds a gas column of nearly 600 m in the P18-2 compartment.

The rest of the overburden is formed by several geological formations, some of which can also be assumed to have good sealing properties. The Vlieland Claystone Formation (Figure 4-5) has proven itself as a good seal, as it forms the seal for the oil-bearing Lower Cretaceous sandstones in the West Netherlands Basin. It is considered here as the secondary caprock. Clayey sequences are also abundant in the North Sea Supergroup, especially in the lower part. These could very well act as secondary seals.

The nomenclature of the caprock as used in the present study is different from the one used in the CATO study of 2011. In the CATO study, the Upper Germanic Trias Group was designated the primary seal, and the Altena Group the secondary seal. In the present study the Altena Group and the Upper Germanic Trias Group are considered to form one seal, since there are no permeable formations in between the two. Therefore, the Upper Germanic Trias Group plus the Altena Group form the primary seal (Figure 4-8), and the Vlieland Claystone Formation the secondary seal.



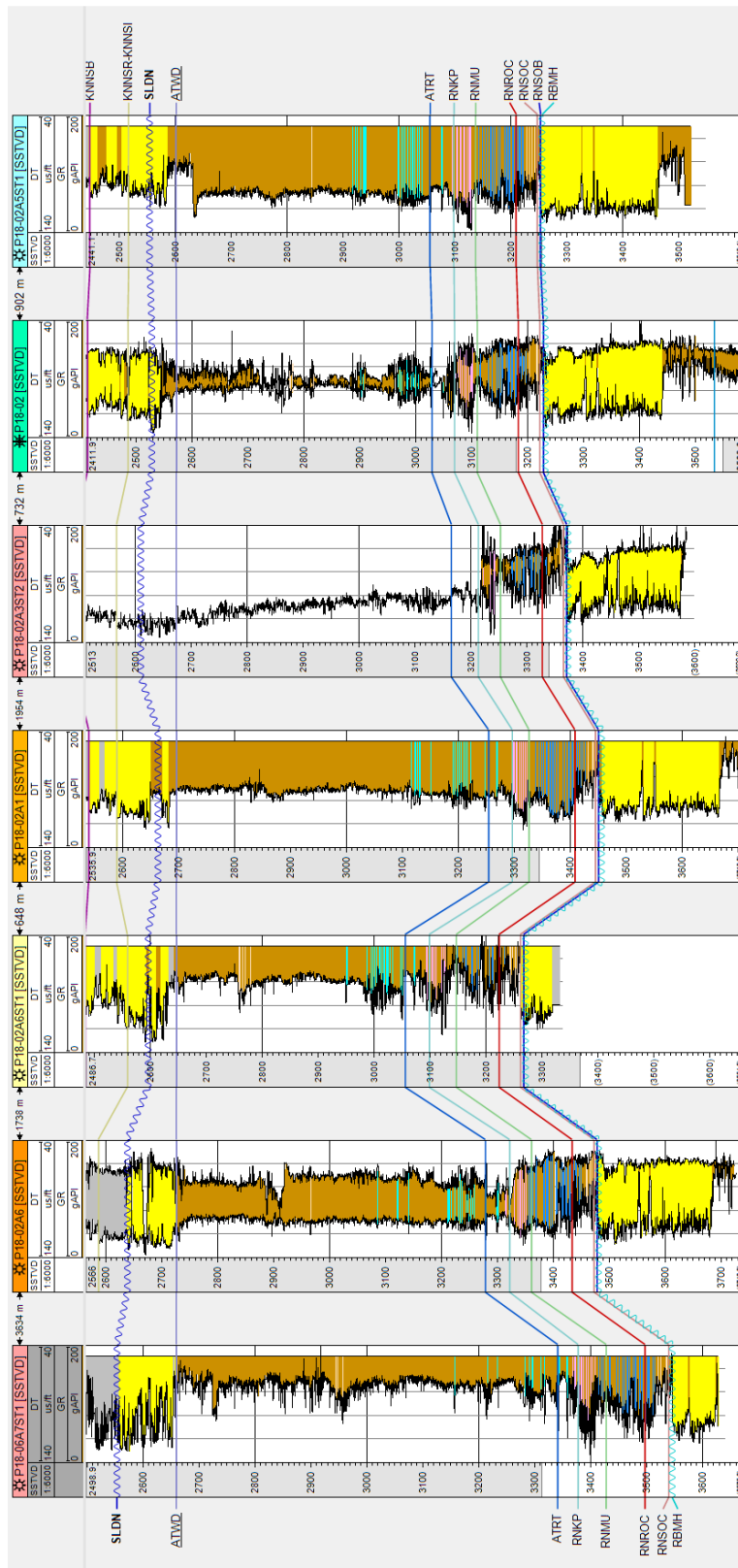


Figure 4-8: Well panel through the P18 wells of the immediate overburden of the Bunter formations showing that the Upper Germanic Trias Group plus the Alتنا Group form one continuous, primary seal over the entire storage complex.

#### 4.4 Naturally sealing formations

Recently the decommissioning of production platforms and infrastructure in the Southern North Sea has begun. A number of studies were initiated to investigate whether parts of the decommissioning process could be done more economically. One of these studies focused on well decommissioning, and specifically on the question whether naturally occurring ductile formations could be utilised to provide economic, self-healing and durable long-term sealing of wellbores. The outcome of the study, essentially based on existing literature, was that in the southern North Sea some formations are indeed suitable for creating effective annular barriers (Fischer et al., 2016; Geel, 2016). The idea is that if at the time of well abandonment it can be demonstrated that ductile clays or salts are hydraulically isolating the outer annulus and provide zonal isolation, no additional measures need to be taken at that point (as already accepted and practice in Norway and shown by Williams et al, 2009)). Of course, if this sealing behaviour can be demonstrated before CO<sub>2</sub> injection starts, it also reduces the risk of CO<sub>2</sub> leakage outside the well.

The shales from the Lower North Sea Group, The Vlieland Claystone Formation, and the Aalburg Shale were identified as having sufficiently ductile behaviour and swelling potential to create a sufficient seal around the casing (Figure 4-9). In addition, salts and possibly shales from the Upper Germanic Trias Group could have creeping or swelling behaviour.

The fact that all the above mentioned formations occur in the P18 area, it increases the probability that some or all will contribute to sealing the wells long term. This is further dealt with in Section 9.

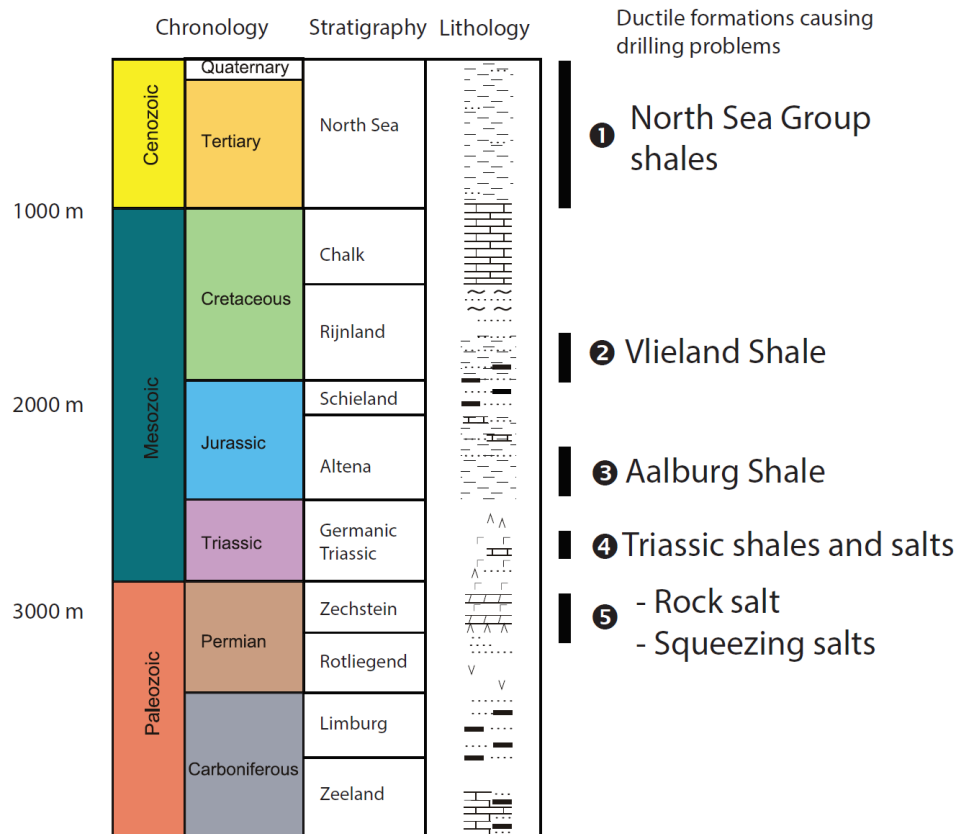


Figure 4-9 Typical stratigraphic column with potential self-sealing formations (Fischer et al, 2016).

#### 4.5 Overview of wells

Table 4-1 gives an overview of the wells that have been drilled in the P18-2 Field. Original holes of wells that were sidetracked (P18-02-A-03, P18-02-A-03ST1, and P18-02-A-05) have been omitted from the table. The trajectories of the proposed injectors are shown in Figure 4-10, and those of well tracks that have been plugged back are shown in Figure 4-11. Well P18-02A6ST1 is included here for the sake of completeness, but is advised in the current report to be plugged and abandoned (see Chapter 9).

Table 4-1: Overview of wells in the P18-2 compartment

NLOG name	Taqa name	Current well status	TDTotal Depth m MD (m)	Potential injectors	Remarks
P18-A-01	P18-02-A-01	Producing	3840	Yes	
P18-A-03S2	P18-02-A-03ST2	Producing	4302	Yes	
P18-A-05S1	P18-02-A-05ST1	Producing	5230	Yes	
P18-A-06	P18-02-A-06	Producing	4805	Yes	
P18-A-06S1	P18-02-A-06ST1	Producing	3954	No	
P18-02	P18-02	Suspended	3766	No	Discovery well

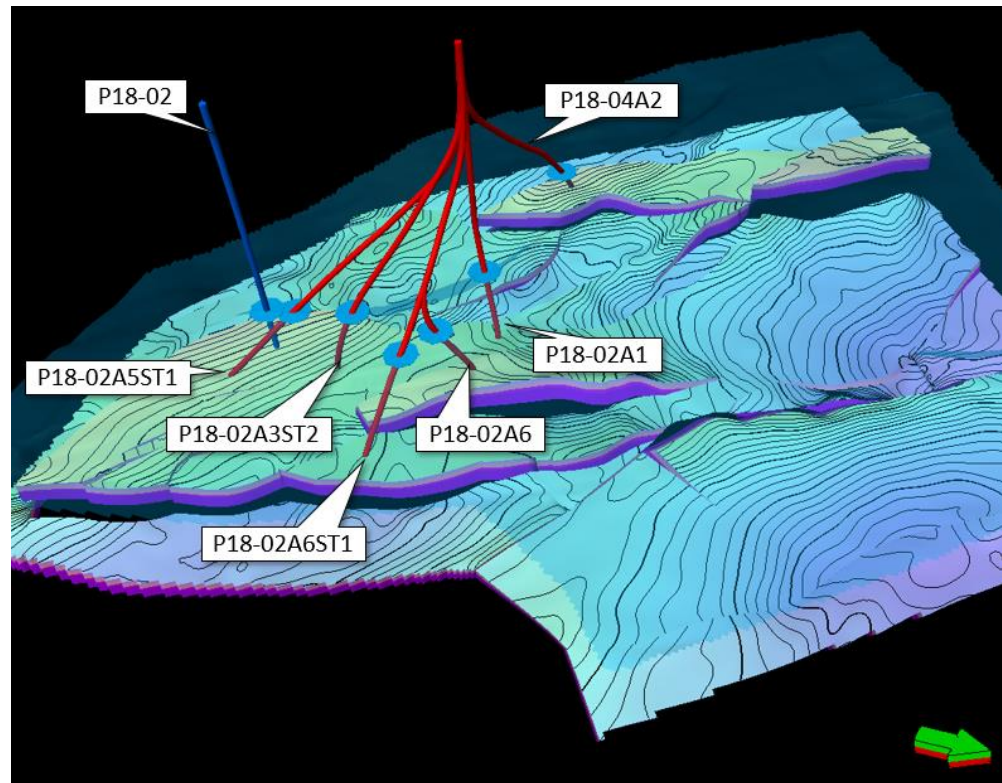


Figure 4-10: Overview of all envisaged injectors (in red) and suspended wells for P18-2. Light blue dishes denote entry points of wells into the caprock (=Base Schieland Gp). View to the southwest.

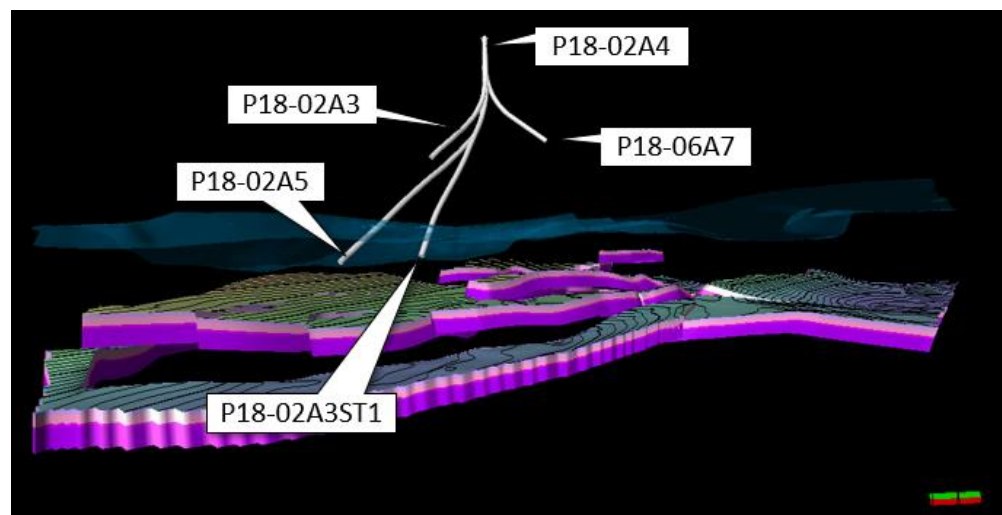


Figure 4-11: Overview of all plugged-back wells and sidetracks (in white) for P18-2. Light blue dishes denote entry points of wells into the caprock (=Base Schieland Gp). View to the west.

## 5 Injection scenario

### 5.1 Injection wells and well completion

Current plans for CO<sub>2</sub> storage in the P18-2, P18-4 and P18-6 fields are to use up to six injection wells. The P18-4 field has a single well, P18-04-A-02, which promises injection rates of the order of 1 Mt/yr (Vandeweijer et al., 2011). The P18-6 field also has a single well, P18-06-A-07, but the expected injection rates are significantly lower (Vandeweijer et al., 2011). Up to four injection wells are foreseen in the P18-2 field (see Table 4-1); in this study, well P18-02-A-06 is considered a back-up injection well and not included in the injection simulations.

The tubings in the existing wells can be replaced prior to injection, and the optimal tubing size needs to be based on dedicated well dynamics simulations (e.g., Belfroid, 2019). Such simulations need to be performed as part of a future study. For the purpose of the current study, for all wells considered for injection the tubing is assumed to have an external diameter of 4.5". This value follows from a trade-off between feasible injection rates at low and high reservoir pressure (Belfroid, 2019).

### 5.2 CO<sub>2</sub> supply scenarios

The future rate of CO<sub>2</sub> supply, to be delivered by emission sources in the Rotterdam harbour area, was uncertain at the time this study was undertaken. Based on the volumes of the CO<sub>2</sub> currently emitted in the harbour area and the volumes that could be captured at relatively low cost, a 'most likely' CO<sub>2</sub> supply profile was created (Figure 5-1).

Assuming that the P18-4 field will accommodate about 1 Mt/yr, or about 25% of the CO<sub>2</sub> supply, the supply profile to the P18-2 field is as given in Figure 5-2. The overall CO<sub>2</sub> supply reaches a plateau rate of 2.8 Mt/yr.

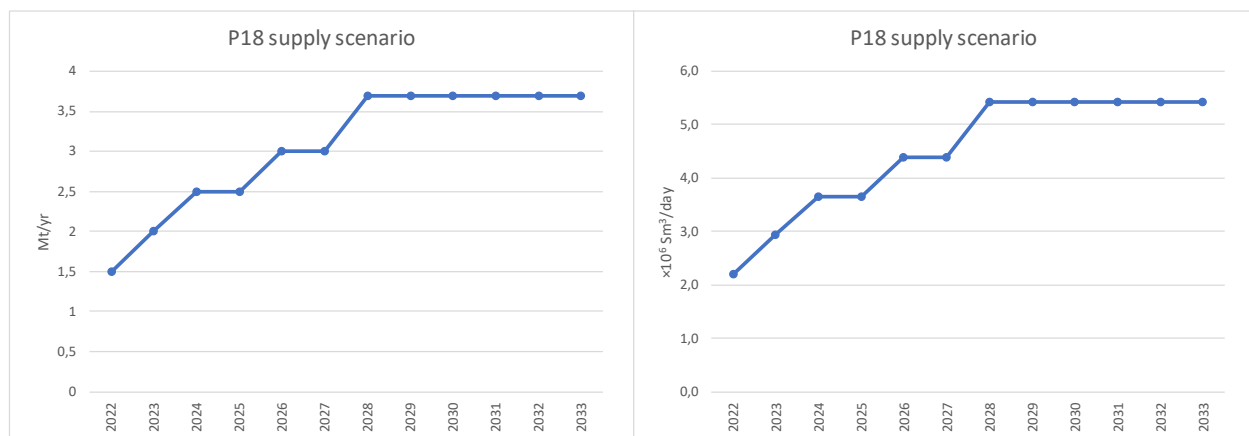


Figure 5-1 Potential future supply scenario for CO<sub>2</sub> from Rotterdam harbour sources. Flow rates increase from 1.5 Mt/yr by 2022 to 3.7 Mt/yr by about 2028 (about  $5.5 \cdot 10^6 \text{ Sm}^3/\text{day}$ ).

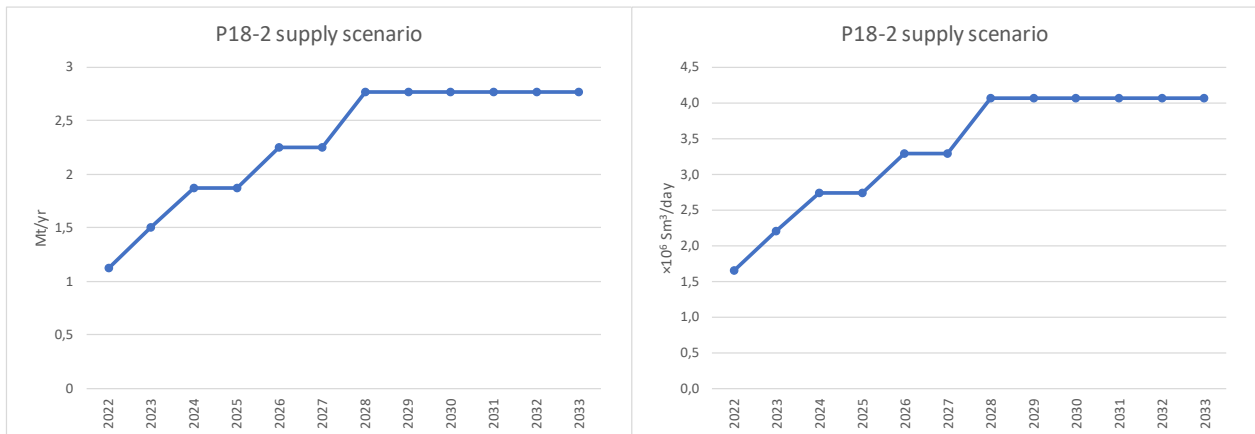


Figure 5-2 Potential future supply scenario for CO<sub>2</sub> to the P18-2 field: it is assumed that the three proposed P18-2 injection wells accommodate 75% of the total flow (Figure 5-1). Total flow rate to the P18-2 wells increases to 2.8 Mt/yr by 2028 (about  $4.1 \cdot 10^6$  Sm<sup>3</sup>/day).

### 5.3 CO<sub>2</sub> quality

At the time of the present study, no information was available about the potential sources of CO<sub>2</sub>. Recent work suggests that most available capture technologies can be expected to deliver CO<sub>2</sub> at a purity of 95% or higher (see, e.g., IEAGHG, 2016); sources in the Rotterdam harbour currently deliver CO<sub>2</sub> of more than 99% purity to the OCAP pipeline for use in greenhouses. While impurities alter the behaviour of CO<sub>2</sub> and may affect elements of the CCS chain, the results presented here were derived assuming pure CO<sub>2</sub>.

Figure 5-3 illustrates the effect of impurities on the phase behaviour of CO<sub>2</sub>. While pure CO<sub>2</sub> has a phase *line* that separates vapour conditions from those in which liquid CO<sub>2</sub> occurs (black curve in the figure), the presence of impurities in the CO<sub>2</sub> changes it into a *region* of pressure and temperature conditions in which the transition from liquid to gas phase occurs. Generally, two-phase flow is to be avoided in the handling of CO<sub>2</sub>, e.g. to prevent slugging. Two-phase flow is expected to occur in CO<sub>2</sub> injection wells without causing issues (Belfroid, 2019), but should be avoid in transport pipelines, risers and compressor. The conclusion that can be drawn from Figure 5-3 is that temperature and pressure should be chosen high enough to avoid the two-phase region of the CO<sub>2</sub> mixture being transported.

Impurities have an impact that extends beyond the phase envelope – for example, changes in density affect the operational window for injection as well as the storage capacity.

In the current study pure CO<sub>2</sub> was assumed in the simulations.

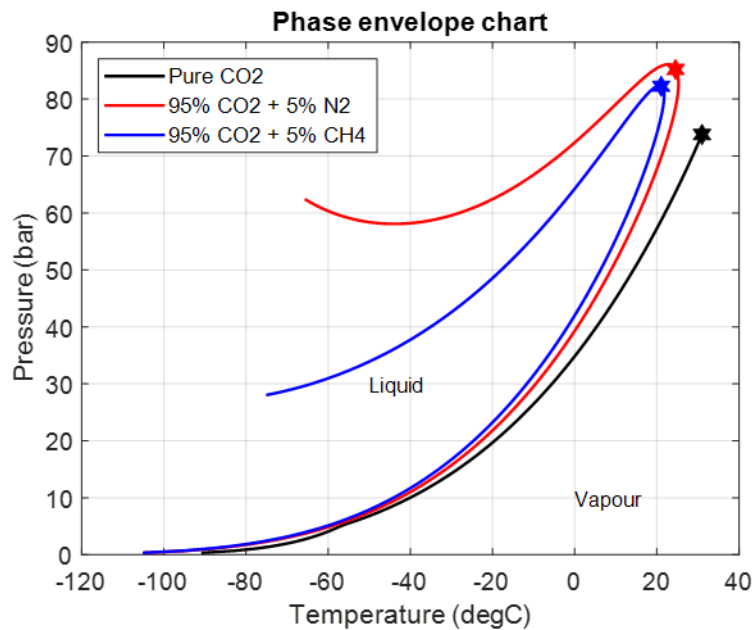


Figure 5-3 Effect of impurities (either 5 wt% N<sub>2</sub> or CH<sub>4</sub>, equal to 7.6 and 12.6 mol% respectively) on the location and shape of the CO<sub>2</sub> phase line. The data was generated using NIST REFPROP v10.

#### 5.4 Summary of injection conditions

To summarise, the injection of CO<sub>2</sub> into the P18-2 reservoir is subject to the following conditions.

- The CO<sub>2</sub> supply follows the profile as shown in Figure 5-2, with a plateau injection rate of 2.8 Mt/yr, distributed over three injection wells based on their injectivity. The three wells are P18-02-A-01, P18-02-A-03ST2 and P18-02-A-05ST1.
- The tubing in all injector wells will be recompleted (pers. comm. EBN, 2019). The external tubing diameter for all four injector wells is assumed to be 4.5". The actual well completion will be decided on at a later date, following a more detailed analysis of the operational window of the wells and the required flexibility in injection rates during the storage project.
- The CO<sub>2</sub> is assumed to contain no impurities. At the time of the present study, no quality/specification information was available about potential sources of CO<sub>2</sub>.

Additional assumptions apply to the conditions in the reservoir and to the downhole conditions of the CO<sub>2</sub>. These are explained in detail in Section 6.

- At the start of injection, the reservoir pressure is 20 bar; see Section 6.3.
- In the injection simulations, the average reservoir pressure will have a maximum that is equal to the initial reservoir pressure; see Section 6.3.
- The maximum downhole pressure is assumed to be equal to the initial pressure in the reservoir, 375 bar; see Section 6.3. This is the highest pressure for which faults and caprock have proven containment of natural gas.
- The minimum downhole temperature of the CO<sub>2</sub> was required to always be above 15 °C, to avoid CO<sub>2</sub> hydrate formation in the well and in the near-well area; see Section 6.4.

## 6 Evaluation of reservoir performance and integrity

### 6.1 Introduction

This section presents the results of an analysis of the process of injecting CO<sub>2</sub> into the P18-2 field. The analysis aims to:

- estimate of the storage capacity of the field (Section 6.3),
- establish the dispersion of CO<sub>2</sub> in the P18-2 field (Section 6.3),
- estimate the pressure and temperature levels in the injection wells and the fields during and after injection (Sections 6.3 and 6.4),
- assess the effects of interaction between CO<sub>2</sub> and the reservoir rock (Section 6.5).

The conclusions reached in this section are the following.

- The P18-2 field can store 32 Mt of CO<sub>2</sub>, assuming a final reservoir pressure of 351 bar (hydrostatic pressure, which is the pressure of the formations surrounding the storage reservoir). If the reservoir pressure is brought back to the initial pressure (375 bar at datum depth 3150 m), the storage capacity is 32.2 Mt of CO<sub>2</sub>.
- The injection wells together (P18-02-A-01, P18-02-A-03ST2 and P18-02-A-05ST1, together with the P18-4A2 well in the P18-4 field) can inject the target CO<sub>2</sub> supply rates given in Section 5.2, for a period of about 10 years from the start of injection. The last two to four years (2031 – 2035) of the target injection scenario would require another storage location.
- CO<sub>2</sub> fills the pore volume that was previously filled with natural gas and does not spill.
- The injection process must be managed to ensure that temperature and pressure in the well and in the near-well area remain outside the hydrate formation window.
- The injection of CO<sub>2</sub> will dry out the reservoir and may lead to salt deposition. The overall effect on permeability is expected to be negligible. Drying out of the reservoir reduces the probability of formation of hydrates.
- Chemical interaction between the CO<sub>2</sub> and the reservoir formation is insignificant.

The analysis presented in this section reveals no barriers to storage of CO<sub>2</sub> in the P18-2 field.

The results are a starting point for the assessment of fault stability (Section 7) and caprock integrity (Section 8).

### 6.2 Setup of injection simulations

Belfroid (2019) shows that the injection of CO<sub>2</sub> into a depleted field at low to very low pressure, such as the P18-2 field, can lead to low temperatures in the well, both at the wellhead and at bottomhole, due to the pressure difference between the high-pressure transport pipeline at the surface and the reservoir. Using a realistic setup for the Porthos compression and transport system and taking into account the phase behaviour of CO<sub>2</sub>, Belfroid (2019) presents injection scenarios for the P18-4 wells that lead to safe conditions at the wellhead and downhole, while meeting the



overall target rate shown in Figure 5-2. These downhole conditions show that CO<sub>2</sub> will be injected at temperatures well below the temperature of the reservoir.

The results show that the operational window for the P18-2 field is large: for a set of well characteristics a wide range of injection conditions is allowed, which do not lead to operational risks and result in feasible fluid velocities in the tubing. For the present study, the range of feasible injection rates is not a key issue; this study focuses on the response of the reservoir to CO<sub>2</sub> injection and on any restrictions for injection.

The simulation of injection of CO<sub>2</sub> into the P18-2 field was performed in two steps. In the first step, the injection and dispersion of CO<sub>2</sub> into the reservoir formations (see Section 4) is modelled using an isothermal simulator. While this ignores the temperature of the CO<sub>2</sub> upon injection, it provides a reliable estimate of the storage capacity of the field, as well as of the dispersion of the CO<sub>2</sub> during and after injection. The results from this first step are presented in Section 6.3.

The second step involves modelling the evolution of temperature within the reservoir formations. This approach takes into account the pressure and temperature of the CO<sub>2</sub>, but uses a less detailed representation of the storage reservoir. The results from this second step are presented in Section 6.4.

## 6.3 CO<sub>2</sub> storage capacity and CO<sub>2</sub> dispersion

### 6.3.1 *Setup of simulations*

This section evaluates the storage capacity of, and the dispersion of CO<sub>2</sub> in the P18-2 field. The injection wells are P18-02-A-01, P18-02-A-03ST2 and P18-02-A-05ST1, as listed in Table 4-1. Well P18-02-A-06 is also listed as injection well in Table 4-1, but is considered a back-up injection well and not included in the injection simulations presented below. The target injection profile is given in Figure 5-2.

### 6.3.2 *Simulation method*

A history matched dynamic model of P18-2 is used, see Section 17.7 for a description of the model. The following assumptions were made in the injection scenarios.

- The injection rate for each of the three injection wells depends on the local reservoir conditions and applied constraints and is calculated by the simulator.
- At the start of injection, the reservoir pressure is approximately 20 bar; the exact pressure distribution is based on the production history match and production forecast.
- The final average reservoir pressure (maximum allowable reservoir pressure) after CO<sub>2</sub> injection is assumed to be 375 bar (datum depth 3400m), which is equal to initial reservoir pressure. This is the highest pressure for which caprock, faults and reservoir have proven containment of natural gas.
- Injection simulations are run to a maximum average reservoir pressure that is equal to the initial gas pressure.
- The wells are constrained on group rate, therefore the total injection is equal to the most likely injection scenario for the P18-2 field (see Figure 5-2), but the distribution is based on the injectivity of the different injection wells.

- The wells are closed, when injection is no longer possible (i.e. when the maximum allowable reservoir pressure has been reached) or the injection rate is below  $5 \cdot 10^5$  Sm<sup>3</sup>/day (~0.03 Mt/yr). Since no leak-off test is available to set the value of maximum allowable reservoir pressure, this value is set equal to the initial pressure of the reservoir.
- It is assumed that the injectivity (used here to refer to the product of permeability and thickness) as derived from production data and information from logs can be used to simulate the CO<sub>2</sub> injection process.
- The maximum bottom hole pressure (BHP) of the injectors is set to 375 bar (equal to initial gas pressure).
- No changes occur in the well completion configuration.
- The saturation curves for gas-water systems are assumed to be the same for CO<sub>2</sub>-water systems.

Two injection scenarios were modelled: a base case and a high case. The base case scenario is the most probable injection scenario by filling up the reservoir up to 375 bar (initial reservoir pressure). In the second scenario, 'high case', injection is continued to an average reservoir pressure up to 450 bar to investigate the flow pattern of CO<sub>2</sub> at reservoir pressure higher than the initial pressure. Table 6-1 summarises the two scenarios.

Table 6-1: P18-2 injection scenarios

Injection Scenario	Target rate	BHP constraint (bar)	Avg reservoir pressure constraint (bar)	Minimum injection rate (Sm <sup>3</sup> /day)
Base case	- Figure 5-2. - Based on group constraint	375	375	$5 \cdot 10^5$
High case	- Figure 5-2. - Based on group constraint	450	450	$5 \cdot 10^5$

All simulations were performed with the Eclipse 300 reservoir simulator, a state-of-the-art compositional model that can handle the behaviour of CO<sub>2</sub> in the reservoir – including phase transitions – and the interactions between CO<sub>2</sub> and residual gas. See also Section 17.7.1.

Eclipse 300 cannot properly handle non-isothermal conditions, water evaporation or CO<sub>2</sub> dissolution. As a consequence the injected CO<sub>2</sub> has the temperature of the reservoir (126 °C), even though the temperature of the CO<sub>2</sub> is likely to be significantly lower (see Section 6.4).

The TOUGH2-ECOMG simulator was used to run non-isothermal injection scenarios (see also Section 6.4.2.1) to estimate the effect of cold CO<sub>2</sub> injection, CO<sub>2</sub> water interaction (water evaporation) and the related risk associated (cold front and dry out zone).

### 6.3.3 Simulation results

The total amount of CO<sub>2</sub> that can be stored in P18-2 is 32.2 Mt, assuming a reservoir pressure limit of 375 bar (initial pressure). Since the three injection wells are on group rate constraint the injection rate is distributed over the three wells based on injectivity (the product of permeability K and reservoir thickness H). An overview of the results of the injected volume and the distribution of injected volumes over the three injection wells is given in Table 6-2.

Table 6-2: P18-2 storage capacity for a final reservoir pressure of 375 bar, which is equal to the initial pressure (i.e., the pressure before production of the gas field).

P18-2 storage	Gas volumes (BCM) / relative contribution of each well (%)	CO <sub>2</sub> mass (Mt) / relative contribution of each well (%)
P18-02-A-01	1.56 / (9%)	2.92 / (9%)
P18-02-A-03ST2	1.31 / (8%)	2.45 / (8%)
P18-02-A-05ST1	14.3 / (83%)	26.8 / (83%)
<b>Total</b>	<b>17.2</b>	<b>32.2</b>

In Figure 6-1 and Figure 6-2 the injection profiles for the three wells are presented for the base case and high-case scenario.

The proposed injection wells together have an injectivity that is high enough to accommodate this target rate until 2033. The solid green curve in the graph labelled 'Field Gas Injection', represents the combined injection in the three wells and reproduces the supply curve in Figure 5-2.

It is observed that well P18-02-A-05ST1 injects more than 80% of the total injected volume; the other two injection wells contribute less than 10% each. This is due to the lower KH derived for the P18-02-A-01 and P18-02-A-03ST2 wells (see also Section 17.8.4.2).

The maximum injectivity is proportional to the pressure difference between the maximum allowable BHP (375 bar) and the reservoir pressure; this difference decreases over time. Until 2033, all CO<sub>2</sub> supplied by the emitters can be accommodated in the P18-2 field. After 2033 the injection becomes constrained by the BHP limit and the total injection rate starts to decline. Also the local reservoir pressure (9-point pressure) is set to 375 bar, which results in a long tail of CO<sub>2</sub> injection. A minimum injection rate was set of  $5 \cdot 10^5$  sm<sup>3</sup>/day. As a result, in 2040, injection ceases in all three injection wells as the reservoir reaches an average pressure of 375 bar (Figure 6-1 and Figure 6-2).

The sharp increase in injection rate that is observed in the profile of well P18-02-A01 around the year 2033 (Figure 6-1) is due to the group constraint set-up of the simulation; at this time the bottomhole limit of 375 bar is reached in well P18-02-A05ST2 and some of the flow is redirected to well P18-02-A01, for a short period until it reaches the bottomhole limit (Figure 6-2).

For completeness also the local reservoir pressure (9p pressure) and injection rate is shown for the two scenarios (base, high case), in Figure 6-3.

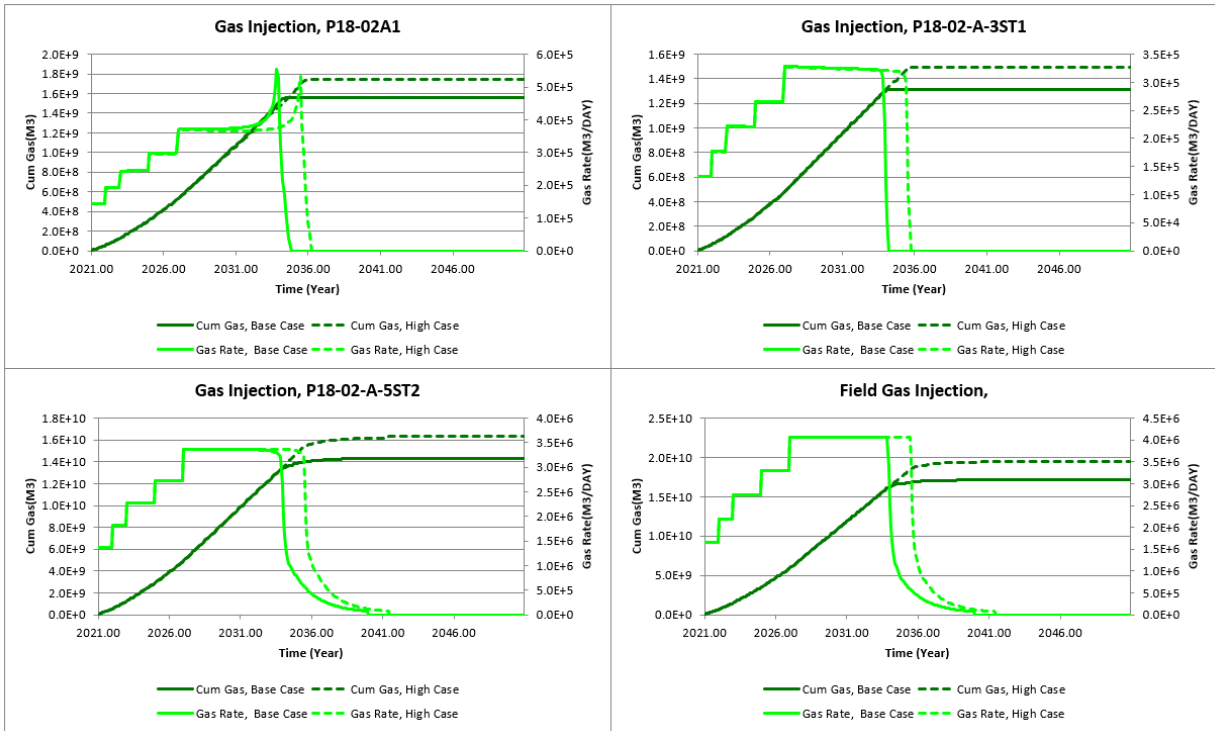


Figure 6-1: Injection rate and cumulative CO<sub>2</sub> mass injected for the three injection wells for a BHP constraint set to 375 (solid curves), representing the base case scenario, or 450 bar (dashed curves), representing the high-case scenario. See Table 6-1 for scenario parameters.

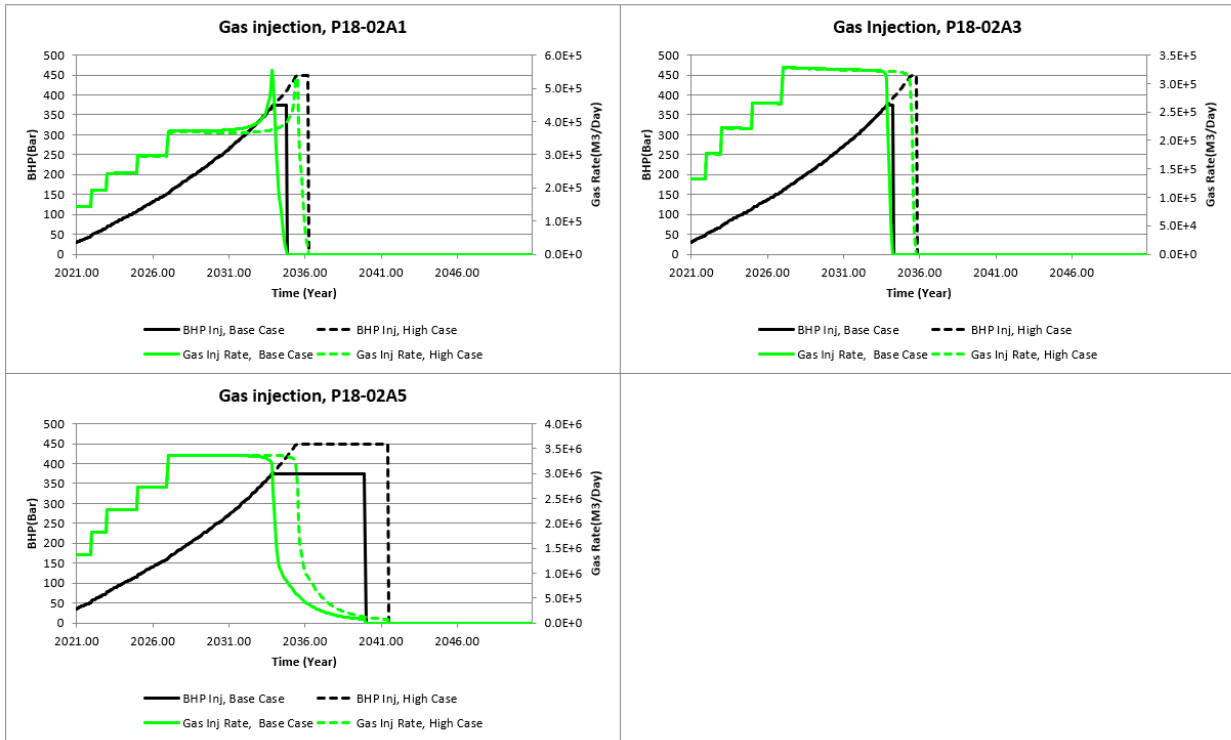


Figure 6-2: Injection rate and BHP for the three proposed injection wells for a BHP constraint set to 375 bar (solid curves), representing the base case scenario, or 450 bar (dashed curves), representing the high-case scenario. See Table 6-1 for scenario parameters.

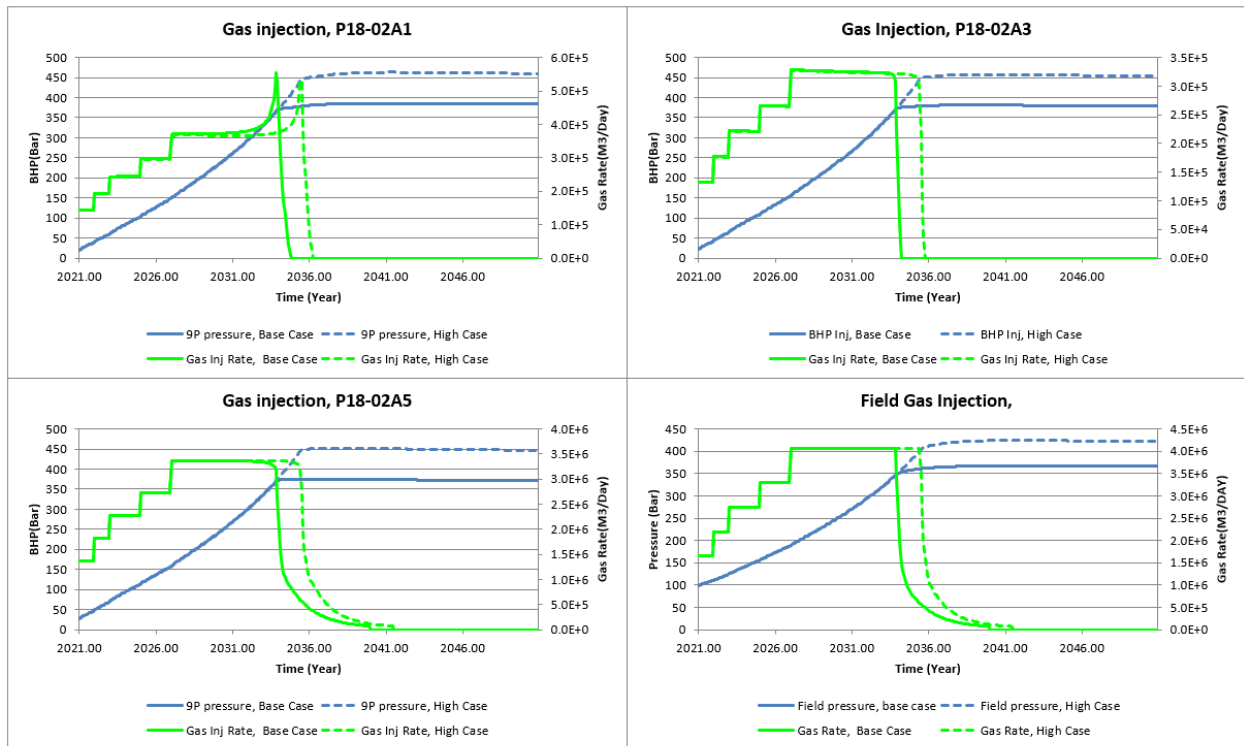


Figure 6-3: Injection rates vs well pressures (9-point pressures). In the right lower pane Injection rates vs field pressures for the three proposed injection wells for a BHP constraint set to 375 (solid curves), representing the base case scenario, or 450 bar (dashed curves), representing the high-case scenario. See Table 6-1 for scenario parameters.

From reservoir engineering perspective reservoir pressure can be brought back to initial pressure (375 bar). However, the results of well integrity analysis (Section 9.3) suggest reservoir pressure could be limited to hydrostatic pressure. Table 6-3 shows the storage capacity of the P18-2 reservoir when the average reservoir pressure after CO<sub>2</sub> injection is equal to hydrostatic pressure (351 bar).

Table 6-3: P18-2 storage capacity at hydrostatic pressure of 351 bar.

P18-2 storage	Gas volumes (BCM) / Relative contribution of each well (%)	CO <sub>2</sub> mass (Mt) / Relative contribution of each well (%)
P18-02-A-01	1.52 / (9%)	2.85 / (9%)
P18-02-A-03ST2	1.30 / (8%)	2.43 / (8%)
P18-02-A-05ST1	13.5 / (83%)	25.3 / (83%)
<b>Total</b>	<b>16.3</b>	<b>30.6</b>

6.3.4 Pressure, residual gas and CO<sub>2</sub> behaviour in the reservoir

For the base case scenario Figure 6-4, Figure 6-5 and Figure 6-6 shows maps of pressure, gas saturation and CO<sub>2</sub> molar density, respectively.

The pressure map (Figure 6-4) is similar at start of production and at the end of injection, which is expected. However there is one exception: at the end of injection compartment III is still at the depleted pressure level corresponding to the end of production (~50-60 bar), since no injection takes place in this particular

compartment and no communication exists with the other compartments (see Section 17.8).

In Figure 6-6, the CO<sub>2</sub> molar density is visible, at first as circular regions around the wells in compartment I (see saturation maps for the years 2021 and 2025). Later, the CO<sub>2</sub> progresses into compartment II. In the final stages of injection, it reaches compartment IV.

A comparison of the first panel in Figure 6-5 (this panel shows the initial GWC) with the panels in Figure 6-6 suggests that CO<sub>2</sub> migration occurs to beyond the initial gas-water contact (GWC) at the NW border of the reservoir. Also Figure 6-7 suggests CO<sub>2</sub> crossing the initial GWC, as well as CO<sub>2</sub> reaching the gas pocket. But, more importantly, the bottom panel of Figure 6-7 indicates that after injection, the CO<sub>2</sub> that crossed the GWC moves back towards the reservoir.

In conclusion the CO<sub>2</sub> might move beyond the GWC, however if so after the end of injection it will return to above the original GWC. The results also show that even though the CO<sub>2</sub> is moving below original GWC spilling is not occurring since the CO<sub>2</sub> is not flowing outside the storage complex, defined earlier.

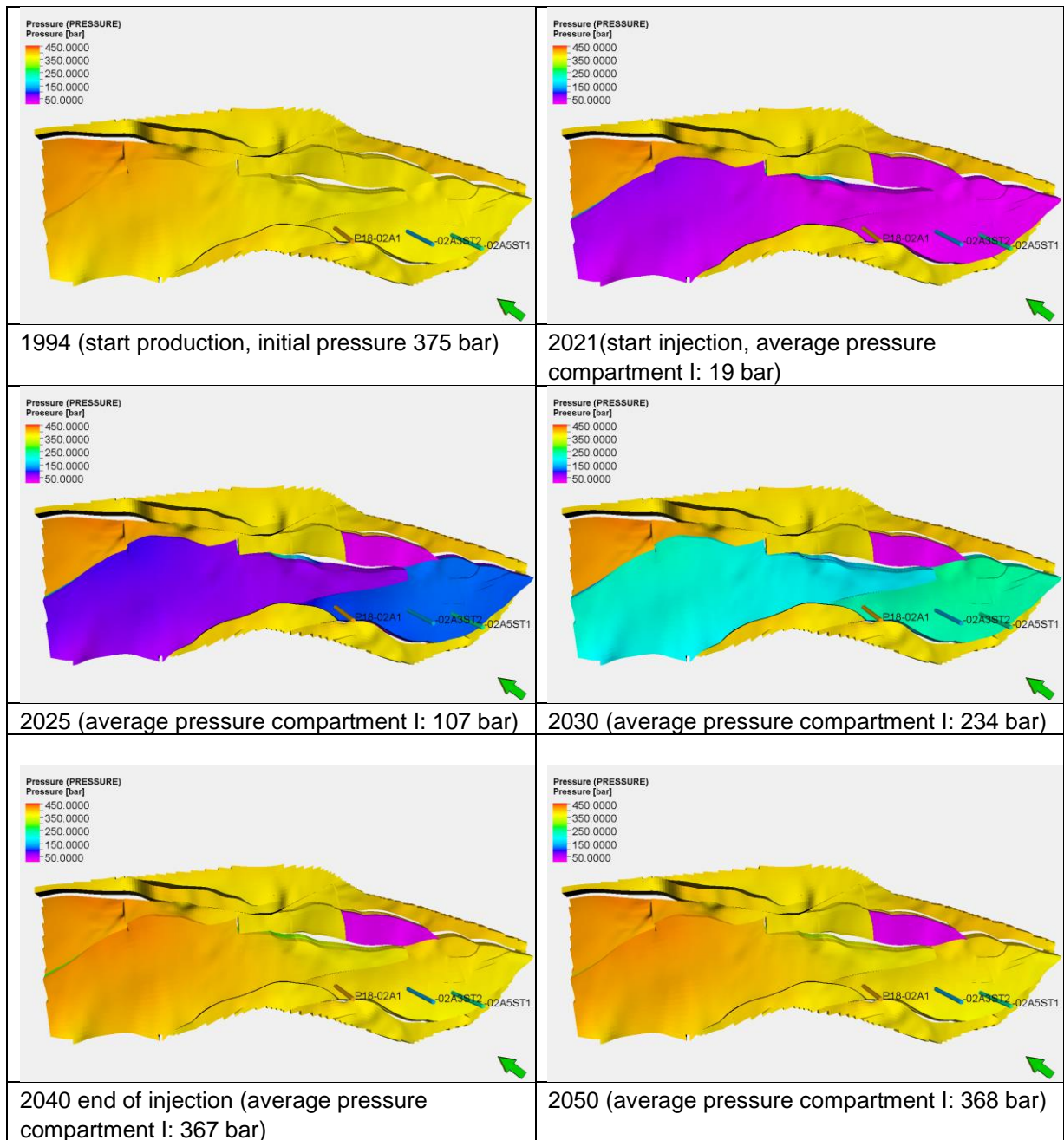


Figure 6-4: Pressure map at different stages of injection into P18-2. Average pressure in the hydrocarbon filled part of the field is about 375 bar in 1994 and in 2040. The map for 2050 shows equilibration in the ten years after injection was ceased. The pressures are HCPV weighted pressure in compartment 1.

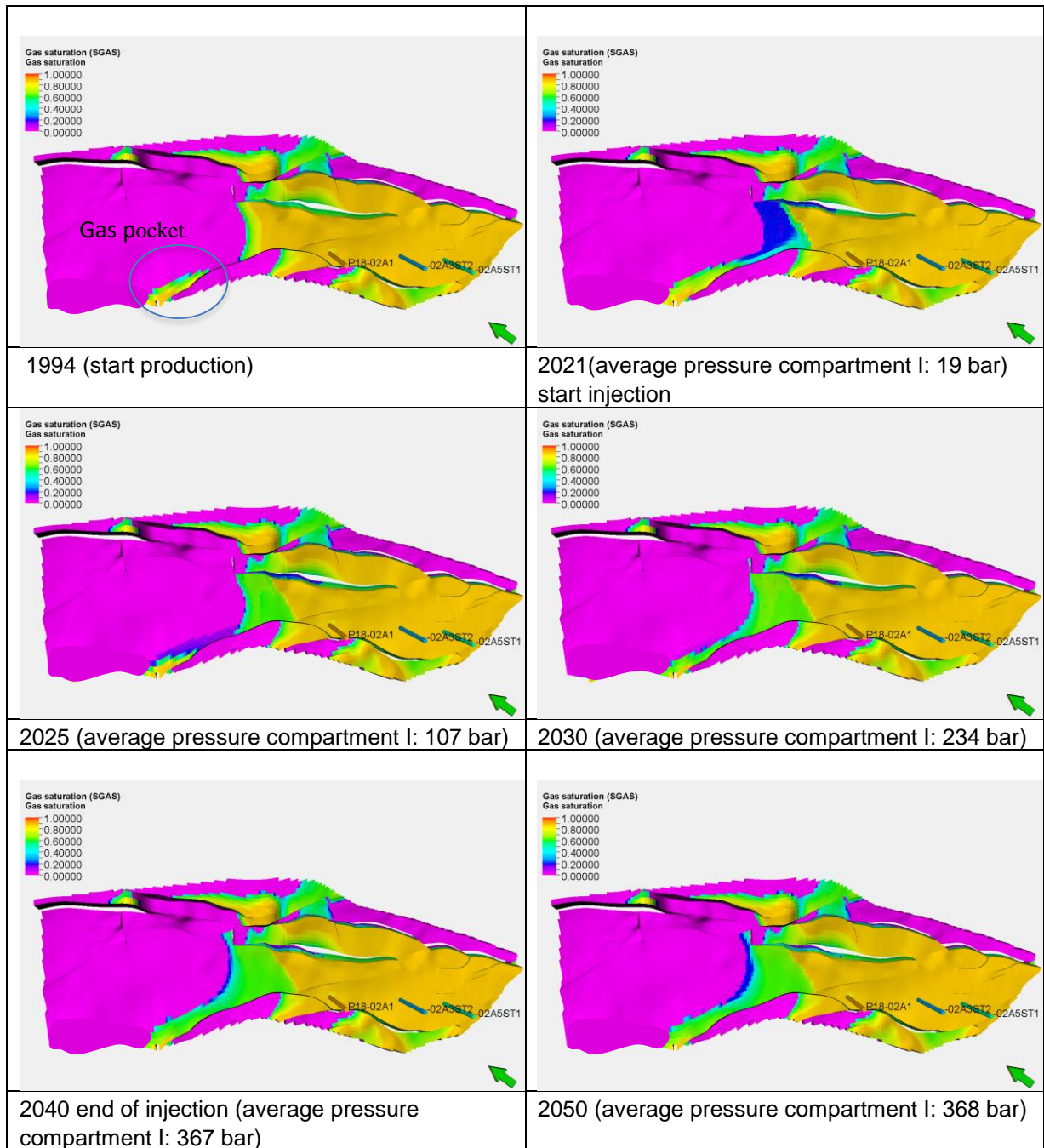


Figure 6-5: Gas saturation map at different stages of injection into P18-2. Gas in the 'gas pocket' near the NW border of the gas reservoir (see panel '1994 (start production)') is pulled towards the production wells; gas from the pocket contributes to the production. During injection, increasing reservoir pressure pushes residual gas back into the pocket.



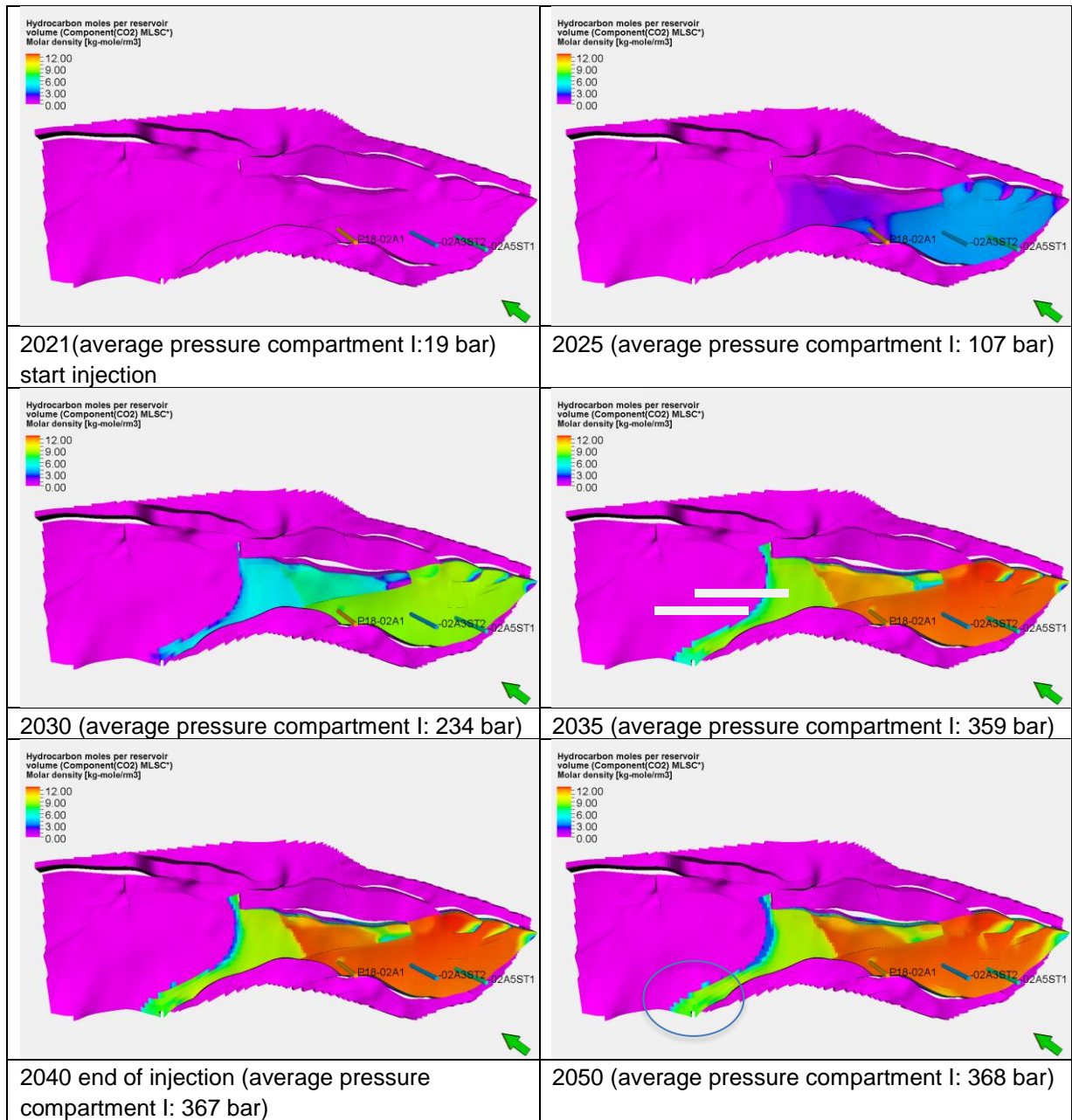


Figure 6-6: CO<sub>2</sub> molar density (kmol/m<sup>3</sup>; “kg-mole/m<sup>3</sup>” in the legend should be “kmol/m<sup>3</sup>”) map at different stages of injection into P18-2. CO<sub>2</sub> migrates beyond the original gas-water contact (compare panels in this figure with the first panel in Figure 6-5) and reaches the gas pocket (pocket indicated in the panel ‘2050’).

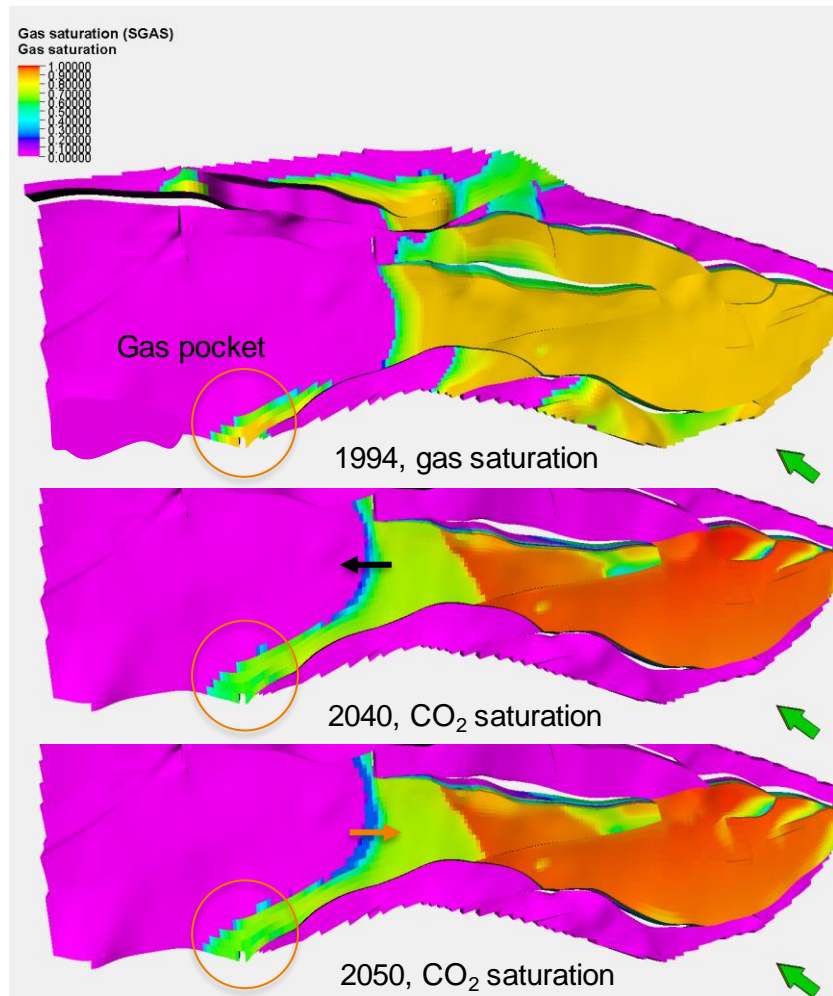


Figure 6-7: As Figure 6-6, now focusing on the period 2040 – 2050 and highlighting the behaviour of CO<sub>2</sub> in the NW corner of the reservoir. Top panel: initial gas saturation in 1994, prior to production, showing the gas-water contact (GWC). Middle panel: CO<sub>2</sub> saturation at the end of injection, in 2040. CO<sub>2</sub> has migrated beyond the initial GWC (black arrow), and has reached the gas pocket (in the circle). Bottom panel: CO<sub>2</sub> saturation in 2050, ten years after the end of injection. CO<sub>2</sub> has started migrating back into the reservoir (orange arrow); the CO<sub>2</sub> that has reached the gas pocket remains trapped. Colour coding indicates natural gas or CO<sub>2</sub> saturation: purple for zero saturation, red for full saturation.

### 6.3.5 Pressure communication with P18-6

Vandeweyer et al. (2011) state, on potential communication between P18-2 and P18-6: “Field P18-06 is located to the northeast of the main compartment. It is bounded by faults F13 and F57, of which only F13 has enough offset to be sealing by juxtaposition”. First of all, the numbering of the P18-2 faults from the Petrel project used in the current study (see e.g. Figure 4-4) is different from Vandeweyer et al. (2011). Fault F13 (a minor, transverse fault) is currently called F500, but F57 has retained its name.

Second, the seismic interpretation of the faults in this boundary area, especially F57, is different from Vandeweyer et al (2011)’s. Although F57’s throw is now much larger, it still suggests potential communication between P18-6 and Compartment II and IV of P18-2 which warrants further examination.

A closer look (Figure 6-8 and Figure 6-9) shows that P18-6 is disconnected from P18-2 by two faults, of which P18-6's boundary fault F57 is the most important one. In between the faults a small graben is filled by overlying caprock shale. The only contact is by Volpriehausen juxtaposition, which has a low permeability (lower than 1 mD). Furthermore, the faults in the graben are likely to have undergone severe cataclasis (Nieuwland, 2012), which reduces the across-fault permeability even further.

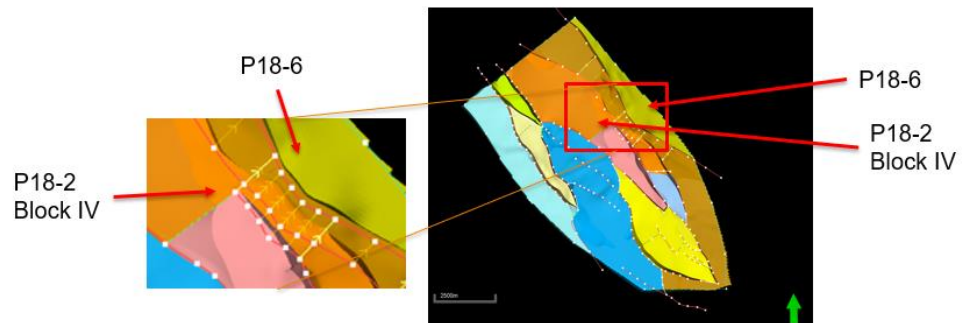


Figure 6-8: Overview fault between P18-2 and P18-6.

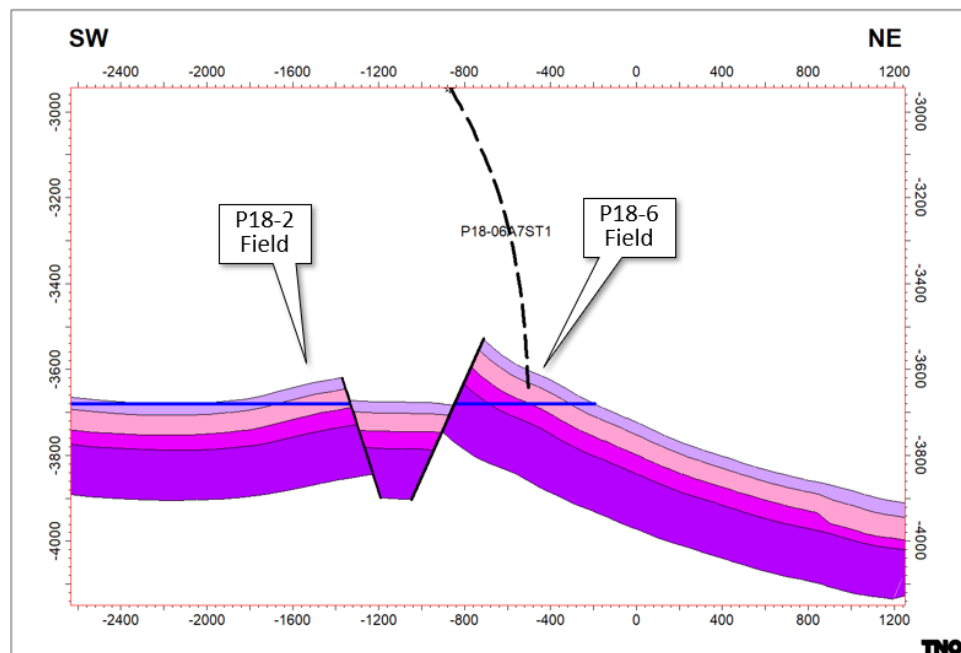


Figure 6-9: Cross section showing faults between P18-2 and P18-6.

The first pressure value from P18-6 was recorded in the end-of-well report (EOWR), available on nlog.nl; a pressure of 378 bar was inferred, in February 2003. A second pressure point is mentioned on nlog.nl: 305 bar, measured on 15-2-2004, after production of 0.074 bcm. Both data points are indicated by a star on the p/z plot in in Figure 6-10.

The data shown in Figure 6-10 suggest that measurements during periods of shut-in could have resulted in too low pressure values, due to relatively short shut-in times. For a poor quality reservoir such as P18-6 (~1 mD) pressure equilibration

requires long shut-in periods. Therefore we expect that in reality the p/z curve is a straight line and P18-6 is a depletion-driven reservoir.

The pressure data in Figure 6-11 show that after about 10 years of production from P18-2, the initial pressure found in the P18-6 reservoir was still about 275 bar higher than that in the P18-2 field. Therefore the conclusion can be drawn that these two compartments are not in pressure communication on a production timescale.

In addition, during the last years of production the pressure behaviour of the main compartment (Compartment I) of P18-2 is different from that of P18-6 (see Figure 6-11), which suggests that there is no pressure communication between the two reservoirs on production time scale.

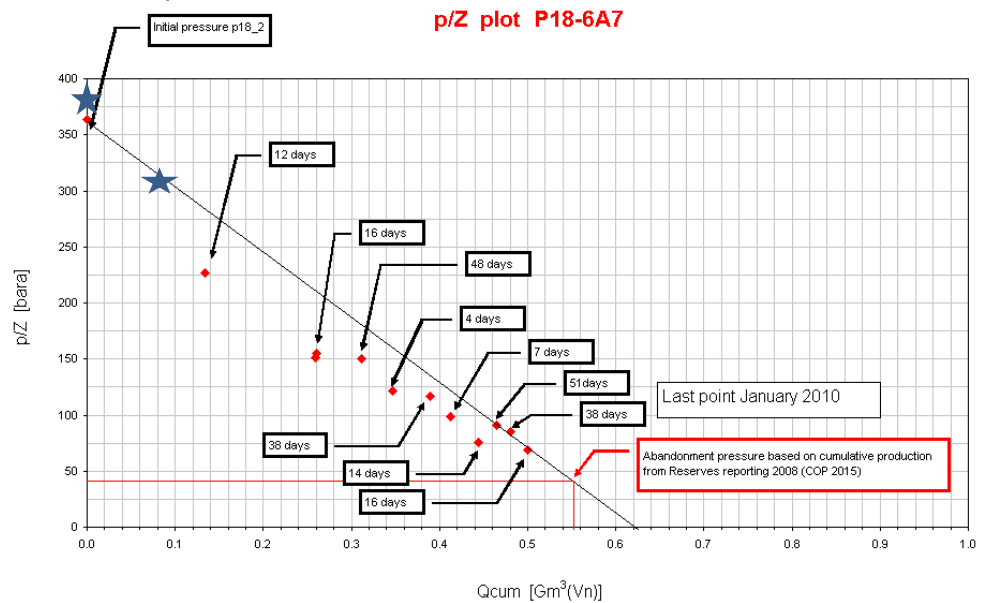


Figure 6-10: P/z plot for P18-6 with shut-in periods. Figure taken from Vandeweijer et al. (2011).). The two stars indicate pressure data reported on nlog.nl: 378 bar from the EOWR and 305 bar after production of 0.074 bcm. As also indicated, the initial pressure of the P18-2 field is added for comparison.

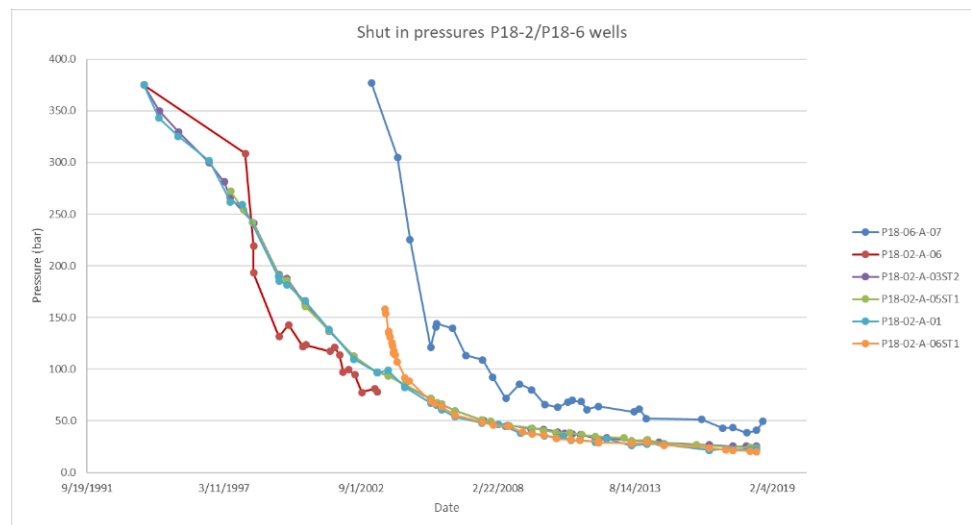


Figure 6-11: Pressure behaviour of P18-2 and P18-6 reservoirs.

### 6.3.6 Conclusions

The injection simulations lead to the following conclusions.

- Assuming a final reservoir pressure of 375 bar (initial reservoir pressure, datum depth 3400 m), the P18-2 field (using compartment I,II and IV) can store 32.2 Mt of CO<sub>2</sub>.
- Assuming hydrostatic reservoir pressure of 351 bar (datum depth 3400 m), the P18-2 field (using compartment I,II and IV) can store 30.6 Mt of CO<sub>2</sub>.
- From the point of view of the reservoir, the target CO<sub>2</sub> supply rates can be injected through the three proposed P18-2 injection wells together (P18-02-A-01, P18-02-A-03ST2 and P18-02-A-05ST1), for a period of about 10 years. The last two to four years (2034 – 2041) of the target injection scenario would require another storage location.
- About 83% of the stored CO<sub>2</sub> is injected through well P18-02-A-05ST1. The other two wells both contribute 8-9% to the total injection amount of CO<sub>2</sub>. It is to be noted that in the results presented here, any restrictions to flow from the tubing the wells is not included; such restrictions can result in a different distribution of flow over the wells.
- With the injection scenario used here, after the year 2033 combined injection capacity decreases to below the target level of about  $4.1 \cdot 10^6$  Sm<sup>3</sup>/day - although timing of the end of the injection plateau rate depends on the injection history and on the final pressure chosen for the reservoir.
- CO<sub>2</sub> fills the pore volume that was previously filled with natural gas. In compartment IV of the P18-2 field, the model employed suggests that CO<sub>2</sub> migrates some distance across the original gas-water contact into the connected aquifer, but does not spill.
- After the end of injection, the CO<sub>2</sub> is retained within the limits of the structures that make up the original P18-2 gas field. Post injection simulations shows gravitational segregation leads CO<sub>2</sub> to move back to the original GWC.

## 6.4 Temperature development in the reservoir

### 6.4.1 Introduction

As explained in Section 6.2, the simulations presented in the previous section do not take into account the temperature difference between the injected CO<sub>2</sub> and the reservoir. This section describes the evolution of the temperature effect in the P18-2 reservoir estimated by numerical simulations by the TOUGH simulator

Using the CO<sub>2</sub> supply scenario shown in Section 5.2 as the target, the conditions of the CO<sub>2</sub> at bottom hole, in the well, prior to inflow into the reservoir, were derived from a flow assurance study performed in parallel to the study presented here (Belfroid, 2019). The key results from the steady-state simulations, which are used for this study, are summarized below. For a full description of the study, including start-up and shut-in simulations, the reader is referred to Belfroid (2019).

The steady-state simulations were performed for a range of well characteristics: flow rates, CO<sub>2</sub> injection temperatures and reservoir pressure conditions. The compressor and transport pipeline to the P18-A platform were taken into account in deriving these results. The downhole temperature was required to always be above 15 °C, to avoid CO<sub>2</sub> hydrate formation in the well (which could happen when brine enters the well during shut-in periods) or in the near-well zone in the reservoir (due to the pressure drop between well and reservoir; see also Section 6.4.3).

Table 6-4 shows a feasible injection scenario over time, in which the mass flow rate is limited to 30 kg/s (about 1 Mt/yr) at the depletion pressure of 20 bar and increases to 60 kg/s (2 Mt/yr) once reservoir pressure increase to 60 bar or higher. At high reservoir pressure the injection rate decreases, due to a downhole pressure limit of 375 bar (see also Section 6.3.1). The downhole temperature (in this case, the temperature inside the wellbore) increases with increasing reservoir pressure. The lowest downhole temperature occurs during the first phase of injection, when the reservoir pressure is at its lowest. The additional pressure and temperature drop in the reservoir near the well is shown in Section 6.3.3.

It is to be noted that Table 6-4 shows results for a single well; Belfroid (2019) also provides injection scenarios with all (four) injector wells in P18-2 and P18-4 open. During injection, the CO<sub>2</sub> supplied to the platform will be distributed over the open wells; the wells will select the rate. The table provides an indication of the potential rates for a single well. Details of the simulations that led to the table are given by Belfroid (2019).

Table 6-4 CO<sub>2</sub> conditions at platform and downhole for several values of reservoir pressure, for a single well.

Reservoir pressure [bar]	Mass flow rate [kg/s]	P Platform [bar]	P Downhole [bar]	T Platform [°C]	T downhole [°C]
20	30	78	32	42	17
60	60	87	75	37	32
100	60	87	110	37	51
200	60	94	206	36	64
300	45	105	303	33	62

## 6.4.2 Setup of simulation

### 6.4.2.1 TOUGH2 simulator

The TOUGH2 simulator is used in combination with the ECO2MG module (Pruess, 2011; Loeve et al., 2014), which is designed to model the behaviour of CO<sub>2</sub> in the presence of brine in both gas reservoirs and aquifers. A key feature of the module is that it considers the transition from low pressure to high pressure across the CO<sub>2</sub> saturation line, which is an important process in the injection of CO<sub>2</sub> into depleted gas field. Also the dry-out zone around the well and salt precipitation is taken into account.

### 6.4.2.2 P18-2 model

A 20-layer radially symmetric model (Figure 6-12) that covers the different geological formations was created to analyse the temperature and pressure field of P18-2 field. The radial direction has 47 cells, which increase exponentially in size away from the well into the reservoir from 0.15 m to 137 m. The grid cell distribution is dense close to the well (left side of Figure 6-13) and also more dense on the interface with the Hardeggen and the caprock to allow a more detailed modelling around this interface. The average permeability of each formation is used in the model (Table 6-5).

Other parameters which are important for the temperature distribution and heat flow in the P18-2 reservoir are the heat conductivity of each formation (2.0 W/m/°C ) and the rock grain specific heat (1000 J/kg/°C for all formations).

Table 6-5: P18-2 properties used in radially symmetric model used to simulate the temperature development in the reservoir.

<i>Formation</i>	<i>Porosity</i>	<i>Permeability (mD)</i>	<i>H (m)</i>
Caprock	0.01	0.01	
Hardegsen	0.11	154	26
Upper Detfurth	0.09	38	49
Lower Detfurth	0.07	31	27
Volpriehausen	0.03	0.02	

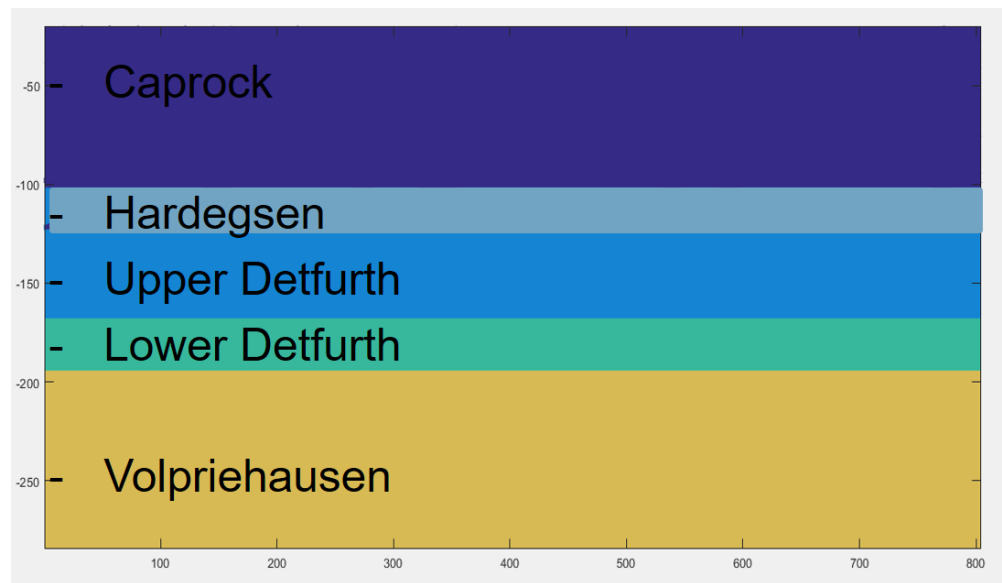


Figure 6-12: Radially symmetric model used for the modelling of the temperature field within the P18-2 reservoir.

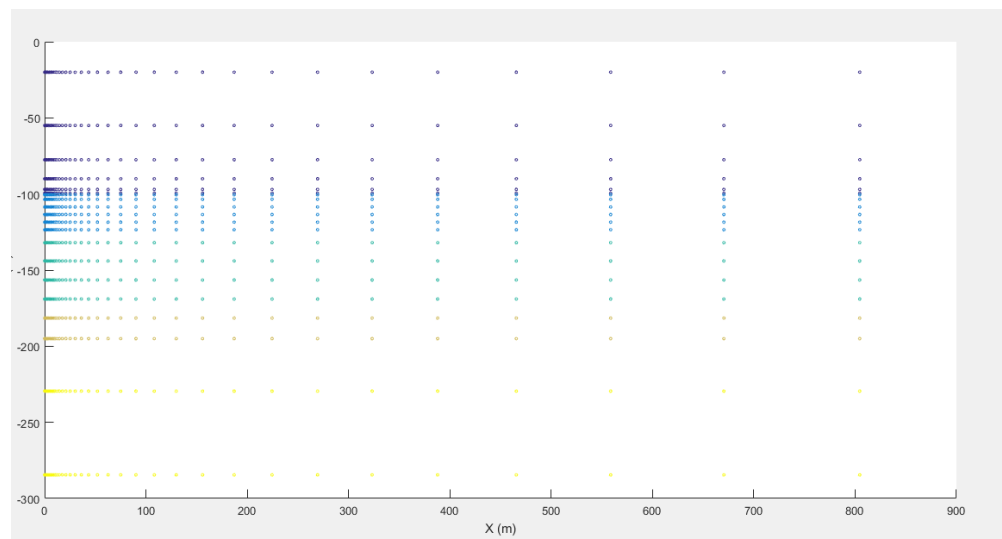


Figure 6-13: Grid cell distribution of the P18-2 radially symmetric model used for the modelling of the temperature field within the P18-2 reservoir; see also Figure 6-12.

### 6.4.2.3 Model settings

The initial reservoir conditions of P18-2 used are listed in Table 6-6.

Table 6-6: Initial conditions used for the modelling of the temperature field within the P18-2 reservoir.

Initial reservoir conditions	value
Reservoir pressure	20 bar
Reservoir temperature	100 °C;
Injection temperature	15 °C;
Injection duration	15 years
Injection rate	1.13 Mt/yr
Initial brine saturation	0.01

The reservoir pressure is set to 20 bar, which is assumed pressure after the production phase. The P8-2 reservoir temperature in reality is 126 °C, but the TOUHG2 simulator is limited to a maximum temperature of 103 °C; therefore the reservoir temperature in TOUGH2 model was set to 100 °C in the simulations. The results of all simulations miss the effect of the last 26 °C (e.g., faster heating of the cold CO<sub>2</sub>, larger effect on the stress changes).

The injection rate of 1.13 Mt/yr/well corresponds to a total injection of 4.5 Mt/yr into four proposed injection wells in the P18-2 and P18-4 reservoirs, which is the maximum injection scenario presented in Section 5.2.

Furthermore, there are two additional reasons why the modelled scenario is the most extreme injection scenario:

- The injection temperature is constant (15 °C) in the model, although the conditions described by Belfroid (2019) show that the temperature of the CO<sub>2</sub> remains close to 15 °C only during the initial phase of injection. In later stages the injection temperature is higher than 15 °C.
- The modelled duration of injection is 15 years with constant injection rate and no shut-in periods (e.g. due to maintenance). In this section, results for the first three years are considered.

The reservoir simulations showed that most of the CO<sub>2</sub> migrates into the Hardegsen Fm. upon injection and much less into the Upper and Lower Detfurth, the injection rates in the thermal simulations were distributed over the three formations accordingly: 60% into the Hardegsen, 28% into the Upper Detfurth and 12% into the Lower Detfurth.

### 6.4.3 Results

The temperature distribution and profiles from the modelling are presented in Figure 6-14 to Figure 6-17, for the injection rate of 1.13 Mt/yr/well. Even though the largest part of the CO<sub>2</sub> is injected in the Hardegsen Formation, the progression of the cold front is faster in the Detfurth Formations. The maximum extent of the cold zone is 400-500 m into the reservoir. The vertical extent of the cold plume into the caprock is less than 100 m), since no temperature effect is observed in Figure 6-15 (represents level '1' in Figure 6-14).

Just above the caprock / Hardegsen interface (10 m above the interface, level '2' in Figure 6-14) a cooling of 55 °C is observed (see Figure 6-16). In the reservoir itself, 60 m below the caprock / Hardegsen interface (level '3' in Figure 6-14) cooling due



to evaporation of brine combined with Joule Thomson effect of CO<sub>2</sub> is observed in the model, leading to temperatures below 10 °C around the injection well (see Figure 6-17).

A close analysis of the temperature effects in the near-well area (up to 50 m from the well) at low-pressure conditions (first 2-3 years at the injection rates used) shows that for the injection scenario the pressure and temperature conditions within the near-well zone are within the hydrate formation window (Figure 6-18).

(residual) pore water is available, hydrates could form and block the pore space, thereby decreasing the injectivity. The minimum temperature in the P18-2 model is 5.4 °C at 40 bar. Note that after 1.5 year of injection the minimum temperature observed in the model is 14 °C, which is outside the hydrate formation window.

However, Figure 6-19 shows that injection at the lower injection rate (0.56 Mt/a) the pressure and temperature conditions in the reservoir remain outside the hydrate forming conditions (Figure 7-1); the minimum simulated temperature is 10 °C at 30 bar.

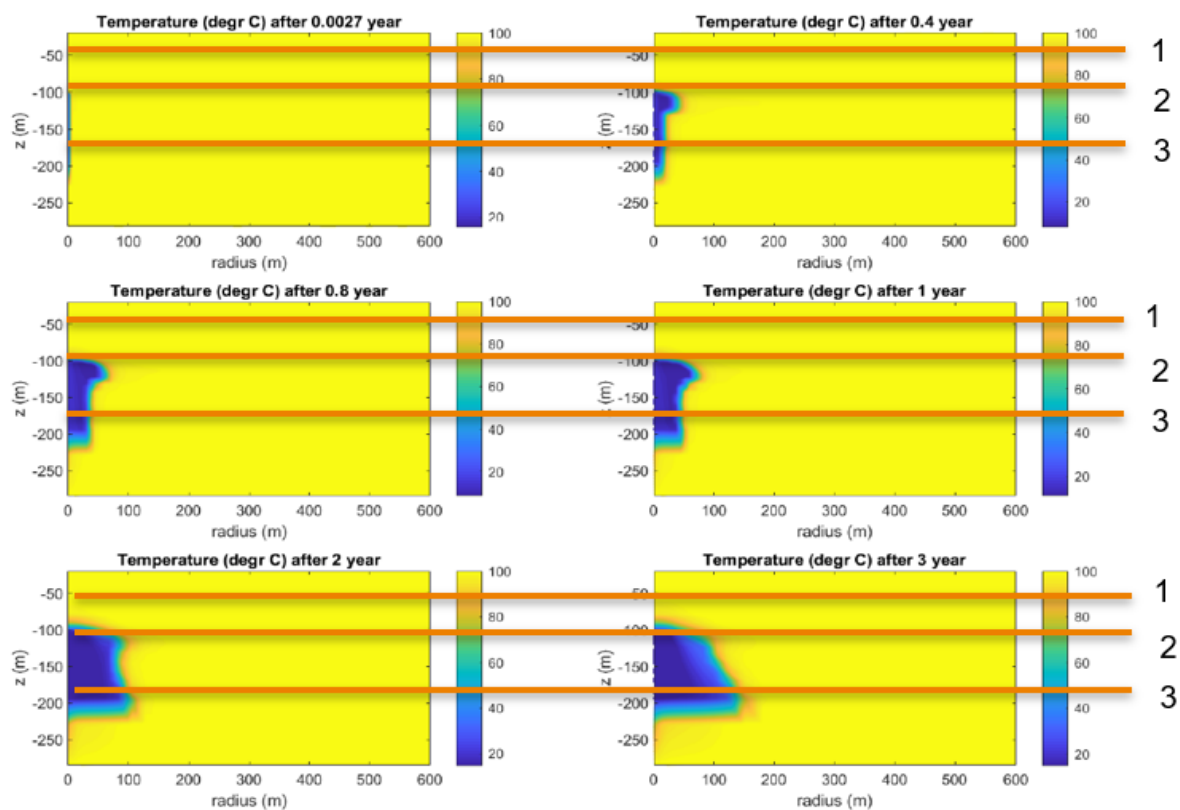


Figure 6-14: Temperature distribution in the P18-2 radially symmetric model for the maximum injection rate scenario 1.13 Mt/year/well. The numbers indicate three vertical levels in the model: level 1 is 100 m above caprock/Hardeggen interface, level 2 is 10 m above caprock / Hardeggen interface and level 3 is 60 m below caprock/Hardeggen interface; i.e., levels 1 and 2 are within the caprock, level 3 is within the reservoir. The injection well is located along the left vertical axis in each panel.

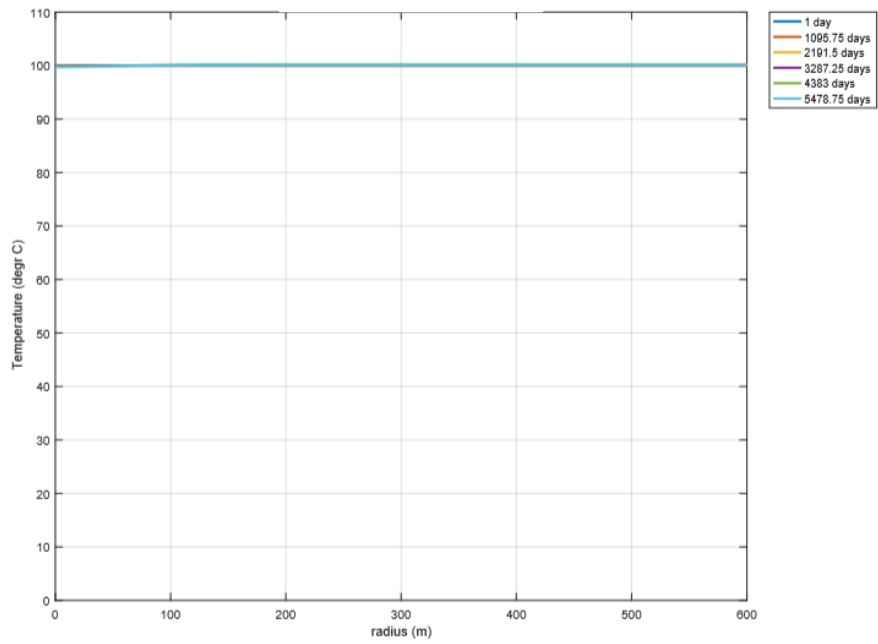


Figure 6-15: Temperature profile in the maximum injection rate scenario for level 1, which is 100 m above caprock / Hardegsen interface. The well is at zero radius.

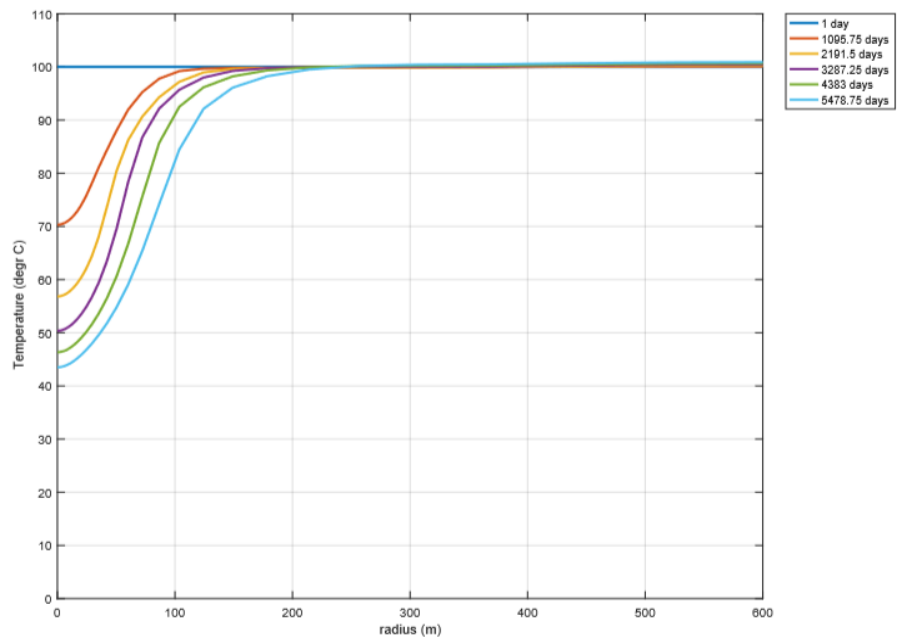


Figure 6-16: Temperature profile in the maximum injection rate scenario for level 2, which is 10 m above caprock / Hardegsen interface. The well is at zero radius.

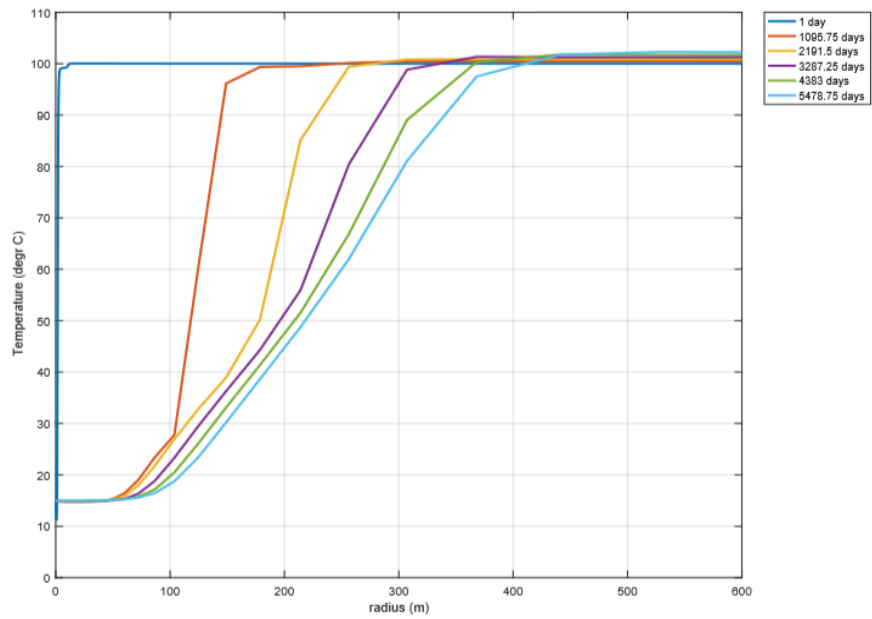


Figure 6-17: Temperature profile in the maximum injection rate scenario for level 3, which is 60 m below caprock / Hardeggen interface. The well is at zero radius.

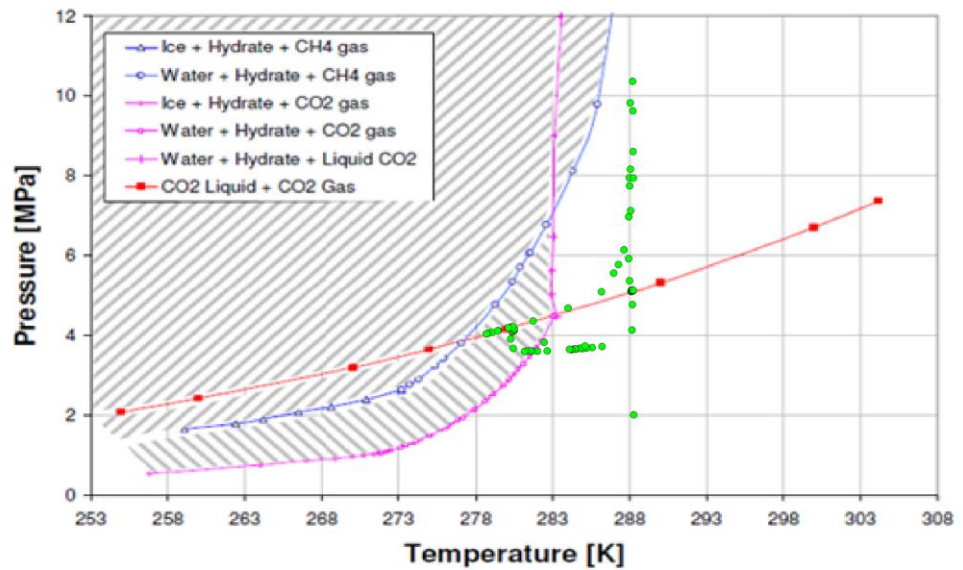


Figure 6-18: Hydrate formation window (hatched area), where hydrates can form, with overlain the temperature in the near-well zone (distance from the well smaller than 50 m): the green dots cover the ranges of temperature and pressure combinations as predicted by the P18-2 TOUGH2 model for the higher injection rate scenario.

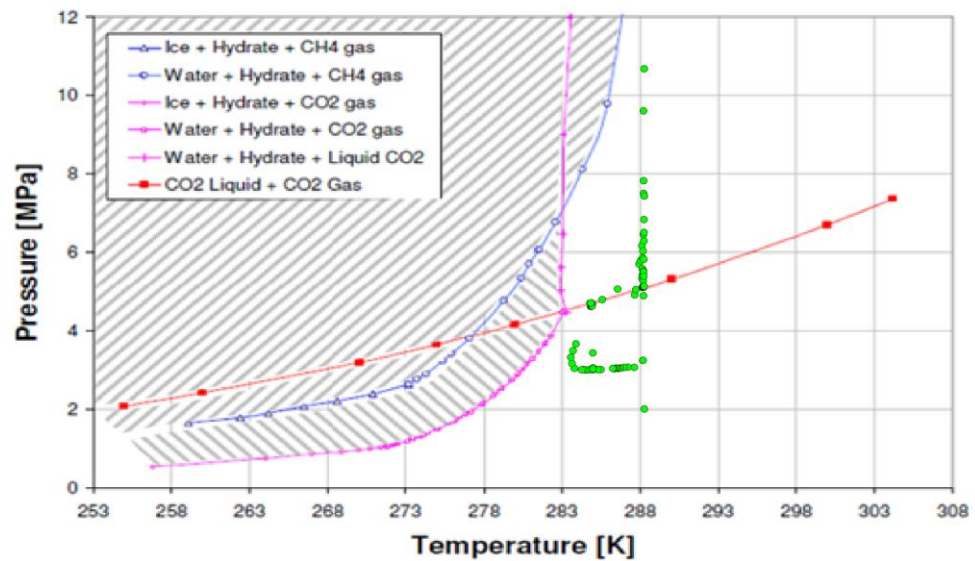


Figure 6-19: Hydrate formation window (hatched area), where hydrates start to occur, with overlain the temperature in the near-well zone (distance from the well smaller than 50 m): the green dots cover the ranges of temperature and pressure combinations as predicted by the P18-2 TOUGH2 model for the lower injection rate scenario.

#### 6.4.4 Risks

The injection scenarios used here were constructed to emphasise the development of a low-temperature zone around an injection well over time. The lowest temperatures of injected CO<sub>2</sub> are expected to occur when reservoir pressure is low (below about 50 bar), which corresponds with the first year at the rates used here. The interpretation should focus on the first few years of the results presented here.

The thermal modelling study identified two main risk factors: hydrate formation and low temperatures in the reservoir.

- When reservoir pressure is low, injection rates of the order of 1 Mt/yr/well and low injection temperature of 15 °C may lead to hydrate formation conditions in the near-well zone. Whether hydrates actually form under these conditions and affect injectivity remains a topic of further research. Hydrate formation does not affect safety or security of CO<sub>2</sub> storage. Hydrate formation due to injection can be avoided by managing injection temperatures and rates.
- The simulation shows a dry-out zone around the well, which results in additional cooling by the evaporation of the brine. In this dry-out zone, hydrates are unlikely to form since they need water. The interplay between drying out and conditions in the reservoir entering the hydrate formation window should be assessed.
- The progression of the cold front is initially fast but slows down with time due to increasing radius of the cold front. For the injection scenarios simulated, the cold front reaches about 100 m distance from the injection well after about two years of injecting low-temperature CO<sub>2</sub>.
- After about two years of injecting cold CO<sub>2</sub>, the cold front has not yet reached the fault that is nearest to an injection well. Well test data suggested that a fault is observed 128-148 m away from The P18-02-A-01 well; according to the static model this distance is 160 m. Section 7.3 investigates the geomechanical implications of a low-temperature front on fault stability.

A reliable modelling of the distribution of the cold plume requires the three-dimensional structure around the well (or wells) to be represented in the model, as well as the historical injection rate and injection temperature over time. Such work is to be done prior to injection, to define the safe injection window from the point of view of temperature development in the reservoir and near faults (see also Section 7.3)

#### 6.4.5 *Conclusions*

The TOUGH2 simulations using a simplified, radially symmetric model, demonstrated that the temperature effects of injecting cold CO<sub>2</sub> for worst case conditions result in:

- Near-well temperatures that could be in the hydrate formation zone. The formation of hydrates could temporarily deteriorate the injectivity. Hydrates, once formed, will disappear once the temperature has increased sufficiently for local conditions to no longer be inside the hydrate formation window. On the other hand the dry out zone around the injection well will prevent to form any hydrates at all by the injected (cold and dry) CO<sub>2</sub>.
- Progression of the cold front into the reservoir. The distance of the cold front depends on the duration and injection rate of injection of cold CO<sub>2</sub>. At high injection rates (over 1 Mt/yr/well) of cold CO<sub>2</sub>, the front is at about 100 m from the injection well in about 2 years. The impact of low temperatures on fault stability are investigated in Section 7.3).

More detailed reservoir simulations with a more advanced, non-isothermal reservoir simulator are needed to improve predictions of the temperature development near each of the three proposed P18-2 injection wells, taking into account the 3D structure of the reservoir.

### 6.5 Chemical interactions

#### 6.5.1 *Introduction*

Within a storage reservoir, physical and chemical interactions between the CO<sub>2</sub>, the formation water and rock minerals will occur during and after CO<sub>2</sub> injection. On the short term, during the injection phase, the risk of porosity and permeability decrease and corresponding injection issues need to be evaluated. On the long term, during the post-abandonment phase, the CCS Directive (EU, 2009) requires evaluation of the fate of CO<sub>2</sub>, for which geochemical reactions play an important role. This section describes the short-term (injection phase) and long-term (post-abandonment phase) CO<sub>2</sub>-water-rock interactions and their impact on the feasibility of CO<sub>2</sub> injection and storage in the P18-2 reservoir, using recent literature. Most of the discussion is general and applicable to CO<sub>2</sub> storage in depleted gas fields. In addition results from previous modelling studies specifically for P18-2 are discussed.

#### 6.5.2 *Injection phase: Effect of dry-out and salt precipitation on injectivity*

During injection of dry CO<sub>2</sub>, whether in an aquifer or a depleted hydrocarbon field, (residual) formation water will evaporate into the CO<sub>2</sub> in the near-well area. A dry-out zone will develop which can extend up to several tens of meters into the reservoir. As this will increase the relative permeability of CO<sub>2</sub>. On the other hand, as the mass of water decreases, the concentration of the aqueous species

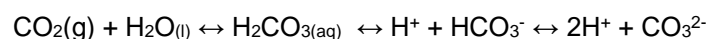
increases and minerals start to precipitate when the remaining water becomes saturated (Miri and Hellevang, 2016). The most common mineral to precipitate is halite salt (NaCl), since formation waters contain mostly Na<sup>+</sup> and Cl<sup>-</sup>, although other minerals such as sulphates or hydroxides can also form. Salt precipitation during CO<sub>2</sub> injection and corresponding permeability reduction and injectivity issues have been studied in the laboratory and by numerical simulations, primarily for the purpose of CO<sub>2</sub> storage in saline aquifers (e.g. Bacci et al., 2011, Kim et al., 2012, Roels et al., 2014). Field evidence of salt precipitation and injectivity impairment was obtained from the Ketzin injection pilot in Germany (Baumann et al., 2014) and the Snøhvit storage site in Norway (Grude et al., 2014). Based on those studies it can be concluded that the key parameter for salt precipitation to result in permeability and injectivity impairment is the availability of saline water for capillary backflow (migration of salt water towards the injection well) and hence continuous supply of salt. In the absence of capillary backflow of saline water, the maximum amount of salt precipitation is constrained by the volume of residual formation water and the concentration of aqueous species. The available species will then precipitate as thin coatings around the rock grains, in the space that was occupied by the residual brine, without significantly affecting the total permeability. This would be a more likely outcome for depleted pressure gas fields

In the P18-2 reservoir the water saturation at the beginning of CO<sub>2</sub> injection will be close to residual and hence it will be immobile. This is supported by the lack of (significant) water (brine) production during the production history of the field (see P18-2 production data at [www.nlog.nl](http://www.nlog.nl)). As a result, capillary backflow of brine during injection will not occur. Production data did not give any evidence for the presence of a strong aquifer support, implying that brine supply from below is also not expected to occur. Tambach et al. (2015a) reported on the modelling of CO<sub>2</sub> injection into a depleted gas reservoir (based on P18 characteristics) and the effect on salt precipitation. In the case of immobile brine the maximum amount of salt precipitation was 2.7% of the pore volume, with corresponding permeability decrease of 23%. Note that the degree of permeability decrease upon a reduction in porosity is highly uncertain, but much higher values than 23% are not to be expected. With permeability values as high as those of the P18-2 reservoir, injectivity impairment by this amount of salt precipitation is not expected to occur. The temperature decrease in the near well area related to the low temperature of injected CO<sub>2</sub> will not have major impact on the extent of salt precipitation.

Overall, the increased relative permeability due to decreased water saturation will have a more significant and positive impact on injectivity than the minor total permeability reduction related to salt precipitation when injecting CO<sub>2</sub> in a depleted gas field such as P18-2.

### 6.5.3 *Injection phase: CO<sub>2</sub>-water-rock interactions*

When CO<sub>2</sub> is injected into the reservoir, it will try to form a new physico-chemical balance with the (residual) formation water. The water starts to evaporate into the dry CO<sub>2</sub>, as described in the previous section, and CO<sub>2</sub> starts to dissolve into the formation water. In the near-well area, the dry-out will progress fast, not leaving any formation water for CO<sub>2</sub> to dissolve in. Beyond the progressing dry-out zone CO<sub>2</sub> dissolves into the formation water and further dissociates by the following reactions:



These reactions lead to an increased acidity of the formation water and a disequilibrium with the rock mineralogy. Both experimental and modelling studies show that on the short term the main reaction is the partial dissolution of carbonates, and potentially sulfides and sulphates, to buffer the pH. Of the carbonates, calcite dissolution is fastest, while the dissolution of other carbonates such as dolomite and ankerite is much slower. The mineralogy of the P18-2 reservoir, reported in the core analysis report for P18-A-01 (P/18-3 well), consists of mainly quartz, with lower amounts of K-feldspar, albite, plagioclase, dolomite, and clay minerals. Only occasionally anhydrite or calcite have been found, in small amounts.

Equilibrium batch reaction modelling with PHREEQC software, performed for the feasibility study of P18 in the CATO-2 project, predicted the dissolution of very small amounts of dolomite and pyrite, with negligible amounts of anhydrite and dawsonite precipitation (Vandeweyer et al., 2011). These reactions present a worst case scenario as the simulation was based on equilibrium modelling and did not consider kinetics. Also, these reactions would not occur in the near well zone where dry-out would occur. Since worst case conditions predict negligible impact of CO<sub>2</sub>-water-rock interactions on porosity, and hence on permeability, in the reservoir beyond the dry-out zone, it can be concluded that geochemical interactions will not negatively impact the injectivity.

#### 6.5.4 *Post-abandonment phase: CO<sub>2</sub>-water-rock interactions*

On the long-term, representative for the post-abandonment phase, the conditions in the reservoir will slowly move towards a chemical equilibrium. This implies that also silicate minerals have time to respond to the change in chemical equilibrium as a result of the high CO<sub>2</sub> partial pressure and partial CO<sub>2</sub> dissolution into the residual formation water beyond the dry-out zone. Since only residual, and thus immobile, formation water is present in the reservoir, a chemical equilibrium will only be obtained on the micro-scale; ions in the formation water can migrate by diffusion through the film of formation water as long as the film is connected. The scale on which formation water is connected is unknown and highly depends on the microstructural characteristics of the rock. Regardless of the scale of connection, diffusion of ions will be very slow, making it most likely to have chemical equilibrium on microscale only. The limited amount of water further slows down the reactions, as water acts as a facilitator for the dissolution-precipitation reactions.

Tambach et al. (2015b) performed simulations with TOUGHREACT to predict long-term mineral reactions and sequestration of CO<sub>2</sub> in carbonate minerals for the P18 reservoir. A key uncertainty in the simulations is whether or not to include dawsonite as a secondary mineral. Dawsonite is a controversial carbonate mineral which, if included in geochemical simulations, is predicted to sequester a large part of the CO<sub>2</sub> on the long term. Also the possibility of magnesite precipitation as a secondary mineral was questioned. In the chemical initialization of the reservoir formations by Tambach et al. (2015b), both dawsonite and magnesite were predicted to be present as initial minerals. Since they were both not measured in any of the P18 reservoir samples analysed, it can be questioned whether the chemical database contains correct chemical constants for these minerals.

In the same study by Tambach et al. (2015b) simulations for long-term CO<sub>2</sub>-water-rock interactions were performed with and without dawsonite and magnesite as secondary minerals. In both cases, long-term mineral reactions include the partial reaction of albite, K-feldspar and kaolinite to illite. In the scenario with dawsonite and magnesite as secondary minerals, the largest part of the CO<sub>2</sub> is predicted to be trapped in carbonate minerals within a few thousand years. In the simulation excluding dawsonite and magnesite as secondary minerals, leaving only calcite and dolomite as potential secondary carbonates, no CO<sub>2</sub> is predicted to be sequestered in carbonate minerals after equilibrium is reached within 10,000 years. Limited CO<sub>2</sub> partial pressure decrease from 365 bar after well closure to 300, 315 and 341 bar for the lower Detfurth, Upper Detfurth and Hardegsen Formation respectively is predicted after 10,000 years, related to a slight overall porosity increase due to dissolution-precipitation reactions. More than 95% of the CO<sub>2</sub> remains in the reservoir in the supercritical state. Hence the impact on Pressure and Temperature medium to long term is negligible

Studies on natural analogues only rarely report on the occurrence of dawsonite, and if present, only in very small amounts. Natural analogues are natural occurrences of CO<sub>2</sub>-rich gas reservoirs in which the CO<sub>2</sub> has had thousands to millions of years to reach chemical equilibrium with the reservoir formation water and mineralogy, and therefore present a unique opportunity to study the long term fate of CO<sub>2</sub> in a depleted hydrocarbon reservoir and validate geochemical models. The absence of large amounts of dawsonite in natural analogues suggests that dawsonite precipitation in geochemical simulators is not well defined.

Two major studies on natural analogues in the US and the UK show that in most cases negligible trapping in carbonate minerals occurred (Baines and Worden, 2004; Gilfillan et al., 2009), which is most likely due to the slow dissolution of silicate minerals which is a rate-limiting step (Baines and Worden, 2004). The study by Gilfillan et al. (2009) identified solubility trapping as the primary sink for the natural CO<sub>2</sub> fields analysed, but this is only possible in case of sufficient availability of formation water, which is not the case in depleted hydrocarbon fields without strong aquifer supports such as the P18-2 reservoir. Based on the insights obtained from natural analogues, the scenario by Tambach et al. (2015b) excluding dawsonite and magnesite as secondary minerals provides a more realistic prediction of the long term fate of CO<sub>2</sub>. We can conclude that almost all of the injected CO<sub>2</sub> will remain in the supercritical state for thousands of years.

## 6.6 Conclusions

### *CO<sub>2</sub> storage capacity, CO<sub>2</sub> injection rates*

The injection simulations lead to the following conclusions.

- Assuming a final reservoir pressure of 316 bar (90% of hydrostatic), the P18-2 field can store 26 Mt of CO<sub>2</sub>.
- From the point of view of the reservoir, the target CO<sub>2</sub> supply rates can be injected through the three proposed P18-2 injection wells together (P18-02-A-01, P18-02-A-03ST2 and P18-02-A-05ST1), for a period of about 10 years from the start of injection. The last two to four years (2031 – 2035) of the target injection scenario would require another storage location.



- About 83% of the stored CO<sub>2</sub> is injected through well P18-02-A-05ST1. The other two wells both contribute 8-9% to the total injection amount of CO<sub>2</sub>.
- With the injection scenario used here, after the year 2033 combined injection capacity decreases to below the target level of about  $4.1 \cdot 10^6$  Sm<sup>3</sup>/day - although timing of the end of the injection plateau rate depends on the injection history and on the final pressure chosen for the reservoir.
- CO<sub>2</sub> fills the pore volume that was previously filled with natural gas.
- CO<sub>2</sub> plume development far away from the injection well requires knowledge of fault transmissibility between Compartments I and II; using P18-02-A6ST1 as an observation well could provide relevant monitoring data.

#### *Near-well hydrate formation*

For a few days/weeks/months in each new injection well CO<sub>2</sub> is likely to be injected at conditions close to those allowing the formation of CO<sub>2</sub>-hydrates. A proper management of injection conditions is needed to ensure that temperature and pressure in the well and in the near-well area remain outside the hydrate formation window. However, dry-out of the near-well region by the CO<sub>2</sub> may prevent hydrate formation anyway. This is an aspect that requires further investigation. It should be noted that hydrate formation does not pose a risk to safe and secure storage of the CO<sub>2</sub>. It may just reduce injectivity temporarily.

#### *Near-well chemical clogging*

Injection of CO<sub>2</sub> into the reservoir will cause drying out of the reservoir. As a result the CO<sub>2</sub> relative permeability will increase. Total permeability decrease related to precipitation of salt will be negligible. Overall the injectivity of CO<sub>2</sub> is expected to increase. Near well clogging due to CO<sub>2</sub>-water-rock interactions in the area beyond the dry-out zone is expected to be insignificant.

#### *Temperature effects*

The injection of CO<sub>2</sub> at low temperature into the P18-2 gas field must be modelled and hence predicted in detail prior to the start of injection. . This is the most important base line conformance measure, and the most important set of lessons to be learned to assist the development of all future pressure depleted gas storage fields The cold CO<sub>2</sub> will affect bottomhole pressure during injection. The pressure in the reservoir will slowly increase as the CO<sub>2</sub> in the reservoir gradually reach initial reservoir temperature. A more detailed analysis is needed prior to the start of injection.

#### *Long-term reservoir integrity*

No significant chemical interactions between the CO<sub>2</sub> and the reservoir rock are expected. CO<sub>2</sub> is expected to remain in supercritical state in the reservoir for a period of the order of thousands of years.

## 7 Fault stability

### 7.1 Introduction

This section focuses on the evaluation of the potential of destabilization of intra-reservoir faults identified in the seismic cube and mapped in the static and dynamic models. The section addresses fault stability in relation to reservoir re-pressurisation (Section 7.2), to the low temperature of the injected CO<sub>2</sub> (Section 7.3) and to geochemical effects of CO<sub>2</sub> (Section 7.4).

The overall conclusion from the work presented in this section is that the risk of fault reactivation due to the injection of CO<sub>2</sub> is low.

The increasing reservoir pressure as a result of injecting CO<sub>2</sub> stabilizes the faults that bound the P18-2 field. CO<sub>2</sub>-related geochemical effects in fault zones are unlikely to lead to reactivation of the faults, or to CO<sub>2</sub> migration along faults.

If low-temperature CO<sub>2</sub> (the temperature can be about 100 °C cooler than the reservoir temperature) reaches a fault, the fault can be locally destabilized. This risk can be mitigated by monitoring and, if necessary, by reducing the injected amount of CO<sub>2</sub> through wells that are close to bounding faults. The well that is closest to a fault (well P18-02-A-01) has low injectivity which may already sufficiently mitigate this risk. Further analysis is needed to define the risk and mitigation requirements in more detail.

### 7.2 Fault stability: pressure effect

For the effects of pressure changes on inter-compartment fault reactivation we use MACRIS (Mechanical Analysis of Complex Reservoir for Induced Seismicity), a TNO-developed semi-analytical approach which allows us to evaluate both the poro-elastic effect and the direct pressure effect on stresses along the mapped faults.

Details of MACRIS are given in an Annex, Section 17.9. The required input for running MACRIS is the ECLIPSE reservoir grid with the flow simulations detailed in Section 6. Taking the ECLIPSE reservoir flow simulations as inputs MACRIS directly computes the stress induced by both the poro-elastic effect (i.e., the reservoir contraction/dilation due to depletion/injection of gas) and the direct pressure effect (i.e., the changes in effective normal stress due to the changes in pore pressure inside the faults). It is important to mention that MACRIS captures the effect of the differential compaction between two offset compartments. For the direct pressure effect, the average pore pressure between the two juxtaposed reservoir compartment at faults has been assumed.

It is not needed to rebuild a new geomechanical mesh with MACRIS; it directly works with the grid of the flow simulation (ECLIPSE). This way, MACRIS is extremely fast. Moreover, it allows the evaluation of stresses in 3D along all the mapped faults with high resolution.

For a simplified 3D single-fault tank reservoir model, the MACRIS stress solution has been compared with the solution given by the Diana FE (Finite Element) simulator. The results are presented in appendix 16.8 and clearly demonstrate the almost perfect match between MACRIS and the FE solution. It is important to keep in mind here that it would not be possible to use an FE approach for the 3D evaluation of the stresses along the multiple faults of the P18-2 field. Solely 2D cross-sections as it has been performed in the previous P18 study (Vandeweyer et al., 2011) could have been performed. Having access to the Coulomb stress distribution in 3D along the fault planes with MACRIS is extremely advantageous, since the along-strike variability is accessible and the area of excess Coulomb stress can be quantified. This area of excess Coulomb stress is key to evaluate the risk of fault reactivation.

All the input parameters used for MACRIS are reported in Table 7-1. One unique set of model parameters has been used in the present analysis; and thus the parameter sensitivity search has not been performed. The stress changes computed in MACRIS must be added to the initial stress tensor. In the West Netherlands Basin the minimum in situ stress is horizontal and the stress regime is extensional or normal-faulting (i.e. the largest principal stress is vertical). The largest vertical stress ( $S_v = S_{max}$ ) is calculated as the overburden weight, from seawater, rock, and pore fluid densities (see Table 7-1). The orientation of the minimum horizontal stress  $S_h$ , determined from borehole breakouts and the World Stress Map, is 55° (N55E). The magnitude of  $S_h$  is defined by applying the ratio of horizontal-to-vertical effective stress  $Ko' = S_h/S_v'$ ; a value of  $Ko' = 0.63$  is used for the analysis. Finally, the magnitude of the maximum horizontal stress  $S_H$  is defined by the ratio  $S_h/S_H = 0.9$ . It is important to note, that a single unique value of each of the parameters controlling the in-situ stress conditions (notably the orientation of  $S_h$ ,  $Ko'$  and  $S_h/S_H$ ) is used for the geomechanical analysis. In other words, a parameter sensitivity search has not been carried out. However, the input parameter values are aligned with the ones used in the geomechanical analysis of Vandeweyer et al. (2011).

Table 7-1 Input model parameters used for the MACRIS semi-analytical approach.

MACRIS model parameters	
<i>S<sub>h</sub> orientation</i>	N55E
$Ko' = S_h/S_v'$	0.63
<i>S<sub>h</sub>/S<sub>H</sub></i>	0.9
$\rho_{rock}$	2260 kg/m <sup>3</sup>
$\rho_{water}$	1150 kg/m <sup>3</sup>
$\rho_{gas}$	200 kg/m <sup>3</sup>
<i>E<sub>reservoir</sub> (Young's modulus)</i>	18GPa
<i>E<sub>overburden</sub> (Young's modulus)</i>	25GPa
<i>E<sub>underburden</sub> (Young's modulus)</i>	28GPa
<i>v (Poisson's ratio)</i>	0.2
$\mu$ (friction coefficient)	0.6
$\alpha$ (Biot's coefficient)	1.0

From the new full stress tensor, including the induced stress changes, one can derive the shear stress  $\tau$  and effective normal stress  $\sigma'$  for any fault orientations. In order to assess the potential reactivation of a fault, one needs to combine both stresses, the shear stress promoting slip whereas the normal is clamping the fault.

One convenient way is generally to calculate the Coulomb stresses  $C$  or the Fault Shear Capacity (FSC), respectively defined as:

$$C = \tau - \mu\sigma' \quad (8.1.1)$$

$$FSC = \frac{\tau}{\tau_{max}} = \frac{\tau}{\mu\sigma'} \quad (8.1.2)$$

where  $\mu = 0.6$  is the friction coefficient. When  $C$  starts to be positive or alternatively FSC reaches unit, a pre-existing fault can be reactivated since the shear stress is larger than the frictional strength defined as  $\mu\sigma'$ .

Figure 7-1 displays the initial negative Coulomb stresses (see equation 8.1.1 for the definition of the Coulomb stress) computed by MACRIS, that is before any pressure depletion. All the faults are coloured mostly in red, meaning that for all the faults and at any locations along these faults, the initial Coulomb stresses are mostly negative around minus 10-15 MPa. These negative Coulomb stresses represent the initial distance to failure, that is the required additional Coulomb stresses for the faults to be reactivated.

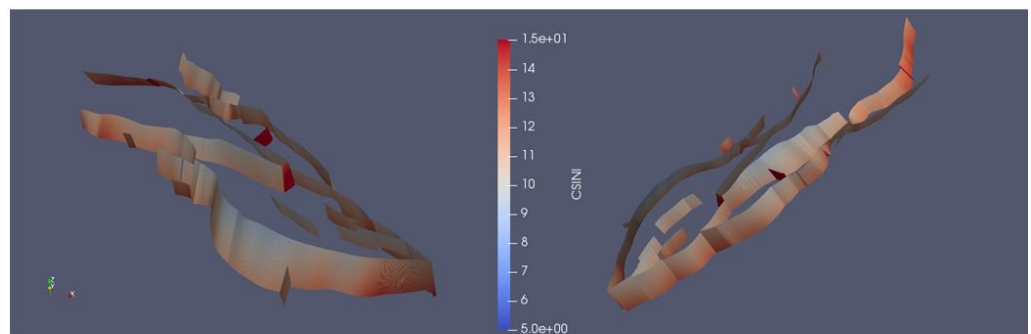


Figure 7-1: Initial distance to failure along the P18-2 faults. Colours indicate the negative Coulomb stress in units of MPa at the initialization of the MACRIS analysis, that is before any pressure depletion.

At the end of the depletion period, elongated areas of large Coulomb stress changes along the strike direction can be localized at the reservoir edges (see Figure 7-2). These areas of high Coulomb stress changes sometimes exceed the failure line (see Figure 7-3) meaning that potentially the concerned fault could be reactivated. However, as observed in Figure 7-3, most of the Coulomb stress peaks exceeding the failure line are expected to disappear during the injection period. The fault pillar displayed in Figure 7-3 is of particular interest, because it is at a close distance from a well. This aspect is further discussed in Section 7.3.

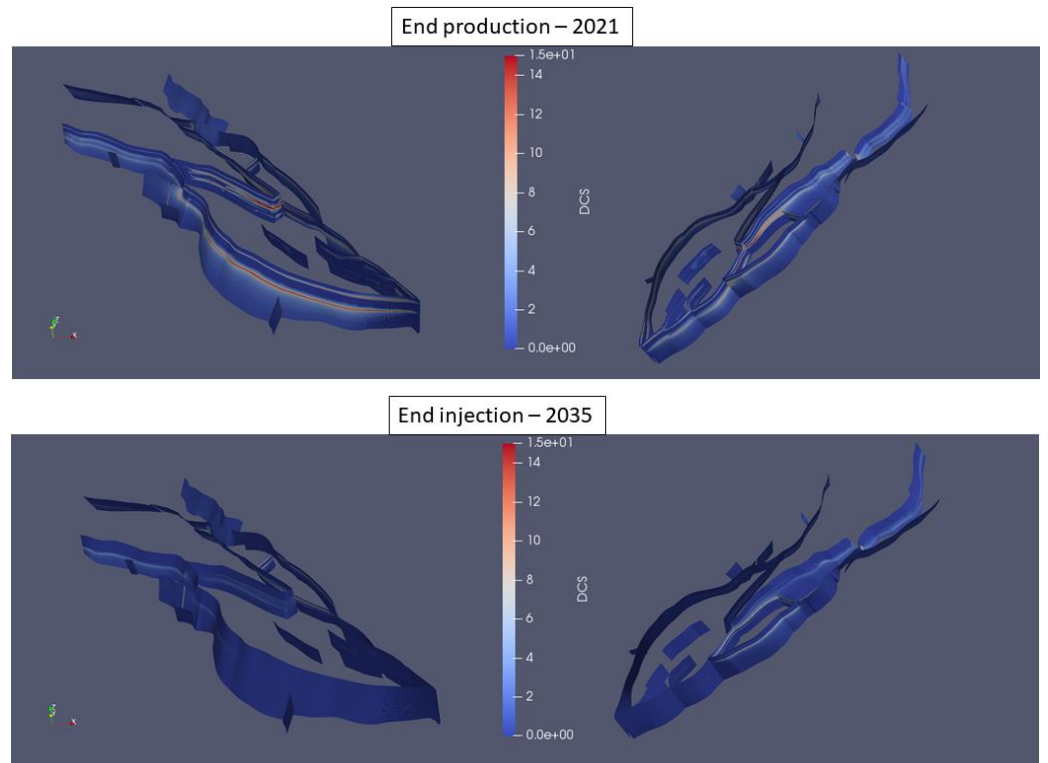


Figure 7-2 Changes in Coulomb stresses in units of MPa along the P18-2 faults inferred from MACRIS analysis.

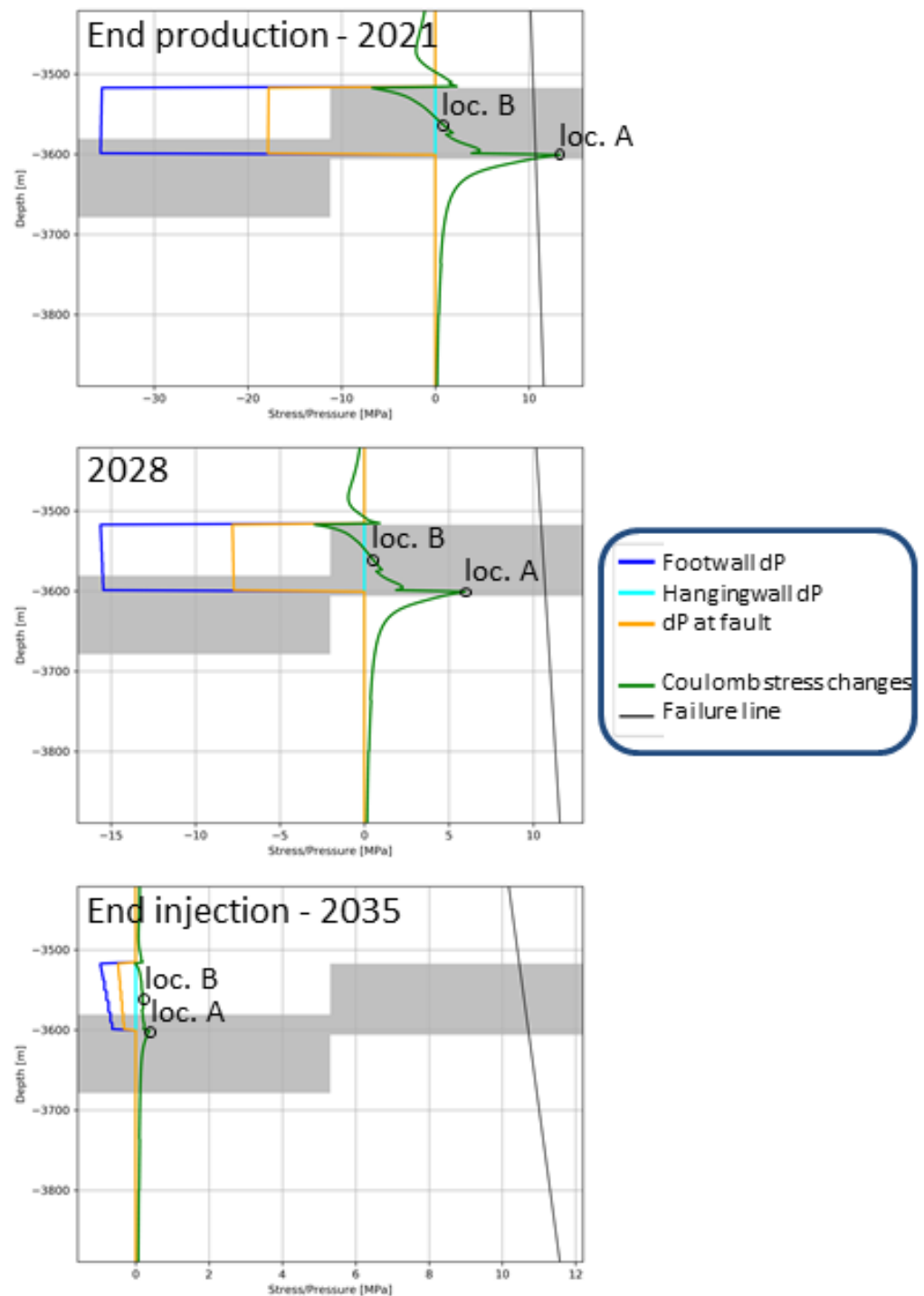


Figure 7-3 Changes in Coulomb stresses and pore pressures (inferred from MACRIS analysis) along representative fault pillars. "Footwall dP" and "Hangingwall dP" represent the changes in pore pressure in the reservoir grid blocks juxtaposed to the fault in the footwall compartment and in the hanging wall compartment, respectively. "dP at fault" corresponds to the pore pressure inside the fault, taken as the average pressure between "Footwall dP" and "Hangingwall dP". The two grey rectangles delineate the two offset reservoir compartments. At the end of the production period, changes of Coulomb stresses exceed the failure locally at one reservoir edge. This Coulomb stress peak vanishes during the injection period. Stress state at locations A and B (loc. A and loc. B) are further detailed in Figure 7-4 and Figure 7-5. For the sake of visibility, the ranges of the x-axis have been separately adjusted for each graphs.

Figure 7-4 and Figure 7-5 give more detail on the changes of the stress state during the production and injection period illustrated by Mohr circles. At locations where the Mohr circle crosses the Coulomb failure envelope, fault instability is expected. Due to the differential compaction effect, even two nearby locations along the same fault pillar can experience a contrasted stress history. Location A, at the reservoir edge, is characterized by a stress path leading to fault reactivation. Instead, for location B, in the centre of the reservoir, the stress path remains parallel to the Coulomb failure envelope.

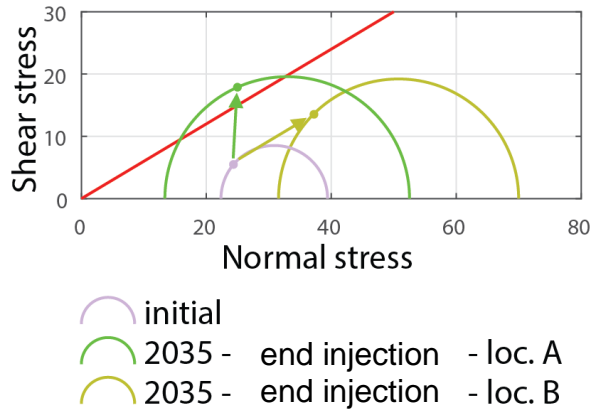


Figure 7-4 Heterogeneity of the stress field (in units of MPa) at the end of the injection period: Mohr-Coulomb analysis for two locations (loc. A and loc. B) along the same fault pillar displayed in Figure 7-3. The Coulomb failure envelope ( $\tau_{max} = \mu\sigma'$  with  $\mu = 0.6$ ) is displayed in red.

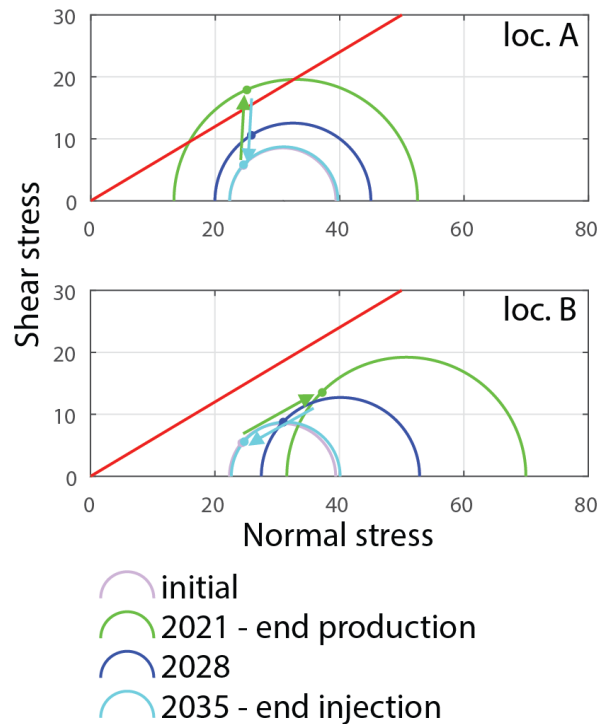


Figure 7-5 Contrast in stress path: Mohr-Coulomb analysis for two locations (loc. A and loc. B) along the same fault pillar displayed in Figure 7-3. The Coulomb failure envelope ( $\tau_{max} = \mu\sigma'$  with  $\mu = 0.6$ ) is displayed in red. In units of MPa.

Figure 7-6 is complementary to Figure 7-2, giving us access to the 3D along-strike variability of the fault reactivation likelihood. Figure 7-6 confirms that at the end of the injection period most (if not all) of the areas where the Fault Shear Capacity FSC (equation 8.1.2) is exceeded, present at the end of the depletion period, disappear. The faults are thus expected to be stable at the end of the injection period. This conclusion would only be disputed in the case of either (1) direct injection inside a reservoir fault or (2) direct flow communication between the well and a reservoir fault. Assuming we are not missing pre-existing faults in the structural reservoir model, one can already confirm that injection inside a reservoir fault is not occurring. The second scenario is also unlikely to happen since unidentified in the reservoir simulations.

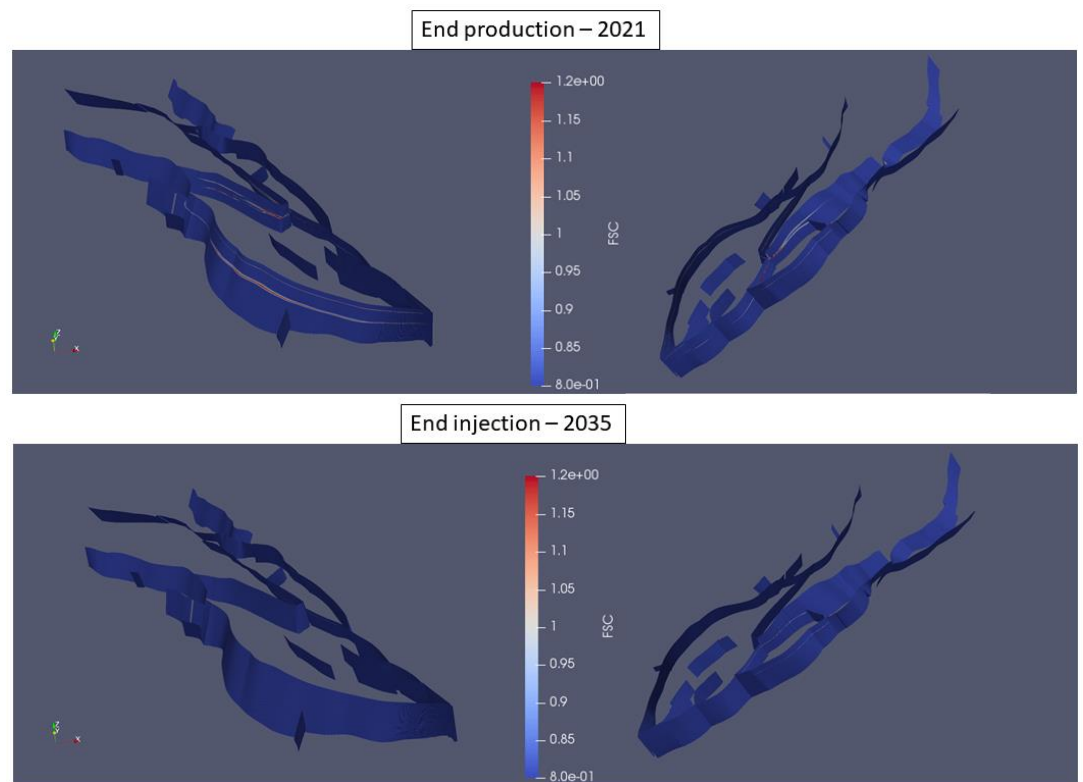


Figure 7-6 Fault Shear Capacity (FSC) along the P18-2 faults inferred from MACRIS analysis. At the end of the production period, only very locally (at the reservoir edges) the Fault Shear Capacity exceeds unity, meaning that the shear stress is larger than the frictional shear strength (“max shear stress”). During the injection period, these very local areas of exceedance of the frictional shear strength disappear.

### 7.3 Fault stability: temperature effect

Up to this point, results of the MACRIS analysis consider the pressure effect only. The temperature effect on the stability of the intra-reservoir faults is now addressed.

To answer this question, we used a TNO-developed geomechanical semi-analytical approach detailed in an Annex, Section 17.9.2. The required input for this approach is the radially symmetric temperature field resulting from the TOUGH2 flow simulation introduced in Section 6. The reader is referred to Table 7-2. for the input parameters required for this analysis. The TOUGH2 flow simulation and the



geomechanical semi-analytical approach should be seen as one-way coupled, and the temperature effect on the fluid viscosity is handled by the TOUGH2 simulator.

Table 7-2 Input model parameters used for the thermo-elastic semi-analytical approach.

Thermo-elastic model parameters	
$\Delta T$	-90°C
<i>Sh orientation</i>	N55E
$Ko' = Sh'/Sv'$	0.63
<i>Sh/SH</i>	0.9
$\rho_{rock}$	2260 kg/m <sup>3</sup>
$\rho_{water}$	1150 kg/m <sup>3</sup>
$\rho_{gas}$	200 kg/m <sup>3</sup>
<i>E (Young's modulus)</i>	18GPa
<i>v (Poisson's ratio)</i>	0.2
$\alpha_T$ ( <i>linear thermal expansion coefficient</i> )	10 <sup>-5</sup> K <sup>-1</sup>
$\mu$ ( <i>friction coefficient</i> )	0.6
$\alpha$ ( <i>Biot's coefficient</i> )	1.0

We take the temperature field after 5 years of injection as representative (see Figure 7-7). We will argue later that this is not a limitation, since the critical parameter for the risk assessment is the distance between the cooling front and a pre-existing fault.

The transient temperature field after 5 years of injection from TOUGH2 is first approximated as an homogenous cylindrical field at a temperature relative to that of the undisturbed reservoir of -90 °C, with a height equal to the reservoir height, and with a radius  $r=200m$  (see Figure 7-7). This approximation of sharp temperature front is often assumed for fast analytical approaches (Candela et al., 2018). The semi-analytical approach, detailed in Section 17.9.2, provides an estimate of the thermo-elastic stresses inside and around the cylindrical field which are induced by cooling.

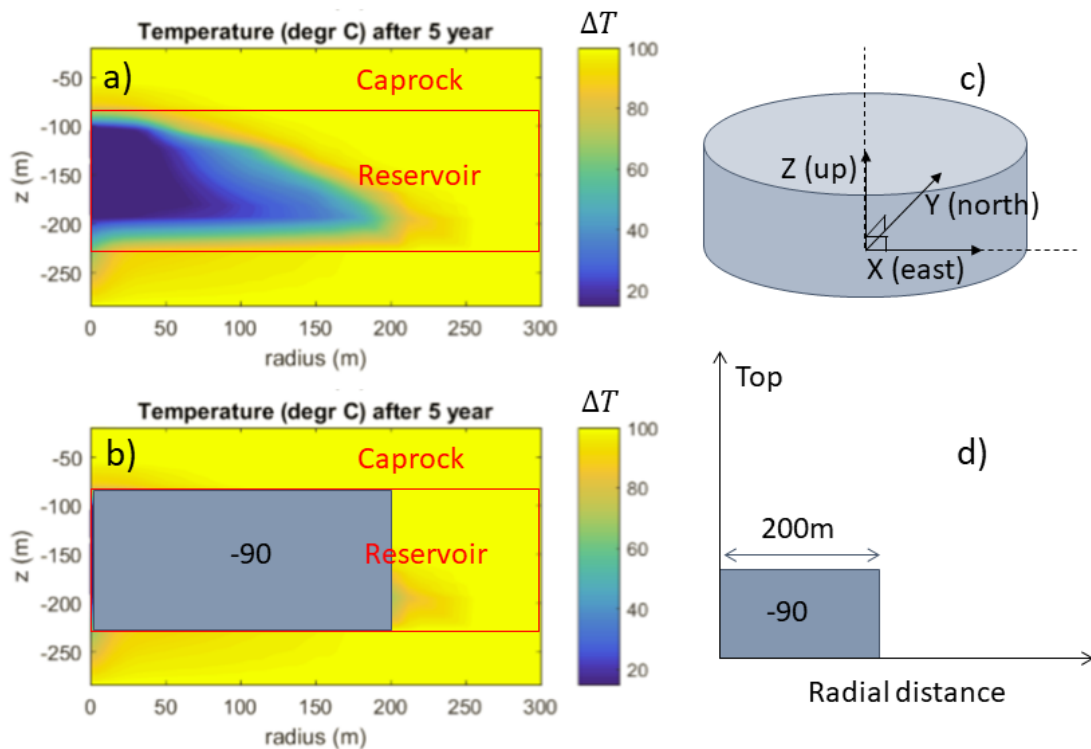


Figure 7-7 Temperature distribution and geometry of the geomechanical semi-analytical approach used to evaluate thermo-elastic stresses. a) Transient temperature field simulated by TOUGH2 (see Section 6.4.3). b) Cylindrical-shape approximation of the transient temperature field in a). The temperature change is homogeneously distributed and fixed at -90 °C. c) and d) Geometry of the geomechanical semi-analytical approach.

Following the semi-analytical approach, faults are not explicitly modelled (as it was the case in the MACRIS analysis for the pressure effect) but the changes in stress which are induced by the reservoir cooling can be calculated at any location inside the reservoir and caprock. From equation 8.1.1 the changes in Coulomb stress induced by the temperature effect at any reservoir fault can be calculated. As soon as the cooling front reaches a fault, Figure 7-8 and Figure 7-9 show that the change in Coulomb stress can reach value as high as 10MPa. This result holds for a range of fault planes orientations whom are relevant for the P18 field. Ahead of the cooling front, the thermally-induced Coulomb stresses rapidly decay; at 100 m from the cooling front the Coulomb stresses are around 2.5 MPa.

It is important to point out that even if the temperature field at the end of 15 years of injection was used as input, (instead of 5 years), the same results are expected in terms of magnitude of change of Coulomb stress inside the cooled reservoir and in terms of stress decay with distance ahead of the cooling front. The distance reached by the cooling front is then the determining parameter for the fault stability analysis. At the end of 15 years of injection, the TOUGH2 simulations (see Section 6.4) predict that the cooling front could extend as far as 300 m from the injection well after 15 years of injection. Given this constraint, only one injection well (P18-02-A-01) can be identified at a radial distance shorter than 300 m from a pre-existing identified fault cross-cutting both the reservoir and caprock (see Figure 7-3). Well P18-02-A-05ST1 is close to fault F35 (230 m), but has not been taken into account because it has a small throw (max 15 m), is an internal fault, and has

two tips. It will therefore form no baffle to flow, will not act as a pressure barrier, and will therefore not change its stress state.

However, in order to conclude about fault reactivation, if any, one needs to add to the changes in Coulomb stress the initial stress situation before injection of cold CO<sub>2</sub>. Figure 7-3 indicates this initial stress situation at the end of the production period and along the fault pillar closest to a well. As pointed before, the initial Coulomb stresses are spatially highly heterogeneous along the fault pillar; at the reservoir edge the Coulomb stresses are already reaching the failure line but some other locations are at more than 10 MPa from the failure line. Adding up the 10 MPa of thermally induced Coulomb stresses to the initial Coulomb stresses induced by the reservoir depletion, one can estimate that almost two-thirds of the fault pillar would overreach the failure line. One can thus conclude that for this particular fault close to a well, the likelihood of reactivation is high. This result will still hold even if the cooling front would reach this fault later during the injection period since the Coulomb stresses solely induced by pressure changes still remain at around 10 MPa from the failure line (see Figure 7-3). Finally it is important to repeat the limitations of TOUGH2 here; indeed, the highest temperature than TOUGH2 can model is 103 °C whereas the initial reservoir temperature was ~126 °C. One can thus expect the change in temperature to be more severe than the -90 °C used in our geomechanical semi-analytical approach; and it results that the modelled change of Coulomb stress could be even higher.

However, it is to be noted that the cooling front modelled here represents a worst-case scenario with a low probability of occurring: the cooling is due to prolonged injection of CO<sub>2</sub> at a temperature equal to the lower limit at bottom hole and at a rate corresponding to the maximum load scenario. Also, in reality one can expect a more gradual temperature front, and thus the area of excess of Coulomb stress relatively to the failure line, will be more limited in space. In other words, the potential of reactivating a pre-existing fault inside the reservoir would be confined to a small area beyond the cooling front. Finally, a solution here is to adjust the injection rate at this particular well located close to a reservoir fault. This way, the extent of the cooling front can be constrained to stay at a safe distance from the fault.

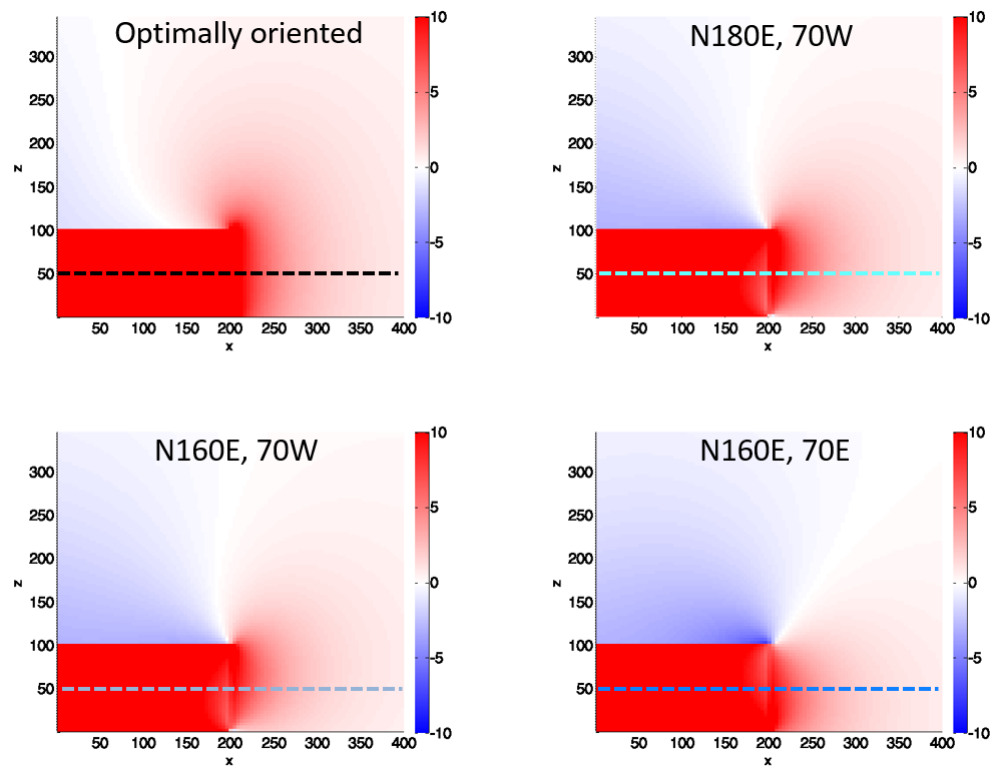


Figure 7-8 Thermo-elastically induced Coulomb stress changes in units of MPa for different fault orientation. Top left: fault planes with the highest Coulomb stress changes; Top right: fault planes with a North-South strike and dipping 70 degrees toward West; Bottom left: fault planes with a N160E strike and dipping 70 degrees toward West; Bottom right: fault planes with a N160E strike and dipping 70 degrees toward East. The model input used to generate these results is the homogenous temperature field presented in Figure 7-7. The horizontal dashed lines in the centre of the reservoir represent the stress profiles displayed in Figure 7-9.

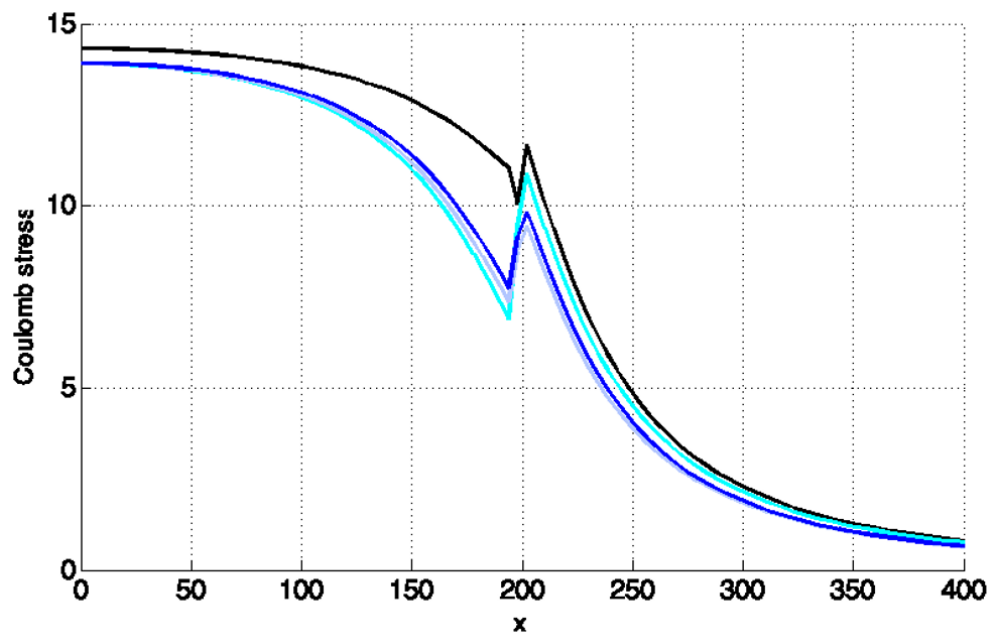


Figure 7-9 Profiles of thermo-elastically induced Coulomb stress changes in units of MPa. Each colour corresponds to each fault families presented Figure 7-8.

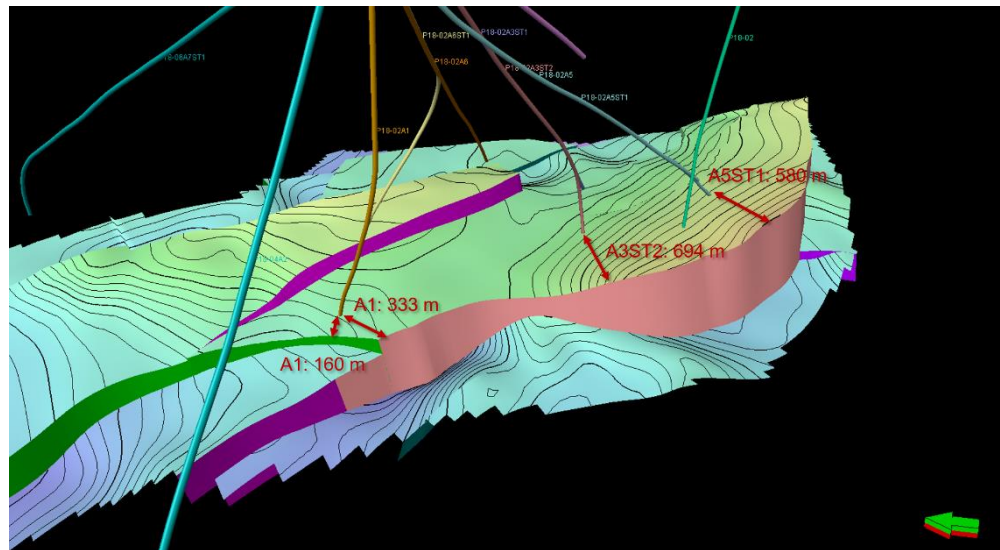


Figure 7-10 Distances faults – wells. Only in the vicinity of one well (P18-02-A-01), one fault is located at a distance smaller than 300 m.

After fault reactivation, a relevant question is about the magnitude of the induced earthquakes. To answer this question, we would need additional modelling results. However, we can shed light here on the expected end-members in terms of event magnitude. One first end-member is the case where a rupture will remain confined to the perturbed zone and thus the induced event would be small (magnitude < 1). The perturbed zone is the area of the fault already included in the cooled domain with the excess Coulomb stress. The second end-member is the case where the rupture will propagate all the way through the fault area extent. In this case, the magnitude of the event would be large (magnitude well above 1). Note here that we do not consider the case where the rupture could jump to another fault and extend even further. The reality is probably between the first and the second end-member. One dominant factor that controls the event propagation and thus its final size is the initial Coulomb stress level at the start of the fault reactivation. This initial Coulomb stress is the one at the end of the depletion period and given by the MACRIS analysis (see Figure 7-2 and Figure 7-3). Due to the differential compaction effect, this initial Coulomb stress level is spatially highly heterogeneous; with only some locations at the reservoir edge close to the failure line or already at the failure line. From this picture one can make the assumption that the propagation of an induced event will remain confined to the perturbed zone and will quickly die out outside because of the lack of high stresses to sustain its propagation. However it is important to point here again that to give a more definitive answer on the potential magnitudes of induced events, we will need to carry out new geomechanical models focusing on this particular matter.

## 7.4 Fault stability: geochemical effects

### 7.4.1 Introduction

The P18 reservoir compartments that have been assigned as potential storage reservoirs are fault bounded. These faults have effectively proven that they do not

allow across-fault fluid flow by the mere fact that they were able to support a large gas column over geologic time span. The compartments are hydraulically isolated from their surroundings due to juxtaposition of the reservoir against impermeable shales. Also several large faults intersect the compartments, such as those that subdivide the three main compartments of P18-2. Some of these faults are sealing, whereas some provide partial communication across the fault (see Section 4.2). Large-scale faults are generally surrounded by an area with a large number of smaller faults and fractures and matrix consisting of fault gouge. Instead of 'faults' we should refer to the 'fault (damage) zone' (Fisher, 2013). If porous rocks or sediments are faulted in early stages of consolidation, the damage zone generally has a lower permeability than the undeformed material (Fisher, 2013).

For storage integrity purposes, a difference should be made between sealing *across* and *along* the fault zone. Juxtaposition against a sealing formation can result in hydraulic isolation due to sealing across the fault. Yet, if the fault zone extends to above the caprock and the fault gouge is permeable, the risk of upward migration exists. In a previous analysis of migration scenarios for P18, shallow gas pockets in the overburden were found, but these most probably originated in the overlying Jurassic Posidonia shales (Vandeweyer et al., 2011). No evidence was found for gas leakage from the P18 reservoir, supporting a conclusion that the fault zones of each of the faults penetrating the caprock are sealing. The non-sealing faults might allow along fault fluid migration, but still not allow leakage towards the overburden if the fault ends within the caprock.

When CO<sub>2</sub> is injected in the reservoir, geochemical reactions between CO<sub>2</sub> and minerals within the fault might change the sealing capacity (in case of sealing faults) and/or cause reactivation. The geochemical effects of CO<sub>2</sub> on the faults, and the impact of these effects on its sealing integrity and reactivation potential need to be evaluated to assess the risk of leakage through the faults of the P18-2 reservoir and the potential of reactivation on the long term. These are described based on recent literature.

#### 7.4.2 *Geochemical effects of CO<sub>2</sub> on sealing capacity*

Where there is juxtaposition of the reservoir against impermeable shales, we can assume that the fault zone mineralogy of sealing faults is made up of crushed and mixed sandstone and shale components, whereas the non-sealing faults which did not juxtapose the reservoir against impermeable shales is made up of crushed reservoir material only. Although the Triassic sandstones have a relatively high clay content, the intra-compartment faults probably contain less clay than the compartment to shale faults. They will have comparable mineralogy, with variable mineral contents consisting of quartz, feldspars, clay minerals, carbonates, anhydrite and accessory minerals.

Similar to geochemical effects of CO<sub>2</sub> on caprock integrity, the only migration mechanism for CO<sub>2</sub> into sealing faults is by diffusion in dissolved form. Therefore, horizontal and vertical penetration of the geochemically affected zone is of the same order of magnitude as the vertical penetration into the caprock: several meters after 10,000 years. Changes in mineralogy will include partial dissolution of silicate minerals and precipitation of carbonate and clay minerals. Corresponding porosity changes will be too small to affect the sealing capacity.

A non-sealing fault zone might allow migration of supercritical CO<sub>2</sub>. Migration across the fault zones is not an issue if the compartment across the fault is also used as storage reservoir or is part of the storage complex. Migration of CO<sub>2</sub> into the fault zone could lead to enhanced chemical reactions. According to Fisher (2013), the most common type of fault gouge in Triassic reservoirs is cataclastic faults. For 19 Triassic fault gouges, gas permeability values ranged from 0.0007 to 1.8 mD (Fisher, 2013). A non-sealing fault will have a permeability at the high end of this range, but it is still a low permeability. Low flow rates will enhance self-sealing of the leak path by carbonate precipitation, especially in the presence of sufficient clay minerals which can provide the required cations for reaction with dissolved CO<sub>2</sub> to form carbonate minerals. However, the rate of self-sealing is not well known and will probably be highly dependent on many variables and fault characteristics.

#### 7.4.3 *Geochemical effects of CO<sub>2</sub> on reactivation potential*

Chemical interactions between the carbonized brine and fault zone mineralogy will result in slight mineralogical changes. These changes will only occur in the first few meters at the contact with the reservoir for sealing fault zones after thousands of years. In case of non-sealing faults, mineral reactions might have occurred across the fault zone. The chemical reactions on the long term are uncertain and will be affected by local differences in mineralogy. Overall, it is predicted that the carbonate content will increase because of the interaction with dissolved CO<sub>2</sub> with cations in the formation water, and on the long term with cations from silicate minerals. Few geomechanical studies have been done to investigate the effect of carbonate content on mechanical properties of faults. They concluded that with increasing carbonate content, fault gouge has an increased friction coefficient, indicating lower potential for fault reactivation (Samuelson et al., 2012; Adelinet et al., 2014; Bakker et al., 2016). In case fault reactivation *does* occur, higher carbonate contents increase the tendency for velocity weakening (which makes the fault weaker and sliding can continue, e.g. unstable slip) and can therefore increase the probability of microseismicity to occur (Samuelson et al., 2012). This is supported by an experimental study in which fault gouge from an outcrop which was very heavily altered by CO<sub>2</sub> interactions showed unstable slip at reservoir temperatures, whereas less heavily altered fault gouge resulted in stable slip (Bakker et al., 2016). The permeability of fault gouge material shows a tendency to decrease by orders of magnitude upon displacement during slip (Bakker et al., 2016), although it is not clear whether this occurs for both stable and unstable slip.

#### 7.4.4 *Evidence of leakage from field data*

In Arizona, USA, CO<sub>2</sub> leakage from a large natural CO<sub>2</sub> reservoir through faults was studied in order to quantify leakage rates (Miocic et al., 2019). In this specific area, faults extended from the reservoir up to the surface, and CO<sub>2</sub> rich fluids have been leaking for 420.000 years through fractures present in the damage zones around the faults. It was estimated that the average leakage rate through the faults is up to 36 kt/yr, which is less than 0.01% leakage per year for this reservoir.

In case of the P18-2 storage site, the faults do not reach the surface, but end in the Cretaceous aquifers. In a worst case, that the non-sealing faults turn out to be leakage paths, and self-sealing by carbonate precipitation does not occur, dense-phase or gaseous CO<sub>2</sub> would migrate up to the Cretaceous aquifers and dissolve into the formation water, but only if the reservoir CO<sub>2</sub> pressure is above hydrostatic

conditions (see also Section 9.3.4). From the Arizona study it was concluded that leakage along faults does not negatively impact the suitability of a reservoir from the point of view of CO<sub>2</sub> emission reductions (Miocic et al., 2019).

## 7.5 Conclusions

### *Pressure effect on fault stability*

The 4D distribution of Coulomb stresses has been computed along the mapped faults. Following the MACRIS approach, these Coulomb stresses combined (1) the poro-elastic effect, (2) the direct pressure effect at faults and (3) the effect of the fault offset. This analysis indicates that these Coulomb stresses only exceed the failure line very locally at the reservoir edge and at the end of the production phase. This outcome of our modelling workflow is supported by the fact that no tremors have been detected up to now. During the injection phase, the risk of fault reactivation due to pressure effect is even lower.

### *Temperature effect on fault stability*

In order to model the temperature effect on fault stability a TNO-developed geomechanical semi-analytical approach has been used. The distance reached by the cooling front is the determining parameter for the fault stability analysis. When the cooling front reaches a fault, the induced Coulomb stresses by the temperature effect can be such that locally, at this particular location, the fault can be reactivated. Given this distance criteria, only one single fault close to a well has been identified as potentially locally reactivated by the coupled temperature and pressure effect. Adjusting the injection rate at the particular well close to this fault can be a solution to maintain the distance of the cooling front at a safe distance from the fault. The injection simulations shown in 6.1 suggest that the injection rate in well P18-02-A-01, which is closest to faults, will be significantly lower than that of well P18-02-A-05ST: this may well satisfy this recommendation.

### *Geochemical effects on fault stability*

The impact of geochemical alterations in fault zones is unlikely to lead to CO<sub>2</sub> migration along faults. This, in turn limits the speed and depth of penetration of CO<sub>2</sub> into a fault zone, rendering the impact of chemical alterations insignificant.



## 8 Caprock integrity

### 8.1 Introduction

This section focuses on the potential reactivation of faults in the caprock due to pressure increase during CO<sub>2</sub> injection (Section 8.2), to temperature effects from the injection of low-temperature CO<sub>2</sub> (Section 8.3). Changes in pressure and temperature inside the reservoir can induce different stress changes between intra-reservoir section of the pre-existing faults and their caprock section. Section 8.4 discusses geochemical effects of interaction between CO<sub>2</sub> and the caprock.

The caprock overlying the P18-2 field has a thickness of more than 450 m. Only a few of the faults that exist in the field or that bound the field extend to above the caprock; most of the faults terminate in the caprock. While for the latter the consequences of fault reactivation are likely to be limited, the potential of fault reactivation needs to be quantified for the former.

The conclusion from the results presented below is that the risk of reactivation of faults in the caprock due to the injection of CO<sub>2</sub> is very low. The interaction between CO<sub>2</sub> and the caprock is expected to be insignificant.

### 8.2 Pressure effect on caprock integrity

This section considers the potential of destabilization of pre-existing faults inside the caprock due to the pressure effect. These faults are the ones present inside the reservoir flow model and that extend upward into the caprock. The pressure-induced Coulomb stress changes along the pre-existing fault planes are thus calculated following MACRIS analysis and is detailed in Section 7.2; implicitly it is thus also assumed that generating a new fault will require larger stress changes.

Figure 7-2, Figure 7-3 and Figure 7-6 show that the Coulomb stresses rapidly decay on top of the reservoir inside the caprock. The pressure effect is thus not expected to contribute to the risk of fault reactivation in the caprock.

### 8.3 Temperature effect on caprock integrity

A temperature decrease of reservoir rock due to the injection of relatively cold CO<sub>2</sub> induces contraction of the rock mass and a change in total stress, depending on the boundary conditions. The induced stress changes take place inside the reservoir, but also in the caprock on top of it. This section addresses the magnitude and distribution of temperature-related stress changes in the caprock. The main question addressed in this section is: what are the risks of reactivating a pre-existing fault in the caprock due to the temperature-induced stress changes?

To answer this question we used a TNO-proprietary geomechanical semi-analytical approach detailed in Section 17.9 and already introduced in the previous Section 7.3. We take as input the same temperature field after 5 years of injection as the one considered for intra-reservoir fault reactivation (see Figure 7-7).

According to the semi-analytical approach, and as mentioned previously, faults are not explicitly modelled but the changes in Coulomb stress which are induced by the reservoir cooling can be calculated for any fault orientation and at any location inside the caprock. The Coulomb stress changes are thus defined for any fault plane in the caprock; generating a new fracture will require larger shear stress than those for reactivating a fault plane. The fault planes should therefore be seen as “potential fault planes” since faults have not explicitly been identified in the seismic cube.

The results achieved (see Figure 8-1 and Figure 8-2) indicate that on top of the cooled part of the reservoir, the changes in Coulomb stress are negative. On these locations in the caprock, therefore, there is no risk of fault reactivation due to cooling of the reservoir below it. Only on top of the reservoir beyond the edge of the cooling front, the changes in Coulomb stress start to be positive (see Figure 8-1 and Figure 8-2). For our analysis we decided to pick the optimally oriented fault planes, that is for any location we picked the fault orientations where the Coulomb stress changes are maximum. Consequently, the current approach in terms of risk quantification can be seen as conservative, or worst case. However, Figure 7-8 shows that instead of considering the optimally oriented fault planes but the orientations of the P18 faults cross-cutting both the reservoir and caprock, it would have led to similar changes in Coulomb stress.

To summarize, the potential risk of reactivating a pre-existing fault in the caprock is very low.

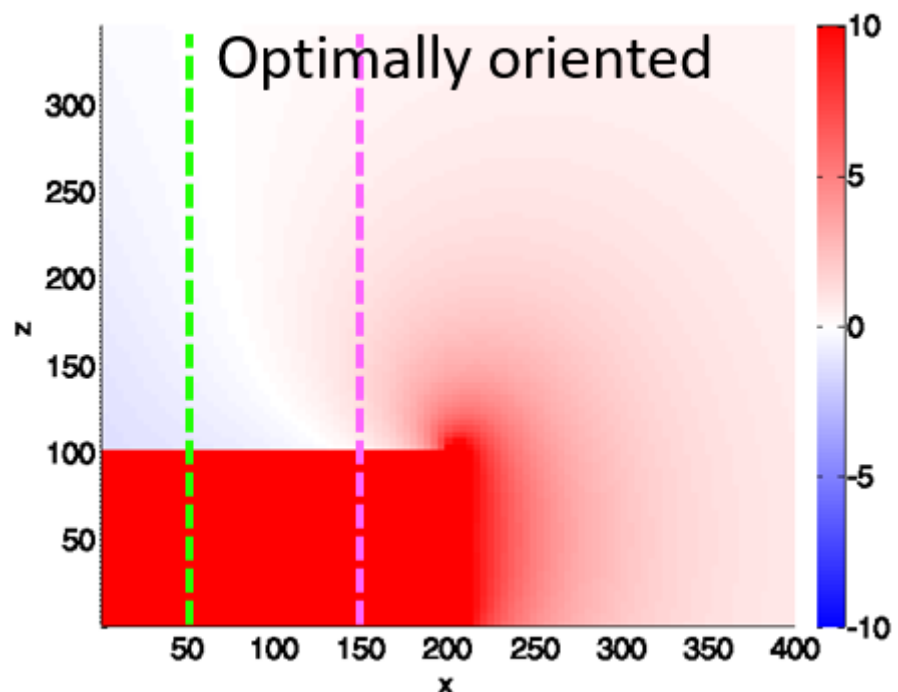


Figure 8-1 Thermo-elastically induced Coulomb stress changes in units of MPa along optimally oriented fault planes. The vertical dashed lines represent the stress profiles displayed in Figure 8-2.

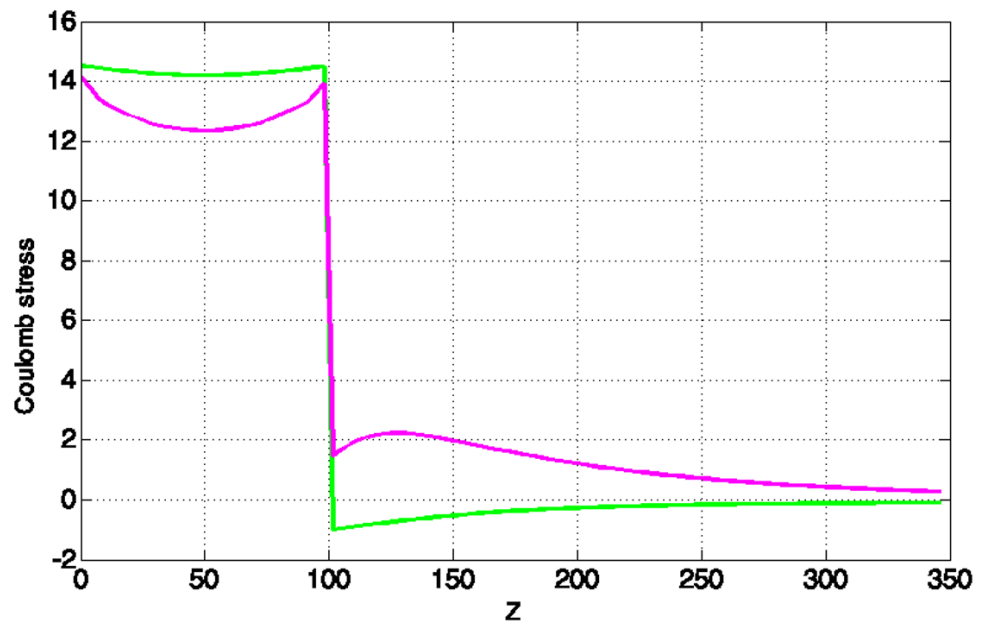


Figure 8-2 Profiles of thermo-elastically induced Coulomb stress changes in units of MPa. Each colour corresponds to different vertical cross-sections for the stress profiles as displayed in Figure 8-1.

## 8.4 Geochemical effects

### 8.4.1 Introduction

Geochemical reactions between CO<sub>2</sub> and caprock minerals can change the sealing capacity. The geochemical effects of CO<sub>2</sub> on the caprock, and the impact of these effects on its sealing integrity need to be evaluated to assess the risk of leakage through the thick caprock of the P18-2 reservoir on the long term. These are described based on recent literature.

### 8.4.2 Geochemical effects of CO<sub>2</sub> on caprock integrity

The caprock of the P18 reservoirs is made up of the Upper Germanic Trias Group and the Jurassic Altona Group. Caprock material of the P18 reservoirs has not been analysed. Caprock material of the nearby Q16 reservoir as analogue for P18 caprock was characterized by Peach et al. (2010). Eight caprock samples from the Solling and Röt Formations (both Formations belong to the Upper Germanic Trias Group) were measured for gas permeability and porosity. All permeability values were below 0.1 mD and porosity ranged between 0.02 and 5.3%. Four samples from the Röt Formation were analyzed by XRD and eight samples of Solling and Röt Formations were analysed by optical microscopy. The samples were carbonate-rich mudrocks with a mineralogy mainly made up of carbonates (ankerite or dolomite), phyllosilicates (mica and clay) and quartz (Peach et al., 2010).

The caprock of both the P18 and the Q16 gas fields has a proven sealing capacity for natural gas. Yet, CO<sub>2</sub> behaves differently than natural gas, both from physical and chemical perspective. The low permeability measured for the Q16 caprock samples justifies the assumption that penetration of CO<sub>2</sub> into the caprock will not occur, as long as the CO<sub>2</sub> pressure in the reservoir remains below the pre-production gas pressure. Specific numbers on safe CO<sub>2</sub> pressures cannot be given. However, as long as the capillary entry pressure of the caprock is not exceeded, the

only way for the CO<sub>2</sub> to migrate into the caprock is by upward diffusion in dissolved state. The diffusion is driven by increased concentration of dissolved CO<sub>2</sub> in the pore water of the reservoir and at the contact with the caprock. Tambach et al. (2012, 2015b) report on 1D reactive transport simulations that were performed with PHREEQC to assess the interaction of dissolved CO<sub>2</sub> during upward migration into the caprock. Due to the lack of detailed caprock mineralogical analysis, the mineralogy was based on samples from the adjacent P15 field, analysed and reported by Spain and Conrad (1997). The detailed analysis showed a much higher quartz content than the analyses by Peach et al. (2010). Dolomite, illite and anhydrite are present in moderate amounts, and small amounts of K-feldspar, albite, siderite and pyrite were identified. The simulation results showed that upward diffusion of dissolved CO<sub>2</sub> and the associated pH decrease is very slow. During the upward migration, mineral reactions occur to buffer the pH and convert the dissolved CO<sub>2</sub> into carbonate minerals. This further slows down the upward migration of the dissolved CO<sub>2</sub>. After 10,000 years some mineral reactions and a minor porosity increase was simulated only in the 5-10 metres above the reservoir-caprock contact (Figure 8-3). A sensitivity study on mineral types and reactive surface areas predicted a porosity increase in the bottom part of the caprock of no more than 0.7%. Only one simulation predicted a porosity decrease of 1.8% in the first metre and porosity increase up to 5 metres into the caprock (Tambach et al., 2012).

Gaus et al. (2005) found similar orders of magnitude for the extent and scale of geochemical reactions in shale caprock at the Sleipner injection site in Norway. These authors predicted either a porosity increase or decrease in the lowest few metres of the caprock, depending on the mineralogical composition of the rock, 3,000 years after injection. The predicted porosity increases are below 0.05%, porosity decreases are up to 2.6%. Depending on the type of plagioclase (albite versus anorthite; generally no distinction is made in mineralogical analyses), the migration of dissolved CO<sub>2</sub> reached either 1.5 or 10 meters into the caprock after 3000 years (Gaus et al., 2005). In the first scenario, the more reactive anorthite was able to sequester the CO<sub>2</sub> in carbonate minerals much faster, thereby retarding the upward migration of dissolved CO<sub>2</sub>. The study shows how sensitive geochemical effects are to the rock mineralogy. Generally, the exact composition of the minor minerals define the reactivity. Yet, even the more reactive compositions will not significantly affect the sealing integrity of caprocks.

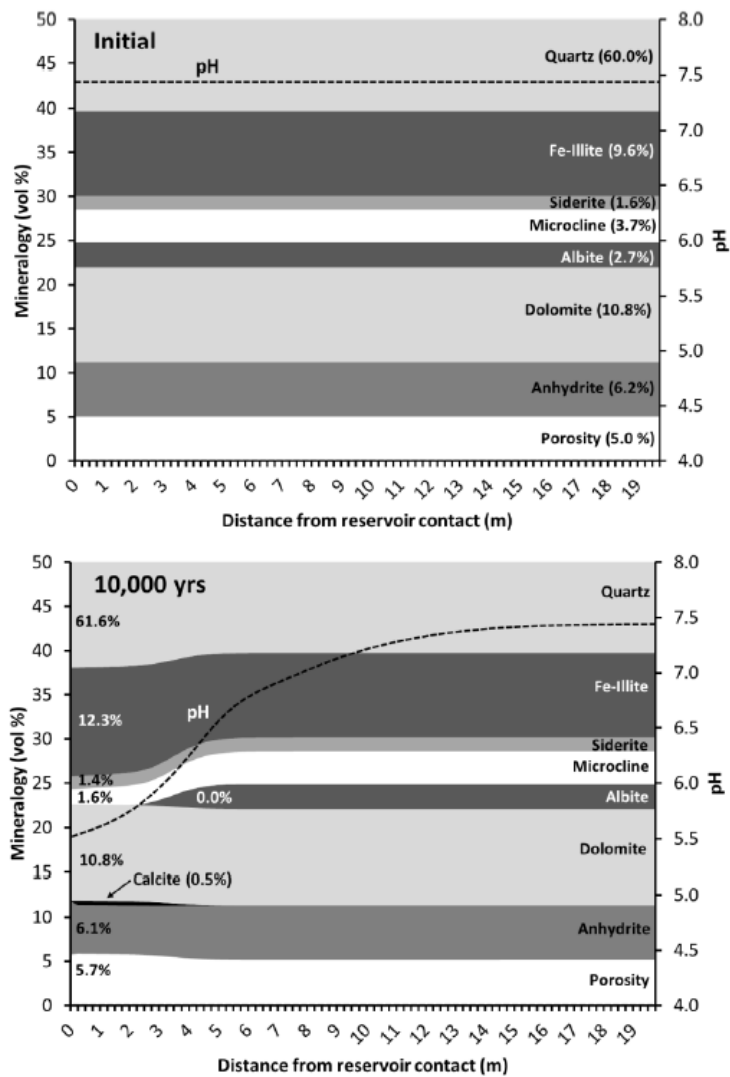


Figure 8-3: Initial mineralogy of the caprock and mineralogy after 10,000 years of simulation as a function of the distance from the reservoir contact. Up to 50 vol% is shown, the remaining part is made up of quartz. From Tambach et al. (2012).

In a more elaborate reactive transport simulation, assessing the impact of heterogeneities in shale caprock, local penetration of scCO<sub>2</sub> was predicted in areas of a caprock with lower sealing capacity (Tian et al., 2019). Local changes in porosity and permeability (both positive and negative) were predicted, related to variations in mineral compositions. Vertical migration of the scCO<sub>2</sub>, in those areas that penetration occurred, reached almost 50 m into the caprock after 500 years (Tian et al., 2019). Migration of small amounts of CO<sub>2</sub> out of the storage would take > 1,000 years (the total caprock thickness for the P18-2 reservoir is several hundreds of meters) Such a scenario represents a worst case condition, as exploration data for the P18-2 did not show any evidence for penetration of gas into the caprock, providing evidence for the overall sealing capacity of the P18-2 caprock.

## 8.5 Conclusions

*Pressure effect on caprock integrity*

Following the MACRIS approach, both induced Coulomb stresses along the intra-reservoir part of the faults and those along the intra-caprock part of the faults have been assessed. These Coulomb stresses rapidly vanish on top of the reservoir inside the caprock; the intra-caprock mapped faults are thus not expected to be reactivated by the pressure effect.

*Temperature effect on caprock integrity*

In order to model the temperature effect on pre-existing faults in the caprock, a TNO-proprietary geomechanical semi-analytical approach has been used. The geomechanical analysis shows that the risk of intra-caprock fault reactivation is very low.

*Geochemical effects on caprock integrity*

CO<sub>2</sub> is not expected to significantly interact with or migrate into the caprock.

## 9 Well integrity

### 9.1 Introduction

The wells relevant in the context of CO<sub>2</sub> injection into the P18-2 block have been evaluated regarding their current status and integrity risks. The wells considered are listed in Table 9-1, which repeats Table 4-1. The wells listed in the table are the wells that penetrate the cap rock (see Figure 4-10); wells that do not penetrate the caprock (shown in Figure 4-11) are not considered in this section.

Well integrity is considered at four levels:

- The integrity of the wells in their current state (Section 9.2);
- Mechanical effects of injecting cold CO<sub>2</sub> on the integrity of the well cement (Section 9.3);
- Geochemical processes acting on the cement (Section 9.3.4);
- Well abandonment (Section 9.4).

Table 9-1: Wells in the P18-2 compartment considered in well integrity analysis (repeats Table 4-1 in Section 4.5).

NLOG name	Taqa name	Current well status	Total Depth (m)	Potential injectors	Remarks
P18-A-01	P18-02-A-01	Producing	3840	Yes	
P18-A-03S2	P18-02-A-03ST2	Producing	4302	Yes	
P18-A-05S1	P18-02-A-05ST1	Producing	5230	Yes	
P18-A-06	P18-02-A-06	Producing	4805	Yes	
P18-A-06S1	P18-02-A-06ST1	Producing	3954	No	
P18-02	P18-02	Suspended	3766	No	Discovery well

The conclusions from the well integrity analysis are the following:

- *Well integrity.* All wells reviewed have the potential to be used safely as CO<sub>2</sub> injectors (with the exception of well P18-02, which is to be decommissioned). Appropriate mitigation measures are proposed to make them fit for storage operations.
- *Effects of injecting cold CO<sub>2</sub> on well integrity.* It is highly likely that de-bonding of cement interfaces will take place upon cold CO<sub>2</sub> injection, creating microannuli. The characteristics of the microannuli and pressure conditions determine whether upward CO<sub>2</sub> migration would actually take place. Keeping the CO<sub>2</sub> pressure in the reservoir below the hydrostatic pressure conditions will reduce the likelihood of leakage through microannuli.
- *Well abandonment.* Appropriate methods should be used for the abandonment of the wells. Given the likelihood of microannuli forming during the injection of cold CO<sub>2</sub>, abandonment methods that remove these potential leakage paths could be considered. As an example, full-bore pancake like plugs would provide formation-to-formation closure of the injection wells.

## 9.2 Status of the well barriers

### 9.2.1 *Well Integrity assessment approach*

Currently there are no specific industry standards for CO<sub>2</sub> injection wells. Therefore the approach followed in this well integrity assessment is to utilize existing oil and gas industry standards that address well integrity for injectors and complement any specific gaps for CO<sub>2</sub> injection wells if required.

The standards on which this well integrity assessment is based are:

1. NORSOK Standard D10, rev. 4 June 2013 - Well integrity in drilling and well operations (NORSOK, 2013);
2. ISO standard 16530-1:2017, March 2017 - Petroleum and natural gas industries - Well integrity, Part 1: Life cycle governance (ISO/TC 67/SC 4 Drilling and production equipment, 2017);
3. NOGEPa industry standard no. 45, 12 October 2016 - Well decommissioning (NOGEPa - OPCOM, 2016).

The reports related to well integrity and CO<sub>2</sub> storage and used for this assessment are:

4. MiReCOL report, February 2015 - D8.1 Description of leakage scenarios for consideration in the work in SP3 (Vrålstad, et al., 2015);
5. Dutch State Supervision of Mines (SSM/SodM), January 2019 – The integrity of onshore wells (SodM, 2019).

For the sake of completeness some relevant sections of the above mentioned standards and reports are presented.

1. The NORSOK D10 standard refers to well integrity by:
  - General principles: A two well barrier concept of primary barrier and secondary barrier for wells penetrating into hydrocarbon bearing formations and/or formations with the potential to flow to surface.
  - Structural integrity: the key components (conductor, guide base, risers) that provide structural integrity of the well during its service life shall be evaluated with respect to loads, wear and corrosion.
  - Injection / disposal wells: The well shall be constructed such that the injected media will be contained within the targeted formation zone (reservoir) without risk of out of zone injection.
  - WBS examples: Permanent well decommissioning (abandonment) is illustrated by a primary well barrier at caprock, secondary well barrier at intermediate section and an open hole to surface barrier.
2. The ISO well integrity standard refers to the NORSOK D10 standard and considers:
  - Structural integrity monitoring: The well operator should establish suitable systems to model or measure degradation in the structural well operating limits. The conductor, surface casing (and supporting formations) and wellhead assembly typically provide structural support for the well. Failure of these structural components can compromise well integrity and escalate to a loss of containment. For each well the well operator should assess the risk of failure of such structural components.



3. The NOGEPa no. 45 standard on well decommissioning has the following statements on well decommissioning.
  - Summarised mandatory requirements for Well Decommissioning:
    - o A permanent barrier shall extend across the full cross section of the well covering all annuli.
    - o The depth of the permanent barrier shall be selected to be adjacent to the caprock of adequate thickness with an estimated formation fracture pressure that exceeds the maximum anticipated pressure at depth.
    - o In case of cement, the permanent barrier length inside the inner wellbore shall be:
      - At least one hundred meters long (100 m), or
      - At least fifty meters (50 m) when placed on top of a tested mechanical support in cased hole.
4. The MiReCOL D8.1 report refers to Norsok D10 and includes the following information on well integrity:
  - The report considers well barrier breaches (CO<sub>2</sub> migration along the well bore) and includes the in-situ formation of the previous casing behind the liner lap as a barrier element to mitigate the risk of out of zone injection (which is conform NORSOK D10).
  - Aging issues with cement degradation, casing corrosion and wear, and thermal loads imposed on the well infrastructure are examples of the most likely causes for well leakages.
5. SodM (2019) categorizes CO<sub>2</sub> storage wells as gas wells from a well integrity perspective with the associated well failure model identifying potential leak paths, see Figure 9-1 (this is based on the ISO 16530 well failure model).

It should be noted that SodM defines the Surface tree (also known as the X-mas tree) as a secondary barrier element and the Surface Controlled SubSurface Safety Valve (SCSSSV) as primary barrier element, which is conform the NORSOK D10 standard. However, they do define failures of the tubing above the SCSSSV, the control line, tubing hanger and feedthroughs (blue items 3, 16 and 17 in Figure 9-1) as primary leakage elements, which is a variation on the NORSOK D10 standard. In this report NORSOK D10 is primarily followed, as a result all elements above the SCSSSV are considered to be secondary barrier elements (because they are isolated in the event of an SCSSSV closure).

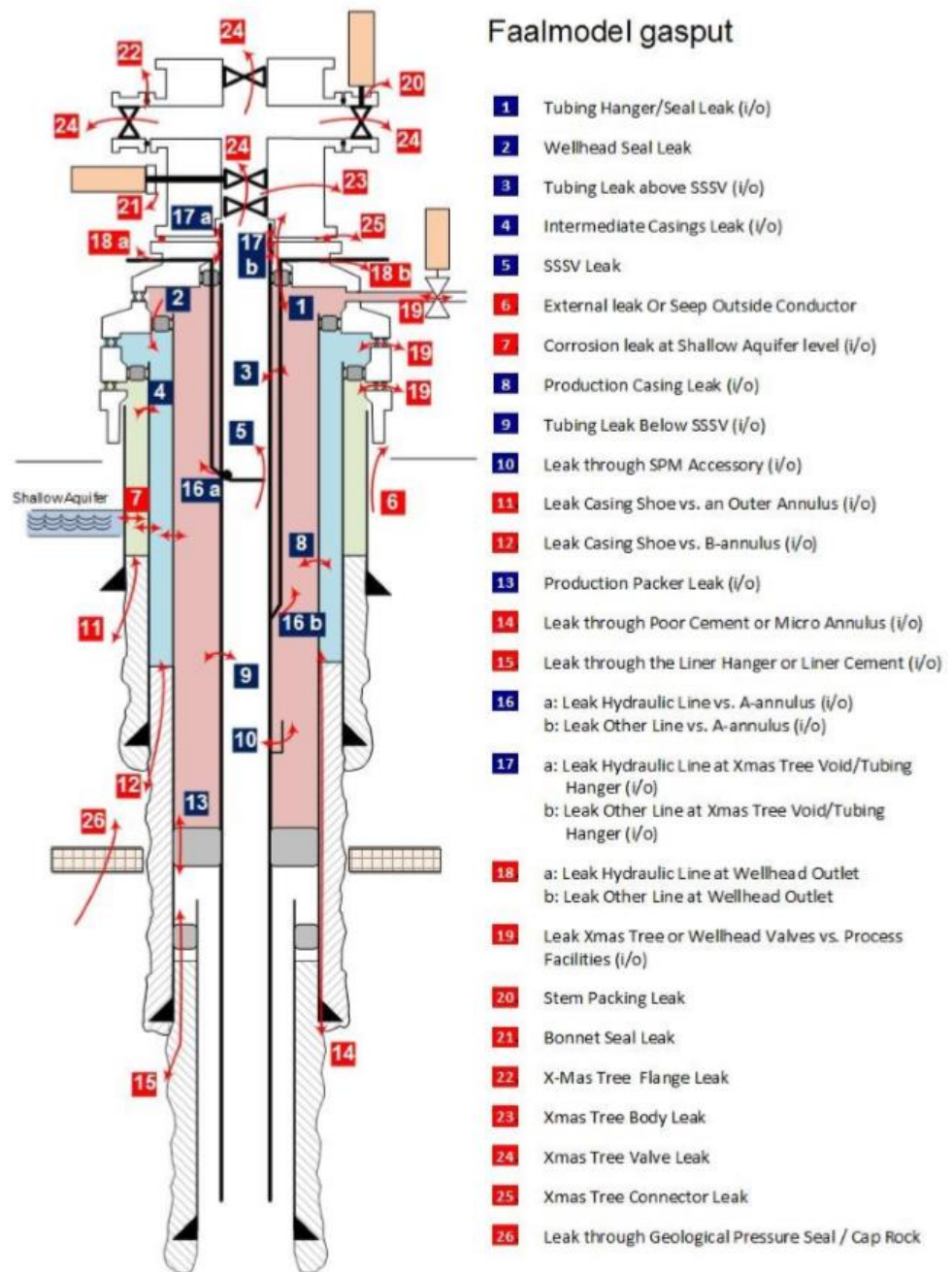


Figure 9-1 Well failure model for gas wells, including storage wells. (SodM, 2019). The blue numbers are primary barrier element failures and the red numbers are secondary barrier element failures.

9.2.1.1 Well integrity assessment concept

Based on the reviewed standards and reports, the scope of the well integrity assessment in this report includes and reviews the following elements:

- a) The primary and secondary well barrier elements from reservoir caprock to surface, conform NORSOK D10.

- b) The risk of out of zone CO<sub>2</sub> injection due to a failure of a primary and/or a secondary barrier, with supporting in-situ formation of the previous casing below the liner lap.
- c) Structural integrity of the load bearing surface casing, conductor or riser.

The definition of the barrier elements for this assessment comes from NORSOK D10.

- Primary well barrier: first well barrier that prevents flow from a potential source of inflow.
- Secondary well barrier: second well barrier that prevents flow from a potential source of inflow.

The structural integrity assessment of the load bearing surface casing is for this assessment limited to a review of the “as built” status, identifying the potential well integrity risk.

It should be pointed out that the assessment of the influence of fatigue or corrosion on well integrity, with the structural load effects and associated thermal and pressure cycles, is not in the scope of the current work. This should be considered as the next fundamental step in assessing the structural well integrity lifecycle for the CO<sub>2</sub> injection program.

#### 9.2.2 *P18-2 well integrity analysis*

The P18 fields have been subjected to CO<sub>2</sub> storage assessment and well integrity evaluations in the CATO-2 R&D programme (Akemu, et al., 2011). The previous well integrity assessment focused on the P18-4 field and identified and evaluated barriers of wells relevant for the foreseen storage operation and identified gaps or uncertainties about barrier status in general. Based on this previous study it was not possible to decide on the suitability of the P18-2 wells for CO<sub>2</sub> injection and storage given the new operating envelope. The present assessment is based upon the previous work and addresses the gaps that were identified earlier. It considers new findings, as well as information that was not available at the time of the first studies.

The present study includes:

- An assessment of the wells penetrating the P18-2 reservoir;
- An assessment of earlier identified gaps, by detailed review of the end-of-well reports (EOWR), newly obtained records and quantification of the relevant barrier elements for the primary, secondary and structural barriers in place;
- Illustrations of well barrier envelope status in well barrier diagrams combined with potential risks for each barrier, with the aim to assist selecting suitable wells for injection of CO<sub>2</sub> in the P18-2 reservoir.

The wells relevant for the planned storage were re-evaluated. The scope of the assessment includes the following wells: P18-2A1, P18-2A3-ST1-2, P18-2A5-ST1, P18-2A6-ST1 and P18-2 (suspended well).

#### 9.2.3 *General well integrity P18-2 and well status issues*

The status of the wells penetrating the P18-2 reservoir that emerges from the review of previous work is as follows:

- a) The wells have not been assessed for the well completion load case for CO<sub>2</sub> injection with respect to temperature and pressure, except for the P18-4A2 well.

- Previous assessment (Akemu, et al., 2011) indicates that the type of retrievable production packers used in P18-2 wells will unseat when injecting cold CO<sub>2</sub>.
- b) The same type of retrievable production packers has been used in the other P18-2 wells identified for CO<sub>2</sub> injection, no well completion load case assessment has been done so far for these wells.
  - c) No assessment records were found on the lifecycle assessment of load bearing surface casing and conductor. External corrosion due to corrosive fluids and metocean induced fatigue of the load bearing casing could reduce its lifecycle load capacity. This is a fundamental requirement to assess the lifecycle of the well and the risk of loss of well integrity.
  - d) The bond logs for cement have been assessed previously (Akemu, et al., 2011); in the review the interpretation method has been verified and found to be correct.
  - e) The expected final CO<sub>2</sub> reservoir pressure for P18-2 is maximised at initial pressure (see Section 5.4); this has been considered in the assessment of individual barriers.
  - f) The surface tree material, trim and temperature classification must be validated against the operating envelope associated with injection of CO<sub>2</sub>.
  - g) The material specifications of the flow wetted barrier elements like surface tree, tubing hangers, completion accessories and seals / elastomers need to be validated against the CO<sub>2</sub> injection operating envelope.
  - h) Akemu et al. (2011) report that 5", 13Cr-L80 completions are installed. However, in this assessment it has been concluded that the completions are actually 5½", 13Cr-L80 for P18-2A1, P18-2A3 and P18-2A6, the P18-2A5 well is completed with a 7", 13Cr-L80 completion combined with a 5 ½", 13 Cr-L80 SCSSSV section.

The assessment of the individual wells is presented in sections 9.2.4 to 9.2.8.

#### 9.2.4 *Well P18-2-A1*

A well barrier diagram with well barrier envelopes and elements defined for well P18-2-A1 is provided in Figure 9-2, the evaluation of the elements can be found in Table 9-2. The evaluation of the well integrity barriers leads to the following observations.

##### Primary barrier

- The EOWR (End of Well Report) states that the 7" liner was run and installed for later production. The cement report in the EOWR of P18-3, that was later renamed to P18-2A1, shows a good cement job with a calculated top of cement reported to be at 3508 m MD. The well status diagram has recorded the TOC at 3477 m MD, this is a discrepancy in the reporting. For this assessment the depth reported in the cement report (3508 m MD) is taken because that represents the worst case scenario (cement report). The cement bond log (CBL) on the 7" liner cement, indicates poor bonding.
- No A-annulus pressures or pressure build-up has been reported, this has also been confirmed by the TAQA annular pressure history.
- The production packer is installed in a liner with a poor cement bond according to the bond log, this puts the packer with liner and liner cement as barrier elements at risk.

##### Secondary barrier

- The liner lap is positioned above the packer, the liner as barrier element is at risk, due to possible corrosion behind the carbon steel liner as a result of the poor cementation (bond log) and presence of CO<sub>2</sub> in the production life of the well and during future CO<sub>2</sub> injection.
- The liner lap was not tested upon installation. However, the liner lap is exposed to a hydrostatic overbalance of completion brine in the production annulus that confirms liner lap integrity. The current overbalance is estimated to be about 4060 psi (~280 bar) based on assumed annulus completion brine with a density of 1.10 s.g. and a reservoir pressure of 1230 psi (85 bar).
- The 9 5/8" casing shoe has a Formation Integrity Tests (FIT) reported that is above the final CO<sub>2</sub> storage reservoir pressure. The EOWR mentions for the cement job of the 9 5/8" casing a bump plug pressure of about 2000 psi (140 bars). There is no top of cement (TOC) reported in EOWR, the well status diagram shows the TOC at seafloor level.
- The 9 5/8" casing penetrates two formations with natural formation sealing potential (natural swelling clay); the Vlieland and Aalburg shales. These could improve the sealing performance over time (Fischer, et al., 2016).

#### Structural well integrity:

- The 13 3/8" casing is placed at 1963 m MD and had a successful FIT of 13.8 ppg, the casing is cemented to 175 m MD (calculated depth).
- The 20" casing is set at 404 m MD and is cemented to seafloor.
- The 30" conductor is piled to 131 m MD.

From a structural load bearing capacity point of view there appears to be adequate cement overlap to transfer the well loads. The 20" casing is cemented to seafloor this leaves the 20" casing inside the conductor exposed to potential risk of corrosion of the fluids in the conductor annulus from wellhead to seafloor, this needs to be verified.

#### Discrepancies:

- Akemu et al. (2011) reports a pressure test of 5000 psi (~345 bar) for the 9 5/8" casing and the 7" liner. The EOWR only reports a 9 5/8" pressure test to 5000 psi (~345 bar) prior to liner installation.
- Akemu et al. (2011) reports the production tubing to be 5", 13Cr-L80, in this study it was confirmed to be 5½", 13Cr-L80.
- The EOWR reports a calculated TOC for the 7" liner at 3508 m MD, the well status diagram shows the TOC at 3477 m MD.
- The EOWR has no report on top of cement (TOC) for 9 5/8" casing, the well status diagram shows the TOC at seafloor.

#### Summary

- The well currently appears to have no apparent leaks.
- From Table 9-2 can be seen that most barrier elements have been validated, except for the cement behind the 7" liner, there is a discrepancy on the TOC level in the 7" liner cement report and well status diagram of 31 m.
- The low quality of the 7" liner cementation at packer depth, combined with the fact that the 7" liner is made of carbon steel material, poses the risk of external degradation due to corrosion from potentially corrosive reservoir fluids. This would require mitigation, possibly by recompletion i.e. repositioning of the production packer into a liner / casing with a good cement bond.

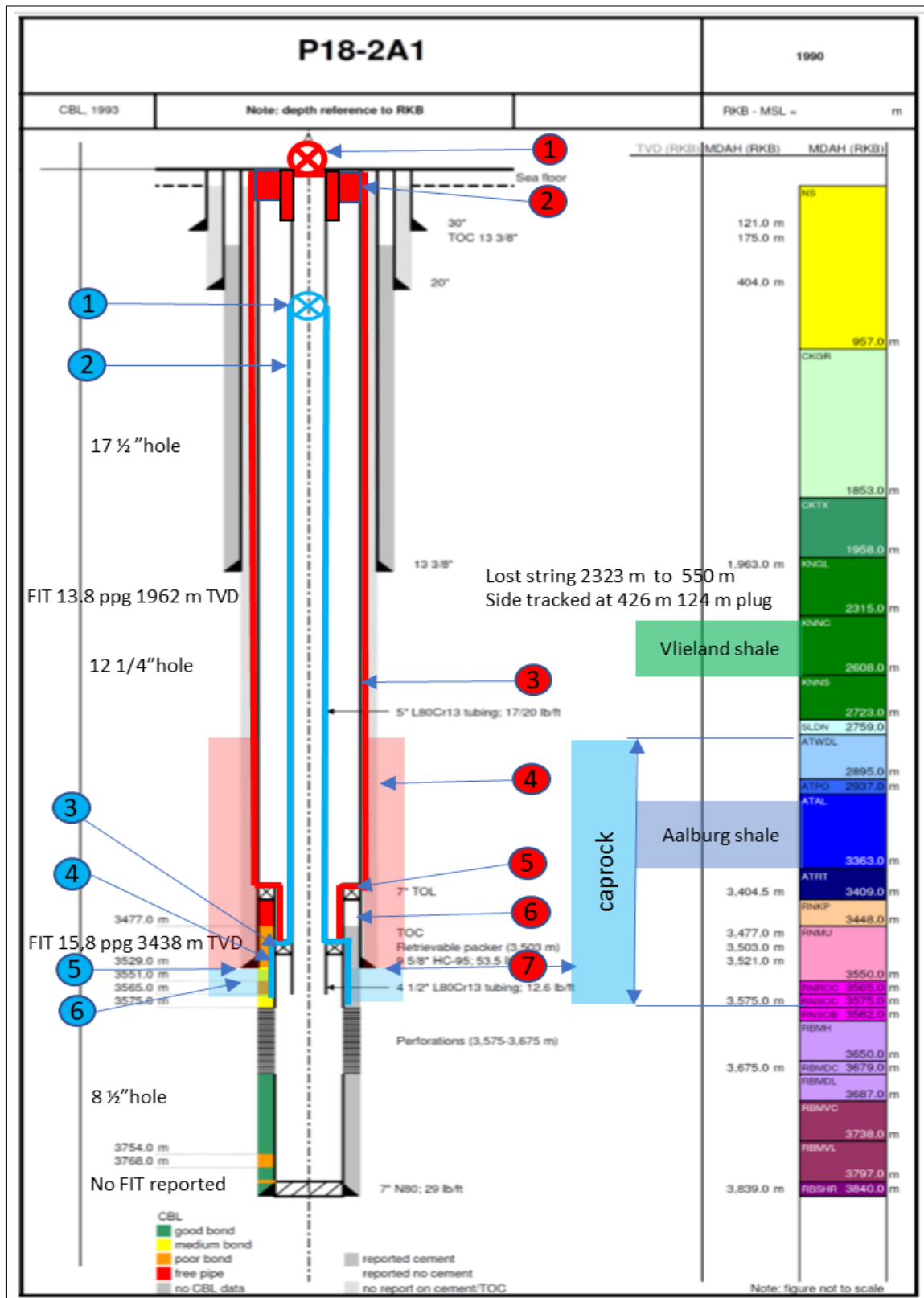


Figure 9-2 Well P18-2A1 barrier diagram with barrier elements defined. See Table 9-2 for a discussion of the barrier elements (indicated by the numbered circles).

Table 9-2 Well P18-2A1 barrier element assessment based on current data set. The numbers in the first column correspond with the numbers in coloured circles in Figure 9-2.

no	P18-2A1 Element	As built	Monitor	Barrier validated	Validation Criteria
<b>Primary well barrier</b>					
1	5 1/2" Scssv	Tested to 5000 psi	Maintained	Yes	Tested & maintained
2	5 1/2" Tubing	Tested to 5000 psi	Annular pressure records	Yes	Tested, no annular pressure build up reported
3	7" Production packer	Installed at 3503 m MD which is 26 m below the TOC in the 7" liner. Tested to 5000 psi	Annular pressure records	Yes	Tested, no annular pressure build up reported.
4	7" Liner	Liner report for P18-3 (previous name of P182A1) The liner covers 50 m of caprock	NA	Yes	The liner and production packer are under continuous high hydrostatic differential pressure of the A annulus. No annular pressure build up recorded
5	In-situ formation (Cap rock)	FIT of 15.8 ppg at 3488 m TVD	NA	Yes	FIT of 15.8 ppg at 3488 m TVD reported
6	7" Liner cement	Cement report of P18-3 (previous well name) reports the TOC at 3508 m MD. The well status diagram shows the TOC at 3477 m MD. The CBL indicates a poor bond	NA	No	The well status diagram shows the TOC 3477 m MD. The CBL indicates a poor bond. The TOL is set at 3404 m MD, this leaves 73 m of uncemented liner combined with poor bond.
<b>Secondary well barrier</b>					
1	Surface tree & tubing hanger	Tested to 5000 psi	Maintained	Yes	Tested & maintained
2	Well head & casing hanger	Tested to 5000 psi	Maintained	Yes	Tested & maintained
3	9 5/8" Casing	Tested to 5000 psi	Annular pressure records	Yes	Tested, no annular pressure build up reported
4	9 5/8" Casing cement	Cement report does not provide a TOC, the report quotes for the 9 5/8" cementation: minimal losses during circulation, cementation in 2 stages with 2000 psi bump plug pressure	Annular pressure records	Yes	Good cement report on placement of cement in caprock NFS potential - Vlieland shale & Aalburg shale
5	7" Liner + liner lap	The CATO-2 report (Akemu et al. 2011) quotes a 5000 psi test that is not mentioned in the end of well report.	Annular pressure records	Yes	The liner is tested by default; the differential pressure from annulus to reservoir by hydrostatic column is approximately 280 bar
6	7" Liner cement	The cement report of P18-3 (previous well name) reports the TOC at 3508 m MD. The well status diagram shows the TOC at 3477 m MD. The CBL indicates a poor bond	Annular pressure records	No	The well status diagram shows the TOC 3477 m MD. The CBL indicates a poor bond. There is 47 m of uncemented liner above the production packer
7	In-situ formation (Cap rock)	FIT of 15.8 ppg at 3438 m TVD	NA	Yes	FIT 15.8 of ppg at 3438 m TVD reported

### 9.2.5 Well P18-2A3-ST2

A well barrier diagram with well barrier envelopes and elements defined for well P18-2A3-ST2 is provided in Figure 9-3, the evaluation of the elements can be found in Table 9-3. The evaluation of the well integrity barriers leads to the following observations.

#### Primary barrier:

- The 7" liner is installed with the casing shoe in the caprock. According to the EOWR it shows a good cement job. The in-situ formation integrity test (FIT) of 15 ppg at 3269 m TVD and a 4000 psi (272 bar) casing test confirmed the integrity of these elements.
- There has been no pressure build-up reported for the A-annulus, this has been confirmed by the TAQA annular pressure history.
- The retrievable production packer has been installed in the 7" liner with a good cement bond at about 200 m below TOC / top of liner.
- The side track (ST-1) was drilled to 3718 m MD and plugged back from 3425 m MD due to a lost drilling assembly with a length of 4.65 m. The well was side tracked (ST-2) again from 3375 m MD, this leaves an 8 1/2" open borehole of ST-1 from 3718 m MD to 3425 m MD that penetrates 177m of caprock. The caprock is present from 3375 m MD to 4070 m MD, given the penetration of 343 m, this leaves 352 m of caprock in place. The production packer (primary barrier) is positioned at 3715 m MD. The ST-1 borehole extends 3 m below this

depth, therefore ST-1 appears to be well isolated and is not considered a risk from a well integrity perspective, mainly because of a good 7" liner cementation.

#### Secondary barrier:

- The 7" liner has a good cementation in accordance with the EOWR, cement was properly displaced and positively pressure tested, the risk of liner lap failure above the production packer is mitigated by the 7" integrity status.
- The 9 5/8" casing shoe has a FIT that is above the final CO<sub>2</sub> storage reservoir pressure. The EOWR reported a good cement job with TOC of 1806 m MD.
- Two formations with natural formation sealing potential are penetrated by the well, the Aalburg shale that covers the 7" liner and the Vlieland shale that covers the 9 5/8" casing shoe, and part of the 7" liner. These could improve the sealing performance over time.
- In the original hole before (ST-1), is a lost drill string positioned with top cemented and cased off. This provides a conduit from 2323 m to 550 m outside the existing wellbore, this conduit does not penetrate the caprock and is not considered as a risk.

#### Structural well integrity:

- The 13 3/8" casing is placed at 1806 m MD and had a successful FIT of 13 ppg, the casing is cemented to 151 m MD calculated.
- The 20" casing is set at 408 m MD and is cemented to seafloor.
- The 30" conductor is piled to 132 m MD.

From a structural load bearing capacity point of view there appears to be adequate cement overlap to transfer the well loads. The 20" casing is cemented to seafloor this leaves the 20" casing inside the conductor exposed to potential risk of corrosion of the fluids in the conductor annulus from wellhead to seafloor, this needs to be verified.

#### Discrepancies:

- Akemu et al. (2011) report the production tubing as 5", 13Cr-L80 but it was confirmed in this study to be 5½", 13Cr-L80.

#### Summary

- The well currently appears to have no apparent leaks.
- From Table 9-3 can be seen that all barrier elements have been validated.
- The CO<sub>2</sub> injection load case capacity and the material compatibility for the retrievable packer to be assessed and potentially to be mitigated to make this well a suitable CO<sub>2</sub> injector.



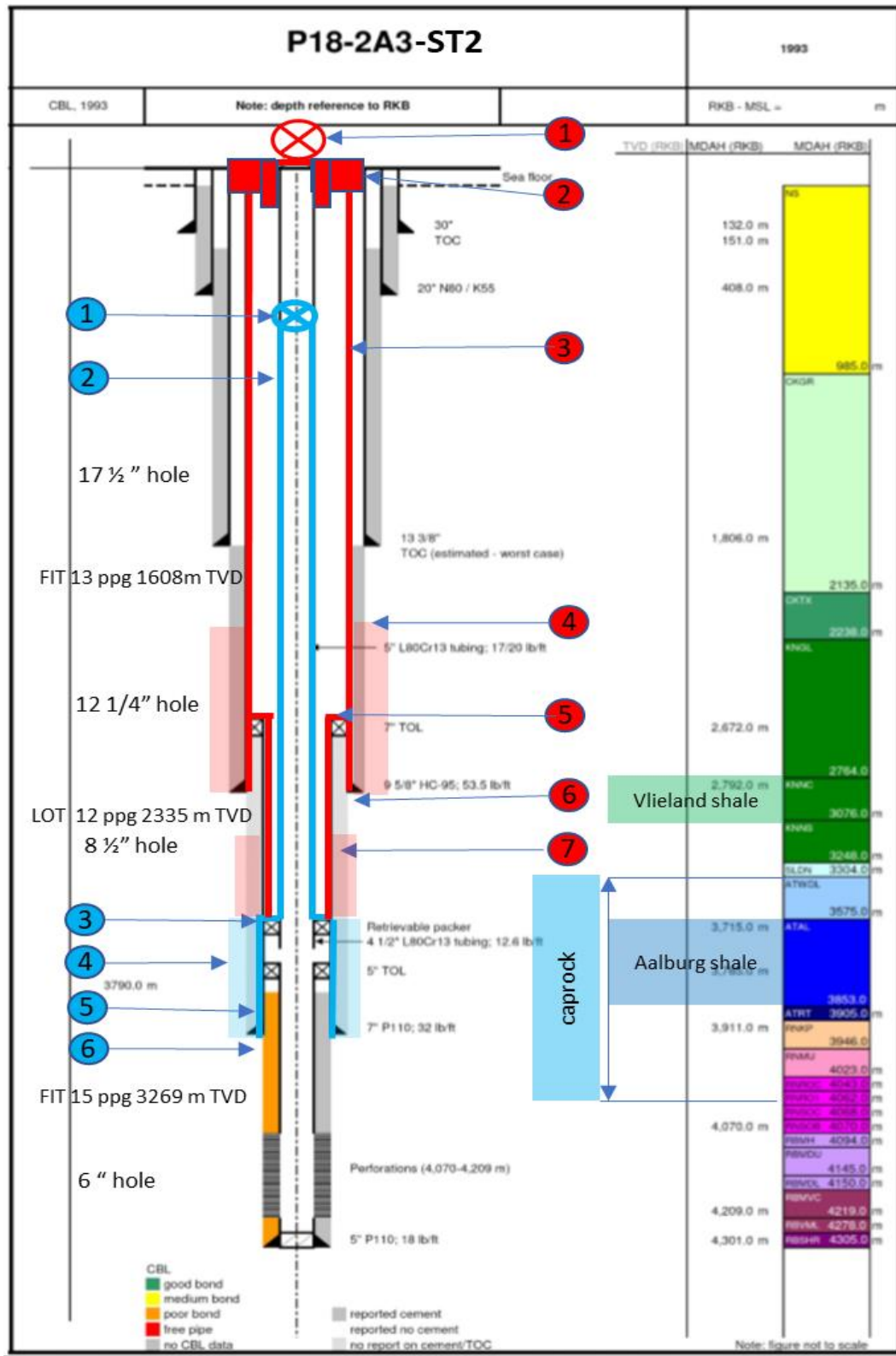


Figure 9-3 Well P18-2A3-ST2 barrier diagram with barrier elements defined. See Table 9-3 for a discussion of the barrier elements (indicated by the numbered circles).

Table 9-3 Well P18-2A3-ST2 barrier element assessment based on current data set. The numbers in the first column correspond with the numbers in coloured circles in Figure 9-3.

no	P18-2A3-ST2 Element	As built	Monitor	Barrier validated	Validation Criteria
<b>Primary well barrier</b>					
1	5 1/2" Scsssv	Tested to 5000 psi	Maintained	Yes	Tested & maintained
2	5 1/2" Tubing	Tested to 5000 psi	Annular pressure records	Yes	Tested & no annular pressure build up reported
3	7" Production packer	Retrievable packer that is tested	Annular pressure records	Yes	Tested & no annular pressure build up reported
4	7" Liner cement	Cement was fully displaced	Annular pressure records	Yes	Good cement report Identified NFS potential - Aalburg shale
5	7" Liner	Tested to 4000 psi	Annular pressure records	Yes	Tested & no pressure in annulus reported
6	In-situ formation (Caprock)	FIT of 15 ppg at 3269 m TVD	NA	Yes	FIT of 15 ppg at 3269 m TVD reported The plugged back side track 1 did not fully penetrate the caprock, there is 468 m of undisturbed caprock in place
<b>Secondary well barrier</b>					
1	Surface tree & tubing hanger	Tested to 4000 psi	Maintained	Yes	Tested & maintained
2	Wellhead & casing hanger	Tested to 4000 psi	Maintained	Yes	Tested & maintained
3	9 5/8" Casing	Tested to 4000 psi	Annular pressure records	Yes	Tested to 4000 psi, no annular pressure build up reported
4	9 5/8" Casing Cement	The TOC is estimated to be at 1806 m MD. A top up job of 13 3/8" by 9 5/8" annulus has been reported	Annular pressure records	Yes	Cement was displaced and tested
5	7" Liner + liner lap	Tested to 4000 psi	Annular pressure records	Yes	Tested to 4000 psi, no annular pressure build up reported
6	In-situ formation	LOT of 12 ppg at 2335 m TVD	NA	Yes	LOT of 12 ppg at 2335 m TVD reported Identified NFS potential - Vlieland shale
7	7" Liner cement	The TOC is calculated to be at the top of liner at 2672 m MD. The plug is bumped with 800 psi pressure, the reported over-displacement pressure was 2400 psi	Annular pressure records	Yes	Good cement report Identified NFS potential - Aalburg shale

### 9.2.6 Well P18-2A5-ST1

A well barrier diagram with well barrier envelopes and elements defined for well P18-2A5-ST1 is provided in Figure 9-4, the evaluation of the elements can be found in Table 9-4. The evaluation of the well integrity barriers leads to the following observations.

#### Primary barrier

- The 7" liner is placed almost entirely in the caprock. The liner has a good cement report and CBL assessment. The TOC was calculated to be at 3805 m MD and this has been confirmed by a log, the liner was tested to 5000 psi (~345 bar).
- The Aalburg shale, a potential naturally sealing formation, covers the 7" liner and potentially provides additional support for the good cement.

#### Secondary barrier

- There is a sustained casing pressure reported up to 610 psi (42 bar), that is bled down to 100 psi (7 bar). In the annular pressure history has been found that this pressure has been up to 98 bar, which is within the Maximum Allowable Annular Surface Pressure (MAASP) of 1650 psi (114 bar). The source of the annular pressure build-up is assumed to be from the casing side as the hydrostatic pressure in the production casing exceeds the tubing pressure at packer depth. Mainly fluid returns were found when bleeding off the pressure. No further investigation has been undertaken to date.

- The 9 5/8" casing has a good cement job with the TOC reported at 2338 m MD.
- The 9 5/8" casing shoe has a FIT that is above the final CO<sub>2</sub> storage reservoir pressure.
- The potential natural sealing formation Vlieland shale covers part of the 9 5/8" casing.

It should be pointed out that the original bore hole has a lost drilling assembly that is plugged back with cement and is positioned with the top of fish at 3900 m to 4404 m MD, this penetrates the caprock to 4404 m. The bottom of the caprock is at 4800 m MD, this leaves 400 m of undisturbed caprock in place and is not considered a risk.

#### Structural well integrity:

- The 13 3/8" casing is placed at 2488 m MD and had a successful FIT of 12.3 ppg, the casing is cemented to 991 m MD calculated, an ECP is set at 942 m MD.
- The 20" casing is set at 991 m MD and is cemented to main sea level according to well status diagram, the EOWR does not contain a cement report on the 20" casing.
- The 30" conductor is piled to 131 m MD.

From a structural load bearing capacity point of view there appears to be adequate cement overlap to transfer the well loads, the 20" casing is cemented to main sea level this leaves the 20" inside the conductor exposed to potential risk of corrosion of the fluids in the conductor annulus from wellhead to mean sea level, this needs to be verified.

#### Discrepancies:

- Akemu et al. (2011) reports the production tubing to be 5", 13Cr-L80, but it was confirmed in this study to be a 7", 13Cr-L80 completion, with a 5 1/2", 13Cr-L80 SCSSSV and a 5 1/2", 13Cr-L80 tubing to surface.

#### Summary

- From Table 9-4 it can be seen that most barrier elements have been validated, with the exception of the secondary barrier 9 5/8" casing due to the sustained casing pressure.
- The sustained A-annulus pressure, is managed within the Maximum Operating Pressure (MOP) for the current natural gas production situation. The risk associated with multi barrier failure and out of zone injection of CO<sub>2</sub> may require mitigations to the current well status, i.e. the A-annulus pressure needs investigation / recompletion.

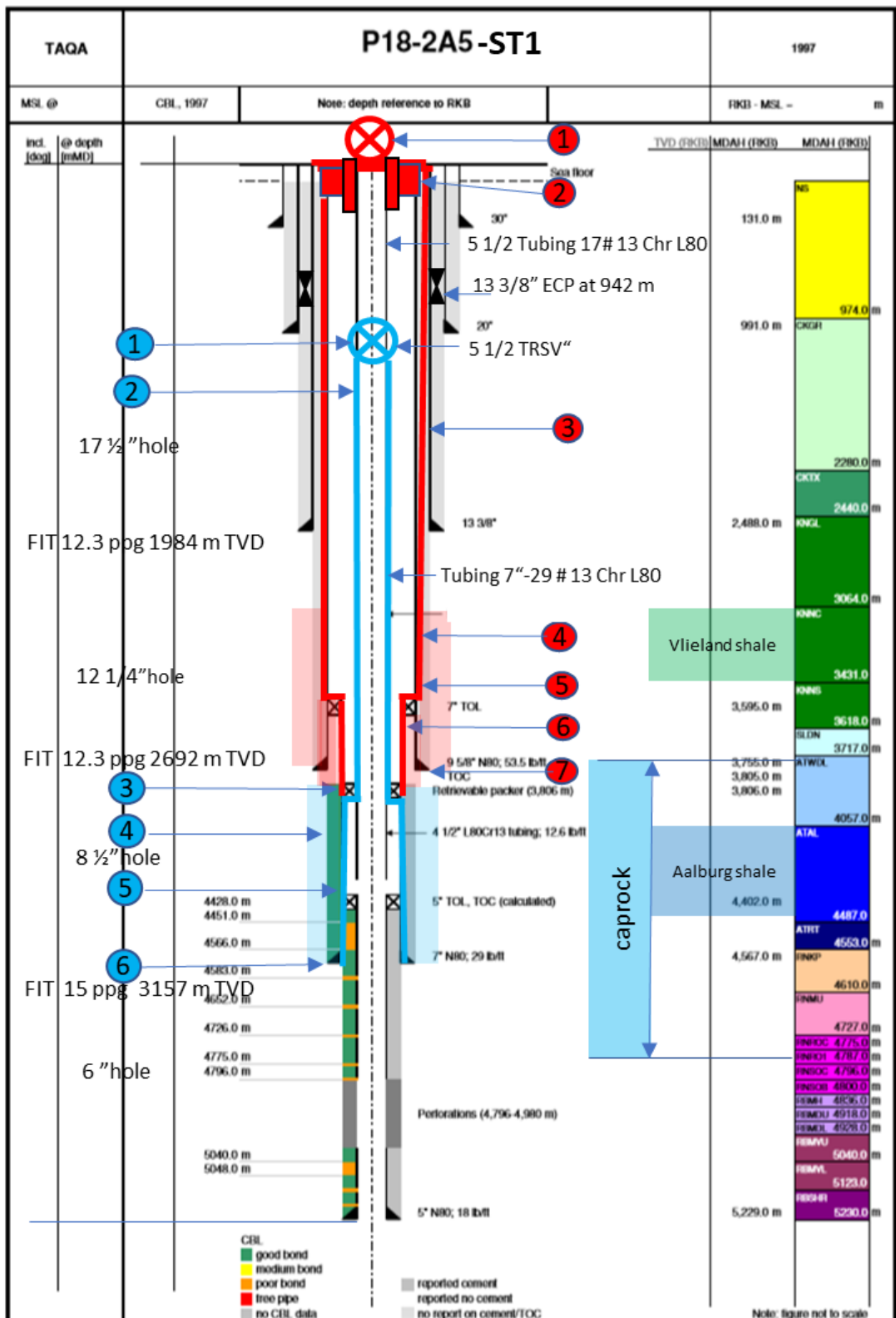


Figure 9-4 Well P18-2A5-ST1 barrier diagram with barrier elements defined. See Table 9-4 for a discussion of the barrier elements (indicated by the numbered circles).

Table 9-4 Well P18-2A5-ST1 barrier element assessment based on current data set. The numbers in the first column correspond with the numbers in coloured circles in Figure 9-4.

no	P18-2A5-ST1 Element	As built	Monitor	Barrier validated	Validation Criteria
<b>Primary well barrier</b>					
1	5 1/2" Scssv	Tested	Maintained	Yes	Tested & maintained
2	7" Tubing	Tested	Annular pressures recorded	Yes	Tested, some annular pressure reported but no gas bled off
3	7" Production packer	Tested, the retrievable packer is installed at 3806 m MD, the TOC is reported to be at 3805 m MD	The sustained annular pressure in the A annulus is within MOP	Yes	The A annulus has a sustained pressure of 40 bar on average, there was only liquid bled off. The source is not from producing reservoir because pressure is too low to be able to leak into the hydrostatic fluid column in the annulus. A possible source of pressure is the formation behind the casing or liner lap, this is not certain
4	7" Liner cement	The TOC is at 3805 m MD, no detailed cement report available. The cement is fully displaced to 43 m MD above the 7" shoe. Good cement bond log	Annular pressures recorded	Yes	Tested and fully displaced cement job Good cement bond log
5	7" Liner	Test reported with no value	Annular pressures recorded	Yes	Liner is tested and exposed to hydrostatic overbalance of annulus
6	In-situ formation (Caprock)	FIT of 15 ppg at 3157 m TVD The original borehole penetrates the top of the caprock for 28 m with a stuck drilling assembly, it is plugged back leaving 960 m of undisturbed caprock in place	NA	Yes	FIT of 15 ppg at 3157 m TVD reported Identified NFS potential - Aalborg shale
<b>Secondary well barrier</b>					
1	Surface tree & tubing hanger	Tested at 5000 psi	Maintained	Yes	Tested & maintained
2	Wellhead & casing hanger	Tested at 5000 psi	Maintained	Yes	Tested & maintained
3	9 5/8" Casing	Tested at 5000 psi	The sustained annular pressure in the A annulus is within MOP	No	The A annulus has a sustained pressure of 40 bar on average, there was only liquid bled off. The source is not from producing reservoir because pressure is too low to be able to leak into the hydrostatic fluid column in the annulus. A possible source of pressure is the formation behind the casing or liner lap, this is not certain
4	9 5/8" Casing cement	The TOC is calculated to be at 2338 m MD, the cement is fully displaced to 104 m above the shoe	Annular pressures recorded	Yes	A cement top up job is reported for the 13 3/8" by 9 5/8" annulus. Identified NFS potential - Vlieland shale
5	7" Liner + liner lap	A test is reported without pressure value	Annular pressures recorded	Yes	The liner lap is exposed to annular pressure and hydrostatic brine column
6	7" Liner cement	The TOC is at 3805 m MD, no detailed cement report is available. The cement is fully displaced to 43 m above the 7" line shoe. The CBL indicates a good cement bond	Annular pressures recorded	Yes	Tested and fully displaced cement job Good cement bond log
7	In-situ formation	FIT of 12.3 ppg at 2692 TVD	NA	Yes	FIT of 12.3 ppg at 2692 TVD reported

### 9.2.7 Well P18-2A6 + ST

Well barrier diagrams with well barrier envelopes and elements defined for well P18-2A6 MB (mother bore) and P18-2A6-ST are provided in Figure 9-5 and Figure 9-6, whereas the evaluation of the elements can be found in Table 9-5. The evaluation of the well integrity barriers leads to the following observations.

#### Primary barrier

- The 9 5/8" retrievable production packer is installed at 2145 m MD and tested. This is above the 9 5/8" tieback at 2223 m MD that is tested.
- The 9 5/8" tie-back casing is cemented and tested, the EOWR mentions a good cement job. The TOC is reported to be at 1631 m MD, there is a cement report from Halliburton that states that the cement slurry is placed to 2022 m MD, this cement report has been taken as TOC in this assessment (worst case scenario).

- The tubing and SCSSSV are tested, no annular pressures have been observed or reported.
- This defines the primary barrier above the production packer as validated.
- The side track window is uncemented which has implications for the well integrity:
  - The EOWR reported the TOC to be at top of liner (TOL). The cement across the 7" side track liner was logged from the 7" liner shoe at 3711 m MD to 2180 m MD (approximately 308 m above the 9 5/8" casing. The bond log of the 7" side track liner across the 9 5/8" side track exit window at 2495 m MD shows "ratty" cement across the window down to 2753 m MD. The cement bond is poor from 2753 m MD to an approximate depth of 3158 m MD. From 3158 m MD to the 7" liner shoe (at 3709 m MD) the cement bond quality appears to be very good.
  - The 7" side track liner is perforated at the depth of the hollow whip-stock, this connects both the mother bore and the side track reservoirs through the uncemented side track window and the surrounding open borehole formation at the casing window.
  - The 9 5/8" casing is uncemented from 3000 m MD (TOC) to 2284 m MD (the 13 3/8" casing shoe). The 7" side track liner has "ratty" cement (no bond) from 2753 m MD to 2284 m MD (the 13 3/8" casing shoe). This results in a section of +/- 1185 m of uncemented formation; 716 m of 12 1/4" hole and 469 m of 8 1/2" side track.
  - The in-situ formation has been tested at 1961 m MD TVD to 12 ppg (pounds per gallon), equivalent to 4060 psi (280 bar) pressure.
  - The above compromises the integrity of the primary barrier in mother bore and side track below the production packer.

#### Secondary barrier:

- The secondary barrier consists out of the 9 5/8" tieback casing that is tied back to below production packer and is tested.
- The top of the 9 5/8" casing cement inside the tieback annulus is reported in the EOWR to be at 1613 m MD. The well status diagram has two depths for TOC: the 9 5/8" tie-back packer TOC is calculated to be at 2022 m MD and the TOC of the 9 5/8" casing at 1631 m MD. The TOC reported in the EOWR (at 2022 m MD) has been taken in this assessment (worst-case scenario).
- The annular pressure is monitored and recorded, no sustained annular pressures are reported confirming integrity.

#### Structural well integrity:

- The 13 3/8" casing is placed at 2284 m MD and had a successful FIT of 12 ppg at 1961 m TVD, the casing is cemented to 200 m MD estimated with a multistage packer at 932 m.
- The 20" casing is set at 987 m MD and is cemented with cement returns to surface.
- The 30" conductor is piled to 131 m MD.

From a structural load bearing capacity point of view there appears to be adequate cement overlap to transfer the well loads, the 20" casing is cemented to surface and partly washed out, this leaves a small top portion of the 20" inside the conductor exposed to potential risk of corrosion of the fluids in the conductor annulus, this needs to be verified.

#### Discrepancies

- Akemu et al. (2011) reports the production tubing as 5" 13Cr-L80, it has been confirmed to be 5 1/2", 13 Cr-L80 .
- The EOWR repeatedly reports for the 9 5/8" a top of cement at 1631 m MD, the cement report and final well status diagram show 2022 m MD.
- The EOWR reports on the 7" side track liner a top of cement at top of liner, the bond log shows no or "ratty" cement from top of 7" side track liner to 2753 m MD.

#### Summary

- The well primary barrier is limited to the production packer set above the tieback packer and the side track window.
- The producing reservoir formations from the side track and the mother bore connect at the side track window that is not isolated. Although this imposes a risk of out of zone injection below the primary and secondary barrier envelop; about 1185 m of uncemented borehole (open formation) is exposed.
- For this well to be used as CO<sub>2</sub> injector the primary well integrity barrier has to be restored to the caprock of the mother bore reservoir and the integrity of the window has to be restored. This has most likely to be done by plug and abandonment (P&A) of the side track and installing a cemented scab or tie back liner to restore the mother bore integrity.
- The mother bore original primary and secondary barrier can be restored, it has a good cementation and in-situ formation at caprock level.
- The 13 3/8" casing has 25% casing wear and therefor the burst rating has been reduced from 3860 to 2500 psi (262-170 bar). A 9 5/8" tieback has been installed to mitigate the risk of exceeding the reduced burst rating for drilling the next section.

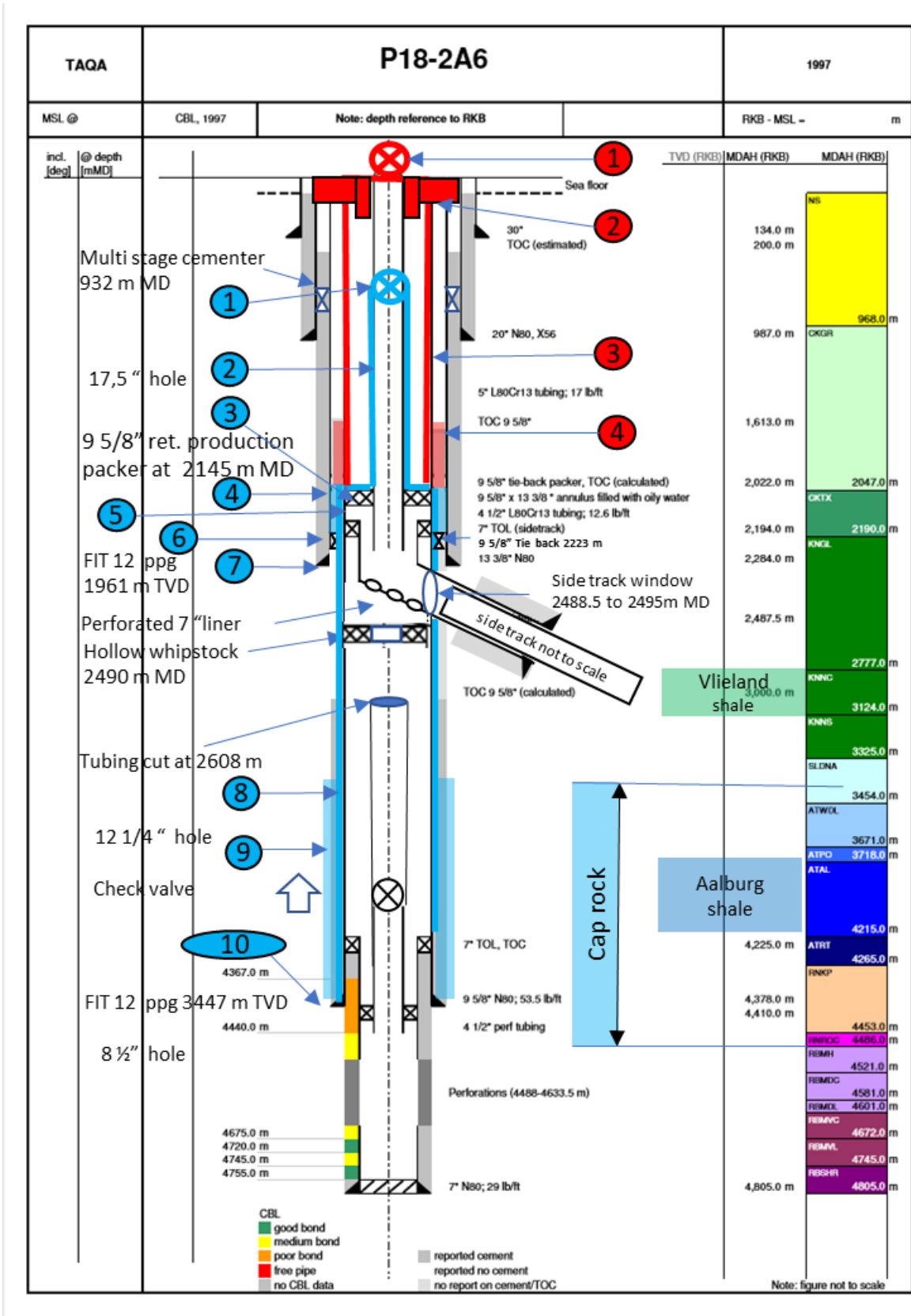


Figure 9-5 Well P18-2A6 barrier diagram with barrier elements defined. See Table 9-5 for a discussion of the barrier elements (indicated by the numbered circles).



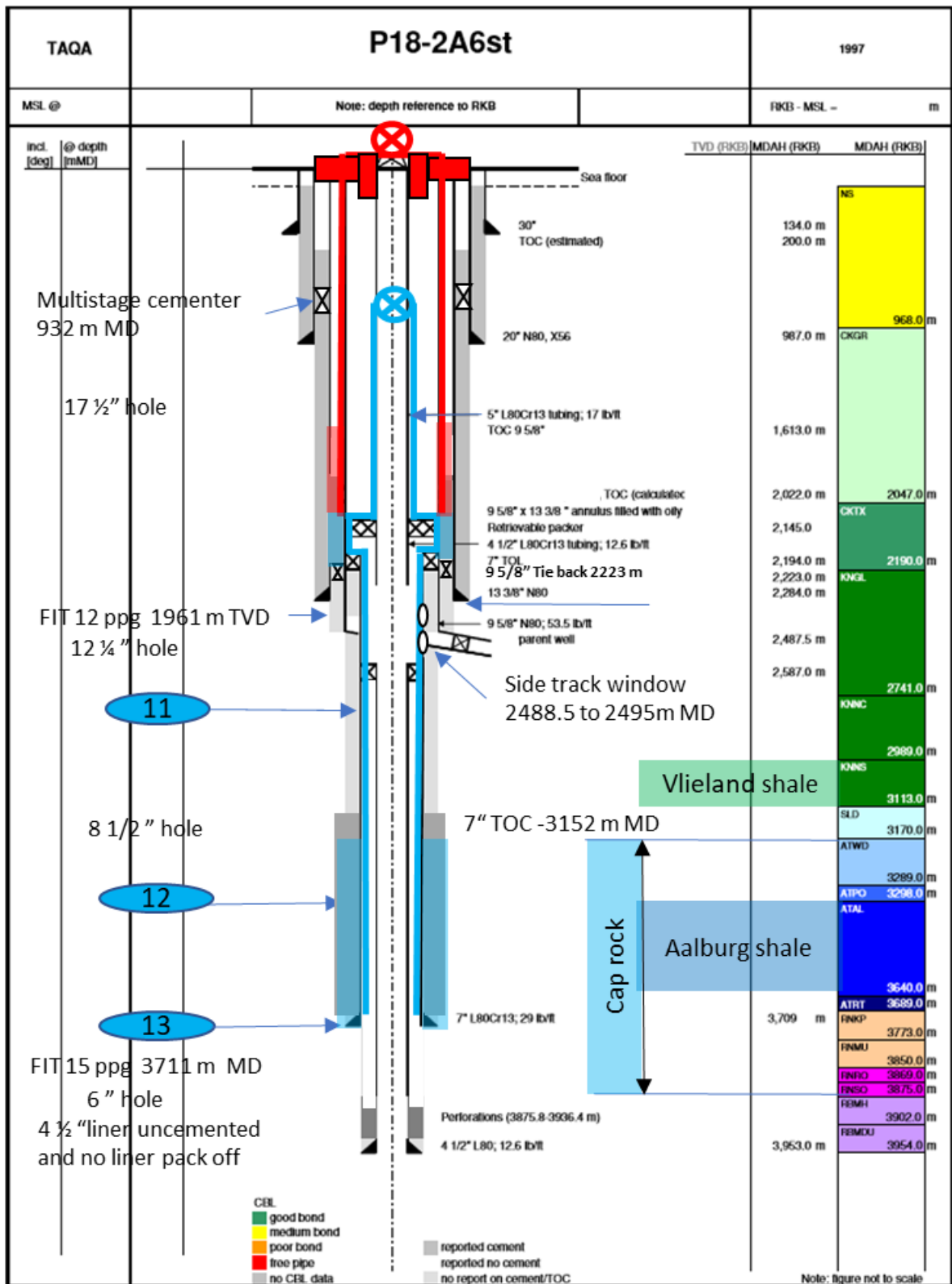


Figure 9-6 Well P18-2A6-ST1 barrier diagram with barrier elements defined. See Table 9-5 for a discussion of the barrier elements (indicated by the numbered circles).

Table 9-5 Wells P18-2A6 and P18-2S6-ST1 barrier element assessment based on current data set. The numbers in the first column correspond with the numbers in coloured circles in Figure 9-5 and Figure 9-6.

no	P18-2A 6-ST1 Element	As built	Monitor	Barrier validated	Validation Criteria
<b>Primary well barrier</b>					
1	5 1/2" Scssv	Tested at 5000 psi	Maintained	Yes	Tested & maintained
2	5 1/2" Tubing	Tested at 5000 psi	Annular pressures recorded	Yes	Tested, no annular pressure build up reported
3	9 5/8" Retrievable production packer	Set at 2144 m MD and tested	Annular pressures recorded	Yes	Tested, no annular pressure build up reported
4	9 5/8" Tie-back casing cement	The 9 5/8" casing cement is part of the tieback packer that is set at 2233 m MD. The top of the production packer is at 2145 m MD, the total length of the primary seal is 78 m.	Annular pressures recorded	Yes	There is a good cement report on the 9 5/8" tie-back casing. The TOC is reported in the EOWR to be at 1613 m MD. The Halliburton cement report indicates the TOC to be at 2022 m MD, this is a conflict in the reports. In this report 2022 m MD has been used as this is the worst case scenario with total length of the primary seal of 78 m
5	9 5/8" Tie-back casing	Tested, this is the 9 5/8" contingency tieback for the risk of casing wear risk of the 13 3/8" casing	Annular pressures recorded	Yes	Tested, no annular pressure build up reported
6	9 5/8" Tie-back packer	Tested to 5000 psi together with the 7" liner before the side track	NA	Yes	Tested
7	In-situ formation	FIT of 12 ppg at 1961 m TVD	NA	Yes	FIT of 12 ppg at 1961 m TVD reported
8	9 5/8" Casing	Tested before side track window is created to 5000 psi	NA	No	Integrity compromised by uncemented side track window Identified NFS potential - Vlieland and Aalborg shales
9	9 5/8" Casing cement	Cement report indicates good cement to 3000 m MD	NA	No	The integrity is compromised by the uncemented side track window
10	In-situ formation (caprock motherbore)	FIT of 12 ppg at 3447 m TVD	NA	Yes	FIT of 12 ppg at 3447 m TVD reported Note: The FIT is affected by the uncemented window and the reported FIT is at 12 ppg at 1961 m TVD
11	7" Side track liner	The liner is perforated at the side track window to facilitate commingled flow	NA	No	The integrity is compromised by the uncemented side track window
12	7" Side track liner cement	The EOWR states cement to the top of liner. The CBL reports the TOC at 3152 m MD, this is about 660 m MD below the sidetrack window	NA	No	The Integrity is compromised by the uncemented side track window and perforated section at the side track window Identified NFS potential - Vlieland and Aalborg shales
13	In-situ formation (caprock side track)	FIT of 15 ppg at 3711 m TVD	NA	No	The FIT is compromised by the uncemented window and the FIT of 12 ppg at 1961 m TVD
<b>Secondary well barrier</b>					
1	Surface tree & tubing hanger	Tested to 5000 psi	Maintained	Yes	Tested & maintained
2	Wellhead & casing hanger	Tested to 5000 psi	Maintained	Yes	Tested & maintained
3	9 5/8" Tie back casing	Tested to 5000 psi	Annular pressures recorded	Yes	Tested, no annular pressure build up reported
4	9 5/8" Casing cement	Tieback string is mitigating the risk of wear of the 13 3/8" casing The EOWR calculated the TOC at 1613 m MD and at 2022 m MD	Annular pressures recorded	Yes	There is a good cement report on the 9 5/8" tie-back casing. The TOC is reported in the EOWR to be at 1613 m MD. The Halliburton cement report indicates the TOC to be at 2022 m MD, this is a conflict in the reports. In this report 2022 m MD has been used as this is the worst case scenario with total length of the primary seal of 78 m

### 9.2.8 Well P18-02

The P18-02 well is suspended and left with a mud line suspension in place to allow potential re-entry. The well is plugged at various depths with a total of 4 plugs. The well was re-assessed in view of CO<sub>2</sub> storage with following results (see also Figure 9-7 and Table 9-6).

The assessment is done based on current standards in place; Norsok D10 section 9.6.5.1 (permanent abandonment open hole) and NOGEP A 45. The NOGEP A 45 standard is currently under review with reference to decommissioning requirements for CO<sub>2</sub> storage wells, this implies that this assessment has to be reviewed when the updated NOGEP A 45 standard is available.

#### Primary barrier

- The 7" liner EZSV (trademark of a drillable plug) is installed above top perforations at 3300 m MD with a 1.5 m cement plug from 3300 m to 3298.5 m. This is below the caprock bottom which is located at 3275 m MD. Therefore the plug is not considered to be a primary barrier element as it is located below the cap rock (see section 9.2.1.1 point a).
- The second 7" mechanical plug is installed in the 7" liner at 3006 m MD and tested to 2000 psi (~140 bar). The cement plug is placed from 3006 m MD to above the top of the 7" liner with a TOC of 2956 m MD in the 9 5/8" casing. Resulting in 50 m cement.
- The 7" liner is cemented to 3005 m MD TOC, this is 49 m below the top of the liner at 2956 m MD, this implies that, at the depth of the cement plug, there is no cement behind the 7" liner. Therefore there is no cement across all annuli at this depth.
- The cement plug covers the 9 5/8" over a length of 60 m, from the top of liner at 2896 m MD to the TOC of the plug at 2956 m MD. The 9 5/8" cementation is reported to be good in the cement report, but the CBL indicates poor bonding.
- The in-situ formation (Caprock) was tested by a FIT to 14.8 ppg at 3711 m TVD.

#### Secondary barrier

- The mechanical plug is set in the 9 5/8" casing at 1915m MD and tested to 2000 psi. The cement plug is placed from 1915 m MD to 1846 m MD with a total length of 59 meter.
- The 9 5/8" cementation was done in 2 stages with the multistage cement packer at 1893 m MD and with the TOC of the first stage cementation at 1932 m MD. This implies that there is no cement in the 9 5/8" by 13 3/8" annulus from 1932 m MD to 1893 m MD.
- The EOWR reports a premature landing of the shut of plug ahead of the cement that resulted in a failed placement of the first stage cement job. The bond log shows no cement at plug depth, the second stage cementation is from 385 m MD to 69 m MD TOC.

#### Open hole barrier

- There are no specific requirements for the open hole barrier, it has been assessed based on the NORSOK D10 9.6.5.1 barrier diagram example for permanent abandonment for open hole wells.
- The open hole barrier has a 65 m cement plug placed on a mechanical plug from 154 m MD to 85 m MD. There is no cement in the 9 5/8" by 13 3/8" annulus at this depth, the 13 3/8" by 20" annulus is cemented.

#### Structural integrity

All wellheads are removed and the 9 5/8", 13 3/8" and 20" casings were backed out and removed at the mudline hanger. A casing stick up protector has been placed at seabed.

#### Discrepancies

- The well status diagram shows that the 13 3/8" casing is cemented with the TOC at 1627 m MD, while the final well report indicates there is no cement placed at the first stage cementation.
- Akemu, et al., (2011) did not address the discrepancy of the uncemented 13 3/8" casing at cement plug depth.

### Summary

- From Table 9-6 it can be seen that multiple barrier elements for this suspended well could not be validated, the well needs to be planned for re-assessment and decommissioning conform the updated NOGEPa 45 standard for CO<sub>2</sub> storage decommissioning when these are available.

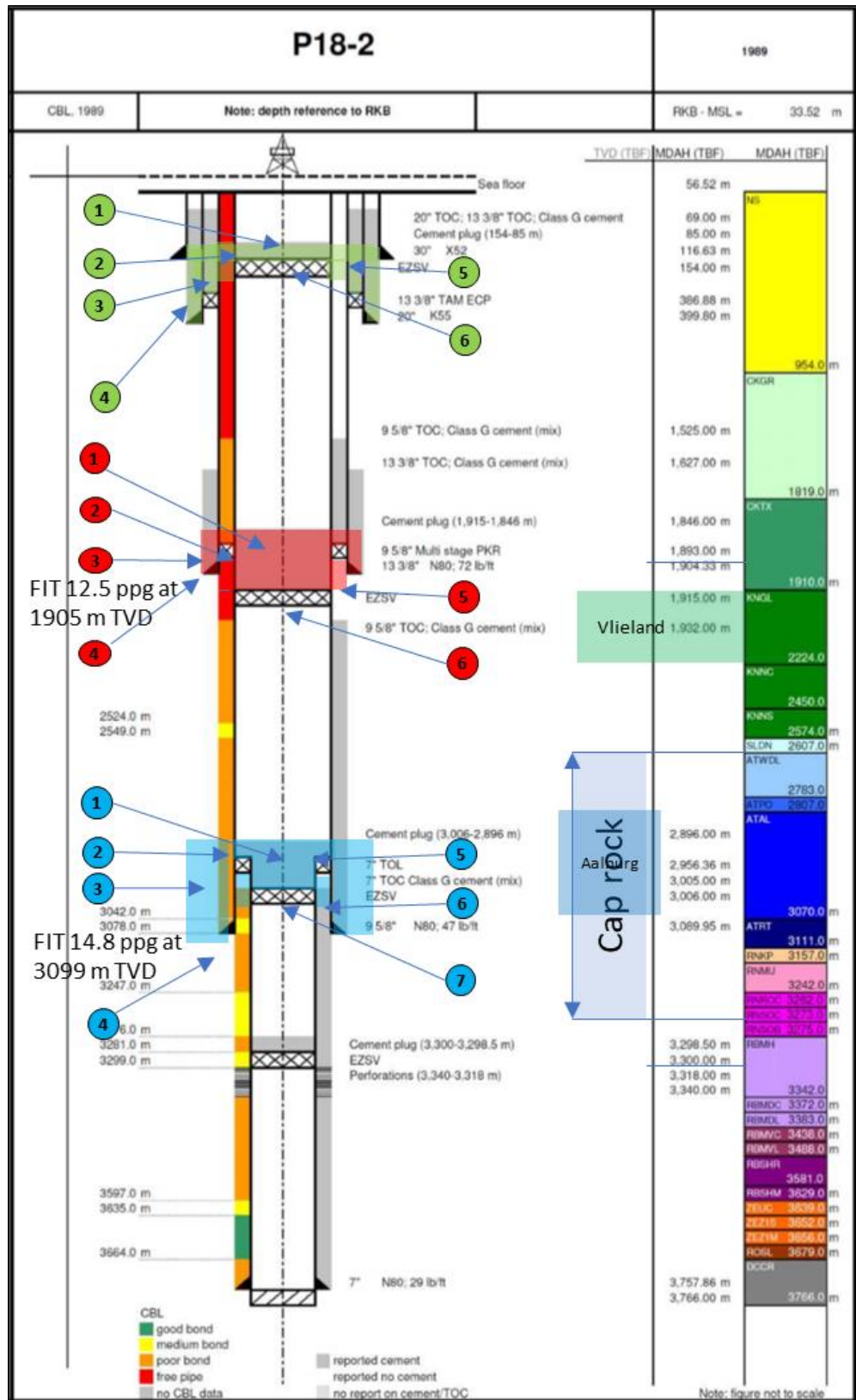


Figure 9-7 Well P18-2 barrier diagram with barrier elements defined. See Table 9-6 for a discussion of the barrier elements (indicated by the numbered circles).

Table 9-6: Wells P18-02 barrier element assessment based on current data set. The numbers in the first column correspond with the numbers in coloured circles in Figure 9-7.

no	P18-2A1 Element	As built	Monitor	Barrier validated	Validation Criteria
<b>Primary well barrier</b>					
1	5 1/2" Scssv	Tested to 5000 psi	Maintained	Yes	Tested & maintained
2	5 1/2" Tubing	Tested to 5000 psi	Annular pressure records	Yes	Tested, no annular pressure build up reported
3	7" Production packer	Installed at 3503 m MD which is 26 m below the TOC in the 7" liner. Tested to 5000 psi	Annular pressure records	Yes	Tested, no annular pressure build up reported.
4	7" Liner	Liner report for P18-3 (previous name of P182A1) The liner covers 50 m of caprock	NA	Yes	The liner and production packer are under continuous high hydrostatic differential pressure of the A annulus. No annular pressure build up recorded
5	In-situ formation (Cap rock)	FIT of 15.8 ppg at 3488 m TVD	NA	Yes	FIT of 15.8 ppg at 3488 m TVD reported
6	7" Liner cement	Cement report of P18-3 (previous well name) reports the TOC at 3508 m MD. The well status diagram shows the TOC at 3477 m MD. The CBL indicates a poor bond	NA	No	The well status diagram shows the TOC 3477 m MD. The CBL indicates a poor bond. The TOL is set at 3404 m MD, this leaves 73 m of uncemented liner combined with poor bond.
<b>Secondary well barrier</b>					
1	Surface tree & tubing hanger	Tested to 5000 psi	Maintained	Yes	Tested & maintained
2	Well head & casing hanger	Tested to 5000 psi	Maintained	Yes	Tested & maintained
3	9 5/8" Casing	Tested to 5000 psi	Annular pressure records	Yes	Tested, no annular pressure build up reported
4	9 5/8" Casing cement	Cement report does not provide a TOC, the report quotes for the 9 5/8" cementation: minimal losses during circulation, cementation in 2 stages with 2000 psi bump plug pressure	Annular pressure records	Yes	Good cement report on placement of cement in caprock NFS potential - Vlieland shale & Aalburg shale
5	7" Liner + liner lap	The CATO-2 report (Akemu et al. 2011) quotes a 5000 psi test that is not mentioned in the end of well report.	Annular pressure records	Yes	The liner is tested by default; the differential pressure from annulus to reservoir by hydrostatic column is approximately 280 bar
6	7" Liner cement	The cement report of P18-3 (previous well name) reports the TOC at 3508 m MD. The well status diagram shows the TOC at 3477 m MD. The CBL indicates a poor bond	Annular pressure records	No	The well status diagram shows the TOC 3477 m MD. The CBL indicates a poor bond. There is 47 m of uncemented liner above the production packer
7	In-situ formation (Cap rock)	FIT of 15.8 ppg at 3438 m TVD	NA	Yes	FIT 15.8 of ppg at 3438 m TVD reported

### 9.2.9 Conclusion on current well status

The selected wells relevant in the context of CO<sub>2</sub> injection into the P18-2 field have been evaluated regarding their current status and well integrity risks. All wells reviewed have the potential to be used safely as CO<sub>2</sub> injectors. Appropriate mitigations can make them fit for storage operations as given below.

#### 9.2.9.1 Generic well integrity issues of the wells

- The currently installed production packers are retrievable and need to be replaced based on the expected CO<sub>2</sub> injection load case. The workover would include the change or refurbishment of the surface tree and associated sealing components, which should be suitable for the CO<sub>2</sub> injection operating envelope, i.e. pressure, temperature, CO<sub>2</sub> composition and flow rate.
- The operating temperatures for equipment are specified in the API standards with specific requirement for extreme (cold) conditions, all materials should be checked for suitability for the expected low temperatures.
- Seals and pack-offs that have been reported as leaking could be restored with appropriate sealing arrangements; this holds for the non-flow-wetted operational envelope.

- The well load cases must be assessed for CO<sub>2</sub> injection and evaluated against the status of the load bearing surface casing and completion design, considering sudden load changes during start-up / shut-down of CO<sub>2</sub> injection.
- Where flow-wetted components have been exposed to production fluids, like casing or liners, these may need to be assessed for corrosion of wet CO<sub>2</sub> (presence of water / brine).
- The condition of these liners may require recompletion below the current packer depths or above the liner laps depending on the identified risks to mitigate the risk of potential failure of the liner due to wear or corrosion.

#### 9.2.9.2 Summary

All wells reviewed P18-2A1 / 2A3-ST2 / 2A5-ST1 / 2A6 + ST could be re-used safely for CO<sub>2</sub> injection if the risks identified are mitigated properly; see overview in Table 9-7.

Table 9-7 Overview of P18-2 CO<sub>2</sub> injector wells selection.

Well	Status	Integrity for CO <sub>2</sub> injector	Remarks
P18-2A1	Producer	Yes	Needs recompletion and repositioning of production packer in liner / casing with good cement bond
P18-2A3-ST2	Producer	Yes	Retrievable packer CO <sub>2</sub> injection load case and material compatibility are the components to be mitigates to make this well a suitable CO <sub>2</sub> injector
P18-2A5-ST1	Producer	Yes	'A'-annulus pressure needs investigation / recompletion for CO <sub>2</sub> injection
P18-2A6 + ST	Producer	Yes	Needs restoration of the side track window in order to be able to use it for CO <sub>2</sub> injection.
P18-2	Suspended	No	Requires to be re-assessed against new CO <sub>2</sub> storage abandonment requirements (Nogepa / SodM) and decommissioned in accordance to this standard.

### 9.3 Influence of cooling on well cement

Injection of CO<sub>2</sub> at a lower temperature than the temperature of the surrounding rock can cause thermal contraction of the materials and associated stress reduction of the surrounding rock in the near-well area that may affect the structural integrity of the well barriers. The operating envelope of P18 CO<sub>2</sub> injection wells needs to consider cooling effects, which are not part of the current operating envelope designed for natural gas production.

In this section we provide an estimate of the effects of cooling due to cold CO<sub>2</sub> injection on the structural integrity of the injection well, focussing on the integrity of annular cement behind the casing, and discuss the risk of leakage along the outside of the well. Potential failure modes of the sealant (cement sheath) that can create potential continuous leakage pathways up the well across the caprock are of primary interest (Figure 9-8). The most likely leakage mechanism is related to the flow of fluids along a microannulus formed by de-bonding of the cement-casing interface or the cement-formation interface.

Note that, in order for CO<sub>2</sub> to migrate and eventually leak to the overburden through a microannulus, several events have to take place and several constraints with regard to subsurface conditions have to be met. The likelihood of cement-casing or cement-rock debonding to take place during injection of cold CO<sub>2</sub> in a P18-2 well is investigated using a numerical model based on the DIANA finite elements<sup>6</sup>. Subsequently, the likelihood that a continuous microannulus forms along the entire caprock level towards the overburden, and the conditions that need to be met for CO<sub>2</sub> to migrate through a microannulus into the overburden are discussed. For a worst-case scenario where all events occur and all conditions are met, an estimate of the leakage rate will be given and this will be discussed in the context of the total storage capacity in P18-2.

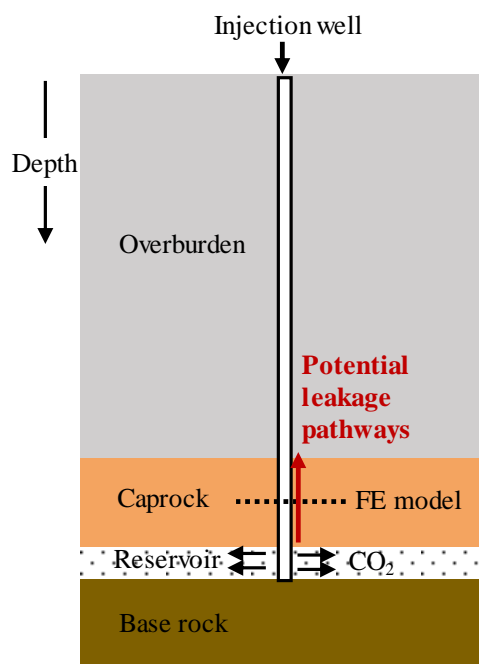


Figure 9-8: Sketch of an injection well showing the location of a finite element (FE) model for well integrity analysis at the caprock level. The model represents a cross-section of the near-wellbore area normal to the well axis at the analysis depth (see ).

### 9.3.1 *Pressure and temperature in the CO<sub>2</sub> injection well*

The initial flow assurance study for the Porthos consortium by Belfroid (Belfroid, 2019) presents several scenarios and sensitivities that can be used to estimate the possible variation of pressure and temperature conditions in CO<sub>2</sub> injection wells for different reservoir and injection conditions. This flow assurance work will be repeated and refined throughout well and project design and regularly throughout the injection years. Here we focus on CO<sub>2</sub> injection in a single well and present pressure and temperature (P&T) profiles obtained using the OLGA simulator. The OLGA model includes the entire pipeline and considers the reservoir conditions relevant for the P18-2 CO<sub>2</sub> injection (Table 9-8). Well geometry is based on an idealized well (P18-4A2) and is considered to be representative for other planned injection wells.

<sup>6</sup> See [dianafea.com](http://dianafea.com).



Steady-state simulations were performed for six scenarios (or cases in (Table 9-8) with an injection rate of 30 kg/s (~1 Mt/yr).

Table 9-8: Overview of steady-state cases of well flow simulations.

Case name	Mass flow rate (kg/s)	Reservoir pressure (bar)	Pipeline pressure control (bar)	Compressor outlet temperature (°C)
Case_b1	30	20	85	80
Case_b2	30	60	85	40
Case_b3	30	80	85	40
Case_b4	30	100	85	40
Case_b5	30	200	85	40
Case_b6	30	20	30	80

Simulated pressure profiles in the well for steady-state injection conditions are plotted in Figure 9-9. For a very low reservoir pressure of 20 bar and two-phase flow in the well, the wellhead pressure is higher than the bottom hole pressure (cases P\_b1 and P\_b2 in Figure 9-9). In other cases with a higher reservoir pressure the flow is mostly or fully single-phase and the bottom hole pressure exceeds the well head pressure due to the weight of the column of supercritical CO<sub>2</sub> in the well.

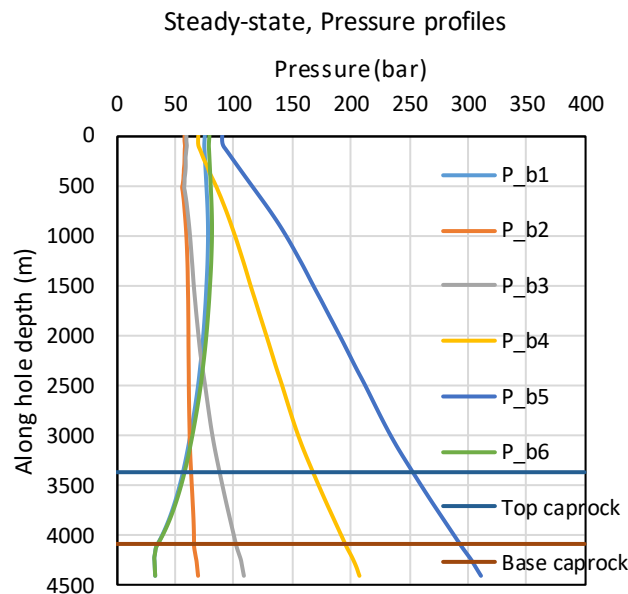


Figure 9-9: Pressure profiles in the well as a function of the along hole depth for the cases of steady-state CO<sub>2</sub> injection from Table 9-8.

The corresponding simulated temperature profiles for steady-state injection conditions are plotted in Figure 9-10. In the upper part of the well, at the depth range of 500 to 1500 m, temperature of injected CO<sub>2</sub> is higher than that of the surrounding rock. The temperature of the tubing, casing, annular cement and surrounding rock formation will increase, i.e. heating. At larger depths, below 500 to 1500 m, the temperature of the tubing, casing, annular cement and surrounding rock formation will decrease, i.e. cooling. For steady-state conditions, cooling is

most severe in the case of a low reservoir pressure of 20 bar and occurs at the level of the caprock (cases T\_b1 and T\_b6 in Figure 9-10). The CO<sub>2</sub> inside the well at the caprock level is 70°C to 100°C colder than the surrounding formation. For higher reservoir pressure, the degree of cooling decreases to 30°C to 40°C.

Figure 9-10 shows temperature profiles for steady-state conditions; the temperature in the well during a non-steady-state operation (such as a shut-in procedure) may lead to lower temperatures of the CO<sub>2</sub> in the well, but the heat capacity of the well system (such as liner and annulus fluid) prevents those short-lived low-temperature events from significantly changing the temperature of the cement and casing in the deeper parts of the well<sup>7</sup>. The profiles shown in Figure 9-10 can be used as a reliable estimate of the conditions in the well.

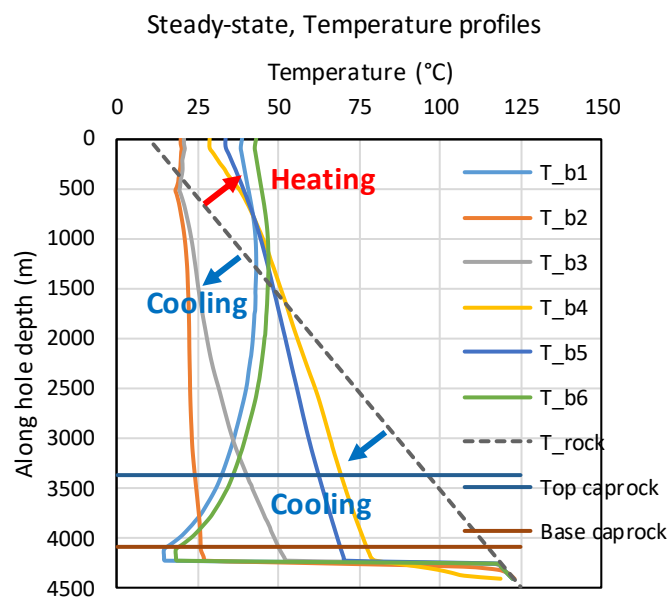


Figure 9-10: Temperature profiles as a function of the along hole depth for the cases of steady-state CO<sub>2</sub> injection from Table 9-8. Dashed black line denotes the formation temperature (T<sub>rock</sub>).

### 9.3.2

#### *Numerical modelling of the effects of cold CO<sub>2</sub> injection on well cement integrity*

A numerical model was developed to investigate the impact of thermal effects on well integrity, in particular on the integrity of annular cement behind the casing. Thermo-mechanical non-linear finite element analyses considered a section of a CO<sub>2</sub> injection well across the caprock (Figure 9-11), to evaluate whether failure of the well barriers could result in debonding of the annular cement with the casing and/or rock interfaces at caprock level, thereby creating a microannulus. In a worst case scenario, when such a microannulus is continuous from reservoir to above the caprock, a leakage path is formed.

<sup>7</sup> S. Belfroid, personal communication, 2019.

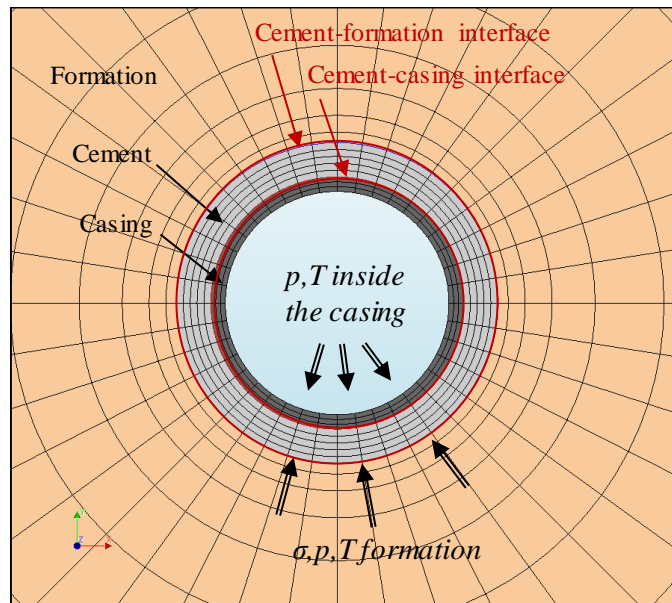


Figure 9-11: Mesh for a 2D finite element model of a cross-section of the near-well area.

The non-linear finite element simulator DIANA was used to generate meshes for 2D numerical models of the well system and run simulations. The workflow for well integrity analysis is automated through a dedicated user interface called the DIANA SEALEC application. Based on the user input in DIANA SEALEC, meshes of the well system can be generated automatically and well integrity analyses mimicking the entire lifetime of a well can be conveniently defined and executed.

The numerical model of the near-well area was developed on a cross-sectional area normal to the well axis. The model comprises well casing(s), cement sheath(s) and the surrounding rock formation. Two models with different well completion geometries were developed: completion with a single casing (Figure 9-12a) and completion with a double casing (or a liner lap; (Figure 9-12b). Chosen sizes and characteristics of casings in the models are representative of the P18-2 wells. The possible injection wells are completed over the caprock depth interval with a 9 5/8" casing and a 7" liner, and in some cases with a 5" liner.

Complete plane strain elements are used for bulk materials and zero-thickness interface elements are used for the casing-cement and the cement-formation interfaces. All materials in the model are assumed to be elastic and the well material interfaces are assumed to be rigid. The model input parameters are given in Table 9-9.

Table 9-9: Model input parameters.

Parameter	Unit	Caprock	Cement	Casing	Interface
E Young modulus	GPa	26	8.3	200	rigid
$\nu$ Poisson coefficient	-	0.3	0.1	0.3	-
Thermal expansion coeff.	$K^{-1}$	$1 \cdot 10^{-5}$	$1 \cdot 10^{-5}$	$1.3 \cdot 10^{-5}$	-
Volumetric specific heat	$Jm^{-3} K^{-1}$	$2.24 \cdot 10^6$	$4 \cdot 10^6$	$4 \cdot 10^6$	-
Thermal conductivity	$Wm^{-1} K^{-1}$	2.3	0.87	15	-

The effects of cooling were assessed by applying a temperature load of  $-1^{\circ}\text{K}$  ( $-1^{\circ}\text{C}$ ) on the inner side of the casing instantly at the start of the analysis. As all the well materials in the model were assumed elastic, the magnitude of induced thermo-mechanical stresses ( $\sigma_{\Delta T}$ ) scales linearly with the degree of cooling ( $\Delta T$ ), i.e. the stress magnitude due to cooling by  $\Delta T < -1^{\circ}\text{K}$  is obtained simply by multiplying  $\Delta T$  with the stress magnitude predicted by the model ( $\sigma_{\Delta T = -1\text{K}}$ ). A staggered heat flow and mechanical analysis is then performed. First a transient temperature field is calculated for a change in temperature of  $-1^{\circ}\text{K}$  ( $-1^{\circ}\text{C}$ ) and then the related thermo-mechanical stresses caused by this temperature change.

Note that the model is initially stress-free, i.e. the initial stress state in the cement sheath is set to zero as our aim is to estimate the net thermo-mechanical stress induced by cooling. Estimating the initial, i.e. present day (compressive) stress in annular cement of gas producing wells is difficult: direct in-situ measurement of stress in cement at downhole conditions is not possible; stress estimates can only be obtained by modelling the entire well history, taking into account the different phases in the lifetime of a well, cement material properties, quality of executed cement job, interactions with the surrounding rock formation, etc.. Modelling well histories is beyond the scope of this task, which focusses on the thermo-mechanical effects of cooling on well cement integrity.

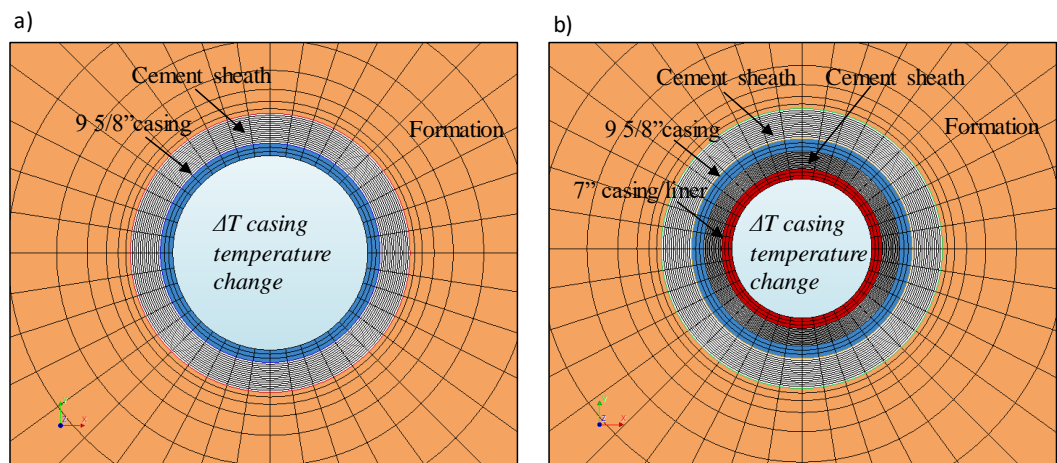


Figure 9-12: Meshes for 2D finite element models of the near-well area at the level of caprock for well sections completed with (a) a single casing and (b) a double casing (liner lap).

Simulation results show gradual extension of the cooled area radially into the surrounding rock (Figure 9-13 and Figure 9-14). After 1 year of injection, the radial extent of cooled area is about 10 m and has reached the edge of the model. The largest drop in temperature occurs within a radius of 1-3 m from the injection well (Figure 9-14).

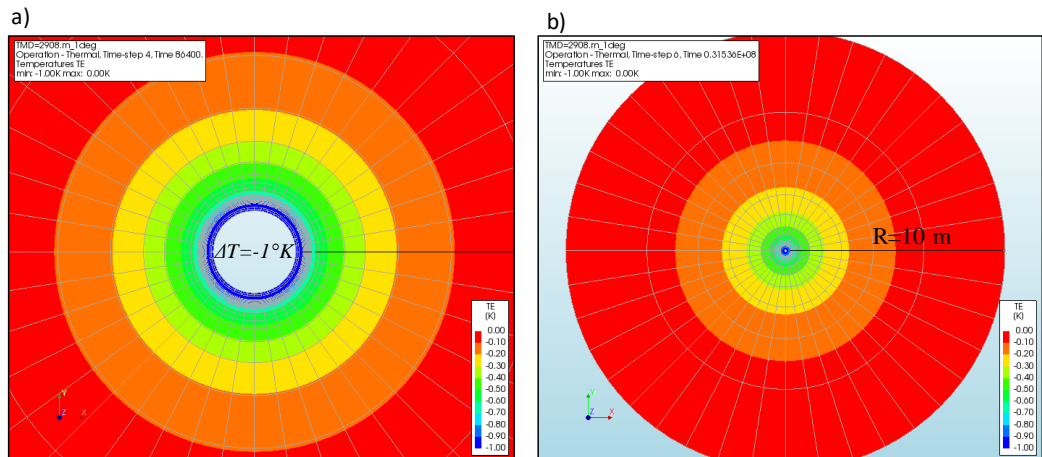


Figure 9-13: Contours of temperature change in the near-well area due to a casing temperature change of  $-1^{\circ}\text{K}$  (or  $-1^{\circ}\text{C}$ ) after (a) 1 day and (b) 1 year. The contour interval is  $0.1^{\circ}\text{K}$ .

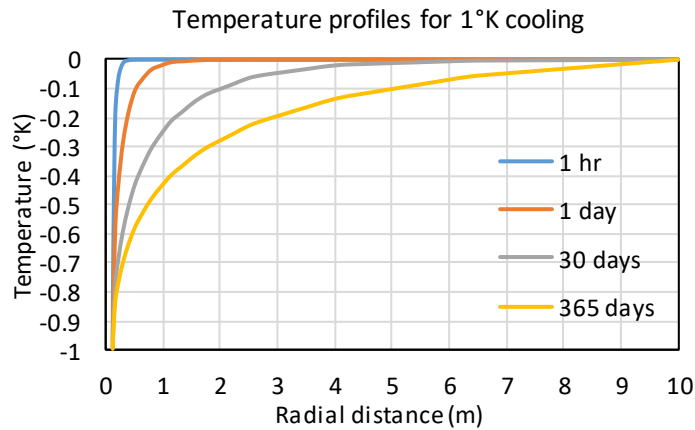


Figure 9-14: Profiles of temperature change as a function of radial distance from the well due to a casing temperature change of  $-1^{\circ}\text{K}$  (or  $-1^{\circ}\text{C}$ ) for different times.

Cooling induces thermal contraction which in turn induces thermo-mechanical tensile stresses in the radial direction. As expected, the magnitude of tensile stress increases with time, as the cooling front propagates deeper into the surrounding formation, and decreases with the radial distance from the well casing.

For a single casing well model, the magnitude of tensile stresses is larger at the casing-cement interface, which is closer to the inner side of the casing than at the cement-formation interface (blue bar and orange bar, respectively in Figure 9-15). The magnitudes of tensile stresses range between  $0.1$  and  $0.17 \text{ MPa}/1^{\circ}\text{C}$ . For a decrease of casing temperature by  $100^{\circ}\text{C}$ , tensile stresses at the interfaces will be thus 100 times higher and can reach 10 to 17 MPa. If the initial stress in cement is less than these values, de-bonding of the interfaces will occur.

In a double casing well model there are four well interfaces and the evolution of tensile stresses at the interfaces with time is more complex (Figure 9-16). Initially, just after the start of cooling, the magnitude of tensile stresses at the interfaces decreases with the distance from the inner casing (Figure 9-16, 1hr). This pattern was also observed in the single casing well model. However, for longer cooling

times, from 1 day onwards, the largest magnitude of tensile stresses occurs at a more distant interface between the 9 5/8" casing and cement (grey bar in Figure 9-16). These magnitudes of  $\sim 0.19$  MPa per  $1^\circ\text{C}$  cooling are larger than in the case of a single casing well model (grey bar for 365 days in Figure 9-16). Overall, the magnitude of thermal stresses is dependent on the values of elastic and thermal properties for the well materials (casing, cement and rock) and their interfaces.

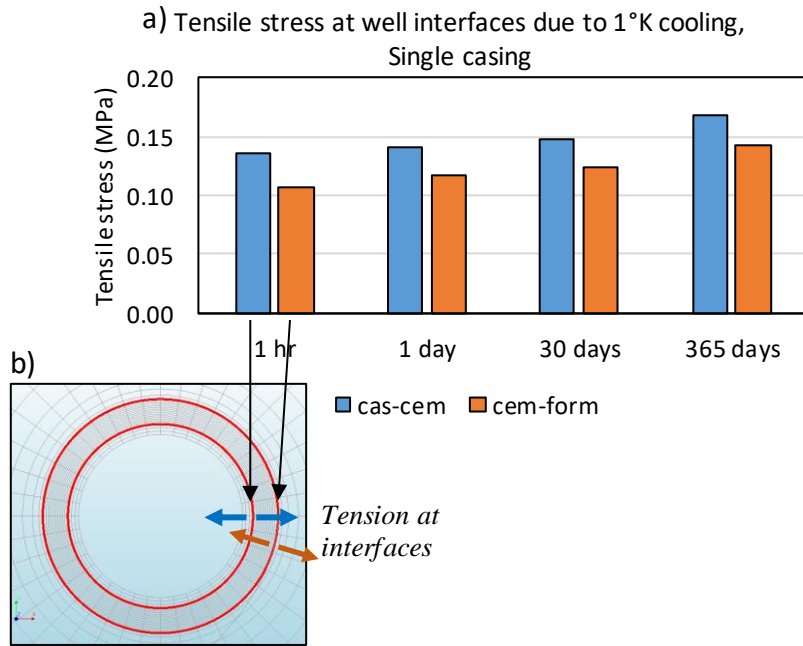


Figure 9-15: (a) Tensile stresses at the well interfaces due to a casing temperature change of  $-1^\circ\text{K}$  (or  $-1^\circ\text{C}$ ) after 1 hour, 1 day, 30 days and 365 days. (b) Sketch showing locations of the monitoring points at the two interfaces in a single casing well model.

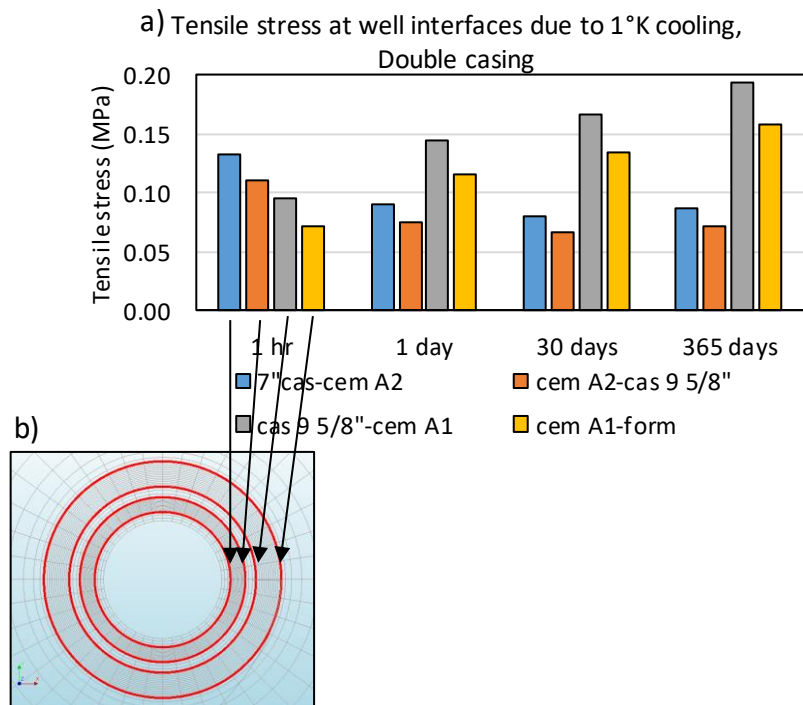


Figure 9-16: (a) Tensile stresses at the well interfaces due to a casing temperature change of  $-1^{\circ}\text{K}$  (or  $-1^{\circ}\text{C}$ ) after 1 hour, 1 day, 30 days and 365 days. (b) Sketch showing locations of the monitoring points at the four interfaces in a double casing well model.

### 9.3.3 *Implications of debonding on formation of potential leakage pathway*

Annular cement across the caprock in the P18-2 wells consists of sections with good cement and sections with poor/absent cement. Sections with poor cement are not considered to be sealing. Sections with good cement, which are in many cases a few tens of meters long, are most sensitive to debonding. For creation of a leakage pathway from reservoir to overburden, across the entire caprock thickness, de-bonding needs to occur along all sections with good cement, in order to connect sections with poor cement. Debonding of good cement is likely to occur at the level of caprock due to cooling by  $60\text{-}100^{\circ}\text{C}$  because of:

- large induced thermo-mechanical tensile stresses, which tend to cause de-bonding ( $\sim 10\text{-}20\text{ MPa}$ );
- very low tensile strength of the well cement interfaces (that counteracts the tensile stress) of  $0.1\text{-}3\text{ MPa}$  for a good cement bond and  $\sim 0\text{ MPa}$  for a poor cement bond;
- possibly low, largely uncertain magnitudes of the radial compressive stress in the annular cement (that counteracts the tensile stress).

The actual permeability and therefore also the flow rate is stress-dependent. The microannulus may be open and act as a conduit or closed and act as a seal. The permeability of circumferential microannulus created by debonding depends on the effective normal stress acting on that fracture ( $\sigma_n'$ ) and the fluid pressure inside the microannulus ( $p$ ); when  $p > \sigma_n'$ , the microannulus is open and acts as a conduit, when  $p < \sigma_n'$  the microannulus is closed and acts as a seal.

The effective normal stress  $\sigma_n'$  is either:

- The radial stress in annular cement ( $\sigma_n'\text{-cem}$ ) acting on the casing-cement interface. The  $\sigma_n'\text{-cem}$  is largely uncertain and could be low especially in the case of cement sheath located in-between two casings. The  $\sigma_n'\text{-cem}$  could possibly be lower than the hydrostatic stress ( $< 0.10\text{-}0.11\text{ bar/m}$ ). This implies that the hydrostatic fluid pressure inside the microannulus could keep the leakage path at the casing-cement interface open. Although a microannulus at the casing-cement interface can be kept open under a pressure lower than the hydrostatic pressure, the hydrostatic pressure conditions will still exist at the tip of a microannulus transecting the caprock. Keeping the  $\text{CO}_2$  pressure in the reservoir below the hydrostatic pressure conditions will prevent the  $\text{CO}_2$  from displacing the brine in the micro-annulus, as discussed in more detail in the next section.
- The radial stress in the rock formation ( $\sigma_n'\text{-rock}$ ) acting on the cement-rock interface. The  $\sigma_n'\text{-rock}$  could be:
  - (i) lower than the minimum in-situ horizontal stress  $Sh_{min}$  ( $0.17\text{-}0.18\text{ bar/m}$ ), but likely larger than the hydrostatic pressure ( $\sim 0.10\text{ to }0.11\text{ m/bar}$ ), if a plastic zone was formed in the (brittle) rock formation surrounding the wellbore;
  - (ii) close to the  $Sh_{min}$  ( $0.17\text{-}0.18\text{ bar/m}$ ) if the wellbore is surrounded by naturally sealing formations, which are either ductile (Aalburg Shales) or viscous (Röt salt, halitic parts). Potential advantage of naturally sealing formations is that they can improve annular sealing around non-cemented or poorly cemented parts of casing strings simply by moving or creeping onto the casing strings. Additional advantage is an increase in the compressive stresses in the near-well area, which could become equal to the far-field stresses in

these naturally sealing formations (0.17-0.18 bar/m in shales and 0.21 bar/m in halite). This implies that the hydrostatic fluid pressure inside the microannulus cannot keep the leakage path at the cement-formation interface open. The microannulus is closed and acts as a seal. Several shale layers and potentially salt layers in the caprock of the P18-2 reservoir have been identified as natural sealing formations. Local sealing of a microannulus could make the leakage path discontinuous and therefore prevent leakage.

Leakage risk and the effect of chemistry

#### 9.3.4 *Leakage risk and the effect of chemistry*

The well integrity simulations demonstrated that de-bonding of the well interfaces is likely to occur at the good cement sections of the P18-2 wells due to the mechanical stress related to cooling on the well materials and interfaces. In a worst case scenario, de-bonding could result in the formation of a leakage path (a microannulus), connecting the storage reservoir with the overburden, as discussed in the previous section.

Figure 9-17 gives a schematic representation of the pressure evolution in the reservoir and overburden in the various stages of the reservoir from initial (pre-production) to post-CO<sub>2</sub> injection. The initial reservoir conditions at the start of the gas production phase show the equilibrium of the water and gas pressure as developed during the geologic time of its existence. The hydrocarbon buoyancy pressure anywhere in the reservoir above the water-gas contact, equal to the average capillary pressure, is higher than the water pressure. Because of the capillary entry pressure of the caprock, which is higher than the prevailing buoyancy pressure if leakage does not occur, the gas remains in the reservoir.

In the gas production phase, both the water and the gas pressure in the reservoir decrease to low and sometimes very low levels. In case of a 'tank reservoir' where (strong) aquifer support is absent, the pressure remains low after production has ceased.

At the reservoir-caprock interface, a sharp water pressure transition exists because the water in the caprock is practically immobile on the time scale of hydrocarbon production and CO<sub>2</sub> injection. During CO<sub>2</sub> injection, both the water and gas pressure in the reservoir increase. As long as the gas pressure remains below the hydrostatic conditions at the base of the caprock, the gas will not be able to displace the water column in the overburden and leakage will not occur, even if a leakage path such as a microannulus exists. Over time, the reservoir conditions will move towards an equilibrium state due to water influx from the over- and underburden into the reservoir, implying re-pressurisation of the reservoir. In case of a tank reservoir, this influx is very small and it will take thousands of years before the gas pressure in the reservoir will become higher than the overlying hydrostatic column. This implies, that even if a leakage path such as a microannulus exists, a CO<sub>2</sub> leakage mechanism is absent.

In the unfortunate event that the gas pressure does increase to above the hydrostatic pressure, it is still uncertain whether CO<sub>2</sub> would migrate through a microannulus. Microannuli with small apertures will have a capillary entry pressure, similar to caprocks. The gas pressure has to be higher than the sum of the hydrostatic pressure at the base of the caprock and the entry pressure.



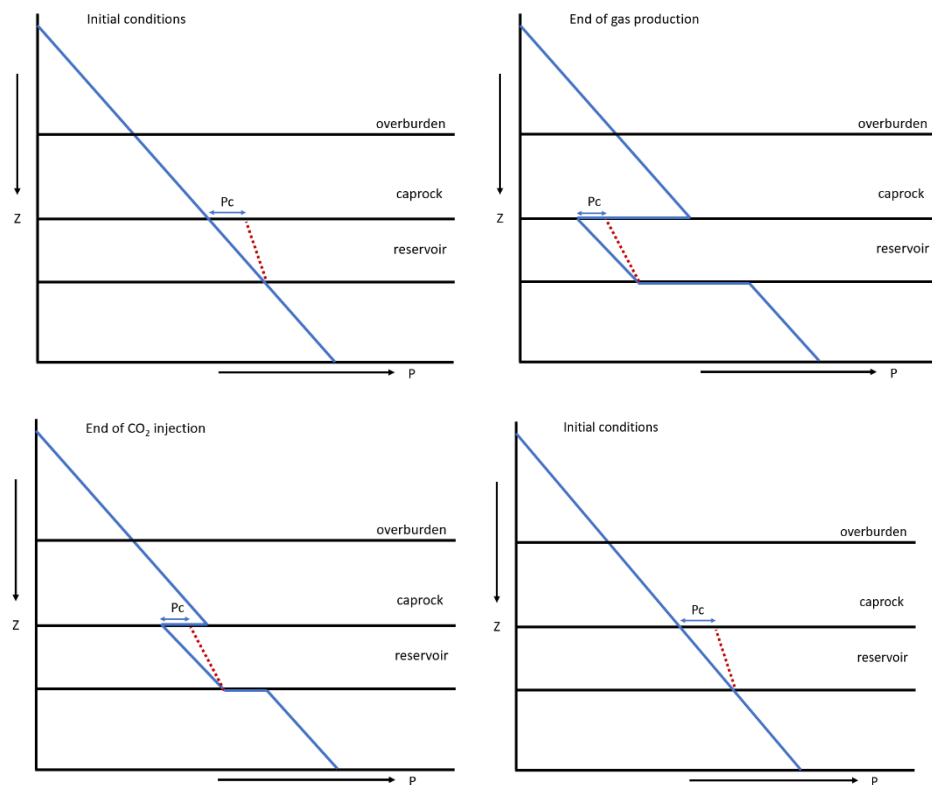


Figure 9-17: Pressure conditions in the various stages of the reservoir.

If CO<sub>2</sub> could displace the water column within the microannulus and starts migrating upwards, chemical interaction will take place with the cement. Assuming that the cement is of good quality, horizontal migration of CO<sub>2</sub> into the cement will take place by diffusion in dissolved state. Cement, which has a very high pH, is susceptible to interaction with carbonized water as cement minerals can quickly dissolve when the pH of the pore water decreases. The complex chemical interaction between cement minerals and carbonized brine is described in many publications (e.g., Kutcho et al., 2007; Rimmelé et al., 2008; Duguid et al., 2010). The most important reactions involve the dissolution of portlandite (CaOH<sub>2</sub>), the decalcification of Ca-silicate hydrate (CSH) and the precipitation of calcite (CaCO<sub>3</sub>) (Figure 9-18). Depending on the location of calcite deposition, complete pore clogging of the cement can occur, preventing further diffusion of carbonized brine and thereby further degradation of the cement. The upward flow of CO<sub>2</sub> through the microannulus adds another complicated component to the process, and has been described in Koenen and Wasch (2018). Instead of calcite precipitation in the pore spaces of cement, the calcite can accumulate within the microannulus and block the leakage path. The potential presence of sulfate in the caprock formation water can result in anhydrite precipitation in the microannulus, supporting the microannulus clogging by calcite (Koenen and Wasch, 2018). Whether clogging occurs depends on the upward flow rate of the CO<sub>2</sub> and the width of the microannulus. A low flow rate and/or small microannulus will allow calcite (and anhydrite) deposit to grow and block the leakage path. A high flow rate and/or large microannulus will not allow calcite growth, and instead, the leakage path will get worse in time due to cement mineral dissolution. This is illustrated in Figure 9-19. The worst case conditions for a microannulus of 100 micron and a CO<sub>2</sub> pressure 10 bar above hydrostatic conditions give a migration rate of CO<sub>2</sub> towards the overburden in the order of 10<sup>-6</sup>

kg/s, adding up to slightly more than 30 kg per year (Koenen and Wasch 2018). Compared to storage volumes in the order of megatonnes, this amount of leakage can be considered as negligible.

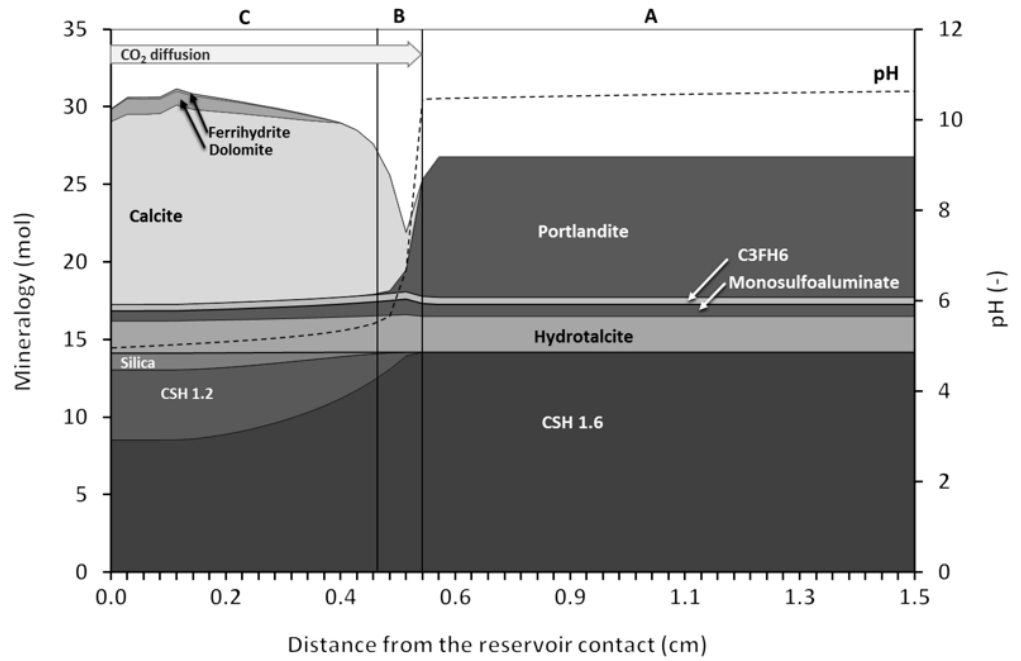


Figure 9-18: Simulated cement mineralogy with distance from the reservoir (or brine) contact after 300 days of inward diffusion of dissolved CO<sub>2</sub> and kinetic mineral reactions (PHREEQC software). Three zones develop: A: original cement, B: dissolution front, C: carbonated zone. The porosity of the cement decreases in the carbonated zone. From Koenen et al. (2014).

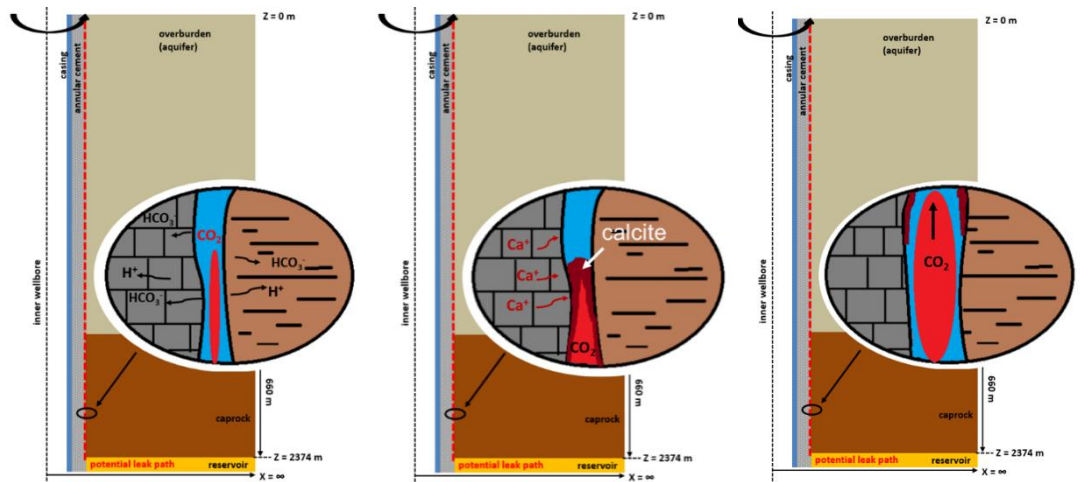


Figure 9-19: Schematic overview of CO<sub>2</sub> migration through a microannulus (red dotted line in between the annular cement and the surrounding rock). Left: initial state of microannulus and CO<sub>2</sub> migration. Middle: at low flow rate and/or small microannulus dissolved calcium migrates to the microannulus and is deposited as calcite, thereby blocking the leakage path. Right: at high flow rate and/or large microannulus the leakage path is enhanced as fast cement dissolution and CO<sub>2</sub> flow prevent calcite deposition. From Koenen & Wasch (2018).

### 9.3.5 Conclusions

Well dynamics simulations provided input on the temperature evolution along the wellbore with time. They showed that the CO<sub>2</sub> inside the injection well is 30 °C to 100 °C colder than the surrounding caprock formation, with largest temperature differences occurring in the initial phase of injection when the reservoir pressure is low (~20 bar) and the temperature of CO<sub>2</sub> at bottom hole is ~17 °C.

Based on performed simulations, debonding of well interfaces in P18-2 CO<sub>2</sub> injection wells is likely to occur due to cold fluid injection, thermal contraction and associated stress reduction in the near-well area. Debonding can, in principle, occur over lengths of tens of meters of caprock sections with good CBL. However, for migration of CO<sub>2</sub> with eventually leakage to occur, a continuous microannulus along the well cemented sections need to connect poorly cemented sections towards the overburden before we can speak of a leakage path. The presence of shale and potentially salt layers in the P18-2 caprock, identified as natural sealing formations could locally interrupt the leakage path. Even if a continuous leakage path would exist, it depends on the microannulus characteristics and pressure conditions whether upward CO<sub>2</sub> migration would actually take place. If the pressure conditions in the reservoir are high enough to overcome the capillary pressure within the microannulus, and migration does take place, the chemical interaction between CO<sub>2</sub> and cement can either prevent or enhance leakage towards aquifers overlying the caprock or towards the surface, also depending on the microannulus characteristics and pressure conditions. Keeping the CO<sub>2</sub> pressure in the reservoir below or at the hydrostatic pressure conditions will prevent the CO<sub>2</sub> from displacing the brine in the microannulus. In that case adequate monitoring during injection operations is required. The decommissioning method and procedures should result in well plugging from formation-to-formation (pancake plug or similar) in case microannulus formation is likely and poorly bonded annulus cement is not accepted as a leakage barrier. Based on performed simulations, debonding of well interfaces in P18-2 CO<sub>2</sub> injection wells is likely to occur due to cold fluid injection, thermal contraction and associated stress reduction in the near-well area. Debonding can, in principle, occur over lengths of tens of meters of caprock sections with good CBL. However, for migration of CO<sub>2</sub> with eventually leakage to occur, a continuous microannulus along the well cemented sections need to connect poorly cemented sections towards the overburden before we can speak of a leakage path. The presence of shale and potentially salt layers in the P18-2 caprock, identified as natural sealing formations could locally interrupt the leakage path. Even if a continuous leakage path would exist, it depends on the microannulus characteristics and pressure conditions whether upward CO<sub>2</sub> migration would actually take place. If the pressure conditions in the reservoir are high enough to overcome the capillary pressure within the microannulus, and migration does take place, the chemical interaction between CO<sub>2</sub> and cement can either prevent or enhance leakage towards aquifers overlying the caprock or towards the surface, also depending on the microannulus characteristics and pressure conditions. Keeping the CO<sub>2</sub> pressure in the reservoir below or at the hydrostatic pressure conditions will prevent the CO<sub>2</sub> from displacing the brine in the microannulus. In that case adequate monitoring during injection operations is required. The decommissioning method and procedures should result in well plugging from formation-to-formation (pancake plug or similar) in case microannulus formation is likely and poorly bonded annulus cement is not accepted as a leakage barrier.

Based on performed simulations, debonding of well interfaces in P18-2 CO<sub>2</sub> injection wells is likely to occur due to cold fluid injection, thermal contraction and

associated stress reduction in the near-well area. Debonding can, in principle, occur over lengths of tens of meters of caprock sections with good CBL. However, for migration of CO<sub>2</sub> with eventually leakage to occur, a continuous microannulus along the well cemented sections need to connect poorly cemented sections towards the overburden before we can speak of a leakage path. The presence of shale and potentially salt layers in the P18-2 caprock, identified as natural sealing formations could locally interrupt the leakage path. Even if a continuous leakage path would exist, it depends on the microannulus characteristics and pressure conditions whether upward CO<sub>2</sub> migration would actually take place. If the pressure conditions in the reservoir are high enough to overcome the capillary pressure within the microannulus, and migration does take place, the chemical interaction between CO<sub>2</sub> and cement can either prevent or enhance leakage towards aquifers overlying the caprock or towards the surface, also depending on the microannulus characteristics and pressure conditions. Keeping the CO<sub>2</sub> pressure in the reservoir below or at the hydrostatic pressure conditions will prevent the CO<sub>2</sub> from displacing the brine in the microannulus. In that case adequate monitoring during injection operations is required. The decommissioning method and procedures should result in well plugging from formation-to-formation (pancake plug or similar) in case microannulus formation is likely and poorly bonded annulus cement is not accepted as a leakage barrier.

Overall, the likelihood of CO<sub>2</sub> leakage through microannuli is small. De-bonding of cement-casing and cement-rock interface is very likely, but a leakage path requires a continuous microannulus from reservoir to overburden which is less likely. The presence of that natural sealing formations in the caprock could locally seal a microannulus, disconnecting the reservoir from the overburden. If a leakage pathway does exist, the CO<sub>2</sub> pressure in the reservoir should be high enough to displace the water in the microannulus. For a pressure below or at hydrostatic conditions, as is the plan for CO<sub>2</sub> storage in P18-2, this would not happen. In case the CO<sub>2</sub> pressure would be high enough to migrate through the microannulus, chemical interaction between the CO<sub>2</sub> and the cement would stimulate self-sealing of the leakage path by calcite precipitation. In a worst case scenario that self-sealing would not occur, leakage rates would be very low; e.g. <0.00001% of the total amount of CO<sub>2</sub> injected per year in the P18-2 storage plan.

## 9.4 Well abandonment

### 9.4.1 *Abandonment prior to start of injection*

Abandoning non-essential and non-injection wells before the start of CO<sub>2</sub> injection is considered a good practice with known reservoir conditions. This would reduce uncertainties with respect to well control during the well interventions for abandonment, compared to intervention after or during CO<sub>2</sub> injection. There is a strong case to decommission off-platform wells early, P18-02 for example, and sidetracks in platform wells that need isolating before injection begins. However, early decommissioning of platform wells removes them as candidates for monitoring activities.

The wells P18-02 and P18-2A6-ST need to be reworked or abandoned in accordance with P&A standards applicable for CO<sub>2</sub> storage wells (these standards are currently under development).

- The P18-02 well is suspended with P&A plugs, the mud line suspension for tie back strings is still installed. Some deficiencies have been identified for the P&A plugs; these should be managed in accordance with applicable P&A standards.
- For the P18-2A6-ST well some deficiencies have been identified at the side track window. From a reservoir storage aspect the side track should be P&A'd in accordance with applicable P&A standards and the P18-2A6 wellbore integrity has to be restored.

#### 9.4.2 *Abandonment after end of injection*

After completing the CO<sub>2</sub> injection through the P18-2 injection wells, these wells need to be abandoned in a way that conforms to good practice and meets required standards for a CO<sub>2</sub> storage site. After abandonment, the wells should ensure permanent and safe containment of the CO<sub>2</sub> in the reservoir.

Currently cement is the material of choice for annular seals and decommissioning of oil and gas wells. The abandonment plug has to extend across the full cross section of the well (“rock-to-rock”), whilst covering all annuli. If the cement behind the casing(s) is good, this can be achieved by placing a cement plug in the casing. If the quality of the annular seal is not sufficient or cannot be confirmed, pancake plugs have to be installed. This is achieved by removing the casing(s) and potentially cement and thereby creating a so called ‘window’. These are standard O&G practices, clearly described in the decommissioning standards.

Reaction of CO<sub>2</sub> with wellbore cement is a slow process if good construction practices and proper cement materials were used (IEAGHG, 2018). Degradation rates have been found to be proportional to temperature, pressure and the square root of time (Shell, 2015). According to literature the degradation of Portland cements could be up to about 12 m in 10.000 years. It is also reported that the permeability that can be created by the degradation is such that it still is within API criteria for cement (EPA, 2012).

Previous work (Vandeweyer et al., 2011) recommended placing pancake-type abandonment plugs. This approach to the P&A of CO<sub>2</sub> wells was also proposed in the permit application for the P18-4 reservoir. Whether pancake-type plugs will be the method of choice for abandonment of the P18-2 injection wells, and which materials to be used for the plug, depends on future developments until time of abandonment.

## 9.5 **Conclusions**

### *Well integrity*

The wells relevant in the context of CO<sub>2</sub> injection into the P18-2 field have been evaluated regarding their current status and integrity risks. All wells reviewed have the potential to be used safely as CO<sub>2</sub> injectors. Appropriate mitigation measures have been proposed to make them fit for storage operations.

### *Effects of injecting cold CO<sub>2</sub> on well integrity*

It is highly likely that de-bonding of cement interfaces will take place upon cold CO<sub>2</sub> injection, creating microannuli. In the unlikely case that the microannulus forms a continuous leakage path from reservoir to overburden, the characteristics of the

microannuli and pressure conditions determine whether upward CO<sub>2</sub> migration would actually take place. Keeping the CO<sub>2</sub> pressure in the reservoir below or at hydrostatic pressure conditions will prevent the CO<sub>2</sub> from migrating through the microannulus. This justifies the choice of keeping the reservoir pressure below or at hydrostatic conditions (Section 1.1). However, if for some reason the reservoir pressure would be high enough to displace the water column in the microannulus, the chemical interaction between CO<sub>2</sub> and cement can either prevent or enhance leakage, also depending on the microannulus characteristics and pressure conditions. For worst-case conditions, if CO<sub>2</sub> would migrate from the reservoir to the overburden through a microannulus, leakage rates would still be very low; i.e. <0.00001% on an annual basis. Overall, the likelihood and effect of leakage through microannuli is very low and can be considered insignificant.

#### *Well abandonment*

Appropriate methods should be used for the abandonment of the wells. Given the likelihood of microannuli forming during the injection of cold CO<sub>2</sub>, abandonment methods that remove these potential leakage paths would be preferred. As an example, full-bore pancake like plugs would provide formation-to-formation closure of the injection wells. However the choice of employing these techniques should be weighed up against 1) the guarantee that pressure in the reservoir stays below the surrounding pressure, preventing flow out of the reservoir through microannuli 2) even if flow occurred through microannuli the chemical reaction between CO<sub>2</sub> and cement would cause a permanent flow barrier 3) the expansion and elasticity of layers above the reservoir, including the caprock will eventually close around the wellbores squeezing shut any microannuli and guaranteeing permanent storage of the CO<sub>2</sub>. The use of pancake plugs is unlikely to be more successful than any of these effects individually.

## 10 P18-2 storage site and storage complex

### 10.1 Introduction

The assessment of leakage risks for CO<sub>2</sub> storage in the P18-2 field relies on a proper definition of the storage site and storage complex. In this Section we discuss these, based on definitions in the EU Storage Directive and insights from the detailed reservoir, fault, caprock and well evaluations in Sections 6 to 9.

### 10.2 Definitions in the Netherlands Mining Law and the EU Storage Directive

The EU Storage Directive (EU, 2009) introduced the concept of the storage complex in defining rules for environmentally sound and safe geological storage of CO<sub>2</sub>. This is to be accomplished by the characterization and assessment of the storage complex.

The following definition is given of the storage complex, *op. cit.*:

‘storage complex’ means the storage site and surrounding geological domain which can have an effect on overall storage integrity and security; that is, secondary containment formation

According to the Netherlands Mining Law (Mijnbouwwet, 10 April 2019):

“CO<sub>2</sub>-opslagcomplex: opslagvoorkomen voor CO<sub>2</sub> en de omringende geologische gebieden die een weerslag kunnen hebben op de algehele integriteit van de opslag en de veiligheid ervan”.

The definition of “storage complex” in the Netherlands Mining Law does not explicitly refer to “secondary containment formation” like in the EU Storage Directive. For the definition of “storage site” the Netherlands Mining Law uses the term “opslagvoorkomen van CO<sub>2</sub>”. Although it seems that this term can be linked to “storage site” in the EU Directive it is not clear if this will include “the associated surface and injection facilities” as well, like is defined in the EU Storage Directive (see below). For this report we assume that these facilities are part of the storage site. “Opslagvoorkomen” is: een voorkomen dat gebruikt wordt voor opslag”

The storage site according to the EU Directive is defined as, *op. cit.*:

‘storage site’ means a defined volume area within a geological formation used for the geological storage of CO<sub>2</sub> and associated surface and injection facilities  
Leakage then means “*any release of CO<sub>2</sub> from the storage complex*” and migration stands for “*the movement of CO<sub>2</sub> within the storage complex*” according to the EU Directive.

The Storage Directive (EU, 2009: Article 4, para 4) also says:

4. A geological formation shall only be selected as a storage site, if under the proposed conditions of use there is no significant risk of leakage, and if no significant environmental or health risks exist..

We consider the hydraulically connected pore space bordered by flow barriers together representing a physical trap, and we predict by dynamic modelling the dispersion of CO<sub>2</sub> inside the physical trap. Our predictions will be confirmed by operational monitoring (EU, 2009: Article 13).

This implies that monitoring activity should be focused particularly on providing the evidence for the effectiveness of the geological and engineering barriers that prevent significant risk of leakage (migration out of the storage complex).

Note that Guidance document no 2 (EU, 2011) suggests to allow for changes in the specific boundaries of the storage complex during the storage permit review and updating process.

CO<sub>2</sub> movement out of the storage site but remaining in the storage complex is called migration (in the Storage Directive). Movement of CO<sub>2</sub> out of the storage complex is called leakage under the Storage Directive, and if the CO<sub>2</sub> then reaches the atmosphere it is called emission under the implementing regulation of the ETS Directive (ETS directive, 2009; EU, 2018) and emission allowances need to be returned by the storage permit holder to the state. Leaks cannot be measured, they can only be estimated. From the monitoring plan and plan for corrective measures it needs to be defined how to recognise such movement of CO<sub>2</sub> and what actions or corrective measures to take.

### 10.3 Definition of the storage site

The storage site is what contains the CO<sub>2</sub> – the reservoir – and the injecting or not yet decommissioned wells and associated surface installations (wellheads) and injection facilities (tubing in wells). More specifically, the P18-2 storage site comprises the following:

- P18-2 Triassic reservoir rocks of the Volpriehausen Sandstone, Lower and Upper Detfurth Sandstones and the Hardeggen Formation. The lower 3 units are vertically hydraulically disconnected by the presence of low permeable zones in between (baffles). Strongly restricted flow is possible between the Upper Detfurth sandstone and the Hardeggen Formation (see Figure 17-14 and Figure 17-15)The reservoir consists of 4 partly hydraulically connected main compartments and is bounded by faults on all sides except for the northern boundary, which is downdip of the original the GWC. Near faults F14 and Fault1, the northern boundary is in a spill point just to the north of the reservoir (see Figure 10-1; more details are in Section 12.1).
- Wells penetrating the storage complex up to the wellheads;
- Related wellheads measurement equipment and christmas trees.

### 10.4 Definition of the storage complex

In addition to the components of the storage site mentioned in 10.3, the storage complex also includes the formations that seal off CO<sub>2</sub> in the reservoir and any surrounding formation that could contain CO<sub>2</sub>.

The Porthos P18-2 storage complex is proposed to include the following spatial compartments in addition to the storage site components:

- Massive caprock on top of the reservoir consisting of impermeable Upper Germanic Triassic Group and Altena Group with a thickness of 450 to 750 m;
- The formations below the storage reservoir consisting of the Triassic Rogenstein and Main Claystone Members.



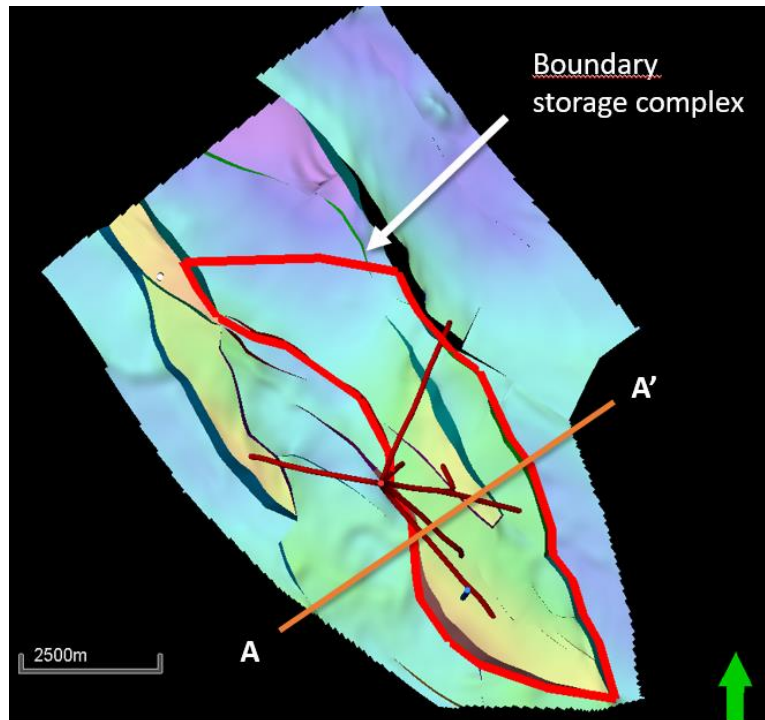


Figure 10-1 Depth map of the top of the reservoir with the proposed boundary of the storage complex at top reservoir level (red line) delimited by the bounding faults and an open boundary downdip of the GWC to the north; line segment A-A' represents the location of the geological cross section shown in Figure 10-2.

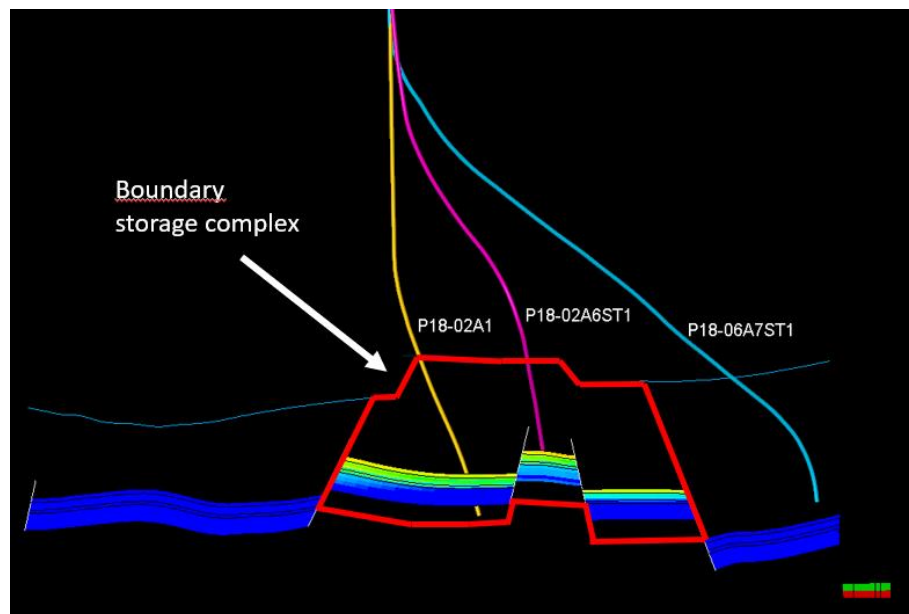


Figure 10-2 Geological cross section of the reservoir and the overburden with indication of the vertical extension of the storage complex (in red); location of cross section is shown in Figure 10-1. Blue line is top caprock (=Base Schieland Gp).

## 10.5 Differences with the P18-4 storage complex definition

In contrast to P18-2, the P18-4 storage complex includes the Lower Cretaceous aquifers and seals as a secondary containment system. The proposal for P18-2 relies on the containment by the massive seal of Triassic and Jurassic formations, which has a very low likelihood of CO<sub>2</sub> leaking out of this caprock sequence and thus complies with the Storage Directive requirement that no significant leakage risk exists or will develop. In addition, the storage reservoir pressure will be kept at or below the initial pressure. For these reasons it is not necessary to add an additional spatial compartment on top of the Triassic and Jurassic caprock sequence to warrant CO<sub>2</sub> containment.

Over a small section reservoir rocks of Compartment 2-IV in P18-2 and the adjacent P18-6 reservoir are juxtaposed. The huge pressure difference between the P18-6 reservoir (378 bar) and the P18-2 reservoir (100 bar) after 9 years of production from the P18-2 reservoir indicates that these reservoirs behave as two separate hydraulic units. Furthermore, Compartment 2-IV very likely is a separate hydraulic unit; CO<sub>2</sub> injected in Compartment 2-I will thus not reach Compartment 2-IV and the adjacent P18-6 reservoir. For these reasons it is concluded that the P18-6 reservoir can be excluded from the P18-2 storage complex (see also Section 6.3.5). In the case of the juxtaposed P18-4 and P15-9 reservoirs this evidence was not available as they were produced simultaneously and a large differential pressure was not built up. For that reason the P15-9 reservoir was included in the P18-4 storage complex.

In contrast to P18-4, P18-2 has two more potential structural spill points, one to the North and one to the Southwest of the P18-2 reservoir. Their acting as true spill points depends among other things on the degree of filling of the reservoir and the lateral hydraulic connectivity near the potential spill zones.

Reservoir simulations with highly exaggerated reservoir pressures up to 450 bar indicate that the CO<sub>2</sub> does not migrate beyond the northern limit of the storage site (see also Section 6.3.4 for more background information).

In a small section to the NW of Compartment I across Fault F14, low permeable Volpriehausen Sands (< 1 mD) are juxtaposed to the Hardegsen Formation. The low permeability makes it highly unlikely that significant amounts of CO<sub>2</sub> migrate across the fault (see also Section 12.1).

## 10.6 Barriers

### 10.6.1 Barriers in the storage complex

The storage complex includes the principle barriers for the permanently stored CO<sub>2</sub> in the P18-2 depleted gas reservoir.

The *geological barrier system* consists of:

- Massive caprock, consisting of Triassic and Jurassic shales, directly located above the reservoir rocks (see also Section 4.3);
- Sealing, reservoir-bounding faults;
- Structural relief trapping of CO<sub>2</sub>, e.g. at the northern boundary of the reservoir.

The *well engineering barrier system* consists of the two barriers, as described in Section 9.

#### 10.6.2 *Evaluating barrier integrity*

The various barriers have been evaluated in detail to further qualify the P18-2 reservoir for permanent CO<sub>2</sub> storage:

- The initial condition of the caprock and the faults is characterized in Section 4 and Appendix B (Section 17).
- The risk of lateral migration (spilling) from the reservoir compartment to the North was assessed in more detail in Section 6.
- The stability of the fault zone under the influence of chemical, mechanical and thermal processes were investigated (see Section 7).
- The possible effects of fracturing and chemical degradation on the integrity of the caprock have been evaluated with semi-analytic thermomechanical modelling and following a literature study, respectively (see Section 8).
- The integrity of all wells penetrating the reservoir have been evaluated and recommendations for qualifying the well for CO<sub>2</sub> storage have been defined (see Section 9).

The results of these investigations have been used to characterize the risks for loss of containment and to propose measures to lower the risk level if necessary (see Section 12). Section 13 describes the monitoring plan, which enables the early identification and intervention of potential issues for CO<sub>2</sub> containment.

# 11 Migration paths

## 11.1 Introduction

The EU storage directive requires an analysis of potential leakage pathways (EU, 2009, Annex I). The results presented in sections 6 through 9 support the conclusion that leakage of CO<sub>2</sub> (i.e., CO<sub>2</sub> moving out of the storage complex) along wells, faults or through the caprock is highly unlikely, if the injection process is conducted within safe limits (see Sections 12 and 14, below). Overfilling the reservoir (i.e., spilling of the CO<sub>2</sub> across a spill point) does not occur, as long as the average reservoir pressure is kept below initial gas pressure.

Nevertheless, with this starting point, an analysis was made of pathways that CO<sub>2</sub> would take in case of a hypothetical leak out of the reservoir, along one of the wells, or through the caprock. The analysis includes the identification of possible secondary containment at the level of the reservoir formations, or in the overburden.

A static overburden model was assembled, based on both 2D and 3D seismic surveys and well information. On the basis of the overburden model and the selected migration pathways, an evaluation of possible migration scenarios was developed.

The conclusions are that in case of overfilling of the reservoir, migration through the Buntsandstein (reservoir formations level), the CO<sub>2</sub> remains trapped and finally will migrate towards the adjacent gas reservoirs. In case of migration of CO<sub>2</sub> into the aquifers of the overburden, caused by a shortcut along the wellbore, it will remain trapped within these aquifers. However, migration of CO<sub>2</sub> along faults in the overburden (above the Altena Group) to a shallower aquifer level cannot to be excluded.

Overall, given the results presented in the previous sections, the conclusion from the analysis presented in this section is that the only potential pathway to the surface of CO<sub>2</sub> stored in the P18-2 field is via leaking wells, leaking directly into the atmosphere and not indirectly via pathways originating in deeper parts of the overburden.

## 11.2 Available data and workflow

A geological model was constructed with Petrel modelling software (Schlumberger). The model comprises an area with a 14 km minimum radius surrounding the P18 gas field.

In vertical direction the model spans the total overburden of the reservoir.

The workflow for building the model is described in *CATO-2-WP3.1-Geological report P18 (December 2010)*: seismic interpretation of the overburden was performed, and subsequently the model was built on the basis of a fault model with a grid cell size of 250m x 250m. The model was converted from time to depth, and tied to the wells.

Figure 11-1 shows the location of the P18 fields, with neighbouring fields and wells.

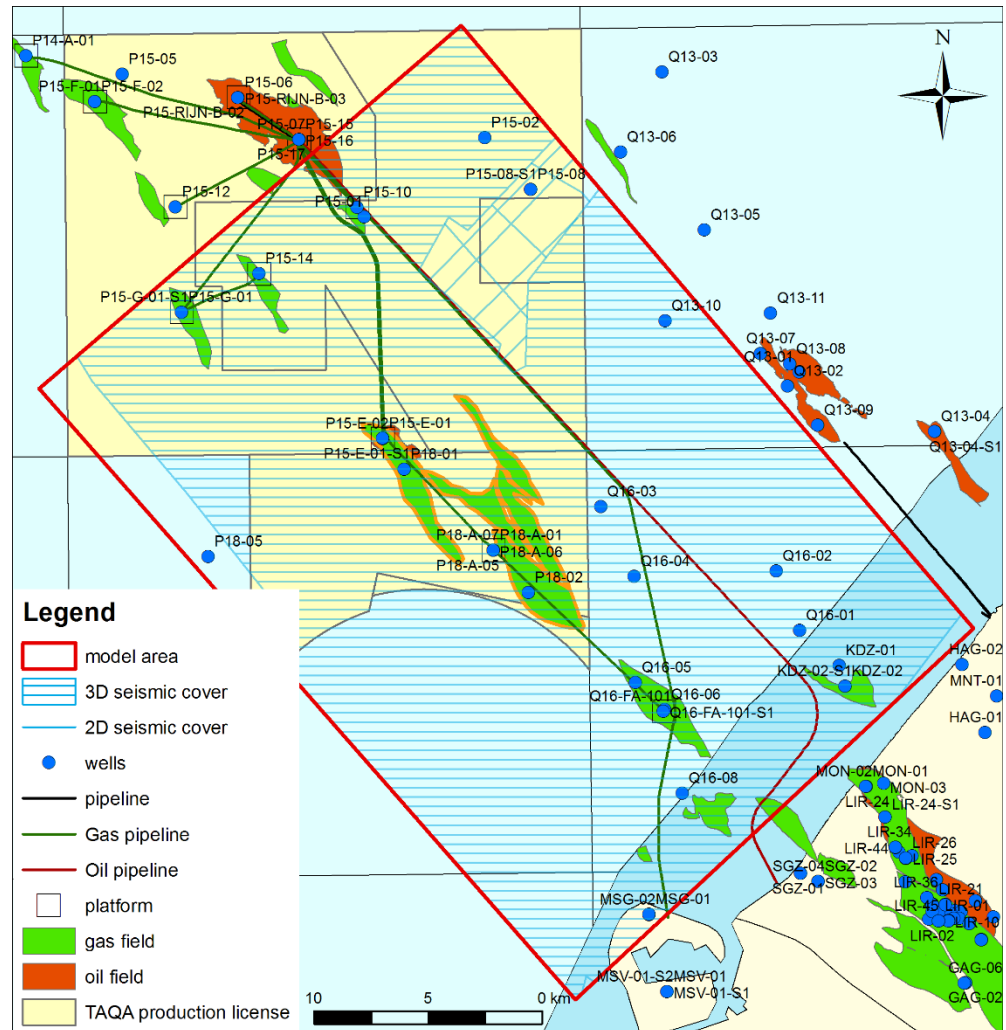


Figure 11-1: Location map of P18 model area. Target P18 gas fields are indicated with an orange boundary.

### 11.3 Geological model of the overburden

#### 11.3.1 Overburden

The primary seal, made up by the Upper Germanic Trias and Altena Group is successively overlain by (see also Figure 11-2):

- The Schieland Group, which consists of shales and (stacked) channel sands of the Nieuwerkerk Fm. (Delft sandstone equivalent). The lateral continuity of the individual sandbodies (thickness 2-5m) is probably very limited.
- Lower Cretaceous Rijnland Group, which consist of marine sandstones, shales and marls. At the base of the Rijnland Group, the Rijn / Rijswijk Fm. is present. This sandstone is widely distributed in the P18 area. It is also known for its oil (P15) and gas (onshore) accumulations within the West Netherlands Basin. The sandstones are interpreted as transgressive sheet sands, with good lateral continuity. In the upper part of the Rijnland succession, the Holland Greensand Member is present. It consists of argillaceous sands and silts. The distribution is limited to the southern margin of the West Netherlands Basin. Although the Holland Greensand has good lateral continuity, permeability is general low.

- Upper Cretaceous Chalk Group, which consist at the base of the formation of sands and marls and a thick layer (900 m) of limestones (Chalk). The distribution of the basal Texel Greensand is limited to the southern basin margin.
- The North Sea Group, which consists of siliciclastic sediments. Two major aquifers can be distinguished; the Dongen sand, a basal transgressive sandstone, and the marine Brussels Sand Member.

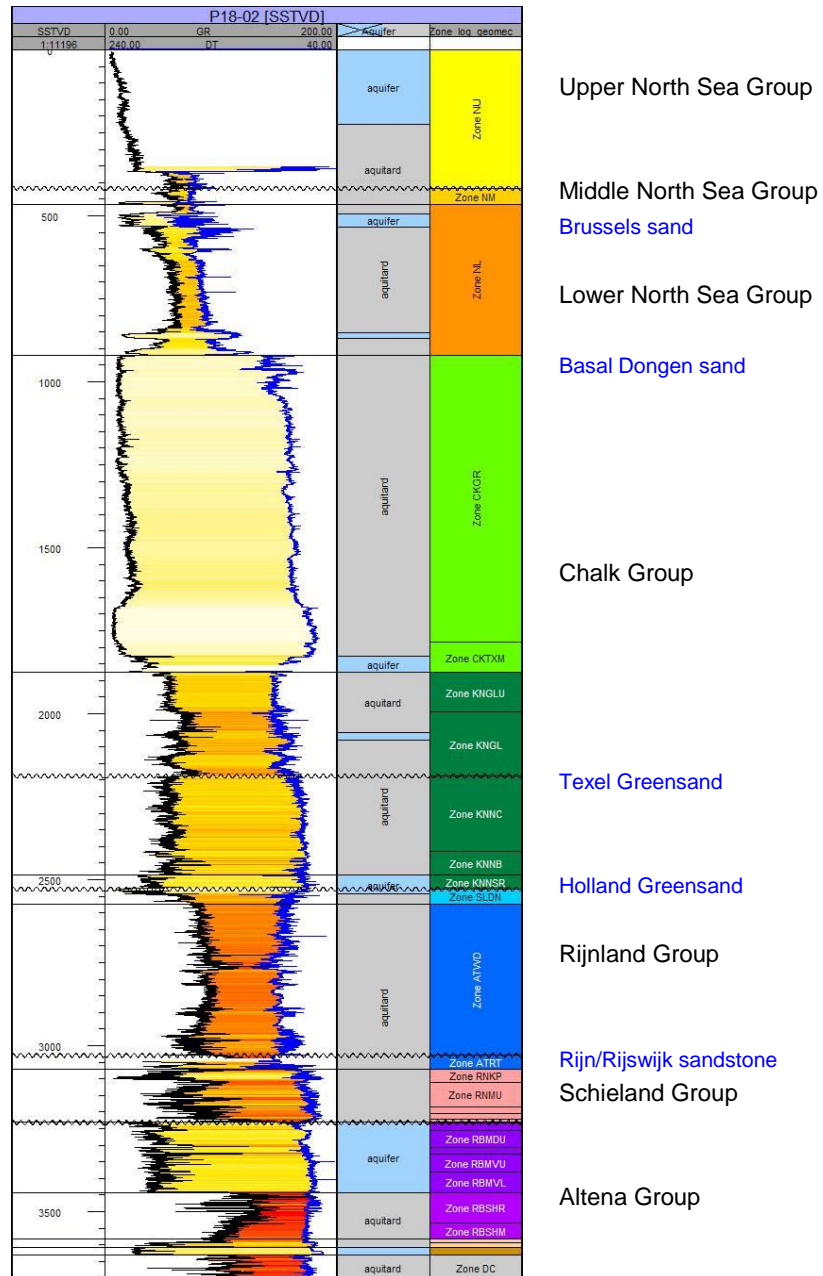


Figure 11-2: Composite well log (GR, DT) of P18-02 with main stratigraphic units and aquifer intervals

### 11.3.2 Faults

Faults present at reservoir level (Buntsandstein) in general continue till the Schieland group (white line) or base Rijnland Group (dark green line in Figure 11-3). Late Cretaceous inversion caused faulting of the sediments above the Base

Cretaceous Unconformity (base Rijnland) These faults (dashed lines Figure 11-3) have limited displacement, but continue to the Upper North Sea Group.

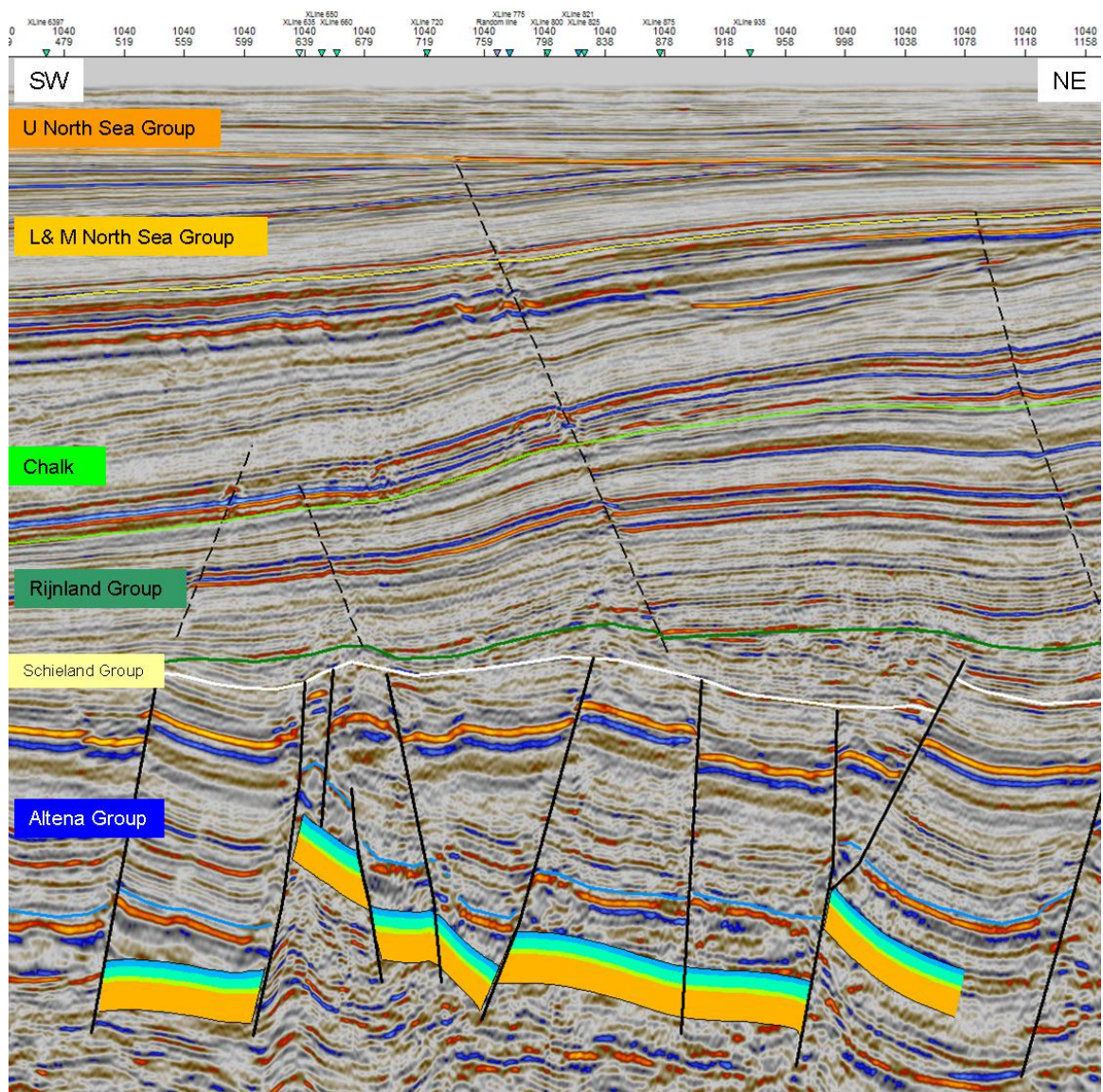


Figure 11-3: Seismic cross-section (inline 1040 of P15P18 seismic cube) through the P18 field, displaying the reservoir interval (coloured layering), the main bounding faults to the reservoirs (bold lines), the main stratigraphic units in the overburden and the faults in the overburden (dashed)

## 11.4 Migration scenarios

For the qualitative analysis three migration scenarios were considered.

- Spilling out of the gas reservoir, due to overfilling. This leads to migration within the Bundsandstein formations beyond the boundaries of the storage complex (hence, this would be classified as leakage). See Section 11.6.1.
- Leakage through the caprock due to fracture formation. This leads to CO<sub>2</sub> entering the Rijn/Rijswijk Sandstone (Section 11.6.2).
- A wellbore shortcut, opening pathways for CO<sub>2</sub> into formations overlying the caprock.

- Migration into Rijn/Rijswijk Sandstone (Section 11.6.2);
- Migration into Holland Greensand (Section 11.6.311.6.3);
- Migration into Texel Greensand (Section 11.6.4);
- Migration into Dongen & Brussel Sandstone (Section 11.6.5).

The sections below investigate the consequences of these scenarios occurring, in spite of their low to very low probability, given the results presented in Sections 6 (spilling out of the reservoir), 8 (caprock integrity) and 9 (well integrity).

## 11.5 Methods

Possible CO<sub>2</sub> migrations pathways were analyzed using the rapid trapping assessment tool PetroCharge Express of IES. With this tool a rapid analysis of the migration pathways based on the layer geometry is performed. The layer geometry was provided by the exported horizons from Petrel (regional scale model). The program uses the input top layer as bounding elements assuming these layers to be impermeable. Although in reality the layers are not completely impermeable the goal is to create a concept model from which migration routes within the layer can be deducted.

It should be noted that PetroCharge only looks at the geometry and does not describe various other aspects of flow. It was therefore decided to “inject” large amounts of CO<sub>2</sub> in the considered leakage scenarios and to focus on the migration paths and final accumulation structures.

## 11.6 Results

### 11.6.1 Migration scenario: Buntsandstein

In case of “overfilling” the gas reservoir with CO<sub>2</sub> (see also the comments in the introduction to this section) it might be possible that the CO<sub>2</sub> will pass by the original closure defined by the initial gas water contact (GWC).

- Overfilling the P18-2 main compartment could lead to migration towards the Q16-4 structure (Figure 11-4, arrow 1) and the P16-FA field (Figure 11-4, arrow 3)
- Overfilling the P18-4 compartment in combination with migration along faults could lead to migration towards the P15-E and P15-14 field (Figure 11-4, arrow 2).

It must be mentioned that the structure drilled by the (dry) exploration wells Q16-04 and Q16-03, only minor amounts of gas were encountered. If the containment were to fail by a mechanism describes above, the most probable failure would be of an absence of sideseal in combination with reservoir juxtaposition with Jurassic sandstones from for instance the Nieuwerkerk Formation.



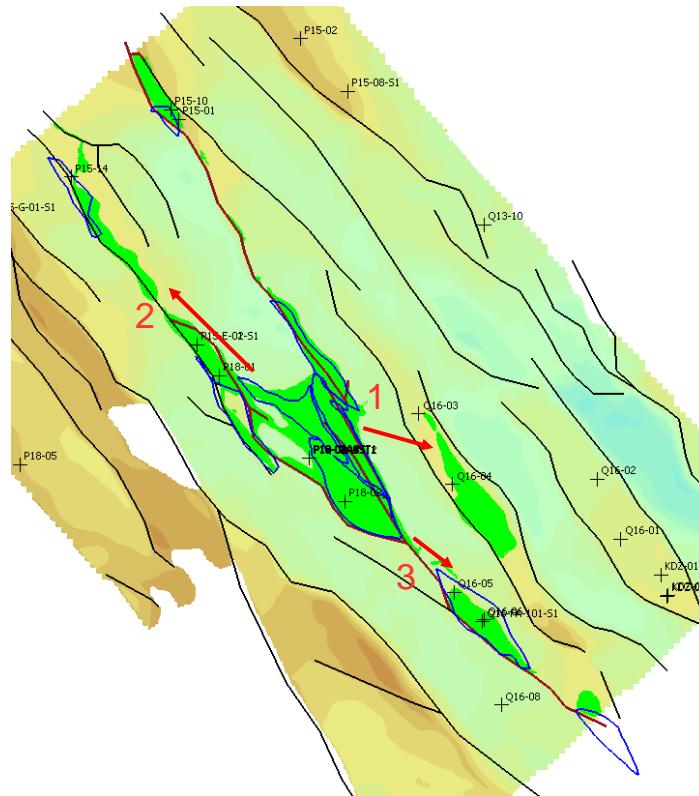


Figure 11-4 Structure map of Top Buntsandstein. Black lines indicate faults. Also shown are boundaries of gas accumulations and location of wells.

#### 11.6.2 Migration scenario: Rijn/Rijswijk sandstone

In case of fault reactivation or shortcut via a wellbore, CO<sub>2</sub> can hypothetically migrate into the Rijn/Rijswijk sandstone aquifer.

- CO<sub>2</sub> leaking along wells P18-02-A-01, P18-02-A-06 or P18-02-A-06-S1 will migrate towards Q16-03 & Q16-04 structure (Figure 11-5, arrow 1).
- Spill originating from wells P18-02, P18-02-A-03, P18-02-A-05 will migrate towards Q16-FA structure (Figure 11-5, arrow 2).

#### 11.6.3 Migration scenario: Holland Greensand

In case of a shortcut via a wellbore, CO<sub>2</sub> can hypothetically also migrate into the Holland Greensand aquifer

- Spill originating from wells P18-02-A-01, P18-02-A-03, P18-02-A-06, P18-02-A-06-S1, P18-06-A-07 will migrate towards Q16-03, Q16-04 structure (Figure 11-6, arrow 1)
- Spill originating from wells P18-02, P18-02-A-05 will migrate towards Q16-FA structure (Figure 11-6, arrow 2)
- Spill originating from P18-A-02 well will migrate towards P15-9 (E) structure (Figure 11-6, arrow 3)

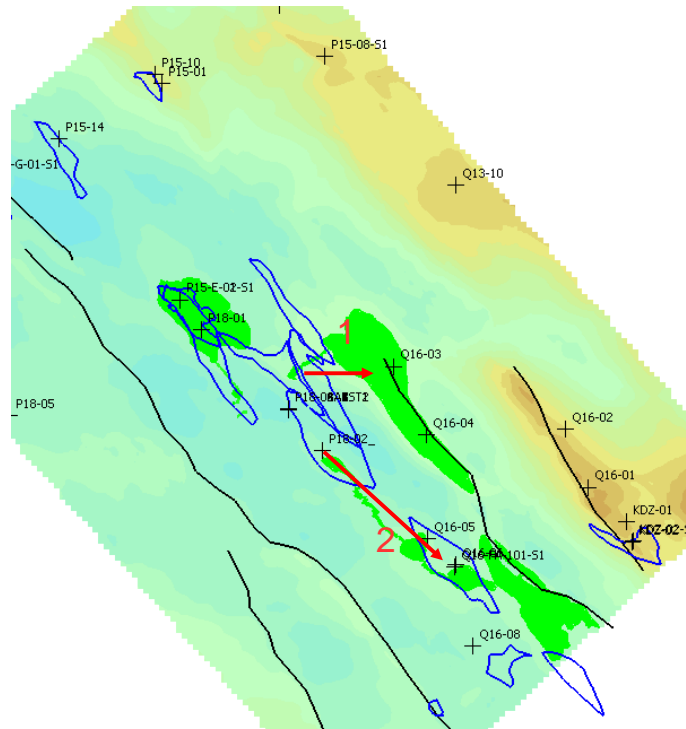


Figure 11-5: Structure map of the Base Rijnland Group. Black lines indicate faults. Also shown are boundaries of gas accumulations and location of wells.

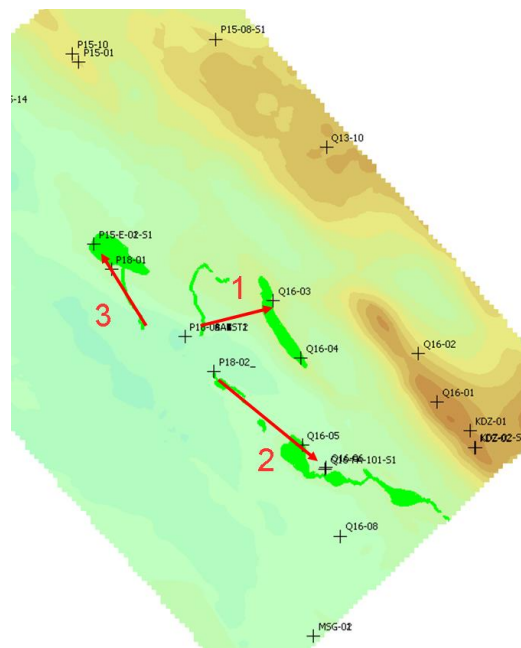


Figure 11-6: Structure map Holland Greensand.

11.6.4 Migration scenario: Texel Greensand

In case of a shortcut via a wellbore, CO<sub>2</sub> can hypothetically migrate into the Texel Greensand aquifer

- Spill originating from P18-A production wells will migrate towards Q16-3 structure and finally Q16-02 (Figure 11-7, arrow 1).

- Spill from the P18-02 well will migrate towards Q16-FA structure and finally Q16-01 (Figure 11-7, arrow 2).

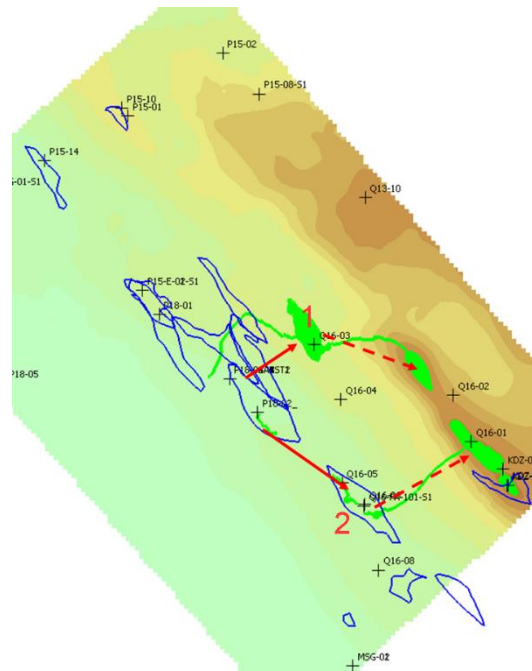


Figure 11-7: Structure map base Chalk Group.

11.6.5 *Migration scenario: Dongen sand & Brussel sandstone*

In case of shortcut via a wellbore, CO<sub>2</sub> can hypothetically migrate into the North Sea Group aquifer

- Spill originating from P18-A production wells will migrate towards Q13-10 structure (Figure 11-8, arrow 2).
- Spill from the P18-02 well will migrate towards Q16-02 structure (Figure 11-8, arrow 2)

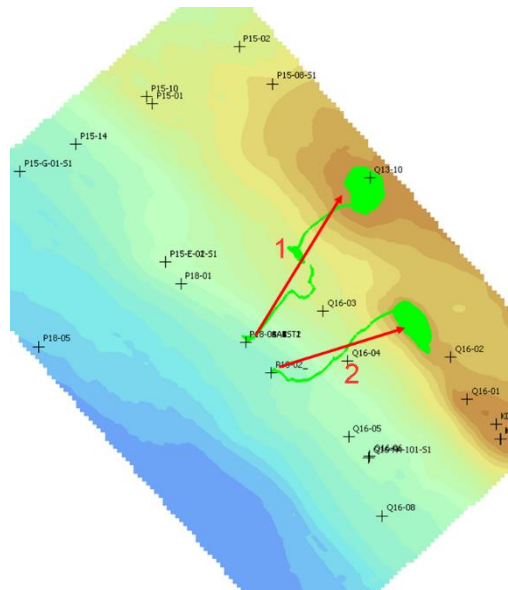


Figure 11-8: Structure map base North Sea Group.

### 11.7 Present day hydrocarbon migration

Inspection of the overburden revealed the possible existence of shallow gas pockets (*CATO-2-WP3.1-D01-Geological report P18 (December 2010)*). The gas most probably is sourced from Jurassic Posidonia shales (van Balen, 2000). The Posidonia shales are situated stratigraphically above the Bunter reservoir and seal, so this hydrocarbon migration is no proof of seal failure/leakage of the P18 Bunter reservoir.

Figure 11-9 shows a seismic section of the overburden, to illustrate hydrocarbon migration, and to illustrate a possible migration pathway for CO<sub>2</sub>. Gas is sourced from the Posidonia shale (strong reflector at the base of the lowest arrow), and migrates via a fault into the sands of the North Sea Group. The red ellipses indicate bright spots, which suggest the presence of gas. Migration is also possible within the Brussels sand, indicated by the arrows in Figure 11-9. At the location where the Brussels sand toplaps against the Upper North Sea Group (Mid Miocene Unconformity, orange line), an increase of amplitudes is observed, which suggest migration from the Brussels sand into the Upper North Sea Group.

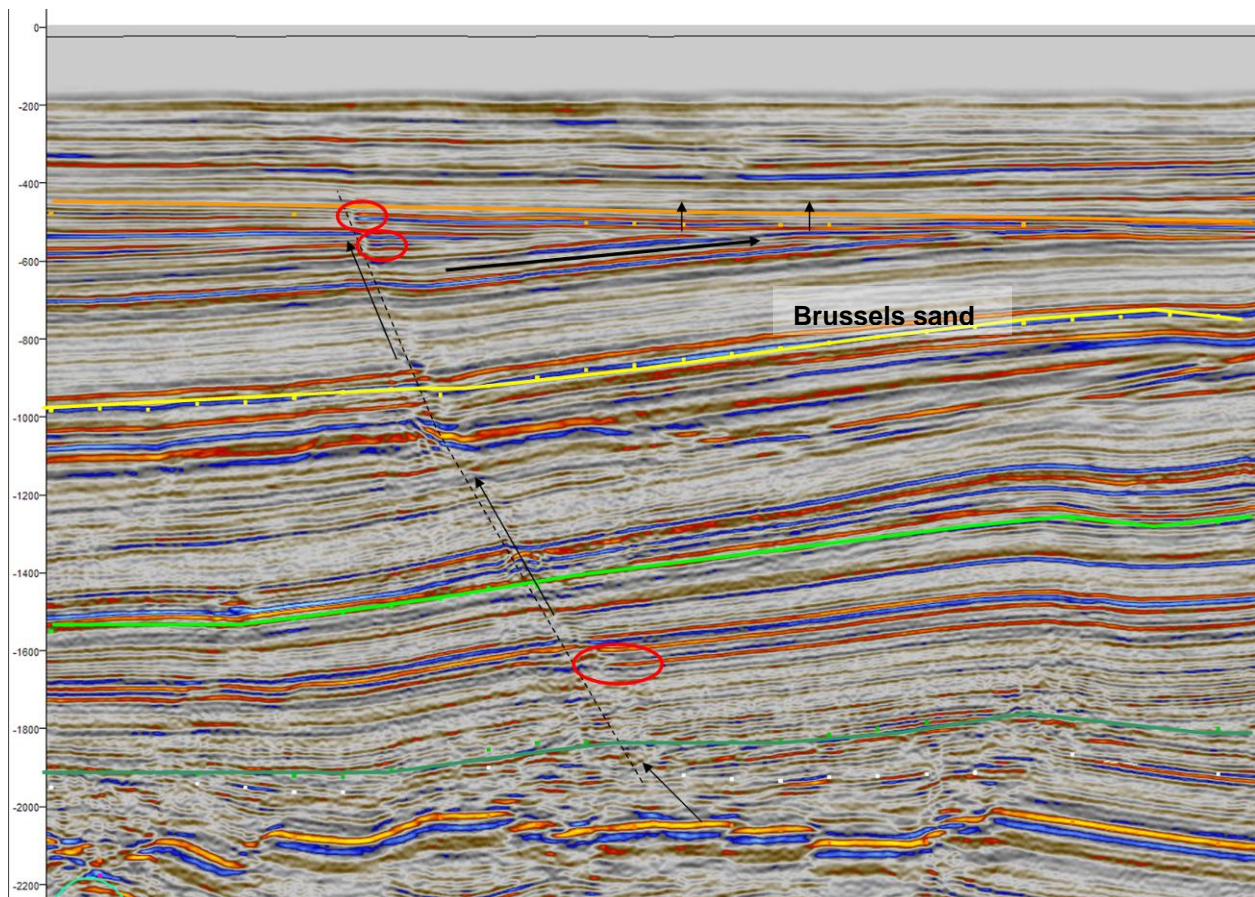


Figure 11-9: Seismic section of the P18 overburden. Arrows indicate hydrocarbon migration along a fault (dashed line). Red ellipses mark bright spots on the right side of the fault. Dark

green line: base Rijnland (BCU), bright green line: base Chalk, yellow line: base North Sea, orange line: base Upper North Sea (MMU).

## 11.8 Conclusions

A Petrel model of the overburden has been constructed, using on publicly available data and data provided by TAQA. Based on the geological model and selected hypothetical migration scenarios, a qualitative evaluation of the possible pathways was developed.

Starting from the results presented in sections 6 through 9, which support the conclusion that leakage of CO<sub>2</sub> (i.e., CO<sub>2</sub> moving out of the storage complex) along wells or faults is highly unlikely if the injection process is conducted within safe limits (see Sections 12 and 14, below), the conclusions are that in case of overfilling of the reservoir, migration through the Buntsandstein (reservoir formations level), the CO<sub>2</sub> remains trapped and finally will migrate towards the adjacent gas reservoirs. Also, in case of migration of CO<sub>2</sub> into the aquifers of the overburden, caused by a shortcut along the wellbore, it will remain trapped within these aquifers. However, migration of CO<sub>2</sub> along faults in the overburden (above the Altena Group) to a shallower aquifer level cannot to be excluded.

Overall, given the results presented in the previous sections, the conclusion from the analysis presented in this section is that the only potential pathway to the surface of CO<sub>2</sub> stored in the P18-2 field is via leaking wells, leaking directly into the atmosphere and not indirectly via pathways originating in deeper parts of the overburden.

## 12 Risk assessment and preventative measures

The current study on the feasibility of CO<sub>2</sub> storage in the P18-2 reservoir made optimal use of earlier work done on the P18 reservoirs, a large part of which was carried out as part of the national CATO2 programme until 2011. The main outcomes of the risk assessment work carried out at that time were presented and discussed during a workshop with representatives from Taqa, EBN, Royal HaskoningDHV and TNO on 12 November 2018. The results were used to verify the completeness of the initial scope of the present feasibility study and if necessary to expand it. This established the basis for the studies (in addition to those already carried out in 2011) presented in Chapters 6 through 9. The central question is where the CO<sub>2</sub> is at any given point in time and whether it could (partially) migrate out of the storage complex. In Section 10 the delimitations of the storage site and the storage complex including the intended storage reservoir have been presented.

After the identification and evaluation of the risks, measures were defined to diminish the risk level. The present chapter provides an extensive summary of this risk management exercise. The risk evaluations are presented for the individual spatial compartments, e.g. reservoir, caprock, fault zones and wells, which together make up the storage complex and leakage barriers. A summary of the risks and their evaluation is provided in the risk register (see Section 0).

The assessment presented here is based on a number of technical conditions (the list below repeats Section 5.4).

- The CO<sub>2</sub> supply profile is shown in Section 5.2; the profile has a plateau injection rate of 2.8 Mt/yr.
- Three wells are available for injection: P18-02-A-01, P18-02-A-03ST2 and P18-02-A-05ST1.
- The tubing in all injection wells will be recompleted (pers. comm. EBN, 2019). The external tubing diameter for all four injector wells is assumed to be 4.5" (Section 5.1).
- Additional conditions apply to the reservoir and the downhole conditions of the CO<sub>2</sub>.
  - At the start of injection, the reservoir pressure is 20 bar.
  - Downhole temperature is required to always be above 15 °C, to avoid CO<sub>2</sub> hydrate formation in the well and in the near-well area (Section 6.4).
- The maximum average reservoir pressure is equal to the initial reservoir pressure.
- The CO<sub>2</sub> is assumed to contain no impurities. At the time of the present study, no quality/specification information was available about potential sources of CO<sub>2</sub>.

The assessment is focused on the functioning of the P18-2 reservoir as a suitable 'container' for the storage of CO<sub>2</sub> to prevent significant leakage from the storage complex as required under the EU Storage Directive (EU, 2009). The permanent containment of CO<sub>2</sub> is provided by a number of geological and technical barriers. It is of great importance that any risk to this containment function is small, can be managed and is acceptable.

The risks of loss of containment relate to possible existing or future defects in the reservoir (pressure evolution and fluid flow leading to lateral flow or spilling of CO<sub>2</sub>), in the caprock (migration pathways, e.g. fractures), bounding faults (re-activation and increased likelihood for CO<sub>2</sub> migration) or the wells (migration pathways as a result of defects in well cement or casing).

The results from the risk assessment together represent a main building block for the Environmental Impact Assessment which is required for the storage permit application.

## 12.1 Reservoir

The P18-2 reservoir is bounded by sealing faults on all sides except for the north-western boundary of Compartment IV of the gas reservoir, which is in direct contact with the water saturated part of the Triassic reservoir rocks more downdip (see Figure 4-2). Along faults F14 and Fault 1 (Figure 4-4) the reservoir has an elongated extension. This extension might be prone to lateral flow or spilling of CO<sub>2</sub> further to the NW. At two other locations near bounding faults CO<sub>2</sub> might spill as in these zones reservoir rocks are juxtaposed to water or gas saturated rocks outside the reservoir.

In summary, three locations with potential hydraulic connections to permeable rocks outside the reservoir have been evaluated in more detail:

- NW margin of Compartment II represented by the outer boundary of the GWC, in particular near Fault 1;
- Small section to the NW of Compartment I across Fault F14;
- Small section along fault F57 between reservoirs P18-2 and P18-6.

### 12.1.1 *Evaluation of spilling at the NW margin of Compartment II*

Results from the reservoir flow simulations show that CO<sub>2</sub> that is injected in Compartment I will start dispersing into the NW elongated extension of the reservoir 9 years after the start of injection (see Section 6.1).

Reservoir simulations with overexaggerated reservoir pressures up to 450 bar show that the CO<sub>2</sub> does not migrate beyond the northern limit of the storage site (see also Chapter 6).

On the basis of the additional simulation work (e.g., Section 0) and proposed risk reduction measures the risk of spilling can be further reduced to a very low likelihood that a negligible amount of CO<sub>2</sub> migrates out of the reservoir and will not flow out of the storage site at all (risk classification A-1; see also Appendix C and Figure 12-1).

### 12.1.2 *Evaluation of spilling at the NW edge of Compartment I*

A small potential spill zone is identified at the NW edge of Compartment I across bounding fault F14 of the reservoir (Figure 4-6). Low-permeable sandstones of the Volpriehausen Formation (< 1 mD) are juxtaposed to permeable sandstones of the Hardegsen Formation across a small zone at fault F14 (Section 4.2).

The potential spill point is very likely not leading to migration of CO<sub>2</sub> out of the reservoir as the very low-permeable Volpriehausen (< 1 mD) and Hardeggen Formations are juxtaposed, hampering the flow of CO<sub>2</sub>.

Proper zonal isolation of wells and prevention of the re-activation of faults which may be present in the area of spilled CO<sub>2</sub> from the reservoir, will avoid vertical migration (see also Fault zone compartment).

The low permeability of the Volpriehausen Sandstone on the other side of Fault 14 juxtaposed to the P18-02 reservoir strongly restrains the lateral migration of CO<sub>2</sub> out of the P18-02 reservoir. This implies that there is a very low likelihood that any CO<sub>2</sub> can migrate out of the reservoir (risk class A-3; see Figure 12-1).

#### 12.1.3 *Evaluation of CO<sub>2</sub> flow between reservoirs P18-2 and P18-6*

Both the static model used during the CATO2 work and the new model for the current feasibility study indicate that there is a small section across the fault zone with juxtaposition of the low-permeable Volpriehausen Sandstone (see Section 6.3.5). The P18-6 reservoir is located directly to the NE of Compartment 2-IV of the P18-2 reservoir. Geological reservoir modelling and pressure history observations indicate that this compartment represents a separate hydraulic unit from the P18-2 reservoir, which implies that no CO<sub>2</sub> will migrate in this part of the reservoir and thus will not end up in the P18-6 reservoir.

The pressure in P18-06 was at the initial level of 377 bar whereas at the same time pressure has dropped to about 100 bar in the producing P18-2 reservoir (June 2003). Apparently, this pressure difference could exist, which indicates absence of flow and no pressure equilibration between the two reservoirs on production time scales. Any pressure communication would only be expressed on geological time scales in the order of 10<sup>3</sup> to 10<sup>6</sup> years.

A fault analysis of the P18 faults revealed that the faults between P18-02 and P18-6 have a high (to very high) probability of being sealing due to the high probability of impermeable fault gouge formation or cataclasis (Nieuwland, 2012).

The pressure difference of about 277 bar between the two reservoirs and the very low permeability of the Volpriehausen Sandstone show that there is a very low likelihood that even a negligible amount of CO<sub>2</sub> will migrate from P18-2 to P18-6 or no CO<sub>2</sub> is flowing out of P18-2 to P18-6 at all (risk class A-1; see Figure 12-1).



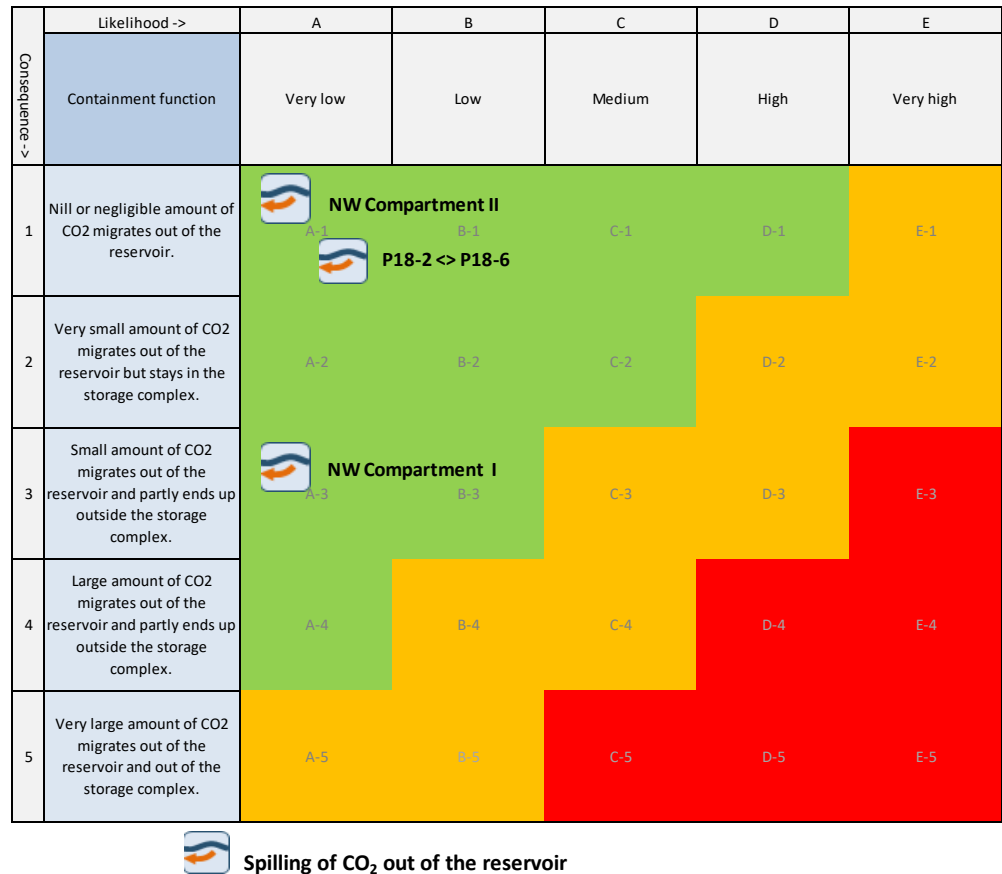


Figure 12-1 Geological risk matrix for the reservoir compartment with inclusion of proposed risk reduction measures.

## 12.2 Caprock

Impermeable shales of the Upper Triassic and Altona Groups overlie the P18-02 reservoir, which represent a good seal for the natural gas reservoir. The sealing capacity is evidenced by the presence of gas in reservoir below the seal with a thickness of 450 m to 750 m and a gas column of about 600 m. The average reservoir pressure after CO<sub>2</sub> injection will be lower than the initial pressure.

### 12.2.1 Initial condition

As the evidence for the initial sealing capacity of the caprock is very strong, it is a good seal for CO<sub>2</sub> storage as well and consequently the risk of CO<sub>2</sub> migration out of the reservoir is low to even negligible (see Figure 12-2).

### 12.2.2 Fracturing

Fractures in the seal may be caused by local stress variations due to initial gas production and subsequent CO<sub>2</sub> injection, and associated pressure and temperature changes. Fractures represent a potential conduit for CO<sub>2</sub> loaded fluids depending on their connectivity and continuity (see also Fault zone).

Semi-analytic modelling (Section 8) has shown that Coulomb stresses as a consequence of pressure build-up due to injection quickly decay inside the caprock. The pressure effect is thus not expected to contribute to the risk of fault reactivation

in the caprock. New fractures or faults will not be generated as they would require even higher Coulomb stresses. This is confirmed by earlier mechanical analysis of seal and fault based on P18-2; no critical factors identified (Vandeweyer et al., 2011: ch6, par 6.7, p108).

Although semi-analytic thermo-mechanical modelling shows that temperature-induced positive Coulomb stresses occur in the caprock near the edges of the cooling front (Section 8.3), they are not sufficiently large to re-activate faults in the caprock, nor will they result in new fractures in the caprock. The likelihood of thermomechanically re-activating a pre-existing fault in the caprock is thus very low.

If fracturing due to pressure increase and/or temperature drop would occur, this will only result in local effects. Considering the huge thickness of the caprock, the likelihood of fracturing the complete caprock is nil and consequently the risk is low to even negligible (Figure 12-2).

### 12.2.3 *Chemical degradation*

CO<sub>2</sub> if dissolved may react with minerals in the caprock near the interface with the CO<sub>2</sub> reservoir. Since the caprock has proven to be a seal for gas, the only way of upward migration is by diffusion of dissolved CO<sub>2</sub>, which is a very slow process. Chemical interaction between dissolved CO<sub>2</sub> and caprock minerals is very slow and has minor effects on porosity and permeability. Hence, no migration path is expected to be formed. The affected zone of migration of dissolved CO<sub>2</sub> and chemical interaction is in the order of several meters in thousands of years (Gaus et al., 2005; Tambach et al., 2012); see also Section 8.4.

Chemical degradation will only marginally influence the sealing properties of the caprock and thus will the overall integrity of the caprock stay intact. The likelihood of degrading the caprock is very low and its consequence will be nil or negligible (Figure 12-2).

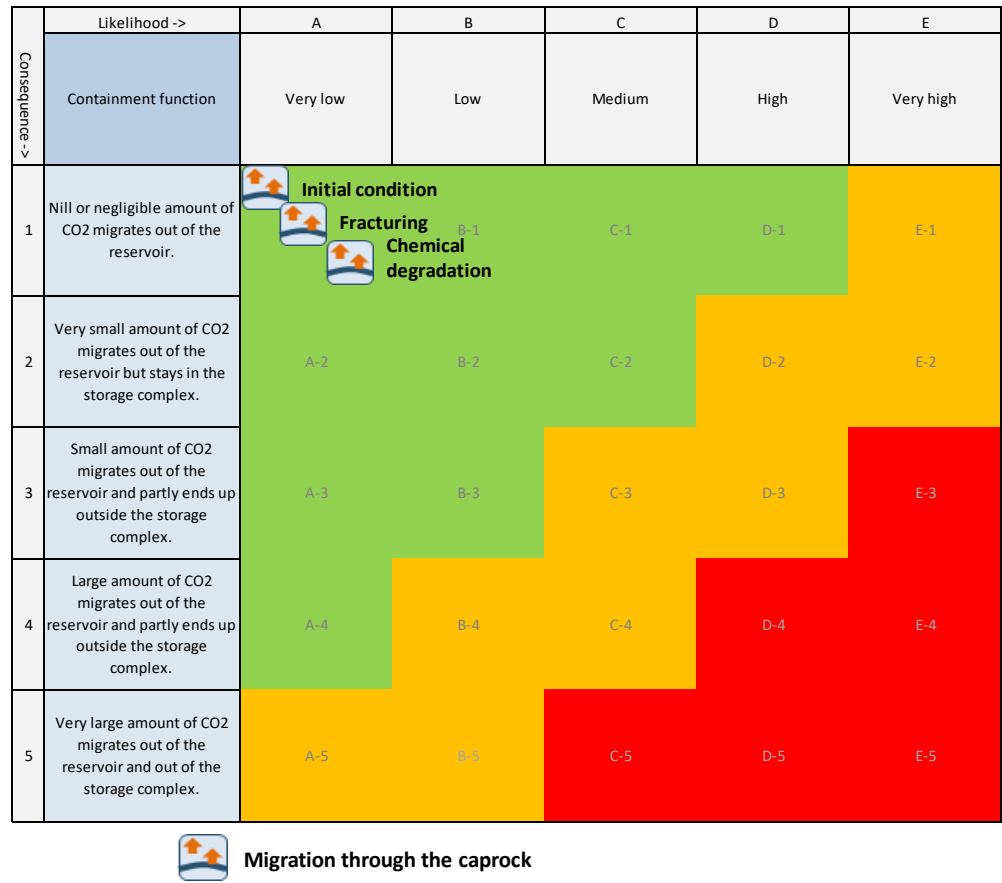


Figure 12-2 Geological risk matrix for the caprock compartment with inclusion of proposed risk reduction measures

### 12.3 Fault zones

#### 12.3.1 Initial condition

The sealing capacity of reservoir boundary faults is high as evidenced by the presence of gas on the reservoir side of the bounding faults and the permeability contrast of juxtaposed claystone and sandstone rocks on both sides of the bounding faults (see Section 4.2).

Bounding faults F19/F20 and F10 (Section 4.2) are effective seals as evidenced by presence of juxtaposed reservoir rock and sealing rock. In two cases reservoir rocks can be juxtaposed over a very small section on both sides of faults but in these cases reservoir rock with very low permeability (< 1 mD) is present on either one or both sides of the fault (see also discussion on reservoir spilling in Section 12.1).

As reservoir rocks next to bounding faults are sealed off by very low permeable rocks on the other side of the fault zone, there is a very low likelihood that a negligible amount of CO<sub>2</sub> will migrate across or along the fault and sealing rock (see Figure 12-3).

### 12.3.2 *Chemical degradation*

Chemical alteration of the fault zone may enhance migration of CO<sub>2</sub> along the fault. Currently, there is no evidence for gas migration from the P18-2 reservoir along the faults to overlying formations. In general, the geochemical reactions between CO<sub>2</sub>, formation water and fault gouge mineralogy will result in precipitation of carbonate minerals. On the longer term, silicate minerals might react, providing additional cations for carbonate precipitation. Porosity and hence permeability effects are predicted to be negligible. Increase of carbonate content in the fault gouge is known to increase the friction coefficient and to decrease potential for fault re-activation (Samuelson et al., 2012; Adelinet et al., 2014; Bakker et al., 2016). That is why it is highly unlikely that chemical degradation in itself leads to the migration of CO<sub>2</sub> across the fault zone (see Figure 12-3). See also Section 7.4.

### 12.3.3 *Fault stability: effects of re-pressurising P18-2*

Due to pressure changes during production and/or injection faults may be re-activated (Vandeweyer et al., 2011: par 6.7, p109) and potentially act as conduits for CO<sub>2</sub>.

No seismic activity during production was observed, based on the KNMI database (Vandeweyer et al., 2011). Semi-analytic modelling has shown that at the end of the injection period most (if not all) of the areas where positive Coulomb stresses which are present at the end of depletion, have disappeared (Section 7.2). The faults are thus expected to be stable at the end of the injection period. Injection of CO<sub>2</sub> is thus a mitigation measure in itself as it reduces the underpressure in the reservoir and consequently the risk of fault re-activation.

Based on the results from the semi-analytic modelling it appears to be highly unlikely that faults will be re-activated due to the increased pressure by CO<sub>2</sub> injection and consequently will not lead to migration of CO<sub>2</sub> along the fault (Figure 12-3).

### 12.3.4 *Fault stability: effects of injecting low-temperature CO<sub>2</sub>*

Injection of a cold CO<sub>2</sub> stream could re-activate a nearby fault and change its fluid transport properties. TOUGH2 simulations have shown that the cooling front could extend to 300 m from the injector after 15 years of injection (Section 7.3). Semi-analytic thermomechanical modelling indicates that the Coulomb stresses rapidly decay to around 2.5 MPa at a distance of 100 m from the cooling front. Thus injection wells at less than 300 to 400 m from a fault may thermomechanically influence its stability, if the cold front reaches the fault.

The above simulations do overestimate the effect as in reality the continuous pressure build-up in the reservoir will have a stabilizing effect on the faults. Secondly, the well P18-2-A1 which is close to a fault, has the worst injectivity and consequently a less pronounced cooling effect.

Lowering the injection rates of wells which are close to faults will reduce the advancement of the cold front and thus diminish the risk of fault re-activation and migration along the fault.

With inclusion of proper management of the injection rates in wells nearby faults the likelihood of thermomechanical fault re-activation leading to the migration of a very small amount of CO<sub>2</sub> out of the reservoir, will be low (Figure 12-3).

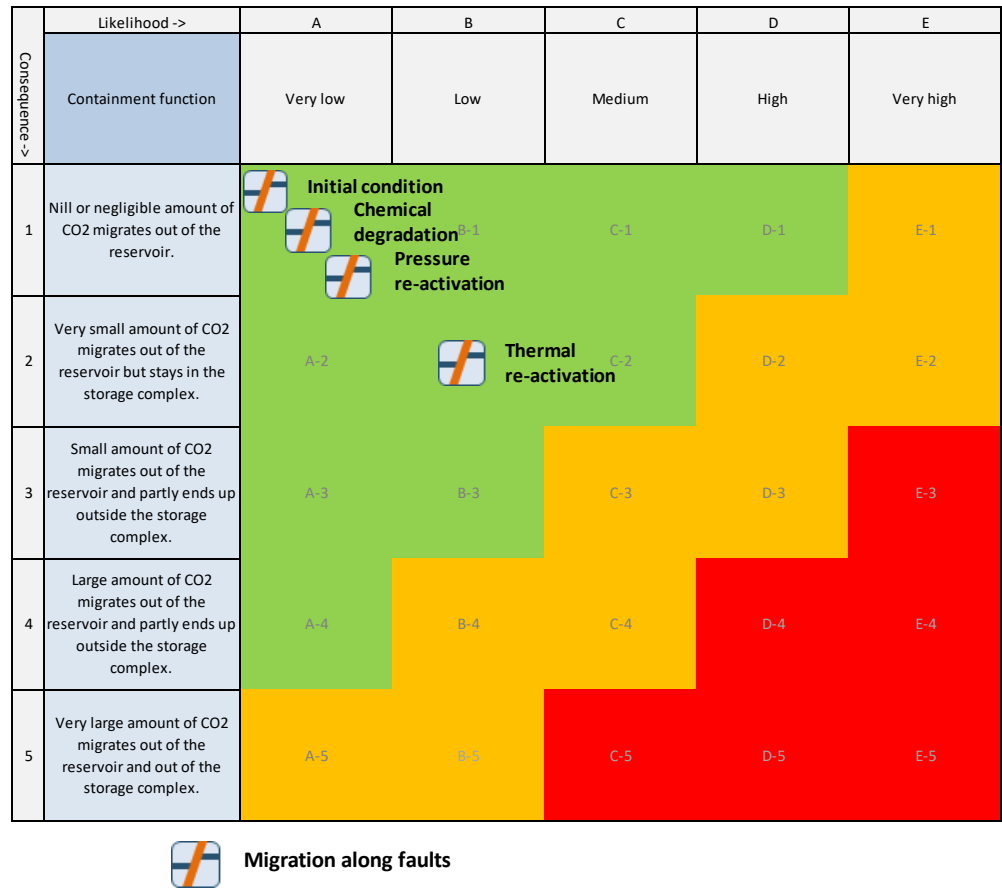


Figure 12-3 Geological risk matrix for the fault zones with inclusion of proposed risk reduction measures.

## 12.4 Wells

The following wells penetrating the P18-2 reservoir, were evaluated in detail:

- P18-02 (exploration well)
- P18-2A-01 (Compartment I)
- P18-2A-03/-S1/-S2 (Compartment I)
- P18-2A-05/-S1 (Compartment I)
- P18-2A-06/-S1 (Compartment III/Compartment II)

### 12.4.1 Surface casing of all injector wells

The condition of the outer casing inside the conductor may be reduced due to external corrosion or to fatigue by the cyclic nature of metoceanic movement. As a consequence the load bearing capacity of the casing and conductor could be reduced and seriously hamper the integrity of the well barriers. All potential injectors have adequate cement overlap in the surface part of the wells in order to transfer the loads.

As no assessment records were found on the load bearing capacity of the surface casing and conductor, it is recommended to perform for example, an external

surface casing corrosion log to confirm the remaining load capacity of the surface casing (see also Section 9.2).

After proper assessment and if needed workover of the injector wells, the likelihood that a negligible amount of CO<sub>2</sub> will migrate out of the reservoir; is characterized as low (see Figure 12-4).

#### 12.4.2 *P18-02 (exploration well)*

P18-02 well is suspended and left with a mud line suspension in place to allow potential re-entry. The well is plugged at various depths with a total of 4 plugs. Several barrier elements for this suspended well could not be validated. That's why the well needs to be planned for re-assessment and decommissioning conform the updated NOGEPa 45 standard for CO<sub>2</sub> storage decommissioning provided that these are available in time.

The current well layout seems to be inadequate for long-term containment of a near original reservoir pressurized CO<sub>2</sub> storage, as it may result in CO<sub>2</sub> migration pathways from the reservoir to shallower levels, bypassing the caprock (see also Section 9.2.8). The likelihood that deficiencies in the cement bond and the quality of the plug will lead to migration out of the reservoir and partly will leak out of the storage complex has been evaluated as medium. After the proposed re-assessment and workover activities, the likelihood that a negligible amount of CO<sub>2</sub> will migrate out of the reservoir is expected to become low (Figure 12-4).

#### 12.4.3 *P18-2A-01 (Compartment I)*

The low quality of the 7" liner cementation at packer depth, combined with the fact that the 7" liner is made of carbon steel material, poses the risk of external degradation due to corrosion by potentially corrosive reservoir fluids and consequently an inadequate hydraulic isolation over parts of the caprock. The production packer is installed across a zone with poor cement bonding. This results in a low likelihood that CO<sub>2</sub> migrates along the well and partly ends up outside the storage complex (see also Section 9.2.4).

By recompletion and repositioning the production packer in a casing or liner section with good cement bond, leakage from the well will be effectively prevented. With the implementation of the proposed measures the likelihood will become low that a negligible amount of CO<sub>2</sub> will migrate out of the reservoir (Figure 12-4).

After definite cessation of injection the well should be plugged according to CO<sub>2</sub> storage abandonment requirements (under development).

#### 12.4.4 *P18-2A-03/-S1/-S2 (Compartment I)*

All primary and secondary barrier elements have been validated and thus pose no significant risk for CO<sub>2</sub> leaking out of the well. The mother borehole and side-track S1 do not end in reservoir and thus do not increase the likelihood of CO<sub>2</sub> migration out of the reservoir.

The CO<sub>2</sub> injection load case capacity and the material compatibility for the retrievable packer are to be assessed and potentially to be mitigated to make this well a suitable CO<sub>2</sub> injector. With the implementation of the proposed measures leakage from the well should be prevented; the likelihood is low that a negligible amount of CO<sub>2</sub> will migrate out of the reservoir (Figure 12-4).

After definite cessation of injection the well should be plugged according to CO<sub>2</sub> storage abandonment requirements (under development).

#### 12.4.5 *P18-2A-05/-S1 (Compartment I)*

The mother bore was drilled to about 200 m TVD above the reservoir. Then the drill pipe parted and 500 m of drill pipe/BHA (Bottom Hole Assembly) was left in the mother bore hole (circulation was possible before the drill pipe parted) with a cement plug on top, after which the well was side tracked. As the mother borehole does not end in reservoir, this does not increase the likelihood of CO<sub>2</sub> migration out of the reservoir.

Sustained casing pressure was measured in the 9 5/8 " production casing, which is being managed by keeping the pressure below the Maximum Operating Pressure (MOP) for the current natural gas production. The current condition of this well indicates that there is a medium likelihood that a small amount of CO<sub>2</sub> migrates along the well and ends up outside the storage complex (see also Section 9.2.6).

The source of sustained pressure in the production casing needs to be investigated and if required being repaired. As a result, the likelihood that a negligible amount of CO<sub>2</sub> will migrate out of the reservoir should be low after the repair (Figure 12-4).

After definite cessation of injection the well should be plugged according to CO<sub>2</sub> storage abandonment requirements (under development).

#### 12.4.6 *P18-2-A-06/-S1 (Compartment II/Compartment III)*

The well connects P18-2 Compartments II and III. The producing reservoir formations from the side track and the mother bore connect at the side track window, which is not isolated.

For this well to be used as CO<sub>2</sub> injector the well barrier of the mother bore and the integrity of the side-track window have to be restored. This has most likely to be done by plug and abandonment (P&A) of the side track and installing a cemented scab or tie back liner to restore the mother bore integrity. The original primary and secondary barriers of the mother bore can be restored; it has a good cementation and in-situ formation at caprock level.

The current condition of this well indicates that there is a medium likelihood that a small amount of CO<sub>2</sub> migrates along the well and ends up outside the storage complex (see also Section 9.2.7). With the proposed measures the double barrier could be re-instated such that it sufficiently reduces the risk of leakage. As a result, the likelihood that a negligible amount of CO<sub>2</sub> will migrate out of the reservoir should be mitigated to low (Figure 12-4).

After definite cessation of injection the well will be plugged according to CO<sub>2</sub> storage abandonment requirements (under development).

#### 12.4.7 *Cooling of P18 injector wells*

Injection of cold CO<sub>2</sub> leads to thermal contraction of the wells. The induced tensile stresses can exceed the bonding strength and thus lead to debonding at the well-cement interface. The resulting micronannuli represent a potential pathway for CO<sub>2</sub>

migration which could be further enhanced by chemical interaction of CO<sub>2</sub> and the cement around the microannuli (see Sections 9.3 and 9.3.4).

Although the creation of microannuli is considered to be highly likely, the migration of CO<sub>2</sub> is prevented by the pressure of CO<sub>2</sub> which is to be maximised at the hydrostatic pressure. At the end of the injection phase an appropriate formation-to-formation plug is recommended.

A small to negligible amount of CO<sub>2</sub> may migrate through the thermally induced microannuli of the P18 injector wells and partly end up outside the storage complex (risk class C-3; see Figure 12-4). After appropriate abandonment of the injector wells the risk will be reduced to a low likelihood that a small amount of CO<sub>2</sub> migrates out of the reservoir (risk class B-1).

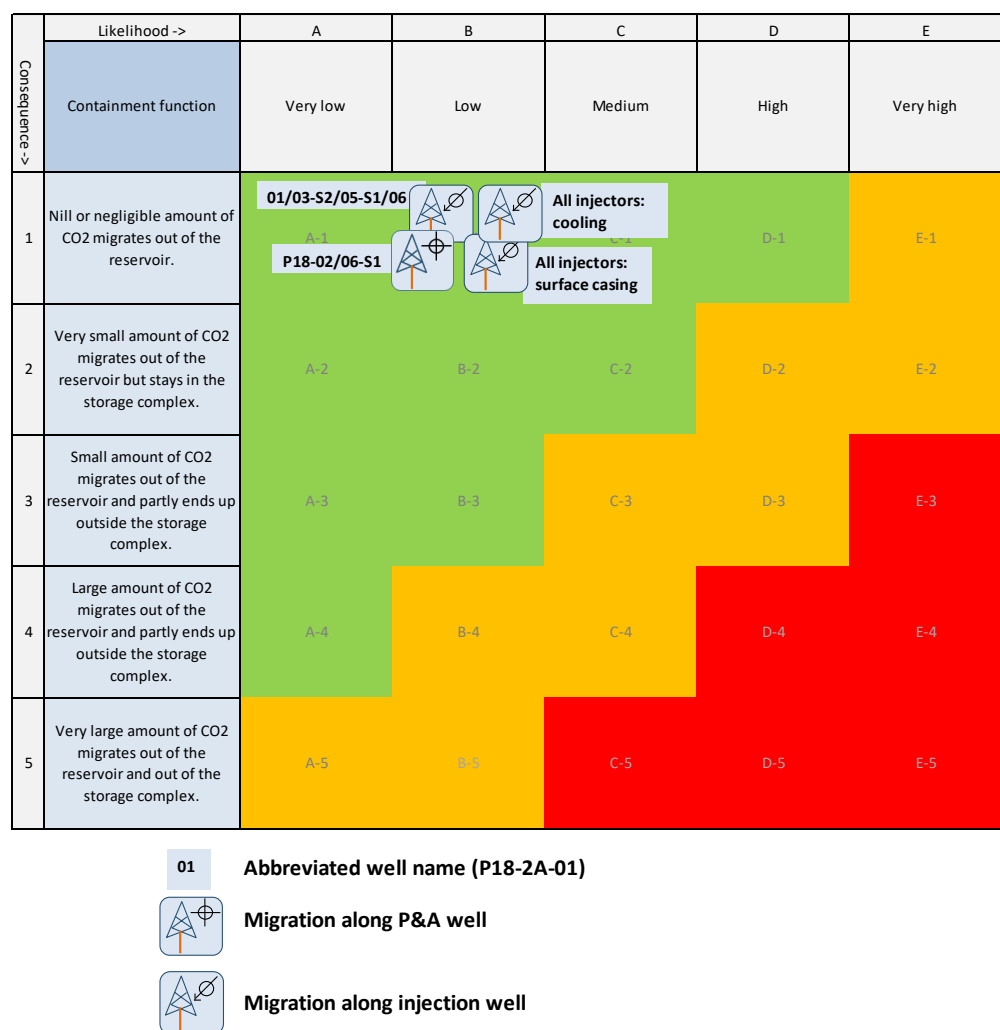


Figure 12-4 Well risk matrix after implementation of risk reduction measures; most well names are abbreviated: for example “01” stands for “P18-2A-01”.

## 12.5 Conclusion

*All risks can be reduced to acceptable, low levels*



All geological and subsurface well engineering risks in the P18-2 field can be reduced to acceptable, low levels, with no significant environmental impacts if the store is properly designed, managed and abandoned. The conclusion is that there are no prohibitive risks to storing CO<sub>2</sub> in the P18-2 field. All risks can be managed so that their risk level is low and acceptable.

#### *Well workovers required*

All selected wells will need workover activities to some degree to qualify them for CO<sub>2</sub> injection and storage. Proper management of injection rate and temperature is necessary to prevent undesired effects of cooling on faults nearby wells and re-heating of the near well area on the pressure evolution in the reservoir in the post-injection phase. For that purpose pressure, temperature and flow rate of injected CO<sub>2</sub> should be monitored (see Section 13).

#### *Reservoir pressure after injection*

As mentioned above, all risks identified here can be reduced to acceptable, low levels, provided the storage site is properly designed, managed and eventually closed. Part of this is the design of safe injection scenarios and management of pressure and temperature in the wells and reservoir. It should be noted that the simulation of the injection of CO<sub>2</sub> into the reservoir, the integrity of the caprock and the stability of faults pose no limits to the average reservoir pressure at the end of injection (apart from the maximum given by the initial pressure, which represents the maximum pressure at which the reservoir, caprock and faults have proven containment). Safe and secure storage is possible for reservoir pressure up to initial pressure (i.e., the pressure that existed in the field prior to production).

However, the study did identify a risk that requires reservoir pressure to be maximised at hydrostatic pressure. The potential migration of CO<sub>2</sub> through microannuli formed between casing (liner) and cement due to the low temperature of the injected CO<sub>2</sub> becomes small to negligible when reservoir pressure is kept below hydrostatic pressure.

## 13 Monitoring and corrective measures plan

### 13.1 Introduction

A thorough risk based approach to monitoring is adopted. This means that the elaboration of the plan depends on the results of the location-specific risk assessment, which is laid out in the previous sections.

A risk-based monitoring plan:

- Aims to ensure the safety and integrity of the storage complex;
- Reveals the necessary information for transfer of responsibility to government after the end of injection;
- Can supply and incorporate additional learning with respect to large-scale CCS;
- Should be able to prove the effectiveness of corrective measures;
- Provide a balance between efficiency and costs.

New techniques and equipment will be included whenever judged appropriate, provided that these techniques do not add to the complexity associated with operating an offshore unmanned installation.

The monitoring and corrective measures plans are part of a set of related plans that are part of the storage permit. The location specific risk assessment (Section 10) is the main input for the corrective measures and closure plans. The development of the monitoring plan is also based on a location specific risk analysis and has strong links with the corrective measures plan. Figure 13-1 illustrates the links and the consistency between the plans.

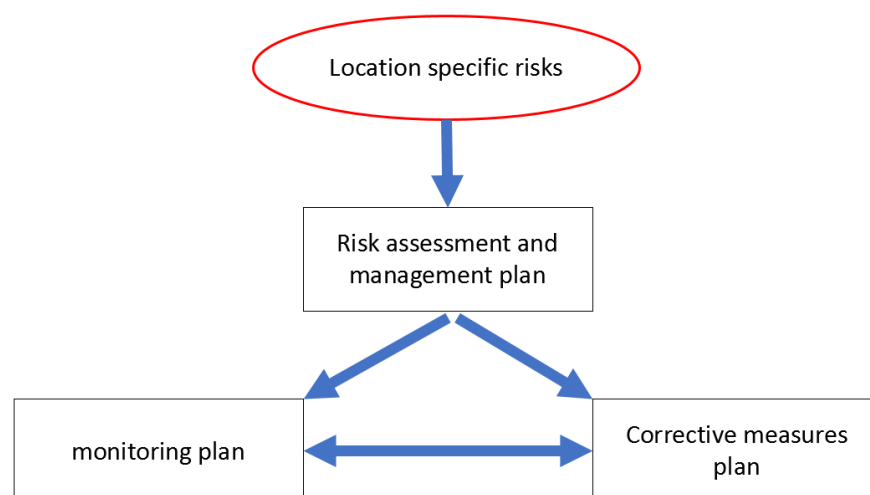


Figure 13-1. Consistency between risk management, monitoring and corrective measures plans.

Monitoring requirements of the CCS Directive 2009/31/EC and OSPAR are framed around enabling the operator to understand and to demonstrate understanding of

ongoing site processes, to predict future site behavior and to identify any leakage. Further requirements of the monitoring include early identification of deviations from predicted site behavior, provision of information needed to carry out remediate actions and the ability to progressively reduce uncertainty.

#### 13.1.1 *Reading Guide*

The foundation of the plan is given first. This refers to the legislation, regulations and other preconditions that have been taken into account. Then the philosophy of the monitoring plan is explained. Finally, the elaboration of the operational monitoring plan is explained, while the detailed monitoring plan is documented in Section 19. The cross-references to the corrective measures plan are explicitly indicated.

The plan described here represents the draft monitoring plan, to be updated and detailed prior to the start of injection.

### 13.2 **Foundation of the monitoring and corrective measures plan**

For the P18-2 storage project the monitoring plan needs to comply with the following regulations and requirements:

- Provisions of two key regulatory treaties governing CO<sub>2</sub> storage in the European offshore area, which are the OSPAR Guidelines (OSPAR, 2007) and the European Storage Directive (EU, 2009) and its implementation in the Dutch Mining Law.
- Requirements of the EU Emissions Trading System (ETS), as defined under the EU Monitoring and reporting Guidelines (EU, 2017), which deals with the accounting of leaked emissions from storage sites.
- Specific requirements to the P18-2 storage project as a first of a kind project for The Netherlands.

The starting point for developing the monitoring and corrective measures plan is an adequate characterization and risk assessment.

The general requirements for both site characterization and risk assessment are given in the Dutch mining law, the EC Storage Directive and its Annexes. Clarifying details are provided in the EU guidance documents (EU, 2011).

The detailed site characterization benefited from the fact that the storage reservoir is part of a larger natural gas field which has been produced for more than two decades. This has led to an abundance of information on the site.

The monitoring plan must relate to preventative and corrective measures. In the adopted template in this report, potential risks, monitoring techniques and mitigation measures are linked together.

With respect to the phases of a storage operation, the plan describes a 'workflow' for monitoring activities during the pre-injection (site qualification), injection (operation), post-injection (closure and post-closure) phases and after transfer of responsibility (long-term stewardship). However, monitoring in the different stages of a project is not fundamentally different. The philosophy of the monitoring plan is that it must be complete, transparent, consistent, and verifiable.

An additional requirement for the P18-2 storage project is that the monitoring plan may also serve the first of a kind character of the project, in combination with CO<sub>2</sub> injection in the P18-4 field and, potentially, the P18-6 field. This could mean gathering more data for a deeper understanding of the storage process, learning of findings.

#### 13.2.1 *General requirements from Directive 2009/31/EC*

A monitoring plan should meet the requirements according to the EU CCS Directive (EU, 2009; Annex II), as listed below.

##### **Initial plan**

The monitoring plan shall provide details of the monitoring to be deployed during the main stages of the project, including baseline, operational and post-closure monitoring.

The following shall be specified for each phase:

- 1 Parameters monitored;
- 2 Monitoring technology employed and justification for technology choice;
- 3 Monitoring locations and spatial sampling rationale;
- 4 Frequency of application and temporal sampling rationale.

For the purpose of:

- Comparing actual and modelled behaviour of CO<sub>2</sub> and brine
- Detecting significant irregularities
- Detecting CO<sub>2</sub> migration
- Detecting CO<sub>2</sub> leakage
- Detecting significant negative effects for environment, drinking water, nearby residents, the biosphere
- Evaluating the effectiveness of corrective measures taken in case of leakage
- Proving safety and integrity of the storage complex, including the assessment of complete and permanent storage.

The parameters to be monitored are identified so as to fulfil the purposes of monitoring. However, the plan shall in any case include continuous or intermittent monitoring of the following items:

- Fugitive emissions of CO<sub>2</sub> at the injection facility;
- CO<sub>2</sub> volumetric flow at injection wellheads;
- CO<sub>2</sub> pressure and temperature at injection wellheads (to determine mass flow);
- Chemical analysis of the injected material;
- Reservoir temperature and pressure (to determine CO<sub>2</sub> phase behavior and state).

The choice of monitoring technology shall be based on best practice available at the time of design. The following options shall be considered and used as appropriate:

- Technologies that can detect the presence, location and migration paths of CO<sub>2</sub> in the subsurface and at surface;
- Technologies that provide information about pressure-volume behaviour and areal/vertical saturation distribution of CO<sub>2</sub> to refine numerical 3-D-simulation

to the 3-D-geological models of the storage formation established pursuant to Article 4 and Annex I of the Storage Directive (EU, 2009);

- Technologies that can provide a wide areal spread in order to capture information on any previously undetected potential leakage pathways across the areal dimensions of the complete storage complex and beyond, in the event of significant irregularities or migration of CO<sub>2</sub> out of the storage complex.

### Updated plan

The monitoring system initially installed and related procedures need to be updated on the basis of the evaluation and modelling activity, or the verification results. Monitoring plans must be updated, at least every five years, to take into account changes to assessed risk of leakage, changes to assessed risks to environment and human health, new scientific knowledge, and improvements in the best available technology. National authorities may set a more stringent frequency.

According to Annex II of the Storage Directive one has the following updating requirements:

- a. The data collected from the monitoring shall be collated and interpreted. The observed results shall be compared with the behaviour predicted in dynamic simulation of the 3-D-pressure-volume and saturation behaviour undertaken in the context of the security characterization.
- b. Where there is a significant deviation between the observed and the predicted behaviour, the 3-D-model shall be recalibrated to reflect the observed behaviour. The recalibration shall be based on the data observations from the monitoring plan, and where necessary to provide confidence in the recalibration assumptions, additional data shall be obtained.
- c. Steps 2 and 3 of Annex I of the Storage Directive shall be repeated using the recalibrated 3-D model(s) so as to generate new hazard scenarios and flux rates and to revise and update the risk assessment.
- d. Where new CO<sub>2</sub> sources, pathways and flux rates or observed significant deviations from previous assessments are identified as a result of history matching and model recalibration, the monitoring plan shall be updated accordingly.

Post-closure monitoring shall be based on the information collected and modelled as in a) through d). The plan must now also provide information needed for the transfer of responsibilities to the competent authority (long-term stewardship). Especially the site's permanent containment must be indicated, based on all available evidence.

### 13.2.2 Emissions accounting for ETS

The Monitoring and Reporting Guidelines for CCS under the ETS describe the method for quantifying potential CO<sub>2</sub> emissions from a storage project.

Potential sources for CO<sub>2</sub> emissions from the geological storage of CO<sub>2</sub> include:

- Fuel use at booster stations and other combustion activities such as on-site power plants;
- Venting at injection or at enhanced hydrocarbon recovery operations;
- Fugitive emissions at injection;
- Breakthrough CO<sub>2</sub> from enhanced hydrocarbon recovery operations;

- Leakage from the storage complex.

Quantitative monitoring for ETS will only be required if there is an indication of leakage. There is no requirement for emissions accounting as long as there is no evidence that the site leaks. However, in case irregularities are observed for example in the downhole pressure and temperature measurements, the need for additional monitoring to detect migration pathways out of the storage complex becomes stringent.

The key question for quantitative monitoring is of course to what extent the state-of-the-art technology allows for an accurate quantification. In that perspective NSBTF (2009) suggests choosing a combination of a model-driven approach in combination with a monitoring strategy to best estimate the leakage for ETS purposes.

In the unlikely event that there is evidence for CO<sub>2</sub> flow out of the storage complex, or that irregularities occur that give rise to the need to check for anomalies outside of the storage reservoir, a strategy would be to detect leakage to the surface by geophysical methods like seismic data (detection of gas chimneys) or sea-bottom sonar techniques (detection of pockmarks) and then carry out in situ gas measurements and/or sample these leakage areas for direct CO<sub>2</sub> detection. Based on these observations an estimate can be made of leakage rates for the area. However, it should be noted that in the case of CO<sub>2</sub> storage in depleted gas fields, seismic methods have limited value. Most currently operational CO<sub>2</sub> storage projects use saline aquifers, such as Sleipner and Snøhvit in Norway, in which case seismic methods provide an efficient way to monitor the development of the CO<sub>2</sub> plume in the storage reservoir and verify containment by the caprock (e.g., Furre et al., 2017). Seismic methods cannot be used to monitor the distribution of CO<sub>2</sub> in a depleted gas field, as seismic waves cannot discriminate between CO<sub>2</sub> and residual natural gas in the reservoir. In addition, gas fields offer high certainty that CO<sub>2</sub> will be contained in the depleted reservoir (as shown here in Sections 4 through 8), effectively removing the need to check for anomalies above the caprock. Only in case of evidence of unforeseen circumstances or non-conformance would seismic methods be considered as monitoring tool for CO<sub>2</sub> in depleted gas fields.

### 13.2.3 *Specific requirements for the P18-2 storage project*

CO<sub>2</sub> storage is the main objective of the P18-2 storage project. For the project, and the storage permit in particular, the monitoring plan serves to make supported statements about the following:

- Safety and integrity, regarding possible damage to the environment or the soil. Monitoring will have to support that the CO<sub>2</sub> remains stored in the reservoir and does not end up in the biosphere. The lasting quality of the structure of the reservoir and the sealing layer must also be clear. Monitoring offers the opportunity to take action if anomalies occur.
- Demonstration character of the project, learning of findings, some situations can be better understood through measurements.
- Commercially, regarding the ETS and the amounts stored. Monitoring must show that the captured CO<sub>2</sub> is in fact permanently out of circulation and no emission rights for this CO<sub>2</sub> need to be surrendered.
- Legally, regarding the delineation of the storage location. Monitoring must show that the CO<sub>2</sub> does not enter other reservoirs for which no storage permit has been issued.

- Offer a foundation to support the transfer of responsibility after injection is concluded.

### 13.3 Philosophy of the monitoring plan

Besides meeting all legal requirements, the monitoring plan should be based on a balance between efficiency and costs.

#### 13.3.1 *Regular measurements*

A significant part of the monitoring program is measuring primary operational parameters and verifying the underlying model of the subsurface.

A plan has been devised that includes regular measurements, such as flow, pressure and temperature. These parameters will be used to test whether the injection program is proceeding according to plan and the extent to which anomalies occur with respect to the modelled behavior.

#### **Traffic light model**

The measurement program uses the so-called traffic light model. This means that for the measurements, the expected values are indicated in ranges: green, yellow and red. Quantification of these monitoring value ranges is a key element of the monitoring plan update prior to the start of injection.

In the traffic light model, a green zone is given for each operational parameter; the value of the parameter falls within this range, when the operation is proceeding as expected. Outside of this range, threshold 1 (see Table 19-1), a yellow zone exists, indicative of a deviation from the predicted behaviour, without a direct need for corrective measures. When values fall within this range, it is important that insight is gained into the cause of the anomalous results. For that reason, additional measurements should be taken (extra measurements and/or the use of other measuring techniques, depending on the circumstances). Finally, there is a red zone, threshold 2 (see Table 19-1), indicating measurements that are so far outside of the expected range that corrective measures are probably necessary. If such an unexpected event occurs, undesired effects may develop. In order to limit such consequences as much as possible, corrective measures may be deployed. The monitoring program serves to indicate the effectiveness of these corrective measures.

#### **Business as usual**

When the injection proceeds as predicted, with measured values consistent with predicted values (green zone), the frequency of measurements could gradually be decreased.

#### **Scale-up**

If the measurements deviate from the expected values (yellow zone), this will lead to a higher frequency of measurements, or the introduction of other types of measurements. If this does not provide sufficient illumination of the situation, the monitoring program will be expanded further.

#### **Adjusting the model**

Monitoring data can also provide (new) information and insights about the subsurface; this information should be used to adjust and calibrate any models used. The adjusted models can be used to predict future behavior with higher reliability, so that the behavior of the CO<sub>2</sub>, the well, the reservoir and the sealing layer can be predicted more accurately as the injection process proceeds.

### 13.3.2 *Special measurements*

Pre- injection, injection and post-injection monitoring do not differ in intent. Risks may be deemed higher in (parts of) the injection phase, notably the beginning of the injection activities. The monitoring plan reflects higher degrees of risk through more frequent and / or different monitoring techniques. Besides the measurements for the verification of predicted behavior during injection, there are a number of special measurements included in the monitoring program. These concern baseline measurements, measurements before closure and transfer, as well as measurements under special circumstances during the injection process.

#### **Baseline measurements**

In the pre-injection phase there will be a period of monitoring in order to determine the current status of the storage site. During this period baseline data will be gathered. It is of key importance to identify all possible baseline data that might be needed later in the injection and post-injection phases both for required monitoring and for contingency monitoring.

The baseline data will serve as a reference for monitoring during and after the injection process.

Baseline and repeat measurement acquisition, processing and interpretation are part of the monitoring plan (Table 19-1), where the relation with risk assessment and preventive/corrective measures is also described.

#### **Measurements before closure and transfer**

Measurements should be made before the closure of the reservoir and before the transfer to the competent authority. Their purpose is:

- Measurements to determine whether the behaviour of the CO<sub>2</sub> stored in the reservoir is such that the well can be abandoned.
- Measurements necessary after the conclusion of injection to establish whether the CO<sub>2</sub> stored is in or moving towards a stable situation so that it is possible to transfer responsibility to the government.

#### **Measurements under special circumstances**

During CO<sub>2</sub> injection, the pressure in the reservoir increases; the temperature, pressure and flow rate through each well are chosen such that injection can take place safely. During the injection process, the injection rates of CO<sub>2</sub> will vary, with occasional interruptions. Part of the monitoring program is to measure the conditions that arise during such transient operations.

The period required for monitoring after abandonment of the wells and prior to decommissioning of the platform is not defined yet, neither is the period between decommissioning of the platform and transfer of liability to the state authorities. The required lengths of these periods need to be established in agreement with State Supervision of the Mines (SodM).



### 13.3.3 *Direct and indirect determination of possible leakage*

Two ways can be distinguished to enable verification of the points above. On the one hand, there are direct detection methods that can be used to demonstrate the presence of CO<sub>2</sub> migration from the reservoir. An example of this can be CO<sub>2</sub> measurements at wells.

On the other hand, there are also indirect detection methods available, which can be used to verify that the CO<sub>2</sub> injected is behaving as predicted. The predictions are derived from static and dynamic models created beforehand, but also from updates to these models based on available monitoring data (such as pressure measurements in the reservoir). For this reason, important parameters have been included in the monitoring plan for the purpose of indirect monitoring. These include:

- pressure and temperature measurement in the wells;
- annular pressures of the wells;
- volume of injected CO<sub>2</sub>;
- composition of the injected gas;
- well integrity measurements ;
- measurements of irregularities at the seabed.

### 13.3.4 *Different stages*

Different stages can be distinguished throughout the lifetime of the CO<sub>2</sub> storage project. This leads to different monitoring requirements through the lifetime of the project. The different stages are listed below.

- Pre-injection

Prior to actual injection, the monitoring focuses on recording the starting situation (baseline monitoring).

- Injection

In the operational phase CO<sub>2</sub> is injected until the reservoir is filled to an extent that further injection is not desired or allowed, or until no more CO<sub>2</sub> is delivered and a decision is made to conclude CO<sub>2</sub> injection.

- Post-injection

After CO<sub>2</sub> injection has stopped, there is a period of observation. During this period, it will be decided whether a stable end situation will be reached. If this is the case, the well will be closed with a plug. If the plug is shown to be of an acceptable quality, the wells will be sealed.

- Post-injection — abandonment

If the seal is shown to be of acceptable quality, the wells will be permanently abandoned. Later, responsibility can be transferred to the government.

- Post-injection — transfer of liability

Once a stable situation is achieved, the responsibility of the filled reservoir may be transferred to the competent authority. After the transfer, the developments in the reservoir will be followed periodically. The competent authority is responsible for a monitoring period of 30 years from the moment of transfer.

For each stage, the monitoring plan (Table 19-1) indicates the parameters to be measured, the frequency, the technology used and the location for each activity. The expected duration of each monitoring period is also indicated.

### 13.3.5 *Report monitoring results*

Prior to the start of injection activities, a baseline report will be compiled, describing the starting state of the wells and the storage site. This is the basis that will be used to map any changes.

An annual report of the monitoring results will be presented to the competent authority. The report should hold operational information, possible anomalous situations and information towards closure and transfer.

Prior to both site closure and site transfer a report is compiled, recording the state of both the well and the subsurface.

### 13.3.6 *Conclusion*

#### **Deviations from expectations**

Deviations from any expected behaviour of the storage complex may indicate migration or leakage of the injected CO<sub>2</sub>. In the P18-2 case the main activities in determining such deviations from the expected behaviour consist of monitoring the CO<sub>2</sub> pressure and temperature.

A thorough and reliable history match has been established. Deviations from the expected pressure development (p/Z curve) throughout and after the operational phase, could be an indicator of migration of CO<sub>2</sub> from the reservoir or leakage from the storage complex. To this end the pressures at the top of the wells are measured in any case (in the wellhead) as well as the pressures at the bottom of the wells (downhole).

Should unexpected deviations be measured and migration of CO<sub>2</sub> from the reservoir be suspected, measures need to be taken. Taking into account the comments about the application of seismic methods in the case of CO<sub>2</sub> storage in depleted gas fields given in Section 13.2.2, these may include time-lapse seismic monitoring, which allows possible migration paths or shallow CO<sub>2</sub> accumulations to be detected with an expected observation threshold of several tens of kilotons. The detection limit and measurement precision will be specified with the submission of the revised monitoring plan prior to injection and after detailed engineering.

The shallower the gas accumulation occurs, the better the chance that it can be detected. Baseline monitoring prior to injection will be used to make an inventory of pockmarks already present. This will allow the change with respect to the initial situation to be determined in case of a possible migration or leakage.

#### **Well integrity**

Various techniques are used to monitor the integrity of the (injection) wells. These include:

- Logging across the depth of the well;
- Measurement of the pressures in the annuli;
- Periodic analysis of the liquids in the annuli, in order to test for the presence of CO<sub>2</sub>.

Prior to the commencement of CO<sub>2</sub> injection, each injection well will be worked over and its state will be recorded as the baseline for later determinations of the integrity

of the well. After injection, the well will be safely sealed and permanently abandoned. However, before the well is entirely abandoned, there will first be a period in which the integrity of the plug (FFP) is measured at seal level. These measurements consist of tests monitoring the annular pressures, logs and taking samples of the liquids from the well above the seal in order to analyse for the presence of CO<sub>2</sub>.

#### **Monitoring of the seabed**

Finally, there is monitoring of the seabed. This is mainly in order to show that there are no changes and therefore there is no migration of CO<sub>2</sub> to the seabed. Various acoustic technologies (multibeam echo sounding, side scanning sonar, etc.) can be used to identify changes in and at the seabed as a result of changes in the deep underground (often in the shape of pockmarks) and possible CO<sub>2</sub> bubble streams in the water column. In addition, seabed samples (via coring) can be used to establish the presence or absence of leaking CO<sub>2</sub>.

### **13.4 Interpretation**

Abovementioned aspects have led to the monitoring plan presented here. The following aspects will be monitored:

- Injection process
- Well integrity
- Reservoir integrity
- Environmental monitoring (for leakage of CO<sub>2</sub> from the storage complex)

#### **13.4.1 Categories**

Monitoring of CO<sub>2</sub> storage can be achieved either by measuring the absence of any leakage through direct detection methods, or by verifying indirectly that the CO<sub>2</sub> is behaving as expected in the reservoir based on static and dynamic modelling and updating thereof corroborated by monitoring data. The main challenge for measuring absence of any leakage consists of spatial and temporal coverage of the monitoring method, i.e. "Where and when do we need to monitor in order to be sure that no leakage occurs". The strategy should therefore be based on identified risks.

For the indirect model-based monitoring the emphasis is more on scenario confirmation. As long as monitoring data demonstrates that the storage system is behaving according to the predictive models, the understanding of both the processes occurring and the behaviour of the storage complex can be considered sufficient. In case of significant deviations, one should find the causes of the deviations and where necessary recalibrate the models and perform new predictive simulations. If however the deviations fall well beyond the uncertainty ranges of the predictive models, then additional monitoring and possibly contingency measures need to be taken.

In practice often a combination of approaches is applied required and the optimum monitoring plan will be guided by the risk assessment and the site characterization.

Following the NSBTF (2009) and the draft EU guidance documents (EU, 2011), the following categories for monitoring are identified:

1. Mandatory monitoring: in any case for all sites. A number of parameters to be monitored is mandatory based on the EU storage directive (EU, 2009).

2. Required monitoring: site specific. This monitoring group is directed to gathering evidence for containment in the reservoir and to demonstrate integrity of seal, fault and wells in case of regular development.
3. Contingency monitoring. The third group refers to a contingency monitoring system which will only be installed if irregularities show up. In the CCS Directive a “significant irregularity” is defined as ‘...any irregularity in the injection or storage operations or in the condition of the storage complex itself, which implies the risk of a leakage or risk to the environment or human health’.

It is to be noted that these three categories as such have not been implemented in Dutch legislation, therefore the term *mandatory* should be read as “mandatory following the CCS Directive”. Similar for the term *required*, which is not as such defined in legislation. Required in the context of this report means a preliminary proposal of essentially risk-based monitoring with the current state of knowledge.

The quantification of a leakage at the sea bottom for ETS purposes is considered as part of the contingency monitoring. Quantitative monitoring for ETS will only be required, if there is an indication of leakage. For the North Sea the strategy suggested by NSBTF (2009) would be to detect leakage to the surface by geophysical methods like seismic data (detection of gas chimneys) or sea-bottom echo-sounding (detection of pockmarks) and then sample these leakage areas for direct CO<sub>2</sub> detection repeatedly. Based on the sampling profiles an estimate can be made of leakage rates over time for the area. In case of wellbore leakages an additional monitoring program in and around the well is suggested.

In the operational execution, the following categories are distinguished, and for each category the measurements performed for general testing are indicated, as well as the measurements that relate to gaining insight into deviations and to conclusion and transfer.

### 13.5 The monitoring plan

Following NSBTF (2009) and the draft EU guidance documents (EU, 2011), Table 13-1 lists the categories for monitoring that have been identified, as well as the aspects to be monitored. Table 13-2 gives a summary of the monitoring plan describing the equipment or method that can be used to measure certain processes.

The complete monitoring plan for P18-2, in the form of a table, is given in Table 19-1. Below is a description of the parameters mentioned in the table. These parameters follow both from the mandatory monitoring obligations as stipulated by the storage directive and the risk assessment.

#### Column 1

The first column describes the parameters to be monitored. These parameters follow both from the mandatory monitoring obligations as stipulated by the storage directive and from the risk assessment.

Table 13-1. Summarized monitoring classification table.

	<b>Mandatory (Mandatory monitoring according to Annex II of the EU directive)</b>	<b>Required (Preliminary estimation of required monitoring)</b>	<b>Contingency monitoring</b>
<b>Injection process</b>	Flow, pressure, temperature and composition of injected CO <sub>2</sub>		
<b>Well integrity</b>	Various Integrity measurements, well head pressure & temperature	Various baseline measurements, plug integrity measurements	
<b>Reservoir integrity</b>	Flowing pressure and temperature measurements	Stabilized pressure and temperature measurements	Seismic survey in case of irregularities
<b>Environmental monitoring</b>		Various baseline measurements, Microseismic monitoring	Various surveys in case of irregularities

**Column 2**

The second column indicates the proposed technique adopted to measure the parameter. A more detailed description of the technique is provided outside the table.

**Column 3**

The third column indicates the category of monitoring (mandatory according to the EU directive, required, contingency).

**Column 4 and 5**

The fourth and fifth columns give a description of both the temporal frequencies (column 4) and spatial coverage (column 5) of the data acquisition foreseen in the different phases of the project (pre-injection, injection and post-injection including long-term stewardship after transfer of responsibility). The rationale behind the monitoring strategy related to the identified risks is described in the following section.

**Column 6**

Column six provides a description of the expected values that indicate normal behavior and of the expected accuracy of the monitoring method. Expected values and therefore this column is colored green.

**Column 7**

The seventh column indicates threshold values, where normal behavior as anticipated stops and where irregularities start. As long as the measured values remain below these threshold values, no actions are required (green column). In case threshold values exceeded, the seventh column (colored orange) defines specific actions. Upon exceeding threshold values, monitoring data suggest that the behavior of the storage system starts to deviate from expectations. This could for

example lead to recalibration of the models, but when persisting to more stringent measures.

### Column 8

In case the monitor values exceed the threshold defined in the eighth column (colored red), the highest alert phase starts and immediate actions (or contingency measures) as defined in the second sub column of column eight are required.

Table 13-2. Summary of specific monitoring equipment and methods to be used for monitoring of certain processes.

	<b>Injection process</b>	<b>Measurement equipment / method</b>
1	Injection rate	Flow meter
2	Injection stream CO <sub>2</sub> concentration	Samples & analysis: online system
3	Injection stream composition	Samples & analysis: Additional samples for calibration
4	Water measurement	Water measurement
5	Discontinuous emissions through leakage, venting or incidents	Combination of techniques
<b>Well integrity</b>		
6	Annular pressure	Pressure device (with alarm value)
7	Well integrity	Wireline Logging (selection of tool: CBL, PMIT, EMIT, USIT, WAF, optical)
8	Well head pressure	Pressure device
9	Well head temperature	Temperature device
10	Plug integrity	Pressure test and additional inspections
<b>Reservoir integrity</b>		
11	Reservoir pressure (FBHP) (see also line 8)	pressure device
12	Reservoir Temperature (FBHT) (see also line 9)	thermometer or DTS
13	Stabilized pressure (CIBHP) (gradient) during shut-in period	pressure device combined with shut-in
14	Stabilised temperature (CIBHT) (gradient) during shut-in period	thermometer or DTS combined with shut-in
15	Suspected leakage	Surface seismic survey
<b>Environmental monitoring</b>		
16	Pockmarks at the seabed	Multi-beam echosounding
17	Presence of shallow gas or gas chimneys in the subsurface	Baseline seismic data
18	Migration pathways for gas in the shallow subsurface	Time-lapse seismic data acquisition (2D or 3D)
19	CO <sub>2</sub> in soil at pockmarks	Gas samples using vibrocore + lab analysis
20	Bubble detection at wellhead	Acoustic bubble detector
21	Microseismic monitoring	Permanent geophones or DAS in monitoring wells

### Items to be monitored

The next part of the monitoring plan describes the different items or events to be monitored (Injection process, Well integrity, Reservoir Integrity, Environmental Monitoring) and over which time frame (Pre-injection, Injection, Post-injection, etc). See Table 19-2.

It is noted that the timing for monitoring of the post injection period including the abandonment of the wells and the decommissioning of the platform and the period to the transfer of liability to the state have not been defined in this plan. The definition of these periods will be subject of discussion with State Supervision of the Mines (SodM).

#### 13.5.1 *Proposed monitoring methods*

This section provides more detailed background information on the rationale behind the selection of the proposed monitoring techniques. For each section corresponding to an identified actor in the risk analysis the primary relevant monitoring techniques are referred to between brackets by their number as appearing in the first column in Table 19-1. Monitoring techniques for contingency monitoring are not given between the brackets, this to not overcomplicate the overview below. Techniques relevant for contingency monitoring are indicated in Table 19-1.

##### 13.5.1.1 *Reservoir / injection process (1,2,3,4,5,8,9,11,12,13,14)*

The risk identified from leakage of CO<sub>2</sub> out of the reservoir / storage site where:

- Spilling (via spill point), or
- Sealing capacity of fault zone between P18-2 and P18-6.

Based on the history match of the P18-2 reservoir the field can be considered as a “tank model”, without an active aquifer drive. Therefore CO<sub>2</sub> is expected to disperse throughout the original gas reservoir.

Often – and this applies only to storage of CO<sub>2</sub> in saline aquifers - the key tool for reservoir / CO<sub>2</sub> plume imaging is 3D surface seismic, however this technique is not deemed suitable for P18-2. This is because of the considerable depth of the P18-2 storage reservoir, which renders surface seismic methods less effective.

Additionally, for P18-2 the presence of (residual) gas within the reservoir makes the feasibility of repeated seismic surveys for the monitoring of CO<sub>2</sub> dispersion questionable, as seismic data cannot discern between CO<sub>2</sub> and residual gas.

The main components for monitoring deviations in expected behaviour indicating potential migration out of the reservoir or storage complex consist of pressure (and temperature) monitoring. After proper history matching, a deviation from the expected pressure trend (P/z curve) during and after the operational phase is an indicator for potential migration out of the storage complex. As for the P18-2 reservoir, pressure monitoring has the potential to be a powerful tool, since there is no strong aquifer drive masking potential deviations. A rough estimation of the threshold of the mass of CO<sub>2</sub> migration out of the reservoir that can be detected is in the order of 2-10 ktonnes of CO<sub>2</sub>. The exact value depends on the quality of the P/z curves with proper and reliable pressure measurements. Factors like water influx, communication with neighboring compartments or CO<sub>2</sub> dissolution in water

have a negative effect on the detectability. In addition, the measurement accuracy of inflow rates should be taken into account.

Proper pressure measurements can be obtained from the injection well after a shut-in, or continuously from a “monitoring” well. The latter is the preferred option allowing a continuous measurement of the reservoir pressure in equilibrium. In case the reservoir pressure is measured in the injection well after a shut-in, pressure equilibration should be measured over a time interval in the order of days. Based on the latter, the equilibrium pressure can be extrapolated (if it has not already been reached in this period).

Migration in the reservoir can be followed by additional geophysical logs (RST logs) well tests and downhole fluid samples at monitoring wells to detect CO<sub>2</sub> breakthrough. During the injection phase, microseismic monitoring and innovative pulse testing techniques may provide data on the location of the advancing CO<sub>2</sub> temperature front by detecting thermal fracturing (if any), and density/viscosity differences. The latter is not considered as an absolutely required measurement for CO<sub>2</sub> tracking, but is recommended. Furthermore the CO<sub>2</sub> can be traced as it closes in on boundary faults or moves toward spill points.

#### 13.5.1.2 *Well integrity (6,7,8,9,10,11,12,13,14,16)*

The key tool for monitoring well integrity is logging, aimed both directly at the wellbore (cement bond logging, etc.), but also at the surrounding formations (saturation logging). Pressure-temperature logging and downhole fluid chemistry are also potentially very useful. Non-well-based tools include 2D or 3D surface seismic for volumetric imaging of the overburden around the wellbores and multibeam echosounding to detect surface changes around the wellbore. During the injection stage, well-based microseismic monitoring can also provide information on flow and degradation processes around the wellbores.

#### 13.5.1.3 *Caprock/overburden (11,12,13,14,16,17,21)*

Caprock integrity is assumed intact as long as no abnormal behaviour of the pressure is observed. In case significant deviations are observed, contingency monitoring is required; potentially useful techniques include time-lapse seismic surveys to detect migration pathways (chimneys) or shallow gas accumulations. 2D surface seismic surveys may be a cost-effective alternative to full 3D, but will not provide full areal coverage of the top seal.

The threshold value of seismically detectable shallow accumulations of CO<sub>2</sub> is in the order of 10's of ktonnes under the condition that CO<sub>2</sub> accumulates as a concentrated gas pocket. The shallower the CO<sub>2</sub> accumulates, the better the chances of picking up the signal.

During the injection phase, microseismic monitoring provides data on whether the top seal is being geomechanically compromised. The feasibility of using wells as monitoring wells for microseismic monitoring has not been thoroughly explored yet, but may be regarded as a option, for example during periods when an injection well is shut in.

#### 13.5.1.4 *Faults (11,12,13,14,21)*

Thermal reactivation of faults is identified as a risk with risk classification B-2 (Section 12.3). If the cold front of the injected CO<sub>2</sub> reaches a fault, the likelihood of activation increases. In order to reduce this risk, the advancement of the cold front



from the injector wells to nearby faults needs to be managed and monitored.

Pressure and temperature monitoring data needs to be used in combination with non-isothermal reservoir simulations to assess whether the cold front stays away from the faults within and bounding reservoir compartments.

During the injection phase, microseismic monitoring as well as advanced well tests (pulse testing) may provide data on the location of the migrating CO<sub>2</sub> front. Geophysical logs would not provide reliable indications of generalized CO<sub>2</sub> migration, except where free CO<sub>2</sub> accumulates in very close proximity to the wellbores.

The threshold value of seismically detectable accumulations of CO<sub>2</sub> in the overburden is in the order of 10's of ktonnes, depending on the depth and geophysical properties of the reservoir and surrounding rocks. In the P18-2 case this is considered a contingency measurement. Just like sampling fluids of shallower aquifers can show traces of leaking CO<sub>2</sub>. To detect the absence of migration to the seabed, various types of surveys are an option. These will be able to identify pockmarks or bubbles and check for composition and origin.

#### 13.5.1.5 *Calibration of flow simulations (1,2,3,4,5,8,9,11,12,13,14)*

The calibration of flow simulations combines aspects of several of the above aims, effective reservoir management, accurate pressure and temperature monitoring and insights into fine-scale and geochemical processes. Likely tools are downhole pressure/temperature measurements, RST logs and monitoring breakthrough in monitoring wells. For P18-2 where 3D seismic imaging of CO<sub>2</sub> in the reservoir is considered difficult if not impossible, downhole pressure/temperature is the key technology. As in a number of cases above, microseismic monitoring and pulse testing (an advanced way of well testing) may be useful in the injection phase.

## 13.6 **Conclusion**

The adopted monitoring approach for CO<sub>2</sub> storage in P18-2, builds on the results of the site characterization and the risk assessment. The reservoir has been classified as suitable for CO<sub>2</sub> storage; the reservoir offers stable long-term containment. This conclusion is essentially based on a) the fact that natural gas has been contained in these reservoirs for millions of years, b) the knowledge of the reservoirs obtained during exploration and production of the fields, c) the fact that at the end of injection the pressure in the reservoir will be lower than that of surrounding formations.

The monitoring plan proposed is designed to verify CO<sub>2</sub> containment and storage reservoir integrity while and after the storage facility is in operation. This is achieved by both measuring the absence of any leakage through direct detection methods (for example at the wells), and by verifying indirectly that the CO<sub>2</sub> is behaving as expected in the reservoir by collecting pressure, temperature and injection rate data that feed in to static and dynamic modelling. The design includes therefore the collection of data such as representative storage pressures and annuli pressures, injected volumes and gas qualities, well integrity measurements, reservoir conditions, micro seismicity and sea bottom measurements.

The main component for monitoring deviations in expected behaviour indicating potential migration out of the reservoir consists of pressure and temperature monitoring. After proper history matching any deviations from the expected pressure trend (P/z curve) during and after the operational phase is a potential

indicator for migration out of the storage reservoir. Reservoir pressures will be determined regularly via shut-in of injection wells or monitoring wells. Downhole pressure tests are envisaged to verify the storage pressures and to verify the conversion of the wellhead pressures to downhole pressures.

Only in case irregularities are observed in seismicity pressure, or the temperature behaviour and when migration in the overburden is suspected, additional monitoring is proposed, like time-lapse seismic monitoring to detect possible migration pathways (chimneys) or shallow gas accumulations. The threshold value of seismically detectable accumulations of CO<sub>2</sub> is of the order of 10's of ktonnes under the likely condition that CO<sub>2</sub> accumulates as a concentrated gas pocket in shallower aquifers. The shallower the CO<sub>2</sub> accumulates, the better the chances of picking up the signal.

The key tools for monitoring well integrity consist of (repeated) logging, measuring the annuli pressures and regular analysis of the annuli fluids for the presence of gas or CO<sub>2</sub>. Prior to CO<sub>2</sub> injection a proper assessment of the current state of the existing wells is carried out, as well as work-overs. Before abandonment, wells will be suspended for a period of time to verify the quality of the plugs at caprock level by gas tests, monitoring of annuli pressures and possibly sampling of fluids from the well to monitor for the presence of CO<sub>2</sub>.

Finally, shallow monitoring, to detect the absence of migration to the seabed, in the form of multi-beam echosounding, side scanning sonar or high-resolution 3D surveys can be considered for identifying pockmarks or bubbles. Furthermore, sampling fluids in the soil at the sea bottom (via cores) can be used to verify the absence of traces of migrating CO<sub>2</sub>. The locations of the sampling will essentially be associated with the well positions, but additional locations can be selected based on multi-beam echosounding results.

In both cases, echosounding and fluid sampling, these types of monitoring should be performed when there is reason to suspect loss of containment and significant leakage out of the storage complex.

## 14 Conclusions

All risks identified that are related to the potential leakage of CO<sub>2</sub> out of the P18-2 storage site during or after CO<sub>2</sub> injection have been studied in detail and classified in a risk register. Most of the risks have been classified as 'low', with 'very low likelihood' that 'nil to negligible amount of CO<sub>2</sub> migrates out of the reservoir' (risk classification A-1). The remaining risks with slightly higher likelihood and/or consequence are related to (1) lateral CO<sub>2</sub> migration out of the storage reservoir, (2) the integrity of the wells in the field, and (3) the stability of the faults in the storage system.

- (1) Simulation of the behaviour of CO<sub>2</sub> after injection into the storage formations shows that there is a possibility for the CO<sub>2</sub> to move into the attached water-filled formation (but remain within the storage complex). Simulations show that when CO<sub>2</sub> injection is stopped before the initial reservoir pressure is reached the CO<sub>2</sub> is retained within the original gas-filled reservoir and will not leave the storage complex.
- (2) Analysis of available data on the integrity of the wells in the P18-2 field shows that a workover is required for each of the injection wells. Once these are performed, the risk of CO<sub>2</sub> leaking along wells, based on pre-injection status, is considered low.

The initial low reservoir pressure leads to low temperature of the CO<sub>2</sub> at the bottom of the well, causing significant temperature gradients in the well. These might lead to de-bonding of well liner (casing) and cement, potentially allowing leakage pathways to form (micro-annuli) for CO<sub>2</sub>. However, only when the pressure in the reservoir is above hydrostatic pressure could CO<sub>2</sub> enter these micro-annuli and potentially migrate into overlying aquifers. Therefore, the pressure in the reservoir is to be maximized at hydrostatic pressure, to reduce the likelihood of CO<sub>2</sub> flowing through these micro-annuli to small to negligible.

- (3) The cold CO<sub>2</sub> is injected into the reservoir formations, where it will create a low-temperature zone around the injection wells. If this zone could reach faults that are present in the reservoir, fault stability might be affected; however, at the same time, faults become more stable during the injection process due to increasing reservoir pressure. Monitoring of injection rate and temperature is required to track the pressure and temperature development in the reservoir and ensure that faults remain stable. All analysis points to small to negligible probability of fault reactivation; the caprock of 450 m to 750 m thick ensures that, fault destabilization, if any, will not lead to CO<sub>2</sub> movement through the caprock.

### *Recommendations*

- (1) In the study presented here the modelling of the injection process was performed with an isothermal reservoir simulator that could not simultaneously handle pressure and temperature variations in the reservoir. The impact of the low temperature of the injected CO<sub>2</sub> was estimated through the use of an additional simulator and analytical approaches and of scenarios that bring out potential effects. While the results are considered sufficient for the assessment

of the risks associated with CO<sub>2</sub> storage, detailed simultaneous modelling of pressure and temperature in the storage formations is required prior to the start of injection. This is needed for pressure and temperature predictions that are sufficiently reliable for the management of the injection process and for the interpretation of monitoring data.

- (2) The aim of the present study was to provide the basis for a storage permit application, by understanding the response of the storage formations, the caprock, the faults and the wells to the injection of CO<sub>2</sub>. The study established that conditions can be found under which CO<sub>2</sub> can be injected and stored safely and securely in the P18-2 field. The study did not aim to arrive at a complete and detailed description of these conditions. Such an 'operational plan' for CO<sub>2</sub> injection into the P18-2 field will be required prior to the start of injection, as a basis for the detailed monitoring plan and for the operational management of the injection process. The present study is the first step towards the P18-2 operational plan.

## 15 References

- Adelinet M., Nauroy J-F., Graham C.C., Cuss R.J., Wiseall A.C., Bakker E., Spiers C.J. and Hangx S.J.T. (2014). Progress report with data on processes, constitutive relations and parameters for modelling work. EU FP7 UltimateCO<sub>2</sub> Deliverable D4.5.
- Akemu O., Miersemann U., Benedictus T., Nepveu M. and Desroches J. (2011). Well integrity assessment of the P18 gas field (TAQA), CATO2 report WP3.4-D22.
- Ames R. and Farfan P.F. (1996). The environments of deposition of the Triassic Main Buntsandstein Formation in the P and Q quadrants, offshore the Netherlands. In: Rondeel H.E., Batjes D.A.J., Nieuwenhuijs W.H. (eds) *Geology of Gas and Oil under the Netherlands*. Springer, Dordrecht. pp 167-178.
- Bacci G., Korre A. and Durucan S. (2011). An experimental and numerical investigation into the impact of dissolution/precipitation mechanisms on CO<sub>2</sub> injectivity in the wellbore and far field regions. *International Journal of Greenhouse Gas control* 5, 579-588.
- Baines S.J., and Worden R.H. (2004). *Geological Storage of Carbon Dioxide*. Geological Society, London, Special Publications 233, 59-85.
- Barnes J. and Hut P. (1986). A hierarchical O(N log N) force-calculation algorithm. *Nature*, 324, 446-449.
- Bakker E., Hangx S.J.T., Niemeijer A.R. and Spiers C.J. (2016). Frictional behaviour and transport properties of simulated fault gouges derived from a natural CO<sub>2</sub> reservoir. *International Journal of Greenhouse Gas Control* 54, 70-83.
- Baumann G., Henniges J. and De Lucia M. (2014). Monitoring of saturation changes and salt precipitation during CO<sub>2</sub> injection using pulsed neutron-gamma logging at the Ketzin pilot site. *International Journal of Greenhouse Gas Control* 28, 134-146.
- Belfroid, S. (2019). Porthos – CO<sub>2</sub> injection, TNO report TNO 2019 R10335.
- BP (2007). P/18 Field Petrophysical Study. Company report, 13 p.
- Candela, T., van der Veer, E.F., Fokker, P.A. (2018). On the importance of thermo-elastic stressing in injection-induced earthquakes, *Rock Mechanics and Rock Eng.*, 51 (12), 3925-3936.
- Duguid A. and Scherer G.W. (2010). Degradation of oilwell cement due to exposure to carbonated brine. *International Journal of Greenhouse Gas Control* 4, 546-560.
- Energy Institute (2019). Hearts and Minds toolkit – Risk assessment matrix. website, version 15 Oct 2019. <https://publishing.energyinst.org/heartsandminds/toolkit/RAM>.
- EPA (2012). *Geologic Sequestration of Carbon Dioxide Underground Injection Control (UIC) Program Class VI Well Construction Guidance* (May 2012).
- ETS directive (2009): DIRECTIVE 2009/29/EC OF THE EUROPEAN PARLIAMENT AND OF THE COUNCIL of 23 April 2009 amending Directive 2003/87/EC so as to improve and extend the greenhouse gas emission allowance trading scheme of the Community EU Guidance Document 2 (draft 2010): Site Characterisation, CO<sub>2</sub> Stream Composition, Monitoring and Corrective Measures. Draft document for consultation version June 17, 2010.

- EU (2009): DIRECTIVE 2009/31/EC OF THE EUROPEAN PARLIAMENT AND OF THE COUNCIL of 23 April 2009 on the geological storage of carbon dioxide and amending Council Directive 85/337/EEC, European Parliament and Council Directives 2000/60/EC, 2001/80/EC, 2004/35/EC, 2006/12/EC, 2008/1/EC and Regulation (EC) No 1013/2006.
- EU (2011). Implementation of Directive 2009/31/EC on the Geological Storage of Carbon Dioxide. Guidance document 2: Characterisation of the storage complex, CO<sub>2</sub> Stream Composition, Monitoring and Corrective Measures.
- EU (2017). EU Guidance Document (MRGs); The Monitoring and Reporting Regulation – General guidance for installations; Updated November 2017.
- EU (2018). Commission Implementing Regulations (EU) 2018/2066 of 19 December 2018 on the monitoring and reporting of greenhouse gas emissions pursuant to Directive 2003/87/EC of the European Parliament and of the Council and amending Commission Regulation (EU) No 601/012.
- Fisher Q. (2013). Collection of petroleum field analogues data and description of risks of CO<sub>2</sub> leakage along faults. EU FP7 UltimateCO<sub>2</sub> Deliverable D4.1.
- Fischer, H., Orlic, B., Osinga, S., Hopmans, P., Wollenweber, J., Geel, K. (2016). Options to initiate and enhance ductile properties of shale for well bore sealing. “TKI Plugging wells by enhanced formation ductility” - Deliverable report D5.1; TNO report 2016 R10970.
- Furre, A.-K., Eiken, O., Alnes, H., Vevatne, J.N., Kiær, A.F. (2017). 20 years of monitoring CO<sub>2</sub>-injection at Sleipner, Energy Procedia, 114, 3916-3926.
- Gaus I., Zazroual M. and Czernichowski-Lauriol I. (2005). Reactive transport modelling of the impact of CO<sub>2</sub> injection on the clayey cap rock at Sleipner (North Sea). Chemical Geology 217, 319-337.
- Geel, C.R. (2016). Geological screening of ductile formations. “TKI Plugging wells by enhanced formation ductility” - Deliverable report D4.1; TNO report 2016 R10273.
- Geertsma, J. (1973). A basic theory of subsidence DUE to reservoir compaction: The homogeneous case. Verhandelingen Koninklijk Nederlandsch Geologisch Mijnbouwkundig Genootschap 2S, 43-61.
- Gilfillan S.M.V., Lollar B.S., Holland G., Blagburn D., Stevens S., Schoell M., Cassidy M., Ding Z., Zhou Z., Lacrampe-Couloume G. and Ballentine C.J. (2009). Solubility trapping in formation water as dominant CO<sub>2</sub> sink in natural gas fields. Nature 458, 2 April 2009, doi:10.1038/nature07852.
- Grude S., Landrø M. and Dvorkin J. (2014). Pressure effects caused by CO<sub>2</sub> injection in the Tubåen. Fm., the Snøhvit field. International Journal of Greenhouse Gas Control 27, 178-187.
- IEAGHG (Greenhouse Gas Programme) (2016). Impact of impurity on CO<sub>2</sub> compression, liquefaction and transportation, Report 2016/01.
- IEAGHG (2018). Well Engineering and Injection Regularity in CO<sub>2</sub> Storage wells, IEAGHG Technical Report, 2018-08.
- ISO/TC 67/SC 4 Drilling and production equipment. (2017). *ISO 16530-1:2017: Petroleum and natural gas industries - Well integrity - Part 1: Life cycle governance*. bsi.
- Kim K.-Y., Han W.S., Oh J., Kim T. and Kim J.-C. (2012). Characteristics of salt precipitation and the associated pressure build-up during CO<sub>2</sub> storage in saline aquifers. Transport in Porous Media 92, 397-418.
- Koenen M., Wasch L., Wollenweber J. and Tambach T. (2014). CATO-2 Deliverable WP3.4-D12. Experimental and modelling study into chemical

- degradation mechanisms and rates of cement subjected to aqueous and supercritical CO<sub>2</sub> at in-situ reservoir conditions.
- Koenen M. and Wasch L. (2018). The potential of CO<sub>2</sub> leakage along de-bonded cement-rock interface. 14th International Conference on Greenhouse Gas Control Technologies, GHGT-14. 21<sup>st</sup> – 25<sup>th</sup> October 2018, Melbourne, Australia.
- Kutchko B.G., Strazisar B.R., Dzombak D.A., Lowry G.V. and Thaulow N. (2007). Degradation of well cement by CO under geologic sequestration conditions. *Environmental Science and Technology* 41 (13), p4787-4792
- Loeve, D., Hofstee C. and Maas J.G.,(2014). Thermal effects in a depleted gas field by cold CO<sub>2</sub> injection in the presence of methane, *Energy Procedia*, Volume 63, p. 5378-5393.
- Mijnbouwwet, <https://wetten.overheid.nl/jci1.3:c:BWBR0014168&z=2019-04-10&g=2019-04-10>
- Mindlin, R.D. (1936). Force at a point in the interior of a semi-infinite solid, *Physics*, 7(5), 195–202.
- Miocic J.M., Gilfillan S.M.V., Frank N., Schroeder-Ritzrau A., Burnside N.M. and Haszeldine R.S. (2019). 420,000 year assessment of fault leakage rates shows geological carbon storage is secure. *Scientific Reports*, DOI:10.1038/s41598-018-36974-0.
- Miri R. and Hellevang H. (2016). Salt precipitation during CO<sub>2</sub> storage – A review. *International Journal of Greenhouse Gas Control* 51, 136-147.
- Myklestad, N.O. (1942). Two problems of thermal stress in the infinite solid, *Journal of Applied Mechanics*, 9, 136-143.
- Neele, F., Delpart-Jannaud, F., et al. (2013). Site characterization workflow, SiteChar report D1.4.
- Nepveu, M, Neele, F, Delprat-Jannaud, F, Akhurst, M, Vincké, O, Volpi, V, Lothe, A, Brunsting, S, Pearce, J, Battani, A, Baroni, A, Garcia, B, Hofstee, C, And Wollenweber, J. 2015. CO<sub>2</sub> storage feasibility: a workflow for site characterization, *Oil and Gas Science and Technology* 70, 4, 555–566.
- Nieuwland, D. A. (2012) Fault Seal Prediction in Sandstone Reservoirs - A quantitative and calibrated geomechanical method, 3rd International Conference on Fault and Top Seals - From Characterization to Modelling, Montpellier, France 1-3 October, 2012.
- NOGEP A - OPCOM. (2016, October 12). Industry Standard no. 45 - Well Decommissioning. NOGEP A.
- NORSOK. (2013). *Norsok standard D-010: Well integrity in drilling and well operations*
- North Sea Basin Task Force (NSBTF), 2009, Monitoring Verification Accrediting and Reporting (MVAR) Report for CO<sub>2</sub> storage deep under the seabed of the North Sea.
- Okada, Y. (1992). Internal deformation due to shear and tensile faults in a half-space, *Bull. Seism. Soc. Am.*, 82(2), 1018–1040.
- OSPAR (2007). OSPAR Guidelines for Risk Assessment and Management of Storage of CO<sub>2</sub> Streams in Geological Formations (Reference Number: 2007-12), Meeting of the OSPAR Commission, Ostend, 25-29 June 2007.
- Peach C.J., de Bresser J.H.P., van der Kroef R.F.M., Mols A., Verberne B.A. and Samuelson J. (2010). Site-representative caprock and fault rock samples acquired and characterised (1st Year Progress Report). CATO-2 Deliverable WP 3.03-D06.

- Pruess, K., (2011). ECO2M: A TOUGH2 Fluid Property Module for Mixtures of Water, NaCl, and CO<sub>2</sub>, Including Super- and Sub-Critical Conditions, and Phase Change Between Liquid and Gaseous CO<sub>2</sub>. LBML, Univ. Berkeley, Berkeley, CA (Updated Sept 2013).
- Rimmelé G., Barlet-Gouédard V., Porcherie O., Goffé B. and Brunet F. (2008). Heterogeneous porosity distribution in Portland cement exposed to CO<sub>2</sub>-rich fluids. *Cement and Concrete Research* 38, 1038-1048.
- ROAD (2018). Rotterdam capture and storage demonstration project, <https://ccsnetwork.eu/projects/road-project-rotterdam>.
- Roels S.M., Ott H. and Zitha P.L.J. (2014).  $\mu$ -CT analysis and numerical simulation of drying effects of CO<sub>2</sub> injection into brine-saturated porous media. *International Journal of Greenhouse Gas Control* 27, 146-154.
- Samuelson J., Spiers C., Koenen M. and Tambach T. (2012). Lab evaluation of the reactivation potential of simulated faults under CO<sub>2</sub> storage conditions – implications for system integrity and seismic risk. CATO-2 Deliverable WP 3.3 – D13.
- Shell (2015). Peterhead CCS Project, Well Technical Specification, Doc No.: PCCS-05-PT-ZW-7770-00001, 20/05/2015.
- SodM. (2019). *De integriteit van onshore putten*. SodM
- Spain D.R. and Conrad C.P. (1997). Quantitative analysis of top-seal capacity: offshore Netherlands, southern North Sea. *Geologie en Mijnbouw* 76, 217-226.
- Tambach T., van Bergen F., Gutierrez-Neri M., Hostee C., Koenen M., Kooi H., Loeve D., Maas J., Plug W.-J., Ranganathan P., Roels S., van der Meer B., Wasch L. and Zitha P. (2012). Models describing near-well clogging and mineralization to support feasibility and long-term integrity. CATO-2 Deliverable WP3.02-D13.
- Tambach T.J., Loeve D., Hofstee C., Plug W.-J. and Maas J.G. (2015a). Effect of CO<sub>2</sub> injection on brine flow and salt precipitation after gas field production. *Transport in Porous Media* 108, 171-183.
- Tambach T.J., Koenen M., Wasch L.J. and van Bergen F. (2015b). Geochemical evaluation of CO<sub>2</sub> injection and containment in a depleted gas field. *International Journal of Greenhouse Gas Control* 32, 61-80.
- TAQA (2009). CO<sub>2</sub> Offshore Storage Source to Sink. Presentation given by TAQA Energy B.V., 3 July 2009.
- TAQA (2018) Geophysical Evaluation P18. TAQA Internal report, 6 p.
- Tian H., Xu T., Zhu H., Yang C. and Ding F. (2019). Heterogeneity in mineral composition and its impact on the sealing capacity of caprock for a CO<sub>2</sub> geological storage site. *Computers and Geosciences* 125, 30-42.
- Van Balen, R.T., Van Bergen, G., De Leeuw, C., Pagnier, H.J.M., Simmelink, H., Van Wees, J.D., Verweij, J.M. (2000). Modeling the hydrocarbon generation and migration in the West Netherlands Basin, the Netherlands. *Netherlands Journal of Geosciences* 79, 29-44.
- Van Eijs, R., Kuijper, M. and Bisschop, R. (2011). Containment demonstration for the Barendrecht CO<sub>2</sub> storage project, *Energy Procedia*, 4, 4092-4099.
- Vandeweijer V. et al. (2011). Feasibility study P18 (final report). CATO2-WP3.01-D06.
- Vrålstad, T., Todorovic, J., Wollenweber, J., Abdollahi, J., Karas, D., & Buddensiek, M. (2015). *D8.1 - Description of leakage scenarios for consideration in the work in SP3*.



Williams, S., T. Carlsen, K. Constable, & A. Guldahl (2009) Identification and qualification of shale annular barriers using wireline logs during plug and decommissioning operations. SPE paper 119321, 15 p.

## 16 Appendix A. compliance with EU Storage Directive site characterisation and assessment

This appendix presents the links between the site characterisation and assessment elements in the EU Storage Directive (EU, 2009) and the site characterisation elements workflow pursued in the P18-2 feasibility study. Annex I of the EUSD is used here as a reference. This annex consists of three steps, each of which consists of a list of items. The Guidance Document #2 to the EU Storage Directive provides an explanation of all the list elements; there is no need to repeat that here. The table below is modified after the Site characterisation workflow in Appendix I of the SiteChar report D1.4 (Neele *et al.*, 2013).

### 16.1 Data collection (step 1)

	Storage Directive elements in step 1	Sections of the P18-2 feasibility study	Comments
(a)	Geology and geophysics	17 Appendix B	
(b)	Hydrogeology (in particular existence of ground water intended for consumption)	-	n.a.
(c)	Reservoir engineering (including volumetric calculations of pore volume for CO <sub>2</sub> injection and ultimate storage capacity)	17 Appendix B	
(d)	Geochemistry (dissolution rates, mineralisation rates)	-	Based on earlier studies
(e)	Geomechanics (permeability, fracture pressure)	17 Appendix B	
(f)	Seismicity	17 Appendix B	Related to fault stability in 12.3.3, 12.3.4
(g)	Presence and condition of natural and man-made pathways, including wells and boreholes which could provide leakage pathways	17 Appendix B	
(h)	Domains surrounding the storage complex that may be affected by the storage of CO <sub>2</sub> in the storage site	-	Based on earlier studies
(i)	Population distribution in the region overlying the storage site	-	n.a.
(j)	Proximity to valuable natural resources (including in particular Natura 2000 areas pursuant to Council Directive 79/409/EEC of 2 April 1979 on the conservation of wild birds(1) and Council Directive 92/43/EEC of 21 May 1992 on the conservation of natural habitats and of wild fauna and flora(2) ,	-	Addressed in EIA

	potable groundwater and hydrocarbons)		
(k)	Activities around the storage complex and possible interactions with these activities (for example, exploration, production and storage of hydrocarbons, geothermal use of aquifers and use of underground water reserves)	-	Addressed in EIA
(l)	Proximity to the potential CO <sub>2</sub> source(s) (including estimates of the total potential mass of CO <sub>2</sub> economically available for storage) and adequate transport networks	-	Not known at time of study; assumptions provided by client

## 16.2 Building the 3-D static geological earth model (step 2)

	Storage Directive elements in step 2	Sections of the P18-2 feasibility study	Comments
(a)	Geological structure of the physical trap	4.2, Appendix B: 17.1-17.5	
(b)	Geomechanical, geochemical and flow properties of the reservoir overburden (caprock, seals, porous and permeable horizons) and surrounding formations	4.2, 4.3, 4.4, 8.2, 8.3 Appendix B: 17.4	Geochemical properties based on earlier work
(c)	Fracture system characterisation and presence of any human-made pathways	4.2, 4.5, 9 Appendix B: 17.4	
(d)	Areal and vertical extent of the storage complex	10	
(e)	Pore space volume (including porosity distribution)	Appendix B: 17.4.3-17.4.5	
(f)	Baseline fluid distribution	Appendix B: 17.8	
(g)	Any other relevant characteristics	Appendix B: 17.7.5, 17.8.2, 17.8.3, 17.8.6	Gas production data, PVT, RFT and PLT data
(all)	The uncertainty associated with each of the parameters used to build the model shall be assessed by developing a range of scenarios for each parameter and calculating the appropriate confidence limits. Any uncertainty associated with the model itself shall also be assessed.	6.3.4 6.3.5 6.5.4 9.3 17.8.5	Injection rate Salt precipitation Mineral assemblage Cement bonding Well cross flow

### 16.3 Characterisation of storage dynamic behaviour, sensitivity characterisation, risk assessment (step 3)

Step 3 consists of several parts, which are discussed separately.

#### 16.3.1 Characterisation of the storage dynamic behaviour (step 3.1)

	<b>Storage Directive elements in step 3, characterisation of the storage dynamic behaviour</b>	<b>Sections of the P18-2 feasibility study</b>	<b>Comments</b>
(a)	Possible injection rates and CO <sub>2</sub> stream properties	5.2, 5.3, 6.2	
(b)	Efficacy of coupled process modelling (that is, the way various single effects in the simulator(s) interact)	6.3, 6.4 7.2, 7.3, 8.2, 8.3, 9.3	Thermohydraulic Thermomechanical
(c)	Reactive processes (that is, the way reactions of the injected CO <sub>2</sub> with in situ minerals feedback in the model)	6.5, 7.4, 9.3	
(d)	Reservoir simulator used (multiple simulations may be required in order to validate certain findings)	6.3.2, 6.4.2	
(e)	Short and long-term simulations (to establish CO <sub>2</sub> fate and behaviour over decades and millennia, including the rate of dissolution of CO <sub>2</sub> in water)	6.3 6.5	Short term Long term geochem.

#### 16.3.2 Insights from dynamic modelling (step 3.1)

	<b>Storage Directive elements in step 3, insights from dynamic modelling</b>	<b>Sections of the P18-2 feasibility study</b>	<b>Comments</b>
(f)	Pressure and temperature of the storage formation as a function of injection rate and accumulative injection amount over time	6.3, 6.4	
(g)	Areal and vertical extent of CO <sub>2</sub> vs time	6.3	
(h)	Nature of CO <sub>2</sub> flow in the reservoir, including phase behaviour	6.3, 6.4	
(i)	CO <sub>2</sub> trapping mechanisms and rates (including spill points and lateral and vertical seals)	4, 6.3, 10	
(j)	Secondary containment systems in the overall storage complex	10, 11	
(k)	Storage capacity and pressure gradients in the storage site	6.3, 6.4	
(l)	Risk of fracturing the storage formation(s) and caprock	7.2, 7.3, 8.2, 8.3, 12.2, 12.3	
(m)	Risk of CO <sub>2</sub> entry into the caprock	4.3, 8.3, 8.4, 12.2	

(n)	Risk of leakage from the storage site (for example, through abandoned or inadequately sealed wells)	12	
(o)	Rate of migration (in open-ended reservoirs)	11, 12.1	
(p)	Fracture sealing rates <sup>8</sup>	12.3.2	Qualitative; no rates
(q)	Changes in formation(s) fluid chemistry and subsequent reactions (for example, pH change, mineral formation) and inclusion of reactive modelling to assess affects	6.5, 7.4, 8.4, 9.3.4	
(r)	Displacement of formation fluids	-	
(s)	Increased seismicity and elevation at surface level	7	

### 16.3.3 Sensitivity characterisation (step 3.2)

This element of the EU Storage Directive reads: “Multiple simulations shall be undertaken to identify the sensitivity of the assessment to assumptions made about particular parameters. The simulations shall be based on altering parameters in the static geological earth model(s), and changing rate functions and assumptions in the dynamic modelling exercise. Any significant sensitivity shall be taken into account in the risk assessment.”

Sections of the P18-2 feasibility study: 6.3.4, 6.3.5, 8.4.2

Comments: Sensitivity to temperature, injection rate, mineral types

### 16.3.4 Risk assessment: hazard characterisation (step 3.3.1)

This element of the SDEU reads: “The hazard characterisation shall cover the full range of potential operating conditions to test the security of the storage complex. Hazard characterisation shall be undertaken by characterising the potential for leakage from the storage complex, as established through dynamic modelling and security characterisation described above. This shall include consideration of [the items in the table below]. The hazard characterisation shall cover the full range of potential operating conditions to test the security of the storage complex.”

	Elements of Storage Directive Risk assessment: hazard characterisation (step 3.3.1)	Sections of the P18-2 feasibility study	Comments
(a)	potential leakage pathways	9, 11, 12	
(b)	potential magnitude of leakage events for identified leakage pathways (flux rates)	7.4.4	Mostly qualitative
(c)	critical parameters affecting potential leakage (for example maximum reservoir pressure, maximum injection rate, temperature, sensitivity to various	12	

<sup>8</sup> The EU Guidance Document #2 does not offer an explanation as to the meaning of ‘fracture sealing rates’. Here, fracture sealing is assumed to be a combination of chemical reactions (resulting in mineral deposition in injection-induced fractures) and geomechanical processes (resulting in fractures closing).

	assumptions in the static geological Earth model(s))		
(d)	secondary effects of storage of CO <sub>2</sub> , including displaced formation fluids and new substances created by the storing of CO <sub>2</sub>	6.5, 7.4, 8.4	Displaced formation fluids: New substances
(e)	any other factors which could pose a hazard to human health or the environment (for example physical structures associated with the project)	-	n.a.

16.3.5 *Risk assessment: exposure assessment (step 3.3.2)*

This element of the SDEU reads: “Based on the characteristics of the environment and the distribution and activities of the human population above the storage complex, and the potential behaviour and fate of leaking CO<sub>2</sub> from potential pathways identified under Step 3.3.1.”

Sections of the P18-2 feasibility study: -

Comments: Not in scope of present study

16.3.6 *Risk assessment: effects characterisation (step 3.3.3)*

This element of the SDEU reads: “Based on the sensitivity of particular species, communities or habitats linked to potential leakage events identified under Step 3.3.1. Where relevant it shall include effects of exposure to elevated CO<sub>2</sub> concentrations in the biosphere (including soils, marine sediments and benthic waters (asphyxiation; hypercapnia) and reduced pH in those environments as a consequence of leaking CO<sub>2</sub>). It shall also include an assessment of the effects of other substances that may be present in leaking CO<sub>2</sub> streams (either impurities present in the injection stream or new substances formed through storage of CO<sub>2</sub>). These effects shall be considered at a range of temporal and spatial scales, and linked to a range of different magnitudes of leakage events.”

Sections of the P18-2 feasibility study: -

Comments: Not in scope of present study

16.3.7 *Risk assessment: risk characterisation (step 3.3.4)*

This element of the EU Storage Directive reads: “This shall comprise an assessment of the safety and integrity of the site in the short and long term, including an assessment of the risk of leakage under the proposed conditions of use, and of the worst-case environment and health impacts. The risk characterisation shall be conducted based on the hazard, exposure and effects assessment. It shall include an assessment of the sources of uncertainty identified during the steps of characterisation and assessment of storage site and when feasible, a description of the possibilities to reduce uncertainty.”

Sections of the P18-2 feasibility study: Chapter 12

Comments: Directed to characterisation of subsurface hazards

## 17 Appendix B. Subsurface model descriptions

### 17.1 Static model

#### 17.1.1 *New geological model – reasons*

Since the completion of the storage feasibility assessment for the P18-4 field (Vandeweyer et al., 2011), which produced a 3D reservoir model of all P18 fields, a number of developments necessitated the building of a new 3D reservoir model. Around 2014, the operators and co-owners of the P15-P18 blocks had the P15-P18 3D seismic survey reprocessed. A pre-stack, depth migrated (PSDM) version of the cube was now available, both in time and depth, as well as a velocity cube. An initial comparison of the Top Bunter interpreted from that cube with the one from the P18-4 study (Vandeweyer et al., 2011) revealed several important differences.

The most important differences were the location of the SW boundary fault of P18-2, particularly near the intended injector wells. In the new interpretation, the intended injector wells were at a larger distance from the fault, which might have a positive effect on the geomechanical behaviour of the fault when exposed to cold-CO<sub>2</sub> injection.

Another item that showed changes was the Top Bunter horizon, particularly in low-lying areas such as in the hanging walls of the boundary faults. Again, this might impact the geomechanical behaviour of these faults, as the vertical throw is now larger.

Further reasons for critically reviewing the P18-2 reservoir model are that in the 2011 P18-4 study (Vandeweyer et al., 2011) the emphasis was on the P18-4 compartment rather than the P18-2 compartment, and that since 2010 new production data have become available for all P18 compartments. It was therefore decided to build a new reservoir model, based on a seismic interpretation on the new, reprocessed 3D cube.

### 17.2 Seismic interpretation

A substantial part of the Top Bunter and Top Keuper had already been interpreted by TAQA. Only a few blank areas needed to be done. After a review of the TAQA horizon and fault interpretations, the remaining blank areas of the reprocessed cube were interpreted. This was mostly the southeastern tip of the P18-2 compartment and its surroundings (Figure 17-1). In some places, TAQA's interpretation was slightly changed, e.g. Compartment 2-II of P18-2 (Well P18-02-A6ST1). This was mostly done in combination with the interpretation of the overlying Top Keuper, a conspicuous reflector.

Faults interpreted by TAQA were inspected and generally found to agree with the seismic data, although in some instances modifications were made on some of the faults. A few new faults were interpreted, mostly in the P18-2 compartment. This was partly done using the variance attribute with a 5x5x50 computing window (Figure 17-2). During the interpretation it was found that boundary fault F20 (see Figure 17-7) displaces the entire caprock, and even cuts through the Base

Cretaceous Unconformity where it displaces the Lower Cretaceous sands (Figure 17-3).

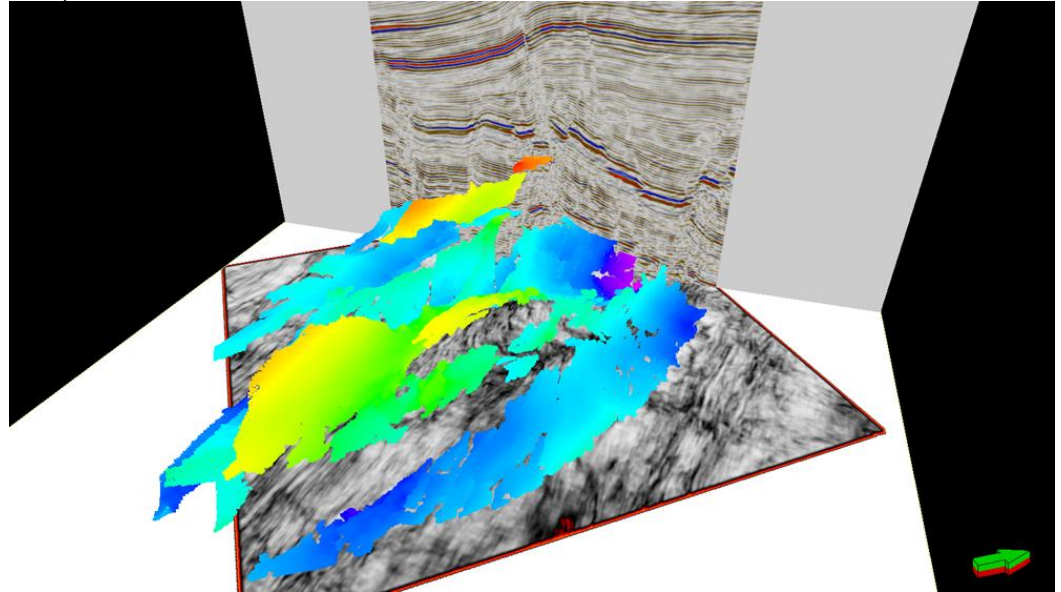


Figure 17-1: Oblique view on seismic interpretation of Top Bunter on the reprocessed P15-P18 3D cube.

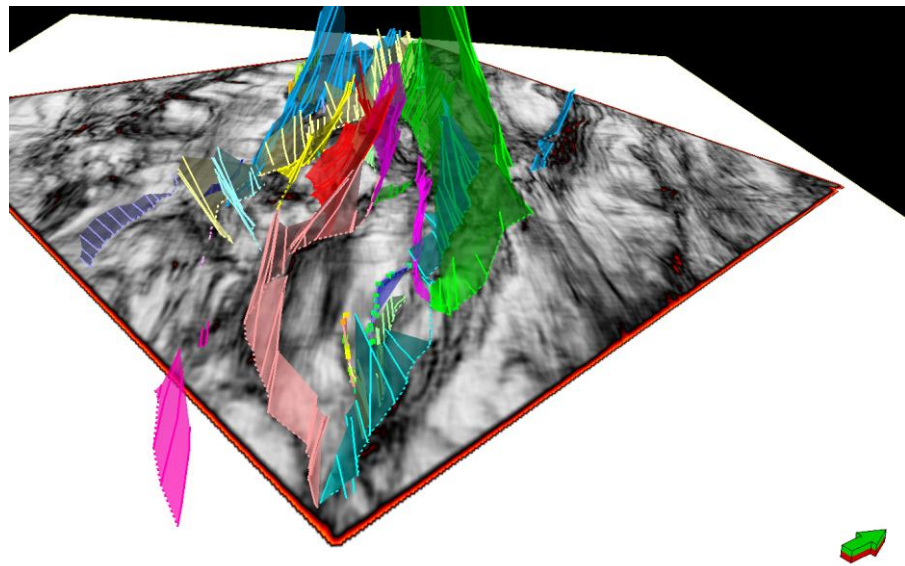


Figure 17-2: Checking existing fault interpretation and identifying additional faults with the variance attribute (5x5x50). Time slice through variance cube with interpreted faults.



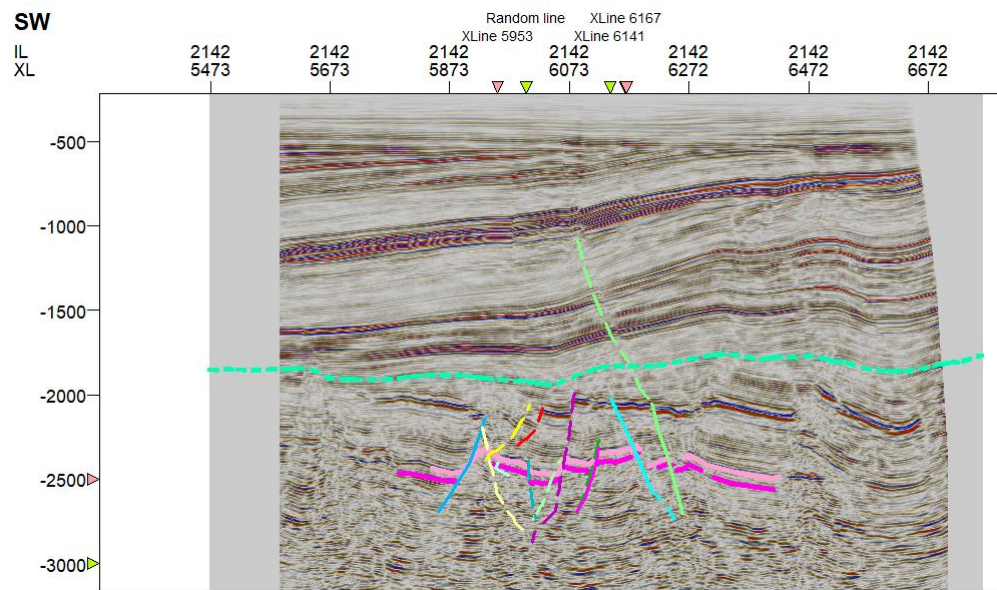


Figure 17-3: Seismic inline 2142 showing the top Bunter (purple horizon), Top Keuper (pink), and Base Cretaceous Unconformity (light green). Boundary Fault F20 (green) cuts through BCU.

### 17.3 Time-depth conversion

After consulting TAQA, it was found that the reprocessed P15-P18 cube came with a strongly improved velocity cube. It was therefore decided to adopt TAQA's velocity model which for the current project only contains two horizons: Top Keuper and Top Bunter (Table 17-1). In contrast to the velocity model that was used in the 2011 CATO study which was based on VELMOD and used six horizons, in the present model the entire overburden velocities above the Triassic are taken from the velocity cube (TAQA, 2018). For the Upper Germanic Trias itself a constant velocity of 4568 m/s was applied.

Table 17-1: Velocity model from TAQA as used in the current study

Interval	Top	Base	TZ conversion method
Overburden	MSL	Top Keuper	PSDM velocities
Upper Triassic	Top Keuper	Top Hardegsen	Constant velocity: 4568 m/s
LowerTr.-Perm.	Top Hardegsen	Top Carboniferous	Constant velocity: 4694 m/s

### 17.4 Petrel model building

Figure 17-4 shows the workflow that was followed to build the new static model. Apart from the newly interpreted faults, the horizons, and the new velocity model, all the necessary steps to build a reservoir model needed to be done. Thus, the horizons and zones were created, and a layering. For the property modelling the same procedure was followed as in the 2011 CATO model.

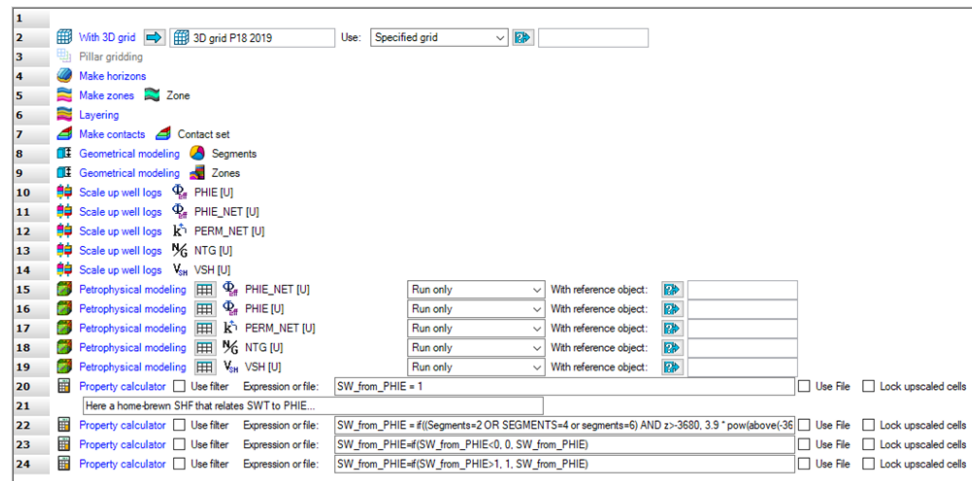


Figure 17-4: Petrel workflow that builds and populates the reservoir model.

#### 17.4.1 Fault model, gridding

All depth-converted faults from TAQA were converted to model faults. However, several faults from the fault model were deleted, either because they were outside the area of interest, or because they were too small to be modelled. Quite some effort was spent on the creation of the fault model and pillar grid of the P18 area in order to ensure a smooth and regular grid that would cause as little problems in ECLIPSE as possible. Most slopes are faulting so the pillar grid needs to be vertically cut close to the base and top of the reservoir model. When the faults reach too shallow or too deep they tend to cross each other, after which Y-faults need to be constructed which usually ends in gridding and geometric problems. Figure 17-5 and Figure 17-7 show the end result of the fault construction and pillar gridding process. Names of the faults used in the current model are displayed in Figure 17-7. For the pillar gridding (Figure 17-6) an average X and Y increment of 50 m was specified.

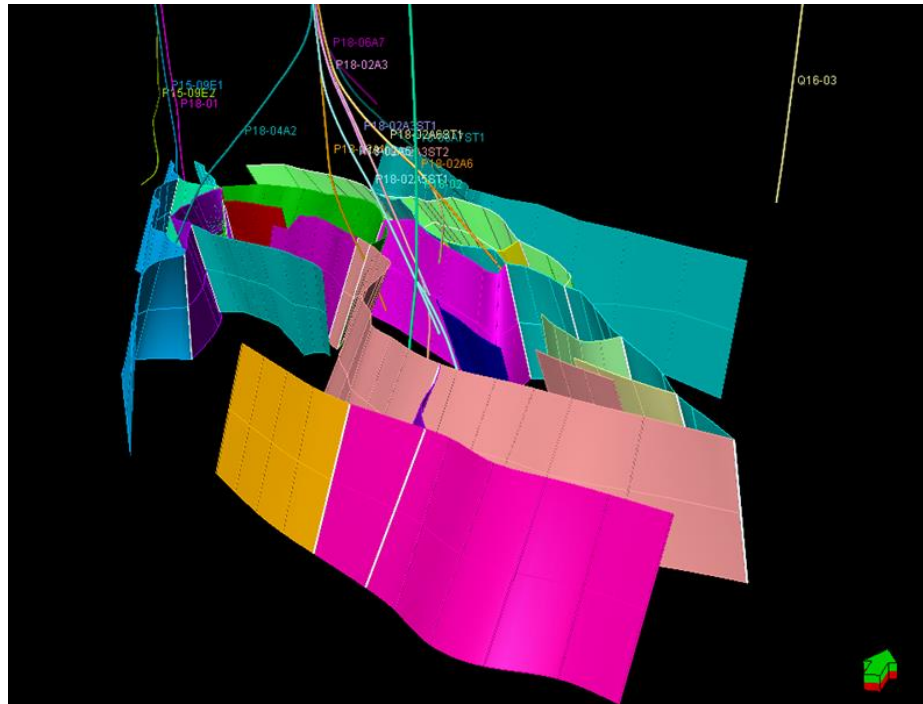


Figure 17-5: 3D view of all faults that have been incorporated in the pillar grid of the Petrel reservoir model.

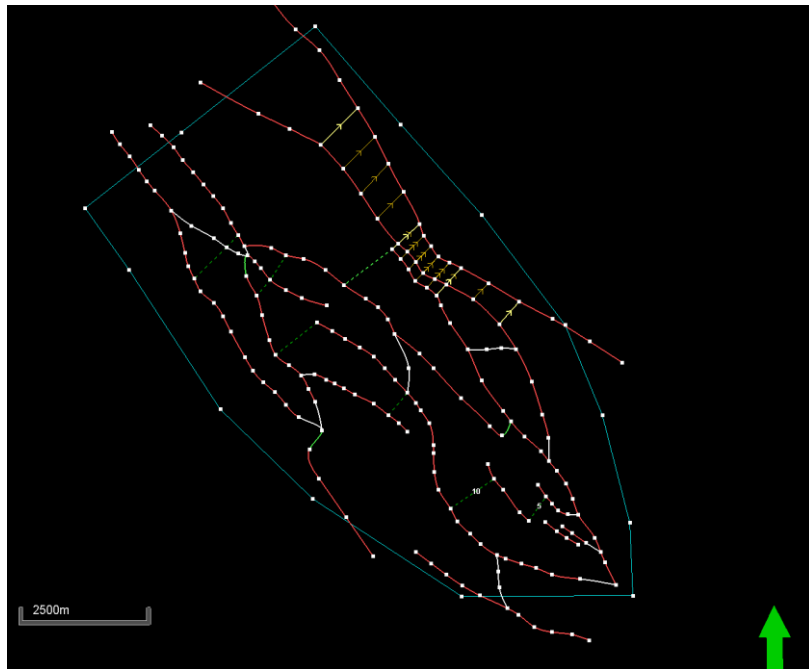


Figure 17-6: Map view of all faults and trends used in the pillar gridding.

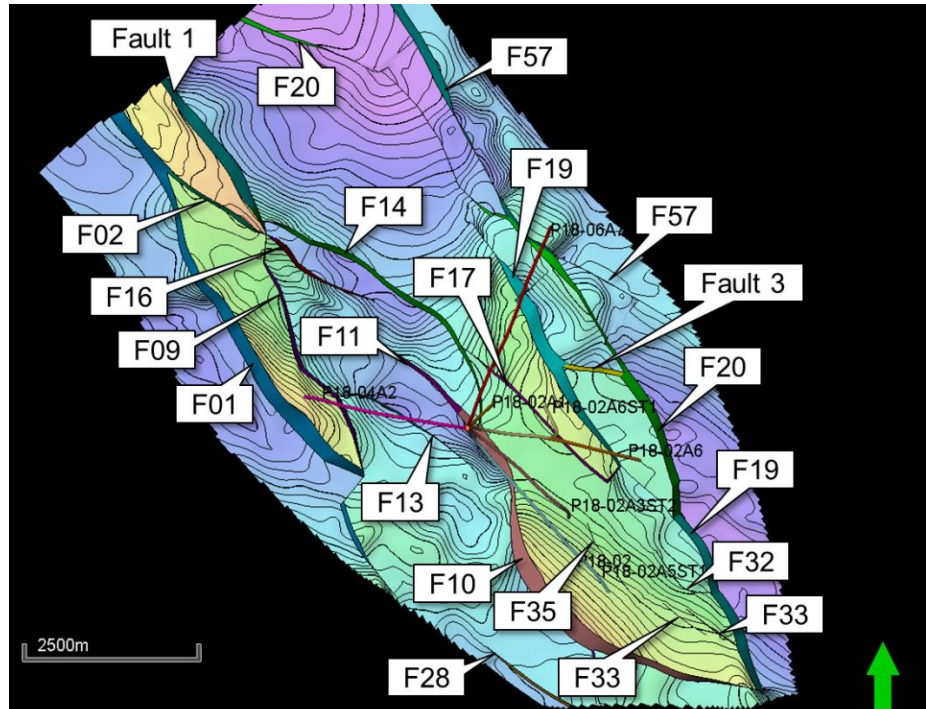


Figure 17-7: Nomenclature of all faults that have been incorporated in the pillar grid of the Petrel reservoir model.

17.4.2 *Make Horizons / Make Zones*

The new model has a different approach towards the construction of the reservoir formations compared to the P18 model from 2011. In the previous model, all Lower Triassic formation tops had a separate horizon as input in the ‘Make Horizons’ process. In combination with the many faults this led to geometrical problems such as rapidly thinning and thickening formations. The current model utilises only one horizon for the reservoir formations (Top Bunter; Figure 17-8).

The 2011 P18 model subdivision into formations was maintained, from top to base: Hardegsen, Upper Detfurth, Lower Detfurth, and Volpriehausen Formation. The rest of the horizons were created using isopachs (Figure 17-10, Figure 17-11, Figure 17-12). The result is a smooth reservoir model where formation thickness changes across the field are kept to a minimum. Figure 17-9 contains a list of all faults that have been incorporated in the pillar gridding process and subsequently in the ‘Make Horizons’ process.

The layering was done as follows: Hardegsen 5, Upper Detfurth 4, Lower Detfurth 3, and Volpriehausen 5 layers. All layers were assigned the type ‘proportional’.

Index	Horizon name	Color	Calculate	Horizon type	Conform to another horizon	Status	Smooth iterations	Use horizon fault lines	Well tops	Input #1
1	Top-Keuper		<input checked="" type="checkbox"/> Yes	Conformable	No	1	5	<input checked="" type="checkbox"/> Yes	Top-Keuper (Well tops TAQA)	06_NearKeuper_P18-ctd_PSDMTime_JakuR2014_grid [Converted] (Cropped Volume for TNO) smoothed (Z)
2	Top-Bunter		<input checked="" type="checkbox"/> Yes	Conformable	No	1	5	<input checked="" type="checkbox"/> Yes	Top-Bunter (Well tops TAQA)	07_TBunter_P18-ctd_SGSH_PSDMTime_JakuR2014_grid [Converted] (Cropped Volume for TNO) smoothed (Z)

Figure 17-8: Dialog box of the ‘Make Horizons’ process of the Petrel reservoir model.

Fault name	Distance	Displacement
<input type="checkbox"/> Use default	Distance: 100	Displacement: Min: 0, Max: 100
<input checked="" type="checkbox"/> Active fault	<input type="checkbox"/> Diff. sides	<input type="checkbox"/> Allow hinge
<input type="checkbox"/> Growth fault		<input checked="" type="checkbox"/> Smooth: 5
<input type="checkbox"/> Tolerance: 1		
<b>Default for all faults</b>	100	Smooth N: 5
<b>Default for each fault</b>		
P18-04 - SGS F01	100	Smooth N: 5
P18-04 - SGS F02	100	Smooth N: 5
P18-04 - SGS F09	100	Smooth N: 5
P18-04 - SGS F10	200/200	Smooth N: 5
P18-04 - SGS F11	100	Smooth N: 5
P18-04 - SGS F13	150	Smooth N: 5
P18-04 - SGS F14	100	Smooth N: 5
P18-04 - SGS F16	100	Smooth N: 5
P18-04 - SGS F17	100	Smooth N: 5
P18-04 - SGS F19	150/100	Smooth N: 5
P18-04 - SGS F20	200	Smooth N: 5
P18-04 - SGS F23	100	Smooth N: 5
P18-04 - SGS F24	100	Smooth N: 5
P18-04 - SGS F28	100	Smooth N: 5
P18-04 - SGS F32	50	Smooth N: 5
P18-04 - SGS F33	50	Smooth N: 5
P18-04 - TNO F34	50	Smooth N: 5
P18-04 - TNO F35	50	Smooth N: 5
Fault 1	100	Smooth N: 5
Fault 2	100	Smooth N: 5
Fault 3	100	Smooth N: 5
F57.xyz	100	Smooth N: 5
Top-Keuper		
Top-Bunter		

Figure 17-9: Detailed list of all faults that have been included in the 'Make Horizons' process of the Petrel reservoir model.

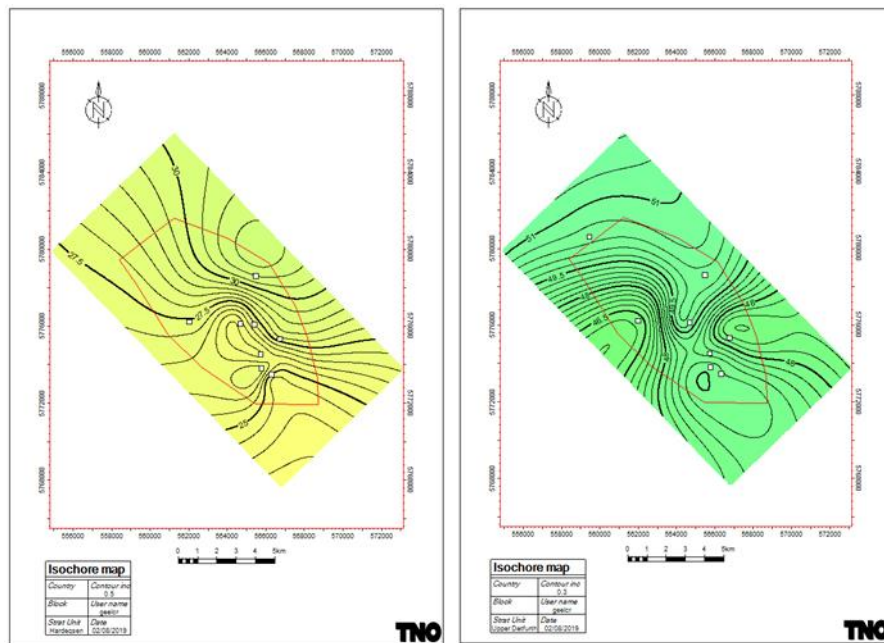


Figure 17-10: Isochore maps of the Hardegsen Fm (left) and the Upper Detfurth (right). Well values on which the isochore maps are based are shown as white squares.

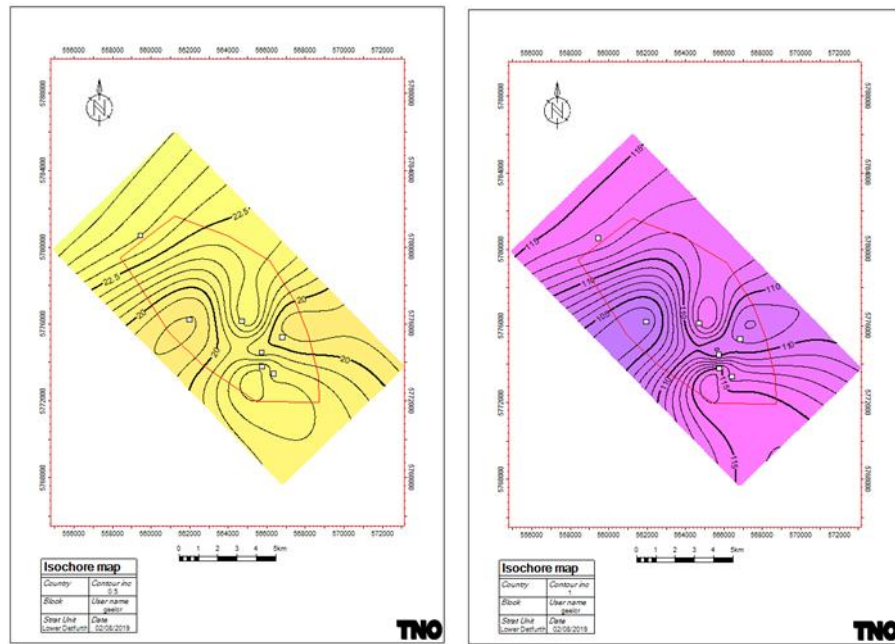


Figure 17-11: Isochore maps of the Lower Detfurth Fm (left) and the Volpriehausen Fm (right). Well values on which the isochore maps are based are shown as white squares.

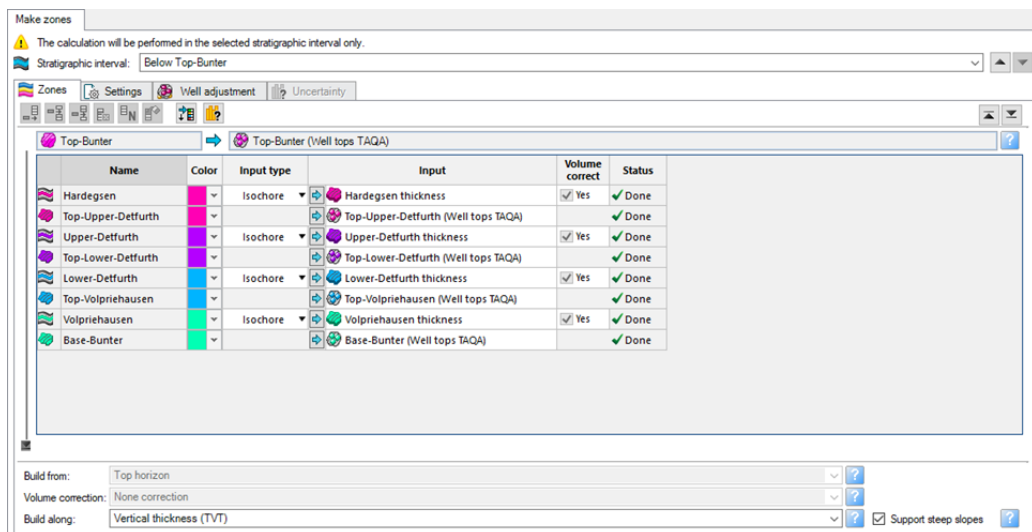


Figure 17-12: Creation of the various reservoir zones in the Petrel reservoir model.

### 17.4.3 Reservoir properties

A detailed petrophysical study on the P15-P18 area was done by BP (2007). Relationships between porosity and permeability in this study were established on the basis of rock types (lithofacies). The origin of these rock types is not readily apparent from this study but seems to have been generated by the Baker Hughes “Horizon” software package (see Ames & Farfan, 1996). On the basis of well log readings, this software package classifies depth intervals into rock types that have been calibrated against lithofacies from core descriptions.

For the P18 area these rocktypes are:

- Rock Type 1: Eolian Dune

- Rock Type 2: Interdune
- Rock Type 3: Eolian Dolomitic
- Rock Type 4: Shales

For each of these rock types a separate porosity-permeability relation has been established (BP, 2007).

- Rock Type 1:  $K_{calc} = 10^{(-3.3+0.58 \cdot PH_{calc} - 0.01229(PH_{calc})^{**2})}$
- Rock Type 2:  $K_{calc} = 10^{(-2.75+0.464 \cdot PH_{calc} - 0.011(PH_{calc})^{**2})}$
- Rock Type 3:  $K_{calc} = 10^{(-3.003+0.358 \cdot PH_{calc} - 0.0068(PH_{calc})^{**2})}$
- Rock Type 4:  $K_{calc} = 0.01$

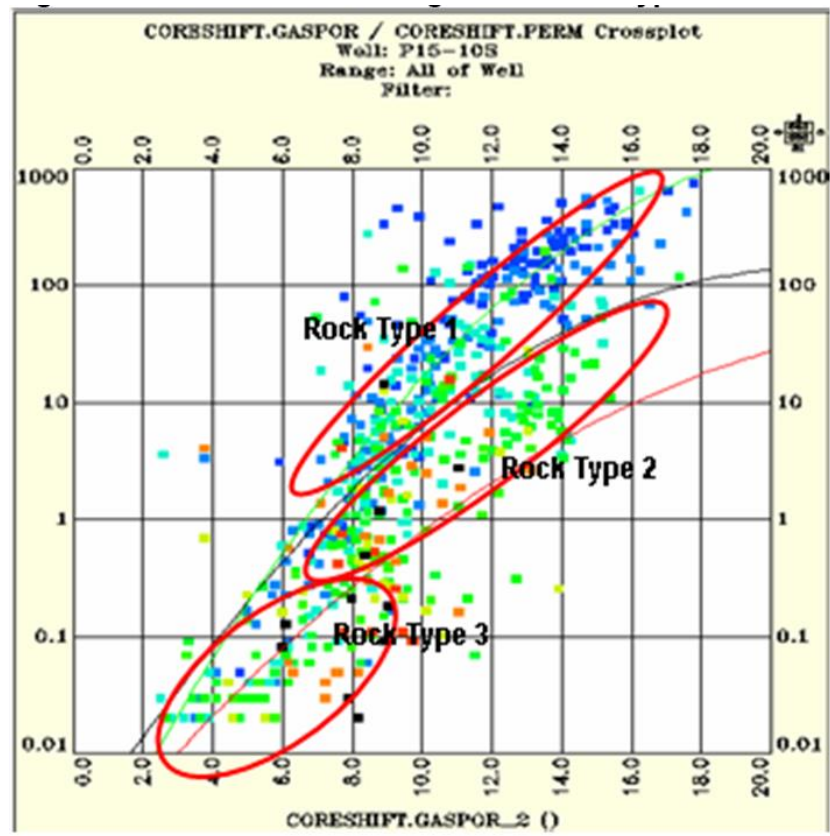


Figure 17-13: Relationship between porosity and permeability for three rock types (lithofacies):  
 1 = Aeolian Dune, 2 = Interdune, 3= Aeolian Dolomitic. Not shown in this graph is rock type 4 = shales. From BP (2007).

There are two field-wide no-flow boundaries or baffles (possibly even pressure boundaries), between Upper and Lower Detfurth Fm, and between Lower Detfurth and Volpriehausen (Figure 17-14). These have impact on pressure behaviour, as illustrated in Figure 17-15. The implementation in the reservoir model was done in ECLIPSE using reduced transmissibility multipliers between the lowermost layer of Upper Detfurth and uppermost layer of Lower Detfurth, and between the lowermost layer of Lower Detfurth and uppermost layer of Volpriehausen Fm.

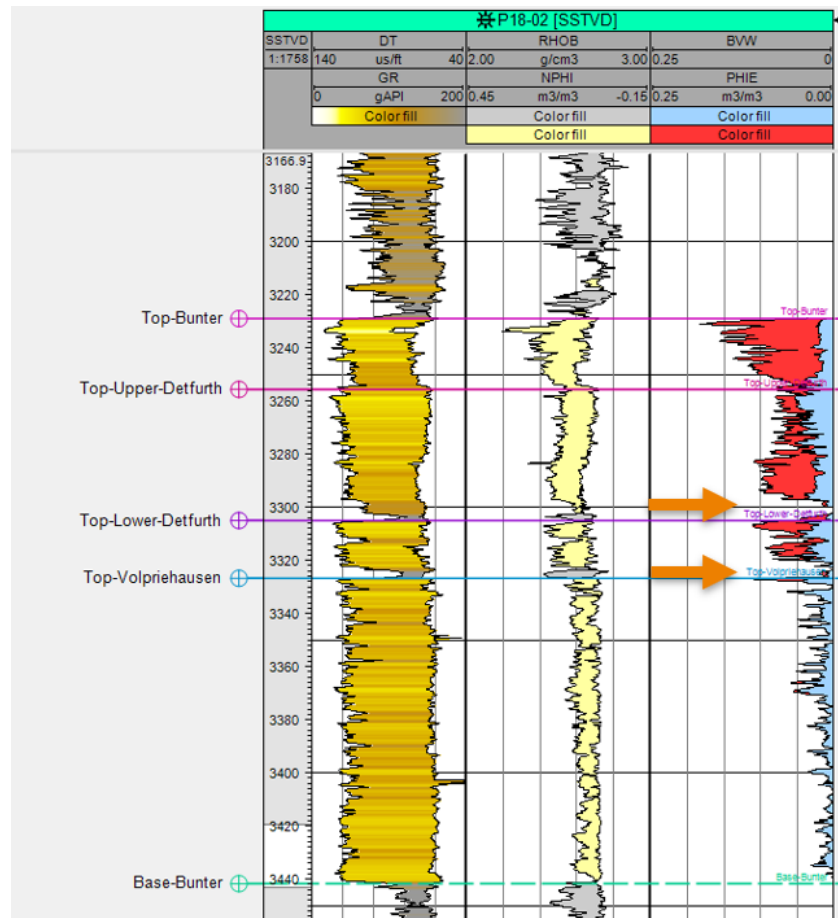


Figure 17-14: Well P18-02 showing the occurrence of two field-wide barriers (orange arrows) separating the Upper and Lower Detfurth Fm, and the Lower Detfurth and Volpriehausen Fm.

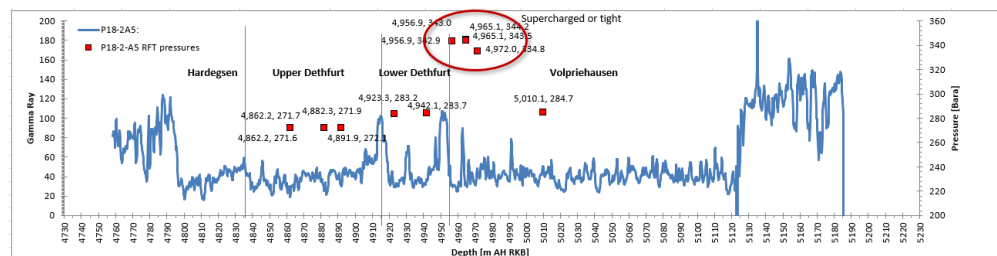


Figure 17-15: RFT measurements in Well P18-A5ST1 (red squares) showing differential depletion. Average pressure in the Upper Detfurth Fm is 272 Bara, in the Lower Detfurth Fm 283.5 Bara, and 284.7 Bara in the Volpriehausen Fm. Encircled points are either supercharged or tight.

17.4.4 Modelling of reservoir properties

Essentially, the same procedure for the distribution of reservoir properties as in the 2011 CATO model was followed. The following logs were arithmetically upscaled:

- PHIE (effective porosity)
- PERM (permeability)
- VSH (Shale volume)



- NTG (Net to gross; log is either one or zero, depending on cutoffs PHIE 8% and VSH 35%)
- PHIE\_NET (Net effective porosity. Log has the value of PHIE or is undefined, depending on the NTG log)
- PERM\_NET (Net permeability. Log has the value of PERM or is undefined, depending on the NTG log)

All properties were distributed using Kriging, with an isotropic variogram range of 5 km. In order to investigate the effect of anisotropy, a second realisation was done for the porosity and permeability using Kriging with an elongated variogram: long axis 5 km, short axis 2.5 km, long axis strikes NW-SE (135-315).

Figure 17-16 to Figure 17-19 show histograms of the distribution of porosity, permeability, and net porosity and net permeability. Ideally, all histograms should be identical. Although there are minor differences, most of the histograms are comparable.

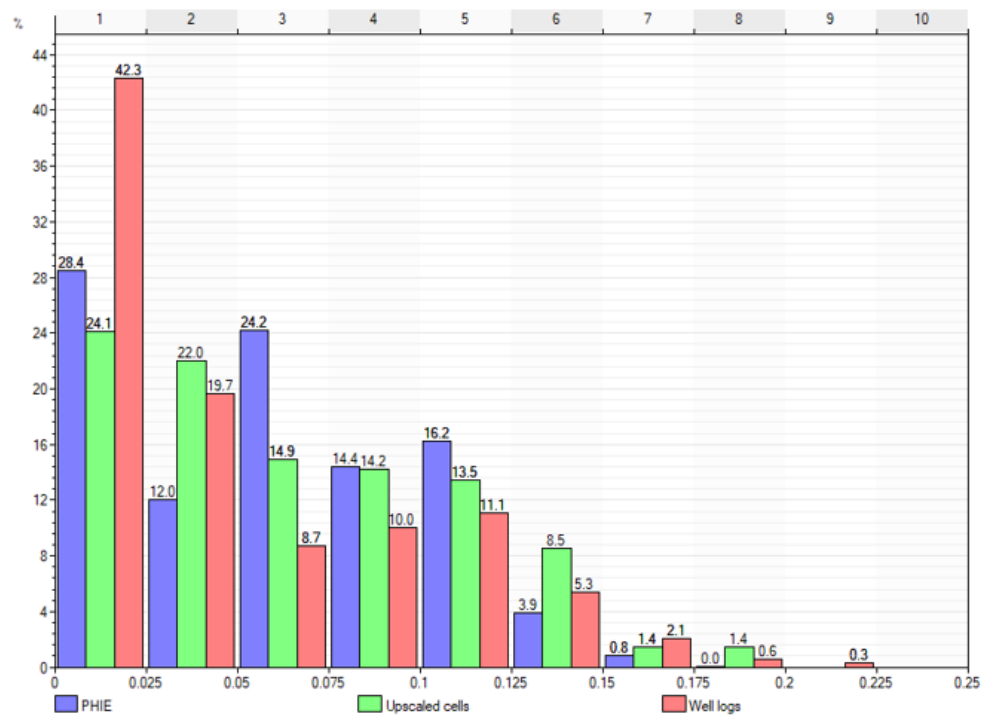


Figure 17-16: Comparison of the distributions of effective porosity (PHIE) in well logs, upscaled well logs, and as 3D property.

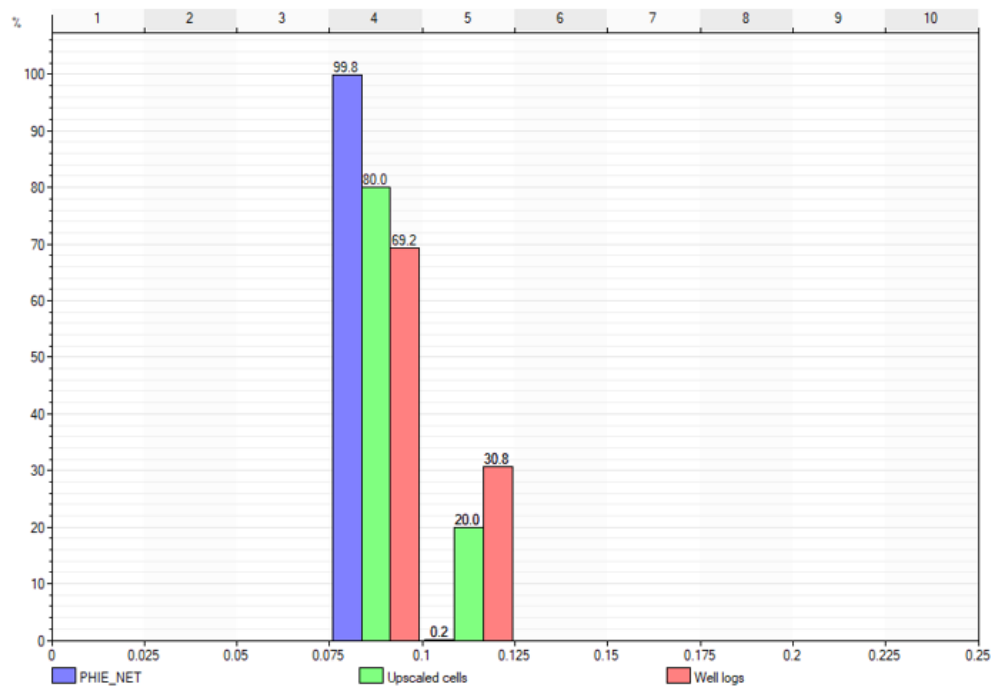


Figure 17-17: Comparison of the distributions of net effective porosity (PHIE\_NET, based on a cutoff of 8%) in well logs, upscaled well logs, and as 3D property.

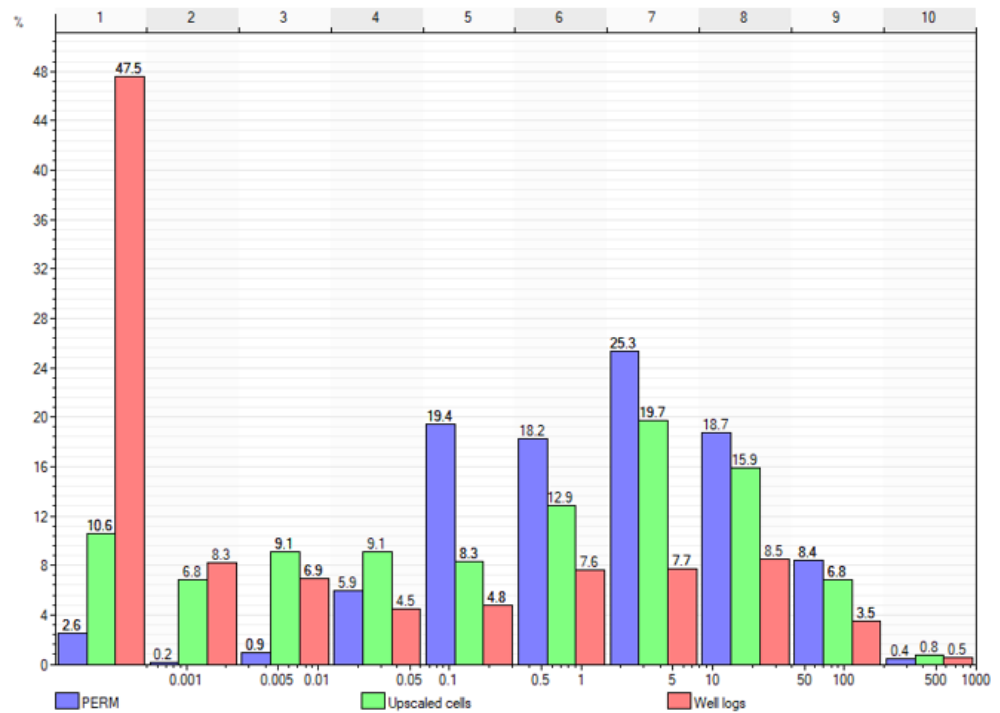


Figure 17-18: Comparison of the distributions of permeability (PERM) in well logs, upscaled well logs, and as 3D property.

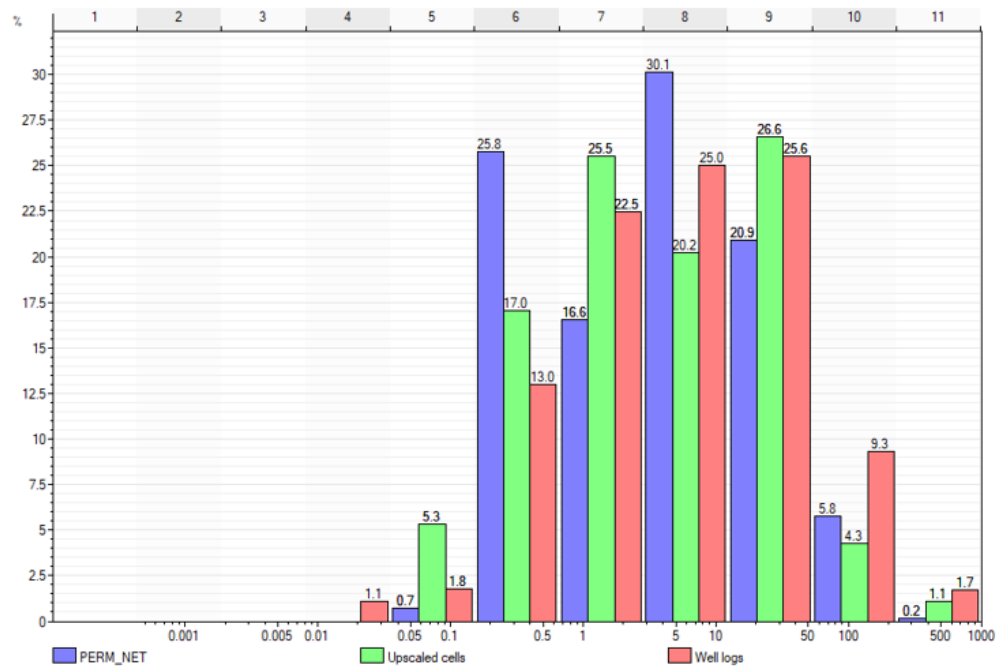


Figure 17-19: Comparison of the distributions of net permeability (PERM\_NET, based on a cutoff of 8% PHIE and 35% VSH) in well logs, upscaled well logs, and as 3D property.

In order to compare the static gas in place with the dynamic gas in place, it is necessary to calculate the water saturation in the field. A Lambda saturation-height function was developed by matching the water saturation logs from resistivity logs with a water saturation log calculated from porosity and height above free water level. The best match yielded the following Lambda saturation-height function (Figure 17-20):

$$S_w = 3.9 HAFWL^{-2.7} Phie^{-0.22}$$

Figure 17-21 and Figure 17-22 show the result of using PHIE or PHIE\_NET for calculating water saturation. In the latter case water saturations in the Volpriehausen Fm are higher. However, because the net to gross is lower the end result is a lower GIIP (see below).

Figure 17-23 to Figure 17-25 show cross plots of the upscaled well logs for water saturation. The Total Water Saturation (from the 2010 model; logs provided by TAQA) is cross plotted against TNO's saturation-height function. All cross plots show the same behaviour, with the majority of the points falling around the  $y=x$  line, and a tail towards higher water saturations for SWT. This can be easily explained by the fact that SWT is calculated for total porosity, hence represents total water saturation which includes all clay-bound water. Apart from this, the match is good, and the currently used water saturations used by TNO in the static model do not underestimate the gas in place, at least not in comparison to the original SWT.

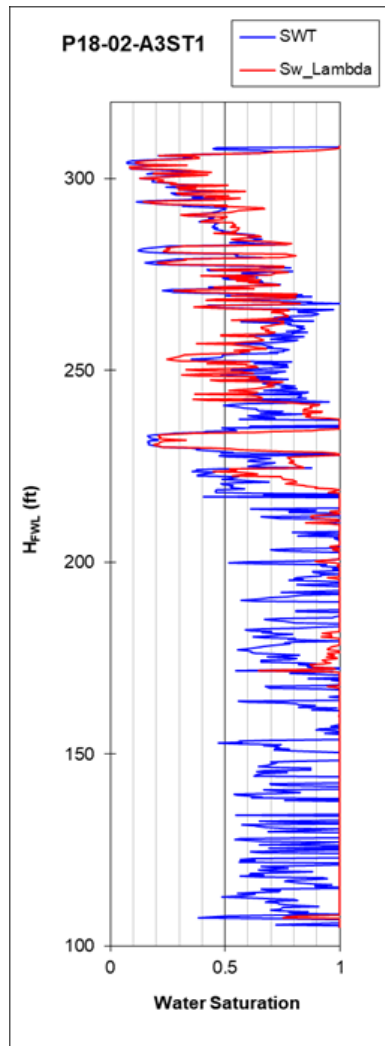


Figure 17-20: Comparison of log-derived water saturation (STW; blue line) and water saturation calculated with a saturation-height function (SW\_Lambda; red line).

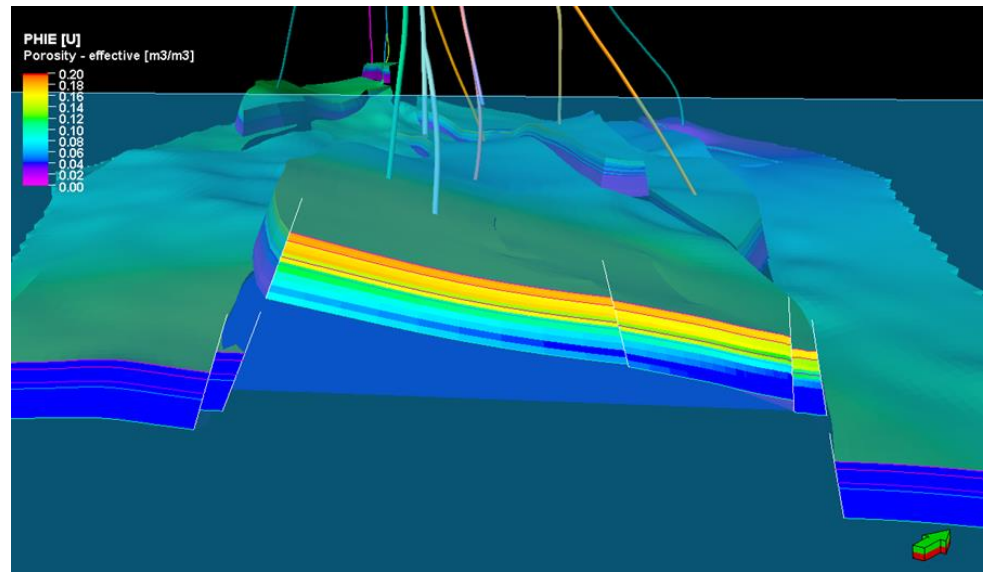


Figure 17-21: Water saturation in Compartment P18-2 without cutoffs on PHIE and VSH. Note the high water saturations in the Volpriehausen Formation. Legend as in Figure 17-22.

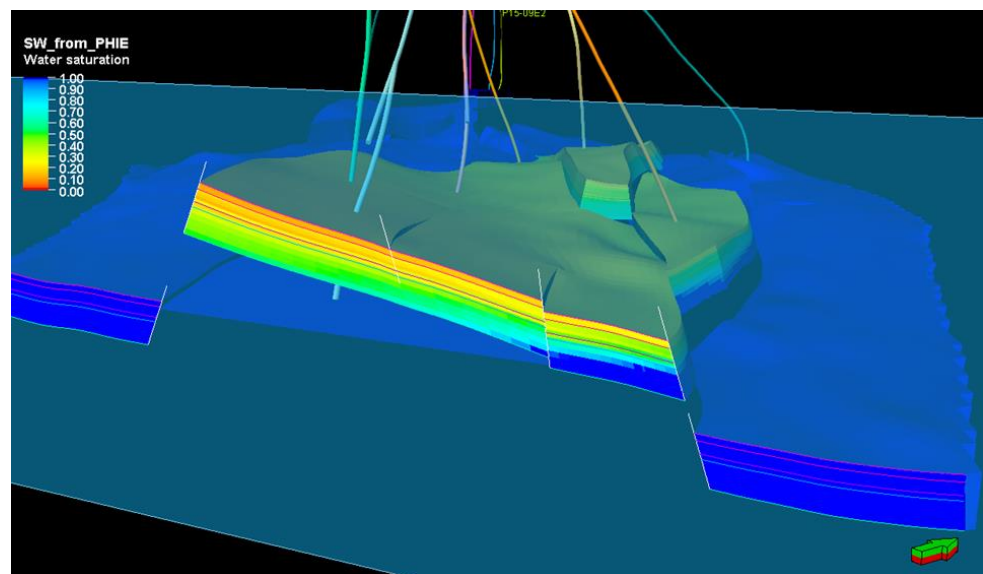


Figure 17-22: Water saturation in Compartment P18-2 with PHIE cutoff of 8% and a cutoff of 35% on VSH.

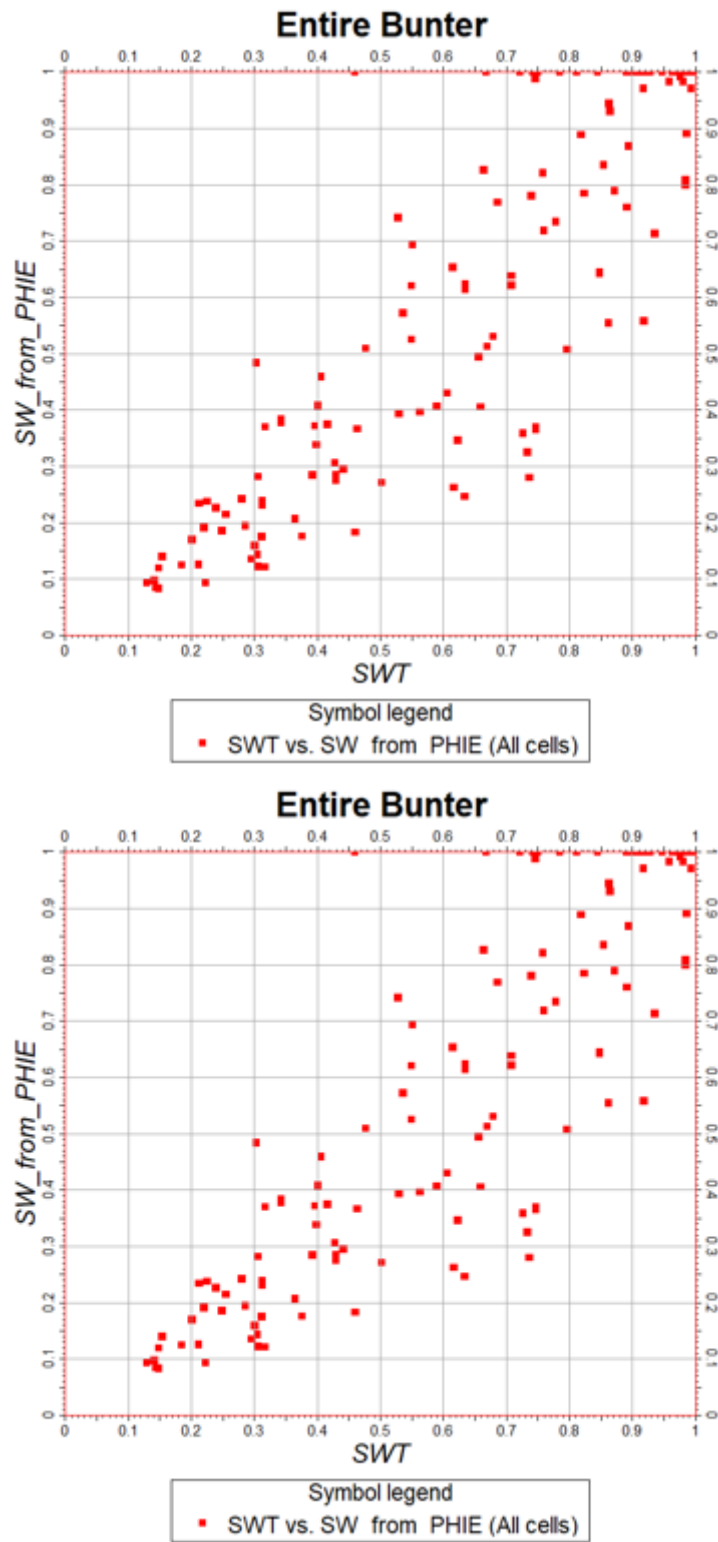


Figure 17-23: Crossplot of upscaled water saturation logs SWT (personal communication TAQA, 2010) and TNO's 2019 saturation-height function SW\_from\_PHIE, for all four Bunter formations.

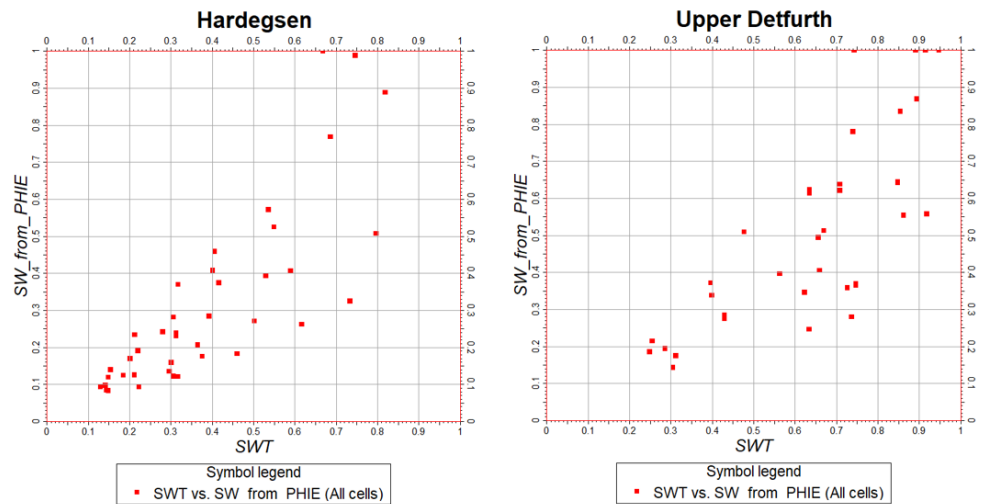


Figure 17-24: Crossplot of upscaled water saturation logs SWT (personal communication TAQA, 2010) and TNO’s 2019 saturation-height function SW\_from\_PHIE, for the Hardegsen and Upper Detfurth formations.

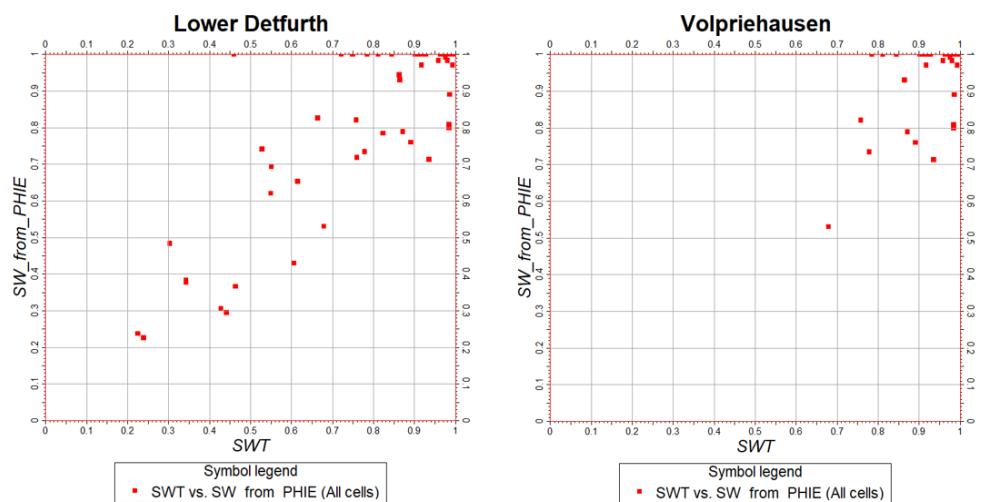


Figure 17-25: Crossplot of upscaled water saturation logs SWT (personal communication TAQA, 2010) and TNO’s 2019 saturation-height function SW\_from\_PHIE, for the Lower Detfurth and Volpriehausen Formations.

17.4.5 GIIP

The actual volumetrics are done during the ECLIPSE history match, but to see whether the geometry and properties of the reservoir model are sufficiently close, the GIIP for the various compartments was calculated.

GIIP was calculated without cutoffs on PHIE or VSH, so with a Net to Gross of 1.0, and with a cutoff on porosity and VSH. Two cutoffs on porosity were examined: 6% and 8%. VSH cutoff was set to 35%. The gas expansion factor Bg was set to 0.0040. Cutoffs of 8% and 35% were derived from BP’s petrophysical evaluation report (BP, 2007).

Table 17-2 shows the results of the GIIP calculations. A realistic scenario with a 35% cutoff on VSH and 8% cutoff on PHIE results in a total GIIP of 13 bcm, which

is on the low side in comparison to the P/Z volumes that sum up to 14.5 bcm. However, the fact that they are in the same range justifies the use of the current model for reservoir simulations. Table 17-3 compares the static volumes from the 2010 and 2019 models.

Table 17-2: Result of static GIIP calculations using various cutoffs. (N.B. for Block read Compartment in this study)

P18-2 Compartment Scenario	2-I GIIP [bcm]	2-II GIIP [bcm]	2-III GIIP [bcm]	Total [bcm]
No cutoffs	11	3	0.9	15
6% Phie, 35% Vsh	10	3	0.9	14
8% Phie, 35% Vsh	9	3	0.8	13

Table 17-3: Comparison of the volumes from the 2010 CATO models and the 2019 model. (N.B. for Compartment read Compartment in this study)

3Dmodel	Block	Bulk volume [*10 <sup>6</sup> m <sup>3</sup> ]	Net volume [*10 <sup>6</sup> m <sup>3</sup> ]	Pore volume [*10 <sup>6</sup> m <sup>3</sup> ]	HCPV gas [*10 <sup>6</sup> m <sup>3</sup> ]	GIIP [*10 <sup>6</sup> sm <sup>3</sup> ]	Total GIIP [*10 <sup>6</sup> sm <sup>3</sup> ]
2010 38 layers	Block I	1512	1245	83	37	9262	12711
	Block II	450	379	24	10	2400	
	Block III N	140	116	6	1	249	
	Block III M	199	127	8	3	718	
	Block III S	24	20	1	0	82	
2010 14 layers	Block I	1512	1246	83	36	9123	12266
	Block II	449	379	24	8	2114	
	Block III N	140	117	6	1	332	
	Block III M	199	128	8	2	620	
	Block III S	24	20	1	0	77	
2019, SW_PHIE, no cutoff	Block 2-I	2262	2262	76	42	10603	15912
	Block2-II	858	858	30	14	3444	
	Block2-III	355	355	10	4	880	
	Block2-IV	917	917	13	4	985	



## 17.5 Differences with 2010 model and implications

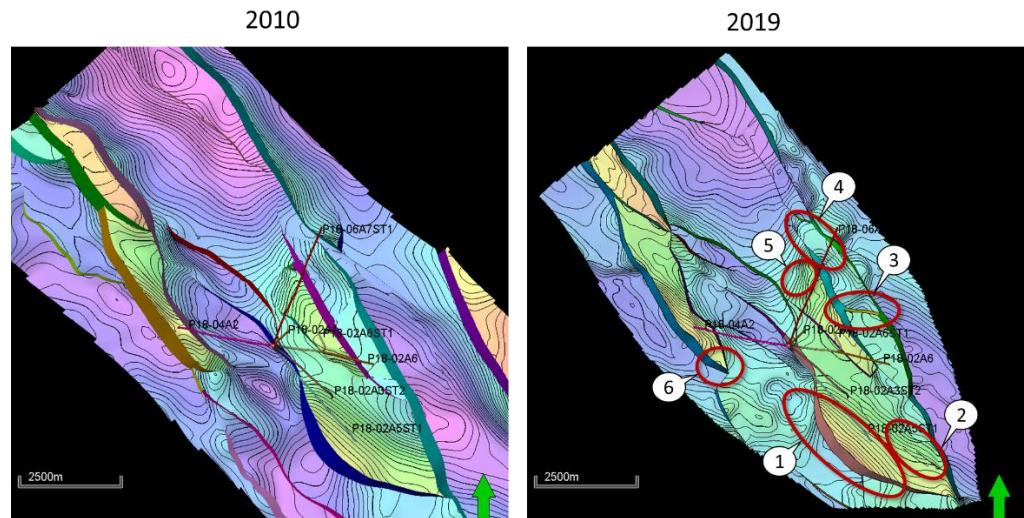


Figure 17-26: Comparison of the 2011 (left) and 2019 (right) Petrel models.

Although in the new model many faults and properties remained the same as in the 2010 TNO model (Vandeweyer et al., 2011), there a number of relevant differences.

These are highlighted in Figure 17-26 and are listed below, with their implications.

- 1) The location of the SW boundary fault (F10) has moved, so the proposed injection wells P18-02-A3 and P18-02-A5 are now further away from that fault. This probably has a positive effect on the geomechanical behaviour of the fault during CO<sub>2</sub> injection.
- 2) A number of small-offset faults are introduced. Because of the small vertical throw they are not expected to have an effect.
- 3) The internal fault in compartment 2-III now has a different orientation. Also, its throw is much larger, so that it is probably sealing.
- 4) The Top Bunter in P18-2 adjacent to P18-6 is now interpreted shallower. That means that the previous interpretation where the P18-6 reservoir was sealed off from the P18-2 reservoir by a simple juxtaposition of Upper Triassic and Altona shales is no longer valid. However, P18-6 is still likely to be separated from P18-2 because of a peculiar constellation of faults (Figure 17-27 to Figure 17-31). Two faults (F20 and F57, which form a synthetic-antithetic fault system) separate P18-6 and P18-2. Wherever Bunter is juxtaposed against Bunter, one of the two is invariably the low-permeable and water-filled Volpriehausen Fm, making across-fault fluid flow extremely unlikely. Fault 57 is a sinistral wrench fault, which increases the likelihood that Fault 57 contains a substantial amount of smeared Solling Clay, increasing the capillary entry pressure of that fault. Therefore, any fluid flowing across Fault 57 needs to surpass that capillary pressure.
- 5) The fault that sealed off Compartment 2-II from its downdip aquifer is no longer in the model. A small-throw fault (around 15 m) could be interpreted, but that would have little consequences for the fluid flow. This means that Compartment 2-II is in pressure communication with its downdip, lateral aquifer.

- 6) The SE tip of the P18-4 field has been slightly modified. Partly based on seismic interpretation of Top Bunter and the faults surrounding the tip, and partly on constraints by Petrel's pillar gridding.

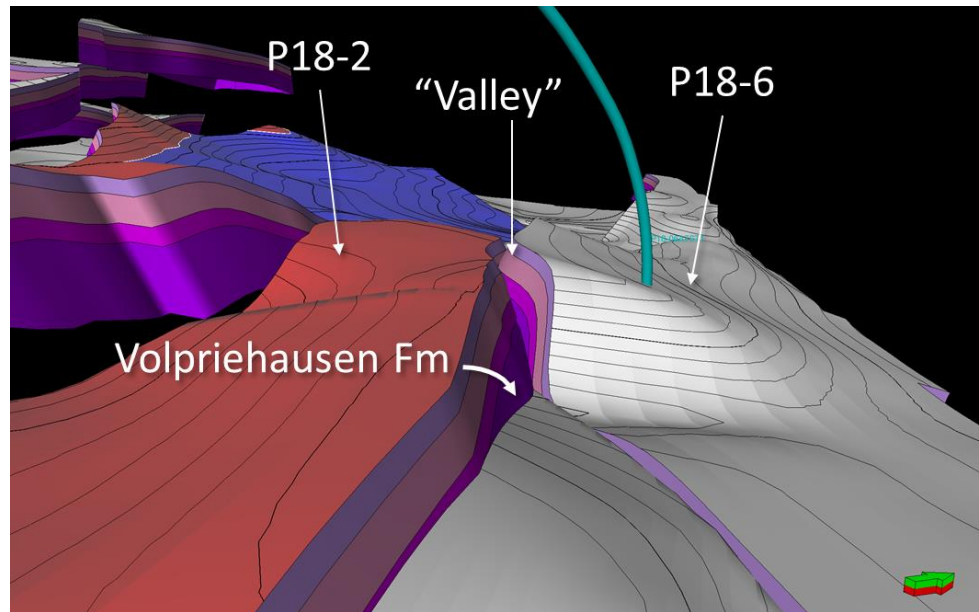


Figure 17-27: Oblique view toward the NW on the boundary between the P18-2 and P18-6 fields. Two horizontally cross-cutting faults create a "valley" between the two fields that is filled with Upper Triassic and Alتنا shales, thus providing an effective seal. Direct contact would only be through the tight Volpriehausen Fm.

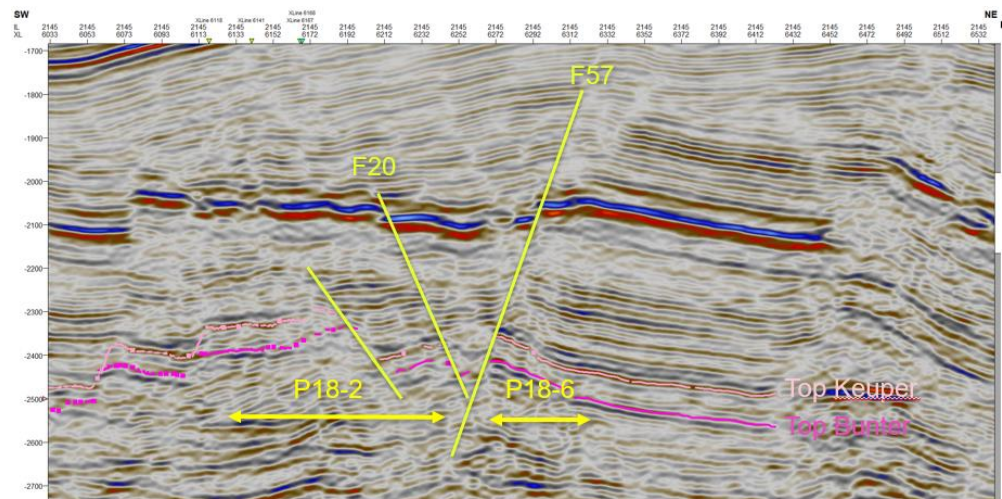


Figure 17-28: Seismic inline 2145 showing the fault configuration that separates the P18-06 accumulation from P18-02.

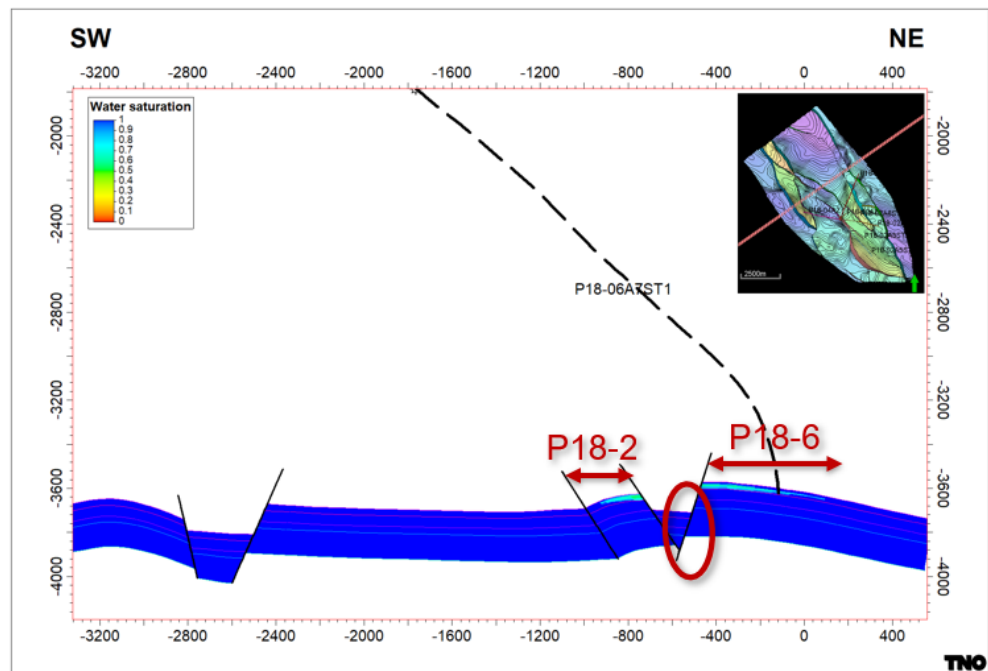


Figure 17-29: Model cross-section through P18-6 and P18-2 showing the original water saturation in the two accumulations. Note that Volpriehausen Fm in P18-6 is juxtaposed against Hardegsen and Detfurth Fm in P18-2.

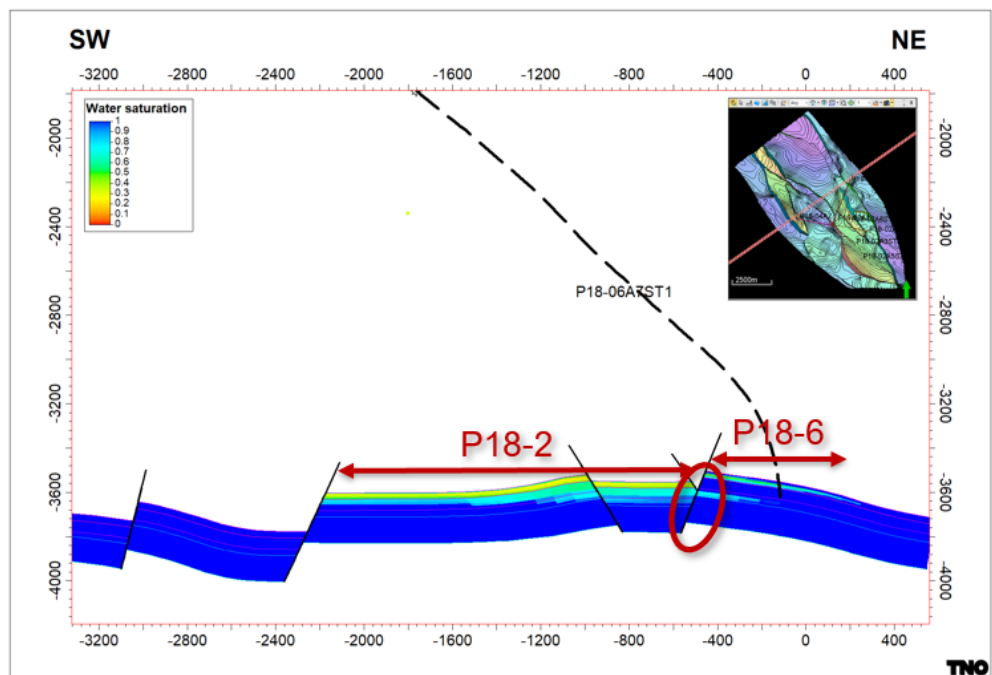


Figure 17-30: Model cross-section through P18-6 and P18-2 showing the original water saturation in the two accumulations. Note that Lower Detfurth in P18-6 is juxtaposed against Upper Detfurth in P18-2, and Hardegsen in P18-6 is juxtaposed against Upper Triassic seal in P18-2.

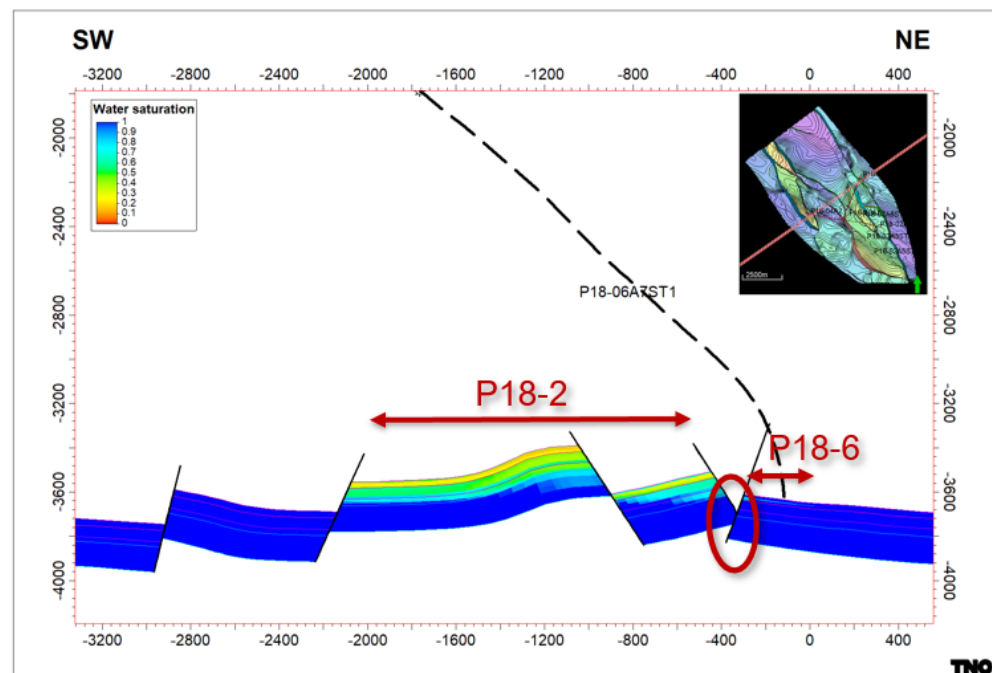


Figure 17-31: Model cross-section through P18-6 and P18-2 showing the original water saturation in the two accumulations. Bunter in P18-6 is juxtaposed against Upper Triassic seal, or Volpriehausen.

## 17.6 Adjustments made to the static model

During the history matching process and after discussions with TAQA and EBN, a modification was made in the dynamic model. A flow boundary was imposed near the GWC in Compartment 4. During the ECLIPSE simulations the question arose whether there was a possibility that Compartment 4 was not in pressure communication with the water-bearing part of Compartment 2 (indicated by “Aquifer” in Figure 17-32 ). Close inspection of the seismic in that area and the fact that the nearby well P18-06A07ST1 has very poor reservoir properties leads to the conclusion that the narrow passage around the GWC of Compartment 4 (red ellipse) is heavily faulted and forms therefore most likely a flow barrier to the down dip aquifer. This was implemented in the ECLIPSE grid.

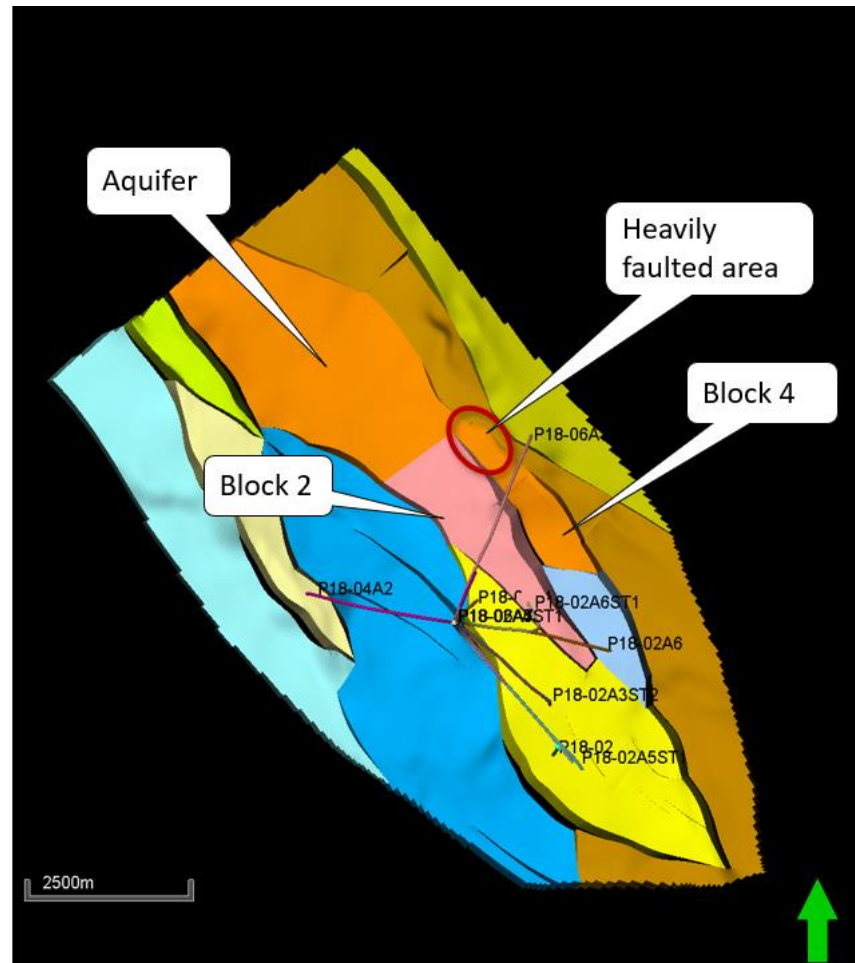


Figure 17-32: The narrow passage around the GWC of Compartment 4 (red ellipse) is heavily faulted and forms therefore most likely a flow barrier to the down dip aquifer.

## 17.7 Dynamic model

### 17.7.1 Reservoir simulator

For the dynamic modelling Eclipse 300 was used. Alternatives were to use the Eclipse 100 simulator or the Shell proprietary reservoir simulator MoReS. The compositional Eclipse simulator was used for the following reasons:

- A black oil simulator cannot handle gas to gas interactions, which is needed for CO<sub>2</sub> injection into a gas (methane) reservoir.
- MoReS was used for P18-2 and P18-4 modelling in a previous study (Vandeweyer et al (2011)). Since that study, the workflow Petrel-Eclipse-Macris has been developed and is considered to be state of the art.

### 17.7.2 Data

For any dynamic reservoir simulation, including Eclipse, the following sets of data are required:

- General run data: grid dimensions, phases present, components present.
- Grid geometry data: specification of geometry of computational grid (location of grid block corners).
- Reservoir rock properties: porosity, net-to-gross, absolute permeability in each grid block.

- PVT data: properties of reservoir and stock tank fluids such as density, viscosity and saturation pressure.
- Saturation and pressure dependent rock properties: relative permeabilities and capillary pressures as function of phase saturations, and rock compressibility.
- Initial conditions in the reservoir: pressure, temperature, phase saturations and phase compositions.
- Regions: specification of regions that splits the computational grid into regions for calculation of PVT properties, saturation properties, initial conditions, and fluids in place.
- Operations data: specification of the wells (location, productivity index, etc.) and the operations to be simulated (production and injection controls and constraints).

These data describe the dynamic characteristics of the P18 reservoir. Each of these sets of data will be discussed in the following sections

### 17.7.3 General simulation data

As mentioned in section 17.7.1 the Eclipse 300 simulator is used with two reservoir fluid phases namely water and gas, and six components namely H<sub>2</sub>O, N<sub>2</sub>, CO<sub>2</sub>, C<sub>1</sub>, C<sub>2</sub>, C<sub>3P</sub>.

The geological grid as described in Section 17.1 - 17.4 was not upscaled to the dynamic 2019 model, however directly from the logs a new dynamic grid was generated, with a cut-off of 6% of the porosity. Table 17-4 below gives an overview of the grid dimensions. The size of the grid blocks do vary in size in each individual direction but are in the order of 50x50x4m (XYZ).

Table 17-4 – Overview of grid dimensions in the geological model and in the simulation model. The '2010 model' refers to the model used in Vanderweijer et al. (2011).

	Number grid blocks x-direction NX	Number grid blocks y-direction NY	Number grid blocks z-direction NZ	Total number of grid blocks	Number active grid blocks
<b>Geological grid 2010 model</b>	51	149	38	3472820	n/a
<b>Simulation grid 2019 model</b>	63	170	17	182070	118504

### 17.7.4 Reservoir Rock properties

This is described in previous sections of Section 17.

### 17.7.5 PVT data

#### 17.7.5.1 Gas PVT data

An equation of state is generated for Eclipse 300 with the composition at 1 m depth listed in Table 17-5.

Table 17-5 – Overview of composition at 1 m depth.

	Composition
N <sub>2</sub>	0.01508
CO <sub>2</sub>	0.01288

C <sub>1</sub>	0.9411
C <sub>2</sub>	0.02376
C <sub>3P</sub>	0.0718

#### 17.7.5.2 Water PVT data

The water formation volume factor is 1.0223 m<sup>3</sup>/Sm<sup>3</sup> at a reference pressure of 215 bar. The water compressibility is 4.1483·10<sup>-5</sup>/bar and water viscosity is 0.32929 cP, also at reference pressure of 215 bar.

#### 17.7.6 Saturation and pressure dependent rock properties

Relative permeability and capillary pressure (Special Core Analysis - SCAL - data) are not available for P18 field. In this study the final parameters used to describe the individual curves are described see Table 17-6 and Figure 17-33 and was part of the history match study. Previous saturation curves used in the CATO-2 study showed the GWC was rising to fast and the water was penetrating from compartment II to compartment-I. The high water saturation basically was disconnecting the two individual compartments, which was in reality not the case. The final parameters used showed a slower movement of the GWC and therefore a improved history match

The most used description of the relative permeability curves is the Corey parametrization according to equation (17-1):

$$k_{r,i}(S_i) = k_{r,end,i} \left( \frac{(S_i - S_{irr,i})}{(1 - S_{irr,i} - S_{irr,j})} \right)^{n_i} \quad (17-1)$$

Where

- $k_{r,i}$  = relative permeability of phase  $i$
- $k_{r,end,i}$  = end-point relative permeability of phase  $i$
- $S_i$  = saturation of phase  $i$
- $S_{irr,i}$  = irreducible or connate saturation of phase  $i$
- $n_i$  = Corey exponent for phase  $i$

The values used to describe the relative permeabilities are listed in Table 17-6.

Table 17-6 – Parameters for calculation of gas-water relative permeabilities

Parameter	Description	Value used in dynamic model
$S_{wc}$	Connate water saturation	0.13
$S_{grw}$	Residual gas saturation in gas/water system	0.20
$n_w$	Corey exponent for water	3.5
$n_o$	Corey exponent for gas	1.5
$k_{rwor}$	Water end-point relative permeability	0.35
$k_{rgcw}$	Gas end-point relative permeability	1

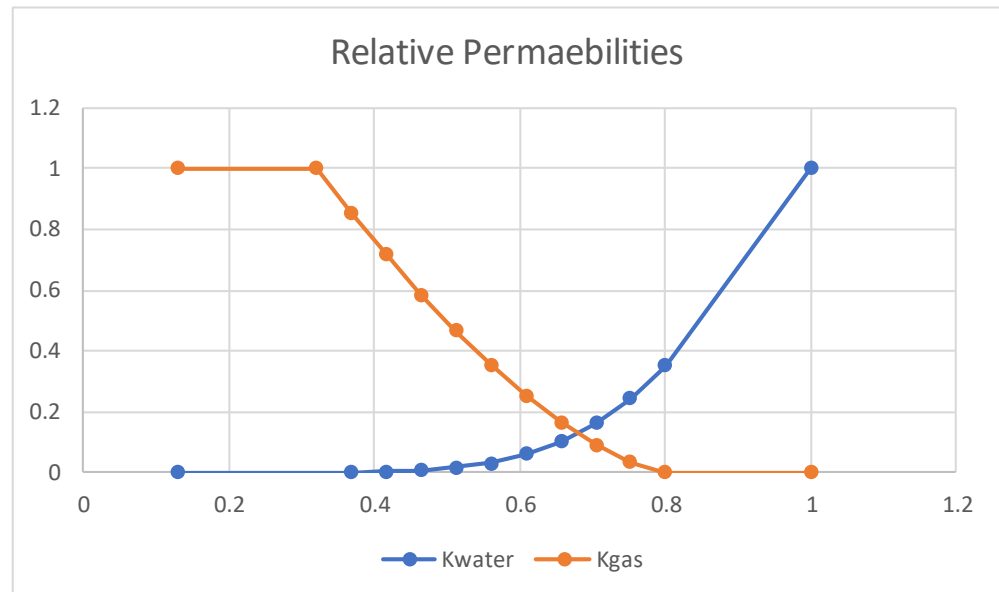


Figure 17-33: Relative permeabilities used in the P18-2 study.

The capillary pressure curves were based on a J-function corresponding to equation 17-2. The J-function itself was provided by TAQA. The reason for using the J-function rather than the saturation height functions from the static model is described in section 17.8.5. Capillary pressure is given by

$$P_c = J(s) \cdot ST \cdot \left( \frac{por}{perm} \right)^{\frac{1}{2}} \cdot U_{cons} \quad 17-2$$

Where

$P_c$  = capillary pressure

$J(s)$  = J-function (shown in Figure 17-34)

ST = surface tension (water gas) set to 76 dynes/cm (typical value for water gas system, petrowiki)

Por = porosity

Perm = permeability

$U_{cons}$  = constant depending on the unit system (Eclipse reference manual)



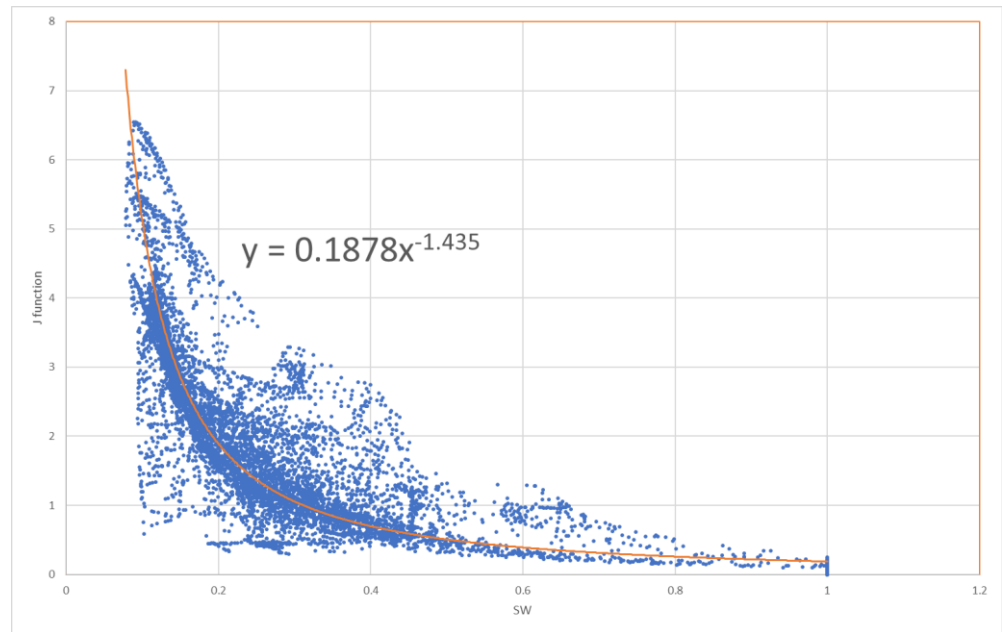


Figure 17-34: The J-function used (orange line) and the saturations of the P18 reservoir (blue dots).

After initialisation with these saturation functions the modelled water saturations were compared to the saturations based on the logs (Figure 17-35). Based on the comparison there is room for improvement, however note that the logs visualise the total water saturation and not the effective water saturation.

figure

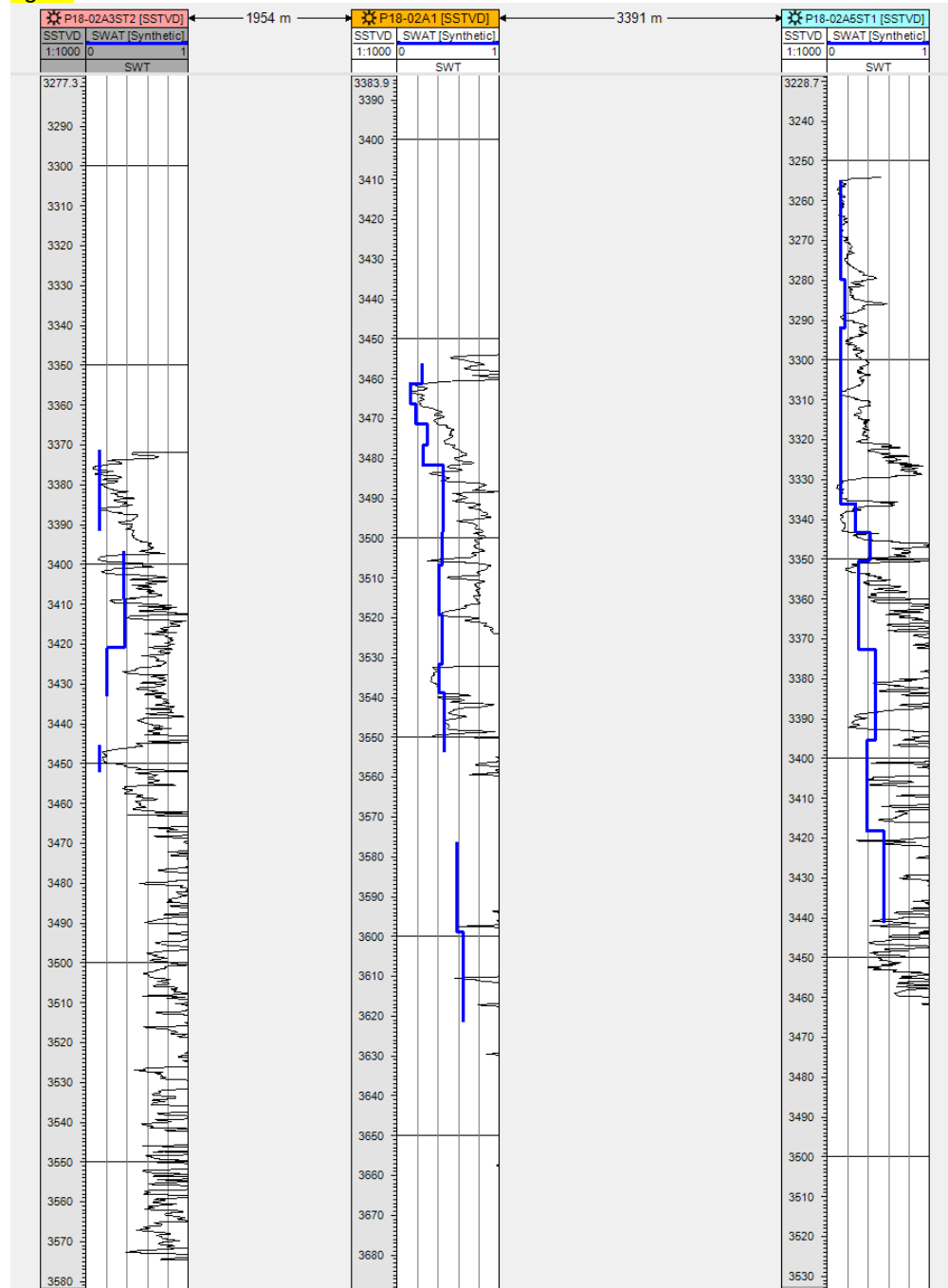


Figure 17-35: total water saturation based on logs (black) and synthetic log based on the jfunction (blue).

17.7.7 Pore compressibility

As no pore compressibility measurements are available for the P18-2 field, a correlation is used<sup>9</sup>. The compressibility is (also) dependent on the porosity according to:

$$Cr(\Phi) = 7.248 \cdot 10^{-6} / (\Phi + 0,000001) - 0.26 \cdot 10^{-5}$$

<sup>9</sup> Personal communication, NAM.

Where

$C_r$  = pore compressibility,

$\Phi$  = porosity.

### 17.7.8 Regions

In the dynamic model regions are specified based on porosity classes for rock properties described in section 17.7.6. and to split the computational grid into regions for calculation. Furthermore regions are used to evaluate the gas initial in place (GIIP) for the different compartments separated by faults or boundaries (see Figure 17-36) .

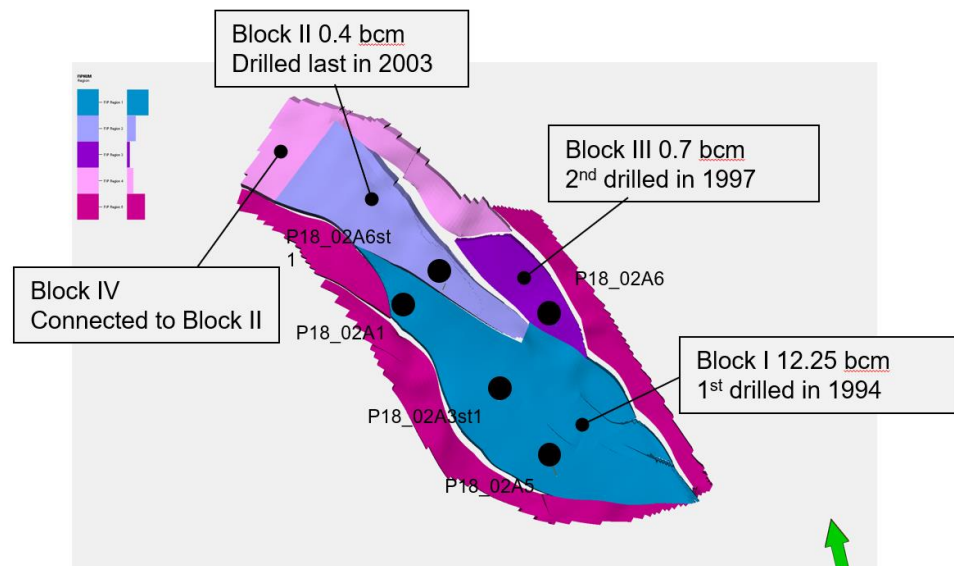


Figure 17-36: Four different regions specified to evaluate GIIP. (N.B. for Block read Compartment in this study)

### 17.7.9 Initial condition in the reservoir

The reservoir is a mechanical and thermodynamic system and hence its (initial) conditions are fully defined by the following state variables at any point in the reservoir or grid block in the simulator:

- Temperature;
- Pressure;
- phase compositions;
- phase saturations.

Initialization of these variables is discussed below.

#### 17.7.9.1 Temperature

An isothermal model is used, all temperature dependent fluid and rock properties are assume to be specified at reservoir temperature of 126 °C degrees.

#### 17.7.9.2 Pressure

The initial (gas) reservoir pressure is 375 bar at datum depth 3150 m. It is important to note that in fact each phase has its own pressure and that each phase pressure

is assumed to be in hydrostatic equilibrium. Phase pressures and phase saturations are coupled through capillary pressure between phases. The capillary pressure is based on the J-function defined in equation 17-2.

#### 17.7.9.3 Gas water Contact

The gas water contact (taken as free water level, i.e.  $P_c = 0$ ) is at 3680 m depth.

#### 17.7.10 General remarks

Petrel 2018 was used to generate an input deck for dynamic model the reservoir engineering module offers options such as specification of fluid and rock properties, specification of historic production data.

There a few manual adaptations in the input files:

- PVT data generated by Petrel are overwritten by TNO's PVT data, in other words an equation of state is used;
- Saturation functions generated by Petrel are overwritten by TNO's saturation functions;
- History match multipliers.

### 17.8 History Match of the dynamic model

#### 17.8.1 Introduction

In the previous chapter the data required to describe the reservoir have been described. In this chapter the data required to define the operations and resulting reservoir behavior will be discussed. These data are:

- Specification of wells: location, trajectory, casing data, perforation data, productivity index, etc.;
- Production and injection data:
  - Water and gas production rates;
  - Bottom hole pressures;
  - Reservoir pressures.

Next the adaption of the reservoir parameters to arrive at an acceptable history match is discussed in detail.

#### 17.8.2 Well data and production data

##### 17.8.2.1 Well Location and trajectory

For all wells well head coordinates and deviation data have been received and imported in Petrel. (see section 17.4).

##### 17.8.2.2 Well completions and perforations

Based on the received well test reports the completion perforation and skin data was gathered shown in Table 17-7.

Table 17-7 - Well test, completion and perforation data.

Well name	Completion size (inch)	Productivity index (Nm <sup>3</sup> /day)/bar	Perforations (m)	KH (mDm) from well test	Skin from well test
P18-02-A-01	4 ½	26.72	3580-3695	1847	0.6-0.9
P18-02-A-03S2	4 ½	31.89	4070-4209	-	2.1-3.3
P18-02-A-05S1	7	37.33	4798-4980	25249	3.19
P18-02-A-06	4 ½	14	4488-4633	3686	2
P18-02-A-06ST1	4 ½	22.28	3376-3936	-	-
P18-4A-02	4 ½	40.95	4085-4199	8208	-
P18-6A-07	4 ½	6.83	4975-5065	-	-

### 17.8.2.3 RFT and PLT data

For well P18-02-A-6ST1 (Figure 17-37) and for well P18-2-A-05st1(Figure 17-38) RFT are available; for the latter also PLT data (Table 17-8) was available.

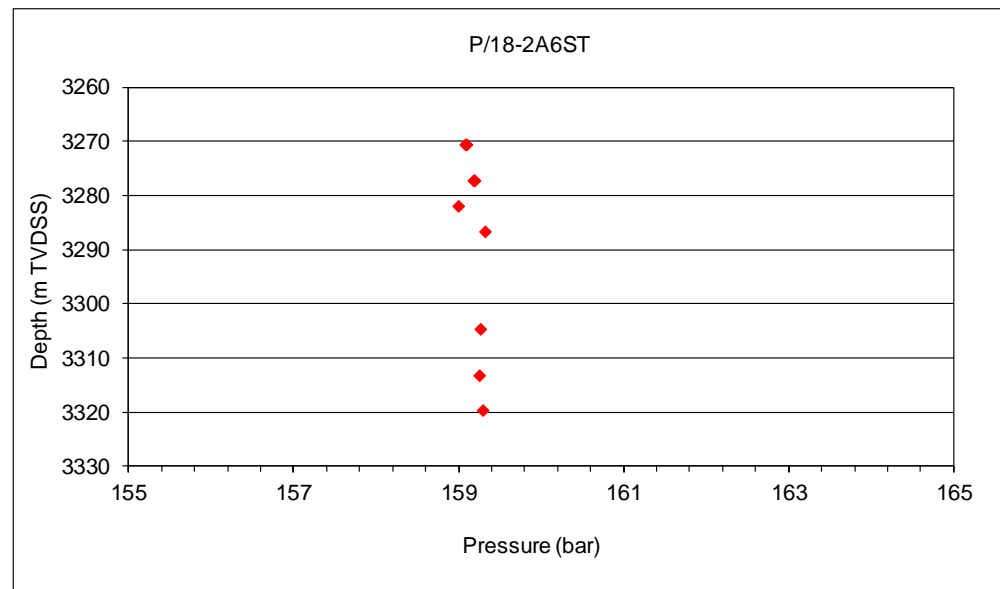


Figure 17-37: RFT data of P18-2-A-6ST1.

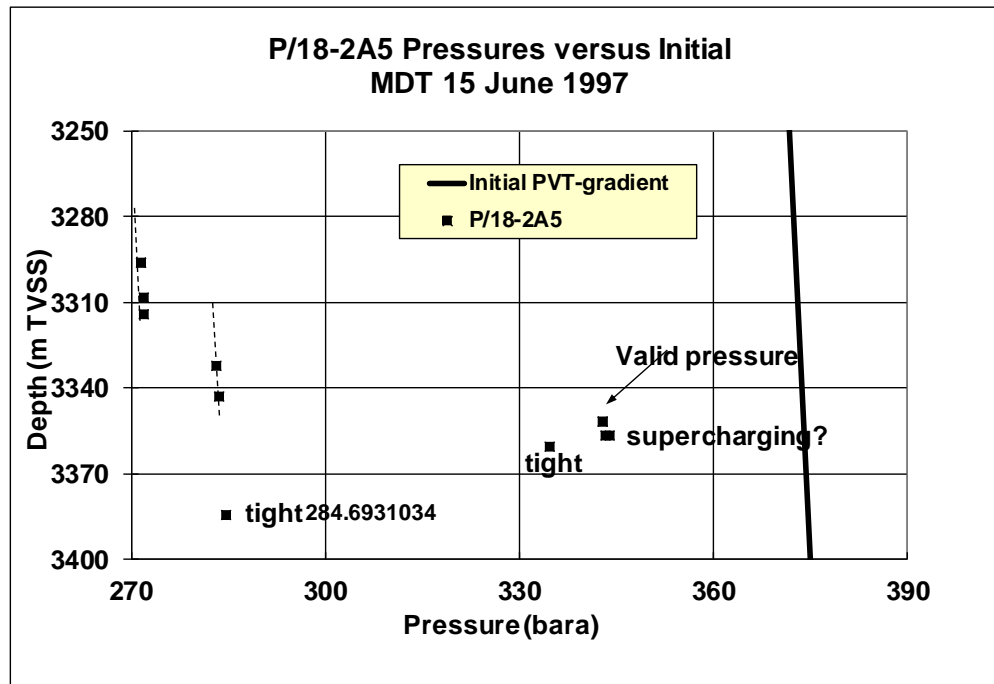


Figure 17-38: RFT data of P18-A-6ST1, note that the vales in the Volpriehausen formation (between 3350-3400 m depth) are more uncertain since the values of the measured pressure values broad range.

Table 17-8: PLT results of P18-2-A5ST1.

Formation	P18-2-A5ST1 (%)
Hardeggen	83
Detfurth Claystone	4
Lower Detfurth Sandstone	13
Volpriehausen	< 1

17.8.2.4 Historic Well Production data

Daily gas and condensate production data was provided by the operator for each individual well.

In Figure 17-39 to Figure 17-43 the daily gas production data of production wells is shown. The received data was improved and used after the following manual editing:

- Daily production data from well P18-02-A-01 and P18-02-A-03ST2 are considered unreliable in the period between 1993 and 1997 → decided to use average production rate for these wells within this particular period.
- In 2003 a sidetrack was drilled from P18-02-A-06 and all production data was assigned to the new production well P18-2-A-06ST1 only. However in 2005 the whipstock is perforated and the production data is not only from P18-02-A-06ST1 but also from P18-02-A-06, therefore crossflow is allowed in this well. From 2005 on the pressure values have to be interpreted with special care since the pressure measurement is a result of two wells drilled and perforated in different compartments in the P18-2 reservoir.

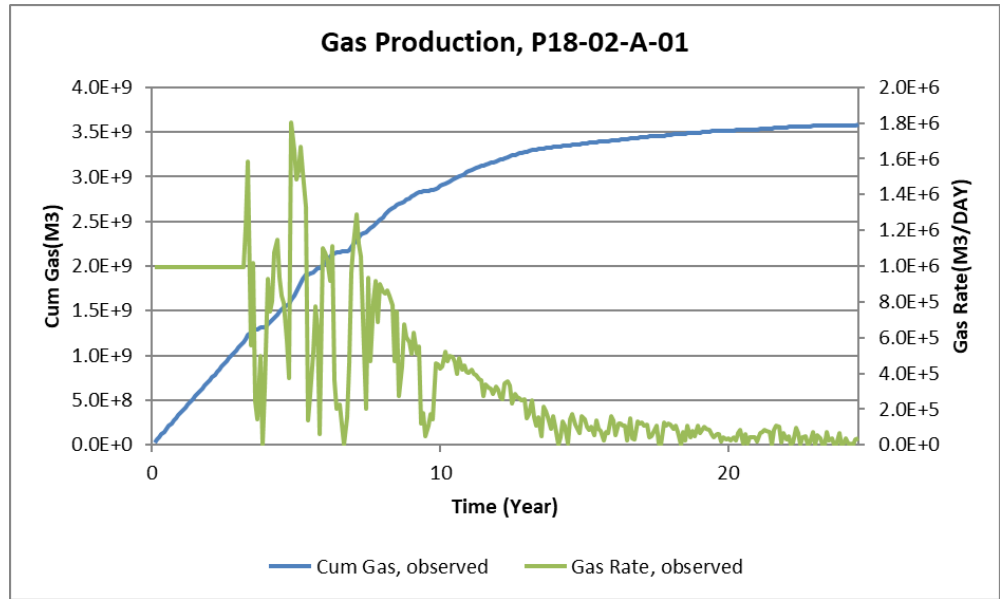


Figure 17-39: Gas production of well P18-02-A-01.

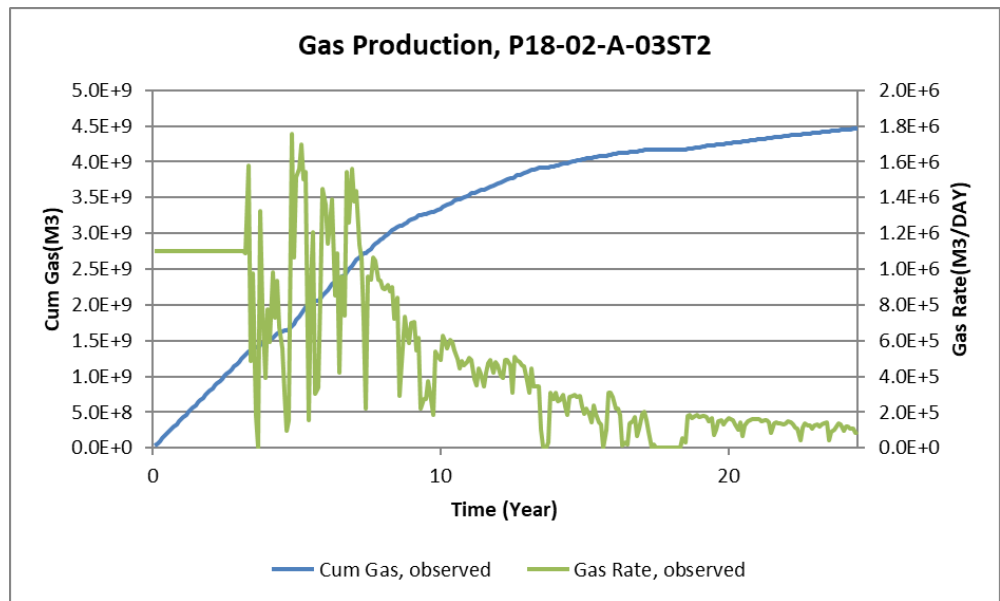


Figure 17-40: Gas production of well P18-02-A-03ST2.

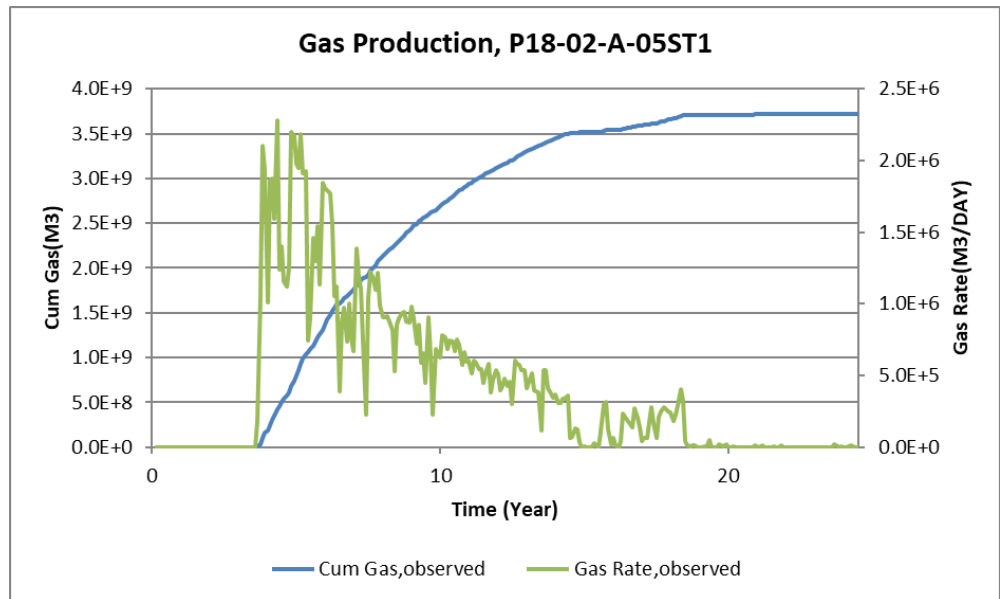


Figure 17-41: Gas production of well P18-02-A-05ST1.

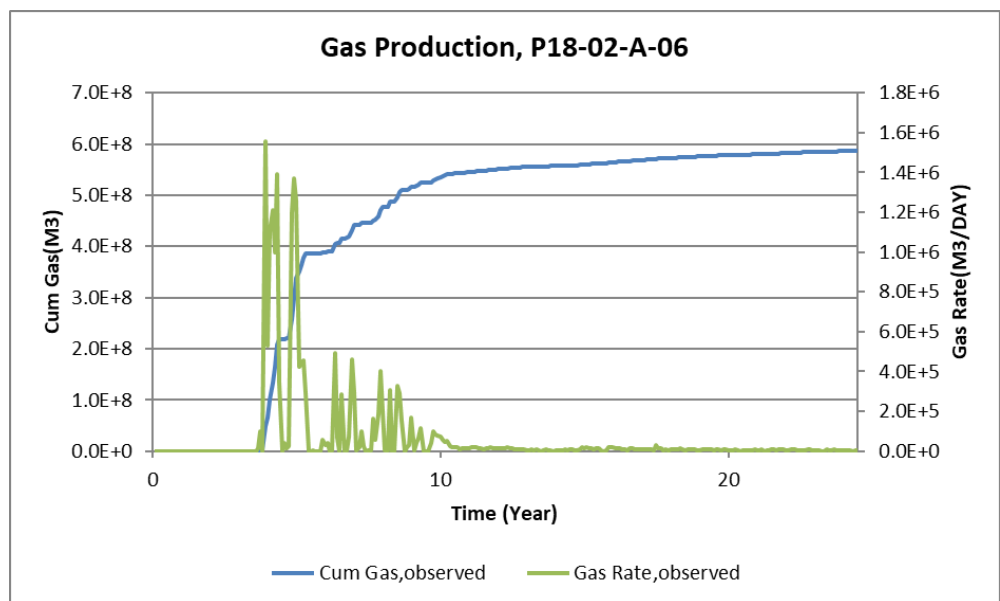


Figure 17-42: Gas production of well P18-02A6.



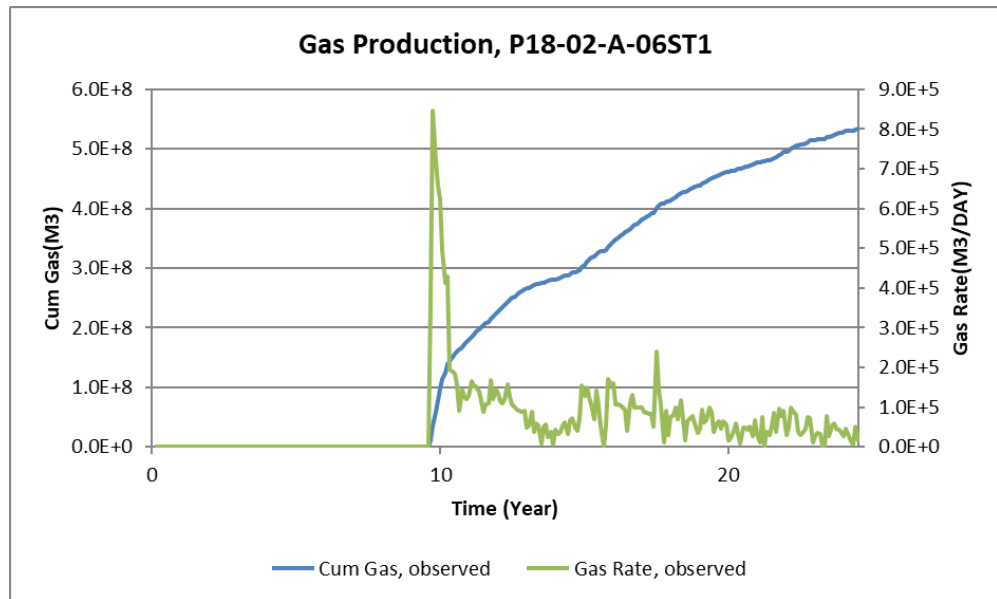


Figure 17-43: Gas production of well P18-02-A-06ST1.

17.8.2.5 Historic pressure data

Daily tubing head pressure (THP) data and on irregular basis shut in pressure data was provided. A bottom hole pressure (BHP) is generally not measured directly. Instead, the (THP) is measured and BHP is calculated from this THP and reported production or injection rates using a well bore flow model. To be able to calculate the BHP from the THP a number of parameters, including completion data and production rates, have to be accurately known by absence of Vertical Lift Performance Relationship (VLP) of each production well the opportunity to convert THP to BHP is not performed.

The measured pressure data (Figure 17-44) suggests a clear communication between compartment I, II and IV, therefore an open fault between compartment I and II is assumed. However compartment III (well P18-02-A-06) has no pressure communication to the other P18 compartments.

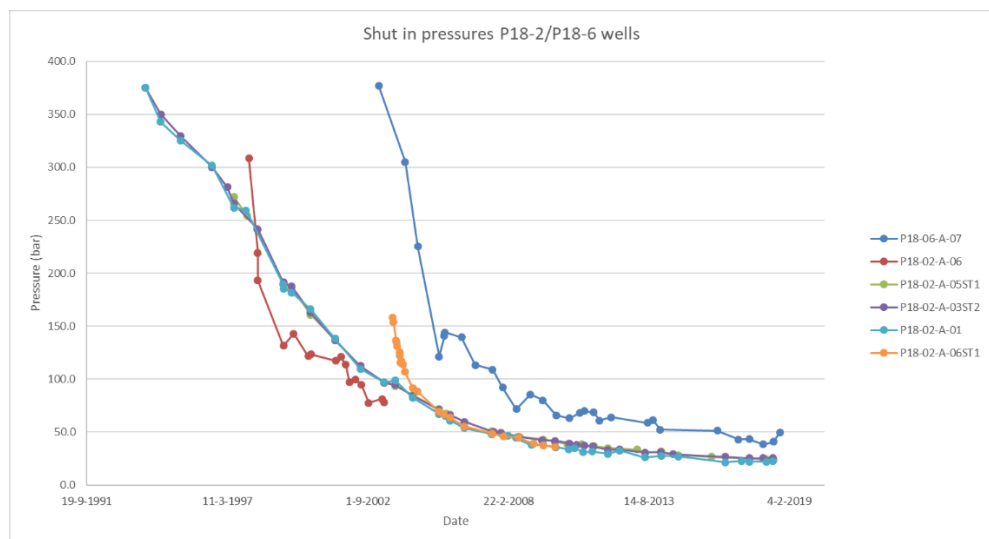


Figure 17-44: Pressure profiles of the five production wells over time.

17.8.3 *P/Z curves*

The standard method to estimate the GIP and driving mechanism (e.g. natural water drive, volumetric depletions) is material balance analysis applied on the production and pressure history. The most used method is the p/z plot shown in

Figure 17-45 and Figure 17-46, which shows a linear profile corresponding to volumetric depletion driving mechanism.

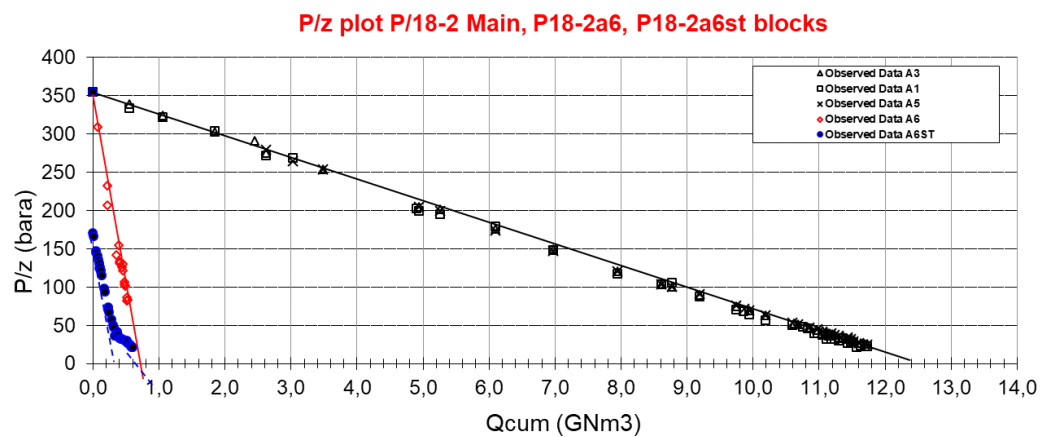


Figure 17-45: P/Z curves of P18-2 field.

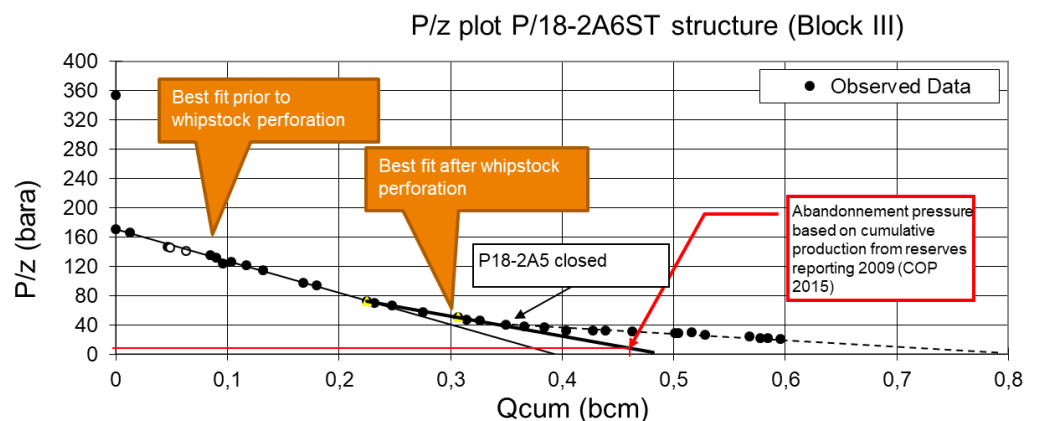


Figure 17-46: P/Z curve of P18-2 compartment, compartment III.

17.8.4 *History matching approach*

As discussed in a previous section (17.8.2.5) no BHP observations are available, therefore the measured shut-in pressures is matches with the 9-point pressure of each individual well. The history match approach is done according to the following procedure:

- The simulations was performed under rate constraint conditions
- Change the GIP of the individual compartments by a pore volume multiplier (if needed)
- Change the permeability of the dynamic model based on porosity – permeability relationship, since the well logs and well test data (KH) do not match.

- Match the measured shut-in pressures with the 9-point pressure of each individual well.

#### 17.8.4.1 History Match of GIIP

The result of the history matching the GIIP is summarized in Table 17-9. The base case is the model without any pore volume multipliers, but with the baffle and adjusted permeability to fit the well test KH as described in 0. The base case model is already close to the GIIP estimated by P/Z analysis, however to improve the pressure behaviour of the different production wells, multipliers in the main compartment (compartment I) and in compartment III are used. Especially the multiplier used in compartment III could indicate further compartmentalisation needed to match. In the HM case the following pore volume multipliers for the different compartments are used:

- Compartment I: 1.10;
- Compartment II: 1.00;
- Compartment III: 0.75;
- Compartment IV: 1.00.

For completeness all volumes for the base case and the HM case are summarised in Table 17-10.

Table 17-9: GIIP results.

	Volume in Compartment I, II and IV (GSm <sup>3</sup> )	Volume in Compartment III (GSm <sup>3</sup> )	Total Volume (GSm <sup>3</sup> )	GWC (m)
P/Z	12.65	0.7	13.35	3680
Base case	12.30	0.97	13.27	3680
HM case	13.2	0.73	13.93	3680

Table 17-10: Overview of the pore volume, Hydrocarbon volume (HC) and GIIP of the base case and History Match case of all compartments in P18-2 reservoir.

		pore volume (10 <sup>6</sup> rm <sup>3</sup> )		HC pore volume (10 <sup>6</sup> rm <sup>3</sup> )		GIIP (10 <sup>6</sup> Sm <sup>3</sup> )	
		static	dynamic	static	dynamic	static	dynamic
Base case	P18-2-compartment-I	46	46	36	37	9.1·10 <sup>3</sup>	9.1·10 <sup>3</sup>
	P18-2-compartment-II	22	22	12	12	3.0·10 <sup>3</sup>	3.0·10 <sup>3</sup>
	P18-2-compartment-III	5	5	4	4	9.0·10 <sup>2</sup>	9.7·10 <sup>2</sup>
	P18-2-compartment-IV	47	47	0	1	1.1·10 <sup>2</sup>	1.9·10 <sup>2</sup>
	Total	120	121	52	54	1.3·10 <sup>4</sup>	1.3·10 <sup>4</sup>
Hm case	P18-2-compartment-I	46	51	36	40	9.1·10 <sup>3</sup>	1.0·10 <sup>4</sup>
	P18-2-compartment-II	22	22	12	12	3.0·10 <sup>3</sup>	3.0·10 <sup>3</sup>
	P18-2-compartment-III	5	4	4	3	9.0·10 <sup>2</sup>	7.3·10 <sup>2</sup>
	P18-2-compartment-IV	47	47	0	1	1.1·10 <sup>2</sup>	1.9·10 <sup>2</sup>

	Total	120	124	52	56	1.3·10 <sup>4</sup>	1.4·10 <sup>4</sup>
--	-------	-----	-----	----	----	---------------------	---------------------

17.8.4.2 History match on pressure data

Not only the GIP is adjusted by the static model also the permeability, which are based on logs and porosity/permeability relationship. However based on the well-test higher values for the permeability are expected (see Table 17-7). Therefore porosity-permeability relationship should be re-evaluated. This porosity-permeability relationship from the BP petrophysical report is based on three rock types based on cores of the Detfurth formation alone. Therefore it is difficult to adjust the relationship for the higher porosities alone. To adjust the relationship the following strategy was used:

- A multiplier of 2 on the permeability of the entire P18-reservoir.
- Since the Hardegsen formation has higher quality than the Detfurth (see PLT) a multiplier of 4 on top of the previous multiplier is used. The permeability of the Hardegsen is probably underestimated because of upscaling process and more importantly the absence of cores from the Hardegsen itself.

Table 17-11 shows the comparison between KH (product of permeability and formation thickness) from well test data and dynamic model; Figure 17-47 shows the distribution of permeability in the P18-2 dynamic model.

Table 17-11: Comparison of model KH and the KH estimated from the well test.

Well Name	Perforations (m)	KH (mDm) based on well test	KH (mDm) in dynamic model 2019
P18-02-A-01	3580-3695	1847	1548
P18-02-A-03ST2	4070-4209	-	1572
P18-02-A-05ST1	4798-4980	25249	15696
P18-02-A-06	4488-4633	3686	3660
P18-02-A6ST1	3376-3936	-	14493

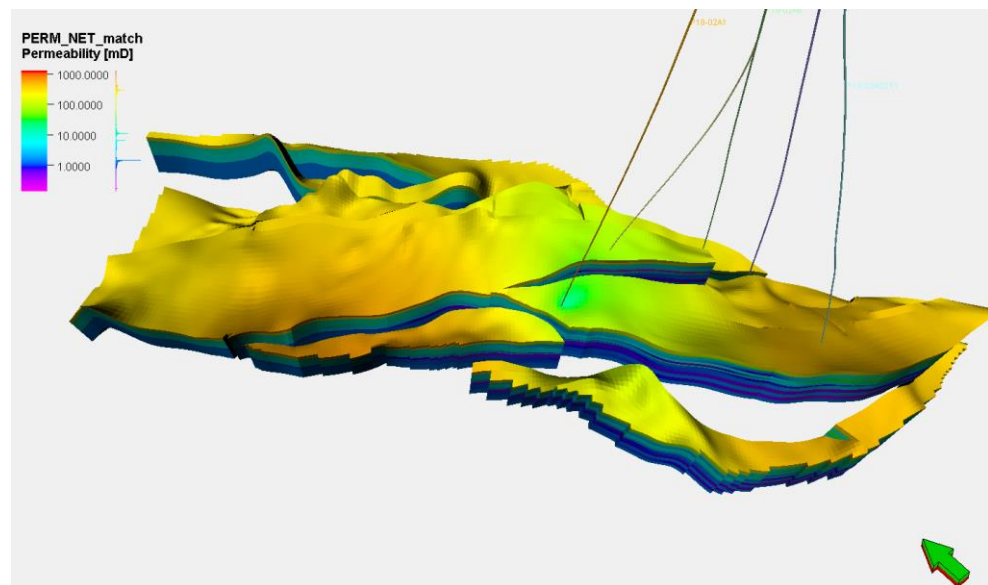


Figure 17-47: Permeability distribution in the P18-2 field.

Based on the pressure data (Figure 17-44) a clear pressure difference is observed between compartment I and compartment II, which suggest a baffle between both compartments. This baffle was modelled by a transmissibility multiplier on the fault between the two compartments with a value of 0.04.

#### 17.8.5 Result of the history match

Based on the parameters described in the previous section the following production and pressure match is achieved (Figure 17-48 through Figure 17-55). In the figures both the base case and the history matched model are presented. The base case have the same volume as the static model, but the baffle between compartment I and II is implemented). In general the match of the production and pressure of all the wells are achieved. The production rate of well P18-02-A-03ST2 is not maintained in the base case, which was the reason (together with the modelled pressures, which were too low) to increase the GIIP by 10% in compartment I.

In particular the match of well P18-02-06ST1 was problematic. From the RFT data which show that the pressure in compartment II had decreased to 159 bar (Table 17-13), it was clear that there is a baffled connection between compartments I and II. This was represented by a multiplier of 0.04. However, the connection between the compartments changes over time due to water inflow at the Hardegsen-Hardegsen juxta-position of the fault between compartments I and II. The dynamic model was mostly able to reproduce the pressure profile of well P18-02-A-06 and P18-02-06ST1 located in compartment II (see Figure 17-55). However, if water inflow is too strong and decreases the transmissibility between the compartments too fast, the pressure match deteriorates. It was found that calculation of the capillary pressure with a J-function gave a better representation of the water saturation and water inflow than the saturation-height function.

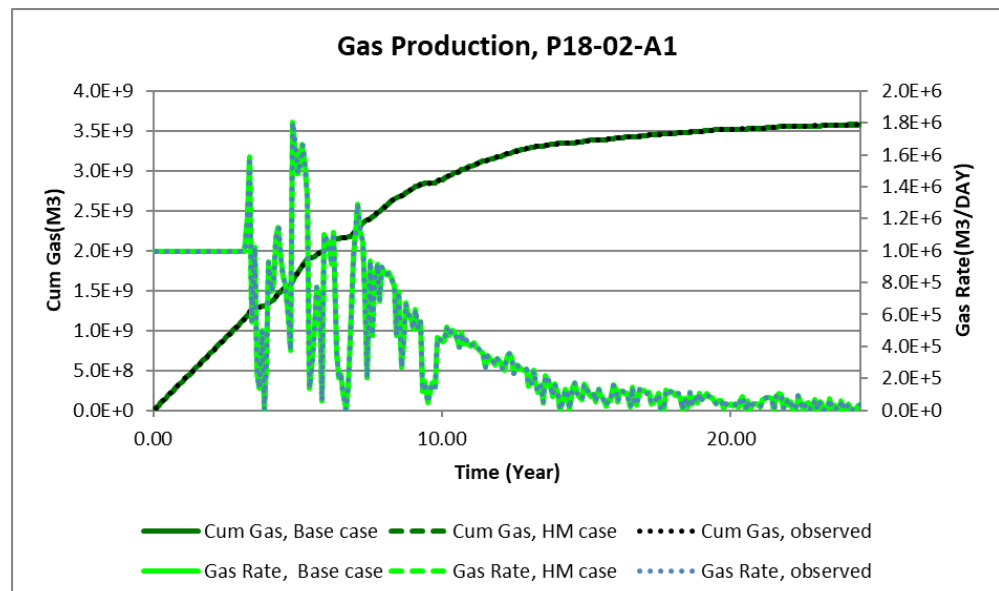


Figure 17-48: History matched production data well P18-02-A-01.

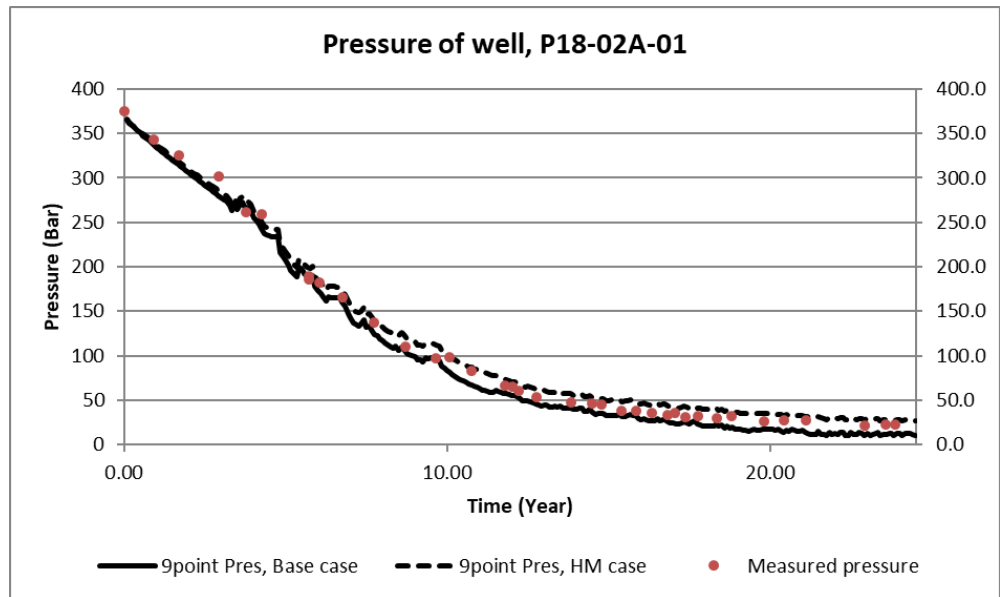


Figure 17-49: History matched pressure data well P18-02-A-01.

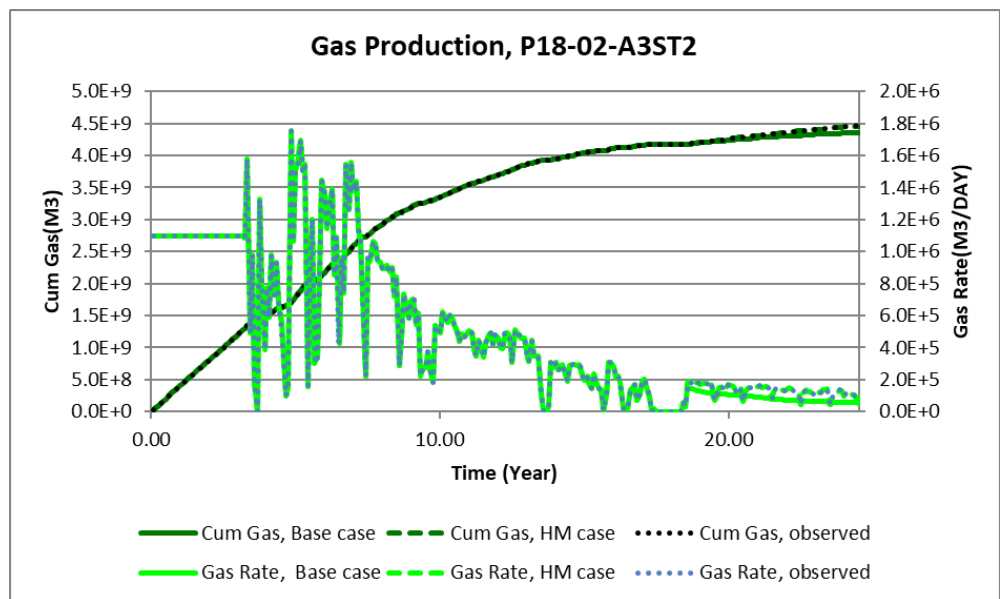


Figure 17-50: History matched production data well P18-02-A3ST2.

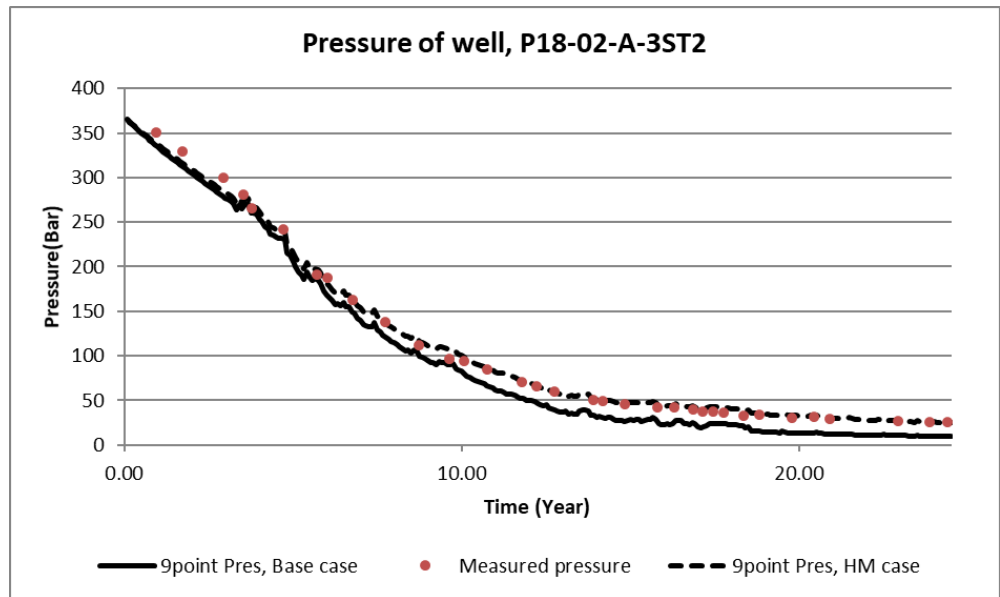


Figure 17-51: History matched pressure data well P18-02-A-03ST2.

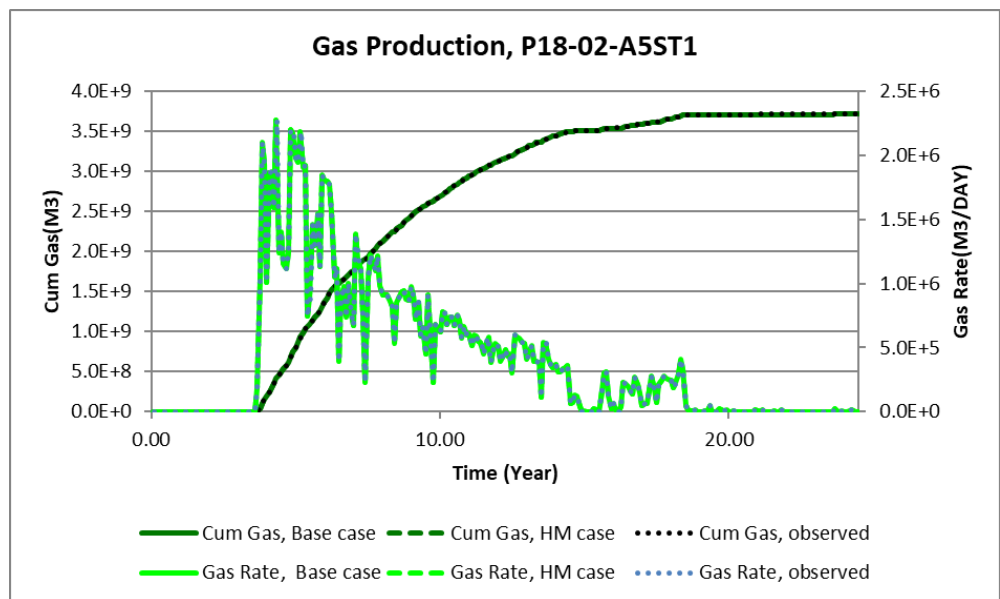


Figure 17-52: History matched production data well P18-02-A-05ST1.

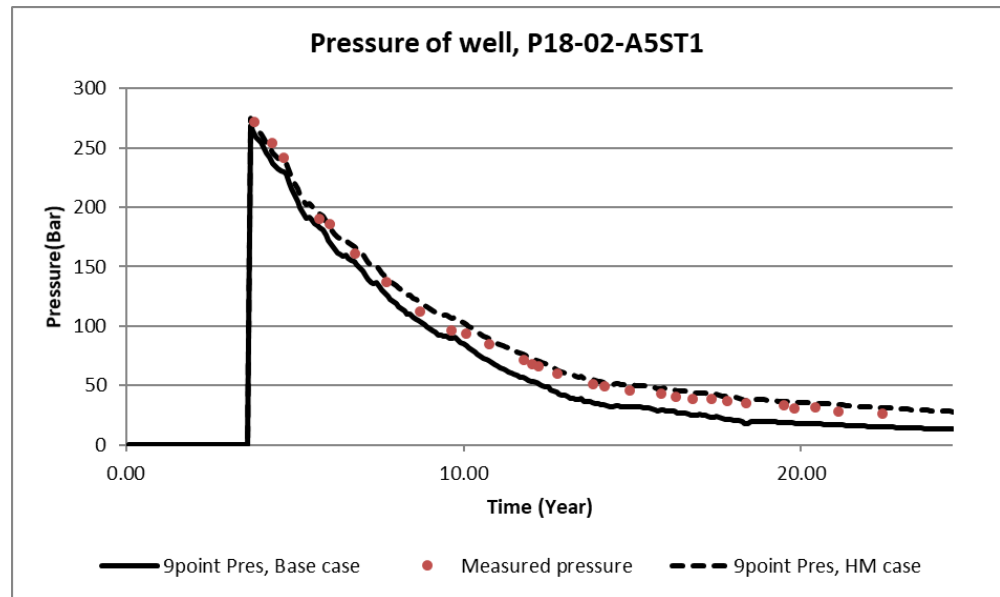


Figure 17-53: History matched pressure data well P18-02-A-05ST1.

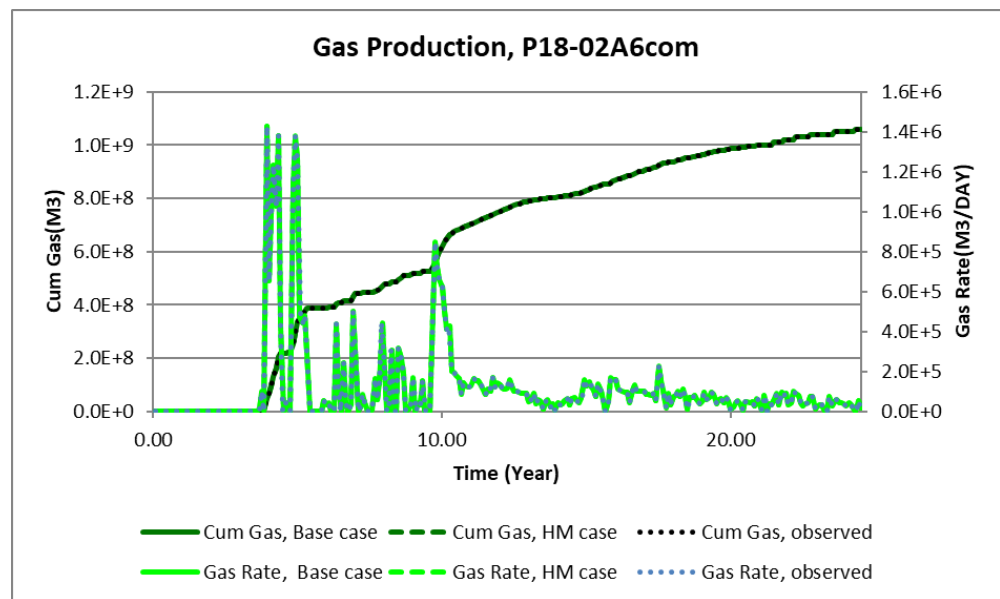


Figure 17-54: History matched production data well P18-02A6 and P18-02-A6ST1.



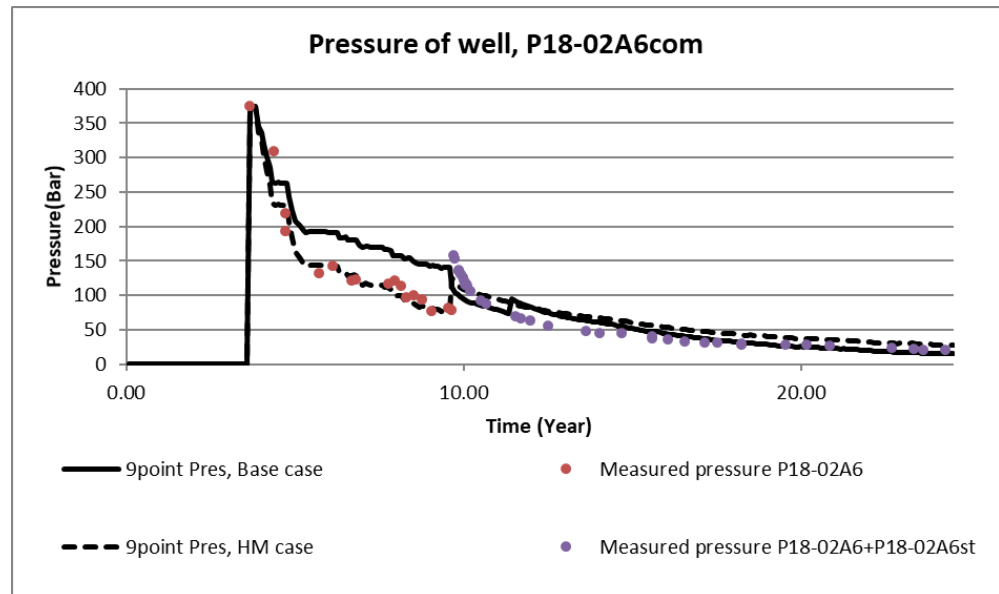


Figure 17-55: History matched pressure data for wells P18-02A6 and P18-02A6st. Note in 2003 (after 10 years the well P18-02A6 is closed and P18-02A6st is opened. In 2005 (after 12 years) the whipstock is perforated and production is from both wells at the same time. The pressure measurements from 2005 (after year 12 in the figure) and later are difficult to interpret because of simultaneous production from the two compartments.

17.8.6 History Match on RFT and PLT data

The modelled and observed RFT data from well P18-02-A5ST1 are in agreement, although it was difficult to obtain a match for P18-02-A6ST1. The reservoir model allows for crossflow between the wells P18-02-A6ST1 and P18-02-A6, but the rate of crossflow is highly uncertain. A better match was obtained with a model without crossflow.

Table 17-12: PLT results of P18-2-A5ST1.

Formation	P18-2-A5-str1 measured (%)	P18-2-A5-str1 modelled (%)
Hardegsen	83	84
Detfurth Claystone	4	13
Lower Detfurth Sandstone	13	2
Volpriehausen	< 1	1

Table 17-13: RFT data observed and modelled, for wells P18-02-A5ST1 and P18-02-A6ST1.

Formation	RFT P18-02-A5ST1		RFT P18-02-A6ST1		TNO model without crossflow (bar)
	Observed (bar)	TNO model (bar)	Observed (bar)	TNO model with crossflow (bar)	
Hardegsen		275	159	127	136
Upper Detfurth	270	276	159	127	136
Lower Detfurth	280	277	159	127	136
Volpriehausen	340*	280	159	127	136

#### 17.8.7 *History match conclusion*

- The dynamic model reproduces production rates and most of the pressure data. The start of P18-02-A-6ST1 well was more difficult to capture in this model.
- Compartment I and II are partly connected.
- Compartment III is likely to be disconnected and probably further compartmentalized.
- A pressure measurement in the well P18-02-A6ST1 should make clear whether crossflow happened. For the purpose of this study we assumed the model with crossflow, which is the basis for the injection scenarios.
- The dynamic model reproduces the pressure behaviour of the proposed injection wells, despite the unknown parameters (compressibility, saturation curves).

### 17.9 **Geomechanical model**

#### 17.9.1 *MACRIS – Poro-elastic model*

We detail here the TNO-developed semi-numerical approach (MACRIS, Mechanical Analysis of Complex Reservoirs for Induced Seismicity) to handle pressure effects along multiple faults. More specifically MACRIS is designed to compute 3D stress changes along faults induced by: (1) poro-elastic effect (contraction/inflation of the reservoir due to fluid pressure depletion/injection), (2) direct pressure effect (changes of the fluid pressure intra-faults can induce changes in effective normal stress), (3) differential compaction effect due to the fault offset.

MACRIS is a mesh-free approach where there is no need to build a dedicated grid for the geomechanical analysis. MACRIS takes directly as input the grid of the reservoir flow simulation; in our case: the 3D pressure fields of the P18-2 field at a yearly sampling rate. Each grid block of the reservoir flow simulation is considered as a compacting nucleus of strain (center of compression; Mindlin 1936; Geertsma, 1973; Okada, 1992). The contribution of each of these nuclei is integrated to compute the poro-elastic stress changes along each fault of the P18-2 field with a meter-scale spatial resolution. The restriction that we presently still have is that only one-way coupling is considered. We deem this acceptable for gas reservoirs, where the effect of compaction on the gas pressures in the pores is small. The Barnes-Hut algorithm (Barnes and Hut, 1986) is used for re-discretizing the initial reservoir grid for two purposes: (i) clustering the nuclei of strain close to the faults in order to increase the spatial stress resolution, and (ii) shortening the computation time.

MACRIS thus computes the poro-elastic normal and shear stress changes induced by the reservoir compaction for every observation point along each fault.

Observation points are placed on fault pillars (i.e. sub-vertical lines along the fault dip direction), which in turn make up the 3D geometry of a fault (see Figure 17-56).

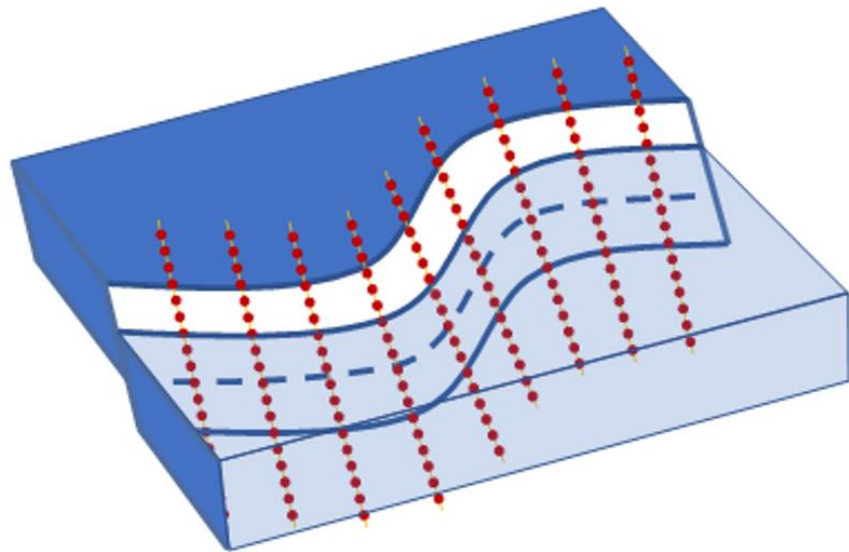


Figure 17-56: Schematic of the distribution of the observation points (where the stress solution is evaluated) along fault pillars.

In order to account for the direct pressure effect, we still need to define the pore pressure changes inside the faults to calculate the effective normal stress changes and derive the Coulomb stress changes. This intra-fault pore pressure is defined as the average fluid pressure between the two juxtaposed reservoir compartments.

MACRIS has been validated by comparison with relatively slow finite-element (FE) numerical computations (DIANA), with excellent results (van Wees et al., 2018). This benchmarking exercise has been carried on using single-fault tank models; for MACRIS it was a 3D model and for DIANA it was a 2D plane strain model. For the present study we extended this benchmarking exercise by comparing the 3D MACRIS model with this time a full 3D DIANA model. Results of this exercise are presented in Figure 17-57. The 3D single-fault model mimics the P18-2 field at the end of the depletion period, that is with an initial pressure of 330 bars and a decrease of pressure of -300bars at the end of the depletion period. The MACRIS results closely match the FE DIANA solution. Deviations between both solutions are less than 3%.

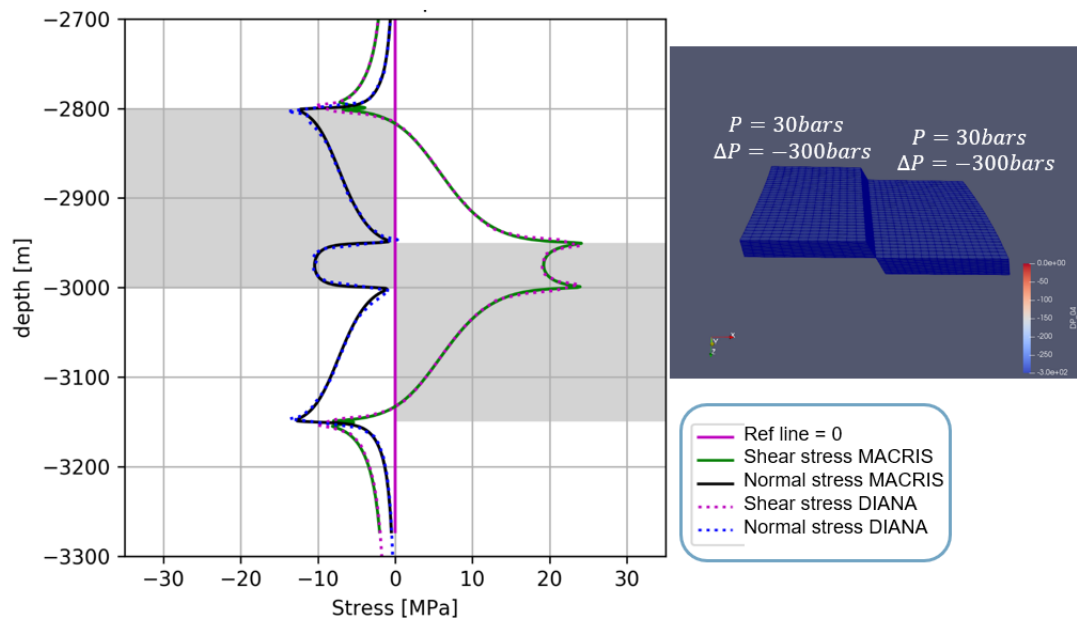


Figure 17-57: Comparison MACRIS vs. Diana FEM package. Right: 3D single-fault model with offset. Both compartments start with the same initial pressure (330 bars) and are depleted of the same amount (-300 bars). Left: Stress solution along the central pillar of the model. The changes in shear and normal stresses induced by the poro-elastic effect are almost identical between both solutions. For this particular example, the pore pressure inside the fault remains at the initial pore pressure.

### 17.9.2 Thermo-elastic model

The TNO-developed semi-analytical approach to model thermo-elastic stresses due changes in temperature of reservoir rock is based on Myklestad (1942). Myklestad (1942) derived equations for all the components of the stress tensor as induced by heating a semi-infinite cylinder to a constant temperature difference with respect to the ambient reservoir temperature using elliptical integrals in a cylindrical coordinate system. Candela et al. (2018) contains all the details of the derivation.

This approach gives us the tensor of stress changes inside and outside the reservoir in the cylindrical coordinate system. This tensor of stress changes thus needs to be translated to Cartesian coordinates using standard cylindrical coordinate transformation. The initial stress state is then added to the tensor of stress changes to obtain the stress tensor in Cartesian coordinates (see Figure Figure 17-58 and Figure 17-59).

We consider faults uniformly distributed in our model. In other words, each location inside and outside the reservoir (in the caprock) can potentially host a fault. More specifically, from the stress tensor, at each location, one can calculate the Coulomb stress changes for any fault plane orientations.

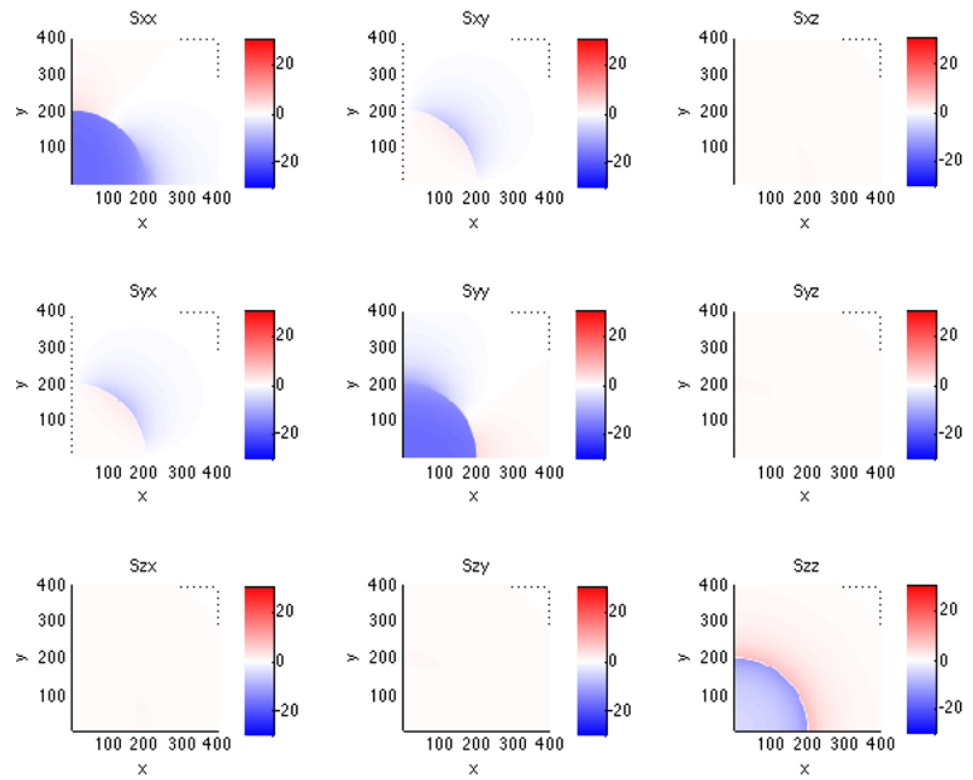


Figure 17-58: Horizontal [XY] spatial distribution of each component of the tensor of stress changes.

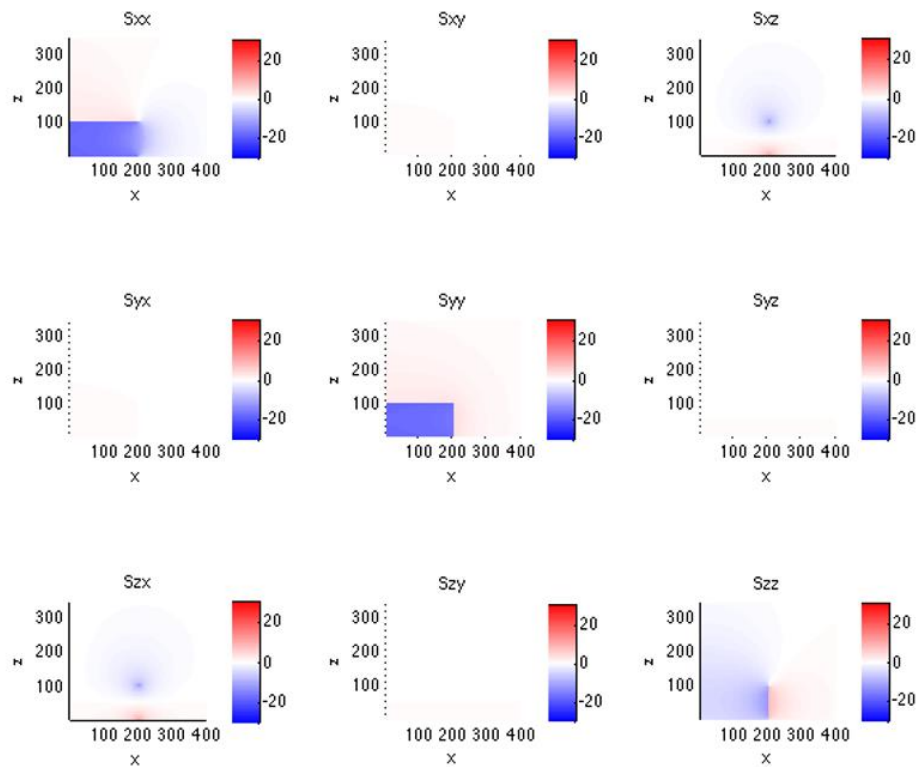


Figure 17-59: Vertical [XZ] spatial distribution of each component of the tensor of stress changes.

### 17.10 Well degradation model

The nonlinear finite element simulator DIANA<sup>10</sup> is used to generate meshes for 2D numerical models of the well system and run structural and heat transfer simulations. The workflow is automated by a dedicated user interface DIANA SEALEC: the user-defined input and model parameters are used to generate meshes and define the complete non-linear (phased, staggered) analysis, which mimics the different loads acting on the well system throughout the entire lifetime of a well, from the drilling phase, well completion, testing, operations and abandonment (Figure 17-60).

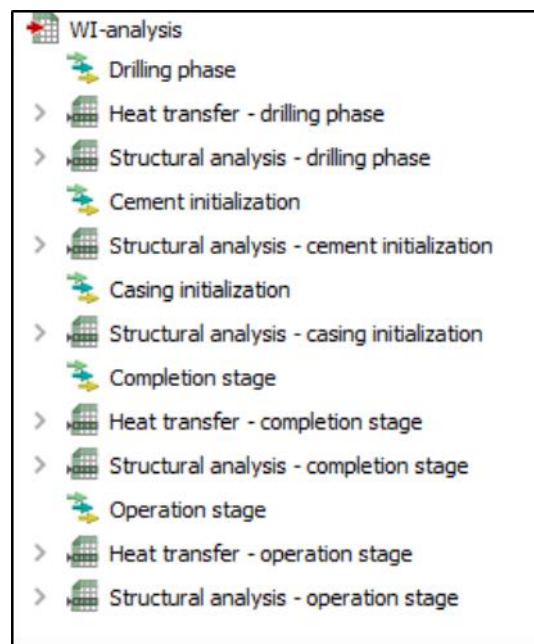


Figure 17-60: Example of steps in the wellbore integrity analysis.

The model of the well system, representing a cross-section normal to the well axis, comprises the casing, the cement and the surrounding rock formation. The chosen 2D modelling approach is computationally efficient and simulations can easily be repeated for various depths along the wellbore. Complete plane strain elements are used for bulk materials. Zero-thickness interface elements are used for the casing-cement and the cement-formation interfaces. The well materials can be modelled with different constitutive models; for example a von Mises elasto-plastic material model for the steel casing; a combination of the Mohr-Coulomb elasto-plastic model and the multi-directional fixed crack model for the cement; a Mohr-Coulomb elasto-plastic model for the rock formation; and the Coulomb friction model with a tension cut-off for the interfaces between materials. Different failure modes can be simulated, for example: plastic deformation of casing, plastic deformation and cracking of the cement sheath, plastic deformation of formation and debonding of cement interfaces (Figure 17-61). Specific deformational behaviour of materials can be modelled such as shrinkage of cement and the creep behaviour of viscous rock salt formation.

<sup>10</sup> See [dianafea.com](http://dianafea.com).

Structural, heat transfer and fluid flow analyses are typically needed for wellbore integrity assessment. Results from finite element analyses are typically displacements, stresses and strains in different formulations.

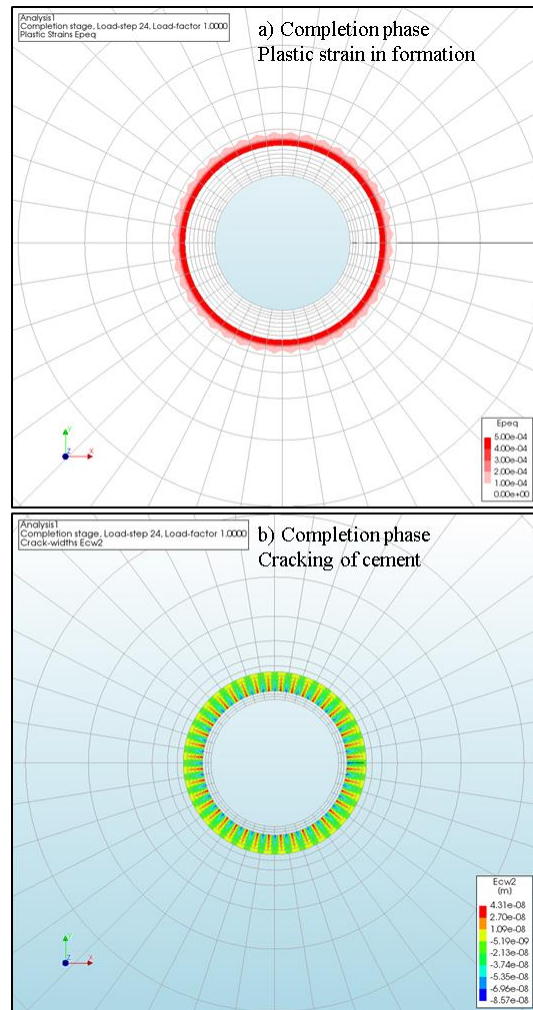


Figure 17-61: (a) Plastic strain in the formation and (b) cracking of annular cement in the completion phase.

# 18 Appendix C. Risk Register

## Caprock

Identified risk	Description	Positive evidence for integrity	Risk reduction measures	Risk characterisation	Risk classification
Initial condition	Impermeable shales of the Upper Triassic and Altona Groups overlie the P18-02 reservoir, which represent a good seal for the natural gas reservoir.	Effective seal as evidenced by the presence of gas in reservoir below the seal; 50 m of primary caprock and 100s of metres of secondary caprock; gas column of 581 m	Reservoir pressure after CO2 injection equal to or lower than initial gas reservoir pressure	As the evidence for the initial sealing of the gas reservoir is very strong, it is a good seal for CO2 storage as well and consequently the risk of migration out of the reservoir is low to even negligible when the pressure is kept at or below the initial reservoir pressure.	A-1
Fracturing	Fractures in the seal may be caused by local stress variations due to initial gas production, subsequent CO2 injection and associated pressure and temperature changes. Fractures represent a potential conduit for CO2 loaded fluids depending on their connectivity and continuity (see also Fault zone)	Semi-analytic modelling has shown that Coulomb stresses as a consequence of pressure build-up due to injection quickly decay on top of the reservoir inside the caprock. The pressure effect is thus not expected to contribute to the risk of fault reactivation in the caprock. New fractures or faults will not be generated as they would require even higher Coulomb stresses. This is confirmed by earlier mechanical analysis of seal and fault based on P18-2; no critical factors identified (Vandeweyer et al., 2011: ch6, par 6.7, p108). Although temperature-induced positive Coulomb stresses occur in the caprock near the edges of the cooling front, they are not sufficiently large to re-activate faults in the caprock nor will they result in new fractures in the caprock. The likelihood of re-activating a pre-existing fault in the caprock is thus very low. A similar conclusion was drawn for P18-4 at a depth 3190 m (Peters et al., 2014).	Keep the pressure below fracturing condition and appropriate management of thermal effects	If fracturing due to pressure increase and/or temperature drop will occur, this will only result in local effects if any. Considering the huge thickness of the caprock, the likelihood of fracturing the complete caprock is nil and consequently the risk is low (to even negligible).	A-1
Chemical degradation	CO2 if dissolved may react with minerals in the caprock near the interface with the CO2 reservoir.	Since the caprock has proven to be a seal for gas, the only way of upward migration is by diffusion of dissolved CO2, which is a very slow process. Chemical interaction between dissolved CO2 and caprock minerals is very slow and has minor effects on porosity and permeability. Hence, no migration path is expected to form. The affected zone of migration of dissolved CO2 and chemical interaction is in the order of several meters in thousands of years (Gaus et al., 2004; Tambach et al., 2012).	Reservoir pressure after CO2 injection at or lower than initial gas reservoir pressure, to prevent CO2 from entering the caprock in gaseous/supercritical state thereby enhancing geochemical reactions.	Chemical degradation will only marginally influence the sealing properties of the caprock and thus will the overall integrity of the caprock stay intact. The likelihood of degrading the caprock is very low and its consequence will be nil or negligible.	A-1



**Fault zone**

Identified risk	Description	Positive evidence for integrity	Risk reduction measures	Risk characterisation	Risk classification
Initial condition	Sealing capacity of reservoir boundary faults determined by juxtaposed claystone and reservoir rocks (Vandeweyer et al., 2011: par3.5.1, p20 and Fig. 3:8 on p23)	Bounding faults F19/F20 and F40 are effective seals as evidenced by presence of juxtaposed gas reservoirs and sealing rock. In two cases reservoir rocks can be juxtaposed over a very small section on both sides of faults but in these cases reservoir rock with very low permeability (< 1mD) is present on one or both sides of the fault (see also discussion on communication between P18-2 and P18-6 for the reservoir compartment).	Manage pressure gradient across fault	As reservoir rocks next to bounding faults are sealed off by very low permeable rocks on the other side of the fault zone, it has a very low likelihood that a negligible amount of CO2 will migrate across or along the fault and sealing rock.	A-1
Chemical degradation	Chemical degradation of material in fault zone	Currently, there is no evidence for gas migration from the P18-02 reservoir along the faults to overlying formations. In general, the geochemical reactions between CO2, formation water and fault gouge mineralogy will result in precipitation of carbonate minerals. On the longer term, silicate minerals might react, providing additional cations for carbonate precipitation. Porosity and hence permeability effects are predicted to be negligible. Increase of carbonate content in the fault gouge is known to increase the friction coefficient and to decrease potential for fault re-activation.		Chemical degradation leads to lowering of the porosity and permeability of the fault gouge and increases the friction coefficient of faults. Therefore it is highly unlikely that chemical degradation in itself leads to the migration of CO2 across the fault zone.	A-1
Pressure re-activation	Due to pressure changes during production and/or injection faults may be re-activated (Vandeweyer et al., 2011: par 6.7, p109) and potentially act as conduits for CO2.	No seismic activity was encountered during production, based on the KNMI database (Vandeweyer et al., 2011) Semi-analytic modelling has shown that at the end of the injection period most (if not all) of the areas where positive Coulomb stresses which are present at the end of depletion, have disappeared. The faults are thus expected to be stable at the end of the injection period.	Injection of CO2 is a mitigation measure in itself as it reduces the underpressure in the reservoir and consequently the risk of fault re-activation.	Based on the results from the semi-analytic modelling it appears to be highly unlikely that faults will be re-activated due to the increased pressure by CO2 injection and consequently will not lead to migration of CO2 along the fault.	A-1
Thermal re-activation	Cold injection stream could re-activate a nearby fault and change its fluid transport properties.	TOUGH2 simulations have shown that the cooling front could extend to 300 m from the injector after 15 years of injection. Semi-analytic modelling indicates that the Coulomb stresses rapidly decay to around 2.5 MPa at a distance of 100 m from the cooling front. Thus injection wells at less than 300 to 400 m from a fault may thermomechanically influence its stability.	Managing the advancement of the cold front near faults by adjusting the injection rates of wells which are within a distance of 300 to 400 m from a major fault. More detailed thermomechanical assessment may reduce the uncertainty in the consequence of cooling for fault re-activation.	With inclusion of proper management of the injection rates in wells nearby faults the likelihood of thermomechanical fault re-activation leading to the migration of a very small amount of CO2 out of the reservoir will be low.	B-2

Cont. improvement
ALARP
Intolerable

**Reservoir**

Identified risk	Description	Positive evidence for integrity	Risk reduction measures	Risk characterisation	Risk classification
Spilling NW of compartment II	Overfilling could lead to lateral migration (spilling) of CO2 to neighbouring Buntsandstein aquifers and gas reservoirs. Subsequently, CO2 may migrate to Lower Cretaceous or Lower Tertiary aquifers in case the wells are not well isolated. A potential spill zone is identified at the NW edge of compartment II of the reservoir near Fault 1.	The final pressure state of the reservoir will be at or below the initial pressure. A simulation scenario with strong overpressurization during injection does not show spilling.	Spilling prevented by keeping the reservoir pressure at or below the initial pressure and limiting the total mass of injected CO2. Proper zonal isolation of wells and preventing re-activation of faults to avoid vertical migration (see also Fault compartment)	Keeping the average reservoir pressure at or below the initial pressure at the end of injection and the robustness of flow simulations indicate a very low likelihood that a negligible amount of CO2 migrates out of the reservoir.	A-1
Spilling NW of compartment I	Overfilling could lead to lateral migration (spilling) of CO2 to neighbouring Buntsandstein gas reservoirs and aquifers. Subsequently, CO2 may migrate to Lower Cretaceous or Lower Tertiary aquifers via non isolated wells or permeable faults if any. A second small potential spill zone is identified at the NW edge of compartment I (across fault F14) of the reservoir. Low permeable sandstones of the Volpriehausen Formation (< 1 MD) and permeable sandstones of the Hardegsen Formation are juxtaposed across fault F14.	The final pressure state of the reservoir will be at or below the initial reservoir pressure. The potential spill point is very likely not leading to migration of CO2 out of the reservoir as the very low permeable Volpriehausen (< 1 MD) and Hardegsen are juxtaposed hampering the flow of CO2.	Spilling prevented by keeping the reservoir pressure at or below the initial pressure and limit the total mass of injected CO2. Proper zonal isolation of wells and preventing re-activation of faults to avoid vertical migration (see also Fault zone compartment)	The very low permeability of the Volpriehausen Sandstone on the other side of Fault 14 prevents lateral migration of CO2 out of the P18-2 reservoir. This implies that there is a very low likelihood that a small amount of CO2 migrates out of the reservoir.	A-3
Flow between P18-2 and P18-6 reservoirs	Over a small section across the fault zone between the P18-2 and P18-6 reservoirs, reservoir rocks of the Volpriehausen Sandstone are juxtaposed, which may lead to migration of CO2 from P18-2 to P18-6.	As the permeability of the Volpriehausen Sandstone is very low, the migration and pressure equilibration will be very slow. An assessment of the fault zone indicates that there is a very high probability of an impermeable gouge being present in the fault zone (Nieuwland, 2011). The pressure in P18-6 was at 378 bar before starting injection whereas at the same time pressure has dropped to about 100 bar in the producing P18-2 reservoir (June 2003). Apparently, this enormous pressure difference could exist indicating that there is virtually no flow and pressure equilibration between the two reservoirs on production time scales. Geological information indicates that compartment 2-IV, which is directly adjacent to the P18-6 reservoir is a separate hydraulic unit.		The pressure difference of about 278 bar between the two reservoirs, the very low permeability of the Volpriehausen Sandstone and the hydraulic isolation of compartment 2-IV show that the likelihood of a negligible amount of CO2 migrating from P18-2 to P18-6 is very low.	A-1

Low: Cont. improvement
Medium: ALARP
High: Intolerable

**Wells**

Well	Evaluation of integrity	Risk characterisation (before application of measures)	Risk classification (before application of measures)	Risk reduction measures	Risk characterisation (after application of measures)	Risk classification (after application of measures)
P18-02	P18-02 well is suspended and left with a mud line suspension in place to allow potential re-entry. The well is plugged at various depths with a total of 4 plugs. Several barrier elements for this suspended well could not be validated.	A medium likelihood that deficiencies in the cement bond and the quality of the plug will lead to migration out of the reservoir and partly out of the storage complex	C-3	Re-assessment of the cement and plug and restore the P&A plug integrity for CO2 storage conditions if needed	Re-assessment and adequate restoration of the plug integrity will prevent leakage of CO2. The likelihood is low that a negligible amount of CO2 will migrate out of the reservoir.	B-1
P18-2A-01	Information from available cement bond logs suggests poor casing-cement bond across part of 7" liner; production packer is set across a zone with poor bonding.	Low likelihood that CO2 migrates along the well and partly ends up outside the storage complex.	B-3	Replace packer in casing or liner section with good cement bond. After definite cessation of injection the well will be plugged according to existing p&a standards.	With the implementation of the proposed workover activities leakage from the well will be prevented. The likelihood is low that a negligible amount of CO2 will migrate out of the reservoir.	B-1
P18-2A-03/-S1/-S2	All primary and secondary barrier elements have been validated and thus pose no significant risk for CO2 leaking out of the well. Mother borehole and S1 do not end in reservoir and thus do not pose a problem for CO2 migration from the reservoir.	Low likelihood that CO2 migrates along the well and partly ends up outside the storage complex.	B-3	After definite cessation of injection the well will be plugged according to existing p&a standards.	With the implementation of the proposed workover activities leakage from the well will be prevented. The likelihood is low that a negligible amount of CO2 will migrate out of the reservoir.	B-1
P18-2A-05/-S1	The mother bore was drilled to about 200 m TVD above the reservoir. Then the well was side tracked. As the mother borehole does not end in reservoir, this does not increase the likelihood of CO2 migration out of the reservoir. Sustained casing pressure was measured in production casing.	Medium likelihood that a small amount of CO2 migrates along the well and ends up outside the storage complex	C-3	Investigate and if required repair source of sustained pressure in production casing. After definite cessation of injection the well will be plugged according to existing p&a standards.	With the implementation of the proposed risk reduction measures leakage from the well will be prevented. The likelihood is low that a negligible amount of CO2 will migrate out of the reservoir.	B-1
P18-2A-06/-S1	The producing reservoir formations from the side track and the mother bore connect at the side track window, which is not isolated.	Medium likelihood that a small amount of CO2 migrates along the well and ends up outside the storage complex	C-3	The integrity of the well barriers in the mother bore and the sidetrack window has to be restored. Most likely to be done by plug and abandonment (P&A) of the side track and installing a cemented scab or tie back liner to restore the mother bore integrity. After definite cessation of injection the well will be plugged according to existing p&a standards.	With the implementation of the proposed workover activities leakage from the well will be prevented. The likelihood is low that a negligible amount of CO2 will migrate out of the reservoir.	B-1
All anticipated injector wells: cooling	Injection of cold CO2 leads to the creation of a micro-annulus well at the casing-cement interface which may be enhanced by chemical interaction with CO2.	A medium likelihood exists that a small amount of CO2 migrates along the micro-annulus and partly ends up outside the storage complex.	C-3	Keeping the max average reservoir pressure below the hydrostatic pressure. Monitoring during operations and appropriate plugging after ceasing injection.	Low likelihood remains that a negligible amount of CO2 migrates out of the reservoir	B-1
All anticipated injector wells: status of casing in conductor	Condition of outer casing inside conductor may be reduced due to external corrosion and fatigue due to me to seismic movement. This may jeopardize the integrity of the primary and secondary well barriers.	A medium likelihood exists that a small amount of CO2 migrates along the micro-annulus and partly ends up outside the storage complex.	C-3	External surface casing corrosion log to confirm remaining load capacity of surface casing for CO2 injection load case and if necessary perform necessary workover activities	After the corrosion logging and optional workover activities leakage from the well will be prevented. The likelihood is low that a negligible amount of CO2 will migrate out of the reservoir.	B-1

Low: Cont. improvement
Medium: ALARP
High: Intolerable

# 19 Appendix D. Monitoring Plan

Table 19-1

No.	Parameter to be Monitored*	Proposed Technique adopted	Category of monitoring	Project phase and frequency	Location	Normal situation	Alert value	Contingency value
			Contingency Required (preliminary estimation) EU directive Mandatory according to	Pre-inj inj Post-inj Post-inj (abandonment) Long-term stewardship		Expectation value Accuracy	> Threshold 1 Action**	> Threshold 2 Contingency measures***
	<b>Injection proces</b>							
1	Injection rate	Flow meter	x	Cont	Near well head or Compressor station	Max rate = 285 ton CO2/uur (80 kg/s or 2.5 Mton CO2/year) and no fluctuations at constant pressure, expected value t.b.d.	Fluctuations at constant pressure or value above max. rate	Fluctuations at constant pressure or value above max. safety margins Find cause, solve problem and if necessary reduce injection until flow < threshold 1 value again
2	Injection stream CO2 concentration	Samples & analysis: online system	x	Cont or 1-3 hourly sampling combined with online analysis system Quarterly	Near well head or Compressor station	Defined % for the CO2 concentration of the stream	Allowed fluctuations reached Additional measurements	Above allowed fluctuations Adapt stream composition, reduce injection temporarily
3	Injection stream composition	Samples & analysis: Additional samples for calibration	x	Quarterly	Near well head or Compressor station	Defined % for the composition of the gas	Allowed fluctuations reached Additional measurements, find cause, adapt gas composition, potentially reduce injection rate	Above allowed fluctuations Find cause, adapt stream composition, potentially reduce or stop injection temporarily
4	Water measurement	Water measurement	x	Cont	Near well head or Compressor station	Specification value	In case specification value is reached Consultation with the CO2 provider, check dehydration system	In case value is above specification value and creates a safety issue Stop CO2 delivery, investigate at the CO2 provider the cause, start delivery if value OK again
5	Discontinuous emissions through leakage, venting or incidents	Combination of techniques	x	Yearly	Potential leakage points like joints or ventstacks			

No.	Parameter to be Monitored*	Proposed Technique adopted	Category of monitoring	Project phase and frequency	Location	Normal situation	Alert value	Contingency value
			Mandatory according to EU directive	Pre-inj Inj Post-Inj (abandonment) Post-Inj (abandonment) Long-term stewardship	Expectation value Accuracy		> Threshold 1	> Threshold 2
			Contingency Required (preliminary estimation)					Contingency measures**
	<b>Well integrity</b>							
6	Annular pressure	Pressure device (with alarm value)	x	Baseline date prior to operations Continuously with remote system for online reading	At the well head	Constant pressure	Increase or decrease in pressure within safety margins Additional measurements like logging or sampling + analysis of fluids to detect CO2	Increase or decrease in pressure above safety margins Investigate causes (sampling) and options to remediate (in the extreme case well abandonment)
7	Well integrity	Wireline Logging (selection of tool: CBL, PMIT, EMIT, USIT, WAF, optical)	x	Baseline Every 5 years. If advanced technology is available, more measurements are aimed for.	Well	Measurements within the expected range	Measurements above expectation values Additional measurements (such as repeat) to corroborate observations, potentially seismic contingency measurements in case values large enough to be detected by seismics	Measurements significantly above expectation values Stop injection, additional measurements and seismic contingency measurements to identify shallow gas accumulations, investigate options to remediate (in the extreme case well abandonment)
8	Well head pressure	Pressure device	x	Baseline Continuous Continuous Continuous	At the well head (injection skid)	Measurements within the expected range, no large fluctuations expected at constant flow rates	Loss or increase of pressure with respect to expected values Additional measurements to determine the cause	No recovery of injection pressure after lowering or increasing injection flow Stop injection, investigate the cause and evaluate whether conditions are safe
9	Well head temperature	Temperature device	x	Baseline Continuous Continuous Continuous	At the well head (injection skid)	Determine operational limits for temperature range	In case temperature reaches the determined operational limits (high or low) Additional measurements to determine the cause	In case temperature reaches the determined operational limits Stop injection until the cause of the temperature change is clarified and safe
10	Plug integrity	Pressure test and inspection	x	Test during abandonment to assess the quality of the plug	In the well above the plug	No pressure changes	Minimal pressure changes Investigate cause with other measurements (e.g. check wellbore, fluid sample)	Significant pressure changes Redo the plug

No.	Parameter to be Monitored*	Proposed Technique adopted	Category of monitoring	Project phase and frequency	Location	Normal situation	Alert value	Contingency value
			Mandatory according to EU directive Required (preliminary estimation) Contingency	Pre-inj Inj Post-inj Post-inj (abandonment) Long-term stewardship		Expectation value Accuracy	> Threshold 1 Action**	> Threshold 2 Contingency measures**
	<b>Reservoir integrity</b>							
11	Reservoir pressure (FBHP) (see also line 8)	pressure device	(x)	Baseline data Cont (TH cont, BH cont or monthly in case memory gauges) Cont (TH cont, BH cont or monthly in case memory gauges) as long as the well is not suspended	Calculated from FTHP continuous, AND downhole permanent sensor (large risk of failure) OR downhole memory gauges	Flowing bottomhole pressure in agreement with simulations	Deviation from expected values Recalibration of the reservoir simulation model until satisfactory history match	Significant deviation from expected values Re-evaluate reservoir model, in case no explanation can be provided, stop injection
12	Reservoir Temperature (FBHT) (see also line 9)	thermometer or DTS	(x)	Baseline data Cont (TH cont, BH cont or monthly in case memory gauges) as long as the well is not suspended	Calculated from FHT AND potentially downhole permanent sensor / same	Flowing bottomhole temperature in agreement with well model	Deviation from expected values Recalibration of the well model until satisfactory history match	Significant deviation from expected values Re-evaluate well model, in case no explanation can be provided, stop injection
13	Stabilized pressure (CBHP) (gradient) during shut-in period	pressure device combined with shut-in	x	Baseline data Every year Every year as long as the well is not suspended	Calculated from THP, AND permanent downhole sensor (large risk of failure) or downhole memory gauges, combined with shut-in	Pressure data in agreement with expected simulation model and P/z curve	Deviation from expected values Recalibration of the reservoir simulation model until satisfactory history match	Significant deviation from expected values Re-evaluate reservoir model, in case no explanation can be provided, stop injection
14	Stabilised temperature (CBHT) (gradient) during shut-in period	thermometer or DTS combined with shut-in	x	Baseline data Every year Every year as long as the well is not suspended	DTS for permanent installation or memory gauges combined with shut-in AND if available in monitoring well	Temperature data in agreement with expected well model	Deviation from expected values Recalibration of the well model until satisfactory history match	Significant deviation from expected values Re-evaluate well model, in case no explanation can be provided, stop injection
15	Suspected leakage	Surface seismic survey	x	Baseline data Other monitoring indicates leakage Only when other monitoring indicates leakage Only when other monitoring indicates leakage Survey can be considered for the transfer of liability	Marine vessel (seismic acquisition using streamers)	No changes in the presence of shallow gas pockets or gas chimneys	Shallow gas pockets Determine the origin of the gas	Re-evaluate well model, in case no explanation can be provided, stop injection

No.	Parameter to be Monitored*	Proposed	Category of	Project phase and frequency					Location	Normal situation	Alert value		Contingency value
				Pre-inj	Inj	Post-Inj (abandonment)	Post-Inj (stewardship)	Long-term			> Threshold 1	> Threshold 2	
Environmental monitoring													
16	Pockmarks at the seabottom	Multi-beam echosounding	Mandatory according to EU directive Required (preliminary estimation) Contingency	Pre-inj	Inj	Post-Inj (abandonment)	Post-Inj (stewardship)	Long-term	Marine vessel	No pockmarks	Expectation value	Accuracy	Contingency measures***
17	Presence of shallow gas or gas chimneys in the subsurface	Baseline seismic data	x	Baseline	Contingency	Contingency	Contingency	Contingency	Marine vessel (seismic acquisition using streamers)	No bright spots or chimneys in the subsurface	No pockmarks	Accuracy	Contingency measures***
18	Migration pathways for gas in the shallow subsurface	Time-lapse seismic data acquisition (2D or 3D)	x	Contingency	Contingency	Contingency	Contingency	Contingency	Marine vessel	No changes in bright spots or chimneys in the subsurface	No pockmarks	Accuracy	Contingency measures***
19	CO2 in soil at pockmarks	Gas samples using vibrocore + lab analysis	x	Contingency	Contingency	Contingency	Contingency	Contingency	Sampling from a marine vessel	In case of leakage detection at the seabottom by geophysical methods	In case of leakage detection at the seabottom by geophysical methods	Accuracy	Contingency measures***
20	Bubble detection at wellhead	Acoustic bubble detector	x	Contingency	Contingency	Contingency	Contingency	Contingency	Install at the seabottom	No bubbles	No bubbles	Accuracy	Contingency measures***
21	Microseismic monitoring	Permanent geophones or DAS in monitoring wells	x	Baseline data	Cont	Cont	Cont	Cont	Injection well at caprock and reservoir level	No large events in caprock or at faults (re-activation)	No large events in caprock or at faults	Accuracy	Contingency measures***

\*Follows from the risk assessment  
 \*\* t.b.d. by operator, examples are updating model, additional monitoring, ...  
 \*\*\* t.b.d. by operator, examples are stop injection, back-production, well workover, contingency monitoring

Table 19-2 P18-2 CO<sub>2</sub> storage base case monitoring plan, by injection phase.

**P18-2 CO<sub>2</sub> storage base-case monitoring plan**

Decommissioning of the platform

			Pre-injection	Injection	Post-injection	Post-injection (Abandonment)	Post-injection (Transfer of liability)
<b>Injection Proces</b>							
1	Injection rate	Flow meter		Continuous			
2	Injection stream CO <sub>2</sub> concentration	Gas samples & analysis: online system		Continuous or 1-3 hourly			
3	Injection stream composition	Gas samples & analysis: Additional samples for calibration		Quarterly			
4	Water measurement	Gas measurement		Continuous			
5	Discontinuous emissions through leakage, venting or incidents	Combination of techniques		Yearly reporting according to protocol			
<b>Well Integrity</b>							
6	Annular pressure	Pressure device	Baseline	Continuous			
7	Well integrity	Wireline Logging (selection of tools like: CBL, PMIT, EMIT, USIT, WAF, optical)	Single baseline before start of the injection	Frequency should be determined and adapted during the course of the project			
8	Well head pressure	Pressure device		Continuous			
9	Well head temperature	Temperature device		Continuous			
10	Plug integrity	Pressure test and inspection			Assessment of the quality of the plug		
<b>Reservoir Integrity</b>							
11	Reservoir pressure (FBHP) (see also line 8)	pressure device		Continuous or monthly with memory gauges (frequency can be adapted according to findings) - (Calculated from FTHT, AND potentially downhole permanent sensor (large risk of failure) or downhole memory gauges)			
12	Reservoir Temperature (FBHT) (see also line 9)	thermometer or DTS		Continuous or monthly with DTS or memory gauges (frequency can be adapted according to findings) - (Calculated from FTHT AND potentially downhole permanent sensor (large risk of failure) or downhole memory gauges)			
13	Stabilized pressure (CIBHP) (gradient) during shut-in period	pressure device (wireline tool or memory gauge) combined with shut-in		Shut-in pressure measurement every year			
14	Stabilised temperature (CIBHT) (gradient) during shut-in period	thermometer or DTS (wireline tool or memory gauge) combined with shut-in		Shut-in temperature measurement every year (DTS for permanent installation or memory gauges)			
15	Suspected leakage	Surface seismic survey			Survey in case of irregularities		
<b>Environmental Monitoring</b>							
16	Pockmarks at the seabottom	Multi-beam echosounding	Baseline			survey	survey
17	Presence of shallow gas or gas chimneys in the subsurface	Baseline seismic data	Interpretati can be on existing data				
18	Migration pathways for gas in the shallow subsurface	Time-lapse seismic data acquisition (2D or 3D)			Survey in case of irregularities		
19	CO <sub>2</sub> in soil at pockmarks	Gas samples using vibrocore + lab analysis			Survey in case of irregularities		
20	Bubble detection at wellhead	Acoustic bubble detector			Survey in case of irregularities		
21	Microseismic monitoring	Permanent geophones or DAS in (monitoring) wells		Continuous in monitoring or injection well (considered required monitoring but subject to technical feasibility)			





Princetonlaan 6  
3584 CB Utrecht  
P.O. Box 80015  
3508 TA Utrecht  
The Netherlands

[www.tno.nl](http://www.tno.nl)

T +31 88 866 42 56

## TNO report

TNO 2019 R11212

# CO<sub>2</sub> storage feasibility in the P18-6 depleted gas field

Date	March 2020
Author(s)	Filip Neele Ton Wildenborg Kees Geel Daniel Loeve Lies Peters Siavash Kahrobaei Thibault Candela Mariëlle Koenen Paul Hopmans Kaj van der Valk Bogdan Orlic Vincent Vandeweyer
Number of pages	192 (incl. appendices)
Number of appendices	
Sponsor	
Project name	P18-6 feasibility study
Project number	060.40697

All rights reserved.

No part of this publication may be reproduced and/or published by print, photoprint, microfilm or any other means without the previous written consent of TNO.

In case this report was drafted on instructions, the rights and obligations of contracting parties are subject to either the General Terms and Conditions for commissions to TNO, or the relevant agreement concluded between the contracting parties. Submitting the report for inspection to parties who have a direct interest is permitted.

© 2019 TNO

## Summary

### *Objective*

This study presents the results from a CO<sub>2</sub> storage feasibility study on the P18-depleted gas field that is located in the Netherlands offshore. The aim of the study was to understand the risks associated with injecting CO<sub>2</sub> into the field, to outline injection strategies that lead to safe and secure storage and, finally, to propose an approach to risk management and monitoring during injection. The results from this study are to form the geoscientific basis for a CO<sub>2</sub> storage permit application.

### *Background*

The study was carried out for the Porthos consortium that plans to transport CO<sub>2</sub> from several industrial sources in the Port of Rotterdam to three P18 fields operated by Taqa: P18-2, P18-4 and P18-6. TAQA already obtained a storage permit for the P18-4 field in 2013, with the aim to store CO<sub>2</sub> for the ROAD project, with a mass of about 5 Mt. However, the ROAD project was cancelled in 2017.

The Porthos consortium builds onto the work done by the ROAD project. The consortium plans to transport and store more CO<sub>2</sub> than the 5 Mt target of the ROAD project and, hence, will need storage capacity in addition to that offered by the already permitted P18-4 field. Operated from the same P18-A platform and also close to the end of production, the P18-2 and P18-6 fields represent a maximum storage capacity 32.3 Mt and 1.5 Mt (in both cases for a final reservoir pressure of just under original gas pressure). The current study is directed to the P18-6 field only.

In 2011 a CO<sub>2</sub> storage feasibility study of the P18 fields was performed. The present study provides an update for the P18-6 field based on new data and improved methods and workflows to investigate the response of the depleted field to injection of CO<sub>2</sub>.

### *Study approach*

The requirements for a CO<sub>2</sub> storage permit application are set out in the Dutch Mining Act, which was amended in 2011 to include a transposition of the EU Storage Directive (EU Directive 2009/31/EC). The results presented in this report cover the requirements described in the EU Storage Directive. The present study follows a workflow that was developed in a consortium of several EU Member States, building on combined experience in CO<sub>2</sub> storage feasibility assessments.

The workflow is risk-based, with the aim to understand the site-specific risks associated with CO<sub>2</sub> storage, to reduce them to a level that is as low as reasonably possible through site-specific design of injection scenarios and to develop a monitoring program and mitigation plan aimed at the most relevant, remaining risks.

### *Overall conclusion regarding storage of CO<sub>2</sub> in the P18-6 field*

The overall conclusion of the study is that CO<sub>2</sub> can be stored safely and securely in the P18-6 field. The CO<sub>2</sub> can be injected into the field in a way that is safe; during and after the end of injection, the P18-6 field will retain the CO<sub>2</sub> securely. There is no reason to assume that CO<sub>2</sub> could migrate out of the field after proper decommissioning of the injection well after the end of injection.

### *Managing relevant risks*

The identified risks that are related to the potential leakage of CO<sub>2</sub> out of the P18-6 storage complex during or after CO<sub>2</sub> injection have been studied in detail and classified in a risk register. Most of the risks have been classified as 'very low', with 'very low likelihood' that a small ('nil to negligible') amount of CO<sub>2</sub> could migrate out of the reservoir'; this corresponds with the lowest possible risk class. The risks associated with the injection well have been classified as 'low', with a 'low likelihood' and a small ('nil to negligible') amount of CO<sub>2</sub> could migrate out of the reservoir.

The risks assessed are related to (1) lateral CO<sub>2</sub> migration out of the storage reservoir, (2) the integrity of the well in the field, (3) the stability of the faults in the storage system and integrity of the caprock.

- (1) Simulation of the flow of CO<sub>2</sub> during injection into the storage formations shows that the injected CO<sub>2</sub> will be retained within the confines of the original gas field. There is no risk of CO<sub>2</sub> spilling, even when the pressure in the reservoir is brought back to the initial pressure.
- (2) Analysis of available data on the integrity of the well in the P18-6 field shows that a workover is required for the existing well, P18-A-07-S1. Once this is performed, the risk of CO<sub>2</sub> leaking along the well, based on pre-injection status, is considered low.

The initial low reservoir pressure leads to low temperature of the CO<sub>2</sub> at the bottom of the well, causing significant temperature gradients in the well. These might lead to de-bonding of well liner (casing) and cement, potentially allowing leakage pathways to form (micro-annuli) for CO<sub>2</sub>. However, only when the pressure in the reservoir is above hydrostatic pressure could CO<sub>2</sub> enter these micro-annuli and potentially migrate into overlying aquifers. Therefore, the pressure in the reservoir is to be maximized at hydrostatic pressure, to reduce the likelihood of CO<sub>2</sub> flowing through these micro-annuli to 'low', with an amount of CO<sub>2</sub> that is 'small to negligible'.

- (3) The cold CO<sub>2</sub> is injected into the reservoir formations, where it will create a low-temperature zone around the injection well. In case injection into the P18-6 reservoir on a continuous basis, this zone could reach faults that are present in the reservoir, affecting fault stability; however, at the same time, faults become more stable during the injection process due to increasing reservoir pressure. If the P18-6 reservoir is only used to store the cold contents of the surface transport pipeline after a shut-in period, the mass of injected (colder) CO<sub>2</sub> is small and the low-temperature front does not reach faults near the well. In both modes of operation, monitoring of injection rate and temperature is recommended to measure the pressure and collect the information to track the temperature development in the reservoir through modelling and ensure that faults remain stable. However, all analysis points to small to negligible impact of fault reactivation; none of the faults in the P18-6 reservoir extend to above the caprock of 450 m to 750 m thick. This ensures that, fault destabilization, if any, will not lead to CO<sub>2</sub> movement through the caprock.

The likelihood that CO<sub>2</sub> injection in the P18-6 reservoir affects caprock integrity is very low.

#### *Recommendations*

- (1) In the study presented here the modelling of the injection process was performed with an isothermal reservoir simulator that could not simultaneously handle pressure and temperature variations in the reservoir. The impact of the low temperature of the injected CO<sub>2</sub> was estimated through the use of an additional simulator and analytical approaches. While the results obtained thus far are considered sufficient for the assessment of the risks associated with CO<sub>2</sub> storage, detailed coupled modelling of pressure and temperature in the storage formations is required prior to the start of injection. This is needed for pressure and temperature predictions that are sufficiently reliable for the management of the injection process and for the interpretation of monitoring data.
- (2) The aim of the present study was to provide the basis for a storage permit application, by understanding the current status of the storage formations, the caprock, the faults and the wells, and their response to the injection of CO<sub>2</sub>. The study established that conditions can be established under which CO<sub>2</sub> can be injected and stored safely and securely in the P18-6 field. The study did not aim to arrive at a complete and detailed description of these conditions. Such an 'operational plan' for CO<sub>2</sub> injection into the P18-6 field will be required prior to the start of injection, as a basis for the detailed monitoring plan and for the operational management of the injection process. The present study is the first step towards the P18-6 operational plan.

# Contents

	<b>Summary .....</b>	<b>2</b>
<b>1</b>	<b>Introduction.....</b>	<b>8</b>
<b>2</b>	<b>Reading guide.....</b>	<b>10</b>
2.1	Definitions.....	10
<b>3</b>	<b>Methodology .....</b>	<b>12</b>
3.1	Legal background .....	12
3.2	Feasibility study .....	12
3.3	Risk assessment .....	13
<b>4</b>	<b>P18-6 field overview .....</b>	<b>16</b>
4.1	Introduction.....	16
4.2	Geological description .....	16
4.3	Caprock .....	19
4.4	Naturally sealing formations .....	22
<b>5</b>	<b>Injection scenario .....</b>	<b>24</b>
5.1	Injection wells and well completion .....	24
5.2	CO <sub>2</sub> supply scenarios .....	24
5.3	Injection of CO <sub>2</sub> in P18-6 .....	25
5.4	CO <sub>2</sub> quality .....	25
5.5	Summary of injection conditions .....	26
<b>6</b>	<b>Evaluation of reservoir performance and integrity .....</b>	<b>28</b>
6.1	Introduction.....	28
6.2	CO <sub>2</sub> conditions at bottomhole .....	28
6.3	Reservoir injection performance and risks .....	32
6.4	Reservoir behaviour: temperature effect.....	41
6.5	Chemical interactions .....	49
6.6	Conclusions .....	52
<b>7</b>	<b>Fault stability .....</b>	<b>54</b>
7.1	Introduction.....	54
7.2	Fault stability: pressure effect .....	54
7.3	Fault stability : temperature effect.....	59
7.4	Fault stability: geochemical effects .....	64
7.5	Conclusions .....	66
<b>8</b>	<b>Caprock integrity .....</b>	<b>67</b>
8.1	Introduction.....	67
8.2	Pressure effect on caprock integrity.....	67
8.3	Temperature effect on caprock integrity.....	67
8.4	Geochemical effects .....	69
8.5	Conclusions .....	71
<b>9</b>	<b>Well integrity .....</b>	<b>73</b>
9.1	Introduction.....	73

9.2	Status of the well barriers .....	73
9.3	Influence of cooling on well integrity .....	82
9.4	Well decommissioning .....	93
9.5	Conclusions .....	94
<b>10</b>	<b>P18-6 storage site and storage complex .....</b>	<b>95</b>
10.1	Introduction .....	95
10.2	Definitions in the Netherlands Mining Law and the EU Storage Directive .....	95
10.3	Definition of the storage site .....	96
10.4	Definition of the storage complex .....	96
10.5	Barriers .....	98
<b>11</b>	<b>Migration paths .....</b>	<b>100</b>
11.1	Introduction .....	100
11.2	Available data and workflow .....	100
11.3	Geological model of the overburden .....	101
11.4	Migration scenarios .....	103
11.5	Methods .....	104
11.6	Results .....	104
11.7	Present day hydrocarbon migration .....	108
11.8	Conclusions .....	109
<b>12</b>	<b>Risk assessment and preventative measures .....</b>	<b>111</b>
12.1	Reservoir .....	111
12.2	Caprock .....	113
12.3	Fault zones .....	115
12.4	Wells .....	117
12.5	Conclusion .....	119
<b>13</b>	<b>Monitoring and corrective measures plan .....</b>	<b>121</b>
13.1	Introduction .....	121
13.2	Foundation of the monitoring and corrective measures plan .....	122
13.3	Philosophy of the monitoring plan .....	126
13.4	Interpretation .....	130
13.5	The monitoring plan .....	131
13.6	Conclusion .....	136
<b>14</b>	<b>Conclusions .....</b>	<b>138</b>
<b>15</b>	<b>References .....</b>	<b>140</b>
<b>16</b>	<b>Appendix A: compliance with EU Storage Directive site characterisation and assessment .....</b>	<b>145</b>
16.1	Data collection (step 1) .....	145
16.2	Building the 3-D static geological earth model (step 2) .....	146
16.3	Characterisation of storage dynamic behaviour, sensitivity characterisation, risk assessment (step 3) .....	147
<b>17</b>	<b>Appendix B. Subsurface model descriptions .....</b>	<b>151</b>
17.1	Static model .....	151
17.2	Seismic interpretation .....	151
17.3	Time-depth conversion .....	152

17.4	Petrel model building .....	153
17.5	Adjustments made to the static model .....	164
17.6	Dynamic model.....	164
17.7	History Match of the dynamic model.....	170
17.8	Geomechanical model.....	177
17.9	Well degradation model.....	181
<b>18</b>	<b>Appendix C. Risk Register.....</b>	<b>183</b>
<b>19</b>	<b>Appendix D. Monitoring Plan.....</b>	<b>187</b>



# 1 Introduction

This report presents the results of a study into the technical feasibility of storing CO<sub>2</sub> in the depleted offshore gas field P18-6. This field is one of several fields in the P18 cluster. The Porthos consortium<sup>1</sup> is developing plans for a multi-user CO<sub>2</sub> transport and storage network that connects industrial emitters of CO<sub>2</sub> in the Rotterdam harbour area with geological storage capacity in the Dutch sector of the North Sea. The consortium is targeting the P18 cluster as the first candidate for CO<sub>2</sub> storage. Operation of the network is planned for 2022 / 2023<sup>2</sup>.

The Porthos network is still in its planning stage and no certainty exists at this point in time regarding the supply of CO<sub>2</sub>. A recent study of the P18 gas field cluster suggested that the fields P18-2, P18-4 and P18-6 together can accommodate a supply rate of the order of 2-3 Mt/yr (million tonnes per year) and possibly up to 5 Mt/yr (Vandeweyer et al., 2011). With a combined storage capacity of approximately 37 Mt, storage at a rate of 2-3 Mt/yr could continue for about 15 years.

The P18-4 gas field has a CO<sub>2</sub> storage permit in place. This permit was awarded irrevocably in 2013. The P18-4 field was planned to be part of the “Rotterdam afvang en opslag demonstratieproject” (ROAD), which aimed to capture CO<sub>2</sub> at a coal-fired power plant at the Maasvlakte, compress the CO<sub>2</sub> and transport it by offshore pipeline to the P18-A platform, located at a distance of about 20 km from the Maasvlakte. The ROAD project was cancelled in 2017; all close-out reports are available online (ROAD, 2018).

The Porthos consortium now builds onto the ROAD legacy. The Porthos network is planned to be a multi-user transport and storage network, building up to much higher CO<sub>2</sub> supply rates than those considered in the ROAD project. In addition, the Porthos network has a longer operational phase planned. This means that more depleted gas fields are required for storage, in addition to P18-4. The first candidates are the P18-2 and, potentially, the P18-6 gas fields.

The starting point of the present study was the storage feasibility study of the P18 cluster that was performed under the CATO-2 R&D programme (Vandeweyer et al., 2011). While the scope of that study was the entire P18 complex – including the P18-2, P18-4 and P18-6 compartments – the focus of the analyses was on the P18-4 structure. The P18-4 storage feasibility study was used in a storage permit application that resulted in the permit granted in 2013. The analyses of the P18-2 and P18-6 compartments presented by Vandeweyer et al. (2011) were not sufficient for a subsequent storage permit application for these compartments.

The storage feasibility analysis of the P18-2 field was recently completed, building onto the work presented by Vandeweyer et al., (2011) and using up-to-date tools and workflows, to support a storage permit application (Neele et al, 2019).

---

<sup>1</sup> See <https://rotterdamccus.nl/>.

<sup>2</sup> See Notitie Reikwijdte en Detailniveau – Rotterdam CCUS Project (Porthos), available at <https://www.rvo.nl/sites/default/files/2019/02/Porthos%20concept%20NRD%20-%20versie%20finaal.pdf>

This report presents the results of a technical CO<sub>2</sub> storage feasibility study of the P18-6 structure. The aim of the feasibility study is to identify risks for the containment of CO<sub>2</sub> in the storage complex, how to minimize those risks and the best way to monitor remaining risks. The study, which extends the analyses and results of the CATO-2 study by using the latest production data and deploying state-of-the-art workflows and tools, provides the necessary input for a CO<sub>2</sub> storage permit application under the Dutch Mining Act and a 'Milieu Effect Rapportage' (MER) (which is a required element for the permit application). In 2011, the Dutch Mining Act transposed the EU Storage Directive (EU, 2009), thus ensuring that a storage permit application submitted under the Dutch Mining Act will comply with European legislation concerning CO<sub>2</sub> storage.

The work presented in this report follows the workflow that was used for the P18-2 feasibility study (Neele et al., 2019).

## 2 Reading guide

This report presents the results of a technical CO<sub>2</sub> storage feasibility study for the P18-6 depleted gas field. The structure of the report is as follows.

Sections 3 through 5 set the scene for the storage feasibility study. Section 3 introduces the risk-based approach taken in assessing the feasibility of storing CO<sub>2</sub> in the P18-6 field. The geological setting of the P18-6 field is described in Section 4. Section 5 describes some of the key boundary conditions and assumptions used in the study: the CO<sub>2</sub> supply profile until 2035, as well as the preliminary approach to the injection process. Section 5 also provides a brief summary of relevant results from a flow assurance study that was performed previously; this includes the conditions of the CO<sub>2</sub> at the bottom of the injection well, which follow from the modelling of CO<sub>2</sub> flow from the compression station, through a subsea pipeline and down the injection well. These conditions are used in the present study as the starting point for the modelling of the behaviour of the CO<sub>2</sub> inside the reservoir.

Sections 6 through 11 present the results from the storage feasibility analysis. The behaviour of CO<sub>2</sub> in the reservoir and its effect on the temperature and pressure distribution is presented in Section 6. Sections 7 and 8 discuss the impact of injecting CO<sub>2</sub> on reservoir and caprock integrity and stability of the faults within and bounding the reservoir. Well integrity is covered in Section 9, evaluating the current status of the well and discussing simulation results on the effect of CO<sub>2</sub> injection on the long-term structural integrity. Section 10 defines the storage site and storage complex and contains a description of the barriers in the storage site to CO<sub>2</sub> migration. Section 11 presents an analysis of potential migration of CO<sub>2</sub>, if it leaves the storage complex. All results are pulled together in Section 12 to assess the risks associated with injecting CO<sub>2</sub> into the P18-6 field.

Section 13, finally, outlines the system that will be designed to monitor the injection process and the behaviour of the CO<sub>2</sub> in the subsurface.

### 2.1 Definitions

The following definitions are used throughout this document.

<b>Block</b>	An area on a map (e.g., block P18)
<b>License areas</b>	Part or all of a block (e.g., P18a)
<b>Field</b>	A bounded structure where the hydrocarbons were discovered and produced from and includes the sealing faults, rocks, gas-water contact (GWC) and other structural elements (e.g., P18-6)
<b>Reservoir</b>	Part of the field where the reservoir fluids are contained and where the CO <sub>2</sub> will be stored, i.e. the porous rock
<b>Compartment</b>	Part of a field and includes the bounding elements, (e.g. three compartments in P18-2 field)
<b>Storage Site</b>	Defined under the CO <sub>2</sub> Storage Directive and under the Dutch Mining Act and includes the storage reservoir and the wellbores penetrating the storage reservoir

<b>Storage Complex</b>	Includes the storage reservoir, the wellbores penetrating the reservoir and the surrounding and bounding formations and faults which make up the storage field.
<b>Migration of CO<sub>2</sub></b>	Movement out of the storage reservoir but remaining in the storage complex
<b>Leakage of CO<sub>2</sub></b>	Under the CO <sub>2</sub> Storage Directive means movement of CO <sub>2</sub> out of the storage complex
<b>Emission of CO<sub>2</sub></b>	Under the ETS Directive means escape of CO <sub>2</sub> from the storage site to the atmosphere or the water column
<b>Injection facilities</b>	Include well completions and wellheads; <i>not</i> included are other facilities on the platform, nor the platform itself.

## 3 Methodology

### 3.1 Legal background

This technical CO<sub>2</sub> storage feasibility study aims to provide the basis for a permit application for CO<sub>2</sub> storage in the P18-6 field. The Dutch Mining Act sets out the requirements for a storage permit application. A transposition of the EU Storage Directive (EU, 2009) was included in the Mining Act in 2011<sup>3</sup>. Previous work on the P18-4 field (Vandeweyer et al., 2011) resulted in a successful application for a CO<sub>2</sub> storage permit, proving that the workflow used provided a basis that was both sufficiently detailed and complete.

The present study follows the workflow that was used by Vandeweyer et al. (2011), and that was described in detail by Nepveu et al. (2015), who combined experience from several EU Member States in CO<sub>2</sub> storage feasibility assessments. The workflow covers the full list of requirements set out in Annex II of the EU Storage Directive (EU, 2009). Section 16 shows the link between the elements of site characterisation mentioned in Annex I of the EU Storage Directive and the present report.

### 3.2 Feasibility study

The workflow is risk-based and site specific, with the aims to understand the storage risks involved, to reduce them to a level that is as low as reasonably possible through site-specific design of injection scenarios and to develop a monitoring program aimed at the most relevant, remaining risks.

This study uses the workflow described by Nepveu et al. (2015) as illustrated in Figure 3-1 and outlined below:

- Phase 1 of the workflow represents a screening study, to find one or multiple sites that meet selection criteria, such as location, storage capacity or expected cost of storage.
- Phase 2 of the workflow represents the detailed CO<sub>2</sub> storage feasibility study, which is presented in this report for the P18-6 depleted gas field. The first part of phase 2 is a 'quick scan' of available data. The purpose of the quick scan is to identify the key risks to storage and 'showstoppers', if any, before entering the detailed assessment, which represents the second part of phase 2. This detailed assessment is shown in the diagram in the figure as the central, large rectangle labelled 'RA' (risk assessment), with several disciplines revolving around the RA. This is the key element of a storage feasibility assessment, with several disciplines analysing the response of the storage system on the injection of CO<sub>2</sub>.

For this study, screening was already completed and outside the scope of this report. In addition, a 'quick scan' of available data was already performed in a previous study of the P18 gas fields (Vandeweyer et al., 2011). No showstoppers were identified for the P18-6 field. However, as that study was focused on the P18-4 depleted gas field, the detailed assessment of the P18-6 was incomplete; the

---

<sup>3</sup> See <https://www.nlog.nl/en/licences-and-legislation> for links to relevant government internet sites.

present report repeats the previous assessment with improved tools and experience where possible and fills the gaps where needed.

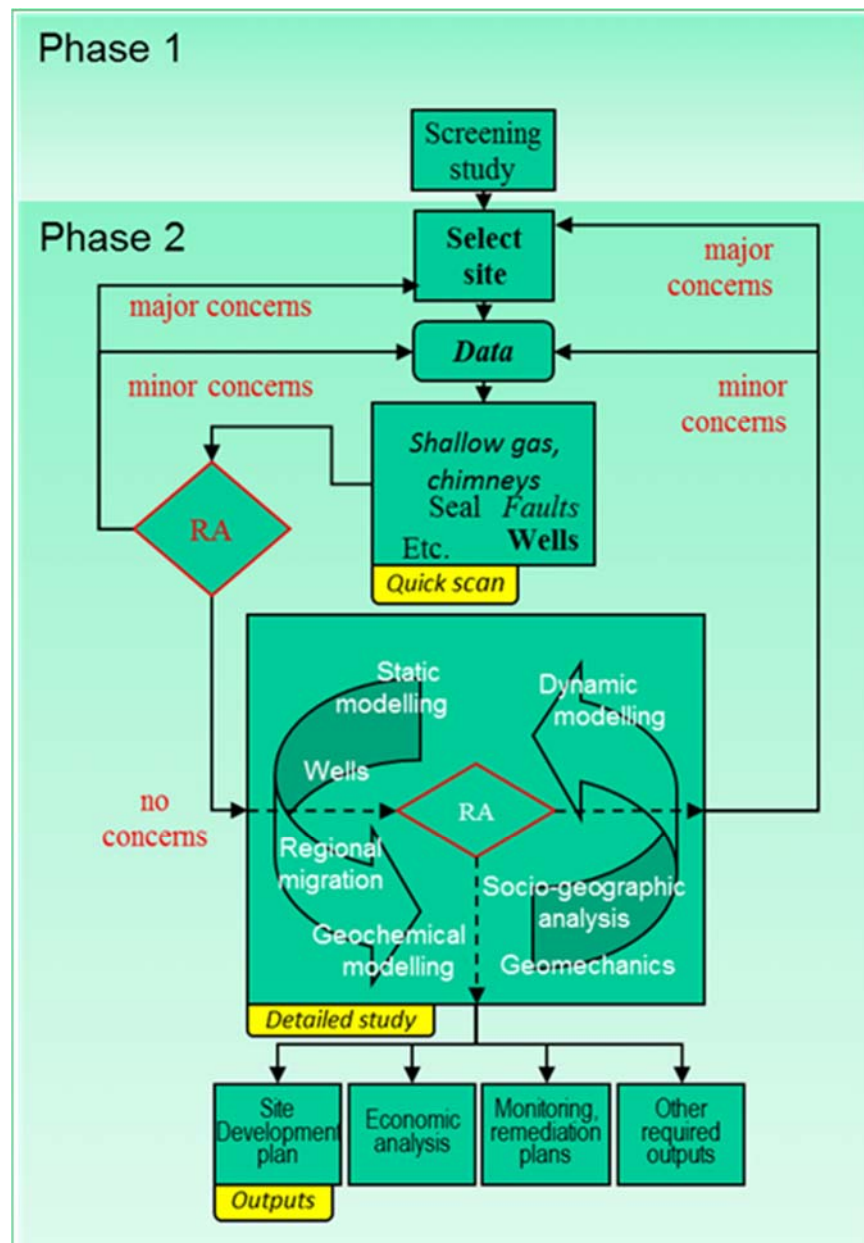


Figure 3-1 Workflow for site screening and characterization (Nepveu et al., 2015). RA is Risk Assessment

### 3.3 Risk assessment

The approach pursued in the risk assessment, (i.e., the assignment of risk classes) is qualitative in nature and expert-based, although the underlying information used is often of a quantitative nature, e.g. output from model simulations or measurements of physical parameters like pressure.

The risk assessment consists of the following steps:

1. Identification of (a combination of) factors, which directly influence the containment of CO<sub>2</sub>
2. Detailed assessment of these (combined) factors and definition of potential risk reduction measures
3. Risk classification

Step 1 was performed in a workshop prior to the project in order to define the required assessment. Step 2, the detailed assessment of the risk factors and definition of potential risk reduction measures, is reported in Sections 6 to 9; step 3 is described in Section 12.

Typically, the results of the risk characterisation and classification are listed in a risk register (see Section 18) and summarized in accompanying risk matrices. For the classification of the risks, a risk matrix with classes of likelihood and consequences has been designed (see Figure 3-2), which is inspired by the work done by Van Eijs et al. (2011) and the risk assessment matrix included in the toolkit of the Energy Institute (website, version 15 Oct 2019). The definition of the classes of consequences has been linked to the concept and definition of the storage complex as described in the EU Storage Directive (EU, 2009).

As shown in Figure 3-2 the following definitions are used for this study:

Five classes of likelihood have been defined with the following definitions:

Very low	Positive evidence for containment and large safety factor
Low	No positive evidence and large safety factor
Medium	Positive evidence and no large safety factor
High	No positive evidence and no large safety factor
Very high	No positive evidence and small or nil safety factor

The classes of consequence have been defined as follows:

Negligible	Within natural variation and cannot be monitored
Very small	Can be monitored and no impact on biosphere
Small	Can be monitored and possible minor impact on biosphere
Large	Can be monitored and possible impact on biosphere
Very large	Can be monitored and possible adverse impact on biosphere

The resulting risk classes have been split in three categories):

Low risk	Strive for continuous improvement; monitoring and risk reduction are optional;
Medium risk	Apply monitoring and risk reduction measures according to ALARP (As Low As Reasonably Practicable) principle;
High risk	Risk reduction to acceptable levels and monitoring are obligatory.

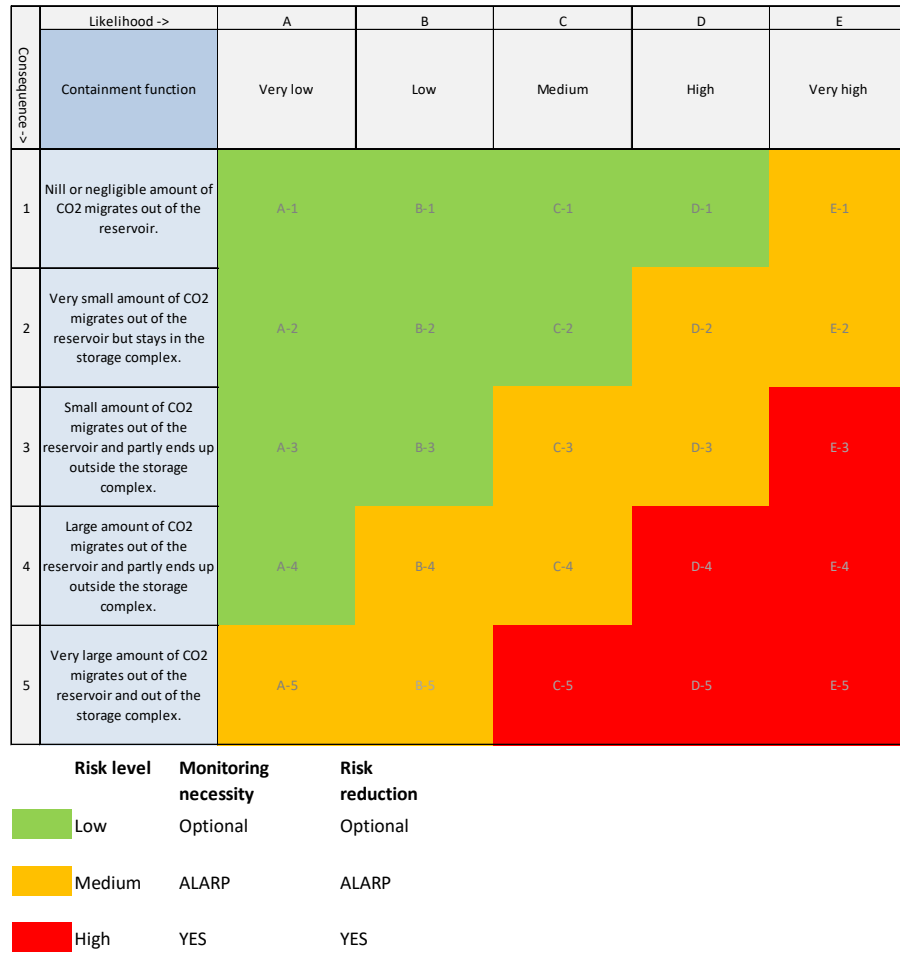


Figure 3-2 Proposed risk matrix nomenclature (modified after Van Eijs et al., 2011; Energy Institute, 2016)



## 4 P18-6 field overview

### 4.1 Introduction

The gas fields P18-2, P18-4, and P18-6, drilled from platform P18-A, are situated at approximately 3500 m depth below sea level and are located some 20 km NW from the port of Rotterdam (Figure 4-1). The reservoir rocks consist of sandstones which belong to the Triassic Main Buntsandstein Subgroup. The primary seal for the gas fields consists of unconformably overlying siltstones, claystones, evaporites and dolostones. The P18 gas fields are located in a heavily faulted area and consist mainly of fault bounded compartments, which are (at least on production time scales) hydraulically isolated from their surroundings. The bounding faults (which are well defined and clear to see on seismic) are sealing on a geological time scale due to juxtaposition of reservoir rock against impermeable rock.

High-calorific gas has been produced from these reservoirs since 1993. The gas is produced through the P18-A satellite platform and the P15-ACD processing and accommodations facilities in the adjacent P15 block, from where it is then transported to the coast by a 40-km-long gas pipeline.

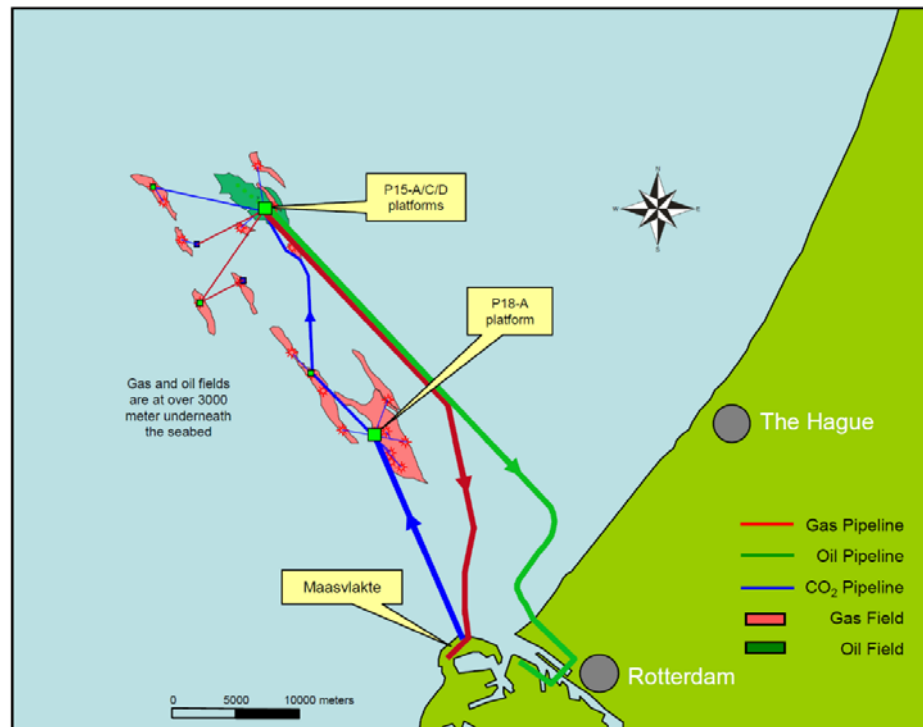


Figure 4-1: Overview of the locations of P15 and P18 fields (After TAQA, 2009)

### 4.2 Geological description

The P18 cluster consists of three fields, the P18-2, P18-4 and P18-6 fields (Figure 4-2). P18-2 was discovered in 1989 with the exploration well P18-02. It consists of four compartments, 2-I, 2-II, 2-III, and 2-IV. Compartment 2-I came on stream first,

in 1993. It contains three production wells: P18-A-01, P18-A-03-S2, P18-A-05-S1, and the exploration well P18-02. Compartment 2-III contains one production well, P18-02-A6, and came on stream in 1997. Compartment 2-II came on stream in 2003, and also contains one production well, P18-A-06-S1. For a while this side track produced from compartment 2-II only. After the whipstock had been perforated in 2005, well P18-A-06 produced simultaneously from the 2-II and 2-III compartments. The P18-4 Field was discovered in 1991 and production started from well P18-A-02 in 1993. The P18-6 Field was discovered in 2003 and production started from well P18-A-07-S1 in 2003.

The P-18 cluster reached peak production in 1998, with a cumulative annual production of 2.2 bcm. At the end of June 2018, the total cumulative production of all P18 fields was 13.5 bcm. According to the updated Winningsplan from 2016, decommissioning of the different fields is expected in 2024. Recovery factors by that time are expected to be 98% for P18-2 and P18-4, and 90% for P18-6.

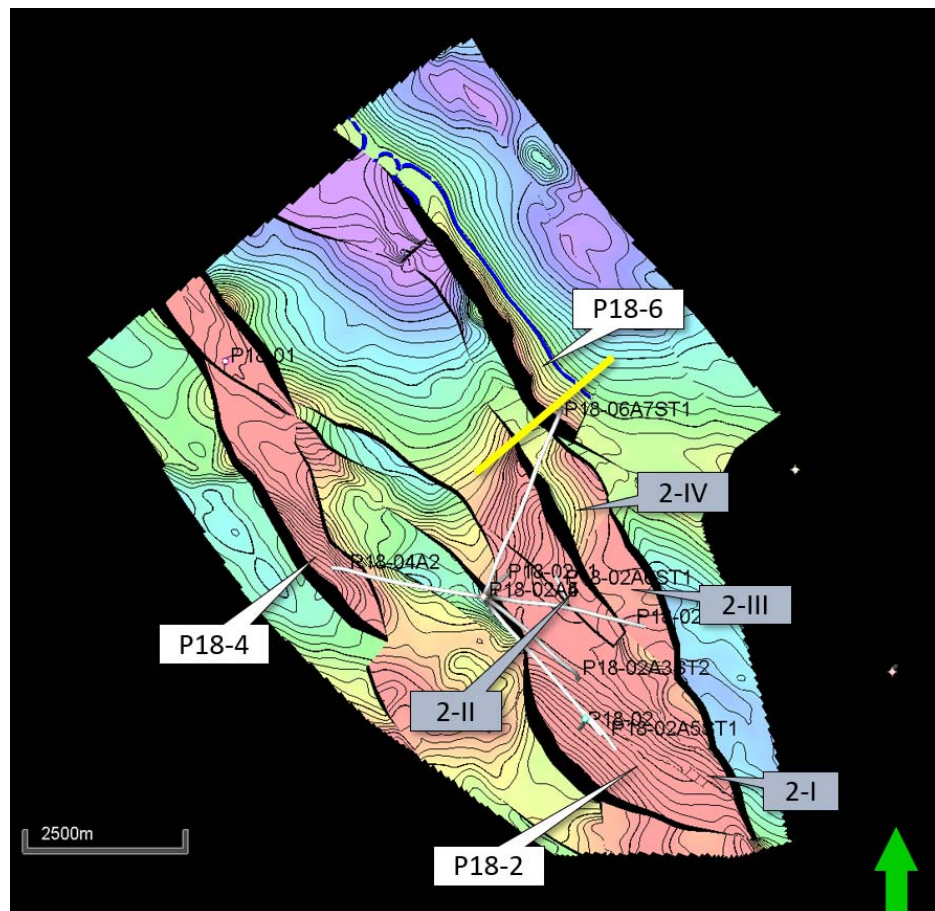


Figure 4-2: Overview of the three P18 fields (P18-2, P18-4, and P18-6), and the compartments of the P18-2 Field (2-I, 2-II, 2-III, and 2-IV). Original gas water contact in P18-6 is indicated by a blue line. Yellow line indicates the position of the cross section shown in Figure 4-3.

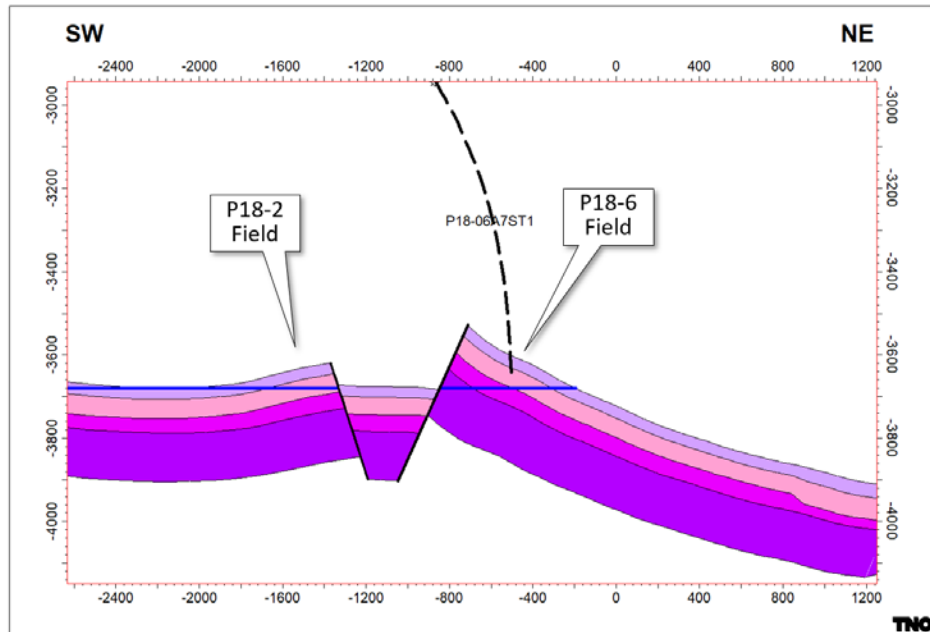


Figure 4-3: Cross section through the P18-6 field with well P18-6-A7 (projected) and a part of the P18-2 field. The various Bunter formations are indicated by different colours, from top to base: Hardegsen, Upper Detfurth, Lower Detfurth, and Volpriehausen Formations. The blue line indicates the original gas water contacts. The location of the cross section is shown in Figure 4-2. Vertical exaggeration is 2x.

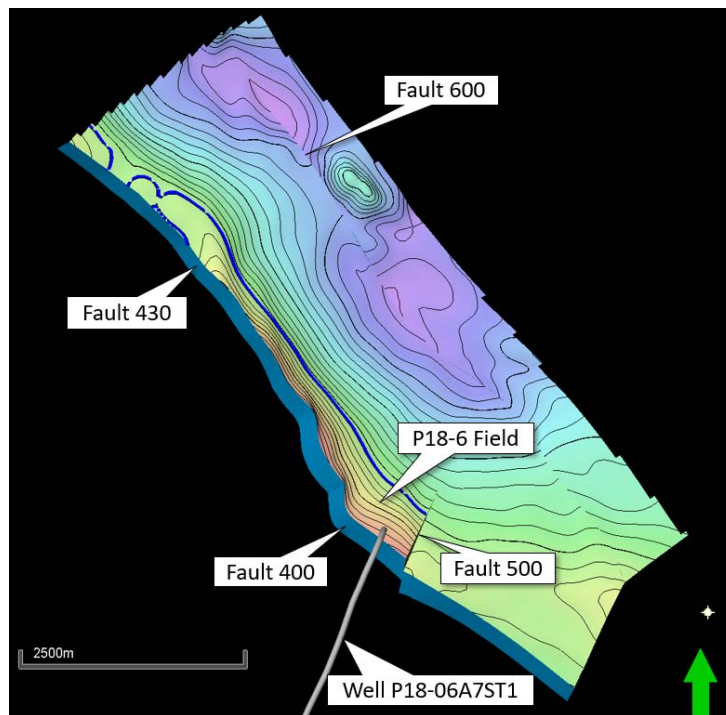


Figure 4-4: Map view of the Top Bunter in the P18-6 area with fault names used in this report.

The structures that contain the reservoirs are bound by a system of NW-SE oriented faults in a horst and graben configuration, with a sinistral strike-slip component. The top of the P18-6 field lies at a depth of 3514 m below sea level and the gas-water contact is at 3680 m below sea level.

The P18-6 Field consists of a NW-SE elongated, tilted fault block. It is bounded to the SW by a large-offset fault and on the SE by a smaller, transverse fault. Both faults are sealing due to juxtaposition of the reservoir zones against impermeable shales of the overlying Upper Triassic and Altena Groups. Figure 4-3 illustrates this for the SW boundary fault.

The reservoir rocks of the P18 fields consist of four sandstone formations that belong to the Lower Germanic Trias Group, informally called Bunter. From top to base these are the Hardegsen, Upper Detfurth, Lower Detfurth and Volpriehausen Formations (Figure 4-5). Each formation has highly variable porosity and permeability values. The Hardegsen Formation has in general the best reservoir properties. Well P18-A-07-S1 has poor reservoir properties, but away from the well reservoir properties must be much better, as testified by the produced gas volume.

### 4.3 Caprock

The seal to the P18 reservoirs is formed by the Upper Germanic Trias Group and the Jurassic Altena Group. The Upper Germanic Trias Group consists of siltstones, claystones, evaporites and dolostones. In well P18-02 it has a thickness of approx. 155 m. Directly above the Upper Germanic Trias Group lies the approx. 500 m thick Altena Group (Figure 4-5), a thick succession of marine claystones, siltstones and marls of Early Jurassic age with excellent sealing quality.

The total thickness of the P18 reservoir's caprock varies between 450 m and 750 m. The seal is excellent, as proven by the fact that it holds a gas column of nearly 600 m in the P18-2 compartment.

The rest of the overburden is formed by several geological formations, some of which can also be assumed to have good sealing properties. The Vlieland Claystone Formation (Figure 4-5) has proven itself as a good seal, as it forms the seal for the oil-bearing Lower Cretaceous sandstones in the West Netherlands Basin. It is considered here as the secondary caprock. Clayey sequences are also abundant in the North Sea Supergroup, especially in the lower part. These could potentially act as secondary seals.

The nomenclature of the caprock as used in the present study is different from the one used in the CATO study of 2011. In the CATO study, the Upper Germanic Trias Group was designated the primary seal, and the Altena Group the secondary seal. In the present study the Altena Group and the Upper Germanic Trias Group are considered to form one seal, since there are no permeable formations in between the two. Therefore, the Upper Germanic Trias Group plus the Altena Group form the primary seal (Figure 4-6), and the Vlieland Claystone Formation the secondary seal.

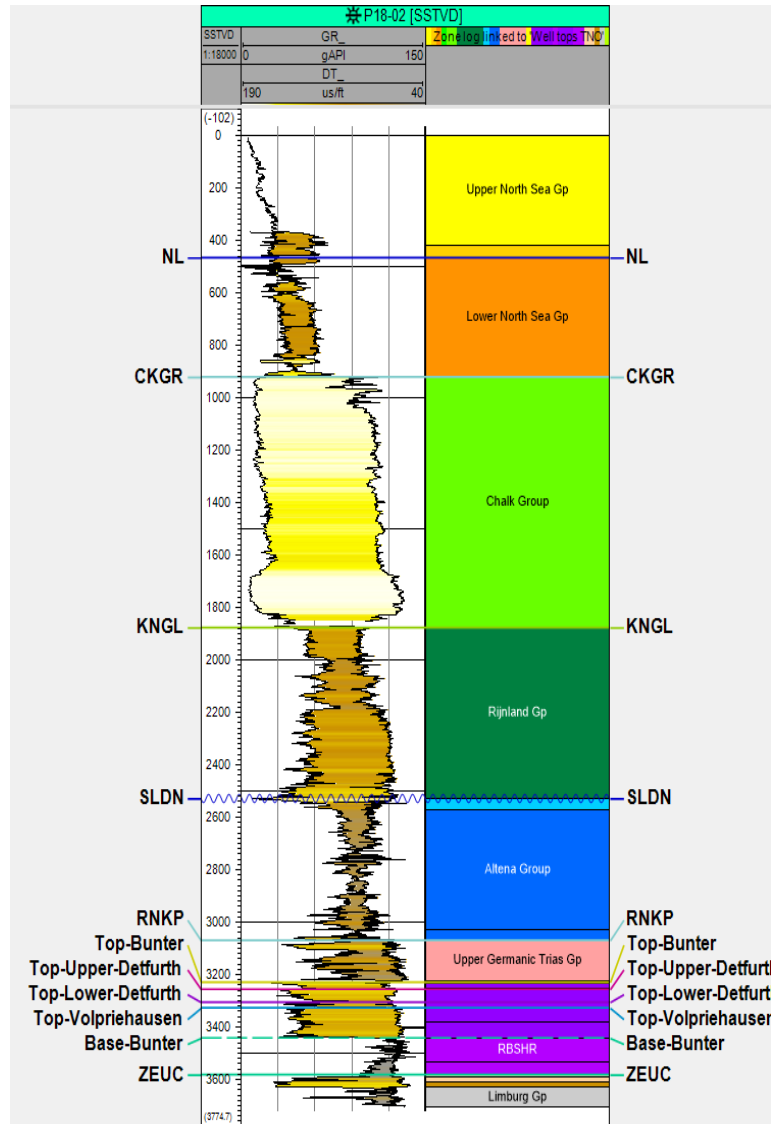


Figure 4-5: Stratigraphy and well logs of the reservoir interval and overburden of the P18 area; well P18-02.

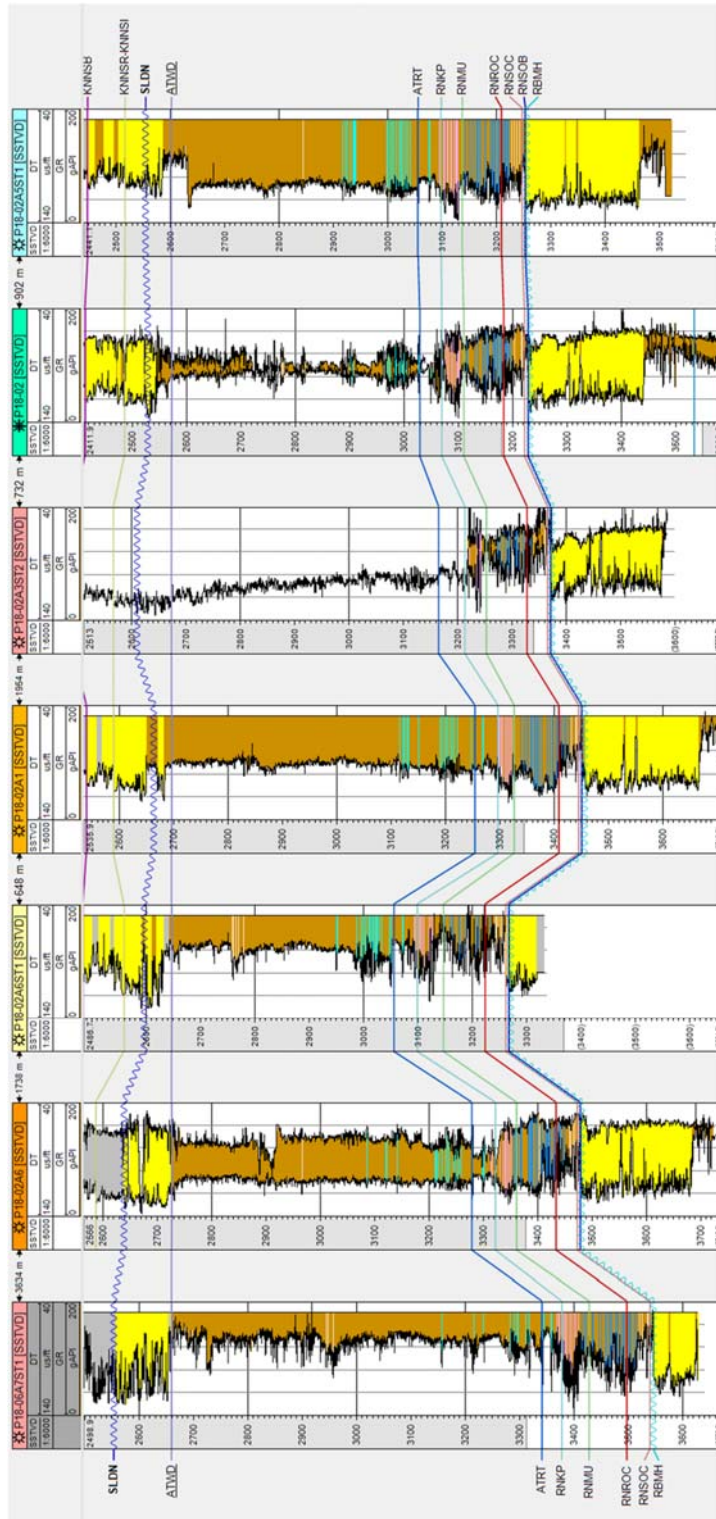


Figure 4-6: Well panel through the P18 wells of the immediate overburden of the Bunter formations showing that the Upper Germanic Trias Group plus the Altena Group form one continuous, primary seal over the entire storage complex.

#### 4.4 Naturally sealing formations

The decommissioning of production platforms and infrastructure in the Southern North Sea has recently begun. A number of studies were initiated to investigate whether parts of the decommissioning process could be done more economically. One of these studies focused on well decommissioning, and specifically on the question whether naturally occurring ductile formations could be utilised to provide economic, self-healing and durable long-term sealing of wellbores. The outcome of the study, essentially based on existing literature, was that in the southern North Sea some formations are indeed suitable for creating effective annular barriers (Fischer et al., 2016; Geel, 2016). The idea is that if at the time of well decommissioning it can be demonstrated that ductile clays or salts are hydraulically isolating the outer annulus and provide zonal isolation, no additional measures need to be taken at that point (as already accepted and practice in Norway and shown by Williams et al. (2009)). Of course, if this sealing behaviour can be demonstrated before CO<sub>2</sub> injection starts, it also reduces the risk of CO<sub>2</sub> leakage outside the well.

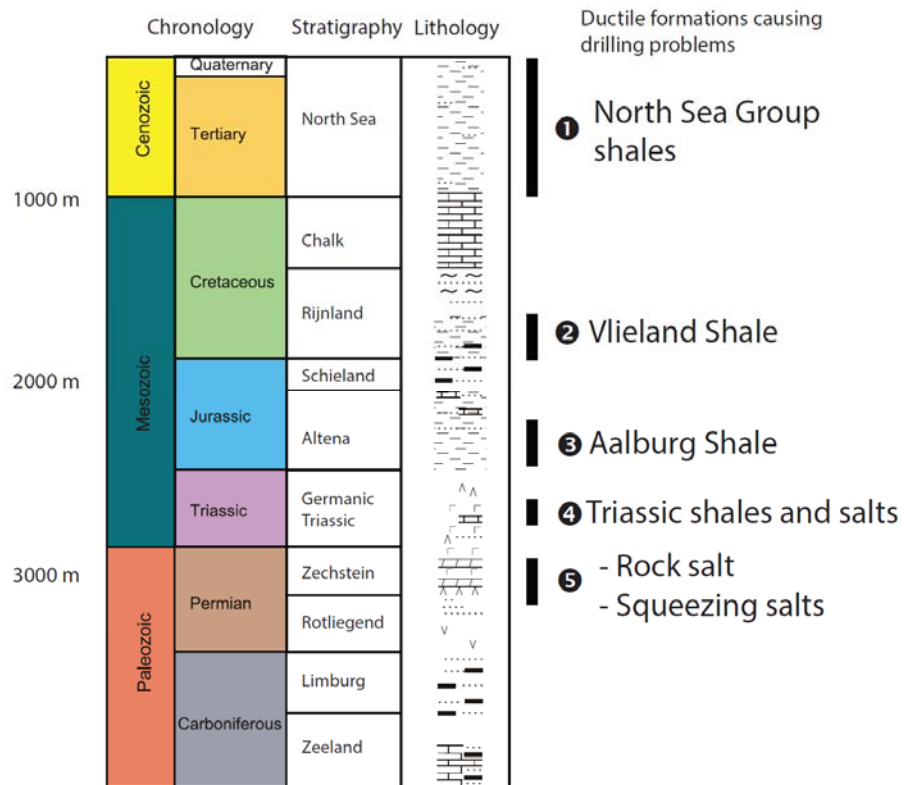


Figure 4-7 Typical stratigraphic column with potential self-sealing formations (Fischer et al, 2016).

The shales from the Lower North Sea Group, The Vlieland Claystone Formation, and the Aalburg Shale were identified as having sufficiently ductile behaviour and swelling potential to create a sufficient seal around the casing (Figure 4-7). In addition, salts and possibly shales from the Upper Germanic Trias Group could have creeping or swelling behaviour.

The fact that all the above mentioned formations occur in the P18 area, it increases the probability that some or all will contribute to sealing the wells in the long term. This is further dealt with in Section 9.



## 5 Injection scenario

### 5.1 Injection wells and well completion

Current plans for CO<sub>2</sub> storage in the P18-2, P18-4 and P18-6 fields are to use up to six injection wells. The P18-4 field has a single well, P18-A-02, which has predicted injection rates in the order of 1 Mt/yr (Vandeweijer et al., 2011). The P18-6 field also has a single well, P18-A-07-S1, but the expected injection rates according to the previous study are significantly lower. This well with a TD of 5066 m is still producing, according to [www.nlog.nl](http://www.nlog.nl) web site (P18-A-07-S1, 15 Oct 2019). Up to four injection wells are expected to come online in the P18-2 field (Neele et al., 2019).

The tubing in the existing well (see section 9 for more details) can be replaced prior to injection, and the optimal tubing size needs to be based on dedicated well dynamics simulations (see, for a dynamic simulation of the P18-2 wells Belfroid, 2019). Such simulations for the P18-6 well need to be performed as part of a future study. For the purpose of the current study, the P18-6 well tubing during injection is assumed to be as it currently is, having mainly an external diameter of 4.5" resulting in an internal diameter of 0.1 m.

### 5.2 CO<sub>2</sub> supply scenarios

The future rate of CO<sub>2</sub> supply, to be delivered by emission sources in the Rotterdam harbour area, was uncertain at the time this study was undertaken. Based on the volumes of the CO<sub>2</sub> currently emitted in the harbour area and the volumes that could be captured at relatively low cost, a 'most likely' CO<sub>2</sub> supply profile was created (Figure 5-1).

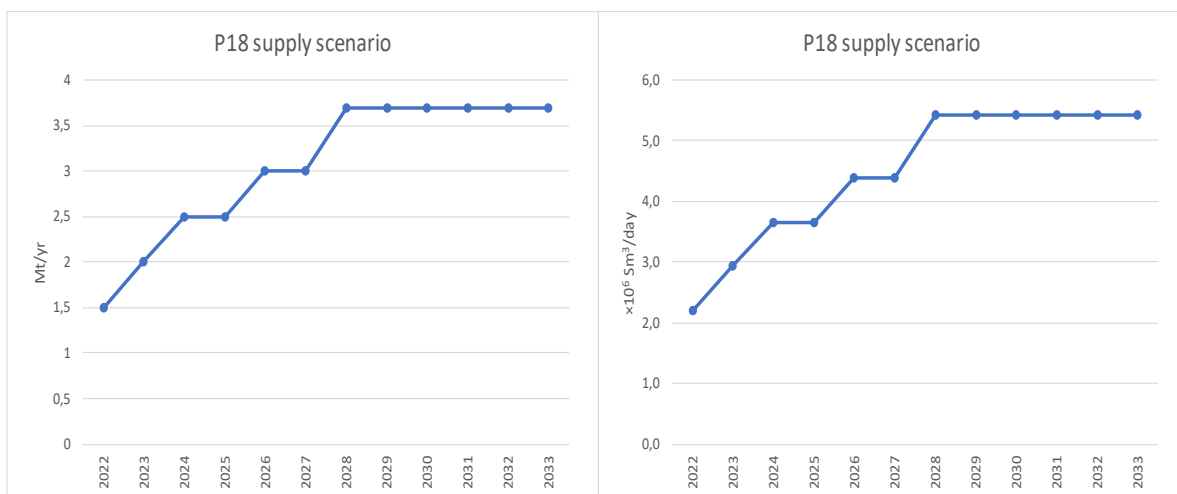


Figure 5-1 Potential future supply scenario for CO<sub>2</sub> from Rotterdam harbour sources. Flow rates increase from 1.5 Mt/yr by 2022 to 3.7 Mt/yr by about 2028 (about  $5.5 \cdot 10^6$  Sm<sup>3</sup>/day). Left: flow rates in Mt/yr; right: flow rates in Sm<sup>3</sup>/day.

### 5.3 Injection of CO<sub>2</sub> in P18-6

Due to the low productivity of the P18-6 field and the limited amount of connected gas, the well P18-A-07-S1 is not planned to be one of the main injection wells. The productivity of the P18-6 field has been relatively low compared to that of the P18-4 and P18-2 fields. The storage feasibility studies of P18-4 (Vandeweyer et al., 2011) and P18-2 (Neele et al., 2019) suggest that the supply profile shown in Figure 5-1 can be accommodated by these two fields. However, a detailed flow assurance study suggests that during the initial phase of injection, when the reservoir pressure in the P18-2 and P18-4 fields is at its lowest level, injection rates during the start-up of a well may be insufficient to store the supplied CO<sub>2</sub> (Belfroid, 2019). The P18-6 field is considered to be used as back-up storage, to be utilised during starting up if the overall injection capacity of the P18-2 and P18-4 wells becomes insufficient.

An alternative scenario for the P18-6 field is related to a start-up after a shut-in of the pipeline. When the transport pipeline to the P18-A platform is shut in, its contents will equilibrate to sea water temperature. During the period of low reservoir pressure in the P18-2 and P18-4 fields, injection of this cold CO<sub>2</sub> is not possible in the P18-2 and P18-4 wells (see Section 6.4). Due to the relatively low injectivity of the P18-6 well (compared to the injectivity of the P18-2 and P18-4 wells), downhole temperature of injected CO<sub>2</sub> is higher. This presents the opportunity of using the well in the P18-6 field for the injection of the contents of the cooled down shut-in pipeline. Once warm CO<sub>2</sub> arrives at the platform (post shut-in), the P18-2 and P18-4 wells can take over.

In both scenarios, the key property of the P18-6 field is the maximum injection rate it can accommodate. This is the driving factor used in the injection scenarios presented in the sections below.

Therefore, CO<sub>2</sub> injection into P18-6 is investigated using the following two scenarios:

1. The storage scenario.  
This scenario is used to determine the storage capacity, injection capacity (i.e., maximum feasible injection rates) and containment in the P18-6 reservoir.
2. The discharge scenario.  
This scenario is only used to estimate downhole conditions of the CO<sub>2</sub>. The aim is to assess the impact on the temperature distribution near the well when injecting CO<sub>2</sub> at a temperature lower than that used in the storage scenario. (Section 6.4.3.2)

### 5.4 CO<sub>2</sub> quality

At the time of the present study, no information was available about the potential sources of CO<sub>2</sub>. Recent work suggests that most available capture technologies can be expected to deliver CO<sub>2</sub> at a purity of 95% or higher (see, e.g., IEAGHG, 2016); sources in the Rotterdam harbour currently deliver CO<sub>2</sub> of more than 99% purity to the OCAP pipeline for use in greenhouses. While impurities alter the behaviour of CO<sub>2</sub> and may affect elements of the CCS chain, the results presented here were derived assuming pure CO<sub>2</sub>.

Figure 5-2 illustrates the effect of impurities on the phase behaviour of CO<sub>2</sub>. While pure CO<sub>2</sub> has a phase *line* that separates vapour conditions from those in which liquid CO<sub>2</sub> occurs (black curve in the figure), the presence of impurities in the CO<sub>2</sub> changes it into a transition zone of pressure and temperature conditions in which the transition from gas to liquid phase occurs. In this transition zone two phases (gas and liquid) are present. Generally, two-phase flow is to be avoided in the handling of CO<sub>2</sub>, e.g. to prevent slugging. Two-phase flow is expected to occur in CO<sub>2</sub> injection wells without causing issues (Belfroid, 2019), but should be avoided in transport pipelines, risers and compressor. The conclusion that can be drawn from Figure 5-2 is that temperature and pressure should be chosen high enough to avoid the two-phase region of the CO<sub>2</sub> mixture being transported.

Impurities have an impact that extends beyond the phase envelope alone – for example, changes in densities will affect the operational window for injection, as well as the storage capacity.

In the current study pure CO<sub>2</sub> was assumed in the simulations.

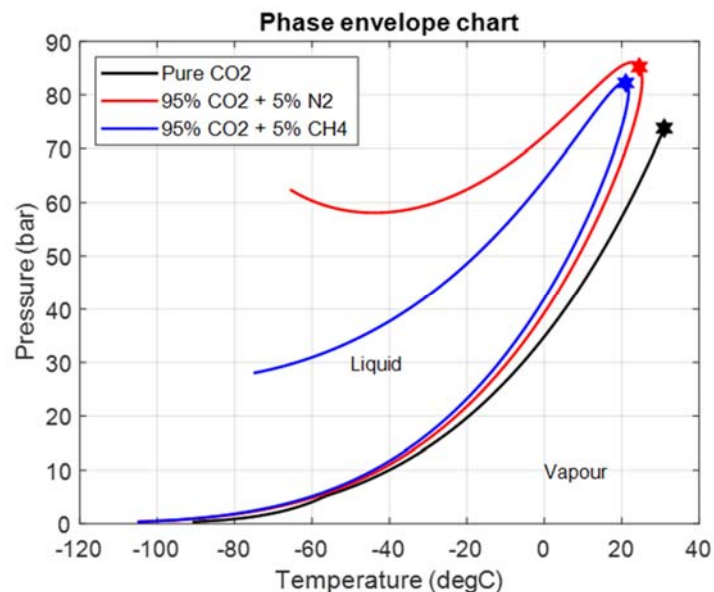


Figure 5-2 Effect of impurities (either 5 wt% N<sub>2</sub> or CH<sub>4</sub>, equal to 7.6 and 12.6 mol% respectively) on the location and shape of the CO<sub>2</sub> phase line. The data was generated using NIST REFPROP v10.

## 5.5 Summary of injection conditions

To summarise, the injection of CO<sub>2</sub> into the P18-6 reservoir is subject to the following conditions.

- The injection simulations are to result in an estimate of the maximum injection rate that the P18-6 reservoir can accommodate at different reservoir pressure levels.
- The tubing in the injection well will be recompleted (pers. comm. EBN, 2019). The external tubing diameter for the injector well is assumed to be 4.5". The actual well completion will be decided on at a later date, following a more

detailed analysis of the operational window of the wells in the P18-2 and P18-4 fields and the required backup capacity of the P18-6 well.

- The CO<sub>2</sub> is assumed to contain no impurities. At the time of the present study, no quality/specification information was available about potential sources of CO<sub>2</sub>.

Additional assumptions apply to the conditions in the reservoir and to the downhole conditions of the CO<sub>2</sub>. These are explained in detail in Section 6.

- At the start of injection, the reservoir pressure is 52 bar; see Section 6.3.
- In the injection simulations, the reservoir pressure will have a maximum that is equal to the initial reservoir pressure; see Section 6.3.
- The maximum downhole pressure is assumed to be equal to the initial pressure in the reservoir, 377 bar; see Section 6.3.
- The minimum downhole temperature of the CO<sub>2</sub> was required to always be above 15 °C, to avoid CO<sub>2</sub> hydrate formation in the well and in the near-well area; see Section 6.4.

## 6 Evaluation of reservoir performance and integrity

### 6.1 Introduction

This section presents the results of an analysis regarding the process of injecting CO<sub>2</sub> into the P18-6 field. The analysis aims to:

- estimate of the storage capacity of the field (Section 6.3),
- establish the flow of CO<sub>2</sub> in the P18-2 field (Section 6.3),
- estimate the pressure and temperature levels in the injection wells and the fields during and after injection (Sections 6.2 and 6.4),
- assess the effects of interaction between CO<sub>2</sub> and the reservoir rock (Section 6.5).

Section 6.2 outlines the set-up and assumptions made for the simulation of the injection process.

The conclusions reached in this section are the following:

- The P18-6 field can store 1.3 Mt of CO<sub>2</sub>, assuming a bottomhole pressure during injection that does not exceed initial pressure (i.e., the pressure prior to production of the natural gas).
- CO<sub>2</sub> fills the pore volume that was previously filled with natural gas and does not spill (i.e. flow laterally beyond the storage complex boundaries).
- The injection process must be managed to ensure that temperature and pressure in the well and in the near-well area remain outside the hydrate formation window.
- The injection of CO<sub>2</sub> will dry out the reservoir and may lead to salt deposition although the overall effect on permeability is expected to be negligible. Drying out of the reservoir reduces the probability of formation of hydrates.
- Chemical interaction between the CO<sub>2</sub> and the reservoir formation is insignificant.

The analysis presented in this section reveals no barriers regarding storage performance and integrity to storage of CO<sub>2</sub> in the P18-6 field.

The results are a starting point for the assessment of fault stability (Section 7) and caprock integrity (Section 8).

### 6.2 CO<sub>2</sub> conditions at bottomhole

The conditions of the CO<sub>2</sub> at bottomhole, inside the wellbore, upon flow into the reservoir, were derived from a flow assurance study performed in parallel to the study presented here. This section gives an overview of how the conditions of the CO<sub>2</sub> at bottomhole (in the wellbore) are determined. These results are used in the analysis of the effect of the low-temperature CO<sub>2</sub> in the reservoir (Section 6.4). The distribution of the cold CO<sub>2</sub> is the starting point for the evaluation of fault stability and caprock integrity due to thermal stresses in Sections 7 and 8.

## 6.2.1 Method

### 6.2.1.1 The simulator

The simulations of downhole CO<sub>2</sub> conditions have been done using OLGA 2017.1.0 simulator with the single component CO<sub>2</sub> module using the pressure-enthalpy methodology. This method is a tabulation format, properties (viscosity, densities etc.) are tabulated with independent variables pressures and enthalpy. All simulations are done in transient mode, with a long enough simulation to reach steady-state conditions (if achievable).

### 6.2.1.2 Boundary conditions

The pressure in the transport pipeline is assumed to be 85 bar or 120 bar, depending on the reservoir pressure.

At mid to high reservoir pressures (40 to 300 bar), the pipeline temperature arriving at the platform is set to 30 °C. The setting is an optimization between cooling power and compressor power.

The following boundary conditions/assumptions are set in the project:

- The pipeline temperature arriving at the platform is set at 30°C.
- The reservoir pressure at the start of injection is 40 bar (which is slightly below the expected minimum reservoir pressure of 52 bar); the maximum reservoir pressure is 377 bar.
- Pipeline operation is preferred to be in single liquid phase condition.
- The downhole temperature (inside the borehole) has a minimum of 15 °C, to avoid hydrate formation, both inside the wellbore (in case of water influx during well shut-in periods), and in the reservoir near the well where expansion of the CO<sub>2</sub> leads to temperature decrease (see Section 6.4).
- The temperature of the topside piping in the well should remain higher than -10°C. Although the tolerance for low temperatures can be improved by using different materials, this limit was assumed to be representative of current facilities.
- Parameters not considered at this stage of the simulations are erosion, tubing vibrations and thermal gradients in the well.

### 6.2.1.3 Model description

The inputs for the model are productivity index, temperature and pressure (PI, T, P), which are based on the Eclipse 300 simulations and shown in Table 6-2. Productivity index or PI is a measure of the ability of a well to produce fluids and is equal to the rate of fluid production divided by the pressure drawdown, all based on measurements at the well.

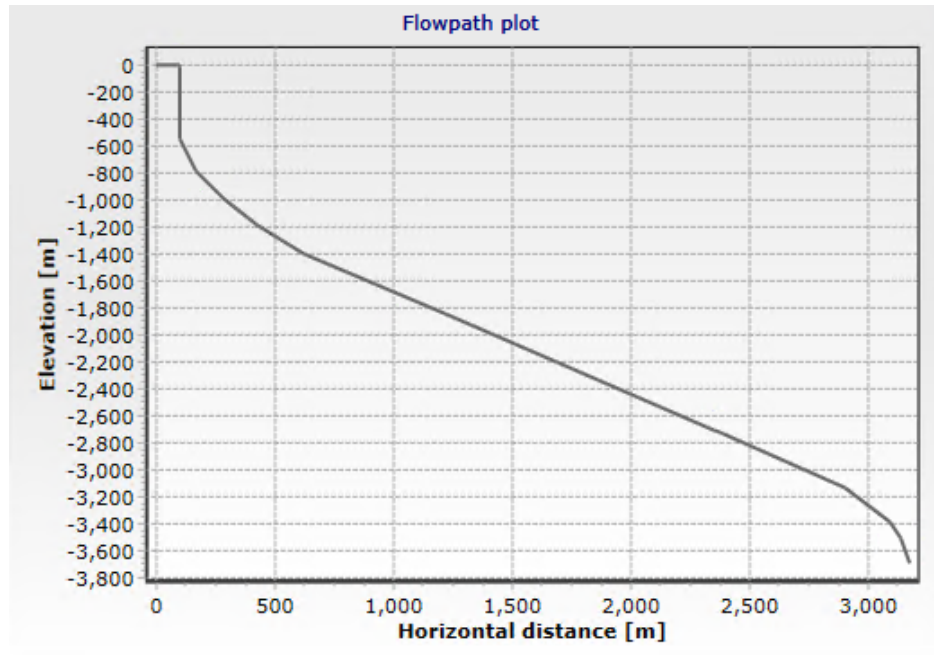


Figure 6-1 Flow path of the well.

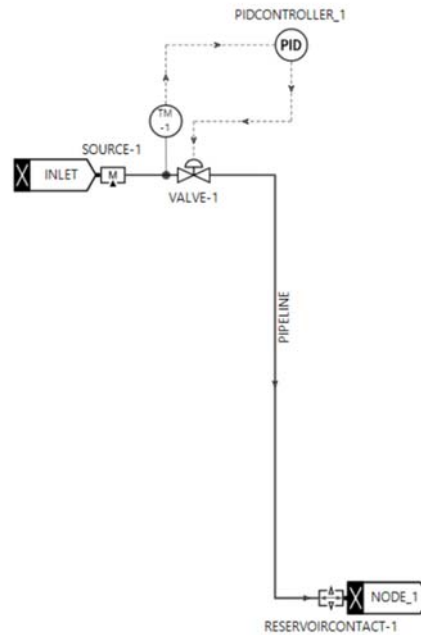


Figure 6-2 Pipeline-well model with control valve.

The model includes 100 m of topside piping (diameter 0.15 m). A mass flow controller is also added to the pipeline. Well inclination is included (Figure 6-2) and as already mentioned a tubing diameter of 0.1 m.

The heat transfer in the well is modelled using a single heat transfer coefficient along the entire well. The heat capacity of the walls is not included, but for steady-state scenarios this produces reliable results. The vertical thermal gradient around the well ranges from 10 °C to 117 °C, with a heat transfer coefficient of 9.5 W/m<sup>2</sup>/K. The pipeline heat transfer coefficient is taken as 6 W/m<sup>2</sup>/K with an ambient temperature (sea water) of 4 °C.

### 6.2.2 Steady-state flow simulations for the storage scenario

The steady-state simulations were conducted for a large range of well characteristics, flow rates, CO<sub>2</sub> temperatures (at the wellhead) and reservoir pressure conditions. The results show that the operational window for the P18-6 reservoir is limited to a maximum injection rate of about 30 kg/s (Table 6-1). At these rates, there is no risk of operational issues or well material degradation.

Pipeline pressure is assumed to be 85 bar and at reservoir pressure above about 200 bar the pipeline pressure is assumed to increase to 120 bar. The temperature of the CO<sub>2</sub> at the wellhead is assumed to be 30 °C.

Table 6-1 shows one feasible injection scenario, in which the mass flow rate is limited to 15 kg/s at the depletion pressure of 40 bar and increases to 20-30 kg/s in the medium to high pressure range (60 to 200 bar). When reservoir pressure approaches initial pressure the injection rate decreases again.

Table 6-1 provides the input for the temperature dependent simulations of injection into the P18-6 reservoir (Section 6.4).

Table 6-1 CO<sub>2</sub> conditions at the platform and downhole for several values of reservoir pressure, for a single well in the storage scenario. Note that the operational pipeline pressure and temperature are 85/120 bar <sup>4</sup> and 30 °C, respectively. PI: productivity index.

Reservoir pressure [bar]	Max mass flow rate [kg/s]	P Pipeline [bar]	P Downhole [bar]	T Pipeline [°C]	T downhole [°C]	PI used [kg/s/Pa]
40	14.5	85	353	30	72.5	4.6·10 <sup>-7</sup>
60	20	85	338	30	69.7	7.14·10 <sup>-7</sup>
100	25.7	85	318	30	68.0	1.17·10 <sup>-6</sup>
200	31.1	120	360	30	62.3	1.94·10 <sup>-6</sup>
300	21.3	120	395	30	65.0	2.12·10 <sup>-6</sup>
350	14.2	120	412	30	68.5	2.26·10 <sup>-6</sup>

### 6.2.3 Steady-state flow simulations for the discharge scenario

The discharge of a 21 km pipeline filled with CO<sub>2</sub> at 10°C results in downhole temperatures in the range of 43°C to 50°C, for a reservoir pressure of 30 bar up to 300 bar. Table 6-2 lists the conditions of the CO<sub>2</sub> at the wellhead and downhole in the pipeline discharge scenario at different reservoir pressures.

<sup>4</sup> 85 bar for reservoir pressure below 200 bar and 120 bar for reservoir pressures above 200 bar.



Table 6-2 CO<sub>2</sub> conditions at platform and downhole for several values of reservoir pressure, for a single well for the discharge scenario. Note that the operational pipeline pressure and temperature are 85 bar and 10 °C, respectively.

Reservoir pressure [bar]	Mass flow rate [kg/s] max	P Pipeline [bar]	T Pipeline [°C]	P Downhole [bar]	T downhole [°C]	PI used [kg/s/Pa]
30	15.5	85	10	396	51.7	$4.20 \cdot 10^{-7}$
40	21.1	85	10	386	47.3	$6.03 \cdot 10^{-7}$
50	24.7	85	10	377	45.3	$7.47 \cdot 10^{-7}$
60	23.2	85	10	383	46.3	$7.14 \cdot 10^{-7}$
100	30.6	85	10	361	43.4	$1.17 \cdot 10^{-6}$
200	31.0	85	10	359	43.2	$1.94 \cdot 10^{-6}$
300	20.3	85	10	391	48.3	$2.12 \cdot 10^{-6}$

#### 6.2.4 Conclusion

- During steady state injection conditions (Table 6-1), the bottomhole conditions of the CO<sub>2</sub> inside the wellbore are typically a temperature of 70 °C at a rate of 20 kg/s. These conditions serve as input for the thermal simulations of injection in the storage scenario.
- During a discharge of the contents of a cooled down pipeline, again a flow rate of 20 kg/s is typical, with a downhole temperature of 43 °C. This applies for reservoir pressures up to about 60 bar.

### 6.3 Reservoir injection performance and risks

#### 6.3.1 Introduction

This section evaluates the storage capacity and the containment within the reservoir of the injected CO<sub>2</sub>. The CO<sub>2</sub> injection into the P18-6 reservoir does not follow the supply scenario shown in Section 5.2, but uses the maximum flow rate that can be injected into the reservoir, as explained in Section 5.3. In these simulations the limitations as evaluated in the flow assurance study (Section 6.2) are not taken into account. In this section, all simulations are done at reservoir temperature (isothermal) and thermal effects are discussed in Section 6.4.

#### 6.3.2 Simulation method

For the simulations in this study a history matched dynamic reservoir model of the P18-6 field is used. (See Section 17.6 for a description of the model and the history match.) The following assumptions were made.

- At the start of injection, the reservoir is depleted to an near-well pressure of 20 bar (shut-in pressure) and 52 bar field average gas pressure of the connected gas (see Section 17.7.7).
- The maximum pressure in the reservoir should not exceed the initial pressure anywhere. Since the reservoir simulation only calculates the grid block average pressure and not the local maximum at the well, this is achieved by setting the maximum bottom hole pressure (BHP) of the well to the initial gas pressure of 377 bar.
- The maximum injection rate is set at 30 kg/s (about 1 Mt/yr), for consistency with the flow assurance results presented in Section 6.2.

- The injection simulation will be conducted isothermally at reservoir temperature (see remarks on the simulator used below).
- It is assumed that the near-well reservoir properties (characterised here by the product of permeability and thickness) as derived from production data and information from logs can be used to simulate the CO<sub>2</sub> injection process.
- No changes occur in the well completion configuration at reservoir level (the relevant factors here are the well diameter and the length of the perforations).
- The saturation curves for gas-water systems are assumed to be the same for CO<sub>2</sub>-water systems.

An additional scenario is run in which the maximum BHP is set to 450 bar. This scenario is used to evaluate CO<sub>2</sub> flow paths and containment in case of overfilling the reservoir.

All simulations were performed with the Eclipse 300 reservoir simulator, a state-of-the-art compositional model that can handle the behaviour of CO<sub>2</sub> in the reservoir (including phase transitions) and the interactions between CO<sub>2</sub> and residual gas; see also Section 17.6.1. CO<sub>2</sub> dissolution into the water phase is not taken into account. The reason for ignoring dissolution is that due to the assumption of equilibrium within a grid block, the amount of CO<sub>2</sub> dissolution is considerably overestimated at field scale (Zang, 2013). Evaporation of water into the gas phase is not handled.

Eclipse 300 cannot handle non-isothermal conditions for CO<sub>2</sub> injection. This means that in all results presented in this section the CO<sub>2</sub> is injected at reservoir temperature, even though the temperature of the CO<sub>2</sub> is likely to be significantly lower (see Section 6.2). The TOUGH2 simulator was used to run non-isothermal injection scenarios for the evaluation of fault stability (Section 7.3) and caprock integrity (Section 8.3). See Section 6.4 for the description of the thermal simulations.

### 6.3.3 Simulation results

The total amount of CO<sub>2</sub> that can be stored in P18-6 for a BHP of 377 bar (initial pressure; field average gas pressure is 379 bar) and injection period of 5.5 years is 1.3 Mt, assuming that before the start of injection the near-well pressure is depleted to 20 bar (shut-in pressure), with field average gas pressure of the connected gas at 52 bar. See Section 17.7.7 for a description of the simulation of the final depletion stage.

Figure 6-3 below shows the injection rate and cumulative mass of CO<sub>2</sub> injected over time. The initial injection rate of 30 kg/s is maintained for approximately three months (for injection at reservoir temperature) and subsequently decreases due to a rapid rise in near well reservoir pressure (Figure 6-4). Figure 6-4 shows the corresponding pressures: BHP, near well pressure and field average gas pressure of the connected gas (i.e. in Hardegsen and Upper-Detfurth) over the injection period. The average field pressure differs from the near-well pressure due to the presence of 'slow' gas, i.e. gas that is available in low permeability deposits and/or behind flow barriers. The near-well pressure shows the typical pressure behaviour also observed during production, namely a fast initial increase and then a slow tail.

The injection is conducted over a period of 5.5 years. Table 6-3 presents the amount stored at yearly intervals. At the end of the simulated injection period the injection rate has dropped to 1.5 kg/s (less than 50 kt/yr). More than half of the injection is completed during the first year.

Table 6-3. Overview of the amount CO<sub>2</sub> stored and the injection rate at the end of each year.

	Amount CO <sub>2</sub> stored [Mt]	CO <sub>2</sub> injection rate [kg/s]	Average connected gas pressure [bar]
After 1 year of injection	0.7	10.7	207
After 2 years of injection	0.9	5.2	256
After 3 years of injection	1.0	3.6	284
Final (after 5.5 years)	1.3	1.5	331

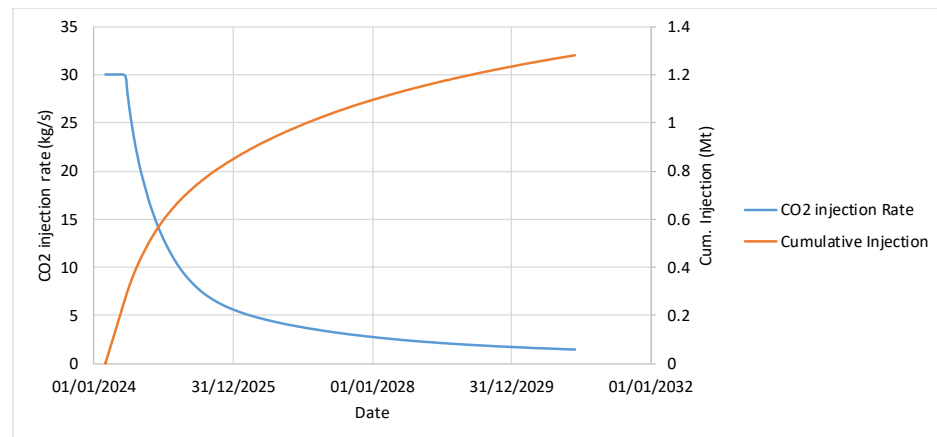


Figure 6-3: Injection rate and cumulative CO<sub>2</sub> mass injected for well P18-06-A7 for a BHP constraint set to 377 bar.

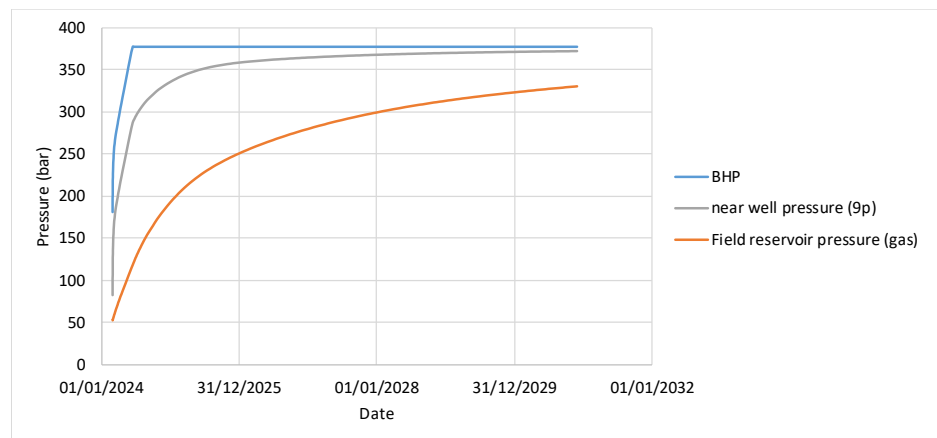


Figure 6-4: BHP, near well reservoir pressure and field average gas pressure during injection.

6.3.4 Pressure, gas and CO<sub>2</sub> behaviour in the reservoir

Figure 6-5, Figure 6-6 and Figure 6-7 show maps of pressure, gas saturation and CO<sub>2</sub> molar density, respectively. Due to the setup of the model, sharp boundaries occur in the model. Section 17.6 gives a detailed description of the model.

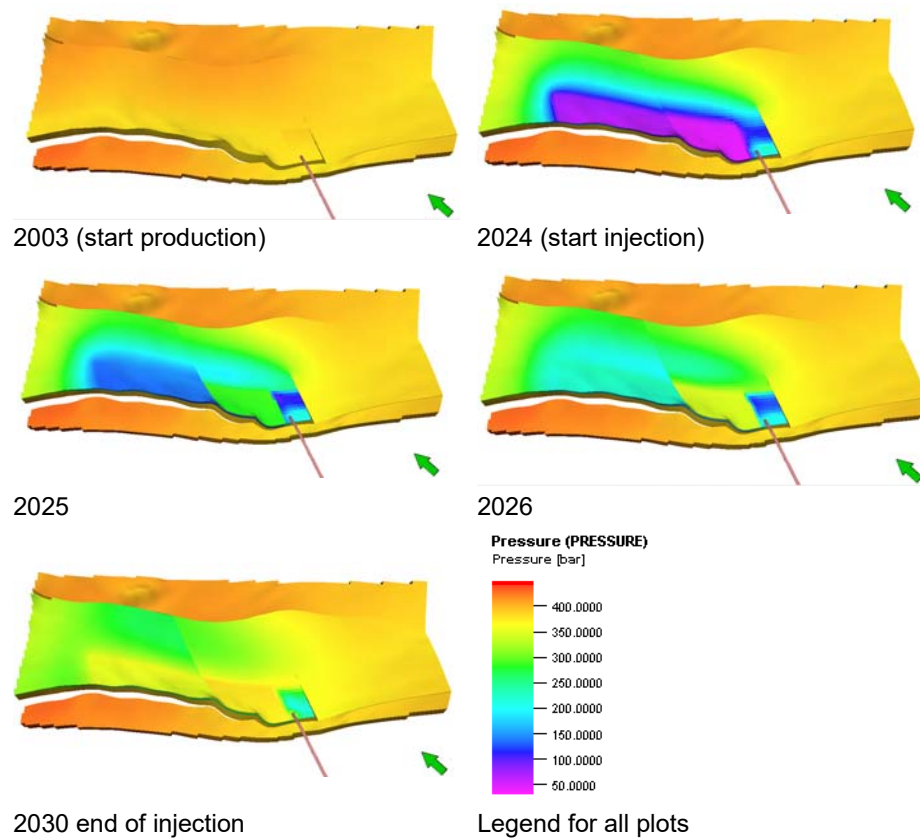


Figure 6-5: Pressure map at different stages of injection into the P18-6 reservoir. The orange line at the bottom of each map represents the well trajectory.

From the history match it was clear that mobility in the aquifer must be limited in order to avoid water production in the well (which is not observed). This is reflected in the pressure behaviour (Figure 6-5), which shows a delayed response in the aquifer: the pressure in the aquifer at the end of injection (in 2030) has hardly increased yet as a result of the injection. In the southern part of the aquifer, pressure has not changed much at all. In the pressure in 2025, the impact of a flow barrier in the gas field which was required to achieve a history match is clearly visible. The field average pressure in the gas filled area of Hardegsen and Upper-Defurth is 52 bar at the start of injection (2024).

In Figure 6-6, it can be seen that the gas saturation in the near well area is lower (i.e. the water saturation is higher) than in the rest of the gas field. This is the result of the poor reservoir flow properties in the near well area. Some water encroachment is visible at the start of injection. The gas distribution at the top of the reservoir at the end of injection is almost the same as the distribution at the start of production.

In Figure 6-7, the CO<sub>2</sub> distribution in the highest permeability layer is shown using the CO<sub>2</sub> molar density. The CO<sub>2</sub> molar density is a measure for the CO<sub>2</sub> gas saturation. Using the molar density gives the opportunity to distinguish between the different fluid components in the P18-6 reservoir. In this high permeable layer, the CO<sub>2</sub> has the widest distribution. A potential spill point in this area is at the end of the small-offset fault near the well that forms the south-eastern limit of the gas-filled

reservoir. Near this fault, the CO<sub>2</sub> migrates to below the original gas-water contact near the well in a downdipping area of the reservoir. However this CO<sub>2</sub> does not move far (even in case of overfilling, see also Figure 6-8) and will migrate back up the slope when injection is stopped. In the north-west corner of the reservoir where there is a spill point, the CO<sub>2</sub> does not move beyond the original gas-water contact.

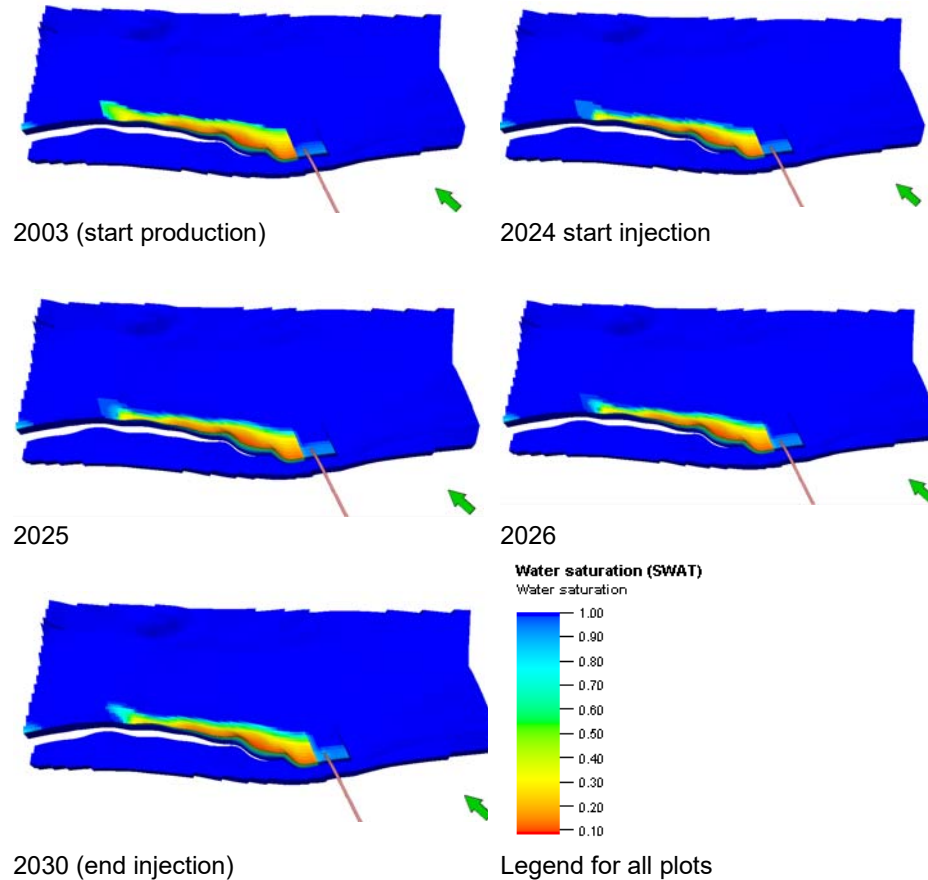


Figure 6-6: Water saturation map at different stages of injection into P18-6. The orange line at the bottom of each map represents the well trajectory.

To investigate the flow paths of the CO<sub>2</sub> further, the CO<sub>2</sub> injection was also done with a maximum BHP of 450 bar to increase the amount of CO<sub>2</sub> injected. Now in total 1.52 Mt CO<sub>2</sub> was injected resulting in a final average reservoir pressure of 389 bar. Figure 6-8 shows the distribution of the CO<sub>2</sub> at the end of injection. The insert shows that even in this case of overfilling the CO<sub>2</sub> does not move beyond the small fault next to the well. Thus once injection is stopped, the CO<sub>2</sub> will move back up the slope into the original gas field. In Figure 6-9, the initial and final gas saturation at the spill point in the north-west is shown. Also here CO<sub>2</sub> does not move beyond the original contact.

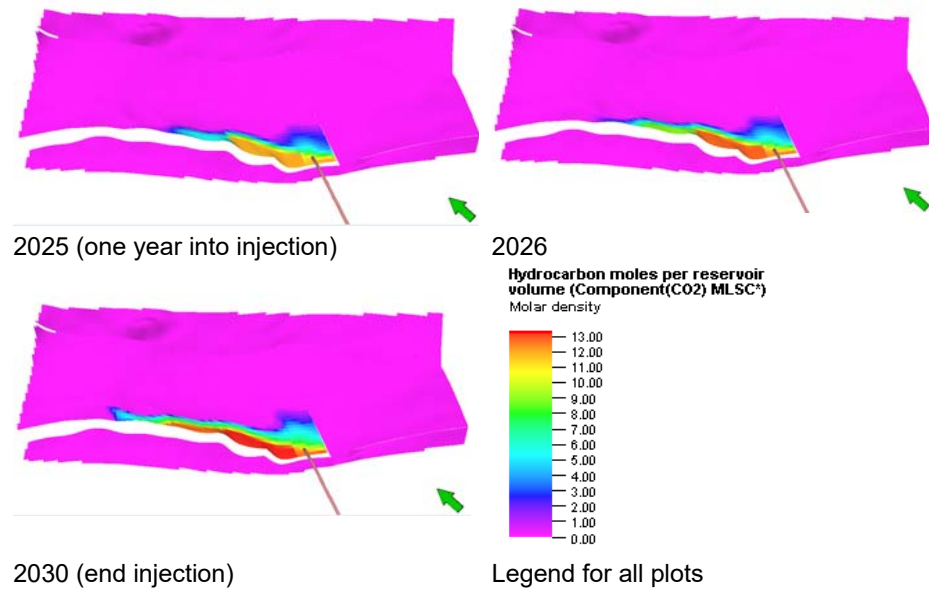


Figure 6-7: CO<sub>2</sub> molar density (kmole/m<sup>3</sup>) map at different stages of injection into P18-6 in the highest permeability layer (layer 11). CO<sub>2</sub> migrates beyond the original gas-water contact (compare panels in this figure with the first panel in Figure 6-6).

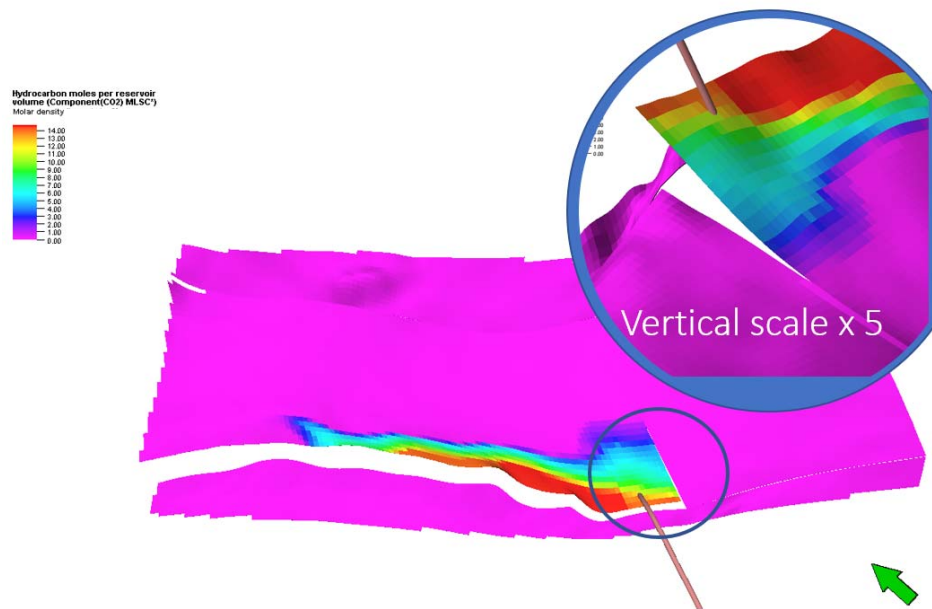


Figure 6-8: CO<sub>2</sub> molar density (kmole/m<sup>3</sup>)<sup>5</sup> in the highest permeability layer (layer 11), after overfilling the P18-6 reservoir (1.52 Mton injected and average gas pressure is 389 bar). CO<sub>2</sub> migrates beyond the original gas-water contact (compare panels in this figure with the first panel in Figure 6-6), but does not reach the end of the near-well fault.

<sup>5</sup> Molar Density represents the number of moles of a molecule present in a unit of volume, common units are mole/m<sup>3</sup> or kmole/m<sup>3</sup>

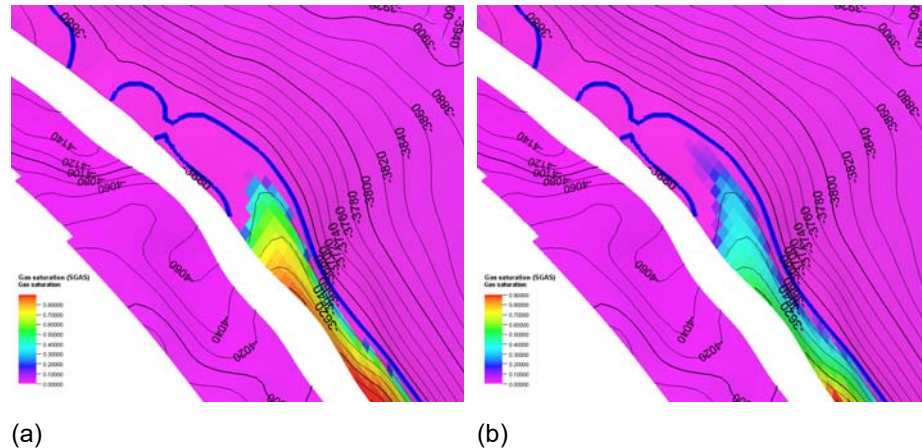


Figure 6-9: (a) Initial gas saturation and (b) gas saturation after overfilling the P18-6 reservoir (1.52 Mton injected and average gas pressure is 389 bar) in the highest-permeability layer (layer 11). The bold blue line indicates the free water level. Contours indicate depth (TVDSS).

### 6.3.5 Discussion on sources of uncertainty

Both the injection rate and total amount injected are sensitive to choices made in the history match and the final depletion phase. In the history match, a multiplier of two on the well productivity was applied to match the final production phase. No transmissibility or skin estimate are available from well tests, resulting in uncertainty in the productivity of the well. The injectivity is thus also uncertain, even when the impact of the low temperature injection is not taken into account.

For the total amount of CO<sub>2</sub> that can be stored, several factors are important: the uncertain well injectivity, the choices for the final depletion phase and the duration of the injection period. The choices for the final depletion phase determine how far the reservoir is depleted before the start of injection. In general, the more depleted the reservoir, the more CO<sub>2</sub> can be stored. Due to the low permeability of the field, both the depletion phase and the injection can take a long time. Since for neither of these phase stopping criteria are available, final values of the CO<sub>2</sub> storage capacity may differ from the estimates presented here. Also intermittent production or injection has not been included in the current analysis, because the impact on storage capacity is expected to be minor.

Also not included in the current simulation is the impact of a shut-in period at the end of depletion before the start of injection. See Section 17.7.7 for a description of the simulation of the final depletion stage. Due to the nature of the field with slow gas and some aquifer drive, pressure will increase during shut-in. In Table 6-4, the impact of a shut-in period is shown for the final production phase. The history match period runs up to 15 May 2019, when total production was 696 Msm<sup>3</sup>. In Table 6-4 the pressure is listed for shut-in periods of 15 days and 1 year for one and two additional years of production and for the end of the simulated production period (five years to 1 April 2024). Figure 6-10 shows the development of the pressure during the last production phase (two more years of production after the end of the history match at 15 May 2019) and during a shut-in. Slow aquifer support causes gradually increasing pressure (curve 'field average p') in the figure.

Table 6-4. Increase in near well gas pressure (9-point average, at well datum) after shut-in of the well for different stages of depletion.

	Total produced volume [M sm <sup>3</sup> ]	Pressure after 15 days of shut-in [bar]	Pressure after 1 year of shut-in [bar]
After 1 additional year of production	717	32.5	47.7
After 2 additional years of production	732	26.0	39.4
Final (5 years to 1 April 2024)	756	20.4	29.7

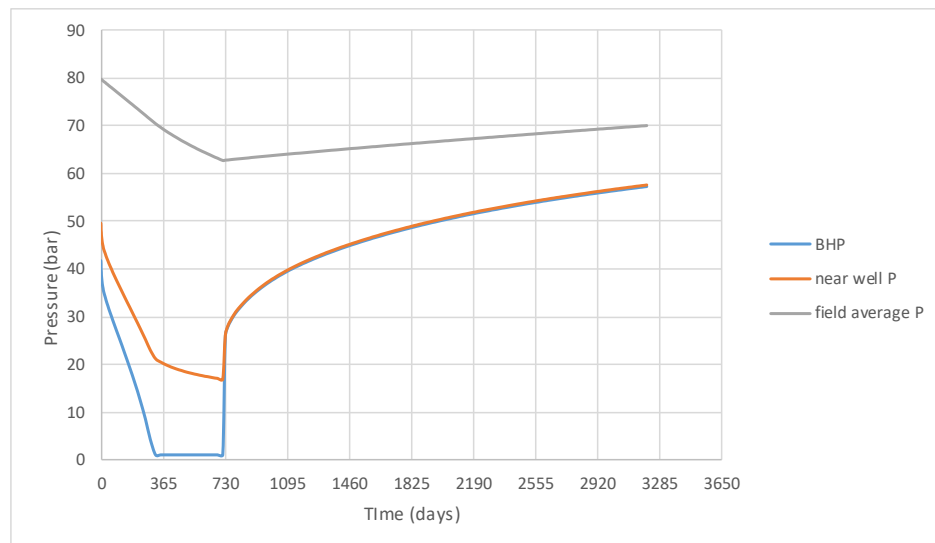


Figure 6-10. Development of the pressure (BHP, near well pressure and field average gas pressure of the connected gas) in case of shut-in after two additional years of production.

### 6.3.6 Pressure communication with P18-2

Vandeweyer et al. (2011) state, on the potential communication between P18-2 and P18-6: "Reservoir P18-06 is located to the northeast of P18-2 reservoir. It is bounded by faults F13 and F57, of which only F13 has enough offset to be sealing by juxtaposition". This suggests potential communication between P18-6 and Compartment II / Compartment IV of P18-2. An overview is given in Figure 6-11 and Figure 6-12.

A closer look shows that P18-6 is disconnected from P18-2 by two faults, of which P18-6's boundary fault Fault 400 / 430 is the most important one. In between the faults a small graben is filled by overlying shale. The only contact is by Volpriehausen juxtaposition, which has a low permeability (lower than 1 mD).



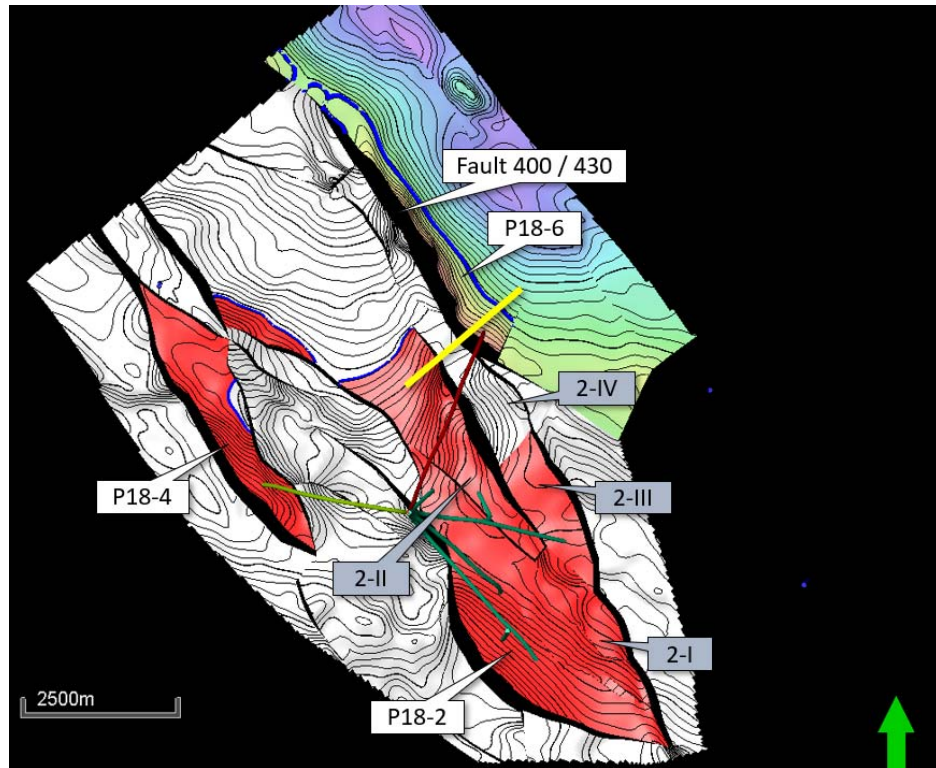


Figure 6-11: Map view of the fault between P18-2 and P18-6.

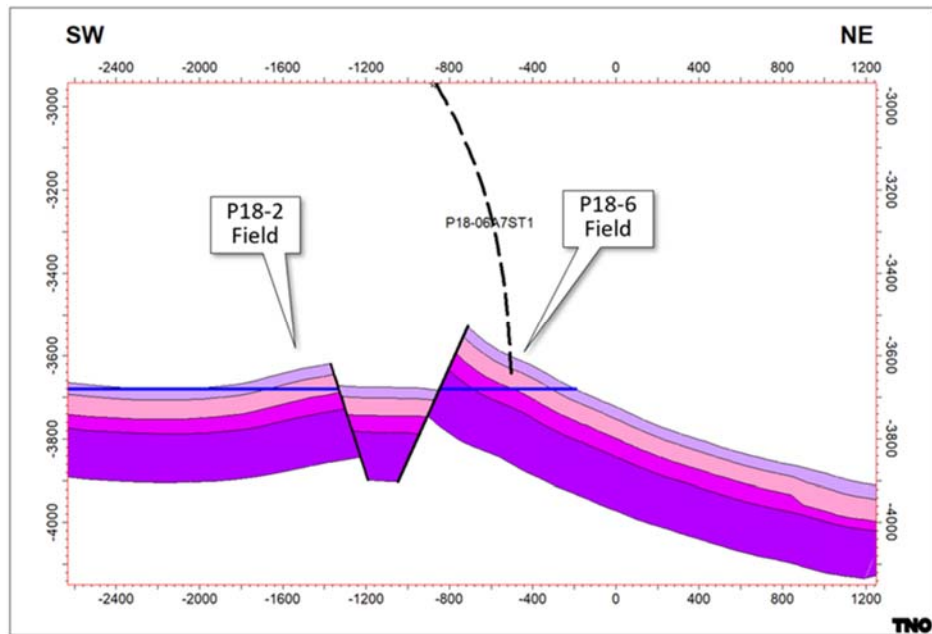


Figure 6-12: Cross section showing fault between P18-2 and P18-6.

The first pressure value from P18-6 was recorded in the end-of-well report (EOWR), available on nlog.nl; a pressure of 378 bar was inferred, in February 2003.

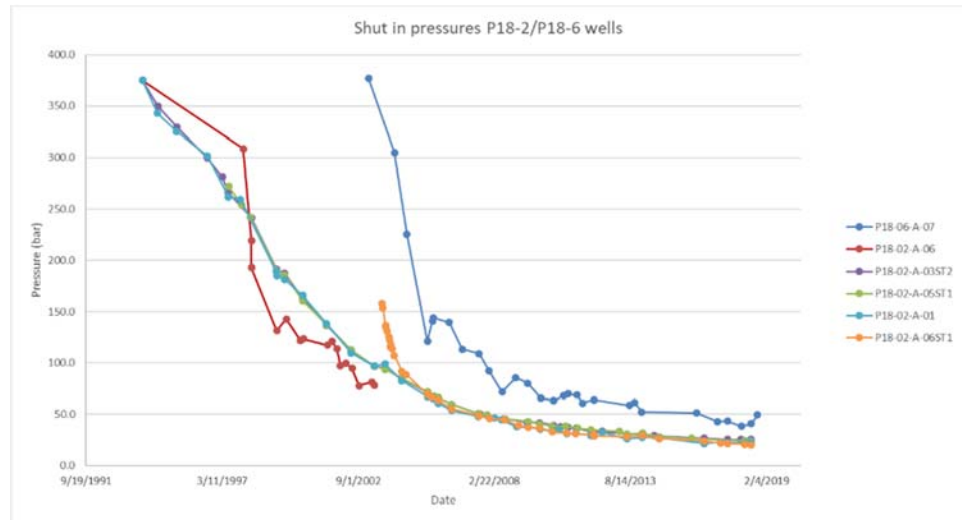


Figure 6-13: Pressure behaviour of P18-2 and P18-6 reservoirs.

The pressure data in Figure 6-13 show that after about 10 years of production from P18-2, the initial pressure found in the P18-6 reservoir was still about 275 bar higher than that in the P18-2 field. This strongly suggests that these two compartments are not in pressure communication.

In addition, during the last years of production the pressure behaviour of the main compartment (Compartment I) of P18-2 is different from that of P18-6 (see Figure 6-13), which suggests that there is no pressure communication between the two reservoirs on production time scale. However, on a geological time scale we cannot exclude pressure communication between both compartments.

### 6.3.7 Conclusions

The injection simulations lead to the following conclusions.

**Storage capacity.** The storage capacity of the P18-6 field is 1.3 Mt of CO<sub>2</sub>, assuming a maximum bottomhole pressure during injection that is equal to the initial pressure (the pressure prior to production of the natural gas).

**Containment.** CO<sub>2</sub> fills the pore volume that was previously filled with natural gas. Only in a small part of the reservoir, the CO<sub>2</sub> moves down-dip below the original gas-water contact. Even when the reservoir is overfilled, i.e., when the average reservoir pressure increases beyond the initial pressure, the CO<sub>2</sub> does not move far and will move back up the slope when injection is stopped. In the north-west corner of the reservoir where a spill point is, the CO<sub>2</sub> does not move beyond the original gas-water contact. Thus, the conclusion is that the reservoir contains the injected CO<sub>2</sub>, without risk of spilling.

## 6.4 Reservoir behaviour: temperature effect

### 6.4.1 Introduction

The simulations presented in the previous section do not take into account the temperature difference between the injected CO<sub>2</sub> and the reservoir, or the evolution of the CO<sub>2</sub> temperature in the reservoir. Water evaporation and the associated

temperature effect was also not taken into account in the previously presented results. The injection scenarios presented in Section 5.2 show that CO<sub>2</sub> is to be injected at a temperature well below that of the reservoir, due to pipeline transport and well operational constraints. The evolution of the temperature field within the reservoir is a key modelling result and input for the geomechanical analysis of temperature induced stress within the storage reservoir.

One of the issues with depleted gas fields in general is the relatively low pressure at the onset of injection. In combination with the low bottomhole temperature of the CO<sub>2</sub>, additional expansion (and, hence, cooling) in the near-well zone could lead to the CO<sub>2</sub> entering into the hydrate formation window, potentially reducing injectivity or even preventing further CO<sub>2</sub> injection completely.

However, hydrate formation is not expected since the injection temperature at the bottomhole (inside the wellbore) is around 70°C (Table 6-1). Furthermore, the quality of the P18-6 field is relatively poor compared to the P18-2 field and the expected abandonment pressure is relatively high (about 40 to 60 bar). As a consequence the Joule Thomson coefficient is relatively small, which results in relatively small cooling effect in the reservoir.

In his chapter two injections scenarios are modelled with a focus on the temperature effects: the storage scenario (Section 6.4.3.1) and the discharge scenario described in Section 6.4.3.2.

The next subsections describe the simulator, the P18-6 model and the results of two injection scenarios.

## 6.4.2 *Method*

### 6.4.2.1 *TOUGH2 simulator*

The TOUGH2 simulator is used in combination with the ECO2MG module (Pruess, 2011; Loeve et al., 2014). The ECO2MG module is designed to model the behaviour of CO<sub>2</sub> in the presence of brine in both gas reservoirs and aquifers, including estimates of the dry out zone around the injection well where possible salt precipitation may occur. A key feature of the ECO2MG module is that it takes into consideration the transition from low to high pressure across the CO<sub>2</sub> saturation line, which is an important process in the injection of CO<sub>2</sub> into a depleted gas field.

### 6.4.2.2 *P18-6 model*

A 26-layer radially symmetric model was created (Figure 6-14) that covers the different geological formations to analyse the temperature and pressure field over time. The radial direction has 47 cells, which increase exponentially in size away from the well into the reservoir from 0.15 m to 137 m. The grid cell distribution is dense close to the well (left side of Figure 6-15) and also more dense on the interface with the Hardegsen and the caprock to allow a detailed modelling around this interface. The average porosity and permeability of the eclipse model is used in the TOUGH2 model (Table 6-5). The values are based on the history matched Eclipse model described in section 17.7.

Other parameters which are important for the temperature distribution and heat flow in the P18-6 reservoir are the heat conductivity of each formation (2.0 W/m/°C for all formations) and the rock grain specific heat (1000 J/kg/°C for all formations).

Table 6-5: P18-6 properties used in the radial symmetric model used for the modelling of the temperature field within the P18-6 reservoir.

Formation	Near Well area		Far well Area	
	Average Porosity	Average Permeability (mD)	Average Porosity	Average Permeability (mD)
Caprock	0.01	0.001	0.01	0.01
Hardegsen	0.023	0.01	0.09	24
Hardegsen-High Perm	0.09	29.6	0.2	550
Upper Detfurth	0.015	0.002	0.075	12.6
Lower Detfurth	0.015	0.002	0.075	0.29

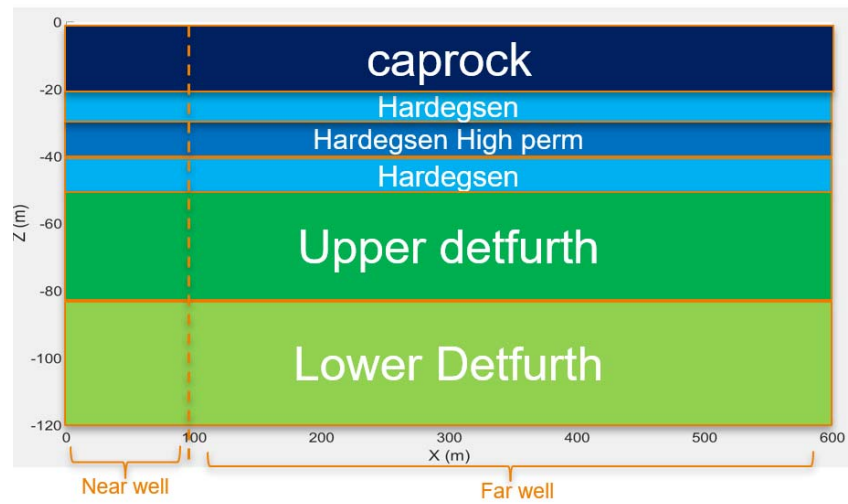


Figure 6-14: Radially symmetric model used for the modelling of the temperature field within the P18-6 reservoir.

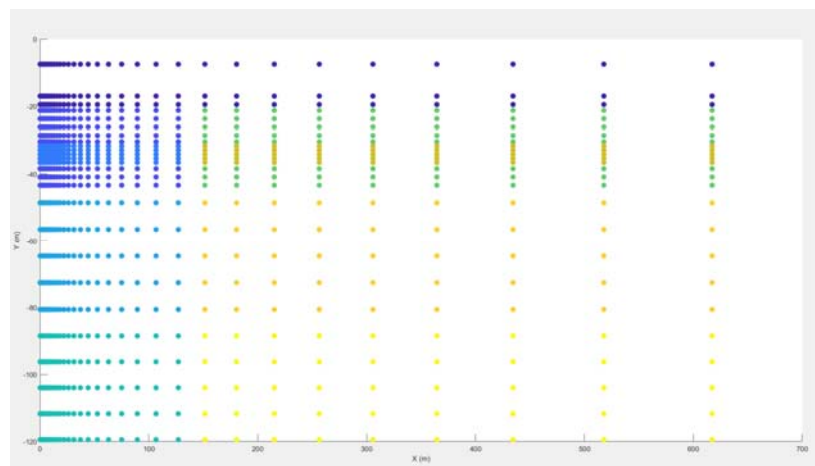


Figure 6-15: Grid cell distribution of P18-6 radially symmetric model; see also Figure 6-14.

The initial reservoir conditions used for the storage scenario are:

- Reservoir pressure 50 bar;
- Reservoir temperature 100 °C;
- Injection temperature 70 °C;
- Injection duration 5 years;
- Constant injection rate of 20 kg/s;
- Initial brine saturation varies according saturation height function shown in (Section 17: equation (17-1)).

The initial reservoir pressure of 50 bar is based on the abandonment pressure of about 52 bar in the Eclipse model (average pressure of the connected gas), see also the discussion in Section 6.3.3.

The reservoir temperature in reality is 117 °C, but the TOUGH2 simulator is limited to a maximum temperature of 103 °C; therefore a reservoir temperature of 100 °C is used in the simulations.

The injection temperature of 70 °C and injection rate is based on the flow assurance simulations (Section 6.2). The injection rate of 0.63 Mt/yr corresponds to constant injection rate of 20 kg/s.

Since the reservoir simulations (see section 6.3.3) showed that most of the CO<sub>2</sub> migrates into the high-permeability part of the Hardegsen Fm upon injection and almost none migrates into the Hardegsen Fm Upper and Lower Detfurth Fm, the injection rates in the thermal simulations were distributed only in the high-permeability layers of the Hardegsen Formation.

### 6.4.3 Results

#### 6.4.3.1 The storage scenario

The temperature distribution and profiles from the modelling for the storage scenario are presented in Figure 6-16 to Figure 6-19. The CO<sub>2</sub> is injected in the high-permeability Hardegsen Fm. The cold zone is demonstrated to be progressing up to 200-250 m into the reservoir in Figure 6-16. In the vertical direction the temperate front is extending symmetrically around the injection area. After four years of injection a few degrees cooling is observed 20m above the bottom of the caprock (Figure 6-17). Just below the caprock a maximum cooling of 15 °C is observed (Figure 6-18). These effects are caused by thermal conductivity of the rock, since almost all CO<sub>2</sub> is in the high-permeability Hardegsen Formation. The Joule-Thomson effect and cooling due to the evaporation of water is only present in the high-permeability Hardegsen Formation (Figure 6-19); the injected CO<sub>2</sub> of 70°C cools down to just below 55°C. The temperatures in the model shows no risk of hydrate formation.

The distance of the fault in P18-6 to the injection well P18-A-7-S1 is 100m. The temperature change at the fault and associated stress changes (see section 7.3 and 7.5) becomes noticeable about 70 days after the start of injection (Figure 6-20). The temperature contrast at the low-temperature front is 30 °C in the TOUGH2 simulations and taking into account that the reservoir temperature is

17 °C higher than can be represented in the TOUGH2 model, the actual temperature contrast at the low-temperature front is close to 50 °C.

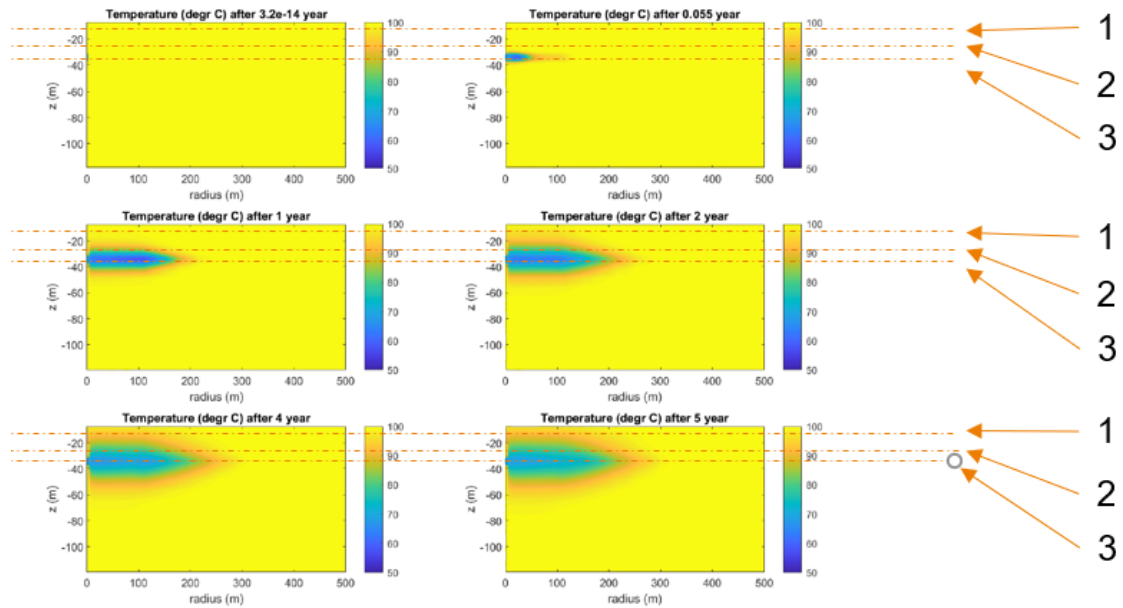


Figure 6-16: Temperature distribution in the P18-6 radially symmetric model for the storage scenario. The numbers indicate three vertical levels in the model: level 1 is 20 m above caprock/Hardegren interface, level 2 is 2.5 m below caprock/Hardegren interface and level 3 is 60 m below caprock/Hardegren interface. 0.055 years is 20 days.

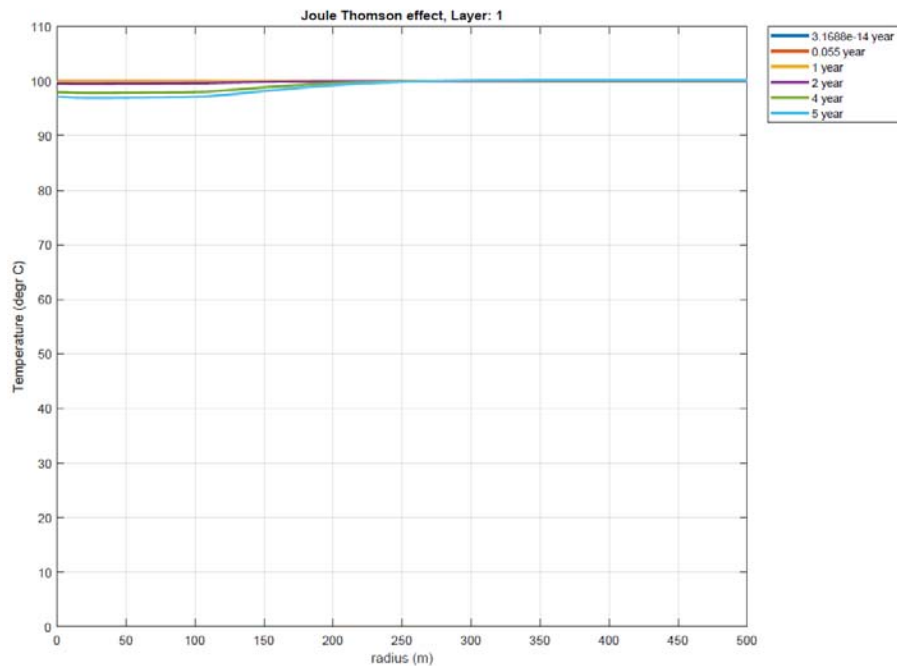


Figure 6-17: Temperature profile in the maximum injection rate scenario for level 1, which is 20 m above the caprock / Hardegren interface.

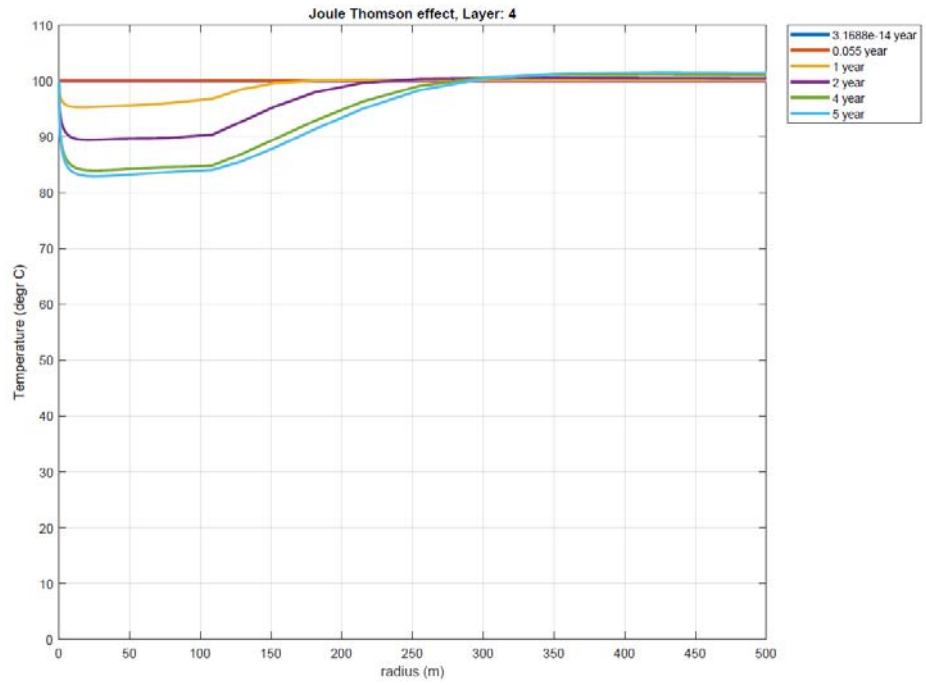


Figure 6-18: Temperature profile in the maximum injection rate scenario for level 2, which is 2.5 m below the caprock / Hardegsen interface.

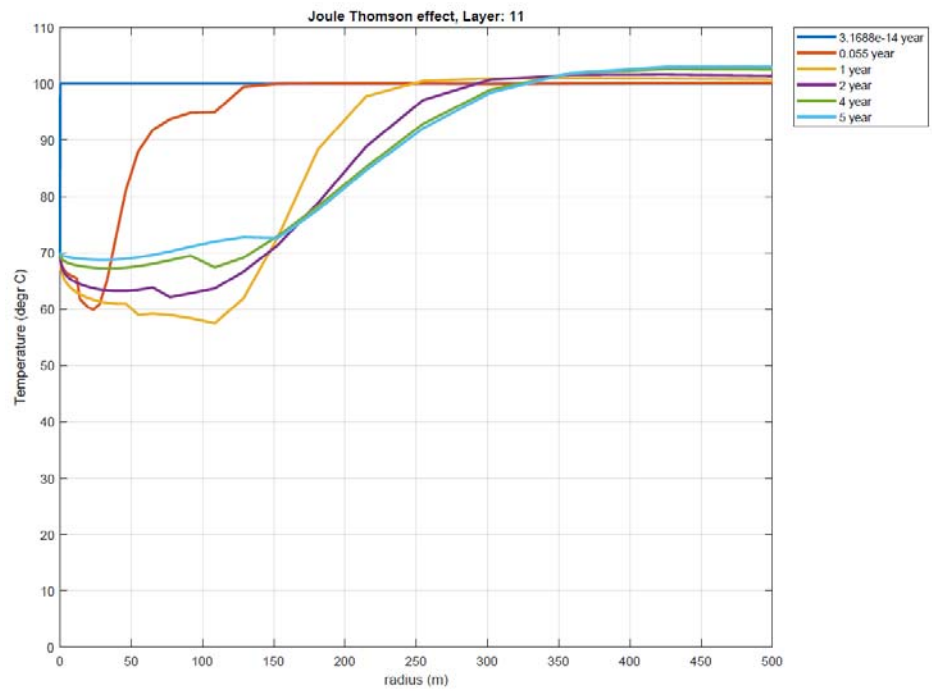


Figure 6-19: Temperature profile in the maximum injection rate scenario for level 3, which is in the middle of the high-permeable Hardegsen Fm.

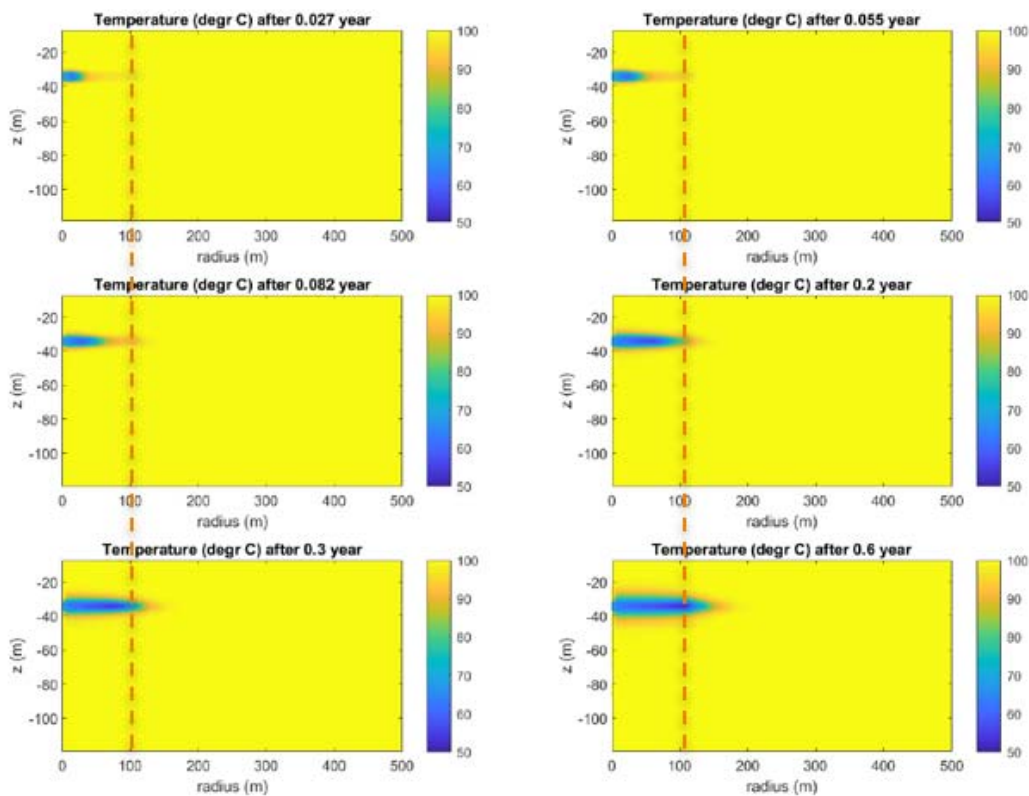


Figure 6-20: Temperature distribution in the P18-6 radially symmetric model for the storage scenario. The orange dashed line is the 100m from the injection well, corresponding to the closest fault to the P18-6-A7 well. After 70 days (0.2 years) the cold CO<sub>2</sub> front arrives at this fault.

#### 6.4.3.2 The discharge scenario

The discharge scenario models a start-up after a shut-in of the pipeline. During the start-up cold CO<sub>2</sub> (10°C) is injected into the P18-6 reservoir. This section estimates the impact of discharging the CO<sub>2</sub> into the P18-6 reservoir with regards to cooling and the location of the cold front.

The total mass of CO<sub>2</sub> in the a 21 km pipeline with a diameter of 16 inch is 2.8 kt<sup>6</sup>. This value was derived assuming that injection starts when the pipeline has been brought back to a pressure of 85 bar; the average temperature in the pipeline will be close to 10 °C. The 2.8 kt is an overestimation of the total volume of cold CO<sub>2</sub>.

The initial reservoir conditions used for the discharge scenario are:

- Reservoir pressure 60 bar;
- Reservoir temperature 100 °C;

<sup>6</sup> Based on CO<sub>2</sub> density of 907 kg/m<sup>3</sup> at 85 bar and 10°C, which is the assumed pressure and temperature of the pipeline.



- Injection temperature 46.3 °C; (see section 6.2)
- Constant Injection rate of 23.2 kg/s;
- Injection duration 1.4 days is needed to empty the total pipeline filled with CO<sub>2</sub>;
- Initial brine saturation varies according saturation height function (equation (17-1)).

The temperature distribution of the discharge scenario is shown in Figure 6-21. The pipeline is fully discharged after 1.4 days at which time the cold front is at about 15 m from the well. The maximum additional cooling is 6°C (i.e. a reservoir temperature of 40°C). After 1.4 days injection stops and it takes about 1.5 years for the cold front to disappear through heat influx from the surrounding formations.

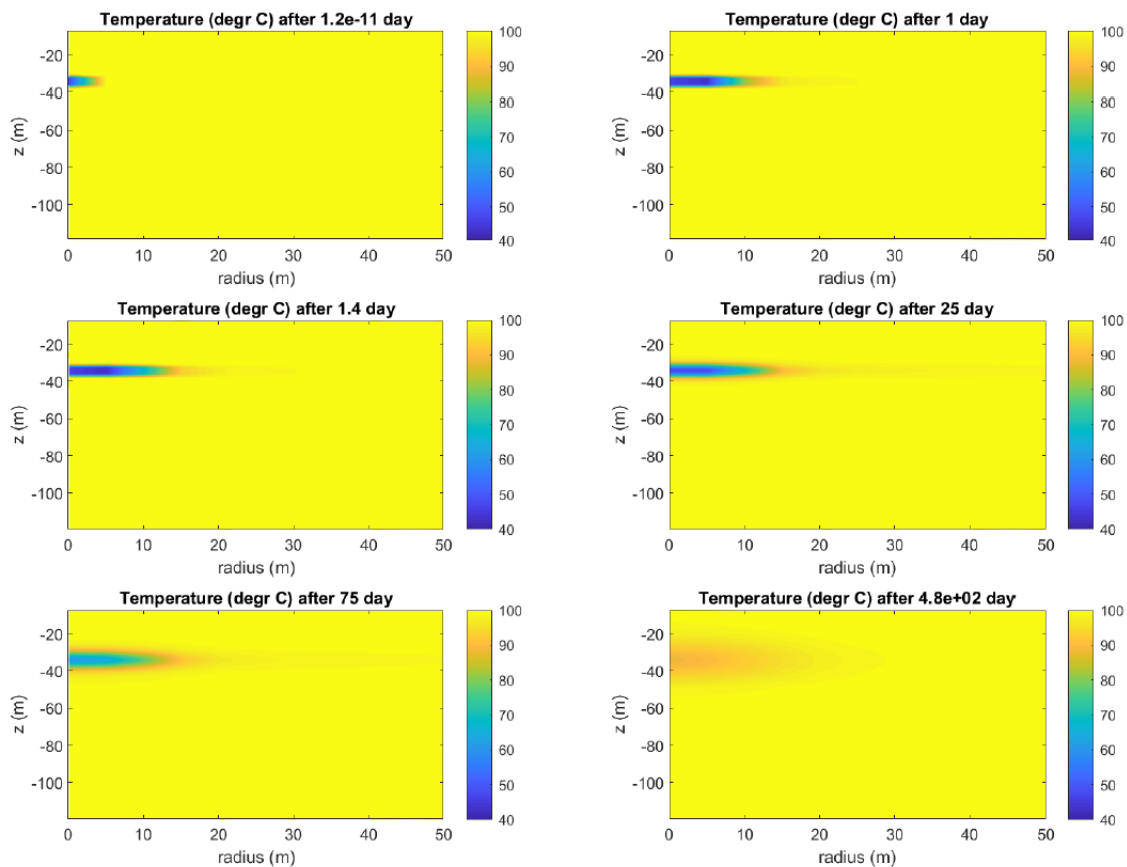


Figure 6-21: Temperature distribution of the discharge scenario. After 1.4 days of injection a cold front of  $\pm 15$ m develops. The minimum temperature observed is 40°C, which corresponds to a maximum cooling of 6.3°C, since the injection temperature is 46.3. After 1.4 days of injection the reservoir starts to equilibrate and after 1.3 years (480 days) the CO<sub>2</sub> is almost at initial reservoir temperature.

#### 6.4.4 Discussion

The cold front of CO<sub>2</sub> and the fluid itself propagates mainly in the high-permeability Hardegsen Fm. The temperature effect in the vertical direction is mainly due to thermal conductivity. At a continuous injection rate of 20 kg/s, the cold front reaches the fault closest to the well; the temperature contrast at the front is about 50 °C.

On the other hand if the purpose of the P18-6 reservoir is to discharge cold CO<sub>2</sub> in the pipeline, the cold front reaches 20 m from the well after a single discharge and a temperature change close to the P18-6 faults is not expected.

Hydrate formation is also not expected in P18-6 since the downhole pressure and temperature ranges expected are outside the possible hydrate formation window.

#### 6.4.5 *Conclusions*

The TOUGH2 simulations used a simplified, radial symmetric model, which demonstrated that the temperature effects of injecting cold CO<sub>2</sub> result in the following conclusions.

- Near-well temperatures and pressures are outside the hydrate zone. No injectivity impairment due to clogging of the reservoir due to hydrates is expected.
- CO<sub>2</sub> injection at a constant rate of 20 kg/s and a temperature of about 70 °C results in a cold front that progresses to about 200 m into the reservoir. The temperature contrast at the front is about 50 °C.
- At the same injection rate and temperature, the cold front reaches the nearest fault after about 70 days.
- Progression of the cold front in a single discharge of the cold pipeline contents is of the order of 20 m.

More detailed reservoir simulations with a more advanced, non-isothermal reservoir simulator are needed to improve predictions regarding:

- the temperature development near the injection wells;
- the temperature development near existing faults, taking into account the geometry of reservoir and faults;
- the post-injection reservoir pressure related to temperature equilibration on the long term.

### 6.5 Chemical interactions

#### 6.5.1 *Introduction*

Within the reservoir, physical and chemical interactions between the CO<sub>2</sub>, the formation water and rock minerals will occur during and after CO<sub>2</sub> injection. On the short term, during the injection phase, the risk of porosity and permeability decrease and corresponding injection issues needs to be evaluated. In the long term, during the post-decommissioning phase, the CCS Directive (EU, 2009) requires evaluation of the fate of CO<sub>2</sub>, for which geochemical reactions play an important role. This section describes the short-term (injection phase) and long-term (post-decommissioning phase) CO<sub>2</sub>-water-rock interactions and their impact on the feasibility of CO<sub>2</sub> injection and storage in the P18-6 reservoir, using recent literature.

#### 6.5.2 *Injection phase: Effect of dry-out and salt precipitation on injectivity*

During the injection of dry CO<sub>2</sub>, (residual) formation water will evaporate into the CO<sub>2</sub> in the near-well area. A dry-out zone will develop which can extend up to several tens of meters into the reservoir. As the mass of water decreases the concentration of the aqueous species increases and minerals start to precipitate when the remaining water becomes saturated (Miri and Hellevang, 2016). The most

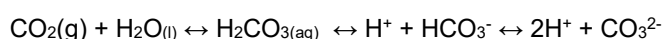
common mineral to precipitate is halite salt (NaCl), since formation waters contain mostly Na<sup>+</sup> and Cl<sup>-</sup>, although other minerals such as sulphates or hydroxides can also form. Salt precipitation during CO<sub>2</sub> injection and the corresponding permeability reduction and injectivity issues have been studied in the laboratory and by numerical simulations for the purpose of CO<sub>2</sub> storage in saline aquifers (e.g. Bacci et al., 2011, Kim et al., 2012, Roels et al., 2014). Field evidence of salt precipitation and injectivity impairment was obtained from the Ketzin injection pilot in Germany (Baumann et al., 2014) and the Snøhvit storage site in Norway (Grude et al., 2014). The key parameter that would allow for salt precipitation to result in permeability and injectivity impairment is the availability of saline water for capillary backflow (migration of salt water towards the injection well) and hence a continuous supply of salt. In the absence of capillary backflow of saline water, the maximum amount of salt precipitation is constrained by the volume of residual formation water and the concentration of aqueous species. The available species will then precipitate as thin coatings around the rock grains in the space that was occupied by the residual brine, without significantly affecting the permeability.

In the P18-6 reservoir the water saturation at the beginning of CO<sub>2</sub> injection will be close to residual and hence it will be immobile. This is supported by the lack of (significant) water (brine) production during the production history of the field (see P18-6 production data at [www.nlog.nl](http://www.nlog.nl)). As a result, capillary backflow of brine during injection will not occur. Production data did not give any evidence for the presence of a strong aquifer support, implying that brine supply from below is also not expected to occur. Tambach et al. (2015a) report on the modelling of CO<sub>2</sub> injection into a depleted gas reservoir (based on P18 characteristics) and the effect on salt precipitation. The report showed that in the case of immobile brine the maximum amount of salt precipitation was 2.7% of the pore volume, with a corresponding permeability decrease of 23%. It should be noted that the extent of permeability decrease upon a reduction in porosity is highly uncertain, but much higher values than 23% are not to be expected. With permeability values as high as those of the P18-6 reservoir, injectivity impairment by this amount of salt precipitation is not expected to occur. The temperature decrease in the near well area related to the low temperature of injected CO<sub>2</sub> will not have major impact on the extent of salt precipitation.

Another effect resulting from the formation of a dry-out zone is that the relative permeability of CO<sub>2</sub> increases when the water saturation decreases. Hence, the absolute permeability reduction due to salt precipitation could be (partially) counteracted by the increased relative CO<sub>2</sub> permeability (Miri and Hellevang, 2016).

### 6.5.3 *Injection phase: CO<sub>2</sub>-water-rock interactions*

When CO<sub>2</sub> is injected into the reservoir, it will try to form a new physico-chemical balance with the (residual) formation water. The water starts to evaporate into the dry supercritical CO<sub>2</sub> (scCO<sub>2</sub>), as described in the previous section, and CO<sub>2</sub> starts to dissolve into the formation water. In the near-well area, the dry-out zone will progress quickly, leaving no formation water for CO<sub>2</sub> to dissolve in. Beyond the progressing dry-out zone, CO<sub>2</sub> dissolves into the formation water and further dissociates by the following reactions:



These reactions result in an increased acidity of the formation water and a disequilibrium with the rock mineralogy. Both experimental and modelling studies show that on the short term the main result is the partial dissolution of carbonates, and potentially sulfides and sulphates, to buffer the pH. Of the carbonates, calcite dissolution is fastest, while the dissolution of other carbonates such as dolomite and ankerite is much slower. The mineralogy of the P18-6 reservoir will be very similar to the mineralogy of the P18-2 reservoir, the latter being reported in the core analysis report for P18-A-01 (P/18-3 well), and consists of mainly quartz, with lower amounts of K-feldspar, albite, plagioclase, dolomite, and clay minerals. Only occasionally anhydrite or calcite have been found, and only in small amounts.

Equilibrium batch reaction modelling with PHREEQC software, performed for the feasibility study of P18 in the CATO-2 project, predicted the dissolution of very small amounts of dolomite and pyrite, with negligible amounts of anhydrite and dawsonite precipitation (Vandeweyer et al., 2011). These reactions present a worst case scenario as the simulation was based on equilibrium modelling and did not consider kinetics. Also, these reactions would not occur in the near well zone where dry-out would occur.

Given that the worst case conditions predict negligible impacts on porosity (and hence on permeability), in the reservoir beyond the dry-out zone from CO<sub>2</sub>-water-rock interactions it can be concluded that geochemical interactions will not negatively impact on injectivity.

#### 6.5.4 *Post-decommissioning phase: CO<sub>2</sub>-water-rock interactions*

In the long-term, during the post-decommissioning phase, the conditions in the reservoir will slowly move towards a chemical equilibrium. This implies that silicate minerals will also have time to respond to the change in chemical equilibrium as a result of the high CO<sub>2</sub> partial pressure and partial CO<sub>2</sub> dissolution into the residual formation water beyond the dry-out zone. Since only residual (and thus immobile) formation water is present in the reservoir, a chemical equilibrium will only be obtained on the micro-scale; ions in the formation water can migrate by diffusion through the film of formation water as long as the film is connected. The scale on which formation water is connected is unknown and highly depends on the microstructural characteristics of the rock. Regardless of the scale of connection, diffusion of ions will be very slow, making it most likely to have chemical equilibrium on microscale only. The limited amount of water further slows down the reactions as water acts as a facilitator for the dissolution-precipitation reactions.

Tambach et al. (2015a) performed simulations with TOUGHREACT to predict long-term mineral reactions and sequestration of CO<sub>2</sub> in carbonate minerals for the P18 reservoir. A key uncertainty in the simulations is whether or not to include dawsonite as a secondary mineral. Dawsonite is a controversial carbonate mineral which, if included in geochemical simulations, is predicted to sequester a large part of the CO<sub>2</sub> in the long term. It is controversial as this mineral is only rarely found in natural CO<sub>2</sub>-rich reservoirs, and if present, only in minor amounts. Most probably, the thermodynamic data in the chemical databases are incorrect, and therefore, dawsonite should not be included in geochemical modelling of CO<sub>2</sub> storage. Also the possibility of magnesite precipitation as a secondary mineral was questioned. In the chemical initialization of the reservoir formations, both dawsonite and magnesite were predicted to be present as initial minerals. Since they were both not measured

in any of the P18 reservoir samples analysed, it can be questioned whether the chemical database contains correct chemical constants for these minerals.

Simulations for long-term CO<sub>2</sub>-water-rock interactions were performed with and without dawsonite and magnesite as secondary minerals. In both cases, long-term mineral reactions include the partial reaction of albite, K-feldspar and kaolinite to form illite. In the scenario which includes dawsonite and magnesite as secondary minerals the largest part of the CO<sub>2</sub> is predicted to be trapped in carbonate minerals within a few thousand years. In the simulation excluding dawsonite and magnesite as secondary minerals, leaving only calcite and dolomite as potential secondary carbonates, no CO<sub>2</sub> is predicted to be sequestered in carbonate minerals after equilibrium is reached within 10,000 years. Limited CO<sub>2</sub> partial pressure decrease from 365 bar after well closure to 300, 315 and 341 bar for the lower Detfurth, Upper Detfurth and Hardegsen Formation respectively is predicted after 10,000 years. This is related to a slight overall porosity increase due to dissolution-precipitation reactions. More than 95% of the CO<sub>2</sub> remains in the reservoir in the supercritical state.

Studies on natural analogues rarely report on the occurrence of dawsonite, and if present, it is only present in very small amounts. Natural analogues include occurrences of CO<sub>2</sub>-rich gas reservoirs in which the CO<sub>2</sub> has had thousands to millions of years to reach chemical equilibrium with the reservoir formation water and mineralogy. These reservoirs therefore present a unique opportunity to study the long term fate of CO<sub>2</sub> in a depleted hydrocarbon reservoir and validate geochemical models. The absence of large amounts of dawsonite in natural analogues suggests that dawsonite precipitation in geochemical simulators is not well defined.

Two major studies on natural analogues in the US and the UK show that in most cases negligible trapping in carbonate minerals occurred (Baines and Worden, 2004; Gilfillan et al., 2009), which is most likely due to the slow dissolution of silicate minerals which is a rate-limiting step (Baines and Worden, 2004). The study by Gilfillan et al. (2009) identified solubility trapping as the primary sink for the natural CO<sub>2</sub> fields analysed, but this is only possible in case of sufficient availability of formation water, which is not the case in depleted hydrocarbon fields without strong aquifer supports such as the P18-2 reservoir. Based on the insights obtained from natural analogues, the scenario by Tambach et al. (2015b) excluding dawsonite and magnesite as secondary minerals provides a more realistic prediction of the long-term fate of CO<sub>2</sub>. We can conclude that almost all of the injected CO<sub>2</sub> will remain in the supercritical state for thousands of years.

## 6.6 Conclusions

The injection simulations lead to the following conclusions.

### *Storage capacity.*

The storage capacity of the P18-6 field is 1.3 Mt of CO<sub>2</sub>, assuming a maximum bottomhole pressure during injection that is equal to the initial pressure (the pressure prior to production of the natural gas).

*Containment.*

CO<sub>2</sub> fills the pore volume that was previously filled with natural gas. The CO<sub>2</sub> only moves down-dip below the original gas-water contact in a small part of the reservoir. Even when the reservoir is overfilled, i.e. when the average reservoir pressure increases beyond the initial pressure, the CO<sub>2</sub> does not move far and will move back up the slope when injection is stopped. In the north-west corner of the reservoir where a spill point is, the CO<sub>2</sub> does not move beyond the original gas-water contact. Thus, the conclusion is that the reservoir contains the injected CO<sub>2</sub>, without risk of spilling.

*Near-well hydrate formation*

Hydrate formation is not expected in P18-6, since the downhole pressure and temperature ranges expected are outside the possible hydrate formation window.

*Near-well chemical clogging*

Injection of CO<sub>2</sub> into the reservoir will cause drying out of the reservoir and the precipitation of salt. This is not expected to lead to clogging of the near-well area but should clogging occur, there is no impact on storage safety or security.

*Temperature effects*

The injection of CO<sub>2</sub> at low temperature into the P18-6 gas field must be modelled in detail prior to the start of injection as the cold CO<sub>2</sub> will affect bottomhole pressure during injection. The pressure in the reservoir will slowly increase as the CO<sub>2</sub> in the reservoir gradually reach initial reservoir temperature. The magnitude of these effects has been estimated in this study; a more detailed analysis is needed prior to the start of injection.

*Long-term reservoir integrity*

No significant interactions between the CO<sub>2</sub> and the reservoir are expected. CO<sub>2</sub> is expected to remain in supercritical state in the reservoir for a period of the order of thousands of years.

## 7 Fault stability

### 7.1 Introduction

This section focuses on the evaluation of the potential of destabilization of intra-reservoir faults identified in the seismic cube and mapped in the static and dynamic models.

The P18 reservoirs, including the P18-6 reservoir, that have been assigned as potential storage reservoirs are fault bounded. These faults are sealing: the compartments are hydraulically isolated from their surroundings due to juxtaposition of the reservoir against impermeable shales. This section investigates the stability of these faults, in both geomechanical terms and geochemical terms. Fault stability in relation to reservoir re-pressurisation is discussed in Section 7.2, then in relation to the low temperature of the injected CO<sub>2</sub> in Section 7.3 and finally in relation to geochemical effects of CO<sub>2</sub> in Section 7.4.

The overall conclusion from the work presented in this section is that the risk of fault reactivation due to the injection of CO<sub>2</sub> is low.

The increasing reservoir pressure, as a result of injecting CO<sub>2</sub> stabilizes the faults that bound the P18-6 field. CO<sub>2</sub>-related geochemical effects in fault zones are unlikely to lead to reactivation of the faults, or to CO<sub>2</sub> migration along faults.

If low-temperature CO<sub>2</sub> (the temperature can be about 60 °C cooler than the reservoir temperature) reaches a fault, the fault can be locally destabilized. This risk can be mitigated by monitoring and, if necessary, reducing the injected amount of CO<sub>2</sub> through wells that are close to bounding faults. Further analysis is needed to define the risk and mitigation requirements in more detail.

### 7.2 Fault stability: pressure effect

To study the effects of pressure changes on intra-reservoir fault reactivation we use MACRIS (Mechanical Analysis of Complex Reservoir for Induced Seismicity), a TNO-developed semi-analytical approach which allows us to evaluate both the poro-elastic effect and the direct pressure effect on stresses along the mapped faults.

Details of MACRIS are given in Section 17.8. The required input for running MACRIS is the ECLIPSE reservoir grid with the flow simulations detailed in Section 6. Taking the ECLIPSE reservoir flow simulations as inputs MACRIS directly computes the stress induced by both the poro-elastic effect (i.e., the reservoir contraction/dilation due to depletion/injection of gas) and the direct pressure effect (i.e., the changes in effective normal stress due to the changes in pore pressure inside the faults). It is important to mention that MACRIS captures the effect of the differential compaction between two offset compartments. For the direct pressure effect, the average pore pressure between the two juxtaposed reservoir compartments at faults has been assumed.

It is not needed to rebuild a new geomechanical mesh with MACRIS as it directly works with the grid of the flow simulation (ECLIPSE). This way, MACRIS is extremely fast. Moreover, it allows the evaluation of stresses in 3D along all the mapped faults with high resolution.

For a simplified 3D single-fault tank reservoir model, the MACRIS stress solution has been compared with the solution given by the Diana FE (Finite Element) simulator. The results are presented in Section 17.8.1 and clearly demonstrate the almost perfect match between MACRIS and the FE solution. It is important to keep in mind that it would not be possible to use an FE approach for the 3D evaluation of the stresses along the multiple faults of the P18-6 field. Only 2D cross-sections, as performed in the previous P18 study (Vandeweyer et al., 2011), can be performed. Having access to the Coulomb stress distribution in 3D along the fault planes with MACRIS is extremely advantageous, since the along-strike variability is accessible and the area of excess Coulomb stress can be quantified. This area of excess Coulomb stress is key to evaluate the risk of fault reactivation.

All the input parameters used for MACRIS are listed in Table 6-1 and are the same as the ones used for the P18-2 field (Neele et al., 2019). One unique set of model parameters has been used in the present analysis and thus the parameter sensitivity search has not been performed. The stress changes computed in MACRIS must be added to the initial stress tensor. In the West Netherlands Basin the minimum in situ stress is horizontal and the stress regime is extensional or normal-faulting (i.e. the largest principal stress is vertical). The largest vertical stress ( $S_v = S_{max}$ ) is calculated as the overburden weight from seawater, rock, and pore fluid densities (see Table 7-1). The orientation of the minimum horizontal stress  $S_h$ , determined from borehole breakouts and the World Stress Map, is 55° (N55E). The magnitude of  $S_h$  is defined by applying the ratio of horizontal-to-vertical effective stress  $K_o' = S_h'/S_v'$ ; a value of  $K_o' = 0.63$  is used for the analysis. Finally, the magnitude of the maximum horizontal stress  $S_H$  is defined by the ratio  $S_h/S_H = 0.9$ . It is important to note, that a single unique value of each of the parameters controlling the in-situ stress conditions (notably the orientation of  $S_h$ ,  $K_o'$  and  $S_h/S_H$ ) is used for the geomechanical analysis. In other words, a parameter sensitivity search has not been carried out. However, the input parameter values are aligned with the ones used in the geomechanical analysis of Vandeweyer et al. (2011) and the previous P18-2 study (Neele et al., 2019).

Table 7-1 Input model parameters used for the MACRIS semi-analytical approach.

MACRIS model parameters	
<i>S<sub>h</sub> orientation</i>	N55E
$K_o' = S_h'/S_v'$	0.63
<i>S<sub>h</sub>/S<sub>H</sub></i>	0.9
$\rho_{rock}$	2260 kg/m <sup>3</sup>
$\rho_{water}$	1150 kg/m <sup>3</sup>
$\rho_{gas}$	200 kg/m <sup>3</sup>
<i>E<sub>reservoir</sub> (Young's modulus)</i>	18 GPa
<i>E<sub>overburden</sub> (Young's modulus)</i>	25 GPa
<i>E<sub>underburden</sub> (Young's modulus)</i>	28 GPa
<i>v (Poisson's ratio)</i>	0.2
$\mu$ (friction coefficient)	0.6
$\alpha$ (Biot's coefficient)	1.0



From the new full stress tensor, including the induced stress changes, one can derive the shear stress  $\tau$  and effective normal stress  $\sigma'$  for any fault orientations. In order to assess the potential reactivation of a fault, both stresses need to be combined, the shear stress promoting slip whereas the normal is clamping the fault. One convenient way to calculate this is using the Coulomb stresses  $C$  or the Fault Shear Capacity (FSC), respectively defined as:

$$C = \tau - \mu\sigma' \quad (7-1)$$

$$FSC = \frac{\tau}{\tau_{max}} = \frac{\tau}{\mu\sigma'} \quad (7-2)$$

where  $\mu = 0.6$  is the friction coefficient. When  $C$  starts to be positive or alternatively FSC reaches unit, a pre-existing fault can be reactivated since the shear stress is larger than the frictional strength defined as  $\mu\sigma'$ .

Figure 7-1 displays the initial negative Coulomb stresses (see equation (7-1) for the definition of the Coulomb stress) computed by MACRIS before any pressure depletion. In MACRIS, the along-fault stresses are evaluated along fault pillars (see Section 17.8.1 for more details) as shown in Figure 7-1. In the previous P18-2 study (Neele et al, 2019), this along-pillar discrete stress distribution was interpolated over a regular grid; here the initial discrete stress distribution is displayed. For all the faults and at any locations along these faults, the initial Coulomb stresses are mostly negative and around minus 10-15 MPa (Figure 7-1). These negative Coulomb stresses represent the initial distance to failure, that is the required additional Coulomb stresses for the faults to be reactivated.

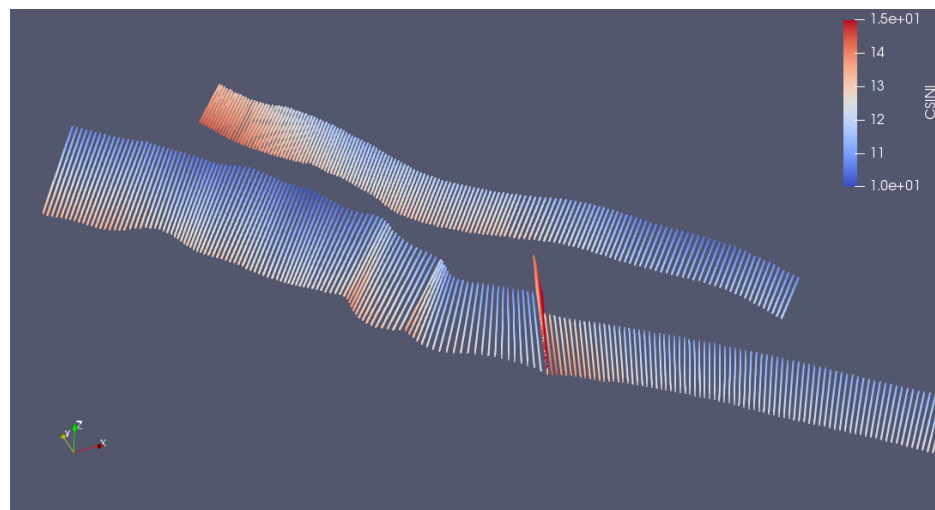


Figure 7-1 Initial distance to failure along the P18-6 faults. Colours indicate the negative Coulomb stress in units of MPa at the initialization of the MACRIS analysis, that is before any pressure depletion.

At the end of the depletion period elongated areas of large positive Coulomb stress changes along the strike direction can be localized at the reservoir edges (see Figure 7-2). These elongated areas of high positive Coulomb stress changes

reduces during the injection phase (see Figure 7-3). Figure 7-4 indicates that these elongated areas of high positive Coulomb stress changes (at the edge of the depleting part of the reservoir) exceed the failure line at the end of the production period, meaning that potentially the concerned fault could be reactivated. However, as observed in Figure 7-4, most of the Coulomb stress peaks exceeding the failure line are expected to disappear during the injection period. The fault pillar displayed in Figure 7-4 is of particular interest, because it is close to a well. This aspect is further discussed in Section 7.3 when the temperature effect is assessed.

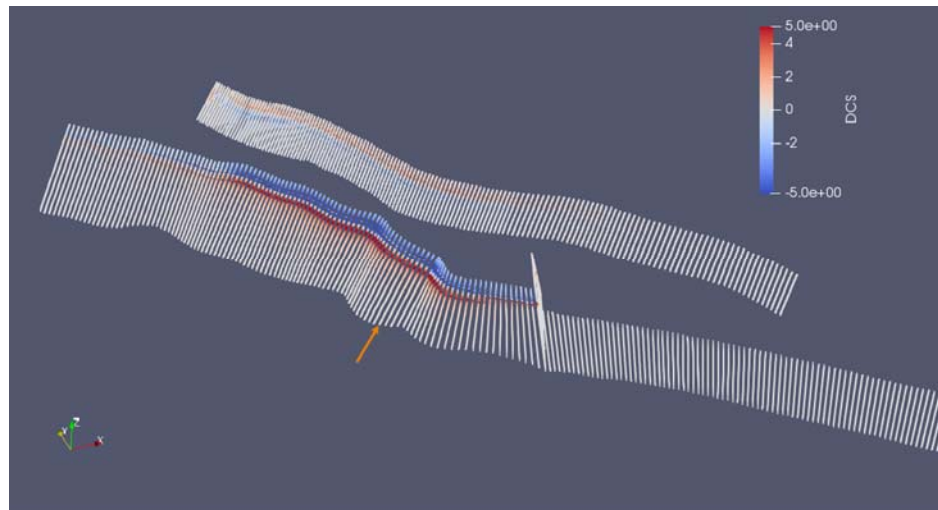


Figure 7-2 Changes in Coulomb stresses (MPa) along the P18-6 faults at the end of the production period inferred from MACRIS analysis. The orange arrow indicates the fault pillar where the stress and pressure changes are displayed in Figure 7-4.

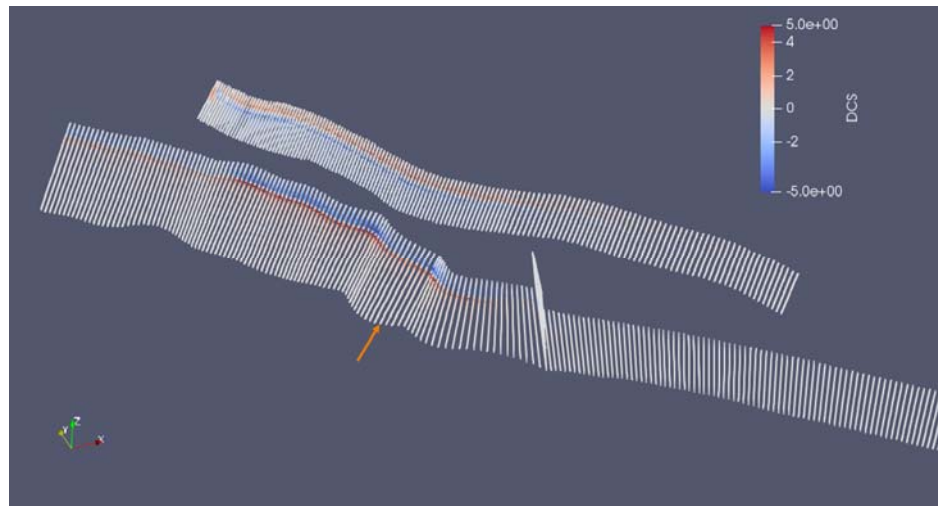


Figure 7-3 Changes in Coulomb stresses (MPa) along the P18-6 faults at the end of the injection period inferred from MACRIS analysis. The orange arrow indicates the fault pillar where the stress and pressure changes are displayed in Figure 7-4.

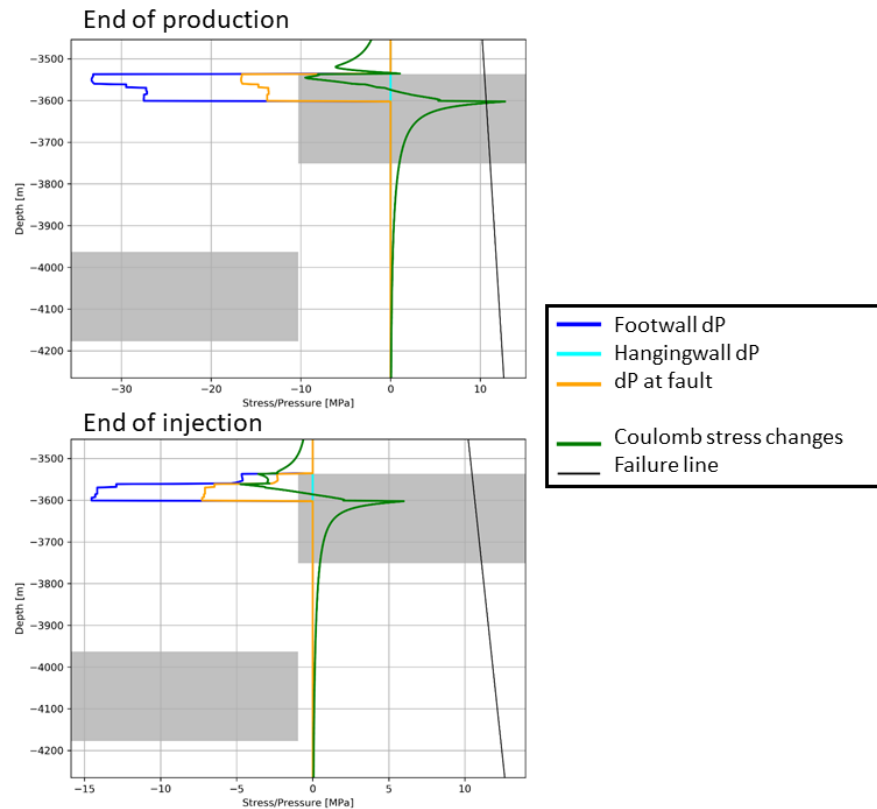


Figure 7-4 Changes in Coulomb stresses and pore pressures (inferred from MACRIS analysis) along one representative fault pillar (location of this pillar is indicated in Figure 7-2 and Figure 7-3. "Footwall dP" and "Hangingwall dP" represent the changes in pore pressure in the reservoir grid blocks juxtaposed to the fault in the footwall compartment and in the hanging wall compartment, respectively. "dP at fault" corresponds to the pore pressure inside the fault, taken as the average pressure between "Footwall dP" and "Hangingwall dP". The two grey rectangles delineate the two offset reservoir compartments. At the end of the production period, changes of Coulomb stresses exceed the failure locally at one reservoir edge. This Coulomb stress peak decreases during the injection period. For the sake of visibility, the ranges of the x-axis have been separately adjusted for each graphs.

Figure 7-5 is complementary to Figure 7-2 and Figure 7-3, giving access to the 3D along-strike variability of the likelihood of fault reactivation occurring. Figure 7-5 confirms that at the end of the injection period most (if not all) of the areas where the Fault Shear Capacity FSC (equation (7-2)) is exceeded, present at the end of the depletion period, disappear. Considering solely the pressure effect, the faults are thus expected to be stable at the end of the injection period. This conclusion would only be disputed in the case of either (1) direct injection inside a reservoir fault or (2) direct flow communication between the well and a reservoir fault. Assuming we are not missing pre-existing faults in the structural reservoir model, this study confirms that injection inside a reservoir fault is not occurring.

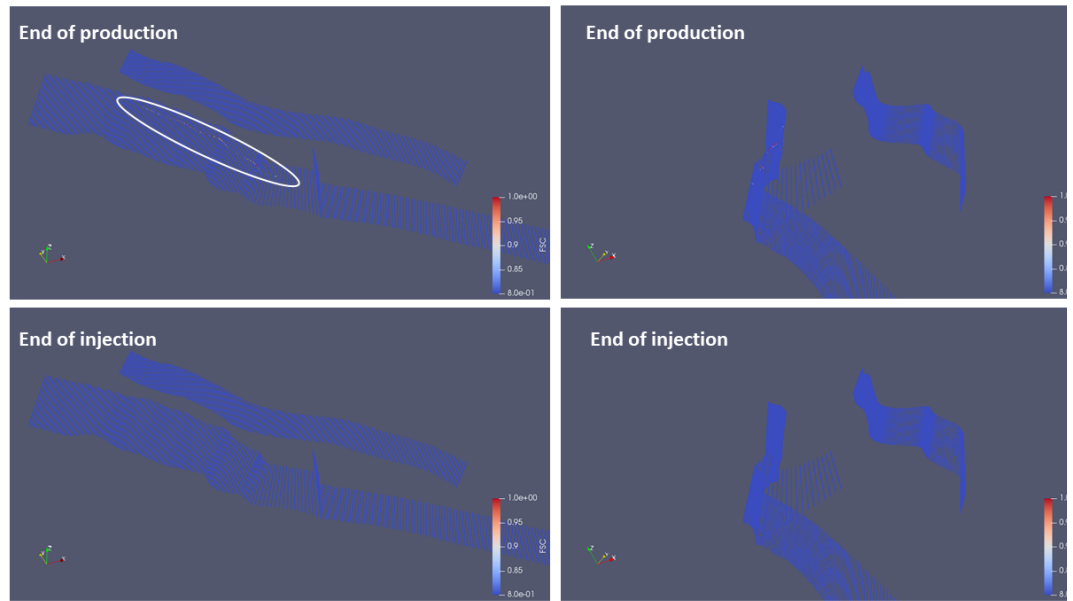


Figure 7-5 Fault Shear Capacity (FSC) along the P18-6 faults inferred from MACRIS analysis. At the end of the production period, the Fault Shear Capacity exceeds unity only very locally (at the reservoir edges and highlighted by the white ellipse) meaning that the shear stress is larger than the frictional shear strength (“max shear stress”). During the injection period, these very local areas of exceedance of the frictional shear strength disappear.

### 7.3 Fault stability : temperature effect

Up to this point, the results of the MACRIS analysis only take into account the pressure effect on fault stability. The temperature effect on the stability of the intra-reservoir faults is now addressed.

Table 7-2 Input model parameters used for the thermo-elastic semi-analytical approach.

Thermo-elastic model parameters	
$\Delta T$	-90°C
<i>Sh orientation</i>	N55E
$Ko' = Sh/Sv'$	0.63
<i>Sh/SH</i>	0.9
$\rho_{rock}$	2260 kg/m <sup>3</sup>
$\rho_{water}$	1150 kg/m <sup>3</sup>
$\rho_{gas}$	200 kg/m <sup>3</sup>
<i>E (Young's modulus)</i>	18 GPa
<i>v (Poisson's ratio)</i>	0.2
$\alpha_T$ (linear thermal expansion coefficient)	10 <sup>-5</sup> K <sup>-1</sup>
$\mu$ (friction coefficient)	0.6
$\alpha$ (Biot's coefficient)	1.0

To answer this question, we used a TNO-proprietary geomechanical semi-analytical approach detailed in Section 17.8.2. The required input for this approach is the radially symmetric temperature field resulting from the TOUGH2 flow simulation introduced in Section 6. Table 7-2 outlines the input parameters required for this

analysis which are the same as used in the P18-2 study (Neele et al., 2019). The TOUGH2 flow simulation and the geomechanical semi-analytical approach should be seen as one-way coupled, and the temperature effect on the fluid viscosity is handled by the TOUGH2 simulator.

The temperature field after 5 years of injection is taken as representative for the amplitude and extent of the cooling in the reservoir (see Figure 7-6). The transient temperature field after 5 years of injection from TOUGH2 is first approximated as an homogenous cylindrical field at a temperature relative to that of the undisturbed reservoir of  $-50\text{ }^{\circ}\text{C}$ , with a height equal to 45m, and with a radius of 200m (see Figure 7-6). This approximation of a sharp temperature front is often assumed for fast analytical approaches (Candela et al., 2018). The semi-analytical approach, detailed in Section 17.8.2, provides an estimate of the thermo-elastic stresses inside and around the cylindrical field which are induced by cooling.

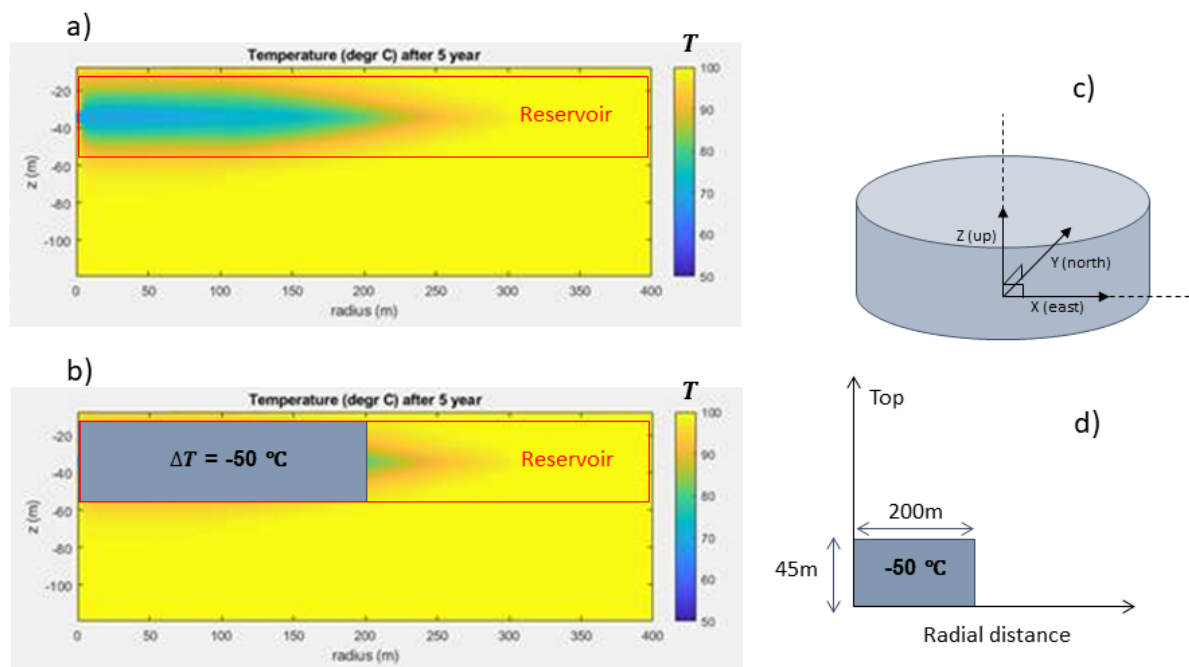


Figure 7-6 Temperature distribution and geometry of the geomechanical semi-analytical approach used to evaluate thermo-elastic stresses. a) Transient temperature field simulated by TOUGH2 (see Section 6.4). b) Cylindrical-shape approximation of the transient temperature field in a). For a) and b) the temperature change is homogeneously distributed and fixed at  $-50\text{ }^{\circ}\text{C}$ . c) and d) Geometry of the geomechanical semi-analytical approach.

Following the semi-analytical approach, faults are not explicitly modelled (as it was the case in the MACRIS analysis for the pressure effect) but the changes in stress which are induced by the reservoir cooling can be calculated at any location inside the reservoir and caprock. From equation (7-1) the changes in Coulomb stress induced by the temperature effect at any reservoir fault can be calculated. As soon as the cooling front reaches a fault, Figure 7-7 and Figure 7-8 show that the change in Coulomb stress can reach a value as high as 9 MPa. This result holds for a range of fault planes orientations which are relevant for the P18-6 field. Ahead of the cooling front, the thermally-induced Coulomb stresses rapidly decay and at 100 m

from the cooling front the Coulomb stresses are around 1.5 MPa. As concluded for the P18-2 study (Neele et al., 2019) the distance reached by the cooling front is the determining parameter for the fault stability analysis. Before reaching the fault, the increase in Coulomb stress in front of the cooling zone is minor, but as soon as the cooling front reaches a fault, the increase in Coulomb stress goes up to ~9 MPa, which is a magnitude capable of reactivating this fault. After 5 years of injection the cooling front is at 200 m from the well which means this scenario might occur (see Figure 7-6) and one of the P18-6 faults cross-cutting both the reservoir and caprock is at a distance of ~100m from a well (Figure 7-9).

However, in order to reach conclusions regarding fault reactivation, the changes in Coulomb stress in the initial stress situation before injection of cold CO<sub>2</sub> need to be added to the thermally induced Coulomb stress. Figure 7-2 and Figure 7-4 display this initial stress situation at the end of the production period and along the fault pillar closest to a well (a distance from well to fault of ~100m). As discussed before, the initial Coulomb stresses (at the end of the production period) are highly heterogeneous spatially along the fault pillar. At the reservoir edge the Coulomb stresses are already reaching the failure line but some other locations are at more than 10 MPa from the failure line. Adding the 9 MPa of thermally induced Coulomb stresses to the initial Coulomb stresses induced by the reservoir depletion, it can be estimated that almost three-fourths of the fault pillar would overreach the failure line (i.e. an along-dip fault section of 150m long might potentially be reactivated). It can therefore be concluded that for this particular fault which is close to a well, the likelihood of reactivation is high.

This last result will still hold, even if the cooling front reaches this fault later during the injection period. The simultaneous reduction in Coulomb stresses induced by pressure changes is expected to stabilize the fault. However this pressure-induced reduction in Coulomb stresses is weak relatively to the temperature-induced increase in Coulomb stresses. Indeed, later during the injection period and if we solely consider the pressure effect, the two-thirds of the fault pillar still remain at less than 9MPa from the failure line (see Figure 7-4). Therefore if we add up the 9 MPa increase of Coulomb stresses due to the temperature effect, two-thirds of the fault pillar will still overreach the failure line even if we combine both temperature and pressure effects.

Finally it is important at this stage to emphasise the limitations of TOUGH2 where the highest temperature that can be modelled is 103 °C whereas the initial reservoir temperature was ~117°C. The change in temperature can therefore be expected to be more severe than the -50 °C used in our geomechanical semi-analytical approach which could result in the modelled change of Coulomb stress being even higher.

The cooling front modelled here represents a realistic scenario where the cooling is due to prolonged injection of CO<sub>2</sub> at a temperature of 70 °C. However, in reality a more gradual temperature front is expected and thus the area of excess Coulomb stress relative to the failure line will be more limited in space. In other words, the potential of reactivating a pre-existing fault inside the reservoir would be confined to a small area beyond the cooling front. Finally, a solution in this scenario is to adjust the injection rate at this particular well located close to a reservoir fault. This way,

the extent of the cooling front can be constrained to maintain a safe distance from the fault.

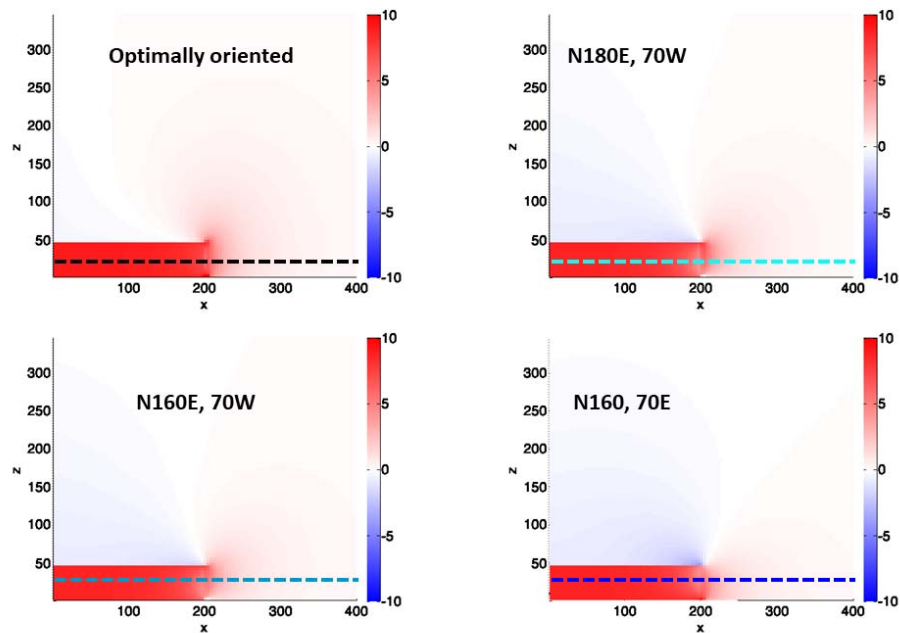


Figure 7-7 Thermo-elastically induced Coulomb stress changes in units of MPa for different fault orientation. Top left: fault planes with the highest Coulomb stress changes; Top right: fault planes with a North-South strike and dipping 70 degrees toward West; Bottom left: fault planes with a N160E strike and dipping 70 degrees toward West; Bottom right: fault planes with a N160E strike and dipping 70 degrees toward East. The model input used to generate these results is the homogenous temperature field presented in Figure 7-6. The horizontal dashed lines in the centre of the reservoir represent the stress profiles displayed in Figure 7-8.

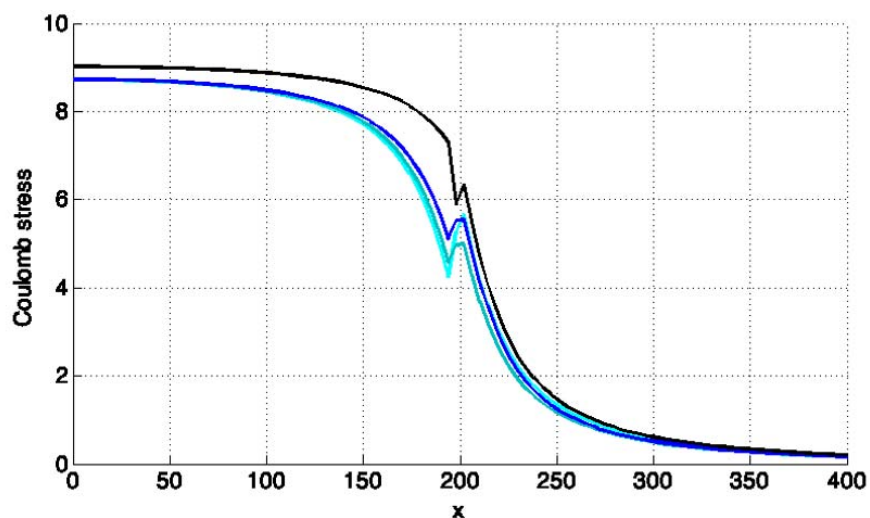


Figure 7-8 Profiles of thermo-elastically induced Coulomb stress changes in units of MPa. Each colour corresponds to each fault family presented in Figure 7-7.

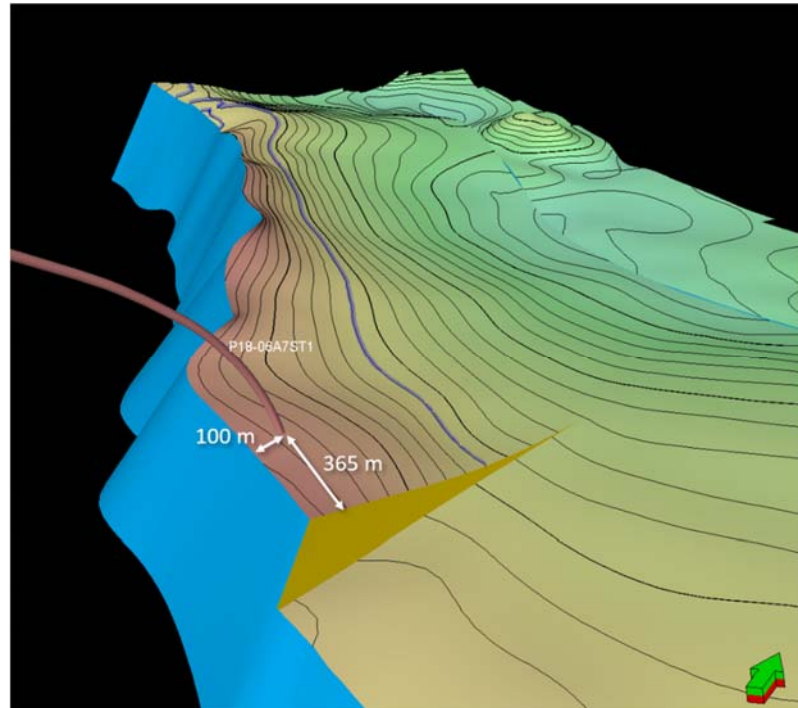


Figure 7-9 Schematic showing the distances from the faults to the wells.

Alongside fault reactivation another important consideration is regarding the potential magnitude of any induced earthquakes should fault reactivation occur. To answer this question additional modelling results are required. However this study can provide insight on the expected end-members in terms of event magnitude. One first end-member is the case where a rupture will remain confined to the perturbed zone and thus the induced event would be small (magnitude <1). The perturbed zone is the area of the fault already included in the cooled domain with the excess Coulomb stress.

The second end-member is the case where the rupture will propagate all the way through the fault area extent. In this case, the magnitude of the event would be large (magnitude well above 1). Note here that the case where the rupture could jump to another fault and extend even further is not considered. The reality is likely to occur between the first and the second end-member. One dominant factor that controls the event propagation and thus its final size is the initial Coulomb stress level at the start of the fault reactivation. This initial Coulomb stress is the one at the end of the production period and given by the MACRIS analysis (see Figure 7-2 and Figure 7-3). Due to the differential compaction effect, this initial Coulomb stress level is highly heterogeneous spatially with only some locations at the reservoir edge close to the failure line or already at the failure line. It can therefore be assumed that the propagation of an induced event will remain confined to the perturbed zone and will quickly die out outside due to the lack of high stresses to sustain its propagation. However it should be emphasised that to give a more definitive answer on the potential magnitudes of induced events, new geomechanical models focusing on this particular matter would need to be developed.



## 7.4 Fault stability: geochemical effects

### 7.4.1 Introduction

The P18 reservoir compartments that have been assigned as potential storage reservoirs are fault bounded. It is assumed that these faults are sealing; the compartments are hydraulically isolated from their surroundings due to juxtaposition of the reservoir against impermeable shales. Large-scale faults are generally surrounded by an area with a large number of smaller faults and fractures and matrix consisting of fault gouge. Instead of 'faults' we should refer to the 'fault (damage) zone' (Fisher, 2013). If porous rocks or sediments are faulted in early stages of consolidation, the damage zone generally has a lower permeability than the undeformed material (Fisher, 2013).

For storage integrity purposes, a difference should be made between sealing *across* and *along* the fault zone. Juxtaposition against a sealing formation can result in hydraulic isolation due to sealing across the fault. Yet, if the fault zone extends to above the caprock and the fault gouge is permeable, the risk of upward migration exists. In the P18-6 area, none of the faults extends upward outside the caprock. In a previous analysis of migration scenarios for P18, shallow gas pockets in the overburden were found, but these most probably originated in the overlying Jurassic Posidonia shales (Vandeweyer et al., 2011). No evidence was found for gas leakage from the P18 reservoir, supporting a conclusion that the fault zones of each of the faults penetrating the caprock are sealing. The question remains why upward gas migration did not occur along the non-sealing faults.

When CO<sub>2</sub> is injected in the reservoir, geochemical reactions between CO<sub>2</sub> and minerals within the fault might change the sealing capacity (in case of sealing faults) and/or cause reactivation. The geochemical effects of CO<sub>2</sub> on the faults, and the impact of these effects on its sealing integrity and reactivation potential need to be evaluated to assess the risk of leakage through the faults of the P18-6 reservoir and the potential of reactivation on the long term. These are described below based on recent literature.

### 7.4.2 Geochemical effects of CO<sub>2</sub> on sealing capacity

Due to juxtaposition of the reservoir against impermeable shales, it is assumed that the fault zone mineralogy of sealing faults is made up of crushed and mixed sandstone and shale components, whereas the non-sealing faults which did not juxtapose the reservoir against impermeable shales comprises crushed reservoir material only. Although the Triassic sandstones have a relatively high clay content, the non-sealing faults probably contain less clay minerals than the sealing faults. Yet, the sealing and non-sealing faults will have very similar mineralogy, with variable mineral contents consisting of quartz, feldspars, clay minerals, carbonates, anhydrite and accessory minerals.

Similar to geochemical effects of CO<sub>2</sub> on caprock integrity, the only migration mechanism for CO<sub>2</sub> into sealing faults is by diffusion in dissolved form. Therefore, horizontal and vertical penetration of the geochemically affected zone is of the same order of magnitude as the vertical penetration into the caprock (several meters after 10,000 years). Changes in mineralogy will include partial dissolution of silicate minerals and precipitation of carbonate and clay minerals. Corresponding porosity changes will be too small to affect the sealing capacity.

The non-sealing fault zones might allow migration of supercritical CO<sub>2</sub> but breakthrough across the fault zones is not an issue if the compartment across the fault is also used as storage reservoir. Upward migration could lead to enhanced chemical reactions. According to Fisher (2013), the most common type of fault gouge in Triassic reservoirs is cataclastic faults. For the 19 Triassic fault gouges studied, gas permeability values ranged from 0.0007 to 1.8 mD (Fisher, 2013). A non-sealing fault will have a permeability at the high end of this range, but it is still a low permeability. Low flow rates will enhance self-sealing of the leak path by carbonate precipitation, especially in the presence of sufficient clay minerals which can provide the required cations for reaction with dissolved CO<sub>2</sub> to form carbonate minerals. However, the rate of self-sealing is not well known and will probably be highly dependent on many variables and fault characteristics.

#### 7.4.3 *Geochemical effects of CO<sub>2</sub> on reactivation potential*

Chemical interactions between the carbonized brine and fault zone mineralogy will result in slight mineralogical changes. These changes will only occur in the first few meters at the contact with the reservoir for sealing fault zones after thousands of years. In the case of non-sealing faults, mineral reactions might have occurred across the fault zone. The chemical reactions in the long-term are uncertain and will be affected by local differences in mineralogy. Overall, it is predicted that the carbonate content will increase because of the interaction with dissolved CO<sub>2</sub> with cations in the formation water, and on the long term with cations from silicate minerals. Few geomechanical studies have been conducted to investigate the effect of carbonate content on mechanical properties of faults. The studies that have been conducted concluded that with increasing carbonate content, fault gouge has an increased friction coefficient, indicating lower potential for fault reactivation (Samuelson et al., 2012; Adelinet et al., 2014; Bakker et al., 2016). In the case where fault reactivation *does* occur, higher carbonate contents increase the tendency for velocity weakening (which makes the fault weaker and sliding can continue, e.g. unstable slip) and can therefore increase the probability of microseismicity to occur (Samuelson et al., 2012). This is supported by an experimental study in which fault gouge from an outcrop which was very heavily altered by CO<sub>2</sub> interactions showed unstable slip at reservoir temperatures, whereas less heavily altered fault gouge resulted in stable slip (Bakker et al., 2016). The permeability of fault gouge material shows a tendency to decrease by orders of magnitude upon displacement during slip (Bakker et al., 2016), although it is not clear whether this occurs for both stable and unstable slip.

#### 7.4.4 *Evidence of leakage from field data*

In Arizona, USA, CO<sub>2</sub> leakage through faults from a large natural CO<sub>2</sub> reservoir was studied in order to quantify leakage rates (Miočic et al., 2019). In this specific area, faults extended from the reservoir up to the surface, and CO<sub>2</sub> rich fluids have been leaking for 420,000 years through fractures present in the damage zones around the faults. It was estimated that the average leakage rate through the faults is up to 36 kt/yr, which is less than 0.01% leakage per year for this reservoir. In case of the P18-6 storage site, the faults do not reach the surface, but end in the Cretaceous aquifers. In a worst case, that the non-sealing faults turn out to be leakage paths, and self-sealing by carbonate precipitation does not occur, supercritical or gaseous CO<sub>2</sub> would migrate up to the Cretaceous aquifers and dissolve into the formation water. From the Arizona study it was concluded that leakage along faults does not

negatively impact the suitability of a reservoir from the point of view of CO<sub>2</sub> emission reductions (Miocic et al., 2019).

## 7.5 Conclusions

### *Pressure effect on fault stability*

The 4D distribution of Coulomb stresses has been computed along the mapped faults. Following the MACRIS approach, these Coulomb stresses combined (1) the poro-elastic effect, (2) the direct pressure effect at faults and (3) the effect of the fault offset. This analysis indicates that these Coulomb stresses only exceed the failure line very locally at the reservoir edge and the risk of fault reactivation due to pressure effect is considered low. The fact that none of the faults in the P18-6 storage site extend to above the caprock reduces the impact of any fault destabilisation.

### *Temperature effect on fault stability*

In order to model the temperature effect on fault stability a TNO-proprietary geomechanical semi-analytical approach has been used. The distance reached by the cooling front is the determining parameter for the fault stability analysis. When the cooling front reaches a fault, the induced Coulomb stresses by the temperature effect can be such that locally, at this particular location, the fault can be reactivated. Given this distance criteria, one P18-6 fault close to a well has been identified as potentially locally reactivated by the coupled temperature and pressure effect. Adjusting the injection rate at the particular well close to this fault can be a solution to maintain the distance of the cooling front at a safe distance from the fault.

### *Geochemical effects on fault stability*

The impact of geochemical alterations in fault zones is unlikely to lead to CO<sub>2</sub> migration along faults. Currently the migration of methane along faults cannot be ruled out but if it happens the cumulative volumes of methane migrating along the fault remain below the detection limit in seismic data, strongly suggesting that flow rates are insignificant, if occurring at all. This, in turn limits the speed and depth of penetration of CO<sub>2</sub> into a fault zone, rendering the impact of chemical alterations insignificant.

## 8 Caprock integrity

### 8.1 Introduction

This section focuses on the potential reactivation of faults in the caprock due to pressure increase during CO<sub>2</sub> injection (Section 8.2), to temperature effects from the injection of low-temperature CO<sub>2</sub> (Section 8.3). Changes in pressure and temperature inside the reservoir can induce different stress changes between intra-reservoir section of the pre-existing faults and their caprock section. Section 8.4 discusses geochemical effects of interaction between CO<sub>2</sub> and the caprock.

The caprock overlying the P18-6 field has a thickness of more than 450 m. None of the faults that exist in the field or that bound the field extend to above the caprock. This means that the consequences of fault reactivation are likely to be limited.

The conclusion from the results presented below is that the risk of reactivation of faults in the caprock due to the injection of CO<sub>2</sub> is very low. The interaction between CO<sub>2</sub> and the caprock is expected to be insignificant.

### 8.2 Pressure effect on caprock integrity

This section considers the potential destabilization of pre-existing faults inside the caprock due to the pressure effect. These faults are the ones present inside the reservoir flow model that extend upward into the caprock. The pressure-induced Coulomb stress changes along the pre-existing fault planes are thus calculated following MACRIS analysis and is detailed in Section 7.1; implicitly it is also assumed that generating a new fault will require larger stress changes.

Figure 7-2, Figure 7-3 and Figure 7-4 show that the Coulomb stresses rapidly decay near the top of the reservoir within the caprock. The pressure effect is thus not expected to contribute to the risk of fault reactivation in the caprock.

### 8.3 Temperature effect on caprock integrity

A temperature decrease of the reservoir due to the injection of relatively cold CO<sub>2</sub> induces contraction of the rock mass and a change in total stress, dependant on the boundary conditions. The induced stress changes take place inside the reservoir, but also within the caprock on top of it. The present section addresses the magnitude and distribution of temperature-related stress changes in the caprock. The main question addressed in this section is: what are the risks of reactivating a pre-existing fault in the caprock due to the temperature-induced stress changes?

To answer this question we used a TNO-proprietary geomechanical semi-analytical approach detailed in Section 17.8.2 and already introduced in Section 7.3. The same temperature field as the one considered for intra-reservoir fault reactivation after 5 years of injection is taken as input (see Figure 7-6).

According to the semi-analytical approach, and as mentioned previously, faults are not explicitly modelled but the changes in Coulomb stress which are induced by the reservoir cooling can be calculated for any fault orientation and at any location

within the caprock. The Coulomb stress changes are thus defined for any fault plane in the caprock; generating a new fracture will require larger shear stress than those for reactivating a fault plane. The fault planes should therefore be seen as “potential fault planes” since faults have not explicitly been identified in the seismic cube.

The results achieved (see Figure 8-1 and Figure 8-2) indicate that on top of the cooled part of the reservoir, the changes in Coulomb stress are negative. On these locations in the caprock, therefore, there is no risk of fault reactivation due to cooling of the reservoir below it. Only on top of the reservoir beyond the edge of the cooling front, the changes in Coulomb stress start to be positive (see Figure 8-1 and Figure 8-2). For this analysis the optimally oriented fault planes were chosen, i.e. for any location the fault orientations where the Coulomb stress changes are maximum were selected. Consequently, the current approach in terms of risk quantification can be seen as conservative, or worst case. However, Figure 8-2 shows that instead of considering the optimally oriented fault planes but the orientations of the P18 faults cross-cutting both the reservoir and caprock, it would have led to similar changes in Coulomb stress.

To summarize, the potential risk of reactivating a pre-existing fault in the caprock is very low.

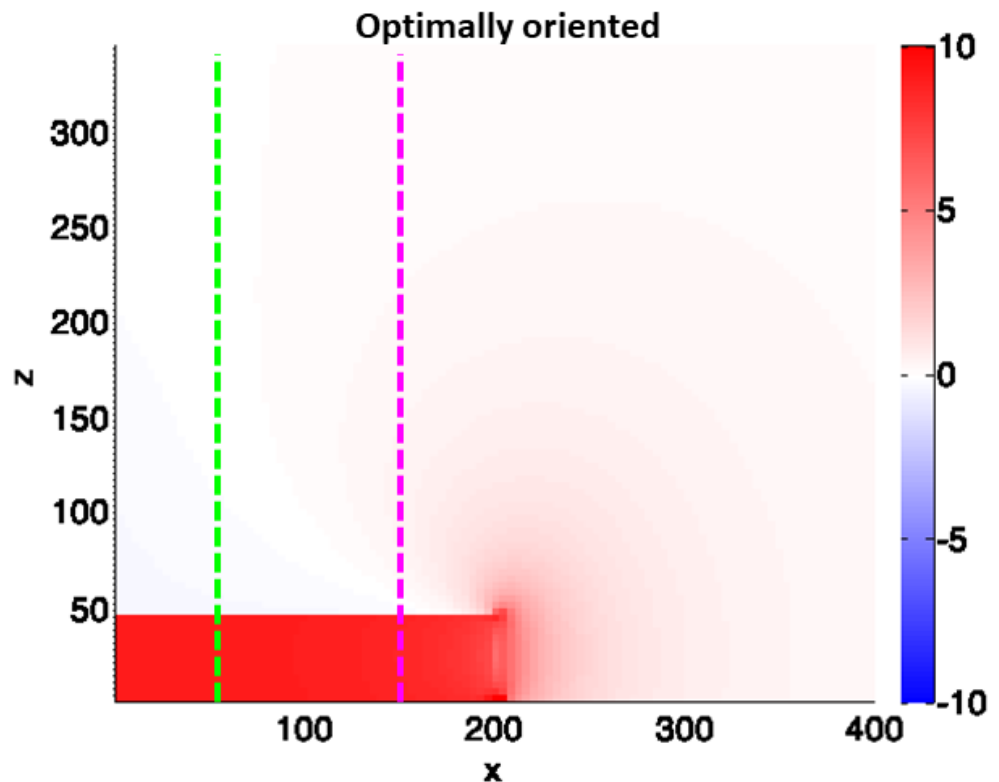


Figure 8-1 Thermo-elastically induced Coulomb stress changes in units of MPa along optimally oriented fault planes. The vertical dashed lines represent the stress profiles displayed in Figure 8-2.

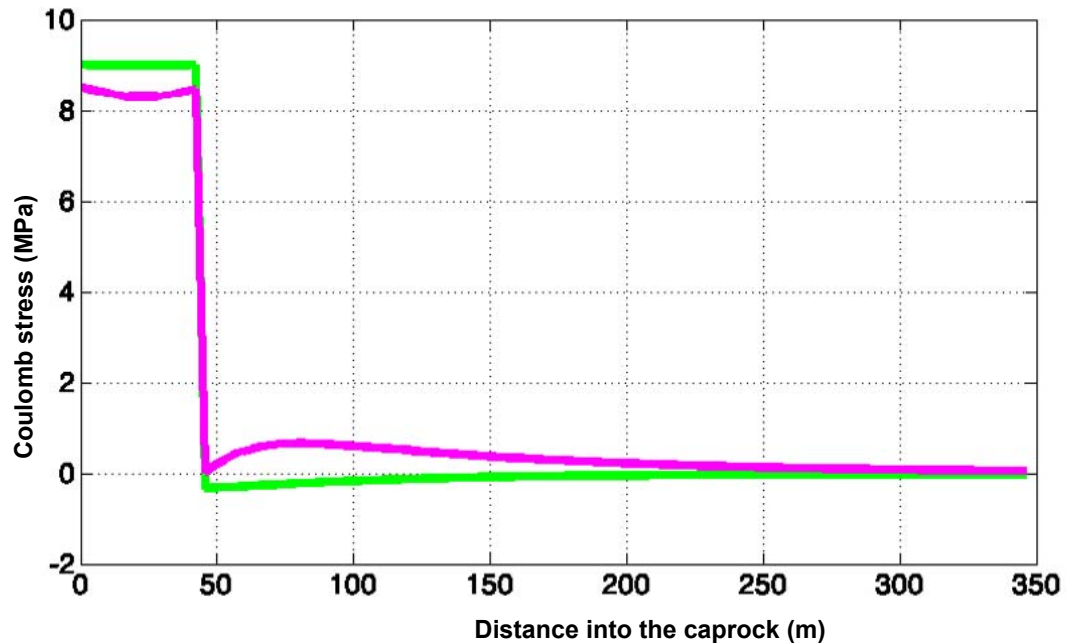


Figure 8-2 Profiles of thermo-elastically induced Coulomb stress changes in units of MPa. Each colour corresponds to different vertical cross-sections for the stress profiles as displayed in Figure 8-1.

## 8.4 Geochemical effects

### 8.4.1 Introduction

Geochemical reactions between CO<sub>2</sub> and the caprock minerals can change the sealing capacity. The geochemical effects of CO<sub>2</sub> on the caprock, and the impact of these effects on its sealing integrity need to be evaluated to assess the risk of leakage through the caprock of the P18-6 reservoir on the long term. These are described below based on recent literature.

### 8.4.2 Geochemical effects of CO<sub>2</sub> on caprock integrity

The caprock of the P18 reservoirs comprises the Solling Claystone Member with the Röt Claystone and Main Evaporite Members situated above. Caprock material of the P18 reservoirs has not been obtained during drilling operations. Caprock material of the nearby Q16 reservoir as analogue for P18 caprock was characterized by Peach et al. (2019). Eight caprock samples from the Solling and Röt Formations were measured for gas permeability and porosity. All permeability values were below 0.1 mD and porosity ranged between 0.02 and 5.3%. Four samples from the Röt Formation were analysed by XRD and eight samples of Solling and Röt Formations were analysed by optical microscopy. The samples were carbonate-rich mudrocks with a mineralogy mainly made up of carbonates (ankerite or dolomite), phyllosilicates (mica and clay) and quartz (Peach et al., 2010).

The caprock of both the P18 and the Q16 gas fields has a proven sealing capacity for natural gas yet, CO<sub>2</sub> behaves differently than natural gas, both from physical

and chemical perspective. The low permeability measured for the Q16 caprock samples justifies the assumption that penetration of supercritical CO<sub>2</sub> (scCO<sub>2</sub>) into the caprock will not occur, as long as the CO<sub>2</sub> pressure in the reservoir remains well below the pre-production gas pressure. The only way for the CO<sub>2</sub> to migrate into the caprock is by upward diffusion in a dissolved state. The diffusion is driven by an increased concentration of dissolved CO<sub>2</sub> in the reservoir pore and at the contact with the caprock. Tambach et al. (2012, 2015b) report on 1D reactive transport simulations that were performed with PHREEQC to assess the interaction of dissolved CO<sub>2</sub> during upward migration into the caprock. Due to the lack of detailed caprock mineralogical analysis, the mineralogy was based on samples from the adjacent P15 field, analysed and reported by Spain and Conrad (1997). The detailed analysis showed a much higher quartz content than the analyses by Peach et al. (2010). Dolomite, illite and anhydrite are present in moderate amounts, and small amounts of K-feldspar, albite, siderite and pyrite were identified. The simulation results showed that the upward diffusion of dissolved CO<sub>2</sub> and the associated pH decrease is very slow. During the upward migration, mineral reactions occur to buffer the pH and convert the dissolved CO<sub>2</sub> into carbonate minerals. This further slows down the upward migration of the dissolved CO<sub>2</sub>. After 10,000 years some mineral reactions and a minor porosity increase was simulated only in the 5-10 metres above the reservoir-caprock contact (Figure 8-3). A sensitivity study on mineral types and reactive surface areas predicted a porosity increase in the bottom part of the caprock of no more than 0.7%. Only one simulation predicted a porosity decrease of 1.8% in the first metre and porosity increase up to 5 metres into the caprock (Tambach et al., 2012).

Gaus et al. (2005) found similar orders of magnitude for the extent and scale of geochemical reactions in shale caprock at the Sleipner injection site in Norway. The authors predicted either a porosity increase or decrease in the lowest few metres of the caprock, depending on the mineralogical composition of the rock, 3,000 years after injection. The predicted porosity increases are below 0.05%, porosity decreases are up to 2.6%. For two different mineral compositions, the migration of dissolved CO<sub>2</sub> reached either 1.5 or 10 meters into the caprock after 3000 years (Gaus et al., 2005). In the first scenario, a more reactive mineral composition was able to sequester the CO<sub>2</sub> in carbonate minerals much faster, thereby retarding the upward migration of dissolved CO<sub>2</sub>. Wang et al. (2019) also predicted minor mineral reactions and porosity increase in shale caprock after 1,000 years and concluded that mineral dissolution and precipitation reactions have 'small to negligible impact on the permeability of the caprock'.

In a more detailed reactive transport simulation, assessing the impact of heterogeneities in shale caprock, local penetration of supercritical CO<sub>2</sub> was predicted in areas of a caprock with lower sealing capacity (Tian et al., 2019). Local changes in porosity and permeability (both positive and negative) were predicted, related to variations in mineral compositions. Vertical migration of the CO<sub>2</sub>, in those areas that penetration occurred, reached almost 50 m into the caprock after 500 years (Tian et al., 2019). With a total caprock thickness for the P18-6 reservoir of several hundreds of meters, migration of small amounts of CO<sub>2</sub> out of the storage would take > 1,000 years. Such a scenario represents a worst case condition, as exploration data for the P18-6 did not show any evidence for penetration of gas into the caprock, providing evidence for the overall sealing capacity of the P18-6 caprock.

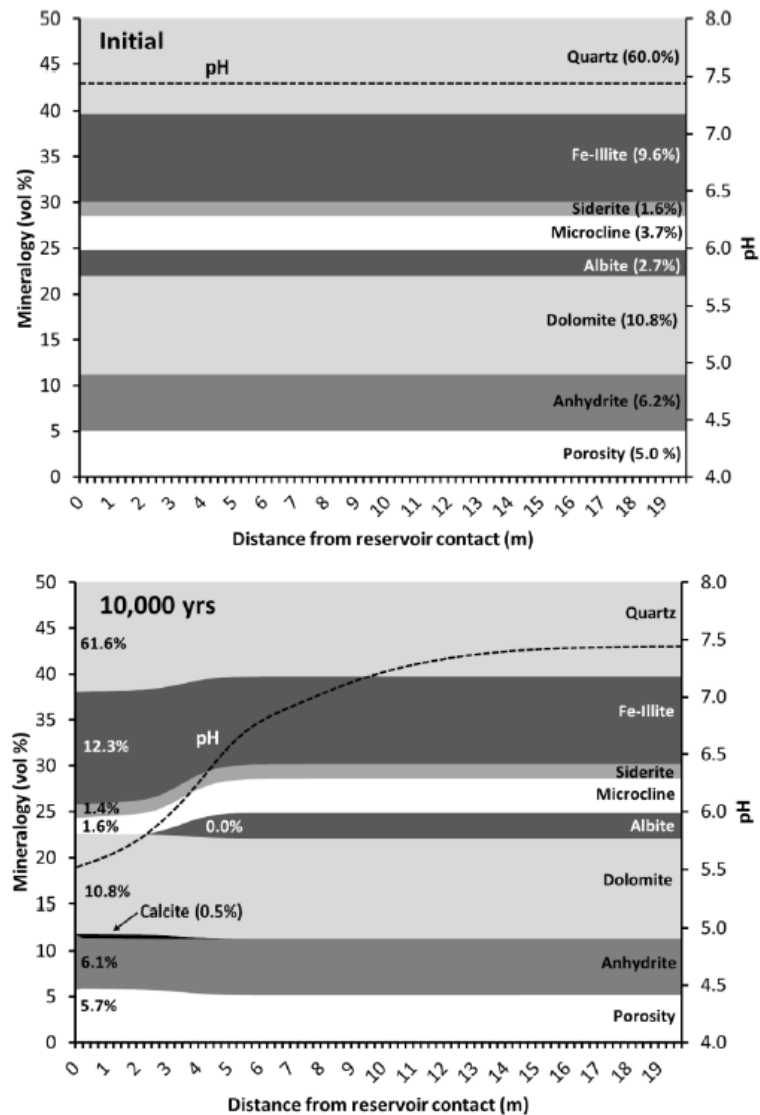


Figure 8-3: Initial mineralogy of the caprock and mineralogy after 10,000 years of simulation as a function of the distance from the reservoir contact. Up to 50 vol% is shown, the remaining part is made up of quartz. From Tambach et al. (2012).

## 8.5 Conclusions

### *Pressure effect on caprock integrity*

Following the MACRIS approach, both induced Coulomb stresses along the intra-reservoir part of the faults and those along the intra-caprock part of the faults have been assessed. These Coulomb stresses rapidly vanish on top of the reservoir inside the caprock; the intra-caprock mapped faults are thus not expected to be reactivated by the pressure effect.

### *Temperature effect on caprock integrity*

In order to model the temperature effect on pre-existing faults in the caprock, a TNO-proprietary geomechanical semi-analytical approach has been used. The geomechanical analysis shows that the changes in Coulomb stresses in the



caprock due to reservoir cooling are negative. The risk of intra-caprock fault reactivation is thus very low.

*Geochemical effects on caprock integrity*

CO<sub>2</sub> is not expected to significantly interact with or migrate into the caprock.

## 9 Well integrity

### 9.1 Introduction

This section presents the analysis of the integrity of the well in the P18-6 field. Well integrity is considered at in the following sections at four levels:

- The integrity of the well in its current state (Section 9.2);
- The effect of injecting cold CO<sub>2</sub> on the integrity of the well (Section 9.2.2);
- Geochemical processes acting on the cement (Section 9.3.4);
- Well decommissioning (Section 9.4).

The conclusions from the well integrity analysis are the following:

- *Well integrity.* The P18-6 well has the potential to be used safely as CO<sub>2</sub> injection. Appropriate mitigation measures are proposed to make the well fit for storage operations.
- *Effects of injecting cold CO<sub>2</sub> on well integrity.* It is highly likely that de-bonding of cement interfaces will take place upon cold CO<sub>2</sub> injection, creating microannuli. The characteristics of the microannuli and pressure conditions determine whether upward CO<sub>2</sub> migration would actually take place. Keeping the CO<sub>2</sub> pressure in the reservoir below hydrostatic pressure conditions will reduce the likelihood of leakage through microannuli.
- *Well decommissioning.* Appropriate methods should be used for the decommissioning of the well. Given the likelihood of microannuli forming during the injection of cold CO<sub>2</sub>, decommissioning methods that remove these potential leakage paths could be considered. As an example, full-bore pancake like plugs would provide formation-to-formation closure of the injection well.

### 9.2 Status of the well barriers

#### 9.2.1 Well Integrity assessment approach

Currently there are no specific industry standards for CO<sub>2</sub> injection wells. Therefore the approach followed in this well integrity assessment is to utilize existing oil and gas industry standards that address well integrity for injectors and complement any specific gaps for CO<sub>2</sub> injection wells if required.

The standards on which this well integrity assessment is based are:

1. Norsok Standard D10, rev. 4 June 2013 - Well integrity in drilling and well operations (NORSOK, 2013);
2. ISO standard 16530-1:2017, March 2017 - Petroleum and natural gas industries - Well integrity, Part 1: Life cycle governance (ISO/TC 67/SC 4 Drilling and production equipment, 2017);
3. NOGEP industry standard no. 45, 12 October 2016 - Well decommissioning (NOGEP - OPCOM, 2016).

The reports related to well integrity and CO<sub>2</sub> storage and used for this assessment are:

4. MiReCOL report, February 2015 - D8.1 Description of leakage scenarios for consideration in the work in SP3 (Vrålstad, et al., 2015);

5. Dutch State Supervision of Mines (SSM/SodM), January 2019 – The integrity of onshore wells (SodM, 2019).

For the sake of completeness some relevant sections of the above mentioned standards and reports are presented.

1. The Norsok D10 standard refers to well integrity by:
  - General principles: A two well barrier concept of primary barrier and secondary barrier for wells penetrating into hydrocarbon bearing formations and/or formations with the potential to flow to surface.
  - Structural integrity: the key components (conductor, guide base, risers) that provide structural integrity of the well during its service life shall be evaluated with respect to loads, wear and corrosion.
  - Injection / disposal wells: The well shall be constructed such that the injected media will be contained within the targeted formation zone (reservoir) without risk of out of zone injection.
  - WBS examples: Permanent well decommissioning (abandonment) is illustrated by a primary well barrier at caprock, secondary well barrier at intermediate section and an open hole to surface barrier.
2. The ISO well integrity standard refers to the Norsok D10 standard and considers:
  - Structural integrity monitoring: The well operator should establish suitable systems to model or measure degradation in the structural well operating limits. The conductor, surface casing (and supporting formations) and wellhead assembly typically provide structural support for the well. Failure of these structural components can compromise well integrity and escalate to a loss of containment. For each well the well operator should assess the risk of failure of such structural components.
3. The NOGEPa no. 45 standard on well decommissioning has the following statements on well decommissioning.
  - Summarised mandatory requirements for Well Decommissioning:
    - o A permanent barrier shall extend across the full cross section of the well covering all annuli.
    - o The depth of the permanent barrier shall be selected to be adjacent to the caprock of adequate thickness with an estimated formation fracture pressure that exceeds the maximum anticipated pressure at depth.
    - o In case of cement, the permanent barrier length inside the inner wellbore shall be:
      - At least one hundred meters long (100 m), or
      - At least fifty meters (50 m) when placed on top of a tested mechanical support in cased hole.
4. The MiReCOL D8.1 report refers to Norsok D10 and includes the following information on well integrity:
  - The report considers well barrier breaches (CO<sub>2</sub> migration along the well bore) and includes the in-situ formation of the previous casing behind the liner lap as a barrier element to mitigate the risk of out of zone injection (which is conform Norsok D10).

- Aging issues with cement degradation, casing corrosion and wear, and thermal loads imposed on the well infrastructure are examples of the most likely causes for well leakages.
5. SodM (2019) categorizes CO<sub>2</sub> storage wells as gas wells from a well integrity perspective with the associated well failure model identifying potential leak paths, see Figure 9-1 (this is based on the ISO 16530 well failure model).

It should be noted that SodM defines the Surface tree (also known as the X-mass tree) as a secondary barrier element and the Surface Controlled SubSurface Safety Valve (SCSSSV) as primary barrier element, which is conform the Norsok D10 standard. However, they do define failures of the tubing above the SCSSSV, the control line, tubing hanger and feedthroughs (blue items 3, 16 and 17 in Figure 9-1) as primary leakage elements, which is a variation on the Norsok D10 standard.

In this report Norsok D10 is primarily followed, as a result all elements above the SCSSSV are considered to be secondary barrier elements (because they are isolated in the event of an SCSSSV closure).

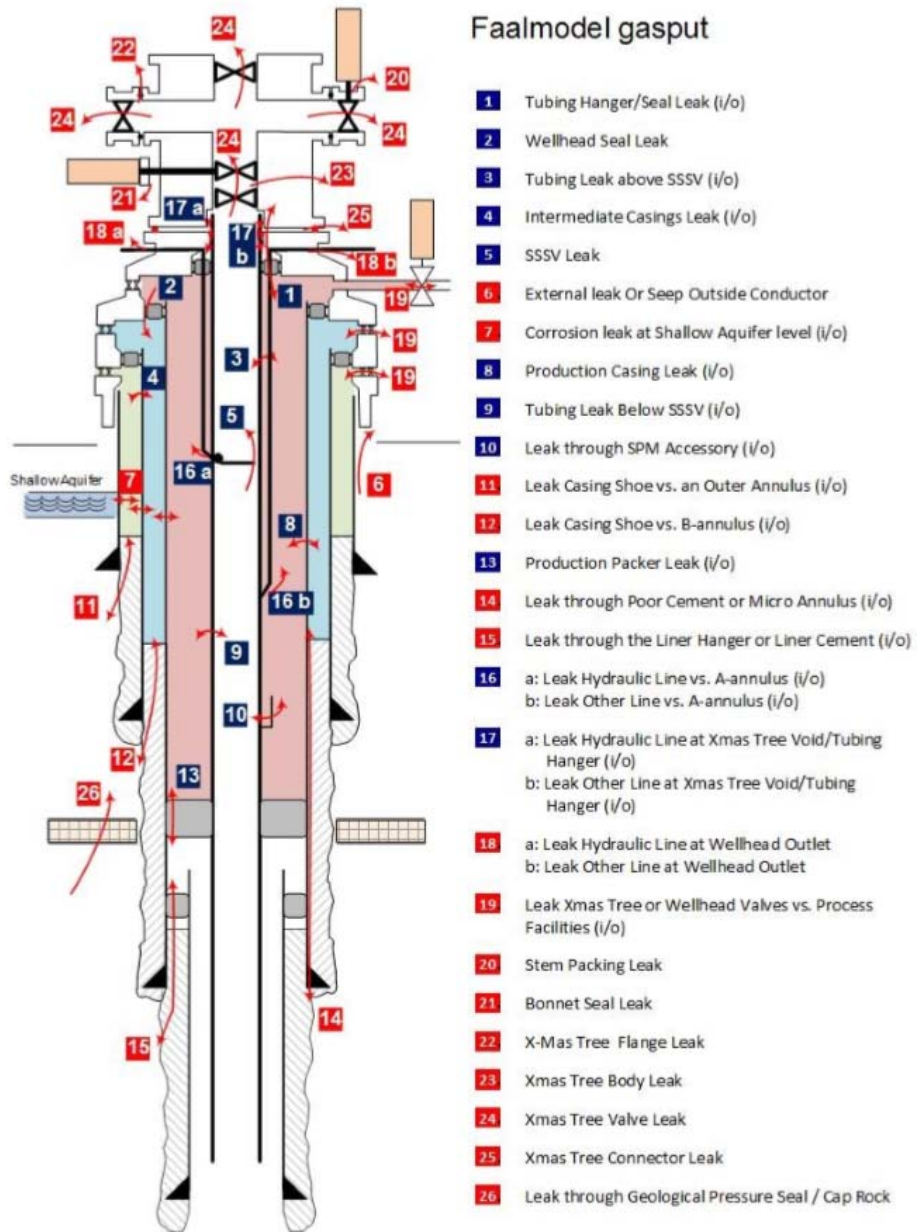


Figure 9-1 Well failure model for gas wells, including storage wells. (SodM, 2019). The blue numbers are primary barrier element failures and the red numbers are secondary barrier element failures.

9.2.1.1 Well integrity assessment concept

Based on the reviewed standards and reports, the scope of the well integrity assessment in this report includes and reviews the following elements:

- a) The primary and secondary well barrier elements from reservoir caprock to surface, conform NORSOK D10.

- b) The risk of out of zone CO<sub>2</sub> injection due to a failure of a primary and/or a secondary barrier, with supporting in-situ formation of the previous casing below the liner lap.
- c) Structural integrity of the load bearing surface casing, conductor or riser.

The definition of the barrier elements for this assessment comes from Norsok D10.

- Primary well barrier: first well barrier that prevents flow from a potential source of inflow.
- Secondary well barrier: second well barrier that prevents flow from a potential source of inflow.

The structural integrity assessment of the load bearing surface casing is for this assessment limited to a review of the “as built” status, identifying the potential well integrity risk.

It should be pointed out that the assessment of the influence of fatigue or corrosion on well integrity, with the structural load effects and associated thermal and pressure cycles, is not in the scope of the current work. This should be considered as the next fundamental step in assessing the structural well integrity lifecycle for the CO<sub>2</sub> injection program.

### 9.2.2 P18-6 well integrity analysis

The P18 fields have been subjected to CO<sub>2</sub> storage assessment and well integrity evaluations in the CATO-2 R&D programme (Akemu, et al., 2011). The previous well integrity assessment focused on the P18-4 field and identified and evaluated barriers of wells relevant for the foreseen storage operation and identified gaps or uncertainties about barrier status in general. Based on this previous study it was not possible to decide on the suitability of the P18-6 well for CO<sub>2</sub> injection and storage given the new operating envelope. The present assessment is based upon the previous work and addresses the gaps that were identified earlier. It considers new findings, as well as information that was not available at the time of the first studies.

The present study includes:

- An assessment of well penetrating the P18-6 reservoir P18-A-07-S1);
- An assessment of earlier identified gaps, by detailed review of the end-of-well reports (EOWR)<sup>7</sup>, newly obtained records and quantification of the relevant barrier elements for the primary, secondary and structural barriers in place;
- Illustration of well barrier envelope status in a well barrier diagram combined with the potential risks for each barrier, with the aim to assist on assessing the suitability of the well for injection of CO<sub>2</sub> in the P18-6 reservoir.

### 9.2.3 General well integrity P18-6 and well status issues

The status of the P18-A-07-S1 well, penetrating the P18-6 reservoir, that emerges from the review of previous work is as follows:

- a) The well has not been assessed for the well completion load case for CO<sub>2</sub> injection with respect to temperature and pressure.
- b) No assessment records were found on the lifecycle assessment of load bearing surface casing and conductor. External corrosion due to corrosive fluids and Metocean induced fatigue of the load bearing casing could reduce

<sup>7</sup> Two end of well reports were used. Well P18-A-04 is the bottom (20" and 30") of well P18-A-07-S1. The well report for well P18-A-04 is Amoco (1993); the EOWR for well P18-A-07 is BP (2003).

- its lifecycle load capacity. This is a fundamental requirement to assess the lifecycle of the well and the risk of loss of well integrity.
- c) The expected final CO<sub>2</sub> reservoir pressure for P18-6 is maximised at initial pressure (see Section 5.5); this has been considered in the assessment of individual barriers.
  - d) The material specifications of the flow wetted barrier elements like surface tree, tubing hangers, completion accessories and seals / elastomers need to be validated against the CO<sub>2</sub> injection operating envelope.

#### 9.2.4 Well P18-A-07-S1

The P18-A-07-S1 well was drilled and completed in the P18-6 block in 2003. The Glomar Adriatic III installed a 20" casing in 1993 in slot 6 with the casing shoe at 416 m MD (reported MDBRT); the well name at that time was P18-2A4. In 2003 a 17 ½" pilot hole was drilled at this slot to 1014 m MD, which was subsequently enlarged to 22" (target depth at 1009 m MD) with an underreamer. A 17" liner was installed with the liner shoe at 1007 m MD.

The original 16" hole was drilled from 1007 m to 1883 m MD. Due to borehole instabilities the drill string got stuck and was cut, the original hole was abandoned. The 16" hole was side tracked from 1025 m MD and completed as a gas producer with a 4 ½" 13Cr-L80 completion. It has been assessed in view of CO<sub>2</sub> storage with the following results (see also Figure 9-2 and Table 9-1).

##### Primary barrier

- The 7" liner is made of P110 (carbon steel) material, it is reported to be successfully cemented, no CBL has been executed. The liner was tested as part of the full (combined) 9 5/8", 7" and 5" well pressure test to 3800 psi (262 bar). The 7" liner shoe was drilled out and a successful FIT of 13 ppg was conducted.
- The 5" liner was installed and cemented with an early bumped plug, most probably due to the top dart/plug bypassing some of the cement. The liner was tested to 3800 psi (262 bar). The 5" liner shoe was drilled out (hard cement) and a successful FIT of 12 ppg was conducted.
- The 5" top of liner was set approximately 35 meters above the cap rock.
- The Aalburg shale that covers part of the 5" liner has natural formation sealing potential. This could improve the sealing performance over time.
- The 5" liner is made of 13Cr-L80 and has no risk for corrosion. It is set in the 7" liner creating a double barrier for the 105 m long section between the top of the 5" liner and the 7" liner shoe, which is set in the cap rock.
- The production packer is located above the caprock and set in the 7" carbon steel liner, the 96 meter section of 7" liner between top of 5" liner and bottom of packer is flow wetted and is exposed to potential corrosion. Failure of this 7" liner section would result in leakage into the overburden (single barrier event).
- The well has a stable 6 bar pressure reported on the production annulus.
- The well has a 3 ½" pre-drilled liner installed, this is uncemented and is therefore not part of the primary barrier.

#### Secondary barrier

- The 7" liner was installed within 68 meters of the cap rock and successfully cemented and tested to 3800 psi (262 bar), combined with the 5" liner test. There has been no CBL executed.
- The 7" liner is covered by the Vlieland shale that has the potential of NFS (natural formation sealing). The 7" shoe track was drilled out and a successful FIT of 13 ppg was conducted in the top of the cap rock.
- The 9 5/8" casing was run and cemented with 175 barrels of cement, with 30 barrels losses during the pumping of the cement. An additional 199 barrels were reported to be lost during displacement. The top of cement (TOC) is calculated to be at 1840 m MD (which corresponds to 1570 m TVD). No CBL has been executed. The casing is tested to 3800 psi (262 bar) combined with the 5" and 7" liner test.
- The 9 5/8" shoe track was drilled out and a successful FIT of 12.3 ppg was conducted.

#### Structural well integrity

- The 13 3/8" casing is placed at 2290 m MD and has a poor cementation, several cement squeezes have been executed after drilling out the shoe, this resulted in a leak off test (LOT) of 9.7 ppg.
- The section between 17" casing shoe at 1007 m MD and the 13 3/8" casing shoe at 2290 m MD is uncemented. The 17" liner was run without a hanger and set on bottom of the 17 1/2" x 22" hole and cemented from the 17" shoe at 1007 m to the top of the 17" liner at 369 m MD.
- The 20" casing shoe is placed at 416 m MD and was cemented to surface (cement returns at spider deck reported in EOWR; Amoco (1993), p.236). Cement has been placed from 351 m to 200 m MD between the 20" and 13 3/8" casings on top of an 13 3/8" inflatable external casing cement packer.
- The conductor is piled to 131 m MD. The conductor is coated underwater and in the splash zone (Amoco (1993), p. 234)..

#### Discrepancies

- The CATO-2 report on the well integrity assessment (Akemu et al., 2011). did not address the discrepancy of the 7" carbon steel liner below the production packer and the associated risk.

#### Summary

- From Table 9-1 it can be seen that the primary and secondary barrier elements could be validated, although no CBL's were executed.
- For the primary barrier the production packer is situated above the caprock, exposing the 7" carbon steel liner to well fluids and thereby introducing the risk of corrosion. This may cause failure and leakage to the overburden above the cap rock, which needs to be evaluated and potentially mitigated.
- The 7" liner shoe is set and cemented in the caprock and tested. The 5" liner is set, cemented and tested, providing a good seal in the caprock.
- The secondary barrier is formed from top of production packer with a 7" liner and 9 5/8" casing string to surface with the 7" liner lap and the 9 5/8" cemented and tested.



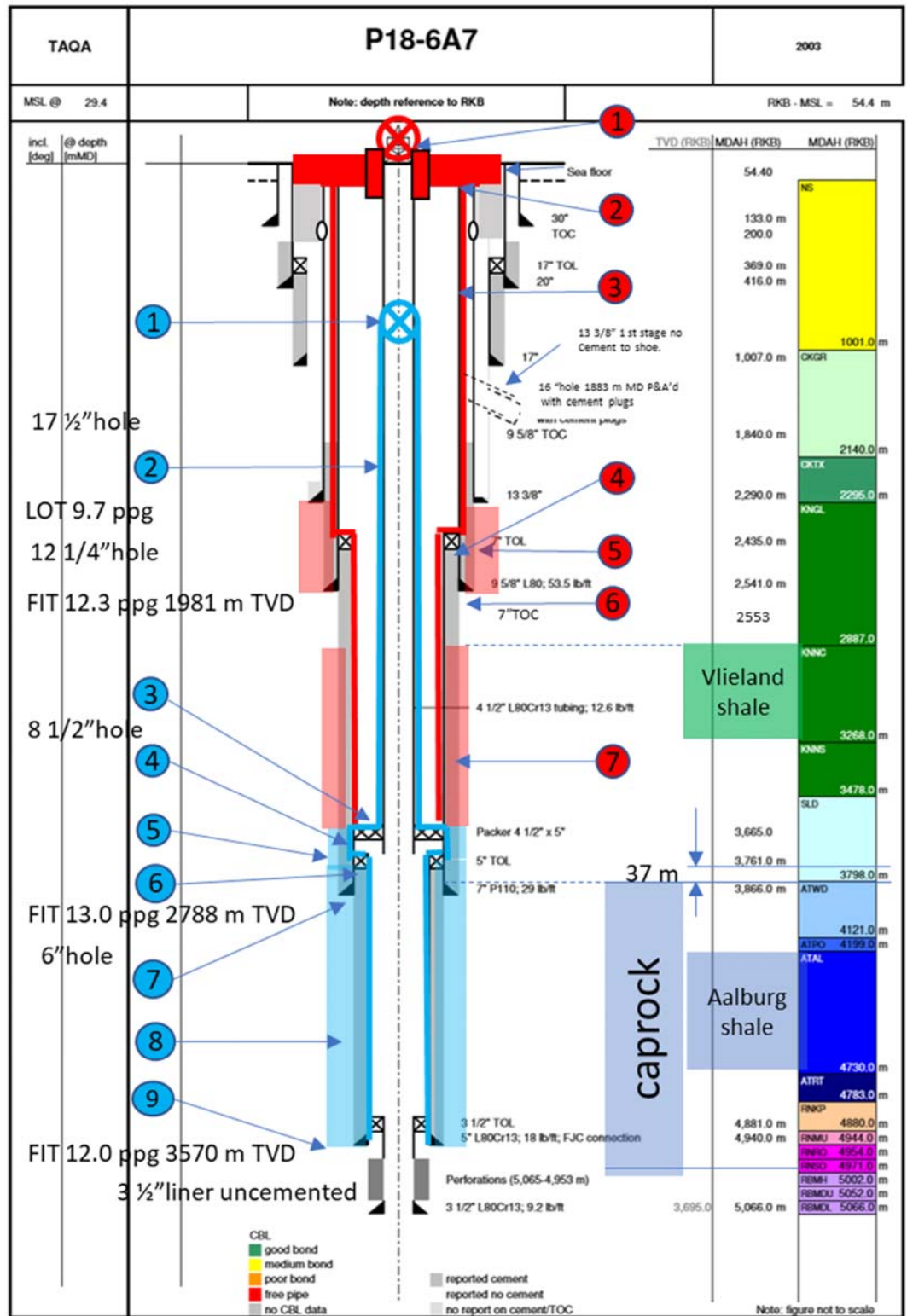


Figure 9-2. Well P18-A-07-S1 barrier diagram with barrier elements defined. See Table 9-1 for a discussion of the barrier elements (indicated by the numbered circles).

Table 9-1 Well P18-A-07-S1 barrier element assessment based on current data set. The numbers in the first column correspond with the numbers in coloured circles in Figure 9-2.

no	P18 6A7	As built	Monitor	Barrier validated	Validation Criteria
<b>Primary well barrier</b>					
1	4 1/2" Scsssv		Maintained	Yes	Tested & maintained
2	4 1/2" Tubing	Tested to 4050 psi	Annular pressure records	Yes	Tested
3	7" Production packer	The permanent packer is set at 3665 m MD and tested, it is positioned 133 m above the caprock	Annular pressure records	Yes	Tested, set 133 m above caprock
4	7" Liner	The 7" liner is flow wetted over 96 meter between the production packer and the 5" liner lap	Annular pressure records	Yes	Pressure tested to 3800 psi. The flow wetted section is a single barrier to the overburden with a length of 96 m, this is above the caprock
5	7" Liner cement	Good cement report, the calculated TOC is at 2553 m MD (118 m below the 7" top of liner) and tested to 4050 psi, no CBL has been executed	NA	Yes	Good cement report and tested
6	5" Liner + liner lap	Tested to 3800 psi. The top of liner is at 3761 m MD, that is 37 m above caprock.	NA	Yes	Tested - installed 96 m below the production packer
7	In-situ formation (Caprock) at 7" liner shoe	FIT 13.0 ppg at 2788 m TVD	NA	Yes	A FIT of 13.0 ppg at 2788 m TVD has been reported
8	5" Liner cement	It is cemented with 14 bbl short of cement due to the wiper plug bypassing cement. It was tested to 3800 psi and there was no CBL executed	NA	Yes	It has a good cement report Identified NFS potential - Aalburg shale
9	In-situ formation (Caprock) at 5" liner shoe	FIT 12.0 ppg 3570 m TVD	NA	Yes	FIT 12.0 ppg 3570 m TVD reported
<b>Secondary well barrier</b>					
1	Surface tree + tubing hanger	Tested to 3800 psi	Maintained	Yes	Tested & maintained
2	Well head + Casing hanger	Tested to 3800 psi	Maintained	Yes	Tested & maintained
3	9 5/8" Casing	Tested to 3800 psi with 7" & 5" liners	Annular pressure records	Yes	Tested to 3800 psi with 7" & 5" liners
4	7" Liner + liner lap	Tested to 4050 psi. The top of liner is at 2435 m MD.	NA	Yes	Tested to 4050 psi
5	9 5/8" Casing cement	Cement report with some losses reported, the TOC of the 9 5/8" casing is calculated to be at 1840 MD (1570 m TVD). No CBL has been executed. It is tested to 3800 psi	Annular pressure records	Yes	Cement report with some losses reported, it has been tested to 3800 psi
6	In-situ formation	FIT 12.3 ppg at 1981 m TVD	NA	Yes	FIT 12.3 ppg at 1981 m TVD reported
7	7" Liner cement	Good cement report, the calculated TOC is at 2553 m MD (118 m below the 7" top of liner). It is tested to 4050 psi, no CBL has been executed	Annular pressure records	Yes	Good cement report and tested Identified NFS potential - Vlieland shale

### 9.2.5 Conclusion on current well status

The P18-A-07-S1 well is relevant in the context of CO<sub>2</sub> injection into the P18-6 reservoir and has been evaluated regarding its current status and well integrity risks. The well has the potential to be used safely as CO<sub>2</sub> injector. Appropriate mitigations can make it fit for CO<sub>2</sub> storage operations as given below.

#### 9.2.5.1 Summary

The P18-A-07-S1 well could be re-used safely for CO<sub>2</sub> injection if the risks identified are mitigated properly; see overview in Table 9-2.

Table 9-2 Overview of P18-6 CO<sub>2</sub> injector well.

Well	Status	Integrity for CO <sub>2</sub> injector	Remarks
P18-A-07-S1	Producer	Yes	The production packer is placed above the caprock, this extends the 7" liner from above the caprock past the production packer. The 7" liner is made of P110 carbon steel and is exposed to corrosion of well bore fluids, with a potential risk of failure and leakage to the overburden. Repositioning of production packer to inside caprock should be considered.

### 9.3 Influence of cooling on well integrity

Injection of CO<sub>2</sub> at a lower temperature than the temperature of the surrounding rock can cause thermal contraction of the materials and associated stress reduction of the surrounding rock in the near-well area that may affect the structural integrity of the well barriers. The operating envelope of P18-6 CO<sub>2</sub> injection well needs to consider cooling effects, which are not part of the current operating envelope designed for natural gas production.

In this section we provide an estimate of the effects of cooling due to cold CO<sub>2</sub> injection on the structural integrity of the injection well, focussing on the integrity of annular cement behind the casing, and discuss the risk of leakage along the outside of the well. Potential failure modes of the sealant (cement sheath) that can create potential continuous leakage pathways up the well across the caprock are of primary interest (Figure 9-3). The most likely leakage mechanism is related to the flow of fluids along a microannulus formed by de-bonding of the cement-casing interface or the cement-formation interface.

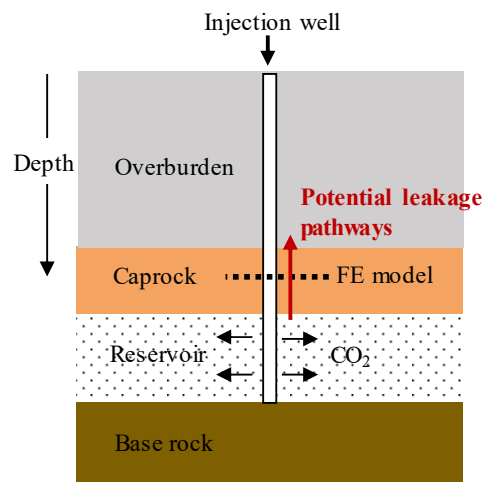


Figure 9-3: Sketch of an injection well showing the location of a finite element (FE) model for well integrity analysis at the caprock level. The model represents a cross-section of the near-wellbore area normal to the well axis at the analysis depth (see Figure 9-6). Please note that the relative sizes of reservoir, caprock and overburden are not to scale.

Note that, in order for CO<sub>2</sub> to migrate and eventually leak to the overburden through a microannulus, several events have to take place and several constraints with regard to subsurface conditions have to be met. The likelihood of cement-casing or cement-rock debonding to take place during injection of cold CO<sub>2</sub> in the P18-6 well is investigated using a numerical model based on the DIANA finite elements<sup>8</sup>. Subsequently, the likelihood that a continuous microannulus forms along the entire caprock level towards the overburden, and the conditions that need to be met for CO<sub>2</sub> to migrate through a microannulus into the overburden are discussed. For a worst-case scenario where all events occur and all conditions are met, an estimate of the leakage rate will be given and this will be discussed in the context of the total storage capacity in P18-6.

### 9.3.1 Pressure and temperature in the CO<sub>2</sub> injection well

Section 6.4.3 presents the results of a limited study of the CO<sub>2</sub> conditions in the well during injection. Figure 9-4 and Figure 9-5 show the pressure and temperature profiles for the storage and discharge scenarios, respectively. Figure 9-5 shows that CO<sub>2</sub> temperatures at bottomhole will be about 50 °C (for the storage scenario) or about 70 °C (for the discharge scenario) below reservoir temperature. The figures show pressure and temperature profiles for steady-state conditions; the temperature in the well during a non-steady-state operation (such as a shut-in procedure) may lead to lower temperatures of the CO<sub>2</sub> in the well, but the heat capacity of the well system (such as liner and annulus fluid) prevents those short-lived low-temperature events from significantly changing the temperature of the cement and casing in the deeper parts of the well<sup>9</sup>. The profiles shown in the figures can be used as a reliable estimate of the conditions in the well.

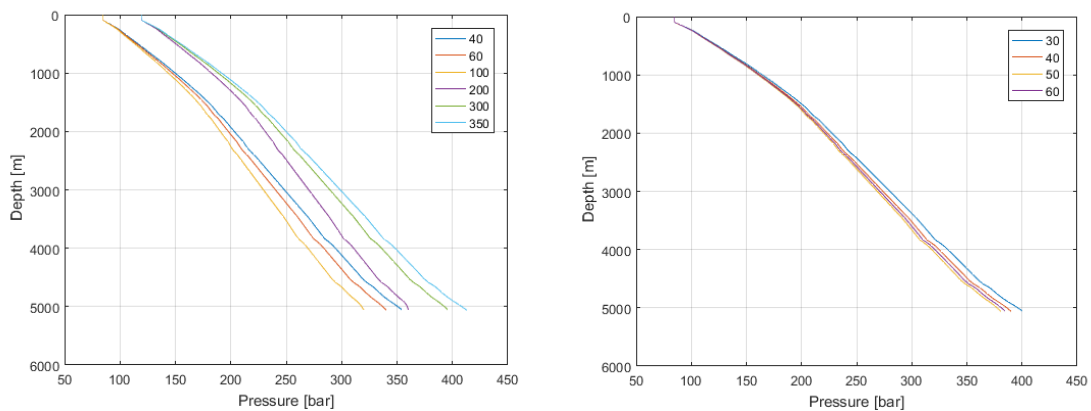


Figure 9-4: Pressure profiles as a function of the along hole depth for the cases of steady-state CO<sub>2</sub> injection from Table 6-1 (left) and pipeline discharge from Table 6-2 (right). Depth along the vertical axis is measured along the borehole.

<sup>8</sup> See [dianafea.com](http://dianafea.com).

<sup>9</sup> S. Belfroid, personal communication, 2019.

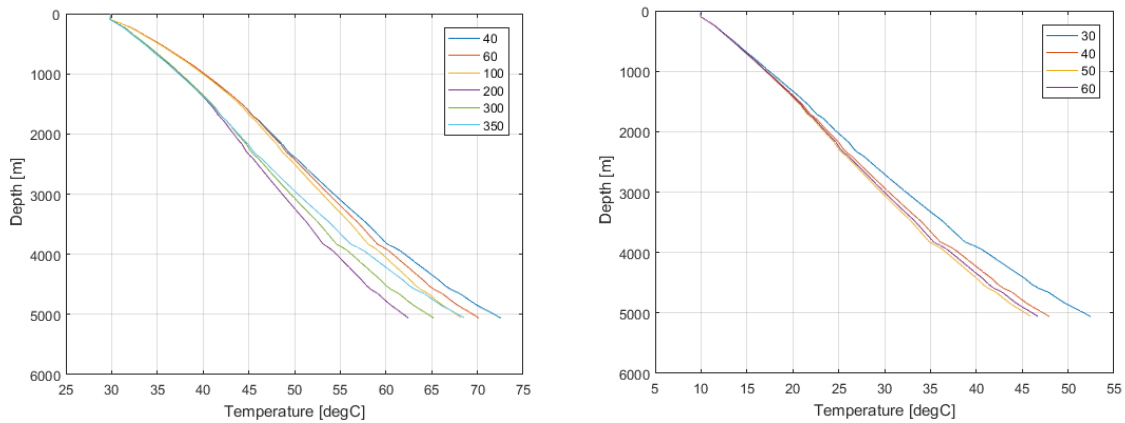


Figure 9-5: Temperature profiles as a function of the along hole depth for the cases of steady-state CO<sub>2</sub> injection from Table 6-1 (left) and pipeline discharge from Table 6-2 (right). Depth along the vertical axis is measured along the borehole. The temperature of the reservoir is 117 °C.

**9.3.2 Numerical modelling of the effects of cold CO<sub>2</sub> injection on well cement integrity**  
 A numerical model was developed to investigate the impact of thermal effects on well integrity, in particular on the integrity of annular cement behind the casing. Thermo-mechanical non-linear finite element analyses considered a section of a CO<sub>2</sub> injection well across the caprock (Figure 9-6), to evaluate whether failure of the well barriers could result in debonding of the annular cement with the casing and/or rock interfaces at caprock level, thereby creating a microannulus. In a worst case scenario, when such a microannulus is continuous from reservoir to above the caprock, a leakage path is formed.

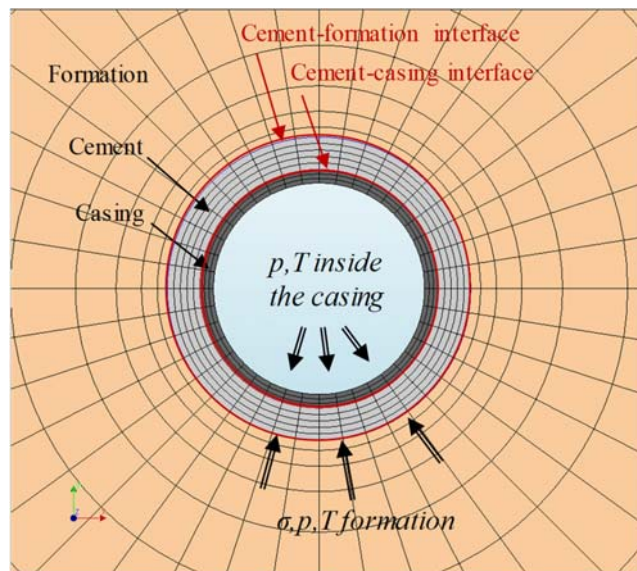


Figure 9-6: Mesh for a 2D finite element model of a cross-section of the near-well area.

Table 9-3: Model input parameters.

Parameter	Unit	Caprock	Cement	Casing	Interface
E Young modulus	GPa	26	8.3	200	rigid
$\nu$ Poisson coefficient	-	0.3	0.1	0.3	-
Thermal expansion coeff.	$K^{-1}$	$1 \cdot 10^{-5}$	$1 \cdot 10^{-5}$	$1.3 \cdot 10^{-5}$	-
Volumetric specific heat	$Jm^{-3}K^{-1}$	$2.24 \cdot 10^6$	$4 \cdot 10^6$	$4 \cdot 10^6$	-
Thermal conductivity	$Wm^{-1}K^{-1}$	2.3	0.87	15	-

The non-linear finite element simulator DIANA was used to generate meshes for 2D numerical models of the well system and run simulations. The workflow for well integrity analysis is automated through a dedicated user interface called the DIANA SEALEC application. Based on the user input in DIANA SEALEC, meshes of the well system can be generated automatically and well integrity analyses mimicking the entire lifetime of a well can be conveniently defined and executed.

The numerical model of the near-well area was developed on a cross-sectional area normal to the well axis. The model comprises well casing(s), cement sheath(s) and the surrounding rock formation. Two models with different well completion geometries were developed: completion with a single casing (Figure 9-7a) and completion with a double casing (or a liner lap; (Figure 9-7b). Chosen sizes and characteristics of casings in the models are representative of the P18-6 well. The possible injection well is completed over the caprock depth interval with a 9 5/8" casing and a 7" liner, and in some cases with a 5" liner.

Complete plane strain elements are used for bulk materials and zero-thickness interface elements are used for the casing-cement and the cement-formation interfaces. All materials in the model are assumed to be elastic and the well material interfaces are assumed to be rigid. The model input parameters are given in Table 9-3.

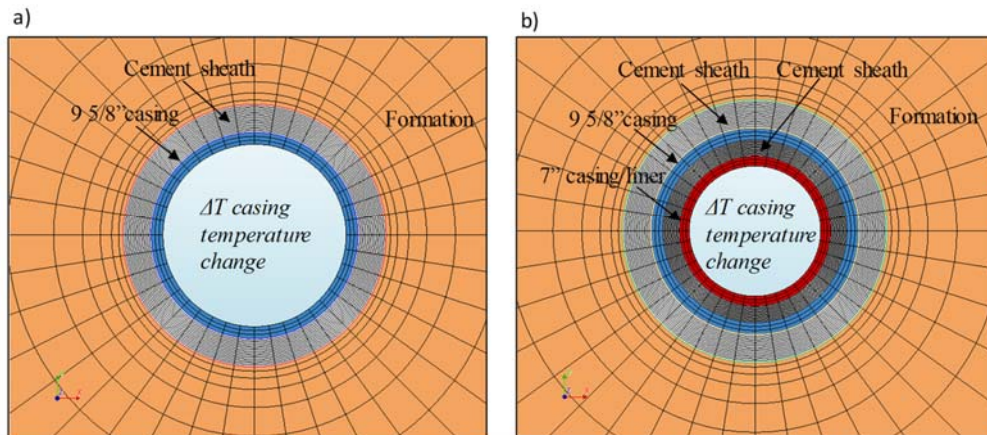


Figure 9-7: Meshes for 2D finite element models of the near-well area at the level of caprock for well sections completed with (a) a single casing and (b) a double casing (liner lap).

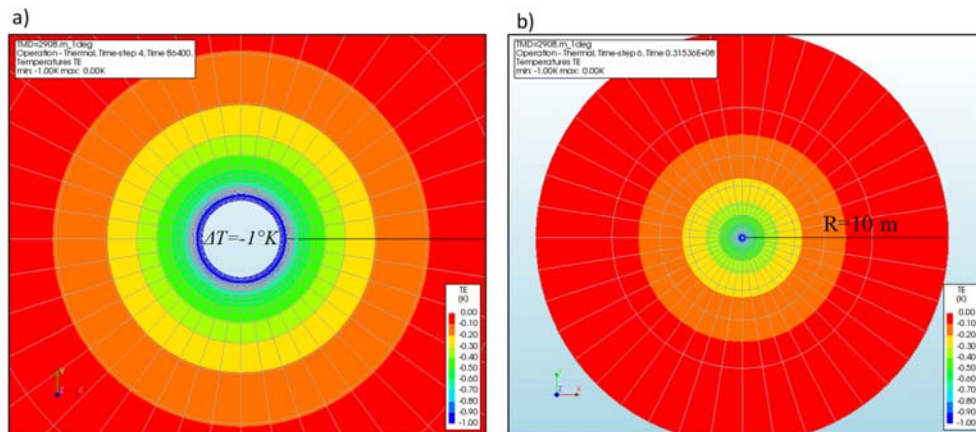


Figure 9-8: Contours of temperature change in the near-well area due to a casing temperature change of  $-1^\circ K$  (or  $-1^\circ C$ ) after (a) 1 day and (b) 1 year. The contour interval is  $0.1^\circ K$ .

The effects of cooling were assessed by applying a temperature load of  $-1^\circ K$  ( $-1^\circ C$ ) on the inner side of the casing instantly at the start of the analysis. As all the well materials in the model were assumed elastic, the magnitude of induced thermo-mechanical stresses ( $\sigma_{\Delta T}$ ) scales linearly with the degree of cooling ( $\Delta T$ ), i.e. the stress magnitude due to cooling by  $\Delta T < -1^\circ K$  is obtained simply by multiplying  $\Delta T$  with the stress magnitude predicted by the model ( $\sigma_{\Delta T} = -1\text{ K}$ ). A staggered heat flow and mechanical analysis is then performed. First a transient temperature field is calculated for a change in temperature of  $-1^\circ K$  ( $-1^\circ C$ ) and then the related thermo-mechanical stresses caused by this temperature change.

Note that the model is initially stress-free, i.e. the initial stress state in the cement sheath is set to zero as our aim is to estimate the net thermo-mechanical stress induced by cooling. Estimating the initial, i.e. present day (compressive) stress in annular cement of gas producing wells is difficult: direct in-situ measurement of stress in cement at downhole conditions is not possible; stress estimates can only be obtained by modelling the entire well history, taking into account the different phases in the lifetime of a well, cement material properties, quality of executed cement job, interactions with the surrounding rock formation, etc.. Modelling well histories is beyond the scope of this task, which focusses on the thermo-mechanical effects of cooling on well cement integrity.

Simulation results show gradual extension of the cooled area radially into the surrounding rock (Figure 9-8 and Figure 9-9). After 1 year of injection, the radial extent of cooled area is about 10 m and has reached the edge of the model. The largest drop in temperature occurs within a radius of 1-3 m from the injection well (Figure 9-9).

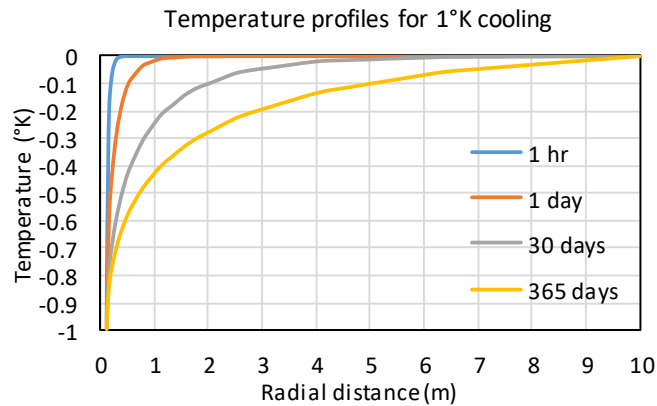


Figure 9-9: Profiles of temperature change as a function of radial distance from the well due to a casing temperature change of -1°K (or -1°C) for different times.

Cooling induces thermal contraction which in turn induces thermo-mechanical tensile stresses in the radial direction. As expected, the magnitude of tensile stress increases with time, as the cooling front propagates deeper into the surrounding formation, and decreases with the radial distance from the well casing.

For a single casing well model, the magnitude of tensile stresses is larger at the casing-cement interface, which is closer to the inner side of the casing than at the cement-formation interface (blue bar and orange bar, respectively in Figure 9-10). The magnitudes of tensile stresses range between 0.1 and 0.17 MPa/1°C. For a decrease of casing temperature by 50°C, tensile stresses at the interfaces will be thus 50 times higher and can reach 5 to 8.5 MPa. If the initial stress in cement is less than these values, de-bonding of the interfaces will occur.

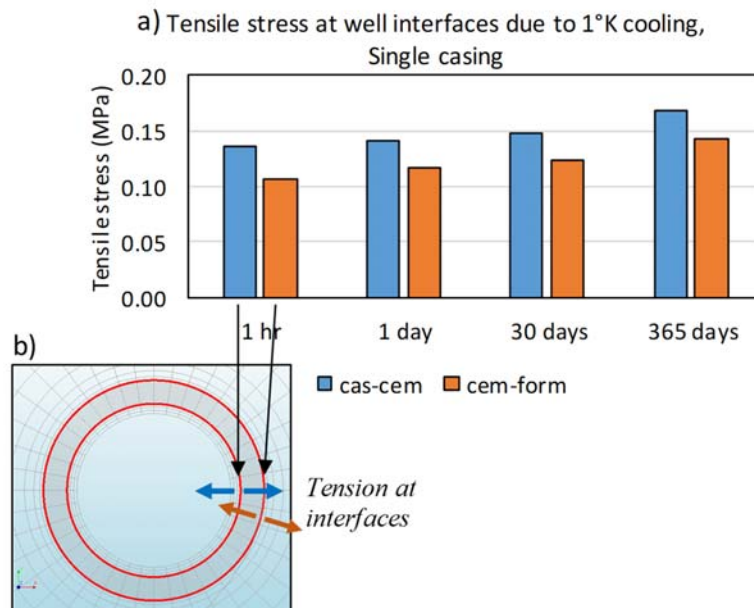


Figure 9-10: (a) Tensile stresses at the well interfaces due to a casing temperature change of -1°K (or -1°C) after 1 hour, 1 day, 30 days and 365 days. (b) Sketch showing locations of the monitoring points at the two interfaces in a single casing well model.



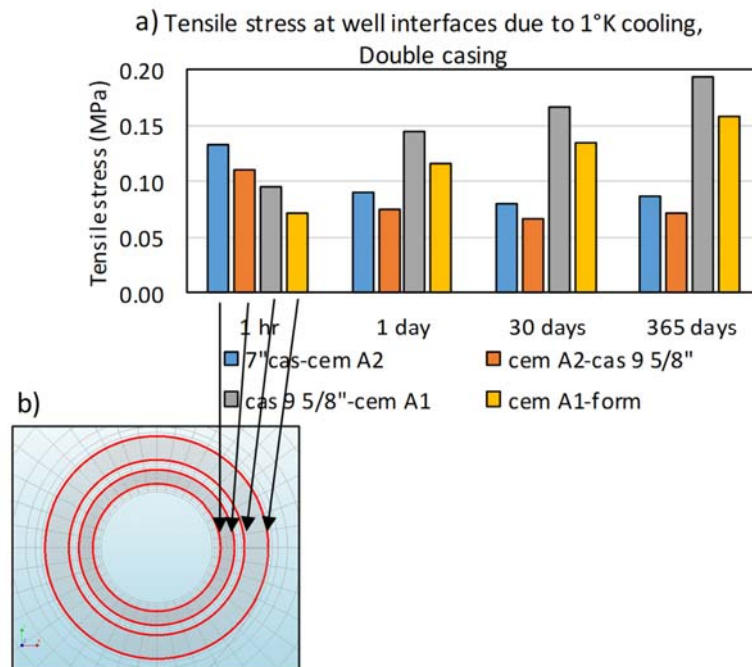


Figure 9-11: (a) Tensile stresses at the well interfaces due to a casing temperature change of -1°K (or -1°C) after 1 hour, 1 day, 30 days and 365 days. (b) Sketch showing locations of the monitoring points at the four interfaces in a double casing well model.

In a double casing well model there are four well interfaces and the evolution of tensile stresses at the interfaces with time is more complex (Figure 9-11). Initially, just after the start of cooling, the magnitude of tensile stresses at the interfaces decreases with the distance from the inner casing (Figure 9-11, 1 hr). This pattern was also observed in the single casing well model. However, for longer cooling times, from 1 day onwards, the largest magnitude of tensile stresses occurs at a more distant interface between the 9 5/8" casing and cement (grey bar in Figure 9-11). These magnitudes of ~0.19 MPa per 1°C cooling are larger than in the case of a single casing well model (grey bar for 365 days in Figure 9-11). Overall, the magnitude of thermal stresses is dependent on the values of elastic and thermal properties for the well materials (casing, cement and rock) and their interfaces.

### 9.3.3 Implications of debonding on formation of potential leakage pathway

Annular cement across the caprock in the P18-6 well could only be assessed with cement reports, no CBLs were run. Based on the P18-2 assessments the well is expected to have sections with good cement and sections with poor/absent cement. Sections with poor cement are not considered to be sealing. Sections with good cement, which are in many cases a few tens of meters long, are most sensitive to debonding. For creation of a leakage pathway from reservoir to overburden, across the entire caprock thickness, de-bonding needs to occur along all sections with good cement, in order to connect sections with poor cement. Debonding of good cement is possible to occur at the level of caprock due to cooling by 50-70°C because of:

- large induced thermo-mechanical tensile stresses, which tend to cause debonding (~5-10 MPa);

- very low tensile strength of the well cement interfaces (that counteracts the tensile stress) of 0.1-3 MPa for a good cement bond and ~0 MPa for a poor cement bond;
- possibly low, largely uncertain magnitudes of the radial compressive stress in the annular cement (that counteracts the tensile stress).

The actual permeability and therefore also the flow rate is stress-dependent. The microannulus may be open and act as a conduit or closed and act as a seal.

The permeability of circumferential microannulus created by debonding depends on the effective normal stress acting on that fracture ( $\sigma_n'$ ) and the fluid pressure inside the microannulus ( $p$ ); when  $p > \sigma_n'$ , the microannulus is open and acts as a conduit, when  $p < \sigma_n'$  the microannulus is closed and acts as a seal.

The effective normal stress  $\sigma_n'$  is either:

- The radial stress in annular cement ( $\sigma_n'$ -*cem*) acting on the casing-cement interface. The  $\sigma_n'$ -*cem* is largely uncertain and could be low especially in the case of cement sheath located in-between two casings. The  $\sigma_n'$ -*cem* could possibly be lower than the hydrostatic stress (< 0.10-0.11 bar/m). This implies that the hydrostatic fluid pressure inside the microannulus could keep the leakage path at the casing-cement interface open.

Although a microannulus at the casing-cement interface can be kept open under a pressure lower than the hydrostatic pressure, the hydrostatic pressure conditions will still exist at the tip of a microannulus transecting the caprock.

Keeping the CO<sub>2</sub> pressure in the reservoir below the hydrostatic pressure conditions will prevent the CO<sub>2</sub> from displacing the brine in the micro-annulus, as discussed in more detail in the next section.

- The radial stress in the rock formation ( $\sigma_n'$ -*rock*) acting on the cement-rock interface. The  $\sigma_n'$ -*rock* could be:
  - (i) lower than the minimum in-situ horizontal stress  $Sh_{min}$  (0.17-0.18 bar/m), but likely larger than the hydrostatic pressure (~0.10 to 0.11 m/bar), if a plastic zone was formed in the (brittle) rock formation surrounding the wellbore;
  - (ii) close to the  $Sh_{min}$  (0.17-0.18 bar/m) if the wellbore is surrounded by naturally sealing formations, which are either ductile (Aalburg Shales) or viscous (Röt salt, halitic parts). Potential advantage of naturally sealing formations is that they can improve annular sealing around non-cemented or poorly cemented parts of casing strings simply by moving or creeping onto the casing strings. Additional advantage is an increase in the compressive stresses in the near-well area, which could become equal to the far-field stresses in these naturally sealing formations (0.17-0.18 bar/m in shales and 0.21 bar/m in halite). This implies that the hydrostatic fluid pressure inside the microannulus cannot keep the leakage path at the cement-formation interface open. The microannulus is closed and acts as a seal. Several shale layers and potentially salt layers in the caprock of the P18 reservoir have been identified as natural sealing formations. Local sealing of a microannulus could make the leakage path discontinuous and therefore prevent leakage.

#### 9.3.4 Leakage risk and the effect of chemistry

The well integrity simulations demonstrated that de-bonding of the well interfaces could possibly occur at the good cement sections of the P18-6 well due to the mechanical stress related to cooling on the well materials and interfaces. In a worst case scenario, de-bonding could result in the formation of a leakage path (a

microannulus), connecting the storage reservoir with the overburden, as discussed in the previous Section.

Figure 9-12 gives a schematic representation of the pressure evolution in the reservoir and overburden in the various stages of the reservoir from initial (pre-production or virgin pressure) to post- $\text{CO}_2$  injection. The initial reservoir conditions at the start of the gas production phase show the equilibrium of the water and gas pressure as developed during the geologic time of its existence. The hydrocarbon buoyancy pressure anywhere in the reservoir above the water-gas contact, equal to the average capillary pressure, is higher than the water pressure. Because of the capillary entry pressure of the caprock, which is higher than the prevailing buoyancy pressure if leakage does not occur, the gas remains in the reservoir.

In the gas production phase, both the water and the gas pressure in the reservoir decrease to low and sometimes very low levels. In case of a 'tank reservoir' where (strong) aquifer support is absent, the pressure remains low after production has ceased.

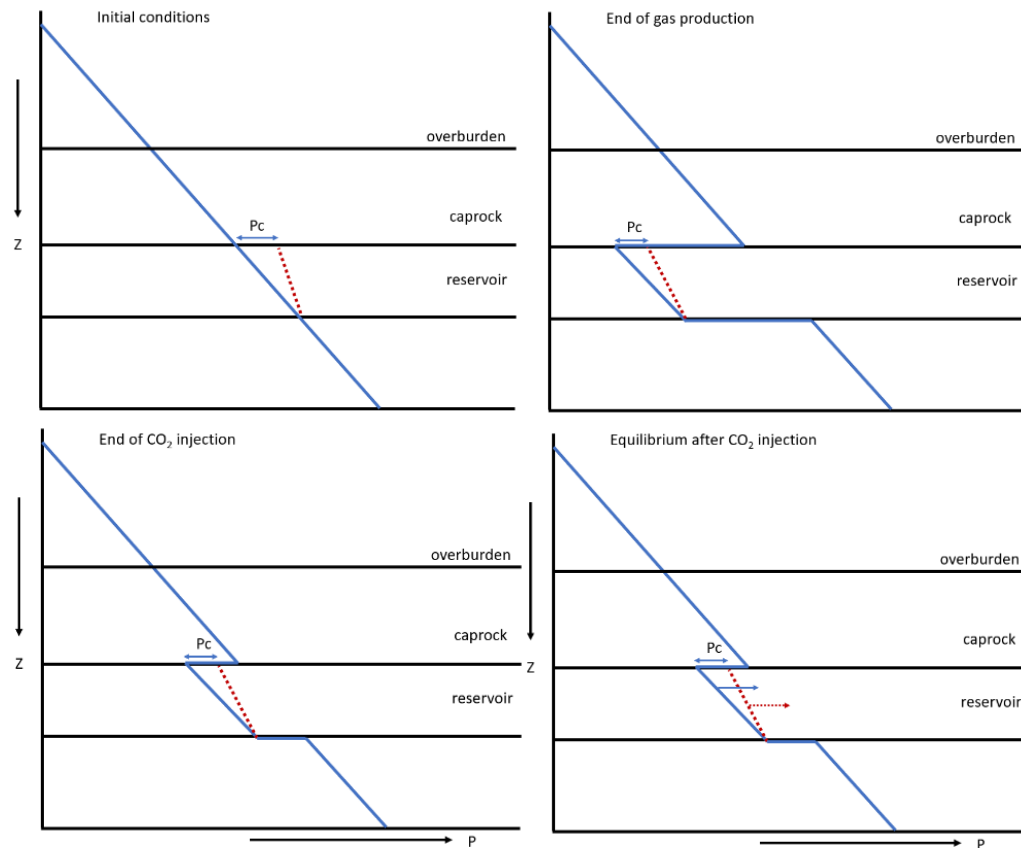


Figure 9-12: Pressure conditions in the various stages of the reservoir.

At the reservoir-caprock interface, a sharp water pressure transition exists because the water in the caprock is practically immobile on the time scale of hydrocarbon production and  $\text{CO}_2$  injection. During  $\text{CO}_2$  injection, both the water and gas pressure in the reservoir increase. As long as the gas pressure remains below the hydrostatic conditions at the base of the caprock, the gas will not be able to

displace the water column in the overburden and leakage will not occur, even if a leakage path such as a microannulus exists. With time, the reservoir conditions will move towards an equilibrium state due to water influx from the over- and underburden into the reservoir, implying re-pressurisation of the reservoir. In case of a tank reservoir, this influx is very small and it will take thousands of years before the gas pressure in the reservoir will become higher than the overlying hydrostatic column. This implies, that even if a leakage path such as a microannulus exists, a CO<sub>2</sub> leakage mechanism is absent.

In the unfortunate event that the gas pressure does increase to above the hydrostatic pressure, it is still uncertain whether CO<sub>2</sub> would migrate through a microannulus. Microannuli with small apertures will have a capillary entry pressure, similar to caprocks. The gas pressure has to be higher than the sum of the hydrostatic pressure at the base of the caprock and the entry pressure.

If CO<sub>2</sub> could displace the water column within the microannulus and starts migrating upwards, chemical interaction will take place with the cement. Assuming that the cement is of good quality, horizontal migration of CO<sub>2</sub> into the cement will take place by diffusion in dissolved state. Cement, which has a very high pH, is susceptible to interaction with carbonized water as cement minerals can quickly dissolve when the pH of the pore water decreases. The complex chemical interaction between cement minerals and carbonized brine is described in many publications (e.g., Kutcho et al., 2007; Rimmelé et al., 2008; Duguid et al., 2010). The most important reactions involve the dissolution of portlandite (CaOH<sub>2</sub>), the decalcification of Ca-silicate hydrate (CSH) and the precipitation of calcite (CaCO<sub>3</sub>) (Figure 9-13). Depending on the location of calcite deposition, complete pore clogging of the cement can occur, preventing further diffusion of carbonized brine and thereby further degradation of the cement.

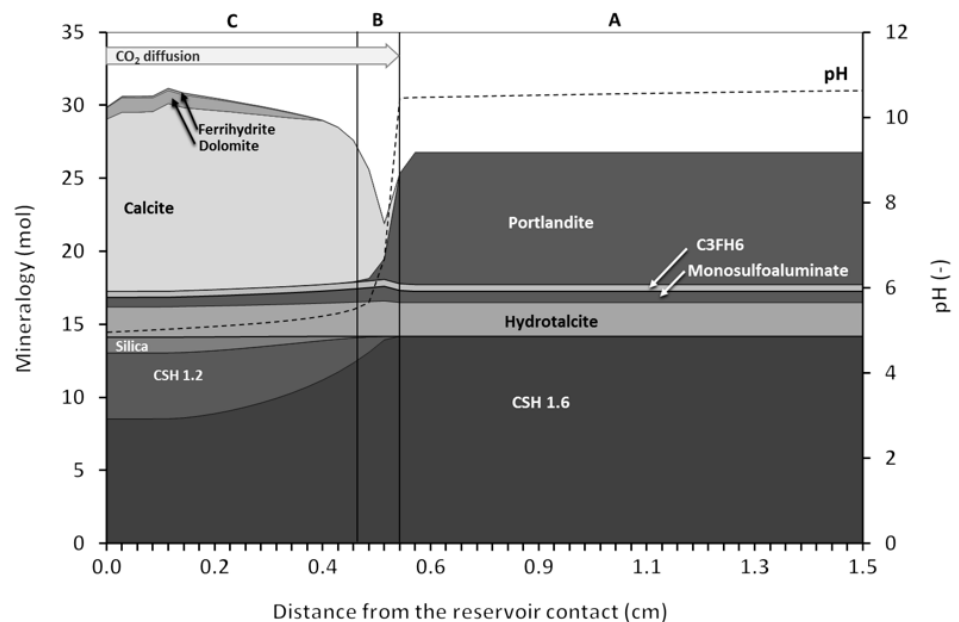


Figure 9-13: Simulated cement mineralogy with distance from the reservoir (or brine) contact after 300 days of inward diffusion of dissolved CO<sub>2</sub> and kinetic mineral reactions (PHREEQC software). Three zones develop: A: original cement, B: dissolution front, C: carbonated zone. The porosity of the cement decreases in the carbonated zone. From Koenen et al. (2014).

The upward flow of CO<sub>2</sub> through the microannulus adds another complicated component to the process, and has been described in Koenen and Wasch (2018). Instead of calcite precipitation in the pore spaces of cement, the calcite can accumulate within the microannulus and block the leakage path. The potential presence of sulfate in the caprock formation water can result in anhydrite precipitation in the microannulus, supporting the microannulus clogging by calcite (Koenen and Wasch, 2018). Whether clogging occurs depends on the upward flow rate of the CO<sub>2</sub> and the width of the microannulus. A low flow rate and/or small microannulus will allow calcite (and anhydrite) deposit to grow and block the leakage path. A high flow rate and/or large microannulus will not allow calcite growth, and instead, the leakage path will get worse in time due to cement mineral dissolution.

This is illustrated in Figure 9-14. The worst case conditions for a microannulus of 100 micron and a CO<sub>2</sub> pressure 10 bar above hydrostatic conditions give a migration rate of CO<sub>2</sub> towards the overburden in the order of 10<sup>-6</sup> kg/s, adding up to slightly more than 30 kg per year (Koenen and Wasch 2018). Compared to the storage volume of ~1.3 Mtonne, this amount of leakage can be considered as negligible.

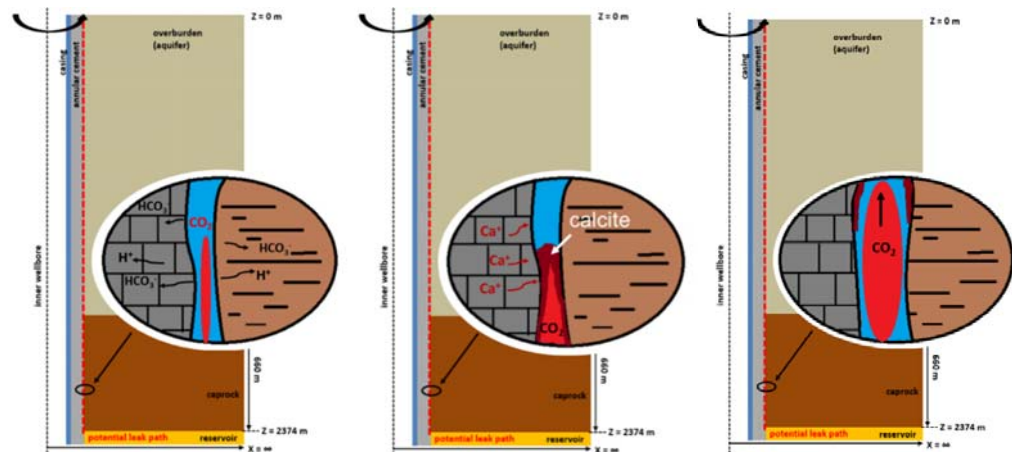


Figure 9-14: Schematic overview of CO<sub>2</sub> migration through a microannulus (red dotted line in between the annular cement and the surrounding rock). Left: initial state of microannulus and CO<sub>2</sub> migration. Middle: at low flow rate and/or small microannulus dissolved calcium migrates to the microannulus and is deposited as calcite, thereby blocking the leakage path. Right: at high flow rate and/or large microannulus the leakage path is enhanced as fast cement dissolution and CO<sub>2</sub> flow prevent calcite deposition. From Koenen & Wasch (2018).

### 9.3.5 Conclusions

Well dynamics simulations provided input on the temperature evolution along the wellbore with time. They showed that the CO<sub>2</sub> inside the injection well is 50 °C to 70 °C colder than the surrounding caprock formation, with largest temperature differences occurring in the initial phase of injection when the reservoir pressure is low (~60 bar) and the temperature of CO<sub>2</sub> at bottom hole is 60-70 °C.

Based on performed simulations, debonding of well interfaces in the P18-6 CO<sub>2</sub> injection well is possible to occur due to cold fluid injection, thermal contraction and associated stress reduction in the near-well area. Debonding can, in principle, occur

over lengths of tens of meters of caprock sections with good CBL. However, for migration of CO<sub>2</sub> with eventually leakage to occur, a continuous microannulus along the well cemented sections need to connect poorly cemented sections towards the overburden before we can speak of a leakage path. The presence of shale and potentially salt layers in the P18-6 caprock, identified as natural sealing formations could locally interrupt the leakage path. Even if a continuous leakage path would exist, it depends on the microannulus characteristics and pressure conditions whether upward CO<sub>2</sub> migration would actually take place. If the pressure conditions in the reservoir are high enough to overcome the capillary pressure within the microannulus, and migration does take place, the chemical interaction between CO<sub>2</sub> and cement can either prevent or enhance leakage towards aquifers overlying the caprock or towards the surface, also depending on the microannulus characteristics and pressure conditions. Keeping the CO<sub>2</sub> pressure in the reservoir below or at the hydrostatic pressure conditions will prevent the CO<sub>2</sub> from displacing the brine in the microannulus. In that case adequate monitoring during injection operations is required. The decommissioning method and procedures should result in well plugging from formation-to-formation (pancake plug or similar) in case microannulus formation is likely and poorly bonded annulus cement is not accepted as a leakage barrier.

Overall, the likelihood of CO<sub>2</sub> leakage through microannuli is small. De-bonding of cement-casing and cement-rock interface is very likely, but a leakage path requires a continuous microannulus from reservoir to overburden which is less likely. The presence of that natural sealing formations in the caprock could locally seal a microannulus, disconnecting the reservoir from the overburden. If a leakage pathway does exist, the CO<sub>2</sub> pressure in the reservoir should be high enough to displace the water in the microannulus. For a pressure below or at hydrostatic conditions, as is the plan for CO<sub>2</sub> storage in P18-6, this would not happen. In case the CO<sub>2</sub> pressure would be high enough to migrate through the microannulus, chemical interaction between the CO<sub>2</sub> and the cement would stimulate self-sealing of the leakage path by calcite precipitation. In a worst case scenario that self-sealing would not occur, leakage rates would be very low; e.g. <0.00001% of the total amount of CO<sub>2</sub> that can be stored in P18-6 on an annual basis.

## **9.4 Well decommissioning**

### **9.4.1 *Decommissioning after the end of injection***

After completing the CO<sub>2</sub> injection through the P18-6 injection well, it needs to be decommissioned in a way that conforms to good practice and meets required standards for a CO<sub>2</sub> storage site. After decommissioning, the well should ensure permanent and safe containment of the CO<sub>2</sub> in the reservoir.

Currently cement is the material of choice for annular seals and decommissioning of oil and gas wells. The abandonment plug has to extend across the full cross section of the well (“rock-to-rock”), whilst covering all annuli. If the cement behind the casing(s) is good, this can be achieved by placing a cement plug in the casing. If the quality of the annular seal is not sufficient or cannot be confirmed, pancake plugs have to be installed. This is achieved by removing the casing(s) and potentially cement and thereby creating a so called ‘window’. These are standard O&G practices, clearly described in the decommissioning standards.

Reaction of CO<sub>2</sub> with wellbore cement is a slow process if good construction practices and proper cement materials were used (IEAGHG, 2018). Degradation rates have been found to be proportional to temperature, pressure and the square root of time (Shell, 2015). According to literature the degradation of Portland cements could be up to about 12 m in 10.000 years. It is also reported that the permeability that can be created by the degradation is such that it still is within API criteria for cement (EPA, 2012).

Previous work (Vandeweyer et al., 2011) recommended placing pancake-type abandonment plugs. This approach to the P&A of CO<sub>2</sub> wells was also proposed in the permit application for the P18-4 reservoir. Whether pancake-type plugs will be the method of choice for decommissioning of the P18-6 injection well, and which materials to be used for the plug, depends on future developments until time of decommissioning.

## 9.5 Conclusions

### *Well integrity*

The P18-A-07-S1 well has been evaluated in the context of CO<sub>2</sub> injection into the P18-6 reservoir regarding its current status and integrity risks. The reviewed well has the potential to be used safely as CO<sub>2</sub> injector. Appropriate mitigation measures have been proposed to make it fit for CO<sub>2</sub> storage operations.

### *Effects of injecting cold CO<sub>2</sub> on well integrity*

It is possible that de-bonding of cement interfaces will take place upon cold CO<sub>2</sub> injection, creating microannuli. In the unlikely case that the microannulus forms a continuous leakage path from reservoir to overburden, the characteristics of the microannuli and pressure conditions determine whether upward CO<sub>2</sub> migration would actually take place. Keeping the CO<sub>2</sub> pressure in the reservoir below or at hydrostatic pressure conditions will prevent the CO<sub>2</sub> from migrating through the microannulus. This justifies the choice of keeping the reservoir pressure below or at hydrostatic conditions. However, if for some reason the reservoir pressure would be high enough to displace the water column in the microannulus, the chemical interaction between CO<sub>2</sub> and cement can either prevent or enhance leakage, also depending on the microannulus characteristics and pressure conditions. For worst-case conditions, if CO<sub>2</sub> would migrate from the reservoir to the overburden through a microannulus, leakage rates would still be very low; i.e. <0.00001% on an annual basis. Overall, the likelihood and effect of leakage through microannuli is very low and can be considered insignificant.

### *Well decommissioning*

Appropriate methods should be used for the decommissioning of the well. Given the likelihood of microannuli forming during the injection of cold CO<sub>2</sub>, decommissioning methods that remove these potential leakage paths would be preferred. As an example, full-bore pancake like plugs would provide formation-to-formation closure of the well.

## 10 P18-6 storage site and storage complex

### 10.1 Introduction

The assessment of leakage risks for CO<sub>2</sub> storage in the P18-6 field relies on a robust definition of the storage site and storage complex. In this Section these definitions are discussed, based on definitions in the EU Storage Directive and insights from the detailed reservoir, fault, caprock and well evaluations in Sections 6 to 9.

### 10.2 Definitions in the Netherlands Mining Law and the EU Storage Directive

The EU Storage Directive (EU, 2009) introduced the concept of the 'storage complex' when defining rules for environmentally sound and safe geological storage of CO<sub>2</sub>. The directive states that safe storage is to be accomplished by the characterization and assessment of the storage complex.

The following definition is given of the storage complex, *op. cit.*:

'storage complex' means the storage site and surrounding geological domain which can have an effect on overall storage integrity and security; that is, secondary containment formation

According to the Netherlands Mining Law (Mijnbouwwet, 10 April 2019):

*"CO<sub>2</sub>-opslagcomplex: opslagvoorkomen voor CO<sub>2</sub> en de omringende geologische gebieden die een weerslag kunnen hebben op de algehele integriteit van de opslag en de veiligheid ervan"*. The definition of "storage complex" in the Netherlands Mining Law does not explicitly refer to "secondary containment formation" like in the EU Storage Directive.

For the definition of "storage site" the Netherlands Mining Law uses the term *"opslagvoorkomen van CO<sub>2</sub>"*. Although it seems that this term can be linked to "storage site" in the EU Directive it is not clear if this will include "the associated surface and injection facilities" as well, like is defined in the EU Storage Directive (see below). For this report it is assumed that these facilities are part of the storage site. *"Opslagvoorkomen is: een voorkomen dat gebruikt wordt voor opslag"* according to the Netherlands Mining Law meaning "an occurrence which is used for storage".

The storage site according to the EU Directive is defined as, *op. cit.*:

"storage site" means a defined volume area within a geological formation used for the geological storage of CO<sub>2</sub> and associated surface and injection facilities  
Leakage then means *"any release of CO<sub>2</sub> from the storage complex"* and migration stands for *"the movement of CO<sub>2</sub> within the storage complex"* according to the EU Directive.

The Storage Directive (EU, 2009: Article 4, para 4) also says:

*"4. A geological formation shall only be selected as a storage site, if under the proposed conditions of use there is no significant risk of leakage, and if no significant environmental or health risks exist."*



The hydraulically connected pore space bordered by flow barriers together representing a physical trap is considered, and the dispersion of CO<sub>2</sub> inside the physical trap is predicted by dynamic modelling. Our predictions will be tested by operational monitoring. This implies that monitoring activity should be focused particularly on providing the evidence for the effectiveness of the geological and engineering barriers that prevent significant risk of leakage (migration out of the storage complex).

Note that Guidance document no 2 (EC, 2011) suggests to allow for changes in the specific boundaries of the storage complex during the storage permit review and updating process.

CO<sub>2</sub> movement out of the storage site but remaining in the storage complex is called migration (in the Storage Directive). Movement of CO<sub>2</sub> out of the storage complex is called leakage under the Storage Directive, and if the CO<sub>2</sub> then reaches the atmosphere it is called emission under the implementing regulation of the ETS Directive (ETS Directive, 2009; EU 2018) and emission allowances need to be returned by the storage permit holder to the state. Leaks cannot be measured, they can only be estimated. From the monitoring plan and plan for corrective measures it needs to be defined how to recognise such movement of CO<sub>2</sub> and what actions or corrective measures to take.

### 10.3 Definition of the storage site

The storage site is what contains the CO<sub>2</sub> (i.e. the reservoir), the injecting or not yet decommissioned wells, the associated surface installations (wellheads) and injection facilities (tubing in wells). More specifically, the P18-6 storage site comprises the following:

- P18-6 Triassic reservoir rocks of the Volpriehausen Sandstone, Lower and Upper Detfurth Sandstones and the Hardegsen Formation. The lower 3 units are vertically hydraulically disconnected by the presence of low permeable zones in between (baffles). Strongly restricted flow is possible between the Upper Detfurth sandstone and the Hardegsen Formation (see Figure 17-11). The reservoir is bounded by faults on the SW and SE sides and dip closure on the NW and NE sides downdip of the GWC (see Figure 10-1; more details are in Section 12.1).
- Well P18-A-07-S1 penetrating the storage site up to the wellheads;
- Related wellheads, measurement equipment and christmas tree.

### 10.4 Definition of the storage complex

In addition to the components of the storage site mentioned in Section 10.3, the storage complex also includes the formations that seal off CO<sub>2</sub> in the reservoir and any surrounding formation that could contain CO<sub>2</sub>.

The Porthos P18-6 storage complex is proposed to include the following spatial compartments in addition to the storage site components:

- Massive caprock on top of the reservoir consisting of impermeable rocks of the Upper Germanic Triassic Group and Altena Group with a total thickness of 450 to 750 m;

- The formations below the storage reservoir consisting of the Triassic Rogenstein and Main Claystone Members.

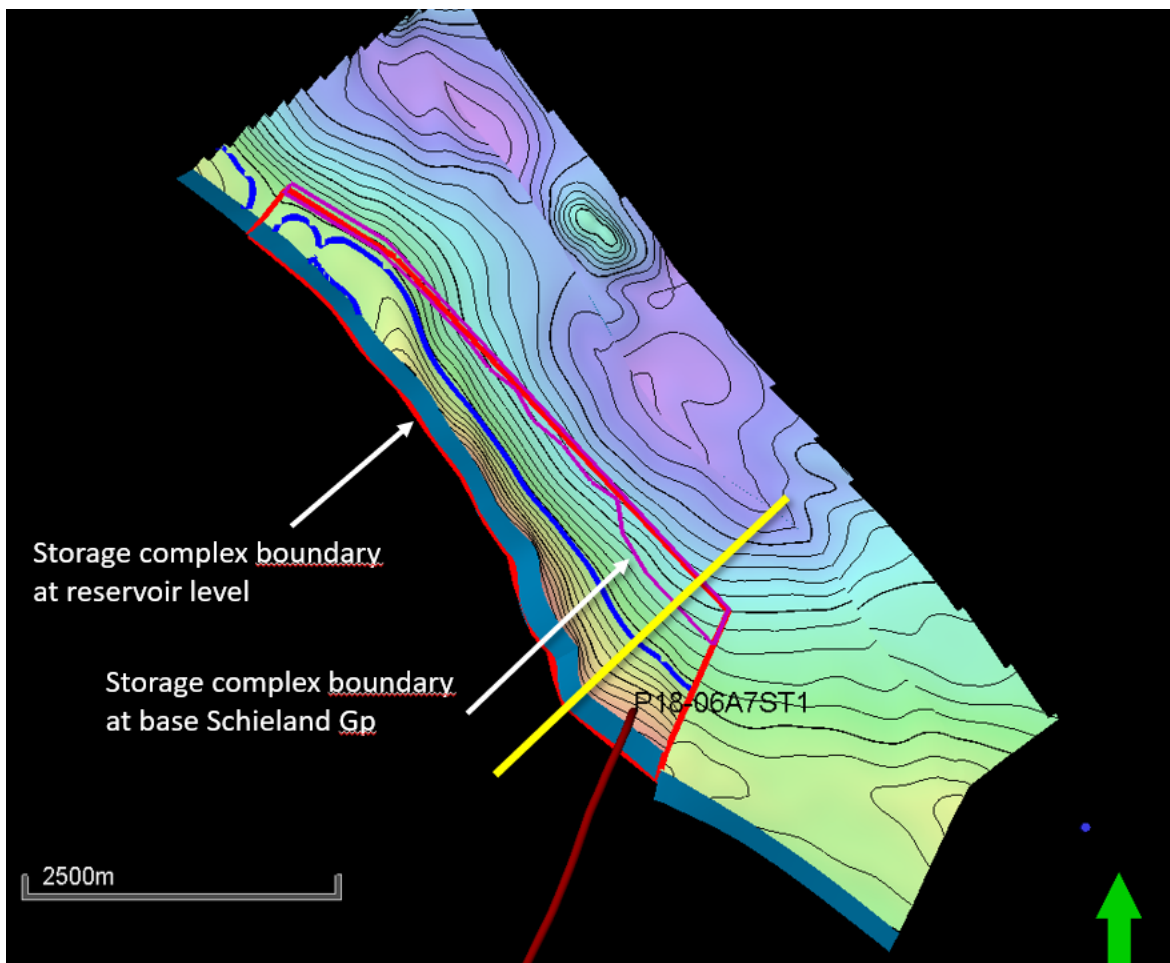


Figure 10-1 Depth map of the top of the reservoir with the proposed boundary of the storage complex at top reservoir level (red line) delimited by the bounding faults and an open boundary down-dip of the GWC to the north; purple line indicates storage complex boundary at the top of the caprock (Base Schieland Gp). Yellow line represents the location of the geological cross section shown in Figure 10-2.

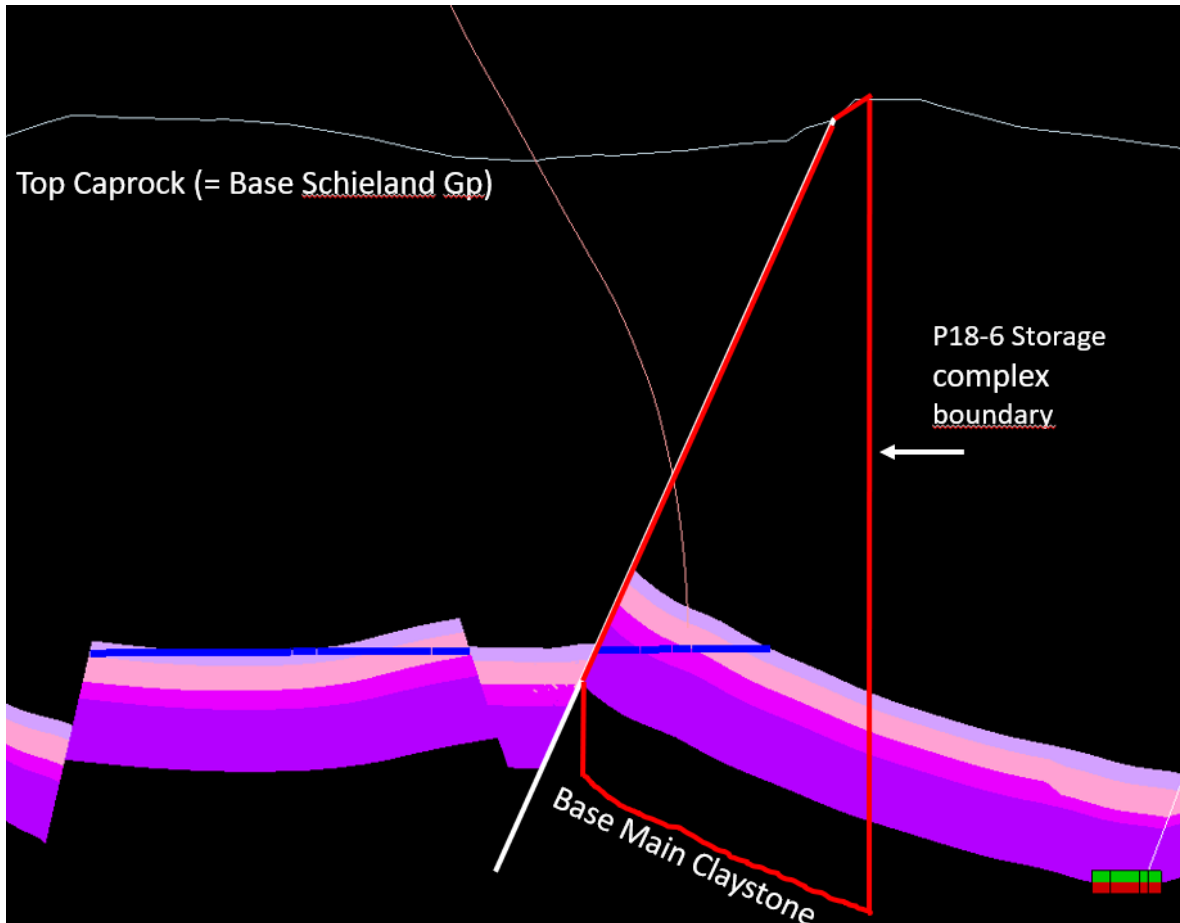


Figure 10-2 Geological cross section of the reservoir and the overburden with indication of the vertical extension of the geological compartments and the wells determining the storage complex); location of cross section is shown in Figure 10-1.

## 10.5 Barriers

### 10.5.1 Barriers in the storage complex

The storage complex includes the principle barriers for the permanently stored CO<sub>2</sub> in the P18-6 depleted gas reservoir.

The *geological barrier system* consists of:

- Massive caprock, consisting of Triassic and Jurassic shales, directly located above the reservoir rocks (see also Section 4.3);
- Sealing, reservoir-bounding faults;
- Structural relief trapping of CO<sub>2</sub>, e.g. at the NW and NE boundaries of the reservoir.

The *well engineering barrier system* consists of the two barriers described in Section 9.

-

### 10.5.2 *Evaluating barrier integrity*

The various barriers have been evaluated in detail to further qualify the P18-6 reservoir for permanent CO<sub>2</sub> storage:

- The initial condition of the caprock and the faults is characterized in Section 4 and Section 17.
- The risk of lateral migration (spilling) from the reservoir compartment to the North was assessed in more detail in Section 6.
- The stability of the fault zone under the influence of chemical, mechanical and thermal processes were investigated (see Section 7).
- The possible effects of fracturing and chemical degradation on the integrity of the caprock have been evaluated with semi-analytic thermomechanical modelling and following a literature study, respectively (see Section 8).
- The integrity of the well P18-A-07-S1 penetrating the reservoir have been evaluated and recommendations for qualifying the well for CO<sub>2</sub> storage have been defined (see Section 9).

The results of these investigations have been used to characterize the risks for loss of containment and to propose measures to lower the risk level if necessary (see Section 12). Section 13 describes the monitoring plan, which enables the early identification and intervention of potential issues for CO<sub>2</sub> containment.

# 11 Migration paths

## 11.1 Introduction

The EU storage directive requires an analysis of potential leakage pathways (EU, 2009, Annex I). The results presented in sections 6 through 9 support the conclusion that leakage of CO<sub>2</sub> (i.e. CO<sub>2</sub> moving out of the storage complex) along wells, faults or through the caprock is highly unlikely, if the injection process is conducted within safe limits (see Sections 12 and 13). Overfilling the reservoir (i.e., spilling of the CO<sub>2</sub> across a spill point) does not occur as long as the average reservoir pressure is kept below initial gas pressure.

Nevertheless, with this starting point, an analysis was made of pathways that CO<sub>2</sub> would take in case of a hypothetical leak out of the reservoir, along one of the wells, or through the caprock. The analysis includes the identification of possible secondary containment at the level of the reservoir formations, or in the overburden.

A static overburden model was assembled, based on both 2D and 3D seismic surveys and well information. On the basis of the overburden model and the selected migration pathways, an evaluation of possible migration scenarios was developed. The scenarios shown below focus on (hypothetical) migration paths relevant for the P18-6 field.

The conclusions are that in the case of overfilling of the reservoir and migration through the Buntsandstein (reservoir formations level), the CO<sub>2</sub> remains trapped and finally will migrate towards the adjacent gas reservoirs. In the case of migration of CO<sub>2</sub> into the aquifers of the overburden, caused by a shortcut along the wellbore, it will remain trapped within these aquifers. However, migration of CO<sub>2</sub> along faults in the overburden (above the Altena Group) to a shallower aquifer level cannot to be excluded.

Overall, given the results presented in the previous sections, the conclusion from the analysis presented in this section is that the only potential pathway to the surface of CO<sub>2</sub> stored in the P18-6 field is via leaking wells, leaking directly into the atmosphere and not indirectly via pathways originating in deeper parts of the overburden.

## 11.2 Available data and workflow

A geological model was constructed with Petrel modelling software (Schlumberger). The model comprises an area with a 14 km minimum radius surrounding the P18 gas fields. In vertical direction the model spans the total overburden of the reservoir.

The workflow for building the model is described in *CATO-2-WP3.1-Geological report P18 (December 2010)*: seismic interpretation of the overburden was performed, and subsequently the model was built on the basis of a fault model with a grid cell size of 250m x 250m. The model was converted from time to depth, and tied to the wells.

Figure 11-1 shows the location of the P18 fields, with neighbouring fields and wells.

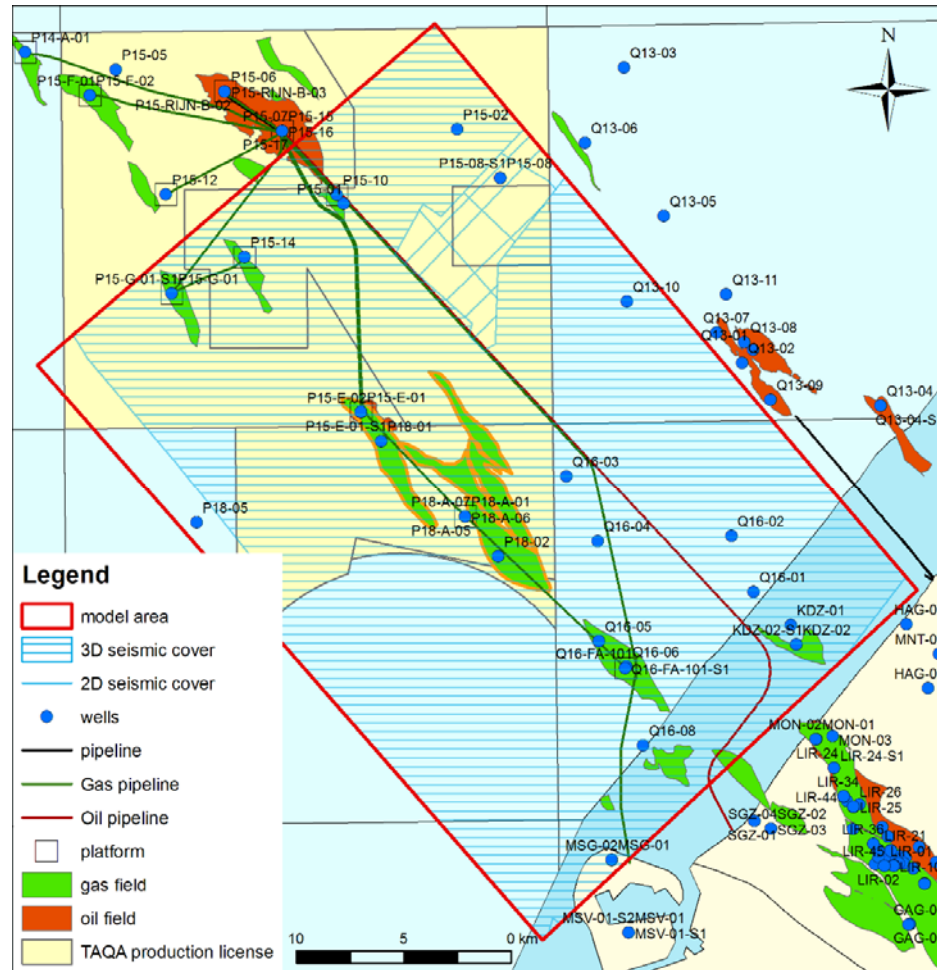


Figure 11-1: Location map of P18 model area. Target P18 gas fields are indicated with an orange boundary.

### 11.3 Geological model of the overburden

#### 11.3.1 Overburden

The primary seal, made up of the Upper Germanic Trias and Altema Groups is successively overlain by (see also Figure 11-2):

- The Schieland Group, which consists of shales and (stacked) channel sands of the Nieuwerkerk Fm. (Delft sandstone equivalent). The lateral continuity of the individual sand bodies (thickness 2-5m) is probably very limited.
- Lower Cretaceous Rijnland Group, which consist of marine sandstones, shales and marls. At the base of the Rijnland Group, the Rijn / Rijswijk Fm. is present. This sandstone is widely distributed in the P18 area. It is also known for its oil (P15) and gas (onshore) accumulations within the West Netherlands Basin. The sandstones are interpreted as transgressive sheet sands, with good lateral continuity. In the upper part of the Rijnland succession, the Holland Greensand Member is present. It consists of argillaceous sands and silts. The distribution is limited to the southern margin of the West Netherlands Basin. Although the Holland Greensand has good lateral continuity, permeability is general low.

- Upper Cretaceous Chalk Group, which consist at the base of the formation of sands and marls and a thick layer (900 m) of limestones (Chalk). The distribution of the basal Texel Greensand is limited to the southern basin margin.
- The North Sea Group, which consists of siliciclastic sediments. Two major aquifers can be distinguished; the Dongen sand, a basal transgressive sandstone, and the marine Brussels Sand Member.

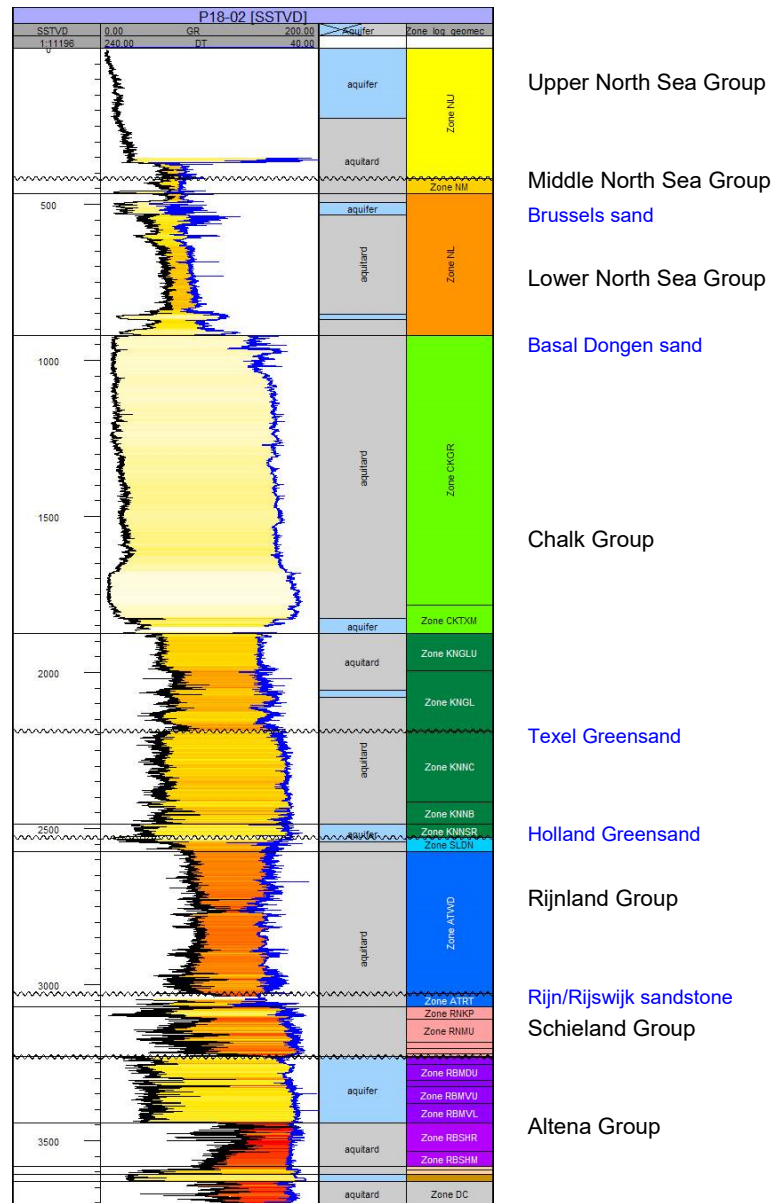


Figure 11-2: Composite well log (GR, DT) of P18-02 with main stratigraphic units and aquifer intervals

### 11.3.2 Faults

Faults present at reservoir level (Buntsandstein) in general continue till the Schieland group (white line) or base Rijnland Group (dark green line in Figure 11-3). Late Cretaceous inversion caused faulting of the sediments above the Base Cretaceous Unconformity (base Rijnland) These faults (dashed lines Figure 11-3) have limited displacement, but continue to the Upper North Sea Group.

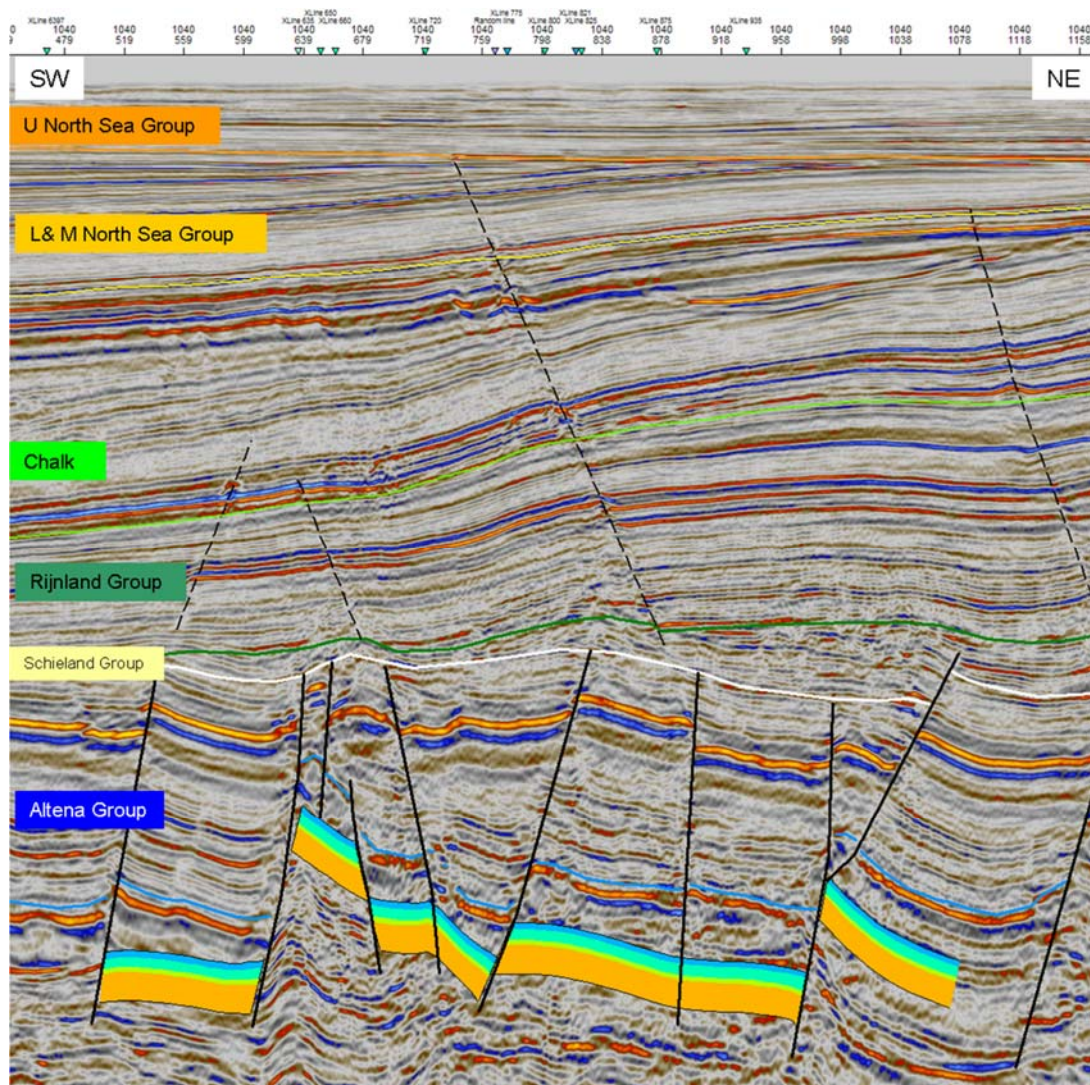


Figure 11-3: Seismic cross-section (inline 1040 of P15P18 seismic cube) through the P18 field, displaying the reservoir interval (coloured layering), the main bounding faults to the reservoirs (bold lines), the main stratigraphic units in the overburden and the faults in the overburden (dashed)

## 11.4 Migration scenarios

For the qualitative analysis three migration scenarios were considered.

1. Spilling out of the gas reservoir, due to overfilling. This leads to migration within the Buntsandstein formations beyond the boundaries of the storage complex (hence, this would be classified as leakage). See Section 11.6.1.



2. Leakage through the caprock due to fracture formation. This leads to CO<sub>2</sub> entering the Rijn/Rijswijk Sandstone (Section 11.6.2).
3. A wellbore shortcut, opening pathways for CO<sub>2</sub> into formations overlying the caprock.
  - Migration into Rijn/Rijswijk Sandstone (Section 11.6.2);
  - Migration into Holland Greensand (Section 11.6.3);
  - Migration into Texel Greensand (Section 11.6.4);
  - Migration into Dongen & Brussel Sandstone (Section 11.6.5).

The sections below investigate the consequences of these scenarios occurring, in spite of their low to very low probability, given the results presented in Sections 6 (spilling out of the reservoir), 8 (caprock integrity) and 9 (well integrity).

## 11.5 Methods

Potential CO<sub>2</sub> migrations pathways were analyzed using the rapid trapping assessment tool PetroCharge Express of IES. With this tool a rapid analysis of the migration pathways based on the layer geometry is performed. The layer geometry was provided by the exported horizons from Petrel (regional scale model). The program uses the input top layer as bounding elements assuming these layers to be impermeable. Although in reality the layers are not completely impermeable the goal is to create a concept model from which migration routes within the layer can be deducted.

It should be noted that PetroCharge only looks at the geometry and does not describe various other aspects of flow. It was therefore decided to “inject” large amounts of CO<sub>2</sub> in the considered leakage scenarios and to focus on the migration paths and final accumulation structures.

## 11.6 Results

### 11.6.1 Migration scenario: Buntsandstein

In case of “overfilling” the gas reservoir with CO<sub>2</sub> it might be possible that the CO<sub>2</sub> will pass by the original closure defined by the initial gas water contact (GWC).

- Overfilling the P18-6 reservoir could lead to migration towards the Q16-4 structure (Figure 11-4, arrow 1);
- Overfilling the P18-6 compartment could lead to migration towards the P15-10 field (Figure 11-4, arrow 2).

It must be noted that in the structure drilled by the (dry) exploration wells Q16-04 and Q16-03, only minor amounts of gas were encountered. If the containment were to fail by a mechanism described above, the most probable failure would that be of an absence of a side-seal in combination with reservoir juxtaposition with Jurassic sandstones from for instance the Nieuwerkerk Formation.

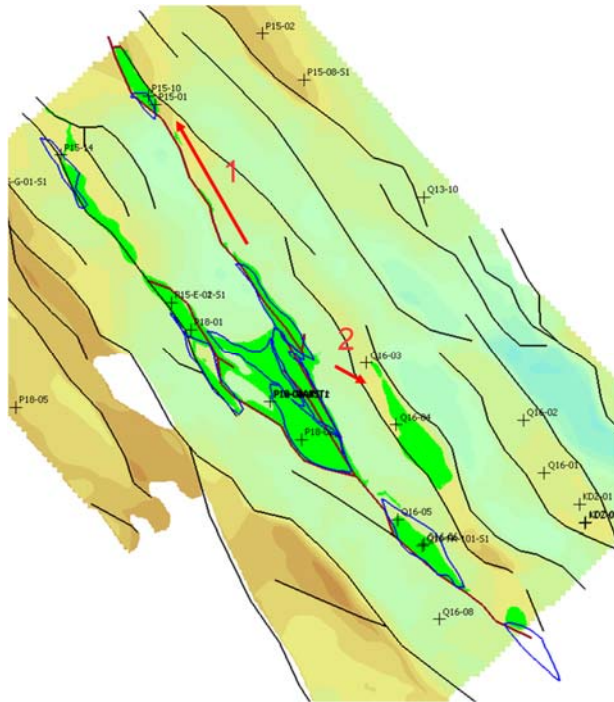


Figure 11-4 Structure map of Top Buntsandstein. Black lines indicate faults. Also shown are boundaries of gas accumulations and location of wells.

#### 11.6.2 Migration scenario: Rijn/Rijswijk sandstone

In the case of fault reactivation or a shortcut occurring via a wellbore, CO<sub>2</sub> can hypothetically migrate into the Rijn/Rijswijk sandstone aquifer.

- Spill originating from well P18-A-07-S1 will migrate towards Q16-03 & Q16-04 structure (Figure 11-5, arrow 1).

#### 11.6.3 Migration scenario: Holland Greensand

In the case of a shortcut via a wellbore, CO<sub>2</sub> can hypothetically also migrate into the Holland Greensand aquifer

- Spill originating from well P18-A-07-S1 will migrate towards Q16-03, Q16-04 structure (Figure 11-6, arrow 1)

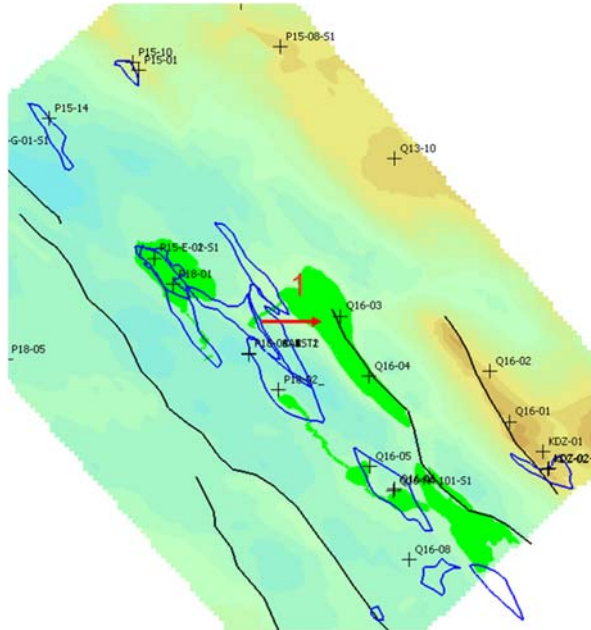


Figure 11-5: Structure map of the Base Rijnland Group. Black lines indicate faults. Also shown are boundaries of gas accumulations and location of wells.

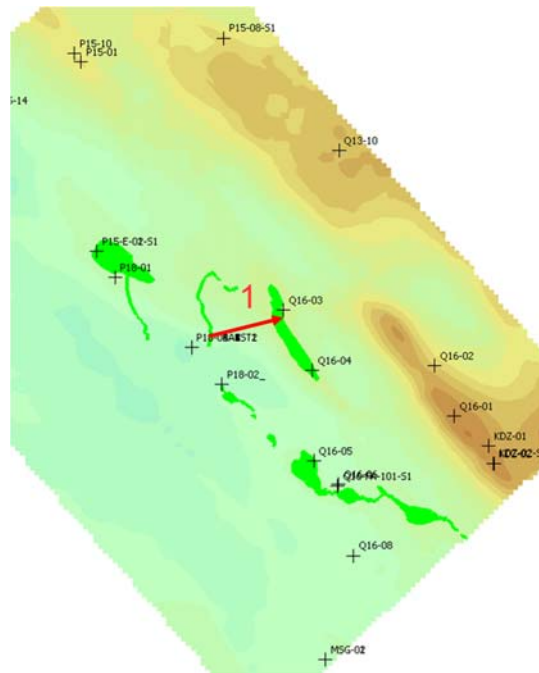


Figure 11-6: Structure map Holland Greensand.

11.6.4 Migration scenario: Texel Greensand

In the case of a shortcut via a wellbore, CO<sub>2</sub> can also hypothetically migrate into the Texel Greensand aquifer

- Spill originating from P18-A production wells will migrate towards Q16-3 structure and finally Q16-02 (Figure 11-7, arrow 1).

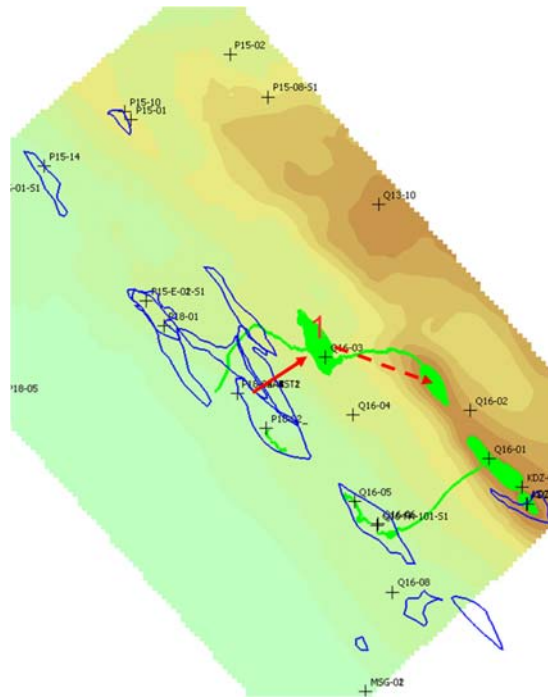


Figure 11-7: Structure map base Chalk Group.

#### 11.6.5 Migration scenario: Dongen sand & Brussel sandstone

In the case of a shortcut occurring via a wellbore, CO<sub>2</sub> can hypothetically migrate into the North Sea Group aquifer

- Spill originating from P18-A production wells will migrate towards Q13-10 structure (Figure 11-8, arrow 2).

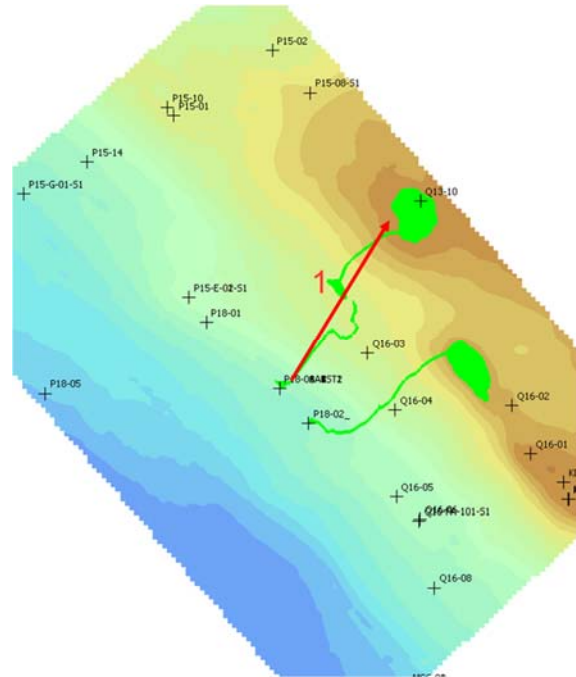


Figure 11-8: Structure map base North Sea Group.

### 11.7 Present day hydrocarbon migration

Inspection of the overburden revealed the possible existence of shallow gas pockets. (*CATO-2-WP3.1-D01-Geological report P18 (December 2010)*). The gas is most probably sourced from Jurassic Posidonia shales (van Balen et al., 2000). The Posidonia shales are situated stratigraphically above the Bunter reservoir and seal, so this hydrocarbon migration provides no proof of seal failure/leakage within the P18 Bunter reservoir.

Figure 11-9 shows a seismic section of the overburden, to illustrate hydrocarbon migration, and to illustrate a possible migration pathway for CO<sub>2</sub>. Gas is sourced from the Posidonia shale (the strong reflector at the base of the lowest arrow), and migrates via a fault into the sands of the North Sea Group. The red ellipses indicate bright spots, which suggest the presence of gas. Migration is also possible within the Brussels sand and is indicated by the arrows in Figure 11-9. At the location where the Brussels sand toplaps against the Upper North Sea Group (Mid Miocene Unconformity, orange line), an increase of amplitudes is observed, which suggest migration from the Brussels sand into the Upper North Sea Group.

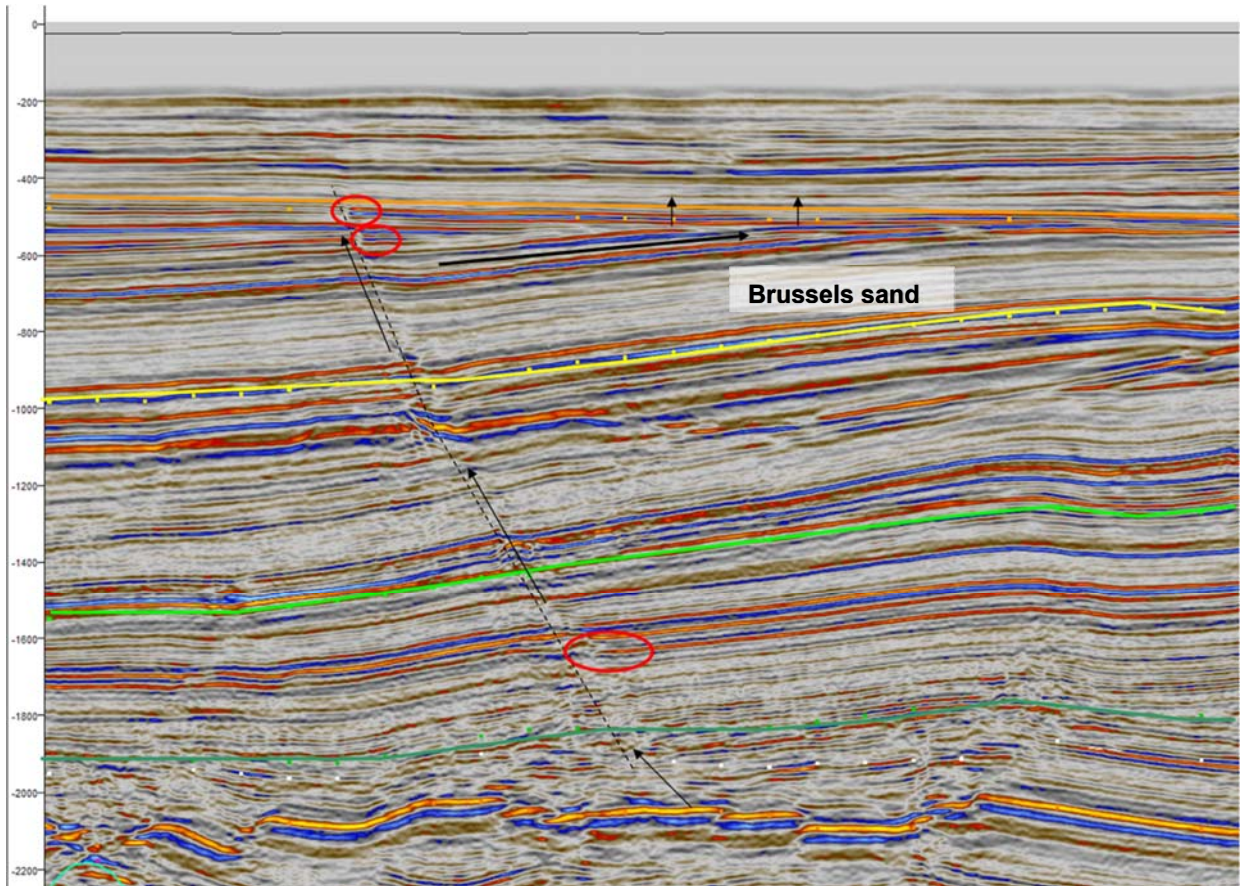


Figure 11-9: Seismic section of the P18 overburden. Arrows indicate hydrocarbon migration along a fault (dashed line). Red ellipses mark bright spots on the right side of the fault. Dark green line: base Rijnland (BCU), bright green line: base Chalk, yellow line: base North Sea, orange line: base Upper North Sea (MMU).

## 11.8 Conclusions

A Petrel model of the overburden has been constructed, using publicly available data and data provided by TAQA. Based on the geological model and selected hypothetical migration scenarios a qualitative evaluation of the possible pathways was developed.

This assessment was based on the results presented in sections 6 through 9, which support the conclusion that leakage of CO<sub>2</sub> (i.e., CO<sub>2</sub> moving out of the storage complex) along wells or faults is highly unlikely. If the injection process is conducted within safe limits (see Sections 12 and 13), the conclusions from this assessment are that in case of overfilling of the reservoir the CO<sub>2</sub> remains trapped in the Buntsandstein (reservoir formations level) and finally will migrate towards the adjacent gas reservoirs. Also, in case of migration of CO<sub>2</sub> into the aquifers of the overburden, caused by a shortcut along the wellbore, it will remain trapped within these aquifers. However, migration of CO<sub>2</sub> along faults in the overburden (above the Altena Group) to a shallower aquifer level cannot to be excluded in the unlikely case that leakage along the well does occur.

Overall, given the results presented in the previous sections, the conclusion from the analysis presented in this section is that the only potential pathway to the surface of CO<sub>2</sub> stored in the P18-6 field is via leaking wells, leaking directly into the atmosphere and not indirectly via pathways originating in deeper parts of the overburden.

## 12 Risk assessment and preventative measures

The current study on the feasibility of CO<sub>2</sub> storage in the P18-6 reservoir made optimal use of earlier work done on the P18 reservoirs, a large part of which was carried out as part of the national CATO2 programme until 2011 and specific work on the P18-2 field (Neele et al., 2019). The risk assessment work for P18-6 was built on the assessment for P18-2 and where relevant the assessment was adjusted or expanded. The risks identified for CO<sub>2</sub> storage in the P18-6 reservoir are based on detailed investigations which are presented in Chapters 6 through 9, and on earlier work for the P18 reservoirs (Vandeweyer et al., 2011; Neele et al., 2019). The central question is where the CO<sub>2</sub> is at any given point in time and whether it could (partially) flow out of the storage complex. In Section 10 the delimitations of the storage site and the storage complex which includes the intended storage reservoir, have been presented.

After the identification and evaluation of the risks, measures were defined to diminish the risk level. The present chapter provides an extensive summary of this risk management exercise. The risk evaluations are presented for the individual spatial compartments, e.g. reservoir, caprock, fault zones and wells, which together make up the storage complex including the flow barriers. A summary of the risks and their evaluation is provided in the risk register (see Section 18).

The assessment presented here is based on a number of technical conditions which are presented in Chapter 5.5. The assessment is focused on the functioning of the P18-6 reservoir as a suitable 'container' for the injected CO<sub>2</sub> to prevent significant leakage from the storage complex as required under the EU Storage Directive (EU, 2009). The permanent containment of CO<sub>2</sub> is provided by a number of geological and technical barriers. It is of great importance that any risk to this containment function is small, can be managed and is acceptable.

The risk of loss of containment relates to possible existing or future defects in the reservoir (pressure evolution and fluid flow leading to lateral flow or spilling of CO<sub>2</sub>), in the caprock (migration pathways, e.g. fractures), bounding faults (re-activation and increased likelihood for CO<sub>2</sub> migration) or the wells (migration pathways as a result of defects in well cement or casing).

The results from the risk assessment represent a main building block for the Environmental Impact Assessment which is required for the storage permit application.

### 12.1 Reservoir

The P18-2 reservoir is bounded by sealing faults on SW and SE sides and is marked by dip closure on the NE and NW sides, where there is direct contact with the low permeable water saturated part of the Triassic reservoir rocks more downdip (see Figure 4-2). In the zones with dip-closure there is a risk of lateral migration of CO<sub>2</sub> or spilling. In addition there may be flow between the P18-2 and P18-6 reservoirs, which was already assessed for in the feasibility study for the P18-2 reservoir (Neele et al., 2019).



In summary, three locations with potential hydraulic connections to permeable rocks outside the reservoir have been evaluated in more detail:

- Tip of bounding cross fault (F600) to the SE;
- Dip-closure at NW edge of reservoir;
- Small section along fault F57 between reservoirs P18-2 and P18-6.

#### 12.1.1 *Evaluation of spilling at the tip of the bounding cross fault to the SE*

Information from nearby wells indicate that the aquifer has a low permeability due to illitisation. Dynamic reservoir simulations show no spilling, even in the case of strong over-pressurization, although the CO<sub>2</sub> may migrate beyond the gas-water contact (see Chapter 6).

Keeping the average reservoir pressure at or below the hydrostatic pressure at the end of injection and the robustness of flow simulations indicate a very low likelihood that a negligible amount of CO<sub>2</sub> migrates out of the reservoir (risk classification A-1; see also Section 18 and Figure 12-1).

#### 12.1.2 *Evaluation of spilling at the NW edge of reservoir*

A saddle is present at the NW edge of the P18-6 reservoir. The robustness of flow simulations indicate a very low likelihood that a negligible amount of CO<sub>2</sub> migrates out of the reservoir. Keeping the average reservoir pressure at or below hydrostatic pressure at the end of injection will decrease this likelihood, although the reservoir simulations do not suggest this is necessary.

#### 12.1.3 *Evaluation of CO<sub>2</sub> flow between reservoirs P18-2 and P18-6*

Both the static model used during the CATO2 work and the new model for the current feasibility study indicate that there is a small section across the fault zone with juxtaposition of the low-permeable Volpriehausen Sandstone (see Section 6.3.6). The P18-6 reservoir is located directly to the NE of Compartment 2-IV of the P18-2 reservoir. Geological reservoir modelling and pressure history observations indicate that this compartment represents a separate hydraulic unit from the P18-2 reservoir, which implies that no CO<sub>2</sub> will migrate in this part of the reservoir and thus will not end up in the P18-6 reservoir.

The pressure in P18-06 was at the initial level of 377 bar when pressure had already dropped to about 100 bar in the P18-2 reservoir in June 2003. Apparently, this pressure difference could exist, which indicates absence of both flow and pressure equilibration between the two reservoirs on production time scales. Any pressure communication would only be expressed on geological time scales in the order of 10<sup>3</sup> to 10<sup>6</sup> years.

An analysis of the P18 faults revealed that between P18-02 and P18-6 the faults have a high (to very high) probability of having sealing characteristics due to the high probability of impermeable fault gouge formation or cataclasis (Nieuwland, 2012).

The pressure difference of about 277 bar between the two reservoirs and the very low permeability of the Volpriehausen Sandstone show that there is a very low likelihood that even a negligible amount of CO<sub>2</sub> will migrate from P18-2 to P18-6 or no CO<sub>2</sub> is flowing out of P18-2 to P18-6 at all (risk class A-1; see Figure 12-1).

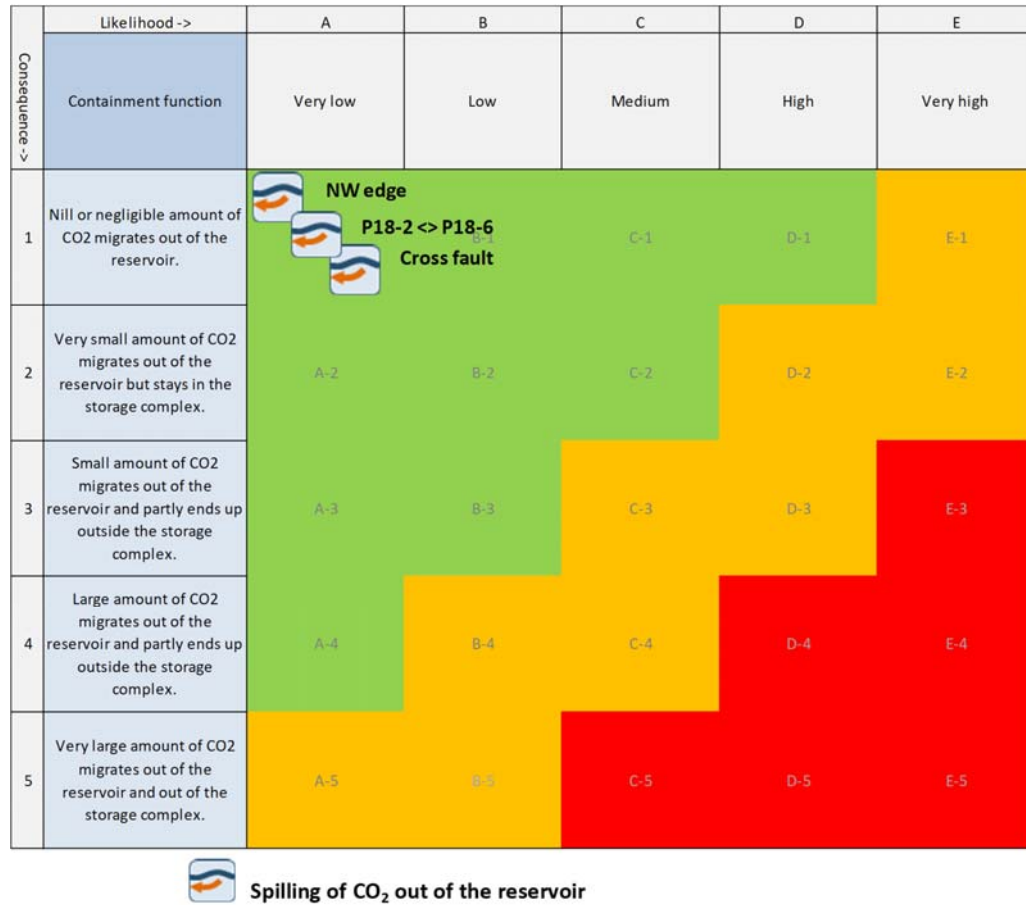


Figure 12-1 Geological risk matrix for the reservoir compartment with inclusion of appropriate risk reduction measures

## 12.2 Caprock

Impermeable shales of the Upper Trias and Altona Groups with a thickness of 450 m to 750 m overlie the P18-6 reservoir, which represent a good seal for the natural gas reservoir. The sealing capacity is evident from the presence of gas in the reservoir below the seal with a gas column of about 170 m.

### 12.2.1 Initial condition

As the evidence for the initial sealing capacity of the caprock is very strong, it is a good seal for CO<sub>2</sub> storage as well and consequently the risk of CO<sub>2</sub> migration out of the reservoir is low to even negligible (see Figure 12-2).

### 12.2.2 Fracturing due to pressurizing the reservoir

Fractures in the seal may be caused by local stress variations due to initial gas production, subsequent CO<sub>2</sub> injection and associated pressure changes. Fractures represent a potential conduit for CO<sub>2</sub> loaded fluids depending on their connectivity and continuity (see also Fault zone).

Semi-analytic modelling has shown that Coulomb stresses as a consequence of pressure build-up due to injection quickly decay on top of the reservoir inside the

caprock. The pressure effect is thus not expected to contribute to the risk of fracture or fault reactivation in the caprock. New fractures or faults will not be generated as they would require even higher Coulomb stresses.

Considering the huge thickness of the caprock and the very rapid decay of the pressure near the top of the reservoir and the basis of the caprock, the likelihood of fracturing the complete caprock is nil and consequently the risk is very low to negligible (Figure 12-2).

#### 12.2.3 *Fracturing due to cooling of the reservoir*

Fractures in the seal may be caused by local stress variations due to initial gas production, subsequent CO<sub>2</sub> injection and associated temperature changes. Fractures represent a potential conduit for CO<sub>2</sub> loaded fluids depending on their connectivity and continuity (see also Fault zone).

Temperature-induced Coulomb stresses in the caprock due to reservoir cooling are negative, and thus do not lead to re-activation of faults or fractures in the caprock nor will they result in new fractures in the caprock. The likelihood of re-activating a pre-existing fault or fracture in the caprock is thus very low.

Temperature drop in the reservoir is very unlikely to lead to re-activation of fractures (or formation of new fractures) and thus will not lead to the migration of CO<sub>2</sub> out of the reservoir. The risk is very low to negligible (Figure 12-2).

#### 12.2.4 *Chemical degradation*

Dissolved CO<sub>2</sub> may react with minerals in the caprock near the interface with the CO<sub>2</sub> reservoir. Since the caprock has proven to be a seal for gas, the only way of upward migration is via diffusion of the dissolved CO<sub>2</sub>, which is a very slow process. Chemical interaction between dissolved CO<sub>2</sub> and caprock minerals is very slow and has minor effects on porosity and permeability. Hence, no migration path is expected to be formed. The affected zone of migration of dissolved CO<sub>2</sub> and chemical interaction is in the order of several meters in thousands of years (Gaus et al., 2005; Tambach et al., 2012).

Chemical degradation will only marginally influence the sealing properties of the caprock and thus will the overall integrity of the caprock stay intact. The likelihood of degrading the caprock is very low and its consequence will be nil or negligible (Figure 12-2).

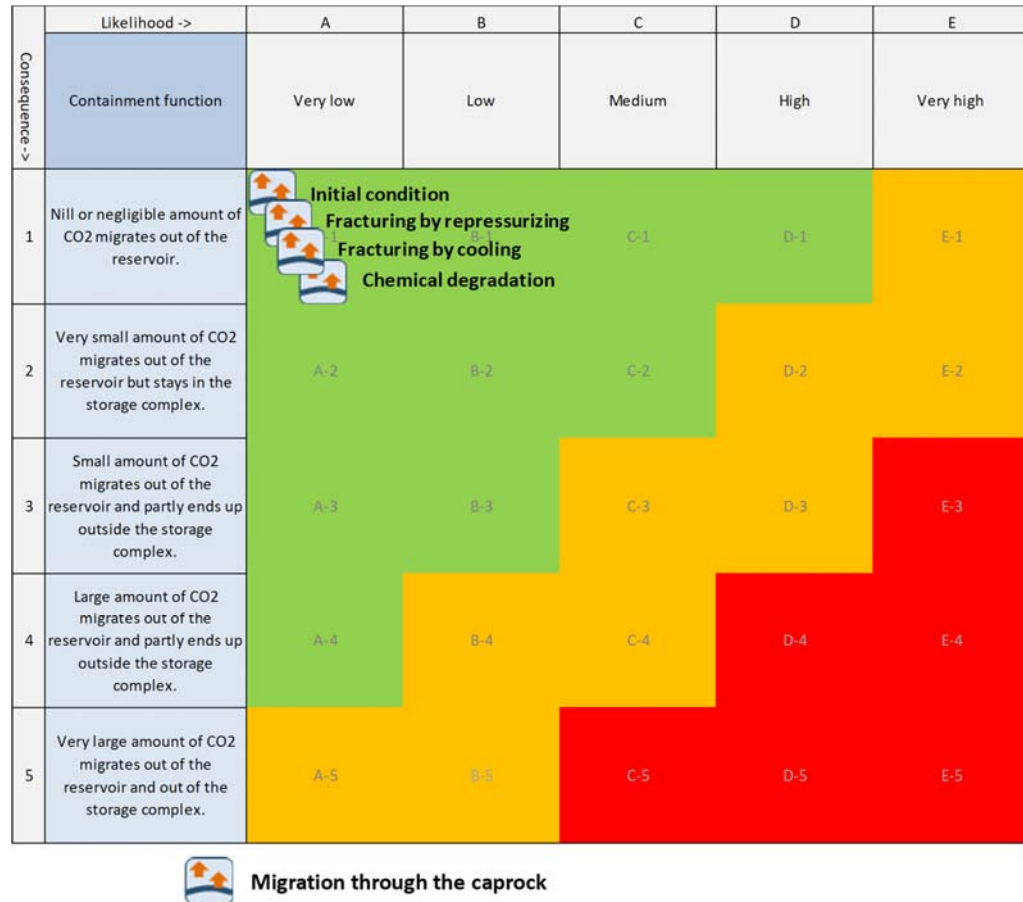


Figure 12-2 Geological risk matrix for the caprock compartment with inclusion of appropriate risk reduction measures

### 12.3 Fault zones

#### 12.3.1 Initial condition

Bounding faults F430 (main fault) and F600 (cross fault; see also Chapter 17.1) are effective seals as evident from the presence of juxtaposed gas reservoirs and sealing rock. As reservoir rocks next to bounding faults are sealed off by very low permeable rocks on the other side of the fault zone, it has a very low likelihood that a negligible amount of CO<sub>2</sub> will migrate across or along the fault and sealing rock (see Figure 12-3).

#### 12.3.2 Chemical degradation

Chemical alteration of the fault zone may enhance migration of CO<sub>2</sub> along the fault. Currently, there is no evidence for gas migration from the P18-6 reservoir along the faults to overlying formations. In general, the geochemical reactions between CO<sub>2</sub>, formation water and fault gouge mineralogy will result in precipitation of carbonate minerals. In the longer term, silicate minerals might react, providing additional cations for carbonate precipitation. Porosity and hence permeability effects are predicted to be negligible. Increase of carbonate content in the fault gouge is known to increase the friction coefficient and to decrease potential for fault re-activation (Samuelson et al., 2012; Adelinet et al., 2014; Bakker et al., 2016). It is therefore

highly unlikely that chemical degradation in itself leads to the migration of CO<sub>2</sub> across the fault zone (see Figure 12-3). See also Section 7.4.

### 12.3.3 *Fault stability: effects of re-pressurising P18-6*

Due to pressure changes during production and/or injection faults may be re-activated (Vandeweyer et al., 2011: par 6.7, p109) and potentially act as conduits for CO<sub>2</sub>.

No seismic activity was encountered during production, based on the KNMI database.<sup>10</sup> Semi-analytic modelling has shown that at the end of the injection period most (if not all) of the areas where positive Coulomb stresses which are present at the end of depletion, have disappeared. The faults are thus expected to be stable at the end of the injection period.

Based on the results from the semi-analytic modelling it appears to be highly unlikely that faults will be re-activated due to the increased pressure by CO<sub>2</sub> injection and consequently will not lead to migration of CO<sub>2</sub> along the fault. The risk is characterized as low (Figure 12-3).

### 12.3.4 *Fault stability: effects of injecting low-temperature CO<sub>2</sub>*

Injection of a cold CO<sub>2</sub> stream could re-activate a nearby fault and change its fluid transport properties. Well P18-A-07-S1 is at a distance of about 100 m from the main bounding fault. Initial TOUGH2 simulations have shown that the cooling front with a temperature drop of about 50 °C could extend to 200 m from the injector after 5 years of injection. Semi-analytic thermomechanical modelling indicates that the Coulomb stresses may reach up to 9 MPa at the edge of the cooling front, which can be sufficient to re-activate the fault. The cold CO<sub>2</sub> from injection wells at less than 200 m from a fault may thermo-mechanically influence its stability.

With time reservoir pressure will increase and the bottomhole injection temperature will increase which will result in making the cooling effect less prominent. Furthermore, the cold area around the well will warm up due to the higher ambient temperature. The pressure increase in itself has a stabilizing effect on the faults. The well P18-2-A1 which is close to a fault, has the worst injectivity and consequently a less pronounced cooling effect. All this will reduce the risk of fault re-activation. On the other hand the effect of cooling may be underestimated as the TOUGH2 simulator has a limit to the temperature of 103 °C whereas the ambient reservoir temperature is 14 °C higher.

The advancement of the cold front near faults can be managed by adjusting the injection rate of well P18-A-07-S1, which is in close distance of the main bounding fault.

Additional simulations with TOUGH2 for a limited period of time of injection (content of pipeline as defined in the discharge scenario) show that the advance of the cold front is strongly limited to 20 m from the well and thus cannot thermo-mechanically reactivate a fault at 100 m from the well. This is considered to be a more representative case for the use of P18-06 field as a backup injection site.

---

<sup>10</sup> KNMI Seismic and Acoustic Data Portal, 2 Oct 2019: doi:10.21944/e970fd34-23b9-3411-b366-e4f72877d2c5).

With inclusion of appropriate management of the injection rate in the well faults the likelihood of thermomechanical fault re-activation leading to the migration of a negligible amount of CO<sub>2</sub> out of the reservoir will be very low or no migration of CO<sub>2</sub> out of the reservoir at all. (Figure 12-3).

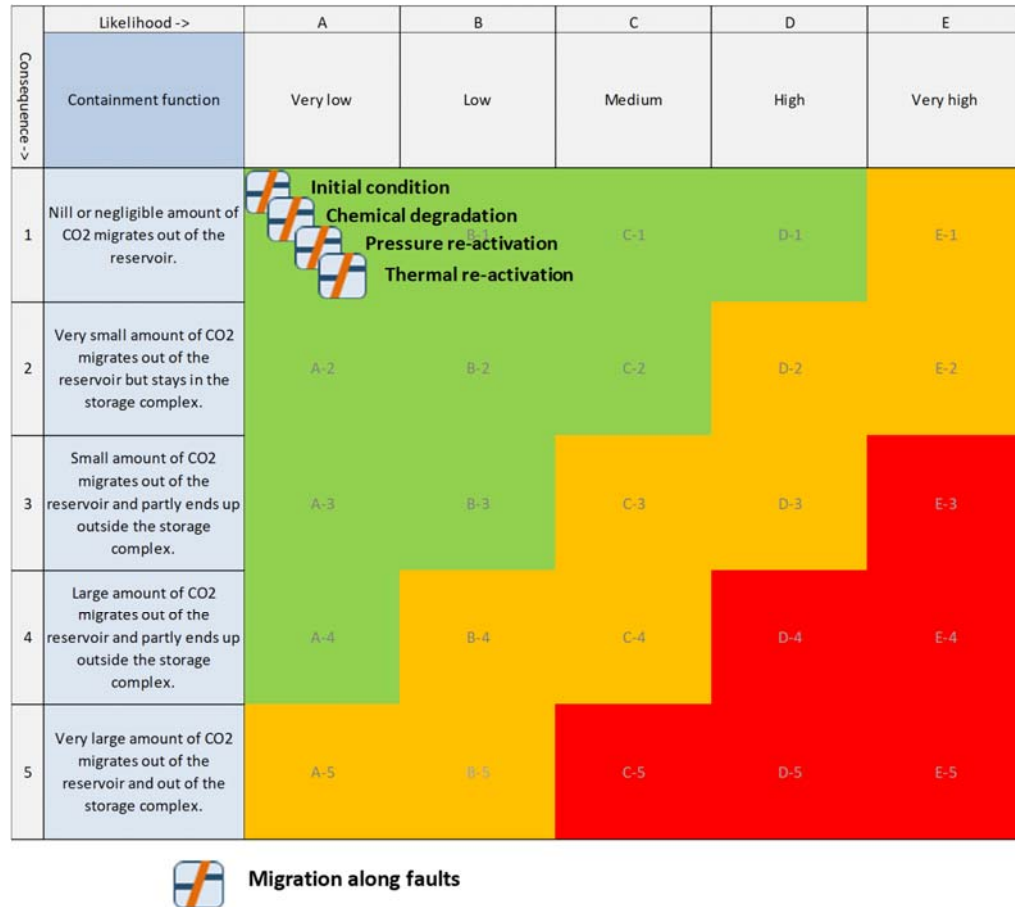


Figure 12-3 Geological risk matrix for the fault zones with inclusion of appropriate risk reduction measures.

## 12.4 Wells

The P18-6A-07-S1 well penetrating the P18-6 reservoir, was evaluated in detail:

### 12.4.1 Outer casing inside conductor

The surface casing in the conductor might be subjected to external corrosion or fatigue induced by metoceanic movement. The presence and quality of the cementation of the conductor and the 20" casing could not be fully ascertained. After evaluation of the presence and quality of the cementation and the implementation of any additional measures, the likelihood that a negligible amount of CO<sub>2</sub> will migrate out of the reservoir; is characterized as low (see Figure 12-4).

#### 12.4.2 *Production packer in 7" liner*

A short stretch of the 7" liner (and cement) above the 5" Top of Liner (TOL) and below the production packer in the 7" liner is just above the caprock in the Schieland Group and may be exposed to corrosive fluids. The 7" liner is P110 carbon steel and is exposed to well bore fluids and represents a single barrier in this small depth window. In the event of presence of water or brine in the wellbore fluids, the risk of corrosion may lead to loss of the primary barrier with potential leakage to the overburden.

With the implementation of adequate measures, leakage from the well will be prevented. The likelihood will be low that a negligible amount of CO<sub>2</sub> will migrate out of the reservoir (see Figure 12-4).

#### 12.4.3 *Cooling*

Injection of cold CO<sub>2</sub> leads to thermal contraction of the wells. The induced tensile stresses can exceed the bonding strength and thus lead to debonding at the well-cement interface. The resulting micro-annuli represent a potential pathway for CO<sub>2</sub> migration which could be further enhanced by chemical interaction of CO<sub>2</sub> and the cement around the micro-annuli (see Sections 9.2.2 and 9.3.4). The effect of cooling at P18-6 will be less than at P18-2 because of the higher pressure and lower temperature drop in P18-6.

Although the creation of micro-annuli is considered to be likely, the migration of CO<sub>2</sub> is prevented by the pressure of CO<sub>2</sub> which is to be maximised at the hydrostatic pressure (at datum level of 3400 m). At the end of the injection phase an appropriate formation-to-formation plug is recommended.

After appropriate decommissioning of the injector wells the risk will be reduced to a low likelihood that a small amount of CO<sub>2</sub> migrates out of the reservoir (risk class B-1; see Figure 12-4).

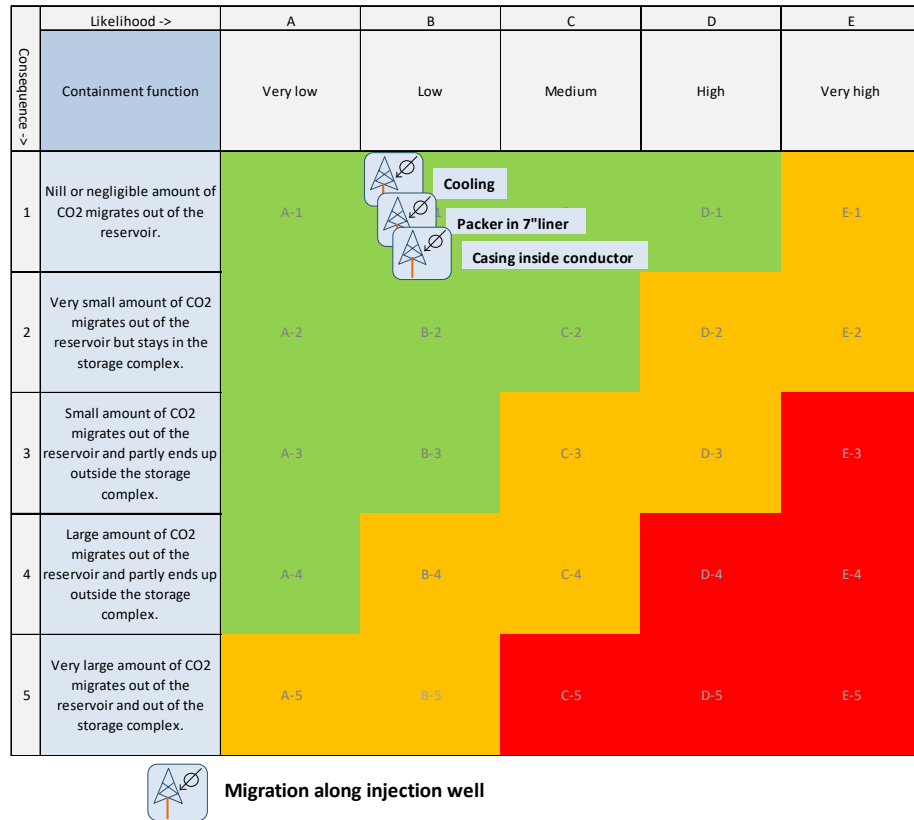


Figure 12-4 Risk matrix for well P18-6A-07-S1 after implementation of appropriate risk reduction measures including any workover activities.

## 12.5 Conclusion

### *All risks can be reduced to acceptable, low levels*

All geological and subsurface well engineering risks in the P18-6 field can be reduced to acceptable, low levels, with no significant environmental impacts if the storage site is properly designed, managed and decommissioned. The conclusion is that there are no prohibitive risks to storing CO<sub>2</sub> in the P18-6 field. All risks can be managed so that their risk level is low and acceptable.

### *Well workovers required*

Well P18-A-07-S1 will require workover activities to some degree to qualify as a CO<sub>2</sub> injector. Proper management of injection rate and temperature is necessary to prevent undesired effects of cooling on wells and nearby wells. For that purpose pressure, temperature and flow rate of injected CO<sub>2</sub> should be monitored (see Section 13).

### *Reservoir pressure after injection*

As mentioned above, all risks identified here can be reduced to acceptable, low levels if the storage site is properly designed, managed and eventually closed. This will require the development of safe injection scenarios and the management of pressure and temperature in the wells and reservoir. It should be noted that the simulation of the injection of CO<sub>2</sub> into the reservoir, the behaviour of CO<sub>2</sub> inside the reservoir, the integrity of the caprock and the stability of faults do not result in limits



to the average reservoir pressure at the end of injection (apart from the maximum given by the initial pressure, which represents the maximum pressure at which the reservoir, caprock and faults have proven containment). Safe and secure storage is possible for reservoir pressure up to initial pressure (i.e., the pressure that existed in the field prior to production).

However, the study did identify a risk that requires reservoir pressure to be maximised at hydrostatic pressure. The potential migration of CO<sub>2</sub> through micro-annuli formed between casing (liner) and cement due to the low temperature of the injected CO<sub>2</sub> becomes small to negligible when reservoir pressure is kept below hydrostatic pressure.

## 13 Monitoring and corrective measures plan

### 13.1 Introduction

A thorough risk based approach to monitoring is adopted. This means that the elaboration of the plan depends on the results of the location-specific risk assessment, which is laid out in the previous sections.

A risk-based monitoring plan will:

- Aim to ensure the safety and integrity of the storage complex;
- Reveal the necessary information for transfer of responsibility to government after the end of injection;
- Be able to supply and incorporate additional learning with respect to large-scale CCS;
- Be able to prove the effectiveness of corrective measures;
- Provide a balance between efficiency and costs.

New techniques and equipment will be included whenever judged appropriate, provided that these techniques do not add to the complexity associated with operating an offshore unmanned installation.

The monitoring and corrective measures plans are part of a set of related plans that are part of the storage permit. The location specific risk assessment (Section 12) is the main input for the corrective measures and closure plans. The development of the monitoring plan is also based on a location specific risk analysis and has strong links with the corrective measures plan. Figure 13-1. illustrates the links and the consistency between the plans.



Figure 13-1. Consistency between risk management, monitoring and corrective measures plans.

Monitoring requirements of the CCS Directive 2009/31/EC and OSPAR are framed around enabling the operator to understand and to demonstrate understanding of

ongoing site processes, to predict future site behaviour and to identify any leakage. Further requirements of the monitoring include early identification of deviations from predicted site behaviour, provision of information needed to carry out remediate actions and the ability to progressively reduce uncertainty.

#### 13.1.1 *Reading Guide*

In the following section the monitoring and corrective measures plan is outlined. The foundation of the plan is given first which refers to the legislation, regulations and other preconditions that have been taken into account. Then the philosophy of the monitoring plan is explained. Finally, the elaboration of the operational monitoring plan is explained, while the detailed monitoring plan is documented in Section 19. The cross-references to the corrective measures plan are explicitly indicated.

The plan described here represents the draft monitoring plan, to be updated and detailed prior to the start of injection.

### 13.2 **Foundation of the monitoring and corrective measures plan**

For the P18-6 storage project the monitoring plan needs to comply with the following regulations and requirements:

- Provisions of two key regulatory treaties governing CO<sub>2</sub> storage in the European offshore area, which are the OSPAR Guidelines (OSPAR, 2007) and the European Storage Directive (EU, 2009) and its implementation in the Dutch Mining Law.
- Requirements of the EU Emissions Trading System (ETS), as defined under the EU Monitoring and reporting Guidelines (EC, 2018), which deals with the accounting of leaked emissions from storage sites.
- Specific requirements to the P18-6 storage project as a first of a kind project for The Netherlands.

The starting point for developing the monitoring and corrective measures plan is an adequate characterization and risk assessment. Although the monitoring and corrective measures plan presented here also makes optimal use of earlier work done on the P18 reservoirs.

The general requirements for both site characterization and risk assessment are given in the Dutch mining law, the EC Storage Directive and its Annexes. Clarifying details are provided in the EU guidance documents.

The detailed site characterization benefited from the fact that the storage reservoir is part of a larger natural gas field which has been produced for more than two decades. This has led to an abundance of information on the site.

The monitoring plan must relate to preventative and corrective measures. In the adopted template in this report, potential risks, monitoring techniques and mitigation measures are all linked together.

With respect to the phases of a storage operation, the plan describes a 'workflow' for monitoring activities during the pre-injection (site qualification), injection (operation), post-injection (closure and post-closure) phases and after transfer of

responsibility (long-term stewardship). However, monitoring in the different stages of a project is not fundamentally different. The philosophy of the monitoring plan is that it must be complete, transparent, consistent, and verifiable.

An additional requirement for the P18-6 storage project is that the monitoring plan may also serve the first of a kind character of the project, in combination with CO<sub>2</sub> injection in the P18-4 field and, potentially, the P18-2 field. This could mean gathering more data for a deeper understanding of the storage process, learning of findings.

### 13.2.1 *General requirements from Directive 2009/31/EC*

A monitoring plan should meet the requirements according to the EU CCS Directive (EU, 2009; Annex II), as listed below.

#### **Initial plan**

The monitoring plan shall provide details of the monitoring to be deployed during the main stages of the project, including baseline, operational and post-closure monitoring.

The following shall be specified for each phase:

1. Parameters monitored;
2. Monitoring technology employed and justification for technology choice;
3. Monitoring locations and spatial sampling rationale;
4. Frequency of application and temporal sampling rationale.

For the purpose of:

- Comparing actual and modelled behaviour of CO<sub>2</sub> and brine
- Detecting significant irregularities
- Detecting CO<sub>2</sub> migration
- Detecting CO<sub>2</sub> leakage
- Detecting significant negative effects for environment, drinking water, nearby residents, the biosphere
- Evaluating the effectiveness of corrective measures taken in case of leakage
- Proving safety and integrity of the storage complex, including the assessment of complete and permanent storage.

The parameters to be monitored are identified so as to fulfil the purposes of monitoring. However, the plan shall in any case include continuous or intermittent monitoring of the following items:

- Fugitive emissions of CO<sub>2</sub> at the injection facility;
- CO<sub>2</sub> volumetric flow at injection wellheads;
- CO<sub>2</sub> pressure and temperature at injection wellheads (to determine mass flow);
- Chemical analysis of the injected material;
- Reservoir temperature and pressure (to determine CO<sub>2</sub> phase behaviour and state).

The choice of monitoring technology shall be based on best practice available at the time of design. The following options shall be considered and used as appropriate (texts taken from the Directive):

- Technologies that can detect the presence, location and migration paths of CO<sub>2</sub> in the subsurface and at surface;
- Technologies that provide information about pressure-volume behaviour and areal/vertical saturation distribution of CO<sub>2</sub> to refine numerical 3-D-simulation to the 3-D-geological models of the storage formation established pursuant to Article 4 and Annex I of the Storage Directive (EU, 2009);
- Technologies that can provide a wide areal spread in order to capture information on any previously undetected potential leakage pathways across the areal dimensions of the complete storage complex and beyond, in the event of significant irregularities or migration of CO<sub>2</sub> out of the storage complex.

### Updated plan

The monitoring system initially installed and its related procedures need to be updated on the basis of the evaluation and modelling activity, or the verification of results. Monitoring plans must be updated, at least every five years, to take into account changes to the assessed risk of leakage, changes to the assessed risks to environment and human health, new scientific knowledge, and improvements in the best available technology. National authorities may set a more stringent frequency.

According to Annex II of the Storage Directive one has the following updating requirements:

- a. The data collected from the monitoring shall be collated and interpreted. The observed results shall be compared with the behaviour predicted in dynamic simulation of the 3-D-pressure-volume and saturation behaviour undertaken in the context of the security characterization.
- b. Where there is a significant deviation between the observed and the predicted behaviour, the 3-D-model shall be recalibrated to reflect the observed behaviour. The recalibration shall be based on the data observations from the monitoring plan, and where necessary to provide confidence in the recalibration assumptions, additional data shall be obtained.
- c. Steps 2 and 3 of Annex I of the Storage Directive shall be repeated using the recalibrated 3-D model(s) so as to generate new hazard scenarios and flux rates and to revise and update the risk assessment.
- d. Where new CO<sub>2</sub> sources, pathways and flux rates or observed significant deviations from previous assessments are identified as a result of history matching and model recalibration, the monitoring plan shall be updated accordingly.

Post-closure monitoring shall be based on the information collected and modelled as in a) through d). The plan must now also provide information needed for the transfer of responsibilities to the competent authority (long-term stewardship). Especially the site's permanent containment must be indicated, based on all available evidence.

### 13.2.2 Emissions accounting for ETS

The Monitoring and Reporting Guidelines for CCS under the ETS describe the method for quantifying potential CO<sub>2</sub> emissions from a storage project.

Potential sources for CO<sub>2</sub> emissions from the geological storage of CO<sub>2</sub> include

- Fuel use at booster stations and other combustion activities such as on-site power plants;
- Venting at injection or at enhanced hydrocarbon recovery operations;
- Fugitive emissions at injection;
- Breakthrough CO<sub>2</sub> from enhanced hydrocarbon recovery operations;
- Leakage from the storage complex.

Quantitative monitoring for ETS will only be required if there is an indication of leakage. There is no requirement for emissions accounting as long as there is no evidence that the site leaks. However, in case irregularities are observed (for example in the downhole pressure and temperature measurements) the need for additional monitoring to detect migration pathways out of the storage complex becomes stringent.

The key question for quantitative monitoring is to what extent the state-of-the-art technology allows for an accurate quantification. In that perspective NSBTF (2009) suggests choosing a combination of a model-driven approach in combination with a monitoring strategy to best estimate the leakage for ETS purposes.

In the unlikely event that there is evidence for CO<sub>2</sub> flow out of the storage complex, or that irregularities occur that give rise to the need to check for anomalies outside of the storage reservoir, a strategy would be to detect leakage to the surface by geophysical methods like seismic data (detection of gas chimneys) or sea-bottom sonar techniques (detection of pockmarks) and then carry out in situ gas measurements and/or sample these leakage areas for direct CO<sub>2</sub> detection. Based on these observations an estimate can be made of leakage rates for the area. However, it should be noted that in the case of CO<sub>2</sub> storage in depleted gas fields, seismic methods have limited value. Most currently operational CO<sub>2</sub> storage projects use saline aquifers, such as Sleipner and Snøhvit in Norway, in which case seismic methods provide an efficient way to monitor the development of the CO<sub>2</sub> plume in the storage reservoir and verify containment by the caprock (e.g., Furre *et al.*, 2017). Seismic methods cannot be used to monitor the distribution of CO<sub>2</sub> in a depleted gas field, as seismic waves cannot discriminate between CO<sub>2</sub> and residual natural gas in the reservoir. In addition, gas fields offer high certainty that CO<sub>2</sub> will be contained in the depleted reservoir (as shown here in Sections 4 through 8), effectively removing the need to check for anomalies above the caprock. Only in case of evidence of unforeseen circumstances or non-conformance would seismic methods be considered as monitoring tool for CO<sub>2</sub> in depleted gas fields.

### 13.2.3 *Specific requirements for the P18-6 storage project*

CO<sub>2</sub> storage is the main objective of the P18-6 storage project. For the project, and the storage permit in particular, the monitoring plan serves to make supported statements about the following:

- Safety and integrity, regarding possible damage to the environment or the soil. Monitoring will have to support that the CO<sub>2</sub> remains stored in the reservoir and does not end up in the biosphere. The lasting quality of the structure of the reservoir and the sealing layer must also be clear. Monitoring offers the opportunity to take action if anomalies occur.
- Demonstration character of the project, learning of findings, some situations can be better understood through measurements.

- Commercially, regarding the ETS and the amounts stored. Monitoring must show that the captured CO<sub>2</sub> is in fact permanently out of circulation and no emission rights for this CO<sub>2</sub> need to be surrendered.
- Legally, regarding the delineation of the storage location. Monitoring must show that the CO<sub>2</sub> does not enter other reservoirs for which no storage permit has been issued.
- Offer a foundation to support the transfer of responsibility after injection is concluded.

### 13.3 Philosophy of the monitoring plan

Besides meeting all legal requirements, the monitoring plan should be based on a balance between efficiency and costs.

#### 13.3.1 Regular measurements

A significant part of the monitoring program is measuring primary operational parameters and verifying the underlying model of the subsurface.

A plan has been devised that includes regular measurements, such as flow, pressure and temperature. These parameters will be used to test whether the injection program is proceeding according to plan and the extent to which anomalies occur with respect to the modelled behaviour.

#### Traffic light model

The measurement program uses the so-called traffic light model. This means that for the measurements, the expected values are indicated in ranges: green, yellow and red. Quantification of these monitoring value ranges is a key element of the monitoring plan update prior to the start of injection.

In the traffic light model, a green zone is given for each operational parameter; the value of the parameter falls within this range, when the operation is proceeding as expected. Outside of this range, threshold 1 (see Table 19-1), a yellow zone exists, indicative of a deviation from the predicted behaviour, without a direct need for corrective measures. When values fall within this range, it is important that insight is gained into the cause of the anomalous results. For that reason, additional measurements should be taken (extra measurements and/or the use of other measuring techniques, depending on the circumstances). Finally, there is a red zone, threshold 2 (see Table 19-1), indicating measurements that are so far outside of the expected range that corrective measures are probably necessary. If such an unexpected event occurs, undesired effects may develop. In order to limit such consequences as much as possible, corrective measures may be deployed. The monitoring program serves to indicate the effectiveness of these corrective measures.

#### Business as usual

When the injection proceeds as predicted, with measured values consistent with predicted values (green zone), the frequency of measurements could gradually be decreased.

**Scale-up**

If the measurements deviate from the expected values (yellow zone), this will lead to a higher frequency of measurements, or the introduction of other types of measurements. If this does not provide sufficient illumination of the situation, the monitoring program will be expanded further.

**Adjusting the model**

Monitoring data can also provide (new) information and insights about the subsurface; this information should be used to adjust and calibrate any models used. The adjusted models can be used to predict future behaviour with higher reliability, so that the behaviour of the CO<sub>2</sub>, the well, the reservoir and the sealing layer can be predicted more accurately as the injection process proceeds.

**13.3.2 Special measurements**

Pre- injection, injection and post-injection monitoring do not differ in intent. Risks may be deemed higher in (parts of) the injection phase, notably the beginning of the injection activities. The monitoring plan reflects higher degrees of risk through more frequent and / or different monitoring techniques. Besides the measurements for the verification of predicted behaviour during injection, there are a number of special measurements included in the monitoring program. These concern baseline measurements, measurements before closure and transfer, as well as measurements under special circumstances during the injection process.

**Baseline measurements**

In the pre-injection phase there will be a period of monitoring in order to determine the current status of the storage site. During this period baseline data will be gathered. It is of key importance to identify all possible baseline data that might be required later in the injection and post-injection phases both for required monitoring and for contingency monitoring.

The baseline data will serve as a reference for monitoring during and after the injection process.

Baseline and repeat measurement acquisition, processing and interpretation are part of the monitoring plan (Table 19-1), where the relation with risk assessment and preventive/corrective measures is also described.

**Measurements before closure and transfer**

Measurements should be made before the closure of the reservoir and before the transfer to the competent authority. Their purpose is:

- to determine whether the behaviour of the CO<sub>2</sub> stored in the reservoir is such that the well can be decommissioned.
- to establish whether the CO<sub>2</sub> stored is in or moving towards a stable situation, after the conclusion of injection, so that it is possible to transfer responsibility to the government.

**Measurements under special circumstances**

During CO<sub>2</sub> injection, the pressure in the reservoir increases; the temperature, pressure and flow rate through each well are chosen such that injection can take place safely. During the injection process, the injection rates of CO<sub>2</sub> will vary, with



occasional interruptions. Part of the monitoring program is to measure the conditions that arise during such transient operations.

The period required for monitoring after decommissioning of the wells and prior to decommissioning of the platform is not defined yet, neither is the period between decommissioning of the platform and transfer of liability to the state authorities. The required lengths of these periods need to be established in agreement with State Supervision of the Mines (SodM).

### 13.3.3 *Direct and indirect determination of possible leakage*

Two ways can be distinguished to enable verification of the points above. On the one hand, there are direct detection methods that can be used to demonstrate the presence of CO<sub>2</sub> migration from the reservoir. An example of this can be CO<sub>2</sub> measurements at wells.

On the other hand, there are also indirect detection methods available, which can be used to verify that the CO<sub>2</sub> injected is behaving as predicted. The predictions are derived from static and dynamic models created beforehand, but also from updates to these models based on available monitoring data (such as pressure measurements in the reservoir). For this reason, important parameters have been included in the monitoring plan for the purpose of indirect monitoring. These include:

- pressure and temperature measurement in the wells;
- annular pressures of the wells;
- volume of injected CO<sub>2</sub>;
- composition of the injected gas;
- well integrity measurements ;
- measurements of irregularities at the seabed.

### 13.3.4 *Different stages*

Different stages can be distinguished throughout the lifetime of the CO<sub>2</sub> storage project. This leads to different monitoring requirements through the lifetime of the project. The different stages are listed below.

- Pre-injection

Prior to actual injection, the monitoring focuses on recording the starting situation (baseline monitoring).

- Injection

In the operational phase CO<sub>2</sub> is injected until the reservoir is filled to an extent that further injection is not desired or allowed, or until no more CO<sub>2</sub> is delivered and a decision is made to conclude CO<sub>2</sub> injection.

- Post-injection

After CO<sub>2</sub> injection has stopped, there is a period of observation. During this period it will be decided whether a stable end situation will be reached. If this is the case, the well will be closed with a plug. If the plug is shown to be of an acceptable quality, the wells will be sealed.

- Post-injection — decommissioning

If the seal is shown to be of acceptable quality, the wells will be permanently decommissioned. Later, responsibility can be transferred to the government.

- Post-injection — transfer of liability

Once a stable situation is achieved, the responsibility of the filled reservoir may be transferred to the competent authority. After the transfer, the developments

in the reservoir will be followed periodically. The competent authority is responsible for a monitoring period of 30 years from the moment of transfer.

For each stage, the monitoring plan (Table 19-1) indicates the parameters to be measured, the frequency, the technology used and the location for each activity. The expected duration of each monitoring period is also indicated.

#### 13.3.5 *Report monitoring results*

Prior to the start of injection activities a baseline report will be compiled, describing the starting state of the wells and the storage site. This is the basis that will be used to map any changes.

An annual report of the monitoring results will be presented to the competent authority. The report should hold operational information, possible anomalous situations and information towards closure and transfer.

Prior to both site closure and site transfer a report is compiled, recording the state of both the well and the subsurface.

#### 13.3.6 *Conclusion*

##### **Deviations from expectations**

Deviations from any expected behaviour of the storage complex may indicate migration or leakage of the injected CO<sub>2</sub>. In the P18-6 case the main activities in determining such deviations from the expected behaviour consist of monitoring the CO<sub>2</sub> pressure and temperature.

A thorough and reliable history match has been established. Deviations from the expected pressure development (p/Z curve) throughout and after the operational phase, could be an indicator of migration of CO<sub>2</sub> from the reservoir or leakage from the storage complex. To this end the pressures at the top of the wells are measured in any case (in the wellhead) as well as the pressures at the bottom of the wells (downhole).

Should unexpected deviations be measured and migration of CO<sub>2</sub> from the reservoir be suspected, measures need to be taken. Taking into account the comments about the application of seismic methods in the case of CO<sub>2</sub> storage in depleted gas fields given in Section 13.2.2. These may include time-lapse seismic monitoring, which allows possible migration paths or shallow CO<sub>2</sub> accumulations to be detected with an expected observation threshold of several tens of kilotons. The detection limit and measurement precision will be specified with the submission of the revised monitoring plan prior to injection and after detailed engineering.

The shallower the gas accumulation occurs, the better the chance that it can be detected. Baseline monitoring prior to injection will be used to make an inventory of pockmarks already present. This will allow the change with respect to the initial situation to be determined in case of a possible migration or leakage.

##### **Well integrity**

Various techniques are used to monitor the integrity of the (injection) wells. These include:

- Logging across the depth of the well;
- Measurement of the pressures in the annuli;
- Periodic analysis of the liquids in the annuli, in order to test for the presence of CO<sub>2</sub>.

Prior to the commencement of CO<sub>2</sub> injection, each injection well will be worked over and its state will be recorded as the baseline for later determinations of the integrity of the well. After injection, the well will be safely sealed and permanently decommissioned. However, before the well is entirely decommissioned, there will first be a period in which the integrity of the plug (FFP) is measured at seal level. These measurements consist of tests monitoring the annular pressures, logs and taking samples of the liquids from the well above the seal in order to analyse for the presence of CO<sub>2</sub>.

#### **Monitoring of the seabed**

Finally, there is monitoring of the seabed. This is mainly in order to show that there are no changes and therefore there is no migration of CO<sub>2</sub> to the seabed. Various acoustic technologies (multibeam echo sounding, side scanning sonar, etc.) can be used to identify changes in and at the seabed as a result of changes in the deep underground (often in the shape of pockmarks) and possible CO<sub>2</sub> bubble streams in the water column. In addition, seabed samples (via coring) can be used to establish the presence or absence of leaking CO<sub>2</sub>.

### **13.4 Interpretation**

Abovementioned aspects have led to the monitoring plan presented here. The following aspects will be monitored:

- Injection process
- Well integrity
- Reservoir integrity
- Environmental monitoring {for leakage of CO<sub>2</sub> from the storage complex}

#### **13.4.1 Categories**

Monitoring of CO<sub>2</sub> storage can be achieved either by measuring the absence of any leakage through direct detection methods, or by verifying indirectly that the CO<sub>2</sub> is behaving as expected in the reservoir based on static and dynamic modelling and updating thereof corroborated by monitoring data. The main challenge for measuring absence of any leakage consists of spatial and temporal coverage of the monitoring method, i.e. "Where and when do we need to monitor in order to be sure that no leakage occurs". The strategy should therefore be based on identified risks.

For the indirect model-based monitoring the emphasis is more on scenario confirmation. As long as monitoring data demonstrates that the storage system is behaving according to the predictive models, the understanding of both the processes occurring and the behaviour of the storage complex can be considered sufficient. In case of significant deviations, one should find the causes of the deviations and where necessary recalibrate the models and perform new predictive simulations. If however the deviations fall well beyond the uncertainty ranges of the predictive models, then additional monitoring and possibly contingency measures need to be taken.

In practice often a combination of approaches is applied required and the optimum monitoring plan will be guided by the risk assessment and the site characterization.

Following the NSBTF (2009) and the draft EU guidance documents (2010), the following categories for monitoring are identified:

1. Mandatory monitoring: in any case for all sites. A number of parameters to be monitored is mandatory based on the EU storage directive (EU, 2009).
2. Required monitoring: site specific. This monitoring group is directed to gathering evidence for containment in the reservoir and to demonstrate integrity of seal, fault and wells in case of regular development.
3. Contingency monitoring. The third group refers to a contingency monitoring system which will only be installed if irregularities show up. In the CCS Directive a “significant irregularity” is defined as ‘...any irregularity in the injection or storage operations or in the condition of the storage complex itself, which implies the risk of a leakage or risk to the environment or human health’.

It is to be noted that these three categories as such have not been implemented in Dutch legislation, therefore the term *mandatory* should be read as “mandatory following the CCS Directive”. Similar for the term *required*, which is not as such defined in legislation. Required in the context of this report means a preliminary proposal of essentially risk-based monitoring with the current state of knowledge.

The quantification of a leakage at the sea bottom for ETS purposes is considered as part of the contingency monitoring. Quantitative monitoring for ETS will only be required, if there is an indication of leakage. For the North Sea the strategy suggested by NSBTF (2009) would be to detect leakage to the surface by geophysical methods like seismic data (detection of gas chimneys) or sea-bottom echo-sounding (detection of pockmarks) and then sample these leakage areas for direct CO<sub>2</sub> detection repeatedly. Based on the sampling profiles an estimate can be made of leakage rates over time for the area. In case of wellbore leakages an additional monitoring program in and around the well is suggested.

In the operational execution, the following categories are distinguished, and for each category the measurements performed for general testing are indicated, as well as the measurements that relate to gaining insight into deviations and to conclusion and transfer.

### 13.5 The monitoring plan

Following NSBTF (2009) and the draft EU guidance documents (EU, 2011), Table 13-1 lists the categories for monitoring that have been identified, as well as the aspects to be monitored. Table 13-2 gives a summary of the monitoring plan describing the equipment or method that can be used to measure certain processes.

Table 13-1. Summarized monitoring classification table.

	<b>Mandatory (Mandatory monitoring according to Annex II of the EU directive)</b>	<b>Required (Preliminary estimation of required monitoring)</b>	<b>Contingency monitoring</b>
<b>Injection process</b>	Flow, pressure, temperature and composition of injected CO <sub>2</sub>		
<b>Well integrity</b>	Various Integrity measurements, well head pressure & temperature	Various baseline measurements, plug integrity measurements	
<b>Reservoir integrity</b>	Flowing pressure and temperature measurements	Stabilized pressure and temperature measurements	Seismic survey in case of irregularities
<b>Environmental monitoring</b>		Various baseline measurements, Microseismic monitoring	Various surveys in case of irregularities

The complete monitoring plan for P18-6, in the form of a table, is given in Table 19-1. Below is a description of the parameters mentioned in the table. These parameters follow both from the mandatory monitoring obligations as stipulated by the storage directive and the risk assessment.

#### **Column 1**

The first column describes the parameters to be monitored. These parameters follow both from the mandatory monitoring obligations as stipulated by the storage directive and from the risk assessment.

#### **Column 2**

The second column indicates the proposed technique adopted to measure the parameter. A more detailed description of the technique is provided outside the table.

#### **Column 3**

The third column indicates the category of monitoring (mandatory according to the EU directive, required, contingency).

#### **Column 4 and 5**

The fourth and fifth columns give a description of both the temporal frequencies (column 4) and spatial coverage (column 5) of the data acquisition foreseen in the different phases of the project (pre-injection, injection and post-injection including long-term stewardship after transfer of responsibility). The rationale behind the monitoring strategy related to the identified risks is described in the following section.

#### **Column 6**

Column six provides a description of the expected values that indicate normal behaviour and of the expected accuracy of the monitoring method. Expected values and therefore this column is coloured green.

Table 13-2. Summary of specific monitoring equipment and methods to be used for monitoring of certain processes.

	<b>Injection process</b>	<b>Measurement equipment / method</b>
1	Injection rate	Flow meter
2	Injection stream CO <sub>2</sub> concentration	Samples & analysis: online system
3	Injection stream composition	Samples & analysis: Additional samples for calibration
4	Water measurement	Water measurement
5	Discontinuous emissions through leakage, venting or incidents	Combination of techniques
<b>Well integrity</b>		
6	Annular pressure	Pressure device (with alarm value)
7	Well integrity	Wireline Logging (selection of tool: CBL, PMIT, EMIT, USIT, WAF, optical)
8	Well head pressure	Pressure device
9	Well head temperature	Temperature device
10	Plug integrity	Pressure test and additional inspections
<b>Reservoir integrity</b>		
11	Reservoir pressure (FBHP) (see also line 8)	pressure device
12	Reservoir Temperature (FBHT) (see also line 9)	thermometer or DTS
13	Stabilized pressure (CIBHP) (gradient) during shut-in period	pressure device combined with shut-in
14	Stabilised temperature (CIBHT) (gradient) during shut-in period	thermometer or DTS combined with shut-in
15	Suspected leakage	Surface seismic survey
<b>Environmental monitoring</b>		
16	Pockmarks at the seabed	Multi-beam echosounding
17	Presence of shallow gas or gas chimneys in the subsurface	Baseline seismic data
18	Migration pathways for gas in the shallow subsurface	Time-lapse seismic data acquisition (2D or 3D)
19	CO <sub>2</sub> in soil at pockmarks	Gas samples using vibrocore + lab analysis
20	Bubble detection at wellhead	Acoustic bubble detector
21	Microseismic monitoring	Permanent geophones or DAS in monitoring wells

**Column 7**

The seventh column indicates threshold values, where normal behaviour as anticipated stops and where irregularities start. As long as the measured values remain below these threshold values, no actions are required (green column). In case threshold values exceeded, the seventh column (coloured orange) defines specific actions. Upon exceeding threshold values, monitoring data suggest that the behaviour of the storage system starts to deviate from expectations. This could for example lead to recalibration of the models, but when persisting to more stringent measures.

**Column 8**

In case the monitor values exceed the threshold defined in the eighth column (coloured red), the highest alert phase starts and immediate actions (or contingency measures) as defined in the second sub column of column eight are required.

### Items to be monitored

The next part of the monitoring plan describes the different items or events to be monitored (Injection process, Well integrity, Reservoir Integrity, Environmental Monitoring) and over which time frame (Pre-injection, Injection, Post-injection, etc). See Table 19-2.

It is noted that the timing for monitoring of the post injection period including the decommissioning of the wells and the decommissioning of the platform and the period to the transfer of liability to the state have not been defined in this plan. The definition of these periods will be subject of discussion with State Supervision of the Mines (SodM).

#### 13.5.1 *Proposed monitoring methods*

This section provides more detailed background information on the rationale behind the selection of the proposed monitoring techniques. For each section corresponding to an identified actor in the risk analysis the primary relevant monitoring techniques are referred to between brackets by their number as appearing in the first column in Table 19-1. Monitoring techniques for contingency monitoring are not given between the brackets, this to not overcomplicate the overview below. Techniques relevant for contingency monitoring are indicated in Table 19-1.

##### 13.5.1.1 *Reservoir / injection process (1,2,3,4,5,8,9,11,12,13,14)*

The risk identified from leakage of CO<sub>2</sub> out of the reservoir / storage site where:

- Spilling (via spill point), or
- Sealing capacity of fault zone between P18-2 and P18-6.

Based on the history match of the P18-6 reservoir the field can be considered as a “tank model”, without an active aquifer drive. Therefore CO<sub>2</sub> is expected to disperse throughout the original gas reservoir.

Often – and this applies only to storage of CO<sub>2</sub> in saline aquifers - the key tool for reservoir / CO<sub>2</sub> plume imaging is 3D surface seismic, however this technique is not deemed suitable for P18-6. This is because of the considerable depth of the P18-6 storage reservoir, which renders surface seismic methods less effective. Additionally, for P18-6 the presence of (residual) gas within the reservoir makes the feasibility of repeated seismic surveys for the monitoring of CO<sub>2</sub> dispersion questionable, as seismic data cannot discern between CO<sub>2</sub> and residual gas.

The main components for monitoring deviations in expected behaviour indicating potential migration out of the reservoir or storage complex consist of pressure (and temperature) monitoring. After proper history matching, a deviation from the expected pressure trend (P/z curve) during and after the operational phase is an indicator for potential migration out of the storage complex. As for the P18-6 reservoir, pressure monitoring has the potential to be a powerful tool, since there is no strong aquifer drive masking potential deviations. A rough estimation of the threshold of the mass of CO<sub>2</sub> migration out of the reservoir that can be detected is in the order of 2-10 kt of CO<sub>2</sub>. The exact value depends on the quality of the P/z curves with proper and reliable pressure measurements. Factors like water influx, communication with neighbouring compartments or CO<sub>2</sub> dissolution in water have a

negative effect on the detectability. In addition, the measurement accuracy of inflow rates should be taken into account.

Proper pressure measurements can be obtained from the injection well after a shut-in, or continuously from a “monitoring” well. The latter is the preferred option allowing a continuous measurement of the reservoir pressure in equilibrium, but for the P18-6 reservoir hardly an option. In case the reservoir pressure is measured in the injection well after a shut-in, pressure equilibration should be measured over a time interval in the order of days. Based on the latter, the equilibrium pressure can be extrapolated (if it has not already been reached in this period).

Migration in the reservoir can be followed by additional geophysical logs (RST logs) well tests and downhole fluid samples at monitoring wells in the same reservoir to detect CO<sub>2</sub> breakthrough. During the injection phase, microseismic monitoring (not necessarily from a well in the same reservoir, but in the direct vicinity of the reservoir), and innovative pulse testing techniques may provide data on the location of the advancing CO<sub>2</sub> temperature front by detecting thermal fracturing (if any), and density/viscosity differences. The latter is not considered as an absolutely required measurement for CO<sub>2</sub> tracking, but is recommended. Furthermore the CO<sub>2</sub> can be traced as it closes in on boundary faults or moves toward spill points.

#### 13.5.1.2 *Well integrity (6,7,8,9,10,11,12,13,14,16)*

The key tool for monitoring well integrity is logging, aimed both directly at the wellbore (cement bond logging, etc.), but also at the surrounding formations (saturation logging). Pressure-temperature logging and downhole fluid chemistry are also potentially very useful. Non-well-based tools include 2D or 3D surface seismic for volumetric imaging of the overburden around the wellbores and multibeam echosounding to detect surface changes around the wellbore. During the injection stage, well-based microseismic monitoring can also provide information on flow and degradation processes around the wellbores.

#### 13.5.1.3 *Caprock/overburden (11,12,13,14,16,17,21)*

Caprock integrity is assumed intact as long as no abnormal behaviour of the pressure is observed. In case significant deviations are observed, contingency monitoring is required; potentially useful techniques include time-lapse seismic surveys to detect migration pathways (chimneys) or shallow gas accumulations. 2D surface seismic surveys may be a cost-effective alternative to full 3D, but will not provide full areal coverage of the top seal.

The threshold value of seismically detectable shallow accumulations of CO<sub>2</sub> is in the order of 10's of ktonnes under the condition that CO<sub>2</sub> accumulates as a concentrated gas pocket. The shallower the CO<sub>2</sub> accumulates, the better the chances of picking up the signal.

During the injection phase, microseismic monitoring could provide data on whether the top seal is being geomechanically compromised. The feasibility of using wells as monitoring wells for microseismic monitoring has not been thoroughly explored yet, but may be regarded as a option, especially now DAS systems become ever more sensitive.

#### 13.5.1.4 *Faults (11,12,13,14,21)*

Thermal reactivation of faults is identified as a risk with risk classification B-2 (Section 12.3). If the cold front of the injected CO<sub>2</sub> reaches a fault, the likelihood of



activation increases. In order to reduce this risk, the advancement of the cold front from the injector wells to nearby faults needs to be managed and monitored. Pressure and temperature monitoring data needs to be used in combination with non-isothermal reservoir simulations to assess whether the cold front stays away from the faults within and bounding reservoir blocks.

During the injection phase, microseismic monitoring as well as advanced well tests (pulse testing) may provide data on the location of the migrating CO<sub>2</sub> front. Geophysical logs would not provide reliable indications of generalized CO<sub>2</sub> migration, except where free CO<sub>2</sub> accumulates in very close proximity to the wellbores.

The threshold value of seismically detectable accumulations of CO<sub>2</sub> in the overburden is in the order of 10's of ktonnes, depending on the depth and geophysical properties of the reservoir and surrounding rocks. In the P18-6 case this is considered a contingency measurement. Just like sampling fluids of shallower aquifers can show traces of leaking CO<sub>2</sub>. To detect the absence of migration to the seabed, various types of surveys are an option. These will be able to identify pockmarks or bubbles and check for composition and origin.

#### 13.5.1.5 *Calibration of flow simulations (1,2,3,4,5,8,9,11,12,13,14)*

The calibration of flow simulations combines aspects of several of the above aims, effective reservoir management, accurate pressure and temperature monitoring and insights into fine-scale and geochemical processes. Likely tools are downhole pressure/temperature measurements, RST logs and monitoring breakthrough in monitoring wells. For P18-6 where 3D seismic imaging of CO<sub>2</sub> in the reservoir is considered difficult if not impossible, downhole pressure/temperature is the key technology. As in a number of cases above, microseismic monitoring and pulse testing (an advanced way of well testing) may be useful in the injection phase.

### 13.6 **Conclusion**

The adopted monitoring approach for CO<sub>2</sub> storage in P18-6, builds on the results of the site characterization and the risk assessment. The reservoir has been classified as suitable for CO<sub>2</sub> storage; the reservoir offers stable long-term containment. This conclusion is essentially based on a) the fact that natural gas has been contained in these reservoirs for millions of years, b) the knowledge of the reservoirs obtained during exploration and production of the fields, c) the fact that at the end of injection the pressure in the reservoir will be lower than that of surrounding formations.

The monitoring plan proposed is designed to verify CO<sub>2</sub> containment and storage reservoir integrity while and after the storage facility is in operation. This is achieved by both measuring the absence of any leakage through direct detection methods (for example at the wells), and by verifying indirectly that the CO<sub>2</sub> is behaving as expected in the reservoir by collecting pressure, temperature and injection rate data that feed in to static and dynamic modelling. The design includes therefore the collection of data such as representative storage pressures and annuli pressures, injected volumes and gas qualities, well integrity measurements, reservoir conditions, micro seismicity and sea bottom measurements.

The main component for monitoring deviations in expected behaviour indicating potential migration out of the reservoir consists of pressure and temperature monitoring. After proper history matching any deviations from the expected

pressure trend (P/z curve) during and after the operational phase is a potential indicator for migration out of the storage reservoir. Reservoir pressures will be determined regularly via shut-in of injection wells or monitoring wells. Downhole pressure tests are envisaged to verify the storage pressures and to verify the conversion of the wellhead pressures to downhole pressures.

Only in case irregularities are observed in seismicity pressure, or the temperature behaviour and when migration in the overburden is suspected, additional monitoring is proposed, like time-lapse seismic monitoring to detect possible migration pathways (chimneys) or shallow gas accumulations. The threshold value of seismically detectable accumulations of CO<sub>2</sub> is of the order of 10's of ktonnes under the likely condition that CO<sub>2</sub> accumulates as a concentrated gas pocket in shallower aquifers. The shallower the CO<sub>2</sub> accumulates, the better the chances of picking up the signal.

The key tools for monitoring well integrity consist of (repeated) logging, measuring the annuli pressures and regular analysis of the annuli fluids for the presence of gas or CO<sub>2</sub>. Prior to CO<sub>2</sub> injection a proper assessment of the current state of the existing wells is carried out, as well as work-overs. Before decommissioning, wells will be suspended for a period of time to verify the quality of the plugs at caprock level by gas tests, monitoring of annuli pressures and possibly sampling of fluids from the well to monitor for the presence of CO<sub>2</sub>.

Finally, shallow monitoring, to detect the absence of migration to the seabed, in the form of multi-beam echosounding, side scanning sonar or high-resolution 3D surveys can be considered for identifying pockmarks or bubbles. Furthermore, sampling fluids in the soil at the sea bottom (via cores) can be used to verify the absence of traces of migrating CO<sub>2</sub>. The locations of the sampling will essentially be associated with the well positions, but additional locations can be selected based on multi-beam echosounding results.

In both cases, echosounding and fluid sampling, these types of monitoring should be performed when there is reason to suspect loss of containment and significant leakage out of the storage complex.

## 14 Conclusions

The identified risks that are related to the potential leakage of CO<sub>2</sub> out of the P18-6 storage complex during or after CO<sub>2</sub> injection have been studied in detail and classified in a risk register. Most of the risks have been classified as 'very low', with 'very low likelihood' that a small ('nil to negligible') amount of CO<sub>2</sub> could migrate out of the reservoir'; this corresponds with the lowest possible risk class. The risks associated with the injection well have been classified as 'low', with a 'low likelihood' and a small ('nil to negligible') amount of CO<sub>2</sub> could migrate out of the reservoir.

The risks assessed are related to (1) lateral CO<sub>2</sub> migration out of the storage reservoir, (2) the integrity of the well in the field, (3) the stability of the faults in the storage system and integrity of the caprock.

- (1) Simulation of the flow of CO<sub>2</sub> during injection into the storage formations shows that the injected CO<sub>2</sub> will be retained within the confines of the original gas field. There is no risk of CO<sub>2</sub> spilling, even when the pressure in the reservoir is brought back to the initial pressure.
- (2) Analysis of available data on the integrity of the well in the P18-6 field shows that a workover is required for the existing well, P18-A-07-S1. Once this is performed, the risk of CO<sub>2</sub> leaking along the well, based on pre-injection status, is considered low.

The initial low reservoir pressure leads to low temperature of the CO<sub>2</sub> at the bottom of the well, causing significant temperature gradients in the well. These might lead to de-bonding of well liner (casing) and cement, potentially allowing leakage pathways to form (micro-annuli) for CO<sub>2</sub>. However, only when the pressure in the reservoir is above hydrostatic pressure could CO<sub>2</sub> enter these micro-annuli and potentially migrate into overlying aquifers. Therefore, the pressure in the reservoir is to be maximized at hydrostatic pressure, to reduce the likelihood of CO<sub>2</sub> flowing through these micro-annuli to 'low', with an amount of CO<sub>2</sub> that is 'small to negligible'.

- (3) The cold CO<sub>2</sub> is injected into the reservoir formations, where it will create a low-temperature zone around the injection well. In case injection into the P18-6 reservoir on a continuous basis, this zone could reach faults that are present in the reservoir, affecting fault stability; however, at the same time, faults become more stable during the injection process due to increasing reservoir pressure. If the P18-6 reservoir is only used to store the cold contents of the surface transport pipeline after a shut-in period, the mass of injected (colder) CO<sub>2</sub> is small and the low-temperature front does not reach faults near the well. In both modes of operation, monitoring of injection rate and temperature is recommended to measure the pressure and track the temperature development in the reservoir and ensure that faults remain stable. However, all analysis points to small to negligible impact of fault reactivation; none of the faults in the P18-6 reservoir extend to above the caprock of 450 m to 750 m thick. This ensures that, fault destabilization, if any, will not lead to CO<sub>2</sub> movement through the caprock.

The likelihood that CO<sub>2</sub> injection in the P18-6 reservoir affects caprock integrity is very low.

#### *Recommendations*

- (1) In the study presented here the modelling of the injection process was performed with an isothermal reservoir simulator that could not simultaneously handle pressure and temperature variations in the reservoir. The impact of the low temperature of the injected CO<sub>2</sub> was estimated through the use of an additional simulator and analytical approaches. While the results obtained thus far are considered sufficient for the assessment of the risks associated with CO<sub>2</sub> storage, detailed coupled modelling of pressure and temperature in the storage formations is required prior to the start of injection. This is needed for pressure and temperature predictions that are sufficiently reliable for the management of the injection process and for the interpretation of monitoring data.
- (2) The aim of the present study was to provide the basis for a storage permit application, by understanding the current status of the storage formations, the caprock, the faults and the wells, and their response to the injection of CO<sub>2</sub>. The study established that conditions can be established under which CO<sub>2</sub> can be injected and stored safely and securely in the P18-6 field. The study did not aim to arrive at a complete and detailed description of these conditions. Such an 'operational plan' for CO<sub>2</sub> injection into the P18-6 field will be required prior to the start of injection, as a basis for the detailed monitoring plan and for the operational management of the injection process. The present study is the first step towards the P18-6 operational plan.

## 15 References

- Adelinet M., Nauroy J-F., Graham C.C., Cuss R.J., Wiseall A.C., Bakker E., Spiers C.J. and Hangx S.J.T. (2014). Progress report with data on processes, constitutive relations and parameters for modelling work. EU FP7 UltimateCO<sub>2</sub> Deliverable D4.5.
- Akemu, O., Miersemann, U., Benedictus, T., Nepveu, M., Desroches, J. (2011). Well integrity assessment of the P18 gas field (TAQA), CATO2 report WP3.4-D22.
- Ames R., Farfan P.F. (1996). The environments of deposition of the Triassic Main Buntsandstein Formation in the P and Q quadrants, offshore the Netherlands. In: Rondeel H.E., Batjes D.A.J., Nieuwenhuijs W.H. (eds) *Geology of Gas and Oil under the Netherlands*. Springer, Dordrecht. pp 167-178.
- AMOCO (1993). Final well report, well P/18-2A3(z) & well P/18-2A4.
- Bacci G., Korre A. and Durucan S. (2011). An experimental and numerical investigation into the impact of dissolution/precipitation mechanisms on CO<sub>2</sub> injectivity in the wellbore and far field regions. *International Journal of Greenhouse Gas control* 5, 579-588.
- Baines S.J., and Worden R.H. (2004). *Geological Storage of Carbon Dioxide*. Geological Society, London, Special Publications 233, 59-85.
- Barnes, J. and Hut, P. (1986). A hierarchical O(N log N) force-calculation algorithm. *Nature*, 324, 446-449.
- Bakker E., Hangx S.J.T., Niemeijer A.R. and Spiers C.J. (2016). Frictional behaviour and transport properties of simulated fault gouges derived from a natural CO<sub>2</sub> reservoir. *International Journal of Greenhouse Gas Control* 54, 70-83.
- Baumann G., Henniges J. and De Lucia M. (2014). Monitoring of saturation changes and salt precipitation during CO<sub>2</sub> injection using pulsed neutron-gamma logging at the Ketzin pilot site. *International Journal of Greenhouse Gas Control* 28, 134-146.
- Belfroid, S. (2019). Porthos – CO<sub>2</sub> injection, TNO report TNO 2019 R10335.
- BP (2007). P/18 Field Petrophysical Study. Company report, 13 p.
- BP (2003). End of well drilling & completion report – P18-6A7, Feb – June 2003.
- Candela, T., van der Veer, E.F., Fokker, P.A. (2018). On the importance of thermo-elastic stressing in injection-induced earthquakes, *Rock Mechanics and Rock Eng.*, 51 (12), 3925-3936.
- Duguid A. and Scherer G.W. (2010). Degradation of oilwell cement due to exposure to carbonated brine. *International Journal of Greenhouse Gas Control* 4, 546-560.
- Energy Institute (2019). Hearts and Minds toolkit – Risk assessment matrix. website, version 15 Oct 2019. <https://publishing.energyinst.org/heartsandminds/toolkit/RAM>
- EPA (2012). *Geologic Sequestration of Carbon Dioxide Underground Injection Control (UIC) Program Class VI Well Construction Guidance* (May 2012).
- ETS directive, 2009: DIRECTIVE 2009/29/EC OF THE EUROPEAN PARLIAMENT AND OF THE COUNCIL of 23 April 2009 amending Directive 2003/87/EC so as to improve and extend the greenhouse gas emission allowance trading scheme of the Community EU Guidance Document 2 (draft 2010): Site Characterisation, CO<sub>2</sub> Stream Composition, Monitoring and Corrective Measures. Draft document for consultation version June 17, 2010.

- EU, 2009: DIRECTIVE 2009/31/EC OF THE EUROPEAN PARLIAMENT AND OF THE COUNCIL of 23 April 2009 on the geological storage of carbon dioxide and amending Council Directive 85/337/EEC, European Parliament and Council Directives 2000/60/EC, 2001/80/EC, 2004/35/EC, 2006/12/EC, 2008/1/EC and Regulation (EC) No 1013/2006.
- EU (2011). Implementation of Directive 2009/31/EC on the Geological Storage of Carbon Dioxide. Guidance document 2: Characterisation of the storage complex, CO<sub>2</sub> Stream Composition, Monitoring and Corrective Measures.
- EC (2018). II (Non-legislative acts) Regulations – Commission implementing regulation (EU) 2018/2066 of 19 December 2018 on the monitoring and reporting of greenhouse gas emissions pursuant to Directive 2003/87/EC of the European Parliament and of the Council and amending Commission Regulation (EU) No 601/2012, Official Journal of the European Union, L 334/1-93
- Fisher Q. (2013). Collection of petroleum field analogues data and description of risks of CO<sub>2</sub> leakage along faults. EU FP7 UltimateCO<sub>2</sub> Deliverable D4.1.
- Fischer, H., Orlic, B., Osinga, S., Hopmans, P., Wollenweber, J., Geel, K. (2016). Options to initiate and enhance ductile properties of shale for well bore sealing. "TKI Plugging wells by enhanced formation ductility" - Deliverable report D5.1; TNO report 2016 R10970
- Gaus I., Zazroual M. and Czernichowski-Lauriol I. (2005). Reactive transport modelling of the impact of CO<sub>2</sub> injection on the clayey cap rock at Sleipner (North Sea). *Chemical Geology* 217, 319-337.
- Geel, C.R. (2016). Geological screening of ductile formations. "TKI Plugging wells by enhanced formation ductility" - Deliverable report D4.1; TNO report 2016 R10273.
- Geertsma, J. (1973). A basic theory of subsidence DUE to reservoir compaction: The homogeneous case. *Verhandelingen Koninklijk Nederlandsch Geologisch Mijnbouwkundig Genootschap* 2S, 43-61.
- Gilfillan S.M.V., Lollar B.S., Holland G., Blagburn D., Stevens S., Schoell M., Cassidy M., Ding Z., Zhou Z., Lacrampe-Couloume G. and Ballentine C.J. (2009). Solubility trapping in formation water as dominant CO<sub>2</sub> sink in natural gas fields. *Nature* 458, 2 April 2009, doi:10.1038/nature07852.
- Grude S., Landrø M. and Dvorkin J. (2014). Pressure effects caused by CO<sub>2</sub> injection in the Tubåen. Fm., the Snøhvit field. *International Journal of Greenhouse Gas Control* 27, 178-187.
- Hulten, F.F.N. van (2006) Reservoir quality distribution as tool for better exploration prospect evaluation and estimation of the resource base in the Netherlands. In: Hulten, F.F.N. van & Lutgert, J.E. (comp.). *Tight gas fields in the Netherlands*, workshop EBN-TNO, September 19, Utrecht (The Netherlands), 13 p.
- IEAGHG (Greenhouse Gas Programme) (2016). Impact of impurity on CO<sub>2</sub> compression, liquefaction and transportation, Report 2016/01.
- IEAGHG (2018). Well Engineering and Injection Regularity in CO<sub>2</sub> Storage wells, IEAGHG Technical Report, 2018-08.
- ISO/TC 67/SC 4 Drilling and production equipment. (2017). *ISO 16530-1:2017: Petroleum and natural gas industries - Well integrity - Part 1: Life cycle governance*. bsi.
- Kim K.-Y., Han W.S., Oh J., Kim T. and Kim J.-C. (2012). Characteristics of salt precipitation and the associated pressure build-up during CO<sub>2</sub> storage in saline aquifers. *Transport in Porous Media* 92, 397-418.

- Koenen M., Wasch L., Wollenweber J. and Tambach T. (2014). CATO-2 Deliverable WP3.4-D12. Experimental and modelling study into chemical degradation mechanisms and rates of cement subjected to aqueous and supercritical CO<sub>2</sub> at in-situ reservoir conditions.
- Koenen M. and Wasch L. (2018). The potential of CO<sub>2</sub> leakage along de-bonded cement-rock interface. 14th International Conference on Greenhouse Gas Control Technologies, GHGT-14. 21<sup>st</sup> – 25<sup>th</sup> October 2018, Melbourne, Australia.
- Kutchko B.G., Strazisar B.R., Dzombak D.A., Lowry G.V. and Thaulow N. (2007). Degradation of well cement by CO under geologic sequestration conditions. *Environmental Science and Technology* 41 (13), p4787-4792
- Loeve, D., Hofstee C. and Maas J.G.,(2014). Thermal effects in a depleted gas field by cold CO<sub>2</sub> injection in the presence of methane, *Energy Procedia*, Volume 63, p. 5378-5393.
- Mijnbouwwet, <https://wetten.overheid.nl/jci1.3:c:BWBR0014168&z=2019-04-10&g=2019-04-10>
- Mindlin, R.D. (1936). Force at a point in the interior of a semi-infinite solid, *Physics*, 7(5), 195–202.
- Miocic J.M., Gilfillan S.M.V., Frank N., Schroeder-Ritzrau A., Burnside N.M. and Haszeldine R.S. (2019). 420,000 year assessment of fault leakage rates shows geological carbon storage is secure. *Scientific Reports*, DOI:10.1038/s41598-018-36974-0.
- Miri R. and Hellevang H. (2016). Salt precipitation during CO<sub>2</sub> storage – A review. *International Journal of Greenhouse Gas Control* 51, 136-147.
- Myklestad, N.O. (1942). Two problems of thermal stress in the infinite solid, *Journal of Applied Mechanics*, 9, 136-143.
- Neele, F., Delpart-Jannaud, F., et al. (2013). Site characterization workflow, SiteChar report D1.4.
- Neele, F., Wildenborg, T., Geel, K., Loeve, D., Peters, L., Kahrobaei, S., Candela, T., Koenen, M., Hopmans, P., van der Valk, K., Orlic, B. and V. Vandeweyer, CO<sub>2</sub> storage feasibility in the P18-2 depleted gas field, TNO report, 2019.
- Nepveu, M., Neele, F., Delprat-Jannaud, F., Akhurst, M., Vincké, O., Volpi, V., Lothe, A., Brunsting, S., Pearce, J., Battani, A., Baroni, A., Garcia, B., Hofstee, C. And Wollenweber, J. (2015). CO<sub>2</sub> storage feasibility: a workflow for site characterization, *Oil and Gas Science and Technology* 70, 4, 555–566.
- Nieuwland, D. A. (2012) Fault Seal Prediction in Sandstone Reservoirs - A quantitative and calibrated geomechanical method, 3rd International Conference on Fault and Top Seals - From Characterization to Modelling, Montpellier, France 1-3 October, 2012.
- NOGEP - OPCOM (2016). Industry Standard no. 45 - Well Decommissioning. NOGEP.
- NORSOK (2013). *Norsok standard D-010: Well integrity in drilling and well operations*.
- North Sea Basin Task Force (NSBTF), 2009, Monitoring Verification Accrediting and Reporting (MVAR) Report for CO<sub>2</sub> storage deep under the seabed of the North Sea.
- Okada, Y. (1992). Internal deformation due to shear and tensile faults in a half-space, *Bull. Seism. Soc. Am.*, 82(2), 1018–1040.
- OSPAR (2007). OSPAR Guidelines for Risk Assessment and Management of Storage of CO<sub>2</sub> Streams in Geological Formations (Reference Number: 2007-12), Meeting of the OSPAR Commission, Ostend, 25-29 June 2007.

- Peach C.J., de Bresser J.H.P., van der Kroef R.F.M., Mols A., Verberne B.A. and Samuelson J. (2010). Site-representative caprock and fault rock samples acquired and characterised (1st Year Progress Report). CATO-2 Deliverable WP 3.03-D06.
- Pruess, K., (2011). ECO2M: A TOUGH2 Fluid Property Module for Mixtures of Water, NaCl, and CO<sub>2</sub>, Including Super- and Sub-Critical Conditions, and Phase Change Between Liquid and Gaseous CO<sub>2</sub>. LBML, Uni. Berkeley, Berkeley, CA (Updated Sept 2013).
- Rimmelé G., Barlet-Gouédard V., Porcherie O., Goffé B. and Brunet F. (2008). Heterogeneous porosity distribution in Portland cement exposed to CO<sub>2</sub>-rich fluids. *Cement and Concrete Research* 38, 1038-1048.
- ROAD (2018). Rotterdam capture and storage demonstration project, <https://ccsnetwork.eu/projects/road-project-rotterdam>.
- Roels S.M., Ott H. and Zitha P.L.J. (2014).  $\mu$ -CT analysis and numerical simulation of drying effects of CO<sub>2</sub> injection into brine-saturated porous media. *International Journal of Greenhouse Gas Control* 27, 146-154.
- Samuelson J., Spiers C., Koenen M. and Tambach T. (2012). Lab evaluation of the reactivation potential of simulated faults under CO<sub>2</sub> storage conditions – implications for system integrity and seismic risk. CATO-2 Deliverable WP 3.3 – D13.
- Shell (2015). Peterhead CCS Project, Well Technical Specification, Doc No.: PCCS-05-PT-ZW-7770-00001, 20/05/2015.
- SodM (2019). *De integriteit van onshore putten*. SodM
- Tambach T., van Bergen F., Gutierrez-Neri M., Hostee C., Koenen M., Kooi H., Loeve D., Maas J., Plug W.-J., Ranganathan P., Roels S., van der Meer B., Wasch L. and Zitha P. (2012). Models describing near-well clogging and mineralization to support feasibility and long-term integrity. CATO-2 Deliverable WP3.02-D13.
- Tambach T.J., Loeve D., Hofstee C., Plug W.-J. and Maas J.G. (2015a). Effect of CO<sub>2</sub> injection on brine flow and salt precipitation after gas field production. *Transport in Porous Media* 108, 171-183.
- Tambach T.J., Koenen M., Wasch L.J. and van Bergen F. (2015b). Geochemical evaluation of CO<sub>2</sub> injection and containment in a depleted gas field. *International Journal of Greenhouse Gas Control* 32, 61-80.
- TAQA (2009) CO<sub>2</sub> Offshore Storage Source to Sink. Presentation given by TAQA Energy B.V., 3 July 2009.
- TAQA (2018) Geophysical Evaluation P18. TAQA Internal report, 6 p.
- Tian H., Xu T., Zhu H., Yang C. and Ding F. (2019). Heterogeneity in mineral composition and its impact on the sealing capacity of caprock for a CO<sub>2</sub> geological storage site. *Computers and Geosciences* 125, 30-42.
- Van Balen, R.T., Van Bergen, G., De Leeuw, C., Pagnier, H.J.M., Simmelink, H., Van Wees, J.D., Verweij, J.M. (2000). Modeling the hydrocarbon generation and migration in the West Netherlands Basin, the Netherlands. *Netherlands Journal of Geosciences* 79, 29-44.
- Van Eijs, R., Kuijper, M. and Bisschop, R. (2011). Containment demonstration for the Barendrecht CO<sub>2</sub> storage project, *Energy Procedia*, 4, 4092-4099.
- Vandeweyer V. et al. (2011). Feasibility study P18 (final report). CATO2-WP3.01-D06.
- Vrålstad, T., Todorovic, J., Wollenweber, J., Abdollahi, J., Karas, D., & Buddensiek, M. (2015). *D8.1 - Description of leakage scenarios for consideration in the*



*work in SP3. <https://mirecol-co2.eu/download/D08.1%20-%20Description%20of%20leakage%20scenarios.pdf>.*

- Wang Y., Zhang L., Soong Y., Dilmore R., Liu H., Lei H. and Li X. (2019). From core-scale experiment to reservoir-scale modeling: A scale-up approach to investigate reaction-induced permeability evolution of CO<sub>2</sub> storage reservoir and caprock at a U.S. CO<sub>2</sub> storage site. *Computers and Geosciences* 125, 55-68.
- Williams, S., T. Carlsen, K. Constable, & A. Guldahl (2009) Identification and qualification of shale annular barriers using wireline logs during plug and decommissioning operations. SPE paper 119321, 15 p.
- Zang, W., (2013) Effect of modeling factors on the dissolution-diffusion-convection process during CO<sub>2</sub> geological storage in deep saline formations, *Front. Earth Sci.* 2013, 7(2): 238–256 DOI 10.1007/s11707-013-0359-x.

## 16 Appendix A: compliance with EU Storage Directive site characterisation and assessment

This appendix presents the links between the site characterisation and assessment elements in the EU Storage Directive (EU, 2009) and the site characterisation elements of the P18-6 feasibility study. Annex I of the EU Storage Directive, used here as a reference, consists of three steps, each of which consists of a list of items. The Guidance Document #2 to the EU Storage Directive provides an explanation of all the list elements; this is not repeated here. The tables below are modified after the Site characterisation workflow in Appendix I of the SiteChar report D1.4 (Neele *et al.*, 2013).

### 16.1 Data collection (step 1)

	Storage Directive elements in step 1	Sections of the P18-6 feasibility study	Comments
(a)	Geology and geophysics	17 Appendix B	
(b)	Hydrogeology (in particular existence of ground water intended for consumption)	-	n.a.
(c)	Reservoir engineering (including volumetric calculations of pore volume for CO <sub>2</sub> injection and ultimate storage capacity)	17 Appendix B	
(d)	Geochemistry (dissolution rates, mineralisation rates)	-	Based on earlier studies
(e)	Geomechanics (permeability, fracture pressure)	17 Appendix B	
(f)	Seismicity	17 Appendix B	Related to fault stability in 12.3.3, 12.3.4
(g)	Presence and condition of natural and man-made pathways, including wells and boreholes which could provide leakage pathways	17 Appendix B	
(h)	Domains surrounding the storage complex that may be affected by the storage of CO <sub>2</sub> in the storage site	-	Based on earlier studies
(i)	Population distribution in the region overlying the storage site	-	n.a.
(j)	Proximity to valuable natural resources (including in particular Natura 2000 areas pursuant to Council Directive 79/409/EEC of 2 April 1979 on the conservation of wild birds(1) and Council Directive 92/43/EEC of 21 May 1992 on the conservation of natural habitats and of wild fauna and flora(2) ,	-	Addressed in EIA

	potable groundwater and hydrocarbons)		
(k)	Activities around the storage complex and possible interactions with these activities (for example, exploration, production and storage of hydrocarbons, geothermal use of aquifers and use of underground water reserves)	-	Addressed in EIA
(l)	Proximity to the potential CO <sub>2</sub> source(s) (including estimates of the total potential mass of CO <sub>2</sub> economically available for storage) and adequate transport networks	-	Not known at time of study; assumptions provided by client

## 16.2 Building the 3-D static geological earth model (step 2)

	Storage Directive elements in step 2	Sections of the P18-6 feasibility study	Comments
(a)	Geological structure of the physical trap	4.2, Appendix B: 17.1-17.5	
(b)	Geomechanical, geochemical and flow properties of the reservoir overburden (caprock, seals, porous and permeable horizons) and surrounding formations	4.1, 4.2, 4.4, 8.2, 8.3 Appendix B: 17.4	Geochemical properties based on earlier work
(c)	Fracture system characterisation and presence of any human-made pathways	4.2, 4.5, 9 Appendix B: 17.4	
(d)	Areal and vertical extent of the storage complex	10	
(e)	Pore space volume (including porosity distribution)	Appendix B: 17.4.3-17.4.5	
(f)	Baseline fluid distribution	Appendix B: 17.7	
(g)	Any other relevant characteristics	Appendix B: 17.6.5, 17.7.2, 17.7.3, 17.7.6	Gas production data, PVT, RFT and PLT data
(all)	The uncertainty associated with each of the parameters used to build the model shall be assessed by developing a range of scenarios for each parameter and calculating the appropriate confidence limits. Any uncertainty associated with the model itself shall also be assessed.	6.3.5 6.3.6 6.5.4 9.3 17.7.5	Fault sealing, salt precipitation, mineral assemblage, cement bonding, well cross flow

### 16.3 Characterisation of storage dynamic behaviour, sensitivity characterisation, risk assessment (step 3)

Step 3 consists of several parts, which are discussed separately.

#### 16.3.1 Characterisation of the storage dynamic behaviour (step 3.1)

	<b>Storage Directive elements in step 3, characterisation of the storage dynamic behaviour</b>	<b>Sections of the P18-6 feasibility study</b>	<b>Comments</b>
(a)	Possible injection rates and CO <sub>2</sub> stream properties	5.2, 5.3, 6.2	
(b)	Efficacy of coupled process modelling (that is, the way various single effects in the simulator(s) interact)	6.3, 6.4 7.2, 7.3, 8.2, 8.3, 9.3	Thermohydraulic Thermomechanical
(c)	Reactive processes (that is, the way reactions of the injected CO <sub>2</sub> with in situ minerals feedback in the model)	6.5, 7.4, 9.3	
(d)	Reservoir simulator used (multiple simulations may be required in order to validate certain findings)	6.3.3, 6.4.2	
(e)	Short and long-term simulations (to establish CO <sub>2</sub> fate and behaviour over decades and millennia, including the rate of dissolution of CO <sub>2</sub> in water)	6.3 6.5	Short term Long term geochem.

#### 16.3.2 Insights from dynamic modelling (step 3.1)

	<b>Storage Directive elements in step 3, insights from dynamic modelling</b>	<b>Sections of the P18-6 feasibility study</b>	<b>Comments</b>
(f)	Pressure and temperature of the storage formation as a function of injection rate and accumulative injection amount over time	6.3, 6.4	
(g)	Areal and vertical extent of CO <sub>2</sub> vs time	6.3	
(h)	Nature of CO <sub>2</sub> flow in the reservoir, including phase behaviour	6.3, 6.4	
(i)	CO <sub>2</sub> trapping mechanisms and rates (including spill points and lateral and vertical seals)	4, 6.3, 10	
(j)	Secondary containment systems in the overall storage complex	10, 11	
(k)	Storage capacity and pressure gradients in the storage site	6.3, 6.4	
(l)	Risk of fracturing the storage formation(s) and caprock	7.2, 7.3, 8.2, 8.3, 12.2, 12.3	
(m)	Risk of CO <sub>2</sub> entry into the caprock	4.3, 8.3, 8.4, 12.2	

	<b>Storage Directive elements in step 3, insights from dynamic modelling</b>	<b>Sections of the P18-6 feasibility study</b>	<b>Comments</b>
(n)	Risk of leakage from the storage site (for example, through decommissioned or inadequately sealed wells)	12	
(o)	Rate of migration (in open-ended reservoirs)	11, 12.1	
(p)	Fracture sealing rates <sup>11</sup>	12.3.2	Qualitative; no rates
(q)	Changes in formation(s) fluid chemistry and subsequent reactions (for example, pH change, mineral formation) and inclusion of reactive modelling to assess affects	6.5, 7.4, 8.4, 9.3.4	
(r)	Displacement of formation fluids	-	
(s)	Increased seismicity and elevation at surface level	7	

#### 16.3.3 Sensitivity characterisation (step 3.2)

This element of the EU Storage Directive reads: *“Multiple simulations shall be undertaken to identify the sensitivity of the assessment to assumptions made about particular parameters. The simulations shall be based on altering parameters in the static geological earth model(s), and changing rate functions and assumptions in the dynamic modelling exercise. Any significant sensitivity shall be taken into account in the risk assessment.”*

Sections of the P18-6 feasibility study: 6.3.5, 6.3.6, 6.3.5, 8.4.2

Comments: Sensitivity to temperature, injection rate, mineral types

#### 16.3.4 Risk assessment: hazard characterisation (step 3.3.1)

This element of the SDEU reads: *“The hazard characterisation shall cover the full range of potential operating conditions to test the security of the storage complex. Hazard characterisation shall be undertaken by characterising the potential for leakage from the storage complex, as established through dynamic modelling and security characterisation described above. This shall include consideration of [the items in the table below]. The hazard characterisation shall cover the full range of potential operating conditions to test the security of the storage complex.”*

	<b>Elements of Storage Directive Risk assessment: hazard characterisation (step 3.3.1)</b>	<b>Sections of the P18-6 feasibility study</b>	<b>Comments</b>
(a)	potential leakage pathways	9, 11, 12	
(b)	potential magnitude of leakage events for identified leakage pathways (flux rates)	7.4.4	Mostly qualitative

<sup>11</sup> The EU Guidance Document #2 does not offer an explanation as to the meaning of ‘fracture sealing rates’. Here, fracture sealing is assumed to be a combination of chemical reactions (resulting in mineral deposition in injection-induced fractures) and geomechanical processes (resulting in fractures closing).

	<b>Elements of Storage Directive Risk assessment: hazard characterisation (step 3.3.1)</b>	<b>Sections of the P18-6 feasibility study</b>	<b>Comments</b>
(c)	critical parameters affecting potential leakage (for example maximum reservoir pressure, maximum injection rate, temperature, sensitivity to various assumptions in the static geological Earth model(s))	12	
(d)	secondary effects of storage of CO <sub>2</sub> , including displaced formation fluids and new substances created by the storing of CO <sub>2</sub>	6.5, 7.4, 8.4	New substances
(e)	any other factors which could pose a hazard to human health or the environment (for example physical structures associated with the project)	-	n.a.

#### 16.3.5 *Risk assessment: exposure assessment (step 3.3.2)*

This element of the SDEU reads: *“Based on the characteristics of the environment and the distribution and activities of the human population above the storage complex, and the potential behaviour and fate of leaking CO<sub>2</sub> from potential pathways identified under Step 3.3.1.”*

The site characterization study will yield probability density functions for CO<sub>2</sub> fluxes, times... as deemed necessary by experts in HSE research and industrial safety. See 4.10 for details.

Sections of the P18-6 feasibility study: -

Comments: Not in scope of present study

#### 16.3.6 *Risk assessment: effects characterisation (step 3.3.3)*

This element of the SDEU reads: *“Based on the sensitivity of particular species, communities or habitats linked to potential leakage events identified under Step 3.3.1. Where relevant it shall include effects of exposure to elevated CO<sub>2</sub> concentrations in the biosphere (including soils, marine sediments and benthic waters (asphyxiation; hypercapnia) and reduced pH in those environments as a consequence of leaking CO<sub>2</sub>). It shall also include an assessment of the effects of other substances that may be present in leaking CO<sub>2</sub> streams (either impurities present in the injection stream or new substances formed through storage of CO<sub>2</sub>). These effects shall be considered at a range of temporal and spatial scales, and linked to a range of different magnitudes of leakage events.”*

Sections of the P18-6 feasibility study: -

Comments: Not in scope of present study

#### 16.3.7 *Risk assessment: risk characterisation (step 3.3.4)*

This element of the EU Storage Directive reads: *“This shall comprise an assessment of the safety and integrity of the site in the short and long term, including an assessment of the risk of leakage under the proposed conditions of use, and of the worst-case environment and health impacts. The risk characterisation shall be conducted based on the hazard, exposure and effects assessment. It shall include an assessment of the sources of uncertainty identified during the steps of characterisation and assessment of storage site and when feasible, a description of the possibilities to reduce uncertainty.”*

The site characterization study will yield probability density functions for CO<sub>2</sub> fluxes, times, as deemed necessary by experts in HSE research and industrial safety. See 4.10 for details.

Sections of the P18-6 feasibility study: Section 12

Comments: Directed to characterisation of subsurface hazards

## 17 Appendix B. Subsurface model descriptions

### 17.1 Static model

#### 17.1.1 New geological model – reasons

Since the completion of the storage feasibility assessment for the P18-4 field (Vandeweyer et al., 2011), which produced a 3D reservoir model of all P18 fields, a number of developments necessitated the building of a new 3D reservoir model. Around 2014, the operators and co-owners of the P15-P18 blocks had the P15-P18 3D seismic survey reprocessed. A pre-stack, depth migrated (PSDM) version of the cube was now available, both in time and depth, as well as a velocity cube. An initial comparison of the Top Bunter interpreted from that cube with the one from the P18-4 study (Vandeweyer et al., 2011) revealed several important differences, enough to justify a new seismic interpretation, as well as a new geological reservoir model.

It was therefore decided to build a new reservoir model, based on a seismic interpretation on the new, reprocessed 3D cube.

### 17.2 Seismic interpretation

A substantial part of the Top Bunter and Top Keuper had already been interpreted by TAQA. Only a few blank areas needed to be done. After a review of the TAQA horizon and fault interpretations, the remaining uninterpreted areas of the reprocessed cube were interpreted. This was mostly the southeastern tip of the P18-2 field and P18-6 in its entirety (Figure 17-1).

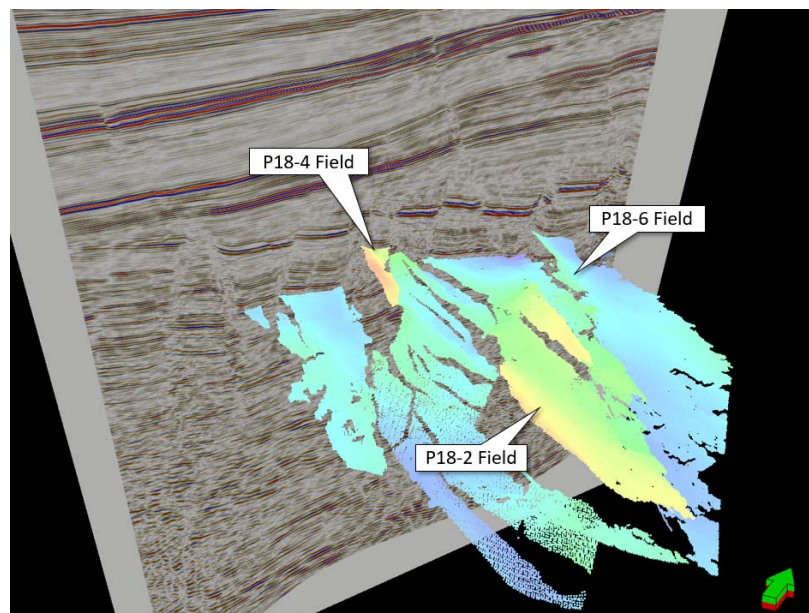


Figure 17-1 Oblique view on seismic interpretation of Top Bunter on the reprocessed P15-P18 3D cube.



Faults interpreted by TAQA were inspected and generally found to agree with the seismic data, although in some instances modifications were made on some of the faults. The P18-6 faults were completely newly interpreted (Figure 17-2). None of the P18-6 boundary faults extends upward to the Base Cretaceous Unconformity.

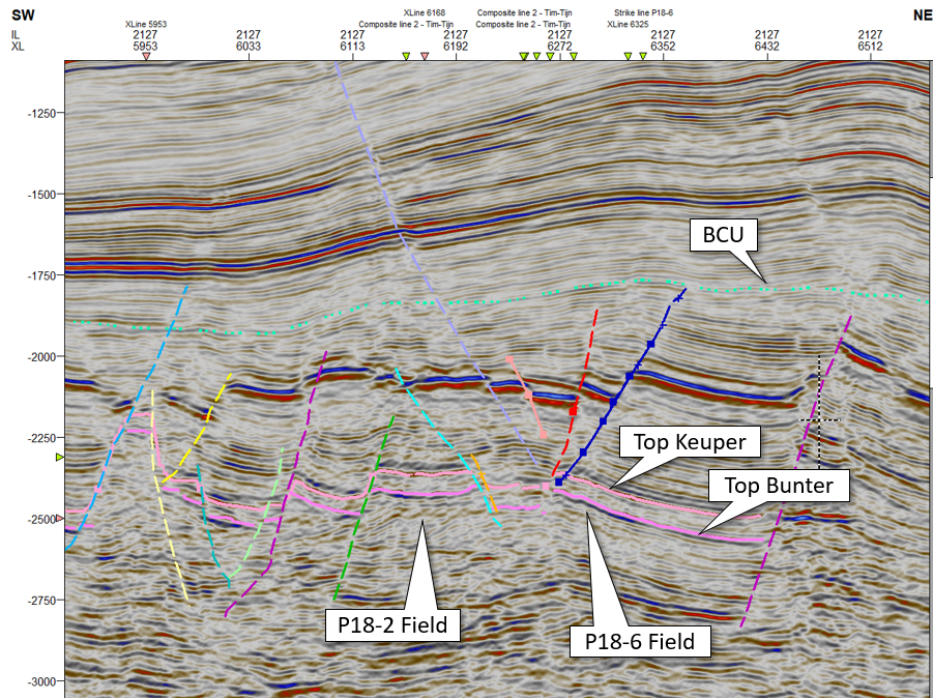


Figure 17-2: Seismic inline 2127 showing the top Bunter (purple horizon), Top Keuper (pink), and Base Cretaceous Unconformity (light green). Note that P18-6 Boundary Fault 400 (dark blue) does not extend upward into the Base Cretaceous Unconformity (BCU).

### 17.3 Time-depth conversion

After consulting TAQA, it was found that the reprocessed P15-P18 cube came with a strongly improved velocity cube. It was therefore decided to adopt TAQA's velocity model which for the current project only contains two horizons: Top Keuper and Top Bunter (Table 17-1). In contrast to the velocity model that was used in the 2011 CATO study which was based on VELMOD and used six horizons, in the present model the entire overburden velocities above the Triassic are taken from the velocity cube (TAQA, 2018). For the Upper Germanic Trias Group itself a constant velocity of 4568 m/s was applied.

Table 17-1: Velocity model from TAQA as used in the current study

Interval	Top	Base	TZ conversion method
Overburden	MSL	Top Keuper	PSDM velocities
Upper Triassic	Top Keuper	Top Hardegsen	Constant velocity: 4568 m/s
LowerTr.-Perm.	Top Hardegsen	Top Carboniferous	Constant velocity: 4694 m/s

## 17.4 Petrel model building

Although initially a model was populated with porosity, permeability, and water saturation from upscaled logs, during the history matching process it became apparent that the reservoir properties away from well P18-A-07-S1 needed major changes in order to match produced volumes, rates, and pressures (see below). Therefore, only the values at the well position were retained in the reservoir simulation model. Since the original static property model was not used for the final model, only the properties resulting from the history match are described here.

### 17.4.1 Fault model, gridding

The P18-6 Field consists of a NW-SE elongated, tilted fault block. It is bounded to the SW by a large-offset fault (Fault 400 and 430) and on the SE by a smaller, transverse fault (Fault 500). All in all, it is a straightforward structure, and no difficulties were encountered during the gridding process.

Figure 17-3 shows the end result of the fault construction and pillar gridding process. Names of the faults used in the current model are also shown in Figure 17-3. For the pillar gridding (Figure 17-4) an average X and Y increment of 50 m was specified.

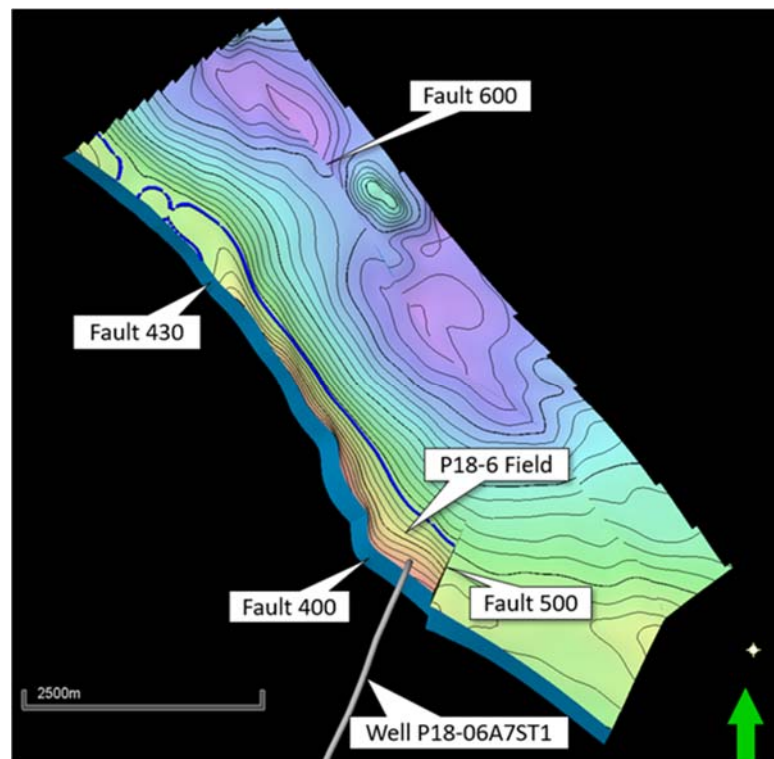


Figure 17-3: Map view of all faults that have been incorporated in the pillar grid of the P18-6 Petrel reservoir model.

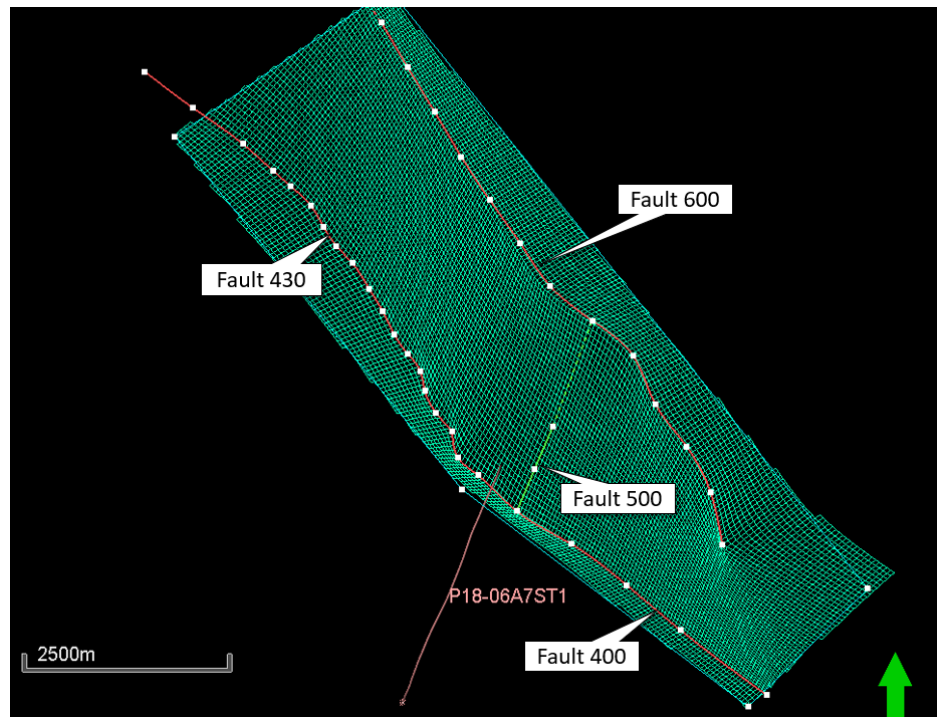


Figure 17-4: Map view of all faults and trends used in the pillar gridding, and the resulting grid.

#### 17.4.2 Make Horizons / Make Zones

The new model has a different approach towards the construction of the reservoir formations compared to the P18 model from 2011. In the previous model, all Lower Triassic formation tops had a separate horizon as input in the 'Make Horizons' process. In combination with the many faults this led to geometrical problems such as rapidly thinning and thickening formations. The current model utilises only one horizon for the reservoir formations (Top Bunter; Figure 17-5).

The 2011 P18 model subdivision into formations was maintained, from top to base: Hardegsen, Upper Detfurth, Lower Detfurth, and Volpriehausen Formation.

The rest of the horizons were created using isopachs (Figure 17-6, Figure 17-7, Figure 17-8). The result is a smooth reservoir model where formation thickness changes across the field are kept to a minimum.

The layering was done as follows: Hardegsen 20, Upper Detfurth 5, Lower Detfurth 5, and Volpriehausen 3 layers. All layers were assigned the type 'proportional'.

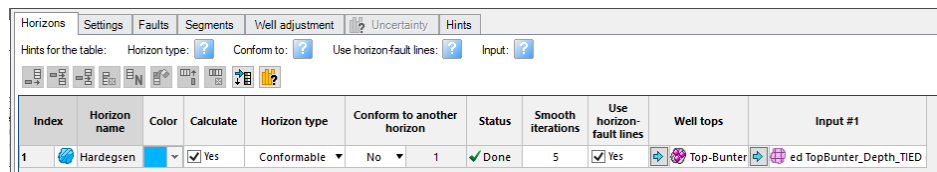


Figure 17-5: Dialog box of the 'Make Horizons' process of the Petrel reservoir model.

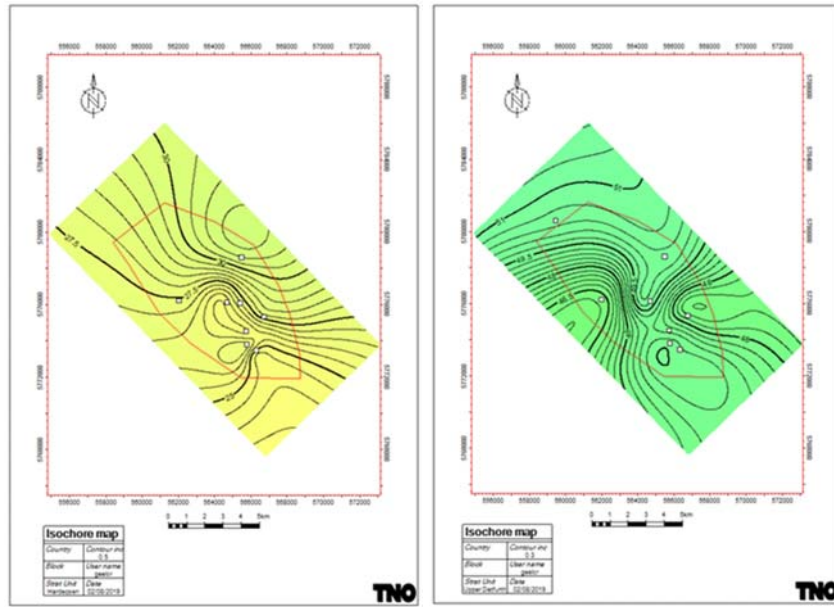


Figure 17-6: Isochore maps of the Hardeggen Fm (left) and the Upper Detfurth Fm (right). Well values on which the isochore maps are based are shown as white squares.

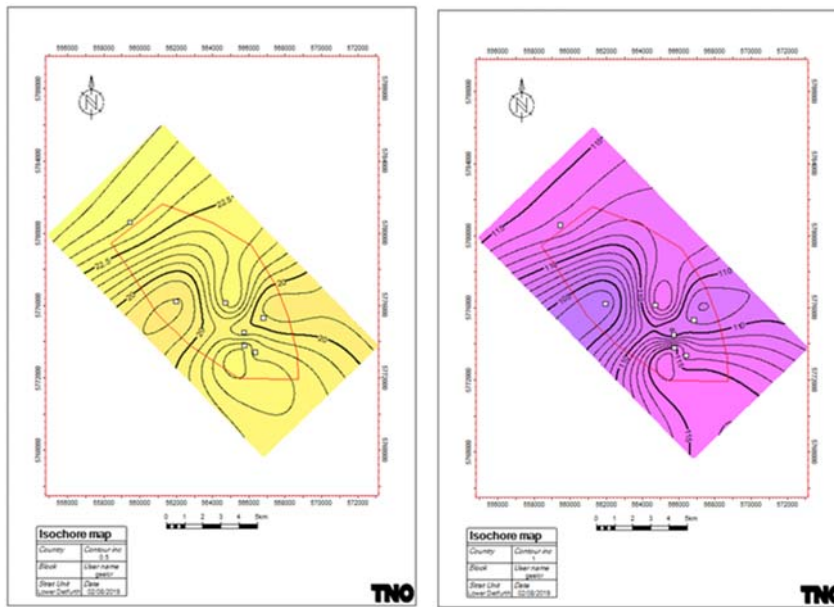


Figure 17-7: Isochore maps of the Lower Detfurth Fm (left) and the Volpriehausen Fm (right). Well values on which the isochore maps are based are shown as white squares.

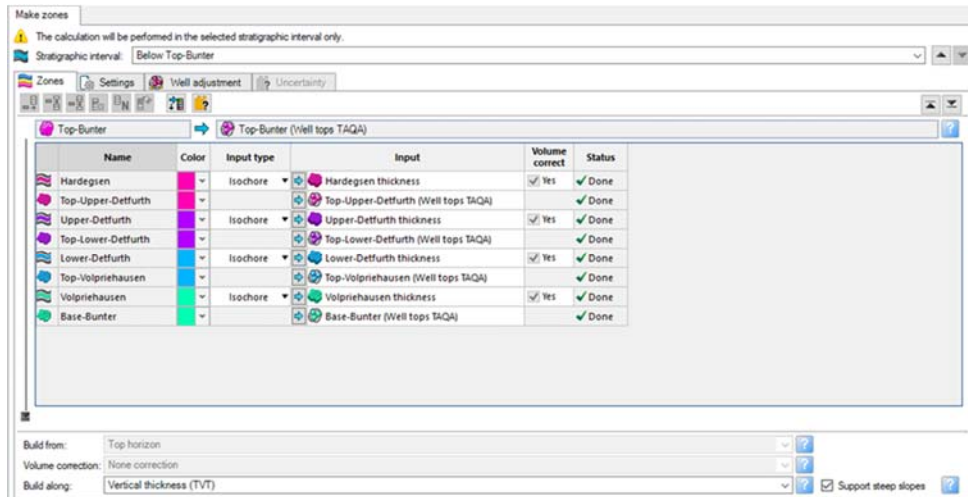


Figure 17-8: Creation of the various reservoir zones in the Petrel reservoir model.

### 17.4.3 Reservoir properties

A detailed petrophysical study on the P15-P18 area was done by BP (2007). Relationships between porosity and permeability in this study were established on the basis of rock types (lithofacies). The origin of these rock types is not readily apparent from this study but seems to have been generated by the Baker Hughes “Horizon” software package (see Ames & Farfan, 1996). On the basis of well log readings, this software package classifies depth intervals into rock types that have been calibrated against lithofacies from core descriptions.

For the P18 area these rocktypes are:

- Rock Type 1: Eolian Dune
- Rock Type 2: Interdune
- Rock Type 3: Eolian Dolomitic
- Rock Type 4: Shales

For each of these rock types a separate porosity-permeability relation has been established (BP, 2007).

- Rock Type 1:  $K_{calc} = 10^{(-3.3+0.58 \cdot PH_{calc} - 0.01229 \cdot (PH_{calc})^2)}$
- Rock Type 2:  $K_{calc} = 10^{(-2.75+0.464 \cdot PH_{calc} - 0.011 \cdot (PH_{calc})^2)}$
- Rock Type 3:  $K_{calc} = 10^{(-3.003+0.358 \cdot PH_{calc} - 0.0068 \cdot (PH_{calc})^2)}$
- Rock Type 4:  $K_{calc} = 0.01$

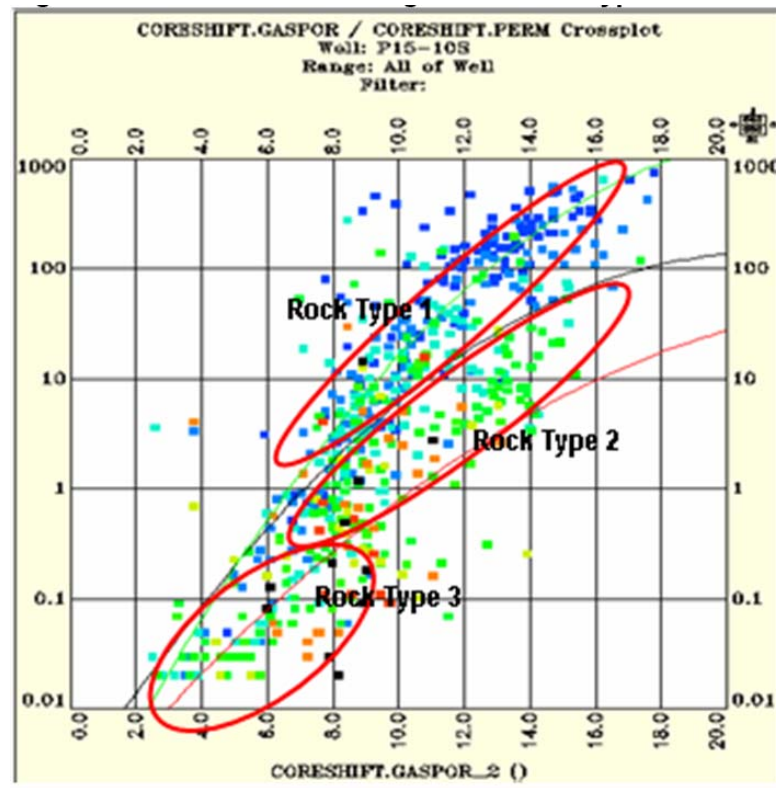


Figure 17-9: Relationship between porosity and permeability for three rock types (lithofacies):  
 1 = Aeolian Dune, 2 = Interdune, 3= Aeolian Dolomitic. Not shown in this graph is rock type 4 = shales. From BP (2007).

For the P18-6 field, because the rock type distribution was not present and for simplicity (see also “modelling of reservoir properties”) a single relation between porosity and permeability was used, which is based on the BP relations (see Figure 17-10). The final relationship was adjusted during the history match (PHIE in %):  

$$K_{calc} = 10^{(-3.5 + 0.57 \cdot PHIE - 0.0129 \cdot (PHIE)^2)}$$

In the P18-2 field, two field-wide no-flow boundaries or baffles were identified, between Upper and Lower Detfurth Fm, and between Lower Detfurth and Volpriehausen (Figure 17-11). It is assumed that these also exist in P18-6 and again these were implemented in the ECLIPSE reservoir model by using transmissibility multipliers between the lowermost layer of Upper Detfurth and uppermost layer of Lower Detfurth, and between the lowermost layer of Lower Detfurth and uppermost layer of Volpriehausen Fm. Also a barrier was identified between the Hardegsen Fm and the Upper Detfurth. The value of this barrier was set in the history match

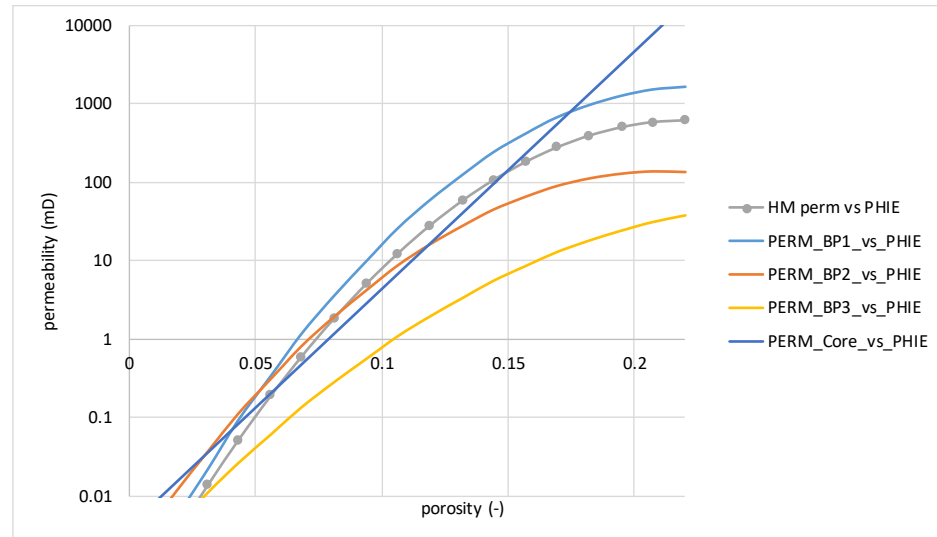


Figure 17-10: Relationship between porosity and permeability used in the history match (HM perm) and for comparison the relationships for the three rock types (lithofacies from BP) on which the used relationship is based.

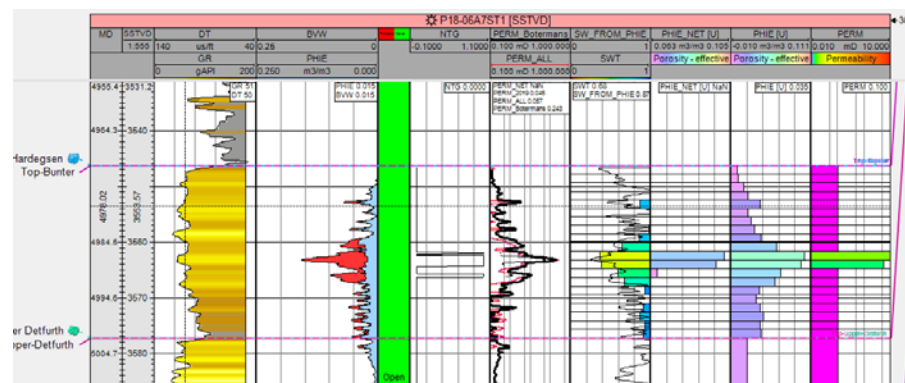


Figure 17-11: Well P18-06-A7 showing the presence of a barrier between the Hardegsen and Upper Detfurth Fm.

#### 17.4.4 Modelling of reservoir properties

For the P18-6 model, for the distribution of the reservoir properties a different approach was used, because:

- The properties observed at P18-A-07-S1 are not representative for the rest of the field, because the observed GIP is far larger than can be expected based on the porosity from the well log.
- The field has only a single well.

Therefore a simplified model approach is chosen in which properties are defined homogeneous per layer (layer-cake model). The layering is based on the upscaled well log and different zones. The advantage of this approach is that a good history match to the dynamic data can be achieved. The disadvantage is that sharp boundaries are implemented that might not be realistic.

Three zones were identified:

- a near well zone with poor properties, which were based on the upscaled well log.
- the gas field which has much better properties than the near-well zone. It is assumed that the high-perm layer present in the well extends also in the gas field.
- the aquifer which has very poor properties. Although the well is drilled close to the aquifer, no significant water production has been observed, indicating low mobility of water in the aquifer. In view of the substantial depth of the aquifer (>3680 m), a reduced permeability is expected due to autigenic illite growth (Van Hulst, 2006).

The properties and distribution of the zones was also part of the history match and will in part be discussed there.

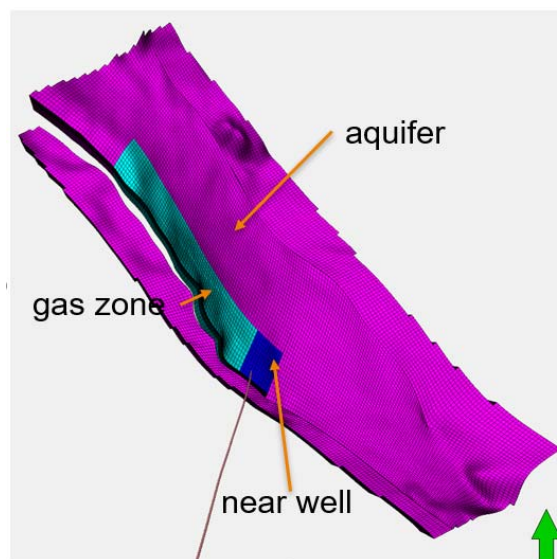


Figure 17-12: distribution of the three zones defined in the P18-6 model.

The log of PHIE (effective porosity) was arithmetically upscaled to the grid resolution of the dynamic model. Figure 17-13 shows the histograms of the upscaled porosity. The upscaled porosity was used for the porosity in the near-well zone (see Table 17-2 for the details). Because the high porosity values were lost due to upscaling, the highest porosity layer (layer 11) was increased to 0.15.



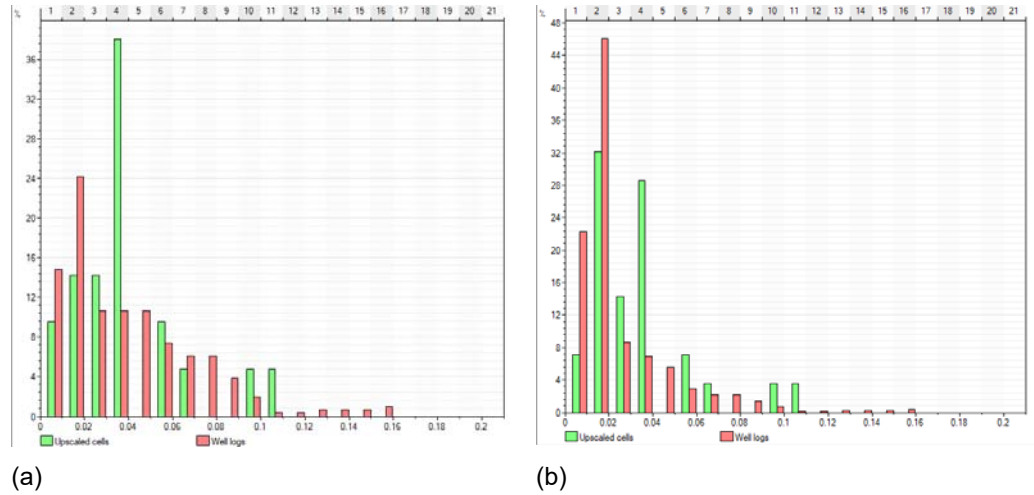


Figure 17-13: Comparison of the distributions of effective porosity (PHIE) in well log and upscaled well log for Hardeggen Fm (a) and the entire well (b).

Table 17-2. Porosity in the different layers and zones (Figure 17-12) of the reservoir model of P18-6.

Model layer	Formation	Por near well	Por gas zone	Por aquifer
1-4	Hardeggen	0.023	0.14	0.07
5-9	Hardeggen	0.023	0.07	0.07
10	Hardeggen	0.059	0.2	0.07
11	Hardeggen	0.15	0.2	0.07
12	Hardeggen	0.097	0.2	0.07
13	Hardeggen	0.066	0.2	0.07
14	Hardeggen	0.057	0.2	0.07
15-20	Hardeggen	0.023	0.07	0.07
21	Upper Detfurth	0.015	0.07	0.07
22-23	Upper Detfurth	0.015	0.12	0.07
24-25	Upper Detfurth	0.015	0.07	0.07
25-33	Lower Detfurth + Volprieausen	0.015	0.06	0.06

In order to compare the static gas in place with the dynamic gas in place, it is necessary to calculate the water saturation in the field. A Lambda saturation-height function was developed by matching the water saturation logs from resistivity logs with a water saturation log calculated from porosity and height above free water level. The best match yielded the following Lambda saturation-height function (Figure 17-14):

$$S_w = 0.001 + 2.8 HAFWL^{-2.9} Phie^{-0.14} \quad (17-1)$$

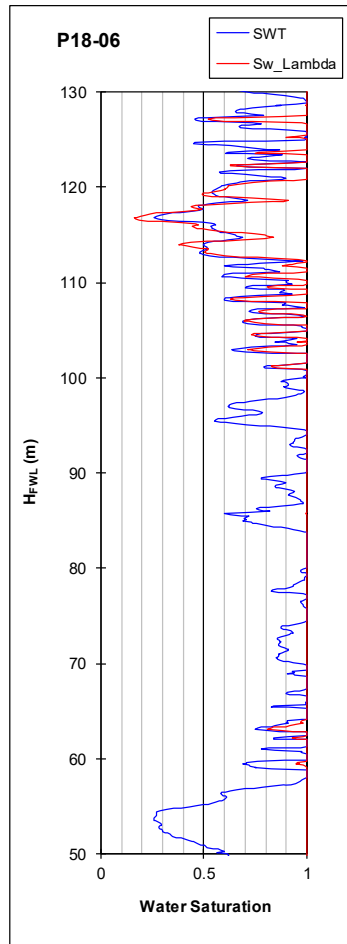


Figure 17-14: Comparison of log-derived water saturation (SWT; blue line) and water saturation calculated with a saturation-height function (SW\_Lambda; red line).

#### 17.4.5 GIIP

The actual volumetrics are done during the ECLIPSE history match, but to see whether the geometry and properties of the reservoir model are sufficiently close, the GIIP was calculated. GIIP was calculated without cutoffs on PHIE or VSH, so with a Net to Gross of 1.0, The gas expansion factor  $B_g$  was set to 0.0040. The GIIP is only calculated for segment 3 in Figure 17-15, which is the only segment which contains gas.

Table 17-3: Result of static GIIP calculations for P18-6 for segment 3 (Figure 17-15).

Formation	HC pore volume [M m <sup>3</sup> ]	GIIP [M sm <sup>3</sup> ]
Hardegsen	2.090	522
Upper Detfurth	1.120	280
Lower Detfurth	0.106	26
Volpriehausen	0.006	2
Total	3.322	831

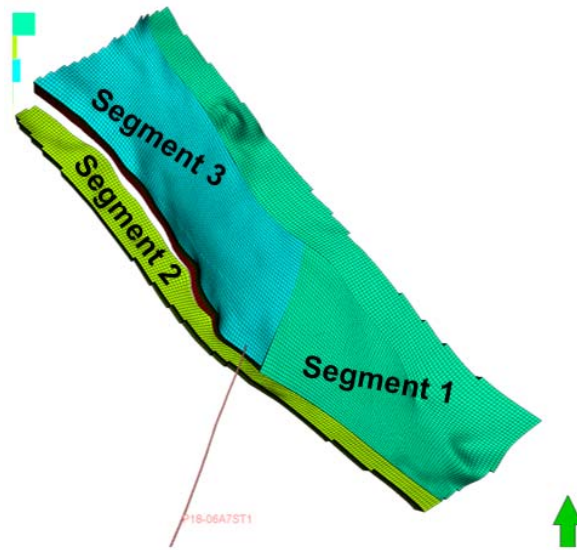


Figure 17-15: Definition of segments for the GIIP calculation.

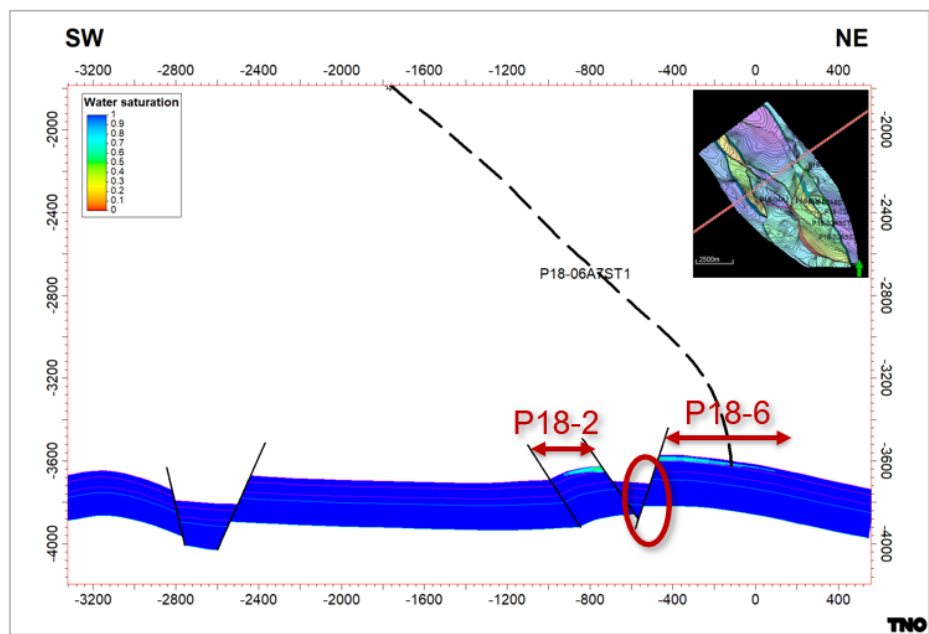


Figure 17-16: Model cross-section through P18-6 and P18-2 showing the original water saturation in the two accumulations. Note that Volpriehausen Fm in P18-6 is juxtaposed against Hardegsen and Detfurth Fm in P18-2.

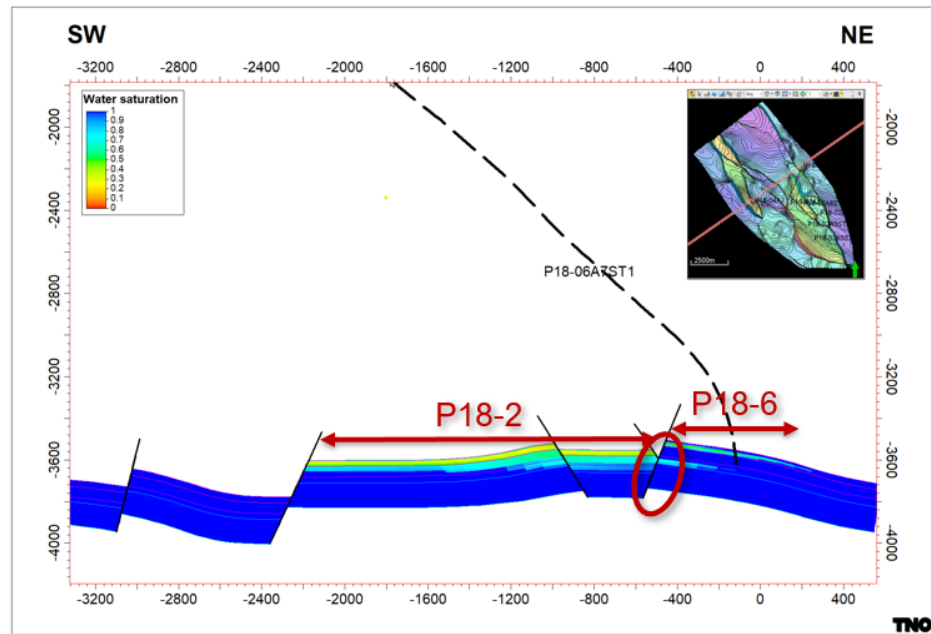


Figure 17-17: Model cross-section through P18-6 and P18-2 showing the original water saturation in the two accumulations. Note that Lower Detfurth in P18-6 is juxtaposed against Upper Detfurth in P18-2, and Hardegens in P18-6 is juxtaposed against Upper Triassic seal in P18-2.

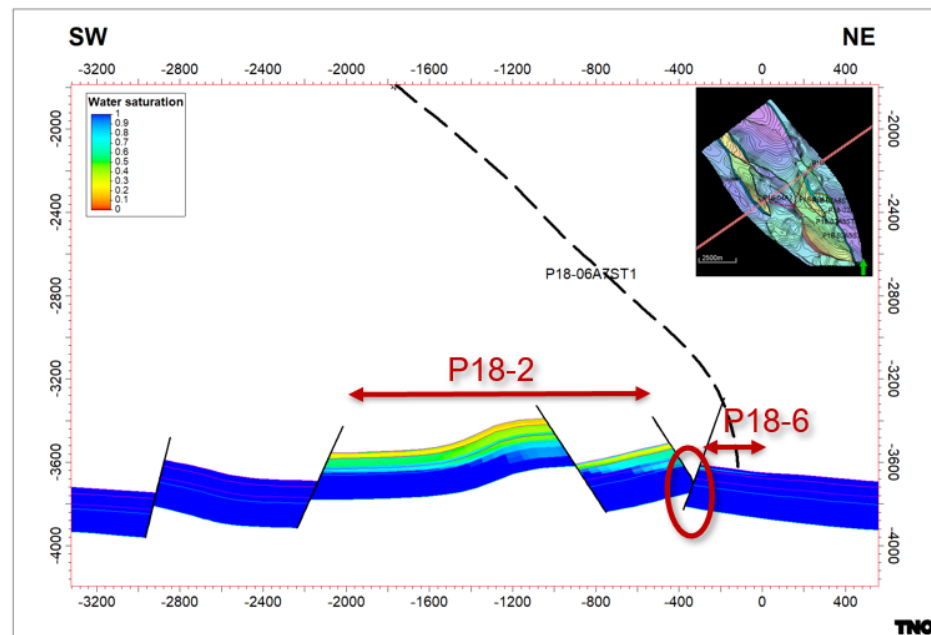


Figure 17-18: Model cross-section through P18-6 and P18-2 showing the original water saturation in the two accumulations. Bunter in P18-6 is juxtaposed against Upper Triassic seal, or Volpriehausen.

## 17.5 Adjustments made to the static model

In the geological model, the fault on the eastern side of the model (Fault 600) is not extended to the boundaries of the model area. Therefore in the north part of the model, the fault is extended in the reservoir model using pore volume multipliers. The southern part of the model is removed, to make sure that the faults extend to the boundaries of the model and because the erroneously high elevations cause gas accumulations in the aquifer which are not real.

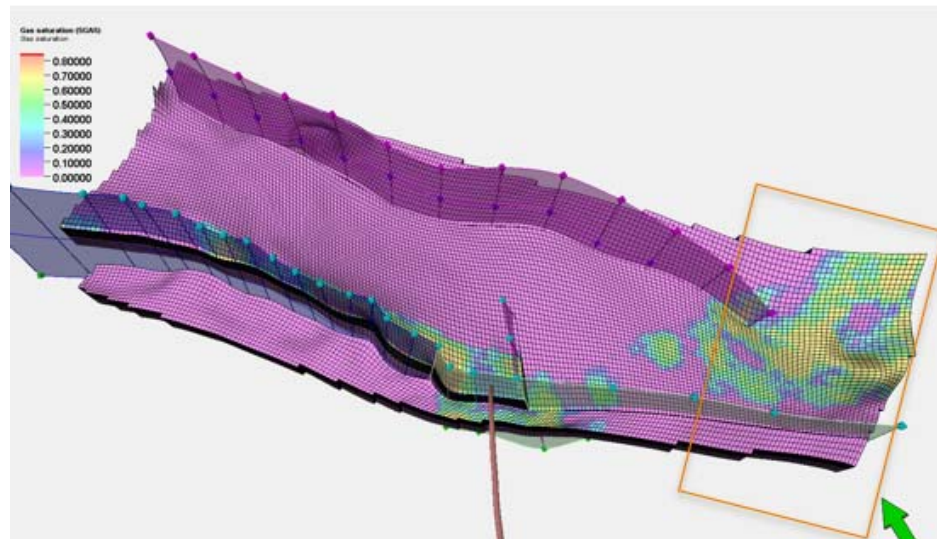


Figure 17-19: Geological model with initial gas saturation. Orange frame indicates the part of the model that is removed.

## 17.6 Dynamic model

### 17.6.1 Reservoir simulator

For the dynamic modelling Eclipse 300 was used. Alternatives were to use the Eclipse 100 simulator or the Shell proprietary reservoir simulator MoReS. The compositional Eclipse simulator was used for the following reasons:

- A black oil simulator cannot handle gas to gas interactions, which is needed for CO<sub>2</sub> injection into a gas (methane) reservoir.
- MoReS was used for P18-2 and P18-4 modelling in a previous study (Vandeweyer et al (2011)). Since that study, the workflow Petrel-Eclipse-Macris has been developed and is considered to be state of the art.

### 17.6.2 Data

For any dynamic reservoir simulation, including Eclipse, the following sets of data are required:

- General run data: grid dimensions, phases present, components present.
- Grid geometry data: specification of geometry of computational grid (location of grid block corners).
- Reservoir rock properties: porosity, net-to-gross, absolute permeability in each grid block.
- PVT data: properties of reservoir and stock tank fluids such as density, viscosity and saturation pressure.

- Saturation and pressure dependent rock properties: relative permeabilities and capillary pressures as function of phase saturations, and rock compressibility.
- Initial conditions in the reservoir: pressure, temperature, phase saturations and phase compositions.
- Regions: specification of regions that splits the computational grid into regions for calculation of PVT properties, saturation properties, initial conditions, and fluids in place.
- Operations data: specification of the wells (location, productivity index, etc.) and the operations to be simulated (production and injection controls and constraints).

These data describe the dynamic characteristics of the P18-6 reservoir. Each of these sets of data will be discussed in the following sections

### 17.6.3 General simulation data

As mentioned in section 17.6.1 the Eclipse 300 simulator is used with two reservoir fluid phases namely water and gas, and five components in the gas phase namely N<sub>2</sub>, CO<sub>2</sub>, C<sub>1</sub>, C<sub>2</sub>, C<sub>3P</sub>.

As explained in Section 17.4, the geological grid was not upscaled to the dynamic 2019 model, however directly from the logs a new dynamic grid was generated. Table 17-4 below gives an overview of the grid dimensions. The size of the grid blocks do vary in size in each individual direction but are in the order of 50x50 m (XY). The layer thickness changes per formation: ~1.2 m for Hardegsen, ~8 m for Detfurth and ~37 m for Volpriehausen.

Table 17-4 – Overview of grid dimensions in the geological model and in the simulation model.

	Number grid blocks x-direction NX	Number grid blocks y-direction NY	Number grid blocks z-direction NZ	Total number of grid blocks	Number active grid blocks
<b>Simulation grid model</b>	63	197	33	409563	300135

### 17.6.4 Reservoir Rock properties

This was described in Section 17.4.3.

### 17.6.5 PVT data

#### 17.6.5.1 Gas PVT data

An equation of state is generated for Eclipse 300 with the composition at 1 m depth listed in Table 17-5. The same values were used as in P18-2.

Table 17-5 – Overview of composition at 1 m depth (mole fractions).

	Composition
N <sub>2</sub>	0.01508
CO <sub>2</sub>	0.01288
C <sub>1</sub>	0.8765
C <sub>2</sub>	0.02376
C <sub>3P</sub> .	0.0718

### 17.6.5.2 Water PVT data

The water formation volume factor is 1.0223  $\text{m}^3/\text{Sm}^3$  at a reference pressure of 215 bar. The water compressibility is  $4.1483 \cdot 10^{-5}/\text{bar}$  and water viscosity is 0.32929 cP, also at reference pressure of 215 bar.

### 17.6.6 Saturation and pressure dependent rock properties

Relative permeability and capillary pressure (Special Core Analysis - SCAL - data) are not available for P18 field. In this study the final parameters used to describe the individual curves are described in Table 17-6 and Figure 17-20 and were part of the history match study. Mobility of water was reduced considerably compared to the values used for P18-2, because otherwise well P18-6-A07 produced water prematurely.

The most used description of the relative permeability curves is the Corey parametrization according to equation

$$k_{r,i}(S_i) = k_{r,end,i} \left( \frac{(S_i - S_{irr,i})}{(1 - S_{irr,i} - S_{irr,j})} \right)^{n_i} \quad (17-2)$$

where

- $k_{r,i}$  = relative permeability of phase  $i$
- $k_{r,end,i}$  = end-point relative permeability of phase  $i$
- $S_i$  = saturation of phase  $i$
- $S_{irr,i}$  = irreducible or connate saturation of phase  $i$
- $n_i$  = Corey exponent for phase  $i$

The values used to describe the relative permeabilities are listed in Table 17-6.

Table 17-6 – Parameters for calculation of gas-water relative permeabilities

Parameter	Description	Value used in dynamic model
$S_{wc}$	Connate water saturation (Hardegsen/Detfurth + Volpriehausen)	0.10/0.25
$S_{grw}$	Residual gas saturation in gas/water system	0.05
$n_w$	Corey exponent for water	4
$n_o$	Corey exponent for gas	1.5
$k_{rwor}$	Water end-point relative permeability	0.05
$k_{rgcw}$	Gas end-point relative permeability	1

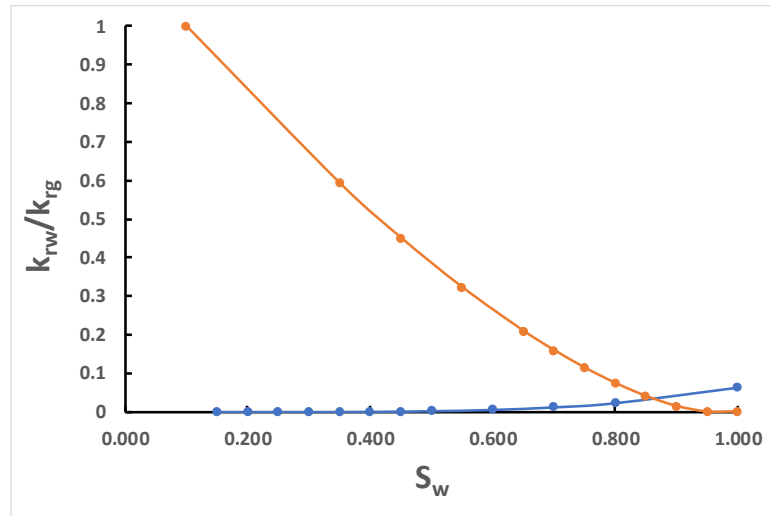


Figure 17-20: Relative permeabilities used in the P18-6 study.

The capillary pressure curves were based on a Leverett J-function corresponding to equation (17-3). The J-function itself was based on the saturation-height functions in Section 17.4.4.  $P_c$  was calculated based on HAFWL and the phase densities. The J-function values (shown in Figure 17-21) were calculated based on the following equation:

$$J(S_w) = \frac{P_c \times \sqrt{\frac{k}{\phi}}}{\sigma U_c} \quad (17-3)$$

Where

- $P_c$  = capillary pressure [bar]
- $\sigma$  = surface tension [dyne/cm] (water gas) set to 72 dynes/cm (is 72 milli N/m) (typical value for water gas system, petrowiki)
- $U_c$  = constant (0.318316 for the given units, Eclipse reference manual)
- $\phi$  = porosity [-]
- $k$  = permeability [mD]

A function was fitted to the cross-plotted values of J and  $S_w$  (Figure 17-21) to parametrize the J-function used in Eclipse (Eq. (17-3).):



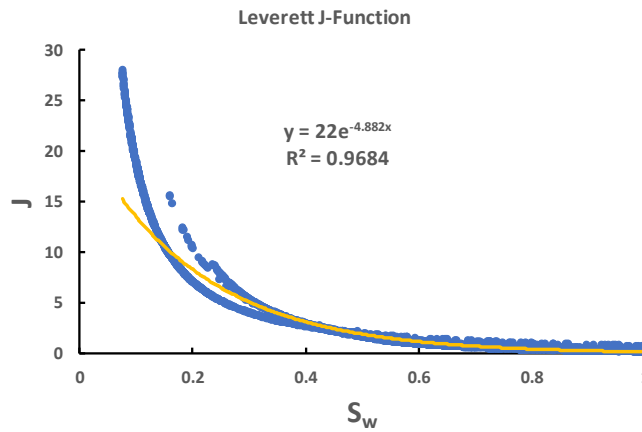


Figure 17-21: The J-function used (orange line) and the saturations of the P18 reservoir (blue dots).

After initialisation with these saturation functions the modelled water/gas saturations were compared to the total water saturations based on the logs (Figure 17-22).

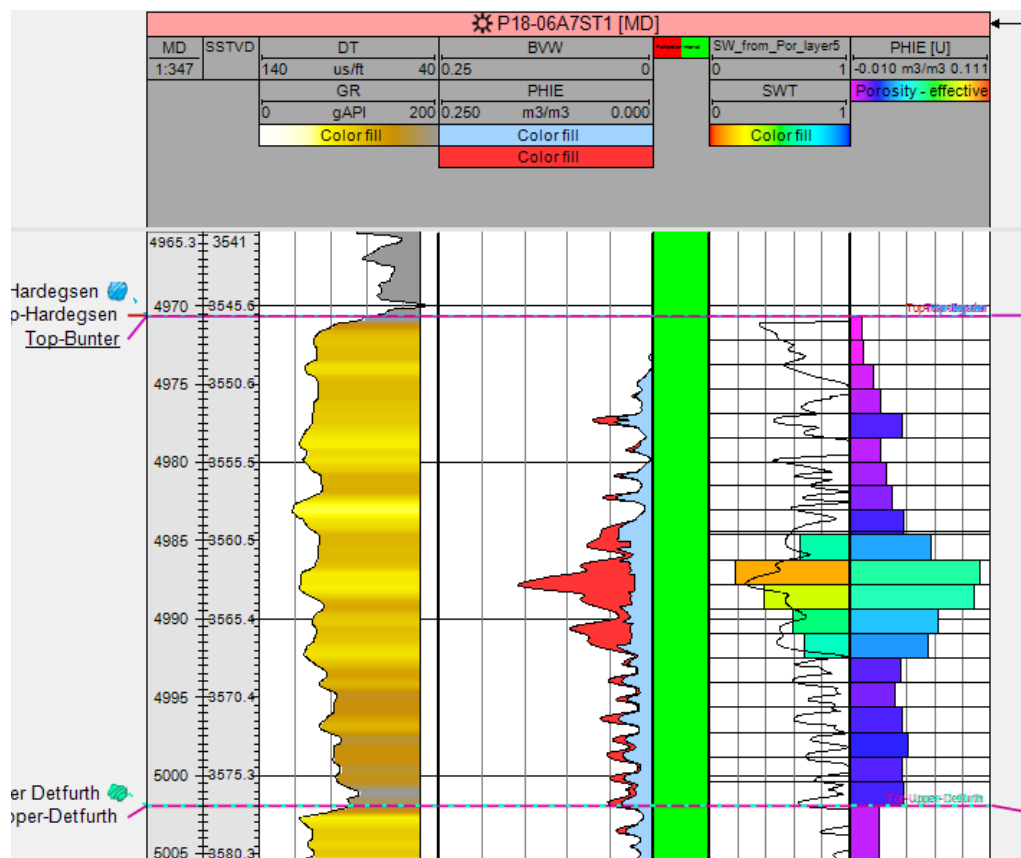


Figure 17-22: Total water saturation based on logs (SWT) and synthetic log based on the j-function (Sw\_from\_Por\_layer5).

### 17.6.7 Pore compressibility

As no pore compressibility measurements are available for the P18-2 field, a correlation is used<sup>12</sup>. The compressibility is (also) dependent on the porosity according to:

$$C_r(\Phi) = 7.248 \cdot 10^{-6} / (\Phi + 0.000001) - 0.26 \cdot 10^{-5}$$

Where

- Cr = pore compressibility,
- Φ = porosity.

Note: in the final review phase, it was discovered that the distribution of the rock compressibility was not updated to the final porosity distribution. Since on average the rock compressibility is correct, this has only minor impact (~2-3 bar) on the history match.

### 17.6.8 Regions

In the dynamic model regions are specified based on porosity classes for rock properties described in section 17.6.6. and to split the computational grid into regions for calculation. Furthermore regions are used to evaluate the gas initial in place (GIIP) for the different compartments separated by faults or boundaries (see Figure 17-15) .

### 17.6.9 Initial condition in the reservoir

The reservoir is a mechanical and thermodynamic system and hence its (initial) conditions are fully defined by the following state variables at any point in the reservoir or grid block in the simulator:

- Temperature;
- Pressure;
- phase compositions;
- phase saturations.

Initialization of these variables is discussed below.

#### 17.6.9.1 Temperature

Since an isothermal model is used, all temperature dependent fluid and rock properties are assumed to be specified at the reservoir temperature of 117 °C degrees.

#### 17.6.9.2 Pressure

Reported initial pressure is 377 bar at 3500 m TVDSS. In the simulator, the initial (gas) reservoir pressure is 380.9 bar at datum depth 3680 m TVDSS. It is important to note that in fact each phase has its own pressure and that each phase pressure is assumed to be in hydrostatic equilibrium. Phase pressures and phase saturations are coupled through capillary pressure between phases. The capillary pressure is based on the J-function defined in equation (17-3).

---

<sup>12</sup> Personal communication, NAM.

### 17.6.9.3 Gas water Contact

The gas water contact (taken as free water level, i.e.  $P_c = 0$ ) is at 3680 m depth in segment 2 (see Figure 17-15 for the definition of the segments). In the other two segments the gas water contact is defined above the reservoir, to ensure that no gas is present in the aquifer. Because the gas water contact was not observed in well P18-A-07-S1, the same contact as in P18-02 was used.

### 17.6.10 General remarks

Petrel 2018 was used to generate an input deck for the dynamic model. The reservoir engineering module offers options such as specification of fluid and rock properties, specification of historic production data.

There are a few manual adaptations in the input files:

- PVT data generated by Petrel are overwritten by TNO's PVT data, in other words an equation of state is used;
- Saturation functions generated by Petrel are overwritten by TNO's saturation functions;
- History match multipliers.

## 17.7 History Match of the dynamic model

### 17.7.1 Introduction

In the previous chapter the data required to describe the reservoir have been described. In this chapter the data required to define the operations and resulting reservoir behaviour will be discussed. These data are:

- Specification of wells: location, trajectory, casing data, perforation data, productivity index, etc.;
- Production and injection data:
  - Water and gas production rates;
  - Bottom hole pressures;
  - Reservoir pressures.

Next the adaptation of the reservoir parameters to arrive at an acceptable history match is discussed in detail.

### 17.7.2 Well data and production data

#### 17.7.2.1 Well Location and trajectory

For all wells well head coordinates and deviation data have been received and imported in Petrel. (see section 17.4).

#### 17.7.2.2 Well completions and perforations

Based on the received well test reports the completion perforation and skin data was gathered shown in Table 17-7.

Table 17-7 Well test, completion and perforation data.

Well name	Completion size (inch)	Productivity index (Nm <sup>3</sup> /day)/bar	Perforations (m)	KH (mDm) from well test	Skin from well test
P18-02-A-01	4 ½	26.72	3580-3695	1847	0.6-0.9
P18-02-A-03S2	4 ½	31.89	4070-4209	-	2.1-3.3
P18-02-A-05S1	7	37.33	4798-4980	25249	3.19
P18-02-A-06	4 ½	14	4488-4633	3686	2
P18-02-A-06ST1	4 ½	22.28	3376-3936	-	-
P18-4A-02	4 ½	40.95	4085-4199	8208	-
P18-A-07-S1	4 ½	6.83	4975-5065	-	-

### 17.7.2.3 RFT and PLT data

For well P18-A-07-S1 no RFT or PLT data are available.

### 17.7.2.4 Historic Well Production data

Daily gas and condensate production data was provided by the operator. In Figure 17-23 the daily gas production data of the production well is shown. The received data was recalculated from Nm<sup>3</sup> to sm<sup>3</sup> which is required for Eclipse and upscaled to monthly time steps (using Petrel).

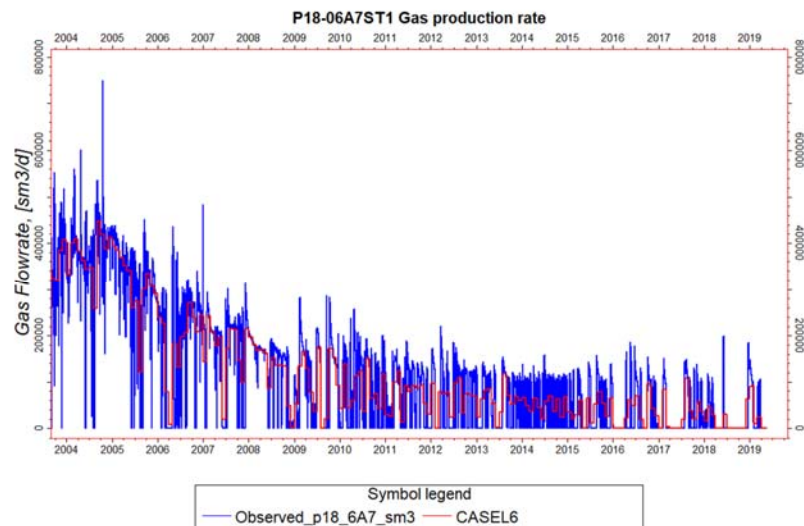


Figure 17-23: Gas production of well P18-A-07-S1 showing the observed daily values and the monthly values used for the simulator (CASEL6).

### 17.7.2.5 Historic pressure data

Daily tubing head pressure (THP) data and on irregular basis shut in pressure data was provided. A bottom hole pressure (BHP) is generally not measured directly. Instead, the (THP) is measured and BHP is calculated from this THP and reported production or injection rates using a well bore flow model. To be able to calculate

the BHP from the THP a number of parameters, including completion data and production rates, have to be accurately known. By absence of Vertical Lift Performance Relationship (VLP) of each production well the opportunity to convert THP to BHP is not performed. The measured initial pressure of 377 bar in 2003 suggests there is no pressure communication with the P18-2 field (Figure 17-16).

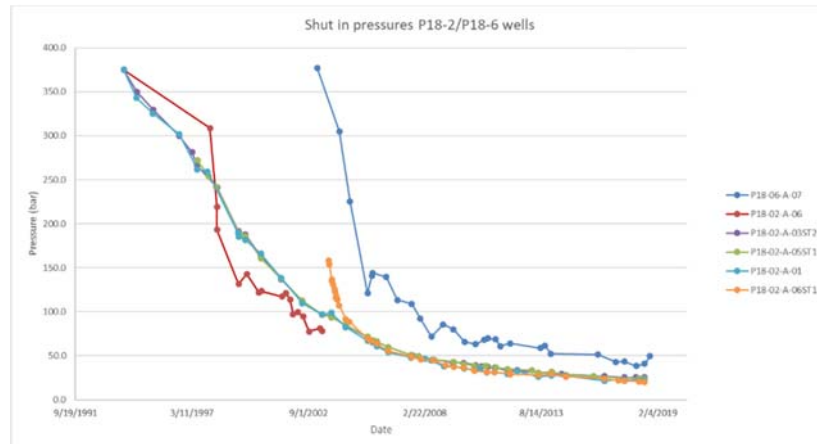


Figure 17-24: Pressure profiles of the production wells over time.

### 17.7.3 P/Z curves

The standard method to estimate the GIIP and driving mechanism (e.g. natural water drive, volumetric depletions) is material balance analysis applied on the production and pressure history. The most used method is the p/Z plot shown in Figure 17-25. This p/Z plot is based on extrapolated build-up profiles rather than direct pressure observations, due to the slow build-ups observed in this well. The GIIP estimated from this curve is 800 MNm<sup>3</sup> (844 M sm<sup>3</sup>).

**p/Z plot P18-6A7**

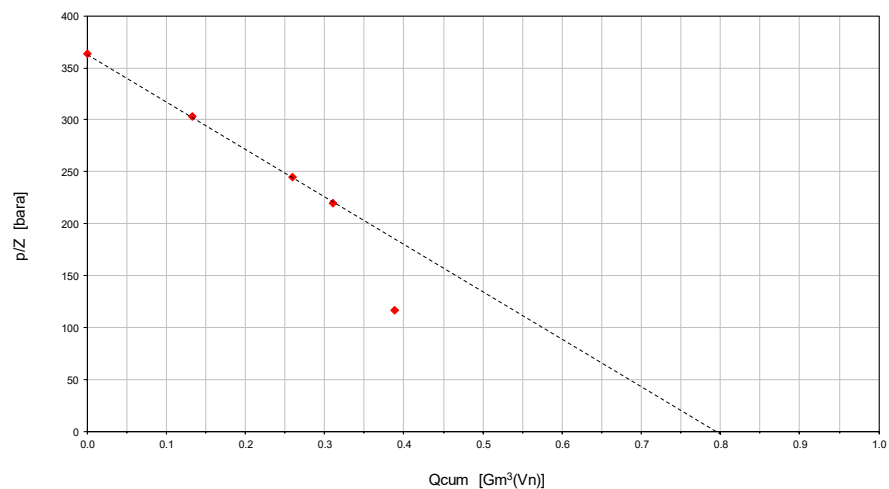


Figure 17-25: P/Z curve of P18-6 field.

#### 17.7.4 History matching approach

As discussed in a previous section (17.7.2.5) no BHP observations are available, therefore the measured shut-in pressures is matches with the 9-point pressure of each individual well. The history match approach is done according to the following procedure:

- The simulations were performed under rate constraint conditions
- Change the GIIP by adjusting the J-function
- Change the permeability of the dynamic model based on porosity – permeability relationship, since no well test data (KH) is available.
- Match the measured shut-in pressures with the 9-point pressure by adjusting the multipliers on flow barriers.

##### 17.7.4.1 History Match of GIIP

The result of the history matching the GIIP is summarized in Table 17-8 for segment 3 (Figure 17-15). The other segments don't contain gas. The gas present in Lower Detfurth and Volpriehausen is not producible. Connected GIIP in the dynamic model is 826 Msm<sup>3</sup> which is close the GIIP estimate of 844 M sm<sup>3</sup> from the p/Z curve.

Table 17-8: GIIP results for segment 3 (Figure 17-15).

Formation	Pore volume [M rm <sup>3</sup> ]		HC pore volume [M rm <sup>3</sup> ]		GIIP [M sm <sup>3</sup> ]	
	static	dynamic	static	dynamic	static	dynamic
Hardeggen	20	20	2.091	2.102	523	541
Upper Detfurth	30	30	1.120	1.122	280	289
Lower Detfurth	24	24	0.106	0.091	26	23
Volpriehausen	69	69	0.006	0.006	2	2
Total	143	142	3.324	3.321	831	856

##### 17.7.4.2 History match on pressure data

In the initial models, connectivity in the gas zone was too large and permeability near the well was too small. Water production occurred too fast in the initial models compared to actual observations (no significant water production has been observed in the well). To achieve a history match on the pressure data, the following adjustments were made:

- To reduce water inflow into the well low porosity and permeability in the aquifer has been assumed and water mobility in the relative permeability has been reduced.
- Increase in permeability in the near well zone by increasing porosity in the highest porosity layer to 0.15, increasing permeability in the near well area in the high permeability layer by 1.5 and a PI multiplier of 2.
- Permeability in vertical direction was set to 0.01 x permeability in horizontal direction.
- The multiplier between the Hardeggen Fm and Upper Detfurth Fm was adjusted to a final value of 0.08. Gas from the Upper Detfurth Fm is produced via the Hardeggen. Although the well has perforations in the Upper Detfurth, due to the low permeability in the near-well zone, the gas flow to the well via the Hardeggen.
- The pressure behaviour in well P18-A-07-S1 shows a very rapid decline initially and a much slower tail. This was interpreted as 300 to 400 M Nm<sup>3</sup> of fast gas and the rest of the gas is available at a much lower rate (interpretations

received from TAQA). Since the amount of gas present in the (well-connected) Hardegsen is more than  $500 \text{ M sm}^3$ , an intra-Hardegsen flow barrier is inferred. After evaluating both a vertical and a horizontal barrier, finally a vertical barrier was implemented by using a multiplier on the horizontal flow of 0.0015 (Figure 17-26).

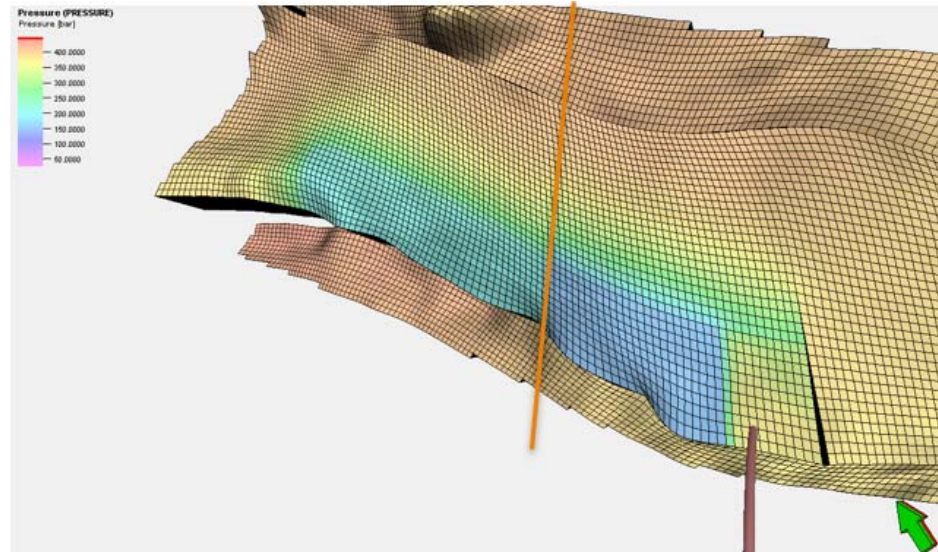


Figure 17-26: Position of the intra-Hardegsen flow barrier indicated by the orange line.

The match of the near well permeability for well P18-A-07-S1 is uncertain because no estimate of the KH from well tests is available. Only one estimate of the Productivity Index (PI) from 2010 (~2500 d after start of production) is available:  $6830 \text{ Nm}^3/\text{day}/\text{bar}$ . The PI from the final history matched Eclipse model is presented in Figure 17-27. These PI values are higher, however the definition is also somewhat different.

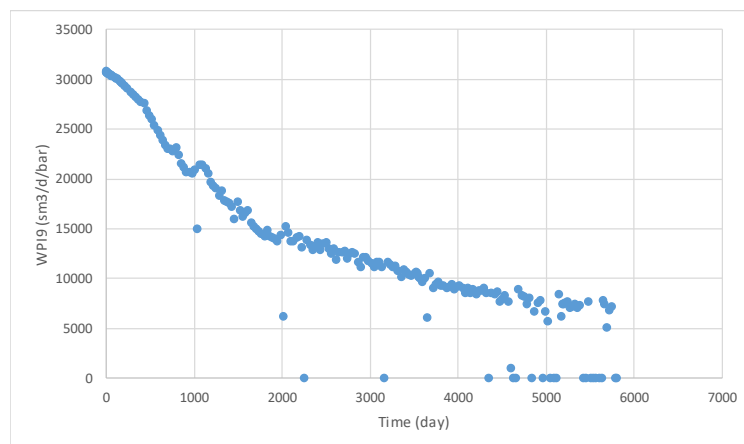


Figure 17-27. Productivity Index of well P18-6-A7-ST1 estimated by Eclipse using the 9-point pressure during production.

When comparing P18-A-07-S1 to the wells in P18-2 and P18-4 (Table 17-7), it is clear that P18-A-07-S1 is the poorest well and that the PI is a factor 2 to 6 lower than the others. However, the initial values for the KH from the model were 40 mDm, which is almost two orders of magnitude lower than for the other wells. The history matched KH from the Eclipse model is 216 mDm (excluding the PI multiplier of 2), which is more in line with the other wells.

#### 17.7.5 Result of the history match

Based on the parameters described in the previous section the following production and pressure match is achieved (Figure 17-28 and Figure 17-29). The observed gas production was fully matched.

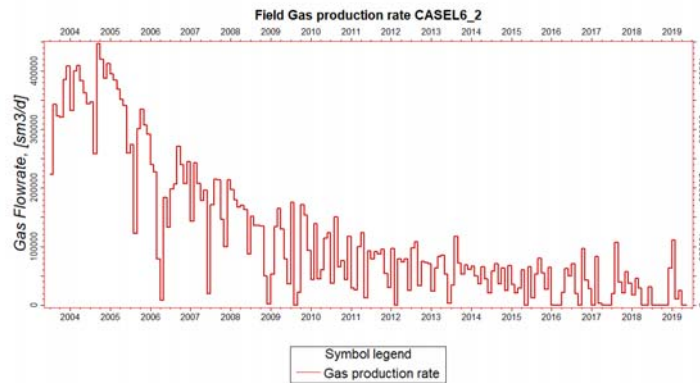


Figure 17-28: History matched production data well P18-A-07-S1.

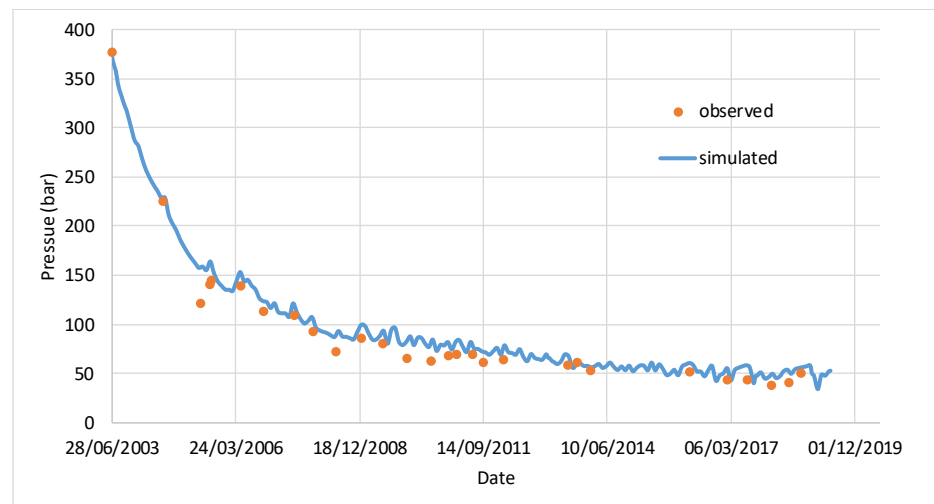


Figure 17-29: History matched pressure data well P18-A-07-S1.

No RFT or PLT data were available for matching. However, three build-ups were extrapolated by TAQA to estimate the reservoir pressure. The observed build-ups had not stabilized yet, because of the slow response of the field. Table 17-9 shows the pressure values estimated by TAQA from the extrapolated build-up profiles and simulated using the Eclipse model. The simulated values are higher than the extrapolated ones. Since the GIIP in the model is the same as the GIIP estimated



from the p/Z curve based on these extrapolated build-up profiles (Figure 17-25), the discrepancy might be due to aquifer support in the simulation model. This is not represented in the extrapolated build-up profiles. From the currently available data it is not possible to verify whether this aquifer support is realistic or not.

Table 17-9. Estimated pressure (at datum depth of 3500 m SSTVD) from extended (extrapolated) build-ups and from Eclipse simulation.

Date	Qcum	P extrapolated	Simulated P*
	Gm <sup>3</sup>	bar	bar
Initial	0	377	
15/08/2004	0.13	301	305
26/08/2005	0.26	232	242
29/04/2006	0.31	206	223

\* Value depends on the duration of the simulated build-up

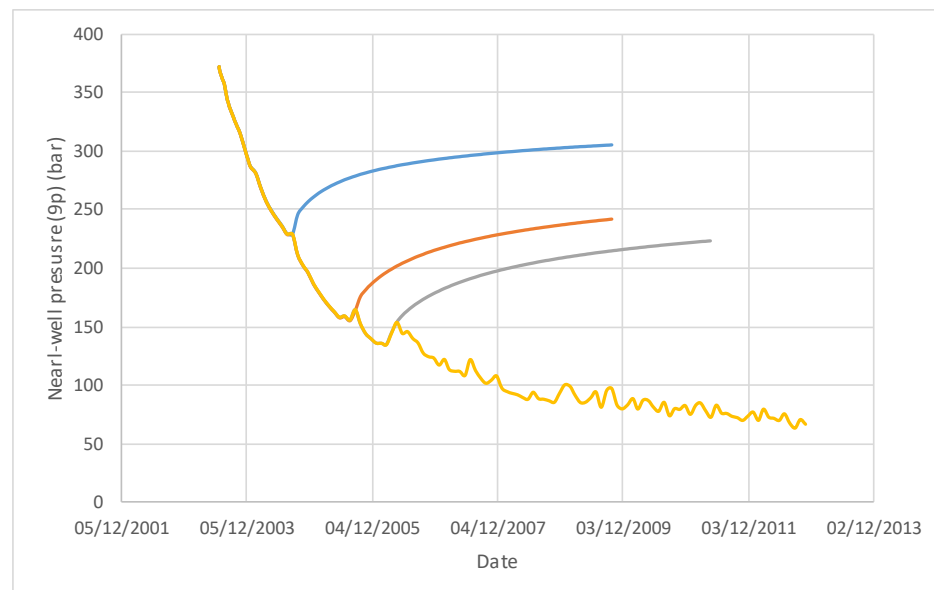


Figure 17-30. Simulated near well pressure for three extended pressure build-ups.

#### 17.7.6 History match conclusion

- The dynamic model reproduces production rates and most of the pressure data.
- An intra-Hardegsen flow barrier was required to achieve a history match on the pressure data (fast initial response and slow tail).
- Aquifer permeability and water mobility were both reduced compared to the initial estimates to reduce water inflow into the well.

#### 17.7.7 Simulation of final production phase

The proposed CO<sub>2</sub> injection will not start at the end of the history match period. To start the injection scenarios at the right initial conditions, a further simulation period is required, namely the final production phase. For P18-6, this final production phase is simulated using a rate constraint of  $6 \cdot 10^4$  sm<sup>3</sup>/d and BHP constraint of 1

bar. Although in reality well P18-A-07-S1 is produced intermittently, the simulation assumed continuous production for simplicity. The production was continued for another five years to 1 April 2024. At the end of this production period, the rate has dropped to  $1.8 \cdot 10^4$  sm<sup>3</sup>/d, the near well pressure is 20.4 bar (after 15 days of shut-in), the field average gas pressure is 62 bar (or 52 bar if only the connected gas is considered). These conditions will be used for the start of injection.

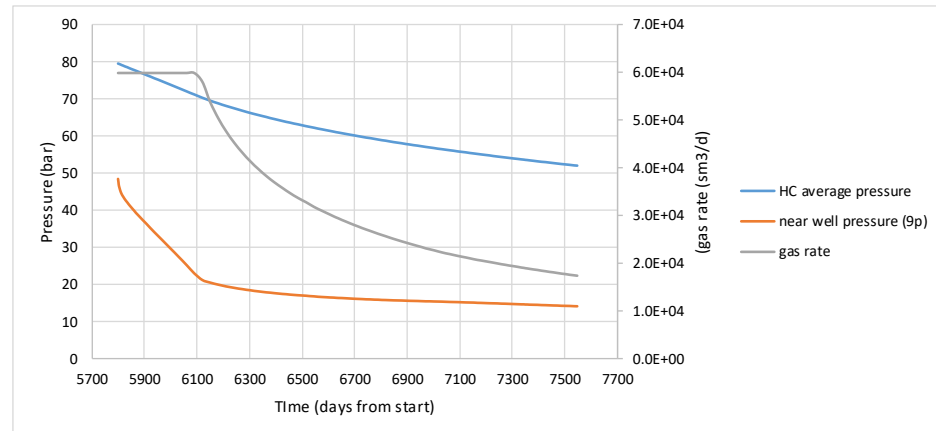


Figure 17-31. Near well pressure, field average gas (HC) pressure of the connected gas and gas rate during the simulated final production phase.

## 17.8 Geomechanical model

### 17.8.1 MACRIS – Poro-elastic model

We detail here the TNO-developed semi-numerical approach (MACRIS, Mechanical Analysis of Complex Reservoirs for Induced Seismicity) to handle pressure effects along multiple faults. More specifically MACRIS is designed to compute 3D stress changes along faults induced by: (1) poro-elastic effect (contraction/inflation of the reservoir due to fluid pressure depletion/injection), (2) direct pressure effect (changes of the fluid pressure intra-faults can induce changes in effective normal stress), (3) differential compaction effect due to the fault offset.

MACRIS is a mesh-free approach where there is no need to build a dedicated grid for the geomechanical analysis. MACRIS takes directly as input the grid of the reservoir flow simulation; in our case: the 3D pressure fields of the P18-6 field at a yearly sampling rate. Each grid block of the reservoir flow simulation is considered as a compacting nucleus of strain (center of compression; Mindlin 1936; Geertsma, 1973; Okada, 1992). The contribution of each of these nuclei is integrated to compute the poro-elastic stress changes along each fault of the P18-6 field with a meter-scale spatial resolution. The restriction that we presently still have is that only one-way coupling is considered. We deem this acceptable for gas reservoirs, where the effect of compaction on the gas pressures in the pores is small. The Barnes-Hut algorithm (Barnes & Hut, 1986) is used for re-discretizing the initial reservoir grid for two purposes: (i) clustering the nuclei of strain close to the faults in order to increase the spatial stress resolution, and (ii) shortening the computation time.

MACRIS thus computes the poro-elastic normal and shear stress changes induced by the reservoir compaction for every observation point along each fault.

Observation points are placed on fault pillars (i.e. sub-vertical lines along the fault dip direction), which in turn make up the 3D geometry of a fault (see Figure 17-32).

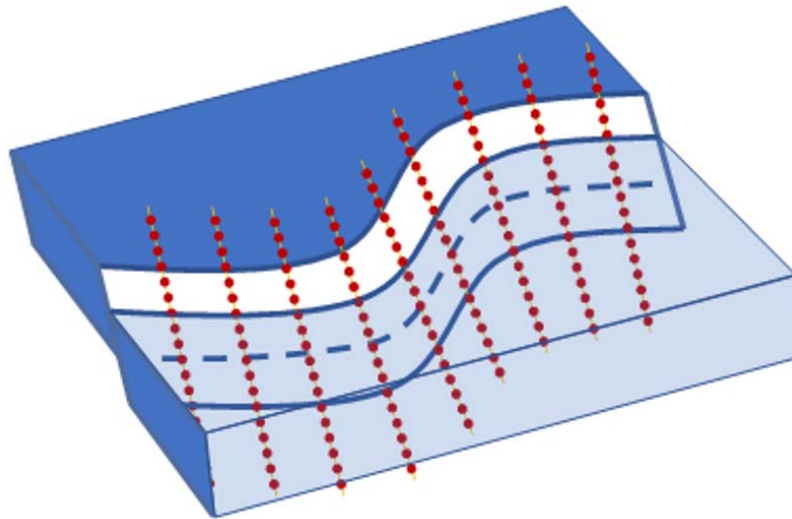


Figure 17-32: Schematic of the distribution of the observation points (where the stress solution is evaluated) along fault pillars.

In order to account for the direct pressure effect, we still need to define the pore pressure changes inside the faults to calculate the effective normal stress changes and derive the Coulomb stress changes. This intra-fault pore pressure is defined as the average fluid pressure between the two juxtaposed reservoir compartments.

MACRIS has been validated by comparison with relatively slow finite-element (FE) numerical computations (DIANA), with excellent results (van Wees et al., 2018). This benchmarking exercise has been carried on using single-fault tank models; for MACRIS it was a 3D model and for DIANA it was a 2D plane strain model. For the present study we extended this benchmarking exercise by comparing the 3D MACRIS model with this time a full 3D DIANA model. Results of this exercise are presented in Figure 17-33. The 3D single-fault model mimics the P18-6 field at the end of the depletion period, that is with an initial pressure of 330 bars and a decrease of pressure of -300bars at the end of the depletion period. The MACRIS results closely match the FE DIANA solution. Deviations between both solutions are less than 3%.

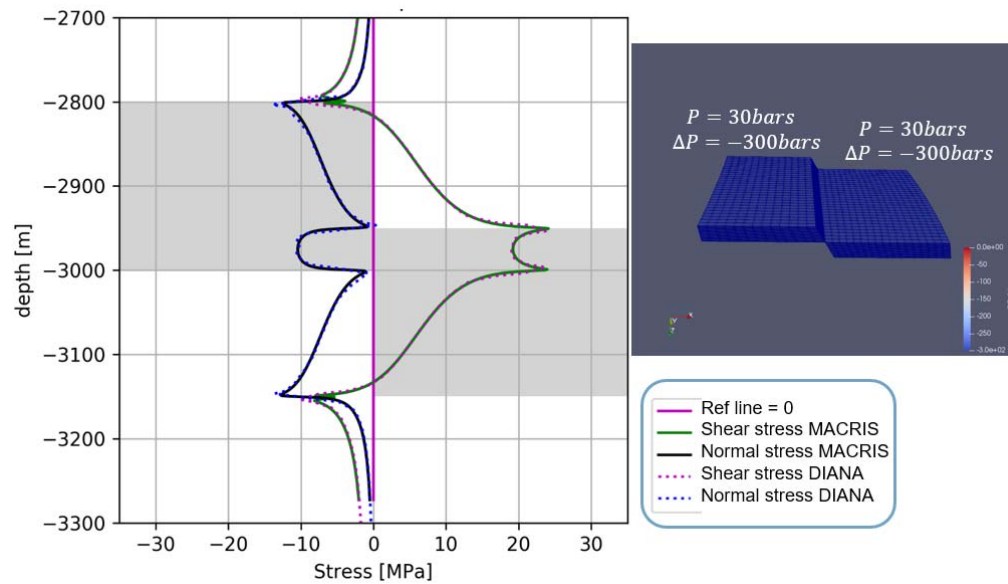


Figure 17-33: Comparison MACRIS vs. Diana FEM package. Right: 3D single-fault model with offset. Both compartments start with the same initial pressure (330 bars) and are depleted of the same amount (-300 bars). Left: Stress solution along the central pillar of the model. The changes in shear and normal stresses induced by the poro-elastic effect are almost identical between both solutions. For this particular example, the pore pressure inside the fault remains at the initial pore pressure.

### 17.8.2 Thermo-elastic model

The TNO-developed semi-analytical approach to model thermo-elastic stresses due changes in temperature of reservoir rock is based on Myklestad (1942). Myklestad (1942) derived equations for all the components of the stress tensor as induced by heating a semi-infinite cylinder to a constant temperature difference with respect to the ambient reservoir temperature using elliptical integrals in a cylindrical coordinate system. Candela et al. (2018) contains all the details of the derivation.

This approach gives us the tensor of stress changes inside and outside the reservoir in the cylindrical coordinate system. This tensor of stress changes thus needs to be translated to Cartesian coordinates using standard cylindrical coordinate transformation. The initial stress state is then added to the tensor of stress changes to obtain the stress tensor in Cartesian coordinates (see Figure 17-34 and Figure 17-35).

We consider faults uniformly distributed in our model. In other words, each location inside and outside the reservoir (in the caprock) can potentially host a fault. More specifically, from the stress tensor, at each location, one can calculate the Coulomb stress changes for any fault plane orientations.

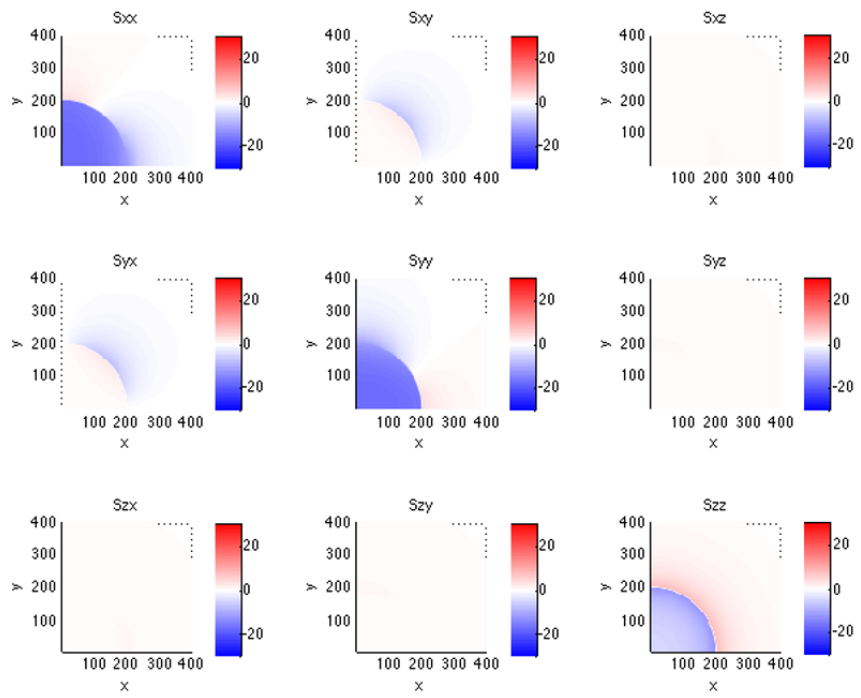


Figure 17-34: Horizontal [XY] spatial distribution of each component of the tensor of stress changes.

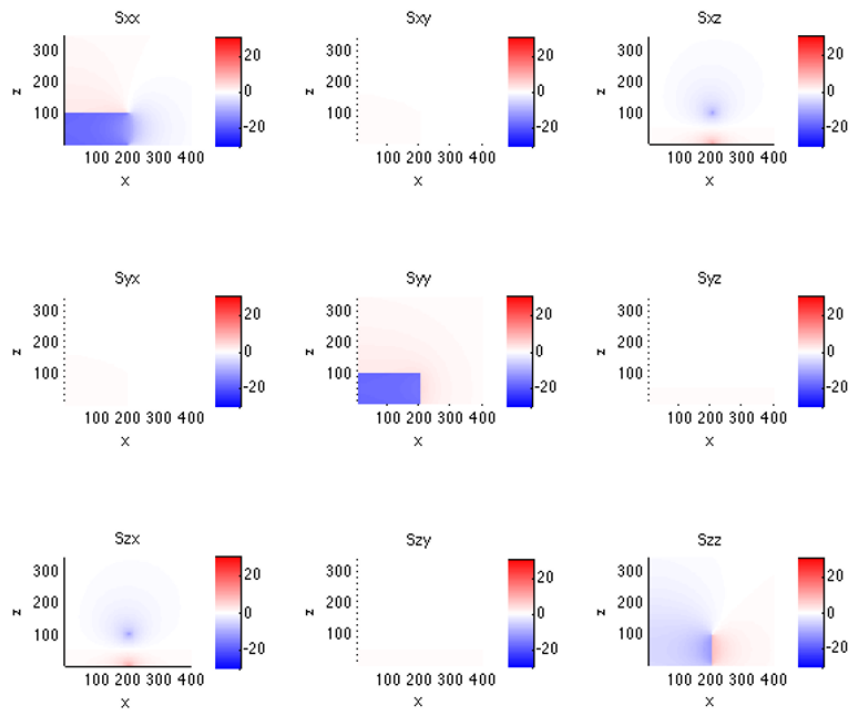


Figure 17-35: Vertical [XZ] spatial distribution of each component of the tensor of stress changes.

## 17.9 Well degradation model

The nonlinear finite element simulator DIANA<sup>13</sup> is used to generate meshes for 2D numerical models of the well system and run structural and heat transfer simulations. The workflow is automated by a dedicated user interface DIANA SEALEC: the user-defined input and model parameters are used to generate meshes and define the complete non-linear (phased, staggered) analysis, which mimics the different loads acting on the well system throughout the entire lifetime of a well, from the drilling phase, well completion, testing, operations and decommissioning (Figure 17-36).

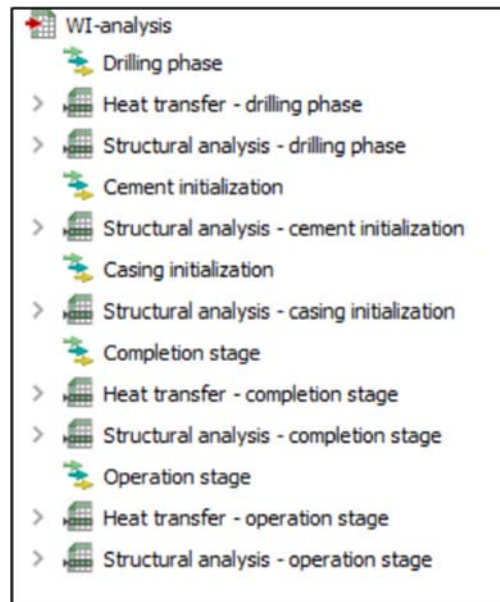


Figure 17-36: Example of steps in the wellbore integrity analysis.

The model of the well system, representing a cross-section normal to the well axis, comprises the casing, the cement and the surrounding rock formation. The chosen 2D modelling approach is computationally efficient and simulations can easily be repeated for various depths along the wellbore. Complete plane strain elements are used for bulk materials. Zero-thickness interface elements are used for the casing-cement and the cement-formation interfaces. The well materials can be modelled with different constitutive models; for example a von Mises elasto-plastic material model for the steel casing; a combination of the Mohr-Coulomb elasto-plastic model and the multi-directional fixed crack model for the cement; a Mohr-Coulomb elasto-plastic model for the rock formation; and the Coulomb friction model with a tension cut-off for the interfaces between materials. Different failure modes can be simulated, for example: plastic deformation of casing, plastic deformation and cracking of the cement sheath, plastic deformation of formation and debonding of cement interfaces (Figure 17-37). Specific deformational behaviour of materials can be modelled such as shrinkage of cement and the creep behaviour of viscous rock salt formation.

<sup>13</sup> See [dianafea.com](http://dianafea.com).

Structural, heat transfer and fluid flow analyses are typically needed for wellbore integrity assessment. Results from finite element analyses are typically displacements, stresses and strains in different formulations.

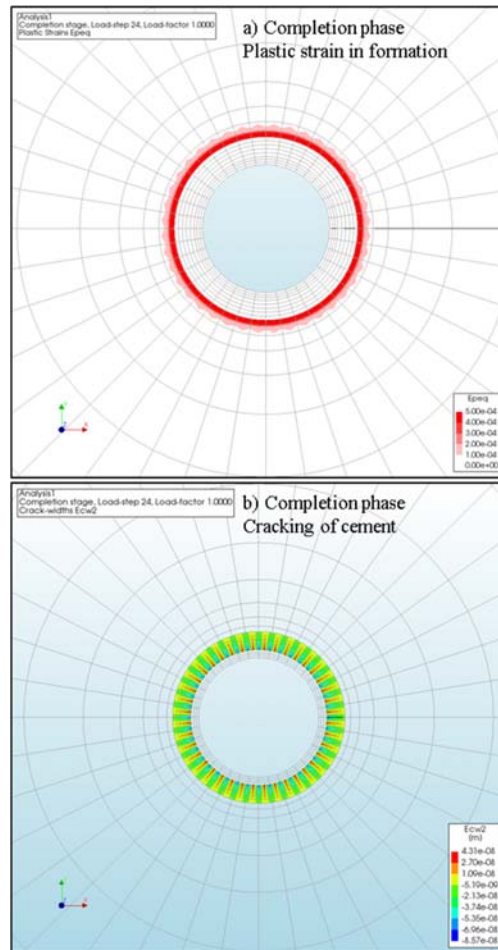


Figure 17-37: (a) Plastic strain in the formation and (b) cracking of annular cement in the completion phase.

# 18 Appendix C. Risk Register

## Caprock

Identified risk	Description	Positive evidence for integrity	Risk reduction measures	Risk characterisation	Risk classification
Initial condition	Impermeable shales of the Upper Triassic and Altona Groups overlie the P18-06 reservoir, which represent a good seal for the natural gas reservoir.	Effective seal as evidenced by the presence of gas in reservoir below the seal with a total thickness between 450 and 750 m and gas column of about 170 m (the latter based on a GWC at 3680 m SSTVD, assumed to be similar to P18-2)	Average reservoir pressure at the end of CO2 injection equal to or lower than hydrostatic pressure	As the evidence for the initial sealing of the gas reservoir is very strong, it is a good seal for CO2 storage as well and consequently the risk of migration out of the reservoir is low to even negligible when the pressure is kept at or below the hydrostatic pressure.	A-1
Pressure fracturing	Fractures in the seal may be caused by local stress variations due to initial gas production, subsequent CO2 injection and associated pressure changes. Fractures represent a potential conduit for CO2 loaded fluids depending on their connectivity and continuity (see also Fault zone).	Semi-analytic modelling has shown that Coulomb stresses as a consequence of pressure build-up due to injection quickly decay on top of the reservoir inside the caprock. The pressure effect is thus not expected to contribute to the risk of fault reactivation in the caprock. New fractures or faults will not be generated as they would require even higher Coulomb stresses.	Keep the pressure below fracturing condition	Considering the huge thickness of the caprock and the very rapid decay of the pressure near the top of the reservoir and the basis of the caprock, the likelihood of fracturing the complete caprock is nil and consequently the risk is very low to negligible.	A-1
Thermal fracturing	Fractures in the seal may be caused by local stress variations due to initial gas production, subsequent CO2 injection and associated temperature changes. Fractures represent a potential conduit for CO2 loaded fluids depending on their connectivity and continuity (see also Fault zone).	Temperature-induced Coulomb stresses in the caprock due to reservoir cooling are negative, and thus do not lead to re-activation of faults or fractures in the caprock nor will they result in new fractures in the caprock. The likelihood of re-activating a pre-existing fault or fracture in the caprock is thus very low.	Appropriate management of thermal effects	Temperature drop in the reservoir is very unlikely to lead to re-activation of fractures (or formation of new fractures) expected to lead will occur and thus will not lead to the migration of CO2 out of the reservoir. The risk is very low to negligible.	A-1
Chemical degradation	CO2 if dissolved may react with minerals in the caprock near the interface with the CO2 reservoir.	Since the caprock has proven to be a seal for gas, the only way of upward migration is by diffusion of dissolved CO2, which is a very slow process. Chemical interaction between dissolved CO2 and caprock minerals is very slow and has minor effects on porosity and permeability. Hence, no migration path is expected to form. The affected zone of migration of dissolved CO2 and chemical interaction is in the order of several meters in thousands of years (Gaus et al., 2004; Tambach et al., 2012).	Reservoir pressure after CO2 injection at or lower than initial gas reservoir pressure, to prevent CO2 from entering the caprock in gaseous/supercritical state thereby enhancing geochemical reactions.	Chemical degradation will only marginally influence the sealing properties of the caprock and thus will the overall integrity of the caprock stay intact. The likelihood of degrading the caprock is very low and its consequence will be nil or negligible.	A-1

Cont. improvement
ALARP
Intolerable



**Fault zone**

Identified risk	Description	Positive evidence for integrity	Risk reduction measures	Risk characterisation	Risk classification
Initial condition	Sealing capacity of main reservoir bounding fault to the SW and bounding cross fault to the SE mainly determined by juxtaposed reservoir rocks and sealing rocks	Bounding faults F430 (main fault) and F600 (cross fault) are effective seals as evidenced by presence of juxtaposed gas reservoirs and sealing rock.	Manage pressure gradient across fault	As reservoir rocks next to bounding faults are sealed off by very low permeable rocks on the other side of the fault zone, it has a very low likelihood that a negligible amount of CO2 will migrate across or along the fault and sealing rock.	A-1
Chemical degradation	Chemical degradation of material in fault zone	Currently, there is no evidence for gas migration from the P18-02 reservoir along the faults to overlying formations. In general, the geochemical reactions between CO2, formation water and fault gouge mineralogy - if present - will result in precipitation of carbonate minerals. On the longer term, silicate minerals might react, providing additional cations for carbonate precipitation. Porosity and hence permeability effects are predicted to be negligible. Increase of carbonate content in the fault gouge is known to increase the friction coefficient and to decrease potential for fault re-activation.		Chemical degradation leads to lowering of the porosity and permeability of the fault gouge and increases the friction coefficient of faults. Therefore it is highly unlikely that chemical degradation in itself leads to the migration of CO2 across the fault zone.	A-1
Pressure re-activation	Due to pressure changes during production and/or injection faults may be re-activated (Vandeweyer et al., 2011: par 6.7, p109) and potentially act as conduits for CO2.	No seismic activity was encountered during production, based on the KNMI database (KNMI Seismic and Acoustic Data Portal, 2 Oct 2019: doi:10.21944/e970fd34-23b9-3411-b366-e4f72877d2c5). Semi-analytic modelling has shown that at the end of the injection period most (if not all) of the areas where positive Coulomb stresses which are present at the end of depletion, have disappeared. The faults are thus expected to be stable at the end of the injection period.	Injection of CO2 is a mitigation measure in itself as it reduces the underpressure in the reservoir and consequently the risk of fault re-activation.	Based on the results from the semi-analytic modelling it appears to be highly unlikely that faults will be re-activated due to the increased pressure by CO2 injection and consequently will not lead to migration of CO2 along the fault. The risk is characterized as low.	A-1
Thermal re-activation	Cold injection stream could re-activate a nearby fault and change its fluid transport properties.	Well P18-6A-07-S1 is at a distance of about 100 m from the main bounding fault. Initial TOUGH2 simulations have shown that the cooling front with a temperature drop of about 50 °C could extend to 200 m from the injector after 5 years of injection. Semi-analytic thermomechanical modelling indicates that the Coulomb stresses may reach up to 9 MPa at the edge of the cooling front, which can be sufficient to re-activate the fault. The cold CO2 plume from injection wells at less than 200 m from a fault may thermomechanically influence its stability. Note that the actual temperature drop could be about 14 °C lower due to limitations of the TOUGH2 simulator.	Managing the advancement of the cold front near faults by adjusting the injection rate of well P18-6A-07-S1, which is in close distance of the main bounding fault. Additional simulations with TOUGH2 for a limited period of time of injection (content of pipeline as defined in the discharge scenario) show that the advance of the cold front is strongly limited to 20 m from the well and thus cannot thermomechanically reactivate a fault at 100 m from the well. This is considered to be a more representative case for the use of P18-06 field as a backup injection site.	With inclusion of appropriate management of the injection rate in the well faults the likelihood of thermomechanical fault re-activation leading to the migration of a negligible amount of CO2 out of the reservoir will be very low or no migration of CO2 out of the reservoir at all.	A-1

Cont. improvement
ALARP
Intolerable

**Reservoir**

Identified risk	Description	Positive evidence for integrity	Risk reduction measures	Risk characterisation	Risk classification
Spilling in SE at tip of cross fault	Overfilling could lead to lateral migration (spilling) of CO2 to neighbouring Buntsandstein aquifers and gas reservoirs. Subsequently, CO2 may migrate to Lower Cretaceous or Lower Tertiary aquifers via non isolated wells or faults if any. A potential spill zone is identified at the northern tip of the SE boundary fault of the P18-6 field.	Information from nearby well indicate that the aquifer has low permeability due to illitisation. Dynamic reservoir simulations show no spilling, even in the case of strong overpressurization. although the CO2 may migrate beyond the GWC.	Spilling prevented by keeping the reservoir pressure at or below the initial pressure and by limiting the total mass of injected CO2. Proper zonal isolation of wells and preventing re-activation of faults to avoid vertical migration (see also Fault compartment).	Keeping the average reservoir pressure at or below the initial pressure at the end of injection and the robustness of flow simulations indicate a very low likelihood that a negligible amount of CO2 migrates out of the reservoir.	A-1
Spilling at NW edge near saddle	Overfilling could lead to lateral migration (spilling) of CO2 to neighbouring Buntsandstein gas reservoirs and aquifers. Subsequently, CO2 may migrate to Lower Cretaceous or Lower Tertiary aquifers via non isolated wells or permeable faults if any. A potential spill zone is identified at the NW edge of the P18-6 field, represented by a saddle.	Information from nearby well indicate that the aquifer has low permeability due to illitisation. Dynamic reservoir simulations show no spilling, even in the case of strong overpressurization. although the CO2 may migrate beyond the GWC.	Spilling prevented by keeping the reservoir pressure at or below the initial pressure and limit the total mass of injected CO2. Proper zonal isolation of wells and preventing re-activation of faults to avoid vertical migration (see also Fault zone compartment)	Keeping the average reservoir pressure at or below initial pressure at the end of injection and the robustness of flow simulations indicate a very low likelihood that a negligible amount of CO2 migrates out of the reservoir.	A-1
Flow between P18-2 and P18-6 reservoirs	Over a small section across the fault zone between the P18-2 and P18-6 reservoirs, reservoir rocks of the Volpriehausen Sandstone are juxtaposed, which may lead to migration of CO2 from P18-2 to P18-6.	As the permeability of the Volpriehausen Sandstone is very low, the migration and pressure equilibration will be very slow. An assessment of the fault zone indicates that there is a very high probability of an impermeable gouge being present in the fault zone (Nieuwland, 2011). The pressure in P18-6 was at 378 bar before starting injection whereas at the same time pressure has dropped to about 100 bar in the producing P18-2 reservoir (June 2003). Apparently, this enormous pressure difference could exist indicating that there is virtually no flow and pressure equilibration between the two reservoirs on production time scales. Geological information indicates that Block 2-IV, which is directly adjacent to the P18-6 reservoir is a separate hydraulic unit.		The pressure difference of about 278 bar between the two reservoirs, the very low permeability of the Volpriehausen Sandstone and the hydraulic isolation of Block 2-IV show that the likelihood of a negligible amount of CO2 migrating from P18-2 to P18-6 is very low.	A-1

Low: Cont. improvement
Medium: ALARP
High: Intolerable

**Well**

Identified risk	Evaluation of integrity	Risk characterisation (before workover)	Risk classification (before workover)	Risk reduction measures	Risk characterisation (after workover)	Risk classification (after workover)
P18-6A-07-S1: production packer in 7"liner	A short stretch of the 7" liner (and cement) above the 5" TOL and below the production packer in the 7" liner is just above the caprock in the Schieland Group and may be exposed to corrosive fluids.	The 7" liner is P110 carbon steel and is exposed to well bore fluids and represents a single barrier in this small depth window. In the event of presence of water or brine in the wellbore fluids, the risk of corrosion may lead to loss of the primary barrier with potential leakage to the overburden. The likelihood that a small amount of CO2 leaks to the overburden is estimated to be medium.	C-3	Appropriate measures, to reinstate the dual barrier function at the level of the 7" liner above the caprock	With the implementation of adequate measures, leakage from the well will be prevented. The likelihood will be low that a negligible amount of CO2 will migrate out of the reservoir.	B-1
P18-6A-07-S1: status outer casing inside conductor	The surface casing in the conductor might be subjected to external corrosion and/or fatigue induced by metoceanic movement.	As the cementation of the conductor and 20" casing could not be sufficiently ascertained, the likelihood that a small amount of CO2 leaks to the overburden is estimated to be medium.	C-3	Verification of the presence and quality of cementation of the conductor and 20" casing and adequate measures if needed.	With the implementation of adequate measures, leakage from the well will be prevented. The likelihood will be low that a negligible amount of CO2 will migrate out of the reservoir.	B-1
P18-6A-07-S1: cooling	Injection of cold CO2 may lead to the creation of a micro-annulus at the casing-cement interface which may be enhanced by chemical interaction with CO2.	Although the pressure and temperature conditions are more favourable than for P18-2, a micro-annulus may still be formed. A medium likelihood exists that a small amount of CO2 migrates along the micro-annulus and partly ends up outside the storage complex.	C-3	Logging during operations, appropriate management of the temperature in the wellbore zone and keeping the reservoir pressure below the hydrostatic pressure (at datum level of 3,400 m)	Low likelihood remains that a negligible amount of CO2 migrates out of the reservoir	B-1

Low: Cont. improvement
Medium: ALARP
High: Intolerable

# 19 Appendix D. Monitoring Plan

Table 19-1 – P18-6 Base case monitoring plan

No.	Parameter to be Monitored*	Proposed Technique adopted	Category of monitoring		Project phase and frequency					Location	Normal situation		Alert value		Contingency value		
			EU directive	Mandatory according to Required (preliminary estimation)	Contingency	Pre-inj	Inj	Post-hj	Post-hj (abandonment)		Long-term stewardship	Expectation value	Accuracy	> Threshold 1	Action**	> Threshold 2	Contingency measures***
<b>Injection proces</b>																	
1	Injection rate	Flow meter	x			Cont				Near well head or Compressor station	Max rate = 105 ton CO2/juur (30 kg/s or 1 Mton CO2/year) and no fluctuations at constant pressure, expected value t.b.d.	Fluctuations at constant pressure or value above max. rate	Verify compressor, find cause of increased rate	Fluctuations at constant pressure or value above max. safety margins	Find cause, solve problem and if necessary reduce injection until flow < threshold 1 value again		
2	Injection stream CO2 concentration	Samples & analysis: online system	x			Cont or 1-3 hourly sampling combined with online analysis system				Near well head or Compressor station	Defined % for the CO2 concentration of the stream	Allowed fluctuations reached	Additional measurements	Above allowed fluctuations	Adapt stream composition, reduce injection temporarily		
3	Injection stream composition	Samples & analysis: Additional samples for calibration	x			Quarterly				Near well head or Compressor station	Defined % for the composition of the gas	Allowed fluctuations reached	Additional measurements, find cause, adapt gas composition, potentially reduce injection rate	Above allowed fluctuations	Find cause, adapt stream composition, potentially reduce or stop injection temporarily		
4	Water measurement	Water measurement	x			Cont				Near well head or Compressor station	Specification value	In case specification value is reached	Consultation with the CO2 provider, check dehydration system	In case value is above specification value and creates a safety issue	Stop CO2 delivery, investigate at the CO2 provider the cause, start delivery if value OK again		
5	Discontinuous emissions through leakage, venting or incidents	Combination of techniques	x			Yearly				Potential leakage points like joints or ventstacks							

No.	Parameter to be Monitored*	Proposed Technique adopted	Category of monitoring			Project phase and frequency					Location	Normal situation		Alert value		Contingency value
			Mandatory according to EU directive	Required (preliminary estimation)	Contingency	Pre-inj	Inj	Post-Inj	Post-Inj (abandonment)	Long-term stewardship		Expectation value	Accuracy	> Threshold 1	Action**	
<b>Well integrity</b>																
6	Annular pressure	Pressure device (with alarm value)		x		Continuously with remote system for online reading					At the well head	Constant pressure	Increase or decrease in pressure within safety margins	Additional measurements like logging or sampling + analysis of fluids to detect CO2	Increase or decrease in pressure above safety margins	Investigate causes (sampling) and options to remediate (in the extreme case well abandonment)
7	Well integrity	Wireline Logging (selection of tool: CBL, PMIT, EMIT, USIT, WAF . optical)		x		Baseline	Frequency should be determined and adapted during the course of the project				Well	Measurements within the expected range	Measurements above expectation values	Additional measurements (such as repeat) to corroborate observations, potentially seismic contingency measurements in case values large enough to be detected by seismics	Measurements significantly above expectation values	Stop injection, additional measurements and seismic contingency measurements to identify shallow gas accumulations, investigate options to remediate (in the extreme case well abandonment)
8	Well head pressure	Pressure device			x	Baseline	Continuous	Continuous	Continuous	At the well head (injection skid)	Measurements within the expected range, no large fluctuations expected at constant flow rates	Loss or increase of pressure with respect to expected values	Additional measurements to determine the cause	No recovery of injection pressure after lowering or increasing injection flow	Stop injection, investigate the cause and evaluate whether conditions are safe	
9	Well head temperature	Temperature device			x	Baseline	Continuous	Continuous	Continuous	At the well head (injection skid)	Determine operational limits for temperature range	In case temperature reaches the determined operational limits (high or low)	Additional measurements to determine the cause	In case temperature reaches the determined operational limits	Stop injection until the cause of the temperature change is clarified and safe	
10	Plug integrity	Pressure test and inspection		x						In the well above the plug	No pressure changes	Minimal pressure changes	Investigate cause with other measurements (e.g. check deformation of the wellbore, fluid sample)	Significant pressure changes	Redo the plug	



No.	Parameter to be Monitored*	Proposed Technique adopted	Category of monitoring				Project phase and frequency					Location	Normal situation		Alert value		Contingency value	
			Mandatory according to EU directive	Required (preliminary estimation)	Contingency		Pre-inj	Inj	Post-inj	Post-inj (abandonment)	Long-term stewardship		Expectation value	Accuracy	> Threshold 1	Action**	> Threshold 2	Contingency measures***
	<b>Environmental monitoring</b>																	
16	Pockmarks at the seabottom	Multi-beam echosounding		x								Acquisition from a ship	No pockmarks	Pockmarks	Additional gas sampling + analysis to identify the origin of potential seepage or leakage. In case of leakage, identify the pathway with time-lapse seismic data. Mitigation to	Detection of bubbles	Additional gas sampling + analysis to identify the origin of potential seepage or leakage. In case of leakage, identify the pathway with time-lapse seismic data. Mitigation to	
17	Presence of shallow gas or gas chimneys in the subsurface	Baseline seismic data		x							survey prior to transfer of liability and every 5 years after handover of liability	Available baseline seismic data	No bright spots or chimneys in the subsurface	Bright spots and/or gas chimneys	Investigate origin of the gas, in case a leakage pathway is suspected, apply time-lapse seismic data	Bright spots and/or gas chimneys to the surface	Additional gas sampling + analysis to identify the origin of potential seepage or leakage. In case of leakage, identify the pathway with time-lapse seismic data. Mitigation to potential leaks	
18	Migration pathways for gas in the shallow subsurface	Time-lapse seismic data acquisition (2D or 3D)			x						Marine acquisition from a vessel	No changes in bright spots or chimneys in the subsurface	Changes in bright spots and/or gas chimneys	Investigate origin of the gas, in case a leakage pathway is suspected, apply time-lapse seismic data	Changes in bright spots and/or gas chimneys to the surface	Additional gas sampling + analysis to identify the origin of potential seepage or leakage. In case of leakage, identify the pathway with time-lapse seismic data. Mitigation to potential leaks		
19	CO2 in soil at pockmarks	Gas samples using vibrocore + lab analysis			x						Sampling from a vessel			In case of leakage detection at the seabottom by geophysical methods	Investigate origin of the gas, in case a leakage pathway is suspected, apply time-lapse seismic data	In case of leakage detection at the seabottom by geophysical methods	Investigate origin of the gas, in case a leakage pathway is suspected, apply time-lapse seismic data	
20	Bubble detection at wellhead	Acoustic bubble detector			x						Install at the seabottom	No bubbles	In case of few bubbles	Investigate origin of the gas, in case a leakage pathway is suspected, apply time-lapse seismic data	Significant bubble stream	Well remediation (workover)		
21	Microseismic monitoring	Permanent geophones or DAS in monitoring wells		x							Injection well at caprock and reservoir level	No large events in caprock or at faults (re-activation)	Large events in the caprock or at faults	Additional measurements like seismic contingency measurements to identify shallow gas accumulations, evaluate whether injection can be continued safely	Very large events in the caprock or at faults	If considered a safety issue then stop injection, additional measurements and seismic contingency measurements to identify shallow gas accumulations, evaluate whether injection can be continued safely		

continued at lower

Table 19-2 – P18-6 Base case monitoring plan, overview of project phases.

			Pre-injection	Injection	Post-injection	Post-injection (Abandonment)	Post-injection (Transfer of liability)
<b>Injection Proces</b>							
1	Injection rate	Flow meter		Continuous			
2	Injection stream CO2 concentration	Gas samples & analysis: online system		Continuous or 1-3 hourly			
3	Injection stream composition	Gas samples & analysis: Additional samples for calibration		Quarterly			
4	Water measurement	Gas measurement		Continuous			
5	Discontinuous emissions through leakage, venting or incidents	Combination of techniques		Yearly reporting according to protocol			
<b>Well Integrity</b>							
6	Annular pressure	Pressure device	Baseline	Continuous			
7	Well integrity	Wireline Logging (selection of tools like: CBL, PMIT, EMIT, USIT, WAF, optical)	Single baseline before start of the injection	Frequency should be determined and adapted during the course of the project			
8	Well head pressure	Pressure device	Continuous				
9	Well head temperature	Temperature device	Continuous				
10	Plug integrity	Pressure test and inspection			Assessment of the quality of the plug		
<b>Reservoir Integrity</b>							
11	Reservoir pressure (FBHP) (see also line 8)	pressure device	Continuous or monthly with memory gauges (frequency can be adapted according to findings) - (Calculated from FTHP, AND potentially downhole permanent sensor (large risk of failure) or downhole memory gauges)				
12	Reservoir Temperature (FBHT) (see also line 9)	thermometer or DTS	Continuous or monthly with DTS or memory gauges (frequency can be adapted according to findings) - (Calculated from FTHT AND potentially downhole permanent sensor (large risk of failure) or downhole memory gauges)				
13	Stabilized pressure (CIBHP) (gradient) during shut-in period	pressure device (wireline tool or memory gauge) combined with shut-in	Shut-in pressure measurement every year				
14	Stabilised temperature (CIBHT) (gradient) during shut-in period	thermometer or DTS (wireline tool or memory gauge) combined with shut-in	Shut-in temperature measurement every year (DTS for permanent installation or memory gauges)				
15	Suspected leakage	Surface seismic survey		Survey in case of irregularities			
<b>Environmental Monitoring</b>							
16	Pockmarks at the seabottom	Multi-beam echosounding	Baseline			survey	survey
17	Presence of shallow gas or gas chimneys in the subsurface	Baseline seismic data	Interpretation can be on existing data				
18	Migration pathways for gas in the shallow subsurface	Time-lapse seismic data acquisition (2D or 3D)		Survey in case of irregularities			
19	CO2 in soil at pockmarks	Gas samples using vibrocore + lab analysis		Survey in case of irregularities			
20	Bubble detection at wellhead	Acoustic bubble detector		Survey in case of irregularities			
21	Microseismic monitoring	Permanent geophones or DAS in (monitoring) wells		Continuous in monitoring or injection well (considered required monitoring but subject to technical feasibility)			







TAQA

# **PORTHOS**

## **Basis of completion design**

ECM Number #: 196564

---

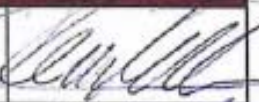




### **TAQA Energy B.V.**

Kruseman van Eltenweg 1,  
1817BC Alkmaar,  
The Netherlands

Date: August 8th, 2019  
Issue No.: Version 2.0

---

**DOCUMENT CONTROL**
**Authorization**

Activity	Name	Function	Date	Signature
Prepared	Hein van Heekeren	Senior Well Engineer	26-8-2019	
Reviewed	Tim-Tijn Scherpenhuijsen	Geologist / CCS Project Manager	24-8-2019	
Reviewed	Willem-Jan Plug	Subsurface Manager	26-8-2019	
Reviewed	Reinout Storm	Manager Drilling & Wells	8-8-2019	R. Storm 
Approved	Isabelle de Vos	Drilling & Completions expert, EBN	28/08/2019	

**Revision record**

Version	Date	Status / Changes
0, Draft	27-2	For review
0.1 Draft	28-2	Incorporated comments from TTS, WJP & RS
0.2	28-2	For approval
0.3	5-3	Incorporated comments Jan-Thijs Keijser
1.0	25-3	Incorporated comments IdV
1.1	12-6	Added wells optional wells P18-2A6 & P18-6a7, for review.
1.2	19-6	Included comments of reviewers, for approval.
2.0	8-8	Included comments IdV and updated to follow ISO specification

## TABLE OF CONTENTS

<b>DOCUMENT CONTROL</b> .....	<b>2</b>
<b>Authorization</b> .....	<b>2</b>
<b>Revision record</b> .....	<b>2</b>
<b>1. INTRODUCTION</b> .....	<b>4</b>
<b>2. DESIGN ASSUMPTIONS</b> .....	<b>5</b>
2.1. Reservoir .....	5
2.2. Regional pore pressure and fracture gradient profiles .....	5
2.3. CO <sub>2</sub> delivery specifications.....	6
2.4. Normal operational parameters and input from the flow assurance study .....	7
2.5. Well integrity.....	8
<b>3. DESIGN REQUIREMENTS</b> .....	<b>10</b>
3.1. Completion configuration .....	10
3.2. Materials .....	11
3.3. Annulus fluids.....	12
3.4. Production Liner & Casing cement .....	12
3.5. Logging requirements .....	12
3.6. Clean-out.....	13
<b>4. CONCLUSIONS AND RECOMMENDATIONS</b> .....	<b>14</b>
<b>5. APPENDICES</b> .....	<b>15</b>
5.1. Appendix A: generalized stratigraphy of the P18 area .....	15
5.2. Appendix B: Static wellhead and reservoir pressures for CO <sub>2</sub> injection well .....	17
5.3. Appendix C: Example CO <sub>2</sub> injection completion P18-4A2 well.....	18
5.4. Appendix D: Example CO <sub>2</sub> injection completion P18-2A3 well .....	19
5.5. Appendix E: Wellhead and Tree.....	20

## 1. INTRODUCTION

As part of the Porthos CCS project it is planned to inject CO<sub>2</sub> in the depleted P18-2 and P18-4 Bunter gas reservoirs. A multidisciplinary well selection workshop\* has been held on the 31<sup>st</sup> of January in the EBN office to select the candidate wells for injection based on reservoir properties and well integrity status. All planned injection wells are located on the normally unmanned P18/A platform and are currently producing gas that is evacuated through the P15/D platform. The below table lists all wells that were selected to serve as an injection well:

Well Name:	Well type	Well type
P18-2A1	P18-A platform	Injector
P18-2A3	P18-A platform	Injector
P18-2A5	P18-A platform	Injector
P18-4A2	P18-A platform	Injector
P18-2A6	P18-A platform	Optional injector*
P18-6A7	P18-A platform	Optional injector*

*\*The mother bore of P18-2A6 well and the P18-6A7 well have been added as optional injection candidates to the basis of completion design in a later phase because the flow assurance study indicated that there may be a benefit in using these wells as “start-up” wells and to increase the total storage capacity.*

The purpose of this document is to prepare a basis of design for re-completion of the wells to make them suitable for CO<sub>2</sub> injection based on current known requirements for the wells. The design will follow ISO standard 27914 “Carbon dioxide capture, transportation and geological storage - Geological storage”.

## 2. DESIGN ASSUMPTIONS

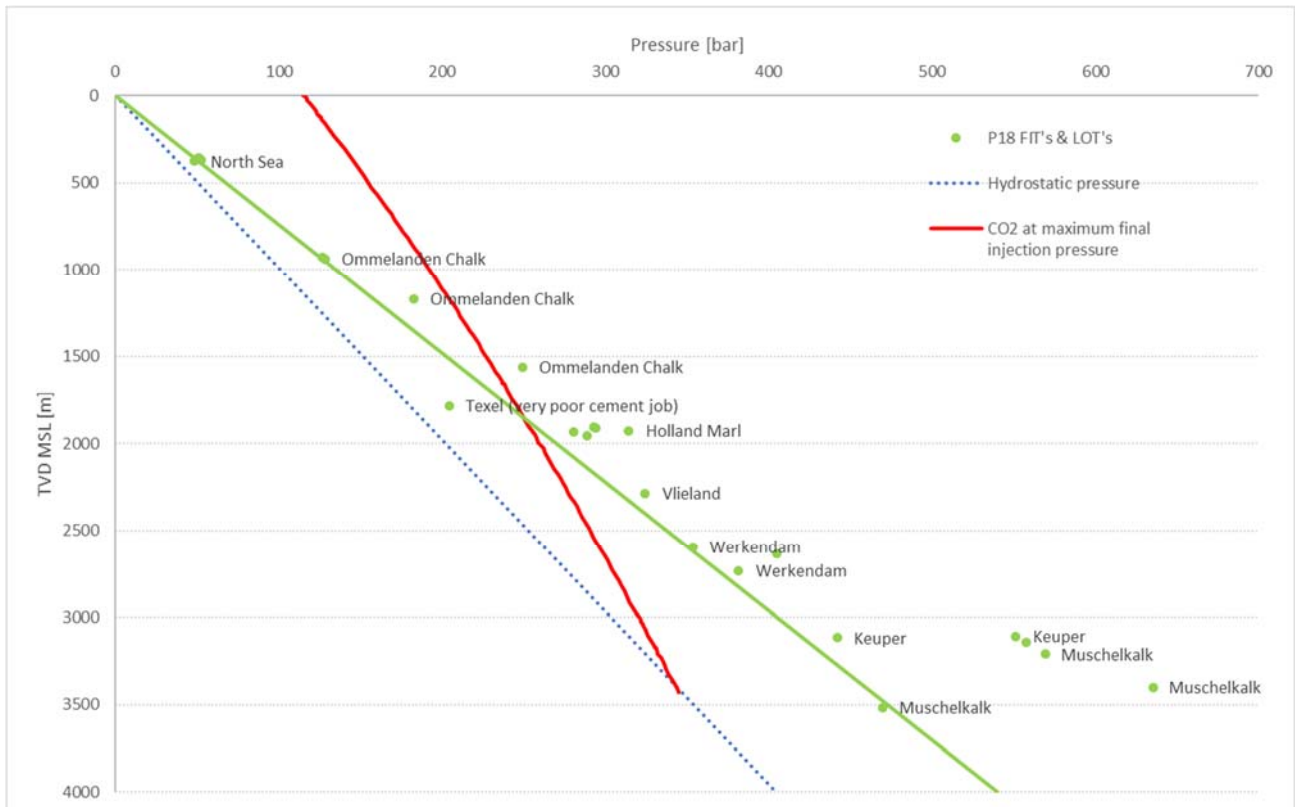
### 2.1. Reservoir

CO<sub>2</sub> is planned to be injected in the Bunter reservoir at a depth of around 3200 m TVD. The caprock consists of the Solling Claystone Member and an >500m TVD thick sequence consisting of the Rot, Muschelkalk, Keuper and various Altona shales. A generalised stratigraphy of the P18 wells can be found in appendix A.

### 2.2. Regional pore pressure and fracture gradient profiles

The pore pressures and formation fracture pressures are displayed in the figure below;

- The minimum fracture gradient is based on P18 limit and leak-off test results, indicated by a Green dot. The Green line connects these dots and is indicative of the formation strength.
- The Blue line shows the hydrostatic pressure line of the formations
- The Red line shows the pressure profile in case the well would be fully filled with CO<sub>2</sub> at the final planned reservoir pressure of 345 bar



### 2.3. CO<sub>2</sub> delivery specifications

Component	Concentration*	Based on
CO <sub>2</sub>	≥ 95%	ISO-27913
H <sub>2</sub> O	≤ 40 ppmv	OCAP ≤40ppmv / Technical Operation ≤50 ppmv <sup>Note 1</sup>
Sum [H <sub>2</sub> +N <sub>2</sub> +Ar+CH <sub>4</sub> +CO+O <sub>2</sub> ]	≤ 4%	ISO-27913 <sup>Note 2</sup>
H <sub>2</sub>	≤ 0.75%	ISO-27913 <sup>Note 2</sup>
N <sub>2</sub>	≤ 2%	ISO-27913
Ar	≤ 1%	ISO-27913
CH <sub>4</sub>	≤ 1%	ISO-27913
CO	≤ 750 ppmv <sup>Note 3</sup>	OCAP
O <sub>2</sub>	≤ 40 ppmv <sup>Note 4</sup>	Storage license P18-4
H <sub>2</sub> S	≤ 5 ppmv <sup>Note 5</sup>	OCAP
SO <sub>x</sub>	≤ 50 ppmv	ISO-27913
NO	≤ 2.5 ppmv	OCAP (emitters do not require additional purification)
NO <sub>2</sub>	≤ 2.5 ppmv <sup>Note 6</sup>	OCAP (emitters do not require additional purification)
NO <sub>x</sub>	≤ 5 ppmv <sup>Note 6</sup>	OCAP NO+NO <sub>2</sub>
C2+ (hydrocarbons)	≤ 1200 ppmv <sup>Note 7</sup>	OCAP (emitters do not require additional purification)
Aromatic hydrocarbons (incl.BTEX <sup>Note8</sup> )	≤ 0.1 ppm	OCAP (emitters do not require additional purification)
Total volatile organic compounds <sup>Note 9</sup>	≤ 350 ppm	Already being sent to OCAP <sup>Note 10</sup>
Ethylene (Etheen)(C <sub>2</sub> H <sub>4</sub> )	≤ 1 ppmv	OCAP (emitters do not require additional purification)
H-cyanide (HCN)	≤ 20 ppmv	OCAP (emitters do not require additional purification)
Carbonyl Sulfide	≤ 0.1 ppmv	OCAP (emitters do not require additional purification)
Dimethyl Sulfide	≤ 1.1 ppmv	OCAP (emitters do not require additional purification)

\*All percentages are mole %. Note: 1 % (mole) = 10 000 ppmv

Note 1: A study of the phase diagram with CO<sub>2</sub> and H<sub>2</sub>O vs. the Porthos operating regimes indicated that solids may form at 100ppm H<sub>2</sub>O, but not at 50ppm. Optimization between these steps has not been done to determine the maximum amount of H<sub>2</sub>O that could be allowed to prevent solid formation.

Note 2: Components lighter than CO<sub>2</sub> shift the phase diagram upwards. This increases the operating costs for compression, but also increases the 2-phase zone which must be avoided in the offshore pipeline. Crossing the 2-phase zone from high pressure to low pressure causes significant temperature drops by the Joule Thompson effect. Hydrogen is the lightest of these components and should therefore be allowed with caution.

Note 3: Next limit: ISO-27913 CO < 0.2%.

Note 4: ISO-27913 stipulates O<sub>2</sub> < 10 ppmv (Petroleum Industry Standard w.r.t. well integrity), although recommendation from material specialist to avoid corrosion is 100ppm. Also, for wells in stainless steel, low levels of O<sub>2</sub> is actually required to form an oxidation layer. Therefore, the specification was slightly relaxed to OCAP composition.

Note 5: Next limit: ISO-27913 and specialist recommendation to avoid corrosion and: H<sub>2</sub>S < 200ppmv.

Note 6: Next limit: ISO-27913 NO<sub>2</sub> < 50 ppmv

Note 7: Next limit: ISO-27913 C2+ < 2.5%

Note 8: BTEX = benzene, toluene, ethylbenzene, xylene

Note 9: Total volatile organic compounds = ethanol, acetaldehyde, ethyl acetaat, traces of n-propanol, isobutanol, acetone, dimethyl ether, propanal, 2-butanol, methanol, n-butanol and isoamyl acetaat

Note 10: OCAP specification on Total volatile organic compounds < 1.2 ppm

## 2.4. Normal operational parameters and input from the flow assurance study

For the flow assurance study (Flow assurance study presentation January 31th 2019, Stefan Belfroid, TNO) the following parameters have been taken into account for steady state injection:

Temperatures:

- Compressor outlet temperature  $35 < T < 80$  °C
- Downhole temperature  $T > 15$  °C
- Topside piping  $T > -10$  °C

Flowrates:

- Desired flow rates 15 – 170 kg/s, (through pipeline) with an objective of 70 kg/s per well
- 4 wells available for injection (1 well in P18-4; 3 wells in P18-2). The optional injection wells P18-2A6 and P18-6A7 were added in the final stage of this study, hence no detailed FAS modelling has been done for these two wells. Therefore, the generalized completion and well design have been applied for both the P18-2A6 and P18-6A7. The recommendation is to update the flow assurance study including these two additional wells to understand the impact on completion and well design due to differences in reservoir properties and injectivity.

Pressure:

- Reservoir pressure prior to start of CO<sub>2</sub> injection: 20 bar (note: The P18-2 and P18-4 reservoir pressures are now around 22 bar and the P18-6 reservoir pressure is around 46 bar)
- Reservoir pressure end of CO<sub>2</sub> injection: 340 bar
- Minimum pipeline pressure 60 bar (minimum discharge pressure compressor)
- Other constraints such as tubing vibrations; thermal/mass flow rate constraints for reservoir, thermal gradients in well (radial and axial)

In order to stay within the above operating boundaries, the flow assurance study has shown that a completion with primarily 5 1/2" tubing is the most optimal. When using a smaller diameter tubing it will be easier to meet the temperature constraints at the topside. On the other hand, it will lead to higher wellhead pressures which implicates that at the final reservoir pressure the desired injection rates cannot be met. When modelling the larger diameter tubing it became apparent that it will be very difficult to meet the temperature requirements at low reservoir temperatures. (Flow assurance study presentation January 31th 2019, Stefan Belfroid, TNO)

During start-up and shut-in, the temperatures of the CO<sub>2</sub> in the well can drop even further. The worst case that is modelled for the flow assurance study is an Emergency Shut Down (ESD) with 20 bar reservoir pressure, below is a graph with the resulting minimum temperature and lowest mean temperature of the CO<sub>2</sub>. When the reservoir pressure increases with injection this temperature effect will reduce and the well will stay at higher temperatures.



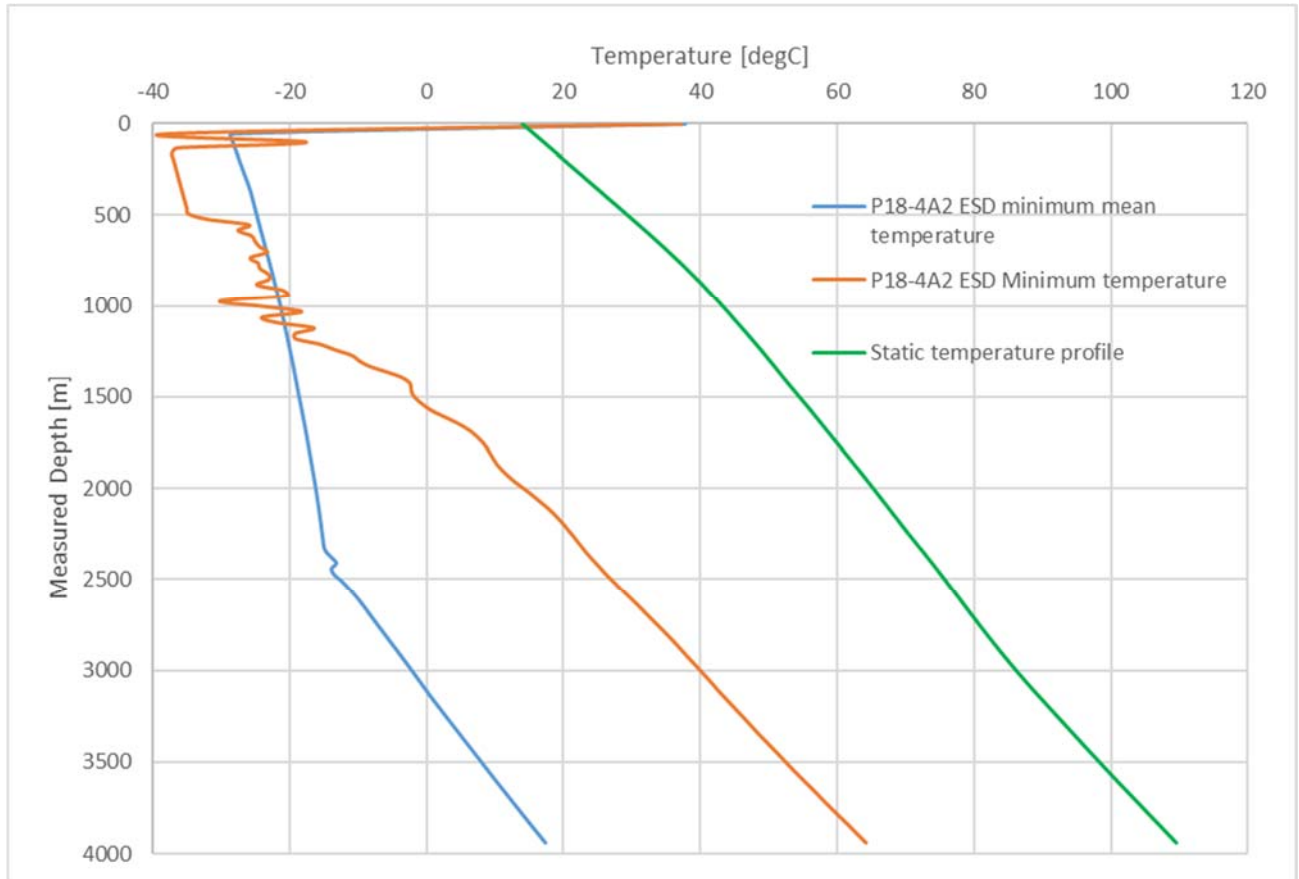


**Figure 1 Static temperature and CO<sub>2</sub> temperature profiles during an ESD**

### Downhole monitoring

The flow assurance modelling has shown that the wellhead pressure will vary very little with increasing reservoir pressure, refer to appendix B for a graph (Flow assurance study presentation January 31th 2019, Stefan Belfroid, TNO). It is therefore recommended to install a downhole pressure gauge to allow for accurate monitoring of the reservoir pressure. Given the large expected temperature variations and the big impact that this will have on the completion it is recommended to install a continuous array of temperature measurements over the tubing to confirm the results of modelling and aid in operating the well in the design envelope. The data gathered in the Porthos project may also be beneficial for future CO<sub>2</sub> storage projects.

### 2.5. Well integrity

A well integrity review has been performed by TNO (Well integrity study presentation January 31th 2019, Paul Hopmans, TNO NB: This review did not consider the P18-6A7 well as a potential injector). The currently installed completions have a retrievable packer which is not deemed suitable for the expected temperature variations and will therefore need to be replaced. The main conclusion of this review, on the well materials that will stay in the well, were:

- No major operational issues during cementing of the production casings and liners which are located at the proposed packer setting area.
- Most of the cement bond logs that were run over the production liners showed poor bonding.
- No annular pressures have been observed during the productive life of the wells except for the P18-2A5 well where there is a sustained pressure slowly building on the A-annulus.
- The formation integrity tests done after cementing show competent casing shoes whereby all casing shoes from the 13 3/8" down can cope with the anticipated maximum CO<sub>2</sub> pressure.

- The P18-2A6 well is a multilateral well, consisting of a lateral which will need to be decommissioned and a mother bore which could be considered as an injection candidate, this will involve retrieving a whipstock and isolation of the lateral section.

A Taqa quick scan of the P18-6A7 well integrity has revealed the following:

- The completion has a permanent packer, in the define phase it could be considered to perform a detailed assessment including a flow assurance study to check whether the completion could be used as is including potential temperature limitations.
- FIT's of the 9 5/8" casing (Holland Marl) down are of sufficient strength to cope with anticipated maximum CO<sub>2</sub> pressure.
- There are no abnormal annular pressures recorded.
- No CBL's were run, the 13 3/8" primary cement job failed due to a blocked bottom plug / float collar, the result of subsequent squeeze jobs was poor.
- Losses were observed during the 9 5/8" casing cement job, the calculated top of cement is inside the 13 3/8" shoe.
- Losses were observed during the 7" liner cement job, the theoretical top of cement was estimated at 118 m below the TOL (spacer returns observed), the liner was rotated during the first part of the displacement.
- During the 5" liner cement job the top wiper plug was bumped 2.2 m<sup>3</sup> early, it was thought that cement had bypassed the wiper plug, therefore only spacer and no cement was observed above the TOL, rotation not reported.

When the annular cement of a production liner is deemed inadequate it could be considered to place the packer above the liner across a caprock in an area with good annulus cement. It is therefore not expected that the current cement status will be an issue for CO<sub>2</sub> injection. However, the prognosed quite extreme temperature cycles may influence the cement bond quality during the well life. A study is being performed by TNO on the effect of the temperature cycles on the cement bond quality, it is advised to take the study results along in the define phase. Remediation for a poor annulus cement is discussed in the design requirements section (section 3.4).

### 3. DESIGN REQUIREMENTS

#### 3.1. Completion configuration

The Flow assurance study shows that 5 1/2" is the optimal tubing size for the injection wells. This will fit in the top part of all injection wells since the top part of the wells consist of 9 5/8" casing. Three of the wells have a 7" liner above the reservoir, 2 wells have a 5" liner over the reservoir and the P18-6A7 has a predrilled 3 1/2" liner over the reservoir. The P18-2A6 well will require decommissioning of the lateral and isolation of the lateral from the motherbore. Various solutions exist which could be used, this is not expected to lead to a reduction in ID smaller than that of the ID of a 7" liner. In the define phase the benefits of using a system with a larger ID which could enable using a larger tubing to deeper in the well could be weighed against potential downsides of such a solution including potential extra cost. Below is a table with the depth of the Top Of Liners (TOL) and the top of the perforations.

	P18-2A1	P18-2A3	P18-2A5	P18-4A2	P18-2A6	P18-6A7
7" TOL [m]	3405	2672	3594	3924	*2200	2435
5" TOL [m]	N/A	3785	4402	N/A	N/A	3761
4 1/2" TOL [m]	N/A	N/A	N/A	N/A	N/A	N/A
Top of perforations [m]	3575	4070	4796	4083	4488	**4953

\* Estimated top of a to be installed scab liner over the window, this could be 7" scab liner or a different size scab liner/patch, this will be decided on in the define phase

\*\* Predrilled holes in 3 1/2" liner

For the wells with a 7" liner over the reservoir there is an opportunity to install the packer across the caprock just above the perforations in case the annulus cement at that level is deemed competent (refer to appendix C for an example completion diagram). This will reduce the amount of liner and casing that is in contact with CO<sub>2</sub>. It will also facilitate the final decommissioning of the well as the packer with a plug installed can be used to isolate the upper part of the well from the reservoir and it can serve as a base for the cement plug. This will reduce decommissioning risks and cost whilst still allowing to set a full-bore cement plug against the caprock (for more details on the decommissioning please refer to the Porthos basis of decommissioning design). The maximum tubing size that will fit in a 7" liner is 4 1/2" when a pressure/temperature monitoring cable is run with the tubing.

For the wells with a 5" liner the packer will need to be installed as deep as possible in the 7" liner across a suitable caprock (refer to appendix D for an example completion diagram). For the P18-6A7 well this means that the packer will be installed just above the caprock (Altena shales). This is not the preferred place since it could allow leakage above the caprock without a possibility to monitor it. However, it could be considered to stab the tailpipe of the completion into the 5" TOL to add an additional barrier to the 7" liner and to monitor the condition of the barrier by regular risk based corrosion logs. Installing a packer in the 5" liner will result in a too small tubing size to allow for the required injection rates. This means that the 5" liners will be exposed to CO<sub>2</sub>. For the P18-6A7 well it may be preferred to install a deeper packer and to accept a reduced injection capacity. In the define phase, it should be confirmed with Flow Assurance calculations that the depth of the packers will not form a too big restriction for injection, this will be an iterative process. Next to pressure and temperature effects, the maximum allowed velocity in the well components to avoid erosion should be considered.

An example of the proposed configurations with a 7" liner and with a 7" & 5" liner can be found in appendix C and D.

#### Packer

It is preferred to install a completion whereby the tubing is fixated to a packer. Given the relatively large impact of pressure fluctuations on well temperatures in CO<sub>2</sub> injection wells it is advised to perform flow assurance calculations based on the final injection parameters for the operating envelope of each specific well. The outcome from the flow assurance study can be used as input to calculate the

loads on the packer and as such to validate the final packer design. For the wells where the packer can be placed just above the perforations permanent packers may be used since these can be left downhole during decommissioning of the wells. However, in case of an unexpected workover due to issues with the new completion this would lead to extra workover cost compared to a retrievable packer.

For wells where the packers cannot be set close enough to the caprock for instance due to poor casing quality, poor annulus cement or unsuitable production liner size it is advised to source retrievable packers with a cut to retrieve option for ease of later decommissioning. In case no retrievable packers of sufficient strength can be sourced, a permanent packer can be installed but this will lead to extra time spend on milling of the packer during the final decommissioning of the wells.

The extreme temperature variations that are modelled in the Flow Assurance study will lead to very high loads on the tubing and packer and will lead to strict specifications for the packer and tubing.

In case the detailed modelling shows that the use of a standard packer completion is not an option it could be considered to select a system where the tubing is allowed to slide in a sealbore. The downside of this option is that given the frequent movement past the seals this is more susceptible to leakages.

### **Subsurface safety valve**

The use of a Surface Controlled SubSurface Safety Valve (TRSCSSSV) is mandatory for self-flowing wells. This safety valve should be suitable for the low anticipated temperatures in the well, it is however expected to be difficult to find a standard safety valve in the market that fulfils this requirement, especially in the top section which is expected to cool down the most, it could be considered to place the safety valve deep in the well where the temperatures will be higher. Next to that the control line fluid may be susceptible to freezing which will hamper the functionality of the TRSCSSSV. Therefore, it could be considered to use an injection valve rather than a TRSCSSSV or a combination of both. An injection valve will always close directly in case of an uncontrolled release whereas a TRSCSSSV closes after a sequence of valves is closed or hydraulic pressure is lost. A downside of injection valves is that they may be more susceptible to erosion and that they are not controllable from surface. A dispensation will need to be requested from the regulator for not installing a TRSCSSSV. The pro's and cons of both options and the effect of the low CO<sub>2</sub> temperature on the control line fluid needs to be investigated in the define phase. A deep-set injection valve which gives backpressure to the system may aid in reducing the ESD loads on the well, this should be investigated in the Flow Assurance study.

### **Downhole monitoring**

In order to get the full temperature profile of the wells a fibre optic Distributed Temperature Sensor (DTS) system could be installed in combination with a downhole pressure gauge. This will lead to restrictions on the tubing size at the bottom of the wells compared to a design where no downhole monitoring is required.

## **3.2. Materials**

### **Tubulars**

For the flow wet tubulars Cr13 material will be required to cope with the proposed CO<sub>2</sub> specification, higher quality super Cr13 variants could be required to cope with the very low temperature requirements. In the define phase this should be discussed with OCTG (tubing) suppliers in order to prepare the material specification.

### **Casing & Liners**

The casing designs of the injector wells will need to be checked against the CO<sub>2</sub> injection load cases. As part of this wellhead movement should be assessed and checked for interference with the platform structure and facilities.

### **Wellhead & X-tree**

The existing wellhead and tree have not been designed (Temperature class PU -20°C to 121 °C) to cope

with the very low expected temperatures. The flow wet components such as the tubing hanger and the X-tree can be changed out, the new equipment will need to be ordered to arctic specification (API temperature class KU -60°C to 121 °C). It will be very difficult to change out the wellhead equipment of the casings, it should however be checked what the temperature effect will be on this equipment and whether the equipment is suitable for this. Also the use of heat tracing could be considered. Refer to Appendix E for wellhead and tree setup for the P18-A wells. Please note that the wellhead & tree of the P18-6A7 well is different than that of the other P18 wellhead and trees.

### **Elastomers**

If elastomers are used in the packer, wellhead or subsurface safety valve these need to be checked against compatibility with the CO<sub>2</sub> specification

### **3.3. Annulus fluids**

Standard oil and gas wells in the Netherlands are completed with a completion brine in the A-annulus, however in these wells the expected low temperatures may lead to freezing of the brine. Also, the outer annuli could be exposed to freezing conditions. In the define phase, the temperature effects on the annulus fluids should be modelled. In case it is apparent that the A-annulus will freeze it should be considered to add anti-freezing agents, use an oil-based annulus fluid and/or nitrogen blanket in the annulus. The use of a nitrogen blanket in the annulus may have the additional benefit of insulation to the outer casing strings and will lead to a continuous overpressure which will allow continuous verification of the barrier envelope. This could be an option in case modelling shows that the outer annuli will be susceptible to freezing conditions since it is not possible to change-out the fluids that are present in the outer annuli. Alternatively, the operating envelope would need to be reduced in order to keep the temperatures of the annuli within acceptable boundaries. Introducing a nitrogen blanket will however make the completion installation a bit more complex and may introduce a potential leak path in the completion.

### **3.4. Production Liner & Casing cement**

The preferred setting depth of the production packer is as close to the perforations as possible where the well geometry allows this. This means that the production liners and the annulus cement will be part of the primary barrier envelope. The CBL's that were done on the production liners just after installation showed poor bonding for most of the wells. However, the isolation of the liner cement is believed to be sufficient for CO<sub>2</sub> injection when the cement job parameters were good and no annulus pressures have been observed during the producing life of the wells. It could be considered to reinterpret the existing CBL's to gain extra confidence in the cement bond logs.

Alternatively the production packer could be installed in the production casing when the cement job parameters were good, a FIT/LOT showed that the shoe is of sufficient strength to cope with the maximum anticipated pressure and no annulus pressures have been observed during the producing life of the wells.

In case that no isolation is present remedial actions could be considered. The best way to remediate a poor cement job would be to decommission the existing production liner with a Full-bore Formation Plug against the caprock and sidetrack back into the reservoir to install a new production liner, this will be an expensive solution.

### **3.5. Logging requirements**

Several logs could be run before running the new completion to verify the condition of the well. During the injection phase production logging may be required to assess the well and the injection performance. As per ISO 27914:2017 standard prior to conversion for CO<sub>2</sub> storage, the long-string casing shall be inspected and tested for integrity over its full length by obtaining and evaluating cement integrity logs and running and evaluating a casing inspection log for casing corrosion or damage.

**Cement bond logs**

A cement bond is typically used during the construction of a new well when there were operational issues with the cementation to check if there is a cement bond behind the casing. Please note however that it is the experience of Taqa that CBL results can be misleading, we have had examples of well sections with poor CBL's and good isolation and well sections with good CBL's where there was an obvious leak path. It is therefore of importance to ensure that the planned cement evaluation tool is suitable for the specific cement/casing situation and that prior to running the tool the evaluation and decision criteria are established.

**Corrosion logs**

Corrosion logs will be run as per the ISO standard. It is important to ensure that the minimum required wall thickness is known prior to running the tools and that the evaluation and decision criteria are established. Special focus areas of the corrosion logs are the proposed packer setting area in the production liner since in cases where this area was exposed to well fluids containing a minor amount of CO<sub>2</sub> during the production life and the P18-2A5 well where irregular A-annulus behaviour has been observed during its productive life.

**Production logs**

When for some wells there are doubts on reservoir performance (injectivity) a production log like an (M)PLT could be considered. The CCS ISO standards also mentions that a baseline saturation log should be obtained to establish gas saturations near the wellbore, the benefits of such a log should be discussed with the subsurface team in the define phase.

**3.6. Clean-out**

Before running a new completion and potentially some logs it is advised to perform a clean-out run with casing scrapers to remove scales, debris and plugging material from the well kill from the casing walls.

#### 4. CONCLUSIONS AND RECOMMENDATIONS

- The 4 initially proposed P18-2 and P18-4 gas wells are suitable to convert to CO<sub>2</sub> injection wells.
- The P18-2A6 well is a multilateral well, consisting of a lateral which will need to be decommissioned and a mother bore which could be considered as an injection candidate, this will involve retrieving a whipstock and isolation of the lateral section.
- The P18-6A7 well could be considered as an injection candidate, it does have a different well architecture and wellhead system than the other P18-A wells which will lead to variations in the design.
- For P18-2A6 and P18-6A7 a flow assurance study needs to be done to understand the impact on completion and well design due to differences in reservoir properties and injectivity.
- The large variation in modelled injection temperature profiles will lead to large loads on the tubing and packer and will require strict specifications and lead to extra cost and longer lead times
- The expected extreme low temperatures will lead to strict specifications for materials and lead to extra cost and longer lead times
- The cyclic temperature loading on the existing cement should be taken into account in the detailed design.
- It is recommended to review options to reduce the temperature loads in order to be able to use a more cost-effective design.
- It is recommended to prepare a flow assurance model for the detailed completion of each well and to update this model with the actual planned start and end reservoir pressures.
- The completions should cater for production logging during the operational stage
- The casing designs of the injector wells will need to be checked against the CO<sub>2</sub> injection load cases.
- Temperature limitations of well elements that cannot be changed-out during a workover such as annulus fluids and wellhead seals must be evaluated as they might impact the operational boundary conditions.
- Wellhead movement should be assessed and checked for interference with the platform structure and facilities.
- In the define phase start engaging equipment vendors for completion items & wellhead / xmas tree to share the project requirements and issue statement of requirements allowing for expert input on dedicated equipment specifications.
- For time and cost estimates please refer to the separate “Porthos CCS P18-2 well options cost estimates” document (ECM#198432)

## 5. APPENDICES

### 5.1. Appendix A: generalized stratigraphy of the P18 area

The Mainbuntsandstein formation “Bunter” in Taqa nomenclature is the only stratigraphic interval in the P18a,c area that has producing gas fields. In the nearby P15 production license, the Rijswijk member “Rijn” in Taqa nomenclature and Delft sandstone member “Delfland” in Taqa nomenclature may contain oil.

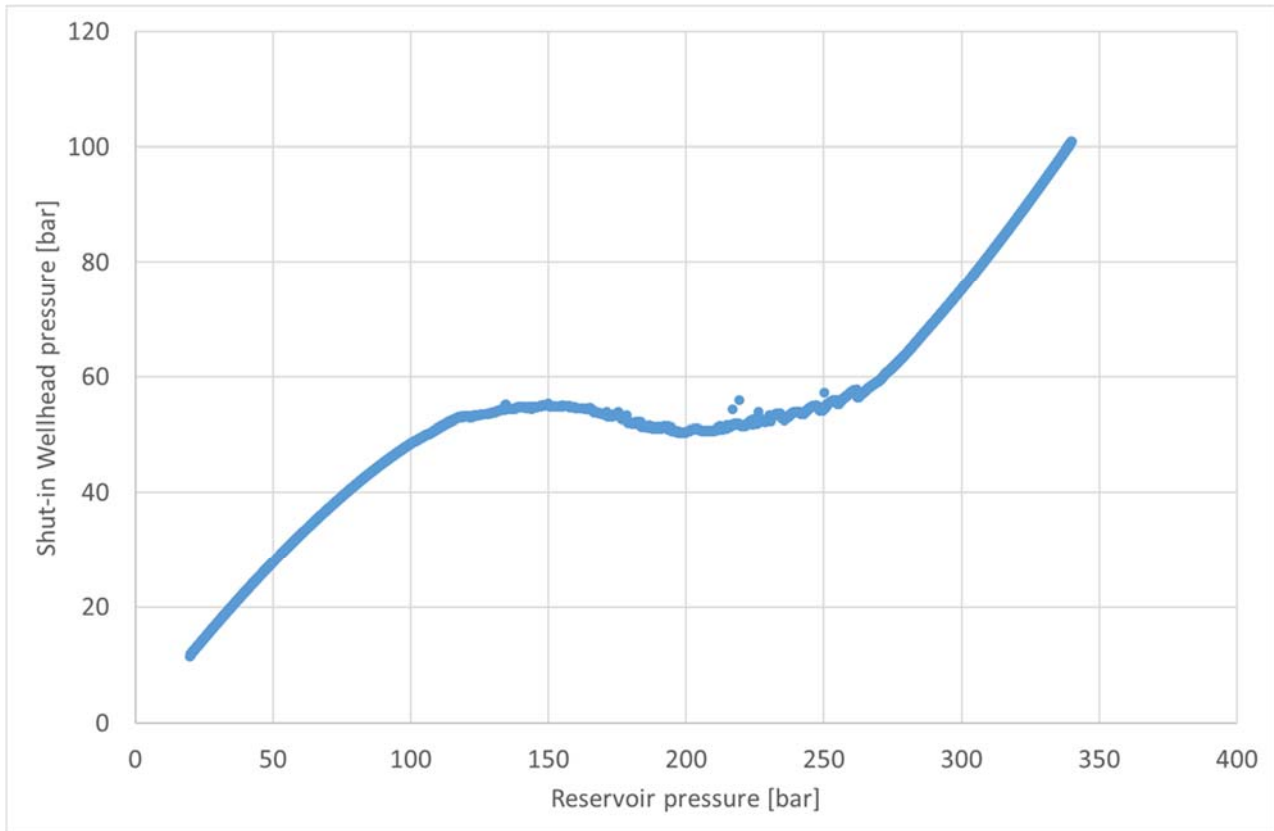
Generalised Stratigraphy of the P18 wells (based on the vertical P18-2 well):

			M TVDSS (+/-)			
Tertiary	Upper North Sea	Undifferentiated	0	The North Sea Group, which consists of siliciclastic sediments. Three major aquifers can be distinguished; the Dongen sand, a basal transgressive sandstone, and the marine Brussels sand and the Berg sand		
		Middle North Sea	Boom Clay		417	
	Berg Sand		456			
	Lower North Sea	Asse Clay	465			
		Brussel sand	489			
		Ieper Clay	530			
		Dongen sand	637			
Landen Clay		870				
Upper Cretaceous	Chalk	Ommelanden Formation	920	Upper Cretaceous Chalk Group, which consist at the base of the formation of sands and marls and a thick layer (900 m) of limestones (Chalk). The distribution of the basal Texel Greensand is limited to the southern basin margin.		
		Texel Marlstone Member	1785			
		Texel Greensand Member	1828			
Lower Cretaceous	Rijnland	Holland	Upper Holland Marl Member	1876	Lower Cretaceous Rijnland Group, which consist of marine sandstones, shales and marls. At the base of the Rijnland Group, the Rijn / Rijswijk sandstone is present. This sandstone is widely distributed in the P18 area. It is also known for its oil (P15) and gas (onshore) accumulations within the West Netherlands Basin. The Rijnland sandstones are interpreted as transgressive sheet sands, with good lateral continuity. The Berkel and IJsselmonde are interpreted as coastal barriers with less lateral continuity. It must be assumed that the Berkel Sand is in connection with the Rijswijk/Rijn member. The IJsselmonde, Berkel and Rijswijk/ Rijn share the same seal which is the Vlieland Claystone and Lower Holland Marl Member.  In the upper part of the Rijnland succession, the Holland Greensand is present. It consists of argillaceous sands and silts. The distribution is limited to the southern margin of the West Netherlands Basin. Although the Holland Greensand has good lateral continuity, permeability is in general low	
			Middle Holland Claystone Member	1996		
			Holland Greensand Member	2056		
		Vlieland	Lower Holland Marl Member	2078		
			Vlieland Claystone Formation	2190		
	IJsselmonde Sandstone Member		2416			
	IJsselmonde Claystone Member		2436			
	Berkel Sandstone Member		2486			
	Jurassic	Schieland	Delfland	Rodenrijs Claystone Member		2544
				Delft Sandstone Member (“Delfland” in Taqa nomenclature)		2562
Altena		Alblasserdam Member	2567			
		Lower Werkendam Member	2573			



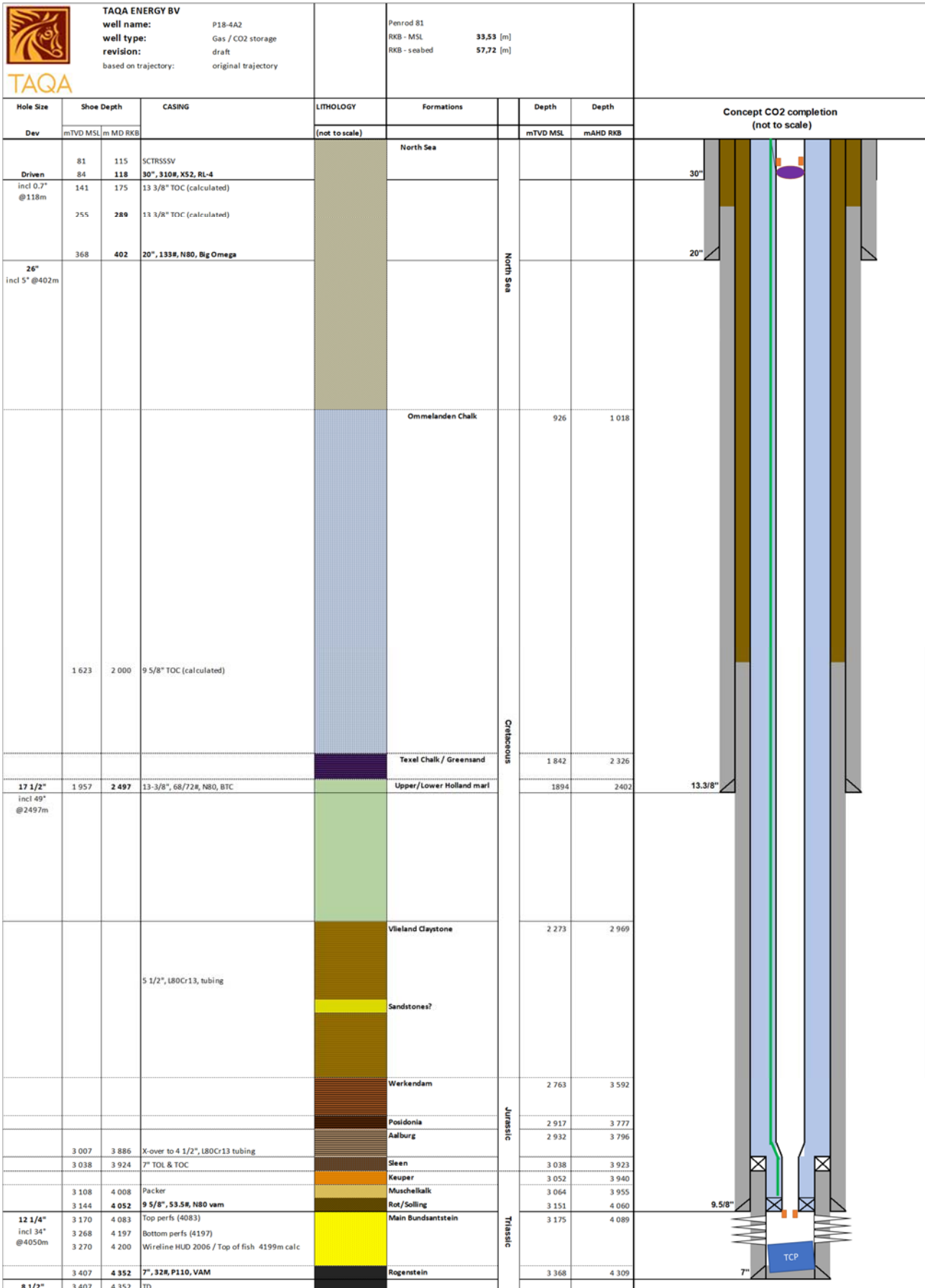
		Posidonia Shale Formation	2747	In the P18-02 well, the Altena Group has a thickness of approx. 500 m.	
		Aalburg Formation	2778		
		Sleen Formation	3036		
Upper Triassic	Upper Germanic Triassic	Upper Keuper Claystone Member	3077	The primary seal to the P18 reservoirs is formed by siltstones, claystones, evaporites and dolostones of the Solling Claystone Member, the Röt Formation, the Muschelkalk Formation, and the Keuper Formation that disconformably overlie the reservoir. The Solling Claystone Member consists of red, green and locally grey claystones that were deposited in a lacustrine setting just after the tectonic movements of Hardegsen phase during a major transgression (Geluk et al., 1996). It is the first laterally extensive claystone above the reservoir rocks of the Main Buntsandstein. In well P18-02, it has a thickness of approx. 5 m (Fig. 11). The Röt Formation consists of thin-bedded claystones, and is approx. 40 m thick. The Muschelkalk Formation consists of claystones, dolomites, and evaporates, and is approx. 70 m thick. All these rocks contain variable amounts of nodular anhydrite cementation (Spain and Conrad, 1997). The Keuper Formation consists of claystones intercalated with zones of anhydrite and gypsum, and is approx. 40 m thick. In total, the thickness of the primary seal in well P18-02 is approx. 155 m.	
		Dolomitic Keuper Member	3086		
		Red Keuper Claystone Member	3111		
		Upper Muschelkalk Member	3123		
		Middle Muschelkalk Marl Member	3145		
		Muschelkalk Evaporite Member	3158		
		Lower Muschelkalk Member	3165		
		Röt Claystone Member	3208		
		Solling Claystone Member	3228		
		Rot Sandstone / Basal Solling Sandstone	3226		Sandstone
Lower Triassic	Lower Germanic Triassic	Main Buntsandstein "Bunter"	Hardegsen Formation	3239	Dominated by reservoir-quality sandstones, depleted gas accumulation
			Detfurth Claystone Member	3308	
			Lower Detfurth Sandstone Member	3338	
			Volpriehausen Clay-Siltstone Member	3349	
			Lower Volpriehausen Sandstone Member	3404	
		Rogenstein Member	3454		
		Main Claystone Member	3547		
Permian	Zechstein	Zechstein Upper Claystone Formation	3595		
		Z1 Fringe Sandstone Member	3605		
		Z1 Middle Claystone Member	3618		
	Rotliegend	Slochteren Formation	3622		
	Carboniferous	Ruurlo Formation	3645		

## 5.2. Appendix B: Static wellhead and reservoir pressures for CO<sub>2</sub> injection well




Source Flow assurance study presentation January 31th 2019, Stefan Belfroid, TNO

### 5.3. Appendix C: Example CO<sub>2</sub> injection completion P18-4A2 well

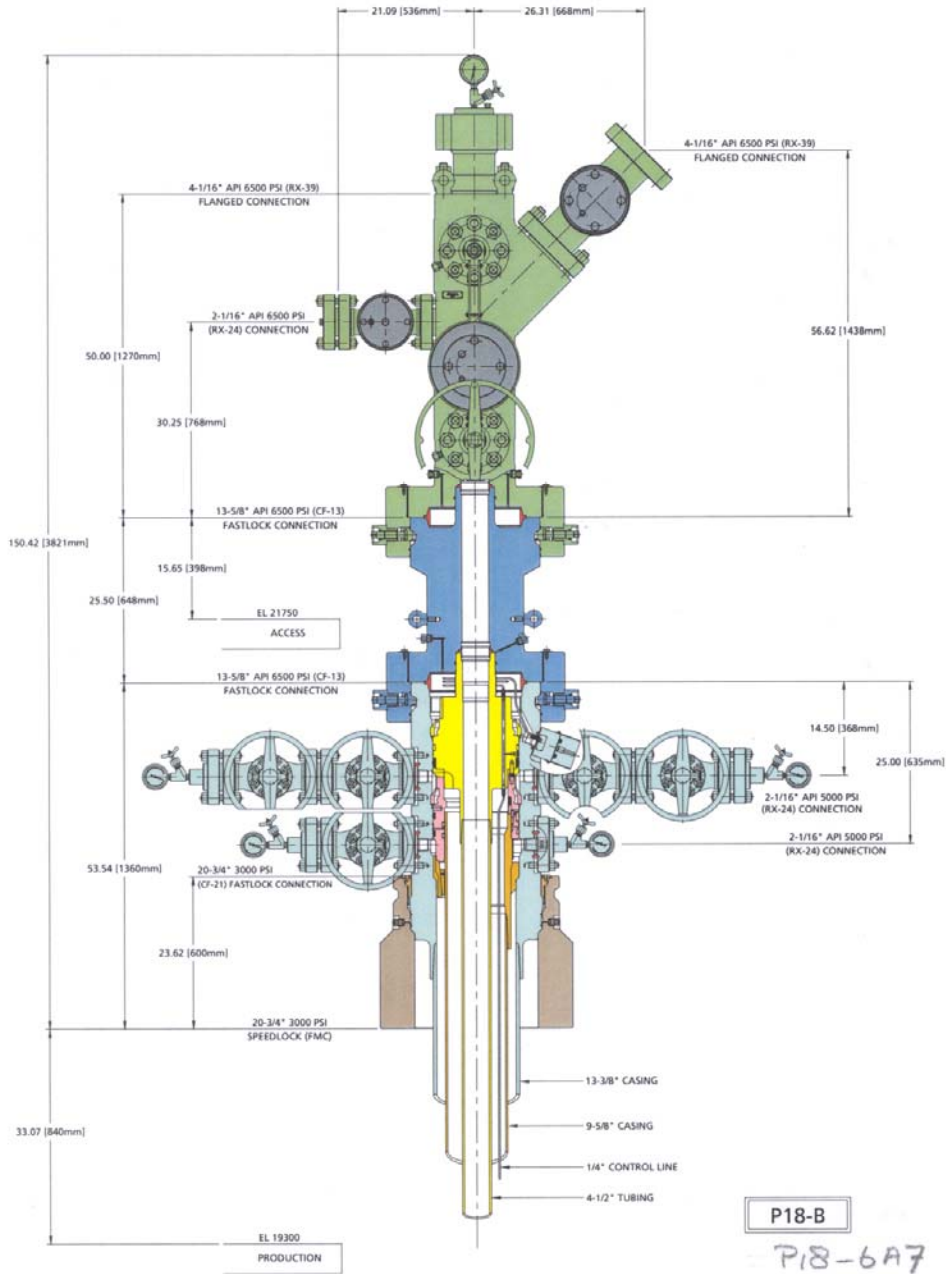


### 5.4. Appendix D: Example CO<sub>2</sub> injection completion P18-2A3 well

 <b>TAQA ENERGY BV</b> well name: P18-2A3z well type: Gas / CO <sub>2</sub> storage revision: draft based on trajectory: original trajectory			Global Marine adriatic III RKB - MSL 47,72 [m] RKB - seabed 71,72 [m]					
Hole Size	Shoe Depth		CASING	LITHOLOGY (not to scale)	Formations	Depth	Depth	Concept CO <sub>2</sub> completion (not to scale)
	Dev	mTVD MSL						
Driven	82	130	TRSCSSV		North Sea			30"
	84	132	30", 310#, X52					
incl 0.5° @132m		103	13 3/8" TOC (calculated)		North Sea			20"
		360	408					
26"	incl 2.3° @408m	378	Sidetrack 16" hole		Ommelanden Chalk		985	13.3/8"
		1560	1806					
17 1/2"	incl 41° @1806m	1560	13-3/8", 72#, N80, BOSS		Texel Chalk / Greensand		2135	
		2130	2632					
12 1/4"	incl 44° @2792m	2198	7" TOL / TOC at 3475 m CBL		Upper/Lower Holland marl		2238	9.5/8"
		2285	2792					
8 1/2"	incl 38° @3211m	3100	5" TOL / TOC		Wieland Claystone		2759	
		3211	3911					
6"		4070	Top perms		Sandstones?			
		4209	Bottom perms					
		4215	HUD, wireline 2014, sample contained salt		Werkendam		3304	
		4301	5", 18#, P110, HFJP					
		4302	TD		Aalburg		3375	
					Sleen		3853	
					Keuper		3905	
					Muschelkalk		3946	7"
					Rot/Solling		4023	
					Main Bundsantstein		4070	
					Rogenstein		4278	5"



<b>Part</b>	<b>Connection</b>	<b>Rating (psi)</b>
Cameron 5 1/8" 5000psi Production tree with manual swab upper and lower master valves and hydraulically actuated wing valve	9" FMC Speedloc	5000
FMC Spacer Spool	13 5/8 FMC Speedloc x 9" FMC Speedloc	5000
FMC 13 5/8" x 13 5/8" Tubing Head Spool	13 5/8" FMC Speedloc x 13 5/8" FMC Speedloc	5000
FMC 20 3/4" x 13 5/8" Intermediate Casing Head Housing	20 3/4" FMC Speedloc x 13 5/8" FMC Speedloc	5000
FMC Sliploc type casing head	20 3/4" FMC Speedloc	3000

**P18-6A7 wellhead and tree**

**BP - NETHERLANDS**

**CUSTOMER ASSEMBLY DETAILS: 13-5/8" 5000 PSI SSMC 2 STAGE COMPACT HOUSING. 13-5/8" 6500 PSI SPACER SPOOL. 4-1/8" 6500 PSI XMAS TREE. 30" CONDUCTOR x 20" x 13-3/8" x 9-5/8" CASING x 4-1/2" TUBING. ONE CONTROL LINE**

SK-118853-01

Part	Connection	Rating (psi)
Cameron 4 1/16" 6500psi production tree with manual swab upper and lower master valves and hydraulically actuated wing valve	13 5/8" Cameron Fastlock	6500
Cameron Spacer Spool	13 5/8" Fastlock x 13 5/8" Fastlock	6500
Cameron 13 5/8" x 13 5/8" SSMC dual stage wellhead	13 5/8" Cameron Fastlock x 20 3/4" Cameron Fastlock	5000
X-over from Cameron to FMC	20 3/4" FMC Speedloc x 20 3/4" FMC Speedloc	3000
FMC Sliploc type casing head	20 3/4" FMC Speedloc	3000



# **P18 Subsidence Evaluation**

**Rapport voor TAQA Energy BV**

Fenix Consulting Delft BV  
C.J. de Pater

Datum  
October 2019



# **P18 Subsidence Evaluation**

Rapport voor TAQA Energy BV

Datum  
October 2019

## **DISCLAIMER**

**Fenix Consulting Delft nor any person acting on behalf of Fenix:**

- **Makes any warranty or representation, express or implied, with respect to the accuracy, completeness, or usefulness of the information contained in this report, or that the use of any apparatus, method, or process disclosed in this report may not infringe privately owned rights; or**
- **Assumes any liability with respect to the use of, or for damages resulting from the use of, any information, apparatus, method, or process disclosed in this report.**

# Executive Summary

The P18 fields will induce seabed subsidence during depletion, which is almost complete. In the injection phase for CO<sub>2</sub> storage, the seabed will rebound, which may only be partial since reservoir rocks often show less rebound compared with compaction during primary depletion.

The subsidence and uplift were computed with the so-called nucleus of strain method developed by Geertsma and Van Opstal. The subsidence evaluation uses the Eclipse grid and from each cell the contribution to total subsidence is added. The effect of a cell is proportional to compaction coefficient, pressure change and cell volume. The compaction coefficient has been computed from the Young's modulus used in the TNO design study of 18GPa and a Biot coefficient of 1.

## Conclusions

- Subsidence at the platform during primary depletion is modest at 0.076m (7.6cm). The maximum subsidence is 0.101m (10.1cm).
- Rebound at the platform during CO<sub>2</sub> injection is 0.076m (7.6cm) when pressure is restored to virgin pressure.
- For partial rebound due to hysteresis of reservoir stiffness, the uplift would be 0.03m (3cm) at virgin pressure.

# Contents

<b>EXECUTIVE SUMMARY .....</b>	<b>III</b>
Contents.....	iv
List of Figures .....	v
List of Tables.....	v
Nomenclature .....	vi
<b>1 INTRODUCTION .....</b>	<b>1</b>
<b>2 RESERVOIR PROPERTIES AND PRESSURE HISTORY.....</b>	<b>4</b>
<b>3 SUBSIDENCE CALCULATION.....</b>	<b>5</b>
Results .....	5
References .....	9

## List of Figures

Figure 1: Overview of the locations of P15 and P18 fields (After TAQA, 2009).....	1
Figure 2: Overview of the three P18 fields (P18-2, P18-4, and P18-6), and the blocks of the P18-2 Field (2-I, 2-II, 2-III, and 2-IV). Red line indicates the position of the cross section shown in Figure 4...1	1
Figure 3: Lithology of the Triassic P18-2 field and overburden. The Hardegsen (Top Bunter) and Detfurth layers comprise the reservoir with a small contribution from the tight Volpriehausen layer. ...2	2
Figure 4: Cross section through the P18-2 field, showing block 2-I with initial water saturation. The location of the cross section is shown in Figure 2. ....2	2
Figure 5: P18 Compartments with FIP numbers assigned to them. ....3	3
Figure 6: Logs and lithology in well P18-04A2. DSI readings from log displays were used to compute the modulus in overburden and reservoir. ....4	4
Figure 7: Maximum subsidence due to depletion of the P18-2 field.....6	6
Figure 8: Maximum subsidence due to depletion of the P18-2 and P18-4 fields.....7	7
Figure 9: Maximum subsidence due to depletion of the P18-2, P18-4 and P18-6 fields. ....7	7
Figure 10: Subsidence at the platform location vs. depletion and repressurization of the P18-2, P18-4 and P18-6 fields. In the case of reservoir hysteresis only 40% of the compaction during depletion is recovered as rebound. ....7	7
Figure 11: Uplift at the platform location vs. depletion and repressurization of the P18-2, P18-4 and P18-6 fields. In the case of reservoir stiffness hysteresis only 40% of the compaction during depletion is recovered as rebound. ....8	8

## List of Tables

Table 1: Reservoir properties. Most properties apply to all three fields, but the pressure and stress changes apply to P18-2. The pressure for the other fields is listed in Table 2. ....4	4
Table 2: Reservoir pressures per field. ....5	5
Table 3: Total Subsidence and uplift (in mm) of platform as a function of pressure. ....8	8
Table 4: Subsidence at the platform and maximum subsidence for different scenarios. Three different scenarios were computed: including all grid cells, only active cells and all cells, but the Volpriehausen cells below the GWC were excluded. ....8	8

## Nomenclature

Units: SI (m= metre, s= second, kPa = $10^3$ Pa, MPa = $10^6$ Pa, GPa = $10^9$ Pa)

Dimensions: m= mass, L= length, t= time

Variable	Description	Units	Dimensions
$A_p$	: Poroelastic coefficient	[-]	(-)
$E$	: Young's modulus	[GPa]	(m/Lt <sup>2</sup> )
$p$	: pressure	[MPa]	(m/Lt <sup>2</sup> )
$V_{res}$	: reservoir volume	[m <sup>3</sup> ]	(L <sup>3</sup> )
$\alpha_B$	: Biot coefficient	[-]	(-)
$\nu$	: Poisson's ratio	[-]	(-)

# 1 Introduction

TAQA is planning (with PORTHOS partners) to use the depleted P18 fields for CO2 storage. The location of the fields and the various reservoir compartments are shown below, Figure 1. The various compartments are indicated in the map of Figure 2. The P18-2 field consists of several compartments, while the P18-4 and P18-6 fields consist of a single compartment. The latter fields are isolated from the P18-2 field.

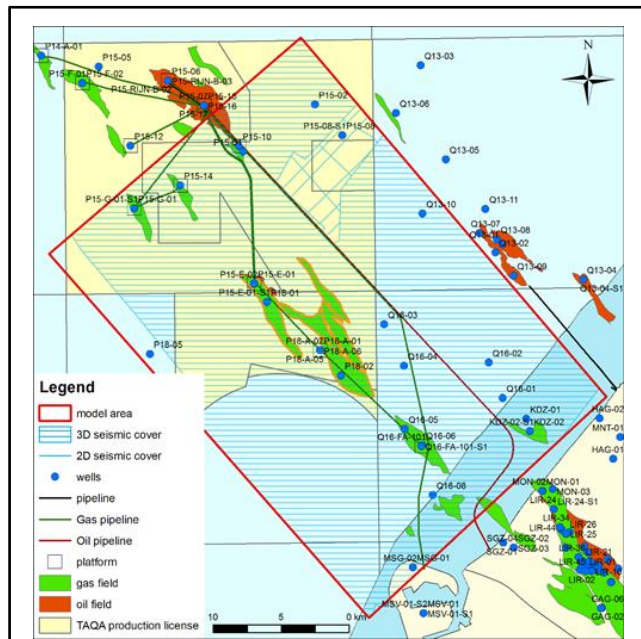


Figure 1: Overview of the locations of P15 and P18 fields (After TAQA, 2009).

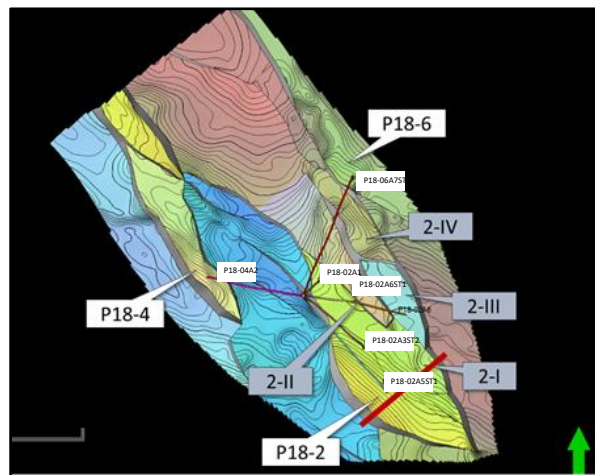
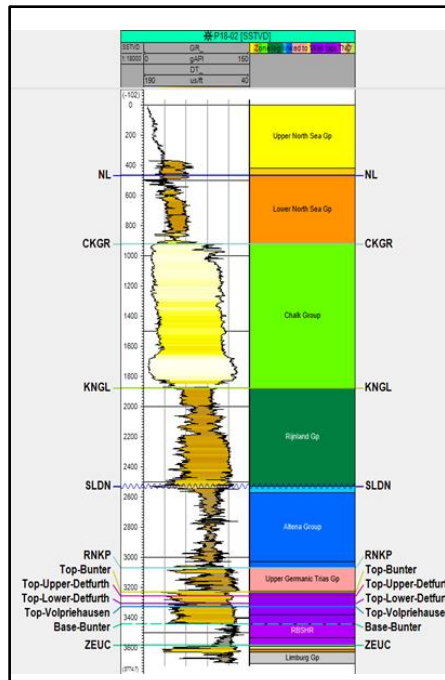


Figure 2: Overview of the three P18 fields (P18-2, P18-4, and P18-6), and the blocks of the P18-2 Field (2-I, 2-II, 2-III, and 2-IV). Red line indicates the position of the cross section shown in Figure 4. (TNO, 2019)

The reservoirs belong to the Triassic Buntsandstein and consist of the Hardegsen, Upper and Lower Detfurth and Volpriehausen. The tight Volpriehausen layer gives only a small contribution to the reservoir storage capacity. However, the full reservoir height of some 220m is included in the geomechanical analyses since these layers will all deplete or repressurize over time.

Figure 4 shows a typical cross-section through the P18-2 field with the bounding faults. The different compartments are shown in Figure 5, which will be used to select the compartments of the P18-2, P18-4 and P18-6 fields for the subsidence evaluation.



**Figure 3: Lithology of the Triassic P18-2 field and overburden. The Hardegsen (Top Bunter) and Detfurth layers comprise the reservoir with a small contribution from the tight Volpriehausen layer. (TNO, 2019)**

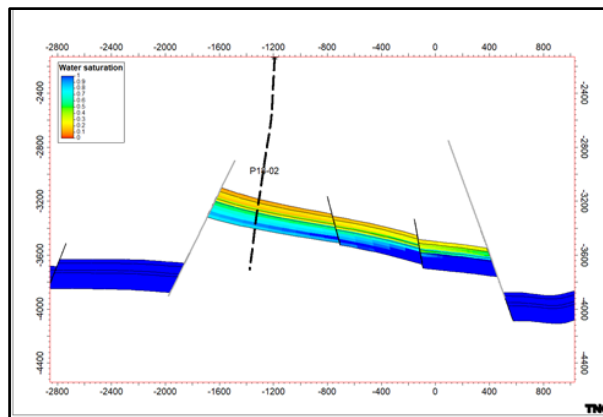


**Figure 4: Cross section through the P18-2 field, showing block 2-I with initial water saturation. The location of the cross section is shown in Figure 2. (TNO, 2019)**

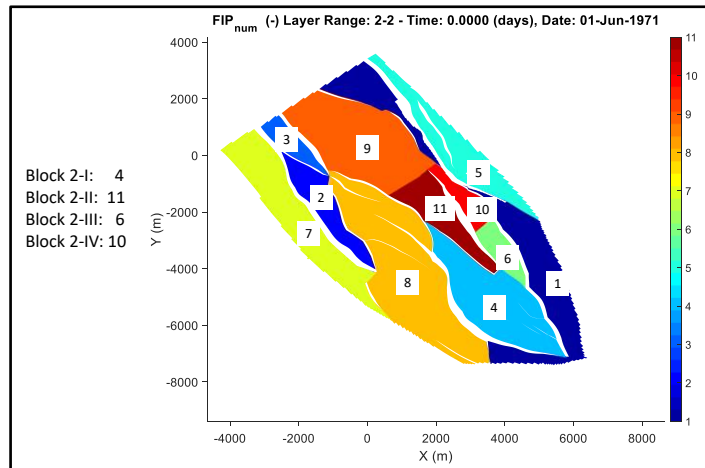


Figure 5: P18 Compartments with FIP numbers assigned to them.



## 2 Reservoir properties and pressure history

The Buntsandstein reservoirs are conventional gas reservoirs with fairly good porosity and permeability. The Young's modulus was determined from a dipole shear sonic log, shown in Figure 6. The average value of the modulus over the reservoir is 37GPa, assuming a ratio of static to dynamic modulus of 75%. We obtain a higher value of the modulus than used in the TNO study, but the lower estimate of 18 GPa will be used, which is equivalent to a conservative estimate of compaction. The reservoir properties are listed in Table 1.

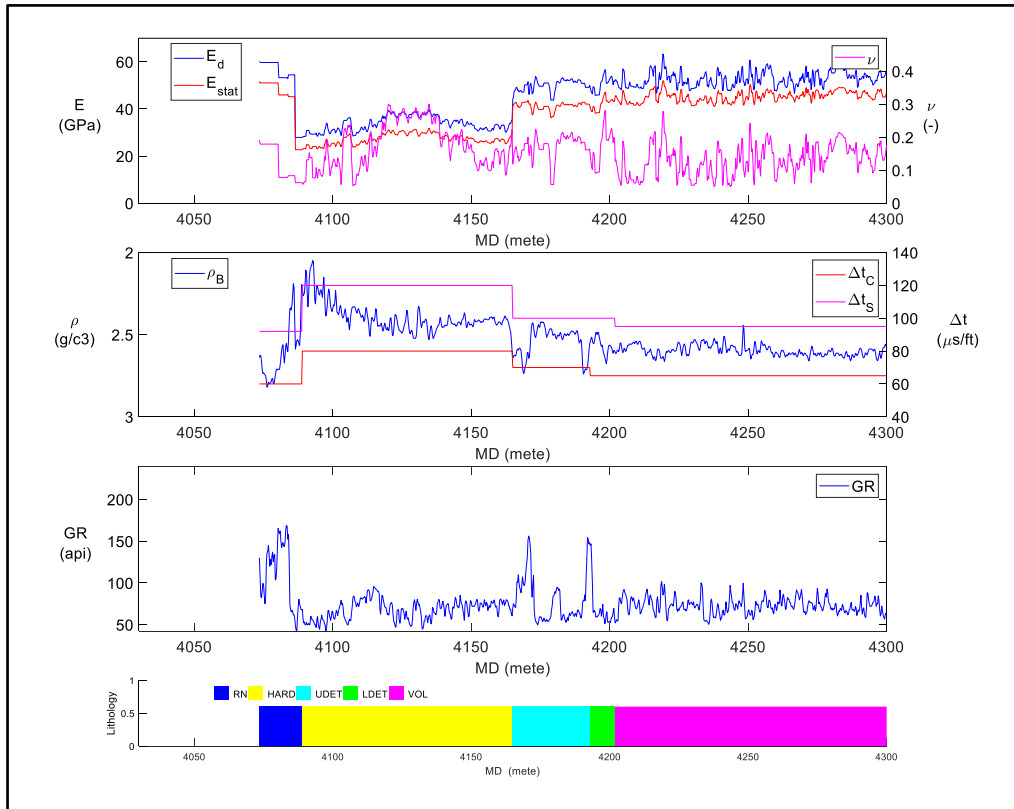


Figure 6: Logs and lithology in well P18-04A2. DSI readings from log displays were used to compute the modulus in overburden and reservoir.

Table 1: Reservoir properties from TNO report (2019), except for stress which was determined from LOT and frac injections. Most properties apply to all three fields, but the pressure and stress changes apply to P18-2. The pressure for the other fields is listed in Table 2.

Modulus		18	GPa	Virgin pressure	375	bar
Poisson ratio		0.25		Depleted pressure	20	bar
Biot Coefficient		1		Pressure drop	-355	bar
Compaction coefficient		0.046	1/GPa	Thermal expansion coefficient	1.00E-05	1/C
Depth		3500	m	Temperature drop	-90	C
Horizontal stress ratio		0.43		Thermal stress coefficient	2.4	bar/C
Stress path coefficient		0.60		Thermal stress drop	-216	bar
Vertical stress gradient		20.30	kPa/m	Poroeleastic coefficient	0.67	
Minimum horizontal stress gradient		14.84	kPa/m	Poroeleastic stress drop	-237	bar
Reservoir pressure gradient		10.71	kPa/m	Stress gradient drop	-6.8	kPa/m

### 3 Subsidence Calculation

Decreasing pressure causes higher effective stress on the reservoir rock so that the rock compacts. A fairly accurate estimate of the reservoir compaction can be obtained by summing the effect of a small volume of the reservoir over the entire reservoir volume (Geertsma, 1973).

For uniaxial compaction the reservoir height change is given by:

$$\Delta H_{res} = c_m \Delta p_{res} H_{res} \quad (1)$$

The surface deformation due to the pore pressure distribution in the reservoir can be calculated by summing the effect of a small volume of the reservoir over the entire reservoir volume. The small volume can be considered as a source (or nucleus) of strain. The surface subsidence can be written as:

$$u_z = \frac{c_m (1-\nu)}{\pi} \frac{d}{(r^2 + d^2)^{3/2}} \Delta V \Delta p_{res} \quad c_m = \alpha_B \frac{(1+\nu)(1-2\nu)}{(1-\nu)E} \quad (2)$$

Where:  $d$ : depth,  $r$ : distance from nucleus, along the surface,  $c_m$ : compaction coefficient,  $\nu$ : Poisson Ratio,  $\Delta p_{res}$ : reservoir pressure change,  $\Delta V$ : volume of nucleus,  $\alpha_B$ : Biot constant,  $E$ : Young's modulus. For a circular reservoir of height  $h$  the subsidence is given by:

$$u_z = 2c_m (1-\nu) h \Delta p_{res} \int_0^\infty e^{-\eta u} J_0(u) J_1(\rho u) du \quad (3)$$

Where:  $\eta = d/R$  and  $\rho = r/R$ ,  $J_0$ : Bessel function of order zero,  $J_1$ : Bessel function of order one.

Alternatively, Eqn 2 can also be directly used to compute subsidence from a pressure simulation. The pressure in each grid block is then used to compute its contribution to subsidence and the sum over all grid cells yields the total subsidence. This can also be done for each time step so that the subsidence (or uplift) is obtained over the course of reservoir recovery.

The method that Opstal developed to take into account the relative stiffness of the underburden was used to apply the nucleus of strain approach to subsidence. The semi-analytical method published by van Opstal was derived for a fixed Poisson Ratio of 0.25. The optimization of the coefficients for other values of the Poisson Ratio outlined in the paper by Van Opstal was used to generalize the computation for any value of the Poisson Ratio.

**Table 2: Reservoir pressures per field.**

	P18-2 (bar)	P18-4 (bar)	P18-6 (bar)
Initial pressure	375	340	377
End production / start injection pressure	20	20	45
90 hydrostatic pressure	316	290	321
100 hydrostatic pressure	351	322	357
Initial pressure	375	340	377

### Results

Two Petrel models and an Eclipse model were provided from which the Eclipse grids of the reservoir were extracted:

- P18\_TNO\_2019-07-21 Stripped (2019-05-15).pet
- P18-6\_reservoir(20190911)\_clean4EBN.pet
- runL28\_FC with CASEL6

Using the grid coordinates per cell, the cell volume was computed and the subsidence was computed over an area around the reservoirs. The first Petrel model contained only the P18-2 and P18-4 fields and the second Petrel model contained the P18-6 field and the Eclipse model contained the pressures computed for the depleted state. The latter pressure distribution was used to compute the reservoir compaction of P18-6.

For reservoir simulation some cells can be made inactive when they have low permeability or porosity. However, even tight layers will be depleted over time and contribute to compaction. So, the subsidence was computed for all cells in the reservoir grid and for the active cells. For P18-2 and P18-4 fields this gave a different result while P18-6 included all cells so only the results for all cells was computed. For P18-6 all cells were active, but the water leg is large and does not contribute to subsidence since it is very tight. So, for P18-6 one scenario is uniform pressure excluding the water leg, but the most accurate estimate is based on simulated pressures. It was found from reservoir simulation that the water bearing part of the Volpriehausen layer does not follow the gas pressure, so that should be excluded from the subsidence computation. All results are listed in Table 4, but the result that excluded the Volpriehausen water leg is plotted in the figures.

For the P18-2 field the subsidence contours are shown in Figure 7 for the scenario in that only excluded the water leg. Subsidence would be reversed for elastic behavior of the reservoir but it is generally observed that after compaction of rock, the rebound is much less due to inelastic behavior. For instance, in the Bergermeer gas storage only a partial rebound was observed after repressurization compared with initial subsidence.

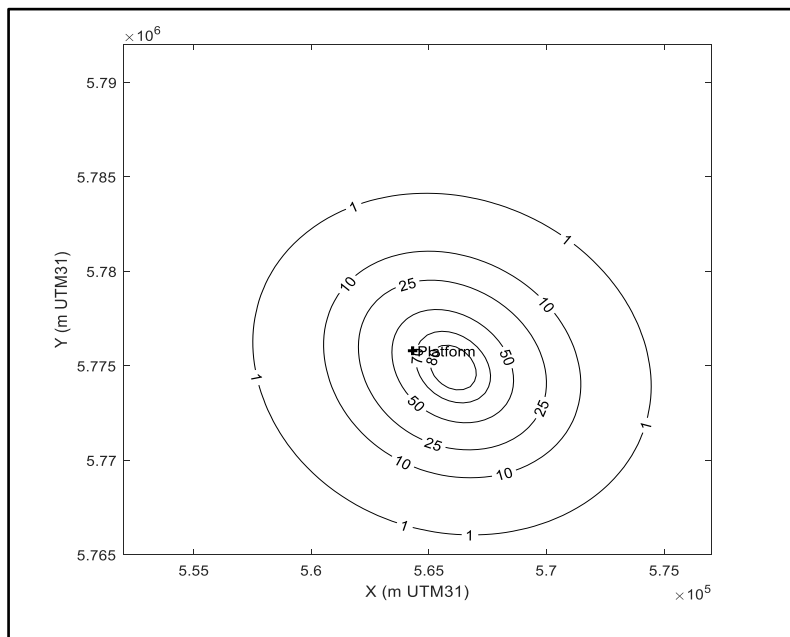


**Figure 7: Maximum subsidence due to depletion of the P18-2 field.**

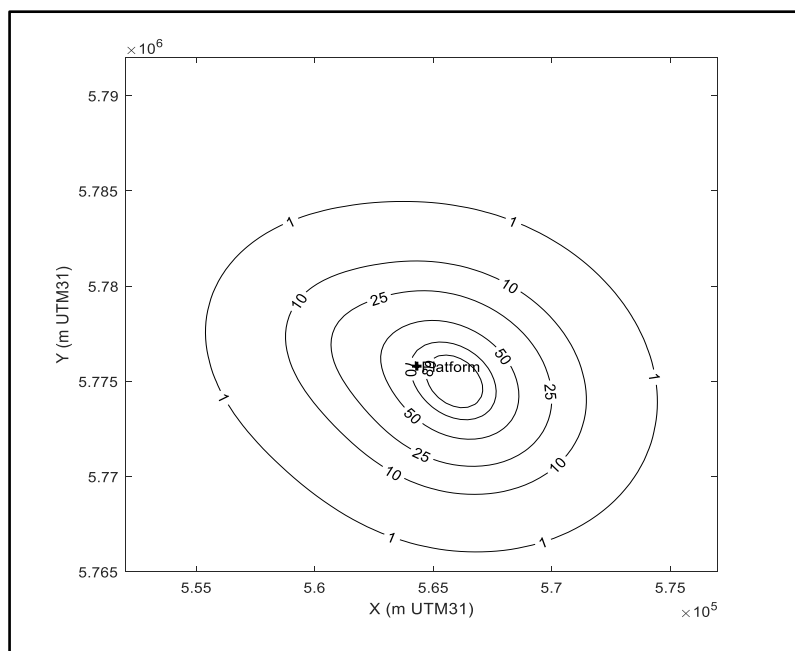


**Figure 8: Maximum subsidence due to depletion of the P18-2 and P18-4 fields.**

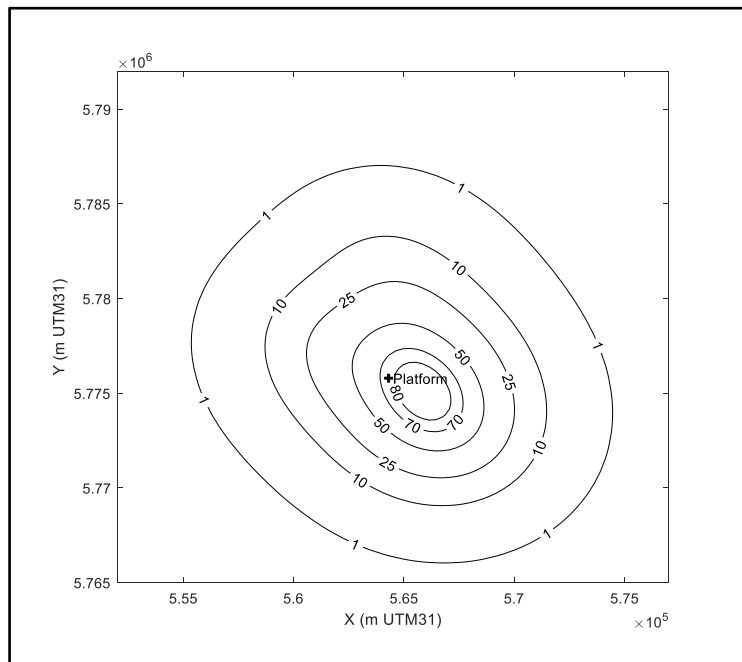


**Figure 9: Maximum subsidence due to depletion of the P18-2, P18-4 and P18-6 fields.**

Therefore, the rebound is given for elastic behavior, which would give a maximum uplift of 7.6cm. As a lower bound hysteresis would give an uplift of only 3cm, which corresponds with 2.5 times larger stiffness during rebound.

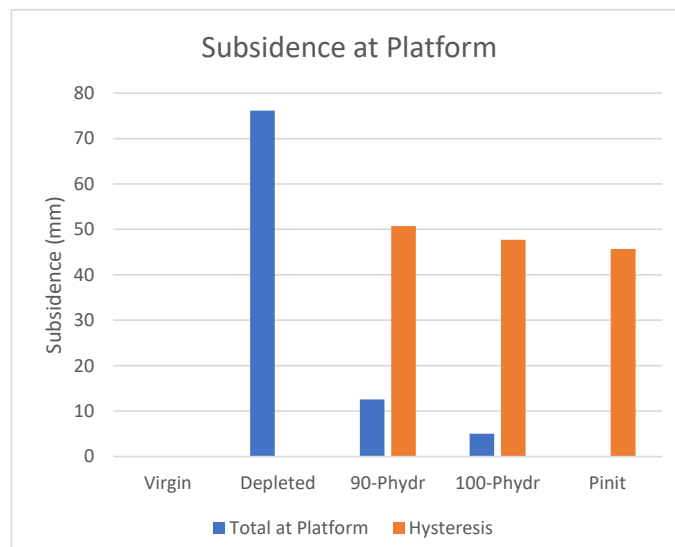


**Figure 10: Subsidence at the platform location vs. depletion and repressurization of the P18-2, P18-4 and P18-6 fields. In the case of reservoir hysteresis only 40% of the compaction during depletion is recovered as rebound.**

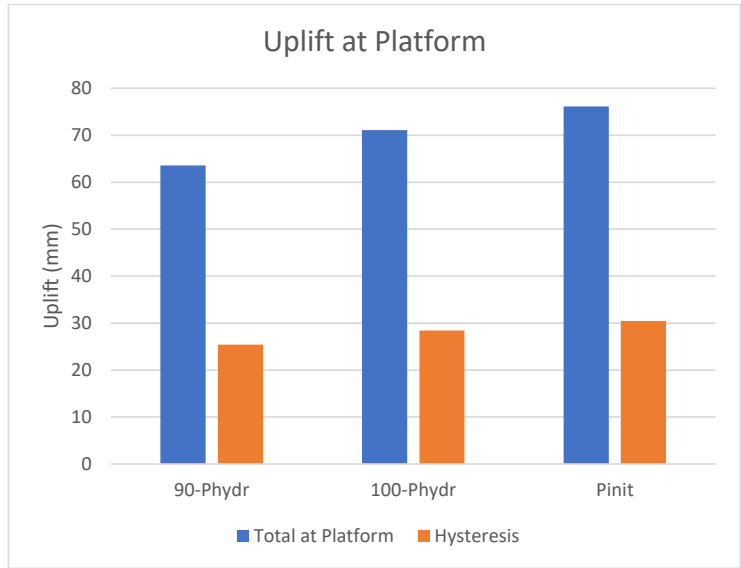


**Figure 11: Uplift at the platform location vs. depletion and repressurization of the P18-2, P18-4 and P18-6 fields. In the case of reservoir stiffness hysteresis only 40% of the compaction during depletion is recovered as rebound.**

**Table 3: Total Subsidence and uplift (in mm) of platform as a function of pressure for the scenario that excluded only the water leg for P18-2 and P18-4. For P18-6 the simulated pressure was used.**

	P18-2	P18-4	P18-6	Total at Platform	Hysteresis	Uplift Platform	Hysteresis
Initial pressure bar	375	340	377	0			
End production / start injection pressure bar	20	20	45	76			
90 hydrostatic pressure bar	316	290	321	13	60	64	16
100 hydrostatic pressure bar	351	322	357	5	58	71	18
Initial pressure bar	375	340	377	0	57	76	19

**Table 4: Subsidence at the platform and maximum subsidence for different scenarios. Three different scenarios were computed: including all grid cells, only active cells and all cells excluding the Volpriehausen cells below the GWC were excluded. For P18-6 all cells were active, but the water leg is large and does not contribute to subsidence since it is very tight. So, for P18-6 one scenario is uniform pressure excluding the water leg, but the most accurate estimate is based on simulated pressure**

Scenario		Subsidence at platform (mm)	Maximum subsidence (mm)
P18-2	All cells	71	89
P18-2	Active	65	81
P18-2	NoWL	67	87
P18-4	All cells	10	26
P18-4	Active	9	24
P18-4	NoWL	7	16
P18-6	NoWL	4	11
P18-6	All cells-Psim	2	12
P18-2 & 4	All cells	81	93
P18-2 & 4	Active	74	84
P18-2 & 4	NoWL	74	89
P18-2 & 4 & 6	All Cells-No WL	76	101

## References

- Geertsma, J. and van Opstal, G. (1973). A Numerical Technique for Predicting Subsidence Above Compacting Reservoirs, Based on the Nucleus of Strain Concept. *Verh. Kon. Ned. Geol. Mijnbouwk. Gen.*, 28, pp. 63-78.
- TNO, (2019), “CO2 storage feasibility in the P18-2 depleted gas field”, August 2019, TNO report 11111, Authors: Neele, F, T. Wildenborg, K. Geel, D. Loeve, L. Peters, S. Kahrobaei, T. Candela, M. Koenen, P.Hopmans, K. van der Valk, B. Orlic, V. Vandeweyer.



# **P18 CCS: Seismic Risk Evaluation**

**Report for TAQA Energy BV**

Fenix Consulting Delft BV  
C.J. de Pater

Date  
November 2019

# **P18 CCS: Seismic Risk Evaluation**

Report for TAQA Energy BV

Date  
November 2019

## **DISCLAIMER**

**Fenix Consulting Delft nor any person acting on behalf of Fenix:**

- **Makes any warranty or representation, express or implied, with respect to the accuracy, completeness, or usefulness of the information contained in this report, or that the use of any apparatus, method, or process disclosed in this report may not infringe privately owned rights; or**
- **Assumes any liability with respect to the use of, or for damages resulting from the use of, any information, apparatus, method, or process disclosed in this report.**



# Executive Summary

TAQA is planning (with PORTHOS partners) to use the depleted P18 fields for CO<sub>2</sub> storage. The location of the fields is just offshore Hoek van Holland.

The various compartments are distinguished as several fields: the P18-2 field (consisting of several compartments), while the P18-4 and P18-6 fields consist of a single compartment. The P18-2 field is isolated from the P18-4 field, which has a much shallower GWC.

Seismicity is mainly a concern because it may lead to upward migration of CO<sub>2</sub> if fault slippage enhances conductivity of the faults. Since the fields are more than 5km from the shoreline, there are no vulnerable surface structures that might be damaged by earthquakes.

In gas fields, the main source of seismicity is differential compaction that causes stress concentrations on the faults. As yet, the reservoirs have been strongly depleted but no recorded seismicity was induced. Upon injection, the reservoir pressure will be restored so that stability of the faults is improved. Other mechanisms of seismicity could be local pressure changes during CO<sub>2</sub> injection and cooling of the reservoir due to injected gas expansion into the low-pressure reservoir.

The excess pressure will be very low, so this is unlikely to induce seismicity. However, extensive cooling will reduce the stress because of reservoir shrinkage. Some injectors are only a few hundred meters from a fault, so the cold front could reach the fault after several years. Fortunately, the thermal stress effect is similar to the differential compaction effect, although thermal stress reduces confining stress on the fault while differential compaction mainly increases shear stress. However, the slippage condition is equivalent and therefore the probability of seismicity by thermal stress reduction is deemed low since no seismicity was observed during compaction of the fields. Although, the CO<sub>2</sub> injection carries a potential hazard of induced seismicity, it follows from the analysis that the probability of seismicity is low and therefore risk is negligible.

Compared with analogous CO<sub>2</sub> injection projects like Sleipner (North Sea), In Salah (Algeria) or Weyburn (Canada), the P18 project falls in a class of low probability of seismicity. In the In Salah project, some weak seismicity was induced (of magnitude 1.7) but this is a low-permeability aquifer that had significant pressure increase. In the Sleipner project, CO<sub>2</sub> is injected into a huge high-permeability aquifer, which ensures that pressure changes are small. This is similar to injection into a depleted gas field like P18, where the excess injection pressure changes are also small so that geomechanical effects are small.

## Conclusions

- The P18 fields have been almost depleted and the reservoir properties also indicate that compaction induced seismicity might be possible. However, no seismicity has been observed, so that maximum magnitude of any seismicity should be less than 1.5.
- Since pressure will be restored during CO<sub>2</sub> injection and no seismicity was induced during depletion, the risk of seismicity during injection is deemed negligible (Teatini *et al.*, 2019).
- Since no seismicity has been observed, the fields fall in the class of negligible risk, so that only monitoring with the regional network is required.
- Fracture propagation during injection is unlikely, but due to thermal stress reduction a fracture could be propagated from the injector, if the modulus or thermal expansion coefficient is higher than expected.
  - An injection fracture will be confined to the cooled zone and it will also propagate along the major faults, in view of the stress orientation. Therefore, hitting a fault or breaching the overburden or underburden is very unlikely.
- Local pressure increase by injection is quite small, so that geomechanical effects of pressure will be negligible. The restoration of pressure will be up to virgin pressure so that stability of the faults is actually improved. In this sense, the P18 field falls in the low-risk category of worldwide CO<sub>2</sub> storage projects, analogous to the Sleipner storage project in the Norwegian sector of the North Sea.

# Contents

<b>EXECUTIVE SUMMARY .....</b>	<b>III</b>
Contents.....	iv
List of Figures .....	v
List of Tables.....	vi
Nomenclature .....	vii
<b>1 INTRODUCTION .....</b>	<b>1</b>
<b>2 MECHANISMS OF SEISMICITY .....</b>	<b>4</b>
<b>3 RESERVOIR PROPERTIES, PRESSURE AND FAULT SYSTEM .....</b>	<b>6</b>
Fault System.....	8
<b>4 STRESS ANALYSIS .....</b>	<b>14</b>
<b>5 FRACTURE SIMULATIONS.....</b>	<b>16</b>
<b>6 RISK ANALYSIS .....</b>	<b>18</b>
Injection Seismicity Risk Analysis.....	22
Risk Classification.....	25
Discussion .....	26
<b>REFERENCES .....</b>	<b>26</b>

## List of Figures

Figure 1: Overview of the locations of P18 and nearby P15 fields (After TAQA, 2009). .....	1
Figure 2: Overview of the three P18 fields (P18-2, P18-4, and P18-6), and the blocks of the P18-2 Field (2-I, 2-II, 2-III, and 2-IV). Red line indicates the position of the cross section shown in Figure 4 (TNO, 2019). .....	1
Figure 3: Lithology of the Triassic P18-2 field and overburden. The Hardegsen (Top Bunter) and Detfurth layers comprise the reservoir with a small contribution from the tight Volpriehausen layer (TNO, 2019). .....	2
Figure 4: Cross section through the P18-2 field, showing block 2-I with initial water saturation. The location of the cross section is shown in Figure 2 (TNO, 2019). .....	2
Figure 5: Correlation between size of rupture area (for a square area) and earthquake magnitude. Using seismic traces the size of the slip area and the stress drop can be inferred. These slip area dimensions are plotted for depletion earthquakes in Bergermeer and Groningen. For a computed maximum slip area, the empirical relation gives a conservative estimate of magnitude. The TNO correlation is based on a theoretical relation and is more conservative. ....	4
Figure 6: Map of gas fields in the Netherlands. Induced earthquakes in the Netherlands are concentrated in two areas: one near the Groningen gas field and another near the Bergermeer field and neighbouring fields that lie on the same trend. The P18 fields belong to a trend of gas fields, extending from Zuid-Holland to offshore P18 and P15 blocks (West-Netherlands Basin) that are seismically quiet. ....	5
Figure 7: Logs and lithology in well P18-04A2. DSI readings from log displays were used to compute the modulus in overburden and reservoir. The Hardegsen reservoir has lower modulus than the overburden. ....	6
Figure 8: Stress gradients derived from P18-1 logs and LOT pressures as well as fracture gradients determined in nearby P15 and P12 fracture injection PFO's. The logs in the P18-2 well yielded the same result for the reservoir stress. ....	7
Figure 9: Stress orientation in the North Sea area near P18 (World Stress Map, 2016). ....	8
Figure 10: Faults in the P18-2 field, with well P18-2-A5. The dashed line indicates the cross-section along the minimum stress direction. ....	9
Figure 11: Faults in a cross-section through well P18-2-A5 along the minimum stress direction. The red ellipse indicates the injection interval. ....	9
Figure 12: Faults in the P18-2 field, with well P18-2-A1. The dashed line indicates the cross-section along the maximum stress direction. ....	10
Figure 13: Faults in a cross-section through well P18-2A1 along the minimum stress direction. The red ellipse indicates the injector. ....	10
Figure 14: Faults in a cross-section through well P18-2A1 along the maximum stress direction. The red ellipse indicates the injector. ....	10
Figure 15: Faults in the P18-2 field, with well P18-2A3. The dashed line indicates the cross-section along the minimum stress direction. ....	11
Figure 16: Faults in a cross-section through well P18-2A3 along the minimum stress direction. The red ellipse indicates the injector. ....	11
Figure 17: Faults in a cross-section through well P18-2A3 along the maximum stress direction. The red ellipse indicates the injector. ....	11
Figure 18: Faults in the P18-4 field, with well P18-4A2. The dashed line indicates the cross-section along the minimum stress direction. ....	12
Figure 19: Faults in the P18-4 field, in a cross-section through well P18-4A2 along the minimum stress direction. The red ellipse indicates the Injection interval in well. ....	12

Figure 20: Faults in the P18-6 field, with well P18-6A7ST1. The dashed line indicates the cross-section along the minimum stress direction. ....	13
Figure 21: Faults in a cross-section through well P18-6A7ST1 along the minimum stress direction. The red ellipse indicates the injector. ....	13
Figure 22: Critical excess pressure above reservoir pressure that is needed to destabilize a fault in the virgin state. ....	14
Figure 23: Critical excess pressure above reservoir pressure that is needed to destabilize a fault, after depletion. ....	14
Figure 24: Mohr Coulomb plot for stresses after depletion in the P18-2 reservoir. For a critically oriented fault, instability could occur with an excess pressure of 5.3MPa in the fault. ....	15
Figure 25: Mohr Coulomb plot for virgin stresses in the P18-2 reservoir. Also, the effect of depletion and cooling by CO <sub>2</sub> injection is plotted. ....	15
Figure 26: Pressure in base case fracture simulation for CO <sub>2</sub> injection into P18-2 field. Since the pressure is much lower than the stress, no fracture propagation is possible. Only if the thermal stress would fall below the BHP a fracture could propagate. ....	16
Figure 27: Pressure in fracture simulation for CO <sub>2</sub> injection into P18-2 field for higher modulus of 30GPa. Since thermal stress is proportional to the modulus, the lower stress facilitates fracturing after a few months injection. ....	17
Figure 28: pressure and temperature fronts in the simulation with fracturing. In agreement with detailed CO <sub>2</sub> simulations, the cold front extends over several hundred meters after 5 years and after 1 year the extent is some 50 m which facilitates an 80 m fracture length. ....	17
Figure 29: Fracture size vs. time, for simulation with high modulus of 30GPa. ....	17
Figure 30: Risk map with surface risk index on the horizontal axis and subsurface risk index on the vertical axis. ....	18
Figure 31: Risk map for injection seismicity with surface risk index on the horizontal axis and subsurface risk index on the vertical axis. ....	24
Figure 32: Decision flow diagram for Seismic Risk Classification proposed by SoDM. There has been no past seismicity in P18 and the risk matrices for compaction as well as injection risk yield risk class I of negligible risk, monitoring with the regional network is sufficient. ....	25

## List of Tables

Table 1: Average reservoir properties. Most properties apply to all three fields, but the pressure and stress changes apply to P18-2. The pressure for the other fields is listed in Table 3. ....	6
Table 2: Average properties of the reservoir layers. ....	7
Table 3: Reservoir pressures per field. ....	7
Table 4: Distance of injectors to nearby faults, within 1km distance. Distances were calculated from the centre of the Hardeggen interval. Yellow colour indicates boundary faults that have become stressed by differential compaction during depletion. ....	8
Table 5: Modulus from DSI log in P18-4 well, with E-factor. ....	19
Table 6: Total fault length and block volume for P18-2, P18-4 and P18-6 fields with the corresponding B-factor. The B-factor was also computed including only the boundary faults, which are most significant, but that yielded also a high value. ....	19
Table 7: Fault length and maximum magnitude of earthquakes that could be sustained by each fault. ....	19

Table 8: Reservoir bulk volumes and maximum magnitude that could be induced based on the compaction energy release. For P18-2 and P18-4 the volume change was computed assuming uniform pressure at full depletion. For P18-6 the volume change was computed with the simulated pressure at full depletion. Since most of the bulk volume of P18-6 experiences no pressure decrease, the volume change is relatively small.....19

Table 9: Subsurface risk factors for seismicity .....20

Table 10: Surface risk factors. The factor for industrial installations was assigned 2, to allow for more platforms or other structures although at the moment no other platforms exist within 5km of the P18 field. ....21

Table 11: Subsurface risk factors for injection seismicity. The weight factor recognizes the large significance of reservoir type for overall risk. ....24

## Nomenclature

Units: SI (m= metre, s= second, kPa = $10^3$ Pa, MPa = $10^6$ Pa, GPa = $10^9$ Pa)

Dimensions: m= mass, L= length, t= time

Variable	Description	Units	Dimensions
$A_p$	: Poroelastic coefficient	[-]	(-)
$c$	: cohesion	[MPa]	(m/Lt <sup>2</sup> )
$E$	: Young's modulus	[GPa]	(m/Lt <sup>2</sup> )
$g$	: Stress gradient	[kPa/m]	(m/L <sup>2</sup> t <sup>2</sup> )
$K_h$	: horizontal stress ratio	[-]	(-)
$M_0$	: seismic moment	[N m]	(mL <sup>2</sup> /t <sup>2</sup> )
$M$	: moment magnitude	[-]	(-)
$p$	: pressure	[MPa]	(m/Lt <sup>2</sup> )
$V_{res}$	: reservoir volume	[m <sup>3</sup> ]	(L <sup>3</sup> )
$R_{crit}$	: Stress ratio: shear stress over effective normal stress	[-]	(-)
$\alpha_B$	: Biot coefficient	[-]	(-)
$\nu$	: Poisson's ratio	[-]	(-)
$\mu$	: friction coefficient	[-]	(-)
$\sigma_{H,max}$	: maximum horizontal stress	[MPa]	(m/Lt <sup>2</sup> )
$\sigma_{h,min}$	: minimum horizontal stress	[MPa]	(m/Lt <sup>2</sup> )
$\sigma_{vert}$	: vertical stress	[MPa]	(m/Lt <sup>2</sup> )
$\sigma_n$	: normal stress on fault plane	[MPa]	(m/Lt <sup>2</sup> )
$\tau$	: shear stress	[MPa]	(m/Lt <sup>2</sup> )



# 1 Introduction

TAQA is planning (with PORTHOS partners) to use the depleted P18 fields for CO<sub>2</sub> storage. The location of the fields and nearby fields are shown below in Figure 1.

The fields are indicated in the map of Figure 2. The P18-2 field consists of several compartments, while the P18-4 and P18-6 fields consist of a single compartment. The P18-2 field is isolated from the P18-4 field, which has a shallower GWC.

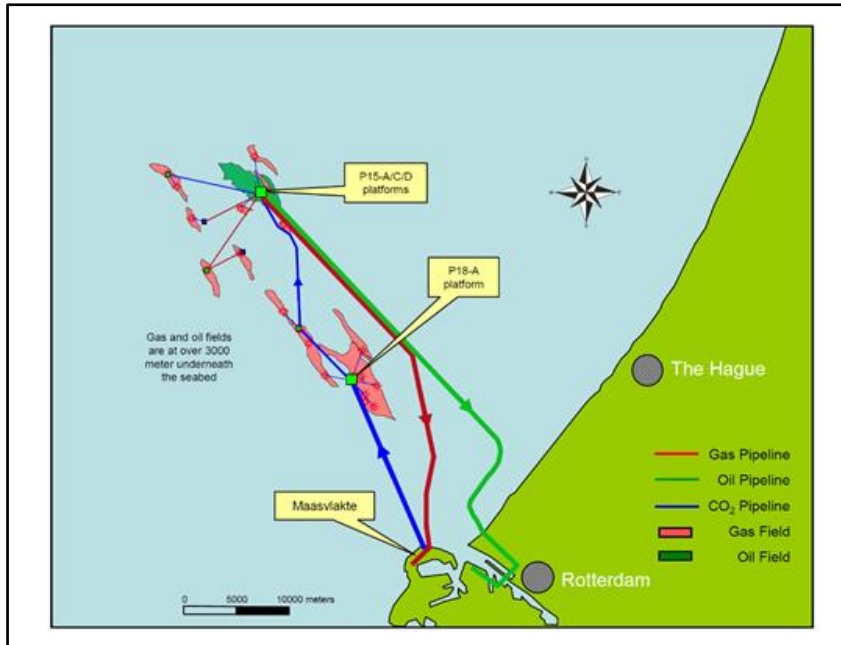


Figure 1: Overview of the locations of P18 and nearby P15 fields (After TAQA, 2009).

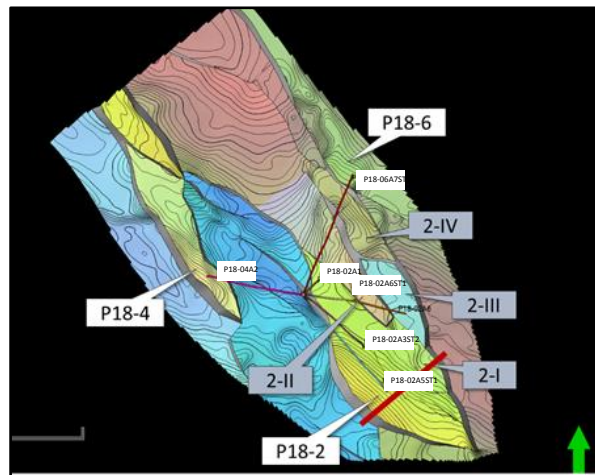


Figure 2: Overview of the three P18 fields (P18-2, P18-4, and P18-6), and the blocks of the P18-2 Field (2-I, 2-II, 2-III, and 2-IV). Red line indicates the position of the cross section shown in Figure 4 (TNO, 2019).

The reservoirs belong to the Triassic Buntsandstein and consist of the Hardegsen, Upper and Lower Detfurth and Volpriehausen. The tight Volpriehausen member gives only a small contribution to the reservoir storage capacity. However, the full reservoir height of some 220m is included in the geomechanical analyses since these layers may all deplete or repressurize over time. This is a conservative assumption for the seismic hazard evaluation.

Figure 4 shows a typical cross-section through the P18-2 field with the bounding faults on which significant stress concentrations can be expected during depletion of the field.

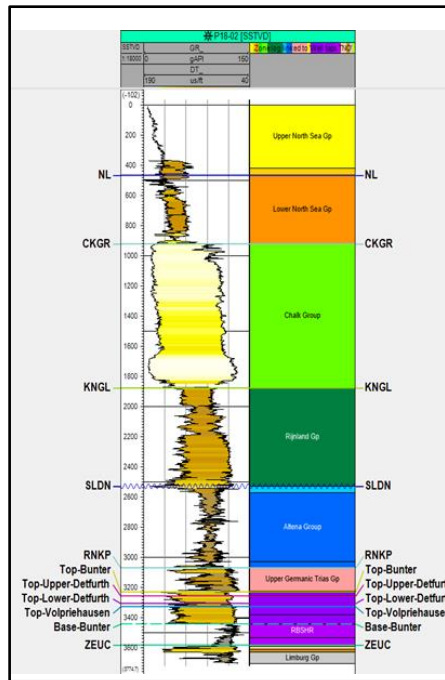


Figure 3: Lithology of the Triassic P18-2 field and overburden. The Hardegsen (Top Bunter) and Detfurth layers comprise the reservoir with a small contribution from the tight Volpriehausen layer (TNO, 2019).

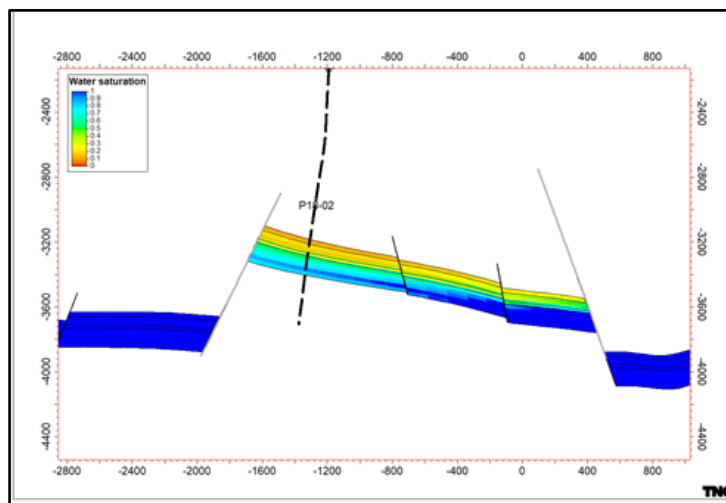


Figure 4: Cross section through the P18-2 field, showing block 2-I with initial water saturation. The location of the cross section is shown in Figure 2 (TNO, 2019).



The main concern with seismicity is not so much the potential damage to surface structures, which is in this case only a few nearby wellhead platforms that should be earthquake resistant. Slippage on faults might also enhance conductivity on faults which could lead to upward migration of CO<sub>2</sub>. Fortunately, the seal overlying the reservoir is 700m thick, so that the probability of any leakage through faults is negligible.

No seismicity has been observed during depletion of the field, which already reached a low pressure, so that seismicity could be expected. However, in the future the stress at the faults will differ from the historical stress, so that in principle an earthquake cannot be excluded.

Several methods will be used to estimate a maximum possible magnitude and the likelihood of such an event. Deterministic risk analysis will be applied to obtain the classification of P18 with respect to perceived risk in Dutch gas fields. Maximum depletion will indicate high risk; in addition, the modulus contrast between reservoir and overburden and the potentially slipping fault surface area will also be determined.

Upon CO<sub>2</sub> injection, with increasing reservoir pressure the seismic risk is expected to decrease with elastic reservoir behavior, as the stress on the faults will decrease. One uncertainty is the stress recovery which might not be elastic. Another new factor is cooling by injection, since adiabatic expansion of the CO<sub>2</sub> will cool the reservoir significantly. This is a recognized risk of injection projects and will be treated separately as one of the injection risk factors.

First, the risk matrix for surface and subsurface risk will be evaluated for differential compaction. Since the standard subsurface risk matrix does not cover injection projects, a separate risk matrix will be used for the perceived risks during injection. For instance, fracturing and thermal stress will also be discussed.

The risk analysis will be based on the design study by TNO and the geomechanical analysis in this report.

## 2 Mechanisms of seismicity

### Fault Stability Criterion: Predicting Seismicity

In the Northern part of the Netherlands (i.e. excluding Brabant and Limburg), there is no record of natural earthquakes indicating that the region is tectonically relaxed, i.e. any strain rate must be very low and fault stress is far from critical. Induced earthquakes are regularly caused by reservoir depletion and compaction and a few earthquakes may have been caused by injection during waterflooding or by drilling losses. Compaction seismicity only occurs after significant pressure depletion of about 30% of virgin pressure (Roest *et al.*, 1993; Bourne *et al.*, 2014). This confirms that Dutch gas fields have no critically stressed faults either at reservoir level or in the deep subsurface. Depletion of the P18 reservoirs will cause some faults to become critical, due to differential compaction. However, injection seismicity depends on critically stressed faults, so that faults with little throw will pose no risk for injection seismicity since they are far from critical.

The criterion for fault slip is simplified to the Mohr-Coulomb criterion, which predicts slippage when the ratio of shear stress to effective normal stress exceeds the friction coefficient:

$$R_{crit} = \frac{\tau}{\sigma_n - p} > \mu \quad (1)$$

Where  $\tau$  is the shear stress on the fault plane,  $\sigma_n$  is the normal stress and  $p$  is the local pore pressure. This shows that three factors could cause slippage: increase of shear stress, decrease of normal stress or increase of local pore pressure in the fault. For instance, depletion will increase the effective normal stress but the increase in shear stress caused by differential compaction can drive the fault into criticality.

Injection induced seismicity is most often caused by increasing pore pressure. This effect has been extensively observed in geothermal and waste water injection. In CO<sub>2</sub> injection, cooling of the reservoir might play a significant role. Furthermore, it is also possible that stress due to opening an injection fracture causes fault instability.

In order to assess the maximum earthquake magnitude, it is necessary to consider the size of the slippage area on a fault since that determines the magnitude, as illustrated in Figure 5.

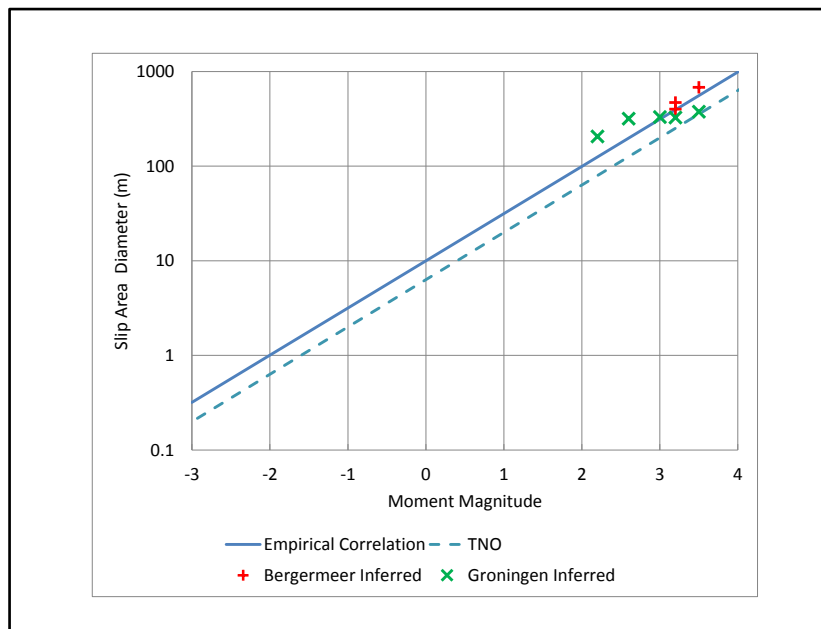


**Figure 5: Correlation between size of rupture area (for a square area) and earthquake magnitude. Using seismic traces the size of the slip area and the stress drop can be inferred. These slip area dimensions are plotted for depletion earthquakes in Bergermeer and Groningen. For a computed maximum slip area, the empirical relation gives a conservative estimate of magnitude. The TNO correlation is based on a theoretical relation and is more conservative.**

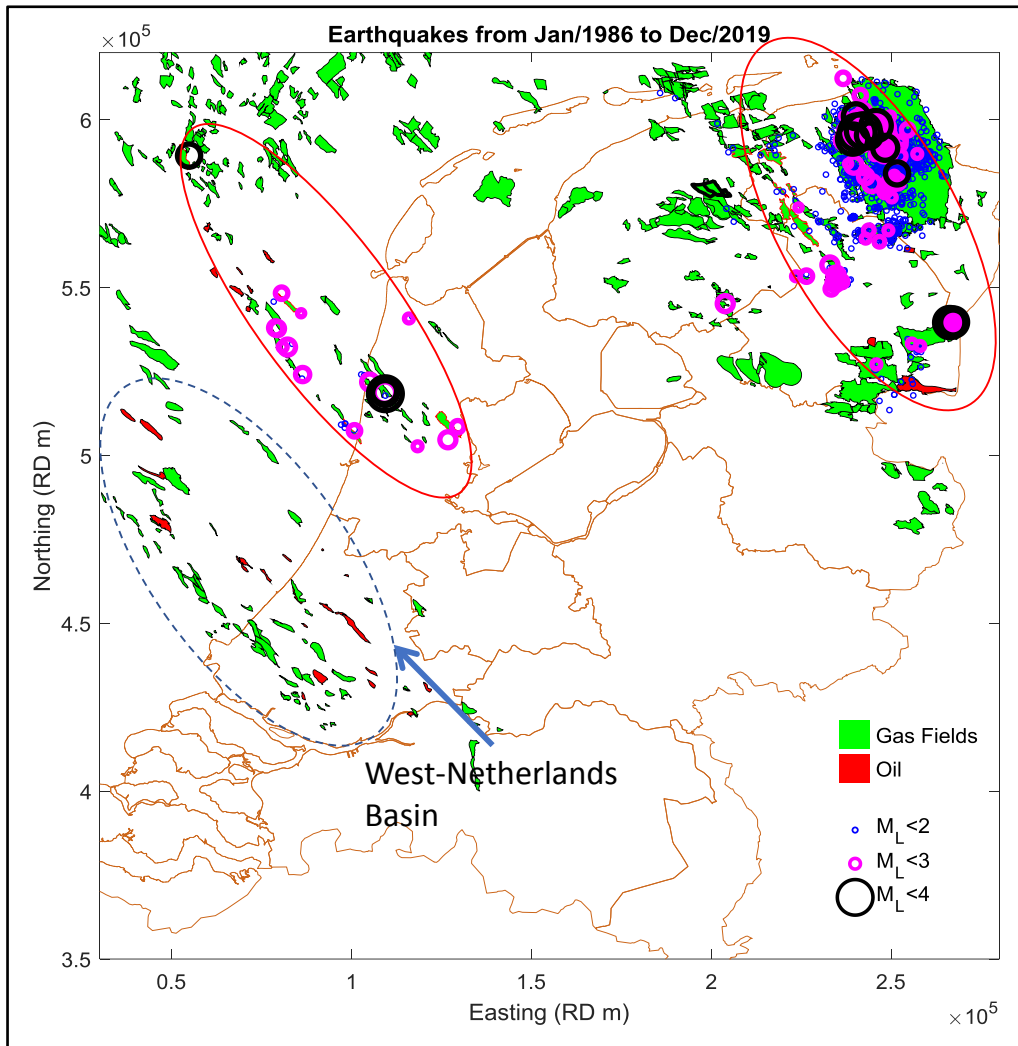


**Figure 6: Map of gas fields in the Netherlands. Induced earthquakes in the Netherlands are concentrated in two areas: one near the Groningen gas field and another near the Bergermeer field and neighbouring fields that lie on the same trend. The P18 fields belong to a trend of gas fields, extending from Zuid-Holland to offshore P18 and P15 blocks (West-Netherlands Basin) that are seismically quiet.**

Figure 6 shows induced seismicity in the Netherlands, which apparently occurs in two clusters of fields. It might be concluded that the gas fields in non-seismic areas just have no faults or faults that never become critically stressed, but that is not the case. The main causes of seismicity are the presence of faults in the reservoirs and significant compaction. A number of fields have such faults and significant depletion so that the faults become critically stressed, so that the absence of seismicity cannot be explained from reservoir properties (Vörös *et al.*, 2019). For instance, the Monster field is fully depleted, but induced no seismicity, while the seismic risk analysis could not exclude seismic risk; see NAM (2013), which assigns a probability of up to 42% for induced seismicity.

As yet, it is unclear what causes the regional variation of seismicity in Dutch gas fields and the non-seismic character of P18, but it can be concluded that even when the faults become critically stressed, the probability of seismicity is very low, since none of the fields in the West-Netherlands Basin have induced any seismicity.

### 3 Reservoir properties, pressure and fault system

The Buntsandstein reservoirs are conventional gas reservoirs with fairly good porosity and permeability, see Table 2. The modulus was determined from a Dipole Shear Sonic log, shown in Figure 7. The average value of the modulus over the reservoir is 37GPa, assuming a ratio of static to dynamic modulus of 75%. For seismic hazard, the ratio of overburden to reservoir modulus is important, so it does not matter how the dynamic modulus from sonic logs is converted to static modulus. However, compaction is proportional to the absolute value. We obtain a higher value of the modulus than used in the TNO study, but the lower estimate of 18 GPa will be used, which is equivalent to a conservative estimate of compaction.

From the density logs, LOT data and past fracture treatments in nearby fields, there is fair control of the vertical and minimum horizontal stress. The maximum horizontal stress is estimated from regional experience based on drilling data as fairly high but still lower than the vertical stress. The stress orientation was assumed to coincide with regional stress: maximum stress at 40degNW from data in the World Stress Map, see Figure 9.

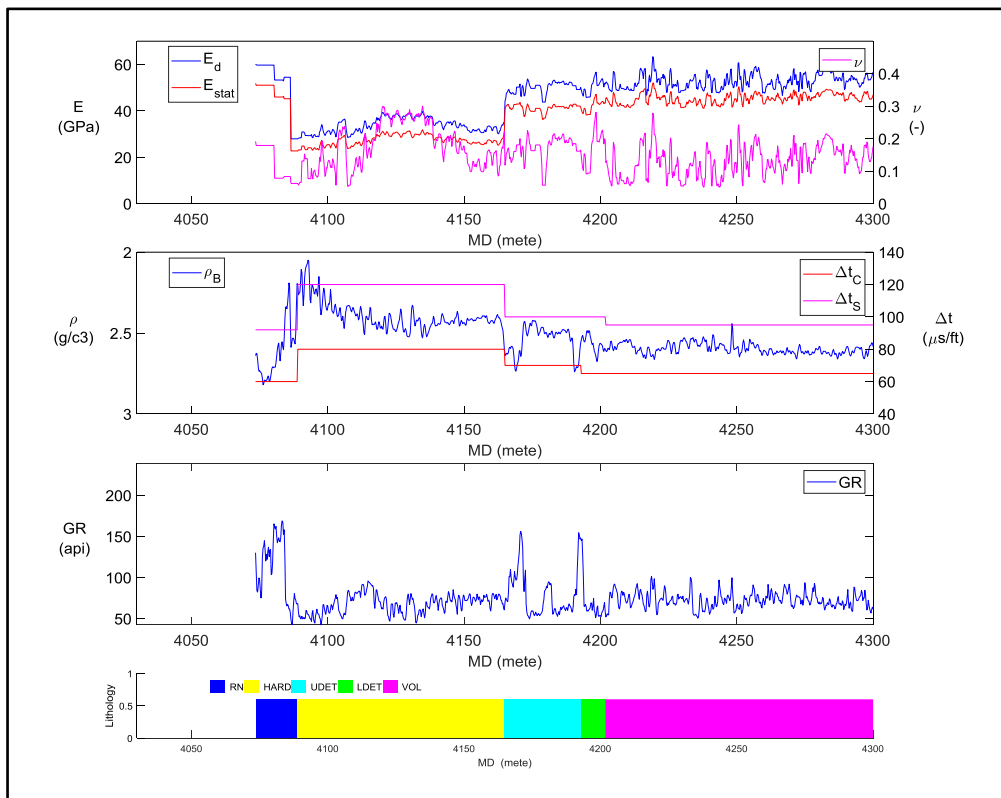


Figure 7: Logs and lithology in well P18-04A2. DSI readings from log displays were used to compute the modulus in overburden and reservoir. The Hardeggen reservoir has lower modulus than the overburden.

Table 1: Average reservoir properties. Most properties apply to all three fields, but the pressure and stress changes apply to P18-2. The pressure for the other fields is listed in Table 3.

Modulus			18	GPa	Virgin pressure	375	bar
Poisson ratio			0.25		Depleted pressure	20	bar
Biot Coefficient			1		Pressure drop	-355	bar
Compaction coefficient			0.046	1/GPa	Thermal expansion coefficient	1.00E-05	1/C
Depth			3500	m	Temperature drop	-90	C
Horizontal stress ratio			0.43		Thermal stress coefficient	2.4	bar/C
Stress path coefficient			0.60		Thermal stress drop	-216	bar
Vertical stress gradient			20.30	kPa/m	Poroeleastic coefficient	0.67	
Minimum horizontal stress gradient			14.84	kPa/m	Poroeleastic stress drop	-237	bar
Reservoir pressure gradient			10.71	kPa/m	Stress gradient drop	-6.8	kPa/m

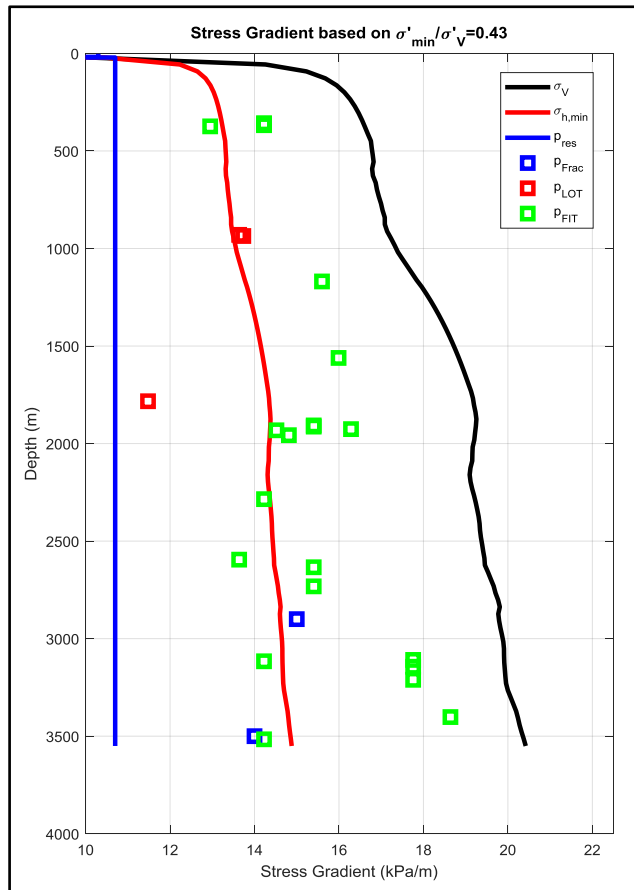


Figure 8: Stress gradients derived from P18-1 logs and LOT pressures as well as fracture gradients determined in nearby P15 and P12 fracture injection PFO's. The logs in the P18-2 well yielded the same result for the reservoir stress.

Table 2: Average properties of the reservoir layers.

	Thickness (m)	Porosity (BV)	Permeability (mD)
Hardeggen	20	0.11	154
Upper Detfurth	50	0.09	38
Lower Detfurth	30	0.07	31
Volpriehausen	85	0.03	0.02

Table 3: Reservoir pressures per field.

	P18-2 (bar)	P18-4 (bar)	P18-6 (bar)
Initial pressure	375	340	377
End production / start injection pressure	20	20	45
90 hydrostatic pressure	316	290	321
100 hydrostatic pressure	351	322	357
Initial pressure	375	340	377

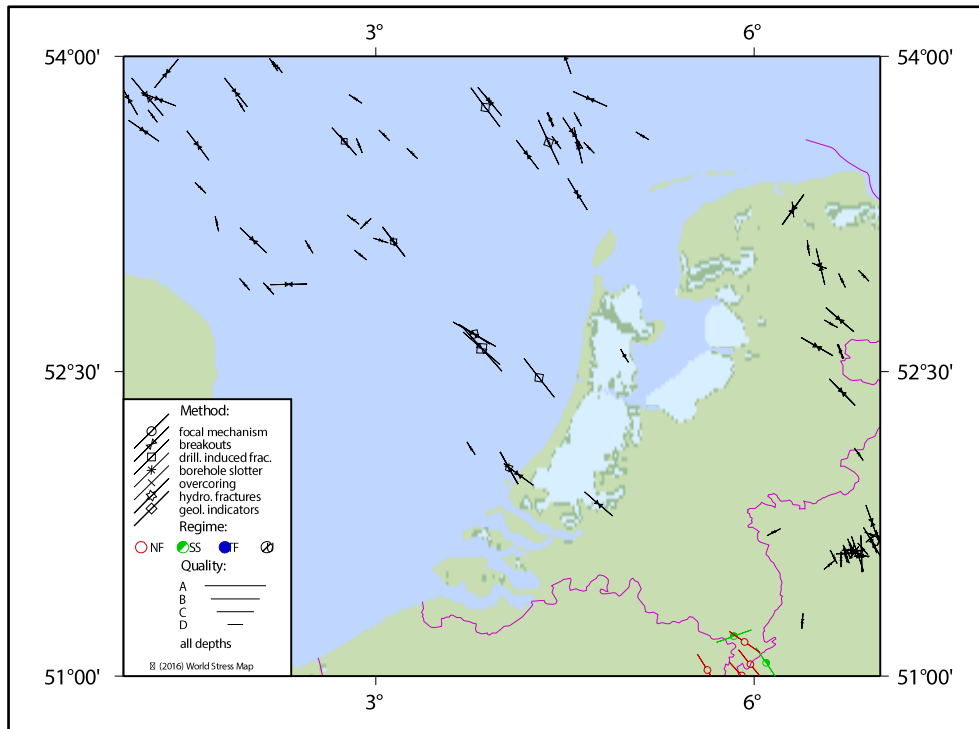


Figure 9: Stress orientation in the North Sea area near P18 (World Stress Map, 2016).

## Fault System

Experience shows that stronger induced earthquakes occur on existing large faults that are activated by compaction or injection. So, it is important to determine the fault size and the distance of the wells from the main faults. This will be restricted to the faults mapped in the seismic interpretation, which only maps the larger faults.

The faults in the P18-2 field are shown in Figure 10. The cross-section through the main injector is shown in Figure 11. The boundary fault 10 is more than 600m from the well, but the intra-block fault 35 is 264m from the well. In the other fields the faults are also steeply dipping, striking close to the maximum stress orientation and some faults are within a few hundred meters from the injector, see Table 4. Fault 35 was not considered in the stress analysis of TNO (2019), since it has little offset, so that differential compaction is small. However, even a fault with little offset can be activated by injection pressure. It is therefore necessary to consider also the intra-reservoir faults for injection seismicity.

Most faults are striking along the maximum horizontal stress, which means that they are favourably oriented for slip. However, any hydrofracs will propagate along maximum stress along the faults, so the fractures would not propagate towards a fault.

In Table 4 the boundary faults that are close to injectors are indicated in yellow. These faults are of interest since depletion will induce high shear stress on these faults by differential compaction.

**Table 4: Distance of injectors to nearby faults, within 1km distance. Distances were calculated from the centre of the Hardeggen interval. Yellow colour indicates boundary faults that have become stressed by differential compaction during depletion.**

P18-02A5		P18-02A1		P18-02A3ST2		P18-04A2		P18-06A7ST1	
FN	Distance	FN	Distance	FN	Distance	FN	Distance	FN	Distance
P18-04-F35	264	P18-04-F14	234	P18-04-F35	271	P18-04-F01	226	Fault400	235
P18-04-F10	614	P18-04-F17	325	P18-04-F10	711	P18-04-F09	309	Fault600	413
P18-04-F24	687	P18-04-F10	341	P18-04-F17	722	P18-04-F13	490	Fault430	666
P18-04-F34	721	P18-04-F11	399						
P18-04-F32	829	P18-04-F13	893						
		P18-04-F19	932						
		Fault3	997						

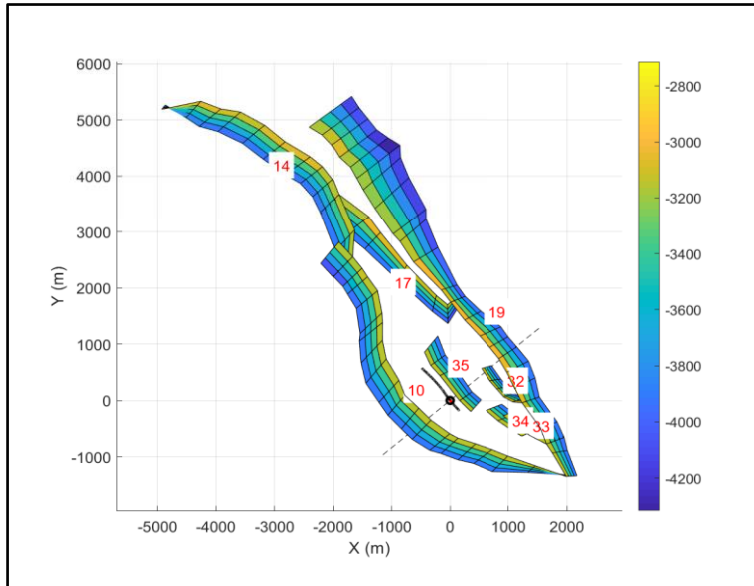


Figure 10: Faults in the P18-2 field, with well P18-2-A5. The dashed line indicates the cross-section along the minimum stress direction.

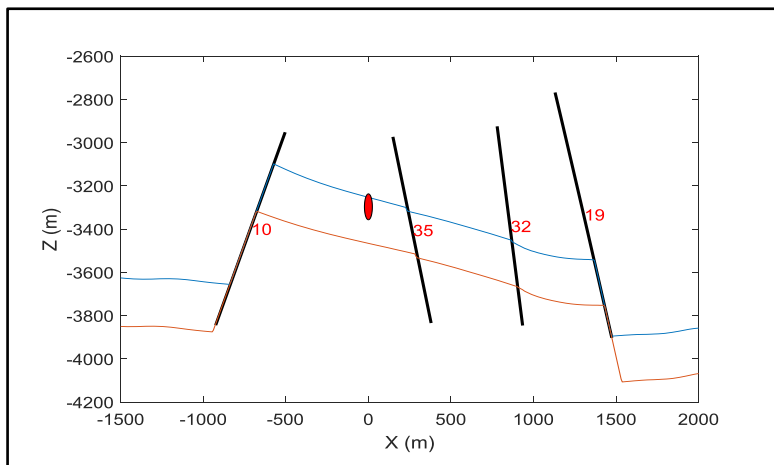
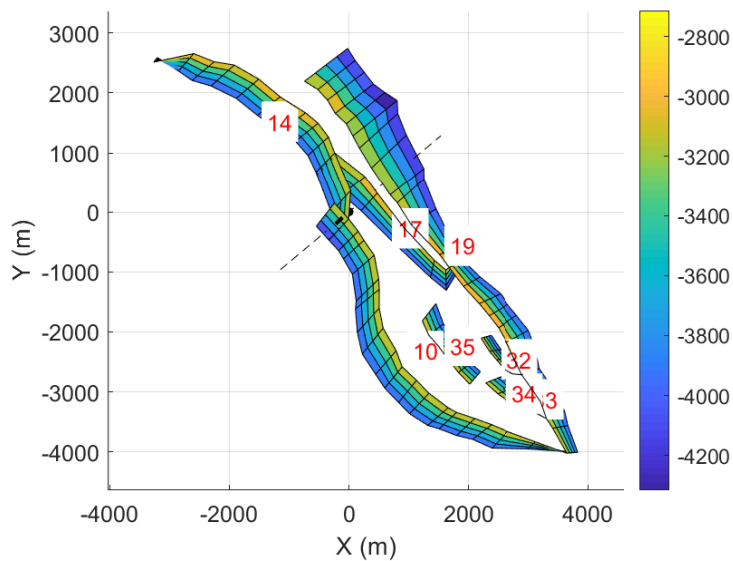
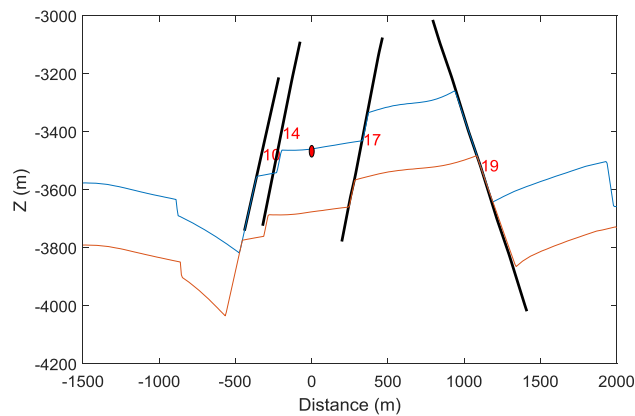


Figure 11: Faults in a cross-section through well P18-2-A5 along the minimum stress direction. The red ellipse indicates the injection interval.

Figure 12 shows the faults near well P18-02A1 and Figure 13 and Figure 14 shows the cross-section along minimum and maximum stress, respectively. This well is quite close to faults 14 and 10 that are boundary faults. These faults obtain high shear stress during depletion of the reservoir (TNO, 2019; Fig 7-2).



**Figure 12: Faults in the P18-2 field, with well P18-2-A1. The dashed line indicates the cross-section along the maximum stress direction.**



**Figure 13: Faults in a cross-section through well P18-2A1 along the minimum stress direction. The red ellipse indicates the injector.**

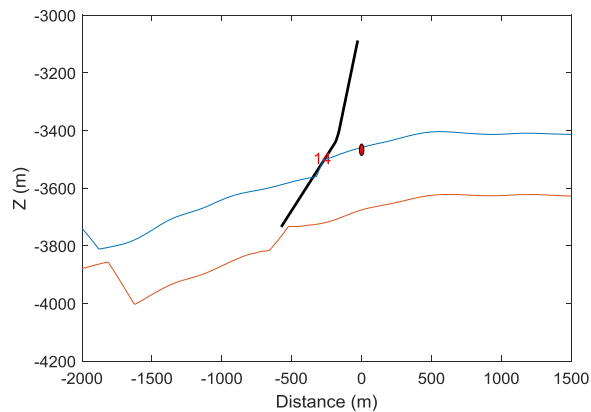


**Figure 14: Faults in a cross-section through well P18-2A1 along the maximum stress direction. The red ellipse indicates the injector.**



Figure 15 shows the faults near well P18-02A3. This well is far from boundary faults, as shown in Figure 16 and Figure 17. The tip of Fault35 is fairly close, but this is an intra-reservoir faults with small throw.

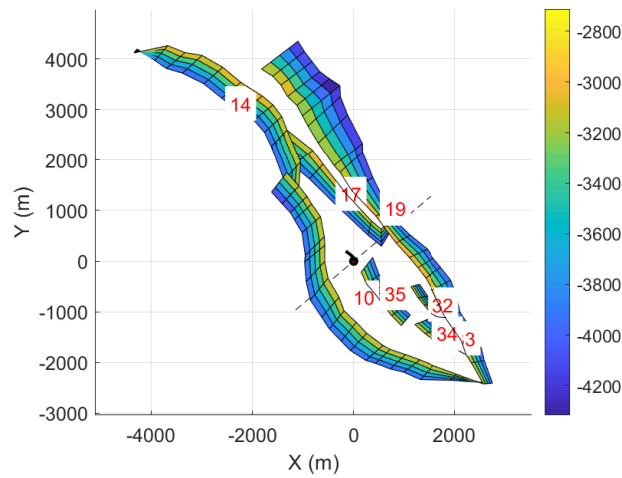


Figure 15: Faults in the P18-2 field, with well P18-2A3. The dashed line indicates the cross-section along the minimum stress direction.

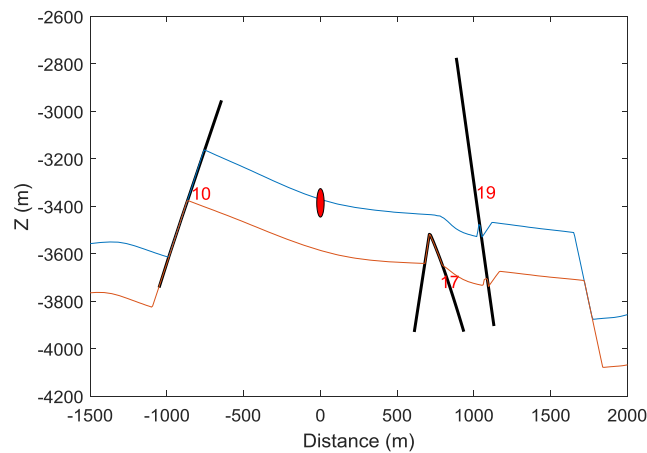


Figure 16: Faults in a cross-section through well P18-2A3 along the minimum stress direction. The red ellipse indicates the injector.

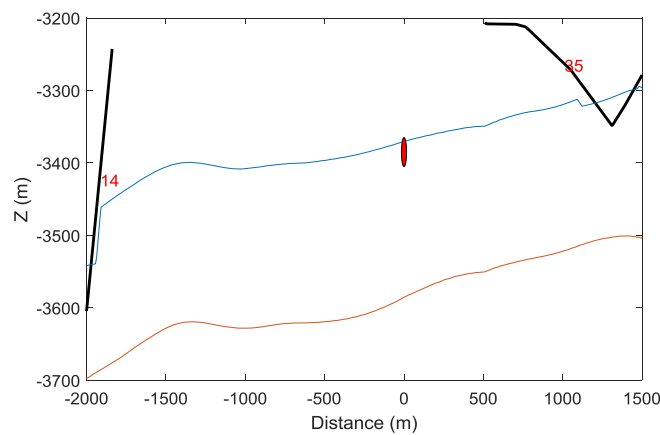


Figure 17: Faults in a cross-section through well P18-2A3 along the maximum stress direction. The red ellipse indicates the injector.

Figure 18 shows the faults that bound the P18-4 field. The cross section is shown in Figure 19.

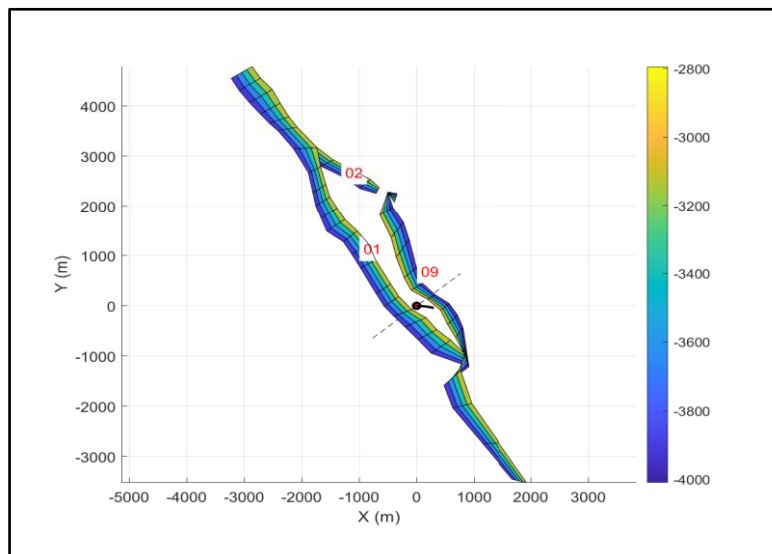


Figure 18: Faults in the P18-4 field, with well P18-4A2. The dashed line indicates the cross-section along the minimum stress direction.

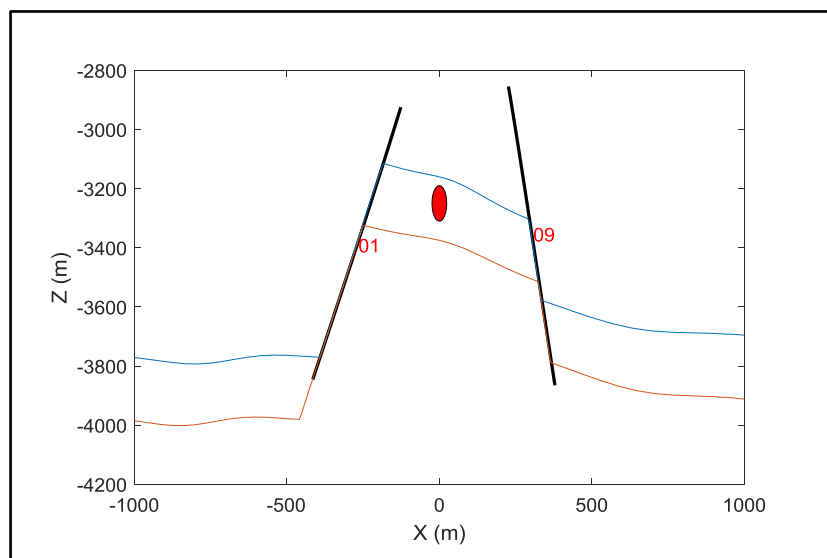


Figure 19: Faults in the P18-4 field, in a cross-section through well P18-4A2 along the minimum stress direction. The red ellipse indicates the Injection interval in well.

Figure 20 shows the P18-6 field faults with cross-section along minimum stress shown in Figure 21. The well is close to the bounding fault 400. Since this is a small field with limited gas zone, the compaction will be small, so that differential compaction will be limited.

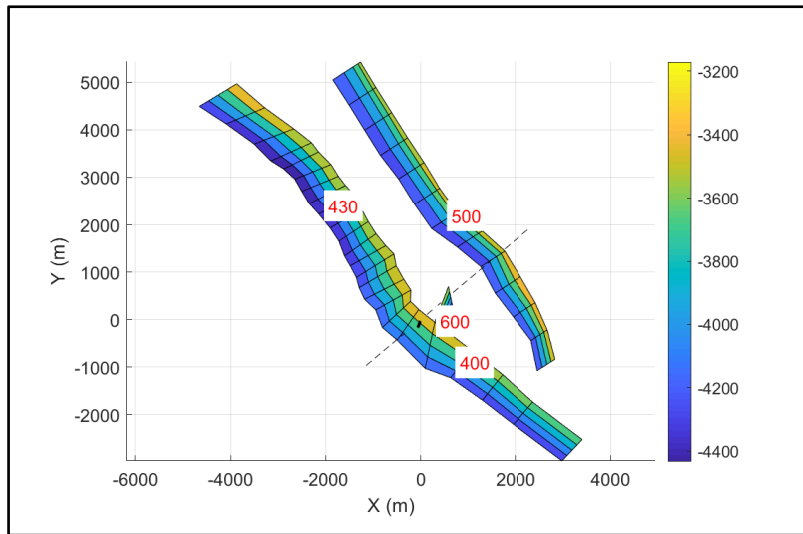


Figure 20: Faults in the P18-6 field, with well P18-6A7ST1. The dashed line indicates the cross-section along the minimum stress direction.

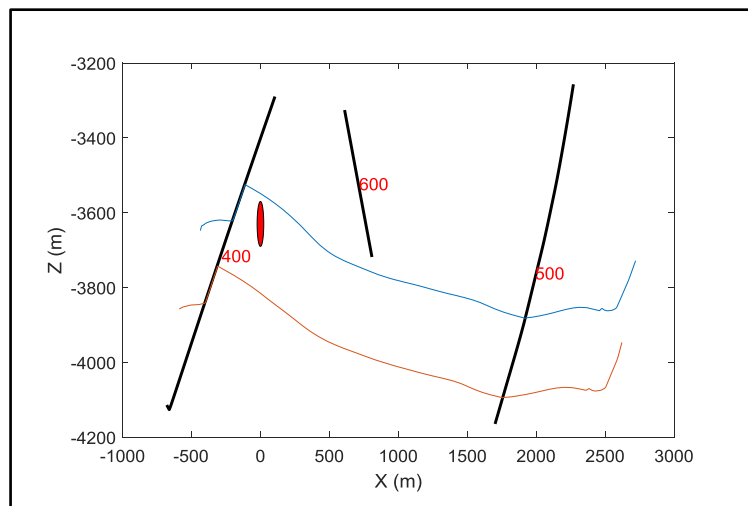
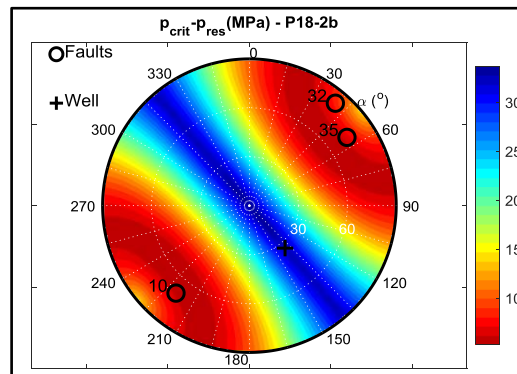


Figure 21: Faults in a cross-section through well P18-6A7ST1 along the minimum stress direction. The red ellipse indicates the injector.

## 4 Stress Analysis

### Virgin Stress and Pore Pressure Effect

Stability of the faults near the well may be influenced by the injection pressure and cooling. First, the stress on the faults in the virgin condition will be analysed. Stability depends on the normal and shear stress on the fault planes. Most faults have a favourable orientation in the stress field, so that the vertical and minimum stress give a large shear stress on the fault. From the fault stability condition, Eqn 1, the excess pressure above reservoir pressure can be computed that would destabilize the fault. This is shown in Figure 22 for virgin stress. In the depleted state the critical pressure is plotted in Figure 23. In these figures, each point in the polar diagram represents the normal to a fault plane. The origin of the plot is the horizontal plane, while the boundary represents vertical planes with different strike. The crosses represent the well axis and the circles correspond with faults in the vicinity of the main injector, P18-2A5, see cross-section Figure 11.



**Figure 22: Critical excess pressure above reservoir pressure that is needed to destabilize a fault in the virgin state.**

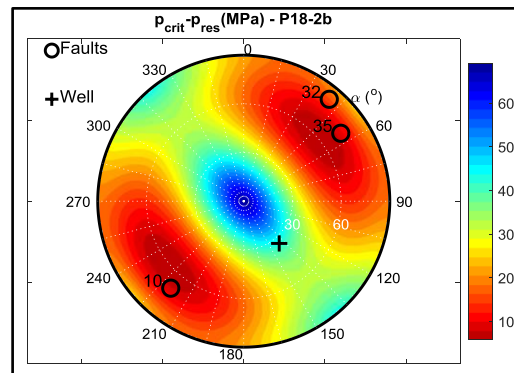


**Figure 23: Critical excess pressure above reservoir pressure that is needed to destabilize a fault, after depletion.**

Assuming a favourably oriented fault, the critical excess pressure would be 5.3MPa as shown in the Mohr circle diagram in Figure 24. The pressure at the fracture entrance is just 3-4 MPa above reservoir pressure (TNO, 2019, pp51-52), so the fracture pressure should be insufficient to destabilize a fault. Moreover, the injection pressure extends only over a small area, since the pressure falls off quickly away from the injector. Figure 25 shows the effect of depletion and cooling. The Mohr diagram confirms that depletion does not have a big effect on stability of the reservoir faults. Of course, differential compaction at the boundaries of reservoir with non-reservoir rock is not captured by the stress changes shown in Figure 25, which only apply to intra-reservoir faults with little offset, such as Fault35. The TNO study indeed showed that some sections of the boundary faults become critically stressed due to reservoir compaction.

Cooling has a much stronger effect on reservoir faults, since the horizontal stress is expected to decrease strongly. The reservoir will not reach the thermal fracturing regime (with negative effective stress), but the confining stress will become very low so that slippage is possible, even for a modest level of the shear stress, shown in Figure 25. For a thermal expansion coefficient of  $10^{-5}$  and  $90^{\circ}\text{C}$  cooling, the stress reduction is about 21MPa, which translates in a Mohr-Coulomb stress increase of about 10MPa. The critical stress would then

be just reached for a cooling of 20°C. Since the TNO study showed that the cooling front can extend several hundred meter from the well, it is likely that the cold zone can reach some faults. TNO (2019) computed the extent of the cold front for the main injector, which is far from the boundary faults. The other injectors are much closer to boundary faults, but these wells inject at a rate that is more than 8 times lower. That gives at least an 8 times slower cold front penetration, so the cold front will not reach the faults in the first years when injection pressure is highest. At the end of the injection project, the pressure is restored which stabilizes the boundary faults, the injection pressure is lower and the cooling effect will be reduced because adiabatic expansion is diminished by the higher background pressure. The cooling presents a new risk since the reservoir has not been cooled in the past, but the critically stressed faults will not be cooled during the first years of the injection. Therefore, the risk of thermally induced seismicity is negligible.

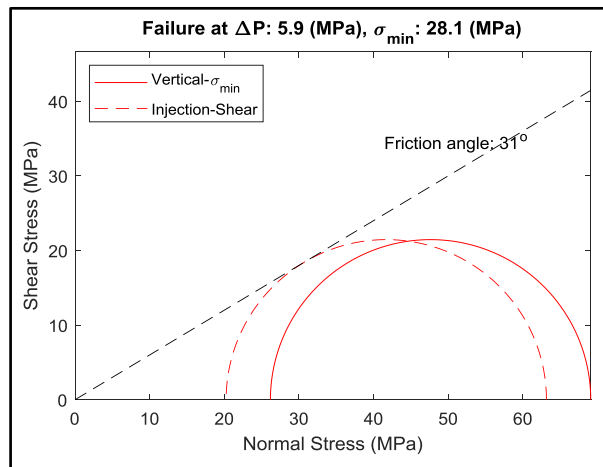


**Figure 24: Mohr Coulomb plot for stresses after depletion in the P18-2 reservoir. For a critically oriented fault, instability could occur with an excess pressure of 5.3MPa in the fault**

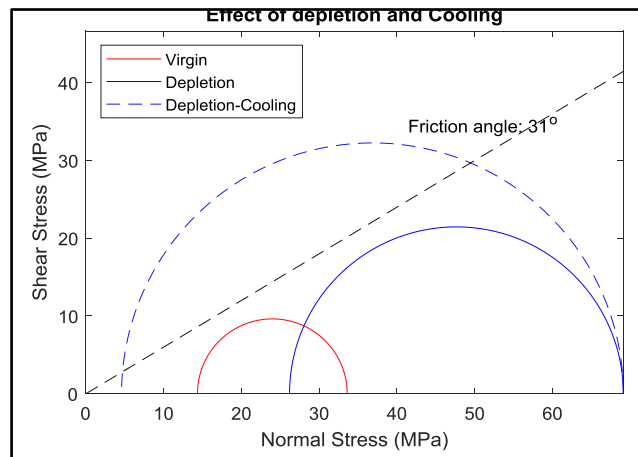


**Figure 25: Mohr Coulomb plot for virgin stresses in the P18-2 reservoir. Also, the effect of depletion and cooling by CO2 injection is plotted.**

## 5 Fracture Simulations

For seismic risk due to injection, an important issue is fracture propagation at the injectors, since a long fracture could not only cause increased pressure at a fault, but also modify the thermal front so that cooling occurs over longer distances. Although injection pressure is quite low, it is still of interest to consider fracture propagation by thermal stress reduction. Simple fracture simulations were performed in 2D using elliptical flow geometry (Hagoort, 1980; Koning, 1988). Only the first year is simulated, since it will be very uncertain to make a long-term forecast. It is assumed that the reservoir is cooled by 90°C and the injection rate is used for the main injector, P18-2A5. The cooling by CO<sub>2</sub> injection happens not only due to the heat capacity of the fluid, but mainly by Joule-Thompson expansion. This effect was added to the thermal model, which was developed for water injection. The simulations were benchmarked to the TOUGH2 simulations by TNO which model the entire thermodynamics of CO<sub>2</sub> injection. The model considers only 100 m reservoir consisting of Hardegsen and Detfurth; the resulting pressure of 3.5 MPa above reservoir pressure matches the TNO results (TNO, 2019, pp52-52). The cooling simulation is shown in TNO (2019; pp 66, Fig 7-7). For the standard input parameters, no fracture is propagated, since the stress remains far above the injection pressure, see Figure 26.

However, the thermal stress depends on the coefficient of thermal expansion (taken as  $10^{-5}\text{C}^{-1}$ ) and the modulus, which could be higher than the estimated value of 18 GPa. The modulus of sandstones with the porosity of the Hardegsen is commonly about 30GPa (English, 2019). For Buntsandstein sandstones Heap (2019) found an average modulus of 25GPa at a porosity of 11%, with a range of 5GPa.

For a higher value of the modulus of 30GPa, the thermal stress reduction is larger and a fracture can be propagated, see Figure 27, Figure 28 and Figure 29. The pressure distribution is hardly affected by the fracture, but the cooled region becomes somewhat elliptical. For these conditions the fracture size is moderate and the cold zone remains almost circular. Quite often, thermal fractures have only an impact on the injectivity and not on the shape of the flood front because both horizontal stresses become very low, so that a fracture network is formed that keeps the flood front circular. However, when the maximum horizontal stress is much larger than the minimum stress, the cold front becomes elliptical with a length that is much larger than the width. No evidence exists for a large horizontal stress difference so that a single fracture

Since the fracture propagates due to cooling it will also be strongly contained in the layers that accept the injected CO<sub>2</sub>. Therefore, there is no risk of upward or downward fracture growth.

Fortunately, the maximum stress orientation is along the major faults, so any fracture would propagate along the faults. Therefore, it is unlikely that a fracture would ever hit a fault. Well P18-2A1 is close to a fault as listed in Table 4, but that well has a much lower injection rate, so that less cooling and even lower injection pressure is expected so that no fracture propagation is possible.

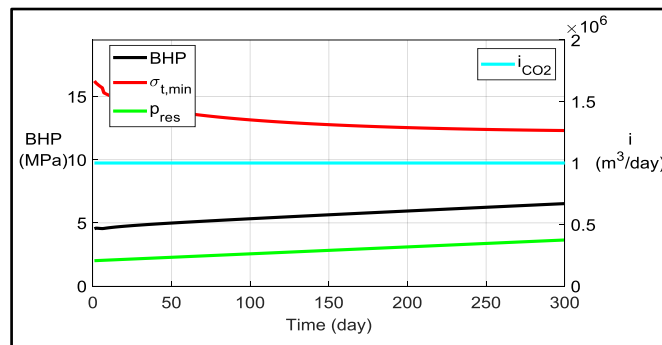


**Figure 26: Pressure in base case fracture simulation for CO<sub>2</sub> injection into P18-2 field. Since the pressure is much lower than the stress, no fracture propagation is possible. Only if the thermal stress would fall below the BHP a fracture could propagate.**

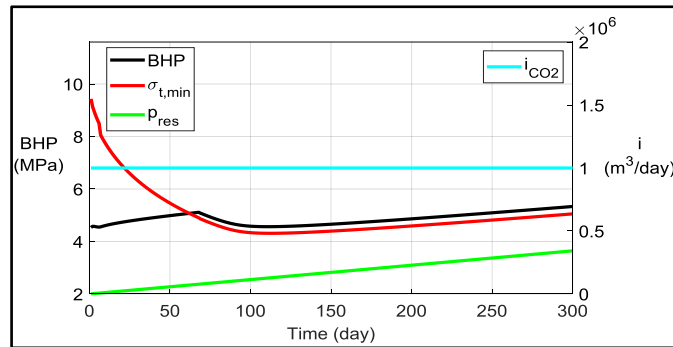


**Figure 27: Pressure in fracture simulation for CO<sub>2</sub> injection into P18-2 field for higher modulus of 30GPa. Since thermal stress is proportional to the modulus, the lower stress facilitates fracturing after a few months injection.**

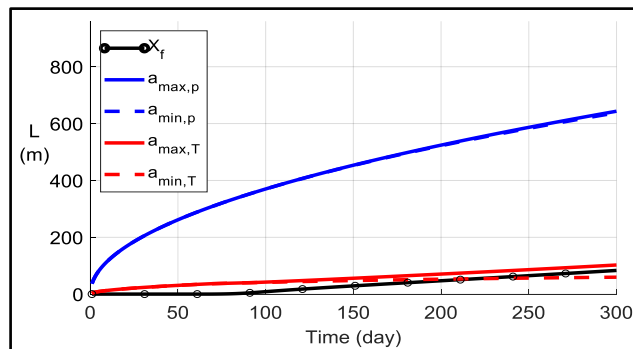


**Figure 28: pressure and temperature fronts in the simulation with fracturing. In agreement with detailed CO<sub>2</sub> simulations, the cold front extends over several hundred meters after 5 years and after 1 year the extent is some 50 m which facilitates an 80 m fracture length.**

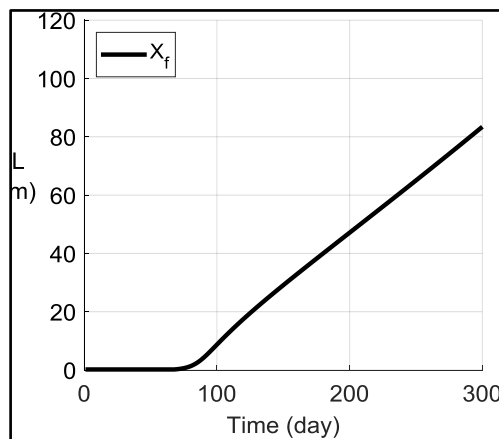


**Figure 29: Fracture size vs. time, for simulation with high modulus of 30GPa.**

For the P18-2 injector, fracturing can be monitored by observing the excess injection pressure (over reservoir pressure), which should rise with time. If injectivity improves, it is an indication of fracturing, so that fracture size should be monitored. It may be feasible to infer fracture size from the injectivity, but the pressure behavior is likely insensitive to fracture size and the usual method of inferring fracture size from Pressure fall-offs is complicated by the phase behavior of the CO<sub>2</sub>. The most important effect may be a larger extent of the cold front compared with matrix injection. This could cause earlier cooling at nearby faults and some pressure increase at a fault. However, since injection pressure is low compared with reservoir stress, the effect of fracture pressure on the faults will be negligible.

## 6 Risk Analysis

### Deterministic Seismic Hazard Analysis

For compaction induced seismicity, the SoDM guideline suggests risk factors for subsurface processes based on a deterministic analysis and a few other factors. Most important is the pressure depletion, for which a threshold of 30% depletion has been determined before the onset of seismicity. P18 fields have been almost completely depleted so this factor is satisfied. The contrast between reservoir stiffness and non-reservoir stiffness is another factor, since differential compaction depends on this ratio. Table 5 lists the modulus of reservoir and overburden: the modulus ratio is 1.3, which exceeds the threshold for seismicity of 1. The E-ratio is just below the upper threshold of 1.34, but it is so close that the highest risk is assigned, which is a conservative approach. Since faults are essential for seismicity, the degree of faulting is another factor. Table 6 lists the ratio of fault area to reservoir volume which results in B-factors for the fields that exceed the threshold for seismicity of 0.86. This would put the P18 reservoirs in the highest seismicity risk class of 42%. The B-factor is computed from fault length,  $L$ , reservoir volume,  $V$  and reservoir height,  $H$  with:

$$B = \frac{H_{res} \sum_{faults} L_{fault,i}}{V_{res}^{2/3}} \quad (2)$$

These factors indicate higher risk of relatively strong seismicity. The combined Risk Index is computed with the sum of all scores,  $s_i$ :

$$I_R = \frac{\sum_{All} s_i}{\sum_{All} \max(s_i)} \quad (3)$$

Table 9 lists the risk factors and scores for the P18 field. Table 10 gives the surface risk factors, which were developed for onshore fields. For offshore fields the vulnerability of surface structures concerns only the nearby wellhead platforms, which are of course earthquake resistant, since their foundations are built to withstand North Sea storms. Here, the guideline by SoDM is followed, which specifies an influence radius of 5km.

Both subsurface and surface risk indices can be combined to derive the risk class, as plotted in Figure 30. Clearly, the field falls in the negligible risk class.

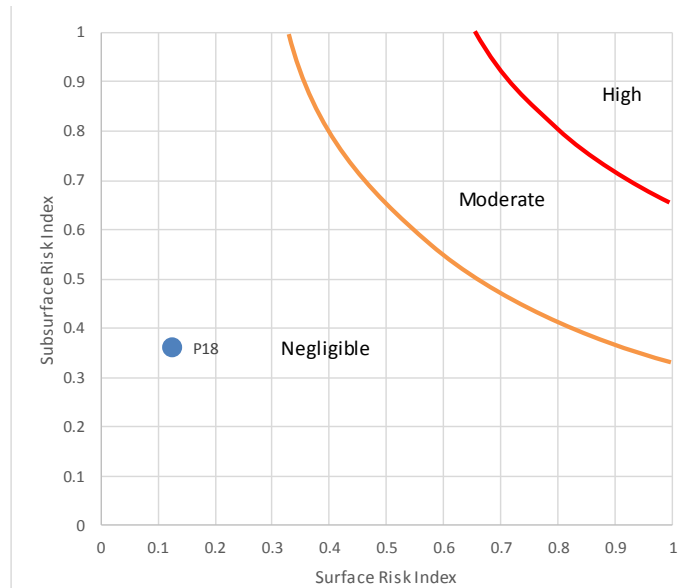


**Figure 30: Risk map with surface risk index on the horizontal axis and subsurface risk index on the vertical axis.**



**Table 5: Modulus from DSI log in P18-4 well, with E-factor.**

	Top (m)	$\rho_B$ (g/c3)	$\Delta t_c$ (ms/ft)	$\Delta t_s$ (\mus/ft)	$E_{dyn}$ (GPa)	$E_{stat}$ (GPa)	$\nu$ (-)
RN	4076	2.67	60	92	56.5	48.3	0.13
HARD	4093	2.40	80	120	34.0	27.6	0.18
UDET	4166	2.52	70	100	50.0	41.0	0.17
LDET	4194	2.57	65	100	50.7	42.1	0.18
VOL	4209	2.59	65	95	52.8	45.3	0.13
E-ratio						1.31	

**Table 6: Total fault length and block volume for P18-2, P18-4 and P18-6 fields with the corresponding B-factor. The B-factor was also computed including only the boundary faults, which are most significant, but that yielded also a high value.**

Block	L (m)	L-Boundary (m)	Hres (m)	Vres (m <sup>3</sup> )	B (-)	B-boundary (-)
P18-2	2.01E+04	1.61E+04	210	2.71E+09	3.2	2.3
P18-4	1.07E+04	1.07E+04	229	6.23E+08	6.2	6.2
P18-6	1.95E+04	1.95E+04	228	5.07E+09	1.9	1.9

**Table 7: Fault length and maximum magnitude of earthquakes that could be sustained by each fault.**

	#	Length (m)	M0 (Nm)	M (-)
P18-2	10	6378.6	1.50E+15	4.1
	14	1180.9	2.78E+14	3.6
	17	3144.1	7.41E+14	3.8
	19	5363.8	1.26E+15	4.0
	32	1022.7	2.41E+14	3.5
	33	890.5	2.10E+14	3.5
	34	765.2	1.80E+14	3.4
	35	1350.0	3.18E+14	3.6
P18-4	1	5235.8	1.23E+15	4.0
	2	1519.0	3.58E+14	3.6
	9	3941.7	9.29E+14	3.9
P18-6	129	7588.2	1.79E+15	4.1
	130	5784.5	1.36E+15	4.0
	131	4997.0	1.18E+15	4.0
	134	1106.3	2.61E+14	3.5
	130-131	10781.4	2.54E+15	4.2

**Table 8: Reservoir bulk volumes and maximum magnitude that could be induced based on the compaction energy release. For P18-2 and P18-4 the volume change was computed assuming uniform pressure at full depletion. For P18-6 the volume change was computed with the simulated pressure at full depletion. Since most of the bulk volume of P18-6 experiences no pressure decrease, the volume change is relatively small.**

	FIPNUM	Volume (m3)	Area (m2)	Height (m)	$\delta$ Volume (m3)	M <sub>0</sub> (Nm)	M (-)
P18-2	4	1.57E+09	7.11E+06	220	2.58E+06	2.47E+14	
P18-2	11	7.68E+08	3.05E+06	252	1.26E+06	1.21E+14	
P18-2	6	3.05E+08	1.43E+06	214	5.01E+05	4.81E+13	
P18-2	10	2.85E+08	1.33E+06	214	4.69E+05	4.50E+13	3.7
P18-4	2	6.23E+08	2.72E+06	229	1.02E+06	9.83E+13	3.3
P18-6		5.07E+09	2.22E+07	228	5.22E+05	5.01E+13	3.1

**Table 9: Subsurface risk factors for seismicity**

	DHAIS	M	Ligging voorkomen	Opslingering	Score
5		Alle methodes >4,5			
4	Bevend veld > 5 bevingen per jaar van $M \geq 1,5$	1 methode > 4,5 én/of Alle methodes 4,1 – 4,5			
3	Bevend veld < 5 bevingen per jaar van $M \geq 1,5$	1 methode 4,1 – 4,5 én/of Alle methodes 3,6 – 4,0		>60% slappe grond ( $V_{s,30} \leq 200\text{m/s}$ ) en/of >30% grondsoort die extra gevoelig zijn voor amplificatie, zoals veenlagen dikker dan 3m en slappe veenlagen met een dikte van 1m-3m gelegen op een stijve ondergrond.	
2	P=42% Of Bevend veld $M < 1,5$	1 methode 3,6 – 4,0 én/of Alle methodes 3,1 – 3,5	Boven de lijn Amsterdam-Arnhem	30-60% slappe grond ( $V_{s,30} \leq 200\text{m/s}$ ) en/of 15-30% grondsoort die extra gevoelig zijn voor amplificatie, zoals veenlagen dikker dan 3m en slappe veenlagen met een dikte van 1m-3m gelegen op een stijve ondergrond.	
1	P=19%	1 methode 3,1 – 3,5 én/of Alle methodes 2,6 – 3,0		10-30% slappe grond ( $V_{s,30} \leq 200\text{m/s}$ ) en/of 5-15% grondsoort die extra gevoelig zijn voor amplificatie, zoals veenlagen dikker dan 3m en slappe veenlagen met een dikte van 1m-3m gelegen op een stijve ondergrond.	
0		1 methode 2,6 – 3,0 én/of Alle methodes $\leq 2,5$	Onder de lijn Amsterdam-Arnhem	<10 % slappe grond ( $V_{s,30} \leq 200\text{m/s}$ ) en/of < 5% grondsoort die extra gevoelig zijn voor amplificatie, zoals veenlagen dikker dan 3m en slappe veenlagen met een dikte van 1m-3m gelegen op een stijve ondergrond.	
	4	5	2	3	14
<b>P18</b>	2	3	0	0	0.36

**Table 10: Surface risk factors. The factor for industrial installations was assigned 2, to allow for more platforms or other structures although at the moment no other platforms exist within 5km of the P18 field.**

	Bevolkingsdichtheid (aantal inwoners per km <sup>2</sup> )	Industriële inrichtingen	Speciale gebouwen En vitale infrastructuur	Dijken	Sum/ Score
<b>4</b>	> 2500	Meerdere direct boven het veld	Meerder ziekenhuizen en/of energievoorzieningen direct boven het veld	Primaire dijken boven het veld	
<b>3</b>	1000-2500 en/of 500-1000 met wijken bestaande uit flats/ appartementen-complexen binnen 5 km rond het veld	1 boven het veld en/of meerdere binnen 5 km rond het veld.	1 ziekenhuis en/of energievoorziening direct boven het veld of meerdere binnen 5 km rond het veld. Meerdere scholen, tehuisen en/of publieksgebouwen direct boven het veld	Primaire dijken binnen 5 km rond het veld en/of secundaire dijken boven het veld	
<b>2</b>	500-1000 en/of 250-500 met wijken bestaande uit flats/ appartementen-complexen binnen 5 km rond het veld	1 binnen 5 km rond het veld.	1 school, tehuis en/of publieksgebouw boven het veld of meerdere binnen 5 km rond het veld.	Secundaire dijken binnen 5 km rond het veld	
<b>1</b>	250-500 en/of <250 met wijken bestaande uit flats/appartementen-complexen binnen 5 km rond het veld	-	1 school, tehuis en/of publieksgebouw binnen 5 km rond het veld.	-	
<b>0</b>	< 250	Geen binnen 5 km rond het veld	Geen boven en/of binnen 5 km rond het veld	Geen dijken binnen 5 km rond het veld	
<b>Max</b>	4	4	4	4	16
<b>Weight</b>	1	1	1	1	
P18	0	3	0	0	0.2
In Salah	1	2	1	0	0.25
Sleipner	0	2	0	0	0.125
Weyburn	1	2	1	0	0.25

## Injection Seismicity Risk Analysis

The potential mechanisms of earthquakes generation by fluid injection have been reviewed by TNO (2014). These are:

- Poro-elastic stress effects as a result of the injection
- Pore pressure increase in a near-critically stressed fault
- Chemical reactions reducing the strength of a fault
- Thermal changes effecting stresses
- Mass changes
- Stress transfer from nearby earthquakes

For long-term injection chemical reactions and mass changes may be relevant but detailed lab studies have shown that chemical interaction of CO<sub>2</sub> with sandstone is negligible (TNO, 2019) and the effect of mass changes can also be neglected since there are no deep fault systems that could be triggered by the additional mass of the CO<sub>2</sub> compared with the virgin reservoir. Since the P18 field is in a seismically quiet area the stress transfer effect can be disregarded.

From water injection projects it is known that thermal stress change may become significant after some months. So, for the long-term injection of CO<sub>2</sub> in a relatively stiff reservoir thermal stress reduction will play a role. Cooling occurs mainly because of Joule-Thomson effect during expansion of the injected CO<sub>2</sub> into the low-pressure reservoir. Simulations by TNO (2019) have shown that the cold front can extend to faults near the injectors. The stress analysis of Figure 25 indicates that slippage may occur because of the reduction in confining stress on the faults.

In some German geothermal projects, seismicity started after injecting for years, which can be explained by cooling of the rock. The well-known Geysers geothermal project shows seismicity that is also presumed to be induced by thermal stress reduction.

For Geothermal injection the following risk factors were identified (Baisch *et al.*, 2014):

- basement connected
- inter-well pressure communication
- re-injection pressure [MPa]
- circulation rate [m<sup>3</sup>/h]
- epicentral distance to natural earth-quakes [km]
- epicentral distance to induced seismicity [km]
- distance to fault [km]
- orientation of fault in current stress field net injected volume [1000 m<sup>3</sup>]

This is aimed at geothermal doublets, although some factors are relevant to all injection projects such as natural seismic activity and proximity to faults.

Experience with injection seismicity, has shown that the factors that govern injection seismicity risk are:

- Natural Seismicity: in seismically quiet regions strong injection seismicity is unlikely, as observed for instance in the Northern Netherlands (Foulger *et al.*, 2019). TNO (2014) found no evidence for felt induced seismicity by Dutch fracture treatments.
- Fault Density/ Location: seismic faults are necessary for induced seismicity
- Stress Regime: Felt induced injection seismicity is almost always observed in strike-slip or reverse faulting stress regimes (Foulger *et al.*, 2019).
- Reservoir Transmissibility and Storage Capacity: Pressure changes are the principal driver of geomechanical changes in CO<sub>2</sub> storage reservoirs, so if any pressure change is small the effects will be small. A CCS project like Sleipner with injection into a huge aquifer where the total injected CO<sub>2</sub> occupies only a tiny fraction of a percent of total storage volume is possibly the best option (Verdon, 2013).

In the P18 reservoirs the faults are likely critically stressed over some sections by differential compaction (TNO, 2019), which might be a risk factor for injection seismicity. However, the absence of seismicity shows

that these faults do not slip in a seismic mode. Therefore, the stressed state of these faults should not be considered as higher risk for injection.

Other factors that enhance risk are:

- Injection Volume: it has been observed that in cases where seismicity is induced the earthquakes get stronger for larger injection volume (McGarr, 1976).
- Thermal Stress reduction

Proximity to basement is a risk factors for injection seismicity, but this is irrelevant for CO<sub>2</sub> injection since no projects exist near basement. Injection volumes are necessarily huge, which presents a significant seismic hazard, but it applies to all CCS projects. The qualification is that the large volume should not be associated with large pressure changes that could cause large earthquakes. A project like Sleipner has very small pressure changes because it injects into a huge aquifer, while In Salah has higher risk because injection induces large pressure changes.

As shown in the section on stress analysis, the main injector is far from any critically stressed faults, so thermal stress will not be relevant. Some minor injectors are close to intra-reservoir faults, but these are not stressed by differential compaction because the throw is small. Therefore, thermal stress effects will be insignificant.

These factors indicate higher risk of relatively strong seismicity. Therefore, the Injection Risk Index is computed with:

$$I_R = \frac{\sum_{All} W_i s_i}{\sum_{All} W_i \max(s_i)}, \quad (4)$$

Where  $s_i$ : risk score,  $W_i$ : weight factor.

Table 11 lists the risk factors and scores for the P18 reservoir. Unfortunately, there is no experience in the Netherlands with CO<sub>2</sub> storage, so it is impossible to compare P18 with nearby CCS projects in the same geological setting. So, for reference, a few well-documented CO<sub>2</sub> injection projects are added in other areas; some of these have induced seismicity, such as In Salah and Weyburn, Canada, while the Sleipner project in the North Sea showed no seismicity. Reviews of the In Salah, Sleipner and the Weyburn CO<sub>2</sub> injection projects are presented by Verdon (2013) and Foulger *et al.* (2018). Sleipner is offshore, while In Salah is in the Algerian desert and Weyburn is in a remote area of Saskatchewan, Canada. Therefore, all three projects present low surface risk, but the storage reservoirs are quite different. Sleipner injects into a large, high-permeability aquifer, so that pressure changes are negligible. Weyburn is a hydrocarbon reservoir with complex stress history where CO<sub>2</sub> is not only stored but also injected for EOR. In Salah is a fairly low-permeability aquifer with limited storage capacity that showed significant pressure increase. Both Weyburn and In Salah have induced weak seismicity of magnitude -1.0 and 1.7, respectively.

Figure 31 shows the risk classes for P18 and the reference cases. Calibration of this classification was based on the documented cases. It can be concluded that the P18 injection project falls in the class with negligible risk, analogous to Sleipner. Both the subsurface conditions indicate very low risk of seismic fault slippage over a large area and the surface risk is also negligible since only a few wellhead platforms are in the range of potential earthquake vibrations.

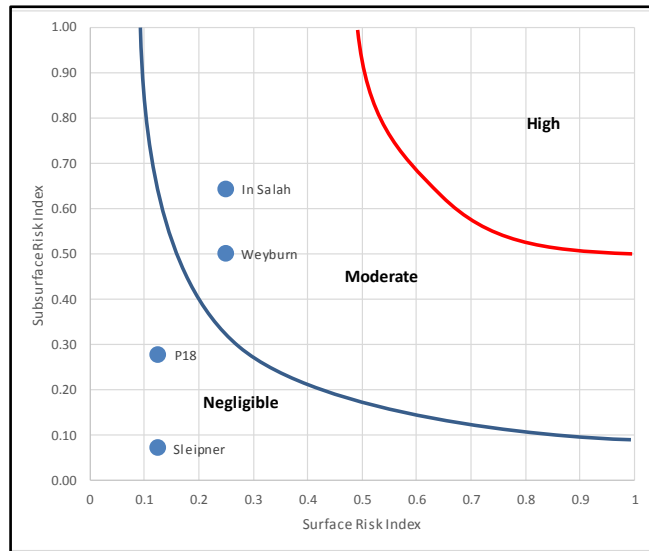


Figure 31: Risk map for injection seismicity with surface risk index on the horizontal axis and subsurface risk index on the vertical axis.

Table 11: Subsurface risk factors for injection seismicity. The weight factor recognizes the large significance of reservoir type for overall risk.

Code	Natural Seismicity	Fracture Density/ Location	Stress Regime	Reservoir Type	Thermal Stress	Score
3						
2	Active: M>6	Near active faults	Overthrust	Aquifer: Increased Pressure	Thermal Fracturing regime	-
1	Moderate: M=3	Many reservoir faults; No active faults	Strike-Slip	Depleted Oil Field with Complex Stress History	Stiff rock/long term	-
0	No record	Few Reservoir Faults; Far from active faults	Normal	High Perm Large Aquifer/Depleted Gas Field	No cooling or soft reservoir	-
Max	2	2	2	2	2	14.0
Weight	1	1	1	3	1	
P18	0	1	0	0	1	0.14
In Salah	0	2	1	2	0	0.64
Sleipner	0	1	0	0	0	0.07
Weyburn	1	2	1	1	0	0.50

## Risk Classification

Apart from compaction and injection, repressurization might also present a seismicity risk. After full depletion, the reservoir pressure will rise by 20bar per year during CO<sub>2</sub> injection (TNO, 2019). This is similar to the refill of a gas storage like Bergermeer (Fenix, 2018), Grijpskerk or Norg. These gas storage reservoirs have induced some seismicity during refill, which could be explained in the case of Bergermeer from the earthquakes that occurred during depletion.

A review of seismic risk in gas storage reservoirs (Teatini *et al.*, 2019) concluded that seismicity during refill is unlikely if no seismicity occurred during primary depletion. The guidelines for safe operation of gas storage reservoirs that never induced seismicity during depletion read:

*“If no seismicity has been recorded during primary production, maximum reservoir pressure can safely be equal to initial pressure. Indeed, the system behaves elastically, and the pressure recovery unloads the faults to their initial criticality condition.*

*If no seismicity has been recorded during primary production and cushion gas injection, reservoir pressure change can safely span the whole pressure change between initial pressure and cushion gas pressure. As above, the system behaves elastically within the pressure range experienced by primary production and cushion gas injection. Therefore, a gas storage reservoir within the same range of pressure variation does not yield the system toward a more critical condition in terms of fault reactivation.”*

It can be concluded that both with regard to compaction/repressurization seismicity and for injection seismicity, the P18 field falls in the class with negligible risk. Both the subsurface conditions indicate very low risk of fault slippage over a large area and the surface risk is also negligible since only a few nearby wellhead platforms are in the range of potential earthquake vibrations. Since the main concern with seismicity is not damage to surface structures, but CO<sub>2</sub> migration due to fault slippage, it can be concluded that the low risk of seismicity results also in low risk of opening migration paths along the faults.

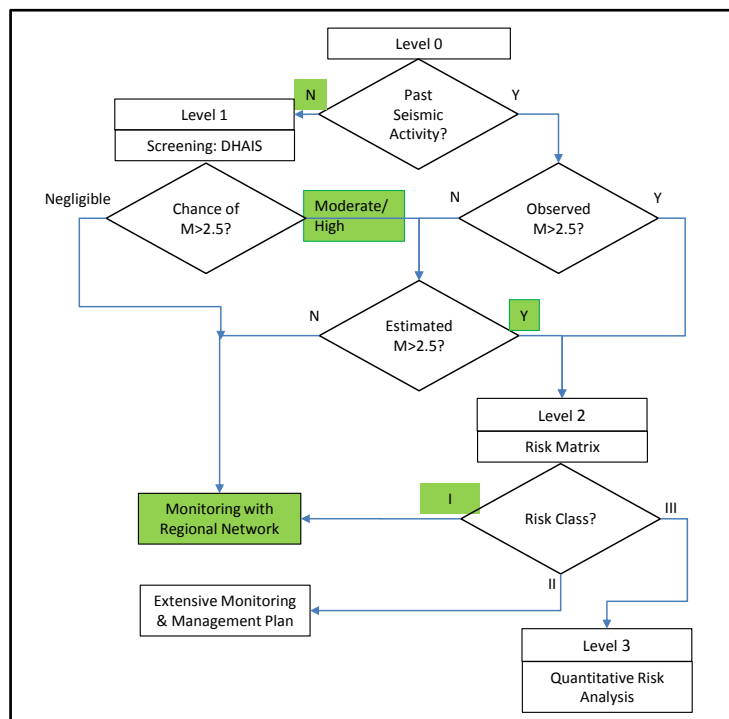


**Figure 32: Decision flow diagram for Seismic Risk Classification proposed by SoDM. There has been no past seismicity in P18 and the risk matrices for compaction as well as injection risk yield risk class I of negligible risk, monitoring with the regional network is sufficient.**

SoDM guidelines for seismic risk analysis outline a decision tree for determining the risk level, shown in Figure 32. Since P18 and neighbouring fields have no history of induced seismicity due to compaction and the risk of injection seismicity is very low, the decision tree yields standard monitoring with the regional network as the appropriate action.

## Discussion

The hazard presented by potential fault slippage is deemed to yield a negligible risk, since seismicity is very unlikely in the P18 field. The guidelines for estimating maximum magnitude of seismicity yield a high value of moment magnitude  $M=4$  for potential earthquakes. However, this is only a possibility if an entire fault would slip. In view of the historical depletion behavior, a realistic estimate of maximum magnitude is  $M=2$  because no seismicity has been observed with the regional monitoring system, while sections along the faults are critically stressed by compaction (TNO, 2019). The injection of CO<sub>2</sub> will raise the pressure, which will stabilize the faults. Any injection seismicity is only observed when faults were already active during depletion, while non-seismic reservoir will also be non-seismic during re-pressurization (Teatini *et al.*, 2019). So, we cannot rule out that the P18 field has fault sections that are critically stressed so that they induce weak earthquakes that have gone undetected. Such weak earthquakes correspond with rather small slippage area. It is not expected that pressure increase will create larger critically stressed fault areas that could induce larger earthquakes.

The absence of seismicity in P18 is likely related to the absence of seismicity in the entire area, which has many producing gas fields. For instance, the Monster field has been fully depleted without inducing seismicity. As yet, the non-seismic character of the faults in the P18 area cannot be explained. It is remarkable that also other areas in the Netherlands show no seismicity while the gas fields in those areas have been fully depleted and also other reservoir properties are similar to gas fields that have induced seismicity (Vörös *et al.*, 2019). Actually, the compaction seismicity is concentrated in two clusters, while gas fields outside these clusters appear to be non-seismic.

Future seismicity cannot be ruled out, because some small faults may still be stressed by cooling of the reservoir. However, any seismic slippage will be confined to the fault area in the vicinity of the reservoir, because only the fault height close to the reservoir will become critically stressed. The seal layers overlying the reservoir are much thicker than the reservoir, so that there is negligible risk of ever breaching the seal by fault slippage, as also concluded in the study by TNO (2019).

## References

- Baisch, S., Koch, C., Stang, H., Pittens, B., Drijver, B., & Buik, N. (2016). Defining the framework for seismic hazard assessment in geothermal projects V0.1. Technical Report, Report No. 161005, Bad Bergzabern, Germany: prepared for KennisAgenda Aardwarmte.
- Bois, A., Mohajerani, M., Dousi, N., & Harms, S. (2013). Inducing Earthquake by Injecting Water In A Gas Field: Water-weakening Effect. SPE Annual Technical Conference and Exhibition, 30 September - 2 October 2013, New Orleans, Louisiana, USA.
- Committee on Induced Seismicity Potential in Energy Technologies. Induced Seismicity Potential in Energy Technologies. The National Academies Press (2013).
- Davies, R., Foulger, G., Bindley, A., & Styles, P. (2013). Induced seismicity and hydraulic fracturing for the recovery of hydrocarbons. *Marine and Petroleum Geology*, 45 (0), 171-185.
- Davis, S. D., & Frohlich, C. (1993). Did (or will) fluid injection cause earthquakes? - criteria for a rational assessment. *Seismological Research Letters*, 64 (3-4), 207-224.
- De Crook, Th., H.W. Haak & B. Dost (1998). Seismich risico in Noord-Nederland. KNMI (Koninklijk Nederlands Meteorologisch Instituut), Techn. Rep., De Bilt, Netherlands.
- Deichmann, N., Kraft, T., & Evans, K. F. (2014). Identification of faults activated during the stimulation of the Basel geothermal project from cluster analysis and focal mechanisms of the larger magnitude events. *Geothermics*, 52 , 84-97.



- Dost, B., Goutbeek, F., van Eck, T., Kraaijpoel, D. (2012) Monitoring induced seismicity in the North of the Netherlands: status report 2010. WR 2012-03.
- Dost, Bernard et al., 2012. Monitoring induced seismicity in the North of the Netherlands: status report 2010,
- Dowrick, David J. and David A. Rhoades, (2004), “Relations Between Earthquake Magnitude and Fault Rupture Dimensions: How Regionally Variable Are They?”, *Bulletin of the Seismological Society of America*, Vol. 94, No. 3, pp. 776–788, June 2004.
- English, J.M., (2012), “Thermomechanical origin of regional fracture systems”, *AAPG Bulletin*, v. 96, no. 9 (September 2012), pp. 1597–1625.
- Fenix Consulting Delft BV (Febr.2016),” Geomechanical Support for BGS+ Storage Plan Permit Application”, Report for TAQA Energy BV.
- Foulger, G. R., Wilson, M. P., Gluyas, J. G., Julian, B. R., & Davies, R. J. (2018). Global review of human-induced earthquakes. *Earth-Science Reviews*, 178 , 438-514.
- Geertsma, J. and van Opstal, G. (1973). A Numerical Technique for Predicting Subsidence Above Compacting Reservoirs, Based on the Nucleus of Strain Concept. *Verh. Kon. Ned. Geol. Mijnbouwk. Gen.*, 28, pp. 63-78.
- Grigoli, F., Cesca, S., Rinaldi, A. P., Manconi, A., López-Comino, J. A., Clinton, J. F., Westaway, R., Cauzzi, C., Dahm, T., & Wiemer, S. (2018). The November 2017 Mw 5.5 Pohang earthquake: A possible case of induced seismicity in South Korea. *Science*, 360 (6392), 1003-1006.
- Hagoort, J.J. (1980), “Modeling the Propagation of Waterflood-Induced Hydraulic Fractures”, SPE-7412-PA.
- Hangx , S.J.T., C.J. Spiers, C.J. Peach, A. ten Hove and A.M.H. Pluymakers, “Mechanical behaviour and transport properties of anhydrite - implications for caprock integrity during long-term storage of CO<sub>2</sub>”, *Geophysical Research Abstracts*, Vol. 14, EGU2012-9379-1, 2012.
- Heap, M.J., M. Villeneuve, A.R.L. Kushnir, J. Farquharson, P. Bauda, T.Reuschlé , (2019), “Rock mass strength and elastic modulus of the Buntsandstein: An important lithostratigraphic unit for geothermal exploitation in the Upper Rhine Graben”, *Geothermics*, Volume 77, January 2019, Pages 236-256
- Houtgast, G. Aardbevingen in Nederland. KNMI report 179. KNMI, de Bilt (1992).
- Kanamori, H. (1994), *Mechanics of Earthquakes*. *Annual Rev. Earth Planet Sci.*, 22, p207-237.
- Kim, K., Ree, J., Kim, Y., Kim, S., Kang, S. Y., & Seo, W. (2018). Assessing whether the 2017 Mw 5.4 Pohang earthquake in South Korea was an induced event. *Science (New York, N.Y.)*, 360 (6392), 1007.
- KNMI, Bernard Dost, Femke Goutbeek, Torild van Eck and Dirk Kraaijpoel, (2010), “Monitoring induced seismicity in the North of the Netherlands: status report 2010””, De Bilt, 2012 | Scientific report; WR 2012-03.
- Koning, E.J.L. (1988), “Waterflooding under fracturing conditions”, PhD thesis TU Delft.
- Kraaijpoel, D. et al., 2008. Location of induced earthquakes in the Netherlands gas fields. In ESC General Assembly 2008, September 7-12, 2008, Hersonissos.
- Logan, J.M., C.A. Dengo, N.G. Higgs, Z.Z. Wang, (1992), “Fabrics of experimental fault zones: their development and relationship to mechanical behaviour”, in *Fault Mechanics and Transport properties of rock*, ed. Evans, Wong), Academic Press.
- McGarr, A., 1976. Seismic Moments and Volume Changes. *Journal of Geophysical Research*, 81(8), pp.1487–1494.
- NAM, (2013), “Winningsplan Monster Field”, NLOG\_FieldAsset\_8243\_wipla\_Gaag\_Monster\_PUB.pdf on <http://www.NLOG.nl>.
- Nicholson, C., R.L. Wesson, (1990), “Earthquake hazard associated with deep well injection- A report to the US Environmental Protection Agency”, USGS 1951, Appendix A, p65.
- Pater, C.J. de and S. Baisch, 2011. Geomechanical Study of Bowland Shale Seismicity. Synthesis Report prepared for Cuadrilla Resources Ltd., 71 pages.
- Roest, J.P.A., Kuilman, W. (1993). Geomechanische Analyse van de lichte aardshokken in het Eleveld reservoir, TU-Delft.
- Roest, J.P.A., Kuilman, W. (1994). Geomechanical analysis of small earthquakes at the Eleveld gas reservoir. In: ‘Eurock ’94; SPE/ISRM international conference, Delft, Netherlands’, pp. 573–580.

- Rutledge, James, Xiaowei Weng, Chris Chapman, Xin Yu, and Scott Leaney, (2015), “Bedding-plane slip as a microseismic source during hydraulic fracturing”, p926, THE LEADING EDGE, August 2015.
- Scholz, Christopher H. Earthquakes and friction laws. *Nature* (1998) 391(1st January 1998): 37-42.
- Segall, P., & Lu, S. (2015). Injection-induced seismicity: Poroelastic and earthquake nucleation effects. *Journal of Geophysical Research: Solid Earth*, 120 (7), 5082-5103.
- STAATSTOEZICHT OP DE MIJNEN, (2016), “METHODIEK VOOR RISICOANALYSE OMTRENT GEÏNDUCEERDE BEVINGEN DOOR GASWINNING TIJDELIJKE LEIDRAAD VOOR ADRESSERING MBB. 24.1.P, VERSIE 1.2”, Den Haag
- Teatini, P., C. Zoccarato, M. Ferronato, A. Franceschini, G. Isotton, M. Frigo, C. Janna, (2019), “KEM-01 Geomechanical factors determining fault criticality during pressure cycling of underground gas storage in (see.
- Thienen-Visser, L van, M. Nepveu, J. Hettelaar “Deterministische hazard analyse voor geïnduceerde seismiciteit in Nederland”, TNO 2012 R10198, (2012),
- TNO (2015), “Quick scan of Induced Seismicity Potential for small onshore depleting gas fields in The Netherlands”, 2015 R10295.
- TNO (2018), “Inventarisatie aantoonbare effecten voor mens en milieu als gevolg van historische conventionele frackoperaties”, TNO2018 R10807 -Eindrapport, 11 september 2018.
- TNO, (2019), “CO2 storage feasibility in the P18-2 depleted gas field”, August 2019, TNO report 11111, Authors: Neele, F, T. Wildenborg, K. Geel, D. Loeve, L. Peters, S. Kahrobaei, T. Candela, M. Koenen, P.Hopmans, K. van der Valk, B. Orlic, V. Vandeweyer.
- Vörös, R., S. Baisch, (2019), “Geomechanical Study – Small Gas Fields in the Netherlands”, State Supervision of Mines (SodM), KEM program report, Version 1, Archive No.: SODM002.



## Feasibility study P18 (final report)

Prepared by: V. Vandeweyer,  
R. Groenberg,  
R. Donselaar,  
M. Pluymaekers,  
D. Loeve,  
C. Hofstee,  
M. Nepveu,  
B. Orlic,  
O. Akemu,  
U. Miersemann,  
T. Benedictus,  
R. Arts,  
F. Neele,  
W. Meindersma,  
M. Dillen

Reviewed by: C. Hofstee

Approved by: J.Brouwer  
(CATO-2 Director)

# Table of Content

3.	RESERVOIR GEOLOGY AND PETROPHYSICS STUDY	10
3.1.	Introduction.....	11
3.2.	Background on P18.....	12
3.3.	Data and methods.....	14
3.3.1.	Sources of data .....	14
3.3.2.	Methods.....	14
	Static reservoir modelling	14
	Quality control	15
	Core and outcrop sampling	16
3.4.	Geological setting.....	16
3.4.1.	Structural history .....	16
	Pre-rift stage	16
	Rift stage	17
	Post-rift/Inversion	18
3.4.2.	Depositional setting.....	19
3.4.3.	Source rock and charging .....	20
3.5.	Reservoir geology .....	20
3.5.1.	Structure and faults .....	20
3.5.2.	Lithologies .....	23
3.5.3.	Petrophysics.....	27
	Wells.....	27
	Model.....	29
3.6.	Seals .....	29
3.6.1.	Primary Seal.....	29
3.6.2.	Secondary and higher seals.....	30
3.6.3.	Shallow gas accumulations .....	33
3.7.	GIIP: estimates and sensitivity .....	36
3.8.	Conclusions and recommendations .....	37
3.8.1.	Conclusions.....	37
3.8.2.	Recommendations .....	39
3.9.	Acknowledgements .....	39
3.10.	References .....	39
4	RESERVOIR STUDY	42
4.1	Introduction.....	42
4.2	Analytical reservoir study .....	42
4.2.1.	Introduction.....	42
4.2.2.	P18 analytical study results.....	42
4.3	Dynamic reservoir study.....	43
4.3.1.	Overview of P18 field .....	43
4.3.2.	Production data .....	45
4.3.3.	Simulation constraints .....	45
4.4.	History match of P18-2.....	45
4.5.	History match of P18-4.....	49
4.6.	History match of P18-6.....	51
4.7.	Discussion and conclusion of the history match .....	52
4.8.	Injection study of P18.....	53
4.8.1.	Introduction.....	53
4.8.2.	Results and discussion.....	53
4.8.3.	Conclusion.....	57

4.9.	Thermal aspects of reservoir modelling of P18.....	57
4.9.1.	Introduction.....	57
4.9.2.	P18 thermal reservoir study .....	57
5.	GEOCHEMICAL STUDY .....	61
5.1.	Geochemical modelling.....	61
5.1.1.	Introduction.....	61
5.1.2.	Stages and scenarios.....	61
5.1.3.	Modelling approach .....	62
5.1.4.	Reservoir and cap rock conditions .....	63
5.1.5.	Pre-operational conditions .....	64
5.2.	Geochemical effects of CO <sub>2</sub> injection.....	66
5.2.1.	Introduction.....	66
5.2.2.	Reservoir rock .....	66
	Short term effects on connate water .....	66
	Carbonate and sulfide mineral reactions (mid term) .....	66
	Full suite of mineral reactions (long term) .....	66
5.2.3.	Cap rock seal .....	68
	Effects on connate water (short term) .....	68
	Carbonate and sulfide mineral reactions (mid-term) .....	68
	Full suite of mineral reactions (long term) .....	68
5.2.4.	Reference scenario; equilibrium assemblage .....	69
5.2.5.	Formation water sensitivity.....	69
5.2.6.	O <sub>2</sub> impurity.....	69
5.3.	Conclusions.....	70
5.4.	References.....	70
6.	TOP SEAL AND FAULT INTEGRITY STUDY .....	71
6.1.	Introduction.....	71
6.1.1.	Background .....	71
6.1.2.	Scope and objective .....	71
6.1.3.	Approach .....	72
6.2.	Geomechanical field characterization .....	72
6.2.1.	Field description .....	72
6.2.2.	Lithological differentiation of the top seal .....	74
6.2.3.	Geomechanical characterization of the top seal and overburden formations .....	76
6.2.4.	In situ stress .....	80
6.3.	Geomechanical numerical model.....	81
6.3.1.	Schematisation and mesh .....	81
6.3.2.	Boundary and initial conditions .....	83
6.3.3.	Pressure loads .....	84
6.3.4.	Calculation scenarios .....	88
6.4.	Top seal integrity assessment.....	89
6.4.1.	Potential for induced fracturing of top seal due to CO <sub>2</sub> injection.....	89
6.5.	Fault seal integrity assessment.....	97
6.5.1.	Fault seal analysis.....	97
6.5.2.	Fault stability analysis .....	99
6.6.	Induced seabed deformation.....	105
6.7.	Conclusions.....	108
7.	WELL INTEGRITY STUDY .....	111
7.1.	Executive summary (restricted).....	111
7.2.	Introduction.....	112

7.2.1.	History of the P18 field .....	112
7.2.2.	Data availability .....	113
7.2.3.	Methodology.....	115
7.3.	Definition of well integrity barriers .....	118
7.4.	Primary cement across the caprock.....	119
7.5.	Production liner .....	119
7.6.	Production casing.....	120
7.7.	Wellhead .....	120
7.8.	Production tubing .....	120
7.9.	Primary cement outside production casing .....	120
7.10.	Production liner hanger .....	120
7.11.	Production packer.....	121
7.12.	Well integrity assessment.....	121
7.12.1.	P18-2A1 .....	121
	Cement barrier across the primary caprock .....	121
	Cement barrier across the secondary caprock.....	121
	Production liner and casing.....	122
	Production tubing and completion .....	122
	Conclusion .....	124
7.12.2.	P18-2A5 .....	124
	Cement barrier across the primary and secondary caprock .....	124
	Production and intermediate liner.....	124
	Production tubing and completion .....	125
	Other criteria.....	125
	Conclusion .....	127
7.12.3.	P18-2A6 .....	127
	Cement barrier across the primary and secondary caprocks .....	127
	Production casing and liner.....	127
	Production tubing and completion .....	127
	Other criteria.....	128
	Conclusion .....	130
7.12.4.	P18-2A6st.....	130
	Cement barrier across the primary and secondary caprocks .....	130
	Production and intermediate liner.....	130
	Production tubing and completion .....	130
	Other criteria.....	130
	Conclusion .....	130
7.12.5.	Well P18-4A2 .....	132
	Cement barrier across the primary and secondary caprocks .....	132
	Production casing and liner.....	132
	Production tubing and completion .....	132
	Other criteria.....	132
	Conclusion.....	132
7.12.6.	Well P18-6A7 .....	134
	Cement barrier across the primary and secondary caprocks .....	134
	Production liner and casing.....	134
	Production tubing and completion .....	134
	Other criteria.....	134
	Conclusion.....	135
7.12.7.	Well P18-2 .....	137
	Cement barrier across the primary and secondary caprocks .....	137
	Abandonment plugs .....	137
	Production liner and casing.....	137
	Conclusion .....	137
7.13.	Summary of integrity assessment of the P18 wells.....	139
7.14.	Long-term well integrity .....	140
7.14.1.	Material degradation.....	140

7.14.2.	Integrity of the P18 wells .....	140
7.15.	Conclusions and recommendations .....	141
7.15.1.	Remediation and mitigation.....	141
7.15.2.	Abandonment.....	142
7.16.	References .....	142
8.	MIGRATION PATH STUDY .....	143
8.1.	Introduction.....	143
8.2.	Available data and workflow.....	143
8.3.	Geological model of the P18 Bunter reservoir and overburden.....	144
8.3.1.	Field description .....	144
8.3.2.	Overburden .....	145
8.3.3.	Faults.....	146
8.4.	Migration scenarios .....	148
8.4.1.	Methods.....	148
8.4.2.	Results .....	148
Migration scenario: Buntsandstein .....	148	
Migration scenario: Rijn/Rijswijk sandstone.....	149	
Migration scenario: Holland Greensand.....	149	
Migration scenario: Texel Greensand.....	151	
Migration scenario: Dongen sand & Brussel sandstone .....	151	
8.5.	Present day hydrocarbon migration .....	152
8.6.	Conclusions.....	153
8.7.	Preliminary monitoring concept.....	154
Introduction .....	154	
8.7.1.	The Eon CCS project .....	154
Introduction .....	154	
Infrastructure .....	154	
Roadmap.....	155	
8.7.2.	The proposed monitoring plan .....	156
8.8.	Geological background information .....	157
8.8.1.	Structure.....	157
8.8.2.	Reservoir properties .....	158
8.8.3.	Overburden properties .....	160
8.9.	Risk assessment of P18.....	161
8.9.1.	Introduction.....	161
8.9.2.	Summary of identified risks .....	161
8.10.	Development monitoring plan.....	162
8.10.1.	Introduction.....	162
Monitoring categories.....	163	
Procedure monitoring plan .....	164	
Monitoring at different stages of the project.....	165	
8.10.2.	Proposed monitoring plan .....	166
8.10.3.	Relation risks – proposed monitoring methods.....	167
Introduction .....	167	
CO <sub>2</sub> Plume imaging (1,8,9,15,16,17,18,19,21,22).....	167	
Top seal integrity (8,9,15,16,17,18,19,20,24,25).....	167	
CO <sub>2</sub> migration in the overburden (19,20,21,23,24,25,26,27).....	168	
Calibration of flow simulations (1,2,3,4,5,8,9,15,16,17,18,21,22) .....	168	
Well integrity (6,7,8,9,10,11,12,13,14,20,23,24,25,27,28).....	168	
8.10.4.	EU Storage Directive / OSPAR .....	168
8.10.5.	Emissions accounting for ETS .....	169
8.11.	Conclusions .....	169
8.12.	References .....	169

9.	SITE DEVELOPMENT PLAN	172
9.1.	Introduction	172
9.2.	Timeline overview	172
9.3.	Detailed timeline overview	174
9.3.1.	Feasibility study and high-level cost estimate ( $\pm 40\%$ )	174
9.3.2.	Concept selection	174
9.3.3.	Environmental Impact Assessment (EIA)	175
9.3.4.	Option on initial storage capacity from 2016	175
9.3.5.	Option on storage capacity from 2018	175
9.3.6.	Option on transport	175
9.3.7.	Apply for NER300 funding	176
9.3.8.	Obtain licenses (national coordination ruling)	176
9.3.9.	FEED	177
9.3.10.	Tendering for detailed Engineering Procurement and Construction	179
9.3.11.	EPC Contract signing	179
9.3.12.	Detailed engineering	180
9.3.13.	Detailed costing	180
9.3.14.	Procurement	180
9.3.15.	Construction: well abandonment and work-over	180
9.3.16.	Construction: equipment of the monitoring well	181
9.3.17.	Construction: platform modification	181
9.3.18.	Construction: pipeline construction	181
9.3.19.	Construction: onshore facilities	181
9.3.20.	Tie-in work and commissioning	181
9.3.21.	Baseline monitoring	181
9.3.22.	Handover	182
9.3.23.	Start injection	182
9.4.	Schematic overview of project timeline	183
11.	APPENDIX A: BASE, TOP AND THICKNESS OF FORMATIONS	188
12.	APPENDIX B: RESERVOIR EMBALLAGE	191
13.	APPENDIX C: OVERVIEW OF DUTCH PERMITS NEEDED FOR CCS PROJECTS	194
14.	APPENDIX D:	195
15.	APPENDIX E: PROJECT TIMELINE	198



### 3. Reservoir geology and petrophysics study

#### Executive Summary

This chapter describes the reservoir geology, overburden and petrophysics of the P18 gas field, which is operated by TAQA Energy B.V. It is located in the offshore part of the Dutch sector, 20km off the coast of the “2e Maasvlakte”, the latest extension to the port of Rotterdam. Here, E.ON is building a coal-fired power plant, of which the emitted CO<sub>2</sub> should be captured, transported, and injected into the (almost) depleted gas reservoirs of the P18 field. Aims of this report are to review the current state of knowledge on the reservoir geology and petrophysics of the reservoirs, estimate their potential storage volume based on GIIP, discuss the properties and sealing quality of the caprock and overburden, and indicate the level of uncertainty in the information provided. The subsurface data on the P18 reservoirs used to compile this report come from four sources: TAQA Energy B.V., the NLOG website (oil- and gas information portal of the Netherlands), the “DINO Loket” database operated by TNO, and TNO itself.

High-caloric gas is being produced from the P18 field since 1993. It is trapped in Triassic-aged sandstones of mixed fluvial/aeolian origin below impermeable layers of clay. The P18 field consists of three blocks that are bound by a system of NW-SE oriented normal faults, which are sealing because of juxtaposition of permeable reservoir intervals with impermeable intervals in the overburden. Block P18-2 has three compartments, whereas blocks P18-4 and P18-6 each have one compartment. The top of the compartments lies at depths between 3175 m and 3455 m below sea level. Production data suggests that most faults between the compartments are sealing, except for the one between compartments P18-02I and P18-02II, which is not sealing in the current situation.

Average gross reservoir thickness in the production wells is 200m. Average NTG of the four individual production zones identified in the reservoir (0.62-0.96) increases from base to top over the reservoir interval. Average porosity is highest in the upper zone (7-13%), is slightly lower in the middle two zones (5-9%), and lowest in the lower zone (3-5%). Permeabilities were calculated based on a porosity-permeability relation, i.e., they follow the same trend. They are highest in the upper zone (2-207mD), lower in the middle two zones (0.1-0.8mD), and lowest in the lower zone (< 0.1mD). Combined thickness of the upper and middle two zones is approx. 100m, as is the thickness of the lower zone. Average water saturations are lowest in the upper (0.24-0.47) and lower of the middle two zones (0.32-0.42), and highest in the lower zone (0.78-0.92).

The primary seal to the P18 reservoirs is 150m thick, and consists of impermeable siltstones, claystones, evaporites and dolostones that directly overlie the reservoir. Closure along the reservoir-bounding faults is obtained by juxtaposition of permeable reservoir intervals with impermeable intervals in the overburden. Most of the bounding faults do not continue further upward into the overburden than the shales of the Altena group, the secondary seal, which is approx. 500m thick. Faults that do penetrate the primary and secondary seal are rare. It is unlikely that their sealing capacity has been compromised, since higher up in the overburden additional seals with substantial thickness are located.

Dynamic GIIP of the P18 field, estimated based on production data, is 17.22BCM. GIIP estimates obtained from the reservoir model are substantially lower: 15.39BCM. For block P18-02, the discrepancy between static and dynamic GIIP is only about 7%, which can easily be attributed to differences in porosity and average water saturation between the wells and the property model. For block P18-04 and P18-06, the discrepancy is much higher, and likely attributed to a combination of under- and overestimated property values (porosity, water saturation) and



Doc.nr: CATO2-WP3.01-D06  
Version: 2011.01.04  
Classification: Confidential  
Page: 11 of 198

## Feasibility study P18

---

structural uncertainty, i.e., reservoir-bounding faults that are slightly off in lateral position and dip compared to the 3D seismic.

### 3.1. Introduction

This chapter describes in detail the reservoir geology, overburden and petrophysics of the P18 gas field that is selected for CO<sub>2</sub>-storage. It forms part of the geological research that is carried out by TU Delft and TNO in work package 3.1 of the CATO-2 project. The P18 field, which is operated by TAQA Energy B.V., is located in the offshore part of the Dutch sector, about 20km off the coast of the “2e Maasvlakte”, the latest extension to the port of Rotterdam (Fig. 1). Here, E.On is building a coal-fired power plant, of which the emitted CO<sub>2</sub> should be captured, transported, and injected into the (almost) depleted gas reservoirs of the P18 field. Aims of this report are to review in detail the current state of knowledge on the reservoir geology and petrophysics of the reservoirs, estimate their potential storage volume based on GIIP, discuss the properties and sealing quality of the caprock and overburden, and indicate the level of uncertainty in the information provided. A potential migration pathway study is described in a separate report by TNO. The information in this report forms the basis for the work in WP3.02 (reservoir simulation), WP3.03 (geomechanical modelling), and WP3.04 (well integrity) of the CATO-2 project.

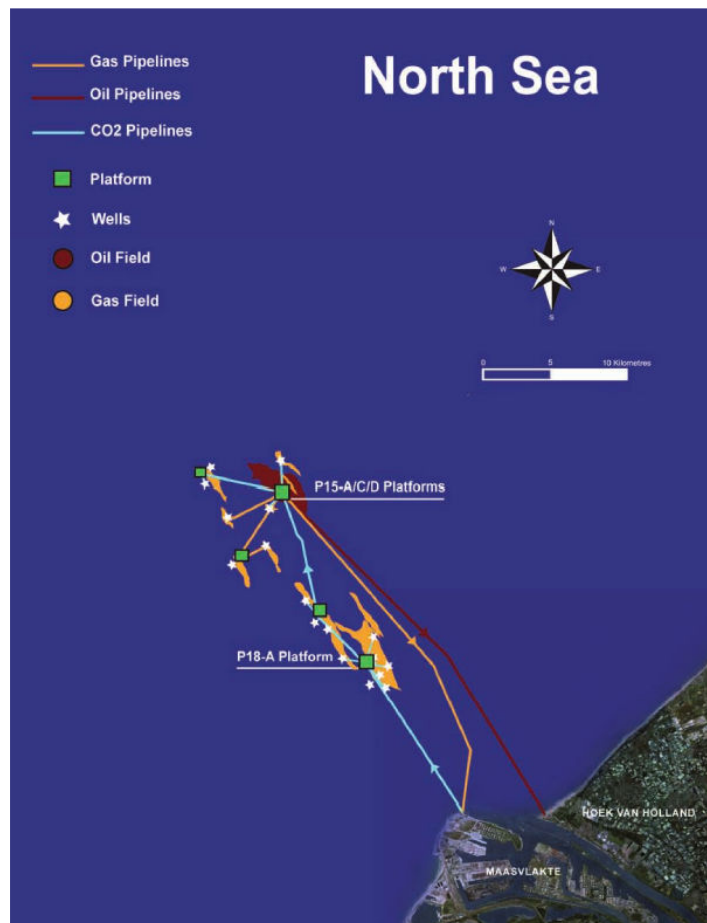


Figure 3.1: P18 gas fields and existing infrastructure (TAQA Energy B.V. 2008)

### 3.2. Background on P18

Rotterdam (Figure 3.1). High-caloric gas is being produced from these reservoirs since 1993. The gas reservoirs consist of sandstones of Triassic age (249-245 Ma; Geluk, 2005), and are sealed by impermeable layers of clay at a depth of 3.5km below the surface. The gas is produced through the P18-A satellite platform, and the P15-ACD processing and accommodations facilities in the adjacent P15 block, from where it is transported to the coast by a 40-km-long gas pipeline.

**Feasibility study P18**

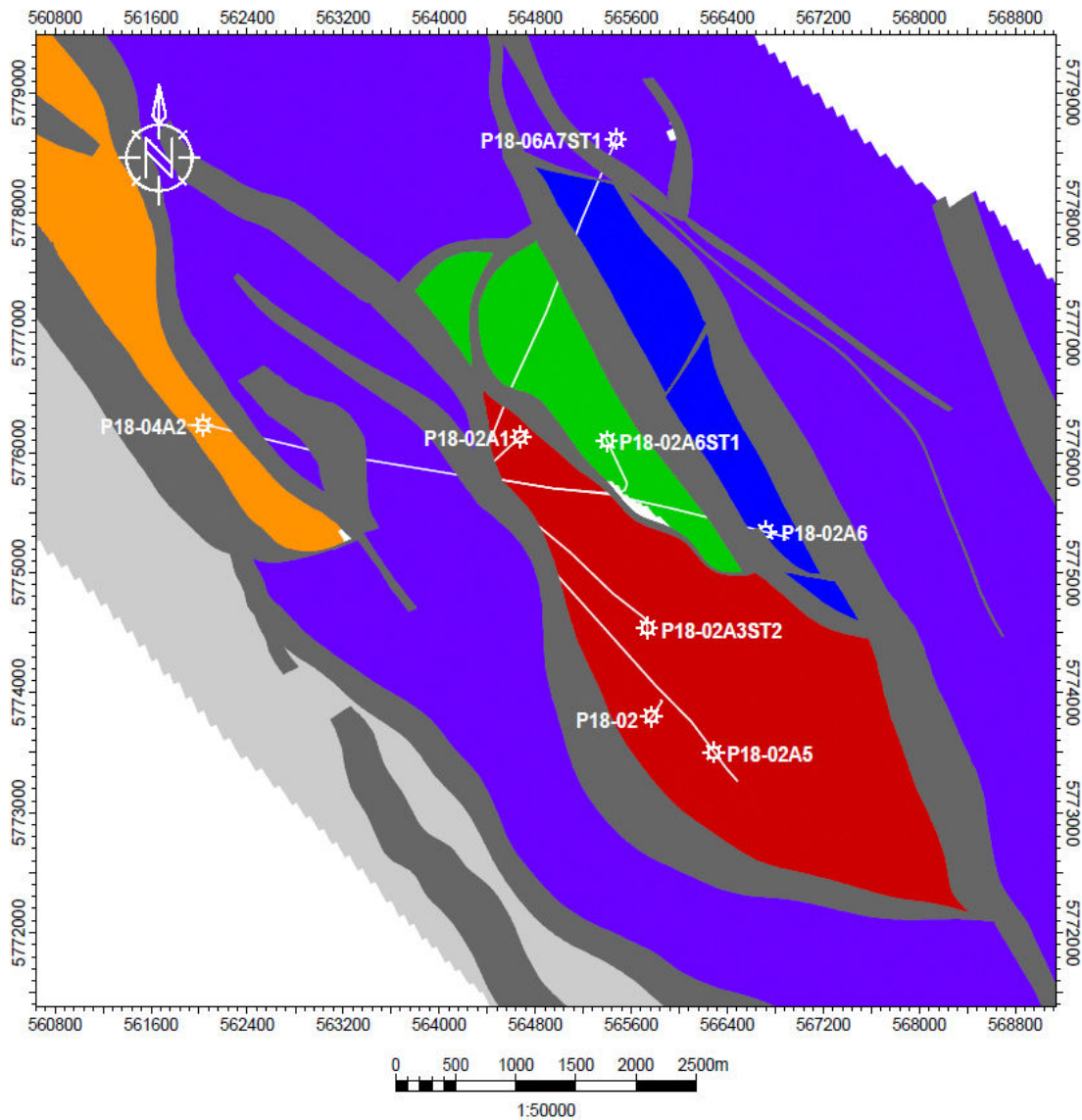


Figure 3.2: Layout of the P18 field, with position of wells at the top of the reservoir interval (top Bunter). Orange: P18-4 block; Red: P18-2, compartment I; Green: P18-2, compartment II; Blue: P18-2, compartment III; P18-6: purple block drilled by P18-06A7ST1.

The P18 field consists of three blocks, the P18-2, P18-4 and P18-6 blocks (Figure 3.2). P18-2 was discovered in 1989 with the exploration well P18-02. It consists of three compartments, P18-2I, P18-2II, and P18-2III.

P18-2I came on stream first, in 1993. It contains three production wells: P18-02-A1, P18-02-A3ST2, P18-02-A5ST1, and the exploration well P18-02. Compartment P18-2III contains one production well, P18-02-A6, and came on stream in 1997. Compartment P18-2II came on stream in 2003, and also contains one production well, P18-02-A6ST1. Since then, this production well produces simultaneously from the P18-02II and P18-02III compartments. Block P18-04 was discovered in 1991, and production started from well P18-04-A2 in 1993. Block P18-6 was discovered in 2003, and production started from well P18-06-A7ST1 in 2003.

**Feasibility study P18**

Peak production was established in 1998, with a cumulative year production of 2.2 Bcm. At the end of 2009, the total cumulative production of all P18 blocks was 17.3 Bcm. The current depletion status is approx. 95% (with respect to the abandonment pressure). Abandonment of the different blocks is expected in the period 2014-2018.

**3.3. Data and methods**

**3.3.1. Sources of data**

The subsurface data on the P18 reservoirs come from four sources (Table 1): TAQA Energy B.V., the NLOG website (oil- and gas information portal of the Netherlands), the “DINO Loket” database operated by TNO, and TNO itself.

Table 1: Sources of data

TAQA	DINO-Loket & NLOG site	TNO in-house/TU Delft
<ul style="list-style-type: none"> <li>• Reservoir model, both in RESCUE, and in RMS format, incl. relevant properties</li> <li>• Fault surfaces, as point data, in depth</li> <li>• Horizons of the reservoir intervals, in time and depth</li> <li>• Well data of the reservoir interval</li> <li>• Formation tops</li> <li>• Completion diagrams</li> <li>• 3D seismic cube <u>in two-way-travel time</u></li> <li>• Production data</li> </ul>	<ul style="list-style-type: none"> <li>• P18 gas extraction plan</li> <li>• 3D seismic cubes of surrounding blocks</li> <li>• Formation water composition</li> <li>• Mineral composition</li> <li>• Gas composition</li> <li>• Core samples</li> </ul>	<ul style="list-style-type: none"> <li>• Regional interpretations of horizons at group level, and faults</li> <li>• Composite well logs</li> <li>• Outcrop samples</li> </ul>

**3.3.2. Methods**

**Static reservoir modelling**

Static reservoir modelling was done in Petrel™, Schlumberger’s reservoir modelling suite, which is selected as the tool to use for this purpose within CATO-2. Because of the different scales the various disciplines within CATO-2 work in, two static geological models were constructed that differ in horizontal and vertical resolution:

1. A reservoir-scale geological model with high resolution (region of interest 18x9km; cell size 50mx50m; 38 equally-spaced layers in the reservoir interval). It is used for the GIIP estimates (see Chapter 7), flow simulation studies and geochemical modelling studies. It focuses on the reservoirs of the P18 field, and forms the basis for the facies-based property modelling that is planned for early 2011. It was completely rebuilt in Petrel because of import problems with the original static reservoir model from TAQA that was

## Feasibility study P18

---

built in RMS, the reservoir-modelling suite from Roxar. In particular, uncorrectable artefacts arose during the import process into Petrel (reservoir modelling software) and MORES (reservoir simulator used for history matching), particularly in relation to the numerous faults, which were not correctly reproduced. Therefore, a new static model was built in Petrel from the original subsurface data from TAQA (Table 1, left column). It has exactly the same resolution as the RMS model, which allowed import of the Gaussian-based property distribution of the RMS model into the Petrel model. Quality control was done by comparing the location of the horizons and faults, the properties, and the GIIP of the different compartments, in the new CATO-2 model to those of the original TAQA model. It was concluded that the differences are negligible (see Chapter 3.7 on uncertainties).

2. A regional-scale model at lower resolution (region of interest 40kmx30km; cell size 250mx250m; layering added in the geomechanical model). This model is larger in size than the reservoir-scale model, and is used in the geomechanical modelling study. It contains the main stratigraphical units of the reservoir and overburden, and the main faults in the reservoir and the overburden. Bounding surfaces that define the stratigraphical units are based on regional interpretations made by TNO. Using well data, 3D and 2D seismic, these interpretations were verified, and adapted when deemed appropriate. For the top and base of the reservoir only (top and base of the Main Buntsandstein Subgroup), the horizons from the higher-resolution reservoir-scale model were inserted to maximize the compatibility between the two models.

### Quality control

Quality control of the reservoir-scale model was done by comparing the depth of the horizons and the location of faults with the 3D seismic data cube supplied by TAQA. The seismic data were supplied in two-way travel times, so a time to depth conversion was needed to compare model with the seismic data. The data on seismic interval velocities provided by TAQA proved to be unusable for the purpose of time-depth conversion because of well-tying of the horizons in the depth domain. Therefore, it was decided to build a new velocity model based on regional-scale velocity modelling work performed in-house at TNO, newly interpreted seismic, and well tops in combination with additional velocity log data from wells. The regional velocity model was built on the basis of velocity information of 22 wells in the area (40 x 30 km) covered by the regional model. Wells were used mainly from the P15, P18, Q13, and Q16 blocks, supplemented by wells KDZ-02-S1, MON-02-S1, and MSG-01. The velocity model is based on a so-called “ $V_{int}-Z_{mid}$ ” relation of the main lithostratigraphic layers. Per layer, a linear velocity function was used:

$$V(z) = V_0 + K * z$$

where V stands for velocity ( $ms^{-1}$ ) and z represents depth (m). The estimate of  $V_0$  and K was made by taking the least squares approximation of  $V_{int}$  as function of  $Z_{mid}$ . Values of  $V_0$  and K thus obtained are given in Table 2.

The new velocity model was used for time-depth conversion of the reinterpreted stratigraphic horizons that were used for the regional-scale model. Quality control of the reservoir-scale model was done by comparing the position of the marker horizons and the position and dip of the faults to the 3D seismic cube provided by TAQA that was depth-converted using our new velocity model. It was concluded that there are small differences, mainly in lateral position and dip of faults, which are not negligible. Differences in fault dip can be attributed to differences in time-depth conversion due to the use of different velocity models. However, differences in the lateral position of faults in the order of 50-100m (1-2 voxels in the reservoir-scale model) can only be traced back

## Feasibility study P18

to the original seismic interpretation. This has implications for GIP estimates, as will be illustrated in Chapter 9.

Table 2: values of  $V_0$  and  $K$  used in the time-depth conversion

Unit ID	Stratigraphic name	$V_0(\text{ms}^{-1})$	$K(\text{s}^{-1})$
N	North Sea Group	1692.6	0.51
CK	Chalk Group	2324.1	0.75
KN	Rijnland Group	1708	0.9
S+AT	Schieland Group and Altena Group	2772.7	0.33
RN	Upper Germanic Trias Group	2788.9	0.45
RB	Lower Germanic Trias Group	2080.4	0.34

### Core and outcrop sampling

In order to facilitate work in other work packages of CATO-2, two core workshops were organized, one at the TNO core facility in Zeist, and one at the core facility of the Nederlandse Aardolie Maatschappij (NAM) in Assen. Purpose of these workshops was to assess the influence of sedimentation processes and diagenesis on the flow properties of the P18 reservoirs. Furthermore, plug samples were taken from the reservoir interval in the core of the P18-02 exploration well, and from the core of well P18-A-01 in the P18-01 field nearby. Plug samples of the caprock, taken from wells Q16-4 and Q16-FA-101, were provided by NAM. Furthermore, rock samples of the reservoir and seal rocks were collected from outcrops in quarries in Germany. Plug and outcrop samples were handed-over to members of WP3.02 and WP3.03 for further study.

## 3.4. Geological setting

### 3.4.1. Structural history

The reservoir rocks of the P18 field are of Triassic age (249-245 Ma; Geluk, 2005), and belong to the Main Buntsandstein Subgroup. The Triassic rocks in the Netherlands represent part of the post-Variscan sedimentary mega-cycle. Its deposition was strongly controlled by a sequence of rift pulses that started in the Late Triassic, and lasted until the Middle Jurassic. It can be subdivided into a pre-rift, syn-rift and post-rift stage.

#### Pre-rift stage

The Early Triassic was characterised by regional, thermal subsidence. During the Early Triassic, sedimentation continued in a gentle northwards dipping basin (Southern Permian Basin) but under semi-arid continental conditions. At the southern margin of this basin, the area of deposition of the rocks of the P18 reservoirs (Figure 3.3), fine-grained lacustrine sediments were laid down initially, followed by a sandy fluvial and aeolian succession: the Main Buntsandstein Subgroup.

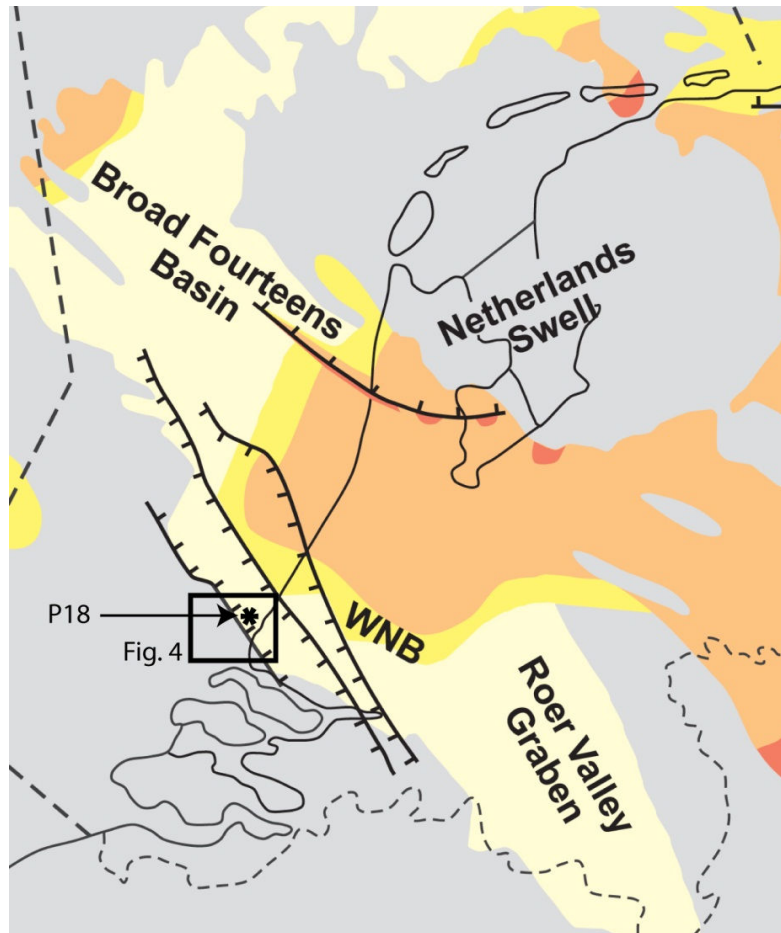


Figure 3.3: (Geluk 2007, after Geluk & Röhring 1997, 1999): Subcrop map of the Hardeggen Unconformity (= top reservoirs P18). Colours indicate formation; red: Lower Buntsandstein Fm., orange: Volpriehausen Fm., yellow: Detfurth Fm., white: Hardeggen Fm., grey: platform areas. WNB: West-Netherlands Basin.

These sediments were derived from the nearby London-Brabant Massif to the south, and the Rhenish massif to the southeast, which formed part of the northern rim of the Variscan orogenic belt (Geluk et al., 1996, Van Balen et al., 2000).

### Rift stage

Active rifting started in the Middle Triassic. Several rift pulses broke up the large basin into a number of NW-SE trending fault-bounded sub-basins (Figure 3.4; De Jager, 2007). One of the sub-basins formed was the West Netherlands Basin (WNB; Figure 3.3), a well-known oil- and gas province in the Netherlands that also contains the P18 gas field. From Middle to Late Triassic, during the *Early Kimmerian* rift phase, the WNB was formed, a structurally rather simple large-scale half-graben, bounded to the north by a major fault zone (Geluk, 1999b). During the Late Triassic to Early Cretaceous, rifting intensified, and faulting caused differential subsidence of the various subunits of the basin (van Balen et al., 2000).



**Feasibility study P18**

The strongest rifting occurred during the Late Jurassic to Early Cretaceous (Van Wijhe, 1987; De Jager et al., 1996; Racero-Baena & Drake, 1996). This caused the breaking-up of the basin into various sub-units, and large thickness variations in the Late Jurassic basin infill, i.e., thick in the basins and thin or absent on the highs.

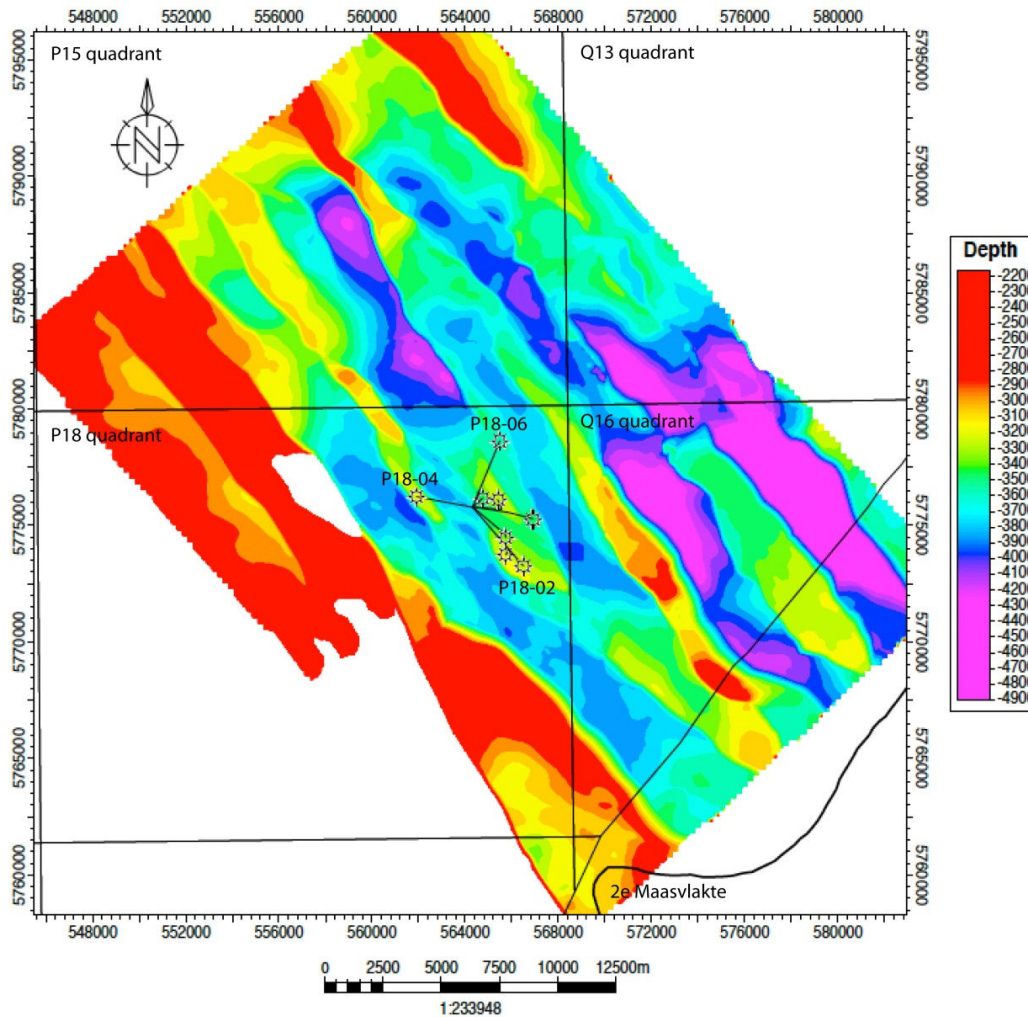


Figure 3.4: Contour map of the top Bunter (= top P18 reservoirs) in the offshore part of the West Netherlands Basin.

The rifting occurred in several discrete pulses of short duration in the time-span from Kimmeridgian to Barremian. Rifting gradually ceased during the Aptian-Albian (Van Wijhe, 1987), but subsidence of the WNB continued into the Late Cretaceous (van Balen et al., 2000).

**Post-rift/Inversion**

Compressional forces during the Late Cretaceous caused the inversion of the West Netherlands Basin (Van Wijhe 1987). On seismic, major fault zones display reverse movements, indicating that older basin-bounding faults were reactivated. Many of the oil-bearing anticlinal structures have been formed during this phase (De Jager et al., 1996; Racero Baena and Drake, 1996). The

**Feasibility study P18**

overall style of the inversion movements, with both a reverse vertical and a horizontal component, suggests they developed in response to transpression (dextral- strike-slip; Van Wijhe, 1987; Dronkers and Mrozek, 1991; Racero Baena and Drake, 1996).

**3.4.2. Depositional setting**

The Triassic sediments are of epicontinental character and were deposited in aeolian, fluvial, lacustrine, coastal and shallow-marine environments (Geluk, 2007). They are subdivided into two groups (Figure 3.5):

- The Lower Germanic Trias Group (Late Permian–Early Triassic), comprising mainly fine-grained clastic deposits with sandstone and oolite intercalations. In the P18 area, it consists predominantly of sandstones.
- The Upper Germanic Trias Group (Middle–Late Triassic) comprising an alternation of fine-grained clastics, carbonates and evaporites with subordinate sandstones.

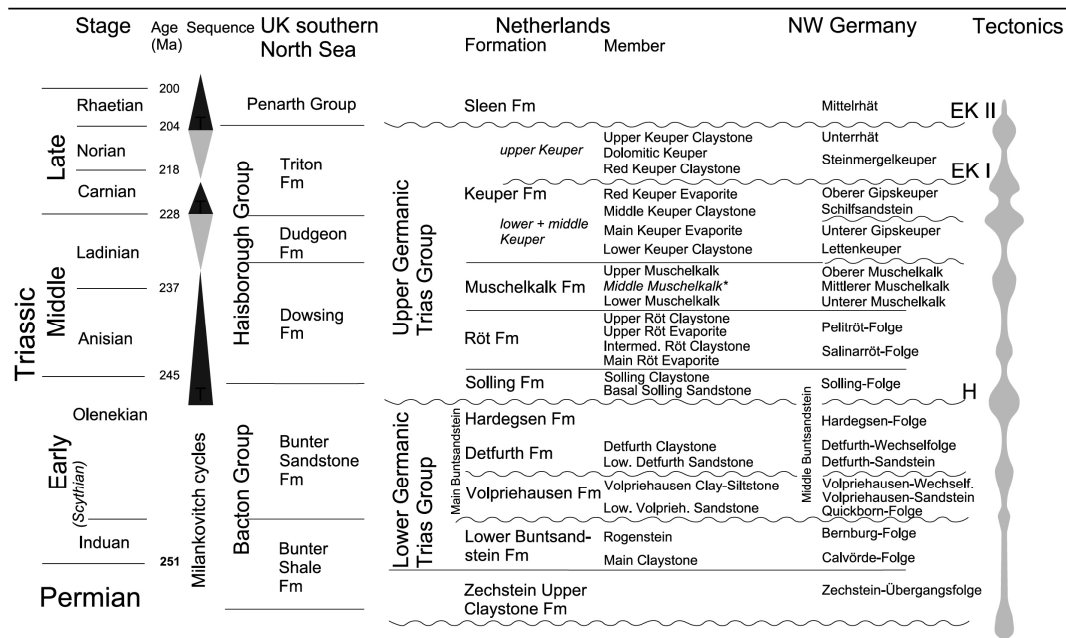


Figure 3.5: (Geluk, 2007; after Van Adrichem Boogaert and Kouwe 1994, Johnson et al. 1994, Geluk 1999 and Kozur, 1999; ages after ISC 2003; sequences after Gianolla and Jacquin 1998): Transgressive sequences in black, regressive sequences in grey. EK I: main Early Kimmerian Unconformity, base Norian; EK II: Early Kimmerian II Unconformity, base Rhaetian; H: Hardegsen Unconformity. \* Middle Muschelkalk comprises the Muschelkalk Evaporite and Middle Muschelkalk Marl.

It is formed by the Hardegsen or Base Solling Unconformity, which forms a regionally well-correlatable event (Ziegler, 1990; Geluk & Röhling, 1997, 1999; Geluk, 2005). Directly above lie the claystones and evaporates of the Solling Claystone and Röt formations that form the caprock to the P18 reservoirs.

### 3.4.3. Source rock and charging

The gases in the P18 and other Triassic reservoirs in the West-Netherlands Basin have either a pure Westphalian (Carboniferous) or a mixed origin (De Jager et al., 1996). Based on the carbon-isotope ratios, carbon molecular gas ratios and nitrogen isotope ratios, Gerling et al. (1999) also concluded that Carboniferous and Upper Permian gas fields in the western part of the Southern North Sea Basin are of a mixed origin, with a low maturity terrestrial source and a more mature marine source. The terrestrial source is a thick succession of Westphalian sediments, which contains humic source rocks in coals and shales. The average coal content of the Westphalian A and B succession is about 5.5% (Dusar et al., 1998), and the TOC of the coals is at least 70% (Van Bergen, 1998). The second source could be a Namurian (Carboniferous) marine source rock.

Generation of the gas and migration into the P18 reservoirs was modelled by van Balen et al. (2000). They concluded that generation set in at about 240 Ma, accelerated at 160 Ma, and levelled out towards the present. In the P18 area, generation continues until now, whereas in the central and northern parts, the generation rate strongly declined at about 150 Ma. The charging occurred between 150 Ma and 80 Ma. This is in agreement with K/Ar dating of diagenetically formed illite, from which the age of gas emplacement for a well in the Broad Fourteens Basin was inferred to be 140 Ma (Lee et al., 1985). As the WNB has a similar tectonic history as the Broad Fourteens Basin (Van Wijhe et al., 1987), the timing of gas emplacement can also have been similar.

## 3.5. Reservoir geology

### 3.5.1. Structure and faults

The structures that contain the reservoirs are bound by a system of NW-SE oriented faults in a horst and graben configuration, with a sinistral strike-slip component (Figure 3.6). The top of the reservoir compartments lies at depths between 3175 m and 3455 m below sea level (Figure 3.7).

Block P18-02 is the main block, and is bounded by two normal faults, the F19 fault and the F20 fault. A closer look at the offsets of these reservoir-bounding faults (Figure 3.8) indicates that they are sealing due to juxtaposition of reservoir zones against impermeable shales of the Altena Group. Inside P18-02, compartment P18-02I, which is the largest compartment of the three, is separated from compartment P18-02II by fault F14, the offset of which is insufficient to be sealing by juxtaposition (Figure 3.8). Indeed, production data suggest that there is partial communication between the two compartments across this fault (pers. comm. N. Vera of TAQA). It is likely that the sealing capacity of this fault depends on a pressure threshold, and that this threshold is exceeded due to depletion of the compartment after production. Compartment P18-02III is separated from P18-02II and P18-02I by fault F18, which has enough offset to be sealing by juxtaposition, except for a small region at the southern end (Figure 3.8). However, no or very minor pressure communication was observed between the P18-02I/ P18-02II compartments and the P18-02III compartment (pers. comm. N. Vera of TAQA), which suggests that the F18 fault is sealing.

Feasibility study P18

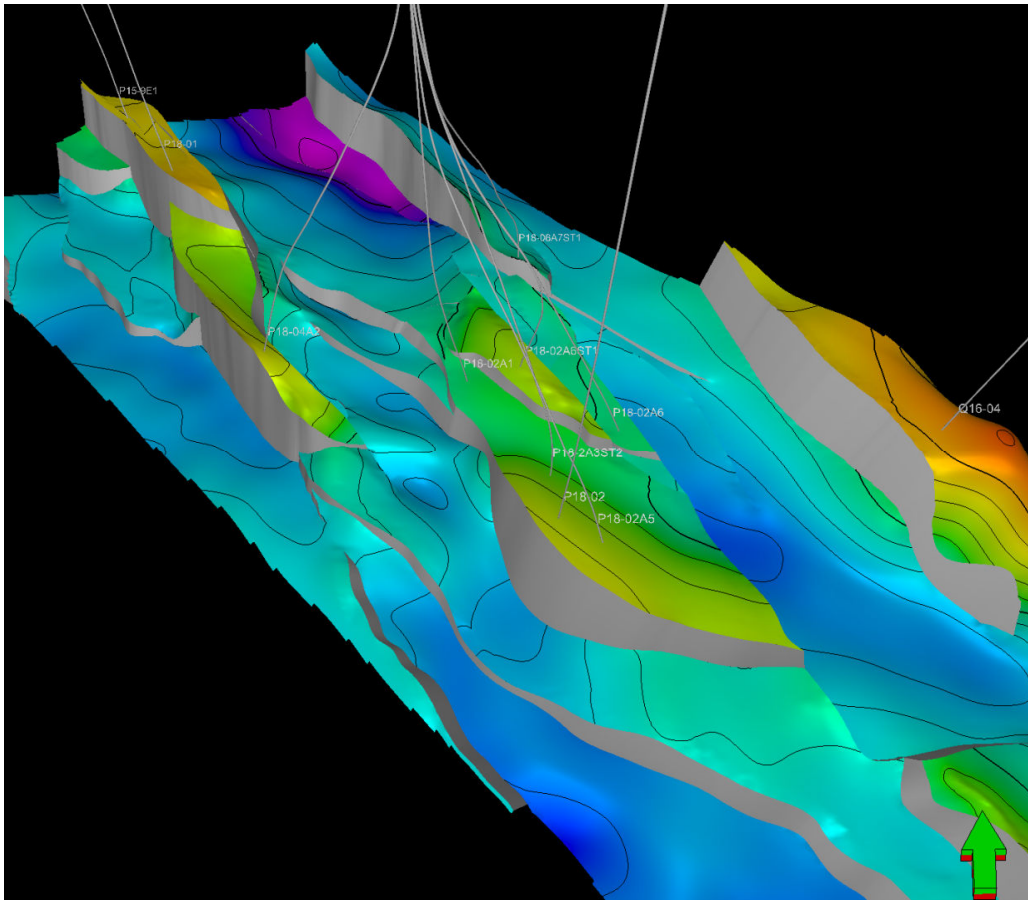


Figure 3.6: 3D view of the top of the P18 reservoirs. Faults are shown in grey.

Feasibility study P18

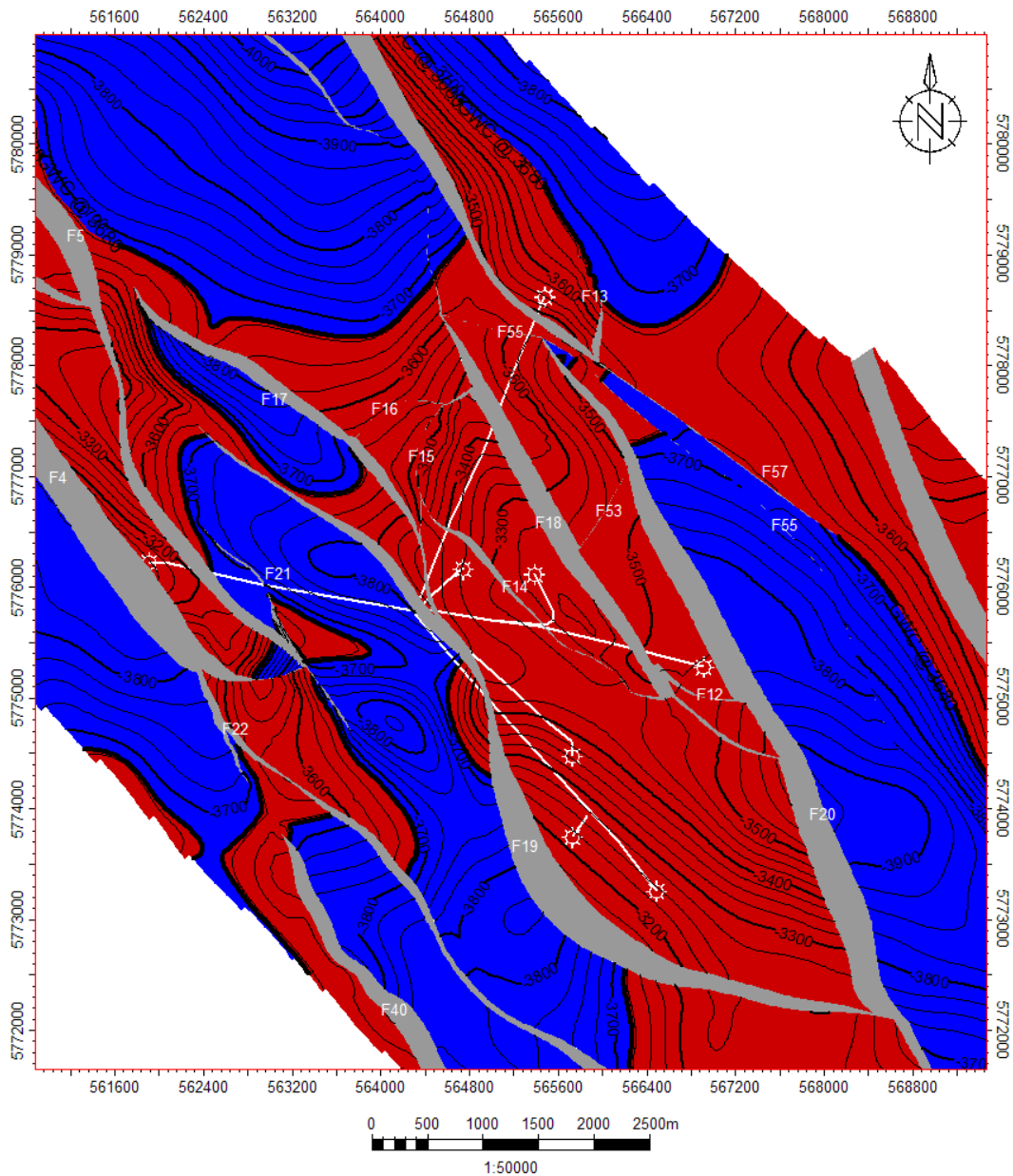


Figure 3.7: Contour map of the top of the reservoir, with faults bounding the compartments in grey. Fault identifiers and locations of the wells at the top of the reservoir are indicated in white. Colouring indicates pore fluid contents based on a GWC of 3680 m SSTVD; red: gas, blue: water

Block P18-04 is located to the northwest of the main block. It is bounded by faults F4 and F5 to the west and east respectively, and separated from the P15-E field by fault F3 (Figure 3.8). All three have sufficient offset to be sealing by juxtaposition, which is supported by production data (e.g. different pressures).

**Feasibility study P18**

Block P18-06 is located to the northeast of the main block. It is bounded by faults F13 and F57, of which only F13 has enough offset to be sealing by juxtaposition.

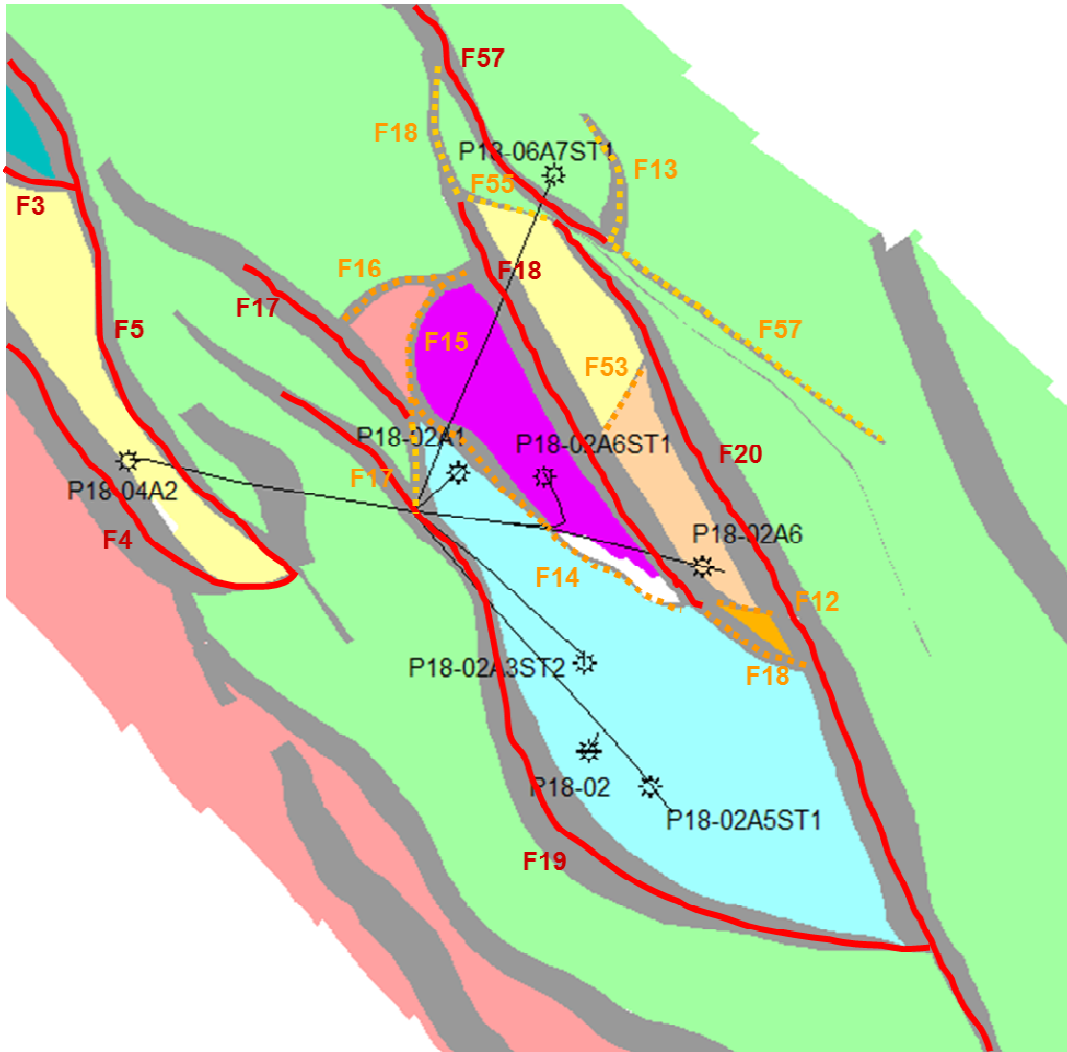


Figure 3.8: Map view of the P18 field, with the different reservoir compartments indicated in different colours. Faults that have enough offset to juxtapose reservoir against non-reservoir are indicated with bold red lines, and faults that do not have enough offset, i.e., where reservoir is juxtaposed against reservoir, are indicated with dotted orange lines.

**3.5.2. Lithologies**

The reservoir rocks of the P18 belong to the Main Buntsandstein Subgroup, a cyclic alternation of (sub-) arkosic sandstones and clayey siltstones. The Volpriehausen Formation is mainly of fluvial origin, but also contains substantial aeolian sediment. It consists of braided river deposits interbedded with dune deposits, and subordinate flood-plain and crevasse-splay deposits (Ames and Farfan, 1996). It is composed of a Lower Volpriehausen Sandstone Member and an Upper Volpriehausen Sandstone Member. The Volpriehausen Formation is a clean sandstone with a blocky appearance on Gamma-ray logs (Figure 3.9 & Figure 3.10) that contains high percentages

**Feasibility study P18**

of calcite and dolomite (Geluk et al., 1996).

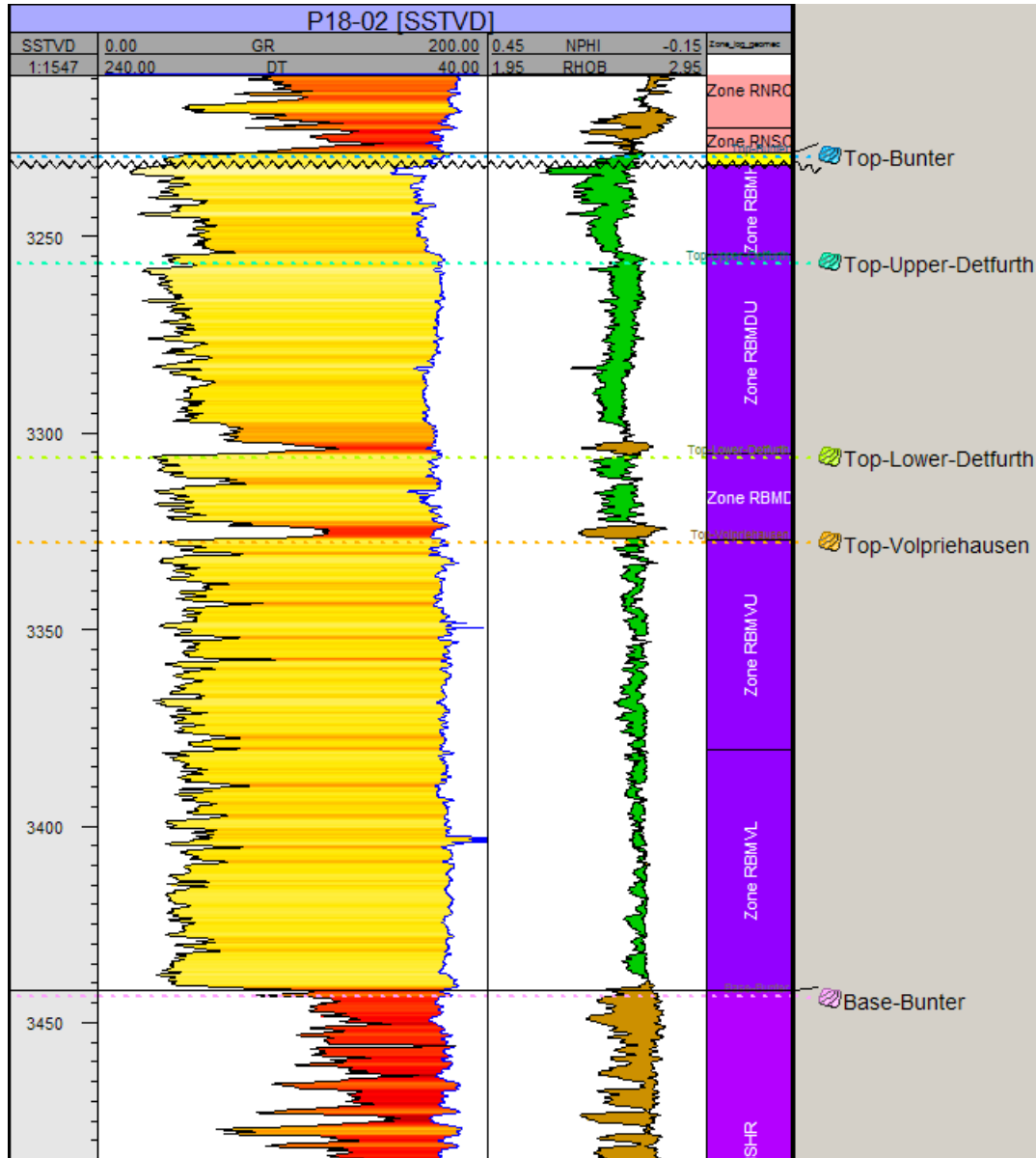


Figure 3.9: GR-log (red-yellow colouring), sonic log (blue), neutron porosity (NPHI) log, and bulk density (RHOB) log over the reservoir interval in the P18-02 exploration well.

On Gamma-ray logs, it is clearly distinguished from the Rogenstein Claystone Member below by a marked increase in Gamma-ray readings. The Rogenstein Claystone member forms the basal seal to the reservoirs (Figure 3.10). Only wells P18-02-A1, P18-02-A2, P18-02-A3ST2, and P18-02-A5 penetrate the entire Volpriehausen Formation. Its thickness in the wells ranges between 101 m and 115 m (Table A1 in Appendix A).



Doc.nr: CATO2-WP3.01-D06  
Version: 2011.01.04  
Classification: Confidential  
Page: 25 of 198

## **Feasibility study P18**

---

The Detfurth Formation is composed of a Lower and an Upper Detfurth Sandstone Member. It consists mainly of aeolian sediment (dunes), and some fluvial deposits (Ames and Farfan, 1996). The Lower Detfurth Sandstone Member forms one of the best reservoir intervals in the P18 fields. It is marked by low gamma-ray values (Figure 3.9 & Figure 3.10) due to its high quartz grain content and because it is quartz-cemented (Geluk et al, 1996). It is distinguished from the Volpriehausen Formation by a well-correlatable interval of high gamma-ray readings (Detfurth Unconformity) and two clearly recognizable coarsening upwards sequences (Figure 3.9 & Figure 3.10).



Feasibility study P18

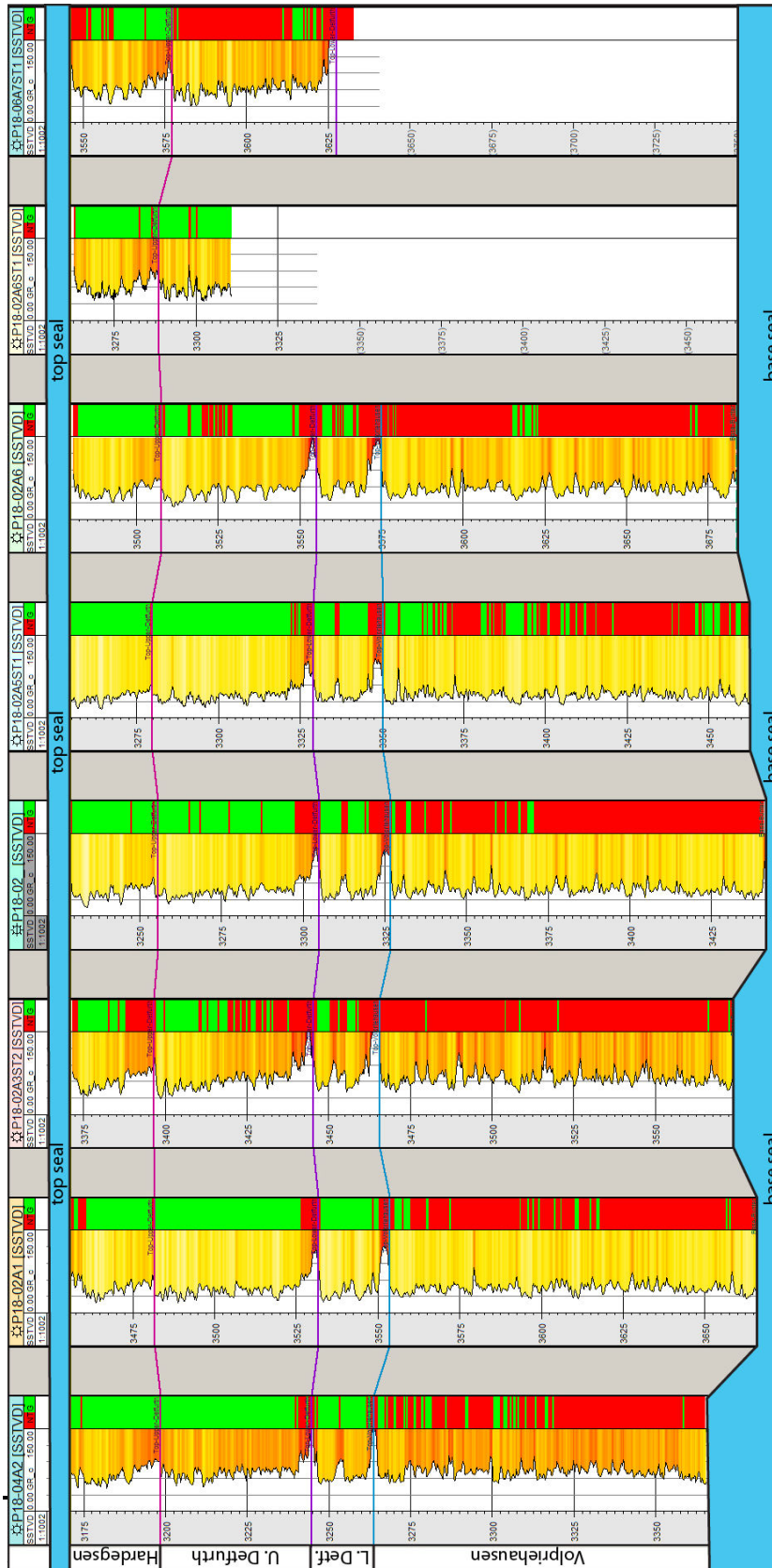


Figure 3.10: Log panel through the production wells of the P18 field. GR-logs on the left side, with colouring indicative of GR reading, yellow: low (sand), red: high (clay). Net Pay logs on the right side, red: no-pay zone, green: pay zone.

## Feasibility study P18

---

It is penetrated by all the wells except well P18-02-A6ST1. Well P18-02-A7ST1 only penetrates the top. Its thickness in the wells ranges between 19 m and 22 m (Table A2 in Appendix A).

The Upper Detfurth Sandstone Member is separated from the Lower Detfurth Sandstone Member by a second well-correlatable interval of high-Gamma-ray readings and a single coarsening-upward sequence (Figure 3.9 & Figure 3.10). It is penetrated by all the wells, although not completely by well P18-2A6ST1. Its thickness ranges between 47 m and 50 m (Table A3 in Appendix A).

The Hardegsen Formation is characterized by sandstones, and is recognized by a marked increase in the Gamma-ray values compared to the underlying Detfurth Formation. Furthermore, it displays a well-developed overall coarsening-upward pattern with low Gamma-ray values towards the top (Figure 3.9 & Figure 3.10). It consists mainly of aeolian deposits and is penetrated by all the wells. Its thickness in the wells ranges between 24 m and 33 m (Table A4 in Appendix). Above the Hardegsen Formation, gamma-ray values increase again, first mildly, and then strongly and abrupt (Figure 3.9). This mild increase is due to the transition from Hardegsen Formation to the Solling Sandstone Member, which here is included in the Hardegsen reservoir zone. The strong increase is due to the transition from the Solling Sandstone Member to the Solling Claystone Member that forms the basal part of the caprock to the P18 reservoirs (Figure 3.10).

### 3.5.3. Petrophysics

#### Wells

Data on the petrophysical properties of the reservoir intervals (N/G, PHI,  $S_w$ ) in the wells were provided by TAQA. They are displayed in tables A5, A6, A7, and A8 in the Appendix A. The Free Water Level (FWL) was determined by TAQA either from pressure-depth gradients or from mapped spill points. However, there is much uncertainty on the actual position of the FWL in the three blocks. For instance, in the P18-02 block, the lowest-known-gas was found at 3506 m (base perforation) in well P18-02A6, but the structural spill point of the P18-02 block is mapped at 3635 m in the NW corner of the block (Figure 3.7). A discussion on the position of the FWL and significance for GIIP estimates and history matching can be found in the report of WP3.02 on the reservoir engineering aspects of this feasibility study.

Average values of porosity and connate water saturation per field are displayed in Table 3. Average porosity in the Hardegsen formation ranges between around 7-13% and in the Detfurth Sandstone Members slightly lower around 5-9%. Maximum porosities encountered in the clean sandy parts of both formations are around 21 %.

The average permeabilities are calculated by TAQA based on the average porosities using a porosity-permeability relation. Although its origin is unclear, it is likely that this relation is based on core measurements. However, an attempt to reproduce this relationship from such measurements failed. Clearly, the permeabilities are highest in the Hardegsen Formation, with a range between 2 and 207 mD. In the Detfurth Sandstone Members they range between 0.1 and 0.8 mD. The combined thickness of both formations is approx. 100 m. The Volpriehausen has a much lower porosity that ranges between 3 and 5%. Permeabilities are very low, i.e., less than 0.1mD. The thickness of the Volpriehausen is also approx. 100 m.

**Feasibility study P18**

Average water saturations range between 0.24 and 0.47 in the Hardegsen Formation, between 0.43 and 0.57 in the Upper Detfurth Sandstone Member, between 0.32 and 0.42 in the Lower Detfurth Sandstone Member, and between 0.78 and 0.92 in the Volpriehausen Formation.

Table 3: Average (arithmetic) petrophysical properties of the reservoir intervals per block in the wells of the P18 field. "N/G" stands for "Net-To-Gross", as calculated by dividing the amount of sand (Vshale cut-off: < 0.35, PHI cut-off: > 0.02) in m by the total thickness of the formation, "PHI" indicates the average porosity (cut-off: > 0.02) of the bulk, "Sw" indicates the average water saturation (Vshale cut-off: < 0.35, PHI cut-off: > 0.02), and "k" indicates the average permeability as calculated using a porosity-permeability relation. "N.F.P." stands for not fully penetrated.

<b>P18-02</b>				
	<b>Hardegsen</b>	<b>Upper Detfurth</b>	<b>Lower Detfurth</b>	<b>Volpriehausen</b>
<b>Thickness (m)</b>	26.4	48.8	21	111
<b>N/G</b>	0.98	0.94	0.79	0.70
<b>PHI</b>	0.125	0.092	0.079	0.039
<b>Sw</b>	0.267	0.428	0.418	0.778
<b>K (mD)</b>	128.0	0.8	0.3	0.0
<b>P18-04</b>				
	<b>Hardegsen</b>	<b>Upper Detfurth</b>	<b>Lower Detfurth</b>	<b>Volpriehausen</b>
<b>Thickness (m)</b>	24	47	19	101
<b>N/G</b>	0.99	0.87	0.81	0.33
<b>PHI</b>	0.131	0.092	0.065	0.049
<b>Sw</b>	0.240	0.470	0.390	0.920
<b>K (mD)</b>	207.0	0.8	0.1	0.0
<b>P18-06</b>				
	<b>Hardegsen</b>	<b>Upper Detfurth</b>	<b>Lower Detfurth</b>	<b>Volpriehausen</b>
<b>Thickness (m)</b>	33	49	N.F.P.	N.F.P.
<b>N/G</b>	0.81	0.91	N.F.P.	N.F.P.
<b>PHI</b>	0.074	0.048	0.059	0.030
<b>Sw</b>	0.470	0.570	0.320	outside gasleg
<b>K (mD)</b>	1.8	0.0	0.1	0.0

## Feasibility study P18

Table 4: Average modelled petrophysical properties of the reservoir intervals per block in the P18 field.

<b>P18-02</b>				
	<b>Hardegsen</b>	<b>Upper Detfurth</b>	<b>Lower Detfurth</b>	<b>Volpriehausen</b>
<b>Thickness (m)</b>	26.6	49.1	21.5	116.2
<b>PHI</b>	0.107	0.077	0.066	0.033
<b>S<sub>w</sub></b>	0.401	0.650	0.624	0.936
<b>P18-04</b>				
	<b>Hardegsen</b>	<b>Upper Detfurth</b>	<b>Lower Detfurth</b>	<b>Volpriehausen</b>
<b>Thickness (m)</b>	29	49	19	111
<b>PHI</b>	0.111	0.076	0.064	0.0245
<b>S<sub>w</sub></b>	0.348	0.61	0.688	0.99
<b>P18-06</b>				
	<b>Hardegsen</b>	<b>Upper Detfurth</b>	<b>Lower Detfurth</b>	<b>Volpriehausen</b>
<b>Thickness (m)</b>	26.9	47.5	19.1	110.7
<b>PHI</b>	0.054	0.029	0.036	0.019
<b>S<sub>w</sub></b>	0.770	0.890	0.660	0.940

## Model

An important step in the quality control of the reservoir model is to verify that the property model honours the original data on the petrophysical properties from the wells, as presented above. Property modelling, i.e., interpolation of measured values of porosity and permeability between the wells, was done by TAQA in RMS assuming that the distribution of the properties resembles a Gaussian distribution. Water saturation was modelled with a height-saturation function. Table 4 displays the average modelled values of thickness, porosity and water saturation for the three blocks in the P18 field. When comparing these values to the average values of thickness, porosity, and water saturation in the wells (Table 3) it can be concluded that the average thicknesses of the reservoir intervals in the model agree well with those in the wells, and that it somewhat underestimates the porosities. Far more striking however is that the model substantially overestimates the water saturation by values ranging between 0.07 and 0.34. Permeabilities in the supplied property model were of low confidence, and have not been included in this report.

## 3.6. Seals

### 3.6.1. Primary Seal

The primary seal to the P18 reservoirs is formed by siltstones, claystones, evaporites and dolostones of the Solling Claystone Member, the Röt Formation, the Muschelkalk Formation, and the Keuper Formation that disconformably overlie the reservoir. The Solling Claystone Member consists of red, green and locally grey claystones that were deposited in a lacustrine setting just after the tectonic movements of Hardegsen phase during a major transgression (Geluk et al., 1996). It is the first laterally extensive claystone above the reservoir rocks of the Main Buntsandstein. In well P18-02, it has a thickness of approx. 5 m (Figure 3.11). The Röt Formation

## Feasibility study P18

---

consists of thin-bedded claystones, and is approx. 40 m thick. The Muschelkalk Formation consists of claystones, dolomites, and evaporates, and is approx. 70 m thick. All these rocks contain variable amounts of nodular anhydrite cementation (Spain and Conrad, 1997). The Keuper Formation consists of claystones intercalated with zones of anhydrite and gypsum, and is approx. 40 m thick. In total, the thickness of the primary seal in well P18-02 is approx. 155 m.

Faults are present in this primary seal. However, these faults appear to be sealing. Reservoir closure is obtained through impermeable zones above and below the reservoir interval (Figure 10), in combination with juxtaposition of permeable reservoir facies against impermeable non-reservoir facies of the Altena Group (secondary seal, see below). A closer look at the 3D seismic reveals that, although most of the reservoir-bounding faults do not continue further upward into the overburden than the shales of the Altena Group, some reverse faults that were formed during the inversion phase appear to originate around the fault tips of the older reservoir-bounding faults (Figure 3.14). However, inversion in the area of the P18 field was relatively weak. Therefore, it is unlikely that these inversion faults are reactivation faults that originate from movement along the older basin-bounding faults. Although impossible to rule out completely, it is not likely that the sealing properties of the basin-bounding faults have been compromised.

### 3.6.2. Secondary and higher seals

Directly above the primary seal lies the Altena Group, a thick succession of marine claystones, siltstones and marls of Early Jurassic age with excellent sealing quality. It also contains the Posidonia Shale Formation that is easily recognized on seismic due to its excellent reflectivity. The Altena Group has a thickness of approx. 500 m in the P18-02 well (Figure 3.14). The rest of the overburden is formed by several geological formations, some of which can also be assumed to have good sealing properties. The North Sea Supergroup is the shallowest succession in the overburden, and consists mostly of siliciclastic sediments. It has a thickness of approx. 1000m, and consists of the Lower, Middle and Upper North Sea Groups. The bases of the Upper and Lower North Sea Groups are marked by distinct unconformities. The Lower North Sea Subgroup comprises Paleocene and Eocene, predominantly marine deposits, the Middle North Sea Group includes mainly Oligocene, marine strata, and the Upper North Sea Group consists of marine to continental, Miocene and younger sediments. The North Sea Supergroup overlies the Chalk Group unconformably. On seismic, it appears as largely unfaulted, although sub-seismic scale faults might be present. Clayey sequences are abundant, especially in the lower part. These could very well act as secondary seals.

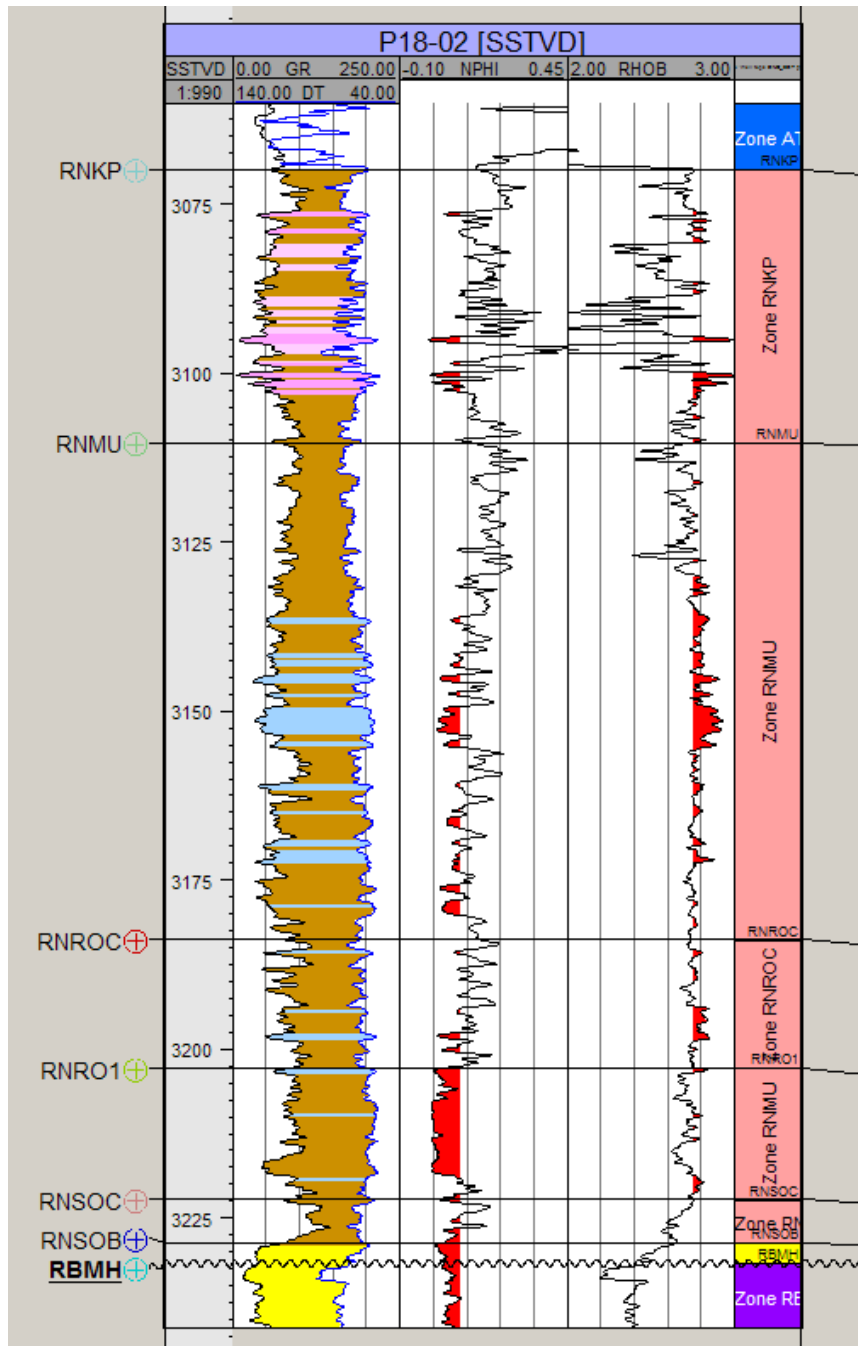


Figure 3.11: GR-log, sonic log, neutron porosity log and bulk density log of the primary seal in the P18-02 exploration well. RBMH: Hardegsen Formation = top reservoir (unconformity). Colouring indicates lithology, yellow: sand, brown: shale, blue: dolomite, light pink: anhydrite, dark pink: gypsum.

Feasibility study P18

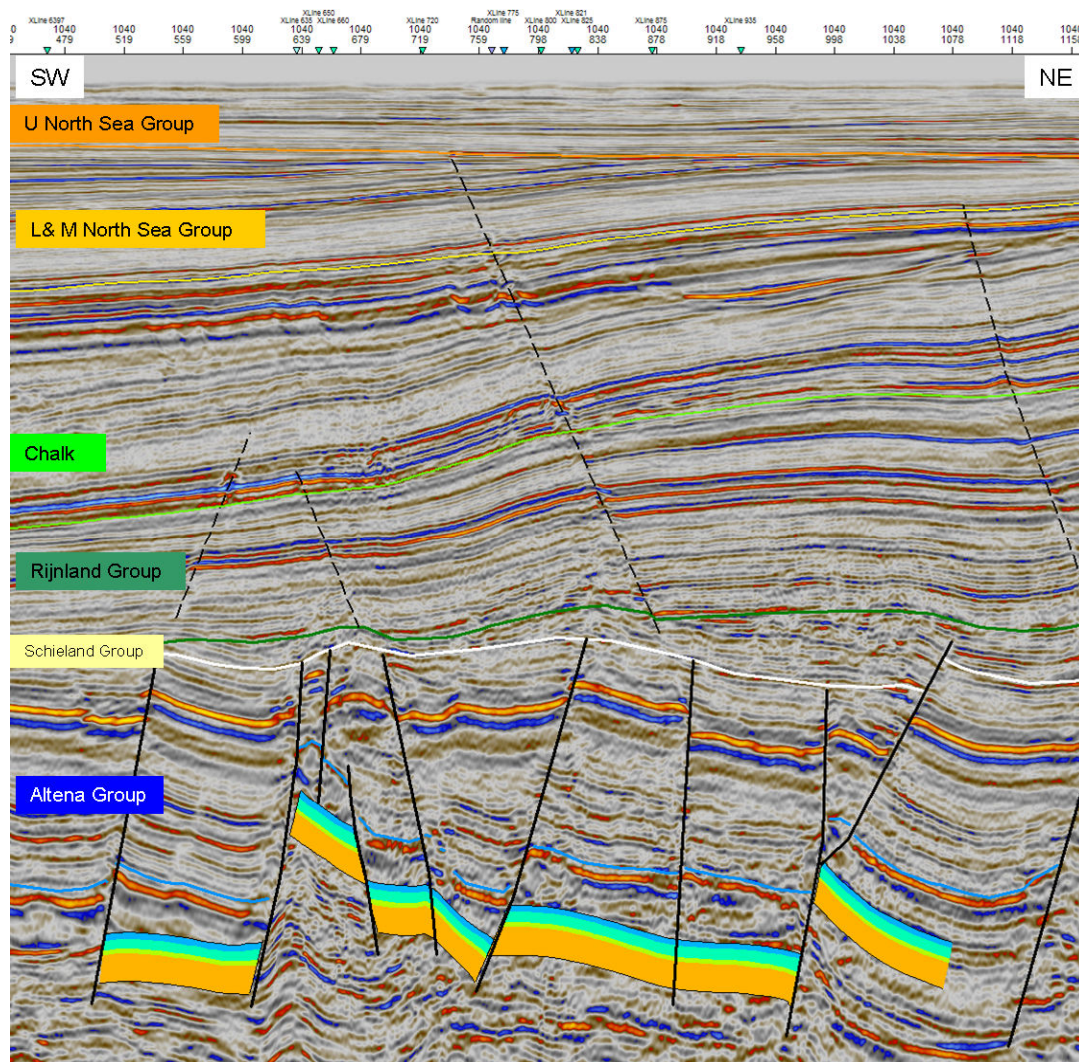


Figure 3.12: Seismic cross-section (inline 1040 in TAQA seismic cube) through the P18 field, displaying the reservoir interval (coloured layering), the main bounding faults to the reservoirs (bold lines), the main stratigraphic units in the overburden and the faults in the overburden (dashed). Position of cross-section is indicated in Figure 3.114.

The Upper Cretaceous Supergroup has a thickness of approx. 1400m and consists of the Ommelanden Formation, the Texel Formation and the Texel Greensand Member. During the Late Cretaceous, the influx of fine-grained clastics into the marine realm (Lower Cretaceous) diminished. A fairly uniform succession of marls and limestones of the Texel and Ommelanden Formations developed. These sediments have an earthy texture and are commonly known as 'chalk'. The sealing properties of these formations are questionable although few of the larger faults penetrate this interval. The Lower Cretaceous Supergroup has a thickness of approx. 1000m, and consists of the Holland Formation, the Vlieland Claystone Formation and the Vlieland Sandstone Formation. At locations in close proximity to the P18 field, some of the sandstone layers present in this interval are gas or oil bearing (e.g. Rijswijk Member, Rijn Member), which demonstrates the sealing quality of the numerous claystone intervals in this succession. The Lower Cretaceous appears largely unfaulted, which further increases the sealing potential of

**Feasibility study P18**

these rocks. However, it is expected that some sub-seismic scale faults are present throughout the Upper and Lower Cretaceous supergroups.

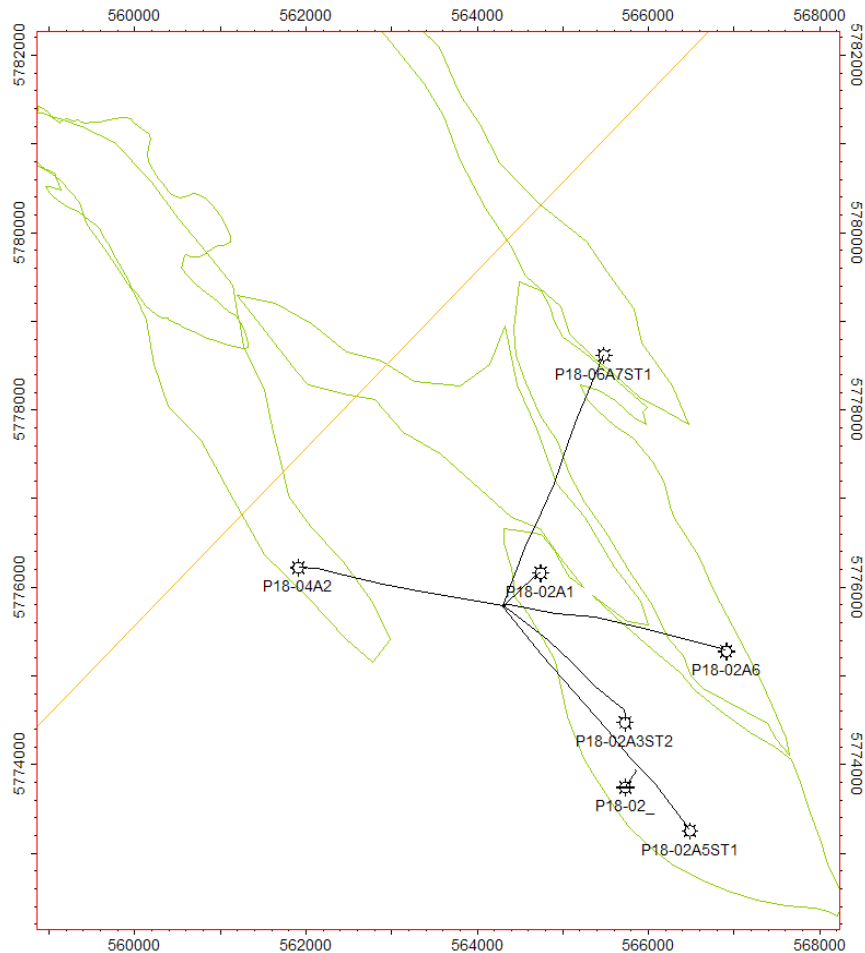


Figure 3.13: Map view of the P18 field, with position of the seismic cross-section of Figure 11 indicated in orange.

**3.6.3. Shallow gas accumulations**

On 3D seismic small bright spots and disturbances (diameter approx. 100m) along and near fault lines can be identified (Figure 3.15). It is likely that these bright spots and disturbances are related to shallow gas. Origin of the gas could be biogenic, but it could potentially also have originated deeper, in which case it must have migrated upward and possibly also laterally through transmissive faults and permeable layers. Considering the excellent sealing quality of the primary seal of the P18 reservoir, and the difference in age and dip of the faults in layers above and below the Altena Group, it is unlikely that these potential shallow gas accumulations are related to the P18 reservoirs from which gas is produced. More likely, it originates from either the Posidonia Shale Formation in the overlying Altena Group, which is responsible for charging many Upper Jurassic and lower Cretaceous reservoirs in the vicinity (De Jager et al., 1996), or from shallower layers by biogenic processes.



Feasibility study P18

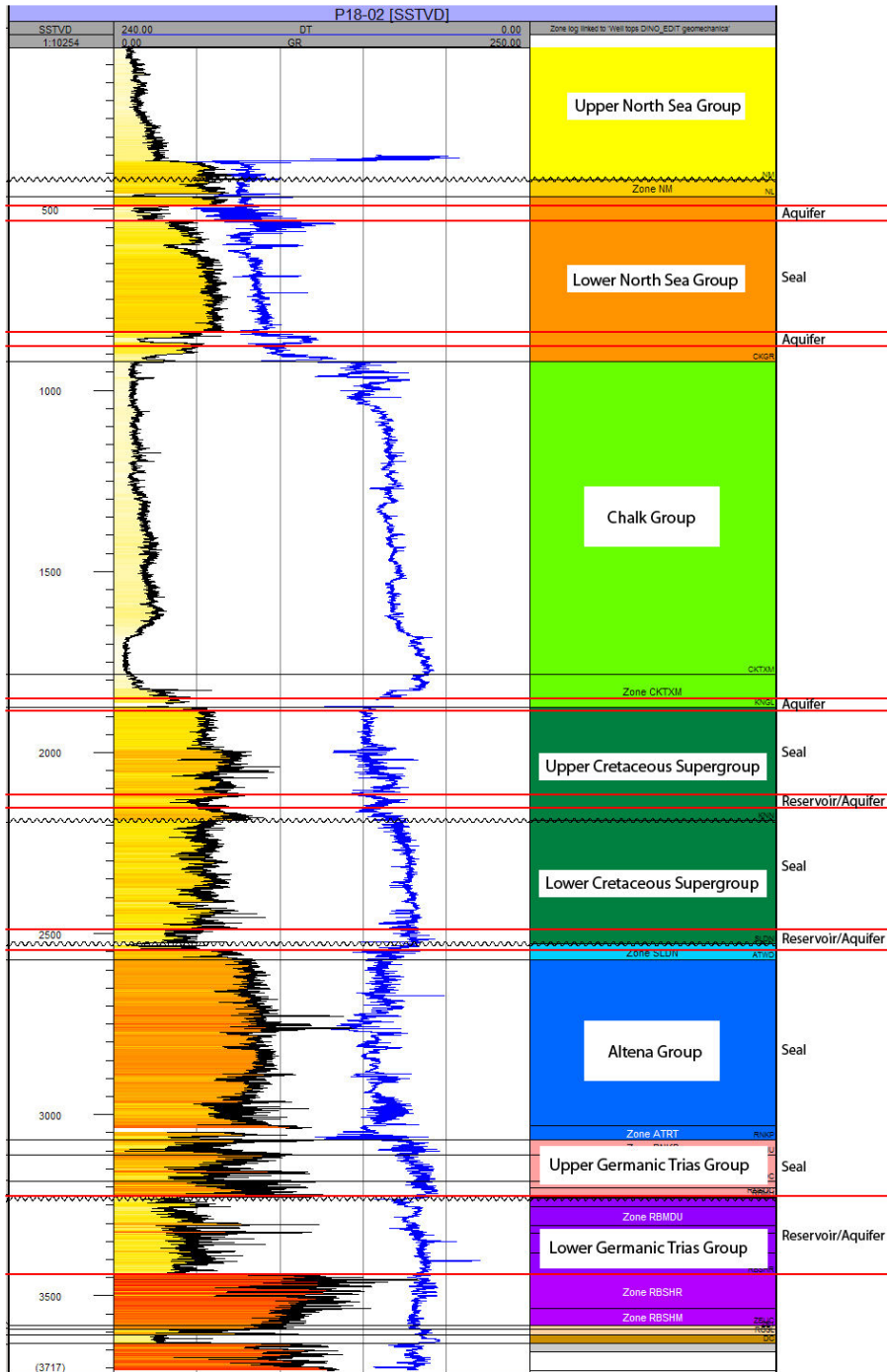


Figure 3.14: Stratigraphy and logs (GR in black with red-yellow colouring, sonic in blue) of the reservoir interval and overburden of the P18 field, with aquifers and seals indicated.

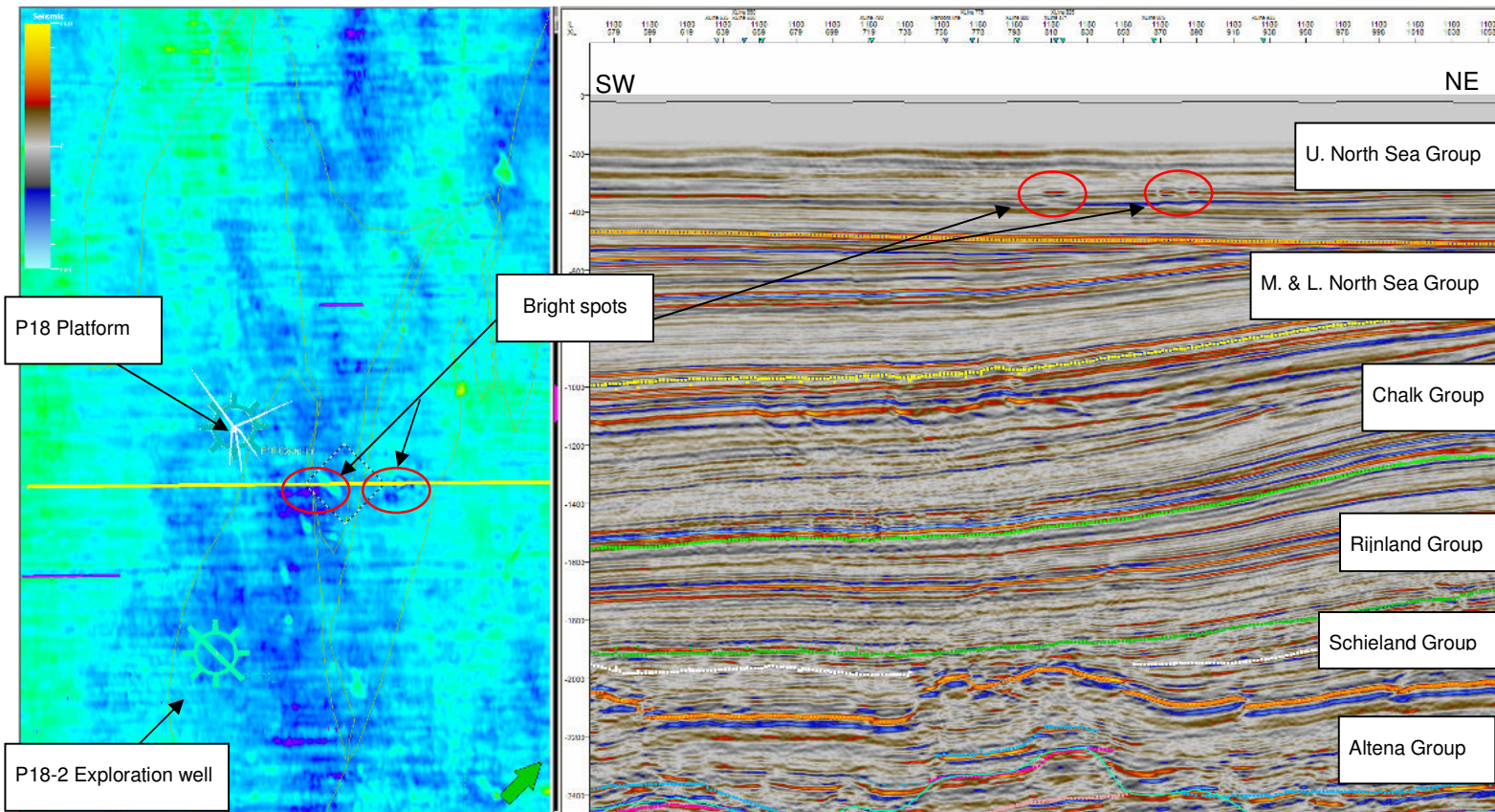


Figure 3.15: Left: map of the RMS amplitude between 250ms and 350ms TWT. Note the greenish blobs slightly east of the P18 structure. Right: Seismic section through the P18 structure, note the elevated amplitudes between 250ms and 350ms TWT.

### 3.7. GIIP: estimates and sensitivity

Estimates of GIIP (Gas Initially In Place) are important, because they are an indication of the volume of CO<sub>2</sub> that can be stored. A GIIP estimate can be made based on different sources of information. Here, two independent sources have been used, a static GIIP estimate based on the static geological model, and a dynamic GIIP estimate, based on production data, i.e., plots of pressure/depth (P/z) vs. cumulative production (see also Chapter 4 reservoir engineering). The GIIP estimate from the production data is very accurate, i.e., it has a low uncertainty attached to it because it is directly based on production. It is a direct indication of the connected volume, i.e., the pore volume connected to the wells. Table 5 displays the GIIP estimates for the three blocks in the P18 field. Static GIIPs for both the original geological model of TAQA (RMS format) and the rebuilt one of CATO-2 (Petrel format) are given to indicate the close match between the two models. Evidently, the static model underestimates the GIIP.

Table 5: Static and dynamic GIIP estimates (in BCM) of the three blocks in the P18 field.

GIIP						
	GWC(m)	Static (TAQA)	Static (CATO-2)	Dynamic	ΔGIIP	%
P18-02	3680	12.40	12.45	13.40	0.95	7.1
P18-04	3377	2.58	2.58	3.20	0.62	19.3
P18-06	3680	0.35	0.36	0.62	0.26	41.9
<b>Sum</b>		15.33	15.39	17.22	1.83	10.6

A sensitivity analysis of the static GIIP estimates was done to assess the sensitivity of the estimates to uncertainty in structure, depth of GWC, porosity and water saturation. For block P18-02, the discrepancy between static and dynamic GIIP is only about 7%, which can easily be attributed to differences in porosity and/or average water saturation between the wells and the property model (see Tables 3, 4). However, for blocks P18-04 and P18-06 the discrepancy is much larger, and can be only partly explained by such differences.

For block P18-04, lowering the water saturation to 0.37, which is on the low side of the average as determined from well P18-04A2, and increasing the porosity to 0.13, which is on the high side of the average as determined from the wells, increases the static GIIP from 2.58 BCM to 2.78 BCM, which still leaves a gap of 0.5 BCM. However, when taking into account the structural uncertainty, this 0.5 BCM can be accounted for, as is shown in Figure 16. Spatial resolution in the reservoir model is 50m, i.e., a single grid cell has sides of 50 m. In the example of Figure 16, the left edge of the reservoir interval, which is formed by a fault (not explicitly shown), falls 50m (one cell) short of the actual position of the fault as identified from seismic. In fact, the position of the fault that bounds the reservoir interval in the model is slightly different from the actual position as identified on seismic. Consequently, a potential GIIP of 0.5 BCM is lost easily in the entire P18-04 block, calculated roughly by multiplying the difference of 50m by the length (3km) and thickness (150m) of the reservoir.

For block P18-06, structural uncertainty adds only 0.07 BCM to the static GIIP due to the low porosity. However, here the water saturation in the reservoir model far exceeds the values as determined from well P18-06A7ST1 (Table 3 & Table 4). Lowering the water saturation from 0.84 (average in the reservoir model) to values in the range of 0.6-0.7 is enough to match the static GIIP with the dynamic GIIP for this block. Furthermore it can be said that the p/Z curve as

## Feasibility study P18

displayed in Figure 4.5 also suggest a low permeability around the producer and a higher permeability elsewhere. This was not reflected in the original geological model as supplied by TAQA.

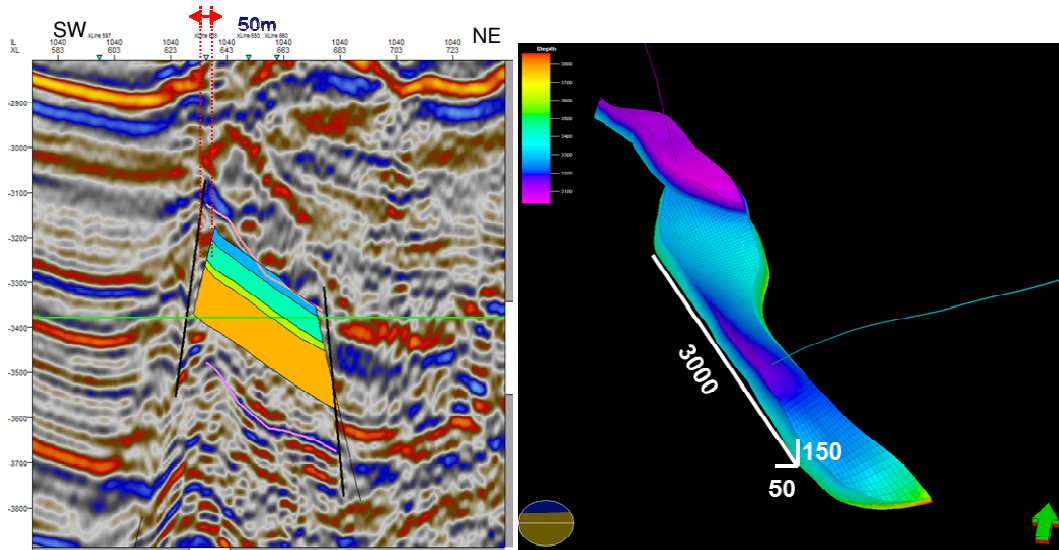


Figure 3.16: Example of structural uncertainty in the reservoir model. Left figure displays a seismic cross-section through block P18-04 (position indicated by red line in right figure), with the modelled reservoir interval in block P18-04 (coloured layering), which does not fully reach up to the faults (solid black lines) as interpreted from the seismic (mismatch approx. 50m). Green line indicates the GWC in this block. Left figure displays a 3D view of the reservoir interval of block P18-04.

## 3.8. Conclusions and recommendations

### 3.8.1. Conclusions

- A new static geological model was built in Petrel to overcome problems with the original model as built by TAQA in RMS. A comparison between the two models (depth and continuity of marker horizons, lateral position and dip of faults, statistics and spatial distribution of petrophysical properties) showed that the differences are negligible, i.e. the new model closely resembles the original model. Findings in this report are based on this new model.
- A velocity model supplied by TAQA proved to be unusable for the purpose of time-depth conversion of the seismic cube supplied by TAQA in two-way-travel time, which was needed to quality control the geological model. Therefore, a new velocity model was built, based on regional-scale velocity modelling work performed in-house at TNO, newly interpreted seismic, and well tops in combination with additional velocity log data from wells.
- Quality control of the new static geological model was achieved by comparing the lateral position and dip of faults and depth and continuity of marker horizons in the model to the depth-converted 3D seismic data. It was concluded that there are small differences, mainly in lateral position and dip of faults, which are not negligible. Differences in fault dip can be attributed to differences in time-depth conversion due to the use of different velocity models. However, differences in the lateral position of faults in the order of 50-100m (1-2 voxels in the reservoir-scale model) can only be traced back to the original seismic interpretation. This has implications for GIIP estimates (see below)

## Feasibility study P18

---

- The structures that contain the P18 reservoirs are bound by a system of NW-SE oriented faults in a so-called “horst and graben” configuration. They subdivide the P18 field into three blocks. Block P18-02 has three compartments, and blocks P18-04 and P18-06 each have one. The top of the compartments lies at depths between 3175 m and 3455 m below sea level. Blocks are bound by normal faults that are sealing because of juxtaposition of permeable reservoir intervals with impermeable intervals above the reservoir. At compartment level, production data suggests that faults are sealing, except for fault F14 between compartments P18-02I and P18-02II, which is not sealing in the current situation.
- The reservoir rocks in the P18 field belong to the Triassic-aged Main Buntsandstein Subgroup, a cyclic alternation of (sub-) arkosic sandstones and clayey siltstones of mixed fluvial/Aeolian origin. Four zones are distinguished in the reservoir; they correspond to the subdivision of the Main Buntsandstein Subgroup into the Volpriehausen Formation, the Upper and Lower Detfurth Formation and the Hardegsen Formation. Gross reservoir thickness in the production wells ranges between 200m and 214m. Average NTG of the individual zones ranges between 0.62 and 0.96, and increases from base to top over the reservoir interval.
- Average porosity in the Hardegsen Formation ranges between around 7-13% and in the Detfurth Formation slightly lower around 5-9%. Maximum porosities encountered in the clean sandy parts of both formations are around 21 %. Permeabilities are highest in the Hardegsen Formation, with a range between 2 and 207 mD. In the Detfurth Formation they range between 0.8 and 0.1 mD roughly. The combined thickness of both formations is approx. 100 m. The Volpriehausen Formation has a much lower porosity that ranges between 3 and 5%. Permeabilities are also low, and range between 0.01-0.05mD. The thickness of the Volpriehausen Formation is also approx. 100 m. Permeabilities were calculated by TAQA using a porosity-permeability relation, the origin of which could not be traced. Average water saturations range between 0.24 and 0.47 in the Hardegsen Formation, between 0.43 and 0.57 in the Upper Detfurth Sandstone Member, between 0.32 and 0.42 in the Lower Detfurth Sandstone Member, and between 0.78 and 0.92 in the Volpriehausen Formation.
- An important step in the quality control of the reservoir model is to verify that the property model honours the original data on the petrophysical properties from the wells. The average thicknesses of the reservoir intervals in the property model agree well with those in the wells, but the property model somewhat underestimates the porosities. Far more important however, especially for GIP estimates, is that the model substantially overestimates the water saturation by values ranging between 0.07 and 0.34. Also, it is not clear how the original property model was populated by TAQA, which severely limits our abilities to reproduce and adapt the property model to improve the match with the well data and the production figures.
- The primary seal to the P18 reservoirs is formed by siltstones, claystones, evaporites and dolostones of the Solling Claystone Member, the Röt formation the Muschelkalk formation, and the Keuper formation that disconformably overlie the reservoir. Total thickness of this primary seal is approx. 150m.
- Faults are present in this primary seal. However, these faults appear to be sealing. Reservoir closure is obtained through impermeable zones above and below the reservoir interval, in combination with juxtaposition of permeable reservoir facies against impermeable non-reservoir facies of the Altena Group (secondary seal). Although most of the reservoir-bounding faults do not continue further upward into the overburden than the shales of the Altena Group, some reverse faults that where formed during the inversion phase appear to originate around the fault tips of the older reservoir-bounding faults. However, inversion in the area of the P18 field was relatively weak. Therefore, it is

## Feasibility study P18

---

unlikely that these inversion faults are reactivation faults that originate from movement along the older basin-bounding faults. Although impossible to rule out completely, it is not likely that the sealing properties of the basin-bounding faults have been compromised.

- Dynamic GIIP of the P18 field, estimated based on production data, i.e., plots of pressure/depth (P/z) vs. cumulative production, is 17.22BCM. GIIP estimates obtained from the static model of the reservoir are substantially lower, 15.39BCM. For block P18-02, the discrepancy between static and dynamic GIIP is only about 7%, which can easily be attributed to differences in porosity and average water saturation between the wells and the property model. For block P18-04 and P18-06, the discrepancy is likely attributed to a combination of under- and overestimated property values (porosity, water saturation) and structural uncertainty, i.e., reservoir-bounding faults that are slightly off in lateral position and dip compared to the 3D seismic.

### 3.8.2. Recommendations

- GIIP estimates as obtained from the static model suffer from structural uncertainty, i.e., reservoir-bounding faults that are slightly off in lateral position and dip compared to the 3D seismic. A reinterpretation of the faults in the reservoir model directly from the 3D seismic data will improve the quality of the reservoir model, and the GIIP estimates.
- GIIP estimates suffer from discrepancies in petrophysical properties such as e.g. porosity and water saturation between the reservoir model and the values from the production wells. An effort can be made to improve the match between the property model and the wells, especially for block P18-06 that is planned to be filled with CO<sub>2</sub> first, where the mismatch in GIIP is 40%.
- Facies-based property modelling will improve the quality of the model by adding heterogeneity to the reservoir based on geological concepts. Such heterogeneity, which is inevitably present in any reservoir, may have large effect on the injection in and subsequent migration of CO<sub>2</sub> through the reservoir.

### 3.9. Acknowledgements

This research has been carried out in the context of the CATO-2-programme. CATO-2 is the Dutch national research program on CO<sub>2</sub> Capture and Storage technology (CCS). The programme is financially supported by the Dutch government (Ministry of Economic Affairs) and its consortium partners. TU Delft acknowledges Schlumberger for the use of Petrel™, Schlumberger's reservoir modelling suite. We thank Andrew van de Weerd en Arie Speksnijder of PanTerra Geoconsultants for valuable comments that improved this report.

### 3.10. References

Ames, R., and Farfan, P.F., 1996. "The environment of deposition of the Triassic Main Buntsandstein Formation in the P and Q quadrants, offshore the Netherlands", in: Rondeel, H.E., Batjes, D.A.J. and Nieuwenhuijs, W.H. (eds): "Geology of Gas and Oil under the Netherlands", Kluwer Academic Publishers (Dordrecht), p. 167–178.

Beutler, G., 1995. "Stratigraphie des Keupers", Bundesanstalt für Geowissenschaften und Rohstoffe (Hannover), Archive number 113087 (unpublished report): 147 pp.

De Jager, J.J., 2007. "Geological Development", in: Wong et al. (eds): "Geology of the Netherlands", Royal Netherlands Academy of Arts and Sciences (Amsterdam), p. 5-26

De Jager, J., Doyle, M.A., Grantham, P.J. and Mabillard, J.E., 1996. "Hydrocarbon habitat of the West Netherlands Basin", in: Rondeel, H.E., Batjes, D.A.J. and Nieuwenhuijs, W.H. (eds): "Geology of gas and oil under the Netherlands", Royal Geological and Mining Society of the Netherlands (KNGMG), Kluwer Academic



Doc.nr: CATO2-WP3.01-D06  
Version: 2011.01.04  
Classification: Confidential  
Page: 40 of 198

## Feasibility study P18

---

Publishers (Dordrecht), p. 191-209.

Dronkers, A.J. and Mrozek, F.J., 1991. "Inverted basins of the Netherlands", *First Break* 9, p. 409-425

Dusar, M., Bless, M.J.M., Burger, K., Demaret, M., Hardy, M., Langenaeker, V., Lie Sun Fan, Paproth, E., Piérart, E., Somers, Y., Streef, M. & Wouters, L., 1998. "De steenkool verkenningsboring Hechtel-Hoef", Geological Survey Belgium Professional Paper 286: 129 pp.

Geluk, M.C., 2007. "Triassic", in: Wong et al. (eds): "Geology of the Netherlands", Royal Netherlands Academy of Arts and Sciences (Amsterdam), p. 85-106

Geluk, M.C., 2005. "Stratigraphy and tectonics of Permo-Triassic basins in the Netherlands and surrounding areas", Ph.D. thesis, Utrecht University, 171pp.

Geluk, M.C., 1999. "Palaeogeographic and structural development of the Triassic in the Netherlands – new insights". In: Bachmann, G.H. & I. Lerche (eds): *The Epicontinental Triassic 1. Zentralblatt für Geologie und Paläontologie*.

Geluk, M.C. and Röhling, H.-G., 1999. "High-resolution sequence stratigraphy of the Lower Triassic Buntsandstein: a new tool for basin analysis", in: Bachmann, G.H. and Lerche, I. (eds): "The Epicontinental Triassic 1". *Zentralblatt für Geologie und Paläontologie* 7-8: p. 545–570.

Geluk, M.C. and Röhling H.-G., 1997. "High-resolution sequence stratigraphy of the Lower Triassic 'Buntsandstein' in the Netherlands and northwestern Germany", *Geologie en Mijnbouw* 76, p. 227–246.

Geluk, M.C., Plomp, A., and van Doorn, Th.H.M., 1996. "Development of the Permo-Triassic succession in the basin fringe area, southern Netherlands", in: Rondeel, H.E., Batjes, D.A.J. & Nieuwenhuijs, W.H. (eds.): "Geology of gas and oil under the Netherlands", Royal Geological and Mining Society of the Netherlands (KNGMG) / Kluwer Academic Publishers (Dordrecht), p. 57-78.

Gerling, P., Geluk, M.C., Kockel, F., Lokhorst, A., Lott, H.K. and Nicholson, R.A., 1999. "NW European gas atlas – new implications for the Carboniferous gas plays in the western part of the Southern Permian Basin", in: Fleet, A.J. and Boldy, S.A.R. (eds.): "Petroleum geology of Northwest Europe – Proceedings of the Fifth Conference", Geological Society (London): 799-808.

Gianolla, P., and Jacquín, Th., 1998. "Triassic sequence stratigraphic framework of Western European Basins", *Mesozoic and Cenozoic Sequence Stratigraphy of European Basins. SEPM Special Publication* 60, p. 643–650.

Johnson, H., Warrington, G. and Stoker, S.J., 1994. "6. Permian and Triassic of the Southern North Sea", in: Knox, R.W.O.B., and Cordey, W.G. (eds): "Lithostratigraphic nomenclature of the UK North Sea", British Geological Survey (Nottingham).

Kozur, H., 1999. "The correlation of the Germanic Buntsandstein and Muschelkalk with the Tethyan scale", In: Bachmann, G.H., and Lerche, I. (eds): "The Epicontinental Triassic", *Zentralblatt für Geologie und Paläontologie* 7–8, p. 701–725.

Lee, M., Aranson, J.L. and Savin, S.M., 1985. "K/Ar dating of time of gas emplacement in Rotliegendes sandstone, Netherlands". *American Association of Petroleum Geologists Bulletin* 69: p. 1381-1385.

Racero-Baena, A., and Drake, S.J., 1996. "Structural style and reservoir development in the West Netherlands oil province". in: Rondeel, H.E., Batjes, D.A.J. & Nieuwenhuijs, W.H. (eds.): "Geology of gas and oil under the Netherlands", Royal Geological and Mining Society of the Netherlands (KNGMG), Kluwer Academic Publishers (Dordrecht), p. 211-227.

TAQA Energy B.V., 2008. "CO<sub>2</sub> offshore Storage Deep Under the Dutch North Sea", promotional material

Van Adrichem Boogaert, H.A., and Kouwe, W.F.P., 1994. "Stratigraphic nomenclature of the Netherlands; revision and update by RGD and NOGEP, Section E Triassic", *Mededelingen Rijks Geologische Dienst* 50.

Van Balen, R.T., Van Bergen, F., De Leeuw, C., Pagnier, H., Simmelink, H., Van Wees, J.D. & Verweij, J.M., 2000. "Modelling of the hydrocarbon generation and migration in the West Netherlands Basin, the Netherlands", *Netherlands Journal of Geosciences* 79, p. 29–44.

Van Bergen, F., 1998. "Basin modelling and hydrocarbon generation in the WNB-an organic petrological and organic geochemical approach", Internal report Netherlands Institute of Applied Geoscience TNO – National Geological Survey (Utrecht) 98-148B: 120 pp.



Doc.nr: CATO2-WP3.01-D06  
Version: 2011.01.04  
Classification: Confidential  
Page: 41 of 198

## **Feasibility study P18**

---

Van Wijhe, D.H., 1987. "Structural evolution of inverted basins in the Dutch offshore", Tectonophysics 137, p. 171-219.

Wolburg, J., 1967. "Zum Wesen der Altkimmerischen Hebung, mit einem Überblick über die Muschelkalk- und Keuper-Entwicklung in Nordwest-Deutschland", Zeitschrift der deutschen Geologischen Gesellschaft 119, p 516–523.

Yeilding, G., 2002. "Hydrocarbon Seal Quantification", in: Koestler, A.G., and Hunsdale, R. (eds.): "NPF Special Publication 11", Norwegian Petroleum Society (NPF), published by Elsevier Science B.V. ( Amsterdam), p. 1-15.

Ziegler, P.A., 1990. "Geological atlas of western and central Europe, part 2", Geological Society Publishing House (Bath), 239 pp.



## 4. Reservoir study

### 4.1. Introduction

In this chapter, reservoir engineering aspects of CO<sub>2</sub> storage in the P18-2, P18-4 and P18-6 reservoirs are discussed. This includes an initial assessment of the storage capacity and maximum injection rates. The dynamic reservoir study comprised both an analytical reservoir study and a reservoir simulation study.

### 4.2. Analytical reservoir study

#### 4.2.1. Introduction

In order to get a basic understanding of the behaviour of the P18 field during CO<sub>2</sub> injection an analytical model is used. The most important aspects of this model are:

- The reservoir is modeled as a single tank that is gradually filled with CO<sub>2</sub>.
- The geometry of the reservoir and the location of the wells are modeled implicitly using an average shape factor and drainage area for the wells.
- The analytical model uses the volume/material balance to calculate the average reservoir pressure given Gas Initially In Place (GIIP), initial reservoir pressure, reservoir pressure at end of production period ("abandonment pressure"), and cumulative CO<sub>2</sub> injected. Well inflow performance (injectivity) is based on the single phase semi steady state inflow model, using pseudo pressure. Given the average pressure from the aforementioned calculation and either BHP or required injection rate, the injection rate or BHP is calculated, respectively. CO<sub>2</sub> injected, average reservoir pressure, and well injectivity are calculated with a time step size of one year.

The model requires a number of basic input parameters with respect to the reservoir. This data includes reservoir depth, size, average thickness, temperature, initial and abandonment pressure, average permeability and required injection rate.

The injection scenario used in this analytical study is 1.1 Mton/year which equals 1.52 MNm<sup>3</sup>/day<sup>1</sup>. Additionally a maximum FBHP constraint is applied, which is case specific and must be determined by the geomechanical engineer.

The most important output of the model will be the cumulative CO<sub>2</sub> injected and the injectivity each year. In section 4.2.2 these resulting injection capacity and rates are presented and discussed for the three compartments of P18.

The next step to improve the accuracy and resolution of the results a reservoir simulator should be used. This will be the subject of section 4.8.

#### 4.2.2. P18 analytical study results

The input as used for the analytical study of P18 is presented Table 6. A summary of the model results is shown in Table 7. In P18-2 and P18-4 the target rate of 1.1 Mt/y is realised and the total injection period needed to fill up the reservoir to the initial pressure is 28 years and 7 years

---

<sup>1</sup> The density of CO<sub>2</sub> at normal conditions (temperature is 0°C and pressure is 1 atmosphere) are used in this study, which equals to 1.9768 kg/m<sup>3</sup>.

## Feasibility study P18

respectively. In contrast the target rate cannot be realised in P18-6. The low permeability gives rise to a high FBHP in order to realise the target rate, exceeding the maximum allowed FBHP.

Table 6: Input parameters for P18

Parameter	Units	P18-2	P18-4	P18-6
Number of wells for injection		1	1	1
First year of injection	Year	2015	2015	2015
Gas initially in place (GIIP)	GNm3	13.35	3.2	0.6
Average depth of reservoir	Meter	3500	3220	3561
Reservoir temperature	°C	126	117	117
Initial pressure	Bar	375	340	377
Abandonment pressure	Bar	20	20	45
Average thickness	Meter	220 m	94.0	70
Average permeability	mDarcy	64	103	0.9
Well Dietz shape factor		0.232	0.232	0.232
Reservoir drainage area	m <sup>2</sup>	2371791	1456000	366600

Table 7: Result analytical study P18

	Units	P18-2	P18-4	P18-6
Cumulative CO <sub>2</sub> injection	Mton	31.83	8.78	1.48
Injection period	Year	2015-2043	2015-2022	2015-2021
Target rate realised?		Yes	Yes	No

### 4.3. Dynamic reservoir study

#### 4.3.1. Overview of P18 field

The P18 field can be divided in 3 independent reservoir compartments, respectively P18-2, P18-4 and P18-6. Static properties of the P18 field as described in Petrel were used as input for the compositional flow simulation in MoReS. The results of these dynamic simulations in MoReS will be discussed in this section. The initial geological model (Roxar) received from TAQA Energy B.V. was converted into a petrel model, the number of gridblocks of which was reduced in order to make it feasible for a reservoir simulation. The actual reservoir appears to have no active aquifer, as the p/Z curve is a straight line. In addition the permeability below the gas-water contact (GWC) is small compared to above the GWC.

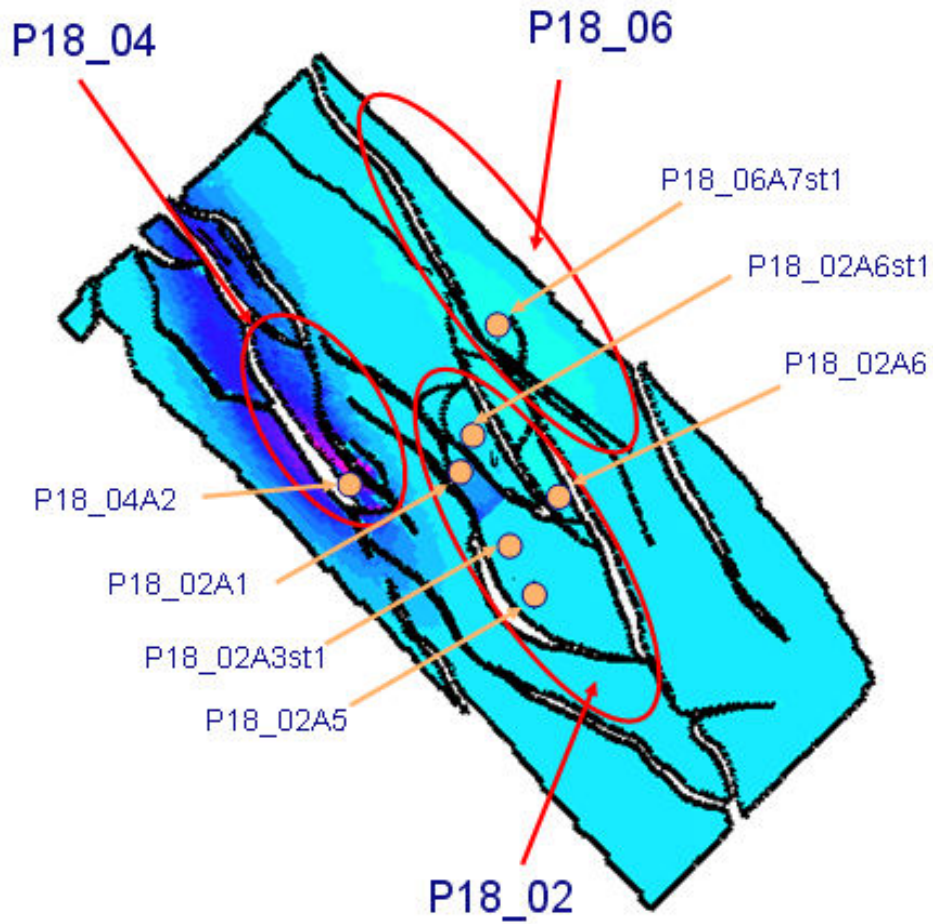


Figure 4.1: Overview of P18 field

## Feasibility study P18

Table 8: below gives a summary of the properties of the P18 field found after the history match.

	Units	P18	P18_2	P18_4	P18_6
Average gridblock dimensions	Meter	i-direction=65 , j-direction=100, k-direction=30			
Simulator grid dimensions		i-direction=77 , j-direction=175, k-direction=4			
Initial fraction of components		C1(0.94), C3p(0.07),C2(0.024),CO <sub>2</sub> (0.013), N <sub>2</sub> (0.015),			
Average permeability	mDarcy	94	64	499	30
Average (volume weighted) porosity		0.068	0.06	0.11	0.08
GWC (gas water contact)	Meter	Depends on compartment	-3680	-3377	-3680
GIIP (gas initially in place)	GNm3	18.7	14.4	3.19	1.1GNm3
Initial pressure	bar	Depends on compartment	375 bar	340 bar	377 bar
Production start datum		1st January 1994	1 <sup>st</sup> January 1994	6 <sup>th</sup> March 1997	15 <sup>th</sup> July 2003

### 4.3.2. Production data

The gas rates provided by TAQA Energy B.V. were daily rates for each well. These rates were averaged to monthly rates to reduce the simulation time. The gas rates for well P18\_02A6 and P18\_2A6ST1 are uncertain, because it was unclear how much gas was produced for each individual well, as only the total combined gas rates of both wells was measured. In the simulations performed the gas rates were divided over the two wells by the ratio of the well KH. For the wells P18\_2A1 and P18\_2A3ST2 the production data before 1997 was considered unreliable. However, the cumulative gas production until this time was known, therefore a constant gas rate between 1994 and 1997 is used during the history match of P18-2. The shut-in pressure measurements of well P18\_6A7ST2 are subject to uncertainty; because the well is perforated in a low permeability environment reliable shut-in pressures need long-shut in periods. The shut-in periods vary from 4 to 51 days. Furthermore the initial pressure is not measured directly but derived from the P18-2 field.

### 4.3.3. Simulation constraints

The MoReS (version 2010.1) reservoir simulator is used to history match the P18 model. The history match simulations were constrained by monthly production data of each individual well and a minimum BHP of 1 bar. It is important to note that non-darcy flow is not modelled in this study.

## 4.4. History match of P18-2

The process of history matching starts with an implementation of the gas production history of each well in the model (as provided by TAQA Energy B.V.).

Feasibility study P18

P/z plot P/18-2 Main, P18-2a6, P18-2a6 blocks

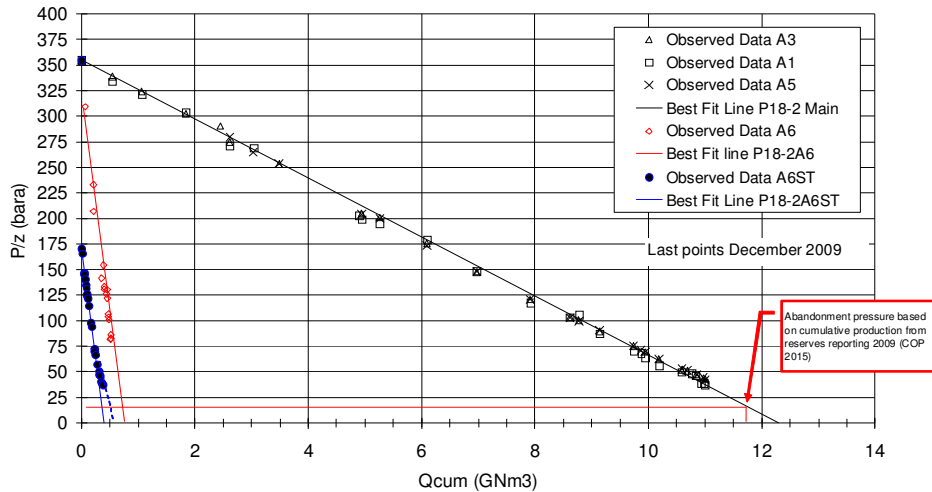


Figure 4.2: Production history for the wells A1, A3ST2, A5, A6 and A6ST1

The gas-initially-in-place and initial pressure are known from the p/z plot derived from field measurements (Figure 4.2). From this linear p/z curve it is assumed there is no active aquifer.

Once a material balance match is achieved, the subsequent step is to match the bottom hole pressures (BHP). Using the provided BHPs over the period of 1994-2010 a match could be achieved by making adjustments to fault transmissibility, well productivity indexes and absolute permeability.

P18-2 consists of three blocks, where block I and II are connected (Figure 4.3). This can be determined from the pressure data from the wells in each individual block. The data show no indication of a connection between block III and the other two blocks.

**Feasibility study P18**

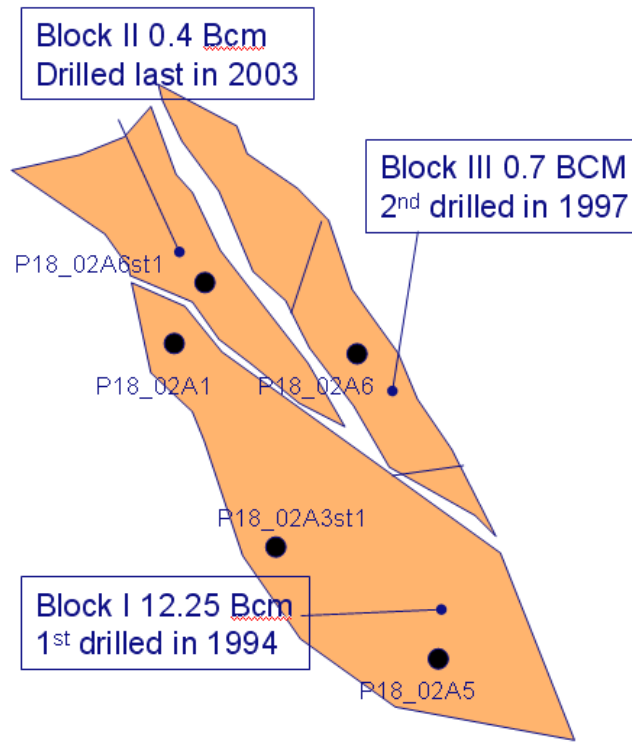


Figure 4.3: Overview block I, II and III in P18-2

In Table 9 an overview is given of the stock tank gas volumes (in GNm<sup>3</sup>) determined by the p/Z curves and determined by the dynamic model. The sensitivity with respect to the gas water contact (GWC) and porosity are shown as well. In order to get the correct mass balance a porosity multiplier very close to one should be applied.

Table 9: Volumes of block I, II and III of P18-2 in GNm<sup>3</sup>

	Volume in Block I and II	Volume Block III	Total Volume Block I, II and III	GWC (m)	porosity multiplier
p/Z	12.65	0.7	13.35		
base case	13.6	0.81	14.4	3680	1
Case 1	13.4	0.78	14.2	3660	1
Case 2	12.9	0.70	13.6	3620	1
Case 3	11.4	0.67	12.0	3680	0.9
Case 4	12.4	0.73	13.1	3680	0.95

In this study the base case is used for further simulation. After the first simulations it became clear additional changes to the permeability and well KH are needed to reproduce the measured shut-in pressures of the wells. In order to get a reasonable history match the fault transmissibility was changed between block I and block II (equal to 0.2). In 2003 the well P18\_02A6ST1 in block II came on stream and the reservoir pressure in this well was equal to 158 bar, which is significant lower than the initial reservoir pressure measured (375 bar) in block I. This observation indicates a connection between both block I and II.

## Feasibility study P18

The permeability around well P18\_02A1 was lower in the original geological model than the average permeability of block I. To increase the flow performance around this well the low permeability region is multiplied by a factor of 5. For the other wells (P18\_02A3ST1 and P18\_02A5) in block I another permeability multiplier was needed to get a reasonable history match, the whole block I was multiplied by a factor of 2. The pressure behaviour of the model corresponds with the measured shut in pressures of the wells in block I (see figure).

In Block II the geological model was not able to produce the measured gas rates, a permeability multiplier of 10 and a well KH multiplier of 5 were applied. Although, the model and measurements are not in perfect agreement; the characteristic behaviour is captured with this model. This block is significantly higher (less deep) then block I and III, it is possible that the absolute permeability is estimated very conservatively, as a result of diagenesis.

In block III no additional changes to the flow performance of the original geological model were made. The measured pressure behaviour is captured well by the dynamic model. The average permeability and porosity of each block of the static model and the history matched model of compartment P18-2 are given in

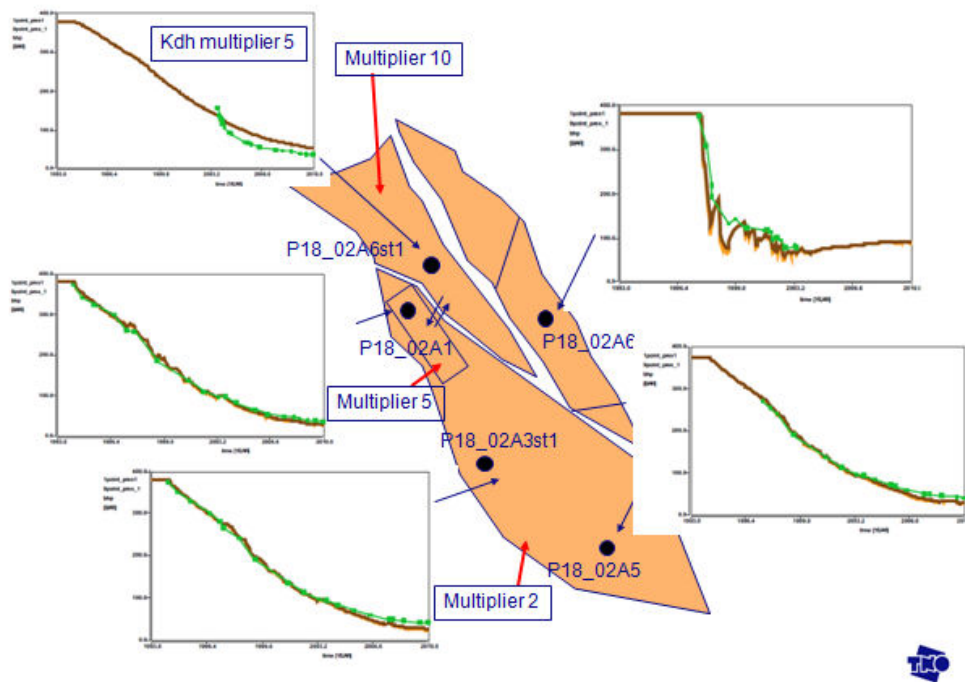


Figure 4.4: Overview P18\_2 of the pressure behaviour of each individual well after applying permeability and well KH multipliers. The green line with markers represents the measured shut-in pressure, the dark lines are the simulated nine-point reservoir pressures.

**Feasibility study P18**

Table 10: Properties of P18-2 of static model and History Matched (HM) model.

	Initial average porosity	averaged porosity in HM model	Initial average permeability (mDarcy)	Average permeability in HM model (mDarcy)
P18_02 block I	0.065	0.065	17.0	43.5
P18_02 block II	0.061	0.061	11.7	117
P18_02 block III	0.057	0.057	7.0	7.0

**4.5. History match of P18-4**

The P18-4 compartment is a reservoir, which consists of one block and is bounded by faults (Figure 4.1). Well P18-04A2 is drilled in the southern part of this compartment. The first step is to get a material balance match; from the p/Z curve the GIIPP was estimated to be 3.2 GNm<sup>3</sup> (Figure 4.5). However the dynamic model had only 2.0 GNm<sup>3</sup> initial in place. This discrepancy can be explained by the interpretation of the fault along the long side of P18-4 compartment. Shifting the south-eastern boundary by the order of 50 meters will give us exact the volume needed to match the material balance. Instead of remodelling the structure of the geological model a porosity multiplier of 1.3 was used to get the correct volume in the dynamic model.

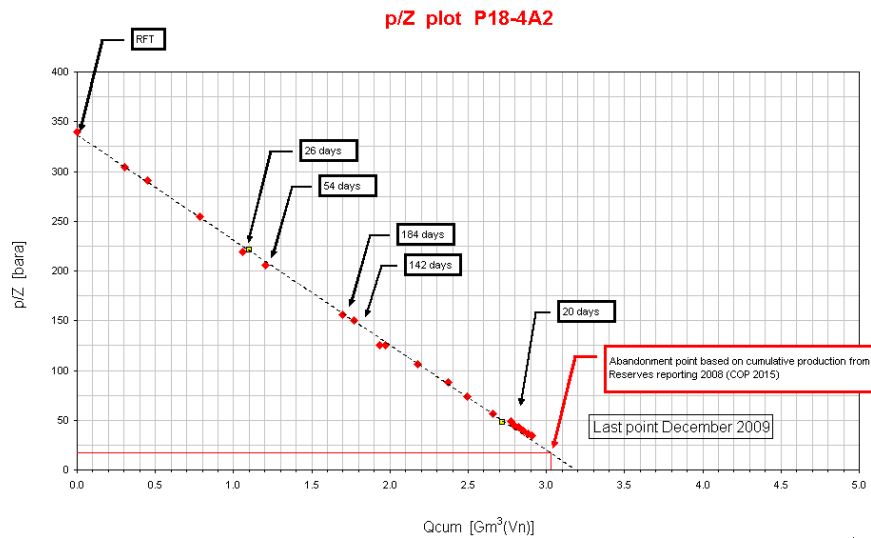


Figure 4.5: p/Z curve of P18-4, the number of days in the black boxes are the shut-in periods



**Feasibility study P18**

Table 11: Volumes of compartment P18-4 in GNm<sup>3</sup>

	Volume P18_4	GWC (m)	porosity multiplier
p/Z	3.2		
base case	2.0	3377	1
Case 1	3.2	3377	1.3
Case 2	2.3	3400	1
Case 3	2.7	3450	1

After simulating Case 1, the reservoir pressure behaviour of P18\_4 corresponds very well with the measured shut in pressures of well P18\_4A2 as can be seen in Figure 4.6. Additional changes to flow parameters (e.g. permeability) are not needed to model the characteristics of the P18-4 field. The average permeability and porosity of the static and history matched model of compartment P18-4 are given in Table 12.

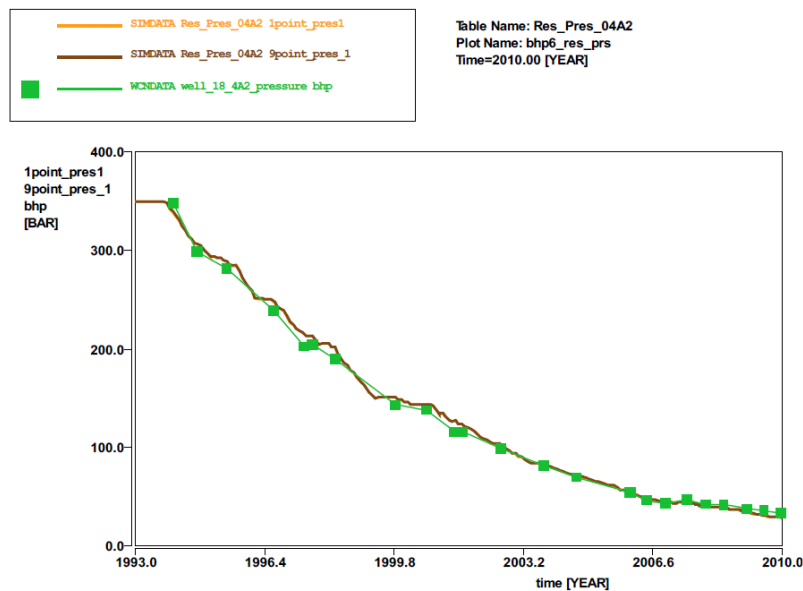


Figure 4.6: Reservoir pressure of the dynamic P18 model (brown line), measured shut in pressures (green markers) of well P18\_4A2.

Table 12: Properties of P18-4 of static model and History Matched (HM) model

	Initial average porosity	averaged porosity in HM model	Initial average permeability (mDarcy)	Average permeability in HM model (mDarcy)
P18_04	0.086	0.111	499.	499

## 4.6. History match of P18-6

P18-6 is a significant lower permeable compartment (Table 8). Well P18\_06A7ST1 is the only well in this compartment and located near the southern boundary, surrounded by faults on the east and southern side. The volumes according to the p/Z curve and the dynamic model are not corresponding with each other. In order to get correct volumes in the dynamic model the GWC or the water saturation ( $S_w$ ) or the porosity or a combination of these could be changed. The GWC is initially at 3680m, however the volumes are not sensitive to the GWC, because the porosity is very low in these lower layers. By changing the porosity with a multiplier 1.4 the volume in the dynamic model corresponds with the volumes from p/Z analysis. However as mentioned before, the p/Z curve is subject of uncertainty because of short shut-in periods (Figure 4.7). An underestimation of the initial volume in place is therefore plausible. In our simulation a porosity multiplier of 1.6 is used, because with smaller volumes an early water breakthrough is observed in the simulations. The absolute permeability was multiplied by 9 and a well KH multiplier of 60 was used to simulate the measured production rates. The physical reason behind the multipliers as described above are discussed in Section 3.7.

In Figure 4.8 the measured and simulated pressures are compared and a reasonable history match is found here. The average permeability and porosity of the static model and the history matched model of compartment P18-6 are given in Table 14.

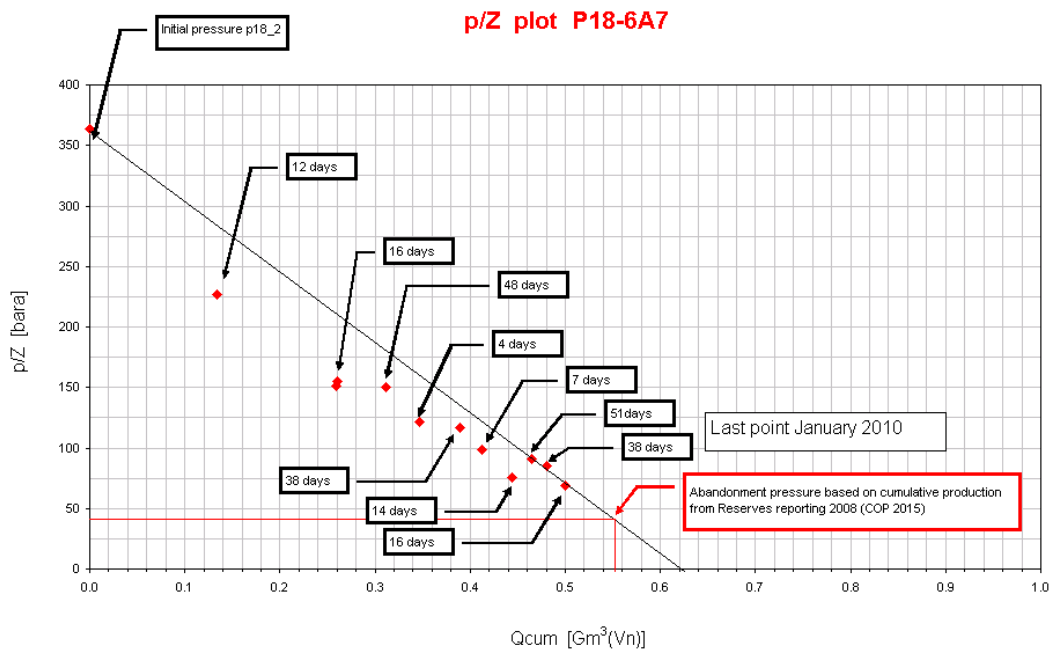


Figure 4.7: p/Z curve of P18-6, the number of days in the black boxes are the shut-in periods

## Feasibility study P18

Table 13: Volumes of compartment P18-6 in GNm<sup>3</sup>

	Volume P18-6	GWC(m)	Porosity multiplier
p/Z	0.62		
base case	0.33	3680	1
Case 1	0.67	3680	1.4
Case 2	1.1	3680	1.6
Case 3	0.36	3700	1
Case 4	0.42	3750	1

Table 14: Properties of P18-4 of static model and History Matched (HM) model

	Initial average porosity	averaged porosity in HM model	Initial average permeability (mDarcy)	Average permeability in HM model (mDarcy)
P18_06	0.047	0.075	3.3646	29.67

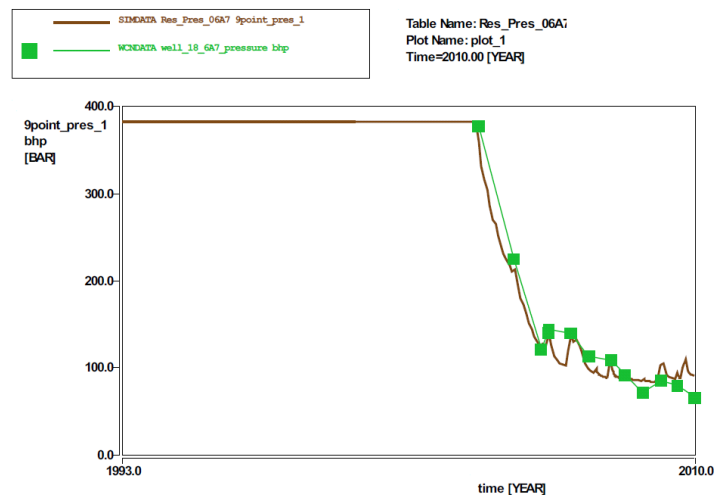


Figure 4.8: Reservoir pressure of the dynamic P18 model (brown line), measured shut in pressures (green markers) of well P18\_6A7ST1.

### 4.7. Discussion and conclusion of the history match

The static model of P18 from TAQA Energy B.V. has large uncertainties (as discussed in the geocological study of P18). The volumes from the p/Z analysis do not correspond with the static model, especially for compartment P18-4 and P18-6. In compartment P18-2 it is not known from which block, which volume is produced, however these are relatively small volumes.

- In P18-2 is permeability the most adapted parameter, in block II a multiplier of 10 is used and a KH multiplier of 5 on the well itself, which means a multiplier on the flow performance of 50. This is an extreme value; therefore the predictive power of the model in this region has a high uncertainty.

## Feasibility study P18

- In P18-4 no adjustment has to be made to the flow performance, the volume balance is incorrect. TNO found an explanation of this mismatch. The structural re-interpretation of this compartment gives the correct volumes of this compartment
- In P18-6 porosity and permeability had to be adapted to get a reasonable history match. The p/Z curve is not a straight line and the initial pressure is not measured directly. Therefore the estimated GIPP are very uncertain. In the dynamic model a higher volume was needed to reproduce the measurements. Furthermore the permeability in the static field of this compartment was multiplied with a factor 9 and the well KH with factor 60. The flow performance of the well is increase by a very extreme factor (520). Using this gives us a reasonable history match, however the uncertainty of this compartment is very high and any prediction taken from this model should be interpreted with care.

## 4.8. Injection study of P18

### 4.8.1. Introduction

The injection study of P18 is performed with the adjustments mentioned earlier in the history matching part in this report (section 4.14, 4.15. and 4.16). The yearly average injection target rate is 34.93 kg/s (equals 1.1 Mton/year) for each individual well, with a maximum of 47 kg/s. The annual injection profile proposed by EON is shown in Figure 4.9. The results with this specific injection rate are similar to the results with a constant injection rate of 1.1Mton/year. In this section the results of a constant injection rate are presented.

In P18 four wells are assigned as injection well, P18\_02A1, P18\_02A6 (because block III is isolated from block I and II), P18\_04A2 and P18\_6A7ST1

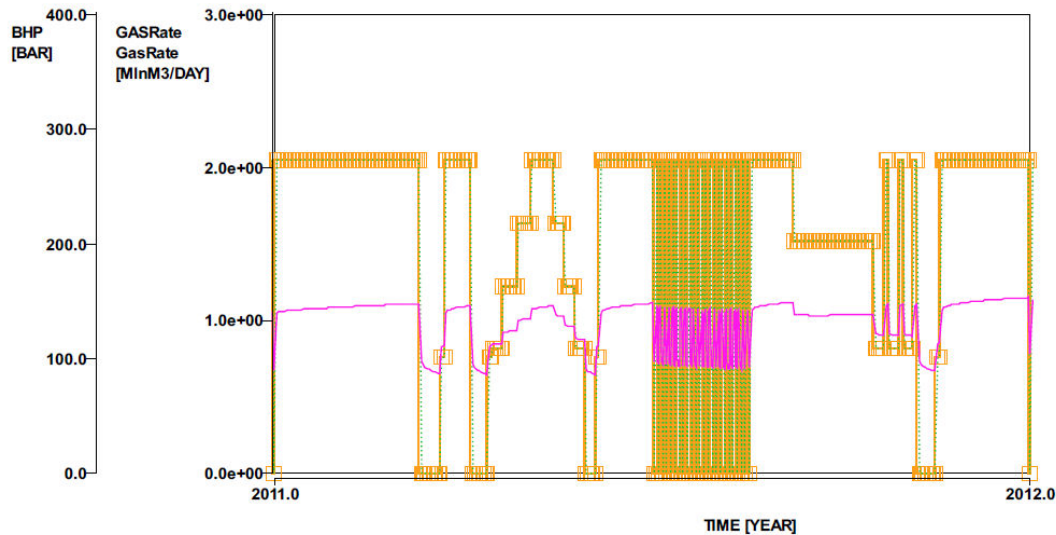


Figure 4.9: Annual injection CO<sub>2</sub> profile proposed by EON with average 1.1 Mton/year. Green dashed line is target rate, the orange line is the simulated injection rate. Pink line is the BHP of the well A1

### 4.8.2. Results and discussion

The forecast injection rate and pressure behaviour of compartment P18-2, P18-4 and P18-6 are shown in Figure 4.10, Figure 4.11 and Figure 4.12 respectively. The forecast shown here is performed with a slow start up phase until 2014 and after that a constant injection rate of 1.1

## Feasibility study P18

Mton/year. Furthermore the injection well is constrained by a maximum BHP pressure equal to the initial reservoir pressure of each particular compartment. The reason for this choice is to prevent the final reservoir pressure (after the CO<sub>2</sub> injection) to become higher than the initial reservoir pressure. If the final reservoir pressure is higher than the initial reservoir pressure this could cause fractures, which can possibly result to a leakage path.

A summary of the capacity of each compartment is given in Table 15: Results compositional reservoir simulation study

As shown earlier in the analytical study the target injection rate in P18\_02A1 and P18\_05A2 is realized and the cumulative CO<sub>2</sub> injection is comparable with previous results from the analytical study.

Well P18\_02A6 in block III can inject the target rate only for a few months. The BHP needed for the target rate is constrained by the maximum allowed BHP (375 bar). It is important to realize that block III is still at a relative high reservoir pressure (90 bar), because it possible to inject more CO<sub>2</sub> in block III if the reservoir pressure is reduced to a lower abandonment pressure. The discrepancy between the analytical study and the simulation study on the cumulative injection can be the reason of this difference.

In P18-6 the low permeability in the area give rise to a low injection rate. In our simulations the injection rate is immediately constraint by the maximum flowing BHP.

The drawdowns (BHP – 9 point pressure) for each injection well are shown in Figure 4.13. For injector P18\_02A6 has a maximum value of 330 bar. This low permeable block (7mDarcy) and a target rate of 47 kg/s give rise to this high drawdown. In contrast to P19\_4A2 a high permeable (499mDarcy) the target rate can be reached by only a maximum drawdown of 5 bar. Furthermore as mentioned before the drawdown of P18\_02A1 and P18A7ST1 is maximum of 50 bar and 8-bar, respectively.

Several processes may increase or decrease the injectivity of the CO<sub>2</sub> with respect to the current simulations. Salt precipitation may decrease, while fracturing may increase the predicted injectivity. Another aspect, which has shown up in field tests is that the change from production to an injection well leads an increased injection. This is possibly due to the small parts which are blown out of the near-well area.

Table 15: Results compositional reservoir simulation study

			P18-2			P18-4	P18-6
		Units	P18_02A1	P18_02A6	Total	P18_04A2	P18_6A7ST1
Cumulative CO <sub>2</sub> injection	Dynamic simulation study	GNm <sup>3</sup> Mton	14.7 29.1	0.7 1.3	15.4 30.4	4.1 8.1	0.3 0.6
	Analytical study	Mton	31.8			8.8	1.5
Target rate realized?			Yes	No		Yes	No

Feasibility study P18

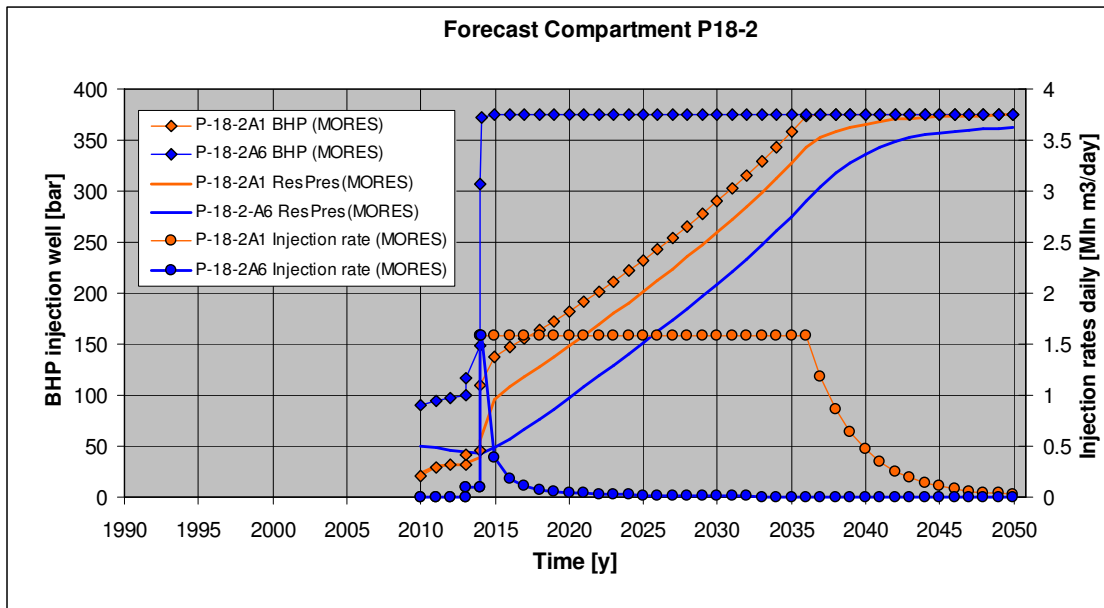


Figure 4.10: Injection behaviour of compartment P18-2, with average injection rate of 1.1 Mton/year

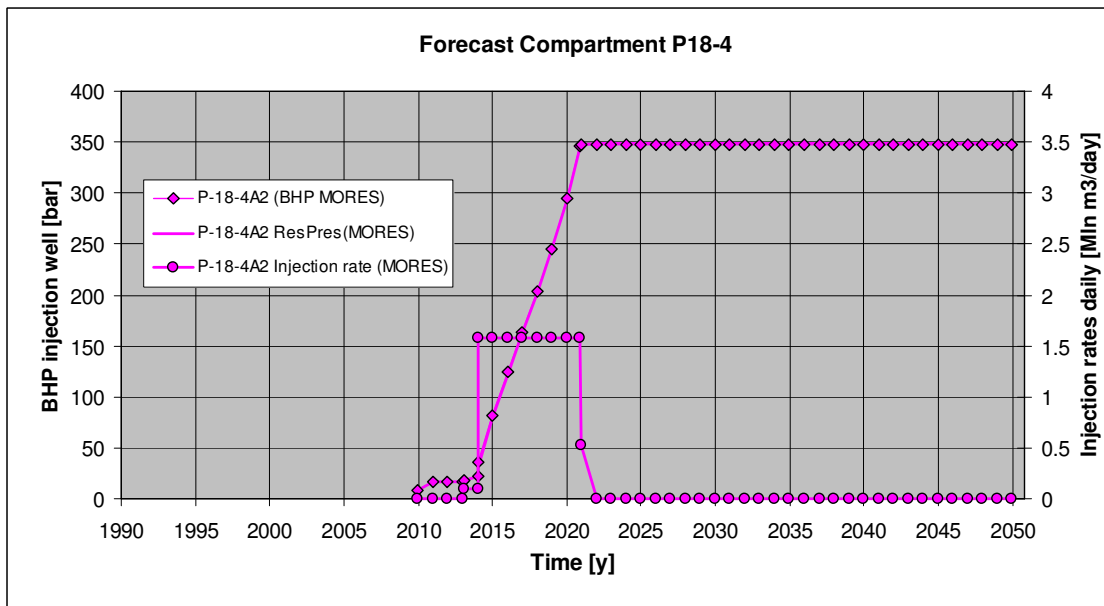


Figure 4.11: Injection behaviour of compartment P18-4, with average injection rate of 1.1 Mton/year

Feasibility study P18

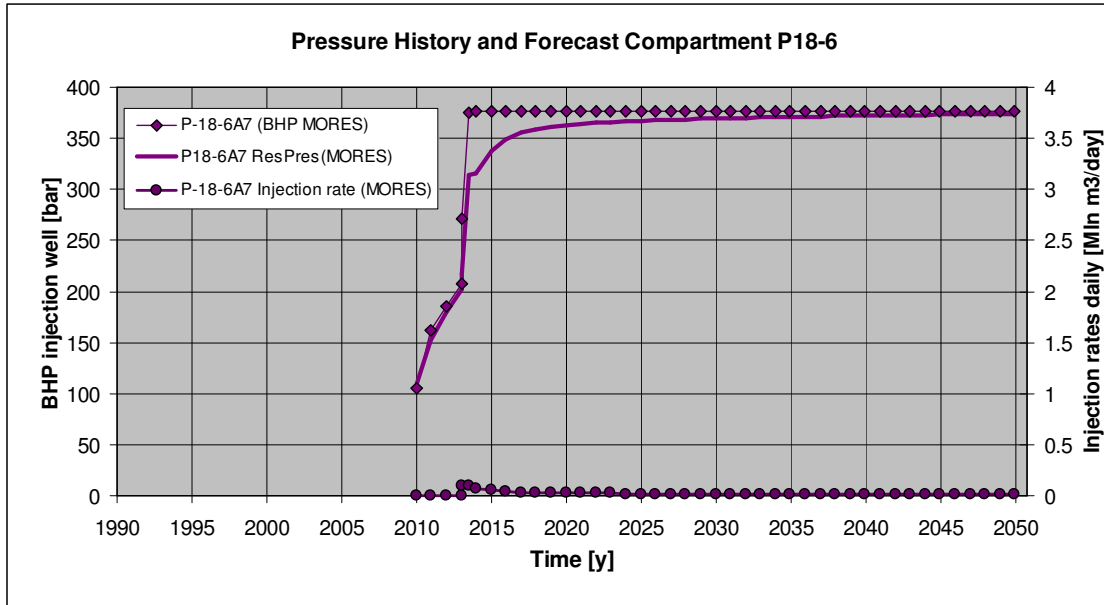


Figure 4.12: Injection behaviour of compartment P18-6, with average injection rate of 1.1 Mton/year

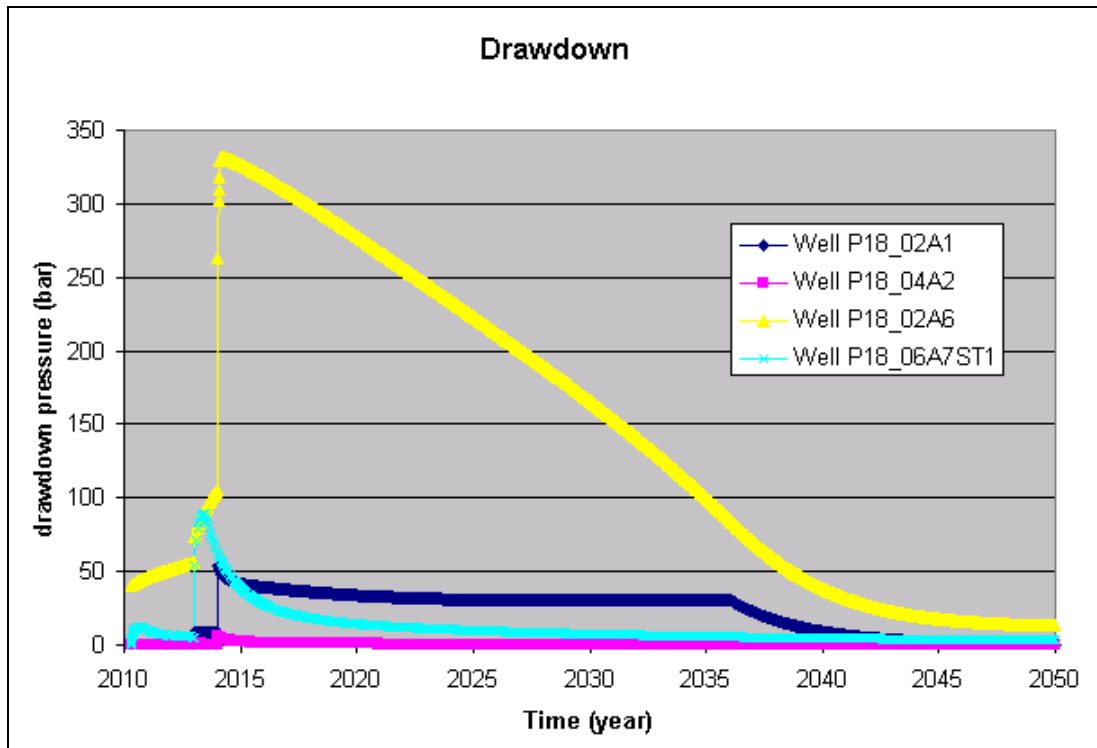


Figure 4.13: Drawdown of each individual well in P18

### **4.8.3. Conclusion**

The conclusions of the injection study of P18 are:

- Simulations show that in P18-2 block I and II the target rate of 1.1 Mton/year is possible and a total of 30.4 Mton CO<sub>2</sub> can be injected.
- In well P18-2A1 the target is possible; however in P18\_2A6 the target rate is not feasible.
- Simulations show that in P18-4 the target rate of 1.1 Mton/year is possible and a total of 8.1 Mton CO<sub>2</sub> can be injected.
- Simulations show P18-6 the target rate is not feasible and a range of 0.5 to 1.6 Mton can be injected in this compartment..

All these conclusions need to be interpreted very carefully, because of the uncertainties in the static and history matched model of P18 as discussed in section 4.17.

## **4.9. Thermal aspects of reservoir modelling of P18**

### **4.9.1. Introduction**

TAQA Energy B.V. plans to inject CO<sub>2</sub> into the various mature P18 compartments. These compartments are deep (over 3 km depth) and quite permeable. This in connection with the off-shore nature of the injected and the associated cooler temperatures of the injected CO<sub>2</sub> means that it is essential to include thermal aspect and processes, such as the Joule-Thompson cooling, impact on induced fracturing etc. in the feasibility study.

Most current reservoir models do not allow to model thermal effects together with a description of the PVT, according to the EOS. In a similar former project, TNO has been successful in modelling the thermal impact of injection into the Barendrecht reservoir. As this was a NAM field, we applied the Shell reservoir model MoReS. TNO at that moment was not allowed to use the Shell model for other producers. It was therefore decided to translate the MoReS input files into those for Eclipse300 (+ thermal). After trying hard with several approaches, and after several talks with Schlumberger it was concluded that the current version of Eclipse cannot properly model the thermal effects of CO<sub>2</sub> injections into a depleted (composition) gas reservoir.

### **4.9.2. P18 thermal reservoir study**

The next approach was to ask Shell to make the MoReS simulator available for TNO reservoir engineers to work on reservoirs within CATO2. Shell agreed to this and allowed the use of MoReS for the P18 and P15 fields operated by TAQA Energy B.V., and the K12-B blocks operated by GDF Suez E7P Nederland B.V. It was therefore possible use the still innovative pseudo-thermal approach as used for the Barendrecht for the P18 fields. During the modelling for P18, we tested the modelling of the C<sub>p</sub> of the liquid phase which was found to be reasonable. Furthermore we changed the way MoReS manages the time steps of the simulation as a function of the temperature changes over all grid blocks in the previous time step.

In other to include small-scale processes in the simulation, a radial sector model was used with very small (1.5 cm) grids directly adjacent to the injection well and much larger grids, further away from the well. The total radius of the flow domain was 2 km. The permeability of the reservoir rock, the initial pressure and temperature were 100 mDarcy, 20 bar and 399 K, respectively.



**Feasibility study P18**

Together with TAQA, a workflow was set up which included integration of the modelling efforts of the TAQA contractor Genesis and TNO. Within the framework, Genesis was responsible for modelling the transport from the on-shore CO<sub>2</sub> source, and the transport/behaviour of CO<sub>2</sub> within the injection well. For various scenarios Genesis modelled the injection rate, bottom hole pressures and temperatures, which subsequently were applied as input data for the reservoir simulation as conducted by TNO.

Genesis provided the data on a number of injection scenarios. Two of these were subsequently modelled by TNO (Bottom Hole Temperatures of 285 K and 259 K, respectively) and an injection rate of 47 kg/s or 1.5 MTon/year.

Figure 4.14 shows the predicted temperatures (BHT = 285 K) around the injection well after 1 day and 1 year of injection, respectively.

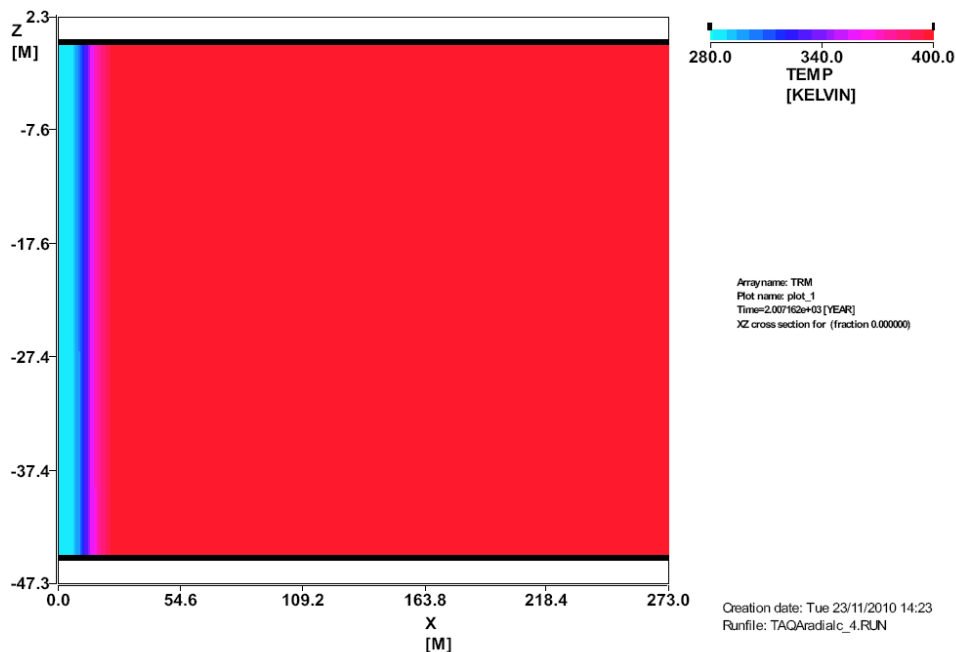


Figure 4.14: Temperature profiles after 1 day of injection.

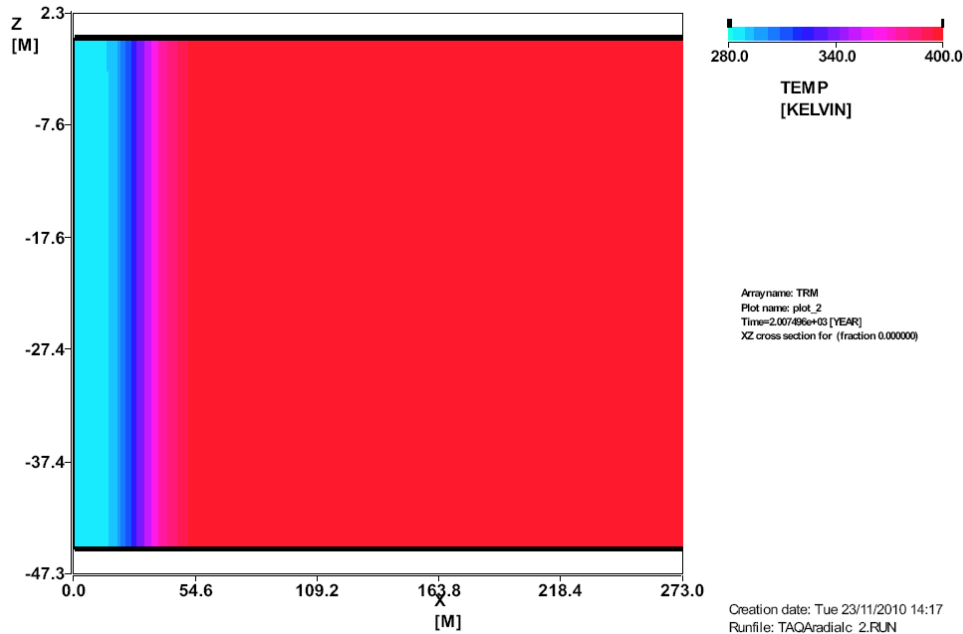


Figure 4.15: Temperature profiles after 1 year of injection.

The temperature propagation in the reservoir depends on the heat capacity of the matrix; the heat capacity used in this study is 2560 kJoule/m<sup>3</sup>/K.

Figure 4.14 shows that temperatures, close to the injection well, drop several degrees within 1 day. Subsequently, the temperature drops rapidly from the initial temperature of the reservoir to that of the injected fluid in the area around the well. The initial cooling is focused on the grid block, directly adjacent to the injection well. Only after this grid has reached the temperature of the injected fluid, the cooling continues in the next grids. After 1 year of injection (Figure 4.15) a very small area near well area has reached a new temperature plateau (at that of the injected fluid). This area will increase with a continued injection under the same conditions. For smaller injection rates the advance of the temperature front will be slower, while for higher rates the speed of advancement will increase. Both figures show a large temperature gradient at the boundary between the new plateau and the rest of the reservoir.

The 12.3 °C of the new temperature plateau is at the high range at which hydrate formation may occur (after the bottom hole has reached 80 bar) Predicting the exact impact of temperature changes and the strong temperature gradient within the reservoir is complex. Not only the fluid properties (for example hydrate formation), but also timescales and degree of drying of the near well area should be considered. Other complicating processes are the thermally induced fracturing and its impact of these fractures on the fluid flow.

The impact of fluctuations of the injection rates and that of a complete shut-in on the temperature profile within the reservoir were also modelled. During the various scenario's, no temperatures below those of the injected fluid were observed. This means that the Joule Thompson effect is neglectable just after the start of the injection as well as right after a shut-in.



Doc.nr: CATO2-WP3.01-D06  
Version: 2011.01.04  
Classification: Confidential  
Page: 60 of 198

## Feasibility study P18

---

As mentioned before the pseudo thermal approach is still under investigation. For certain (more or less random) injection rates, the model was not stable leading to sudden and random stops (due to non-conversion problems) in the middle of a simulation. Investigation this problem, it was found that this was connected with a phase (flash) change within the well bore (for example from vapour to liquid at a certain temperature and pressure. The associated instant changes in density and viscosity of the CO<sub>2</sub> lead to the instability and non-conversion during that time-step. This was solved by slightly changing the injection rates.

The cold injection scenario (159 K) lead to near well temperatures, which rapidly reach 273 K, which resulted in the reservoir simulator to stop (273 K is internal threshold of MoReS). Predicting the impact of freezing conditions within the reservoir is complex. The aforementioned thermal effects are likely to be more pronounced at the lower temperatures. The cold injection may also result in freezing of the connate water in the reservoir.

To the best of our knowledge, it is unknown whether freezing conditions lead to risks or technical problems during the injection. It was therefore concluded that for at the moment some heating of the CO<sub>2</sub> is required before injection in order to stay out of the freezing - and even the hydrate conditions in the near well area. Only after further investigation or a pilot test has shown that colder injection is feasible, it may be possible to reduce the temperature of the injected CO<sub>2</sub>.

## Feasibility study P18

---

conditions of the formation water and mineral assemblage before stage 3, which are used in the model.

### *Stage 3: conditions of P18 reservoir and cap rock after CO<sub>2</sub>*

The effects of CO<sub>2</sub> injection on the reservoir rock and cap rock (seal) are computed in the 'CO<sub>2</sub> scenario'. The results of stage 2 are used with an increase of the CO<sub>2</sub> partial pressure. The following three terms are then modeled:

- No mineral reactions (drop in pH), representing the short-term effects;
- Selection of mineral reactions (carbonates and sulfides), representing the mid-term effects (in the order of years to decades);
- Full suite of mineral reactions, representing the long-term effects (in the order of thousands of years).

### *Stage 4: reference scenario; equilibrium assemblage without CO<sub>2</sub> injection*

Most often, the mineral assemblage of a reservoir or cap rock and the corresponding computed formation water chemistry represent a meta-stable configuration. This is because the reservoir and cap rock are not yet in thermodynamic equilibrium, due to very slow mineral reactions.

Besides, several minerals have not been into contact with formation water due to their presence as inclusions or due to the presence of clay coatings around detrital minerals (Peters, 2009). For this reason, a reference equilibrium assemblage has been modeled in which the final mineral assemblage is computed without CO<sub>2</sub> injection. The resulting mineral assemblage can then be compared to the initial mineralogy and the mineralogy after CO<sub>2</sub> injection. Subsequently, the effect of CO<sub>2</sub> injection on the final reservoir assemblage of the reference equilibrium mineralogy is computed and compared to the initial CO<sub>2</sub> injection assemblage.

Furthermore, the sensitivity of final mineral assemblage to formation water chemistry is shortly investigated (section 5.2.5). This is important since the methodology of the formation water computation holds some uncertainty and subjectivity.

Possible geochemical effects of O<sub>2</sub> impurity in the CO<sub>2</sub> stream are investigated in section 5.2.6

All figures of reservoir and cap rock mineral assemblage are given in Appendix B in such a way that they can be easily compared.

## 5.1.3. Modelling approach

During the modeling, the following constraints were imposed for finding a delicate balance in the mineral-water-gas system:

- A fixed amount of water is available, which is not refreshed (batch reaction in a closed system);
- For each simulation it is checked that the error in the electrical balance between the anions and the cations in the connate water is below 0.05%;
- In the *PHREEQC* model all partial pressures of the gases in the pores are specified and it is assumed that these partial pressures are maintained (i.e. instantaneous supply);
- Ideal gases and ideal gas mixtures are assumed in *PHREEQC*, which is a simplification as CO<sub>2</sub> behaves as a supercritical fluid at the temperature and final pressure conditions at injection depth. Nonetheless, the solubility of CO<sub>2</sub> is corrected for supercritical behaviour by adjusting its partial pressure, using the fugacity coefficient and the Poynting correction. As a result, a lower partial pressure is used as input in order to (artificially) achieve the solubility corresponding to the supercritical behaviour;
- N<sub>2</sub> and CH<sub>4</sub> are present as an inert gas and do not chemically react.

## 5. Geochemical study

### Summary

The effects of CO<sub>2</sub> injection on reservoir and cap rock in the P18 reservoir is predicted by geochemical modeling, using *PHREEQC*. The modeling results show that short-term mineralogical and porosity changes, induced by dissolved CO<sub>2</sub> and corresponding pH decrease, are negligible. On the long-term (thousands of years) mineral reactions will result in a porosity decrease of 0.3 percentage point (pp) for the reservoir and a porosity increase of 0.2 pp for the cap rock. The presence of O<sub>2</sub> as an impurity in the CO<sub>2</sub> stream does not seem to have significant consequences regarding the short-, mid- and long-term geochemical effects of CO<sub>2</sub> storage.

### 5.1. Geochemical modelling

#### 5.1.1. Introduction

TAQA is investigating the possibilities for CO<sub>2</sub> injection in the P18 depleted gas field for geological storage. CO<sub>2</sub> dissolution and subsequent aqueous dissociation will lower the pH of the connate (formation) water, which will influence the chemical equilibrium between gas, connate water and rock mineralogy. Interactions between these three phases will occur, leading to a new equilibrium. This could result in a change in porosity and permeability of the reservoir and cap rock, and affect their storage integrity. Data was collected on the chemical composition of the reservoir and cap rock, on gas currently present and on connate water, together with current and future reservoir conditions like pressure and temperature. This data was used in the geochemical modeling code *PHREEQC* in order to investigate the geochemical effects of CO<sub>2</sub> injection on subsurface characteristics.

*PHREEQC* computes the chemical equilibria of aqueous solutions interacting with mineral assemblages and gases by means of batch-reaction calculations (Parkhurst and Appelo, 1999). The development of the effects in time is considered on a qualitative base; quantification would require further study.

#### 5.1.2. Stages and scenarios

The modeling approach consists of four stages. During the first stage the available data is organized and evaluated. During the following stage the pre-operational (i.e. before CO<sub>2</sub> injection) conditions are established. In the third stage the geochemical consequences of CO<sub>2</sub> injection are computed. Finally a reference scenario without CO<sub>2</sub> injection is also computed.

##### *Stage 1: data inventory and evaluation*

1. Define the mineral composition, porosity and water saturation of the reservoir (Main Buntsandstein) and cap rock;
2. Define the measured composition of the formation water;
3. Define the current gas composition in the formation;
4. Define the pressure and temperature conditions at the injection depth.

##### *Stage 2: pre-operational conditions (before CO<sub>2</sub> injection)*

During the second stage the initial composition of the solution (the speciation of the dissolved ions) and the corresponding rock mineralogy are computed. *PHREEQC* adjusts the pH of the formation water accordingly. Formation water and mineral assemblage are compared to the measured compositions and adjustments are made, if necessary. The results define the

## Feasibility study P18

With respect to the latter constraint we initially observed the following (overall) reaction during our preliminary PHREEQC simulations:



In the case of a relatively high  $\text{CH}_4$  partial pressure and sufficient  $\text{SO}_4^{2-}$  the equilibrium of this reaction will shift to the right. The preliminary simulations predicted that this would lead to dissolution of anhydrite ( $\text{CaSO}_4$ ). It is not considered likely that these reactions will be predominant during the next few thousand years due to two reasons. Firstly the given reaction with  $\text{CH}_4$  and  $\text{SO}_4^{2-}$  requires a very high activation energy and is very slow. Secondly it is frequently observed that anhydrite has been in equilibrium with  $\text{CH}_4$  (for example in the P18 field) for thousands of years. Therefore it is unlikely that anhydrite will dissolve. Rather than eliminating the reactions given above from the PHREEQC database, the problem was solved by replacing  $\text{CH}_4$  by the inert Ar gas in the model.

### 5.1.4. Reservoir and cap rock conditions

The sample analyses of the P18 reservoir (Hardegsen, Upper Dethfurth and Lower Dethfurth formations) show that the average porosity is 8.8% with a water saturation of 0.42 (Cantwell, 1992). The volume percentages of rock, gas and water in the reservoir are therefore 91.2%, 5.1% and 3.7% respectively. In the model 1.0  $\text{dm}^3$  of formation water is used, which corresponds to 1.4  $\text{dm}^3$  of gas and 24.6  $\text{dm}^3$  of minerals.

The porosity of the cap rock is 1% and it is assumed that the water saturation is 100%.

#### Pressure and temperature

The initial pressure in the P18 reservoir is 20 bar. The average temperature is 106°C and total final pressure is defined as 356 bar (20 bar below the initial gas pressure before gas production). The initial and final pressure conditions are shown in Table 16. Pressure and temperature conditions of the cap rock after  $\text{CO}_2$  injection are assumed to be equal to the conditions in the reservoir rock.

Table 16: Initial and final condition of the reservoir gas.

Component	Initial conditions			Final conditions		
	Composition (mol%)	Px (atm)	Log Px (-)	Composition (mol%)	Px (atm)	Log Px (-)
<b>C1</b>	98.26	19.91	1.30	5.52	19.91	1.30
<b>CO<sub>2</sub></b>	1.24	0.25	-0.60	94.45	331.33	2.09
<b>N<sub>2</sub></b>	0.5	0.10	-1.00	0.03	0.10	-1.00
<b>Total</b>	100	20.26			351.34	

#### Rock composition

The reservoir rock composition is defined from several rock samples of the Hardegsen, Upper Dethfurth and Lower Dethfurth formations (Cantwell, 1992). Average values are taken (Table 17). The rock sample from the Volpriehausen formation was excluded as it is expected that  $\text{CO}_2$  will not be injected in this formation, based on porosity measurements. The sealing formation of the P18 Bundsandstein formation consists largely of quartz, with lesser amounts of e.g. dolomite, illite, anhydrite and siderite (Table 18).

## Feasibility study P18

### Gas composition

The composition of the gas phase currently present in the reservoir is known. In the model all alkanes are represented by C1 (CH<sub>4</sub>) (Table 16).

Table 17: Composition of reservoir rock of the P18 field based on sample analyses and experimental mineral densities and mol masses. The volume (dm<sup>3</sup>) and number of moles are in correspondence to a total rock volume of 24.6 dm<sup>3</sup>.

Mineral	Composition (wt%)	Volume (dm <sup>3</sup> )	Amount (Mole)
Quartz	78.1	19.38	856.15
Anorthite	2.3	0.54	5.45
K-feldspar	5.7	1.47	13.59
Dolomite	5.8	1.33	20.66
Anhydrite	0.1	0.02	0.40
Albite	0.1	0.02	0.17
Kaolinite	0.7	0.17	1.63
Clinochlore-14A	1.3	0.32	1.58
Illite	2.8	0.66	4.83
Smectite-Na	3.1	0.66	5.06

Table 18: Composition of cap rock of the P18 field based on sample analyses and experimental mineral densities and mol masses. The volume (dm<sup>3</sup>) and number of moles are in correspondence to a total rock volume of 99 dm<sup>3</sup>.

Mineral	Composition (wt%)	Volume (dm <sup>3</sup> )	Amount (Mole)
Quartz	60.7	62.1	2734.62
Anorthite	2.9	2.8	28.12
K-feldspar	3.7	3.9	35.47
Dolomite	11.8	11.2	173.69
Anhydrite	7.0	6.4	138.57
Pyrite	0.5	0.3	12.19
Siderite	2.4	1.6	55.54
Clinochlore-14A	0.7	0.7	3.55
Illite	10.1	9.9	71.43
Smectite-Na	0.2	0.1	1.0

### 5.1.5. Pre-operational conditions

The balance between rock mineralogy and water chemistry is delicate. Measured compositions of both are subject to local variability and measurement errors. Because the measured salt concentration of the connate water in the P18 field is unexpectedly very low, the formation water of P06-A2, which is located near P18, is used for comparison with the computed chemistry of the formation water in the reservoir. This is done by equilibration of pure water with surplus amounts of minerals present in the reservoir and a NaCl concentration of 130 g/kg water. Subsequently, it is compared to the formation water of P06-A2. It is computed that several minerals show extensive dissolution and precipitation of secondary minerals. To avoid this, the amount of the dissolving minerals is lowered until no significant conversion occurs. Several new minerals are

**Feasibility study P18**

still computed to precipitate in low amounts (glauconite, muscovite and pyrite). Due to the lowering of dissolution of illite, smectite, K-feldspar and anorthite, the amounts of precipitating minerals are so low that they could have been overlooked during mineral analysis. Therefore they are included in the assessment. Mesolite and saponite are computed to dissolve, but these do not naturally occur in regular sandstones. Furthermore, dolomite is computed to transform completely into dolomite-ord and, K-feldspar into microcline. These precipitates and conversions are excluded from the simulation since they do not represent current conditions. Dolomite and K-feldspar thus represent meta-stable phases.

The pH of the computed formation water has a value of 5.8. The computed water chemistry and the measured chemistry of P06-A2 are shown in Figure 5.1. The computed concentration of chloride, magnesium and sodium are close to the measured values of P06-A2. For iron, calcium and potassium, the computed and measured values are significantly different. The high iron concentration in the measured sample(s) might be an artefact caused by corrosion of well material. Other differences might be caused by contamination from, for example, drilling muds. Furthermore, water samples can locally be very different due to local mineralogy differences, and this water sample is from another location. In section 5.2.5 the results of a sensitivity analysis on formation water chemistry are given.

The rock composition corresponding to the computed formation water is shown in Appendix B Figure 12.1.

For the computation of cap rock formation water, the same methodology is used as for the reservoir. Small amounts of albite, diaspore, glauconite and muscovite were predicted to precipitate. These have been included in the modeling since these minerals occur frequently in natural sandstones. The mineral assemblage of the cap rock is shown in Appendix B, Figure 12.4. The pH of the computed formation water has a value of 6.1.

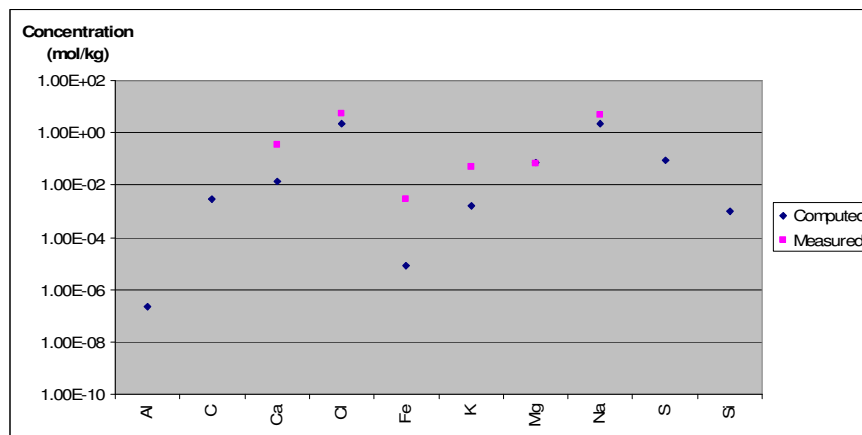


Figure 5.1 Computed and measured formation water composition (initial).



## 5.2. Geochemical effects of CO<sub>2</sub> injection

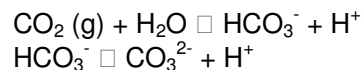
### 5.2.1. Introduction

In this section the effects of CO<sub>2</sub> injection on reservoir and cap rock are described. Three terms were defined describing the qualitative modeling of the processes. The results for the reservoir and cap rock are described in section 5.2.2 and 5.2.3 respectively. Results for the mineral assemblage of reservoir and cap rock, as well as initial rock mineralogy are shown in this section, as well as in Appendix B for easy comparison.

### 5.2.2. Reservoir rock

#### Short term effects on connate water

In this scenario the effect of increased CO<sub>2</sub> partial pressure (356 bar) is computed, while excluding mineral dissolution and precipitation. As expected, the pH of the connate water drops due to the increasing dissolution and dissociation of CO<sub>2</sub>. The following reactions take place:



A relatively high CO<sub>2</sub> partial pressure will shift the first and second reaction more to the right and decreases the pH. The pH in the reservoir is computed to decrease to a value of 3.5, which is expected to be the condition directly after injection. The rates of mineral reactions are assumed to be much slower than the dissolution rate of the CO<sub>2</sub> in the water. Mineral reactions will buffer the pH (see following sections) and a pH of 3.5 is therefore considered to be the minimum. The carbon concentration in the formation water increases as a result of CO<sub>2</sub> dissolution.

#### Carbonate and sulfide mineral reactions (mid term)

On the mid-term the effect of increased CO<sub>2</sub> partial pressure is computed, while also allowing dissolution and/or precipitation of carbonates and sulfides. In the reservoir, a small amount of dolomite and pyrite dissolve (0.03 and 0.17% of the amounts initially present, respectively) due to the dissolution of CO<sub>2</sub>. Some anhydrite and an insignificant amount of dawsonite precipitates. These dissolution and precipitation reactions slightly buffer the pH, to a value of 4.2 but the porosity is not affected. Also, the composition of the formation water does not change significantly, except for an increase in carbon concentration caused by the CO<sub>2</sub> dissolution in the brine.

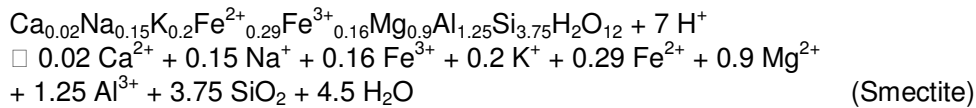
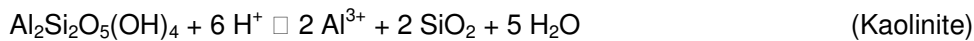
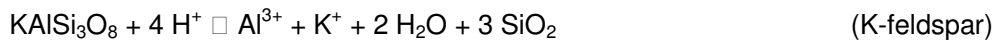
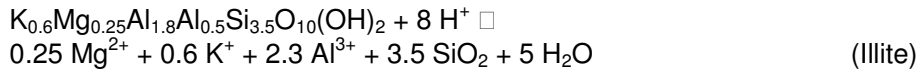
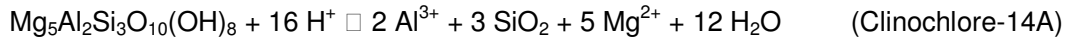
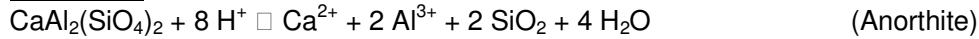
#### Full suite of mineral reactions (long term)

The effect of increased CO<sub>2</sub> partial pressure on the total rock mineralogy describes the conditions of thermodynamic equilibrium. This will take thousands of years to establish since most mineral reactions are very slow. Furthermore, minerals can be (temporarily) inaccessible to formation water due to their presence as mineral inclusions or to clay coatings surrounding them (Peters, 2009).

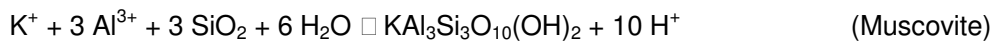
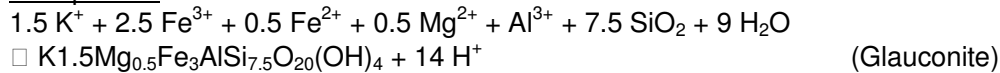
The results on the final formation water, compared to the initial formation water, and the final reservoir mineral assemblage are shown in Figure 5.2 and in Appendix B, Figure 12.2 respectively. The following main reactions occurred:

**Feasibility study P18**

Dissolution



Precipitation



Due to these reactions, *the porosity decreases with 0.3 percentage point (pp) to 8.5%, based on the specific density of the different minerals*. Possible porosity effects due to geomechanical processes are not taken into account. Dissolution of minerals might cause mechanical compaction of the reservoir, thereby causing additional porosity decrease.

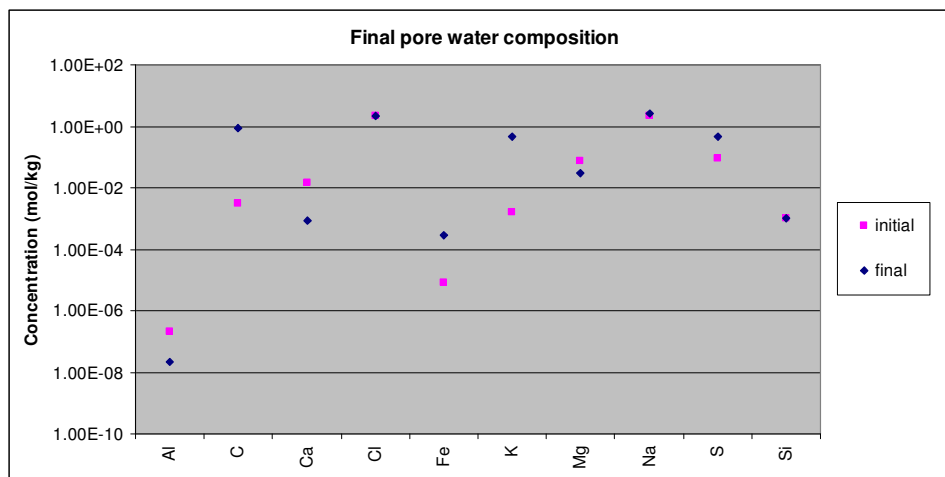


Figure 5.2 Initial and final computed formation water composition.

### 5.2.3. Cap rock seal

#### Effects on connate water (short term)

If CO<sub>2</sub> would dissolve and diffuse into the formation water of the cap rock, the pH could decrease to a value of 3.2. Unlike in the reservoir, the pH drop will not occur throughout the formation within the injectivity period, because a *boundary* between reservoir and cap-rock is affected. We then might expect CO<sub>2</sub> diffusion could start at the reservoir - cap rock boundary, and CO<sub>2</sub> could possibly slowly migrate up, into the cap rock.

#### Carbonate and sulfide mineral reactions (mid-term)

On the mid-term, small amounts of anhydrite and siderite (less than 0.01% of the initial amounts present) will dissolve, thereby buffering the pH to a value of 4.3. Precipitation of other carbonates and sulfides does not occur and the effect of dissolution on porosity is negligible. The iron concentration in the brine increases significantly to a value of  $2.55 \cdot 10^{-3}$  mol/liter due to the dissolution of siderite, but the amount of anhydrite dissolution is too small to have any effect on the calcium concentration.

#### Full suite of mineral reactions (long term)

On the long-term, mineralogical changes are predicted to occur. Illite, K-feldspar, anorthite, clinocllore, and siderite are (almost) completely dissolved, while muscovite, glauconite and diaspore have precipitated in significant amounts (Appendix B, Figure 12.5). *These mineralogical changes correspond to a porosity increase of 0.2 pp (equal to an increase of 20%)*. The final formation water chemistry is shown Figure 5.3.

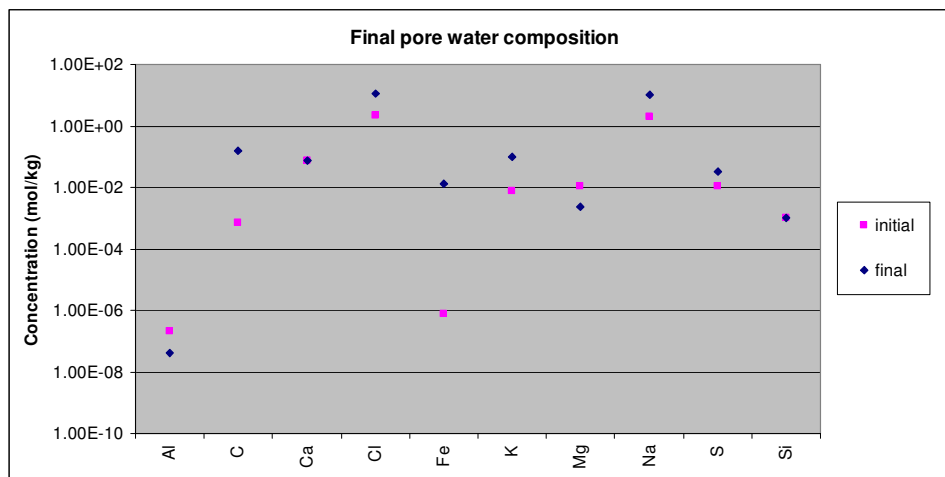


Figure 5.3: Initial and final formation water composition of the cap rock.

#### 5.2.4. Reference scenario; equilibrium assemblage

The computation of the long-term mineralogical changes in the reference scenario show that significant changes would occur in the reservoir and cap rock, even without CO<sub>2</sub> injection, due to their current meta-stable conditions (Appendix B, Figure 12.3 and Figure 12.6 respectively). The porosity of the reservoir increases by 0.1 pp, compared to a decrease of 0.3 pp in the CO<sub>2</sub> scenario. In the equilibrium stage of the cap rock, the porosity is predicted to increase by 0.3 pp, while it increases by 0.2 pp in the CO<sub>2</sub> injection scenario.

CO<sub>2</sub> injection into a reservoir with the computed reference assemblage results in exactly the same mineralogical changes, and thus porosity change, for the reservoir and cap rock as CO<sub>2</sub> injection into a reservoir (with a cap rock) with the meta-stable assemblage (Appendix B, Figure 12.2 and Figure 12.5 respectively). This shows that the meta-stability of the reservoir and cap rock do not affect the mineralogical changes caused by CO<sub>2</sub> injection.

#### 5.2.5. Formation water sensitivity

As explained in section 5.1.5, several minerals are computed to completely dissolve when computing the chemistry of the formation water, thereby supplying the ions required for precipitation of new, secondary minerals. In order to obtain a mineral assemblage close to the measured one, a limited amount of the dissolving minerals was supplied in the calculation of the formation water. For sensitivity analysis, these amounts were multiplied by a factor of ten, allowing the precipitation of larger amounts of secondary minerals. In another run, the precipitation of secondary minerals was excluded. The results show that for both cases there is negligible effect on the mid- and long-term mineral assemblage and the porosity change of the reservoir and cap rock, even if the initial pH is significantly different. Hence, the formation water sensitivity of the P18 reservoir and cap rock is small.

#### 5.2.6. O<sub>2</sub> impurity

The captured CO<sub>2</sub> can contain some O<sub>2</sub>, which is maximally 160 ppm. To study the possible effect of O<sub>2</sub> on the reservoir, 0.05 bar of O<sub>2</sub> is used as input in the model (log P<sub>x</sub> is -1.30), corresponding to 160 ppm.

The model results show that only a fraction of the O<sub>2</sub> is predicted to dissolve on the short-term, having no additional effect on the pH of the formation water compared to the baseline scenario. Mid-term effects are small. Slightly more pyrite and anhydrite will dissolve and precipitate, respectively, compared to the baseline. The iron, in the reduced state, remains in the formation water. All oxygen is used to oxidize sulfur from pyrite for anhydrite precipitation. The effects of these reactions on porosity are negligible.

Increasing the O<sub>2</sub> partial pressure by 10 (corresponding to 1600 ppm O<sub>2</sub> in the CO<sub>2</sub> gas stream), in order to investigate a worse case scenario, would lead to complete pyrite dissolution and slightly more anhydrite precipitation, since more oxygen is in the system to oxidize sulfur from pyrite. The iron from pyrite is oxidized and precipitated as hematite. The porosity change is still negligible.

Long-term effects do not differ from the baseline scenario.

### 5.3. Conclusions

When CO<sub>2</sub> is injected into a reservoir system with cap rock, the pH of the formation water will initially decrease to a value of 3.5 and 3.2 for the reservoir and cap rock respectively, due to the formation of carbonic acid. Dissolution of small amounts of carbonate and sulfides, which is predicted to occur on the mid-term (in the order of years to decades), will buffer the pH to a value of 4.2 and 4.3 respectively. The effects on mineralogy and porosity are negligible. It is predicted that the mineralogical assemblage will have been changed significantly once thermodynamic equilibrium is established, which may take thousands of years. *The corresponding porosity change is a decrease of 0.3 pp (to 8.5%) for the reservoir rock and an increase of 0.2 pp (to 1.2%) for the cap rock.*

Since the initially computed formation water and mineral assemblage of both reservoir and cap rock are not in equilibrium reference calculations were performed to investigate the equilibrium assemblage without CO<sub>2</sub> injection. The results show that the assemblage changes significantly. However, if CO<sub>2</sub> injection would occur in the reference assemblage, the mineralogy and porosity change would be equal to CO<sub>2</sub> injection into a reservoir with cap rock in a meta-stable phase. Furthermore, the final mineral assemblage is relatively insensitive to the methodology of formation water computation.

The presence of O<sub>2</sub> as an impurity in the CO<sub>2</sub> stream is predicted not to have a significant effect on the short-term. On the mid-term the model shows a slight increase in pyrite dissolution and anhydrite precipitation. Effects on porosity are negligible. Long-term effects are similar to the baseline and therefore also to the reference.

### 5.4. References

Cantwell W., 1992. Final Report of Mineralogical Analysis for Amoco Netherlands Petroleum Company, Well number P/18-2 and P/18-3, The Netherlands.

Peters C.A., 2009. Accessibilities of reactive minerals in consolidated sedimentary rock: An imaging study of three sandstones. *Chemical Geology* 265; p198-208

## 6. Top seal and fault integrity study

### 6.1. Introduction

#### 6.1.1. Background

This chapter presents the results of the top seal and fault integrity assessment conducted in the framework of the technical feasibility study of geological CO<sub>2</sub> storage in the depleted P18 Field. The study was undertaken within the framework of CATO-2 project, WP3.3. Caprock and fault integrity.

#### 6.1.2. Scope and objective

CO<sub>2</sub> injection into depleted hydrocarbon reservoirs will change the state of stress in a reservoir-seal system due to various phenomena: poro-mechanical effects caused by changes in the pore fluid pressure; buoyancy effects caused by changes in the pore fluid density; thermal effects caused by changes in the pore fluid temperature; and chemical effects caused by changes in the pore fluid chemistry.

As a result of induced stress changes top seals can be mechanically damaged, pre-existing sealing faults and fractures can be re-activated, or new fracture systems can be created, allowing fluid migration out of the storage complex. Besides the effects on the containment, CO<sub>2</sub> injection could also induce ground movement, which can be either aseismic - in the form of ground surface uplift, or (micro-)seismic - caused by a sudden slip on pre-existing discontinuities or faults.

The objective of this study is to evaluate the impact of induced stress changes, resulting from past gas extraction and future CO<sub>2</sub> injection in P18 Field, on top seals and faults.

The impact on the containment will be evaluated by assessing:

- The mechanical integrity and the potential for induced hydro-fracturing of top seals.
- The mechanical integrity and the potential for re-activation of faults, as fault slip can make previously sealing faults conductive and induce seismic events at the injection site.

The impact on the environment will be evaluated by assessing the induced ground/seabed movement, i.e. subsidence and uplift.

Mechanical and transport rock properties may change over time due to mineral reactions between the injected CO<sub>2</sub> and the rock (reservoir, caprock and fault gouge). Experimental testing program is currently under way at the HPHT lab of Utrecht University to quantify the long-term effects due to CO<sub>2</sub>-rock interaction for P18. The results of these tests were not available at the time when this study was completed and therefore not considered in this report.

### 6.1.3. Approach

The input data for this study were supplied by TAQA Energy B.V.

The following data and models developed within the framework of the CATO-2 project were used in this study:

- Regional geological Petrel model of P18 constructed by TU Delft and reservoir scale Petrel model constructed by TNO.
- Reservoir MoReS model and analytical model developed by TNO.
- Rock mechanics properties of the top seal determined by the experimental testing program at Utrecht University.
- The following tasks and activities were defined and carried out in this study:
- Geomechanical field characterization - by using well logs analysis, experimental rock mechanics tests and in situ stress data analysis.
- Development of geomechanical models - by using a finite element (FE) approach.
- Assessment of top seal mechanical integrity - by using analytical and numerical geomechanical models.
- Assessment of fault seal integrity - by using a fault seal analysis tool based on the Shale-Gouge Ratio, analytical and numerical geomechanical models.
- Assessment of induced ground, i.e. seabed deformation - by using a semi-analytical model for prediction of subsidence/uplift.

## 6.2. Geomechanical field characterization

### 6.2.1. Field description

P18 Field is located in the P block of the Dutch offshore. The reservoir structure of P18 comprises 3 compartments bounded by a system of NW-SE oriented faults in a horst and graben pattern.

The main compartment P18-2 comprises 3 segments (Figure 6.1). The largest segment P18-2 is drained by 3 wells: P18-2A1, P18-2A3 and P18-2A5. Wells P18-2A6 and P18-2A6st drain other two segments. The segment drained by well P18-2A6 is not in communication with other two segments of this compartment. Well P18-2A1 will be used as the CO<sub>2</sub> injector. The initial pressure in P18-2 is 375 bar and GWC is at 3680 m. Reservoir temperature is 126 °C. P18-2 is in production since October 1993.

Compartment P18-4 is drained by one well P18-4A2 which will be used as CO<sub>2</sub> injector. Compartment P18-4 is not in communication with other two compartments. The initial pressure in P18-4 is 340 bar and GWC is at 3377 m. P18-4 is in production since March 1994.

Compartment P18-6 is drained by one well P18-A67 which will be used as CO<sub>2</sub> injector. Compartment P18-6 is not in communication with compartment P18-4 (different GWC) and appears (according to Chapter 4) not to be in communication with compartment P18-2 (equal GWC). The initial pressure in P18-6 is 375 bar and GWC is at 3680 m. P18-6 is in production since March 2004.

## Feasibility study P18

The reservoir rocks consist of sandstones intercalated with thin layers of shale. The reservoir belongs to the Main Buntsandstein Group and comprises the following parts:

- 25 m thick Hardegsen (RBMH), good producer;
- 50 m thick Upper Detfurth (RBMDU), fair producer;
- 25m thick Lower Detfurth (RBMDL), fair producer;
- 120m thick Volpriehausen (RBMVU+RBMVL), poor producer.

Hardegsen and Upper Detfurth are the main gas producers.

The primary top seal overlying the Bunter reservoir is a 50 m thick layer of the lower part of Upper Germanic Trias (RN). This layer comprises (from top to base):

- Röt Claystone Member (Mb) (RNROC),
- Main Röt Evaporite Mb (RNRO1),
- Solling Claystone Mb (RNSOC).

The primary top seal, as defined above, is covered by a 100 m thick upper part of Upper Germanic Trias (Muschelkalk, RNMU and Keuper, RNKP) and a 3-400 m thick Altena Group (AT) which can also be regarded as a part of the primary seal.

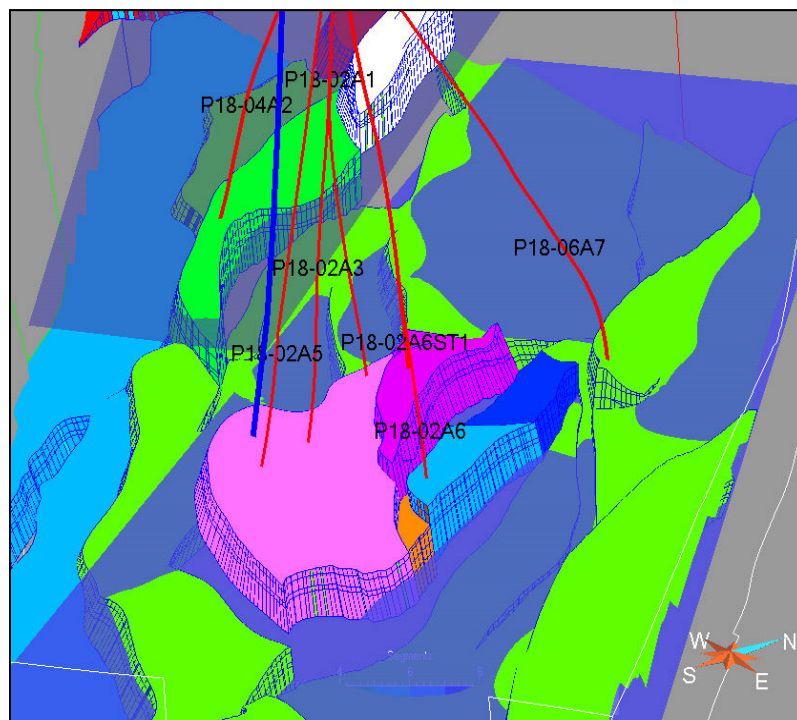


Figure 6.1: Reservoir structure showing compartment P18-2, which consist of 3 segments (in the middle), compartment P18-6 (penetrated by well P18-06A7) and compartment P18-4 (penetrated by well P18-04A2).



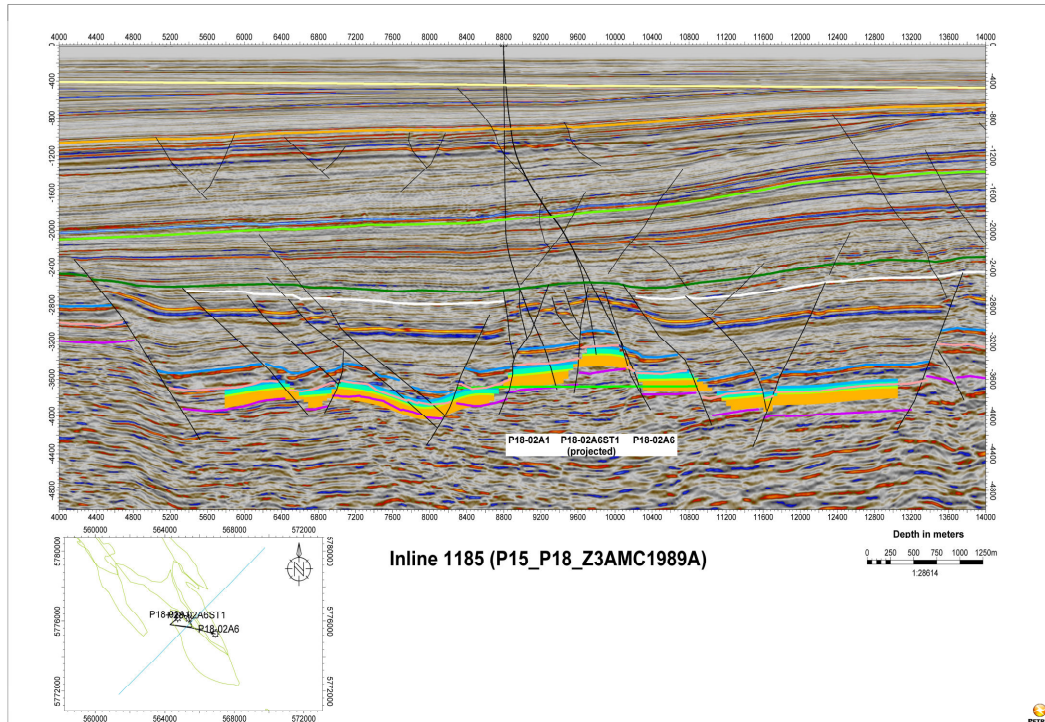


Figure 6.2: Interpreted seismic section along Inline 1185 through the P18 Field. The Bunter reservoir is shown in solid colours.

## 6.2.2. Lithological differentiation of the top seal

Detailed lithological determination of the top seal was performed in order to differentiate various lithologies present in the formations overlying the Bunter P18 reservoir. Bulk top seal lithologies were determined using gamma-ray, density, sonic and neutron-porosity logs. The most complete well-log suites were available from wells P18-2, P18-A-03-S2 and P18-A-06, which we used in analysis. The following lithologies could be resolved: shale, dolomite, anhydrite and gypsum.

The primary top seal overlying the Bunter reservoir is represented by the lower part of Upper Germanic Trias (RN), namely Röt Claystone Mb, Main Röt Evaporite Mb and Solling Claystone Mb. The lithologies present in these layers, according to well logs interpretation, comprise thin beds of shales with anhydritic cementation (Figure 6.3). The average thickness amounts to about 50 m, with a range of 41-68 m. This zone is continuous above compartment P18-2 with variable anhydritic content in shales (Figure 6.4). We assume that the seal above P18-2 is representative for the whole P18 Field.

The core from Röt and Solling (i.e. the primary top seal as defined above) was taken from well P15-14 in the neighbouring block P15 in an earlier study and analysed using standard geologic and petrophysical techniques including mercury-injection capillary-pressure tests (Spain and Conrad, 1997). The results showed that the true top seal for the P15 hydrocarbon accumulations is provided by thinly interbedded and interlaminated shale and very fine-grained sandstone to siltstone. These lithofacies contain type A seals which are capable of supporting gas-column heights in excess of 300 m. The P15-top seal quality may also be representative for the

**Feasibility study P18**

neighbouring P18 block as hydrocarbon accumulations in the Buntsandstein are present in both blocks.

The lower part of Upper Germanic Trias (i.e the top seal as defined above) is covered by a 100 m thick upper part of Upper Germanic Trias (Muschelkalk, RNMU and Keuper, RNKP) and a 3-400 m thick Altena Group (AT) which can also be regarded as a part of primary top seal.

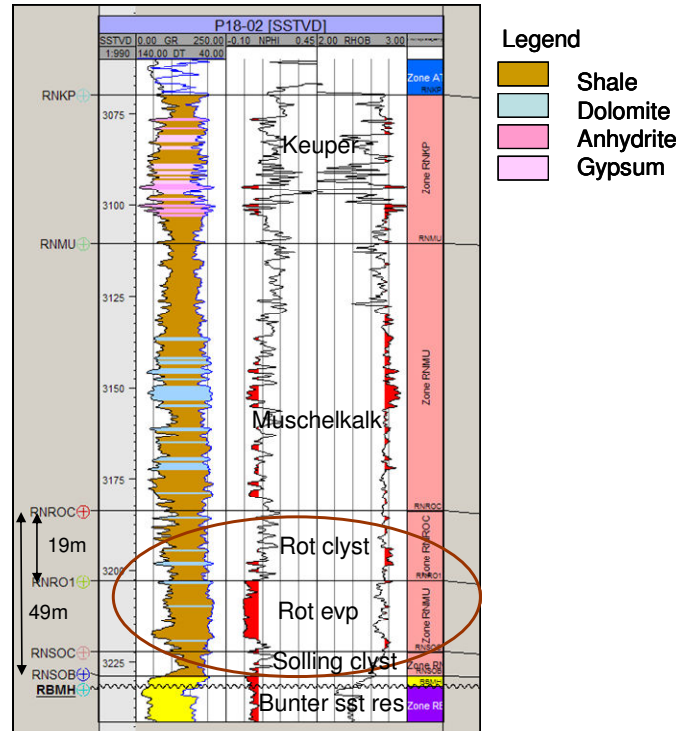


Figure 6.3: Lithological differentiation of the top seal based on well logs from well P18-02. The primary top seal is represented by Solling claystone, Röt evaporites and Röt claystone. Muschelkalk and Keuper could also be regarded as a part of primary top seal.

## Feasibility study P18

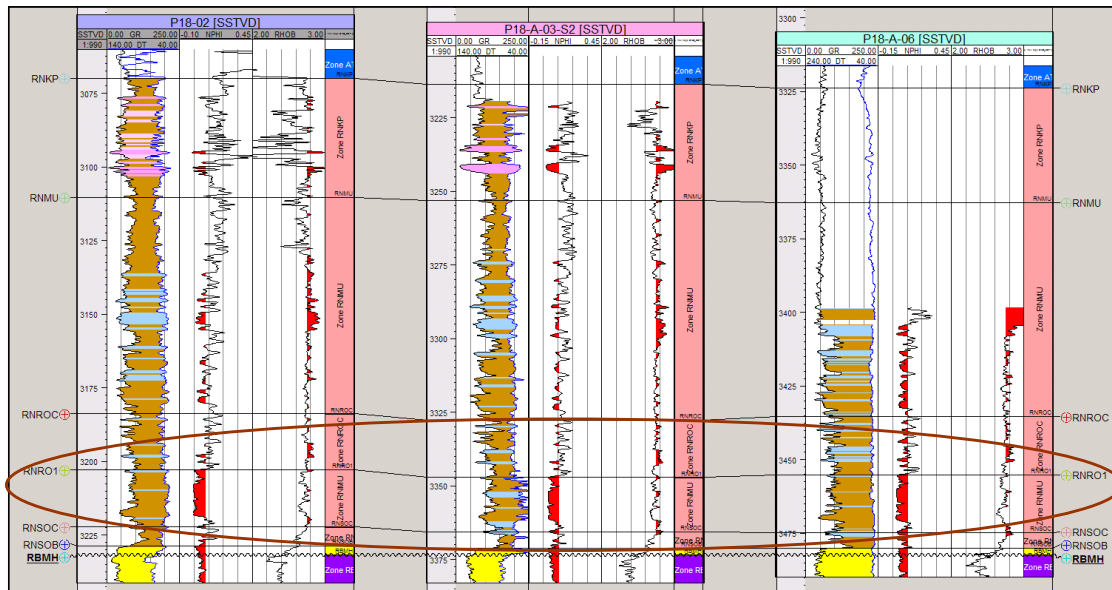


Figure 6.4: Well correlation section showing lithologies of the top seal in compartment P18-2. The primary top seal is represented by Solling claystone, Röt evaporates and Röt claystone. Muschelkalk and Keuper could also be regarded as a part of primary top seal.

### 6.2.3. Geomechanical characterization of the top seal and overburden formations

#### Experimentally derived rock properties

Experimental testing program within the CATO-2 project is currently under way at the HPT lab of Utrecht University to quantify the long-term effects due to CO<sub>2</sub>-rock interaction for P18 (Utrecht University report, 2010). As a part of the testing program, permeabilities of the reservoir rock were measured on samples taken from P18 field. However, caprock core was not available from P18 field. Therefore permeabilities and mechanical properties were measured on samples taken from the Röt/Solling caprocks in the Q16 gas field, which is presumed to be analogous to the P18 field.

First results show that reservoir rocks are generally 2-3 orders of magnitude more permeable than caprocks. For most samples measured permeability of the reservoir rock is on the order of  $10^{-15} \text{ m}^2$  to  $10^{-16} \text{ m}^2$  and permeability of the caprock on the order of  $10^{-18} \text{ m}^2$ .

A summary of the caprock strength properties for the Röt/Solling caprocks from the Q16 gas field is shown in Table 19. Based on the measured properties, the caprock is a hard and competent rock. Generally we find that the mechanical properties fall within a reasonable range for similar materials. At this stage, due to a lack of suitable samples, no analysis has been conducted on the mechanical properties of the reservoir rocks of the P18 gas field.

#### Well log-derived rock properties

Besides the experimental test data on the caprock strength mentioned above, no other experimental data on the strength and elasticity of other formations were available. Therefore, geomechanical properties of the overburden and the underburden required for geomechanical analyses were derived indirectly from the available well logs. The most complete well-log suites were available from wells P18-2, P18-A-02, P18-A-03-S2 and P18-A-06.

**Feasibility study P18**

For determination of dynamic elastic properties both compressional- ( $V_p$ ) and shear ( $V_s$ ) wave velocities are required. Shear velocities were measured in wells P18-A-02 and P18-A-06. They had to be estimated for other two wells using lithology-dependent empirical relationships from the literature (for clastic sediments from Castagna et al., 1985; for anhydrite from Rafavick et al, 1984, and for dolomite from Greenberg and Castagna, 1992).

Dynamic Young's modulus ( $E_{dyn}$ ) was then derived from well logs and converted to the static Young's modulus ( $E_{stat}$ ), which is required in geomechanical analyses, according to the formulas given below:

$$E_{dyn} = \rho V_s^2 \cdot (3V_p^2 - 4V_s^2) / (V_p^2 - V_s^2) \quad (6.1)$$

$$E_{stat} = 0.74 \cdot E_{dyn} - 0.82 \quad (\text{from Eissa and Kazi, 1988}) \quad (6.2)$$

Well-log derived elastic rock properties clearly indicate stiffness contrast (i.e. difference in Young's elasticity modulus) between different lithostratigraphic and geomechanical units. The obtained absolute values of Young's moduli, however, possibly overestimate the expected values and therefore were downscaled by the ratio  $E_{lab} / E_{well-logs}$  for the caprock (as direct measurements of mechanical rock properties were only available for the caprock). This approach gives a value of  $E=20$  GPa for the Bunter sandstone reservoir, which is a realistic value based on analogy with other Bunter reservoirs in the Netherland such as the Barendrecht-Ziedewij gas field (Winningsplan Barendrecht-Ziedewij, 2003).

Summary of the differentiated geomechanical units and their geomechanical properties is given in Table 20. The successive lithostratigraphic units with relatively small thickness, similar in lithology and mechanical properties were joined into one unit.

Table 19: Caprock strength summary. The properties were determined by triaxial tests performed in HPT lab of Utrecht University.  
 $E$ =Young's elasticity, UCS=unconfined compressive strength,  $\mu$ =friction coefficient (corresponds to a friction angle  $\phi=28^\circ$ ),  $C$ =cohesion.

Caprock strength summary, Samples from Q-16 field

Sample #	Lithology	$\sigma_1$ (MPa)	$(\sigma_1 - \sigma_3)_{max}$ (MPa)	$E$ (GPa)	UCS (MPa)	$\mu$	$C$ (MPa)
#57	Röt	5	91.94	21.15	93.315	0.536	27.92
#59	Röt	20	147.74	31.64			
#55	Röt	35	149.87	23.69			
#60	Röt/Solling	50	180.83	29.11			



Feasibility study P18

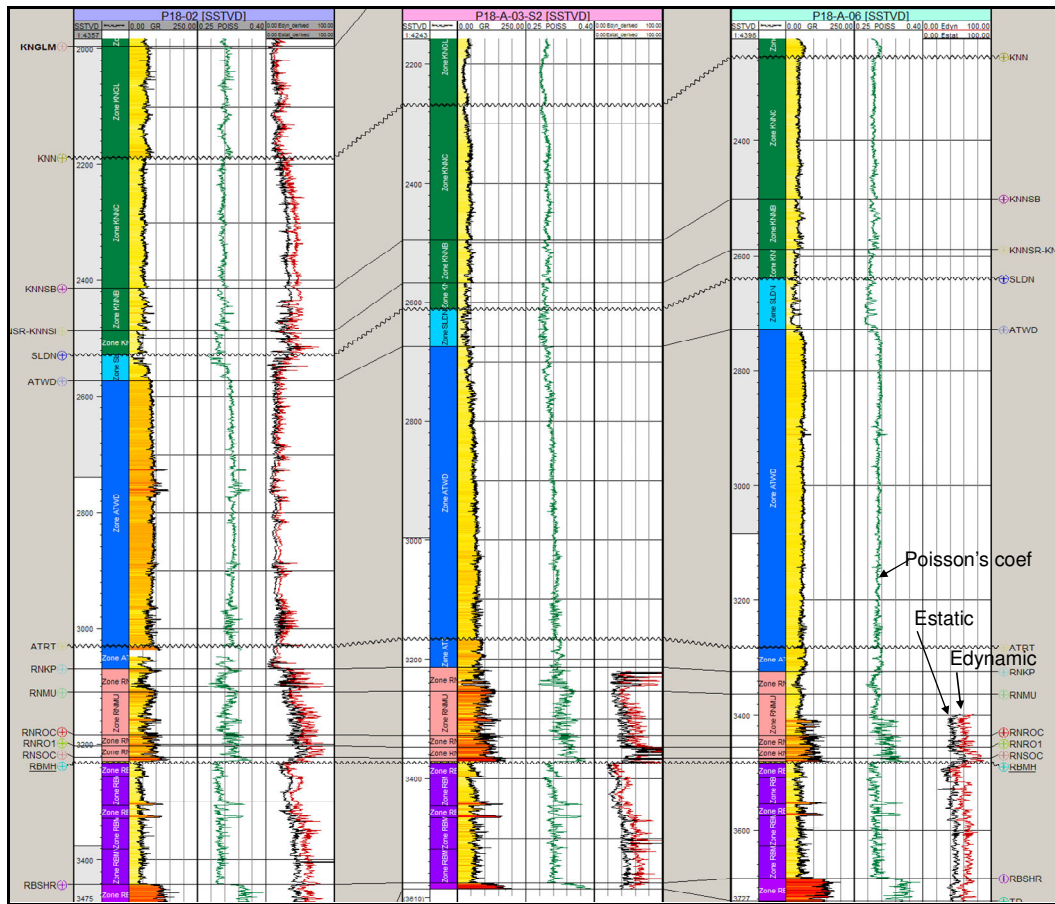


Figure 6.5: Well correlation section showing gamma-ray log and calculated Poisson's coefficient (range from 0.25-0.4) and Young's elasticity modulus (range from 0-100 GPa).

## Feasibility study P18

Table 20: Geomechanical properties for the differentiated geomechanical units in the P18 gas field.

Unit No	Stratigraphic unit	Thickness* [m]	Depth top* mTVDss	Density** [kg/m <sup>3</sup> ]	Young's modulus*** E [GPa]	Poisson's coeff.*** $\nu$ [-]
1	Upper North Sea Group, NU	417	33.5	1960	0.5	0.3
2	Middle and Lower North Sea Group, NM+NL	503	451	2600	5	0.3
3	Chalk Group, CKGR	956	920	2300	20	0.17
4	Rijnland Group, KN	652	1876	2650	17	0.30
5	Schieland Goup, SL	44	2528	2100	13	0.30
6	Altena Group, (AT)	497	2573	2600	15	0.30
7	Upper Germanic Trias (RN) (Keuper Fm, Muschelkalk Fm, Röt Claystone Mb, Röt Evaporite Mb, Solling Claystone Mb) <b>Primary top seal</b>	162	3070	2600	26****	0.30
8	Lower Germanic Trias (RB) = Hardegsen Fm (RBMH) + Upper Detfurth Sandstone Mb (RBMDU) <b>Reservoir, upper part, good producer</b>	74	3232	2600	20	0.2
9	Lower Germanic Trias (RB) = Lower Detfurth Sandstone Mb (RBMDL) + Volpriehausen Sandstone Mb (RBMV) <b>Reservoir, lower part, poor producer</b>	137	3305	2600	25	0.2
10	Rogenstein Mb, RBSHR + Main Clayst Mb, RBSHM (Lower part of Lower Germanic Trias)	140	3442	2600	29	0.30
11	Zechstein Group, ZE (Permian)	27	3582	2100	20	0.35
12	Slochteren Fm, ROSL + Carboniferous, undefined (DC)	>23	3608	2650	30	0.25

\*Thickness and depth based on exploration well P18-02 as this well penetrates all the units down to the Carboniferous base.

\*\*Rock density assumed based on common values for different lithologies.

\*\*\*Elastic rock properties derived indirectly from well logs from P-18-A-02 and P18-2.

\*\*\*\*Young's modulus of the caprock measured in laboratory test on samples from Röt/Solling caprock performed by Utrecht University.

### 6.2.4. In situ stress

The orientations and magnitudes of the principal in situ stresses are the key input parameters required for geomechanical analyses. In the West Netherlands Basin the minimum in situ stress is horizontal and the stress regime is extensional or normal-faulting (i.e. the largest principal stress is vertical).

The regional minimum in situ stress ( $Sh_{min}$ ) orientation in the West Netherlands Basin is in northeast-southwest direction (World Stress Map, Reinecker et al., 2005). Field data from P18 show that  $Sh_{min}$  orientation in well P18-2A6 is 55E - 235NW, which is in agreement with regional stress orientation (Figure 6.6). Determination of stress orientation in well P18-2A6 was based on borehole breakouts analysis (Schlumberger report, 1977).

The magnitude of  $Sh_{min}$  is determined from leakoff test data from wells in P18 (). The estimate is based on a polynomial fit to all but one leakoff test data as a function of depth (D):

$$Sh_{min} = 2.2 * 10^{-6} D^2 + 1.08 * 10^{-2} D \quad (6.3)$$

This relationship fits data better than for example the relationship for the North Sea region provided by Breckels and van Eekelen (1982).

The largest principal vertical stress ( $S_v = S_{max}$ ) is calculated assuming a lithostatic gradient of 2.25 bar/10m. The hydrostatic stress is determined from water density of 1.078 kg/l measured on a sample taken from a neighbouring field. Based on the given stress and pressure gradients, the initial total stresses in the P18 reservoir at a reference depth of 3400 mTVD amount to  $S_v = 765$  bar (76.5 MPa) and  $Sh_{min} = 622$  bar (62.2 MPa). The initial fracturing gradient is  $FG = 1.8$  bar/10m.

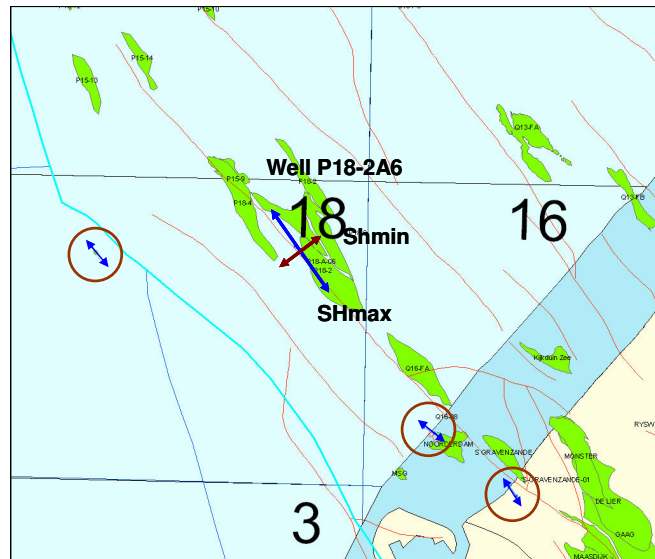


Figure 6.6: Map showing horizontal stress orientations in P18, determined from borehole breakouts in well P18-2A6, and in some neighbouring fields (data from World Stress Map).

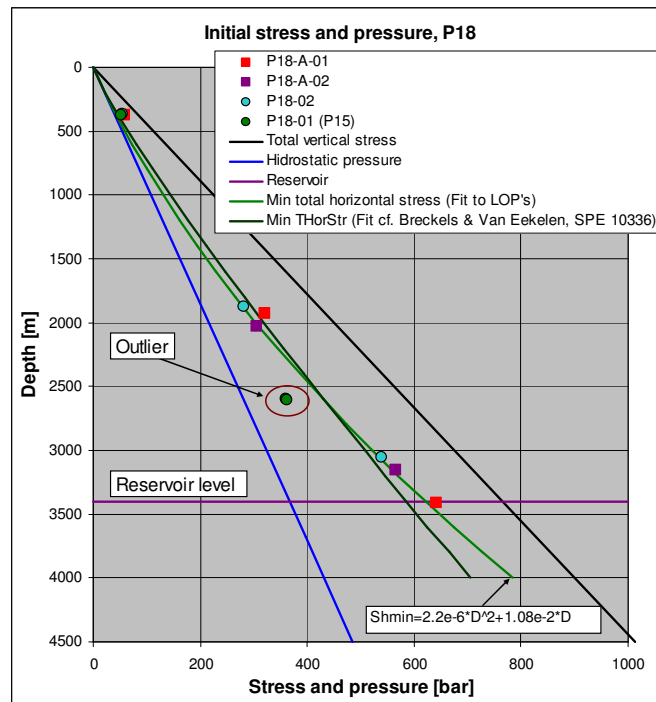


Figure 6.7: Leakoff test data from wells in P18 used to determine magnitude of the minimum total horizontal stress ( $Sh_{min}$ ) as a function of depth ( $h$ ). Total vertical stress is calculated from an assumed lithostatic gradient of 2.25 bar/10m. Hydrostatic pressure is calculated from water density of 1.078 kg/l measured on a sample taken from the neighbouring Q16-8 field.

### 6.3. Geomechanical numerical model

#### 6.3.1. Schematisation and mesh

A two-dimensional (2D) finite element (FE) model of the P18 gas field was developed using a general-purpose FE program DIANA (TNO, 2010). The numerical model represents a plane strain model based on an interpreted seismic cross-section along Inline 1185 running in a SW-NE direction (Figure 6.2).

The location and orientation of the cross-section was chosen in such a way to be able to evaluate the maximum poro-mechanical effects of  $CO_2$  injection on the mechanical seal integrity and fault stability:

- The modelling plane is perpendicular to the maximum horizontal stress, which implies that both the maximum principal (vertical) stress and the minimum horizontal stress lie in the modelling plane.
- The plane is perpendicular to the main geological structure and boundary faults oriented in a NW-SE direction. The (largest) true dip is visible on the modelling plane.
- The plane intersects all three segments of compartment P18-2 which enables studying the overall impact of possibly different pressure increase in each of the three segments.
- The chosen cross-section through compartment P18-2 is also representative for other two compartments P18-4 and P18-6, which are structurally less complex since each of these two compartments forms a single structure compartment.



## Feasibility study P18

General drawback of a 2D modelling approach is that a strike-slip stress regime and strike-slip movement on faults can not be modelled. Current study aims at investigating the potential for normal and reverse faulting, for which a 2D modelling approach is appropriate.

The developed finite element model of P18 preserves the structural complexity of the interpreted seismic cross-section (Figure 6.8 & Figure 6.9). Model dimensions are 10 by 6 km. The model consists of a total of 8,700 elements and 17,700 nodes. Quadratic triangular plane strain elements (the CT12E element type in DIANA notation) were used to model the geomechanical units. 5 boundary faults and 4 faults in the overburden were modelled by using the 1m-thick interface elements which are suitable for modelling the fault slip behaviour (the CL12I element type).

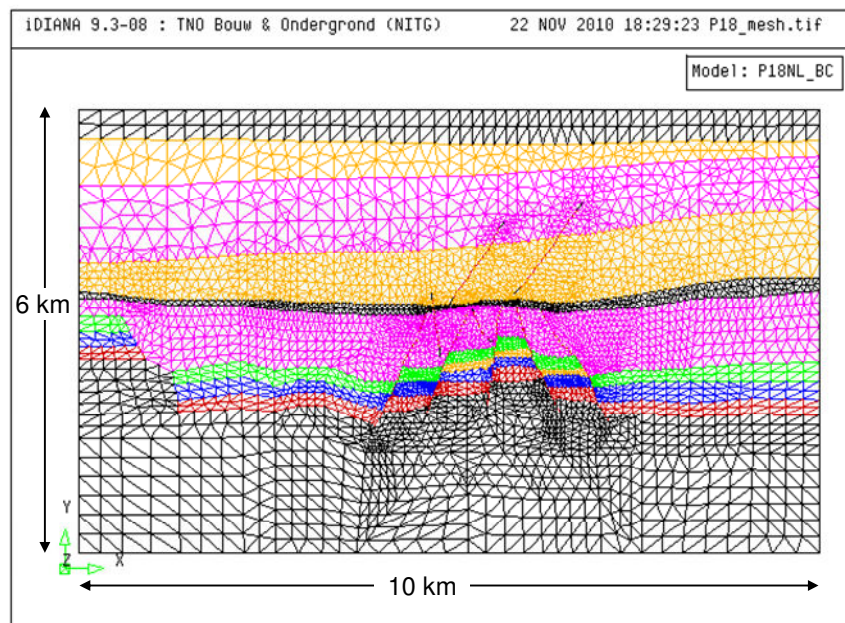


Figure 6.8: Mesh for a two-dimensional plane strain finite element DIANA model of the P18 field.

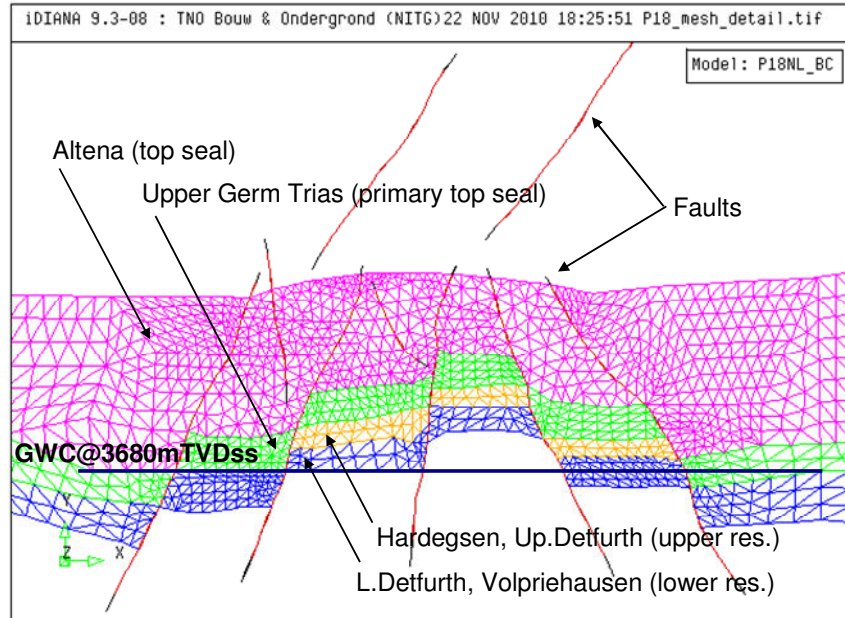


Figure 6.9: Enlarged central part of the mesh showing the main faults, reservoir and top seal.

### 6.3.2. Boundary and initial conditions

Structural boundary conditions were defined by imposing displacement constraints along the model boundaries. Vertical displacements were not allowed along the bottom boundary, while the top boundary was free to move in any direction. The lateral boundaries were constrained in horizontal direction.

The initial vertical stress was introduced in the numerical model by combining the following loads (Figure 6.10):

- The weight of the formations, which is calculated by applying the gravity load on the model.
- The initial pressure of 375 bar in the reservoir above the GWC.
- The hydrostatic pressure in other model units except the reservoir.
- The initial reservoir pressure on the fault segments that laterally bound reservoir blocks.
- Hydrostatic pressure on all other fault segments which do not bound reservoir blocks.

The initial horizontal stress was introduced in the numerical model by defining and applying the ratio of horizontal-to-vertical effective stress  $Ko' = \sigma_3' / \sigma_1' = Sh' / Sv'$ .

A value of  $Ko=0.81$  was used for the total stresses, which is equivalent to a value of  $Ko'=0.63$  for the effective stresses. This value was derived from a minimum horizontal stress gradient of 1.82 bar/10m based on the leakoff test data (Section 6.2.4).

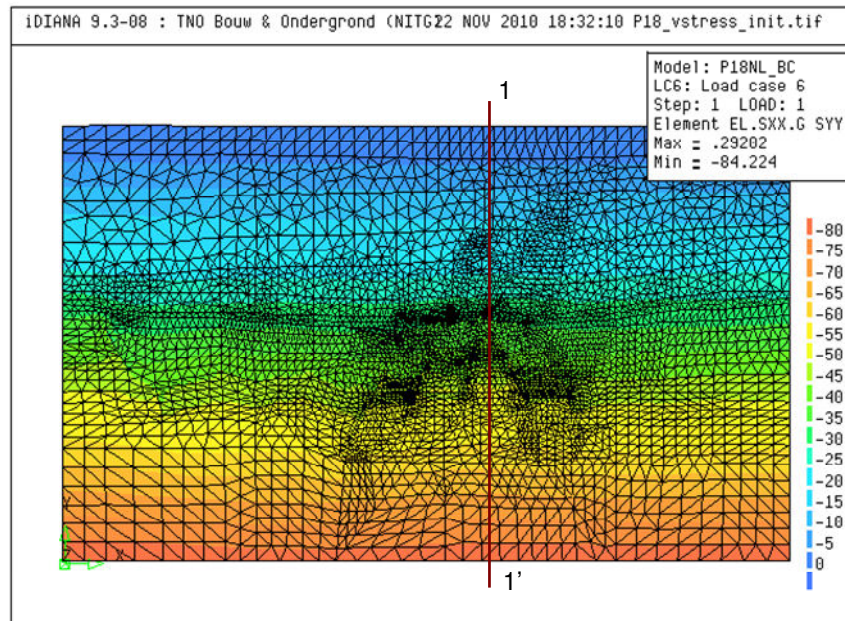


Figure 6.10: Initial vertical effective stress in the finite element model of the P18 field. Compressive stresses are negative.

### 6.3.3. Pressure loads

Pressure histories and pressure forecasts are required for geomechanical analyses. Measured pressure data from all wells in P18 were supplied by TAQA. TNO developed analytical models of CO<sub>2</sub> injection and calculated pressure forecasts for each of the three compartments (Figure 6.11, Figure 6.12 and Figure 6.13). TNO also performed a full-scale reservoir simulation modelling using MoReS. Simulation scenarios assumed that the reservoir compartments will be re-pressurized close to the initial pressure.

Pressures from analytical estimates were used in analytical geomechanical analyses. Pressures from MoReS simulation were used in numerical finite element geomechanical analyses. Besides the BHP in injectors from MoReS simulations (shown in Figure 6.11, Figure 6.12 and Figure 6.13), the average reservoir pressure were also required for FE modelling. This pressure represents the input loads for DIANA FE simulations. The evolution of the average reservoir pressure in each segment of the P18-2 compartment determined from MoReS output is presented in Figure 6.14, Figure 6.15 and Figure 6.16. Note that the pressure evolution in the reservoir is different in the upper part of the reservoir (Hardegsen and Upper Detfurth, which are good producers) from that in the lower part of the reservoir (Lower Detfurth and Volpriehausen, which are poor producers). An overview map showing the location of different compartments and segments in the P18 field is presented in Figure 6.17.

Feasibility study P18

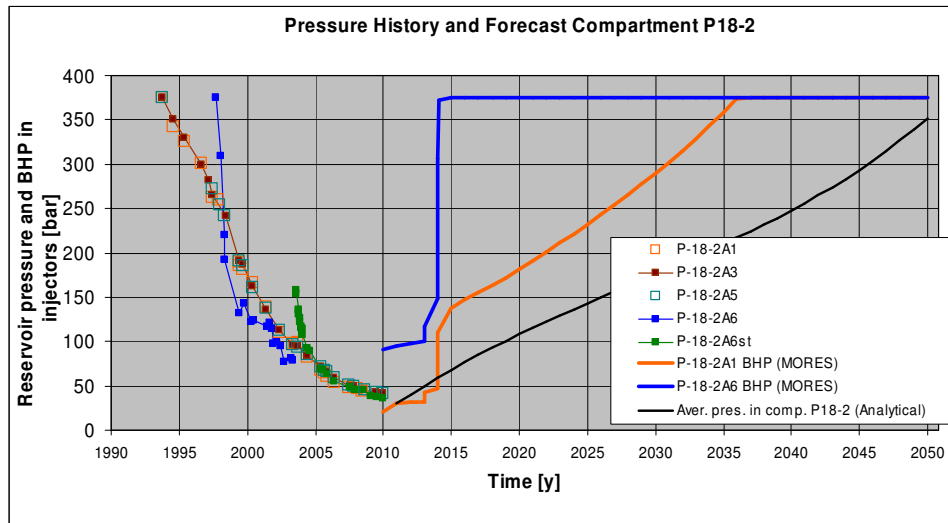


Figure 6.11: Measured pressure data in compartment P18-2 and pressure forecasts based on an analytical model and MoReS simulations performed by TNO.

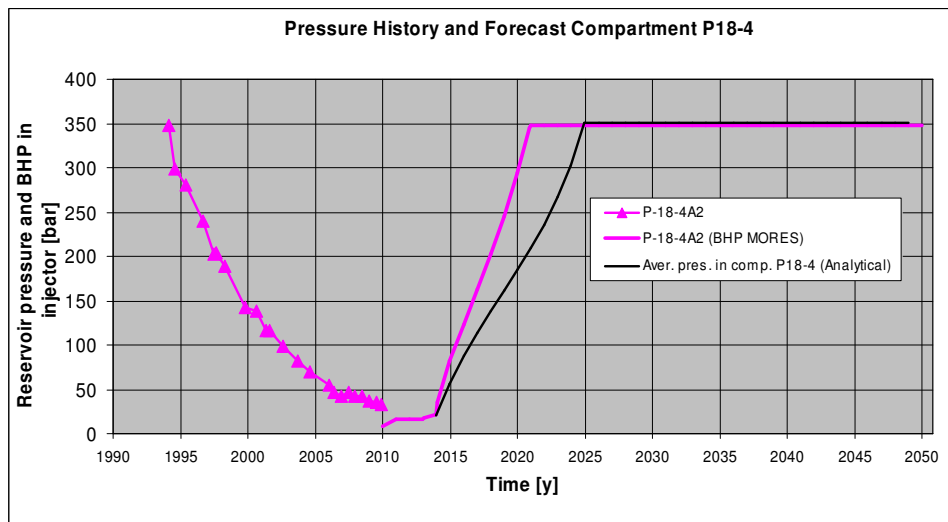


Figure 6.12: Measured pressure data in compartment P18-4 and pressure forecasts based on an analytical model and MoReS simulations performed by TNO.

Feasibility study P18

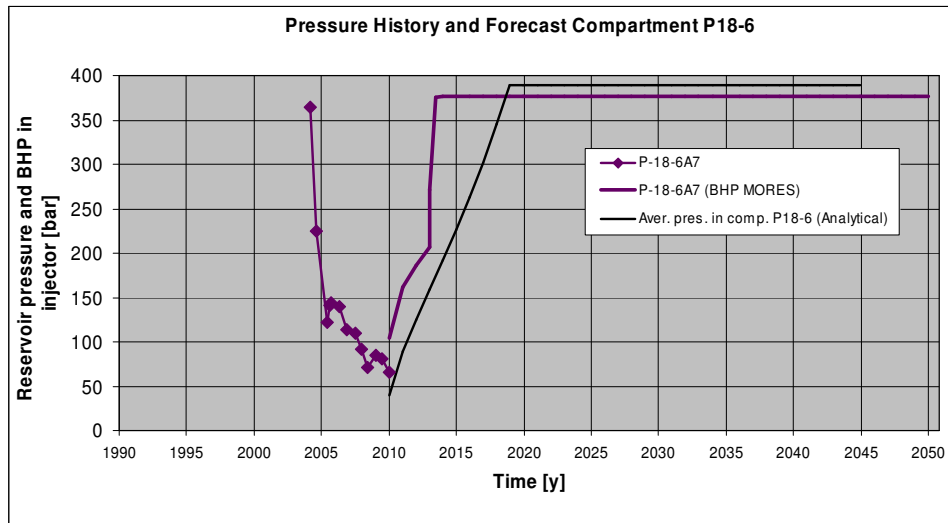


Figure 6.13: Measured pressure data in compartment P18-6 and pressure forecasts based on analytical models of CO<sub>2</sub> injection developed by TNO.

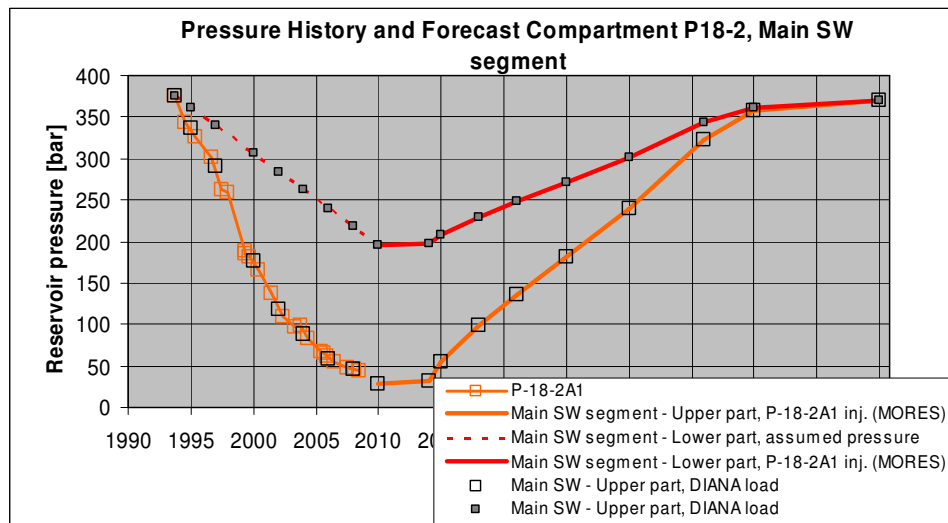


Figure 6.14: Input pressure loads for DIANA FE analysis derived from MoReS simulations. The Main SW segment of compartment P18-2 with the injector P-18-2A1.

Feasibility study P18

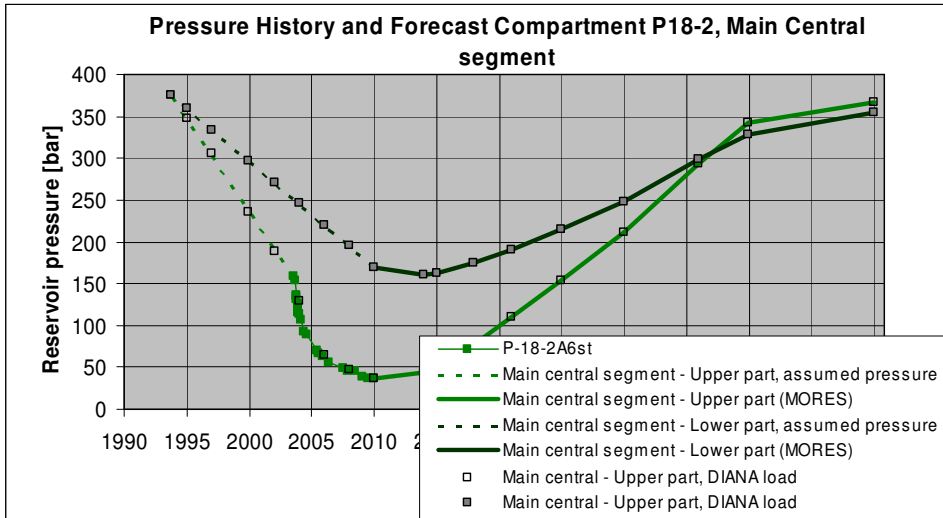


Figure 6.15: Input pressure loads for DIANA FE analysis derived from MoReS simulations. The Main central segment of compartment P18-2 (II) connected to the Main SW segment with the injector P-18-2A1.

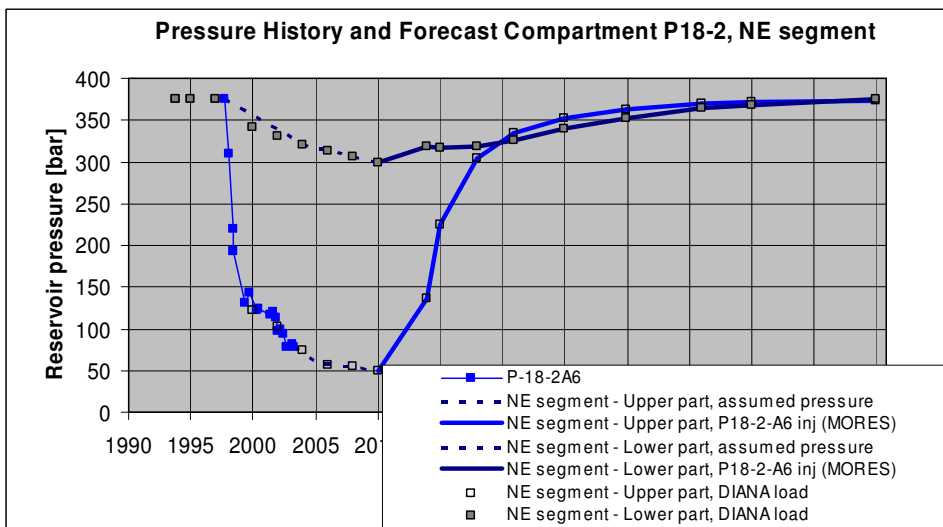


Figure 6.16: Input pressure loads for DIANA FE analysis derived from MoReS simulations. The NE segment of compartment P18-2(III), not connected with the other two segments, with the injector P-18-2A6.

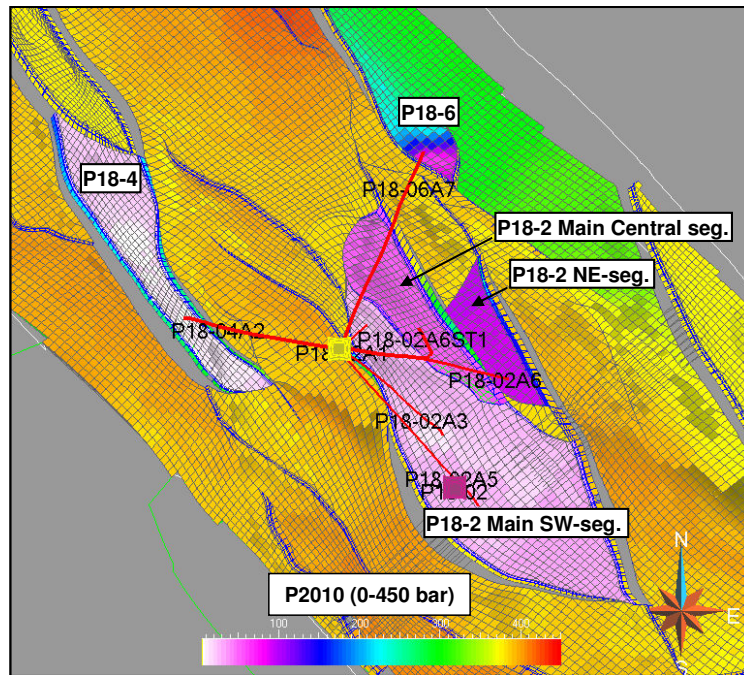


Figure 6.17: Top view of the P18 field showing the location of different compartments and segments. It should be noted that the main central segment and NE seg. are also referred to as sub-compartments P18-2II and P18-2III, respectively.

### 6.3.4. Calculation scenarios

The Base case scenario and four sensitivities were defined and calculated. The material properties for the differentiated geomechanical units and the initial state of stress were the same in all the runs (described in Sections 6.2.3 and 6.2.4). The sensitivities considered the impact of different pressure evolution in various segments of compartment P18-2.

- BC: Base case (BC).  
The pressure evolution is the same in all three segments of compartment P18-2. The pressure evolution is equal to that of the upper part of the Main SW- segment (Figure 6.14).
- S1: Segments re-pressurization sensitivity (S1-NEseg).  
The pressure evolution is the same in the two connected segments of compartment P18-2 (the Main SW-segment and the Main central segment, P18-2II), but different from that in the third, NE-segment. The pressure evolutions are equal to that of the upper part of the Main SW-segment (Figure 6.14) and the upper part of the NE-segment (P18-2III), respectively (Figure 6.15).
- S2: Aquifer depletion sensitivity (S2-NEseg-AQdepl).  
As S1, with addition of pressure change in the aquifer supporting the NE segment.
- S3: Reservoir sub-division sensitivity, with aquifer depletion (S3-NEseg-AQdepl-2LAYres).  
As S2, with addition of differential pressure evolution in the upper and lower part of the reservoir segments.
- S4: Reservoir sub-division sensitivity, without aquifer depletion (S4-NEseg-2LAYres).  
As S3, but without pressure change in the aquifer supporting the NE-segment.

## 6.4. Top seal integrity assessment

### 6.4.1. Potential for induced fracturing of top seal due to CO<sub>2</sub> injection

#### Analytical model

The risks associated with hydraulic fracturing of the reservoir rock are related to the possibility of forming fractures in the top seal allowing vertical CO<sub>2</sub> migration, possible spill paths for lateral CO<sub>2</sub> migration and direct charging of faults by injected CO<sub>2</sub>. Conditions for safe CO<sub>2</sub> injections without fracturing of the reservoir rock are met when the bottom hole pressure (BHP) in the injection well is lower than the minimum in situ stress (Shmin) in the reservoir. Both parameters are dynamic and evolve during depletion and injection period. Evolution of the Shmin was estimated using available data, current practices and methods, while evolution of reservoir and injection pressures (BHP) was based on analytical CO<sub>2</sub> reservoir engineering forecasts. Comparison of the Shmin and the BHP predictions for the Base Case (Figure 6.18) and several variations around it (Figure 6.19) show that the BHP will not exceed the Shmin, which implies that CO<sub>2</sub> injection will not induce fracturing of the reservoir rock in the three compartments under consideration. This conclusion applies to the compartments re-pressurized up to the initial reservoir pressure.

Besides the poro-mechanical effects considered above, it is necessary to consider the impact of thermal effects caused by a difference in temperature between the injected CO<sub>2</sub> and the host reservoir rock. The main consequence of thermal effects is additional decrease of the Shmin in the near-well area promoting easier fracturing of the reservoir rock. Stress reduction due to cooling was estimated analytically using the following expression (Zoback, 2007):

$$\Delta\sigma_T = \alpha E \Delta T / (1 - \nu) \quad (6.4)$$

$\Delta\sigma_T$  is the thermal stress change,  $\alpha$  is the linear coefficient of thermal expansion,  $E$  is the Young's modulus of elasticity of the reservoir rock,  $\nu$  is the Poisson's coefficient and  $\Delta T$  is the temperature difference between the injected fluid and the reservoir rock.

For a value of  $\alpha=1E-5 \text{ } ^\circ\text{C}^{-1}$ ,  $\Delta T=10^\circ\text{C}$  and typical values of the elastic parameters for the Bunter sandstone given in Table 20, the thermal stresses in the near-well area can reach 2.25 MPa. This is the maximum value which is representative for the worst case conditions. In the reality the thermal effects will be lower and can be predicted more accurately with pseudo-thermal MoReS simulator.

Combined poro-mechanical and thermal effects of CO<sub>2</sub> injection suggest that induced fracturing can occur in the latest stage of CO<sub>2</sub> injection, when the pressure in reservoir compartment is approaching the initial pressure. At this stage the BHP can exceed the Shmin if the difference in temperature between the CO<sub>2</sub> and the reservoir rock is more than 50°C (Figure 6.20). In case of fracturing of the reservoir rock, there is a risk of fracture growth into the caprock and mechanical damage of the top seal. Although limited fracture growth into the seal may not be harmful, induced fractures still provide access routes for CO<sub>2</sub> and brine penetration into the seal. The potential for fracture growth into the top seal is dependent on several geological, geomechanical, reservoir and well engineering parameters and has to be studied separately in case of intentional hydro-fracturing of the reservoir.



**Poromechanical effects of gas extraction and CO2 injection**

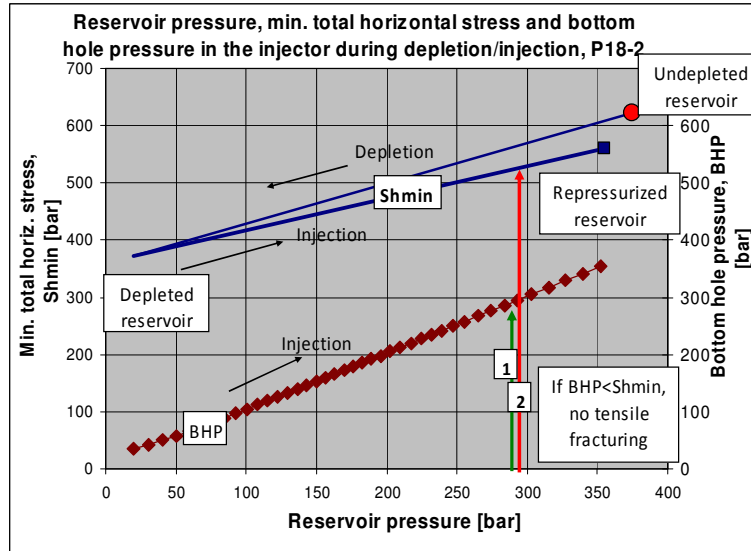


Figure 6.18: Analytical estimates of the maximum admissible injection pressures in compartment P18-2 that will not cause fracturing of the reservoir rock and top seal (excluding thermal effects). The conditions for safe injection are met when the bottom hole pressure (BHP) in the injection well is lower than the minimum in situ stress (Shmin) in the reservoir.

**Poromechanical effects**

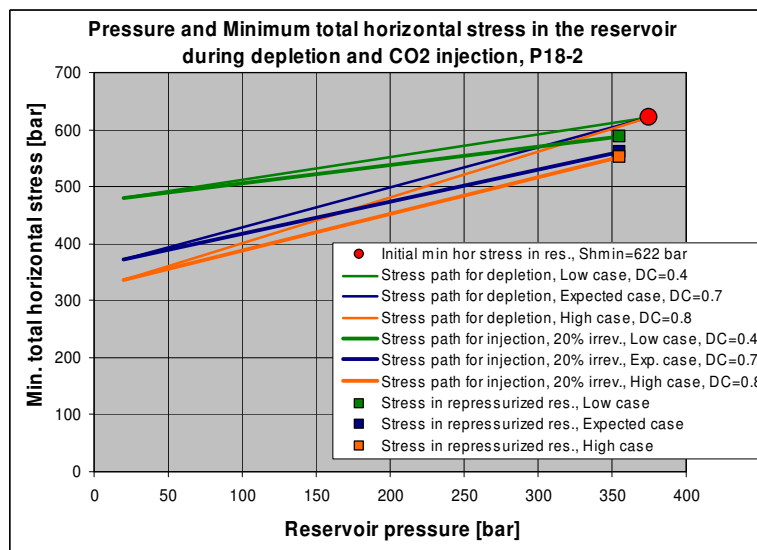


Figure 6.19: Analytical estimates of the possible reservoir stress paths in compartment P18-2 for depletion and injection. DC=depletion constant defined as  $DC = \gamma h = \Delta Sh_{min} / \Delta p$ .

### Poro-mechanical and thermal effects

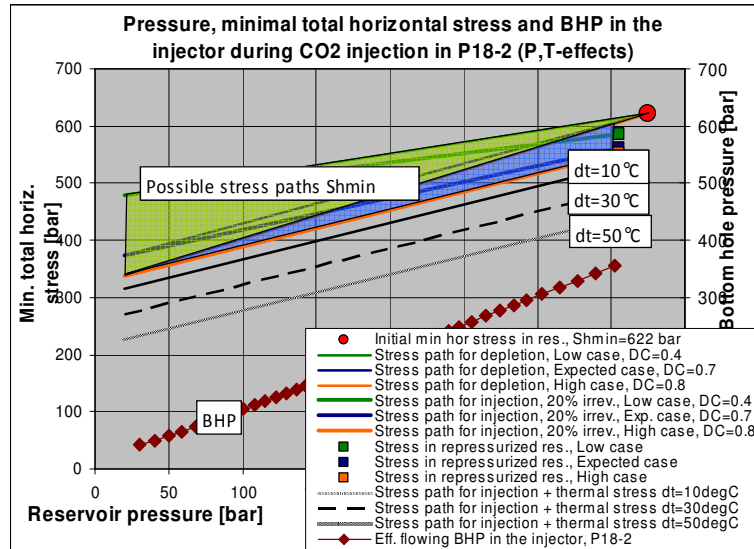


Figure 6.20: Analytical estimates of the maximum admissible injection pressures in compartment P18-2 that will not cause fracturing of the reservoir rock and top seal (combined poro-mechanical and thermal effects). The conditions for safe injection are met when the bottom hole pressure (BHP) in the injection well is lower than the minimum in situ stress (Shmin) in the reservoir decreased by the thermal stresses. DC=depletion constant; dt=temperature difference between injected CO<sub>2</sub> and reservoir rock.

### Numerical model

Numerical analysis was performed to assess the mechanical impact of reservoir depletion and re-pressurization on the reservoir rock and the top seal. The numerical model makes possible investigating the stress perturbations within the reservoir and in its surroundings taking into account the poro-mechanical effects. Note that the model cross-section intersects compartment P18-2 as explained in Chapter 6.3.

In the reservoir, the largest stress change occurs at the end of depletion period (2010), when the reservoir is depleted from the initial 37.5 MPa (375 bar) down to 3 MPa (30 bar). Depletion causes an increase in the (compressive) vertical effective stresses in the depleted reservoir which is approximately equal to the rate of depletion (Figure 6.21 and Figure 6.22). At the same time, the horizontal effective stresses also increase. This increase is, however, much smaller and amounts to about 1/4 the increase in the vertical effective stress. From the elasticity theory it follows that  $dSh' = dSv' \cdot \nu / (1 - \nu)$ , where  $dSh'$ ,  $dSv'$  are the change in the horizontal and vertical effective stresses, respectively, and  $\nu$  is the Poisson's coefficient.

Changes of the vertical, horizontal and shear stress in the reservoir and its surrounding due to depletion are shown in Figure 6.23, Figure 6.24 and Figure 6.25. As discussed above, both the vertical and horizontal effective stresses in the reservoir increase. The rate of stress change is much lower in the surrounding rock than in the reservoir, usually by one order of magnitude. The pattern of vertical stress change shows typical arching effects with stress relaxation above the reservoir (i.e. vertical stress becomes less compressive) and stress concentration at the abutments (stress becomes more compressive, Figure 6.23).

The pattern of horizontal stress change shows the opposite effects with regard to the vertical stress change. Above the reservoir, horizontal stresses become more compressive, while in the abutments horizontal stresses become less compressive (Figure 6.24).

**Feasibility study P18**

The pattern of shear stress change shows the largest changes in the reservoir at the areas where reservoir segments partially overlap (Figure 6.25). In the surrounding rock, the largest change in the shear stress can be observed in the vicinity of the edges of the depleting reservoir (Figure 6.24).

During injection period, the stress development in the reservoir and its surrounding is the opposite of the stress development during depletion. The stress change, which is maximal when the reservoir is fully depleted, gradually reduces as the reservoir is re-pressurized back to the initial pressure. In a hypothetical case of a pure elastic response, production-related stress change would practically vanish at the end of injection period.

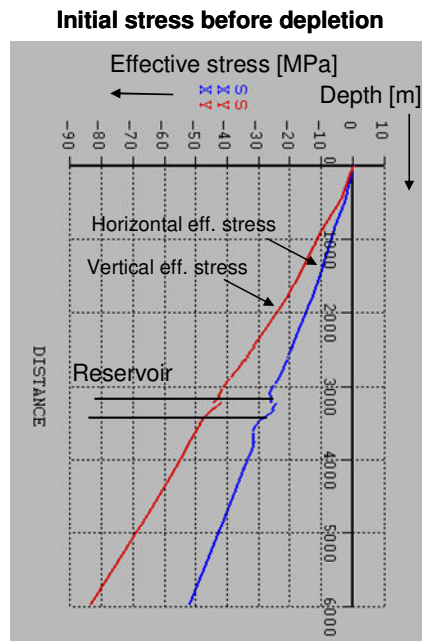


Figure 6.21: Vertical and horizontal effective stress versus depth before depletion.

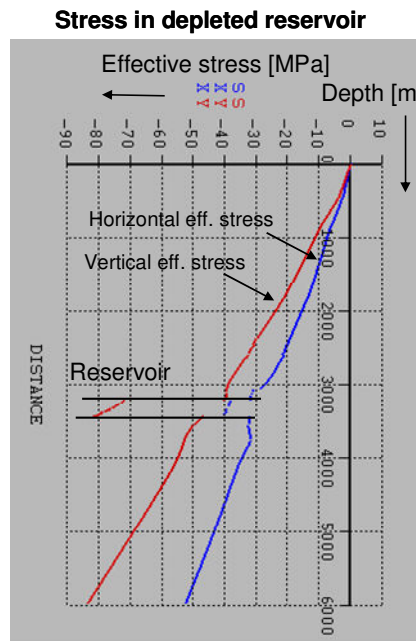


Figure 6.22: Vertical and horizontal effective stress versus depth after depletion.

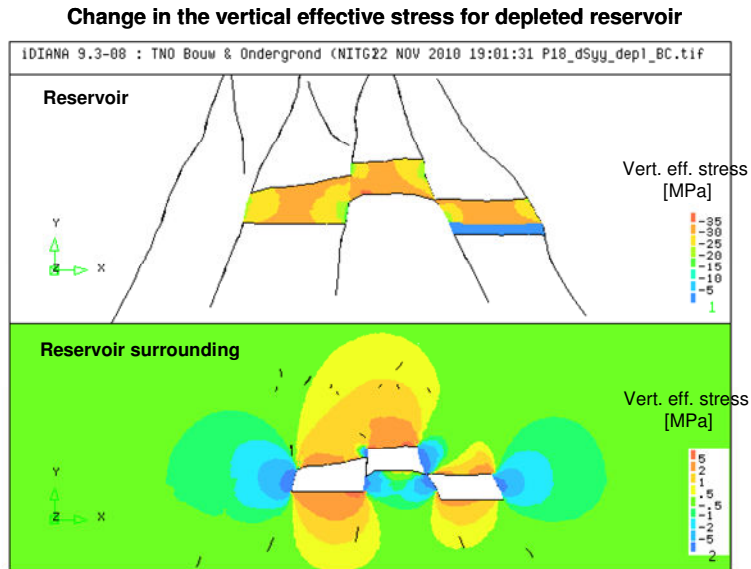


Figure 6.23: Change in the vertical effective stress in the depleted P18 field for the Base Case (compartment P18-2). Compressive stresses are negative.

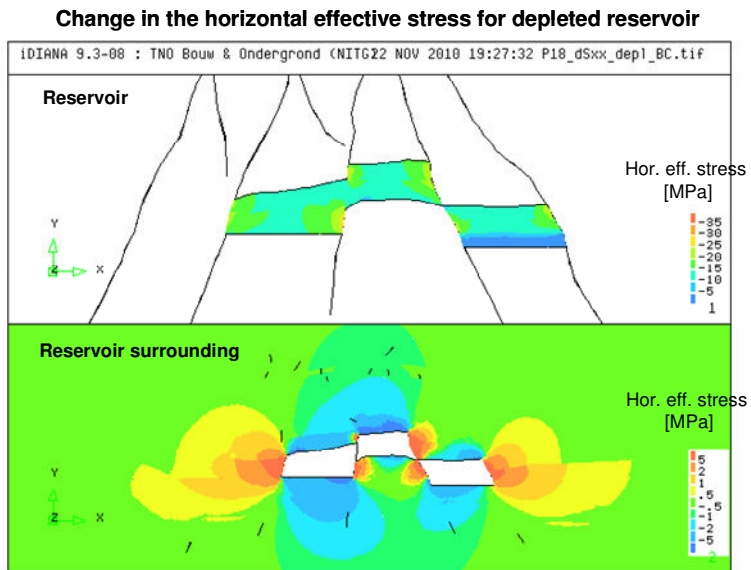


Figure 6.24: Change in the horizontal effective stress in the depleted P18 field for the Base Case (compartment P18-2). Compressive stresses are negative.

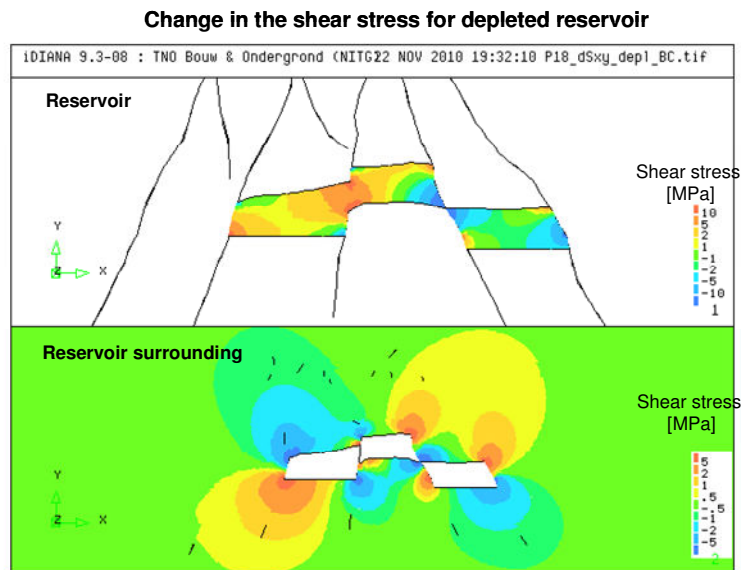


Figure 6.25: Change in the shear stress in the depleted P18 field for the Base Case (compartment P18-2).

Additional analysis was performed to identify locations in the model which are mostly affected by the induced stress changes. We defined a parameter called the mobilised shear strength (MSS) which can be calculated by dividing the shear stress ( $\tau$ ) by the normal effective stress ( $\sigma$ ), i.e.  $MSS = \tau / \sigma$ . By plotting this parameter for the whole model, we can identify locations with the largest MSS values where the rock material is close to, or at failure. For the case of depleted reservoir, the largest values of MSS are nearby the edges of the reservoir segments (Figure 6.26). For a number of monitoring points located in the critical areas we plotted the stress path diagrams (Figure 6.27 to Figure 6.29). The stress path diagrams show the stress evolution during reservoir depletion and future CO<sub>2</sub> injection at the selected monitoring points located in the reservoir and the top seal.

The stress paths for the reservoir rock show a significant increase of both normal effective stress (~ 20 MPa) and shear stress (~10 MPa) during depletion period (Figure 6.27). In order to assess the mechanical effect of depletion on the reservoir rock, we can compare the relative position of the stress paths with the Mohr-Coulomb shear strength criterion thought to be representative for the reservoir rock (cohesion  $c=2$  MPa and friction angle  $F_i=25^\circ$ ). From the comparison it is apparent that the stress paths do not show critical behaviour, i.e. the paths are not converging towards the failure envelope.

During injection, the stress paths development is in the opposite direction, towards the initial state of stress before gas production. In the ideal case of pure elastic behaviour of the reservoir rock and the surrounding rock, re-pressurization of a depleted reservoir back to the initial pressure would undo the production-related stress perturbations.

Hence, the stress change and the related mechanical impact on the reservoir rock are the largest at the time when the reservoir is fully depleted.

**Feasibility study P18**

The stress paths for the top seal show predominantly shear stress change during depletion, while changes in the normal effective stress are minor (Figure 6.28 and Figure 6.29). The direction of shear stress change is, however, different in the top seal (element 226) and the side-seal (elements 325 and 928). The stress development is non-critical, i.e. away from the failure envelope, in the top seal and critical, i.e. towards the failure envelope, in the side seal.

In order to assess the mechanical effect of depletion on the seal, we compare the relative position of the stress paths with the Mohr-Coulomb shear strength criterion based on the experimental data obtained in HPT lab of Utrecht University ( $c=27$  MPa and  $\phi=28^\circ$ ; Figure 6.28 and Figure 6.29). Apparently, the induced stresses can mobilise at most 50% of the shear strength of the seal material, which suggests elastic deformation only. The second failure envelope with  $c=7$  MPa and  $\phi=28^\circ$  is hypothetical and shows the strength of the top seal necessary to initiate shear failure.

During injection, the stress paths development is in the opposite direction, towards the initial state of stress before gas production.

In conclusion, the largest stress changes and the associated mechanical effects affecting the top- and side seal are expected near the edges of the reservoir segments, where stress concentrations occur. Plastic deformation of the reservoir rock and the seal may occur locally at these locations, having in mind the natural variability of (shear) strength which can exist in these rocks.

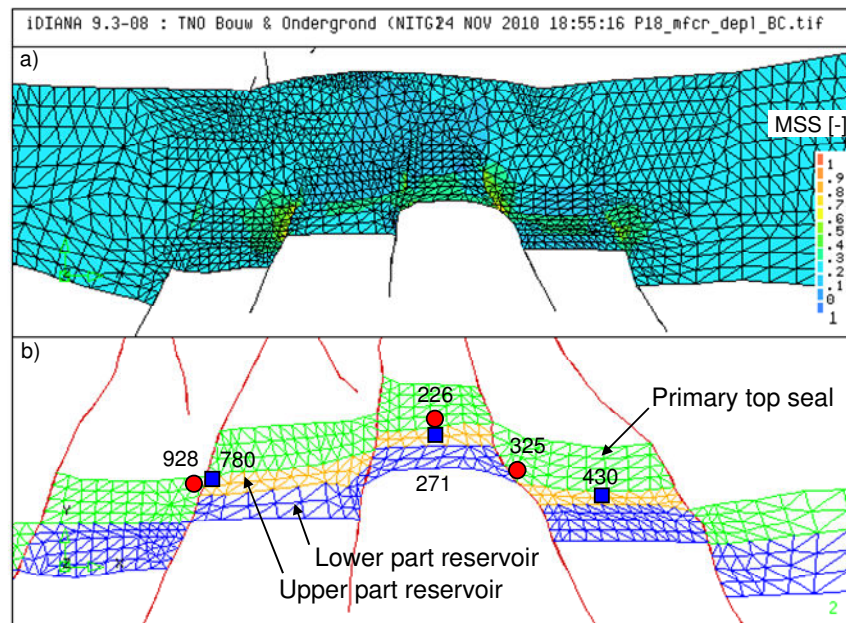


Figure 6.26: Mobilised shear strength (MSS) of the rock for the case of depleted reservoir (MSS=Shear stress / Normal effective stress). b) Location of the selected monitoring points (i.e. the finite elements) used to present the results of FE analysis in Figure 6.28 to Figure 6.29.

**Stress paths for the reservoir rock for depletion, Base case**

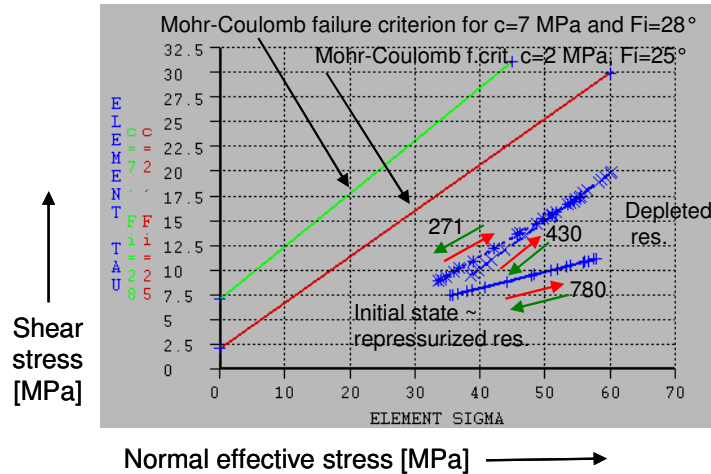


Figure 6.27: Stress paths for the monitoring points in the reservoir for depletion (Base case). The direction of stress development is shown by red arrows. The Mohr-Coulomb failure envelope with  $c=2$  MPa and  $F_i=25^\circ$  for the reservoir rock is based on the assumed shear strength parameters. During injection, the stress paths development is in the opposite direction, towards the initial state before gas production (shown by green arrows).

**Stress paths for the top seal for depletion, Base case**

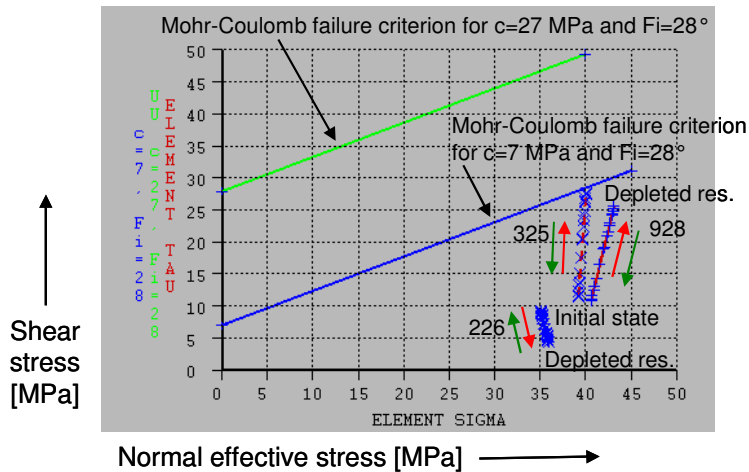


Figure 6.28: Stress paths for the monitoring points in the top seal for depletion (Base Case). The direction of stress development is shown by red arrows. Location of the selected elements is presented in Figure 6.26. The Mohr-Coulomb failure envelope with  $c=7$  MPa and  $F_i=28^\circ$  is based on the experimental data obtained in HPT lab of Utrecht University. The Mohr-Coulomb failure envelope with  $c=27$  MPa and  $F_i=28^\circ$  is hypothetical and shows the strength of the top seal necessary to initiate shear failure. During injection, the stress paths development is in the opposite direction, towards the initial state before gas production (shown by green arrows).

**Stress paths for the top seal for depletion,  
 Sensitivity S4: Reservoir subdivision into lower and  
 upper parts with different pressure evolutions**

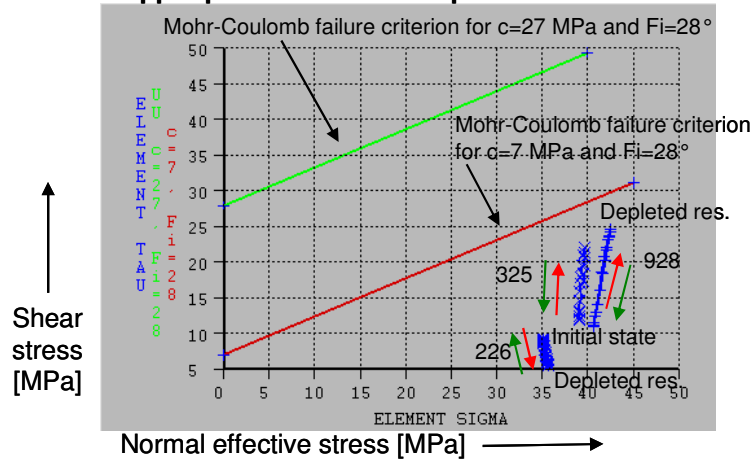


Figure 6.29: Stress paths for the monitoring points in the top seal for depletion (Sensitivity S4). The direction of stress development is shown by red arrows. The Mohr-Coulomb failure envelope with  $c=7$  MPa and  $F_i=28^\circ$  is based on the experimental data obtained in HPT lab of Utrecht University. The Mohr-Coulomb failure envelope with  $c=27$  MPa and  $F_i=28^\circ$  is hypothetical and shows the strength of the top seal necessary to initiate shear failure. Note that the stress path at the monitoring point 325 does not reach the hypothetical failure envelope as in the Base case due to different pressure evolution in the upper and lower part of the reservoir (Figure 6.28).

## 6.5. Fault seal integrity assessment

### 6.5.1. Fault seal analysis

The sealing capacity of the faults that intersect and bound the Bunter reservoir was determined as a function of Shale Gouge Ratio (SGR), i.e. using the clay smear approach (e.g. Yielding, 2002). In the SGR method, hydraulic properties of faults are determined by the amount of shale contained in the fault rock. The SGR depends on the lithology of the host rock and on the throw of a particular point on the fault plane. Continuous smears and significant sealing capacity are present when  $SGR > 0.2$ . Besides the SGR method, juxtaposition maps were made to investigate juxtaposition of different lithologies across the faults and identify potential leak points (Allan, 1989). The SGR analysis and juxtaposition maps were calculated on the reservoir-scale Petrel model of P18.

The boundary faults of all three compartments are found to be sealing (Figure 6.30). Field production data indicate that P18-2, P18-4 and P18-6 represent separate pressure compartments. The boundary faults of the three main compartments of P18 have such large throws that they juxtapose the reservoir Bunter sequence against the sealing Upper Germanic Trias (RN) and occasionally against a lower part of Altona (AT). None of the faults offsets the top of the Altona Group, so that the shales of Altona will always seal off formations below.

The internal faults which split compartment P18-2 into three segments are mostly conductive (Figure 6.31). These faults have much smaller throws than boundary faults. Generally, reservoir sand is juxtaposed against sand across the internal faults and the SGR is low. Most of the internal faults are therefore permeable. The only exceptions are fault F12 and F18, which have a larger SGR and therefore either one, or both of them, are sealing. This was supported by field data which showed the absence of pressure communication between the segment drained by



**Feasibility study P18**

well P18-02A6 and the other two segments of compartment P18-2, which are in mutual pressure communication.

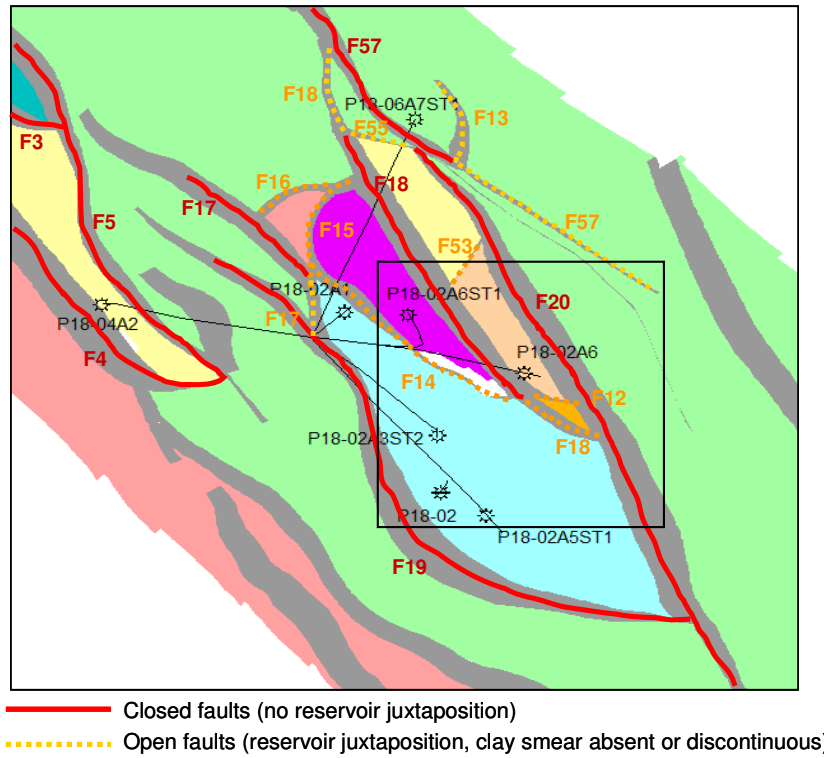


Figure 6.30: Top view of P18 showing sealing capacity of faults determined as a function of Shale Gouge Ratio (SGR).

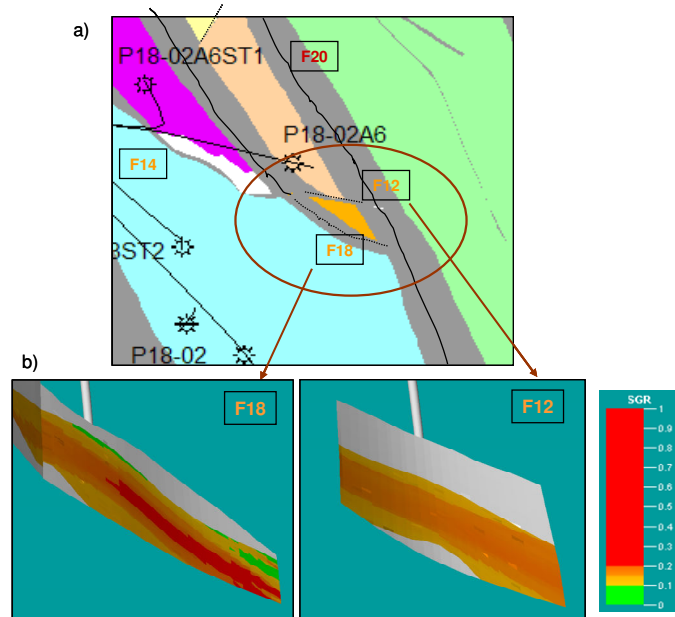


Figure 6.31: a) Top view of a part of compartment P18-2 and b) the Shale Gouge Ratio (SGR) for sealing capacity assessment of faults F12 and F18. According to the SGR, either one or both faults can be sealing (continuous smears and significant sealing capacity are present when  $SGR > 0.2$ ). Field data showed no pressure communication between well P18-02A6 and other wells in compartment P18-2.

## 6.5.2. Fault stability analysis

### Analytical model

Gas extraction and CO<sub>2</sub> injection may cause fault re-activation, i.e. sudden slip movement along faults, which can change their sealing characteristics in such a way that previously sealing faults become conductive to fluid flow. In addition, micro-seismic events (earth tremors) and seismic events of low intensity can occur at the injection site.

The potential for fault re-activation due to gas extraction and CO<sub>2</sub> injection in P18 was estimated by using the Mohr-Coulomb stress circles. A Mohr-Coulomb circle represents the state of stress at the reference depth of 3400mTVDss in undepleted, depleted and re-pressurized compartment P18-2 (Figure 6.32). Note that the effective stresses are used in fault stability analyses. The failure criterion for faults is plotted in the same graph, based on the common shear strength properties of faults (cohesionless faults with a friction coefficient of 0.6).

The initial state of stress in undepleted reservoir, represented by the black circle, is below the Mohr-Coulomb failure line which implies that the fault is stable (Figure 6.32).

During production period, the effective stresses in the reservoir increase and the Mohr-Coulomb stress circles grow in size but do not reach the failure criterion for faults (Figure 6.32). This implies that the faults were stable throughout the production period.

The past history of induced seismicity associated with gas production from fields in the West Netherlands showed no seismic activity in this region.

**Feasibility study P18**

During the injection period, the state of stress is basically reversed with respect to the depletion period. The state of stress in the undepleted reservoir and the repressurized reservoir differ only slightly, depending on the assumptions about the degree of reversibility of the reservoir stress paths (Figure 6.33 and Figure 6.34).

Finally, we present the effects of a hypothetical case of direct CO<sub>2</sub> injection into a fault or fracture zone (Figure 6.35). In this case representative for the worst case conditions, the effective normal stress on fault would decrease as much as the pressure increases, while the shear stress on fault would not change. This means that the reservoir stress path is now horizontal, leading to faster fault reactivation under lower injection pressures than in the previous cases. Once the critical conditions for fault re-activation have been reached, further injection would lead to ongoing fault instability characterized by stress build-up and release and induced seismicity.

**State of stress after depletion**

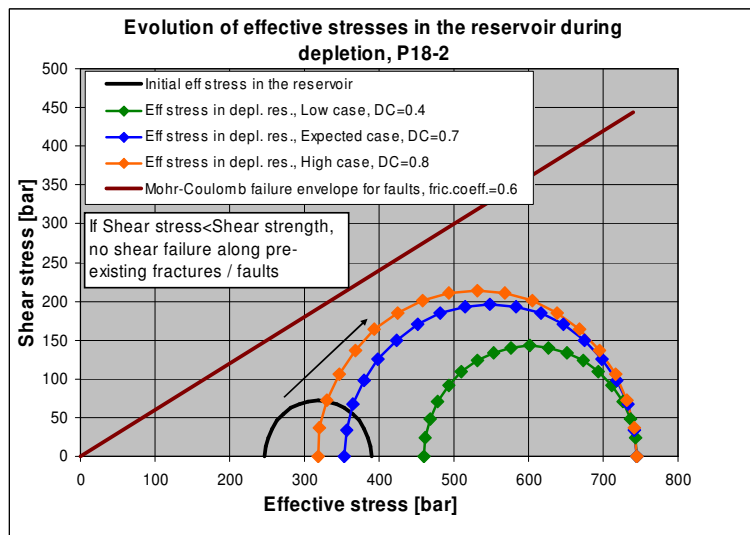


Figure 6.32: Evolution of the effective stresses in the reservoir compartment P18-2 during depletion.

### Stress evolution during injection, fully reversible reservoir stress path

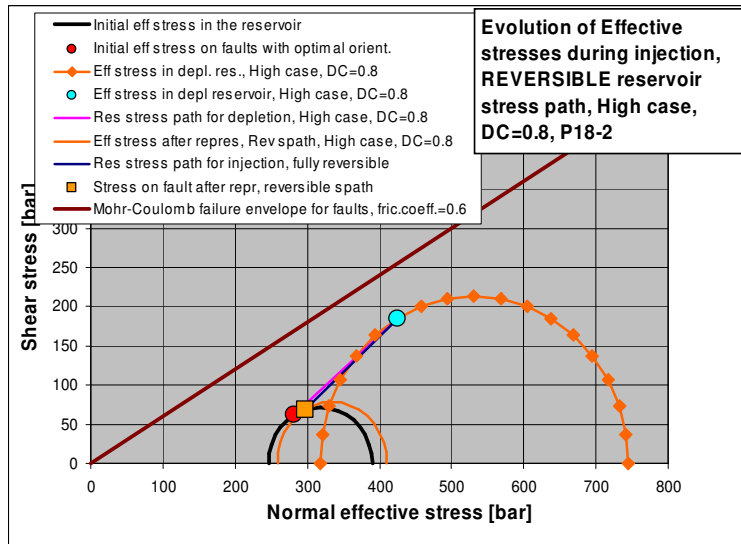


Figure 6.33: Evolution of the effective stresses in the reservoir compartment P18-2 during depletion and subsequent CO<sub>2</sub> injection. The case of fully reversible reservoir stress path.

### Stress evolution during injection, 20% irreversible reservoir stress path

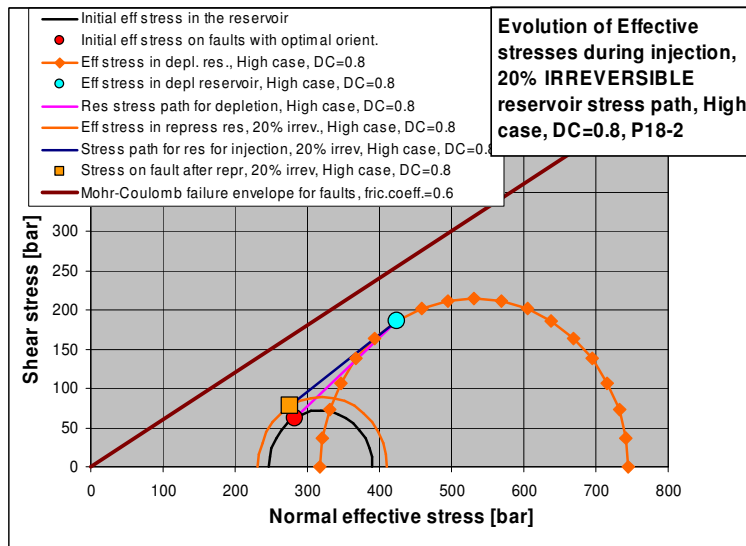


Figure 6.34: Evolution of the effective stresses in the reservoir compartment P18-2 during depletion and subsequent CO<sub>2</sub> injection. The case of 20% irreversible reservoir stress path.

**Stress evolution for a hypothetical case of CO<sub>2</sub> injection directly into fracture / fault zone, Irreversible reservoir stress path**

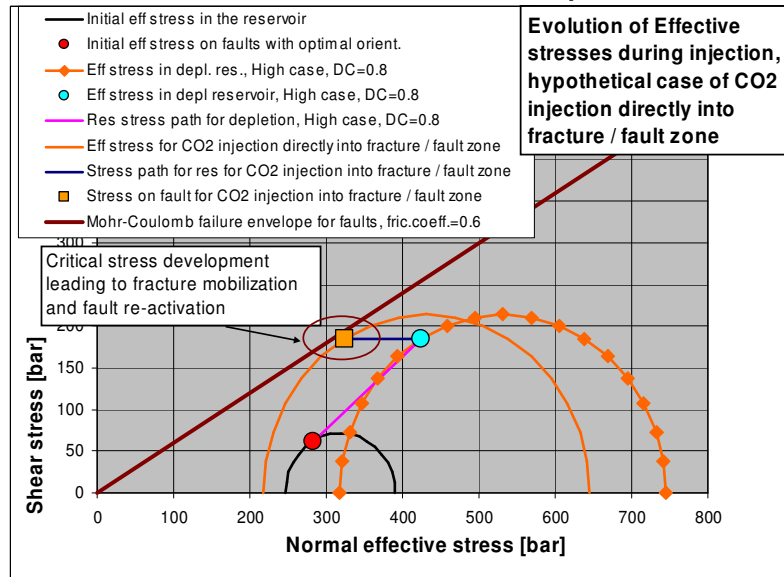


Figure 6.35: Hypothetical case of the effective stress evolution in the reservoir compartment P18-2 during depletion and subsequent CO<sub>2</sub> injection directly into fracture or fault zone. The case of fully irreversible reservoir stress path.

**Numerical method**

Numerical analysis was performed to assess the mechanical impact of production- and injection-related stress changes on the stability of faults. We defined a parameter called the mobilised friction coefficient (MFC) which can be calculated by dividing the shear traction ( $t_s$ ) by the normal traction ( $t_n'$ ), i.e.  $MFC = t_s / t_n'$ . The normal traction is a stress component perpendicular to the fault and the shear traction is a component parallel with the fault. By plotting the MFC we can identify the fault segments with the largest MFC values which are close to, or at failure, indicating fault slip and re-activation. We assumed that the faults are cohesionless, with a friction coefficient of  $\mu = 0.6$ . When the MFC value is approaching the critical value of 0.6, the fault is at risk of failure.

For the case of undepleted reservoir, the values of  $MFC > 0.5$  occur only at two locations in the model, one of which is at the fault tip (Figure 6.36a). For the case of depleted reservoir, the values of  $MFC > 0.5$  occur at several locations nearby the edges of the depleting reservoir segments (Figure 6.36b). However, the average values of MFC calculated for each finite element representing faults do not reach a critical value of 0.6 during depletion period and subsequent repressurization. The MFC values plotted along faults are lower than the critical value of 0.6, which indicates that the faults are stable (Figure 6.37).

We selected a number of monitoring points on the fault segments located in the critical areas to analyze further the induced stress changes (Figure 6.38). The stress path diagrams show that none of the stress paths reaches the assumed Mohr-Coulomb failure envelope for faults, which indicates that the faults are stable (Figure 6.39). Most of the stress paths, however, are converging towards the failure envelope, which means that the stress development is critical.

**Feasibility study P18**

During injection, the stress paths development on the faults is in the opposite direction, towards the initial state of stress before gas production. The effective stresses decrease and, assuming a fully elastic response of the subsurface, return back to the initial state of stress before hydrocarbon production. In such an idealistic case, the stress paths on the fault for depletion and injection fully overlap.

In conclusion, the calculated scenarios show that the potential for reactivation of fault segments bounding the depleting/expanding reservoir compartments is low. The largest stress changes and the associated mechanical effects on faults occur near the edges of the reservoir compartments, where stress concentrations occur. Fault slip may occur locally at these locations, having in mind the natural variability of shear strength in fault rocks and local perturbations of the in situ stress nearby faults.

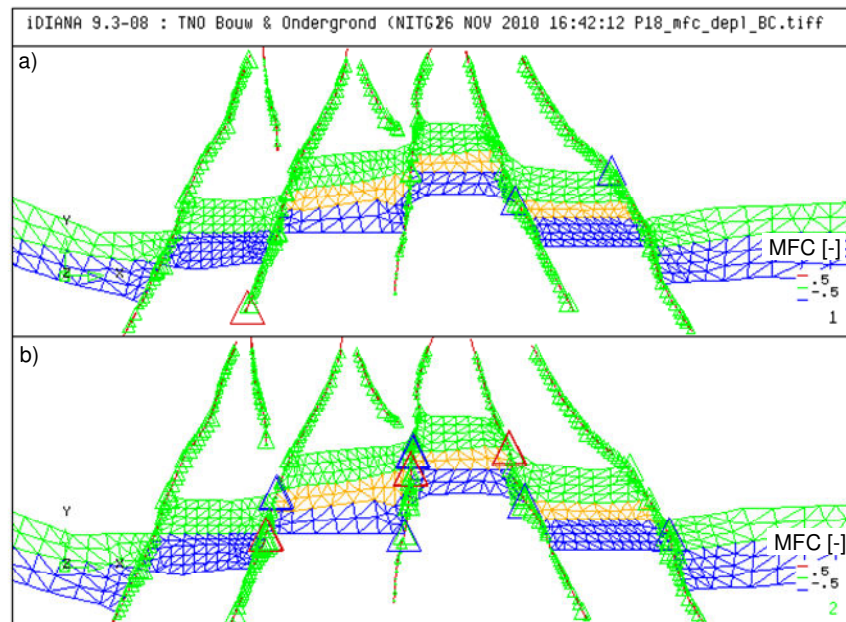


Figure 6.36: a) Mobilised friction coefficient (MFC) on the faults a) for the case of undepleted reservoir, before start of production, and b) for the case of depleted reservoir (Base case).

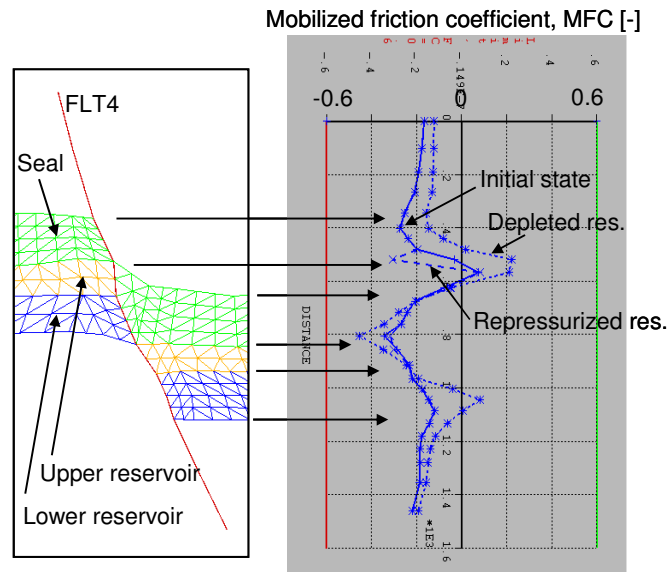


Figure 6.37: Mobilized friction coefficient (MFC) along the fault FLT4 for the initial state of undepleted reservoir, depleted reservoir and repressurized reservoir. Location of FLT4 is presented in Figure 6.38.

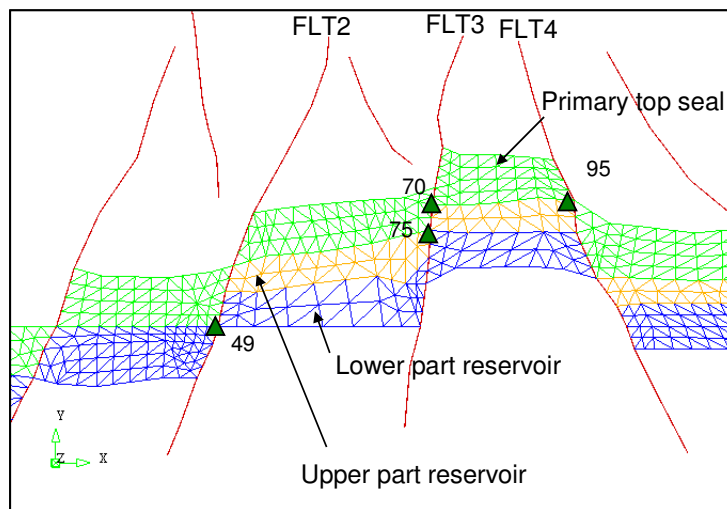


Figure 6.38: Location of the selected monitoring points (i.e. the finite elements) on the faults used to present the results of FE analysis in Figure 6.39.

### Stress paths for the faults for depletion and injection, Base case

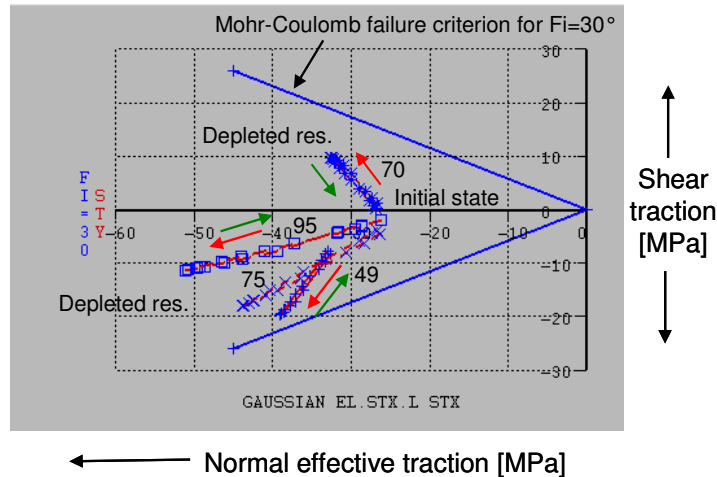


Figure 6.39: Stress paths for the monitoring points on the faults for depletion (Base case). The direction of stress development is shown by red arrows. The Mohr-Coulomb failure envelope with  $F_i=30^\circ$  ( $\mu \sim 0.6$ ) is based on the assumed shear strength parameters for faults. During injection, the stress paths development is in the opposite direction, towards the initial state before gas production (shown by green arrows).

## 6.6. Induced seabed deformation

Production- and injection-related seabed deformation was estimated by using a semi-analytic modelling tool called *AESubs* developed by TNO (Fokker and Orlic, 2006). *AESubs* requires as input the pressure from reservoir simulator, the compaction coefficient ( $C_m$ ) of the reservoir rock and the elastic properties of the overburden and underburden formations. The formations are represented as horizontal layers with elastic, or visco-elastic, properties changing per layer. The forward model for subsidence/uplift prediction uses combinations of analytical solutions to the elastic equations, which approximate boundary conditions. First, a solution is found for a single point source of compaction or expansion. In the following step this solution is integrated over each grid block of the reservoir model to calculate the subsidence/uplift of the ground surface.

In the case of P18 field, the pressures from MoReS simulations were used as input to *AESubs* (Figure 6.40). The elastic properties of the overburden and underburden formations were derived from Table 20 (Figure 6.41).

Data on the compressibility of the reservoir Bunter sandstone in the P18-field were not available. Therefore we used a value from another field with the Bunter reservoir, which is presumed to be analogous to the P18 field.

For the Base case, a value of  $C_m=0.5e-5$  1/bar from the Barendrecht-Ziedewij field was used (Winningsplan Barendrecht-Ziedewij, 2003).

Because the greatest uncertainty in the input parameters for subsidence/uplift calculations usually lies in the compressibility of the compacting/expanding reservoir, we have defined an additional scenario called High case with the compressibility of  $C_m=0.75e-5$  1/bar, which is 50% larger than in the Base case.



**Feasibility study P18**

Input data on reservoir compaction were supplied in the form of compaction/expansion grids with the calculated product of:

$$C_m V dp \quad (6.5)$$

where:

$C_m$  is the coefficient of uniaxial compaction,

$V$  is the compacting/expanding volume, i.e. the volume of each grid block in the reservoir model, and

$dP$  is the pressure change in each grid block with respect to the initial pressure.

The results indicate that the maximum production-related subsidence amounts to 5 to 7.5 cm (Table 21). Such a minor subsidence of seabed is usually considered to be of little practical importance.

During injection period, the production-related subsidence will be reduced due to the injection-related seabed deformation, i.e. uplift. In the case of an elastic reservoir, the subsidence could vanish at the end of injection period when the reservoir is re-pressurized back to the initial pressure. However, it is more likely that injection-related seabed deformation will largely, but not fully, reduce the effects of production-related seabed deformation leaving a few cm of residual subsidence.

Table 21: Maximum subsidence due to gas production and subsequent CO<sub>2</sub> injection in P18.

Time	Maximum subsidence [cm]	
	Base Case, Compaction coefficient $C_m=0.5e-5$ 1/bar	High Case, Compaction coefficient $C_m=0.75e-5$ 1/bar
End production / start CO <sub>2</sub> injection (2010)	5	7.5
Compartment P18-6 : BHP injector P-18-6A7 = Pinit reservoir (2014)	5.1	7.6
Compartment P18-4 : BHP injector P18-4A2 = Pinit reservoir (2021)	3.7	5.5
Compartment P18-2 : BHP injector P18-2A1 = Pinit reservoir (2036)	1.5	2.2
End of injection in all the compartments (2050)	0.6	1

Feasibility study P18

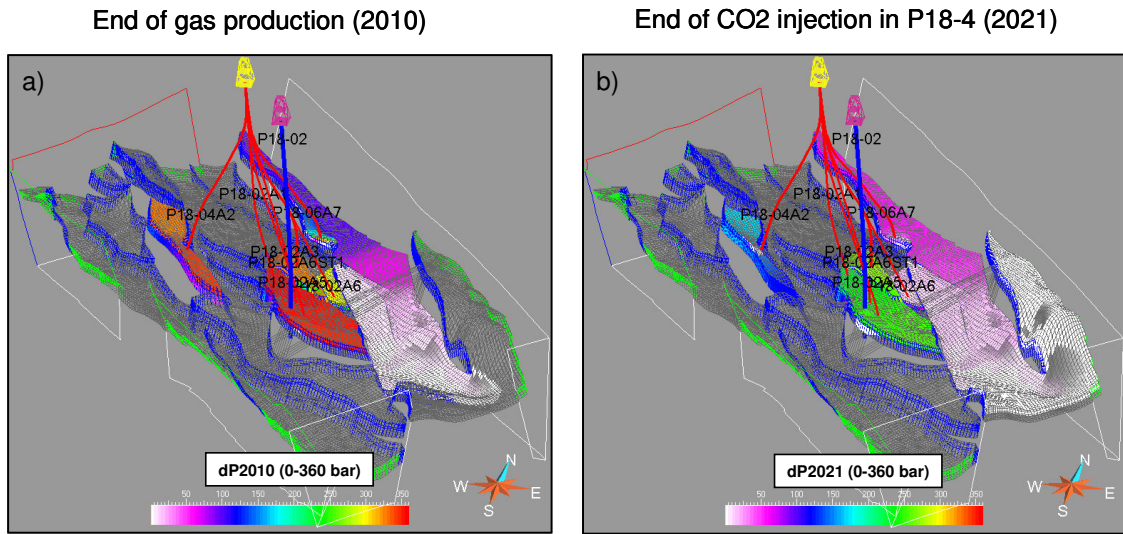


Figure 6.40: Pressure change with respect to the initial pressure in the P18 field a) at the end of gas production period (year 2010) and b) at the end of CO<sub>2</sub> injection in compartment P18-4 (2021). MoReS simulation results.

Base Case, Subsidence 2010,  
 End of gas production,  $C_m=0.5e-5$  1/bar,  
 Max subs = 5 cm

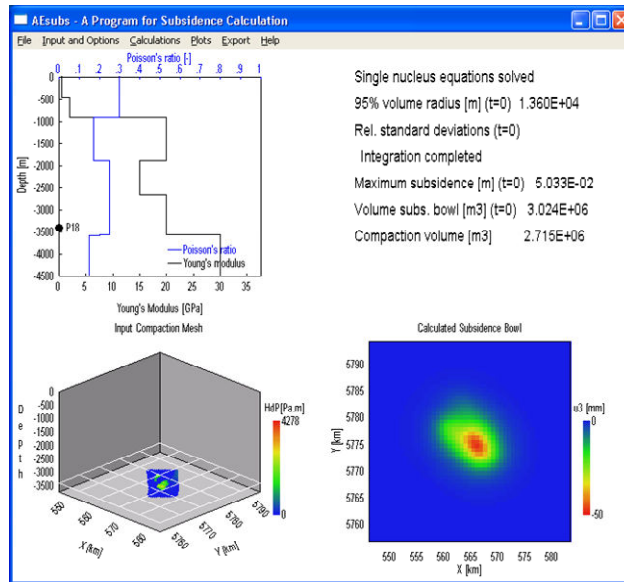


Figure 6.41: Seabed subsidence at the end of reservoir depletion (2010). The input for subsidence calculations are the pressures from MoReS simulations, the compaction coefficient for the reservoir rock  $C_m=0.5 \times 10^{-5}$  1/bar and the elastic properties of different formations in the subsurface. Maximum subsidence amounts to 5 cm.

## 6.7. Conclusions

Top seal integrity and fault stability do not represent critical factors for injection and storage of CO<sub>2</sub> in the depleted P18 field.

The primary top seal overlying the Bunter reservoir is represented by a 50 m thick layer of the lower part of Upper Germanic Trias. The seal comprises (from top to base): Röt Claystone Member, Main Röt Evaporite Mb and Solling Claystone Mb. The primary top seal is covered by a 100 m thick upper part of Upper Germanic Trias (Muschelkalk and Keuper) and a 300-400 m thick Altena Group which also represent sealing formations.

No direct measurements of the sealing characteristics of the primary top seal were available. The measurements on core from Röt and Solling taken from well P15-14 in the neighbouring block P15 can be used as analogue for the P18 field. The true top seal in P15 is provided by thinly interbedded and interlaminated shale and very fine-grained sandstone to siltstone. These lithofacies contain type A seals which are capable of supporting gas-column heights in excess of 300 m.

The anhydrite content in the primary seal is variable. As anhydrite can react with CO<sub>2</sub> in the presence of water, it is necessary to quantify the effects of possible geochemical reactions on the mechanical and transport properties of bulk/intact anhydrite and fault gouge anhydrite material.

The primary top seal (Röt and Solling) is comprised of a hard, brittle and competent rock. The rock strength properties of the top seal were determined by triaxial tests on core in HPT lab of Utrecht University. The value of rock properties are as follows: Young's modulus  $E=20$  to  $30$  GPa, unconfined compressive strength  $UCS=93$  MPa, cohesion  $c=27$  MPa and friction angle  $\phi=28^\circ$ .

The largest stress changes and the associated poro-mechanical effects on the top- and side seals occur when the reservoir is fully depleted. The largest stress changes occur near the edges of the reservoir compartments (and segments) where stress concentrations occur. Due to high strength of the top seal, the poro-mechanical effects on the bulk/intact top seal are expected to be weak. However, plastic deformation of the top seal (and the reservoir rock) may occur locally at the edges of depleting/expanding compartments, having in mind the natural variability of (shear) strength which can exist in these rocks.

Combined poro-mechanical effects, due to pore pressure increase, and the thermal effects, due to injection of cold CO<sub>2</sub> into the hot reservoir, may cause hydro-fracturing of the reservoir rock and possibly, the top- and side seals. The risk of induced hydro-fracturing increases in the later stage of CO<sub>2</sub> injection when the reservoir is almost re-pressurized to the initial pressure.

Risks associated with induced fracturing of the reservoir rock are related to the possibility of forming:

- Fractures in the top seal allowing CO<sub>2</sub> migration out of the containment.
- Possible spill paths for lateral escape of CO<sub>2</sub> from the containment.
- Pathways for direct hydraulic communication between the injection well and faults, leading to direct charging of faults by the injected CO<sub>2</sub> and, consequently, to fault instability and slip, which may affect sealing capacity of faults.

The boundary faults of all three compartments are found to be sealing. These faults have large throws and juxtapose the reservoir Bunter sequence against the sealing Upper Germanic Trias and occasionally a lower part of Altena.

The internal faults which split compartment P18-2 into three segments are mostly conductive.

## Feasibility study P18

---

These faults have much smaller throws than boundary faults. Generally, reservoir sand is juxtaposed against sand across the internal faults and the shale gouge ratio (SGR) is low.

The largest stress changes and the associated poro-mechanical effects on faults occur near the edges of the depleting/expanding reservoir compartments. The potential for fault reactivation generally increases during reservoir depletion, but likely does not lead to fault slip and reactivation. However, fault slip may occur locally at the edges of reservoir compartments, having in mind the natural variability of shear strength properties in fault rocks and local stress perturbations nearby faults.

During injection, the potential for fault reactivation generally decreases providing that the CO<sub>2</sub> is not injected directly into the fault zone and the thermal effects of injection are negligible.

The P18 field was not seismically active during production period, based on the KNMI database of recorded induced seismic events associated with hydrocarbon production in the Netherlands. No production-related induced seismicity has been recorded so far in other hydrocarbon fields in the Western part of the Netherlands. The detection limit of the KNMI seismic network was M2.5 until 1995 and M1-1.5 on Richter scale afterwards.

Current seismic analysis practices do not allow predictions of the magnitude of possible future seismic events related to fluid injection into reservoirs. Quantitative Probabilistic Seismic Hazard Analysis (PSHA) of induced earthquakes associated with CO<sub>2</sub> injection is not yet possible because of lack of data.

The effects of production and subsequent CO<sub>2</sub> injection on seabed deformation are minor. The maximum production-related subsidence amounts to 5 to 7.5 cm, which is considered to be of little practical importance. During injection period, the production-related subsidence will be reduced.

Geomechanical-related risks of fracturing and fault re-activation can be (partially) reduced by:

- Injecting CO<sub>2</sub> with bottom hole pressures (BHP) which are below fracturing condition.
- Avoid overpressurizing the reservoir above the initial pressure.
- Keeping a safe distance between the injection wells and faults to avoid direct charging of faults by injected CO<sub>2</sub> through natural or induced fractures.
- Managing thermal effects of injection



Doc.nr: CATO2-WP3.01-D06  
Version: 2011.01.04  
Classification: Confidential  
Page: 110 of 198

## Feasibility study P18

---

# References

## Papers

- Allan, U.S., 1989. Model for hydrocarbon migration and entrapment within faulted structures. *AAPG Bull.* 73, 803-811.
- Breckels, I.M., van Eekelen, H.A.M., 1982. Relationship between horizontal stress and depth in sedimentary basins. *Journal of Petroleum Technology*, 34(9): 2191-2199. SPE paper 10336.
- Castagna, J.P., Batzie, M.L., Eastwood, R.L., 1985. Relationships between compressional-wave and shear-wave velocities in clastic sillicate rocks. *Geophysics*, Vol. 50, No 4, 571-581.
- DIANA Version 9.3, 2009. Program and User's Documentation. TNO Diana B.V.
- Eissa, E.A. and Kazi, A., 1988. Relation between static and dynamic Young's Modulus of rocks. *Int. J. Rock Mech. Min. Sci.*, Vol. 25, No. 6, 479-482.
- Greenberg, M.L., Castagna, J.P., 1992. Shear-wave velocity estimation in porous rocks: Theoretical formulation, preliminary verification and applications. *Geophysical Prospecting*. 40, 195-209.
- Rafavich, F., Kendall, C.H.St.C., Todd, T.P., 1984. The relationship between acoustic properties and the petrographic character of carbonate rocks. *Geophysics* 49, 1622-1636.
- Spain, D., Conrad, C., 1997. Quantitative analysis of top-seal capacity: offshore Netherlands, southern North Sea. *Geologie en Mijnbouw*, Kluwer, 76: 217-226.
- Reinecker, J., Heidbach, O., Tingay, M., Sperner, B., Müller, B., 2005. *The release 2005 of the World Stress Map* (available online at [www.world-stress-map.org](http://www.world-stress-map.org)).
- Yielding, G., 2002. Shale gouge ratio – calibration by geohistory. In: A.G.Koestler, A.G., Hunsdale, R. (Eds), *Hydrocarbon Seal Quantification*. NPF Spec. Publ. 11, Elsevier, Amsterdam, 1-15.
- Zoback, M. D., 2007, *Reservoir Geomechanics*, Cambridge University Press, 464p.

## Reports

- Winningsplan P18a, P18c, P15c, 2003.
- Winningsplan Barendrecht-Ziedewij, 2003.
- Schlumberger, 1997. Report on processing and interpretation of ultrasonic borehole imager (UBI) data.
- Utrecht University, 2010. Report on mechanical properties and permeability of Röt and Solling claystones from the Q16 gas field and permeability of P18 reservoir rocks. CATO-2 progress report 1.10.2010.

## 7. Well integrity study

### 7.1. Executive summary (restricted)

CO<sub>2</sub> storage is being considered in TAQA's P18 gas field. In the context of the CATO-2 project the suitability of the existing wells in the field is being investigated for injection and long-term storage of CO<sub>2</sub>. The well integrity assessment covers the operational phase of the injection project (decades) and the long-term post-abandonment phase. The study aims at the evaluation of the relevant well system barriers to identify potential showstoppers and recommendations on remedial actions and abandonment strategies. This report presents progress until September 2010, but does not describe the final conclusions of the well integrity assessment of the P18 field. The P18 field comprises 3 reservoir blocks, penetrated by a total of 7 wells, some of which have been sidetracked. One of these sidetracks also penetrates the caprock and the reservoir. One of the wells, P18-2, is plugged with several cement plugs. The current layout of plugs in P18-2 is inadequate for long-term containment of CO<sub>2</sub>, as it provides likely migration pathways from the reservoir to shallower levels, bypassing the caprock. In order to improve the quality of this well, it is required to re-enter the well, which is technical feasible according to TAQA. Subsequently, the existing cement plugs should be drilled out and an abandonment plug of sufficient length should be positioned across the primary and/or secondary caprock. Since cement-to-casing bonding is poor, it is recommended to place pancake-type abandonment plugs. Special attention is drawn to the sidetracked P18-2A6 well. From the limited available data it is uncertain how exactly the parent hole was suspended. It seems that the current layout is unsatisfactory for CO<sub>2</sub> storage. Moreover, since the parent well forms the only penetration to the P18-2 III block, it might be beneficial to not only properly abandon the parent well, but actually use it for CO<sub>2</sub> injection in that block in order to mitigate large pressure differences between the reservoir blocks. This would require adequate abandonment of the P18-2A6st sidetrack and fishing of the whipstock. Subsequently, the P18-2A6 parent well needs to be recompleted to enable CO<sub>2</sub> injection.

All other wells are readily accessible and can be remediated. Most of these show questionable cement sheath quality at caprock level from CBL data or lack data to verify this. Inadequate primary cement poses a risk to long-term integrity, but could also affect the operational phase. However, these wells can be accessed and, in order to prepare them for CO<sub>2</sub> storage, it is recommended to re-evaluate and, if required, remediate the cement sheath quality at least over caprock level.

When considering wells that will be used for CO<sub>2</sub> injection it is recommended to check the packer operating envelope against CO<sub>2</sub> injection scenarios. Potential elastomers and wellhead configuration should also be verified and adapted where required. Moreover, it is suggested to adjust completion materials (tubing, tubing hanger and packer) to corrosive circumstances, in case corrosion mitigation measures are not already in place.

Abandonment - either (re)abandonment of wells that will not play a part in injection or monitoring, or abandonment of injection and monitoring wells after injection ceases - can be designed specifically for CO<sub>2</sub> storage. At present, there are two general options to permanently seal a wellbore for CO<sub>2</sub> containment. If the quality of the primary cement sheath is ensured over critical intervals, traditional abandonment plugs can be positioned and tested at caprock level.

Alternatively, and especially in the case of questionable cement sheaths, pancake plugs can be used at caprock level. This would involve milling out of the casing, annular cement and part of the formation, followed by placement of cement in the cavity. This procedure would effectively reduce the number of material interfaces, which could form potential migration pathways. However, this operation may pose difficulty particularly in horizontal or strongly deviated wells. Both of these

## Feasibility study P18

options should be accompanied by additional plugs higher up the well, according to common practice and as prescribed by governing abandonment regulations.

## 7.2. Introduction

CO<sub>2</sub> storage is being considered in TAQA's P18 gas field. In the context of the CATO-2 project the feasibility of injecting and storing CO<sub>2</sub> in the field is investigated with respect to the existing wells. The well integrity assessment aims to determine whether the existing wells are fit for CO<sub>2</sub> injection and long-term containment as currently planned, covering the operational phase of the injection project (decades) and the long-term post-abandonment phase. The study comprises the identification of potential showstoppers and recommendations on remedial actions and abandonment strategies.

Potential migration from the reservoir along wells is generally considered as the major hazard associated with CO<sub>2</sub> storage (e.g. Gasda et al., 2004; Pruess, 2005; Carey et al., 2007). With respect to the evaluation of long-term integrity of the geological storage system, the quality of wells penetrating the storage reservoir therefore must be taken into account.

The well system forms a potential conduit for CO<sub>2</sub> migration because wellbore cement may be susceptible to chemical degradation under influence of aqueous CO<sub>2</sub> or to mechanical damage due to operational activities. Wet or dissolved CO<sub>2</sub> forms a corrosive fluid that could induce chemical degradation of the oil well cement (e.g. Bruckdorfer, 1986; Scherer et al., 2005; Barlet-Gouédard et al., 2006), potentially enhancing porosity and permeability. It could also stimulate corrosion of steel, which may lead to pathways through the casing steel (Cailly et al., 2005). Furthermore, operational activities (e.g. drilling, pressure and temperature cycles) or natural stresses can result in mechanical degradation of the cement sheath through the development of tensile cracks or shear strain, enabling highly permeable pathways to develop (Shen and Pye, 1989; Ravi et al, 2002). Finally, poor cement placement jobs or cement shrinkage could cause the loss of bonding between different materials (debonding) and lead to annular pathways along the interfaces between cement and casing or host rock (Barclay et al., 2002).

### 7.2.1. History of the P18 field

The P18 field consists of several reservoir blocks. The reservoirs are situated in the Main Buntsandstein Subgroup and are primarily capped by the Solling and Röt Claystone Members (RNSOC and RNROC, respectively). In turn, these are overlain by a secondary caprock, the Muschelkalk and Keuper formations (RNMU and RNKP, respectively). The P18 reservoirs are penetrated by eight wellbores. They are listed in Table 22

Table 22: Overview of reservoirs, compartments and wells in the P18 field

	<i>Reservoir</i>	<i>Block</i>	<i>Well</i>	<i>NLOG-name</i>	<i>Drilled</i>	<i>Comments</i>	<i>Status</i>
1	<b>P18-2</b>	P18-02-I	P18-2	P18-02	1989		Suspended
2		P18-02-I	P18-2A1	P18-A-01	1990	Previously P18-03	Producing
3		P18-02-I	P18-2A3	P18-A-03	1993	Sidetracks -S1,-S2	Producing
4		P18-02-I	P18-2A5	P18-A-05	1997		Producing
5		P18-02-III	P18-2A6	P18-A-06	1997		Shut-in
6		P18-02-II	P18-2A6st	P18-A-06ST	1997	Sidetrack from P18-2A6	Producing
7	<b>P18-4</b>		P18-4A2	P18-A-02	1991		Producing
8	<b>P18-6</b>		P18-6A7	P18-A-07	2003	Sidetrack -S1	Producing

**Feasibility study P18**

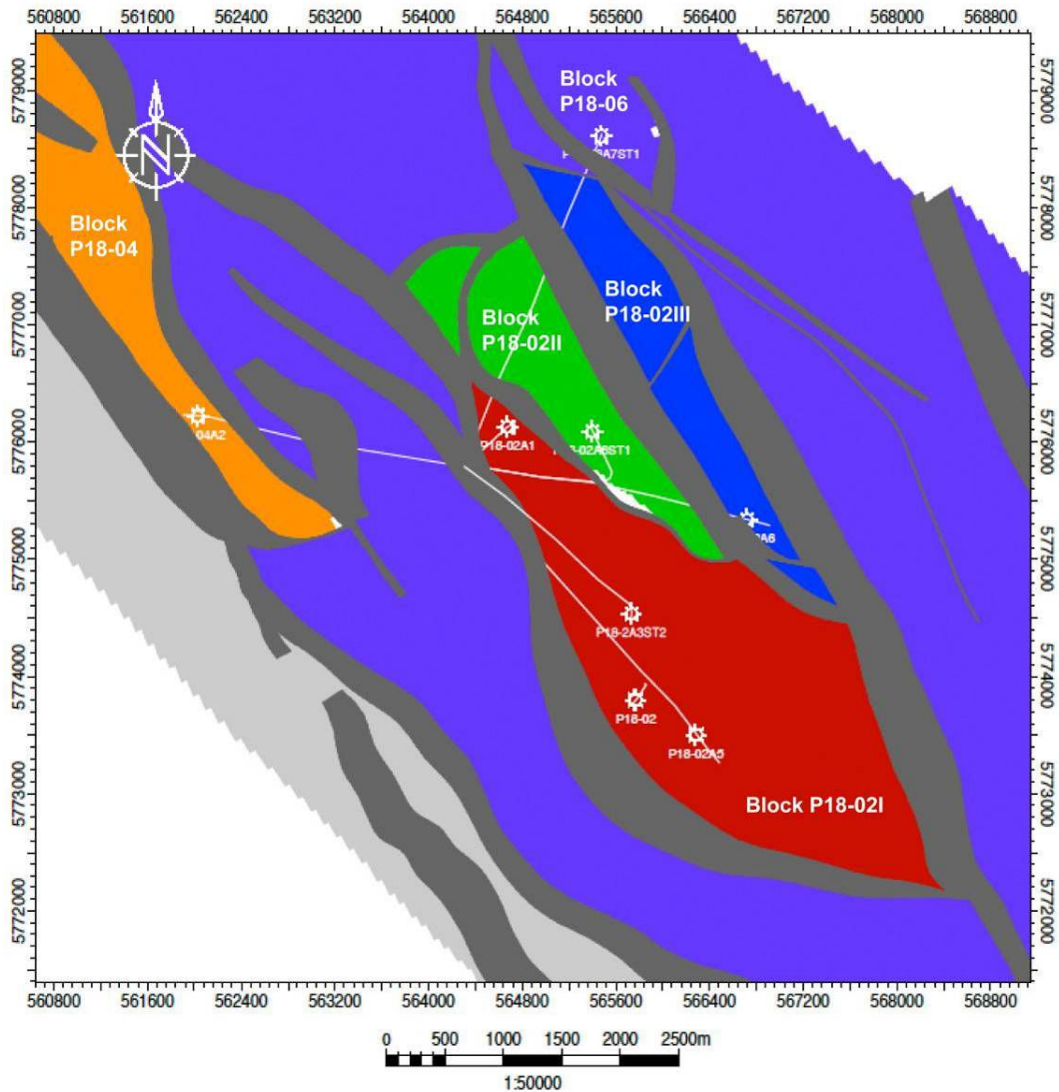


Figure 7.1: Layout of the P18 field, with position of wells at the top of the reservoir interval (top Bunter).

**7.2.2. Data availability**





Doc.nr: CATO2-WP3.01-D06  
Version: 2011.01.04  
Classification: Confidential  
Page: 114 of 198

---

**Feasibility study P18**

---

Table 23 shows the well data that TAQA provided for the study. This data forms the basis of the evaluation presented in this report.



**Feasibility study P18**

Table 23: Data available for the P-18 wells

Wells/boreholes	P18-2A1	P18-2A3	P18-2A5	P18-2A6	P18-6A7	P18-4A2	P18-2
Well status	Producing	Producing	Producing	Producing <sup>1</sup>	Producing	Producing	Abandoned
Spud date	11-1993	14-5-1993	18-11-1993	17-11-1996	7-2003	4-6-1991	11-3-1989
Abandonment date							28-5-1989
Final Well Report	N/A	x	x	x	N/A	x	x
Well/completion diagrams	x	x	x	x	x	x	x
Casing and cementing reports		x		x		x	x
Drilling reports	x	x	x	x		x	x
Well tests	N/A	x	x	x			N/A
Cementing and corrosion logs (mentioned in EOWR)	CBL (7" L)	CBL-VDL (5" L)	USIT-CBL (5" L), CBL-CET (7" L) <sup>2</sup>	USIT-CBL (7" L) <sup>3</sup>	N/A	N/A	CBL (7", 9 5/8")
Openhole logs over reservoir section only	x		x	x	x	x	x
Stratigraphy along the well	x	x	x	x	N/A	x	x
Annulus pressure reports	N/A	N/A	N/A	N/A	N/A	N/A	
Production data	Dec 1993 – March 2010	Dec 1993 – March 2010	Dec 1993 – March 2010	June 1997 – April 2003	Dec 1993 – March 2010	Dec 1993 – March 2010	

<sup>1</sup> Present production from sidetrack P18-2A6st

<sup>2</sup> Cement bond log mentioned in EOWR, but data not physically available

<sup>3</sup> Cement bond log available for pilot hole (P18-2A6) only

**7.2.3. Methodology**

As part of the CATO-2 project, the objective of the current study is to evaluate whether the wells in the P18 field are fit for CO<sub>2</sub> injection and long-term containment of the injected CO<sub>2</sub> as currently envisaged. To this purpose the integrity of the wells in the operational and post-operational period is assessed under the assumptions listed in



Doc.nr: CATO2-WP3.01-D06  
Version: 2011.01.04  
Classification: Confidential  
Page: 116 of 198

## Feasibility study P18

---

Table 24 and using the methodology discussed in Table 25. Note that all well depths in this report are stated in measured depth along hole (MDAH), unless specifically listed otherwise.

**Feasibility study P18**

Table 24: Assumptions of feasibility study

<b>Only existing producing wells will be converted for injection</b>	As a starting point to this study, no information was available on which well(s) will be converted to injection well(s). It is assumed that TAQA will not re-use the abandoned well for injection.
<b>Initial reservoir pressure</b>	The maximum reservoir pressure during the injection project will not exceed the original reservoir pressure (ca. 350bar)
<b>Cold injection</b>	The temperature of the injected CO <sub>2</sub> will be much lower than the ambient temperature in the well (the undisturbed geothermal gradient), i.e. injected CO <sub>2</sub> will not be pre-heated before injection. Therefore, injection will introduce additional thermal-induced stresses to the well tubulars.
<b>Only existing wells</b>	Only existing wells will be evaluated in this study. The evaluation of specifications for (potential) integrity of any future wells that may be drilled in the field is not within the scope of this work..
<b>Dry CO<sub>2</sub> injection</b>	It is assumed that dry CO <sub>2</sub> will be injected.

Table 25: Methodology used in assessing the feasibility of injection using P18 wells

<b>Identify well barriers</b>	Identification of well barriers that keep the well fluids inside the wellbore and prevent uncontrolled discharge to the overburden—above the caprock—and to the atmosphere. These typically include the cement section outside the production casing adjacent to the caprock and the production casing itself.
<b>Assess the evidence for failure</b>	Assessment of potential evidence suggesting failure of the identified barriers, based on information on well history.
<i>Direct evidence</i>	Direct measurements of the quality of the barrier: <ul style="list-style-type: none"> <li>- Measurements that show that the barrier was not installed properly (e.g. cement bond logs, pressure tests)</li> <li>- Measurements that show that the barrier may have been breached during the productive life of the well (annular pressure information).</li> </ul>
<i>Indirect evidence</i>	Indirect evidence that the barrier might be compromised will be used when direct evidence is unavailable (e.g. drilling information on kicks, cement losses).
<b>Define robustness criteria</b>	Robustness criteria will be defined to state which barriers (e.g. wetted areas of pipes) need to be 'upgraded' to be fit-for-CO <sub>2</sub> storage by defining (where applicable).
<b>Data gaps</b>	Data gaps will be identified when insufficient information is available to guide our analysis of the barrier.

### 7.3. Definition of well integrity barriers

This chapter presents the principal well integrity barriers that are investigated in the scope of the present study. The barriers are illustrated for a generic P18 well, which was constructed based on the information provided by TAQA. The evaluation of well barriers includes the definition of failure and robustness criteria applied to the identified barriers in the field. Robustness criteria can be distinguished into two types: mandatory criteria and recommended, “nice-to-have” criteria.

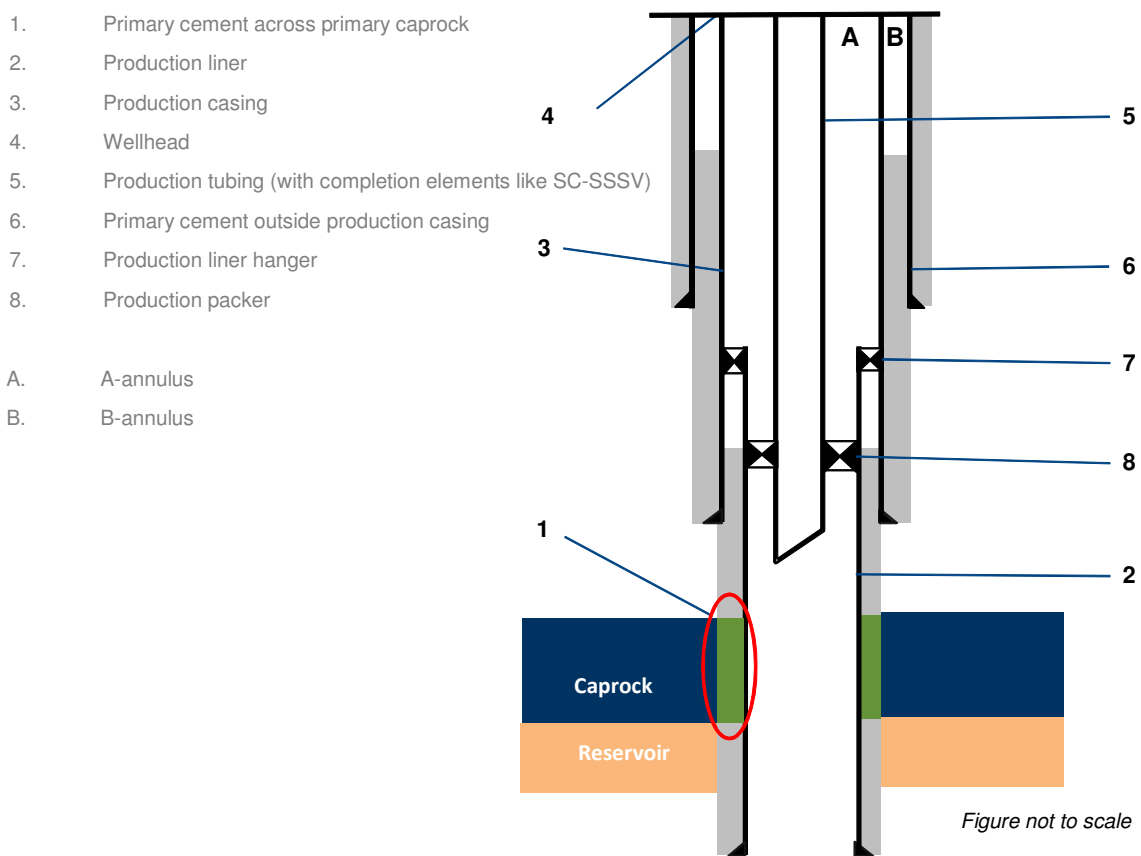


Figure 7.2: Generic P18 well showing the well barriers.

## 7.4. Primary cement across the caprock

The most obvious evidence that the cement across the primary caprock failed during production life is the confirmed presence of reservoir gas in the B-annulus, after the production liner and wellhead are tested OK. The robustness of the primary cement across the caprock is assessed using the criteria summarised in Table 26.

Table 26: Robustness criteria used in assessing quality of primary cement across caprock

		Mandatory	Recommended ("nice-to-have")
<b>Direct evidence</b>	Good (preferably recent) quality cement bond log showing good cement quality across the caprock	×	
<b>Indirect evidence</b>	No prediction of serious defects such as microannuli and cracks created in the cement due to injection of cold CO <sub>2</sub> .	×	
	No large caving/hole washouts in the openhole across caprock		×
	No significant fluid/cement loss during placement		×
	Chemical resistance of the cement to CO <sub>2</sub> attack		×
	No 'high-pressure' well operation that could have compromised the cement across caprock		×
	Good centralisation i.e. if the pipe was well-centralised, then <i>all factors being equal</i> , a better quality cement operations is expected		×

Note 1: The cement bond log does not measure the absolute hydraulic isolation of the cement; it only provides an indication of the quality of the bond from which hydraulic isolation can be inferred. The industry rule of thumb is that good bonding is defined by a CBL reading of about 1-2 mV and a minimum of 3 m of well-bonded cement for a 7" casing/liner. This minimum length does not reflect the potential chemical interaction of acidic fluids with wellbore cement.

Note 2: Hydraulic isolation is best evaluated using the combination of cement bond log and azimuthal cement log. However, azimuthal logs (e.g. USI, Isolation Scanner) are not available for the P18 wells.

## 7.5. Production liner

A pressure test during setting of the liner could tell whether or not the liner itself failed. Failure below the liner hanger is not necessarily a showstopper if the other barriers above the leak still hold. In addition, failure due to any plastic salts in the overburden during the production life of the well was evaluated.

The recommended robustness criterion for the liner for CO<sub>2</sub> injection and storage involves the wetted area of the liner to be made of corrosion-resistant alloy. However, this criterion can be relaxed if the amount of free water in the injected CO<sub>2</sub> stream is expected to be very low.

## 7.6. Production casing

Like the production liner, the production casing is usually tested when it is set. It is investigated whether the casing passed this test. In addition, the impact (if applicable) of plastic salt layers is investigated that may impinge upon the intermediate casing. Direct evidence for failure of the production casing during producing life could include annular pressure communication between the A and B annuli, noise logging and pressure testing of the production casing.

## 7.7. Wellhead

The wellhead provides the main barrier between the well and the atmosphere, and typically is tested during installation and periodically during operation. In this study, the results of these tests are investigated, evaluating whether the wellhead passed the tests. In addition, the materials used to construct the metallic and non-metallic components of the wellhead are investigated to assess if they are fit for CO<sub>2</sub> injection.

## 7.8. Production tubing

The evidence for failure of the production tubing is almost always direct evidence. This includes (but is not necessarily limited to):

- failure of the tubing to hold pressure during initial installation;
- pressure communication between the A-annulus and the tubing;
- reservoir gas-cap on top the A-annulus; and
- depletion of fluid in the A-annulus

The production tubing provides the main wetted surface during CO<sub>2</sub> injection. Due to the corrosive nature of CO<sub>2</sub> (in the presence of free water), the main robustness criteria for the tubing are:

- the wetted areas (the i.d.) be made of CO<sub>2</sub>-resistant material;
- tubing i.d. be sufficient to prevent erosion and high pressure losses due to friction during injection; and
- the tubing be designed to withstand the thermal stresses (due to contraction) that injecting cold fluid will impose on the pipe.

## 7.9. Primary cement outside production casing

The evidence of failure of this cement sheath is similar to that of the primary cement sheath across the caprock, as described in section 0. Particular care should be taken to evaluate the quality of the cement at the shoe, as the quality of the cement there is the primary barrier to an outer annulus becoming a leak path.

## 7.10. Production liner hanger

The production liner hanger is an additional barrier between the reservoir and the production casing. Evidence of failure of the liner hanger could include the presence of reservoir fluids in the A-annulus and/or failure of hanger test during installation.

## 7.11. Production packer

The production packer isolates the corrosive reservoir fluids from the production casing, and 'forces' the fluids to enter the tubing. In addition, the packer may bear some of the tubing loads (depending on how the completion is set). Like the production tubing, evidence for failure of the packer is almost always directly observed. It includes:

- Failure of pressure test during initial installation;
- Loss of annulus fluid levels;
- Presence of reservoir fluids inside the production casing during production life; and
- Pressure communication between the production tubing and the production casing.

There is insufficient information available to distinguish tubing failure from packer failure; therefore, for the remainder of this report, the tubing and production packer will be grouped as one barrier: tubing and completion barrier.

## 7.12. Well integrity assessment

This section involves the application of the defined failure modes and robustness criteria to the wells of the P18 field in order to evaluate their suitability for CO<sub>2</sub> injection and long-term containment.

### 7.12.1. P18-2A1

This well was spudded in 1993 and has produced gas ever since. Available drilling and completion information suggests that no problems occurred during the drilling or completion phase of the well. Refer to the schematic of the well in Figure 7.3.

#### **Cement barrier across the primary caprock**

The 222 m thick Middle Bunter Sandstone (RBM) reservoir is topped by the primary caprock (25m thick), the Solling (RNSOC) and the Röt Claystone (RNROC) members. A cement bond log was run across the 7" liner, covering the reservoir, the primary caprock and the lower part (21 m) of the secondary caprock, with top of cement (TOC) found at 3,477 m. The CBL-VDL log shows poor casing-cement bond in the liner lap above the perforations, including the primary caprock section, and mainly good bonding below the perforations.

#### **Cement barrier across the secondary caprock**

The Muschelkalk (RNMU) and Keuper (RNKP) formations (141 m thick) are believed to act as the secondary caprock. As mentioned above, a cement bond log was run across the lower part of the secondary caprock, showing poor bonding. Across the 9 $\frac{5}{8}$ " casing string, which traverses most of the secondary caprock, no cement bond logs were run.

However, there is indirect evidence suggesting that the casing bond may be adequate. This evidence includes the fact that no problems were encountered during drilling or cementing, such as loss of cement or mud. Furthermore, the well is vertical and the production casing was centralised with at least six centralisers, suggesting good centralisation. There is no information about the condition of the hole, e.g. washouts, or sort of centralisers used.





Doc.nr: CATO2-WP3.01-D06  
Version: 2011.01.04  
Classification: Confidential  
Page: 122 of 198

## Feasibility study P18

---

### Production liner and casing

Both the 7" and 9 $\frac{5}{8}$ " liner/casing strings were pressure tested OK to 5,000 psi for 20 min. The 7" liner consists of 29 lb/ft N-80 casing and the 9 $\frac{5}{8}$ " casing is 53.5 lb/ft HC-95 material. According to reports, neither of the two strings is made of Cr13 steel. There is no data on annulus pressures; therefore, there is no information on possible communication between the completion and casing.

### Production tubing and completion

The completion is 4 $\frac{1}{2}$ "/5" L80 Cr13 tubing. Since it is made of Cr13 steel, it is fit for CO<sub>2</sub> injection. However, a retrievable packer is used. This packer could become unseated during CO<sub>2</sub> injection depending on the packer operating envelope<sup>2</sup>. There is no information available on the wellhead and type of elastomers (if any). Therefore, the suitability of the wetted areas of the wellhead or any elastomers for CO<sub>2</sub> conditions cannot be evaluated.

---

<sup>2</sup> The packer operating envelope shows the tensile, compressional and burst loads that the packer is designed to handle. In essence, it shows the conditions under which the packer can operate. Operating the packer outside this envelope would result in failure of the packer – and loss of well integrity.

Feasibility study P18

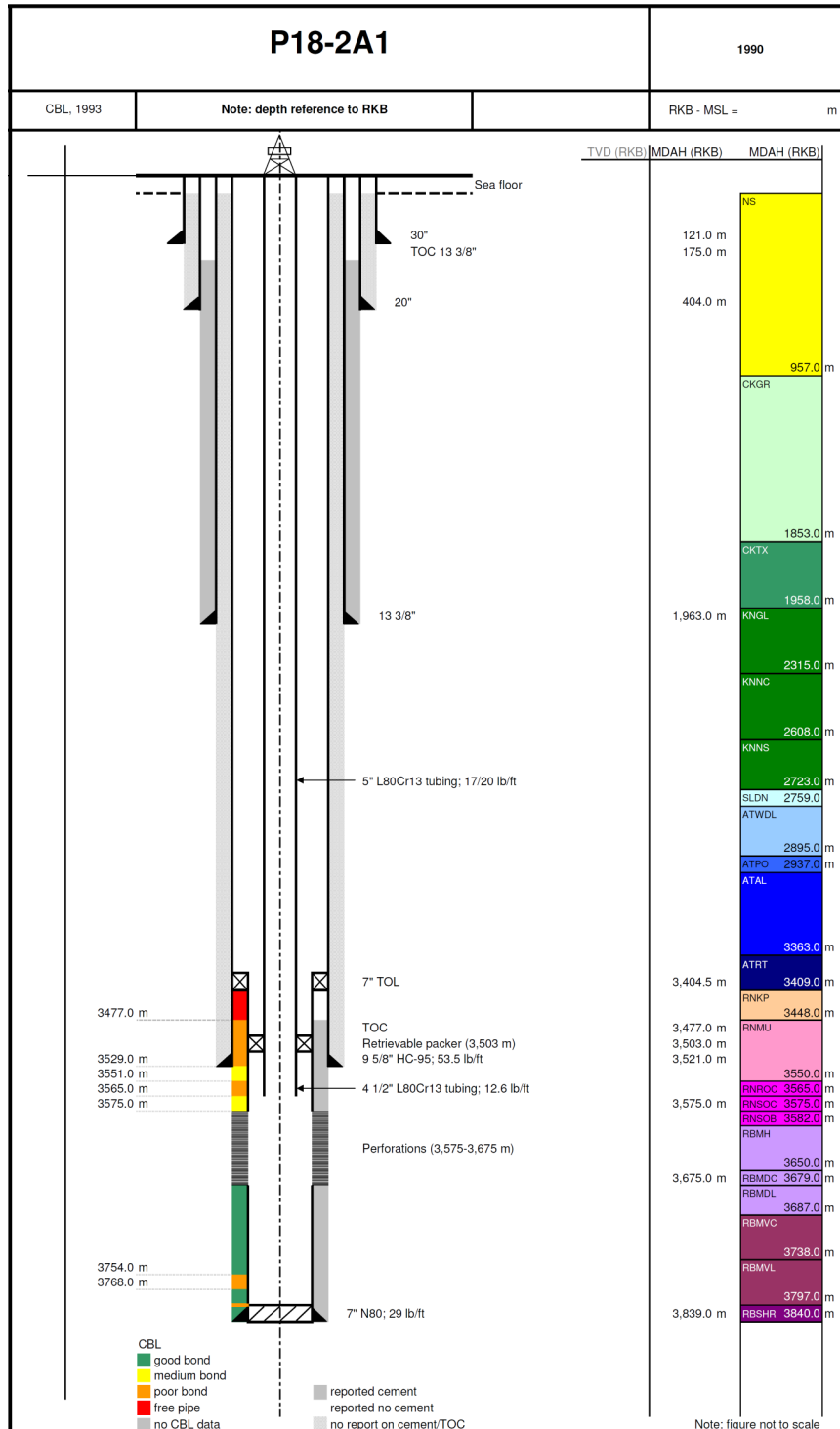


Figure 7.3: P18-2A1 well schematics with CBL interpretation (left hand side) and stratigraphy (right hand side).

## Conclusion

Information from available cement bond logs suggest poor casing-cement bond across the upper part of 7" liner. This implies inadequate hydraulic isolation over the primary caprock and parts of the secondary caprock. No information is available for the 9 $\frac{5}{8}$ " casing cementation. However, successful casing tests, presence of casing centralisers and the absence of cementing and drilling problems provide favourable boundary conditions for a successful cementing job. It is suggested that the cement sheath be re-evaluated before considering it for CO<sub>2</sub> injection by checking annulus pressures or running cement bond logs over the intervals in question. Although the casing strings themselves are not made of Cr13 steel, the completion is and therefore would be fit for CO<sub>2</sub> injection. Furthermore, the packer operating envelope should be checked against CO<sub>2</sub> injection scenarios by performing a tubing stress analysis and if needed workover to be performed. Furthermore, elastomers and wellhead information should also be checked.

### 7.12.2. P18-2A5

Well P18-2A5 was spudded in November 1996. The well was sidetracked once because of wellbore instability problems across the Aalborg (ATAL) shales (4,058m). A cement plug was set from 3,830m to inside the 9 $\frac{5}{8}$ " casing and the 8 $\frac{1}{2}$ " sidetrack drilled below the 9 $\frac{5}{8}$ " casing shoe. After successfully sidetracking the well, a 7 $\frac{5}{8}$ " casing was run without success. The hole was cleaned and a 7" liner run and cemented in place. While drilling the 6" openhole section, mud losses occurred until the mud weight was lowered to 9.1ppg. The well schematic is shown in Figure 5 below.

### Cement barrier across the primary and secondary caprock

The 327m thick Middle Bunter Sandstone (RBM) reservoir is topped by its primary caprock (69m thick), consisting of the Solling Claystone (RNSOC), the Main Röt Evaporite (RNRO1) and Röt Claystone (RNROC) members. The overlying Muschelkalk (RNMU) and Keuper (RNKP) formations (174m thick) are believed to act as the secondary caprock (see Figure 7.4). Conditions for cementing were good. Although mud losses occurred during drilling, no problems were mentioned during the cementing job. The casing string was centralized well by placing 1 centralizer on each joint and 3 m of cement were drilled above the liner top. A cement bond log is available across the 5" liner; it covers the reservoir and the caprocks. The log confirms overall good bonding across the caprocks, represented by low CBL amplitude and good formation arrivals from the variable density log (VDL). Incidentally, short poor-quality zones can be distinguished. The reported calculated top of cement is at 4,398 m (approximately top of the 5" liner).

The end of well report suggests that a cement bond log was also acquired across the 7" liner suggesting good casing-cement bond and top of cement (TOC) 50 m below the 9 $\frac{5}{8}$ " casing shoe. However, the log was not available for analysis. No problems occurred during drilling and cementing operations and the casing was centralized using solid spiral centralizers, providing good cementing conditions and supporting the reported result of the cement bond evaluation.

### Production and intermediate liner

The 7" liner was pressure tested OK to 4,000psi for 15min. The 5" liner is 18 lb/ft N-80 and the 7" liner 29 lb/ft N-80 casing. According to reports, neither of the two strings is made of Cr13 steel.



Doc.nr: CATO2-WP3.01-D06  
Version: 2011.01.04  
Classification: Confidential  
Page: 125 of 198

## Feasibility study P18

---

### **Production tubing and completion**

The well has been in production since Nov 1996. The tubing is 4½"/ 5½" L80Cr13 tubing, which is fit for CO<sub>2</sub> service. Due to the use of a retrievable packer, it is suggested that its operating envelope be checked against CO<sub>2</sub> injection scenarios by performing a tubing stress analysis and if needed workover to be performed. Elastomers and wellhead information was not available but should also be checked.

### **Other criteria**

The pilot hole does not truncate the caprock or the reservoir and therefore should not act as an additional leakage pathway for CO<sub>2</sub>. No information is available about annulus pressures or the cement quality across intermediate aquifer zones.

Feasibility study P18

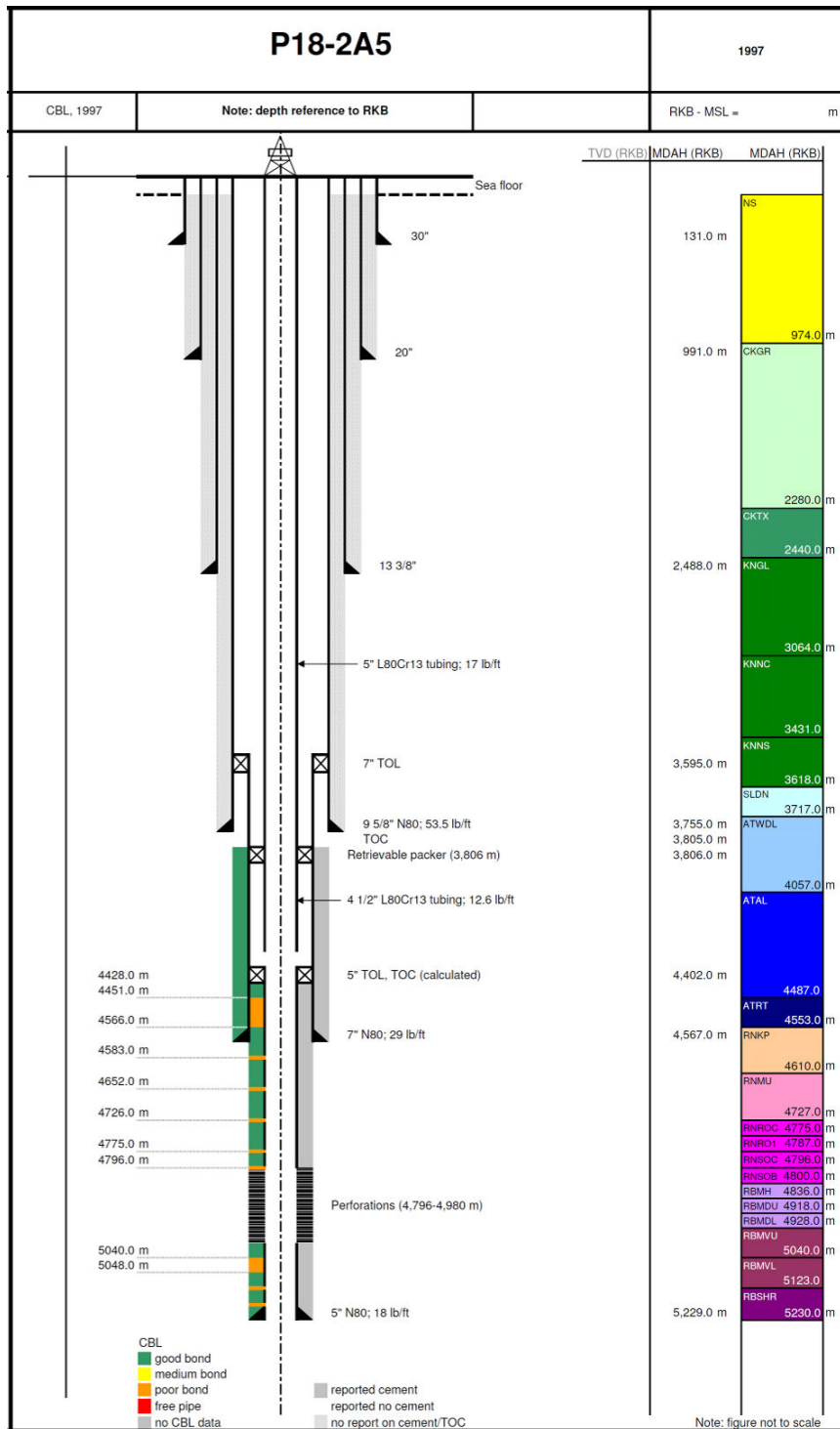


Figure 7.4: P18-2A5 well schematics with CBL interpretation (left hand side) and stratigraphy (right hand side).

## Conclusion

The available information shows that good casing-cement bond exists across the majority of reservoir and caprock formations. Although the casing strings themselves are not made of Cr13 steel, the completion is, and therefore would be fit for CO<sub>2</sub> injection. It is recommended that the packer operating envelope is checked against CO<sub>2</sub> injection scenarios by performing a tubing stress analysis and, if required, workover to be performed. Furthermore, elastomers and wellhead information should be checked.

### 7.12.3. P18-2A6

Well P18-2A6 was spudded in November 1996. Mud losses occurred during drilling of the pilot hole. The bottomhole assembly got stuck at the bottom of the 12<sup>1</sup>/<sub>4</sub>" openhole section in the Triassic Muschelkalk and needed to be fished. After the 9<sup>5</sup>/<sub>8</sub>" liner was set and cemented (TOC = 3,000m), a 13<sup>3</sup>/<sub>8</sub>" casing wear log indicated 25% wear on the casing, so a 9<sup>5</sup>/<sub>8</sub>" tie back casing string was run and cemented (TOC = 1,613m). See Figure 6.

While drilling the 8<sup>1</sup>/<sub>2</sub>" openhole section no problems occurred. The 7" liner was cemented successfully. Both the 9<sup>5</sup>/<sub>8</sub>" casing and the 7" liner were pressure tested OK to 5,000 psi and the well displaced to filtered completion brine.

The well penetrated the P18-2 III reservoir block. The well was sidetracked in 2003 (P18-2A6st, see section 7.12.4) to reach the P18-2 II reservoir block.

### Cement barrier across the primary and secondary caprocks

The 256 m thick Middle Bunter Sandstone (RBM) reservoir is topped by its primary caprock (33 m thick), the Röt Claystone member (RNROC). The above Muschelkalk (RNMU) and Keuper (RNKP) formations (188 m thick) are believed to act as the secondary caprock (Figure 7.5).

A cement bond log is available across the 7" liner of the P18-2A6 well from 4,755 to 4,255m, which covers reservoir and both caprocks. The log suggests good casing-cement bond across several intervals in the reservoir section. However, cement bond is moderate to poor across the caprock with CBL amplitudes ranging between 10 and 30mV.

No cement bond logs are available across the 9<sup>5</sup>/<sub>8</sub>" casing string of the pilot hole. End of well reports indicate that mud losses occurred during drilling and while running the 9<sup>5</sup>/<sub>8</sub>" casing string in hole. This suggests non-ideal cement placement conditions.

### Production casing and liner

Both the 9<sup>5</sup>/<sub>8</sub>" casing and the 7" liner of the pilot hole were pressure tested ok to 5000 psi. The 7" liner consists of 29 lb/ft N-80 and the 9<sup>5</sup>/<sub>8</sub>" casing of 53.5 lb/ft N-80 casing. According to reports neither of the two strings are made of Cr13 steel.

### Production tubing and completion

The P18-2A6 pilot well was in production from June 1997 to April 2003. No information is available on the measures that were taken regarding the pilot hole when sidetracking the well. The pilot well report indicated that a retrievable packer was used in the well. If still applicable, it is suggested that the packer operating envelope be checked against CO<sub>2</sub> injection scenarios by performing a tubing stress analysis and - if needed - workover to be performed. Elastomers and wellhead information was not available, but should also be checked.



Doc.nr: CATO2-WP3.01-D06  
Version: 2011.01.04  
Classification: Confidential  
Page: 128 of 198

## Feasibility study P18

---

### Other criteria

The P18-2A6 pilot hole traverses both the caprock and the reservoir and the available cement-bond log does suggest poor casing-cement bond across the caprock and parts of the reservoir. Due to the missing end of well report for the sidetrack (P18-2A6st), it is not clear how the pilot hole was abandoned. Therefore, there is uncertainty on whether a leak path exists along the original hole. No information is available about annulus pressures or the cement quality across intermediate aquifer zones.

Feasibility study P18

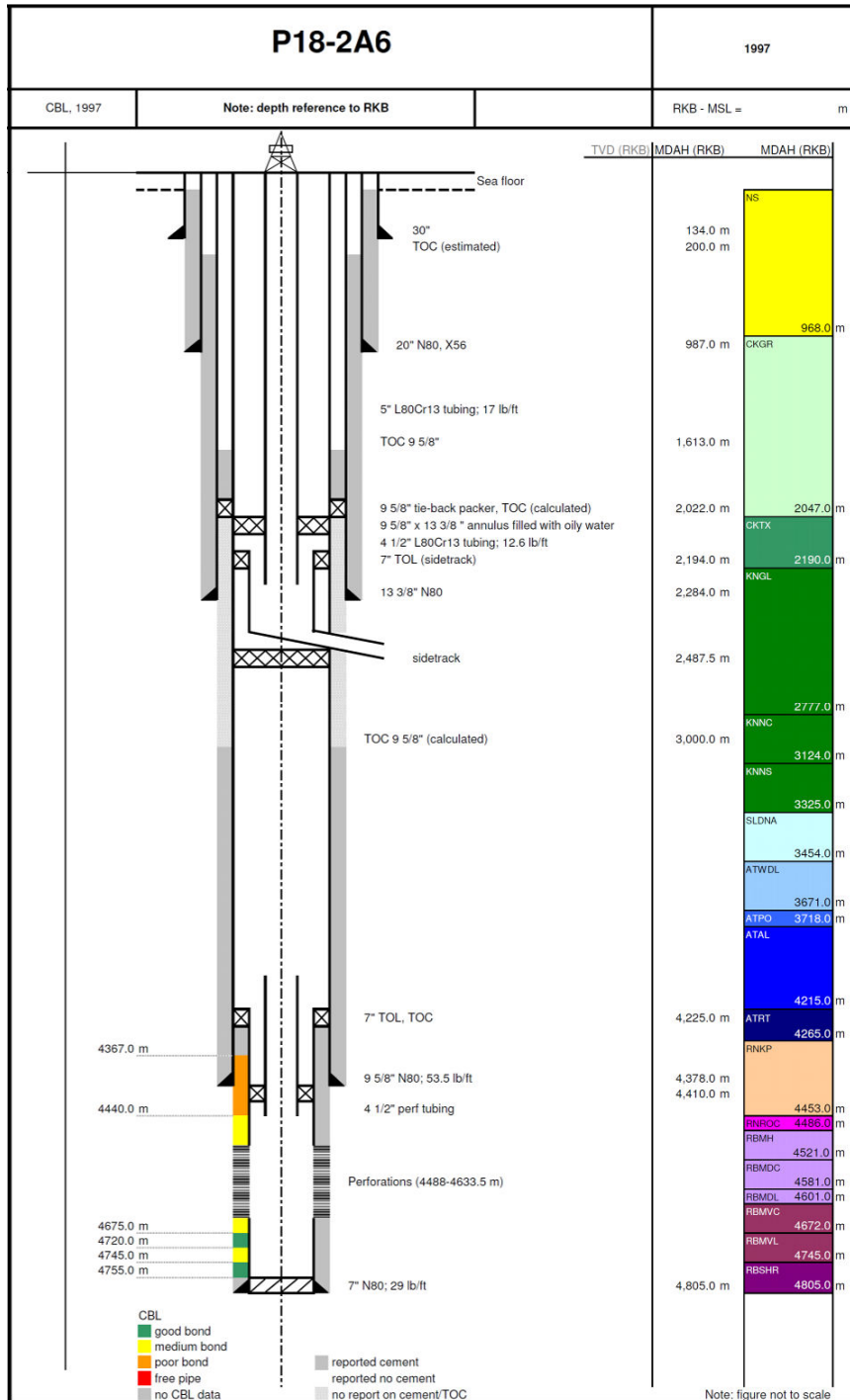


Figure 7.5: P18-2A6 well schematics with CBL interpretation (left hand side) and stratigraphy (right hand side).



## **Conclusion**

Due to the missing information about the sidetracked well and the plugging of the pilot hole, no definite conclusion can be drawn on the suitability of the well for CO<sub>2</sub> storage. The cement bond log across the 7" liner of the pilot hole suggests poor casing-cement bond across the caprock with only a few good intervals across the reservoirs. As this poses a potential threat to long-term CO<sub>2</sub> containment, the abandonment of the pilot hole is crucial for well integrity. However, it is unclear how the pilot hole was abandoned and if the current layout is suitable for CO<sub>2</sub> storage. This issue needs to be clarified before CO<sub>2</sub> injection begins. Without the appropriate data available and proving the contrary, there is a probability that a leakage pathway exists at least along the 7" liner. It is suggested to check the packer operating envelope against CO<sub>2</sub> injection scenarios by performing a tubing stress analysis and if needed workover to be performed. Furthermore, elastomers and wellhead information should also be checked.

### **7.12.4. P18-2A6st**

The P18-2A6 well was sidetracked in 2003 (P18-2A6st). The sidetrack's geometry consists of a 7" liner and a 4½" liner and is presented in Figure 7.6. Unfortunately, the reports on the sidetracked borehole were not available to this study.

### **Cement barrier across the primary and secondary caprocks**

Information about the cementing and casing-cement bond across the 7" and 4½" liner was not obtained.

### **Production and intermediate liner**

No information on pressure tests of the 7" and 4½" liner of the sidetracked borehole is available. The sidetrack's 7" liner consists of L80 Cr13 steel.

### **Production tubing and completion**

The sidetracked well produced since June 2003. The sidetrack's tubing is 4½"/ 5½" L80Cr13 tubing, which is fit for CO<sub>2</sub> service. A retrievable packer is used; therefore, it is suggested that the packer operating envelope be checked against CO<sub>2</sub> injection scenarios by performing a tubing stress analysis and - if needed - workover to be performed. Elastomers and wellhead information on the mother well was not available, but should also be checked.

### **Other criteria**

No information is available about annulus pressures or the cement quality across intermediate aquifer zones.

## **Conclusion**

Due to the missing information about the sidetracked well, no conclusions can be drawn on the suitability of the P18-2A6 well or its sidetrack for CO<sub>2</sub> storage. Specifically, no information is available on the location and bonding quality of the cement in the sidetrack.

In addition, information about the sidetracked wellbore is crucial to decide on its suitability for conversion into a CO<sub>2</sub> injector or for long-term containment of CO<sub>2</sub>. Although the casing strings across the reservoir and caprocks, are not made of Cr13 steel, the completion is and therefore would be fit for CO<sub>2</sub> injection.

It is suggested to check the packer operating envelope against CO<sub>2</sub> injection scenarios by performing a tubing stress analysis and if needed workover to be performed. Furthermore, elastomers and wellhead information should also be checked (as described in section 7.12.3).

Feasibility study P18

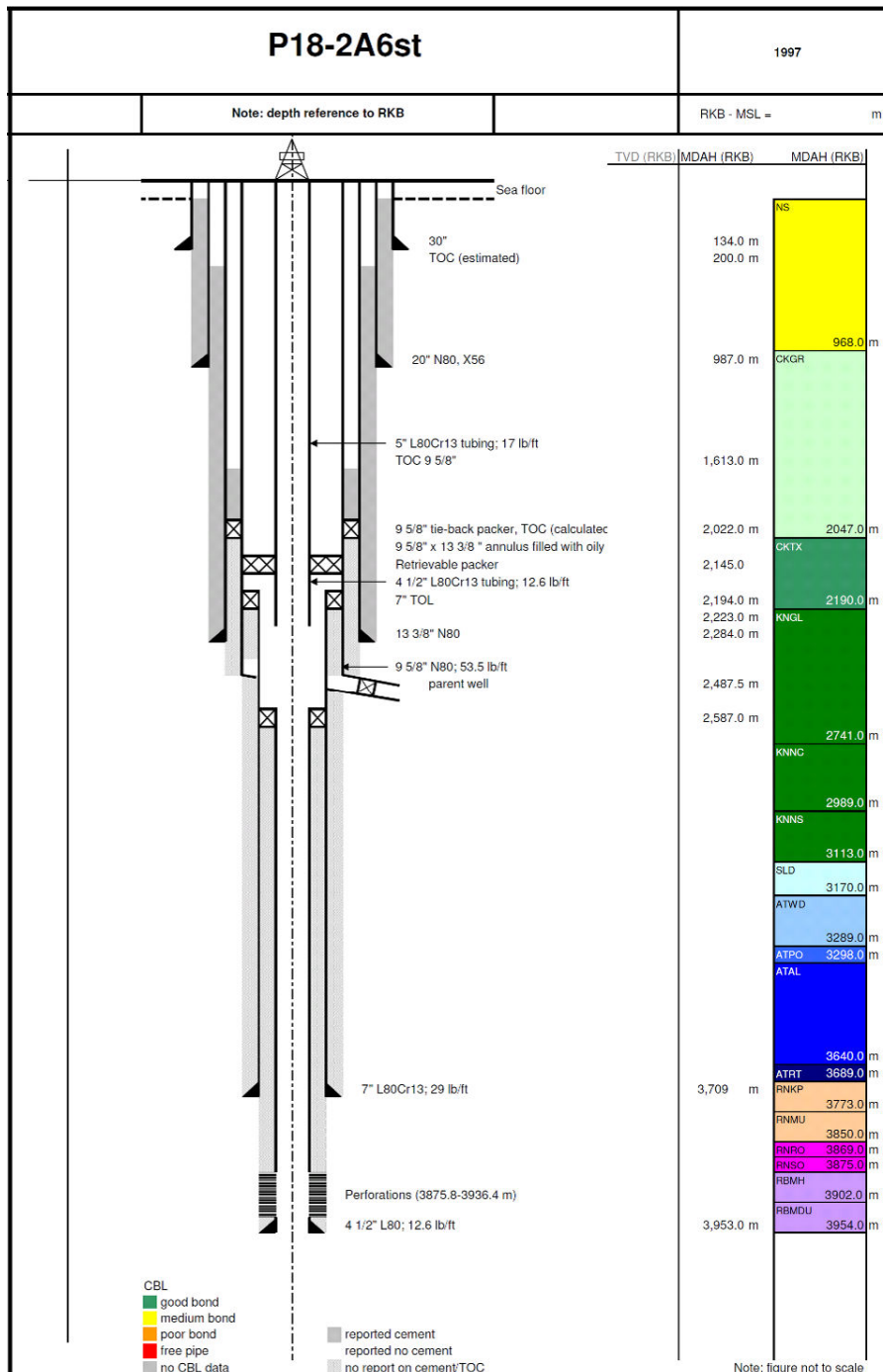


Figure 7.6: P18-2A6st well schematics, CBL interpretation (left hand side) and stratigraphy (right hand side).

### 7.12.5. Well P18-4A2

Well P18-4A2 was spudded in April 1991 and was temporarily suspended with three cement plugs. Subsequently, it was completed and brought on stream in June 2003. The end of well report suggests that no problems occurred during the drilling and cementing operations, except in the 9 $\frac{5}{8}$ " casing string, where mud losses were experienced. Refer to the schematic of the well in Figure 7.7.

#### Cement barrier across the primary and secondary caprocks

The 225 m thick Middle Bunter Sandstone (RBM) reservoir is topped by its primary caprock (24 m thick), the Solling (RNSOC) and Röt Claystone (RNROC) members, and the secondary caprock, the Muschelkalk (RNMU) and Keuper (RNKP) formations (120 m thick).

No cement bond logs are available for the 7" liner and the 9 $\frac{5}{8}$ " casing strings. The 7" liner was set across the reservoir, the primary and the secondary caprock. The end of well report indicates that no mud losses occurred during the drilling of the openhole section and no other problems occurred during the cement job itself. In combination with the in-gauge borehole and evenly spaced casing centralisers, this provides adequate conditions for proper cement placement across the formations of interest. The calculated top of cement is at the top of the 7" liner, at 3,924 m.

The 9 $\frac{5}{8}$ " casing string covers most of the secondary caprock. According to the end of well report 709bbls of mud were lost while setting the casing; moreover only four casing centralizers were used. Top of cement is estimated to be at around 2,000m. This suggests, *all other factors being equal*, the quality of the cement bond across the 9 $\frac{5}{8}$ " casing string to be worse than that across the 7" liner. However, as stated earlier, there is no data available to verify either of the cement bonds.

#### Production casing and liner

No information about pressure testing the 9 $\frac{5}{8}$ " casing and the 7" liner was available. The 7" liner consists is 32 lb/ft P-110 and the 9 $\frac{5}{8}$ " casing of 53.5 lb/ft N-80 casing. Neither string is made of Cr13 steel. Mud across 9 $\frac{5}{8}$ " casing interval showed CO<sub>2</sub>/CaCO<sub>3</sub> contaminations and low to medium corrosion. Corrosion control is reported.

#### Production tubing and completion

The well has been in production since December 1993. The tubing is 4 $\frac{1}{2}$ "/ 5 $\frac{1}{2}$ " L80Cr13 tubing, which is fit for CO<sub>2</sub> service. Since the production packer is a retrievable one, it is suggested that the packer operating envelope be checked (by tubing stress analysis) that it is indeed fit for 'cold' CO<sub>2</sub> service. If needed, thereafter, a workover could be performed.

There was no information on packer/wellhead elastomers; it is recommended that this information be checked before start injection to confirm applicability for CO<sub>2</sub> service.

#### Other criteria

There is no information about annulus pressures or the cement quality across intermediate aquifer zones.

#### Conclusion

Reports indicate overall good cement placement conditions across the 7" liner, suggesting that good hydraulic isolation over the reservoir and the primary caprock and parts of the secondary caprock might exist.

Feasibility study P18

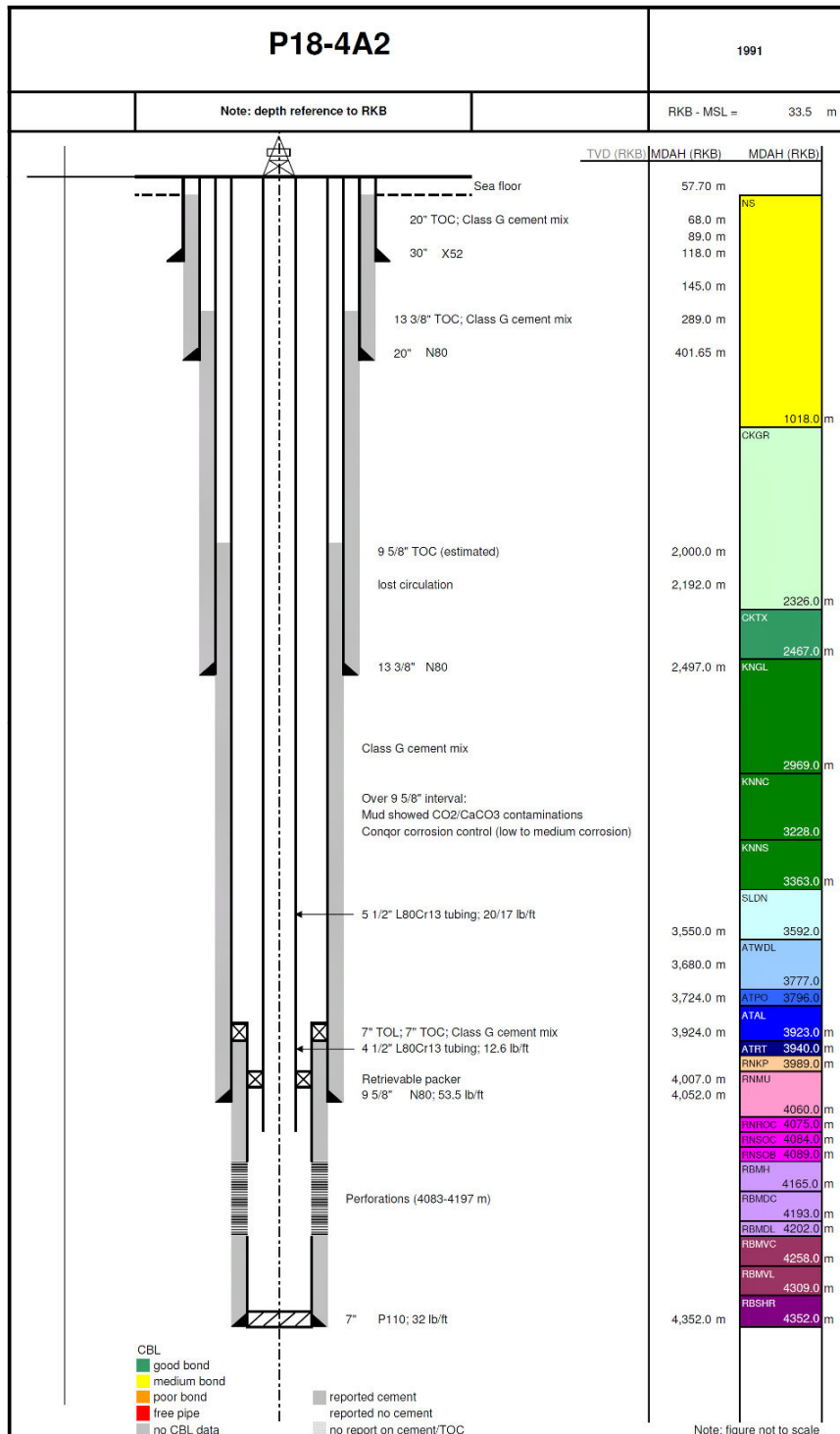


Figure 7.7: P18-4A2 well schematics with CBL interpretation (left hand side) and stratigraphy (right hand side).

Mud losses, which occurred while running, circulating and cementing the 9 $\frac{5}{8}$ " casing, and the limited number of centralisers, suggest that cement placement might not have been optimal. However, these observations are only an indirect inference of cement quality made in the absence of direct measured information; therefore, they need to be verified with the actual data. The casing strings are not made of Cr13 steel. The reported corrosion in the 9 $\frac{5}{8}$ " casing should be verified before converting the well to CO<sub>2</sub> service. However, the completion is made of Cr13 steel and therefore would be fit for CO<sub>2</sub> injection. It is suggested that the packer operating envelope is checked against CO<sub>2</sub> injection scenarios by performing a tubing stress analysis and if needed workover to be performed. Furthermore, elastomers and wellhead information should also be checked.

### **7.12.6. Well P18-6A7**

Well P18-6A7 was spudded February 2003. The pilot well was sidetracked in the Ommelanden Formation (CKGR). The end of well report indicates that the first cementing stage on the 13 $\frac{3}{8}$ " casing did not enter the annulus due to plug problems and that only the second cementing stage was successful. The 3 $\frac{1}{2}$ " liner is not cemented. Refer to the schematic shown in Figure 7.8.

#### **Cement barrier across the primary and secondary caprocks**

The 95 m thick Middle Bunter Sandstone (RBM) reservoir is topped by its primary caprock (27 m thick), the Solling (RNSOC) and Röt Claystone (RNROC) members; the overlying Muschelkalk (RNMU) and Keuper (RNKP) formations (161 m thick) are believed to act as the secondary caprock (see Figure 9).

The 3 $\frac{1}{2}$ " liner covers the reservoir and the primary caprock, whereas the lower section of the 5 $\frac{1}{2}$ " liner is set across the secondary caprock. Casing-cement bond information is not available for the 5" liner and therefore, no statement on its cement quality can be made. The 3 $\frac{1}{2}$ " liner, positioned across the primary caprock, is reported to be uncemented.

#### **Production liner and casing**

No information about pressure testing the 3 $\frac{1}{2}$ " and 5 $\frac{1}{2}$ " liners was available. The 3 $\frac{1}{2}$ " liner consists is 9.5 lb/ft L-80Cr13 and the 5 $\frac{1}{2}$ " liner 18 lb/ft L-80Cr13 material.

#### **Production tubing and completion**

The well has been in production since July 2003. The tubing is 4 $\frac{1}{2}$ " L80Cr13 tubing, which is fit for CO<sub>2</sub> injection. Unlike the other production packer in the other wells, the production packer in well P18-6A7 is not retrievable. However, still it is recommended to confirm that the packer's operating envelope is appropriate for the anticipated CO<sub>2</sub> injection service.

Elastomers and wellhead information was not available and should be checked also.

#### **Other criteria**

There is no information on annulus pressures or the cement quality across intermediate aquifer zones. The well is not located in the immediate vicinity of other boreholes, which truncate the caprock and could provide additional leakage pathways for CO<sub>2</sub>.



Doc.nr: CATO2-WP3.01-D06  
Version: 2011.01.04  
Classification: Confidential  
Page: 135 of 198

## Feasibility study P18

---

### Conclusion

There was limited data available for the P18-6A7 well. Due to missing cementing reports and cement bond logs across the 5½" liner, the casing-cement bond quality across the secondary caprock is highly uncertain. It is recommended to check this before start of injection. The 3½" liner, positioned across the primary caprock, is uncemented.

In addition, both liners and the completion are made out of Cr13 steel and are therefore fit for CO<sub>2</sub> injection. It is recommended that the packer operating envelope is checked against CO<sub>2</sub> injection scenarios by performing a tubing stress analysis and, if required, workover to be performed. Furthermore, elastomers and wellhead information should also be checked.

Feasibility study P18

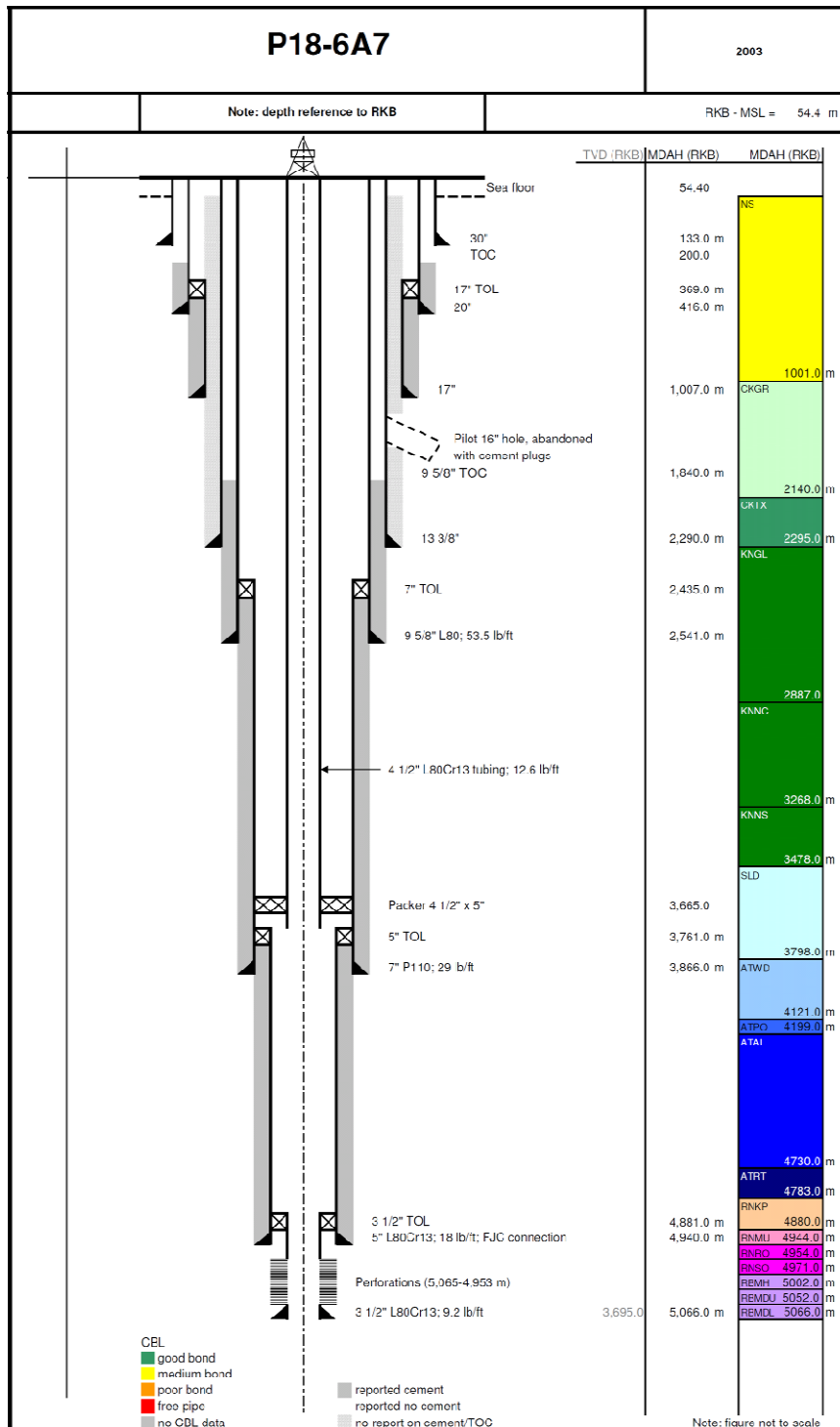


Figure 7.8: P18-6A7 well schematics with CBL interpretation (left hand side) and stratigraphy (right hand side).

### 7.12.7. Well P18-2

This well was spudded in March 1989 and suspended with four cement plugs after a DST test was performed in the Bunter Sandstone Formation. The end of well report does not mention any particular problems during drilling or cementing operations of the 7" liner. The current well configuration is shown in Figure 7.9.

#### Cement barrier across the primary and secondary caprocks

The 213 m thick Middle Bunter Sandstone (RBM) reservoir is topped by its primary caprock (33 m thick), the Solling (RNSOC) and Röt Claystone (RNROC) members; the overlying Muschelkalk (RNMU) and Keuper (RNKP) formations (131m thick) are believed to act as the secondary caprock. Refer to Figure 10.

The 7" liner covers the reservoir and both the primary and secondary caprocks. It was centralized with 47 centralisers within an in-gauge borehole. After running the cement bond log under pressure (1,000 psi), overall poor bonding was recorded with moderate to well bonded sections from 3,664-3,597m and 3,276-3,247 m, with top of cement at around 3,005m MD, inside the 9 $\frac{5}{8}$ " casing. See Figure 10.

The 9 $\frac{5}{8}$ " casing string was centralized with 32 centralisers. A cement bond log was acquired from 2,960 to 100 m, showing overall poor bonding. The top of cement was found at 1,932m and at 1,525 m, separated by a free pipe section on top of a multi-stage packer at 1,893 m.

#### Abandonment plugs

The deepest of the four cement plugs is located across the upper part of the reservoir section (Figure 10), directly above the perforations, but below the caprocks. The cement that was placed on a (presumably) mechanical plug extends only 1.5 m. The remaining cement plugs are located above the caprock intervals. The next plug is positioned at 3,006-2,896 m across the Aalborg Formation (ATAL) at the 7" liner hanger, with a length of 110 m – of which 60 m is situated above the liner hanger. At 1,915-1,846 m a cement plug is placed at the 13 $\frac{3}{8}$ " casing shoe and 9 $\frac{5}{8}$ " multi stage PKR, across the Texel Chalk Formation (CKTX). The uppermost plug extends from 154-85 m, covering the base of the 30" conductor pipe. Each of the cement plugs were pressure tested OK to 2,000 psi.

#### Production liner and casing

The 7" liner and 9 $\frac{5}{8}$ " casing string were pressure tested OK to 4,000 psi and 5,000 psi respectively. The 7" liner consists of 29 lb/ft N-80 and the 9 $\frac{5}{8}$ " casing of 47 lb/ft N-80 casing. Neither of them are made of Cr13 material.

#### Conclusion

Cement bond across the reservoir and caprocks generally shows poor results. The abandonment plugs are situated such that the first plug is positioned across the reservoir, whereas the remaining three are located considerably higher than the primary and secondary caprock. This combination does not provide adequate conditions for CO<sub>2</sub> storage. Aqueous CO<sub>2</sub> could affect the lowermost (1.5m thick) seal or associated poor bonded cement or penetrate the carbon steel casing above the plug, and as a result could easily bypass the primary and secondary caprock. Although the abandonment plugs were pressure tested OK, it is reasonable to expect that, in the long term, CO<sub>2</sub> could bypass the lowermost abandonment plug and migrate through the wellbore to levels above the primary and secondary caprock. Furthermore, the possibility of subsequent upward migration of the CO<sub>2</sub> cannot be excluded, given the poor quality of the cement bond adjacent to the 7" liner and the 9 $\frac{5}{8}$ " casing.



Feasibility study P18

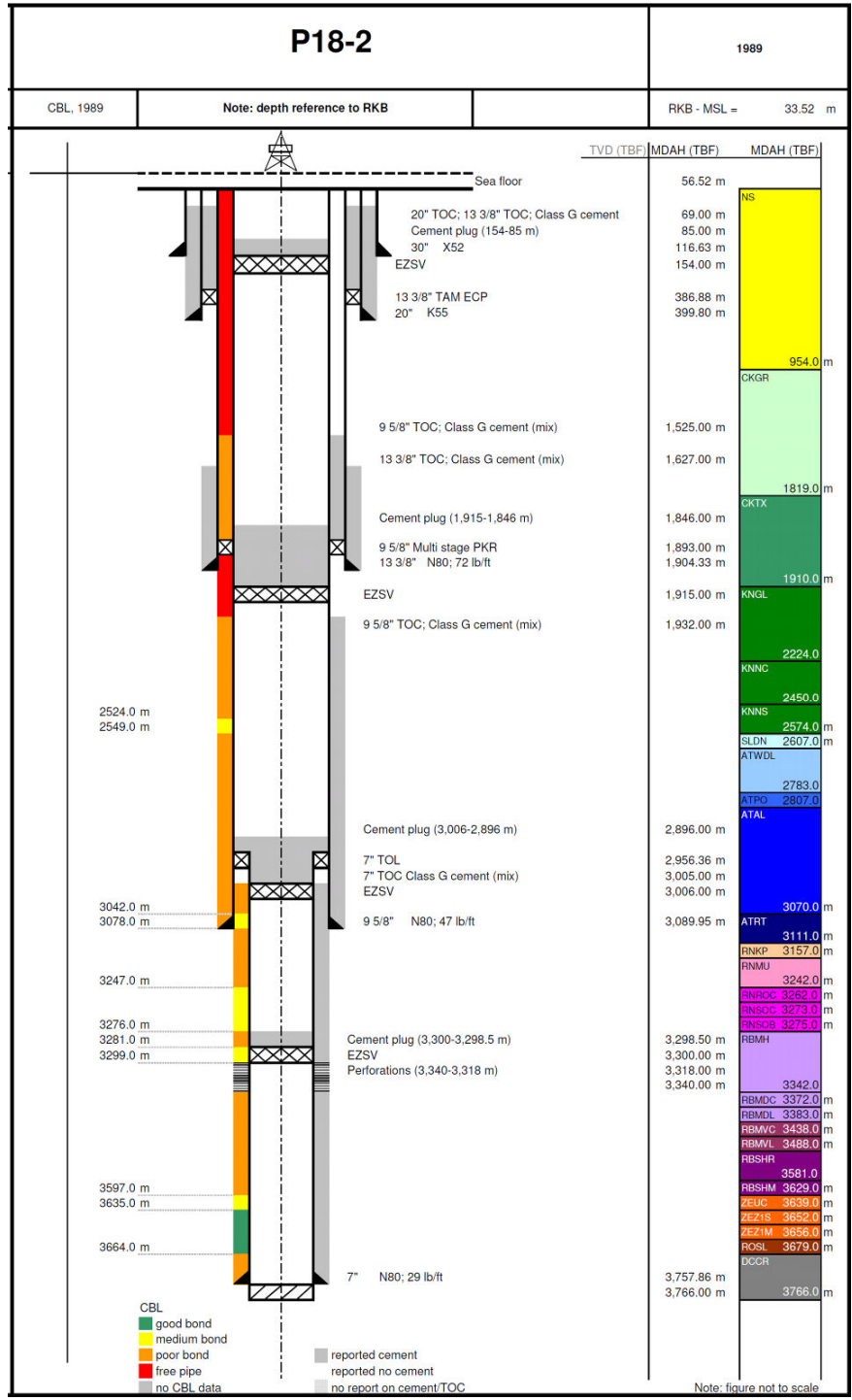


Figure 7.9: P18-2 well schematics with CBL interpretation (left hand side) and stratigraphy (right hand side).

**Feasibility study P18**

### 7.13. Summary of integrity assessment of the P18 wells

In this section, the assessment of the integrity of the seven studied wells is summarized. As discussed in section 7.12, the integrity of the well barriers is evaluated using available direct and indirect evidence. Refer to Table 27 for a summary of the assessment.

Table 27: Summary of P18 well integrity evaluation

Well	P18-2A1	P18-2A3	P18-2A5	P18-2A6	P18-2A6st	P18-4A2	P18-6A7	P18-2
Cement sheath across primary caprock	x	x	✓	x	?	✓	x	x
Cement sheath across secondary caprock	x	x	✓	x	?	x	?	x
Production casing and liner								
	Tested OK?	Y	Y	Y	Y	?	?	Y
	Cr13?	N	N	N	N	Y	Y	N
Production tubing and completion	✓	✓	✓	?	✓	✓	✓	N/A
Production packer	?	?	?	?	?	?	?	N/A
Wellhead	?	?	?	?	?	?	?	?
Abandonment plugs	N/A	N/A	N/A	N/A	N/A	N/A	N/A	x
Comments (see below)	2, 3, 4	2, 3, 4	2, 3, 4	2, 3, 4	1, 2, 3, 4	2, 3, 4	1, 2, 3, 4	

- ✓ Direct evidence suggesting that barrier is of good quality or robust for CO<sub>2</sub> service
- ✓ Indirect evidence suggesting that barrier might be of good quality or robust for CO<sub>2</sub> service
- x Direct evidence suggesting that barrier is not of good quality or robust for CO<sub>2</sub> service
- x Indirect evidence suggesting that barrier might not be of good quality or robust for CO<sub>2</sub> service
- ? No data to suggest quality of barrier or robustness

- 1 No end-of-well report available
- 2 No information on annulus pressure during production life
- 3 Applicability of (retrievable) packer for cold CO<sub>2</sub> injection needs to be confirmed by tubing stress analysis
- 4 Applicability of wellhead and any potential elastomers to CO<sub>2</sub> service unknown

## 7.14. Long-term well integrity

### 7.14.1. Material degradation

Well material degradation can occur by several mechanisms on different timescales. While mechanical deformation of the wellbore may generally be associated with the operational life of the well or field, chemical degradation of well materials will take place on longer timescales. Under certain conditions aqueous CO<sub>2</sub> can chemically interact with well materials. Especially taking into account time spans of thousands of years, these processes may play a crucial role in the integrity of wells and therefore of storage reservoirs.

A review of laboratory experimental studies indicates that diffusion-based chemical degradation rates of cement are relatively low. Extrapolation of the general results shows a maximum of up to a few meters of cement that may be affected in 10,000 years. Even under very high temperatures, extrapolated degradation rates would result in a maximum of 12.4 m of cement plug degradation after 10,000 years of exposure to CO<sub>2</sub>, assuming that diffusion processes define the degradation mechanism. In order to translate the experimental results to field situations, several limiting factors apply. Whereas cement samples in the laboratory in certain cases were immersed in a bath of supercritical CO<sub>2</sub>, well material in reality will be partially surrounded by reservoir rock, limiting the available reaction surface, the supply of CO<sub>2</sub> and the transportation of reaction products. Furthermore, in specific field cases, especially in depleted gas fields, the availability of water necessary for degradation may be far more limited compared to the experiments. Moreover, injected CO<sub>2</sub> will push back the brine present in the storage formation. As dissolution will take place slowly, many wells may not come across the CO<sub>2</sub>-water contact at or near critical levels, such as the cap rock. The presence of only connate water would significantly limit the chemical reactivity of CO<sub>2</sub>, although CO<sub>2</sub> is expected to favourably dissolve water. Finally, higher salinity of formation water will likely decrease the solubility of CO<sub>2</sub> and reaction products, thus reducing cement degradation rates. Especially relative high concentrations of calcium and magnesium in the brine may limit the degradation of wellbore cement. Steel corrosion is much faster than cement degradation with rates up to mm's per year. However, also corrosion rates will be seriously reduced by the limited availability of water. A more detailed discussion is presented in IEA GHG (2009).

As a result of the above, the mechanical integrity and quality of placement of primary cement and cement plugs probably is of more significance than the chemical degradation of properly placed abandonment plugs. The presence or development of fractures or annular pathways in the cement or along material interfaces will strongly affect the bulk permeability of the cement sheath. These phenomena, which may be associated with either operational activities or degradation, will play an important role in leakage mechanisms and may significantly reduce the sealing capacity of the cement. Moreover, degradation in lateral direction, affecting the primary cement sheath and casing steel, is likely to compromise integrity in decades. As previously abandoned wells generally cannot easily be remediated, these wells form an element of especial attention in any prospective CO<sub>2</sub> storage project.

### 7.14.2. Integrity of the P18 wells

In the scope of the present study P18-2 is the only previously abandoned well. The lowermost abandonment plug is very thin and actually positioned below the primary caprock. In case the CO<sub>2</sub> in the reservoir will dissolve present (connate) water, the aqueous CO<sub>2</sub> is likely to interact with the cement sheath and carbon steel casing above this plug. In a timeframe of years to decades, the lateral barrier may be compromised, providing a pathway into the interior casing leading to higher levels, bypassing both the primary and secondary caprock. Given the poor quality of the annular cement sheath along the entire well, leakage pathways through the annulus cannot be excluded.

## Feasibility study P18

---

As described in sections 7.12 and 7.13, most of the P18 wells show questionable cement sheath quality at caprock level from CBL data (i.e. P18-2A1, P18-2A3, P18-2A6, P18-6A7) or lacked data to positively assess these (i.e. P18-2A6st, P18-4A2, P18-6A7). Even if CBL showed good bonding, the evaluated data was acquired prior to production, while bonding could have deteriorated as a result of induced temperature or pressure loading cycles during the production stage. Moreover, CBLs are unable to see thin channels along the material interface and, therefore, even good signal response does not necessarily imply full isolation. In order to prepare the accessible wells for CO<sub>2</sub> storage, cement sheaths should be verified with adequate techniques and if required remediated.

### 7.15. Conclusions and recommendations

From the perspective of well integrity, the feasibility of CO<sub>2</sub> storage in nearly depleted gas fields, is primarily determined by the accessibility of the wells penetrating the prospective storage reservoir. In the P18 reservoir blocks, only the P18-2 well was previously abandoned. The lack of a cement abandonment plug at caprock level and the poor quality of the annular cement, cause the P18-2 well in its current state to be unsuitable for CO<sub>2</sub> storage application. In order to improve the quality of this well, it is required to re-enter the well, which is technical feasible according to TAQA. The existing cement plugs should then be drilled out and an abandonment plug of sufficient length should be positioned across the primary and/or secondary caprock. Since cement-to-casing bonding is poor, it is recommended to place pancake-type abandonment plugs (as described in section 7.15.2). Special attention is drawn to the sidetracked P18-2A6 well. From the limited available data it is uncertain how exactly the parent hole was suspended. It seems that the current layout is unsatisfactory for CO<sub>2</sub> storage. Moreover, since the parent well forms the only penetration to the P18-2 III block, it might be beneficial to not only properly abandon the parent well, but actually use it for CO<sub>2</sub> injection in that block in order to mitigate large pressure differences between the reservoir blocks. This would require adequate abandonment of the P18-2A6st sidetrack and fishing of the whipstock. Subsequently, the P18-2A6 parent well needs to be recompleted to enable CO<sub>2</sub> injection.

#### 7.15.1. Remediation and mitigation

When considering wells for CO<sub>2</sub> injection it is recommended to check the packer operating envelope against CO<sub>2</sub> injection scenarios by performing a tubing stress analysis and, if required, workover to be performed. Furthermore, potential elastomers and wellhead configuration should also be verified and adapted where required. Moreover, it is suggested to adjust completion materials (tubing, tubing hanger and packer) to corrosive circumstances, where applicable. Most of the wells show questionable cement sheath quality at caprock level or lacked data to verify this. Inadequate primary cement imposes a risk to long-term integrity, but could also affect the operational phase. With respect to CO<sub>2</sub> injection and especially long-term containment, it is recommended to re-evaluate the cement sheath quality at least over caprock level by checking annular pressures or running cement bond logs over the intervals in question. Even when subsequent logging showed good bonding, temperature and pressure loading during production could have adversely affected the cement quality. If verification gives cause for remediation, e.g. cement or polymer squeezing should be considered.

### 7.15.2. Abandonment

For P18 all wells are still accessible. P18-2 requires re-abandonment, while all other wells will need abandonment in the future. For these wells abandonment can be designed specifically for CO<sub>2</sub> storage. After the most optimal injection well would be selected, the objectives for the other wells also need to be defined. Although forming a potential conduit to the surface, wells also form an invaluable source of information from the reservoirs. Serious thought should be directed at using specific wells for monitoring purposes, equipped with measurement devices.

At present, there are two general options to permanently seal a wellbore for CO<sub>2</sub> containment. If the quality of the primary cement sheath is ensured over critical intervals, traditional abandonment plugs can be positioned and tested at caprock level. Alternatively, and especially in the case of questionable cement sheaths, pancake plugs can be used at caprock level. This would involve milling out of the casing, annular cement and part of the formation, followed by placement of cement in the cavity. This procedure would effectively reduce the number of material interfaces, which could form potential migration pathways. However, this operation may pose difficulty, particularly in horizontal or strongly deviated wells. Both of these options should be accompanied by additional plugs higher up the well, according to common practice and as prescribed by governing abandonment regulations.

### 7.16. References

- Barclay, I., Pellenberg, J., Tettero, F., Pfeiffer, J., Slater, H., Staal, T., Stiles, D., Tilling, G., Whitney, C., 2002. The beginning of the end: A review of abandonment and decommissioning practices. Oilfield Review, winter 2001/2002, Schlumberger, UK.
- Barlet-Gouédard, V., Rimmelé, G., Goffé, B., Porcherie, O., 2006. Mitigation strategies for the risk of CO<sub>2</sub> migration through wellbores, IADC/SPE Drilling Conference, Miami, USA, February 2006 SPE paper 98924.
- Bruckdorfer, R.A., 1986. Carbon dioxide corrosion in oilfield cements. SPE Rocky Mountain Regional Meeting, May 19-21 1986, Billings, Montana, SPE-15176.
- Cailly, B., Le Thiez, P., Egermann, P., Audibert, A., Vidal-Gilbert, S., Longaygue, X., 2005. Geological Storage of CO<sub>2</sub>: A State-of-the-Art of Injection Processes and Technologies, Oil & Gas Science and Technology – Rev. IFP, Vol. 60, No. 3, pp. 517-525
- Carey, J.W., Wigand, M., Chipera, S., Gabriel, G. W., Pawar, R., Lichtner, P.C., Wehner, S.C., Raines, M.A., Guthrie Jr., G. D., 2007. Analysis and performance of oil well cement with 30 years of CO<sub>2</sub> exposure from the SACROC unit, West Texas, USA, Internat. J. of Greenhouse Gas Contr., 75–85.
- Gasda, S.E., S. Bachu, and M.A. Celia, 2004. The Potential for CO<sub>2</sub> Leakage from Storage Sites in Geological Media: Analysis of Well Distribution in Mature Sedimentary Basins. Environ. Geol., 46 (6-7), 707-720
- IEA Greenhouse Gas R&D Programme (IEA GHG), 2009. Long Term Integrity of CO<sub>2</sub> Storage – Well Abandonment, 2009/08, July 2009.
- Pruess, K., 2005. Numerical Simulations Show Potential for Strong Non-isothermal Effects During Fluid Leakage from a Geologic Disposal Reservoir for CO<sub>2</sub>, In: Dynamics of Fluids and Transport in Fractured Rock, B. Faybishenko, P.A. Witherspoon and J. Gale (eds.), Geophysical Monograph 162, 81–89
- Ravi, K., Bosma, M., Gastbled, O., 2002. Safe and Economic Gas Wells through Cement Design for Life of the Well. SPE Gas Technology Symposium, 30 April - 2 May 2002, Calgary. SPE-75700.
- Shen, J.C. and Pye, D.S., 1989. Effects of CO<sub>2</sub> attack on cement in high-temperature applications. SPE/IADC Drilling Conference, February 28 – March 3 1989, New Orleans, Louisiana, SPE/IADC-18618.
- Scherer, G.W., Celia, M.A., Prévost, J.-H., Bachu, S., Bruant, R., Duguid, A., Fuller, R., Gasda, S.E., Radonjic, M., Vichit-Vadakan, W., 2005. Leakage of CO<sub>2</sub> through abandoned wells: role of corrosion of cement. In: D.C. Thomas & S.M. Benson (eds.): Carbon Dioxide Capture for Storage in Deep Geologic Formations, Vol. 2, pp. 827-848.



## 8. Migration path study

### 8.1. Introduction

In order to assess the risk of migration of CO<sub>2</sub> through the overburden, an analysis is conducted to identify possible secondary containment and migration paths.

A static overburden model was assembled, based on both 2D and 3D seismic surveys and well information. On the basis of the overburden model and the selected migration scenarios, an evaluation of possible migration pathways was developed.

### 8.2. Available data and workflow

A geological model was constructed with Petrel modelling software (Schlumberger). The model comprises an area with a 14 km minimum radius surrounding the P18 gas field. In vertical direction the model spans the total overburden of the reservoir.

The workflow for building the model is described in *CATO-2-WP3.1-Geological report P18 (December 2010)*. In brief: Seismic interpretation of the overburden was performed, and subsequently the model was built on the basis of a fault model with a grid cell size of 250m x 250m. The model was converted from time to depth, and tied to the wells.

**Feasibility study P18**

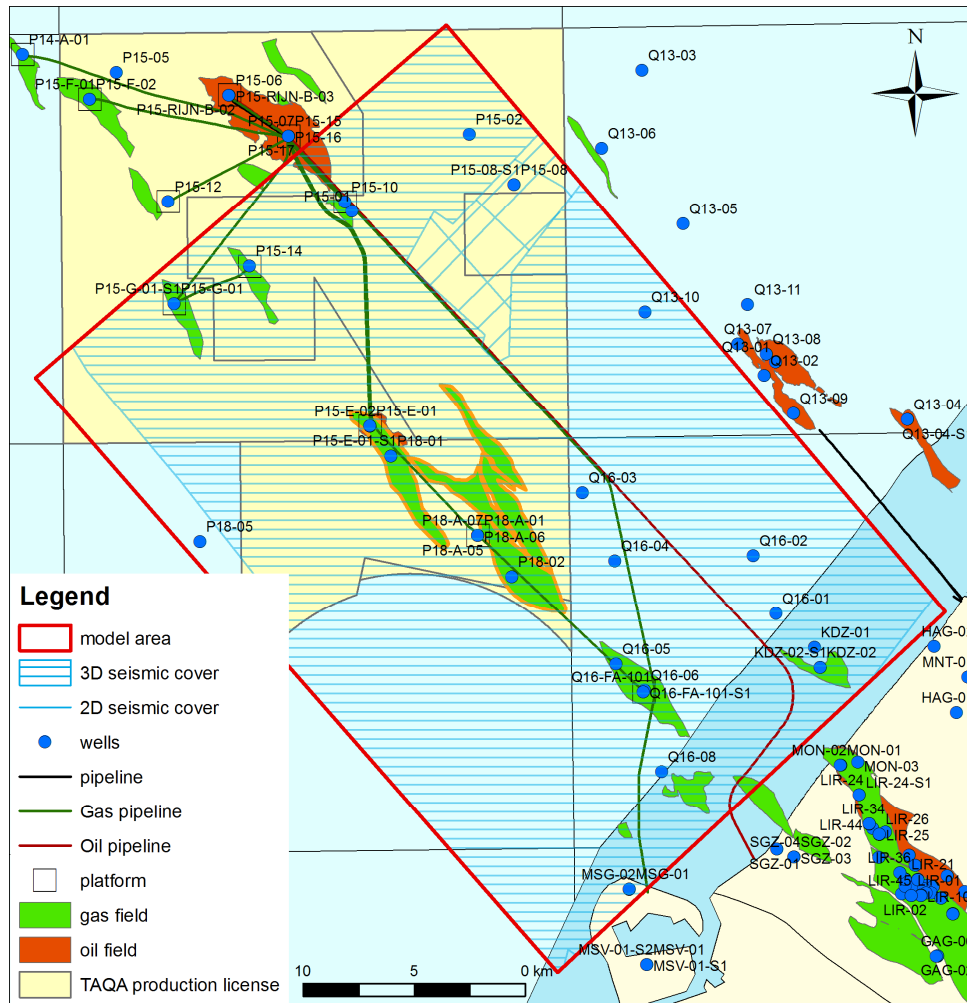


Figure 8.1: Location map of P18 model area. Target P18 gas fields are indicated with an orange boundary.

### 8.3. Geological model of the P18 Bunter reservoir and overburden

#### 8.3.1. Field description

The P18 gas field is located in the P18 block in the Dutch North Sea, approximately 20 km North West of the coastline. The gas field was discovered in 1989 by the P18-02 exploration well, which found the Triassic Buntsandstein gas bearing. Production started in 1993. The 3 separate accumulations of the P18 gas field are being produced by a total of 6 production wells. The current operator of the field is TAQA Offshore B.V.

#### Reservoir

The Main Buntsandstein consists of several successive formations (Table 28). The producing interval is limited to the Hardegsen and Detfurth formation. The combined thickness is approximately 100 m, with an average porosity of around 10%. Average permeabilities range from 2-200 mD. The depth of the reservoir ranges approx. between 3200 m and 3600 m.

**Feasibility study P18**

Table 28: General data on Main Buntsandstein Subgroup sandstones at the P18 location.

Formation	Porosity	Thickness
Hardeggen Fm.	10 % – 12 %	100 m (combined thickness)
Detfurth Fm.	9 % - 11 %	
Volpriehausen Fm.	5 %	100 m

**Seal**

The primary seal of the P18 reservoirs consists of siltstones, claystones, evaporites and dolostones of the Solling Claystone Member, the Röt formation, the Muschelkalk formation, and the Keuper formation. These formations span a total thickness of approximately 155 m.

**8.3.2. Overburden**

Directly above the primary seal, as identified in section 8.3.1, a thick succession of marine claystones, siltstones and marls is present. These sediments have excellent sealing quality and belong to the Altena Group (Jurassic age). In the P18-02 well (Figure 8.2), the Altena Group has a thickness of approx. 500 m.

The Altena Group is successively overlain by:

- The Schieland Group, which consists of shales and (stacked) channel sands of the Nieuwekerk Fm. (Delft sandstone equivalent). The lateral continuity of the individual sandbodies (thickness 2-5m) is probably very limited.
- Lower Cretaceous Rijnland Group, which consist of marine sandstones, shales and marls. At the base of the Rijnland Group, the Rijn / Rijswijk sandstone is present. This sandstone is widely distributed in the P18 area. It is also known for its oil (P15) and gas (onshore) accumulations within the West Netherlands Basin. The sandstones are interpreted as transgressive sheet sands, with good lateral continuity. In the upper part of the Rijnland succession, the Holland Greensand is present. It consists of argillaceous sands and silts. The distribution is limited to the southern margin of the West Netherlands Basin. Although the Holland Greensand has good lateral continuity, permeability is in general low.
- Upper Cretaceous Chalk Group, which consist at the base of the formation of sands and marls and a thick layer (900 m) of limestones (Chalk). The distribution of the basal Texel Greensand is limited to the southern basin margin.
- The North Sea Group, which consists of siliciclastic sediments. Two major aquifers can be distinguish; the Dongen sand, a basal transgressive sandstone, and the marine Brussels sand.



Feasibility study P18

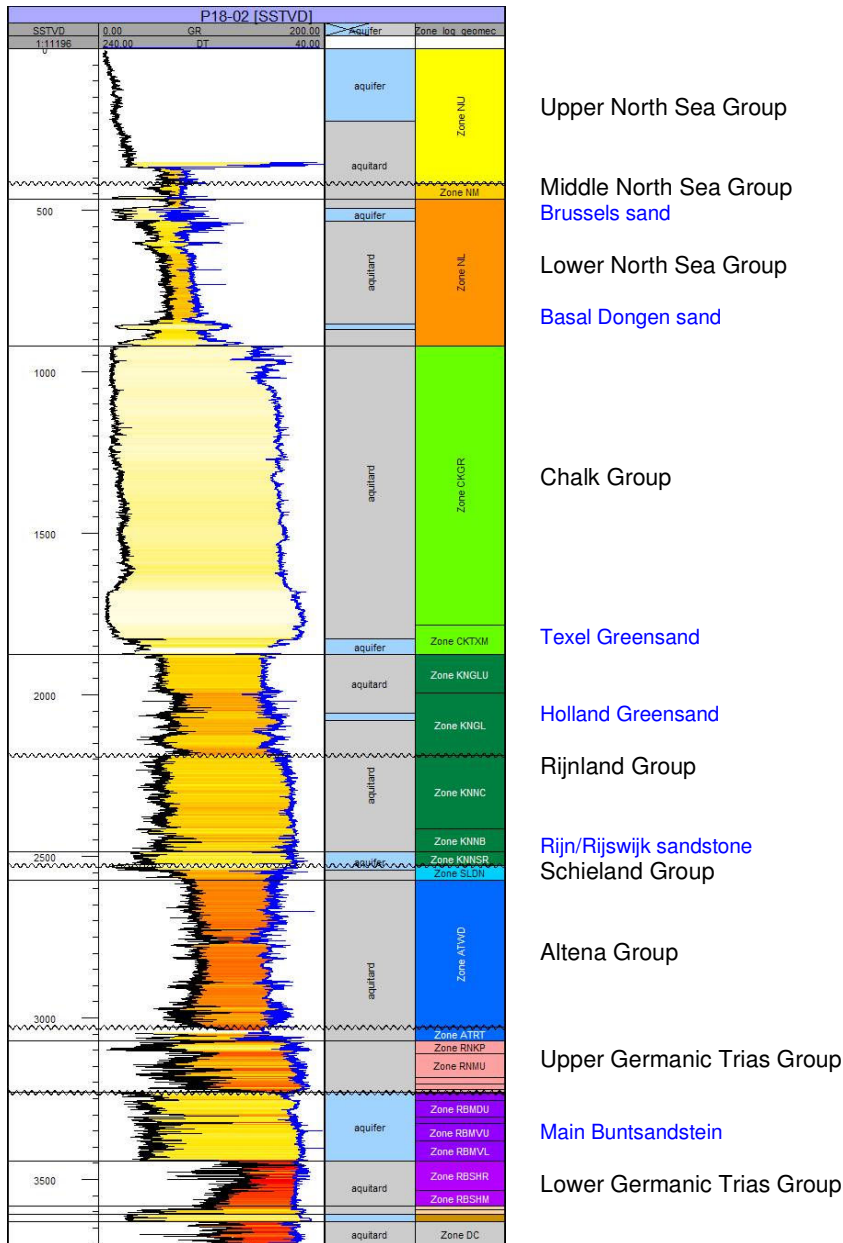


Figure 8.2: Composite well log (GR, DT) of P18-02 with main stratigraphic units and aquifer intervals

### 8.3.3. Faults

Faults present at reservoir level (Buntsandstein) in general continue till the Schieland group (white line) or base Rijnland Group (dark green line in Figure 8.3). Late Cretaceous inversion caused faulting of the sediments above the Base Cretaceous Unconformity (base Rijnland) These faults (dashed lines Figure 8.3) have limited displacement, but continue to the Upper North Sea Group.

**Feasibility study P18**

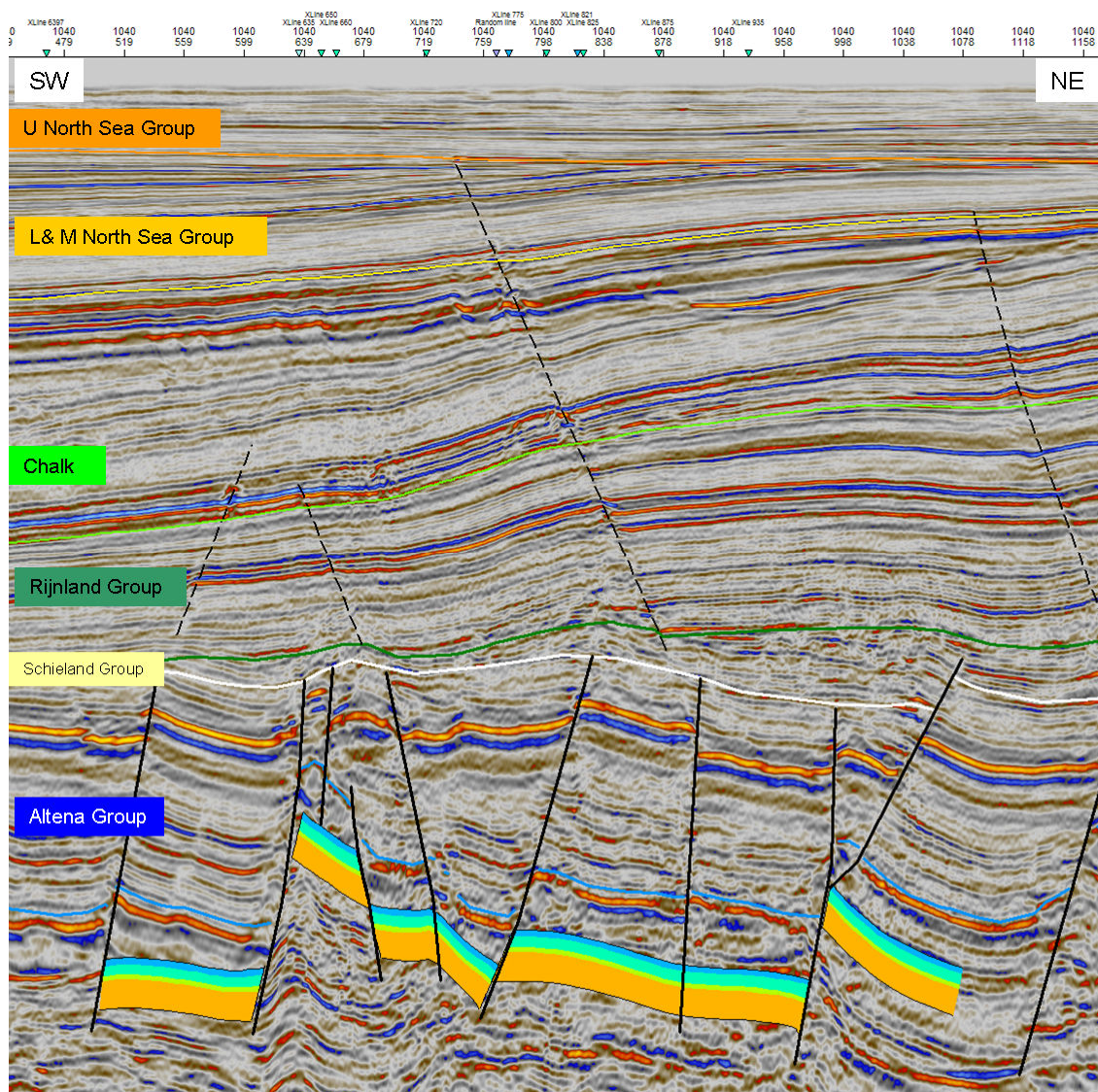


Figure 8.3: Seismic cross-section (inline 1040 of P15P18 seismic cube) through the P18 field, displaying the reservoir interval (coloured layering), the main bounding faults to the reservoirs (bold lines), the main stratigraphic units in the overburden and the faults in the overburden (dashed)

## 8.4. Migration scenarios

For the qualitative analysis three migration scenarios will be considered:

1. Aquifer spill reservoir:
  - a. Buntsandstein
2. Induced fracture caprock:
  - a. Migration into Rijn/Rijswijk sandstone
3. Wellbore shortcut:
  - a. Migration into Rijn/Rijswijk sandstone
  - b. Migration into Holland Greensand
  - c. Migration into Texel Greensand
  - d. Migration into Dongen & Brussel sandstone

### 8.4.1. Methods

Possible CO<sub>2</sub> migrations pathways were analyzed using the rapid trapping assessment tool PetroCharge Express of IES. With this tool a rapid analysis of the migration pathways based on the layer geometry is performed. The layer geometry was provided by the exported horizons from Petrel (regional scale model). The program uses the input top layer as bounding elements assuming these layers to be impermeable. Although in reality the layers are not completely impermeable the goal is to create a concept model from which migration routes within the layer can be deducted.

It should be noted that PetroCharge only looks at the geometry and does not describe various other aspects of flow. It was therefore decided to “inject” unreasonable large amounts of CO<sub>2</sub> within the considered leakage scenarios and to look at the trapping mechanisms in a worst case, when all other processes fail.

### 8.4.2. Results

#### Migration scenario: Buntsandstein

In case of “overfilling” the gas reservoir with CO<sub>2</sub> it might be possible that the CO<sub>2</sub> will pass by the original closure defined by the initial gas water contact. (GWC).

- Overfilling the P18-2 main compartment could lead to migration towards the Q16-4 structure (Figure 8.4, arrow 1) and the P16-FA field (Figure 8.4, arrow 4)
- Overfilling the P18-6 compartment could lead to migration towards the P15-10 field (Figure 8.4, arrow 2).
- Overfilling the P18-4 compartment in combination with migration along faults could lead to migration towards the P15-E and P15-14 field (Figure 8.4, arrow 3).

It must be mentioned that the structure drilled by the (dry) exploration wells Q16-04 and Q16-03, only minor amounts of gas were encountered. If the containment were to fail by a mechanism describes above, the most probable failure would that be of a sideseal in combination with reservoir juxtaposition with Jurassic sandstones from for instance the Nieuwekerk Formation.

**Feasibility study P18**

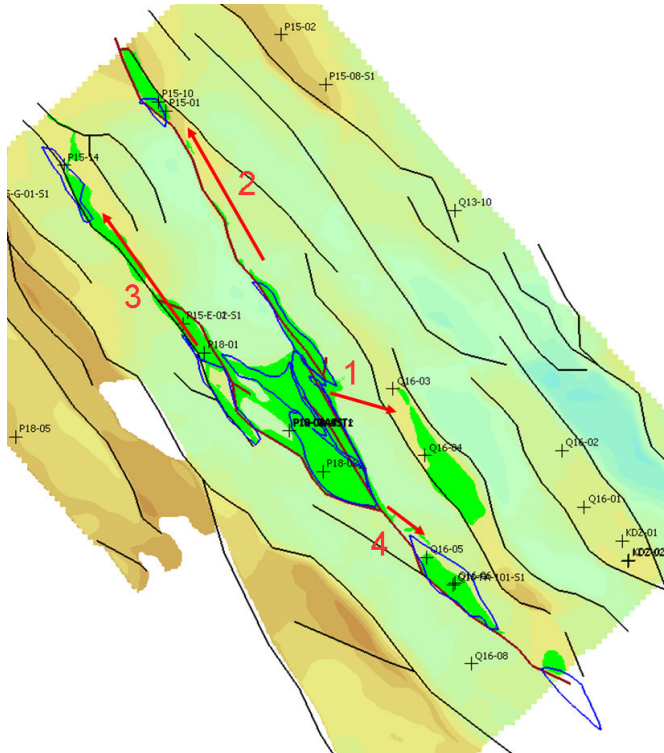


Figure 8.4 Structure map of Top Buntsandstein. Black lines indicate faults. Also shown are boundaries of gas accumulations and location of wells.

**Migration scenario: Rijn/Rijswijk sandstone**

In case of fault reactivation or shortcut via a wellbore, CO<sub>2</sub> can hypothetically migrate into the Rijn/Rijswijk sandstone aquifer.

- Spill originating from wells P18-A-01, P18-A-06 , P18-A-06-S1, P18-A-07 will migrate towards Q16-03 & Q16-04 structure (Figure 8.5, arrow 1).
- Spill originating from wells P18-02, P18-A-03, P18-A-05 will migrate towards Q16-FA structure (Figure 8.5, arrow 2).
- Spill originating from P18-A-02 well will migrate towards P15-9 (E) structure (Figure 8.5, arrow 3).

**Migration scenario: Holland Greensand**

In case of a shortcut via a wellbore, CO<sub>2</sub> can hypothetically also migrate into the Holland Greensand aquifer

- Spill originating from wells P18-A-01, P18-A-03, P18-A-06 , P18-A-06-S1, P18-A-07 will migrate towards Q16-03, Q16-04 structure (Figure 8.6, arrow 1)
- Spill originating from wells P18-02, P18-A-05 will migrate towards Q16-FA structure (Figure 8.6, arrow 2)
- Spill originating from P18-A-02 well will migrate towards P15-9 (E) structure (Figure 8.6, arrow 3)

Feasibility study P18

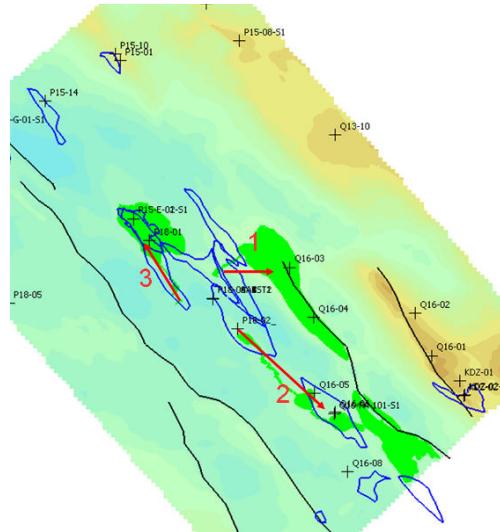


Figure 8.5: Structure map of the Base Rijnland Group. Black lines indicate faults. Also shown are boundaries of gas accumulations and location of wells.

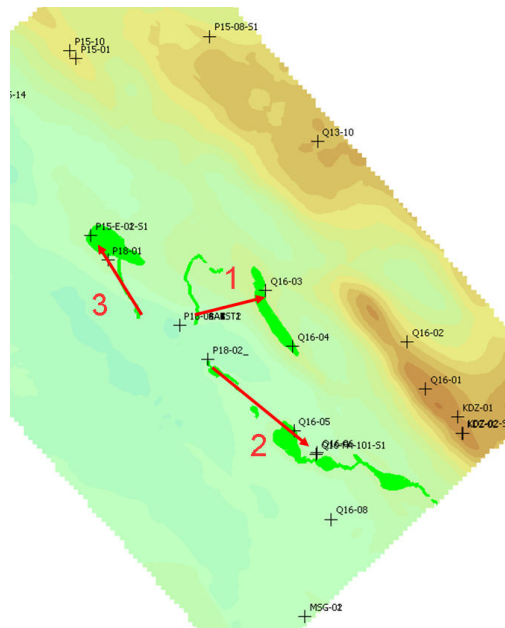


Figure 8.6: Structure map Holland Greensand.

**Feasibility study P18**

**Migration scenario: Texel Greensand**

In case of a shortcut via a wellbore, CO<sub>2</sub> can hypothetically migrate into the Texel Greensand aquifer

- Spill originating from P18-A production wells will migrate towards Q16-3 structure and finally Q16-02 (Figure 8.7, arrow 1).
- Spill from P18-02 well will migrate towards Q16-FA structure and finally Q16-01 (Figure 8.7, arrow 2).

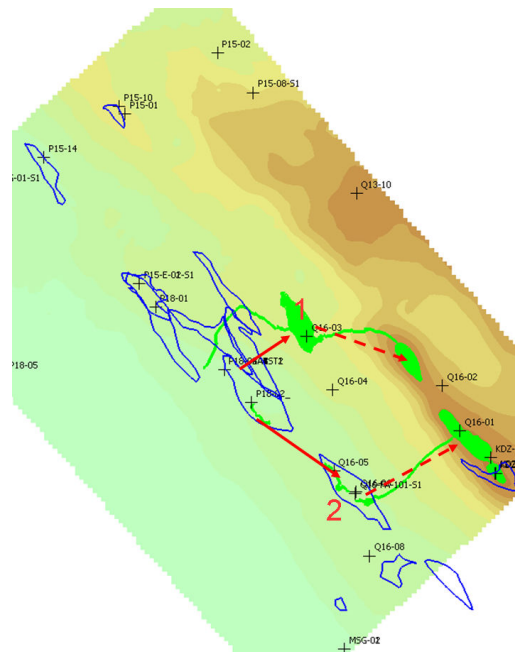


Figure 8.7: Structure map base Chalk Group.

**Migration scenario: Dongen sand & Brussel sandstone**

In case of shortcut via a wellbore, CO<sub>2</sub> can hypothetically migrate into the North Sea Group aquifer

- Spill originating from P18-A production wells will migrate towards Q13-10 structure (Figure 8.8, arrow 2).
- Spill from P18-02 well will migrate towards Q16-02 structure (Figure 8.8, arrow 2)

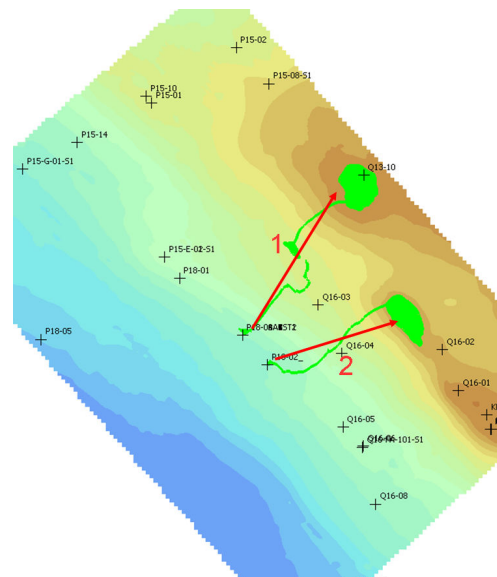


Figure 8.8: Structure map base North Sea Group.

## 8.5. Present day hydrocarbon migration

Inspection of the overburden revealed the possible existence of shallow gas pockets. (*CATO-2-WP3.1-D01-Geological report P18 (December 2010)*). The gas most probably is sourced from Jurassic Posidonia shales (van Baalen, 2000). The Posidonia shales are situated stratigraphically above the Bunter reservoir and seal, so this hydrocarbon migration is no proof of seal failure/leakage of the P18 Bunter reservoir.

Figure 8.9 shows a seismic section of the overburden, to illustrate hydrocarbon migration, and to illustrate a possible migration pathway for CO<sub>2</sub>.

Gas is sourced from the Posidonia shale (strong reflector at the base of the lowest arrow), and migrates via a fault into the sands of the North Sea Group. The red ellipses indicate bright spots, which suggest the presence of gas. Migration is also possible within the Brussels sand, indicated by the arrows in Figure 8.9. At the location where the Brussels sand toplaps against the Upper North Sea Group (Mid Miocene Unconformity, orange line), an increase of amplitudes is observed, which suggest migration from the Brussels sand into the Upper North Sea Group.

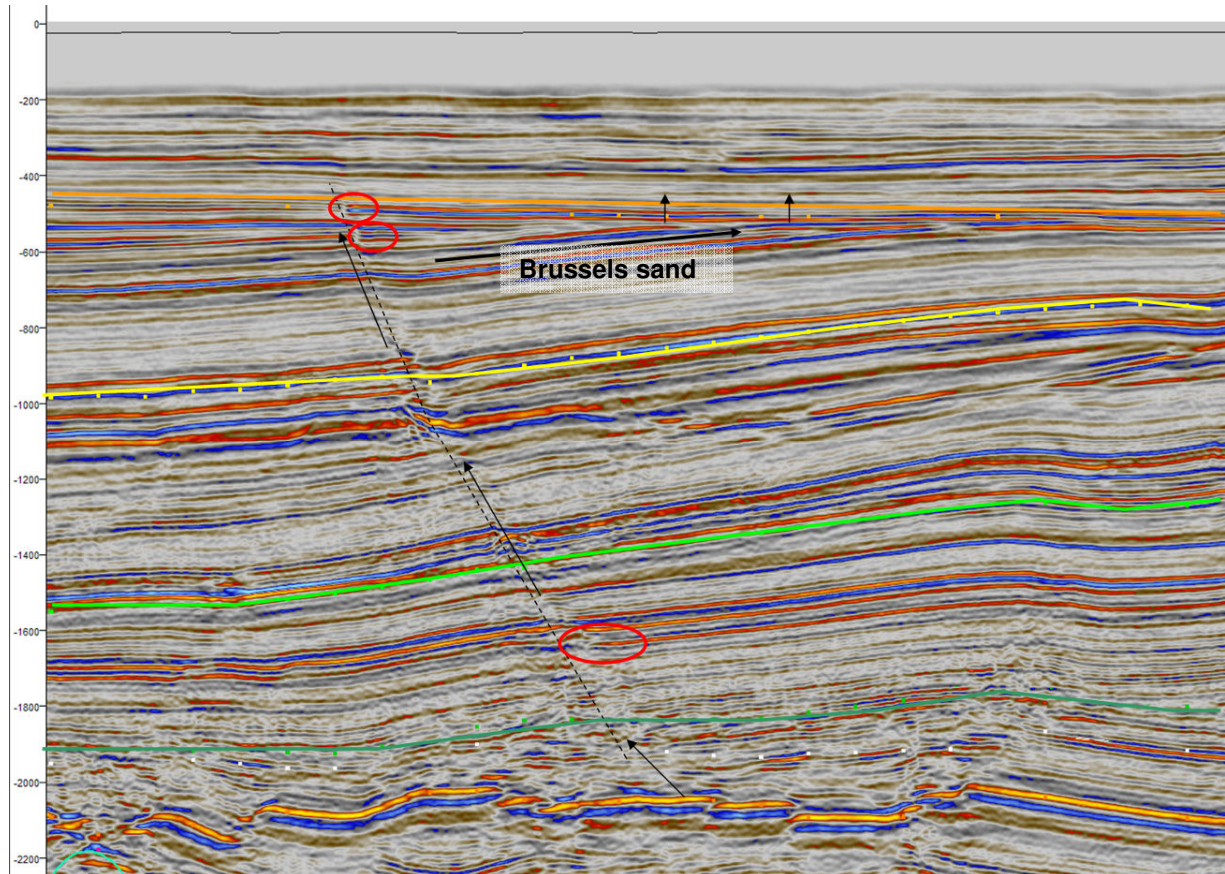


Figure 8.9: Seismic section of the P18 overburden. Arrows indicate hydrocarbon migration along a fault (dashed line). Red ellipses mark bright spots on the right side of the fault. Dark green line: base Rijnland (BCU), bright green line: base Chalk, yellow line: base North Sea, orange line: base Upper North Sea (MMU).

## 8.6. Conclusions

A Petrel model of the overburden has been constructed, which is based on public available data and data provided by TAQA. Based on the geological model and selected hypothetical migration scenarios, a qualitative evaluation of the possible pathways was developed. The main conclusions are that hypothetical migration in the Buntsandstein, caused by overfilling the reservoir, the CO<sub>2</sub> remain trapped within the aquifer and finally will migrate towards the adjacent gas reservoirs. Hypothetical migration of CO<sub>2</sub> in the aquifers of the overburden, caused by a shortcut along the wellbore, will remain trapped within the aquifers. However, migration of CO<sub>2</sub> along faults in the overburden (above the Altena Group) to a shallower aquifer level is not to be excluded.

Overall it can be stated that the most probable pathway to the surface of CO<sub>2</sub> stored in the P18 gasfield is via leaking wells, leaking directly into the atmosphere and not indirectly via pathways originating in deeper parts of the overburden.



## 8.7. Preliminary monitoring concept

### Introduction

This report is meant as input to establish the appropriate final monitoring concept for P18 and is based on the current state of knowledge of the field. This report should not be considered as the final monitoring plan to be submitted for the permit application.

#### 8.7.1. The Eon CCS project

### Introduction

Since 1993 high calorific gas has been produced from the P15 and P18 blocks, offshore the Netherlands. This is done from several platforms, among which the P18-A satellite platform, and the P15-ACD processing and accommodation structure, respectively lie 20 and 40 km NW of Rotterdam (Figure 8.10).

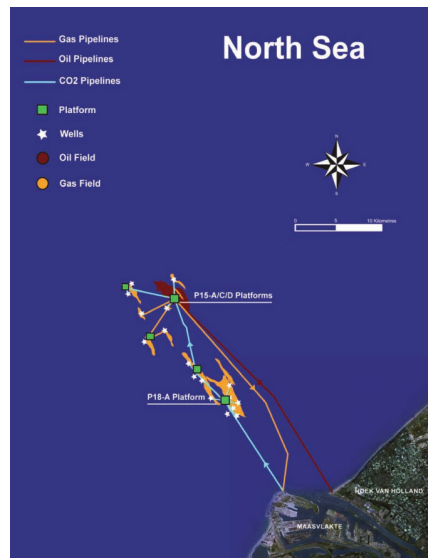


Figure 8.10: Location P15/P18 complex relative to the Dutch shore. Source: CO<sub>2</sub> offshore storage, deep under the Dutch North Sea, (image courtesy TAQA; TAQA, 2009)

The almost depleted gas reservoirs at P15 and P18 are considered suitable for CO<sub>2</sub> storage. They contained large amounts of natural gas under high pressures for millions of years. Furthermore, there is a lot of high quality geological data for these specific structures, to assist in safely storing CO<sub>2</sub>. They are relatively close to large CO<sub>2</sub> emitters and are located offshore, which would likely avoid complex permitting procedures. The CO<sub>2</sub> would be injected into a sandstone formation below impermeable layers of Triassic clay at over 3 km depth.

### Infrastructure

The P18 installation consists of a 4 legged steel jacket (Figure 8.11). Its primary function is the production and transfer of wet gas to the P15-D processing platform some 20 km further offshore (Figure 8.12).



Figure 8.11: P18-A Satellite platform. (Courtesy TAQA; TAQA, 2009)

The P15-ACD installation comprises two 6 legged steel jackets and one 4 legged steel jacket (Figure 8.12). Their functions are:

P15- A	Well production
P15-C	Oil processing and accommodation
P15-D	Gas and condensate processing, compression and transporting to shore, metering and control



Figure 8.12: P15-ACD Processing & Accommodation Platforms. (Courtesy TAQA; TAQA, 2009)

## Roadmap

Injection of CO<sub>2</sub> in the P18 and P15 fields is planned in several phases:

*Phase 1* - From the P18-A platform CO<sub>2</sub> can be injected into several depleted gas reservoirs using multiple injection wells. The combined theoretical storage capacity accessible from this platform amounts to around 41 million tonnes of CO<sub>2</sub>. The effective storage capacity will depend on the maximum permitted reservoir pressure.

*Phase 2* - After natural gas production ceases from the P18-A platform, the existing pipeline to P15-ACD can be used to transport CO<sub>2</sub> to this central facility from where CO<sub>2</sub> can be distributed to the P15 reservoirs, providing an additional 44 million tonnes of theoretical storage capacity.

**Feasibility study P18**

*Phase 3* - When natural gas throughput ceases completely, the 26 inch pipeline can be turned to CO<sub>2</sub> transport duty. The P15-ACD facility could then be used for many years to boost pressure to transport CO<sub>2</sub> north to other depleted gas reservoirs.

This report is solely related to phase 1 of the CO<sub>2</sub> storage project. For phase 1 the intention is to start injection into the P18-6 field, followed by the P18-4 and finally into the P18-2 field. For the Road project the storage capacity for the envisaged 11 Mtonnes CO<sub>2</sub> can be covered by the combination of P18-6 and P18-4.

**8.7.2. The proposed monitoring plan**

This proposed monitoring plan is based upon the EU storage directive (2009) and on the EU ETS directive (2009). Since the directives do not provide details on the format of such a monitoring plan, the EU has started to develop guidance documents. The currently proposed monitoring plan is based upon the (draft) guidance document 2 “Implementation of Directive 2009/31/EC on the Geological Storage of Carbon Dioxide” which is available for public consultation currently. This document has been developed by the European Commission with support from consultants and input from the Information Exchange Group established pursuant to Art. 27(2) of the CCS Directive. It builds on:

- The expertise and experience of the members of the Information Exchange Group, established under the CCS Directive, and the experts involved;
- The results of previous research, methodologies and suggested guidelines.

In the current EU guidance document 2 a global approach is provided for developing a monitoring plan for a storage site. The inventory of monitoring technologies in the document is based on existing literature, essentially the IPCC guidelines for National Greenhouse gas Inventories (2006), the IEA-GHG report (2004), the ASPEN report (2009) and the NSBTF report (2009) as prepared by TNO on behalf of the NSBTF.

The approach adopted in the Aspen report (2009) and the NSBTF report (2009) is inspired on the format for a monitoring plan as produced for the Barendrecht CO<sub>2</sub> storage project by Shell (Shell report, 2008).

Please note, that the proposed format is compliant with the more globally proposed workflow as proposed in the CO<sub>2</sub>QUALSTORE guideline (2010) summarized in Table 29.

Table 29: Workflow to prepare a preliminary monitoring plan and to initiate a baseline monitoring program (taken from the CO<sub>2</sub>QUALSTORE guideline (2010)).

<b>Preliminary monitoring plan. Initiate baseline monitoring program</b>	
Identify monitoring targets based on identified risks and uncertainties	List of proposed monitoring targets
Identify suitable measurement techniques for monitoring of identified targets	List of suggested measurement techniques
Differentiate between base case monitoring and contingency monitoring triggered by early warning signals	Preliminary base case and contingency monitoring programs
Plan and execute baseline monitoring program	Compilation of results from baseline monitoring activities

## 8.8. Geological background information

### 8.8.1. Structure

The reservoir structures comprise multiple compartments bounded by a system of NW-SE oriented faults forming horst and graben structures. The reservoir rocks are of Triassic age, belonging to the Bunter Sandstone ("Main Buntsandstein Subgroup", Van Adrichem Boogaert and Kouwe, 1994, Wong et al., 2007) (Figure 4), and consist of sandstones intercalated with thin layers of shale. The tops of the compartments lie at depths between 3175 m and 3455 m below sea-level (Figure 5).

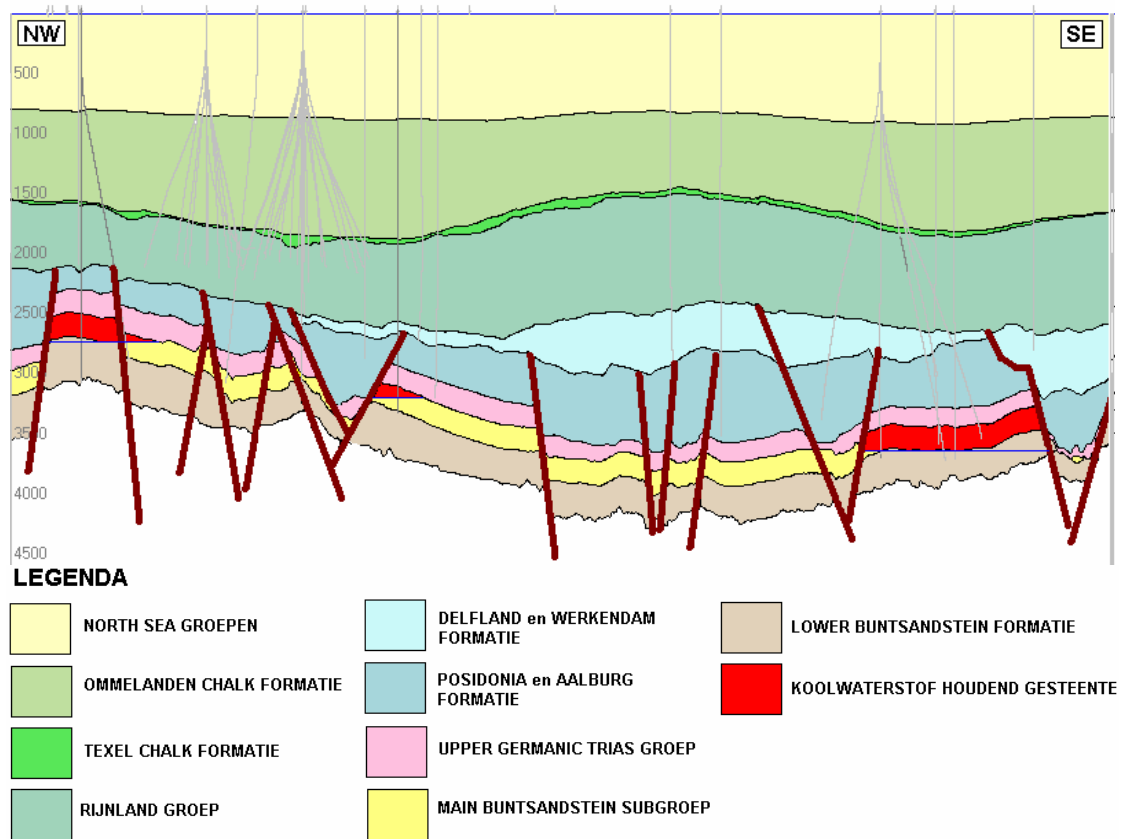


Figure 8.13: Geological cross-section of the P15 field, illustrating the stratigraphy and geological setting. Source: Winningsplan P18a, P18c & P15c.

The reservoir rocks were deposited in a typical desert environment with scarce but intense rainfall. The reservoir consists mainly of dune (aeolian) and river (fluvial) sediments. The aeolian sands have the best reservoir properties, comprising clean, well sorted sands with relatively low shale content.

The source rocks for the natural gas, present in the reservoir structures, are the coal layers from the underlying Carboniferous.

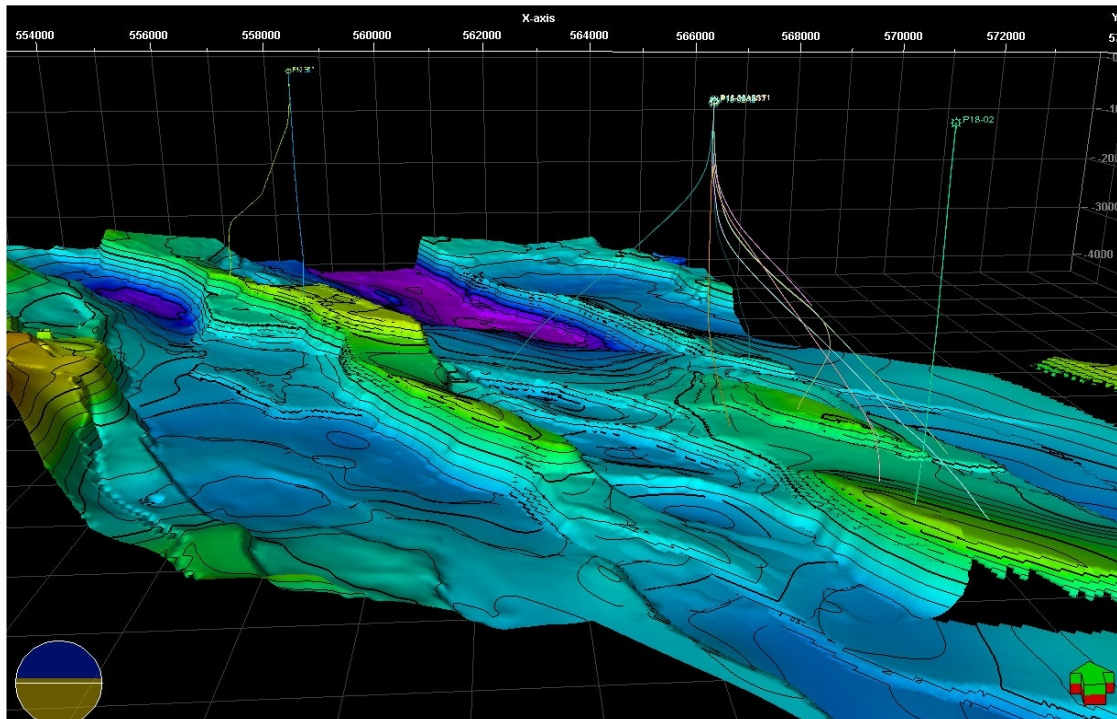


Figure 8.14: 3D view on the top Bunter from a geological model which is still under construction.

## 8.8.2. Reservoir properties

At P18 the Main Buntsandstein Subgroup consists of several units:

- The Hardeggen Fm.
- The Detfurth Fm.
- The Volpriehausen Fm.

Based on well log data the porosity in the Hardeggen Formation varies around 10-12% and in the Deturth Formation it is slightly lower at about 9-11%. Maximum porosities encountered in the clean sandy parts of both Formations are around 21 %. The combined thickness of both Formations is about 100 m and permeabilities range generally from 0.1 -100 mDarcy. The Volperiehausen has a much lower porosity, around 5%, and also lower permeability. The thickness of the Volperiehausen is around 100 m. Table 30 sums up some general data about these Formations at P18. The irreducible water content is around 15 to 20 % and the abandonment pressures for the compartments are about 20 to 30 bars.

Table 30: General data on Main Buntsandstein Subgroup sandstones at the P18 location.

Formation	Porosity	Thickness
Hardeggen Fm.	10 % – 12 %	100 m (combined thickness)
Detfurth Fm.	9 % - 11 %	
Volpriehausen Fm.	5 %	100 m

## Feasibility study P18

For the different reservoir compartments (i.e. P18-2, P18-4 and P18-6) an estimate has been made, based on the gas production history, of the total storage capacity per compartment (Table 31).

Table 31: General data on the compartments at P18.

Compartment	Initial conditions		CO <sub>2</sub> storage capacity (Mt)	Depleted by	wells
	bar	°C			
P18-2	355	126	32	2017	3
P18-4	340	117	8	2015	1
P18-6	364	117	1	2015	1

Much of the general information of the P18 field also applies to the P15 gas field (Table 32) although depletion dates were not readily available. The geological setting is the same. The platform infrastructure is more complex than that at the P18 location, which is merely a satellite platform.

Table 32: General data on the compartments at P15.

Compartment	Initial conditions		CO <sub>2</sub> storage capacity (Mt)	Depleted by	wells
	bar	°C			
P15-9	347	117	11	?	2
P15-10	272	104	1	?	1
P15-11	283	102	16	?	2
P15-12	301	112	2	?	1
P15-13	288	107	9	?	1
P15-14	334	107	2	?	1
P15-15	318	120	1	?	1
P15-16	290	109	1	?	1

### 8.8.3. Overburden properties

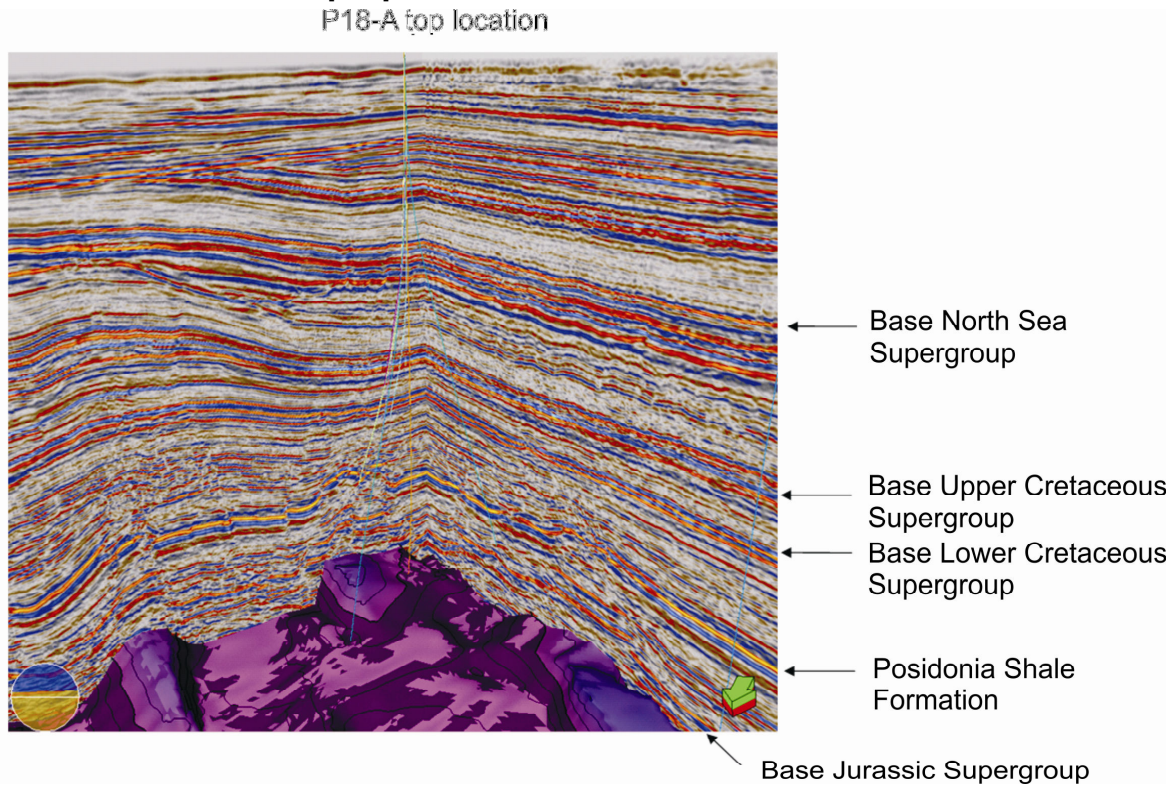


Figure 8.15: Seismic section of the overburden at P18-A. The surface represents the base of the Lower Germanic Trias Group (also base of the reservoir). Note the fractured nature of the Triassic and Jurassic sediments (up to the Posidonia Shale Formation) and the continuity of the Lower Cretaceous and younger sediments.

The overburden at P18-A is formed by several geological formations. The North Sea Supergroup, of Cenozoic age, is the shallowest stratigraphical unit and comprises mostly siliciclastic sediments, from approximately seabed to 1000 m depth. It encompasses the Lower, Middle and Upper North Sea Groups, the bases of which are marked by distinct unconformities. The lower group comprises Paleocene and Eocene strata, predominantly marine deposits, the middle group includes mainly Oligocene marine strata, and the upper group consists of the marine to continental Miocene and younger sediments. The North Sea Supergroup in the area of interest is unfaulted at seismic resolution scale. Clayey sequences are very abundant, especially in the lower parts of the North Sea Supergroup and could very well act as secondary seals. The presence of trap structures has not yet been investigated.

The North Sea Supergroup unconformably overlies the Upper Cretaceous Supergroup, which ranges from approximately 1000 m to 2400 m depth and in this area comprises the Ommelanden Formation, the Texel Formation and the Texel Greensand Member. During the Late Cretaceous, the influx of fine-grained clastics into the marine realm (Lower Cretaceous) diminished. A fairly uniform succession of marls and limestones of the Texel and Ommelanden Formations developed. These sediments have an earthy texture and are commonly known as 'chalk'. The sealing properties of these formations are questionable although this interval is largely unfaulted. The Lower Cretaceous Supergroup consists of the Holland Formation, the Vlieland Claystone Formation and Vlieland Sandstone Formation and ranges from approximately 2400 m to 3400 m

## Feasibility study P18

---

depth. In locations close to P18-A, some of the sandstone layers present in this interval are gas bearing, demonstrating the sealing capacity of various claystone intervals in this succession. In the area of interest the Lower Cretaceous is mainly unfaulted (on seismic resolution scale), improving the likelihood that layers in this level could indeed act as secondary seals. At P18-A the Jurassic Supergroup consists of the Nieuwerkerk Formation, Lower Werkendam Member, Posidonia Shale Formation, Aalburg Formation and the Sleen Formation and ranges in depth from approximately 3400 m to 3900 m. The Nieuwerkerk Formation predominantly comprises continental deposits, whereas the other formations consist of marine sediments mainly in the form of clays which could very well act as secondary (or even primary) seals. The primary seal is formed by clay layers from Triassic and lower Jurassic age (the Upper Germanic Trias and Altena Group). Faults are present in this primary seal, but these do appear to be sealing and in general do not penetrate the caprock further upwards than the Posidonia Shale Formation (Figure 6). Reservoir closure along the bounding faults is obtained by juxtaposition of shale layers of various ages and clay smear. These bounding faults do not continue further upward into the overburden than the shales of the Altena Group (see Chapter 3). Due to the sealing nature of the bounding faults there is no water drive in the compartments.

## 8.9. Risk assessment of P18

### 8.9.1. Introduction

For the P18 field a risk assessment has been carried out by Royal-Haskoning dd. July 7, 2010 in the form of a workshop. Below follows a summary of the identified subsurface related risks.

### 8.9.2. Summary of identified risks

The risks for migration out of the reservoir into the overburden or for leakage at the sea bottom are considered minimal for P18, which is a depleted gasfield with no active aquifer drive. The latter is demonstrated by the straight production P/z curves. Currently the reservoir is well below hydrostatic pressure.

As pointed out in the top seal and fault integrity study (Orlic et al, 2010), geomechanical-related risks of fracturing and fault re-activation are small and can be (partially) reduced by:

- Injecting CO<sub>2</sub> with bottom hole pressures (BHP) which are below fracturing condition.
- Avoid overpressurizing the reservoir above the initial pressure.
- Keeping a safe distance between the injection wells and faults to avoid direct charging of faults by injected CO<sub>2</sub> through natural or induced fractures. Wells closest to faults are wells P18-02A1, P18-02A6, P18-04A2 and P18-06A7ST1. The latter requires most caution, since the injectivity of the P18-06 reservoir is of the least quality.
- Managing thermal effects of injection

During injection, the potential for fault reactivation generally decreases providing that the CO<sub>2</sub> is not injected directly into the fault zone and the thermal effects of injection are negligible. The risk of induced hydro-fracturing increases in the later stage of CO<sub>2</sub> injection when the reservoir is almost re-pressurized to the initial pressure.

Based on the KNMI database of recorded induced seismic events associated with hydrocarbon production in the Netherlands, the P18 field was not seismically active during its production period. The detection limit of the KNMI seismic network was M2.5 until 1995 and M1-1.5 on Richter scale afterwards (Orlic et al., 2010). No major seismic activity is therefore expected.



## Feasibility study P18

---

The caprock has proved to be gas tight based on the production history. However, there are indications on seismic data of natural shallow gas up to the seabottom along and near faults (see Chapter 3). The origin of the shallow gas is unknown. Considering the excellent sealing quality of the primary seal of the P18 reservoir, and the difference in age and dip of the faults in layers above and below the Altena Group, it is unlikely that these potential shallow gas accumulations are related to the P18 reservoirs from which gas is produced. More likely, it originates from either the Posidonia Shale Formation in the overlying Altena Group, which is responsible for charging many Upper Jurassic and lower Cretaceous reservoirs in the vicinity or from shallower layers by biogenic processes.

Furthermore, since the properties of CO<sub>2</sub>, especially in combination with connate water, are different from methane, it means that dissolution and precipitation of minerals, respectively creating or blocking migration pathways, needs to be thoroughly investigated (see Chapter 5).

Furthermore the possibility of fault reactivation needs attention, since the reservoir has been depressured (depleted) and CO<sub>2</sub> injection would involve repressuring. On top of that a possible geochemical-geomechanical interaction must be investigated (see Chapter 6). The modeling results show that short-term mineralogical and porosity changes, induced by dissolved CO<sub>2</sub> and corresponding pH decrease, are negligible. On the long-term (thousands of years) mineral reactions will result in a porosity decrease of 0.3 percentage point (pp) for the reservoir and a porosity increase of 0.2 pp for the cap rock. The presence of O<sub>2</sub> as an impurity in the CO<sub>2</sub> stream does not seem to have significant consequences regarding the short-, mid- and long-term geochemical effects of CO<sub>2</sub> storage (see Chapter 5).

The injectivity of the reservoir is considered to be especially an issue in the P18-6 field (see Chapter 4). The main reservoir is heterogeneous with potentially rapid lateral facies changes typical of a fluvial setting. This may lead to problems during injection such as local pressure build-up. This will be noticed immediately by monitoring the required injection pressure. Apart from geological heterogeneity of the reservoir, near wellbore effects such as salt precipitation or Joule Thompson effects (like freezing) of the CO<sub>2</sub> due to adiabatic expansion do not appear to cause uncontrollable risks (see Chapter 4). The latter may give rise to thermal fracturing. The expectation is, that this will only influence a relatively small part of the reservoir close to the wellbore (see Chapter 4)

In terms of migration of CO<sub>2</sub> into the overburden the main potential pathways considered are along existing or new wellbores. A more detailed analysis of the state of the existing wells has been investigated (see Chapter 7). Characterization and proper abandonment of these wells followed by well integrity measurements is necessary. In the worst case this may require a work-over of one or more of the wells.

Laterally the reservoir is constrained by a structural closure and sealing faults (Orlic et al., 2010). Migration within the reservoir is therefore not a crucial parameter to monitor. However, it does provide input for the predictive simulation models demonstrating a proper understanding of the reservoir and associated flow processes.

## 8.10. Development monitoring plan

### 8.10.1. Introduction

The starting point for developing the monitoring report is an adequate characterization and risk assessment. The general requirements for both site characterization and risk assessment are given in the EC Storage Directive and its Annexes (2009) with further details in the EU guidance

## Feasibility study P18

---

documents (2010). The monitoring report in its turn must be related to preventive and corrective measures.

Therefore in the adopted template in this report potential risks, monitoring techniques and mitigation measures are linked together.

With respect to timing this report describes a 'workflow' for monitoring activities during the pre-injection (site qualification), injection (operation), post-injection (closure and post-closure) phases and after transfer of responsibility (long-term stewardship). However, since monitoring in the different stages of a project is not fundamentally different, they do not play a major role. The philosophy of the monitoring plan is that it must be: complete, transparent, consistent, and verifiable.

### Monitoring categories

Monitoring serves several important purposes, which are confirming containment of CO<sub>2</sub>, alerting for corrective measures in case of increased leakage risk and gathering evidence for the long-term containment of CO<sub>2</sub>.

This can be achieved either by measuring the absence of any leakage through direct detection methods, or by verifying indirectly that the CO<sub>2</sub> is behaving as expected in the reservoir based on static and dynamic modeling and updating thereof corroborated by monitoring data. The main challenge for measuring absence of any leakage consists of spatial and temporal coverage of the monitoring method, i.e. "Where and when do we need to monitor in order to be sure that no leakage occurs". The strategy should therefore be based on identified risks.

For the indirect model-based monitoring the emphasis is more on scenario confirmation. As long as predictive models are behaving in agreement with monitoring data, the understanding of both the processes occurring and the behavior of the storage complex can be considered sufficient. In case of deviations, one should find the causes of the deviations and where necessary recalibrate the models. If however the deviations fall well beyond the uncertainty ranges of the predictive models, then additional monitoring and possibly contingency measures need to be taken.

In practice often a combination of approaches will be required and the optimal monitoring plan will be guided by the risk assessment and the site characterization.

Following the NSBTF (2009) and the draft EU guidance documents (2010), the following categories for monitoring are identified:

1. Mandatory (in any case for all sites) monitoring: A number of parameters to be monitored is mandatory based on the storage directive.
2. Required (site specific) monitoring: This monitoring group is directed to gathering evidence for containment in the reservoir and to demonstrate integrity of seal, fault and wells in case of regular development.
3. Optional contingency monitoring: The third group refers to a contingency monitoring system which will only be installed if irregularities show up. In the Storage directive a "significant irregularity" is defined as '...any irregularity in the injection or storage operations or in the condition of the storage complex itself, which implies the risk of a leakage or risk to the environment or human health'.

Note, that these three categories as such have not been implemented in Dutch legislation yet, therefore the term mandatory should be read as "mandatory following the EU directive". Similar for the term required, which is not as such defined in legislation. Required in the context of this report means a preliminary proposal of essentially risk-based monitoring with the current state of knowledge.

## Feasibility study P18

---

The quantification of a leakage at the seabottom for ETS purposes is considered as part of the contingency monitoring. Quantitative monitoring for ETS will only be required, if there is an indication of leakage.

For the North Sea a sound strategy suggested by the NSBTF (2009) would be to detect leakage to the surface by geophysical methods like seismic data (detection of gas chimneys) or sea-bottom echo-sounding (detection of pockmarks) and then sample these leakage areas for direct CO<sub>2</sub> detection repeatedly. Based on the sampling profiles an estimate can be made of leakage rates in time for the area. In case of wellbore leakages an additional monitoring program in and around the well is suggested.

### Procedure monitoring plan

A monitoring plan drawn up by the operator should meet the following requirements according to the Storage Directive:

#### Initial plan

The monitoring plan shall provide details of the monitoring to be deployed at the main stages of the project, including baseline, operational and post-closure monitoring.

The following shall be specified for each phase:

1. Parameters monitored;
2. Monitoring technology employed and justification for technology choice;
3. Monitoring locations and spatial sampling rationale;
4. Frequency of application and temporal sampling rationale.

The parameters to be monitored are identified so as to fulfil the purposes of monitoring. However, the plan shall in any case include continuous or intermittent monitoring of the following items:

1. Fugitive emissions of CO<sub>2</sub> at the injection facility;
2. CO<sub>2</sub> volumetric flow at injection wellheads;
3. CO<sub>2</sub> pressure and temperature at injection wellheads (to determine mass flow);
4. Chemical analysis of the injected material;
5. Reservoir temperature and pressure (to determine CO<sub>2</sub> phase behaviour and state).

The choice of monitoring technology shall be based on best practice available at the time of design.

The following options shall be considered and used as appropriate:

1. Technologies that can detect the presence, location and migration paths of CO<sub>2</sub> in the subsurface and at surface;
2. Technologies that provide information about pressure-volume behaviour and areal/vertical saturation distribution of CO<sub>2</sub>-plume to refine numerical 3-D-simulation to the 3-D-geological models of the storage formation established pursuant to Article 4 and Annex I;
3. Technologies that can provide a wide areal spread in order to capture information on any previously undetected potential leakage pathways across the areal dimensions of the complete storage complex and beyond, in the event of significant irregularities or migration of CO<sub>2</sub> out of the storage complex.
4. The yearly report to the competent authorities should encompass the above. If needed comment on site-specific monitoring problems.

## Feasibility study P18

---

### Updated plan

The initially installed monitoring system and related procedures need to be updated on the basis of the evaluation and modeling activity, or the verification results. Monitoring plans must be updated, at least every five years, to take into account changes to assessed risk of leakage, changes to assessed risks to environment and human health, new scientific knowledge, and improvements in the best available technology. The national authorities may set a more stringent frequency.

According to Annex II of the Storage Directive one has the following updating requirements:

1. The data collected from the monitoring shall be collated and interpreted. The observed results shall be compared with the behaviour predicted in dynamic simulation of the 3-D-pressure-volume and saturation behaviour undertaken in the context of the security characterisation.
2. Where there is a significant deviation between the observed and the predicted behaviour, the 3-D-model shall be recalibrated to reflect the observed behaviour. The recalibration shall be based on the data observations from the monitoring plan, and where necessary to provide confidence in the recalibration assumptions, additional data shall be obtained.
3. Steps 2 and 3 of Annex I shall be repeated using the recalibrated 3-D model(s) so as to generate new hazard scenarios and flux rates and to revise and update the risk assessment.
4. Where new CO<sub>2</sub> sources, pathways and flux rates or observed significant deviations from previous assessments are identified as a result of history matching and model recalibration, the monitoring plan shall be updated accordingly.
5. Post-closure monitoring shall be based on the information collected and modelled as in a-d. The plan must now also provide information needed for the transfer of responsibilities to the competent authority (long-term stewardship). Especially the site's permanent containment must be indicated, based on all available evidence.

### Monitoring at different stages of the project

Pre- injection, Injection and Post-injection monitoring do not differ in intent. Risks may be deemed higher in (parts of) the injection phase, notably the beginning of the injection activities. The monitoring plan reflects higher degrees of risk with more frequent monitoring.

Baseline and repeat measurement acquisition, processing and interpretation will be commented on in the plan. The relation with risk assessment and preventive/corrective measures is described.

In the pre-injection phase the main issue consists of gathering baseline data. At this stage it is of utmost importance to identify all possible baseline data that might be needed later in the injection and post-injection phases both for required monitoring as well as for contingency monitoring. More precisely, the risk assessment and scenario definition is crucial.

The Storage directive requires the operator to provide a provisional plan with corrective measures. This plan must be produced before any operations have begun. The basis therefore depends largely on modelling exercises performed in the context of site characterization and risk assessment. The operator should comment on how models plus forthcoming data lead him to a diagnosis of the problem – if the suspicion of a problem exists and how corrective measures are taken. This will be largely a site-specific exercise, based on the aforementioned risk assessment.

## Feasibility study P18

---

The period required for monitoring after abandonment of the wells and prior to decommissioning of the platform is not defined yet, neither is the period between decommissioning of the platform and transfer of liability to the state authorities. The required lengths of these periods need to be established in agreement with State Supervision of the Mines (SodM).

### 8.10.2. Proposed monitoring plan

This section describes the actual monitoring plan. The main overview is given by Table 4. The first column describes the parameters to be monitored. These parameters follow both from the mandatory monitoring obligations as stipulated by the storage directive and from the risk assessment.

The second column indicates the proposed technique adopted to measure the parameter. A more detailed description of the technique is provided outside the table.

The third column indicates the category of monitoring (mandatory, required, contingency). The fourth and fifth columns give a description both of the temporal frequencies (column 4) and spatial coverage (column 5) of the data acquisition foreseen in the different phases of the project (pre-injection, injection and post-injection including long-term stewardship after transfer of responsibility). The rationale behind the monitoring strategy related to the identified risks is described in the following section.

Column 6 provides a description of the expected accuracy of the monitoring method and of expected values that indicate normal behavior. Therefore this column is colored green.

The 7th column indicates threshold values, where normal behavior as anticipated stops and where irregularities start. As long as the measured values remain below these threshold values, no actions are required (green column). In case however the values come above the threshold values, one enters the 7th column colored orange with specific actions defined. This stage is considered as an increased alert phase, where behavior starts to deviate from expectations. This could for example lead to recalibration of the models, but when persisting to more stringent measures.

In case the monitor values come above the identified threshold in the 8th column coloured red, the highest alert phase starts and immediate actions (or contingency measures) as defined in the second subcolumn of column 8 are required.

Furthermore the table is divided into different blocks describing the different compartments to be monitored (injection process, injection and monitoring wells, abandoned wells, reservoir integrity, plume tracking, environmental monitoring).

The entire table needs to be updated and submitted to the competent authorities yearly.

Table in Appendix D:Monitoring plan according to the format proposed in the NSBTF (2009) and the draft EU guidance document (2010).

Table in Appendix D:Timeline of the monitoring plan.

Note, that the timing for monitoring of the post injection period including the abandonment of the wells and the decommissioning of the platform and the period to the transfer of liability to the state have not been defined in this plan. The definition of these periods will be subject of discussion with State Supervision of the Mines.

### 8.10.3. Relation risks – proposed monitoring methods

#### Introduction

This section provides more detailed background information on the rationale behind the selection of the proposed monitoring techniques. For each section corresponding to an identified risk/purpose the different techniques relevant for monitoring of it are referred to between brackets by their number as appearing in Table 4.

#### CO<sub>2</sub> Plume imaging (1,8,9,15,16,17,18,19,21,22)

The key tool for plume imaging in general is 3D surface seismic, however this is not deemed suitable for P18. This is because of the considerable depth of the P18 storage reservoir, which renders surface seismic methods less than optimally effective. Additionally, for P18 the presence of (residual) gas within the reservoir makes the feasibility of repeated seismic surveys for plume detection questionable.

Based on the history match of the P18 reservoir the field can be considered as a “tank model” with a good quality straight P/z curve (see Chapter 4) and without an active aquifer drive. Therefore plume migration is expected within the bounds of the original gas reservoir. The main components for monitoring deviations in expected behavior indicating potential migration out of the reservoir or storage complex consist of pressure (and temperature) monitoring. After proper history matching any deviations from the expected pressure trend (P/z curve) during and after the operational phase is a strong indicator for migration out of the storage complex. As for the K12-B reservoir, pressure monitoring has the potential to be a powerful tool at this site, since there is no strong aquifer drive masking potential deviations. A rough estimation of the threshold of the mass of CO<sub>2</sub> migration out of the reservoir that can be detected is in the order of 100-500 ktonnes of CO<sub>2</sub>. The exact value depends heavily on the quality of the P/z curves with proper and reliable pressure measurements. Factors like water influx, communication with neighboring blocks or CO<sub>2</sub> dissolution in water have a negative effect on the detectability.

Proper pressure measurements can be obtained from the injection well after a shut-in, or continuously from a monitoring well. The latter is definitely the preferred option allowing a continuous measurement of the reservoir pressure in equilibrium. In case the reservoir pressure is measured in the injection well after a shut-in care must be taken to take the measurements always at the same time after shut-in or even better, measure the pressure curve over a time interval in the order of days. Based on the curve the equilibrium pressure can be extrapolated (assuming it has not been reached in this period).

Migration in the reservoir can be followed by additional geophysical logs (RST logs) and downhole fluid samples at monitoring wells to detect CO<sub>2</sub> breakthrough. During the injection phase, microseismic monitoring may provide data on the location of the advancing CO<sub>2</sub> temperature front by detecting thermal fracturing. The latter is not considered as an absolutely required measurement for plume tracking, but is recommended.

#### Top seal integrity (8,9,15,16,17,18,19,20,24,25)

As for the plume imaging, the top seal integrity is assumed intact as long as no abnormal behavior of the pressure is observed. In case significant deviations are observed, contingency monitoring is required including time-lapse seismic data acquisition to detect migration pathways (chimneys) or shallow gas accumulations. 2D surface seismic may be a cost-effective alternative to full 3D, but will not provide full areal coverage of the top seal.

## Feasibility study P18

---

The threshold value of seismically detectable accumulations of CO<sub>2</sub> is in the order of 10's of ktonnes under the condition that CO<sub>2</sub> accumulates as a concentrated gas pocket. The shallower the CO<sub>2</sub> accumulates, the better the chances of picking up the signal. During the injection phase, microseismic monitoring provides data on whether the topseal is being geomechanically compromised. The feasibility of using wells from neighbouring blocks as monitoring wells for microseismic monitoring has not been explored yet, but is potentially an option.

### **CO<sub>2</sub> migration in the overburden (19,20,21,23,24,25,26,27)**

The key tool for the detection and imaging of CO<sub>2</sub> migration in the overburden is repeated 3D surface seismic. Note, that this is considered as a contingency measurement, only necessary in case of irregular behaviour. Surface 3D seismic can provide full coverage of the overburden volume and utilise its full imaging/resolution potential in the shallower overburden. During the injection phase, microseismic monitoring may provide data on the location of the migrating CO<sub>2</sub> front. As above, during the injection phase, 2D surface seismic may be a cost-effective alternative to full 3D, but will not provide full areal coverage of the overburden. Geophysical logs would not provide reliable indications of generalised CO<sub>2</sub> migration within the overburden except where free CO<sub>2</sub> accumulates in very close proximity to the wellbores. As mentioned above, the threshold value of seismically detectable accumulations of CO<sub>2</sub> is in the order of 10's of ktonnes. Sampling fluids of shallower aquifers can show traces of leaking CO<sub>2</sub>. To detect the absence of migration to the seabed, multi-beam echosounding is recommended identifying pockmarks or bubbles.

### **Calibration of flow simulations (1,2,3,4,5,8,9,15,16,17,18,21,22)**

The calibration of flow simulations combines aspects of several of the above aims, effective plume imaging, accurate pressure and temperature monitoring and insights into fine-scale and geochemical processes. Likely tools are downhole pressure/temperature measurements, RST logs and monitoring breakthrough in monitoring wells. For P18 where seismic imaging of CO<sub>2</sub> in the reservoir is considered difficult if not impossible, downhole pressure/temperature is the key technology. Downhole fluid chemistry also has a role, particularly in constraining amounts of dissolution. As in a number of cases above, microseismic monitoring may be useful in the injection phase.

### **Well integrity (6,7,8,9,10,11,12,13,14,20,23,24,25,27,28)**

The key tool for monitoring well integrity is clearly logging, aimed both directly at the wellbore (cement bond logging etc), but also at the surrounding formations (saturation logging). Pressure-temperature logging and downhole fluid chemistry are also potentially very useful. Non-well-based tools include 2D or 3D surface seismic for volumetric imaging of the overburden around the wellbores and multibeam echosounding to detect surface changes around the wellbore. During the injection stage, well-based microseismic monitoring can also provide information on flow and degradation processes around the wellbores.

#### **8.10.4. EU Storage Directive / OSPAR**

Monitoring requirements of the European Directive and OSPAR are framed around enabling the operator to understand and to demonstrate understanding of current site processes, to predict future site behaviour and to identify any leakage. Further requirements of the monitoring include early identification of deviations from predicted site behaviour, provision of information needed to carry out remediative actions and the ability to progressively reduce uncertainty.

### 8.10.5. Emissions accounting for ETS

The Monitoring and Reporting Guidelines for CCS under the ETS describe the method for quantifying potential CO<sub>2</sub> emissions from a storage project.

Potential emissions sources for CO<sub>2</sub> emissions from the geological storage of CO<sub>2</sub> include:

- Fuel use at booster stations and other combustion activities such as on-site power plants;
- Venting at injection or at enhanced hydrocarbon recovery operations;
- Fugitive emissions at injection;
- Breakthrough CO<sub>2</sub> from enhanced hydrocarbon recovery operations;
- Leakage from the storage complex.

Quantitative monitoring for ETS will only be required, if there is an indication of leakage. Currently there is no requirement for emission accounting as there is no evidence that the site will leak. However, in case irregularities are observed for example in the downhole pressure and temperature measurements, the need for additional monitoring to detect migration pathways out of the storage complex becomes stringent.

Key question for quantitative monitoring is of course, to what extent does the state-of-the-art technology allow for an accurate quantification. In that perspective the NSBTF (2009) suggests in general choosing a combination of a model-driven approach in combination with a monitoring strategy to best estimate the leakage for ETS purposes.

For P18 a sound strategy would be to detect leakage to the surface by geophysical methods like seismic data (detection of gas chimneys) or sea-bottom sonar techniques (detection of pockmarks) and then carry out in situ gas measurements and/or sample these leakage areas for direct CO<sub>2</sub> detection. Based on these observations an estimate can be made of leakage rates for the area.

In case of wellbore leakages an additional monitoring program in and around the wells is suggested.

### 8.11. Conclusions

Considering the overall philosophy of the EU Directive enshrined in the three minimum geological criteria for transfer of liability:

- Observed behavior of the injected CO<sub>2</sub> is conformable with the modelled behaviour.
- No detectable leakage.
- Site is evolving towards a situation of long-term stability.

one can say, that the three objectives can be covered by the proposed monitoring programme. The main question will be whether characterization of the caprock in combination with reservoir pressure monitoring provides sufficient confidence to omit seismic monitoring for detecting migration out of the storage complex.

### 8.12. References

ASPEN report, 2009. Support to the Introduction of the Enabling Legal Framework on Carbon Dioxide Capture and Storage (CCS), Service Request under the atmospheric emissions Framework contract ENV.C.5/FRA/2006/0071.

CO<sub>2</sub>QUALSTORE 2010: Guideline for Selection and Qualification of Sites and Projects for Geological Storage of CO<sub>2</sub>. DNV Report No.: 2009-1425.





Doc.nr: CATO2-WP3.01-D06  
Version: 2011.01.04  
Classification: Confidential  
Page: 170 of 198

## Feasibility study P18

---

Storage directive, 2009: DIRECTIVE 2009/31/EC OF THE EUROPEAN PARLIAMENT AND OF THE COUNCIL of 23 April 2009 on the geological storage of carbon dioxide and amending Council Directive 85/337/EEC, European Parliament and Council Directives 2000/60/EC, 2001/80/EC, 2004/35/EC, 2006/12/EC, 2008/1/EC and Regulation (EC) No 1013/2006.

ETS directive, 2009: DIRECTIVE 2009/29/EC OF THE EUROPEAN PARLIAMENT AND OF THE COUNCIL of 23 April 2009 amending Directive 2003/87/EC so as to improve and extend the greenhouse gas emission allowance trading scheme of the Community EU Guidance Document 2 (draft 2010): Site Characterisation, CO<sub>2</sub> Stream Composition, Monitoring and Corrective Measures. Draft document for consultation version June 17, 2010.

EU Draft guidance document for consultation (June 17, 2010): Implementation of Directive 2009/31/EC on the Geological Storage of Carbon Dioxide. Draft EU Guidance document 2: Site Characterisation, CO<sub>2</sub> Stream Composition, Monitoring and Corrective Measures.

Intergovernmental Panel on Climate Change (IPCC), 2006, IPCC Guidelines for National Greenhouse Gas inventories, Volume 2 Energy, Chapter 5 Carbon Dioxide, Transport, Injection and Geological Storage.

IEA GHG (Greenhouse Gas Programme), 2004, Overview of Monitoring Requirements for Geologic Storage Project Report PH4/29.

IPCC (2006) Guidelines for National Greenhouse Gas Inventories. Chapter 5: Authors: Sam Holloway (UK), Anhar Karimjee (USA), Makoto Akai (Japan), Riitta Pipatti (Finland), and Kristin Rypdal (Norway) arbon dioxide transport, injection and geological storage.

North Sea Basin Task Force (NSBTF), 2009, Monitoring Verification Accrediting and Reporting (MVAR) Report for CO<sub>2</sub> storage deep under the seabed of the North Sea.

OSPAR (2007). OSPAR Guidelines for Risk Assessment and Management of Storage of CO<sub>2</sub> Streams in Geological Formations (Reference Number: 2007-12), Meeting of the OSPAR Commission, Ostend, 25-29 June 2007.

Shell (2008): Integraal Monitoringsprotocol CO<sub>2</sub>-opslag Barendrecht. Shell report EP200812202493 versie: 2 (8 december 2008).



Doc.nr: CATO2-WP3.01-D06  
Version: 2011.01.04  
Classification: Confidential  
Page: 171 of 198

**Feasibility study P18**

---

## 9. Site development plan

### 9.1. Introduction

This chapter contains an overview of all required steps before CO<sub>2</sub> injection can take place in the P18 field in 2015. This includes information on the key risks at each step along the process and the go / no-go decisions which are involved. The development plan contains three decision gates, where the project is evaluated and has to be approved of in order to enter the following phase in the site development plan. At the end of the chapter, a timeline of the site development plan is included.

### 9.2. Timeline overview

Table 35 displays a concise overview of the different steps involved in the project; the steps are further elaborated below. This chapter also provides the projected dates on when certain steps in the process are expected to be finished. It is important to realize that indications of timing are cyclical in nature and very sensitive to changes in for instance commodity prices of oil or metal.

The timing of the activities shown in the table are sketched in Figure 9.1.

.

## Feasibility study P18

Table 33: Timeline overview for starting CO<sub>2</sub> storage in P18.

	Activities	Timing
1	P18 feasibility study and high level cost estimate	May 2010 - Jan 2011
2	Evaluate site and engineering concept selection	Dec 2010 - Jan 2011
	<b>Decision gate: Site and engineering concept selection</b>	Jan 2011
3	Environmental Impact Assessment (EIA)	Q4 2010 - Q4 2011
4	Option on initial storage capacity from 2016 in the P18 reservoir blocks	Feb 2011
5	Option on storage capacity from 2018 in the P18 reservoir blocks	Feb 2011
6	Option on transport	Feb 2011
	<b>Decision gate: Go ahead with NER300 funding application</b>	Feb 2011
7	Apply for NER300 funding	Feb - May 2011
8	Obtain licenses	Jan 2011 - Q2 2012
9	FEED (Front-End Engineering and Design)	Q3 - Q4 2011
	<b>Decision gate: Final Investment Decision for EPC</b>	Dec 2011
10	Tendering for detailed Engineering Procurement and Construction	Jan - Feb 2012
11	EPC contract signing	Mar 2012
12	Detailed engineering	Apr - Sep 2012
13	Detailed cost statements (+/- 10%)	Q4 2012
14	Procurement (pipelines, platform installations, equipment and workforce)	Q1 - Q3 2013
15	Construction: wells workovers	Q2 - Q3 2014
16	Construction: equipment of the monitoring well (only possible in compartment P18-2)	Q3 2014
17	Construction: platform modification	Q2 - Q3 2014
18	Construction: pipeline	Q2 - Q3 2014
19	Construction: onshore facilities (compressor, pipeline)	Q1 - Q3 2014
20	Tie-in work and commissioning	Q2 2015
21	Baseline monitoring	Q3 2015
22	Handover	Sep 2015
23	Start injection	Q4 2015

## 9.3. Detailed timeline overview

### Start project

#### **9.3.1. Feasibility study and high-level cost estimate ( $\pm 40\%$ )**

This step is Phase 1 part of the Independent Storage Assessment. During this step, the outline of the project is defined. It also includes setting the scope of the project and defining the requirements, implications, benefits and drawbacks of the project.

Furthermore, the stakeholders and their involvement and commitment should be identified. Stakeholders include various layers of the government, emitters, operators and civil society and research institutes.

In a later part of this step, possible sites for the project are outlined. The requirements of the sites and their suitability should be determined, based on a preliminary survey of the options. An assessment is made of the required data for making a more detailed analysis of the suitable sites and constructing a business case, which is the next step of the project. This data includes geological, seismic and economic parameters of the sites.

The feasibility phase should result in the main risks and limitations of transport and storage at a selection of sites. This should also include limitations on injection rates, requirements of number of wells and well sizes, the possibilities on the transport via shipping or pipelines. The requirements on the injection operation strategies are analyzed in the pre-feed and feed phases. The ideal order of studies is starting with the reservoir injection engineering and well integrity study, followed by the conceptual engineering work.

During this step it has been determined that P18 is a suitable candidate for large scale CCS in the period 2015 – 2020. It has been shown that the reservoirs can handle the injection rate of 1.1 Mt/year and no barriers have been identified.

One of the results from this step is a preliminary cost estimate with a margin of uncertainty of the order of 40%.

*Key risk:*

Data is difficult to obtain and often incomplete. There are also large uncertainties involved, which should be accounted for.

#### **9.3.2. Concept selection**

This step entails the study and selection of the concept from the different options of the feasibility study for a specific field such as P18. This step focuses mainly on the technical aspects of the field, making sure the capacity of the fields is adequate and the seal will not leak.

This step results in the selection of a site and the development of a concept for CO<sub>2</sub> storage at this location. This accounts for all aspects of the project, including capture, transport, injection and storage.

## Feasibility study P18

---

### Decision Gate: Site engineering and concept selection

This decision gate follows the first steps of the timeline. This decision gate marks the continuation of the project and allows the other steps to commence. This also means that more funding has to be committed to the project. Criteria in this step:

- Geological factors: capacity, injectivity, containment
- Environmental impact indicators, safety
- Public perception
- Costs

### 9.3.3. Environmental Impact Assessment (EIA)

Environmental Impact Assessments play an important part in project development. The EIA is done based in part on the results of a feasibility study (step 1). A successful EIA is one of the requirements to start the process of obtaining various licenses. The duration of obtaining an EIA after the application is typically between 6 and 12 months, but for large projects this can take up to a year and a half.

### 9.3.4. Option on initial storage capacity from 2016

In this step an option is taken on a field, guaranteeing the availability of the storage site. The current injection plan foresees to start injection in P18-6, after which injection in P18-4 will commence. The capacity with respect to the injection rate is limited in these compartments such that ROAD, which has a priority agreement with TAQA, will need most of the capacity, and only spare capacity is left for third parties. Sufficient additional capacity is available in compartment P18-2 from 2018 onwards when gas production has ceased. For third parties outside ROAD the following options are open, depending on an agreements with TAQA and ROAD, for injection before 2018:

1. Volume-sharing agreement with ROAD for compartments P18-6 and P18-4 for which ROAD has priority in;
2. Agreement with TAQA to use cushion gas N2 during production;
3. Agreement with TAQA to inject in non-producing Block III: requires proper abandonment of the sidetracked well P18-2A6st and re-completion of the parent well P18-2A6.

For the third option it is noted that the CO<sub>2</sub> capacity in Block III is small.

#### *Key risk*

Difficulties in negotiations between operators can delay or impede this procedure.

### 9.3.5. Option on storage capacity from 2018

From 2018 compartment P18-2 would be available, depending on the cessation of production and successful well work-overs. This would give ample storage capacity for third parties.

#### *Key risk*

Difficulties in negotiations between the parties can delay or impede this procedure.

### 9.3.6. Option on transport

## Feasibility study P18

---

The insulated pipeline from the emitters tie-in point to the P18 platform riser is operated by GDFSUEZ. Therefore an agreement with GDFSUEZ must be negotiated in order to get access to the pipeline. For third-parties outside ROAD a tie-in with the ROAD pipeline, including metering and control, must be negotiated.

### **Decision Gate: Go-ahead with the NER300 application**

At this decision gate a decision must be made whether to enter the NER300 application.

### **9.3.7. Apply for NER300 funding**

The NER300, which is a financing instrument from the European Commission for CCS projects, plays an important part in providing funding for the project. The application, for which the details were published in November 2010, should be set in motion as soon as possible, in order to safeguard adequate funding for the project. The deadline for application in the Netherlands is February 9, 2011.

### **9.3.8. Obtain licenses (national coordination ruling)**

During this step, the licenses required for capture, transport, injection and storage of CO<sub>2</sub> should be acquired. There are up to ten legal procedures involved, with a typical duration of around 2 years.

In order to facilitate this process and reduce the amount of time involved in administrative procedures in large scale energy projects, the Dutch government has started an initiative called the "Rijkscoördinatieregeling" or the "National Coordination Ruling", as it is called in English. Responsibility for the coordination of this process lies with the minister of Economic Affairs (EL&I) because the Mining Act is the foremost applicable law for offshore CO<sub>2</sub> storage. Table 34 shows the different phases involved in this process.

For P18, this process has already been set in motion and the first four phases have been completed. Phase 5, the concept decision, is expected to be finished in January, with the exception of the so called "bestemmingsplan", which might need an additional couple of months. In July, phase 6, the review period, should be finished. In August, phase 7, the final decision should be finished. Phase 8, the release of the final decision for review, should start at the end of October. All in all, the process should be complete at the end of 2011, with the exception of step 9, which can require an additional 6 months.

#### **Storage license**

The underground storage of materials requires an appropriate permit from the Dutch Minister of Economic Affairs, Agriculture and Innovation. The procedure to apply for such a permit is outlined in chapter 3 of the Mining Act. Article 1.3.4, appendix 1 and appendix 2 of the Mining Decree contain a summary of the information that must be provided with a permit application.

Outside the territory of the State, i.e., more than 12 nautical miles from the coast, a MER (Dutch Environmental Impact Assessment) is not needed. Environmental regulations are governed by the Dutch Mining Act, Decree and Regulation, the EU Directive, the London Protocol and OSPAR.

**Feasibility study P18**

Table 34: Overview of the different phases in the “National Coordination Ruling”.

Phase	
1	The initiating party reveals its plans concerning a large scale energy project to the Minister of Economic Affairs, Agriculture and Innovation. The law determines which projects fall under the national coordination ruling.
2	The ministry determines whether they will provide a “regional” decision and prepare that decision after consultation with both the initiating party and the concerned authorities.
3	“Agentschap NL” investigates in collaboration with the initiating party and the concerning authorities, which licenses and exceptions are required for the project.
4	The initiating party asks for all licenses and exceptions to the concerned authorities. The coordinating minister discusses a common planning with the various parts of government.
5	The concerned authorities collaborate closely and come to their concept decision. The aforementioned minister also (if so decided) arrives at a concept “rijksinpassingsplan”.
6	The concept decisions are bundled and released for public review. During the review period, everybody can object (in writing). One or more information session are organized in which further feedback can be provided.
7	The authorities process the advice and the feedback, after which the decision are made final.
8	The final decisions are again bundled and released for review. Interested parties can object against these decisions, mostly directed to the “Raad van State”.
9	The department administrative justice of “de Raad van State” comes to a verdict on the appeal against one or more of the decisions. In case of “rijkscoördinatie” with a “rijksinpassingsplan” this happens in a single ruling, within 6 months after receiving appeal of the concerning authorities.

The time needed to obtaining the required licenses is uncertain. Appendix A contains a preliminary list of the Dutch permits required for CCS projects.

*Key risk*

The most important risk is a delay in the permitting procedures. Because CCS is a novel topic in legislature, involving long-term effects and international treaties and hence responsibilities, unexpected delays could occur in obtaining the required licenses. This can jeopardize the progress of the project.

**9.3.9. FEED**

The design phase is generally divided into a FEED (Front End Engineering and Design) phase and the detailed engineering in the EPC (Engineering, Procurement and Construction) phase. The FEED phase concerns the definition of the (transport and storage) system, defining pipeline diameters, transport pressure and compression requirements.



## Feasibility study P18

---

The FEED phase validates the feasibility study, defines the project philosophies and the safety aspects. This phase also includes the full description of injection strategies and procedures such as start-up, shut downs etc. At the end of the phase the system has been designed to a level that allows detailed engineering of the subsystems, such as compressors, pipelines, platform facilities.

The FEED phase is dedicated to the basic engineering and to the cost evaluation (CAPEX and OPEX), as well as the preparation of all technical documents that will constitute the EPC bid package, in order to launch and international tendering for the EPC realization of:

1. CO<sub>2</sub> capture infrastructure at
2. CO<sub>2</sub> transport infrastructure from source to storage site
3. CO<sub>2</sub> injection and storage infrastructure

CO<sub>2</sub> has to be captured and transported from point sources, such as refineries and power plants onshore, to the offshore storage site P18. The CO<sub>2</sub> sources for P18 are located on the industrial area of the Maasvlakte, near Rotterdam. The CO<sub>2</sub> will be transported over a distance of 20 km to the converted CO<sub>2</sub> injection platform P18-A. This also requires investments in onshore facilities.

### Injection installation:

A single 16" riser is foreseen. The subsea pipeline will be operated by GDF Suez. Taqa will take the CO<sub>2</sub> at the platform. At this moment no choice has been made to meter the injection rates per well or only for the total stream. At the flange a fiscal meter will be set-up. At this point composition measurements are also foreseen. The flowline design rate is 47 kg/s with an expected operating arrival pressure of at least 80 bar. The pipeline is insulated such that the arrival temperature at normal operation is 40°C. The goal is to operate the flowline at all times in the liquid or dense phase. Only during start-up scenario's the arrival temperature will be lower. For those cases a start-up heater will be used. At this moment no choice for the type of heating (electrical, gas or diesel) is taken. Start-up is foreseen for 12 times per year with a start-up period of 48 hours. Aside the start-up heater, piping and manifold suitable for cold CO<sub>2</sub> will be placed on board. For this the test-separator will be removed as this doesn't lead to changes in the gas production capabilities. These changes will not require additional mechanical modifications to the platform itself. The CO<sub>2</sub> infrastructure will be part of the total current systems as both injection and production from all wells must be possible.

The FEED phase has the following activities:

1. The determination of injection scenarios and procedures consisting of
  - a. Planning of the remaining gas production. Currently, P18-4 is foreseen to stop production by 2015, whereas P18-2 may produce until 2018.
  - b. Phasing reservoir blocks with respect to start injection. Currently, injection is planned to start in P18-6, then P18-4, and if more capacity is needed, injection could subsequently start in P18-2 from 2018 onwards.
  - c. The phasing of the injection wells.
  - d. Planning of the injection capacity.
  - e. Design of start-up and Emergency Shut-Down (ESD) Procedures.
  - f. Phasing of the well work-overs.
2. The design, planning execution and costing of the well workovers.
3. In case a monitoring well is part of the monitoring plan, the design, planning execution and costing of the monitoring well in compartment P18-2.
4. The design, planning execution and costing of the P18 platform modifications includes
  - a. Retrofit of the riser connecting the pipeline with the platform.
  - b. Installation of a distribution manifold suitable for cold CO<sub>2</sub>.
  - c. Modification of the monitoring and control system

## Feasibility study P18

---

- d. Modification of the Process Control System and safeguarding, safety facilities, etc.
  - e. Revamp of the piping system
  - f. Re-engineer wellheads with suitable materials for cold CO<sub>2</sub> injection
  - g. Installation of well test and control equipment
  - h. Installation of vent and blow down facilities
  - i. Installation of the start-up heater
  - j. Power generation
  - k. Removal of the test separator
5. The design of a monitoring plan
  6. The design, planning execution and costing of the insulated pipeline offshore
  7. The design, planning execution and costing of the onshore facilities which includes
    - a. Dehydration unit
    - b. Compression system
    - c. Pipeline from capture plant to pipeline
    - d. Third-party tie-in to ROAD pipeline including metering and control
  8. Test concept design
  9. Study for optimal change-over production-injection

The FEED phase concerns the breakdown of the transport and storage system into its building blocks. These building blocks, which are now complete in terms of the requirements and interfaces, can be tendered out to contractors, who will perform the detailed design and construction. It has been estimated that this phase (only for transport and storage) takes approximately 4000 hours.

### **Decision Gate: Final Investment Decision for FID**

At this decision gate, the FEED study is complete and the procedures for obtaining the required licenses have been set in motion. Before FID, the project should be evaluated based on current knowledge before proceeding to the EPC tendering, which constitutes the step to the major investments.

At this decision gate, the majority of the preparatory work is finished. By this time, all risks should be clear and appropriately managed. When this decision gate is passed, the actual implementation of the project is set in motion.

### **9.3.10. Tendering for detailed Engineering Procurement and Construction**

Preparation of all technical documents that will constitute the EPC bid package, in order to launch and internationally tender for the EPC realization.

### **9.3.11. EPC Contract signing**

This step entails acquiring all necessary agreements with the parties in the CCS chain as well as awarding and signing the EPC contracts.

#### *Key risk*

The large financial interests involved in the oil and gas business and the insecurities of CCS make it difficult to accurately establish the market value of a (depleted) gas field and its facilities.

## Feasibility study P18

---

This could make negotiation between stakeholders difficult. If no satisfactory agreement is reached, the project can be severely jeopardized.

### 9.3.12. Detailed engineering

Detailed engineering is performed of:

1. Work-overs six existing wells
2. Modifications to the platform facilities
3. Insulated offshore pipeline
4. Onshore facilities (compressors, pipeline)

### 9.3.13. Detailed costing

A detailed costing is conducted such that cost estimated are within +/- 10%.

### 9.3.14. Procurement

This phase involves the procurement of all required elements for the project. The long lead items need to be ordered as soon as possible (potentially in the previous project phase if allowed). This includes materials, such as pipelines and heaters and compressors, and equipment, such as ships and drilling platforms and workforce. Renting a rig is an important part of the procurement phase.

Planning of the well work-overs and laying of the pipeline will require contract signing at least a year before the actual work due to the long procurement periods. This means that contracts need to be signed in the summer of 2012. For timing considerations, it should be kept in mind that constructing pipelines should be done in summer due to the benign weather conditions.

#### *Key risk*

Because the procedures are so costly and time consuming, it is not uncommon in the oil and gas industry to have equipment and workforce reserved for years in advance. A key risk is the availability of required materials and workforce for a sustained period, which would significantly delay the project.

### 9.3.15. Construction: well abandonment and work-over

Deploying a rig in the correct position takes time, depending on the job, and performing a single well work-over it takes between 4 to 10 weeks. During this step, the rig is used for two purposes. First of all, it is used for work-overs on existing wells, which are converted for injection. Secondly, the rig is used to properly abandon wells that are no longer used but which might not have been successfully abandoned.

Required actions of well work-overs at P18:

Required before using P18-2 compartment for CCS

- Rig employment
- Abandonment P18-2 exploration well (current status suspended).
  - Remove cage from seabed.
  - Re-enter well

## Feasibility study P18

---

- Drill out all but bottom plug
- Retrieve top uncemented casing
- Set new cement plugs
- Workover of sidetracked well P18-2A6
  - Abandonment P182-A6st (successful abandonment of this sidetrack would allow for CO<sub>2</sub> storage in the P18-2)
  - Fishing the whip stock in order to get access to parent well and thus compartment III
  - Recompletion of the P18-2A6 parent to enable CO<sub>2</sub> injection in block III

Other injectors in the P18-2 compartment (exception P182-A4) would require:

- new CBL
- Pulling of tubing (using rig)
- In case of bad cement bonding:
  - Perforate casing near poorly cemented area.
  - Perform pressure integrity test
  - Squeeze cement if necessary
  - Isolate created perforation in casing

### 9.3.16. Construction: equipment of the monitoring well

In case a monitoring well is part of the monitoring plan an existing well needs to be converted, equipped and instrumented. Only in compartment P18-2 would a well be available for monitoring.

### 9.3.17. Construction: platform modification

The platform is modified: the test-separator will be removed and new equipment installed. New equipment includes a heaters (used during the first stages of injection and for start-ups), wellhead control and downhole equipment control systems, a retrofit of the riser, a CO<sub>2</sub> manifold, revamp of the piping system and vent and blow down facilities.

### 9.3.18. Construction: pipeline construction

The pipeline with both onshore and offshore sections is constructed. The pipeline will be insulated such that the CO<sub>2</sub> will have a temperature of 40°C. at the well head at normal operations.

### 9.3.19. Construction: onshore facilities

Onshore facilities include the compressor and dehydration systems.

### 9.3.20. Tie-in work and commissioning

This step includes tests to see if everything is working as planned. It results in the handover of the field and the equipment to the new operator.

### 9.3.21. Baseline monitoring

During this step the baseline for the monitoring of the storage during and after injection is collected. It should take place before injection and ideally a short period after the tie in work and commissioning place.



### **9.3.22. Handover**

This step includes tests to see if the chain is working as planned. It results in the handover of the field and the equipment to the new operator.

### **9.3.23. Start injection**

During this phase, injection is started. Injection is planned to take place in 2015.

It is noted that there is an option to continue production of gas after the start of injection, in which case this would become enhanced gas recovery (EGR). At present, this option is not taken into account. The energy requirements on the platform once CO<sub>2</sub> injection is started are limited, and significant only during the first phase of injection, when a heater is used. Gas produced from one of the wells could be used to this end.

Feasibility study P18

9.4. Schematic overview of project timeline

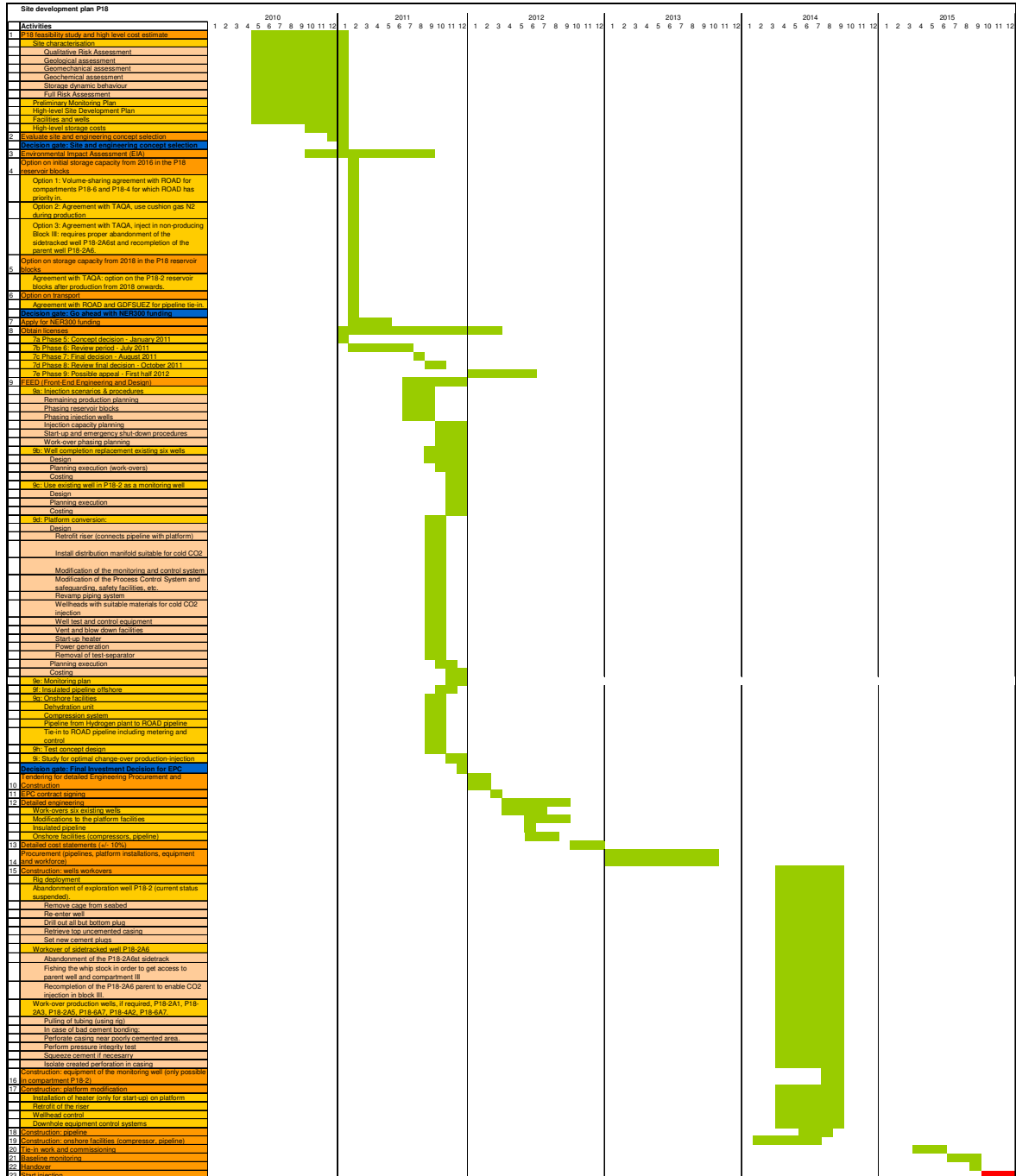


Figure 9.1: Overview of the timeline of activities required to start CO<sub>2</sub> injection at P18, see also Appendix E.



## 11. Appendix A: Base, top and thickness of formations

### Base, top and thickness of the formations (reservoir zones) in the wells

Well ID	Base (m)	Top (m)	Thickness (m)
P18-02 (expl. well)	3441	3326	115
P18-02A1	3665	3553	112
P18-02A3ST2	3575	3465	110
P18-02A5	3464	3350	114
P18-02A6	3683	3575	108
P18-02A6ST1	N.P.	N.P.	-
P18-04A2	3365	3264	101
P18-06A7ST1	N.P.	N.P.	-

Table A1: Data on the base, top and thickness of the Volpriehausen Formation in the P18 wells. N.P. stands for "Not Penetrated".

Well ID	Base (m)	Top (m)	Thickness (m)
P18-02 (expl. well)	3326	3305	21
P18-02A1	3553	3531	22
P18-02A3ST2	3465	3445	20
P18-02A5	3350	3328	22
P18-02A6	3575	3555	20
P18-02A6ST1	N.P.	N.P.	-
P18-04A2	3264	3245	19
P18-06A7ST1	N.P.	3627	-

Table A2: Data on the base, top and thickness of the Lower Detfurth Sandstone Member in the P18 wells. N.P. stands for "Not Penetrated".

Well ID	Base (m)	Top (m)	Thickness (m)
P18-02 (expl. well)	3305	3256	49
P18-02A1	3531	3481	50
P18-02A3ST2	3445	3396	49
P18-02A5	3328	3279	49
P18-02A6	3555	3508	47
P18-02A6ST1	N.P.	3288	-
P18-04A2	3245	3198	47
P18-06A7ST1	3627	3578	49

Table A3: Data on the base, top and thickness of the Upper Detfurth Sandstone Member in the P18 wells. N.P. stands for "Not Penetrated".



**Feasibility study P18**

Well ID	Base (m)	Top (m)	Thickness (m)
P18-02 (expl. well)	3256	3228	28
P18-02A1	3481	3455	26
P18-02A3ST2	3396	3370	26
P18-02A5	3279	3254	25
P18-02A6	3508	3480	28
P18-02A6ST1	3288	3261	27
P18-04A2	3198	3174	24
P18-06A7ST1	3578	3545	33

Table A4: Data on the base, top and thickness of the Hardeggen Formation in the P18 wells. N.P. stands for "Not Penetrated".

**Petrophysical properties of the formations (reservoir zones) in the wells**

Well ID	Top	Base	FWL	BPZ	N/G	PHI	S <sub>w</sub>	PHI_NPZ
P18-02A1	3553	3665	3680	0.96	0.88	0.034	0.93	0.043
P18-02A3	3465	3575	3680	1.00	0.51	0.034	0.91	0.053
P18-02A5	3350	3464	3680	1.00	0.45	0.056	0.46	0.058
P18-02A6	3575	3683	3680	0.79	0.93	0.033	0.81	0.037
P18-04A2	3264	3365	3377	1.00	0.33	0.034	0.92	0.049

Table A5: Average (arithmetic) petrophysical properties of the Volpriehausen Formation in the P18 wells. Values in columns "Top", "Base" and "FWL" (Free Water Level) are in m TVDSS, with FWL as determined from pressure-depth gradients or mapped spill points, "BPZ" stands for "Bulk Pay Zone", and indicates the part of the formation above the FWL, "N/G" stands for "Net-To-Gross", as calculated by dividing the amount of sand (Vshale cut-off: 0.35, PHI cut-off: 0.02) in m by the total thickness of the formation, "PHI" indicates the porosity (cut-off: 0.02) of the bulk, "S<sub>w</sub>" stands for water saturation (Vshale cut-off: 0.35, PHI cut-off: 0.02), and "PHI\_NPZ" indicates the average porosity of the pay zone.

Well ID	Top	Base	FWL	BPZ	N/G	PHI	S <sub>w</sub>	PHI_NPZ
P18-02A1	3531	3553	3680	1.00	0.88	0.073	0.45	0.075
P18-02A3	3445	3465	3680	1.00	0.67	0.084	0.39	0.096
P18-02A5	3328	3350	3680	1.00	0.82	0.108	0.20	0.108
P18-02A6	3555	3575	3680	1.00	0.80	0.051	0.63	0.051
P18-04A2	3245	3264	3377	1.00	0.81	0.065	0.39	0.065
P18-06A7ST1	N.P.	3627	3680	1.00	0.71	0.059	0.32	0.059

Table A6: Average (arithmetic) petrophysical properties of the Lower Detfurth Sandstone Member in the P18 wells. Values in columns "Top", "Base" and "FWL" (Free Water Level) are in m TVDSS, with FWL as determined from pressure-depth gradients or mapped spill points, "BPZ" stands for "Bulk Pay Zone", and indicates the part of the formation above the FWL, "N/G" stands for "Net-To-Gross", as calculated by dividing the amount of sand (Vshale cut-off: 0.35, PHI cut-off: 0.02) in m by the total thickness of the formation, "PHI" indicates the porosity (cut-off: 0.02) of the bulk, "S<sub>w</sub>" stands for water saturation (Vshale cut-off: 0.35, PHI cut-off: 0.02), and "PHI\_NPZ" indicates the average porosity of the pay zone. N.P. stands for "Not Penetrated".





**Feasibility study P18**

Well ID	Top	Base	FWL	BPZ	N/G	PHI	S <sub>w</sub>	PHI_NPZ
P18-02A1	3481	3531	3680	1.00	0.96	0.074	0.35	0.078
P18-02A3	3396	3445	3680	1.00	0.88	0.089	0.56	0.093
P18-02A5	3279	3328	3680	1.00	0.94	0.117	0.31	0.117
P18-02A6	3508	3555	3660	1.00	0.93	0.061	0.72	0.065
P18-04A2	3198	3245	3377	1.00	0.87	0.091	0.47	0.092
P18-02A6ST1	3288	N.P.	3680	1.00	0.99	0.120	0.20	0.120
P18-06A7ST1	3578	3627	3680	1.00	0.91	0.048	0.57	0.048

Table A7: Average (arithmetic) petrophysical properties of the Upper Detfurth Sandstone Member in the P18 wells. Values in columns "Top", "Base" and "FWL" (Free Water Level) are in m TVDSS, with FWL as determined from pressure-depth gradients or mapped spill points, "BPZ" stands for "Bulk Pay Zone", and indicates the part of the formation above the FWL, "N/G" stands for "Net-To-Gross", as calculated by dividing the amount of sand (Vshale cut-off: 0.35, PHI cut-off: 0.02) in m by the total thickness of the formation, "PHI" indicates the porosity (cut-off: 0.02) of the bulk, "S<sub>w</sub>" stands for water saturation (Vshale cut-off: 0.35, PHI cut-off: 0.02), and "PHI\_NPZ" indicates the average porosity of the pay zone. N.P. stands for "Not Penetrated".

Well ID	Top	Base	FWL	BPZ	N/G	PHI	S <sub>w</sub>	PHI_NPZ
P18-02A1	3455	3481	3680	1.00	0.97	0.096	0.35	0.096
P18-02A3	3370	3396	3680	1.00	0.97	0.115	0.31	0.116
P18-02A5	3254	3279	3680	1.00	1.00	0.149	0.18	0.149
P18-02A6	3480	3508	3680	1.00	1.00	0.109	0.36	0.110
P18-04A2	3174	3198	3377	1.00	0.99	0.127	0.24	0.131
P18-02A6ST1	3261	3288	3680	1.00	0.95	0.157	0.14	0.157
P18-06A7ST1	3545	3578	3680	1.00	0.81	0.074	0.47	0.074

Table A8: Average (arithmetic) petrophysical properties of the Hardegsen Formation in the P18 wells. Values in columns "Top", "Base" and "FWL" (Free Water Level) are in m TVDSS, with FWL as determined from pressure-depth gradients or mapped spill points, "BPZ" stands for "Bulk Pay Zone", and indicates the part of the formation above the FWL, "N/G" stands for "Net-To-Gross", as calculated by dividing the amount of sand (Vshale cut-off: 0.35, PHI cut-off: 0.02) in m by the total thickness of the formation, "PHI" indicates the porosity (cut-off: 0.02) of the bulk, "S<sub>w</sub>" stands for water saturation (Vshale cut-off: 0.35, PHI cut-off: 0.02), and "PHI\_NPZ" indicates the average porosity of the pay zone.

## 12. Appendix B: Reservoir emballage

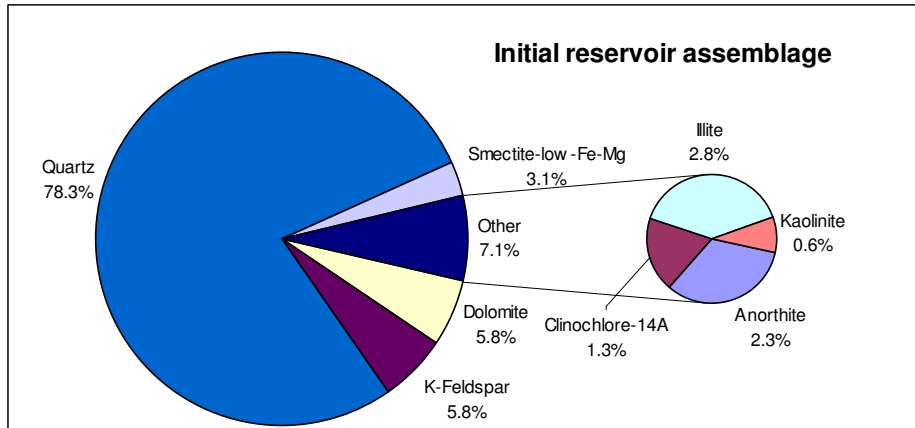


Figure 12.1 Initial, computed reservoir mineralogy (wt%) which deviates slightly from the measured rock composition due to allowance of precipitation of secondary minerals and exclusion of minerals in the diagram with wt% below 0.1 (albite, anhydrite, glauconite, muscovite and pyrite).

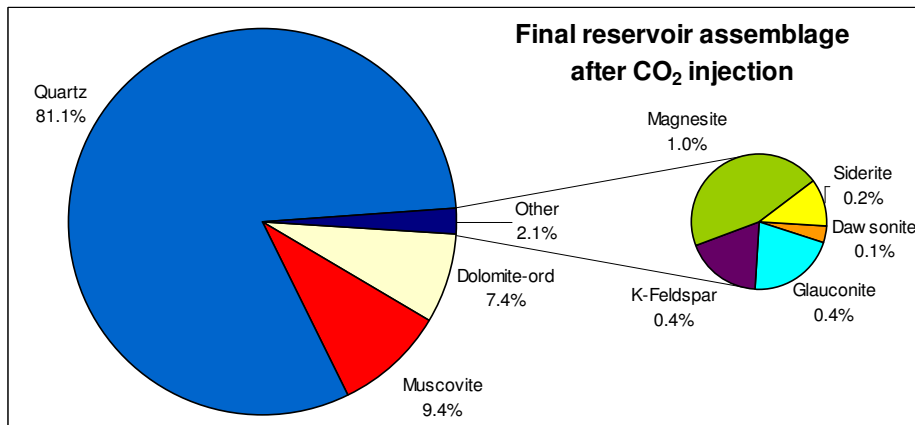


Figure 12.2 Final, computed reservoir assemblage (wt%) after CO<sub>2</sub> injection.

Feasibility study P18

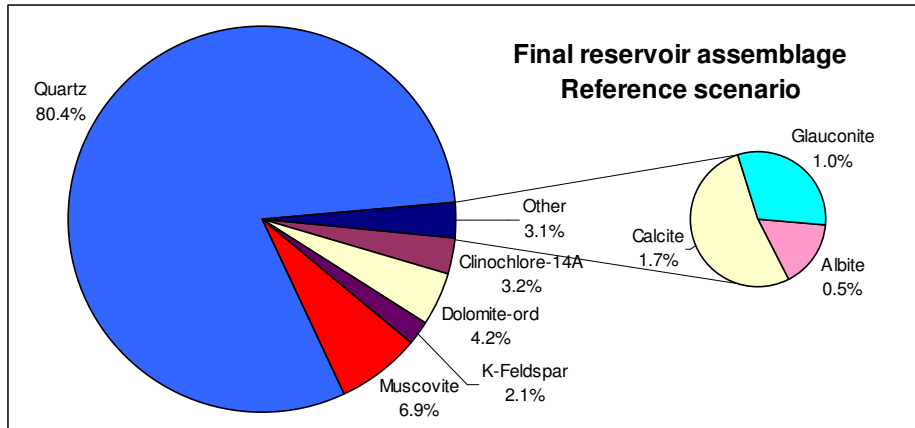


Figure 12.3 Final, computed equilibrium assemblage (wt%) without CO<sub>2</sub> injection.

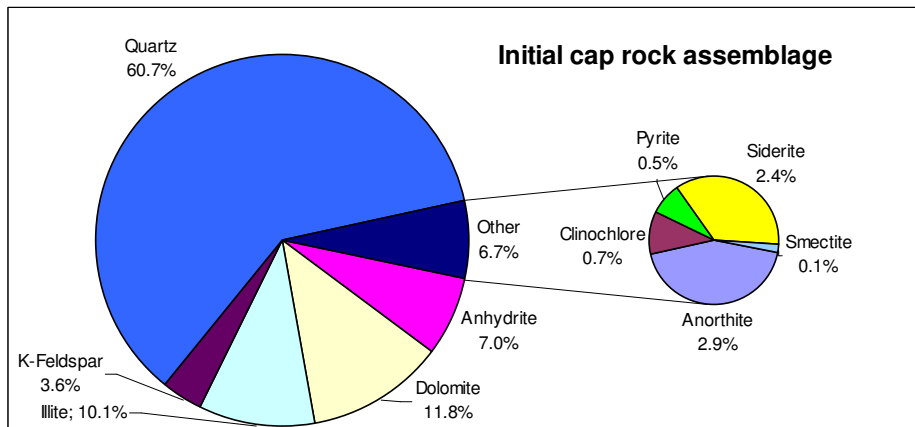


Figure 12.4 Initial cap rock assemblage (wt%). % which deviates slightly from the measured rock composition due to allowance of precipitation of secondary minerals and exclusion of minerals in the diagram with wt% below 0.1 (albite, diaspore, glauconite and muscovite).

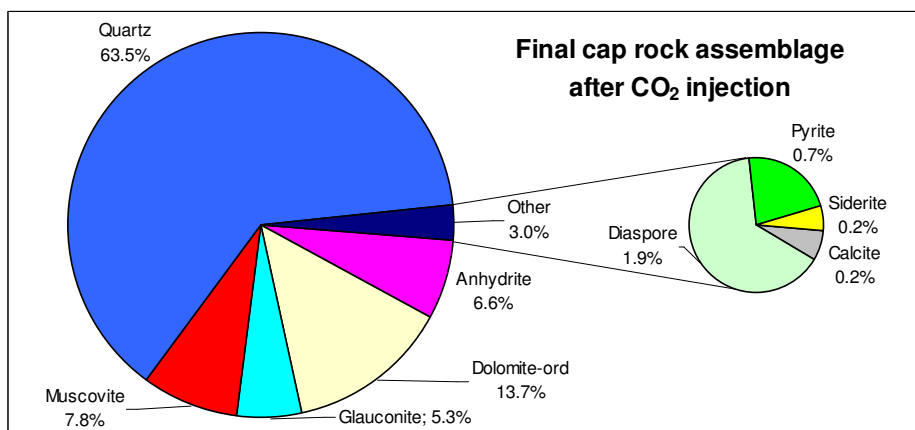


Figure 12.5 Final, computed cap rock assemblage (wt%) after CO<sub>2</sub> injection.

**Feasibility study P18**

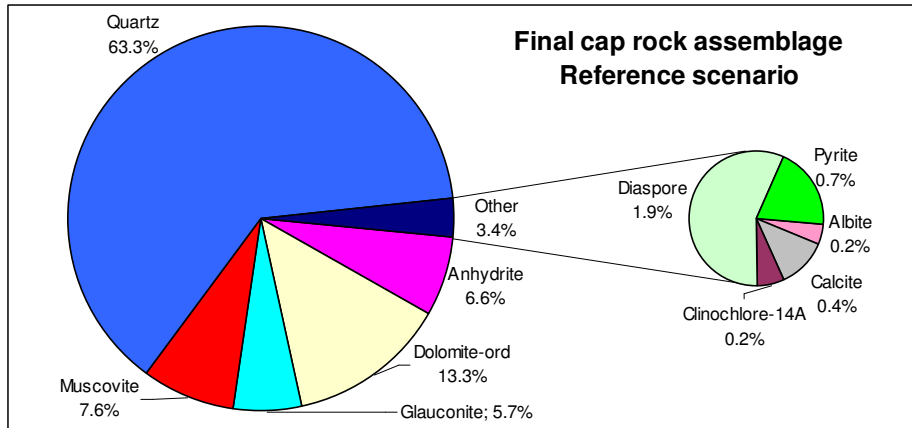


Figure 12.6 Final, computed cap rock assemblage (wt%) without CO<sub>2</sub> injection.

## 13. Appendix C: Overview of Dutch permits needed for CCS projects

The following list, in alphabetical order, gives a preliminary overview of the Dutch permits which are required for CCS projects. Due to the novelty of the concept, it is not yet sure whether this list is complete.

- Act on Environmental Management
- Act on Management of State Hydraulic Works
- Act on Nature Protection
- Act on Spatial Planning
- Circular on Transport of Hazardous Substances
- Construction permit
- Decision on External Safety of Installations
- Flora and Fauna dispensation
- Mining Law
- National Coordination Regulation

## 14. Appendix D:

No.	Parameter to be monitored*	Technique adopted	Category of monitoring	Project phase and frequency					Location	Normal situation		Alert value		Contingency value	
				Pre-inj	Inj	Post-Inj	Post-Inj (abandonment)	Long-term stewardship		Expectation value	Accuracy	> Threshold 1	Action**	> Threshold 2	Contingency measures***
<b>Injection process</b>															
1	Injection rate	Flow meter	X		Cont				Outflow compressor + at well head	Max rate = 169,2 ton CO <sub>2</sub> /hour (47 kg/s or 1,48 Mton CO <sub>2</sub> /year) and no fluctuations at constant pressure, expected value 1 h r	Fluctuations at constant pressure or value above max. rate	Verify compressor, find cause of increased rate	Fluctuations at constant pressure or value above max. safety margins	Stop injection until flow < threshold 1 value again	
2	Injected gas composition	Gas samples & analysis: online system	X		Cont				Compressor station	Defined % for the composition of the gas	Allowed fluctuations reached	Adapt gas composition, reduce injection rate	Above allowed fluctuations	Adapt gas composition, stop injection temporarily	
3	Injected gas composition	Gas samples & analysis: Additional samples for calibration	X		Quarterly				Compressor station	Defined % for the composition of the gas	Allowed fluctuations reached	Adapt gas composition, reduce injection rate	Above allowed fluctuations	Adapt gas composition, stop injection temporarily	
4	Water measurement	Gas measurement	X		Cont				Inlet injection compressor	Specification value	In case specification value is reached	Consultation with the CO <sub>2</sub> provider	In case value is above specification value	Stop CO <sub>2</sub> delivery, investigate at the CO <sub>2</sub> provider the cause, start delivery if value OK again	
5	Discontinuous emissions through leakage, venting or accidents	Combination of techniques	X		Yearly				Potential leakage points like joints or ventstacks						
<b>Injection &amp; monitoring wells</b>															
6	Annular pressure	Pressure device	X		Baseline date prior to operations	Monthly	Monthly		At the well head of all wells (injection and monitoring) penetrating the reservoir	Constant pressure	Increase or decrease in pressure within safety margins	Additional measurements (such as logging or sampling + analysis of fluids to detect CO <sub>2</sub> )	Increase or decrease in pressure above safety margins	Investigate causes (fluid sampling) and options to remediate (in the extreme case well abandonment)	
7	Well integrity	Wireline Logging (CBL, PMIT, EMIT, USIT, WAF, optical)	X		Baseline	Every 2 years	Every 2 years		All wells (injection and monitoring) penetrating the reservoir	Measurements within the expected range	Measurements above expected values	Additional measurements (such as repeat) to corroborate observations, potentially seismic contingency measurements in case values large enough to be detected by seismics	Measurements significantly above expectation values	Stop injection, additional measurements and seismic contingency measurements to identify shallow gas accumulations, investigate options to remediate (in the extreme case well abandonment)	
8	Well head pressure	Pressure device	X		Baseline	Continuous	Continuous	Continuous	At the well head (injection skid)	No fluctuations expected at constant flow rates	Loss of pressure	Lower the injection flow until normal injection pressure is recovered and investigate fracturing	No recovery of injection pressure after lowering injection flow	Stop injection, investigate the cause (fracturing) and evaluate whether conditions are safe	
9	Well head temperature	Temperature device	X		Baseline	Continuous	Continuous	Continuous	At the well head (injection skid)	Determine operational limits for temperature range	In case temperature reaches the determined operational limits (high or low) within 5 to 10 degrees C	Additional measurements to determine the cause	In case temperature reaches the determined operational limits within 5 degrees C	Stop injection until the cause of the temperature change is clarified and safe	
<b>Abandoned wells with pancake plug</b>															
10	Annular pressure	Pressure device	X		Continuous including at least during a month after abandonment				At the well head of all wells (injection and monitoring) penetrating the reservoir	Constant pressure	Increase or decrease in pressure within safety margins	Additional measurements (such as logging or sampling + analysis of fluids to detect CO <sub>2</sub> )	Increase or decrease in pressure above safety margins	Investigate causes (fluid sampling) and options to remediate (in the extreme case well abandonment)	
11	Monitoring 'pancake' plug	Pressure and gastest	X	X	Test after abandonment for wells abandoned at the start of the project		Test after injection period for wells abandoned at the start of the project	Test for wells abandoned after injection period	In the well above the plug	No pressure changes	Minimal pressure changes	Investigate other measurements (e.g. deformation of the wellbore)	Significant pressure changes	Redo the pancake plug	
12	Well head pressure	Pressure device	X		Baseline	Continuous	Continuous	Continuous including at least a test during a month after abandonment	At the well head (injection skid)	No fluctuations expected	Increase or decrease in pressure within safety margins	Additional measurements like logging or analysis of fluids to detect CO <sub>2</sub>	Increase or decrease in pressure above safety margins	Verify the integrity of the pancake plug (pressure and gas test), in case of leakage redo the pancake plug	
13	Well head temperature	Temperature device	X		Baseline	Continuous	Continuous	Continuous including at least a test during a month after abandonment	At the well head (injection skid)	Determine operational limits for temperature range	In case temperature reaches the determined operational limits (high or low) within 5 to 10 degrees C	Additional measurements to determine the cause	In case temperature reaches the determined operational limits within 5 degrees C	Stop injection until the cause of the temperature change is clarified and safe	
14	Composition fluids in wellbore above the pancake plug	Fluid measurement	X		In case pressure changes are observed in the wellbore above the plug				Samples at the well head	Max. CO <sub>2</sub> concentration expected	Increased CO <sub>2</sub> content	Pressure and gastest of the pancake plug			



Feasibility study P18

Reservoir integrity														
15	Reservoir (Bottomhole) pressure	pressure device	(x) x	Baseline data	Cont (monthly with memory gauges)	Cont (monthly with memory gauges)	Cont (monthly with memory gauges)	Downhole permanent sensor or memory gauges	Flowing bottomhole pressure in agreement with simulations	Deviation from expected values	Recalibration of the reservoir simulation model until satisfactory history match	Significant deviation from expected values	Re-evaluate model, in case no explanation can be provided, stop injection	
16	Reservoir (Bottomhole) Temperature	thermometer	x	Baseline data	Cont (monthly with memory gauges)	Cont (monthly with memory gauges)	Cont (monthly with memory gauges)	Downhole permanent sensor or memory gauges	Flowing bottomhole temperature in agreement with well model	Deviation from expected values	Recalibration of the well model until satisfactory history match	Significant deviation from expected values	Re-evaluate well model, in case no explanation can be provided, stop injection	
17	Pressure gradient	pressure device (wireline tool or memory gauge) combined with shut-in	(x) x	Baseline data	6M	6M	6M	Memory gauges combined with shut-in	Pressure data in agreement with expected simulation model and P/z curve	Deviation from expected values	Recalibration of the reservoir simulation model until satisfactory history match	Significant deviation from expected values	Re-evaluate reservoir model, in case no explanation can be provided, stop injection	
18	Temperature gradient	thermometer or DTS (wireline tool or memory gauge) combined with shut-in	(x) x	Baseline data	6M	6M	6M	DTS for permanent installation or memory gauges combined with shut-in	Temperature data in agreement with expected well model	Deviation from expected values	Recalibration of the well model until satisfactory history match	Significant deviation from expected values	Re-evaluate well model, in case no explanation can be provided, stop injection	
19	Microseismic activity in the caprock or at faults	Permanent geophones in monitoring well	x x	Baseline data	Cont	Cont	(Cont)	Monitoring well at caprock and reservoir level	No events in caprock or at faults (re-activation)	Events in the caprock or at faults	Additional measurements like seismic contingency measurements to identify shallow gas accumulations, evaluate whether injection can be continued safely	Large events in the caprock or at faults	Stop injection, additional measurements and seismic contingency measurements to identify shallow gas accumulations, evaluate whether injection can be continued at lower injection rates	
20	Suspected leakage	Surface seismic survey	x	Baseline data already available	Only when other monitoring indicates leakage	Only when other monitoring indicates leakage	Only when other monitoring indicates leakage	Survey can be considered for the transfer of liability	Marine vessel (seismic acquisition using streamers)	No changes in the presence of shallow gas pockets or gas chimneys	~10's of km <sup>2</sup> of CO <sub>2</sub>	Shallow gas pockets	Determine the origin of the gas	
Plume tracking														
21	CO <sub>2</sub> concentrations around the well(s) in the reservoir	RST logging	x	Every 2 years (for gaining experience every half year to year would be preferable)	Every 2 years (for gaining experience every half year to year would be preferable)			Injection well and potentially at monitoring wells						
22	CO <sub>2</sub> breakthrough	Gas measurement	x	Monthly	Monthly			Monitoring well	Breakthrough in agreement with simulations	Breakthrough not in agreement with simulations	Recalibration of the reservoir simulation model until satisfactory history match	N/A	N/A	
Environmental monitoring														
23	Pockmarks at the seabottom	Multi-beam echosounding	x	Baseline	after 5 Years	Survey prior to abandonment	Survey prior to decommissioning of the platform	last survey prior to transfer of liability	Acquisition from a ship	No pockmarks	Pockmarks	Additional gas sampling + analysis to identify the origin of potential seepage or leakage. In case of leakage, identify the pathway with time-lapse seismic data.	Detection of bubbles	Additional gas sampling + analysis to identify the origin of potential seepage or leakage. In case of leakage, identify the pathway with time-lapse seismic data. Mitigation to potential leakage
24	Presence of shallow gas or gas chimneys in the subsurface	Baseline seismic data	x x	Baseline data					Available baseline seismic data	No bright spots or chimneys in the subsurface	Bright spots and/or gas chimneys	Investigate origin of the gas, in case a leakage pathway is suspected, apply time-lapse seismic data	Bright spots and/or gas chimneys to the surface	Additional gas sampling + analysis to identify the origin of potential seepage or leakage. In case of leakage, identify the pathway with time-lapse seismic data. Mitigation to potential leakage
25	Migration pathways for gas in the shallow subsurface	Time-lapse seismic data acquisition (2D or 3D)	x x	Contingency	Contingency	Contingency	Contingency	Contingency	Marine acquisition from a vessel	No changes in bright spots or chimneys in the subsurface	Changes in bright spots and/or gas chimneys	Investigate origin of the gas, in case a leakage pathway is suspected, apply time-lapse seismic data	Changes in bright spots and/or gas chimneys to the surface	Additional gas sampling + analysis to identify the origin of potential seepage or leakage. In case of leakage, identify the pathway with time-lapse seismic data. Mitigation to potential leakage
26	CO <sub>2</sub> in soil	Gas samples using vibrocore + lab analysis	x	Contingency	Contingency	Contingency	Contingency	Contingency	Sampling from a vessel	In case of leakage detection at the seabottom by geophysical methods	Investigate origin of the gas, in case a leakage pathway is suspected, apply time-lapse seismic data	In case of leakage detection at the seabottom by geophysical methods	Investigate origin of the gas, in case a leakage pathway is suspected, apply time-lapse seismic data	
27	CO <sub>2</sub> in soil	Gas samples using vibrocore + lab analysis	x	Yearly	Yearly	Yearly			Measurements around the wellheads	No bubbles				
28	Bubble detection at wellhead	Acoustic bubble detector	x	Contingency	Contingency	Contingency	Contingency	Contingency	Install at the seabottom	No bubbles	In case of few bubbles	Investigate origin of the gas, in case a leakage pathway is suspected, apply time-lapse seismic data	Significant bubble stream	Well remediation (workover)

\*Follows from the risk assessment  
 \*\* t.b.d. by operator, examples are updating model, additional monitoring, ...  
 \*\*\* t.b.d. by operator, examples are stop injection, back-production, well workover, contingency monitoring

**P18 CO2 storage base-case monitoring plan**

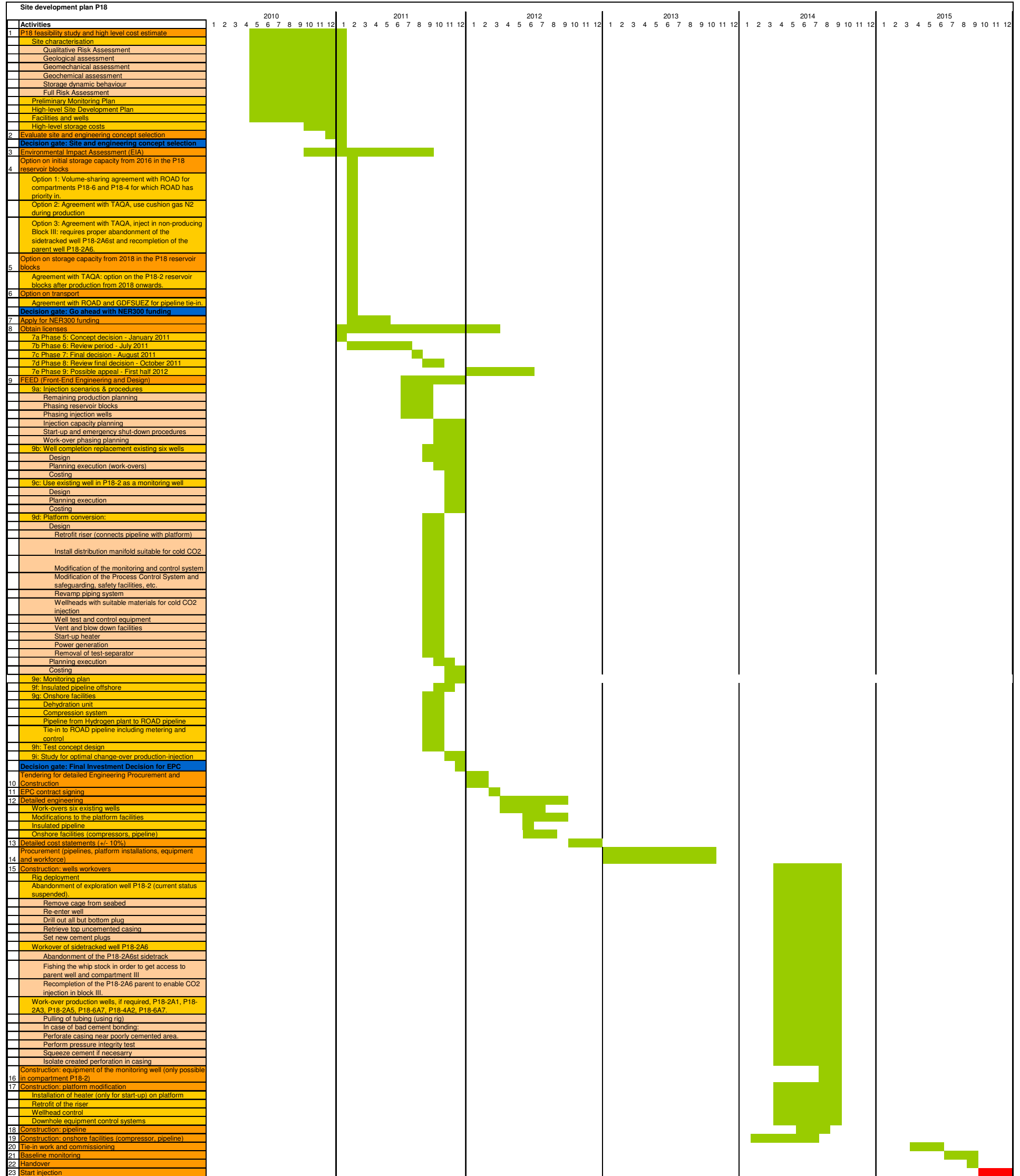
Mandatory monitoring according to Annex II of the EU directive  
 Preliminary estimation of required monitoring  
 Optional contingency monitoring  
↔ Period of time t.b.d. with State Supervision of the Mines (SodM)

↓ Decommissioning of the platform

			Pre-injection				Injection				Post-injection				Post-injection (Abandonment)				Post-injection (Transfer of liability)					
			2011	2012	2013	2014	2015	2016	2017	2018	2019	2020												
<b>Injection proces</b>																								
1	Injection rate	Flow meter	Continuous																					
2	Injected gas composition	Gas samples & analysis: online system	Continuous																					
3	Injected gas composition	Gas samples & analysis: Additional samples for calibration	Quarterly																					
4	Water measurement	Gas measurement	Continuous																					
5	Discontinuous emissions through leakage, venting or accidents	Combination of techniques	Yearly																					
<b>Injection &amp; monitoring wells</b>																								
6	Annular pressure	Pressure device	Baseline				Monthly																	
7	Well integrity	Wireline Logging (CBL, PMIT, EMIT, USIT, WAF, optical)	Single baseline before start of the injection																					
8	Well head pressure	Pressure device	Continuous																					
9	Well head temperature	Temperature device	Continuous																					
<b>Abandoned wells</b>																								
10	Annular pressure	Pressure device	Continuous including at least during a month after abandonment																					
11	Monitoring 'pancake' plug or other used plug	Pressure and gastest	Single baseline test for wells abandoned at the start of the project				Test after injection period for wells abandoned at the start of the project				Test for wells abandoned after injection period													
12	Well head pressure	Pressure device	Continuous including at least a test during a month after abandonment								Continuous including at least a test during a month after abandonment													
13	Well head temperature	Temperature device	Continuous including at least a test during a month after abandonment								Continuous including at least a test during a month after abandonment													
14	Composition fluids in wellbore above the pancake plug	Fluid measurement	In case pressure changes are observed in the wellbore above the plug								In case pressure changes are observed in the wellbore above the plug													
<b>Reservoir integrity</b>																								
15	Reservoir (Bottomhole) pressure	pressure device	Continuous or monthly with memory gauges (frequency can be adapted according to findings)																					
16	Reservoir (Bottomhole) Temperature	thermometer	Continuous or monthly with memory gauges (frequency can be adapted according to findings)																					
17	Pressure gradient	pressure device (wireline tool or memory gauge) combined with shut-in	Shut-in pressure measurement every 6 months																					
18	Temperature gradient	thermometer or DTS (wireline tool or memory gauge) combined with shut-in	Shut-in temperature measurement every 6 months																					
19	Microseismic activity in the caprock or at faults	Permanent geophones in monitoring well	Continuous in available monitoring well (considered contingency monitoring)																					
20	Suspected leakage	Surface seismic survey	Survey in case of irregularities																					
<b>Plume tracking</b>																								
21	CO2 concentrations around the well(s) in the reservoir	RST logging	Every 2 years (for gaining experience every half year to year would be preferable)																					
22	CO2 breakthrough	Gas measurement	Every month																					
<b>Environmental monitoring</b>																								
23	Pockmarks at the seabottom	Multi-beam echosounding	(Existing) baseline				survey				survey				survey				survey					
24	Presence of shallow gas or gas chimneys in the subsurface	Baseline seismic data	Baseline: interpretation on existing data																					
25	Migration pathways for gas in the shallow subsurface	Time-lapse seismic data acquisition (2D or 3D)	Survey in case of irregularities																					
26	CO2 in soil	Gas samples using vibrocore + lab analysis	Survey in case of irregularities																					
27	CO2 in soil	Gas samples using vibrocore + lab analysis	Baseline at risk spots				survey				survey				survey				survey					
28	Bubble detection at wellhead	Acoustic bubble detector	Survey in case of irregularities																					



### 15. Appendix E: Project timeline



Prepared for:

Royal Haskoning B.V. Milieu  
Deelrapport opslag CO<sub>2</sub>  
voor de Milieueffectenrapportage CCS Maasvlakte  
Projectnummer 9V7319.20

*PanTerra Geoconsultants B.V.*  
Weversbaan 1-3  
2352 BZ Leiderdorp  
The Netherlands  
Tel. +31 71 581 35 05  
Fax +31 71 301 08 02  
ABNAMRO bank 49 28 54 319  
E-mail info@panterra.nl

## **Geschiedenis en Beschrijving van de P18 velden**

**A van de Weerd**

**PanTerra Geoconsultants**

**Reviewed: door A. A. Speksnijder**

THIS REPORT contains analyses opinions or interpretations which are based on observations and materials supplied by the client to whom, and for whose exclusive and confidential use, this report is made. The interpretations or opinions expressed represent the best judgement of PanTerra Geoconsultants B.V. (all errors and omissions excepted); PanTerra Geoconsultants B.V. and its officers and employees, assume no responsibility and make no warranty or representations, as to the productivity, proper operations, or profitableness of any oil, gas, water or other mineral well or sand in connection which such report is used or relied upon.

Introductie .....	7
Introductie .....	7
Geschiedenis van de P18 Winingvergunning. ....	9
Geologische Beschrijving van de P/18 velden.....	12
Het West Nederland Bekken.....	12
Tertiair.....	18
Boven Krijt.....	18
Onder Krijt.....	18
Jura.....	18
Trias .....	19
Perm .....	19
Carboon.....	19
De tektoniek van het West Nederland Bekken .....	22
Trias –Midden Jura .....	22
Laat Jura - Vroeg Krijt.....	22
Laat Krijt - Oligoceen.....	22
Oligoceen - nu.....	23
De structuren van de olie en gas velden.....	23
Petroleum systemen van het West Nederland Bekken. ....	23
De structuur van de P18 velden .....	26
Reservoir .....	28
Gascompositie.....	29
De deklaag van de P/18 velden.....	29
De laterale afsluiting van de P/18 velden .....	30
P/18-2 veld.....	31
Reservoir modellen en de vergelijking met de productiegeschiedenis.....	32
P/18-4 veld.....	33
Het P/18-4 geologisch model en de productiegeschiedenis.....	35
Het P/18-6 veld .....	35
Het P/18-6 geologisch model en de productiegeschiedenis.....	36
Bodemdaling en seismische activiteit als gevolg van gasproductie .....	36
De plannen voor CO <sub>2</sub> Injectie .....	36
Opslag capaciteit en injectie tempo van CO <sub>2</sub> in de verschillende velden.....	36
Injectie Plan .....	37
Risico beheersing, CO <sub>2</sub> lekkage mogelijkheden.....	38
Inleiding .....	38
Mogelijke lekkage door de deklaag .....	38
De aard van de afsluitende bovenlagen .....	38
Onderzoek en resultaten mechanische gedrag, afsluitende bovenlagen en breuken .....	39
Onderzoek en resultaten: geochemie van afsluitende bovenlagen (caprock of seal) .....	40
Onderzoek en resultaten: geochemie van het reservoir .....	40
CO <sub>2</sub> lekkage via het overstromingspunt (“spillpoint”) van het reservoir .....	40
Lekkage langs breuken .....	42
Reactivatie van breuken.....	42
Gas migratie te zien op seismische lijnen.....	43

## Beschrijving van de P/18 gasvelden.:

Lekkage mogelijkheden bij de putten. ....	43
Lekkages mogelijkheden aan de buitenkant van de putverbuizing. ....	44
Lekkages aan de binnenkant van de putverbuizing. ....	44
Definitieve afsluiting van de putten. ....	45
Status van de P18 putten. ....	45
Zijtakken (“sidetracks”) ....	46
Samenvatting en aanbevelingen van de put inventarisatie studies ....	47
Referenties ....	48

Figuur 1 Schema van het CO <sub>2</sub> opslag project. ....	7
Figuur 2. Kaart van P18 en directe omgeving. Gas velden en gas pijpleiding zijn rood, olievelen en oliepijpleiding zijn groen. (Kaartje van TAQA.) .....	8
Figuur 3 Kaart van P18, detail van Figuur 2. (Kaartje afkomstig van TAQA.) .....	10
Figuur 4. Jaar productie van de P18a en P18c winningvergunnings. Cumulatieve productie (tot en met 2009) is 17343,5 miljoen standaard M <sup>3</sup> (17.3 Bcm). ....	11
Figuur 5. Kaartje van Nederland met daarin aangegeven de structurele elementen in de diepe ondergrond. De locatie van de P18 velden zijn aangegeven alsook de locatie van Barendrecht. De profiel doorsneden worden getoond in Figuur 6 en 7. ....	12
Figuur 6. Doorsnede door Nederland met het West Nederland Bekken. De kaart van Figuur 5 laat de locatie zien van deze doorsnede. (Figuur naar De Jager, 1997.) ....	13
Figuur 7. Doorsnede door het West Nederland Bekken in de omgeving van Rotterdam. Vergelijk met Figuur 6. De locatie van deze doorsnede is aangegeven in Figuur 5. De olievelen in het Onder Krijt en de gas velden in de Trias zijn aangegeven. (Figuur naar De Jager, 1997.) .....	13
Figuur 8. Sterk vereenvoudigde doorsnede door de P/18 velden. De putten zijn geprojecteerd in het vlak van doorsnede. (Figuur uit TAQA, 2009.) .....	14
Figuur 9. Bovengedeelte van de gesteentekolom in P18 gebaseerd op de verticale P18-1 put. De gele lagen in het Tertiair zijn aquifers. Het ondergedeelte is weergegeven in Figuur 10. ....	15
Figuur 10. Ondergedeelte van de gesteentekolom gebaseerd op de verticale P18-1 put. De roze lagen (Trias en Perm) bevatten gas. In deze put is olie aanwezig in zandstenen van de Nieuwerkerk Formatie en in de Ijsselmonde / Berkel/ Rijswijk Members. In de Holland Greensand Member zijn sporen van olie gevonden. In andere putten in P18 zijn deze lagen watervoerend. (Stratigrafische kolom aangepast naar de "condensed well log" van P18-01.) .....	16
Figuur 11. Gamma Ray en Sonic logs van de P18-2 put. Aangegeven zijn de reservoirs, aquifers en afsluitende laag pakketten (= "seals"). De reservoir-aquifer pakketten kunnen water, olie of gas bevatten. (Figuur uit Vandeweyer et al, 2010.) .....	17
Figuur 12. Profiel met de putten van de P/18 velden. De putten zijn naast elkaar geplaatst zodat ze direct met elkaar kunnen worden vergeleken. De curve is de natuurlijke gamma stralingcurve (GR curve). Gedeeltes van de vier reservoirs zijn goed en gedeeltes zijn niet goed: in de kolom rechts van de curve betekent oranje dat de porositeit laag (niet goed) en dat er geen gas uit is gewonnen, groen is goed. B= barrière, GB = gedeeltelijke barrière. ....	20
Figuur 13. Bepaling van gesteentetype in het afsluitend laagpakket van de Boven Trias door middel van boorgatmetingen. Alleen de top van het Trias gasreservoir is aangegeven. (Figuur uit Vandeweyer et al, 2010.) .....	21
Figuur 14. Mogelijke migratieroute (met pijlen aangegeven) van gas uit de Posidonia Formatie langs een breukzone. (Figuur uit Vandeweyer et al, 2011.) .....	24
Figuur 15., Seismische lijn over de P/18-2 en P/18-6 velden. De gas velden zijn duidelijk te zien als horstblokken op het niveau van de Trias. Ook is duidelijk te zien dat er een zwakke anticlinale structuur is op het niveau van de top Jura (= basis .Krijt). Op deze figuur zijn niet alle breuken ingetekend, vooral in het Krijt zijn maar enkele breuken ingetekend. (Figuur uit Petrel model, Vandeweyer et al, 2011) .....	25

- Figuur 16. Dieptekaart van het P/18-2 veld in het noordoostelijke deel van het P18 Blok. Aan de noord kant is het P15 Blok, aan de oostkant het Q16 blok. De contourlijnen zijn dieptelijnen van de top van het Trias reservoir. Alleen het met gas gevulde Trias reservoir van het P18/-2 veld is op dit kaartje rood gekleurd. Aangegeven op deze kaart zijn de oppervlakte locatie van het P18A platform en de locaties (blauw) waar de putten het reservoir doorboren. Met uitzondering van P18-2 zijn al de putten gedeveerd en geboord vanaf het P18 platform. (Figuur uit TAQA 2009.)..... 26
- Figuur 17. Dieptekaart van de P/18 velden. De contourlijnen zijn dieptelijnen van de top van het Trias reservoir. Het met gas gevulde Trias reservoir is op dit kaartje rood gekleurd, in deze kaart is aangenomen dat het gas-water-contact op een diepte van – 3680 m ligt. Aangegeven op deze kaart zijn de oppervlaktelocatie van het P18A platform en de locaties waar de putten het reservoir doorboren. Met uitzondering van P18-2 zijn al de putten gedeveerd en geboord vanaf het P18 platform. (Figuur uit Vandeweyer,2011.)..... 27
- Figuur 18. Kaartje van de drie P/18 velden met daarin schematisch aangegeven de belangrijke breuken (aangegeven met F en een nummer) en de verschillende reservoir compartimenten aangegeven met verschillende kleuren. Er zijn twee type breuken: 1) in rood de breuken met aan één kant Trias reservoir en aan de andere kant schalie (Trias en/of Jura); 2) bruine stippellijnen zijn breuken met aan beide zijden de Trias reservoir sectie. Naar het NW (in de richting van de breuken F17, F16 en F55) duikt het Trias lagenpakket onder het gas-water-contact. (Figuur uit Vandeweyer et al, 2011.)..... 30
- Figuur 19. Dieptekaart van het Trias reservoir van het P/18-4 veld. Het veld wordt aan de NW kant begrensd door het P15-9E veld. P/18-04 veld en de breuken zijn rood ingekleurd. (Figuur uit TAQA 2009.)..... 31
- Figuur 20. Dieptekaart van het Trias reservoir van het P/18-6 veld. Het langwerpige veld is voor een gedeelte gelegen in het P18 blok en wordt doorboord door de P18-6A7 put. Breuken en het gas-voerende reservoir van het P/18-6 veld zijn rood gekleurd. (Figuur uit TAQA 2009.)..... 34
- Figuur 21. Schematische voorstelling van een put met zijtak (“sidetrack”) en enige terminologie. De dieptes worden gemeten in het boorgat (“along hole”) vanaf een referentie punt in de boorinstallatie, meestal de “rotary table”. De hoogte van dit referentie punt t.o.v. gemiddeld zee niveau wordt gemeten. Met behulp van de deviatie data van de put worden vervolgens dieptes omgerekend naar TVD (**T**otal **V**ertical **D**epth), t.o.v. het gemiddelde zeeniveau is dat TVDSS (=Total Vertical Depth Sub-Sea). ..... 47

Tabel 1. Reservoir eenheden in de P/18 velden.....	28
Tabel 2. Grootte en enkele gemiddelde reservoir eigenschappen van de drie P/18 gas velden. De gasvolumes zijn de volumes in het reservoir omgerekend naar de volumes bij oppervlakte druk en temperatuur). Zie Figuur 4 voor een grafiek met de jaarlijkse productie. Een Bcm is een biljoen kubieke meter (1000.000.000 M <sup>3</sup> ); mD is millidarcy, een maat voor de doorlaatbaarheid van een gesteente. (Data uit TAQA 2009.) .....	28
Tabel 3. P/Z plot data en productie data. Alle p18 velden van Jaarverslagen, Ministerie van Economische Zaken. Cum productie van de velden uit TAQA (2009). Een Bcm is een biljoen kubieke meter, dat is 1000.000.000 M <sup>3</sup> . Een P/Z plot is een druk-volume diagram waaruit het reservoir volume kan worden afgeleid.....	29
Tabel 4. Samenstelling van het gas in de P/18 velden in mol percentages.....	29
Tabel 5. Reservoireigenschappen van het P/18-2 veld. Diktes zijn totale diktes van de formaties (z.g. “gross thickness”) afkomstig van boorprofielen. (Porositeit, permeabiliteit & Sw uit TAQA spreadsheet P18 Bunter-petro-wellAverages.).....	32
Tabel 6. Reservoir eigenschappen van het P/18-04 veld. Dikte is de totale dikte van de formaties (z.g. “gross thickness”), afkomstig van het P18-4A2 boorprofiel. (Porositeit, permeabiliteit & Sw uit TAQA spreadsheet P18 Bunter-petro-wellAverages.) .....	34
Tabel 7. Reservoireigenschappen van P/18-6 veld. Er is een put in het veld, P18-6A7St1. De basis van de Lower Detfurth en de Volpriehausen zijn niet doorboord. (Porositeit, permeabiliteit & Sw uit TAQA spreadsheet P18 Bunter-petro-wellAverages.) .....	35
Tabel 8 Hoeveelheden CO <sub>2</sub> die kunnen worden opgeslagen in de drie velden en de mogelijke injectie capaciteit van vier putten (uit Vandeweyer et al, 2011.) .....	37
Tabel 9. Putten in het P18 Blok. Diepte (TD) van de putten is gemeten langs het boorgat (“along hole”, zie Figuur 21). Zie ook de kaart van Figuur 3, waar alleen de mislukte put P18-2A4 niet op staat.....	46

## Introductie

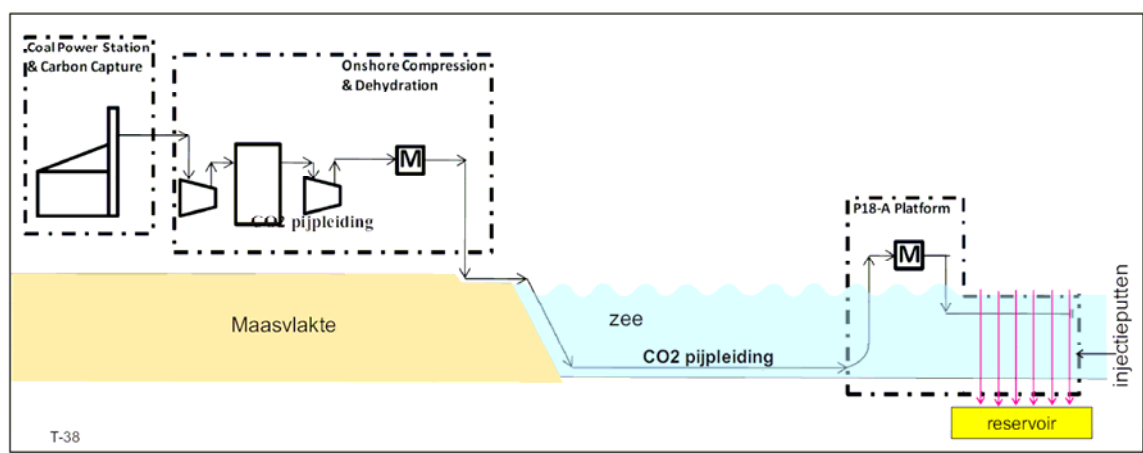
Dit rapport beschrijft de petroleum geologie van de P18 gasvelden. De velden zijn gelegen voor de kust op korte afstand van de Maasvlakte en zijn daarom geschikt voor de opslag van CO<sub>2</sub>. Dit rapport is in het Nederlands geschreven zodat het gebruikt kan worden voor de Milieu Effect Reportage (MER). Er is ook een engelse versie van dit rapport gemaakt.

Het hele opslagproject bestaat uit:

- 1) een CO<sub>2</sub> afvanginstallatie een kolengestookte elektriciteitscentrale,
- 2) pijpleiding naar de lege gasvelden in het P18 Blok voor de kust van de Maasvlakte,
- 3) het P18 platform,
- 4) injectie putten en
- 5) ondergrondse reservoir (zie Figuur 1).

Dit rapport gaat over het reservoir (5) en geeft een samenvatting van de putten. De andere delen van het project zoals, platform, pijpleiding en afvanginstallatie worden hier niet behandeld.

In het P18 offshore blok zijn een drietal gasvelden aanwezig die aan het einde van hun gasproductie zijn; ze zijn bijna leeg en vanwege hun relatief kleine afstand tot de Maasvlakte zijn ze alleen al door hun ligging zeer geschikt voor een CO<sub>2</sub> opslag project. De gasvelden worden beheerd door de maatschappij TAQA en zijn eigendom van TAQA samen met een aantal andere maatschappijen. De elektriciteitscentrale is een samenwerking tussen E-ON en Electrabel. De pijpleiding zal worden aangelegd door GDF-Suez. Samen vormen deze maatschappijen het zogenaamde ROAD<sup>1</sup> project en de Maasvlakte CCS project CV.

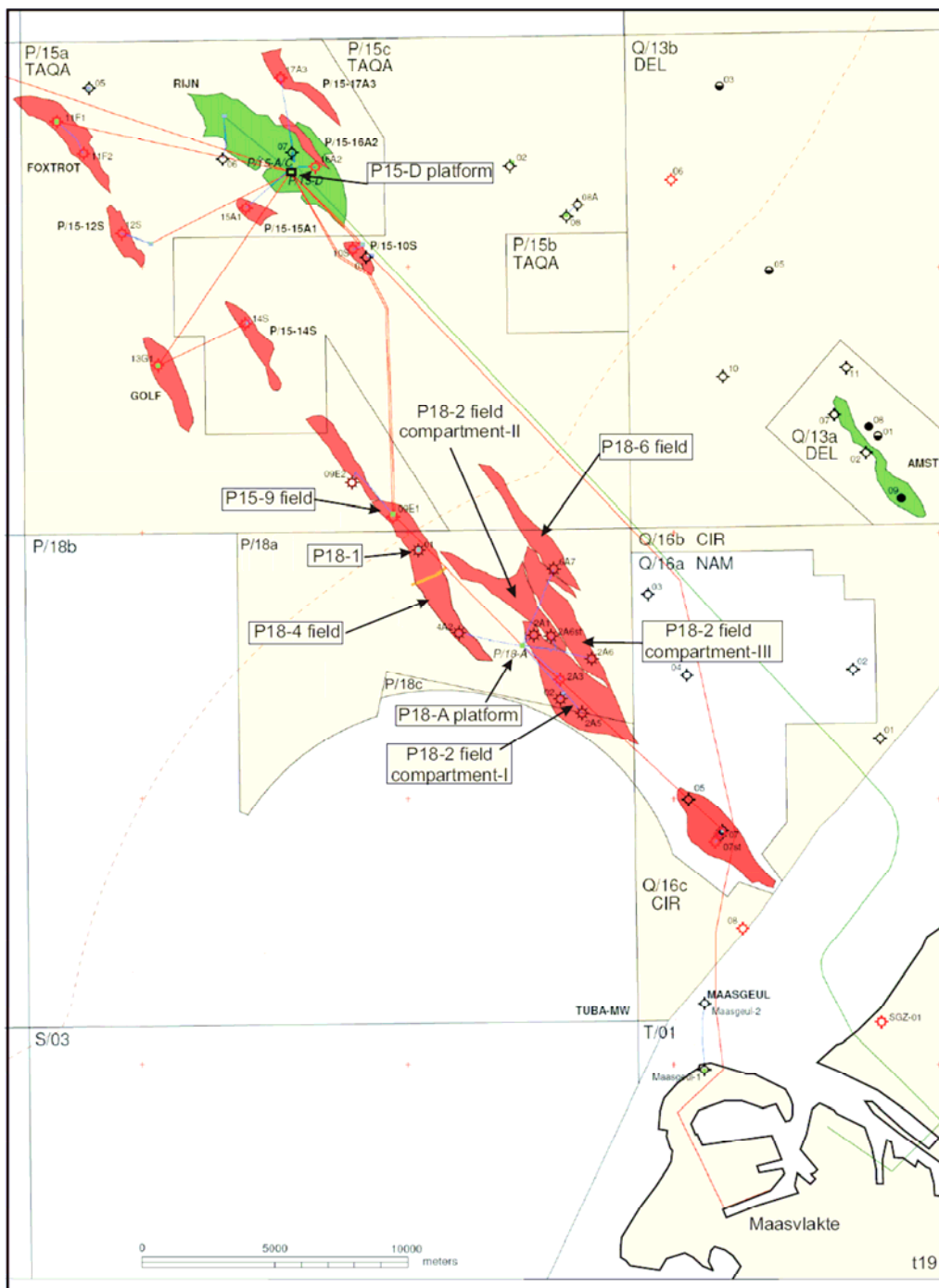


Figuur 1 Schema van het CO<sub>2</sub> opslag project.

<sup>1</sup> Road is een acronym van Rotterdam Opslag en Afvang Demonstratie project.



Beschrijving van de P/18 gasvelden.:



Figuur 2. Kaart van P18 en directe omgeving. Gas velden en gas pijpleiding zijn rood, olievelden en oliepijpleiding zijn groen<sup>2</sup>. (Kaartje van TAQA.).

<sup>2</sup> Internationaal is de conventie om gasvelden rood te kleuren en olie velden groen. Alleen in Nederland (TNO) is dat andersom: gasvelden groen, olie velden rood. TAQA volgt de internationale conventie.

## Geschiedenis van de P18 Winningvergunning.

### 1977-1983: exploratie

De geschiedenis van de P18 activiteiten begint in 1977 toen de maatschappij Amoco Nederland BV een opsporingsvergunning verkreeg voor winningvergunning P18a; deze werd vernieuwd in 1983. De opsporingsvergunning voor P18c is verleend in december 1989.

### 1987-1989: exploratie boringen

De eerste exploratie put, P18-1, werd geboord in de winter van 1987-1988 en ontdekte olie in het Onder Krijt en gas in de Trias. Alleen het gas voorkomen werd getest. De exploratie put P18-2 werd geboord in 1989 en ontdekte gas in de Trias (Figuur 2 & Figuur 3).

### 1990-1993: evaluatie en productie boringen

Naar aanleiding van deze gasvondsten heeft Amoco een winningsvergunning aangevraagd. De winningsvergunning voor P18a werd verleend in april 1992 en voor P18c in juni 1992.

Al voor de winningsvergunning was verleend, was Amoco begonnen met het boren van evaluatie putten. P18-3 (naam later veranderd in P18-2A1) werd geboord in de zomer van 1990 en is een gas vondst. P18-2A2 werd geboord in het voorjaar van 1991 en is eveneens een gasvondst. P18-4 (naam later veranderd in P18-2A4) werd geboord tijdens het voorjaar en zomer van 1993. Het boren van de P18-2A4 put in 1993 mislukte, de put is niet dieper dan 416 meter. Al deze putten werden geboord vanuit de locatie van het (toekomstige) P18A platform.

### 1993: plaatsing P18A platform en constructie pijpleiding.

Het gasproductie platform P18A is geplaatst in 1993. Het is een satelliet van het grote gas behandelplatform P15D. Een pijpleiding van P18A naar platform P15D werd gelegd in 1993. Gas productie begint in 1993.

### 1993-vandaag: gas productie en aanleg van productie putten.

De jaarlijkse gasproductie is weergegeven in de grafiek van Figuur 4. Deze grafiek is gebaseerd op openbare gegevens van TNO en is de totale gasproductie uit alle putten in P18.

Een nieuwe campagne van putten boren werd gestart in 1996. De productieputten P18-2A5, P18-2A6 werden geboord in de winter van 1996-1997. Hun aandeel in de totale gasproductie is te duidelijk zien in de grafiek van Figuur 4.

Een nieuwe zijtak ("sidetrack") werd vanuit P18-2A6 geboord in de zomer van 2003 (P18-2A6-S1), P18-2A7 werd ook die zomer geboord. Deze nieuwe zijtak en nieuwe put leverden een vergroting van de productie op (Figuur 4).

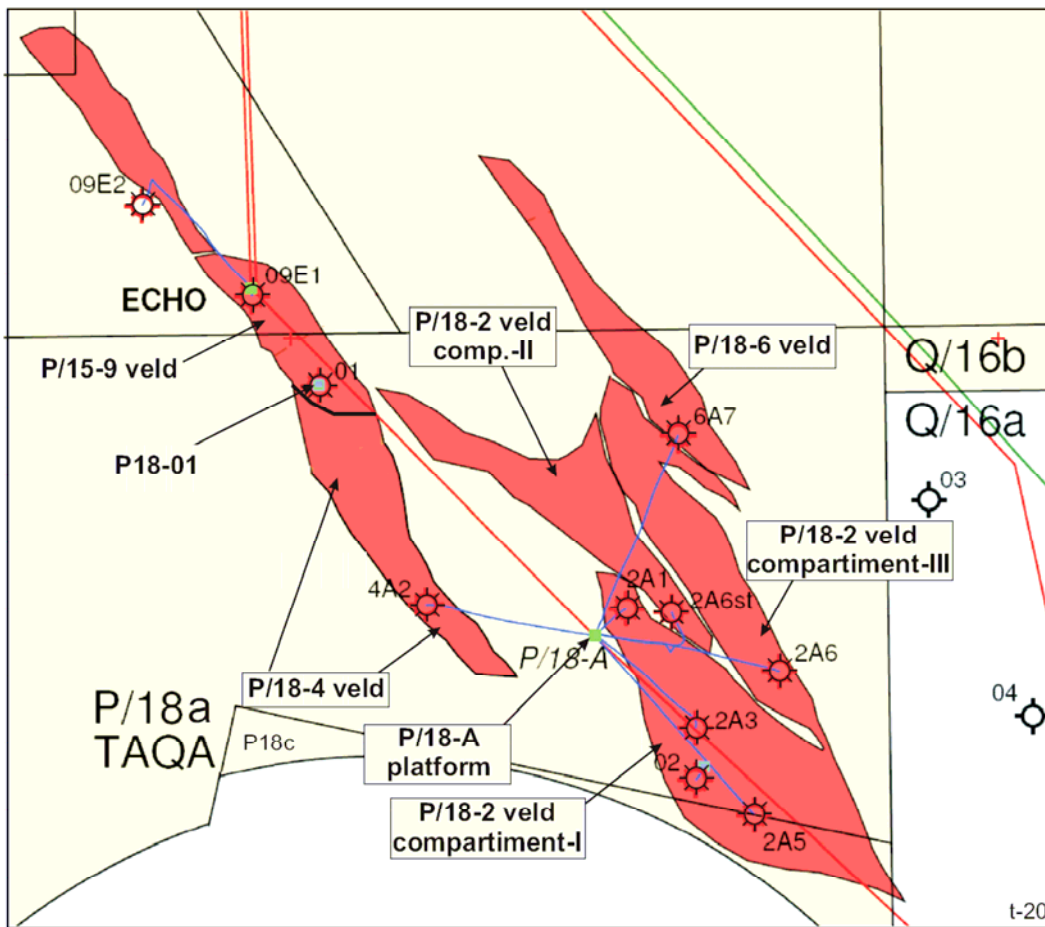
Amoco, inclusief de Nederlandse werkmaatschappijen, werd gekocht door British Petroleum (BP) in 1998. BP verkocht vervolgens de Nederlandse exploratie en productie werkmaatschappij aan TAQA in 2007. De vergunninghouder en uitvoerder voor P18a is

Beschrijving van de P/18 gasvelden.:

nu TAQA. De vergunninghouders van P18c zijn Dana, Dyas en TAQA, terwijl ook hier TAQA de uitvoerder is.

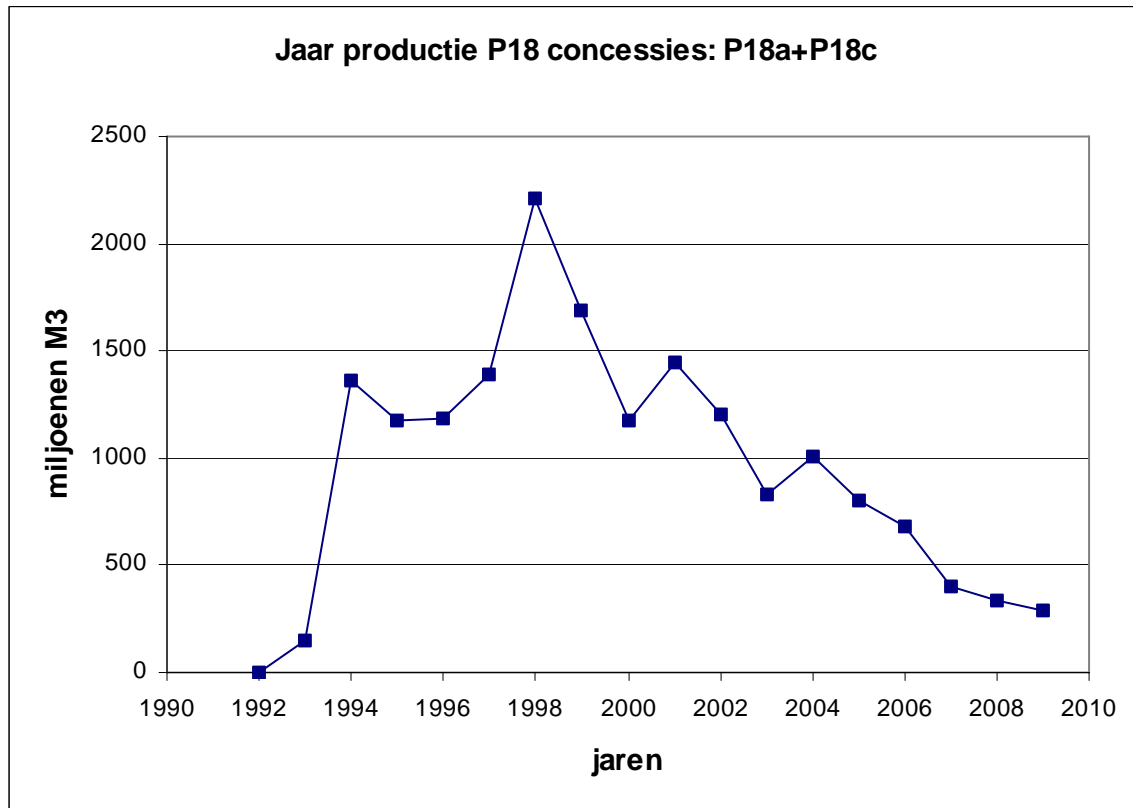
*Conclusie*

In totaal zijn er in het P18 blok drie gasvelden gevonden. Het gas in alle drie de velden is aanwezig in dezelfde Trias reservoirlagen maar de velden zijn van elkaar gescheiden door breuken. De gasvelden waarin CO<sub>2</sub> zal worden opgeslagen zijn P/18-2, P/18-4 en P/18-6. De velden zijn genoemd naar de putten die de velden hebben ontdekt<sup>3</sup>.



Figuur 3 Kaart van P18, detail van Figuur 2. (Kaartje afkomstig van TAQA.)

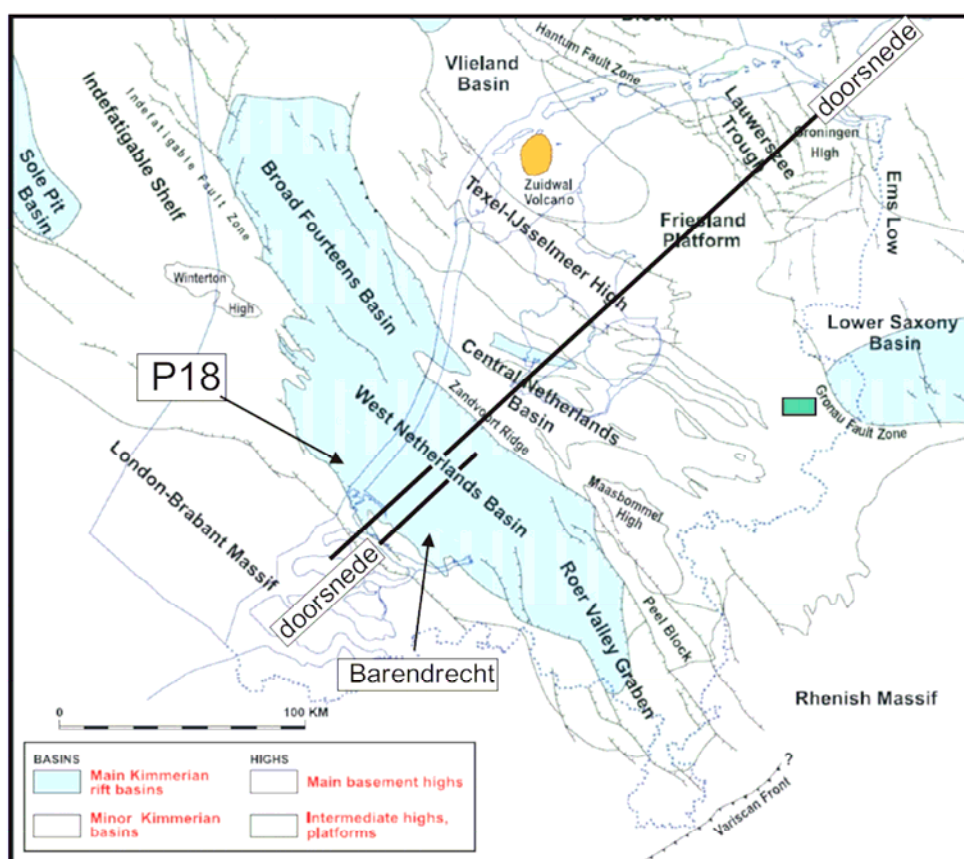
<sup>3</sup> Deze naamgeving is aangehouden door de beheerder van de velden en door het bevoegd gezag. De naamgeving is verwarrend omdat velden en putten dezelfde naam hebben. Als onderscheid tussen put en veld is in dit rapport de volgende conventie ingevoerd: het veld is P/18-2, de put is P18-2.



Figuur 4. Jaar productie van de P18a en P18c winningvergunningen. Cumulatieve productie (tot en met 2009) is 17343,5 miljoen standaard M<sup>3</sup> (17.3 Bcm).

## Geologische Beschrijving van de P/18 velden

Veel gegevens over de ondergrond van Nederland zijn te vinden in “*Geology of the Netherlands*” (een uitgave van de Koninklijke Academie van Wetenschappen uit 2007). Een uitgave in de Nederlandse taal is: “*De ondergrond van Nederland*”, een uitgave van TNO uit 2003. Ook hierin is veel nuttige informatie te vinden over de ondergrond van Nederland. De gegevens waarop dit rapport is gebaseerd zijn afkomstig van TAQA, uit de wetenschappelijke literatuur, uit de openbare gegevens van TNO en uit het haalbaarheid onderzoek uitgevoerd door CATO-2<sup>4</sup> research groepen (Vandeweyer et al, 2011).



Figuur 5. Kaartje van Nederland met daarin aangegeven de structurele elementen in de diepe ondergrond. De locatie van de P18 velden zijn aangegeven alsook de locatie van Barendrecht. De profiel doorsneden worden getoond in Figuur 6 en 7.

### Het West Nederland Bekken.

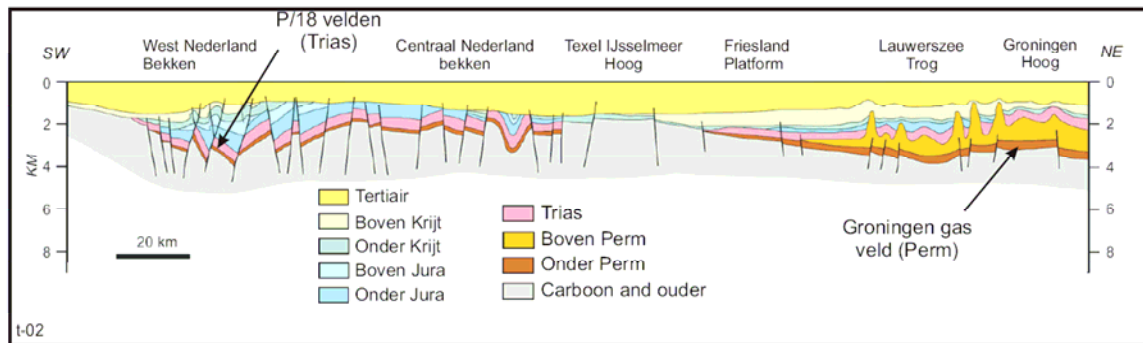
De P/18 velden liggen in het West Nederland Bekken. Dit bekken strekt zich uit in de provincie Zuid Holland en het aangrenzende gebied van de Noordzee (Figuur 5). Naar het zuidoosten toe gaat het bekken over in Roer Vallei Graben. In de Noordzee in het

<sup>4</sup> CATO een acronym van CO<sub>2</sub> Afvang, Transport en Opslag, het nationale onderzoeks programma voor ondergrondse CO<sub>2</sub> opslag.

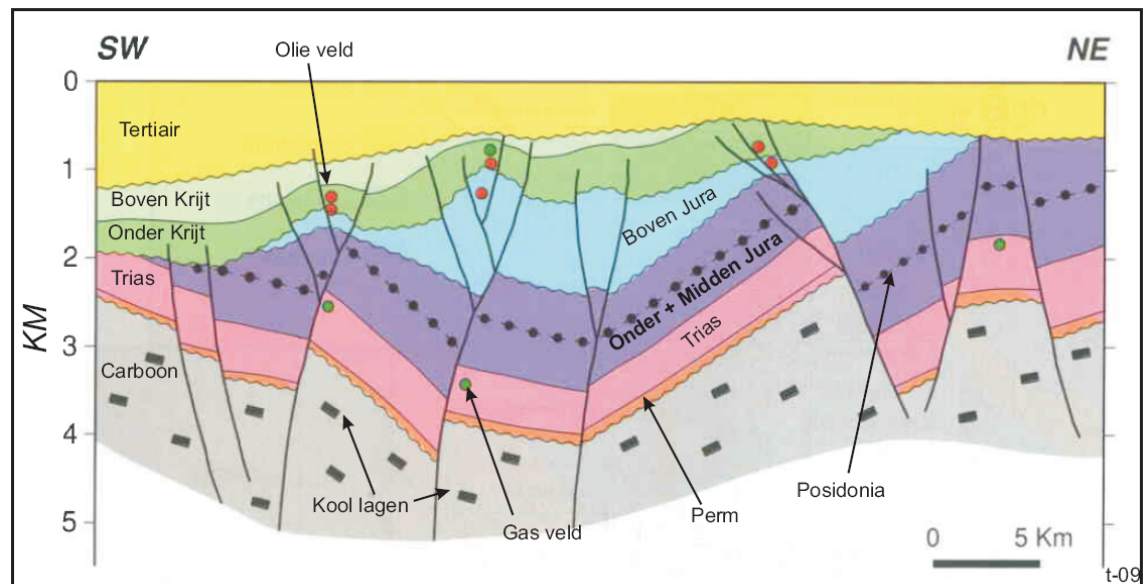
### Beschrijving van de P/18 gasvelden.:

noordwesten grenst het West Nederland Bekken aan het Breeveertien Bekken. Het West Nederland Bekken ontstond in de Laat Jura en werd opgeheven en gedeformeerd in het Laat Krijt. Doorsneden door het bekken zijn te zien in Figuur 6 en 7. Het land gedeelte van dit bekken is uitgebreid beschreven in TNO-NITG, 2002.

In het West Nederland Bekken zijn olie- en gasvelden gevonden; de meeste en grootste gasvelden zijn aanwezig in zandstenen van de Trias, terwijl de olie vooral voorkomt in zandstenen van het Onder Krijt (Figuur 7). De olie- en gasvelden liggen zowel aan land als onder de zeebodem.



Figuur 6. Doorsnede door Nederland met het West Nederland Bekken. De kaart van Figuur 5 laat de locatie zien van deze doorsnede. (Figuur naar De Jager, 1997.)

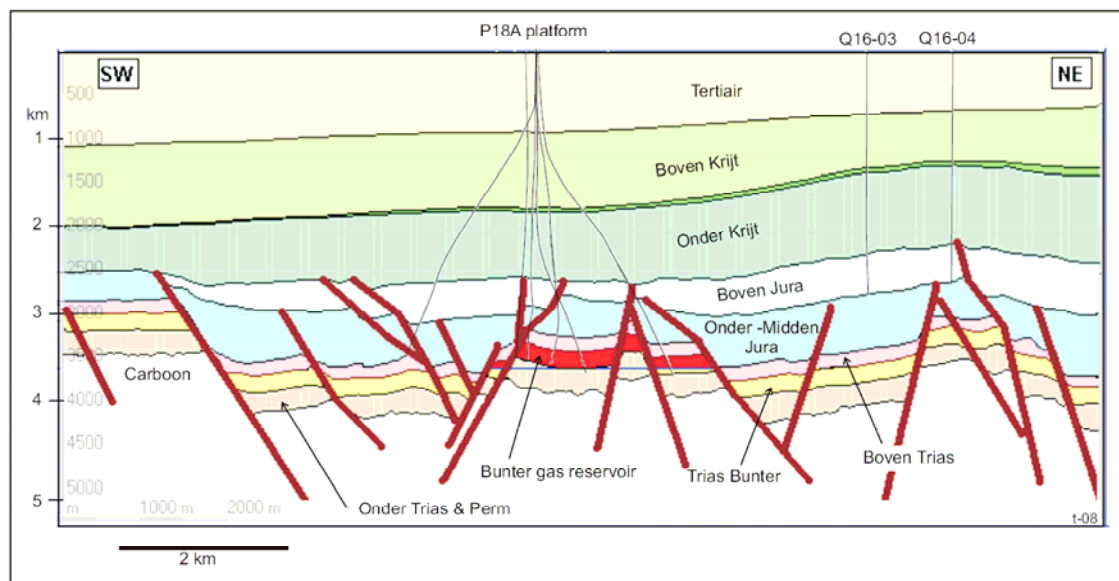


Figuur 7. Doorsnede door het West Nederland Bekken in de omgeving van Rotterdam. Vergelijk met Figuur 6. De locatie van deze doorsnede is aangegeven in Figuur 5. De olievelden in het Onder Krijt en de gas velden in de Trias zijn aangegeven. (Figuur naar De Jager, 1997.)

De olievelden liggen op duizend tot drie duizend meter diepte, terwijl de gasvelden wat dieper zijn gelegen. In P18 zijn de olie voorkomens op ongeveer 2500 m en de gasvelden tussen de drie- en vierduizend meter. De eerste olievelden in het West Nederland Bekken zijn gevonden na de Tweede Wereldoorlog, met de eerste belangrijke vondst in 1953.

## Beschrijving van de P/18 gasvelden.:

Veel olievelden zijn nu uitgeproduceerd (“leeg”) en verlaten, zoals de velden bij Monster, de Lier en IJsselmonde. Aan de noordkant van Rotterdam is het Berkel olieveld nog in productie. De Trias gasvelden liggen dieper (Figuur 7) en zijn ook later gevonden, de meest in de jaren tachtig. De meeste gasvelden zijn in het jaar 2010 nog in productie. De oudste gasvelden zijn nu bijna leeg. De leeg geproduceerde of bijna lege gasvelden van P18 liggen in het West Nederland Bekken voor de kust (Figuur 5). De opbouw van het West Nederland Bekken in de omgeving van P18 lijkt veel op de opbouw van de omgeving bij Barendrecht (zie kaartje in Figuur 5), de afstand beide locatie is ongeveer 50 km. Veel onderzoeken uitgevoerd in het kader van de ondergrondse opslag voor CO<sub>2</sub> in Barendrecht zijn dan ook relevant voor de opslag van CO<sub>2</sub> in P18.



Figuur 8. Sterk vereenvoudigde doorsnede door de P/18 velden. De putten zijn geprojecteerd in het vlak van doorsnede. (Figuur uit TAQA, 2009.)

### *Stratigrafie: Geologische lagen en laagpakketten in de omgeving van P18.*

Hieronder wordt een korte beschrijving geven van de lagen en pakketten die in de omgeving van P18 worden gevonden.

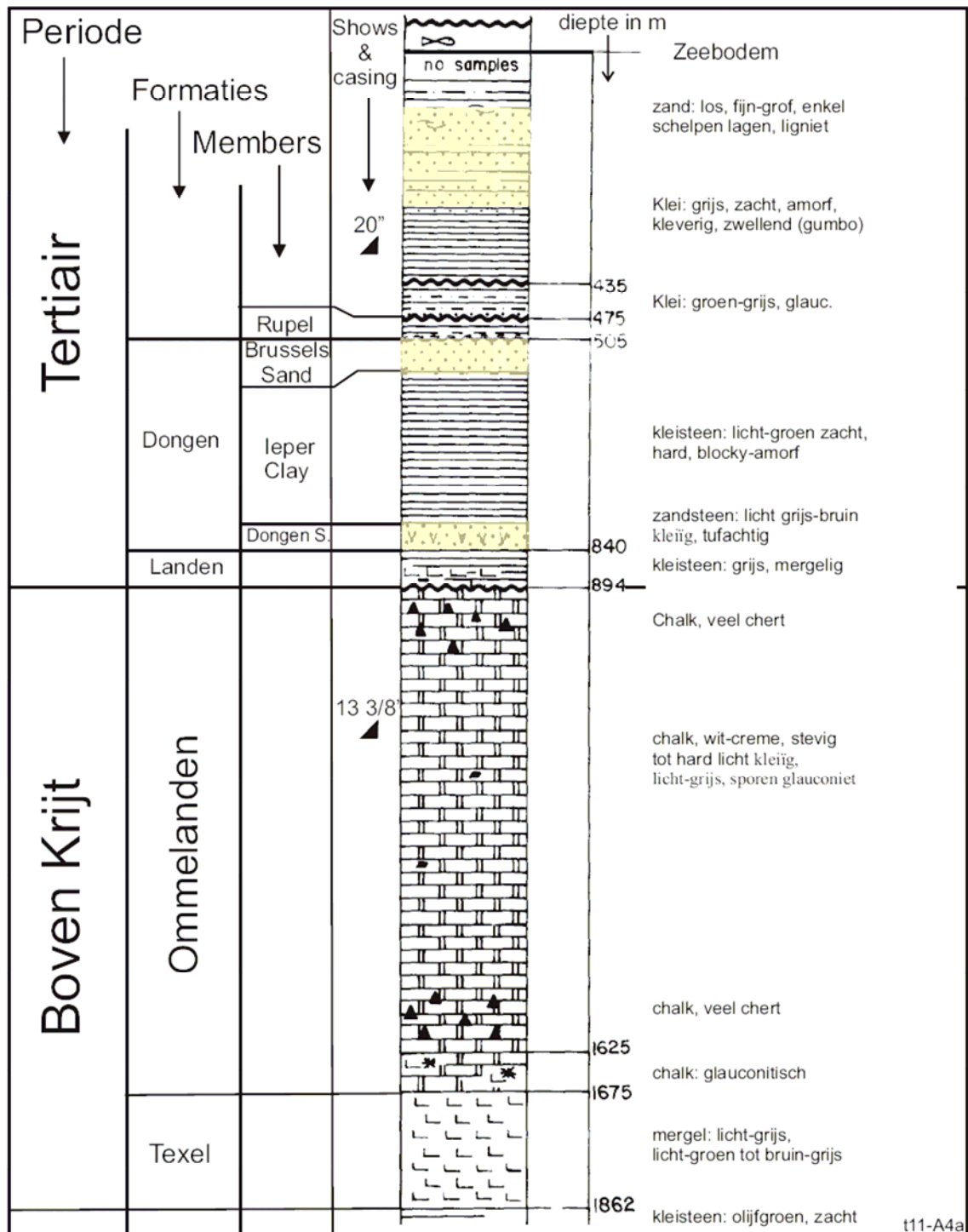
Dankzij de vele boringen en putten is er veel kennis over de lagen en de opeenvolging van de lagen in deze omgeving<sup>5</sup>.

Het laagpakket wordt onderverdeeld op hun ouderdom. We onderscheiden hier van boven naar beneden (dat is van jong naar oud): Tertiair, Krijt, Jura, Trias, Perm en Carboon. Daarnaast worden lagen worden de lagen onderverdeeld in *Groepen*, *Formaties* en

<sup>5</sup> De beschrijving is gebaseerd op putten P18-1 en P18-2. De beschrijving beperkt zich tot de hoofdzaken; voor een gedetailleerde beschrijving van de formele stratigrafie zie van Adrichem Boogaert en Kouwe (1993).

Beschrijving van de P/18 gasvelden.:

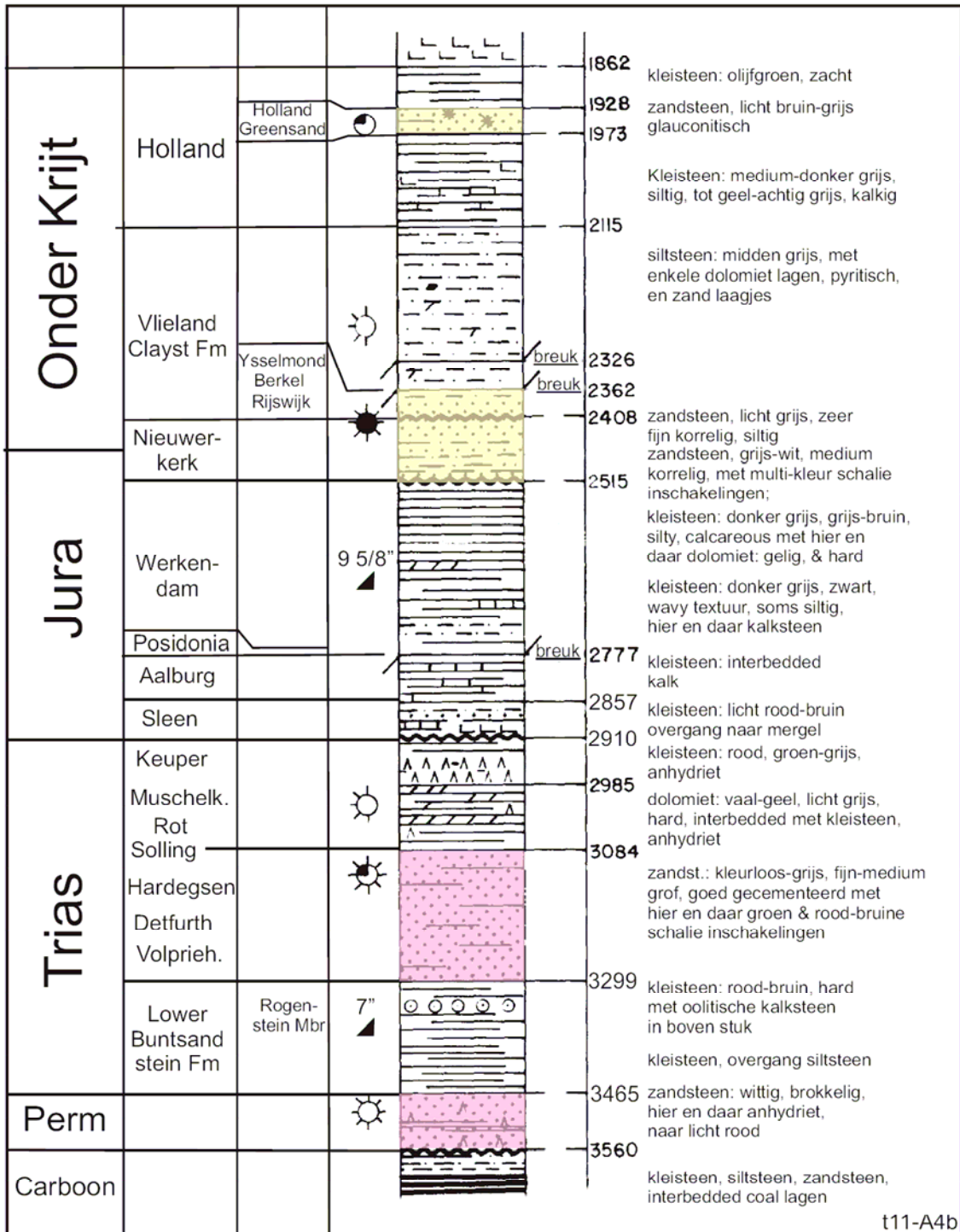
“Members”. Deze onderverdeling is gebaseerd op het soort gesteente, zoals klei, kalk, mergel, zand enzovoort. De hoofdeenheid is de *Formatie*, verschillende formaties kunnen



Figuur 9. Bovengedeelte van de gesteentekolom in P18 gebaseerd op de verticale P18-1 put. De gele lagen in het Tertiair zijn aquifers. Het ondergedeelte is weergegeven in Figuur 10.

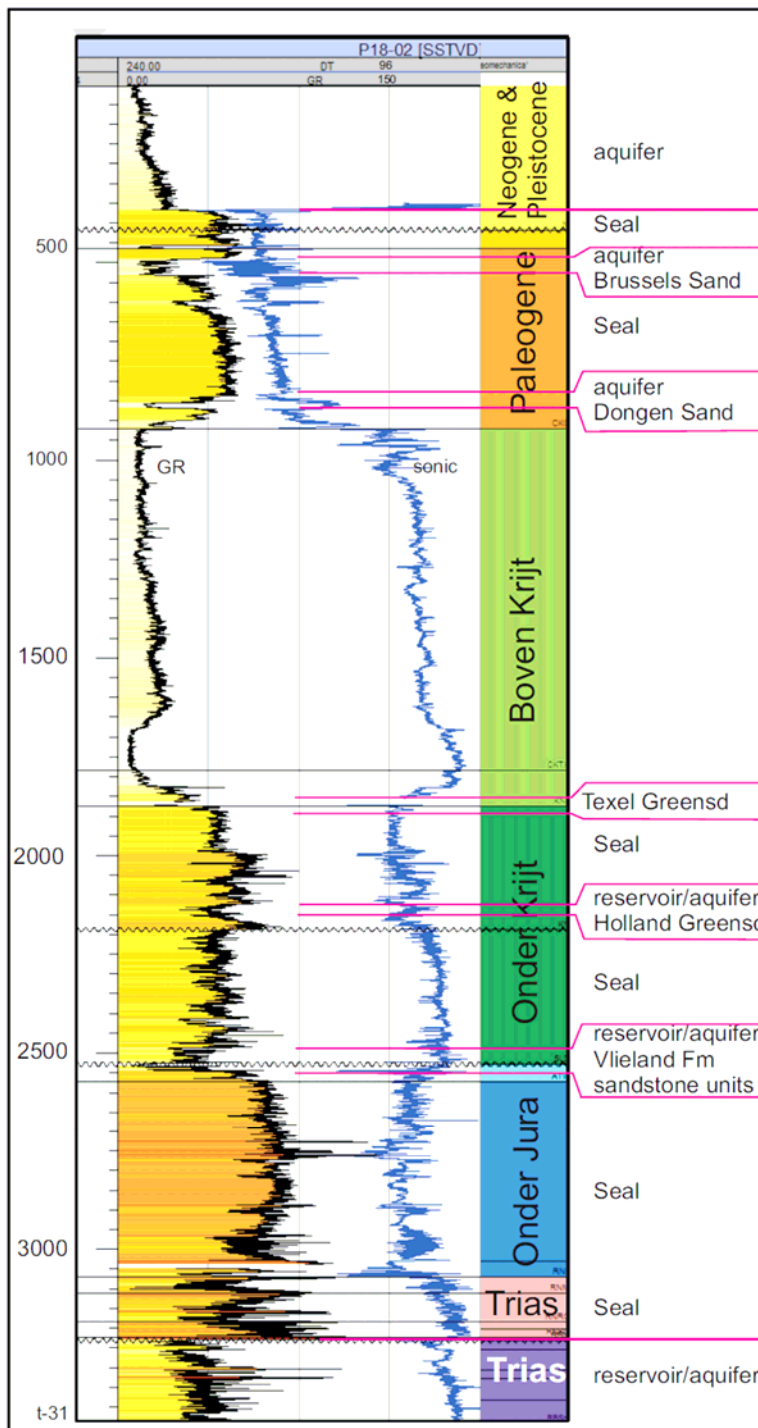


Beschrijving van de P/18 gasvelden.:



Figuur 10. Ondergedeelte van de gesteentekolom gebaseerd op de verticale P18-1 put. De roze lagen (Trias en Perm) bevatten gas. In deze put is olie aanwezig in zandstenen van de Nieuwerkerk Formatie en in de Ijsselmonde / Berkel/ Rijswijk Members. In de Holland Greensand Member zijn sporen van olie gevonden. In andere putten in P18 zijn deze lagen watervoerend. (Het origineel is de "condensed well log" van P18-01.)

Beschrijving van de P/18 gasvelden.:



Figuur 11. Gamma Ray en Sonic logs van de P18-2 put. Aangegeven zijn de reservoirs, aquifers en afsluitende laag pakketten (=“seals”). De reservoir-aquifer pakketten kunnen water, olie of gas bevatten. (Figuur uit Vandeweijer et al, 2010.)

worden samengevoegd in een *Groep*, en een formatie kan worden onderverdeeld in *Members*. Figuur 9 en 10 laten de opeenvolging van formaties zien zoals aangetroffen in de P18-1 put, Figuur 11 toont de P18-2 put.

### *Tertiair*

De zeebodem bevindt zich op ongeveer 20-35 m diepte. Het Boven Tertiair is ongeveer 388 m dik en bestaat uit ongeconsolideerde zanden en kleien van de *Boven Noord Zee Groep*.

Het Onder Tertiair is 458 m dik en bestaat voor het grootste deel uit kleien. Er worden verschillende formaties onderscheiden: de *Rupel Formatie* (95 m dik) en de *Ieper Member* van de *Dongen Formatie* (202 m dik) zijn daarvan de belangrijkste klei formaties; aquifers zijn het Dongen Zand en het Brusselse Zand.

### *Boven Krijt.*

De top van het Krijt bevindt zich op ongeveer 850 - 950m diepte. De basis van het Krijt op 2490-2575 m. Dus het Krijt in het P/18-2 veld is ongeveer 1600 -1700m dik. De dikte van het Krijt kan aanzienlijk variëren in het P18 gebied en daarbuiten. Het Boven Krijt wordt gevormd door de *Ommelanden Formatie* (730-870 m dik) en de *Texel Formatie* (90-95 m dik); beide formaties bestaan uit mergelige kalken (zogenaamde Chalk). In het algemeen hebben deze formaties een lage permeabiliteit, de porositeit is variabel. Het pakket kan zowel afsluitende lagen als reservoirs bevatten.

### *Onder Krijt*

De Holland Formatie (300-400 m dik) bestaat vooral uit mergelige klei, kleisteen en 20-35 m zand van de *Holland Greensand Member*. De *Holland Greensand Member* is een aquifer, maar er kan in dit gebied ook olie voorkomen in dit zand. Hieronder ligt een 200-230 m siltige kleisteen van de *Vlieland Claystone Formation*. Dit wordt gevolgd door 100-125m zandsteen met enkele ingeschakelde kleistenen waarin de *IJsselmonde*, *Berkel* en *Rijswijk Members* worden herkend. In het Rijn olieveld en ook in put P18-1 zijn deze zandstenen verzadigd met olie, elders bevat deze zandsteen alleen water (dus is het een aquifer). De *Nieuwerkerk Formatie* is 30-110 m dik en bestaat uit zanden en ingeschakelde kleien in de putten van het P/18-2 veld, maar seismiek laat zien dat de formatie veel dikker is in de gebieden tussen de velden. De Jura-Krijt grens ligt binnen deze formatie.

### *Jura*

De Jura is hier ongeveer 400 m dik en bestaat uit een viertal formaties. De formaties bestaan voornamelijk uit klei of kleisteen met plaatselijk enkele dunnere inschakelingen van silt en dolomiet. De volgende formaties worden onderscheiden: *Nieuwerkerk Formatie*, *Werkendam Formatie*, *Posidonia Formatie*, *Aalburg Formatie* en *Sleen Formatie*. De *Posidonia Formatie* is het vermelden waard want het is het olie moedergesteente van de olie in het P/15 Rijn veld (Figuur 2) en in de P18-1 put (Figuur 10).

Het Jura laagpakket kan aanzienlijk van dikte verschillen in dit gebied. Over de P/18 gas velden is het in de orde van 400 –500 m dik; naast de velden kan het veel dikker zijn

## Beschrijving van de P/18 gasvelden.:

zoals is te zien in Figuur 8; de verschillen in dikte zijn voornamelijk in de Boven Jura in de Nieuwerkerk Formatie.

### *Trias*

De top van de Trias van de P/18 velden bevindt zich op een diepte tussen 2900-3100m. Buiten de gasvelden is de top van de Trias veel dieper (zie Figuur 8). In de Trias van de P/18 velden kan een driedeling worden herkend:

1) Het bovenste deel, ongeveer 150 tot 175 m dik bestaat voornamelijk uit kleisteen met ingeschakeld dünnere lagen van anhydriet, gips en dolomiet (Figuur 13). Dit is de afsluitende top laag over de P/18 gas velden. Er worden een viertal formaties onderscheiden, van boven naar beneden zijn dat: de *Keuper Formatie* (40m dik), de *Muschelkalk Formatie* (107m dik), de *Röt Formatie* (18m) en de *Solling Claystone Member* (18m).

2) Het middelste deel bestaat overwegend uit zandstenen en is ongeveer 190-215m dik in de P/18 gas velden. Informeel wordt dit pakket wel de Bunter zandstenen genoemd. Er kunnen drie formaties worden onderscheiden: de *Hardegsen Formatie*, de *Detfurth Formatie* en de *Volpriehausen Formatie*.

3) Het diepste deel bestaat voornamelijk uit kleisteen, is 140-170m dik en wordt tot de *Onder Buntsandstein Formatie* gerekend.

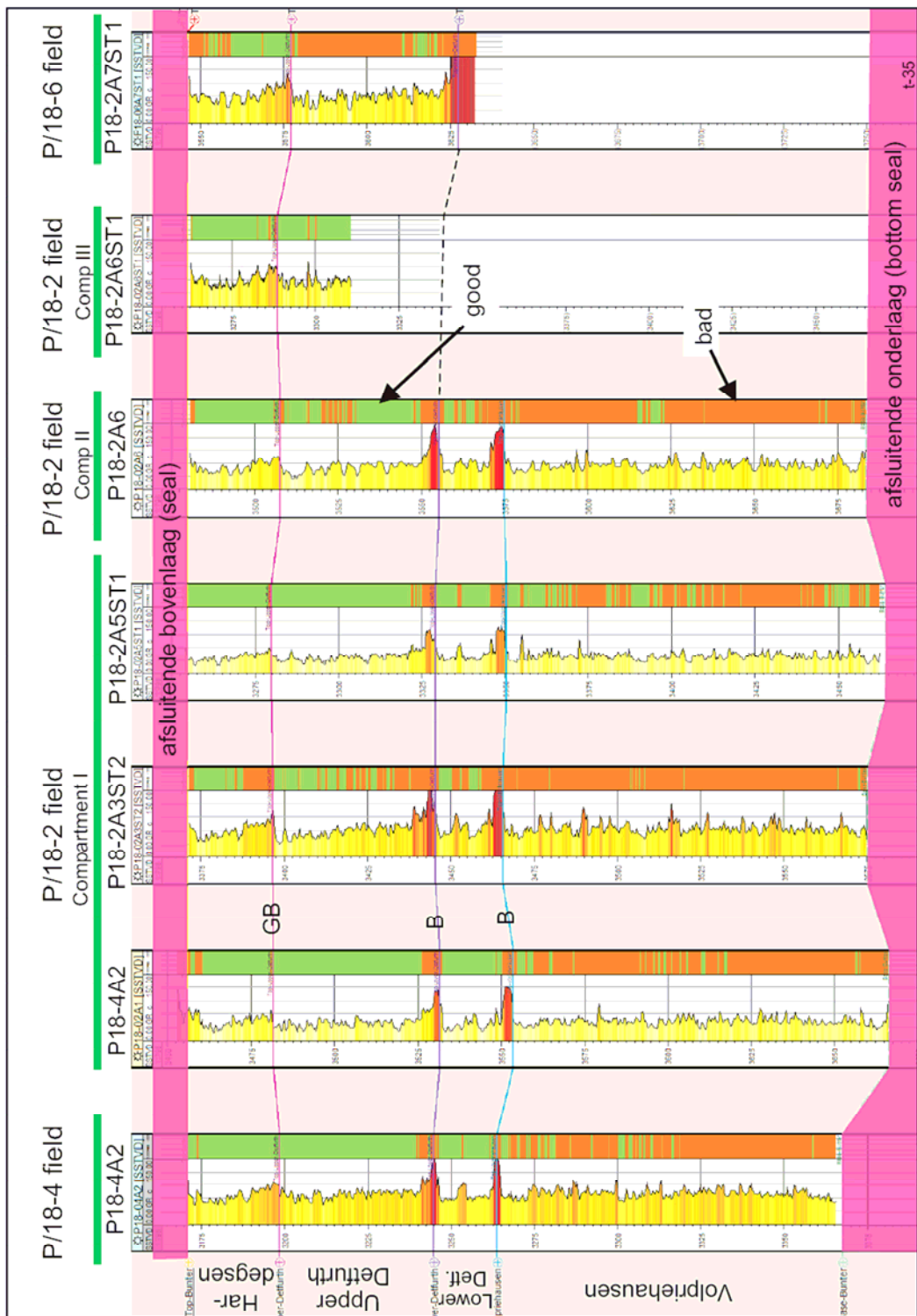
### *Perm*

Het Perm in dit gebied bestaat vooral uit zandsteen en is variabel in dikte. In putten van P18 is 30 tot 95m gemeten.

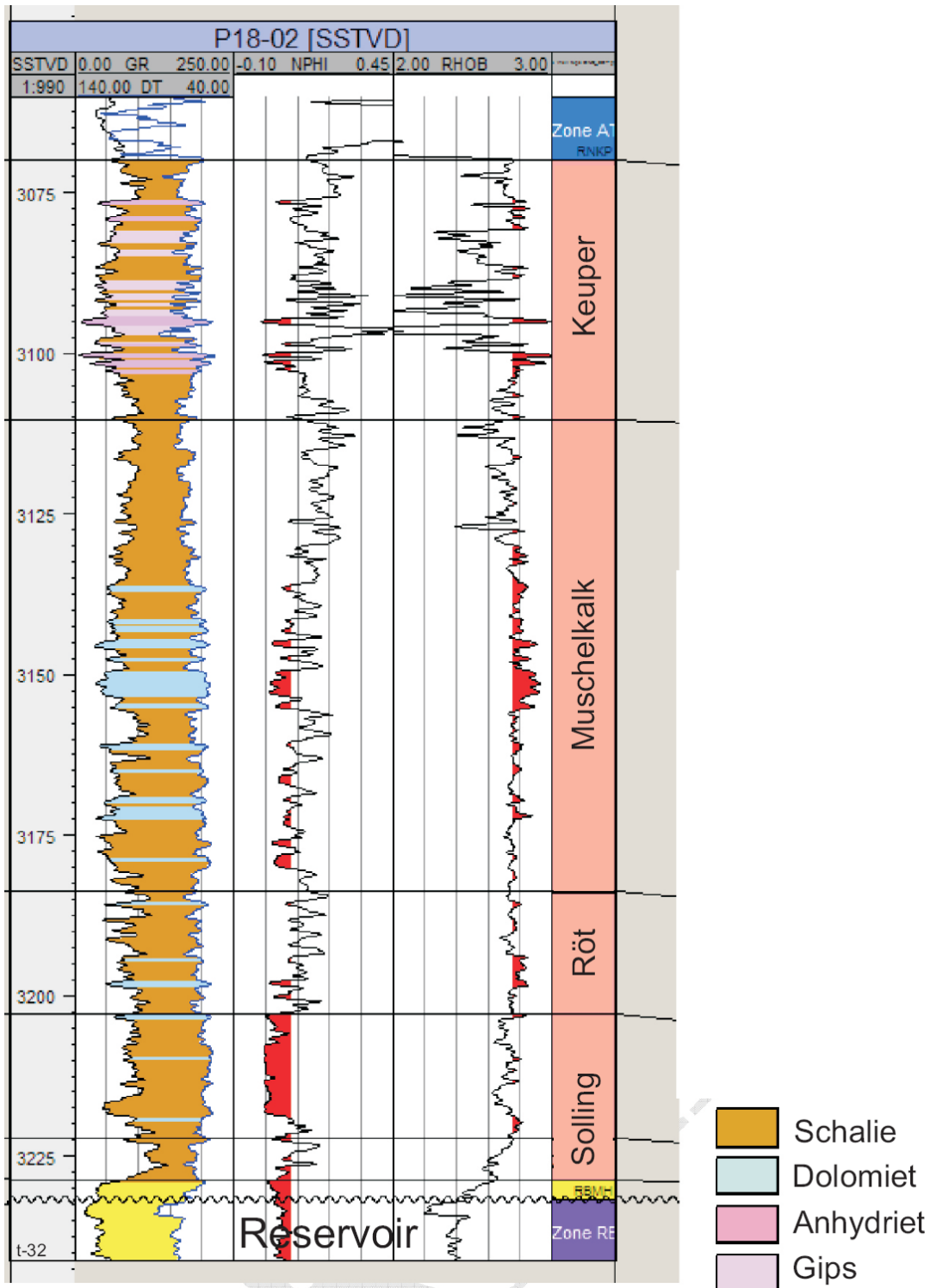
### *Carboon*

De P18-1 en P18-2 putten eindigen in het Carboon. De top van het Carboon werd aangetroffen op een diepte van 3500 tot 3700m.

Beschrijving van de P/18 gasvelden.:



Figuur 12. Profiel met de putten van de P/18 velden. De putten zijn naast elkaar geplaatst zodat ze direct met elkaar kunnen worden vergeleken. De curve is de natuurlijke gamma stralingcurve (GR curve). Gedeeltes van de vier reservoirs zijn goed en gedeeltes zijn niet goed: in de kolom rechts van de curve betekent oranje dat de porositeit laag (niet goed) en dat er geen gas uit is gewonnen, groen is goed. B= barrière, GB = gedeeltelijke barrière.



Figuur 13. Bepaling van gesteentetype in het afsluitend laagpakket van de Boven Trias door middel van boorgatmetingen. Alleen de top van het Trias gasreservoir is aangegeven. (Figuur uit Vandeweyer et al, 2010.)

## De tektoniek van het West Nederland Bekken

In de geschiedenis van het P18 blok kunnen een aantal fasen worden onderscheiden.

### *Trias –Midden Jura*

In de periode van het Trias maakte West Nederland deel uit van een stabiel tektonisch bekken met sedimentatie van duinzanden, rivierzanden en kleien en limnische afzettingen (= afzettingen gevormd in meren). Gedurende de Trias zijn enkele perioden bekend waarin breukbewegingen optraden. Echter in P18 waren deze tektonische activiteiten relatief onbelangrijk zoals blijkt uit de min of meer uniforme dikte en uniforme type afzettingen in de verschillende putten (te zien in Figuur 12). In de Vroeg en Midden Jura zien we vooral marine sedimentatie,

### *Laat Jura - Vroeg Krijt*

De Late Jura markeerde het ontstaan van het West Nederland Bekken. In de Late Jura stond dit gedeelte van Nederland onder trekspanning met uitrekking tot gevolg. Daardoor ontstond er in West Nederland een systeem van normale breuken met een NW-SE oriëntatie, en de daarmee geassocieerde horst blokken en grabens. De grabens zijn gevuld met dikke pakketten gesteenten met een Laat Jura en Vroeg Krijt ouderdom, de Nieuwerkerk Formatie. De dikte van deze formatie is zeer variabel, de formatie is dik in de grabens en dun of zelfs afwezig over de hogere horst blokken. Breukbewegingen gaan door tot in het Vroeg Krijt; in sommige gedeeltes van het West Nederland Bekken is er een grote horizontale component in de breuk bewegingen (zogenaamde zijschuivingen, zie ook Racero-Baena & Drake, 1996).

### *Laat Krijt - Oligoceen*

De volgende tektonische fase vond plaats in het Laat Krijt en het Tertiair. Gedurende deze fase veranderde het tektonische regime van uitrekking naar samendrukking (compressie). Dit omdraaien van tektonisch regime, van uitrekking naar compressie, wordt inversie genoemd. Er ontstaan daardoor nieuwe breukbewegingen die meestal langs de al bestaande breuken plaats vonden; nu zijn het opschuivingen. Ook nu is er een belangrijke horizontale component in de deformatie met zijschuivingen tot gevolg. De eerste breukbewegingen waren tijdens het Krijt (Coniacian, ongeveer 86 miljoen jaar geleden). De laatste breukbewegingen vonden in het Oligoceen plaats (24 miljoen jaargelden, zie de Jager, 2007, fig. 8). Gedurende deze inversie fase werden de structuren van het Krijt aangelegd (o.a. de anticlinale structuur van het P/15 Rijn veld). De tektonische bewegingen van deze inversiefase waren relatief klein in het P18 gebied, naar het NE toe zijn deze bewegingen veel groter geweest.

### *Oligoceen - nu*

Gedurende het Tertiair veranderde tektonische regime weer en ontstond er een regime van trekspanning zoals nu is te meten aan de putten (Vandeweyer et al, 2011; van Balen et al, 2000).

### *De structuren van de olie en gas velden*

De Trias gasvelden zijn aanwezig in de horst blokken die werden gevormd tijdens de Laat Jura - Vroeg Krijt rek fase. Tijdens de volgende fase (de inversie fase) in het Laat Krijt - Vroeg Tertiair worden deze horstblokken in meer of mindere mate verder omhoog geduwd. Er ontstaan dan anticlinale structuren in Onder Krijt lagen. Het P/15 Rijnveld en de olieaccumulatie van de P18-1 put zijn aanwezig in deze Onder Krijt anticlinalen. Figuur 14 laat een seismische lijn zien die het een en ander illustreert.

## **Petroleum systemen van het West Nederland Bekken.**

Een petroleum systeem kan worden gedefinieerd als alle olie- of gasvoorkomens die afkomstig zijn uit een specifiek moedergesteente (“source rock”). De petroleum systemen in het West Nederland Bekken zijn bestudeerd door van Balen et al (2000) en ook beschreven in TNO-NITG (2002). In het West Nederland Bekken hebben we te maken met minimaal twee systemen. Hoewel er plaatselijk verschillen zijn is de geschiedenis van het West Nederland Bekken voldoende uniform om de conclusies van deze studie op P18 te betrekken. De ontwikkeling van het P18 gebied is vooral vergelijkbaar met dat van het gebied bij de Lier in het Westland.

### **Carboon**

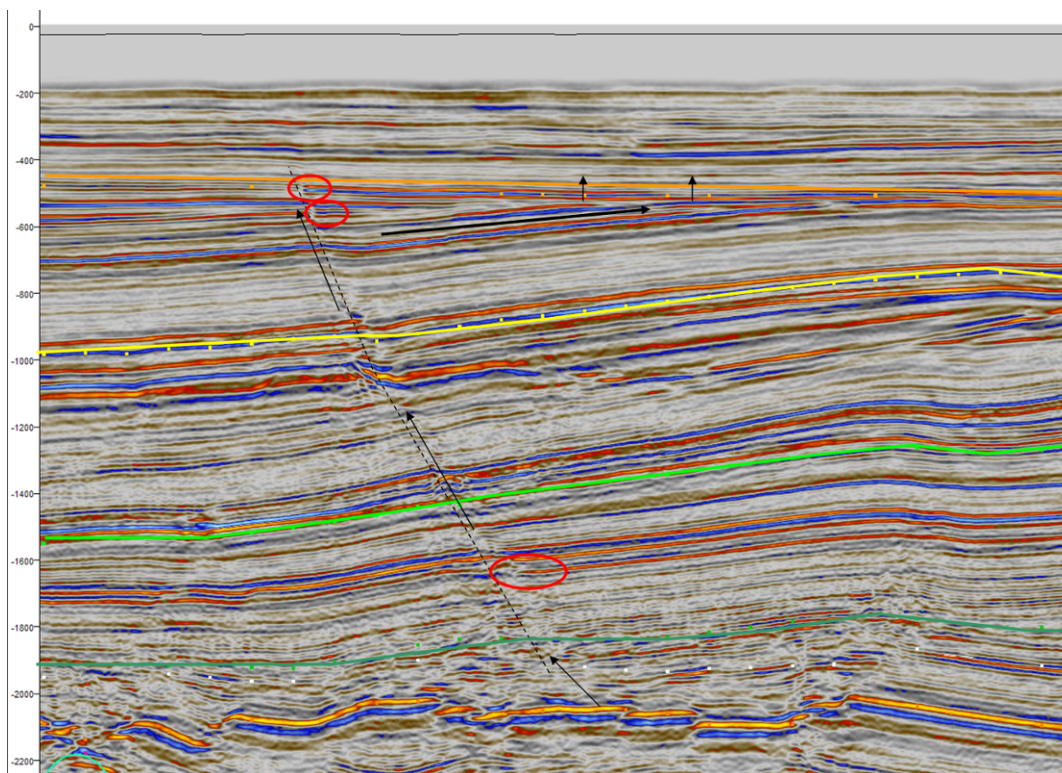
Het oudere petroleumstelsel heeft als moedergesteente de koollagen in het Carboon (Westphalien A and B) en het reservoirgesteente is in de Trias. Dit systeem heeft gas gegenereerd. Er zijn aanwijzingen voor een moedergesteente in dieper gelegen Carboon lagen van het Namurien, ook dit moet gas hebben gegenereerd. Dus het gas in de Trias reservoirs is mogelijk van gemengde afkomst, uit het Namurien en het Westphalien. Model studies (Balen et al, 2000; TNO-NITG, 2002) suggereren dat de gasgeneratie in het Carboon begon in de Trias (240 Ma) en dat kort na het ontstaan van de horstblokken in de Laat Jura periode (150 miljoen jaar geleden) het gas de Trias reservoirs in deze horstblokken kan hebben bereikt. Dit betekent waarschijnlijk ook dat het gas in de Trias reservoir langdurig bewaard bleef, ook tijdens de tektonische inversie periode (86-24 miljoen jaar gelden) toen de grote bewegingen langs de breuken plaatsvonden.

### **Posidonia**

Het jongere petroleum systeem heeft als moedergesteente de Onder Jura Posidonia Formatie en de hieruit ontstane olie is nu te vinden in de reservoirs van het Onder Krijt en bovenste Jura. De oliegeneratie begon ongeveer 130 miljoen jaar geleden en ging door tot ongeveer 40 miljoen jaar geleden. De olie migreerde in de structuren met de Onder Krijt reservoirs onmiddellijk na het ontstaan van de structuren ongeveer 80 miljoen jaar geleden (Laat Krijt). In P18 is er een olieaccumulatie in de put P18-1, echter deze is niet commercieel winbaar. Het Rijn veld in P15 is in productie geweest maar productie is



sinds enkele jaren gestaakt en het veld is op dit moment ingesloten. De Posidonia heeft ook gas gegenereerd (de Jager et al, 1996).

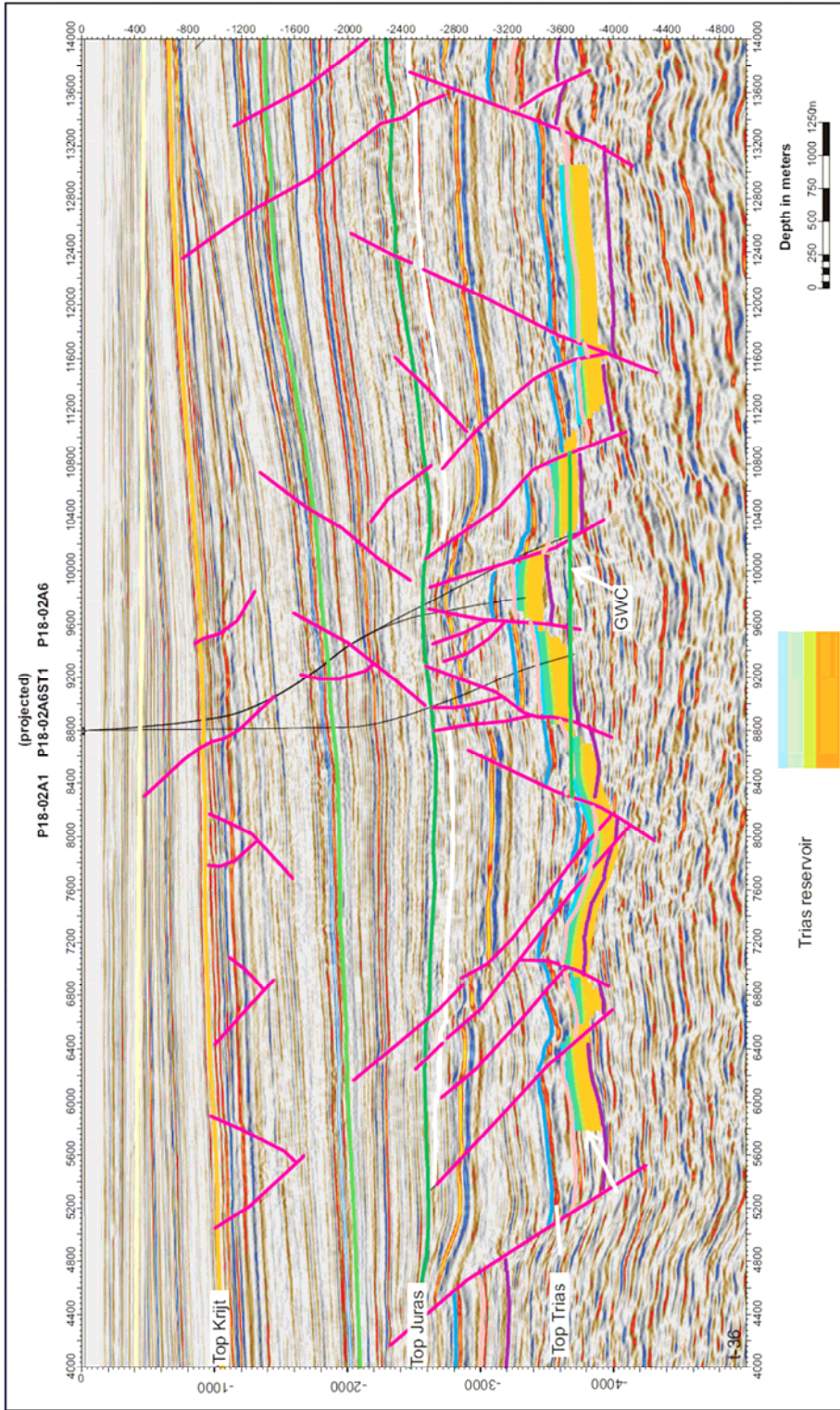


*Figuur 14. Mogelijke migratieroute (met pijlen aangegeven) van gas uit de Posidonia Formatie langs een breukzone. (Figuur uit Vandewijer et al, 2011.)*

### Ondiep gas

Op verschillende plaatsen in Nederland is gas aanwezig op relatief geringe diepte. Dat is meestal gas gegenereerd door bacteriën en dit wordt wel biogeen gas genoemd. Dit gas kan accumuleren in ondiepe gas velden. Seismische anomalieën kunnen aanwijzingen zijn dat er gas aanwezig is in lagen (zogenaamde gasindicatoren). Reeds kleine hoeveelheden gas opgelost in formatiewater kunnen aanzienlijk anomalieën opleveren. Op veel plaatsen in Nederland zowel op land als onder de zeebodem zien we gasindicatoren in ondiepe lagen.. Dat gas indien aanwezig kan biogeen zijn (moerasgas is hiervan een voorbeeld) maar kan ook afkomstig zijn uit de diepe ondergrond en naar boven gemigreerd.

De seismiek over P18 heeft ook gasindicatoren in ondiepere lagen. Deze zijn niet uniek voor P18 maar ook te zien op veel andere plaatsen op het land en onder de zeebodem. Deze anomalieën kunnen betekenen dat er biogeen gas is of dat er gas uit diepe lagen naar boven migreert of in het verleden naar boven is gemigreerd. In P18 zien we mogelijke gasindicatoren ook langs breukvlakken (Vandewijer et al, 2011) en dat suggereert dat er gas uit diepe lagen naar boven migreert. Indien aanwezig langs de breukvlakken is dit gas waarschijnlijk afkomstig uit de Posidonia Formatie (de Jager et al, 1996), maar andere bronnen (zoals kolen in de Schieland Groep) kunnen niet worden uitgesloten.

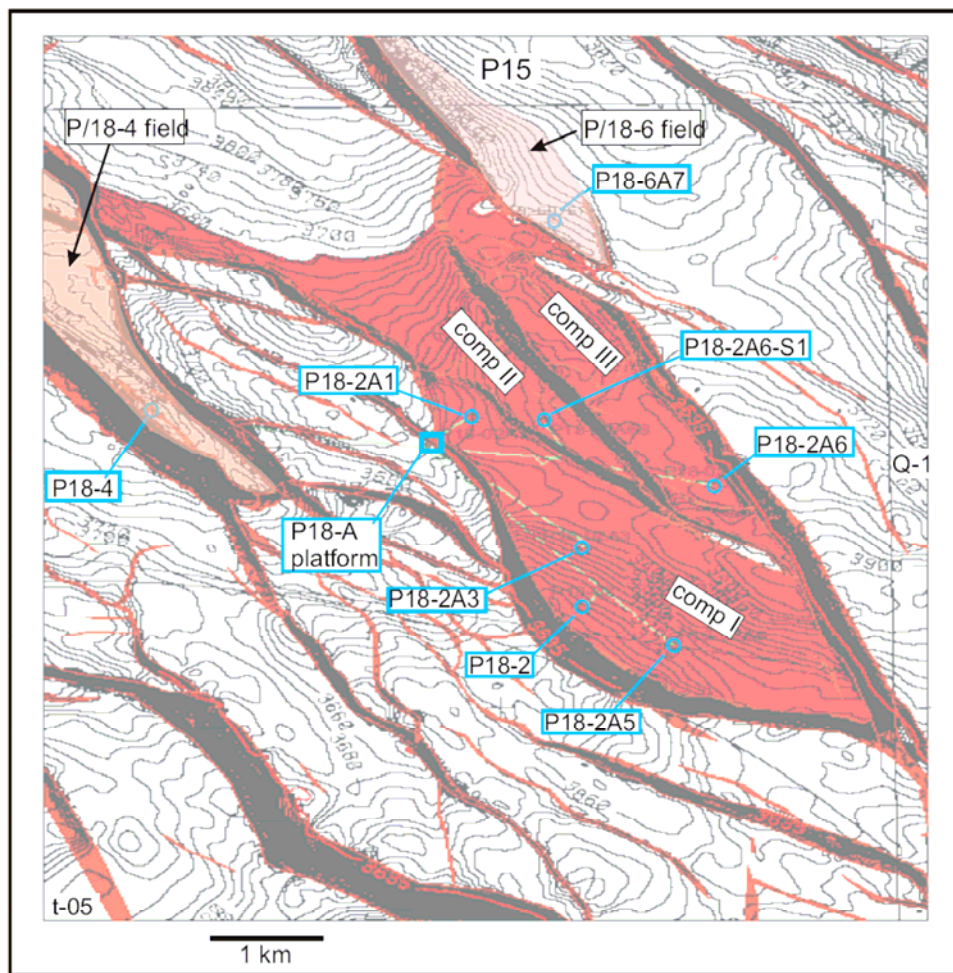


Figuur 15., Seismische lijn over de P/18-2 en P/18-6 velden. De gas velden zijn duidelijk te zien als horstblokken op het niveau van de Trias. Ook is duidelijk te zien dat er een zwakke anticlinale structuur is op het niveau van de top Jura (= basis .Krijt). Op deze figuur zijn niet alle breuken ingetekend, vooral in het Krijt zijn maar enkele breuken ingetekend. (Figuur uit Petrel model, Vandeweijer et al, 2011)

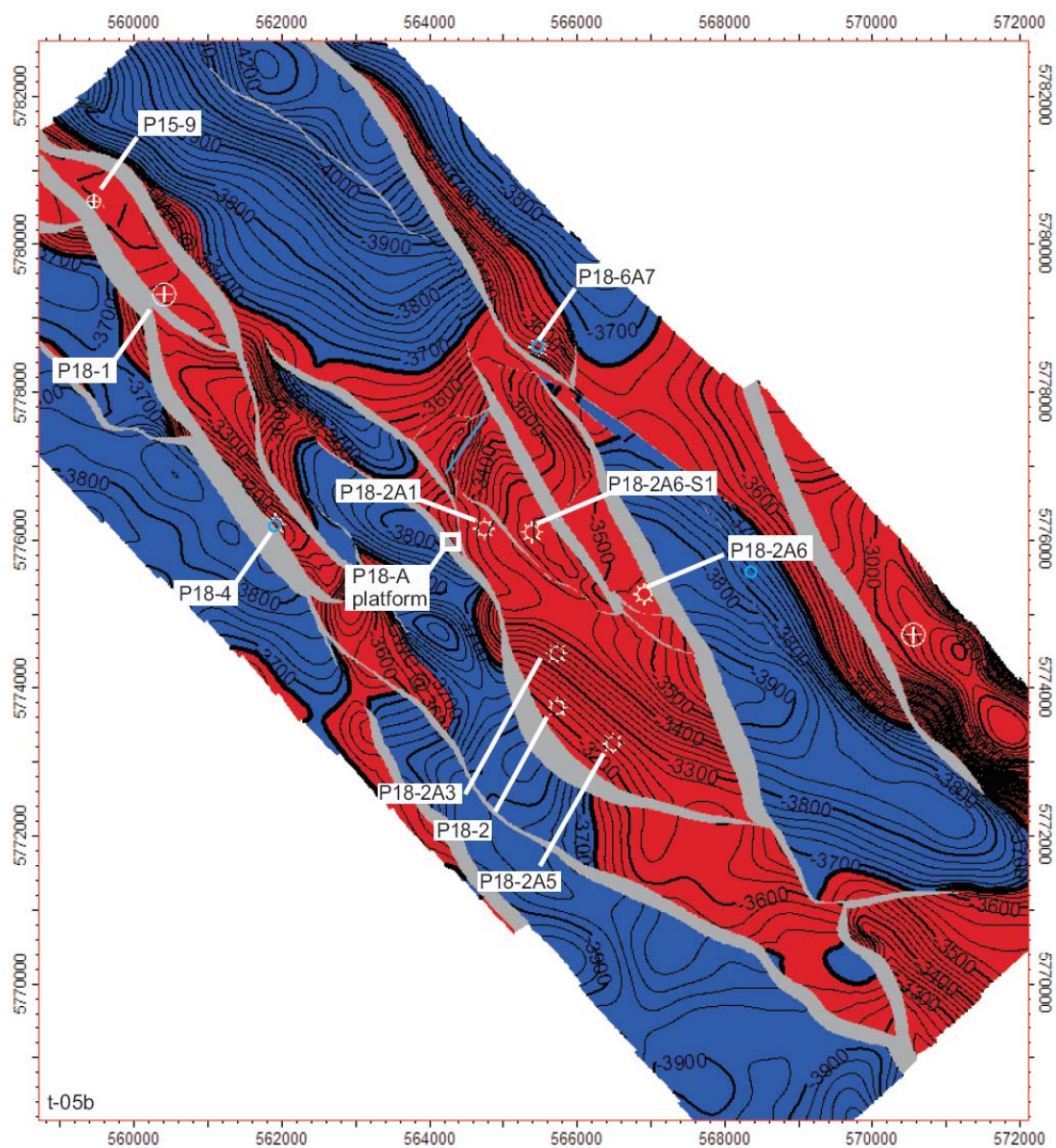
Figuur 14 laat deze anomalieën zien en mogelijke migratiepaden zijn aangegeven. De migratie paden zijn echter zeer hypothetisch. Indien aanwezig zal het gas eerder door aquifers (zoals de Holland Greensand of lagen in de onder Tertiair zanden) naar hogere lagen migreren dan via dit breukvlak.

## De structuur van de P18 velden

De velden in het P18 blok zijn geïsoleerde horst blokken omgeven door breuken. Figuur 8 laat een doorsnede zien door P18 met het P/18-2 veld en een gedeelte van Q16. De breuken in het Trias hebben globaal een NW-ZO richting. De kaarten van de Figuren 15, 16 en 17 laten deze NW-ZO richting van de breuken duidelijk zien.



Figuur 16. Dieptekaart van het P/18-2 veld in het noordoostelijke deel van het P18 Blok. Aan de noord kant is het P15 Blok, aan de oostkant het Q16 blok. De contourlijnen zijn dieptelijnen van de top van het Trias reservoir. Alleen het met gas gevulde Trias reservoir van het P18-2 veld is op dit kaartje rood gekleurd. Aangegeven op deze kaart zijn de oppervlakte locatie van het P18A platform en de locaties (blauw) waar de putten het reservoir doorboren. Met uitzondering van P18-2 zijn al de putten gedevieerd en geboord vanaf het P18 platform. (Figuur uit TAQA 2009.)



Figuur 17. Dieptekaart van de P/18 velden. De contourlijnen zijn dieptelijnen van de top van het Trias reservoir. Het met gas gevulde Trias reservoir is op dit kaartje rood gekleurd, in deze kaart is aangenomen dat het gas-water-contact op een diepte van  $-3680$  m ligt. Aangegeven op deze kaart zijn de oppervlaktelocatie van het P18A platform en de locaties waar de putten het reservoir doorboren. Met uitzondering van P18-2 zijn al de putten gedeveerd en geboord vanaf het P18 platform. (Figuur uit Vandeweijer,2011.)

## Reservoir

In de P/18 velden wordt het reservoir gevormd door zandsteen lagen van de Trias. Dit Trias reservoir wordt informeel Bunter genoemd. De reservoir zandstenen zijn afgezet in een semi-aride continentaal bekken door rivieren en in duinen (Ames & Farfan, 1996). Het totale reservoir pakket is ongeveer 190-215m dik. Binnen dit Bunter reservoir kunnen vier eenheden worden onderscheiden (zie Tabel 1):

Reservoir eenheden	dikte	barrières	opmerkingen
1-Hardegsen	24-33 m		Meest productieve zone
		Dun & gedeeltelijk doorlatende barrière	
2-Boven Detfurth	47-49 m		
		barrière	Schalie laag
3-Onder Detfurth	19-21m		
		barrière	Schalie laag
4- Volpriehausen	101-111 m		Minst productieve zone

Tabel 1. Reservoir eenheden in de P/18 velden.

Aan de basis van de reservoir-eenheden zijn schalielagen aanwezig die functioneren als barrières, de twee barrières aan de basis van de Boven Detfurth en de basis van de onder Detfurth zijn belangrijk. De diepste reservoir-eenheid is het nauwelijks productief. Deze diepe eenheid is relatief heterogeen met verschillende schalielagen. Enkele reservoir eigenschappen van de drie P/18 velden en volumes gas die aanwezig waren voor productie begon worden getoond in Tabellen 2 en 3. Figuur 12 is een stratigrafisch correlatie paneel met alle putten in de drie velden. Het laat zien dat de vier reservoir-eenheden eenvoudig te correleren zijn en ook de schalie lagen aan de basis van de reservoir-zones zijn duidelijk te herkennen.

Gas veld	Gas volume Bcm (oppervlakte condities)	porositeit	Gemiddeld permeabiliteit
P/18-2 veld compartiment I	12.3	5-10%	125 mD
P/18-2 veld compartiment II	0.4	4-8%	
P/18-2 veld compartiment III	0.7	3-7%	
P/18-4 veld	3.2	5-13%	200 mD
P/18-6 veld	0.7	3-7%	2 mD

Tabel 2. Grootte en enkele gemiddelde reservoir eigenschappen van de drie P/18 gas velden. De gasvolumes zijn de volumes in het reservoir omgerekend naar de volumes bij oppervlakte druk en temperatuur). Zie Figuur 4 voor een grafiek met de jaarlijkse productie. Een Bcm is een biljoen kubieke meter (1000.000.000 M<sup>3</sup>); mD is millidarcy, een maat voor de doorlaatbaarheid van een gesteente. (Data uit TAQA 2009.)

gasveld	Cumulatieve productie (Bcm)	Gas volume P/Z plots (Bcm)
P/18-2 veld compartiment I		12.3
P/18-2 veld compartiment II		0.48
P/18-2 veld compartiment III		0.68
Totaal P/18-2	12.5	13.46
P/18-4 veld	3	3.2
P/18-6 veld	0.52	0.62
alle P/18 velden	17.3 *	17.28

Tabel 3. P/Z plot data en productie data. Alle p18 velden van Jaarverslagen, Ministerie van Economische Zaken. Cum productie van de velden uit TAQA (2009). Een Bcm is een biljoen kubieke meter, dat is 1000.000.000 M<sup>3</sup>. Een P/Z plot is een druk-volume diagram waaruit het reservoir volume kan worden afgeleid.

## Gascompositie

De samenstelling van het gas in de P/18 velden wordt getoond in Tabel 4. Condensaat productie voor alle putten is in de orde van 70 M<sup>3</sup> condensaat per miljoen M<sup>3</sup> geproduceerd gas.

stikstof	0.5%
methaan	88.4%
CO <sub>2</sub>	1.2%
hogere koolwaterstoffen	9.9%
totaal	100.0%

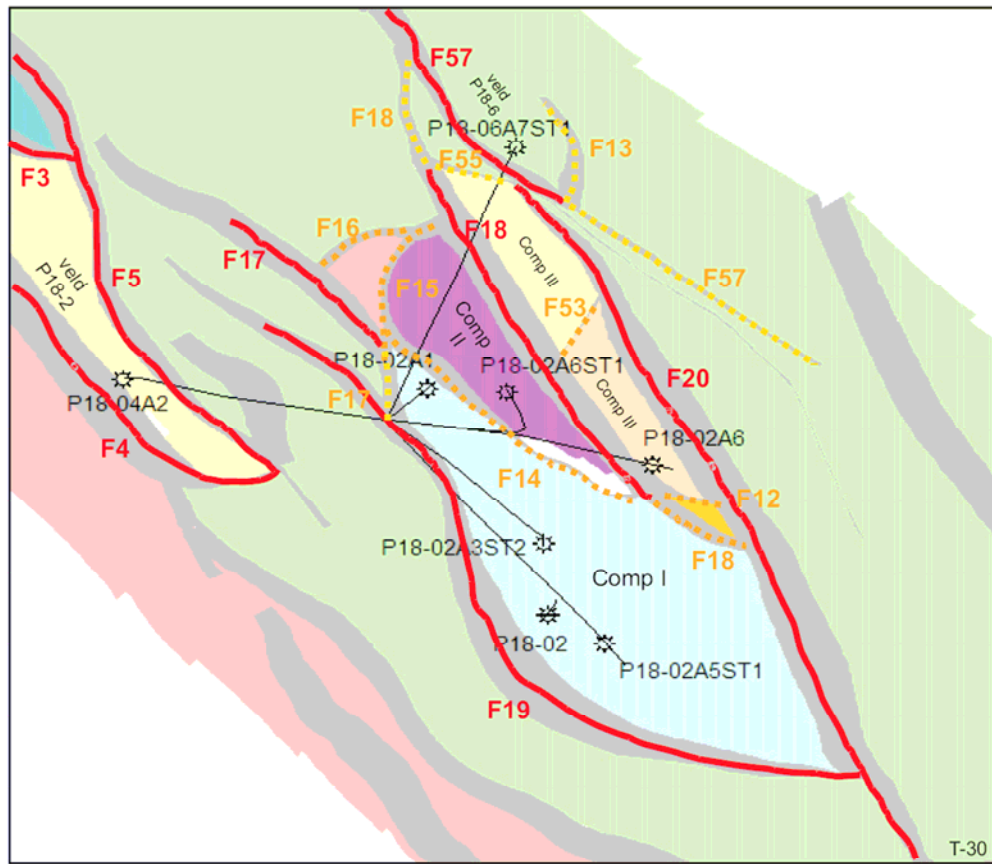
Tabel 4. Samenstelling van het gas in de P/18 velden in mol percentages.

## De deklaag van de P/18 velden

De afsluitende deklaag (seal of caprock) bovenop het gas-voerende reservoir wordt gevormd door een dik pakket schalies van de Trias 150 tot 180 m dik. Eigenschappen van dit Trias pakket zijn beschreven door Spain & Conrad (1997) voor een put in P15 waar de deklaag was gekernd. Spain & Conrad concluderen dat deze deklaag van goede tot excellente kwaliteit is. Bovenop de Trias afdeklaag zorgt ook een 400 tot 500 m dik pakket van Jura kleien voor afsluiting. Ook zijn er dikke kleipakketten aanwezig in het Krijt en in het Tertiair.

## De laterale afsluiting van de P/18 velden

De laterale afsluiting van de P/18 velden is door middel van breuken. Deze breuken worden gekarteerd met behulp van seismiek, alleen de grote breuken zijn gekarteerd. De spronghoogtes (= verticale verzet) van deze breuken zijn nogal verschillend. De breuken met een grote verticale verplaatsing langs de breukvlakken zijn aangegeven in rood in Figuur 18. Bij deze breuken is Trias reservoirzandsteen aanwezig aan de ene kant van het breukvlak en Jura of Trias schalie aan de andere kant. Deze breuken sluiten goed af en laten geen gas door.



Figuur 18. Kaartje van de drie P/18 velden met daarin schematisch aangegeven de belangrijke breuken (aangegeven met F en een nummer) en de verschillende reservoir compartimenten aangegeven met verschillende kleuren. Er zijn twee type breuken: 1) in rood de breuken met aan één kant Trias reservoir en aan de andere kant schalie (Trias en/of Jura); 2) bruine stippellijnen zijn breuken met aan beide zijden de Trias reservoir sectie. Naar het NW (in de richting van de breuken F17, F16 en F55) duikt het Trias lagenpakket onder het gas-water-contact. (Figuur uit Vandeweyer et al, 2011.)

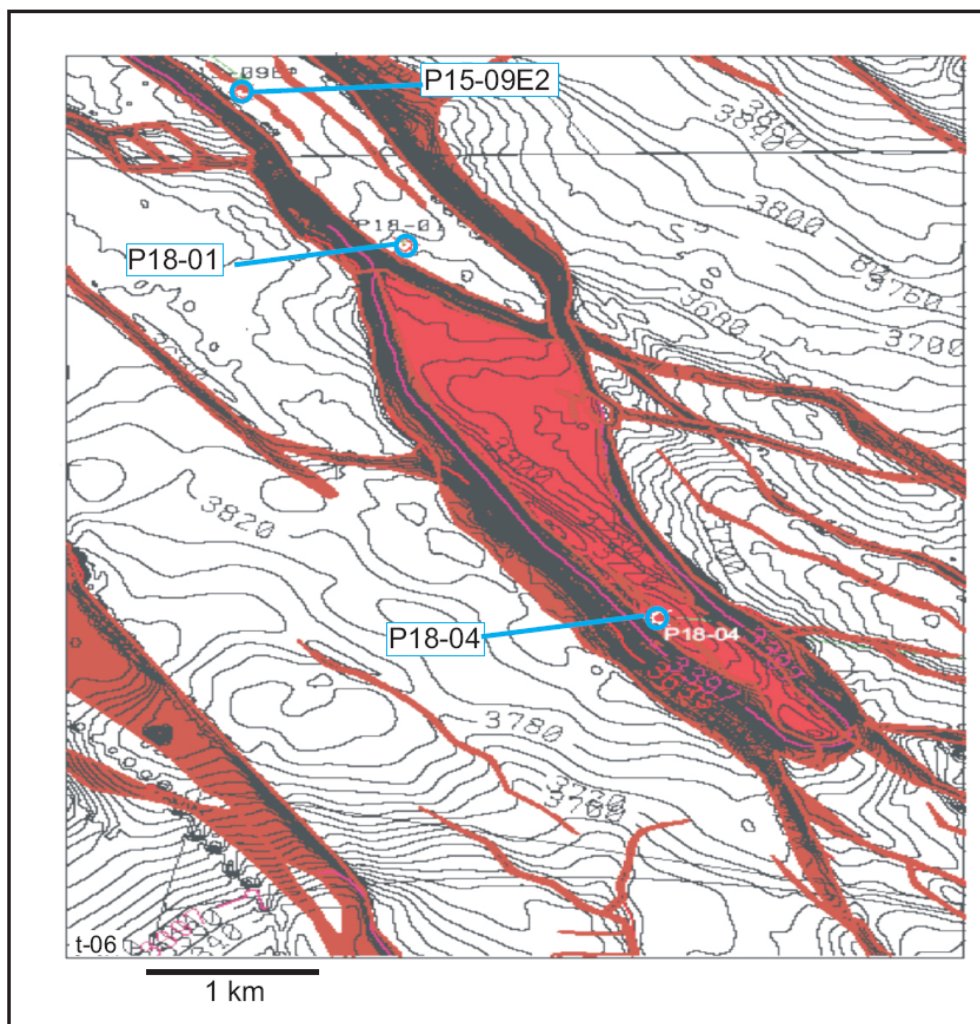
Breuken met een kleinere verticale verplaatsing zijn aangegeven met een bruine stippellijn in Figuur 18. Bij deze breuken is Trias reservoirzandsteen aanwezig aan beide kanten van de breuk. Deze breuken hebben dus een verticale verplaatsing van minder dan 210m. Deze breuken kunnen gas doorlaten; drukmetingen in de reservoirs tijdens de productie periode hebben inderdaad aangetoond dat sommige van deze breuken gas doorlaten (b.v. breuk F14 in Figuur 18; TNO, 2010).

## Beschrijving van de P/18 gasvelden.:

Tijdens de gasproductie kan worden aangetoond dat er geen contact is tussen Compartiment III en Compartiment I, dat wil zeggen dat er de zone met de breuken F12 en F18 (Figuur 18) geen of slechts kleine hoeveelheden gas doorlaat.

### P/18-2 veld

Het P/18-2 veld is het grootste veld in P18 met oorspronkelijk ongeveer 13.5 Bcm gas aanwezig in het reservoir (“original gas in place at surface conditions”). Het veld is opgebroken in drie compartimenten genoemd, I, II en III (zie Figuren 2, 12, 13 en 14). De breuken tussen deze drie compartimenten kunnen gedeeltelijk doorlatend zijn en daarom worden de drie compartimenten als één veld beschouwd.



*Figuur 19. Dieptekaart van het Trias reservoir van het P/18-4 veld. Het veld wordt aan de NW kant begrensd door het P15-9E veld. P/18-04 veld en de breuken zijn rood ingekleurd. (Figuur uit TAQA 2009.)*



Beschrijving van de P/18 gasvelden.:

P/18-2 veld				
	Hardegse	Upper Detfurth	Lower Detfurth	Volpriehausen
Gemiddelde dikte (m)	26.4	48.8	21	111
Gemiddelde N/G	0.98	0.94	0.79	0.70
Gemiddelde porositeit	0.125	0.092	0.079	0.039
Gemiddelde Waterverzadiging	0.267	0.428	0.418	0.778
Gemiddelde permeabiliteit	128.0	0.8	0.3	0.0

Tabel 5. Reservoir eigenschappen van het P/18-2 veld. Diktes zijn totale diktes van de formaties (z.g. "gross thickness") afkomstig van boorprofielen. (Porositeit, permeabiliteit & Sw uit TAQA spreadsheet P18 Bunter-petro-wellAverages.).

Er is onzekerheid tot hoe diep het gas aanwezig is in het P/18-2 veld. In de putten van het P/18-2 veld is het laagste aangetoonde gas op -3506 m diepte in de put P18-2A6, deze diepte is de onderkant van de perforatie in deze put Taqa 2009. Dit betekent dat het gas-water contact dieper is dan -3506 m. De diepte kaarten, gebaseerd op de seismische kartering, suggereren dat het overstroompunt ("spill point") van het P/18-2 veld op een diepte is van ongeveer -3635m. Dit overstroompunt is gelegen in de NW punt van het veld. Het vrije water niveau ("FWL" = free water level) kan niet worden bepaald in het P/18-2 veld. Een betrouwbare watergradiënt is gemeten in put P15-12 (20 km NW van het P18-0 veld). Intersectie van deze watergradiënt met de gasgradiënt van P/18-2 levert een FWL op van -3680 m, aanzienlijk lager dan het structurele lekpunt bepaald op -3635 m. Het hoogste gas is aangetroffen in het P/18-2 veld is gekarteerd op een diepte van ongeveer 3180 m, gecombineerd met een FWL van -3680 suggereert dit een gas kolom van 500 m hoog.

De P/Z plots indiceren dat de producerende putten in compartiment I een volume van totaal 12.3 Bcm bereiken (zie Tabel 3). De twee andere compartimenten zijn veel kleiner. Originele druk van het veld (voor gas productie begon) is 355 bar (TAQA, 2009). Enkele reservoir eigenschappen voor P/18-2 zijn te vinden in Tabel 5.

De putten in de Compartimenten I and II zijn geperforeerd over het gehele interval van de Hardegse, Upper Detfurth, Lower Detfurth en de top 10-20 m van de Volpriehausen Formaties. De zijtak P18-2A6-S1 die in compartiment II is geboord heeft zijn einddiepte in the Lower Detfurth, en is alleen geperforeerd in de Hardegse en Upper Detfurth Formaties.

### *Reservoir modellen en de vergelijking met de productiegeschiedenis*

In het kader van de onderzoeken voor CO<sub>2</sub> opslag in P18 zijn er statische geologische (Petrel) modellen en daarop gebaseerd dynamische modellen gebouwd van de drie P18 velden. Deze zijn gerapporteerd door Vandeweijer et al (2011). De productie geschiedenis van de velden (= het verloop van de druk en de hoeveelheden gas in de verschillende putten die in de tijd worden geproduceerd) wordt in deze modellen gesimuleerd en vergeleken met de werkelijke gebeurde geschiedenis. In het ideale geval zijn er geen verschillen tussen de datasets van het model en de werkelijke gegevens. In de

praktijk zijn er meestal verschillen die het gevolg zijn van incomplete geologische gegevens en moet het model worden aangepast tot dat de simulatie goed overeenkomt met de werkelijkheid. Deze simulatie is dus een test van de betrouwbaarheid van de gebouwde modellen. Als de test geslaagd is kunnen de modellen vervolgens gebruikt worden om de verschillende effecten bij CO<sub>2</sub> injectie na te bootsen.

De reservoirmodellen en de P/Z plots laten zien dat er geen water het reservoir instroomt gedurende de gasproductie in alle drie de compartimenten van het P/18-2 veld. Er is dus geen actieve aquifer aanwezig.

De druk- en productie geschiedenis van de verschillende putten laat zien dat breuk F14 (zie Figuur 18) tussen de compartimenten I en II gas heeft doorgelaten. Echter compartiment III is geheel gescheiden van de compartimenten I en II (Vandeweyer et al (2011)).

De productie- en drukgeschiedenis van drie putten in compartiment I komen redelijk overeen met die van het dynamische model. Enkele aanpassing aan de permeabiliteit in het model moesten worden uitgevoerd om de werkelijke geschiedenis overeen te laten komen met de gesimuleerde geschiedenis in het veld.

Het gas in de compartimenten II en III wordt geproduceerd door één put met twee takken, elk compartiment heeft één tak. De originele put doorboort compartiment III, zes jaar later werd een zijtak geboord naar compartiment II. De originele put in III en de zijtak in II zijn nu samen in productie, maar de hoeveelheden gas zijn niet gescheiden gemeten maar geschat.

Ondanks aanpassingen aan de permeabiliteit van het model van compartiment II kon het model niet helemaal in overeenstemming worden gebracht met de gemeten druk en productie geschiedenis, maar het model is wel bruikbaar om CO<sub>2</sub> injectie na te bootsen. compartiment III gaf geen problemen en het gebouwde model komt redelijk overeen met de gemeten werkelijkheid.

De volgens het model aanwezig gasvolumes in de verschillende veldcompartimenten zijn afhankelijk van de aanpassingen aan het model en verschillen iets met de volumes afgeleid uit de P/Z plots (zie Tabel 3). Het gekozen reservoir model waar mee is gerekend gaan uit van een gas volume die 7% groter is dan dat uit de P/Z plots van Tabel 3 (Vandeweyer et al, tabel 9).

### P/18-4 veld

Dit veld is geheel omgeven door breuken en staat niet in contact met andere velden (zie de Figuren 1, 12 en 13). Bij deze breuken is Trias reservoir aan de ene kant van de breuk niet in contact met Trias reservoirs aan de andere kant van de breuk. Mogelijk is de breuk tussen de P/15-9 en P/18-4 velden hierop een uitzondering, dat kan niet met zekerheid worden vastgesteld. Hier zou de Hardegsen Formatie aan de ene kant in contact kunnen zijn met de Volpriehausen Formatie aan de andere kant van de breuk. Maar de data van de gemeten drukken in de velden suggereren dat de breuk niet doorlaten is.

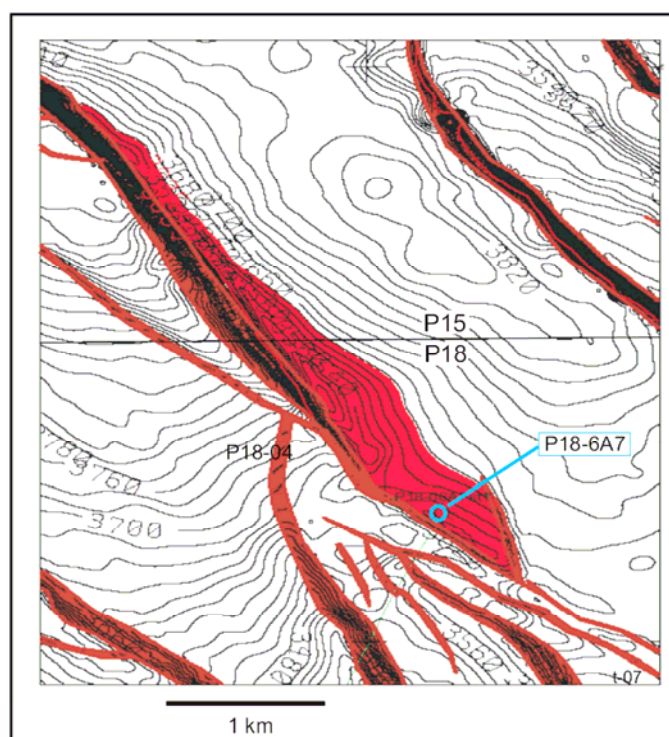
Er is één put in het P/18-4 veld (P18-4A2, zie Tabel 10 en Figuur 16, 17 en 18); deze put heeft geen water in het Trias reservoir aangetroffen. TVD van deze put is -3185 m,

### Beschrijving van de P/18 gasvelden.:

terwijl het vrije water niveau (FWL) op -3377 m is aangenomen. Het vrije water niveau voor de P18-1 put (in het aangrenzende P/15-9 veld) is bepaald op een diepte van -3397 m, het is mogelijk dat -3377 ook het vrije water niveau in het P/18-4 veld is. De initiële druk van het veld is 340 bar (TAQA, 2009).

P/18-4 veld	Hardegsen	Upper Detfurth	Lower Detfurth	Volpriehausen
Gemiddelde dikte (m)	24	47	19	101
Gemiddelde N/G	0.99	0.87	0.81	0.33
Gemiddelde porositeit	0.131	0.092	0.065	0.049
Gemiddelde Waterverzadiging	0.240	0.470	0.390	0.920
Gemiddelde permeabiliteit	207.0	0.8	0.1	0.0

Tabel 6. Reservoir eigenschappen van het P/18-04 veld. Dikte is de totale dikte van de formaties (z.g. "gross thickness"), afkomstig van het P18-4A2 boorprofiel. (Porositeit, permeabiliteit & Sw uit TAQA spreadsheet P18 Bunter-petro-wellAverages.)



Figuur 20. Dieptekaart van het Trias reservoir van het P/18-6 veld. Het langwerpige veld is voor een gedeelte gelegen in het P18 blok en wordt doorboord door de P18-6A7 put. Breuken en het gas-voerende reservoir van het P/18-6 veld zijn rood gekleurd. (Figuur uit TAQA 2009.)

In dit veld bestaat het reservoir uit Trias lagen die vergelijkbaar zijn met het P/18-2 veld en het P/18-6 veld. De porositeit van de Trias gasvoerende lagen ligt tussen de 5 en 13%. De gemiddelde permeabiliteit voor de beste reservoir eenheid, de Hardegsen, is 207 mD. Enkele reservoir eigenschappen zijn te vinden in Tabel 6.

## Beschrijving van de P/18 gasvelden.:

De enige put in het veld (P18-4A2) is geperforeerd over het interval Hardegsen, Upper Detfurth, Lower Detfurth en de top 10m van de Volpriehausen.

### *Het P/18-4 geologisch model en de productiegeschiedenis*

Het P/18-4 veld kwam in productie in 1993; cumulatieve productie tot juli 2010 is 2.9 Bcm. De P/Z plot indiceert dat de put is verbonden met een gasvolume van 3.2 Bcm (zie Tabel 3).

In het kader van de onderzoeken voor CO<sub>2</sub> opslag in P18 is er ook een statisch en een dynamisch model gebouwd van het P/18-4 veld (Vandeweyer et al, 2011).

Vergelijkingen van model met de werkelijke productie laten zien dat het veld 25% meer gas bevat dan het model veronderstelt. Het werkelijke reservoir volume (uit productie cijfers en P/Z plot) zijn dus beter dan het model (gebaseerd op seismische kartering en de put in het veld). Dit is niet ongebruikelijk. Immers, we hebben maar één put en de seismiek over dit veld is moeilijk en laat ruimte voor alternatieve interpretaties. Door aanpassing van de positie van de zuidoost breuk is het reservoir volume in overeenstemming te brengen met de productie cijfers. Ook door een aanpassing van de gemiddelde porositeit in het veld kunnen model en werkelijkheid met elkaar in overeenstemming worden gebracht.

### **Het P/18-6 veld**

Het P/18-6 veld is een langgerekt veld (Figuur 3 en Figuur 20) gelegen aan de noordkant van het P/18-2 veld.

P/18-6 veld				
	Hardegsen	Upper Detfurth	Lower Detfurth	Volpriehausen
Thickness (m)	33	49	N.F.P.	N.F.P.
N/G	0.81	0.91	N.F.P.	N.F.P.
PHI	0.074	0.048	0.059	0.030
S <sub>w</sub>	0.470	0.570	0.320	outside gasleg
K (mD)	1.8	0.0	0.1	0.0

*Tabel 7. Reservoireigenschappen van P/18-6 veld. Er is een put in het veld, P18-6A7St1. De basis van de Lower Detfurth en de Volpriehausen zijn niet doorboord. (Porositeit, permeabiliteit & S<sub>w</sub> uit TAQA spreadsheet P18 Bunter-petro-wellAverages.).*

Er is één put in het veld, P18-6A7S1 (Tabel 10) en ook deze put heeft geen water aangetroffen in het Trias gasreservoir. TVDSS van deze put is -3560 m, het vrije water niveau (FWL) is aangenomen op -3680 m, dus ruim onder de TD van P18-6A7. Enkele reservoir eigenschappen zijn te vinden in Tabel 7. Dit veld heeft de slechtste reservoir eigenschappen van de drie P18 gas velden. De kaart van Figuur 20 suggereert dat gas aanwezig is tot een diepte van -3635 m, maar daarover is geen zekerheid. De initiële druk van het veld is 364 bar (TAQA, 2009).

De put P18-6A7S1 die in dit veld is geboord heeft zijn einddiepte in the Lower Detfurth, en is geperforeerd in de Hardegsen, Upper Detfurth en de top 10 m van de Lower Detfurth Formaties.

### *Het P/18-6 geologisch model en de productiegeschiedenis*

Het P/18-6 veld wordt gekarakteriseerd door lage gemiddelde permeabiliteit. De P/Z plot geeft aan dat put P18-6A7S1 is verbonden met een reservoir gasvolume van 0.62 Bcm. Maar er is onzekerheid over de gemeten drukken daardoor is het mogelijk dat het reservoir volume wordt onderschat. Cumulatieve productie tot juli 2010 is 0.514 Bcm (Tabel 3).

In het kader van de onderzoeken voor CO<sub>2</sub> opslag in P18 is er ook een geologische en dynamisch model gebouwd van het P/18-6 veld (Vandeweyer et al, 2011). In het dynamische model moest porositeit en permeabiliteit aanzienlijk worden aangepast om simulaties in overeenstemming te brengen met de gemeten productie geschiedenis. Dit samen met de onzekerheden van de reservoirvolumes uit de P/Z plots suggereert dat de modelresultaten behoedzaam moeten worden geïnterpreteerd.

### **Bodemdaling en seismische activiteit als gevolg van gasproductie**

Er zijn geen metingen uitgevoerd aan de bodemdaling als gevolg van gasproductie in de P/18 velden. Tot nu toe is er geen seismische activiteit (aardbevingen) gemeten door het meetnet van KNMI. Aardbevingen die ontstaan van gasproductie in velden (z.g. “induced seismic activity”) zijn vrij algemeen in sommige streken van Nederland en daarom heeft het KNMI hiervoor een meetnet. De gevoeligheid van het KNMI meetnet was M2.5 tot 1995 en M1-1.5 na 1995 (Vandeweyer et al, 2011). Dat betekent dat in het P18 blok bevingen van M1.9 nog worden geregistreerd. Ook in andere gedeelten van het West Nederland Bekken met producerende gasvelden in de Trias is geen seismische activiteit waargenomen. Het is onbekend waarom seismische activiteit in het West Nederland Bekken afwezig is (of onder het detectieniveau van het meetnet is).

Theoretisch kan de bodemdaling als gevolg van gasproductie van het P/18-2 veld worden berekend. De maximale berekende bodemdaling als gevolg van gas productie is 5.1-7.6 cm in 2014. Als gevolg van CO<sub>2</sub> injectie gaat de bodem weer stijgen en wordt de bodemdaling bijna geheel te niet gedaan. De berekende maximale bodemdaling (uitgaande van de situatie voor gasproductie begon) zou dan in het jaar 2050 dan slechts 0.6 tot 1 cm kunnen bedragen (Vandeweyer et al, 2011)

## **De plannen voor CO<sub>2</sub> Injectie**

### **Opslag capaciteit en injectie tempo van CO<sub>2</sub> in de verschillende velden**

Het demonstratie- of proefproject gaat uit van injectie van 1.1 miljoen ton CO<sub>2</sub> per jaar. Dit komt overeen met een piek injectiecapaciteit van 47 kg/seconde bij een operatie tijd van 6500 uur per jaar. In een latere fase, als het proefproject een succes is, kan dit project worden omgezet naar injectie van 5 miljoen ton per jaar (158.4 kg/sec, zie Genesis, 2010).

## Beschrijving van de P/18 gasvelden.:

Het dynamische reservoir model (Vandeweyer et al, 2011) heeft ook de injectie van CO<sub>2</sub> gemodelleerd. Uit de modellen kunnen de totale opslag capaciteit en injectiecapaciteit worden berekend (Tabel 8).

De injectiecapaciteit van CO<sub>2</sub> is gesimuleerd voor 4 putten. De compartimenten I and II staan met elkaar in verbinding; dus compartiment II kan gevuld worden met één put in compartiment I, hiervoor is put P18-2A1 gekozen. Compartiment III is geïsoleerd dus dat kan alleen gevuld worden met put P18-2A6; de velden P/18-4 en P/18-6 hebben ook ieder één put (zie Figuur 3).

Van deze vier putten is de injectiecapaciteit van twee putten voldoende om de jaarlijkse hoeveelheid van 1.1 miljoen ton te kunnen injecteren; bij de andere twee putten is die capaciteit onvoldoende. De capaciteit is onvoldoende door de aard van het reservoir (onvoldoende permeabiliteit). Daar komt bij dat de verbuizing van put P18-6A7 ook niet geschikt is om de 47 kg/seconde te kunnen injecteren.

	put/compartiment	unit	veld P/18-2		veld P/18-4	veld P/18-6
			P18-2A1 comp I+II	P18-2A6 comp III	P18-04A2	P18-6A7
Capaciteit	dynamisch model	Bcm	14.7	0.7	4.1	0.3
	dynamisch model	miljoen ton	29.1	1.3	8.1	0.6
	analytisch model	miljoen ton	31.8		8.8	1.5
Injection 1.1 million ton/jaar mogelijk			ja	nee	ja	nee

Tabel 8 Hoeveelheden CO<sub>2</sub> die kunnen worden opgeslagen in de drie velden en de mogelijke injectie capaciteit van vier putten (uit Vandeweyer et al, 2011.)

De totale opslagcapaciteit volgens reservoirmodellen komen goed overeen met eerdere schattingen.

## Injectie Plan

Een injectie plan is januari 2011 nog niet beschikbaar. Er zijn op dit moment (januari 2011) nog te veel onzekerheden om dit plan vast te stellen. Belangrijk bij de vaststelling van dit plan zijn

- Het tijdstip waarop de velden en de putten beschikbaar komen voor injectie,
- De injectie capaciteit van de putten,
- De resultaten van de onderzoeken naar de ombouw van de putten van gas producer naar CO<sub>2</sub> injector.

Ook economische motieven zullen waarschijnlijk een rol spelen bij het vaststellen uiteindelijke injectieplan.

## Risico beheersing, CO<sub>2</sub> lekkage mogelijkheden

### *Inleiding*

Opslag van CO<sub>2</sub> in P18 zal plaats vinden in lege gasreservoirs. Deze reservoirs hebben aangetoond het gas voor geologisch lange perioden te kunnen bevatten. De gasvelden bestaan omdat de deklaag en de afsluitende zijwanden (dit zijn breuken) van de P18 reservoirs geen gas of minimale hoeveelheden gas hebben doorlaten. Ze lijken dus inherent veilig te zijn voor opslag van CO<sub>2</sub>. In de discussie hieronder worden de theoretische en hypothetische mogelijkheden van lekkage van CO<sub>2</sub> uit deze reservoirs besproken. De lekkage mogelijkheden en consequenties daarvan zijn uitvoerig onderzocht voor de P18 velden (Vandeweijer et al, 2011). De conclusies van deze onderzoeken aan het reservoir wijzen erop dat CO<sub>2</sub> opslag in deze velden mogelijk is en mits goed uitgevoerd er geen problemen zullen ontstaan. Ook de resultaten van het onderzoek aan het Barendrecht-Ziedewij Trias veld zijn voor een groot deel toepasbaar op de P18 velden.

De lekkagemogelijkheden kunnen in vier groepen worden onderverdeeld.

- 1) lekkage door de afdichtende bovenlaag.
- 2) Lekkage via het overstromingspunt (“spillpoint”) van het reservoir.
- 3) Lekkage langs de geologische breuken (dat zijn de zijwanden van het reservoir).
- 4) Lekkage langs of door de putten.

### *Mogelijke lekkage door de deklaag*

Lekkage van CO<sub>2</sub> gas door de deklaag (in het Engels is dat “seal” of “caprock”) is een van de hypothetische mogelijkheden. In het Barendrecht MER Deelrapport 3 werden twee mogelijkheden van lekkage door de deklaag onderscheiden:

Door nieuwe scheuren die ontstaan in de deklaag, waardoor grote hoeveelheden CO<sub>2</sub> kunnen weglekken

Langzame lekkage van kleine hoeveelheden CO<sub>2</sub> over langere tijd door de deklaag (bv door diffusie processen). In het Barendrecht MER rapport werd dit langzame lekken sijnepen genoemd.

Newstead et al (2008a) heeft de mogelijkheid van langzame lekkage voor Barendrecht-Ziedewij bestudeerd en gemodelleerd en concluderen dat lekkage onwaarschijnlijk is en dat de hoeveelheden die zouden kunnen lekken verwaarloosbaar klein zijn.

### *De aard van de afsluitende bovenlagen*

De afsluitende bovenlagen (deklagen) in de P18 velden hebben een grote dikte. De afsluitende bovenlagen gerekend tot de Trias zijn 150 tot 180 m dik. Daar onmiddellijk bovenop ligt een 400 tot 500 m dik pakket schalies van de Onder Jura die zelf ook een

goede afdichting vormen. Deze lagen hebben hun afsluitende werking ruimschoots bewezen want zij hebben de Trias gasvelden effectief voor miljoenen jaren opgesloten.

### *Onderzoek en resultaten mechanische gedrag, afsluitende bovenlagen en breuken*

Het mechanische gedrag van het onderste deel van de deklaag (direct bovenop het reservoir ) onder invloed van drukveranderingen is onderzocht en gerapporteerd door Vandeweyer et al (2011). Belangrijk is of er scheuren en scheurtjes kunnen ontstaan door drukveranderingen die plaatsvinden in het reservoir.

Dit onderste gedeelte van de deklaag bestaat uit 41 tot 68 m (gemiddeld ongeveer 50 m) anhydritische kleisteen (=schalies) en dunne dolomiet laagjes. Testen op gesteentemonsters laten zien dat de mechanische effecten op deze kleisteen gering zijn indien de drukken bij de injectieput in het reservoir (de z.g. bottomhole pressure of BHP) binnen de gestelde limieten blijven en bij een normale operatie is dat ook zo. Deze gestelde limieten zijn proefondervindelijk vast gesteld. Ook de temperatuuffecten zijn onderzocht. Bij grote temperatuurverschillen tussen reservoirgesteente en de te injecteren CO<sub>2</sub> kunnen spanningen ontstaan die scheurtjes tot gevolg kunnen hebben. Ook hier geldt dat binnen de gestelde limieten geen scheurtjes zullen ontstaan. Kleine scheurtjes zouden kunnen ontstaan door de gecombineerde effecten van temperatuur en druk in de laatste stadia van het vullen (als het reservoir bijna de vol is) en er de temperatuursverschillen tussen reservoir en CO<sub>2</sub> meer dan 50° C is.

Dit onderzoek concludeert dat alleen al de onderzochte, ongeveer 50 m dikke afsluitlaag, voldoende is om de CO<sub>2</sub> af te sluiten. Bij dit onderzoek aan de deklaag moet men zich ook nog realiseren dat de totale dikte van het afsluitende laagpakket veel groter is, dan de laag die onderzocht is: in totaal tussen de 550 en 780 m. Ook bij overschrijding van de druklimieten bij CO<sub>2</sub> injectie en hoge temperatuurverschillen zullen de afsluitende eigenschappen van het totale laagpakket van 550 tot 780 m dik niet in gevaar komen.

Studies uitgevoerd voor Barendrecht-Ziedewij concluderen dat de risico's verwaarloosbaar gering zijn van scheurvorming in de deklaag als gevolg van CO<sub>2</sub> injectie gedurende het weer op druk brengen van het veld. (Orlic, et al, 2007; Van Eijs & Seeberger, 2008; Wildenburg et al, 2007). Kleine scheuren zouden kunnen ontstaan in de late fase van CO<sub>2</sub> injectie maar blijven beperkt de laagste 15 m van de deklaag ("seal" of "caprock").

Holt & Vasmel (2009) hebben de snelheid van CO<sub>2</sub> migratie berekend bij schade aan de afsluitende bovenlagen van het Barendrecht veld. Dit veld is in het Krijt en vergelijkbaar met het Rijnveld in P15 en de olieaccumulatie in P/18-2. Zij concluderen:

*De modellen van de scenario's waaraan gerekend is, de zogenaamde 'in het slechtste geval'-scenario's, tonen aan dat zelfs in deze gevallen de hoeveelheid CO<sub>2</sub> die naar het oppervlak zou kunnen stromen zeer klein is. Daarnaast komt naar voren dat het bovendien minstens duizenden jaren duurt voordat er überhaupt CO<sub>2</sub> aan het oppervlak verschijnt.*



### *Onderzoek en resultaten: geochemie van afsluitende bovenlagen (caprock of seal)*

De effecten van CO<sub>2</sub> op de afsluitende bovenlagen werd onderzocht door het hoge temperatuur- en druklaboratorium van de Universiteit van Utrecht (Vandeweyer et al, 2011). Dit onderzoek voorspelt dat de effecten op mineralogie en porositeit verwaarloosbaar klein zijn

Voor Barendrecht-Ziedewij (BRTZ) zijn er ook studies uitgevoerd om de chemische veranderingen op de lange en op korte termijn in te schatten (van Bergen et al, 2008; Newstead et al, 2008b. De studies zijn samengevat door de Bruijn (2008a) en Wildenburg et al (2007). De uitkomst is dat chemische verwerking in de deklaag vermoedelijk zal leiden tot een afname van de permeabiliteit, dus tot een verbetering van de afsluitende eigenschappen. Chemische veranderingen in het reservoir kunnen leiden tot een kleine afname van de porositeit. De Bruijn (2008a) merkt verder op dat het Werkendam gasveld (dat 80% CO<sub>2</sub> bevat) in het gas een vergelijkbare afsluitende top laag heeft als Barendrecht-Ziedewij. Deze afsluitlaag werkt perfect en bevestigt dus dat de kans op lekkage (inclusief het “sijpelen” door de deklaag nihil is.

### *Onderzoek en resultaten: geochemie van het reservoir*

De effecten van CO<sub>2</sub> op het reservoir werd onderzocht door het hoge temperatuur- en druklaboratorium van de Universiteit van Utrecht (Vandeweyer et al, 2011). De mogelijk te verwachten verandering op de lange termijn (duizenden jaren) is een kleine afname van de porositeit, van 8.8% naar 8.5 %.

Aan het reservoir van Barendrecht Ziedewij zijn ook veel studies uitgevoerd. Deze studies zijn toepasbaar op de reservoirs in P18 (van Bergen et al, 2008; Newstead et al, 2008b, Seeberger, 2008a; studies samengevat door de Bruijn, 2008a en Wildenburg et al, 2007). De resultaten van deze studies wijzen uit dat veranderingen in het reservoir, op korte termijn en op lange termijn, niet of nauwelijks consequenties hebben voor het reservoir en de daarin opgeslagen CO<sub>2</sub> en dat eventuele risico's verwaarloosbaar klein zijn.

### *CO<sub>2</sub> lekkage via het overstromingspunt (“spillpoint”) van het reservoir*

Hieronder worden een viertal mogelijkheden behandeld die mogelijk lekkage via het overstromingspunt tot gevolg kunnen hebben. Dit zou kunnen gebeuren bij een viertal scenario's:

- 1) overvullen van de P18 CO<sub>2</sub> velden.
- 2) de aanwezigheid in het reservoir van “voorkeurstromen”.
- 3) oplossing van CO<sub>2</sub> in onderliggende waterlagen.
- 4) het ontstaan van drukverhogingen op lange termijn door volumeverandering van het reservoir.

Newstead et al (2008) heeft dit voor Barendrecht-Ziedewij bestudeerd en gemodelleerd en concluderen dat lekkage via het overstromingspunt mogelijk is maar dat de volumes beperkt blijven tot minder dan 2%.

## Beschrijving van de P/18 gasvelden.:

Van de gasvelden in P18 staat vast dat het min of meer afgesloten tanks zijn, er is geen aquifer. Dus de hieronder beschreven mogelijkheden zijn nogal hypothetisch van aard.

### Overvullen

Bij het over-vullen van het reservoir met CO<sub>2</sub> gas kan het (CO<sub>2</sub>) gas-water contact onder het overstromingspunt komen te liggen. Ook bestaat de mogelijkheid dat er een volume verkleining van het reservoir plaats vindt na beëindiging van de CO<sub>2</sub> injectie. Ook hierdoor kan het CO<sub>2</sub>-watercontact onder het overstromingspunt komen te liggen. Echter, de kans op over-vullen van het reservoir met CO<sub>2</sub> wordt gering geacht indien bij het vullen van het reservoir de maximale CO<sub>2</sub> volumes en druk binnen een veilige marge blijven, dat wil zeggen dat de druk van het met CO<sub>2</sub> opgevlude reservoir ruim onder de initiële druk van het gas veld blijft.

### Voorkeurstromen

Het voorkomen van “voorkeurstromen” (door relatief dunne lagen met hoge permeabiliteit) is zeer onwaarschijnlijk. De reservoirmodellen laten geen voorkeurstromen zien.

### CO<sub>2</sub> oplossing

De oplossing van CO<sub>2</sub> in het water onder de CO<sub>2</sub> zal een minimaal effect hebben. Het historische drukverloop gemeten tijdens de gasproductie laat zien dat er slechts kleine tot zeer kleine hoeveelheden water onderin het reservoir aanwezig zijn. Bovendien zal er slechts een klein volume CO<sub>2</sub> oplossen in dit water waarna dit water niet of nauwelijks mobiel zal zijn.

### Drukverhogingen in het reservoir

Drukverhogingen zijn theoretisch mogelijk als gevolg van een aantal mechanismen, zoals reactie van CH<sub>4</sub> met CO<sub>2</sub> en doorgaande gas generatie (in het Carboon) en opvang van dit gas in de P/18 Trias gas reservoirs. Ook deze mogelijkheden zijn onderzocht voor de Barendrecht-Ziedewij (van Bergen et al, 2008; Seeberger et al, 2008b). De theoretische drukverhoging is echter gering en door een veilige druk marge aan te houden kunnen de risico's tot verwaarloosbaar klein worden beperkt.

### Scenario's van CO<sub>2</sub> uitstroom uit het Trias reservoir

Wat er gebeurt met de CO<sub>2</sub> in het hypothetische geval dat het kan uitstromen is onderzocht met structuurkaarten van de top van het reservoir. De kaarten laten zien dat de CO<sub>2</sub> globaal in een viertal richtingen kan uitstromen (Vandeweijer et al, 2011): In alle richtingen migreert het uitstromende CO<sub>2</sub> gas naar andere structuren waar het vanzelf weer opgeslagen wordt onder de Trias en Jura afsluitende bovenlagen. Migratie naar bovenliggende lagen kan alleen gebeuren via putten (Vandeweijer et al, 2011).

Hypothetische migratie stromen zijn ook gemodelleerd voor de Rijn/Rijswijk zandsteen, de Holland Greensand en hogere zandsteen lagen (zie Figuur 9 en 10). Dit om te onderzoeken waar CO<sub>2</sub> naar toe zou migreren in het hypothetische geval dat het zou ontsnappen uit de Trias reservoirs. Theoretisch is het mogelijk dat gas uit deze hogere lagen via breuken naar de oppervlakte zou kunnen migreren, via breuken of via putten.

## Beschrijving van de P/18 gasvelden.:

Ook voor de Barendrecht-Ziedewij zijn deze mogelijkheid van ontsnappen van CO<sub>2</sub> uit het opslag reservoir onderzocht (zie Wildenborg et al, 2007). De conclusies voor Barendrecht-Ziedewij zijn ook dat dit een verwaarloosbaar risico is.

De effecten van een lekkage van CO<sub>2</sub> in Krijt (Chalk) formaties van het Boven Krijt zijn onderzocht voor Barendrecht. Deze formaties zijn ook aanwezig in P18. In Barendrecht is vastgesteld dat oplossing van Krijt (Chalk) door CO<sub>2</sub> opgelost in water kan leiden tot bodemdaling. Model berekeningen suggereren dat deze bodemdalingen beperkt zijn tot enkele centimeters en over een tijdsperiode van honderden jaren plaatsvinden. Gecombineerd met het reeds verwaarloosbare risico dat CO<sub>2</sub> ooit het Krijt (Chalk) bereikt kan dit risico verder worden genegeerd.

### *Lekkage langs breuken*

De opslag van CO<sub>2</sub> zal plaatsvinden in lege gasvelden in het P18 blok. Deze gasvelden hebben bewezen dat het goede gasreservoirs zijn die niet lekken. De zijwanden van deze reservoirs worden gevormd door breuken, dus ook deze breuken hebben bewezen niet doorlatend te zijn voor gas in de reservoirs bij de gemeten initiële drukken (drukken voor dat productie uit deze gasvelden begon). De modelstudies suggereren dat het gas al 150 miljoen jaar geleden het Trias reservoir instroomde en dat dus het gas heel lang in deze reservoirs was opgesloten.

Bij de beoordeling van de breuken is het van belang welk type gesteentes aan het breukvlak grenzen. Er zijn veel soorten breuken, breuken met een geringe verticale verplaatsing (spronghoogte) en breuken met een grote verticale verplaatsing. Globaal zijn twee categorieën van belang:

Type 1: breuken met aan de ene kant van de breuk reservoir zandsteen en aan de andere kant ook reservoir zandsteen. Deze breuken hebben een relatief geringe verticale verplaatsing. Deze breuken vinden we ook binnen de gasvelden en dit soort breuken vormen meestal niet de zijwanden van de gasvelden omdat gas van de ene kant van de breuk naar de andere kant kan stromen.

Type 2: breuken met aan de ene kant van de breuk reservoirgesteente en aan de andere kant schalies. Deze breuken hebben een verticale verplaatsing die groter is dan de dikte van het reservoir, dus groter dan ongeveer 200 m. Deze grote breuken vormen de zijwanden van gasvelden.

Het effect van CO<sub>2</sub> injectie is onderzocht op gesteentes aangetast door breuken. Ook hier kunnen kleine scheurtjes ontstaan (Vandeweyer et al, 2011) indien injectie plaats vindt in de onmiddellijke omgeving van de breuken. Door op een afstand van 150-200 m van de breuken te blijven kunnen de effecten hiervan worden beperkt.

### *Reactivatie van breuken*

Re-activatie van bestaande breuken als gevolg van gaswinning is een veelvoorkomend fenomeen. Als gevolg hiervan treden er kleine aardbevingen op (aardbevingen). Het

KNMI heeft een meetnet in Nederland waar ook deze kleine aardbevingen worden geregistreerd. Echter in Zuid-West Nederland worden geen aardbevingen geconstateerd door de KNMI. Hieruit mag worden geconstateerd dat re-activatie van breuken als gevolg van gasproductie niet of nauwelijks voorkomt in dit gebied.

De mogelijkheid van re-activatie van breuken in P18 is door TNO bestudeerd (Vandeweyer et al, 2011). In het kader van de Barendrecht-Ziedewij opslagplannen is ook gebeurd (Orlic et al, 2007). Voor P18 en Barendrecht-Ziedewijde zijn de conclusies dat de mogelijkheid van re-activatie gering is.

### *Gas migratie te zien op seismische lijnen*

Er zijn aanwijzingen voor aanwezigheid van ondiepe gasaccumulaties en migratie langs breuken (Vandeweyer et al, 2011). Dit gas indien aanwezig, zou afkomstig kunnen zijn uit de Posidonia Fm en /of van biogene gas processen (bacteriën die gas produceren). Dit komt veel voor en is geen bewijs dat P18 afsluitlagen lekken.

### *Lekkage mogelijkheden bij de putten.*

CO<sub>2</sub> lekkage mogelijkheden door de putten en aan buitenzijde van de putwand is uitgebreid beschreven voor het Barendrecht-Ziedewij veld (samenvatting in Wildenberg et al, 2007). Diverse lekkagescenario's zijn in kaart gebracht en onderzocht. Diverse aspecten spelen hierbij een rol. Belangrijk zijn de fysisch-chemische eigenschappen van de vloeistoffen in het reservoir en de toestand van de put tijdens en na beëindiging van de CO<sub>2</sub> injectie.

Hypothetische lekkage mogelijkheden bij putten zijn in detail beschreven door Mulders, et al (2007) voor de Barendrecht en Barendrecht-Ziedewij velden. De maatregelen aanbevolen in deze studie gelden onverkort ook voor de P18 putten. De huidige toestand en status van putten in de P18 velden zijn in kaart gebracht en beschreven in het rapport door Vandeweyer et al, 2011). In deze studie zijn ook aanbevelingen gedaan om de putten geschikt te maken voor CO<sub>2</sub> injectie. De conclusie van deze laatste studie is dat alle putten in de P18 velden in principe geschikt gemaakt kunnen worden voor CO<sub>2</sub> injectie.

Een zestal verschillende theoretische lekkage mogelijkheden zijn in kaart gebracht en geïllustreerd:

1. Aan de buitenkant van de verbuizing (“casing”), tussen verbuizing en het cement aanwezig in de ruimte tussen gesteente en de verbuizing (de cementmantel).
2. Aan de buitenkant van de verbuizing (“casing”), door scheurtjes in het cement dat de ruimte tussen buis en gesteente opvult.
3. Aan de buitenkant van de verbuizing, tussen het gesteente en het cement aanwezig in de ruimte tussen gesteente en de verbuizing.
4. Binnen in de verbuizing (“casing”), tussen de cementplugs en de buis.
5. Binnen in de verbuizing (“casing”), door het cement van de afsluitende cementplugs.
6. Binnen in de verbuizing (“casing”), door de verbuizing als gevolg van corrosie van de verbuizing.

Lekkages kunnen dus optreden aan de buitenkant van de putverbuizing (1, 2, en 3) en aan de binnenkant van de putverbuizing (4, 5, en 6).

Bij lekkage aan de binnenkant van de putverbuizing kan CO<sub>2</sub> ontsnappen naar de atmosfeer en bij lekkage aan de buitenkant van de verbuizing kan CO<sub>2</sub> in de hogere gesteentelagen terecht komen. Beide mogelijkheden worden hier onder beschreven.

#### *Lekkages mogelijkheden aan de buitenkant van de putverbuizing.*

Lekkages aan de buitenkant van de verbuizing kunnen optreden indien de kwaliteit van het cement en de hechting van het cement aan verbuizing en aan het omgevende gesteente niet optimaal is. De effecten van chemische verwerking van het cement als gevolg van de blootstelling aan CO<sub>2</sub> in aanwezigheid van water is beschreven en onderzocht voor Barendrecht-Ziedewij (Mulders et al, 2007, zie ook Newstead et al, 2008a en 2008b). De Bruijn (2008a) in een samenvatting van de geochemische studies stelt dat cementdegradatie als gevolg van blootstelling aan CO<sub>2</sub> gering is; het is ook een langzaam proces en zou eventueel op termijnen langer dan 10,000 jaar een rol kunnen spelen.

Bij lekkage langs de putwand naar boven is het mogelijk dat CO<sub>2</sub> in de zanden van de Boven Jura en Onder Krijt terecht komt<sup>6</sup>.

Deze zanden hebben een uitstekende afsluitende toplaag zoals is aangetoond door de bestaande olievelden die in deze zanden voorkomen (het Rijnveld in P15 en de olie accumulatie in de P18-1 put). De migratie mogelijkheden van CO<sub>2</sub> in de Boven Jura-Onder Krijt zanden zijn onderzocht door Vandeweyer et al (2011). In het onwaarschijnlijke geval dat er CO<sub>2</sub> in voldoende grote hoeveelheden in de Boven Jura-Onder Krijt zanden terecht zou komen, ontstaan er een drietal secundaire CO<sub>2</sub> opeenhopingen. Echter door de goede afsluitende toplaag van deze zanden zullen deze secundaire opeenhopingen een permanent karakter hebben. Ook eventuele verdere migratie paden in hogere zandpakketten zijn onderzocht door Vandeweyer et al (2011). Bij het definitief verlaten van de put en bij twijfel over de cementkwaliteit kan door het plaatsen van een pannekoek plug van tenminste 30 m lengte alle onzekerheid worden weggenomen (Mulders et al, 2007).

#### *Lekkages aan de binnenkant van de putverbuizing.*

Na voltooiing van de CO<sub>2</sub> injectie worden de putten definitief verlaten door het plaatsen van conventionele cement pluggen of pannekoek pluggen. Putten in het CO<sub>2</sub> reservoir die niet gebruikt worden kunnen eerder worden afgesloten. In de studie van Mulders et al (2007) wordt geconcludeerd dat conventionele cement pluggen voldoende zijn bij goede kwaliteit van cementmantels en verbuizing. Indien er twijfels zijn over de kwaliteit van cementmantels en verbuizing kunnen de putten definitief worden afgesloten door pannekoek pluggen.

---

<sup>6</sup> De kans dat CO<sub>2</sub> naar de Boven Jura-Onder Krijt zanden migreert wordt uiterst klein geacht ook door de aanwezigheid van het 500 m dikke pakket Onder Jura schalies. Deze zijn enigszins plastisch en zullen naar verwachting ook bij afwezigheid van cementmantel, de eventuele aanwezige open ruimtes bij de verbuizing dichtdrukken.

Na het plaatsen van conventionele cementpluggen kan lekkage aan de binnenkant van de putverbuizingen optreden door aantasting van de geplaatste cementpluggen. Ook kan door corrosie van de stalen putwand CO<sub>2</sub> in de put terecht komen en naar boven migreren. Dit is onderzocht en beschreven in Mulders et al (2007) en hier wordt geconcludeerd dat deze risico's van CO<sub>2</sub> lekkages verwaarloosbaar klein zijn.

### *Definitieve afsluiting van de putten.*

Definitieve afsluiting van de injectieputten vindt plaats na beëindiging van de CO<sub>2</sub> injectieperiode. De putten kunnen op twee manieren definitief afgesloten worden:

Door het plaatsen van conventionele cementpluggen.

Door het plaatsen van pannekoek pluggen.

Definitieve afsluiting van andere putten in het reservoir (zoals de P/18-2 put) kan plaatsvinden voor dat de injectieperiode wordt beëindigd. Het plaatsen van conventionele cementpluggen kan worden overwogen indien de cementmantel aan de buitenzijde van verbuizing en de verbuizing zelf van voldoende kwaliteit is (Mulders et al (2007)). Het plaatsen van pannekoek pluggen kan worden overwogen indien de kwaliteit van de cementmantel aan de buitenzijde van verbuizing onvoldoende is of indien de kwaliteit van de verbuizing niet kan worden gegarandeerd (Mulders et al, 2007).

De Bruijn (2008b) heeft onderzoek gedaan naar de tijdsduur van complete degradatie (oplossing) van conventioneel cement in afsluitpluggen onder invloed van CO<sub>2</sub> en water en schat deze tijdsduur op groter dan 100,000 jaar. Toepassing van CO<sub>2</sub>-resistent cement zal de levensduur van deze pluggen meer dan verdubbelen.

### **Status van de P18 putten.**

Tabel 11 geeft een overzicht van de putten en uit welk veld en velddeel de putten produceren. In totaal zijn er tien putten in het P18 blok geboord. De bestaande naamgeving van putten en velden is verwarrend. Alle putten met A in de naam zijn geboord vanaf het P18A platform. Het nummer achter de A is een volgorde nummer, eerst A1, daarna A2, daarna A3 etc. Het nummer voor de A refereert naar het veld: P18-2A3 is in het P/18-2 veld en de derde put geboord vanaf platform. P18-4A2 is in het P/18-04 veld en de tweede put geboord vanaf het A platform.

De putten zijn in detail bestudeerd door Vandeweyer et al (2011). Ook Genesis (2010, versie (10 september, 2010) besteed aandacht aan putten.

De conditie van de putten is redelijk tot goed, ook vergeleken met andere putten op het Nederlandse deel van het continentale plat.

P18-1 geboord in 1988 (Tabel 10) doorboort het P/15-9 veld. Een klein deel van dit gasveld is in het P18 blok, het grootste deel is in het P15 Blok. Dit veld maakt geen deel uit van de plannen voor CO<sub>2</sub> injectie in P18.

P18-2 is net als P18-1 niet gedeveerd. De oppervlakte locatie (bovenkant) van P18-2 is niet bij het P18/A platform. Deze put zal definitief worden verlaten.

Beschrijving van de P/18 gasvelden.:

P18-2A4 was een mislukte poging een put te boren. Bij een diepte van 416 m ontstonden er problemen zodat er niet verder kon worden geboord. De put is verlaten.

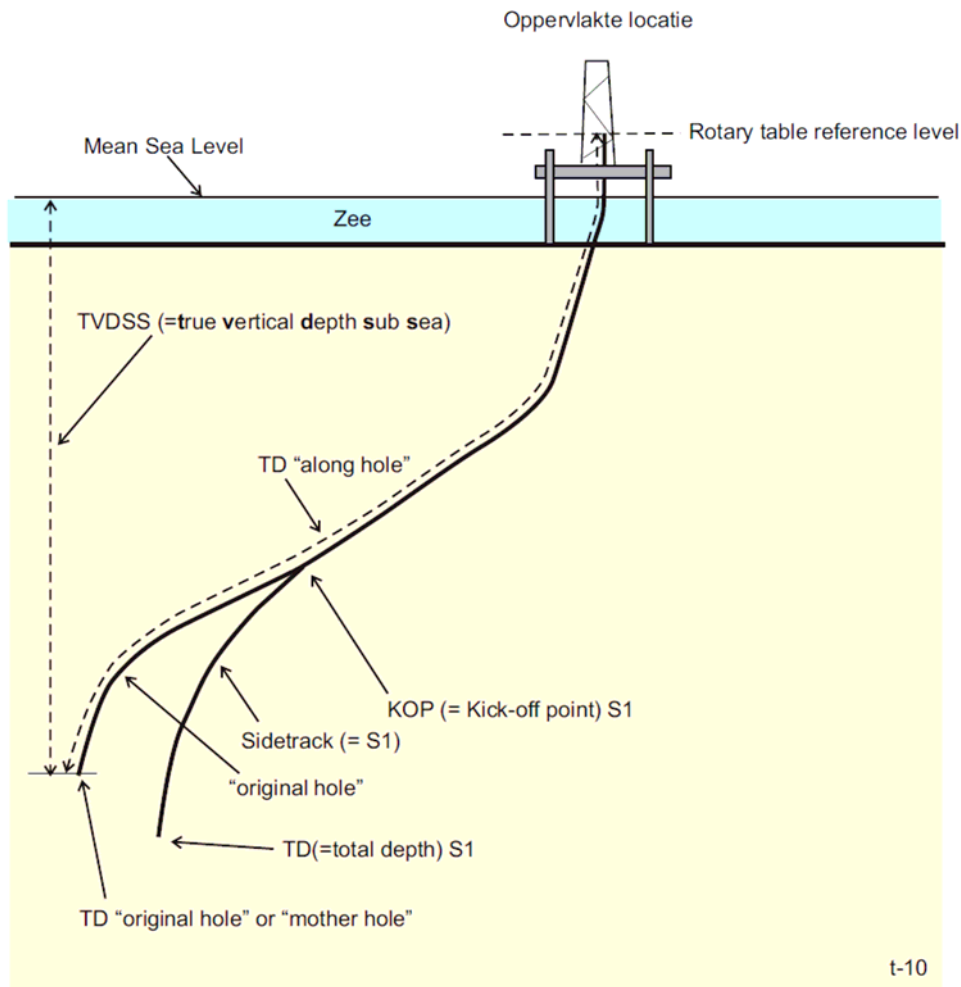
Gas veld	putten	Jaar geboord	Status	TD (m)	opmerkingen
P/15-9	P18-1	1988	“tijdelijk verlaten”	3633	ontdekker P/15-9 veld
P/18-2 veld compartiment I	P18-2	1989	“tijdelijk verlaten”	3766	ontdekker P/18-2 veld; was nooit in productie.
	P18-2A1	1990	productie	3839	
	P18-2A3	1993	productie	4305	Zijtakken S1, S2
	P18-2A4	1993	verlaten	416	put verlaten op 416 m diepte
	P18-2A5	1996-1997	productie	5229	zijtak S1
P/18-2 veld compartiment II	P18-2A6-S1	2003	productie		zijtak van P18-2A6
P/18-2 field compartiment III	P18-2A6	1997	productie	4852	
P/18-4 veld	P18-4A2	1991	productie	4352	oude naam P18-4
P/18-6 veld	P18-6A7	2003	productie	5065	Zijtak S1

Tabel 9. Putten in het P18 Blok. Diepte (TD) van de putten is gemeten langs het boorgat (“along hole”, zie Figuur 21). Zie ook de kaart van Figuur 3, waar alleen de mislukte put P18-2A4 niet op staat.

### Zijtakken (“sidetracks”)

Verskillende putten hebben zijtakken (“sidetracks”), zie Figuur 21 voor enige terminologie. Er zijn twee redenen om een zijtak te boren:

1. Gedwongen doordat er problemen zijn ontstaan tijdens het boren van de put en er niet meer verder kan worden geboord. In dat geval kan er een zijtak worden geboord. Er wordt begonnen met de zijtak ruim boven het niveau waar het probleem aanwezig is en vervolgens in de zijtak verder geboord. De originele tak met het probleem wordt afgesloten en verlaten. Een voorbeeld van dergelijke problemen is put P18-2A5. In deze put is het onderst gedeelte van het boorapparaat (“bottom hole assembly”) losgeraakt en in het boorgat gevallen. Pogingen die weer uit de put te vissen mislukten. Putten met deze zijtakken zijn P18-2A3, P18-2A5 en P18-6A7 (zie Tabel 10). Het hebben van deze zijtakken heeft verder geen consequentie voor de put en kan daarom worden genegeerd.
2. Vrijwillig. In dit geval zijn er geen boorproblemen en wordt er een zijtak geboord om een ander reservoir aan te sluiten. In het geval van P18-2A6 en P18-2A5 is het originele eerste boorgat in het Compartiment III van het P/18-2 veld. Later werd er een zijtak geboord om compartiment II van het P/18-2 veld aan te sluiten. Deze oplossing is veel goedkoper dan een hele nieuwe put te boren. Op dit moment (jaar 2011) zijn beide zijtakken tegelijk in productie.



Figuur 21. Schematische voorstelling van een put met zijtak ("sidetrack") en enige terminologie. De dieptes worden gemeten in het boorgat ("along hole") vanaf een referentie punt in de boorinstallatie, meestal de "rotary table". De hoogte van dit referentie punt t.o.v. gemiddeld zee niveau wordt gemeten. Met behulp van de deviatie data van de put worden vervolgens dieptes omgerekend naar TVD (**T**otal **V**ertical **D**epth), t.o.v. het gemiddelde zeeniveau is dat TVDSS (=Total Vertical Depth Sub-Sea).

### Samenvatting en aanbevelingen van de put inventarisatie studies

De put P18-2 put is afgesloten, maar voor CO<sub>2</sub> opslag is de afsluiting van onvoldoende kwaliteit. Aanbevolen word deze put op een correcte en veilige manier af te sluiten.

Alle putten geboord van het A platform zijn goed toegankelijke en kunnen worden gecontroleerd en zo nodig worden aangepast voor CO<sub>2</sub> injectie. Speciale aandacht moet worden besteed aan P18-2A6 en P18-2A6 S1. Aanbevolen word P18-2A S1 af te sluiten en P18-2A6 om te bouwen tot injector.

Definitieve afsluiting na beëindiging van de CO<sub>2</sub> injectie kan op twee manieren gebeuren: 1) met conventionele cementpluggen of 2) met zogenaamde pannekoek



pluggen. De eerste methode is goedkoper en kan worden uitgevoerd indien er geen twijfels zijn over de status van de put en cement mantels. De twee manier kan worden gekozen indien de cementmantel over de kritieke intervallen van onvoldoende kwaliteit is.

## Referenties

Bisschop, R., F. Seeberger, M. Slaats, R. van Eijs & J. Newstead, 2007, CO2 interaction with Chalk, Doc. no.: EP200709215852.

De Jager, J. M. A. Doyle, P. J. Grantham & J. E. Mabillard, 1996. Hydrocarbon habitat of the est Netherlands Basin. In: Rondeel et al (eds) Geology of Gas and Oil in the Netherlands Kluwer Academic Publishers, p. 191-209.

De Jager, J., 2007, Geological development. In: Wong et al (eds); Geology of the Netherlands. P. 5-26.

De Bruijn, J., 2008a, Geochemical consequences for CO2 storage in the BRT(-Z) fields Summary. EP200810202805.

De Bruijn, J., 2008b, Well cement degradation for CO2 injection fields, EP200710220925.

Genesis, 2010 (versie 10 September), Concept study for transportation & Processing CO2 offshore, Phase 2 report, (versie 10 September), J-71495/A (J71495-A-A-RT-002-B2.docm).

Holt, S & M. Vasmel, 2009, Technisch geologisch onderzoek naar CO2-opslag in het Barendrecht veld. TA3600. Delft University.

Mulders, F.M.M., R. Gouwen, B. Orlic, & T. Benedictus, 2007, Well Integrity for CO2 storage in the fields Barendrecht and Barendrecht-Ziedewij gas fields, TNO report 2007-U-R1057/B.

Newstead, J., H. Priebe, A. Sluijk, M. Lorenzo, M. Slaats, F. Seeberger, R. Bisschop, K. van Ojik, R. Trompert, J. de Bruijn, R. van Eijs, L. Finlayson, L. Haron, 2008a, Leak volume and rate assessment; paragraph 13.7 of Technical Field Development Plan Barendrecht & Barendrecht-Ziedewij CO2 Geostorage. NAM Report No: EP200801218447.

Newstead, J., H. Priebe, A. Sluijk, M. Lorenzo, M. Slaats, F. Seeberger, R. Bisschop, K. van Ojik, R. Trompert, J. de Bruijn, R. van Eijs, L. Finlayson, L. Haron, 2008b; Chapter 6 Chemical Interaction Study of Technical Field Development Plan Barendrecht & Barendrecht-Ziedewij CO2 Geostorage. Report No: EP200801218447.

Orlic, B., P. Fokker, K. Geel, 2007, Caprock and Fault Integrity for CO<sub>2</sub> storage in the Barendrecht and Barendrecht-Ziedewij gas fields. TNO report; 2007-U-R1057/B.

Racero-Baena, A. & S. J. Drake, 1996. Structural style and reservoir development in the West Netherlands oil province. In: Rondeel et al (eds) *Geology of Gas and Oil in the Netherlands* Kluwer Academic Publishers, p. 211-277.

Seeberger, F. 2008a, Estimation of de-hydration effects due to injection of dry CO<sub>2</sub> in Barendrecht and Barendrecht Ziedewij, report EPE 200810202504.

Seeberger, F., 2008b, Estimation of long-term pressure increase due to ongoing gas charge in Barendrecht. Shell EPE report No. EP200810203728.

Spain, D. R. & C. P. Conrad, 1997, Quantitative analysis of top-seal capacity: Offshore Netherlands, Southern North Sea. *Geologie en mijnbouw*, 76, p. 217-1997.

TNO-NITG, 2002, Geological Atlas of the Netherlands, (Explanations to) Mapsheets VII and VIII, Noordwijk-Rotterdam and Amsterdam-Gorinchem. ISBN 90-72869-65-6

TAQA, 2009, Reservoir description P18 fields for CO<sub>2</sub> sequestration. (unpublished) Report constituted for Electrabel/E.on For EEP Application.

Van Adrichem Boogaert, H.A. & W.F.P. Kouwe, 1993, Stratigraphic Nomenclature of the Netherlands, revision and update by the RGD and NOGEP, Mededelingen Rijks Geologische Dienst, No. 50, 1993.

Van Balen, R.T, F. van Bergen, C. de Leeuw, H. Pagnier, H. Simmelink, J.D. van Wees & J. M. Verweij, 2000, Modelling the hydrocarbon generation and migration in the West Netherlands Basin, the Netherlands, *Geologie en Mijnbouw / Netherlands Journal of Geosciences* 79 (1): 29-44 (2000).

Van Bergen, F, T. Tambach, C. Hofstee & P.David, 2008, Geochemical consequences of CO<sub>2</sub> injection in the Barendrecht and Barendrecht-Ziedewij gas fields. TNO report 2007-U-R1057/B – revised Date May 1, 2007 – revised September 2008.

Van Eijs, R., & F. Seeberger, 2008, Barendrecht (BRT) CO<sub>2</sub> sequestration: consequence from a irreversible stress path NAM report EP200803212403.

Vandeweyer, V. R., R. Groenenberg, R. Donselaar, M. Pluymaekers,, D. Loeve, C. Hofstee, M. Nepveu, B. Orlic, A. Akemu, U. Miersemann, T. Benedictus, R. Arts, F. Neele, W. Meindertsma, 2011, Feasibility study P18 (final report). CATO2-WP3.01-D06 report; p.1-197.

Wildenborg, T., F. van Bergen, F. Mulders, T. Benedictus, B. Orlic, C. Hofstee & F. Neele, 2007, Technical investigations supporting the feasibility of effective and safe

### Beschrijving van de P/18 gasvelden.:

storage of CO<sub>2</sub> in the Barendrecht (BRT) and Barendrecht-Ziedewij (BRTZ) gas fields.  
Executive summary, TNO report 2007-U-R1057/B.

Winningsplan P18 velden, 2003. Zie internet:

[http://dinodds51.dinonet.nl/deliverables/sync/NLOG\\_FieldAsset\\_6733\\_20070918-1-01-Pub\\_Public\\_Winningsplan\\_P18.pdf](http://dinodds51.dinonet.nl/deliverables/sync/NLOG_FieldAsset_6733_20070918-1-01-Pub_Public_Winningsplan_P18.pdf)